Zoosystematics and Evolution

101 (2) 2025

PENSOFT

MUSEUM FÜR NATURKUNDE BERLIN

Zoosystematics and Evolution
A Bulletin of Zoology since 1898

Publisher

PENSOFT

Zoosystematics and Evolution

2025. Volume 101. 2 Issue

ISSN: 1435-1935 (print), 1860-0743 (online)
Abbreviated keys title: Zoosyst. Evol.

In Focus

The cover picture shows holotype (SWU 0008699) of *R. medogensis* sp. nov. in situ.

See paper of **Weng S, Liu X, Li J, Yu G, Huang J:** A new species of *Rhacophorus* (Anura, Rhacophoridae) from Xizang, China, with a revision of the distribution of *R. bipunctatus*.

Cover design
Pensoft

Zoosystematics and Evolution
A Bulletin of Zoology since 1898

Content of volume **101** (**2**) 2025

Xiao M-Y, Wang J-J, Luo T, Zhou J-J, Xiao N, Zhou J
Sinocyclocheilus xingrenensis (Cypriniformes, Cyprinidae), a new underground fish from Guizhou Province, Southeastern China 419

Weng S, Liu X, Li J, Yu G, Huang J
A new species of *Rhacophorus* (Anura, Rhacophoridae) from Xizang, China, with a revision of the distribution of *R. bipunctatus* 437

Wu Y-H, Yu Z-B, Yang S-P, Duan Z-P, Zuo A-R, Zhang D-C, Kasyoka Kilunda F, Murphy RW, Che J
Morphological and molecular evidence for a new species of the genus *Leptobrachella* (Anura, Megophryidae) from Gaoligong Mountain Range, Yunnan, China 449

Liu M, Lyu J-B, Du L-N, Chen X-Y
Description of a new loach species, *Yunnanilus triangulus* sp. nov. (Cypriniformes, Nemacheilidae), from Yunnan, China 465

Dong D, Seid CA, Li X, Rouse GW
A new Pacific Ocean species of *Typhlonida* Macpherson & Baba, 2022 (Crustacea, Decapoda, Munididae) from the flank of the emergent seamount Isla del Coco (Costa Rica) with notes on the phylogeny of the genus 473

Pan Y, Liu S, Chen J, Yu G
Underestimated species diversity in *Zhangixalus* (Anura, Rhacophoridae) with a description of two cryptic species from southern China 485

Benchapong T, Enghoff H, Likhitrakarn N, Chanabun R, Aoonkum A, Srisonchai R
Three new species of the millipede genus *Enghoffosoma* Golovatch, 1993 from Thailand (Diplopoda, Polydesmida, Paradoxosomatidae) 509

Jiang C, Fan J, You C, Li W, Huang L
New species of *Tygarrup* centipedes from Xizang, China (Geophilomorpha, Mecistocephalidae) 533

Xie G-L, Zhang G, Meng K, Köhler F
An illustrated type catalogue of *Diplommatina* Benson, 1849 from mainland China, with description of a new species, *Diplommatina yipingica* (Gastropoda, Cyclophoroidea) 551

García-Ruiz M, Abolafia J, Peña-Santiago R
Retrieval of the genus *Capitellus* Siddiqi, 1983, with description of *C. caramborum* sp. nov. (Dorylaimida, Belondiridae) associated with Andalusian (Spain) olive groves 571

Vu TTT, Abolafia J, Nguyen AD, Le TML, Peña-Santiago R
Vastnema crassicutaneum gen. et sp. nov. (Nematoda, Dorylaimida, Dorylaimidae), an interesting new taxon from natural areas of Vietnam 583

Yang S, Xie F, Zhou C, Zhang Z, Wang X, Liu S, Chen S
Molecular phylogeny and taxonomy of the genus *Eozapus* (Mammalia, Rodentia, Zapodidae) with the description of a new speciesh 597

Abstract & Indexing Information

Biological Abstracts® (Thompson ISI)
BIOSIS Previews® (Thompson ISI)
Cambridge Scientific Abstracts (CSA/CIG)
Web of Science® (Thompson ISI)
Zoological Record™ (Thompson ISI)

Zoosystematics and Evolution
A Bulletin of Zoology since 1898

Content of volume **101** (**2**) 2025

Chan T-Y, Yang C-H, Kumar AB, Hurzaid A
On the commercial shrimps of the "*Parapenaeopsis cornuta* (Kishinouye, 1900)" species group (Crustacea, Decapoda, Penaeidae) 609

Liu M, Li J, Zhang Y, Aspe NM, Wu D, Zhao H, Zheng G
A new species of the *Drawida ghilarovi* species complex (Oligochaeta, Moniligastridae) in Changbai Mountain, Northeast China 627

Zhang L-J, Shu S-S, Song X-Y, Naing NH, Oo TN, Chen X-Y
A revision of Bithyniidae (Mollusca, Gastropoda) from the Inle Lake Basin, Myanmar 643

Fang Y, Sun Z, Zhao Y
Taxonomic revision on the *Gobio* group in the Yellow River drainage, with discussion on the validity of the genus *Acanthogobio* (Cypriniformes, Gobionidae) 661

Lei H-T, He L, Huang J-H, Zhou J-J, He D-K
Description of a new cave-dwelling species of *Claea* (Teleostei, Cypriniformes, Nemacheilidae) from the Yangtze River basin in Sichuan, southern China 681

Cao L, Liu Y, Zeng Z, Yi W, Zhang E
Two new species of the loach genus *Homatula* Nichols, 1925 (Pisces, Nemacheilidae) from the upper Chang-Jiang Basin in China 697

Zhang J, Zhang H, Liu J, Yu H, Xu X
A survey of mimetid spiders (Araneae, Mimetidae) from Central Guizhou Province, China 711

Zhang R, Zhou Y, Mao J, Wang C, Zhang D
Hidden diversity of *Freyastera* (Asteroidea, Brisingida, Freyellidae) at great depth: Description of new species and remarks on species boundaries 735

Wu Q, Lin Y-T, Qiu J-W, Xu MY, Xing BP
Two new species of *Idas* (Bivalvia, Mytilidae) from sunken wood in the East China Sea: description, phylogenetic position and symbionts 761

Dai Y-T, Chen Z-G, Ouyang S, Huang X-C, Wu X-P
A new tribe, genus, and species of freshwater mussel from the Changjiang River Basin in China (Bivalvia, Unionidae, Unioninae) 779

Jia C, Xu Z, Li F, Chen L, Wang A, Gao F
Taxonomic status and phylogenetic analyses based on complete mitochondrial genome and microscopic ossicles: Redescription of a controversial tropical sea cucumber species (Holothuroidea, *Holothuria* Linnaeus, 1767) 791

Dai Y-T, Chen Z-G, Li F, Huang X-C, Ouyang S, Wu X-P
A new genus and species of freshwater mussel from the Pearl River Basin in Guangxi, China (Bivalvia, Unionidae, Gonideinae) 805

Knauber H, Schell T, Brandt A, Riehl T
Across trench and ridge: description of five new species of the *Haploniscus belyaevi* Birstein, 1963 species complex (Isopoda, Haploniscidae) from the Kuril-Kamchatka Trench region 813

Turbanov IS, Bolotovskiy AA, Artaev ON, Gandlin AA, Levina MA, Vasil'eva ED, Levin BA
On the border of Europe and Asia: *Gobio uralensis*, a new species of gudgeons (Cypriniformes, Gobionidae) from the Caspian Sea basin 855

Wang Y-R, Sha Z-L
Discovery and taxonomic exploration of *Metopa propoda* sp. nov., a new species of Stenothoidae Boeck, 1871 (Amphipoda, Amphilochoidea) from a seamount of the Caroline Plate, Western Pacific 875

Benito M, Conradie W, Vaz Pinto P, Lobón-Rovira J
A needle in a haystack: Rediscovery and revised description of *Ichnotropis microlepidota* Marx, 1956, from the central highlands of Angola 887

Zoosyst. Evol. 101 (2) 2025, 419–436 | DOI 10.3897/zse.101.141444

PENSOFT

für Natur MUSEUM FÜR NATURKUNDE BERLIN

Sinocyclocheilus xingrenensis (Cypriniformes, Cyprinidae), a new underground fish from Guizhou Province, Southeastern China

Ming-Yuan Xiao[1*], Jia-Jia Wang[2*], Tao Luo[3,4], Jia-Jun Zhou[5], Ning Xiao[6], Jiang Zhou[2]

1 *School of Life Sciences, Guizhou Normal University, Guiyang 550001, Guizhou, China*
2 *School of Karst Science, Guizhou Normal University, Guiyang 550025, Guizhou, China*
3 *School of Life Sciences, Yunnan University, Kunming 650504, Yunnan, China*
4 *Southwest United Graduate School, Kunming 650092, Yunnan, China*
5 *Zhejiang Forest Resource Monitoring Center, Hangzhou 310020, Zhejiang, China*
6 *Guiyang Healthcare Vocational University, Guiyang 550081, Guizhou, China*

https://zoobank.org/F445B038-1840-4CFF-AD1F-A4A5095E1265

Corresponding authors: Ning Xiao (armiger@163.com); Jiang Zhou (zhoujiang@ioz.ac.cn)

Academic editor: Nicolas Hubert ♦ **Received** 10 November 2024 ♦ **Accepted** 16 January 2025 ♦ **Published** 24 February 2025

Abstract

This study describes a new species, *Sinocyclocheilus xingren*ensis **sp. nov.**, collected from a cave near Xingren City, Guizhou Province, China. Morphologically, the new species can be distinguished from the 80 species currently assigned to the genus *Sinocyclocheilus* by a combination of the following characteristics: absence of horn-like structures and indistinct elevation at the head-dorsal junction; body scaleless, with irregular black markings scattered above the lateral line; tip of pectoral fin not reaching the pelvic fin origin; tip of pelvic fin not reaching the anus; lateral line complete and curved, with pores 65–77; tip of maxillary barbel reaching the anterior margin of the operculum; and six rakers on the first gill arch. Phylogenetic trees constructed based on mitochondrial genes indicate that the new species represents an independent evolutionary lineage with relatively large genetic differences of 2.8–9.0% for the mitochondrial Cyt *b* and 2.7–8.5% for ND4.

Key Words

Beipanjiang River, Cavefish, morphology, phylogeny, taxonomy

Introduction

Southwest China is a region of highly developed karst landscapes, with caves that harbor a wide diversity of cave fishes (Wu et al. 2023). The golden-line fish genus *Sinocyclocheilus* Fang, 1936, a typical taxon of cave fishes endemic to China, is primarily distributed in the karst region of Southwestern China (Zhao and Zhang 2009; Xu et al. 2023) in Guangxi, Guizhou, Yunnan, and Hubei Provinces. After the publication of the type species *S. tingi* of the genus *Sinocyclocheilus* in 1936 (Fang 1936), there was no significant progress in the study of the genus for decades. However, the study of *Sinocyclocheilus* accelerated after 1980, with many new species being documented based on morphology. More species of *Sinocyclocheilus* were documented after 2010 with the advent of molecular phylogenetics. To date, the genus has been one of the most diversified genera in the family Cyprinidae, comprising more than 80 species (Zhao and Zhang 2009; Jiang et al. 2019; Xu et al. 2023; Luo et al. 2023; Shao et al. 2024; Fan et al. 2024) (Table 1). Since the discovery of the first species in the genus, *Sinocyclocheilus tingi* (Fang 1936), subsequent research demonstrated that due to the uplift of the Qinghai-Xizang Plateau and resulting

* These authors contributed equally to this paper.

climate change (Wen et al. 2022). A recent phylogenetic study, dividing *Sinocyclocheilus* into five species groups, *S. jii*, *S. angularis*, *S. cyphotergous*, *S. microphthalmus*, and *S. tingi* groups (Wen et al. 2022).

As the main species group in the distribution of *Sinocyclocheilus* on the Yunnan-Guizhou Plateau, the *S. tingi* species group currently includes 27 species (Table 1). These species are mainly found in eastern Yunnan and western Guizhou, including the Nanpanjiang River, Beipanjiang River, Jinshajiang River, Yuanjiang River, and Lancangjiang River (Fig. 1). Currently, three species of this species group are recorded in Guizhou Province, i.e., *S. angustiporus* Zheng & Xie, 1985, *S. robustus* Chen & Zhao, 1988, and *S. xiejiahuai* Luo, Fan, Xiao & Zhou, 2024, have been recorded (Fan et al. 2024) (Fig. 1). Moreover, four new species, *S. longicornus* Luo, Xu, Wu, Zhou & Zhou, 2023; *S. xingyiensis* Luo, Tang, Deng, Duan & Zhang, 2023; *S. guiyang* Shao, Chen, Lu, Zhou & Zeng, 2024; and *S. xiejiahuai*, have recently been described from Guizhou, suggesting that the diversity of the genus in Guizhou may be underestimated.

We collected seven specimens of the genus *Sinocyclocheilus* during fish surveys in southwestern Guizhou Province between 2012 and 2020. These specimens were morphologically similar to *S. angustiporus*, e.g., having irregular black markings above the lateral line (Wu et al. 1989). However, subsequent morphological comparisons and phylogenetic analyses indicated that these seven specimens represented an undescribed species. Here, we provide the formal description of that new species as *Sinocyclocheilus xingrenensis* sp. nov.

Materials and methods

Specimen sampling, morphological comparison, and statistical analysis

Seven specimens were collected from 2012 to 2020 from several caves in Xingren City, Guizhou Province, China. Gill muscle tissues used for the molecular analysis were preserved in 95% alcohol at −20 °C. All specimens were fixed in 10% buffered formalin and then transferred to 75% ethanol for morphological comparison and long-term preservation. The specimens were deposited at Guizhou Normal University, Guiyang City, Guizhou Province, China.

The new species was placed in the *S. tingi* group based on morphology, e.g., absence of horn-like structures and indistinct elevation at the head-dorsal junction, tip of pectoral fins not reaching the pelvic-fin origin, and the presence of serrations along the posterior margin of the last unbranched fin of the dorsal fin (Zhao and Zhang 2009). Therefore, this study focused on morphological comparisons with the 27 species within the *S. tingi* group (Table 2).

We also examined the type and/or materials from the type-localities of *S. aluensis*, *S. angustiporus*, *S. anophthalmus*, *S. grahami*, *S. huaningensis*, *S. huizeensis*, *S. lateristriatus*, *S. macrocephalus*, *S. maitianheensis*, *S. malacopterus*, *S. oxycephalus*, *S. purpureus*, *S. qiubeiensis*, *S. qujingensis*, *S. tingi*, *S. wenshanensis*, *S. xichouensis*, and *S. xiejiahuai* (Appendix 1).

We measured 34 morphometric characters from a total of seven specimens of the new species referenced from Xu et al. (2023). Principal component analysis (PCA) of corrected morphometric measurements and two-dimensional scatter plots were used to explore the relative contributions of specific variables to the morphological variation. Before the PCA analysis, all measurements were normalized using ratios to standard length (standard length being defined as the ratio to the full length) followed by log transformation. PCA analyses were performed in SPSS 21.0 (SPSS, Inc., Chicago, IL, USA).

DNA extraction, PCR amplification, and sequencing

We sequenced six samples from the genus *Sinocyclocheilus*. Genomic DNA was extracted from muscle tissues using a DNA extraction kit (Tiangen Biotech Co., Ltd., Beijing, China). Because the most often used molecular markers for *Sinocyclocheilus* are fragments of the mitochondrial cytochrome b (Cyt *b*) and NADH dehydrogenase subunit 4 (ND4) genes, we selected these fragments for amplification and sequencing. The primers used for Cyt *b* were L14737 (5'-CCACCGTTGTTAATTCAACTAC-3') and H15915 (5'-CTCCGATCTCCGGATTACAAGAC-3'), following Xiao et al. (2005). The primers used for ND4 were L11264 (5'-ACGGGACTGAGCGATTAC-3') and H12346 (5'-TCATCATATTGGGTTAG-3'), following Xiao et al. (2005). PCR amplifications were performed in a 25-µl reaction volume with the following cycling conditions: an initial denaturing step at 95 °C for 3 min; 35 cycles of denaturing at 94 °C for 50 s, annealing at 52 °C (for Cyt *b* and ND4) for 1 min, extension at 72 °C for 1 min, and a final extension step at 72 °C for 10 min. The PCR products were sequenced on an ABI Prism 3730 automated DNA sequencer at Chengdu TSING KE Biological Technology Co., Ltd. (Chengdu, China). All sequences were deposited in GenBank (Table 2).

Phylogenetic analyses and genetic distance

We used a total of 116 mitochondrial sequences for molecular analyses, including 61 Cyt *b* sequences and 55 ND4 sequences. Six samples of muscle tissues from *S. guiyang*, *S. aluensis*, *S. angustiporus*, and the new species were sequenced, and 96 sequences were downloaded from GenBank. We selected *Carassius auratus*, *Cyprinus carpio*, *Garra orientalis*, *Neolissochilus hexagonolepis*, *Schizothorax yunnanensis*, *Barbus barbus*, *Onychostoma simum*, *Pethia ticto*, *Myxocyprinus asiaticus*, and *Danio rerio* as outgroups (Wen et al. 2022).

Table 1. List of 80 currently recognized species of the genus *Sinocyclocheilus* endemic to China and references. Recognized species modified from Jiang et al. (2019) and Xu et al. (2023).

ID	Species	Species group	Province	Rivers	Literature obtained
1	*S. altishoulderus* (Li & Lan, 1992)	*S. angularis* group	Guangxi	Hongshui River	Li and Lan 1992
2	*S. anatirostris* Lin & Luo, 1986	*S. angularis* group	Guangxi	Hongshui River	Lin and Luo 1986
3	*S. angularis* Zheng & Wang, 1990	*S. angularis* group	Guizhou	Beipanjiang River	Zheng and Wang 1990
4	*S. aquihornes* Li & Yang, 2007	*S. angularis* group	Yunnan	Nanpanjiang River	Li et al. 2007
5	*S. bicornutus* Wang & Liao, 1997	*S. angularis* group	Guizhou	Beipanjiang River	Wang and Liao 1997
6	*S. brevibarbatus* Zhao, Lan & Zhang, 2009	*S. angularis* group	Guangxi	Hongshui River	Zhao et al. 2009
7	*S. broadihornes* Li & Mao, 2007	*S. angularis* group	Yunnan	Nanpanjiang River	Li and Mao 2007
8	*S. convexiforeheadus* Li, Yang & Li, 2017	*S. angularis* group	Yunnan	Nanpanjiang River	Yang et al. 2017
9	*S. hyalinus* Chen & Yang, 1994	*S. angularis* group	Yunnan	Nanpanjiang River	Chen et al. 1994
10	*S. longicornus* Luo, Xu, Wu, Zhou & Zhou, 2023	*S. angularis* group	Guizhou	Nanpanjiang River	Xu et al. 2023
11	*S. jiuxuensis* Li & Ran, 2003	*S. angularis* group	Guangxi	Hongshui River	Li et al. 2003c
12	*S. flexuosdorsalis* Zhu & Zhu, 2012	*S. angularis* group	Guangxi	Nanpanjiang River	Zhu and Zhu 2012
13	*S. furcodorsalis* Chen, Yang & Lan, 1997	*S. angularis* group	Guangxi	Hongshui River	Chen et al. 1997
14	*S. mashanensis* Wu, Liao & Li, 2010	*S. angularis* group	Guangxi	Hongshui River	Wu et al. 2010
15	*S. rhinocerous* Li & Tao, 1994	*S. angularis* group	Yunnan	Nanpanjiang River	Li and Tao 1994
16	*S. simengensis* Li, Wu, Li & Lan, 2018	*S. angularis* group	Guangxi	Hongshui River	Wu et al. 2018
17	*S. tianeensis* Li, Xiao & Luo, 2003	*S. angularis* group	Guangxi	Hongshui River	Li et al. 2003d
18	*S. tianlinensis* Zhou, Zhang, He & Zhou, 2004	*S. angularis* group	Guangxi	Nanpanjiang River	Zhou et al. 2004
19	*S. tileihornes* Mao, Lu & Li, 2003	*S. angularis* group	Yunnan	Nanpanjiang River	Mao et al. 2003
20	*S. xingyiensis* Luo, Tang, Deng, Duan & Zhang, 2023	*S. angularis* group	Guizhou	Nanpanjiang River	Luo et al. 2023
21	*S. zhenfengensis* Liu, Deng, Ma, Xiao & Zhou, 2018	*S. angularis* group	Guizhou	Beipanjiang River	Liu et al. 2018b
22	*S. anshuiensis* Gan, Wu, Wei & Yang, 2013	*S. microphthalmus* group	Guangxi	Hongshui River	Gan et al. 2013
23	*S. microphthalmus* Li, 1989	*S. microphthalmus* group	Guangxi	Hongshui River	Li 1989
24	*S. longshanensis* Li & Wu, 2018	*S. microphthalmus* group	Yunnan	Nanpanjiang River	Li et al. 2018
25	*S. aluensis* Li & Xiao, 2005	*S. tingi* group	Yunnan	Nanpanjiang River	Li et al. 2005
26	*S. angustiporus* Zheng & Xie, 1985	*S. tingi* group	Guizhou; Yunnan	Beipanjiang River; Nanpanjiang River	Zheng and Xie 1985
27	*S. anophthalmus* Chen & Chu, 1988	*S. tingi* group	Yunnan	Nanpanjiang River	Chen et al. 1988a
28	*S. bannaensis* Li, Li & Chen, 2019	*S. tingi* group	Yunnan	Luosuojiang River	Li et al. 2019
29	*S. grahami* (Regan, 1904)	*S. tingi* group	Yunnan	Jinshajiang River	Zhao and Zhang 2009
30	*S. guishanensis* Li, 2003	*S. tingi* group	Yunnan	Nanpanjiang River	Li et al. 2003a
31	*S. huaningensis* Li, 1998	*S. tingi* group	Yunnan	Nanpanjiang River	Li et al. 1998
32	*S. huizeensis* Cheng, Pan, Chen, Li, Ma & Yang, 2015	*S. tingi* group	Yunnan	Niulanjiang River	Cheng et al. 2015
33	*S. lateristriatus* Li, 1992	*S. tingi* group	Yunnan	Nanpanjiang River	Li 1992
34	*S. longifinus* Li, 1998	*S. tingi* group	Yunnan	Nanpanjiang River	Li et al. 1998
35	*S. macrocephalus* Li, 1985	*S. tingi* group	Yunnan	Nanpanjiang River	Li 1985
36	*S. maculatus* Li, 2000	*S. tingi* group	Yunnan	Nanpanjiang River	Li et al. 2000a
37	*S. maitianheensis* Li, 1992	*S. tingi* group	Yunnan	Nanpanjiang River	Li 1992
38	*S. malacopterus* Chu & Cui, 1985	*S. tingi* group	Yunnan	Nanpanjiang River	Chu and Cui 1985
39	*S. oxycephalus* Li, 1985	*S. tingi* group	Yunnan	Nanpanjiang River	Li 1985
40	*S. purpureus* Li, 1985	*S. tingi* group	Yunnan	Nanpanjiang River	Li 1985
41	*S. qiubeiensis* Li, 2002	*S. tingi* group	Yunnan	Nanpanjiang River	Li et al. 2002b
42	*S. qujingensis* Li, Mao & Lu, 2002	*S. tingi* group	Yunnan	Nanpanjiang River	Li et al. 2002c
43	*S. robustus* Chen & Zhao, 1988	*S. tingi* group	Guizhou	Nanpanjiang River	Chen et al. 1988b
44	*S. tingi* Fang, 1936	*S. tingi* group	Yunnan	Nanpanjiang River	Zhao and Zhang 2009
45	*S. wenshanensis* Li, Yang, Li & Chen, 2018	*S. tingi* group	Yunnan	Jinshajiang River	Yang et al. 2018
46	*S. wumengshanensis* Li, Mao, Lu & Yan, 2003	*S. tingi* group	Yunnan	Jinshajiang River	Li et al. 2003a
47	*S. xichouensis* Pan, Li, Yang & Chen, 2013	*S. tingi* group	Yunnan	Panlonghe River	Pan et al. 2013
48	*S. yangzongensis* Chu & Chen, 1977	*S. tingi* group	Yunnan	Nanpanjiang River	Zhao and Zhang 2009
49	*S. yimenensis* Li & Xiao, 2005	*S. tingi* group	Yunnan	Yuanjiang River	Li et al. 2005

ID	Species	Species group	Province	Rivers	Literature obtained
50	*S. xiejiahuai* Fan, Luo, Xiao & Zhou, 2024	*S. tingi* group	Guizhou	Beipanjiang River	Fan et al. 2024
51	*S. macroscalus* Li, 1992	*S. tingi* group	Yunnan	Nanpanjiang River	Li 1992
52	*S. brevis* Lan & Chen, 1992	*S. cyphotergous* group	Guangxi	Liujiang River	Chen and Lan 1992
53	*S. cyphotergous* (Dai, 1988)	*S. cyphotergous* group	Guizhou	Hongshui River	Huang et al. 2017
54	*S. donglanensis* Zhao, Watanabe & Zhang, 2006	*S. cyphotergous* group	Guangxi	Hongshui River	Zhao et al. 2006
55	*S. dongtangensis* Zhou, Liu & Wang, 2011	*S. cyphotergous* group	Guizhou	Liujiang River	Zhou et al. 2011
56	*S. gracilicaudatus* Zhao & Zhang, 2014	*S. cyphotergous* group	Guangxi	Liujiang River	Wang et al. 2014
57	*S. huanjiangensis* Wu, Gan & Li, 2010	*S. cyphotergous* group	Guangxi	Liujiang River	Wu et al. 2010
58	*S. hugeibarbus* Li, Ran & Chen, 2003	*S. cyphotergous* group	Guizhou	Liujiang River	Li et al. 2003b
59	*S. lingyunensis* Li, Xiao & Lu, 2000	*S. cyphotergous* group	Guangxi	Hongshui River	Li et al. 2000b
60	*S. longibarbatus* Wang & Chen, 1989	*S. cyphotergous* group	Guizhou; Guangxi	Liujiang River	Wang and Chen 1989
61	*S. luopingensis* Li & Tao, 2002	*S. cyphotergous* group	Yunnan	Nanpanjiang River	Li et al. 2002a
62	*S. macrolepis* Wang & Chen, 1989	*S. cyphotergous* group	Guizhou; Guangxi	Liujiang River	Wang and Chen 1989
63	*S. macrophthalmus* Zhang & Zhao, 2001	*S. cyphotergous* group	Guangxi	Hongshui River	Zhang and Zhao 2001
64	*S. multipunctatus* (Pellegrin, 1931)	*S. cyphotergous* group	Guizhou; Guangxi	Hongshui River; Wujiang River	Zhao and Zhang 2009
65	*S. punctatus* Lan & Yang, 2017	*S. cyphotergous* group	Guizhou; Guangxi	Liujiang River; Hongshui River	Lan et al. 2017
66	*S. ronganensis* Luo, Huang & Wen, 2016	*S. cyphotergous* group	Guangxi	Liujiang River	Luo et al. 2016
67	*S. sanxiaensis* Jiang, Li, Yang & Chang, 2019	*S. cyphotergous* group	Hubei	Yangtze River	Jiang et al. 2019
68	*S. xunlensis* Lan, Zhan & Zhang, 2004	*S. cyphotergous* group	Guangxi	Liujiang River	Lan et al. 2004
69	*S. yaolanensis* Zhou, Li & Hou, 2009	*S. cyphotergous* group	Guizhou	Liujiang River	Zhou et al. 2009
70	*S. yishanensis* Li & Lan, 1992	*S. cyphotergous* group	Guangxi	Liujiang River	Li and Lan 1992
71	*S.guiyang* Shao, Chen, Lu, Zhou, Zeng, 2024	*S. cyphotergous* group	Guizhou	Wujiang River	Shao et al. 2024
72	*S. brevifinus* Li, Li & Mayden, 2014	*S. jii* group	Guangxi	Hejiang River	Li et al. 2014
73	*S. guanyangensis* Chen, Peng & Zhang, 2016	*S. jii* group	Guangxi	Guijiang River	Chen et al. 2016
74	*S. guilinensis* Ji, 1985	*S. jii* group	Guangxi	Guijiang River	Zhao and Zhang 2009
75	*S. huangtianensis* Zhu, Zhu & Lan, 2011	*S. jii* group	Guangxi	Hejiang River	Zhu et al. 2011
76	*S. jii* Zhang & Dai, 1992	*S. jii* group	Guangxi	Hejiang River	Zhang and Dai 1992
77	*S. gracilis* Li, 2014	No assignment	Guangxi	Guijiang River	Li and Li 2014
78	*S. luolouensis* Lan, 2013	No assignment	Guangxi	Hongshui River	Lan et al. 2013
79	*S. pingshanensis* Li, Li, Lan & Wu, 2018	No assignment	Guangxi	Liujiang River	Wu et al. 2018
80	*S. wui* Li & An, 2013	No assignment	Yunnan	Mingyihe River	Li and An 2013

The sequences were revised manually and then aligned using the MUSCLE (Edgar 2004) module in MEGA v.7.0 (Kumar et al. 2016) with default settings. Phylogenetic trees were constructed using both maximum likelihood (ML) and Bayesian inference (BI) methods. The best-fit partitioning scheme and nucleotide substitution models for the sequence matrix were selected within PartitionFinder v.2.1.1 (Lanfear et al. 2017) based on the Bayesian information criterion. The analysis suggested the best partition scheme for each codon position of the Cyt *b* and ND4 genes. Maximum Likelihood analysis was run in IQ-TREE v.1.6.1 (Nguyen et al. 2015) with the best model and 2000 ultrafast bootstrap (UBP) replicates. The BI tree was reconstructed using MrBayes v.3.2.1 (Ronquist et al. 2012). Two independent runs were conducted in the BI analysis, each of which was performed for 10 million generations and sampled every 1000 generations. The first 25% of the run samples were discarded as a burn-in. Convergence of the data runs was assessed using the average standard deviation of split frequencies (below 0.01) and checking effective sample size (more than 200) in Tracer v1.7.1 (Rambaut et al. 2018). Uncorrected *p*-distances (1000 replicates) based on the Cyt *b* and ND4 genes were calculated using MEGA v 7.0 (Kumar et al. 2016).

Results

Phylogenetic reconstruction and genetic divergence

The ML and BI phylogenies were constructed based on two concatenated mitochondrial sequences comprising 1140 bp of Cyt *b* and 1380 bp of ND4. As a result of model selection, GTR+I+G and HKY+I+G were selected as the best models for the 1st codon and 2nd codon of ND4 and Cyt *b*, as well as GTR+I+G and GTR+G as the best models for the 3rd codon of ND4 and Cyt *b*. The ML

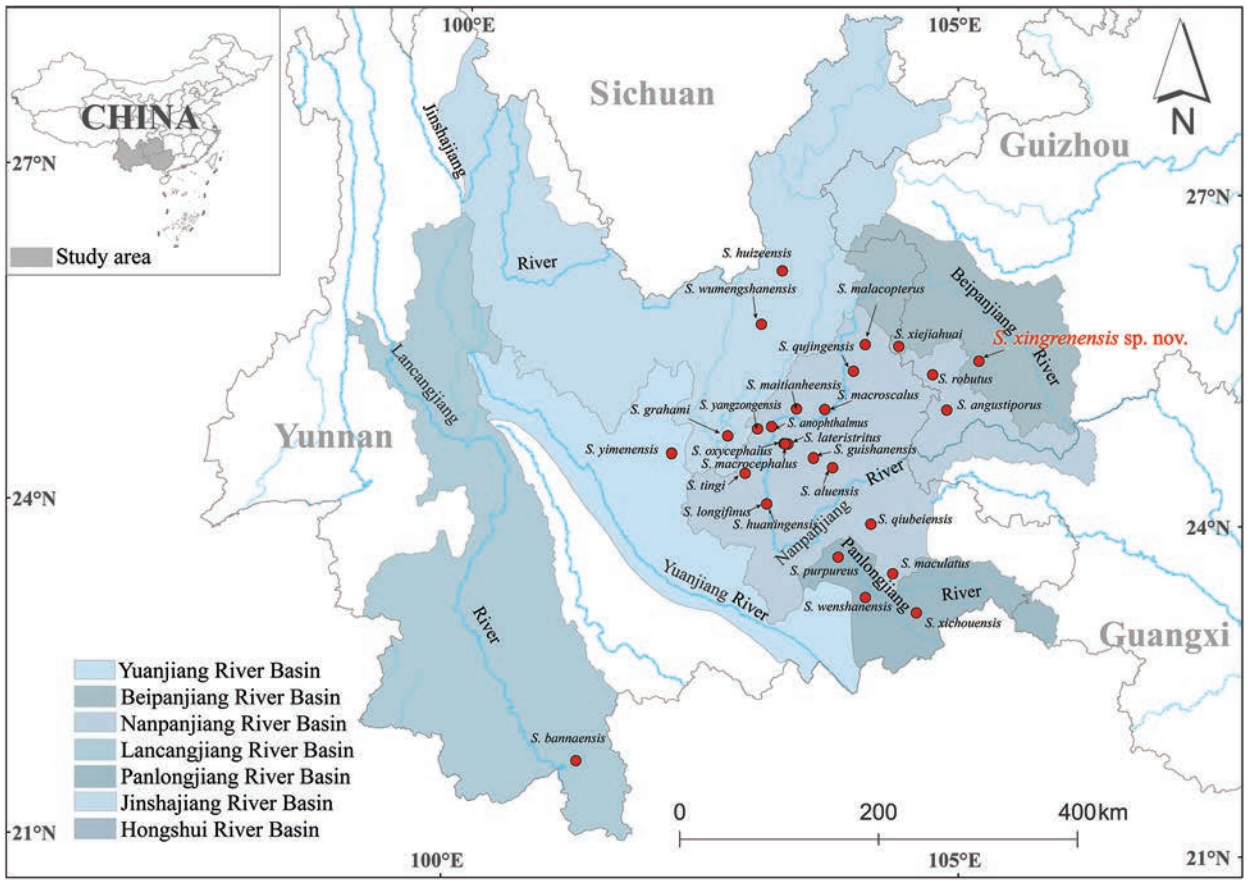

Figure 1. Distribution of 27 species of *S. tingi* group and new species in southwest China.

and BI phylogenetic trees showed identical topologies (Fig. 2). The monophyly of the genus *Sinocyclocheilus* was strongly supported by both phylogenetic analyses. In both analyses, *S. xingrenensis* sp. nov. formed a highly supported clade (BPP/UBP = 0.78/92) (Fig. 2).

We calculated the genetic distance between the new species and the *S. tingi* group using the mitochondrial Cyt *b* and ND4 genes. The smallest *p*-distances between *S. xingrenensis* sp. nov. and other species within the group were 2.8% for Cyt *b* (vs. *S. macrocephalus* and *S. aluensis*) and 2.7% for ND4 (vs. *S. macrocephalus*). These levels of divergence were similar to those between pairs of other recognized species. For example, the Cyt *b* *p*-distance was 2.6% between *S. aluensis* and *S. huaningensis* and 2.7% between *S. guishanensis* and *S. macrocephalus*, while the ND4 *p*-distance was 2.0% between *S. guishanensis* and *S. macrocephalus* and 2.5% between *S. huaningensis* and *S. oxycephalus* (Suppl. materials 1, 2).

Morphological analyses

A total of five principal component factors with eigenvalues greater than one were extracted based on the morphometric data (Suppl. material 3). These accounted for 91.72% of the total variance, with the first principal component (PC1) and second principal component (PC2) accounting for 60.20% and 15.10% of the total variance, respectively. In the scatter plot of PC1 versus PC2, the new species *Sinocyclocheilus xingrenensis* sp. nov. was distinguishable from *S. angustiporus* and *S. robustus* on the PC1 axis (Fig. 3). Major morphometric characters loaded on the PC1 axis included body depth, dorsal fin length, preanal length, anal-fin base length, anal-fin depth, prepectoral length, caudal peduncle length, head depth, head width, eye diameter, upper jaw length, lower jaw length, mouth width, and rostral barbel length (Suppl. material 3). Multivariate analysis of variance showed that, except for body depth, *Sinocyclocheilus xingrenensis* sp. nov. was greater than *S. angustiporus* in the remaining 27 morphometric indices in general, and the differences were significant (Table 4).

Morphological comparisons

Based on phylogeny and morphology, the new species was classified into the *S. tingi* group, incldng indistinct elevation at the head-dorsal junction, last unbranched ray of dorsal fin serrate along posterior margin, absence of horn-like structures and indistinct elevation at the head-dorsal junction, and tip of pectoral fin not reaching the pelvic-fin origin (Zhao and Zhang 2009). Thus, the new species *Sinocyclocheilus xingrenensis* sp. nov. were compared in detail morphologically with literature data for the *S. tingi* group (Table 3).

Table 2. Localities, voucher information, and GenBank numbers for all samples used.

ID	Species	Locality (* type localities)	Voucher number	Cyt *b*	ND4
1	*S. xingrenensis* sp. nov.	Xingren City, Guizhou*	XR01	PQ893907	PQ893904
2	*S. xingrenensis* sp. nov.	Xingren City, Guizhou*	XR02	PV007875	NA
3	*S. xingrenensis* sp. nov.	Xingren City, Guizhou*	XR03	PV007876	NA
4	*S. altishoulderus*	Mashan County, Guangxi	NA	FJ984568	FJ984568
5	*S. aluensis*	NA	NA	PV007877	NA
6	*S. anatirostris*	Leye County, Guangxi	XH1901	AY854708	AY854765
7	*S. angularis*	Baotian Town, Panzhou City, Guizhou*	GZNU20210322001	MZ636514	MZ636514
8	*S. angustiporus*	Xinlongchnag Town, Xingren City, Guizhou	GZNU20210322002	MZ636515	MZ636515
9	*S. angustiporus*	Yunnan	NA	PV007878	NA
10	*S. anophthalmus*	Jiuxiang, Yiliang County, Yunnan	XH3001	AY854715	AY854772
11	*S. anshuiensis*	Lingyun County, Guangxi	NA	KR069120	KR069120
12	*S. bicornutus*	Xinlongchang Town, Xingren City, Guizhou*	NA	KX528071	KX528071
13	*S. brevibarbatus*	NA	GX0064-L20-13	MT373106	MW548423
14	*S. brevis*	NA	GX0155	MT373105	MW548424
15	*S. cyphotergous*	Dongdang Township, Luodian County, Guizhou*	GZNU20150819010	MW024370	MW024370
16	*S. donglanensis*	Hongshuihe River, Donglan County, Guangxi	CA139	AB196440	MW548425
17	*S. furcodorsalis*	Tian'e County, Guangxi	NA	GU589570	GU589570
18	*S. grahami*	Haikou, Kunming City, Yunnan	NA	GQ148557	GQ148557
19	*S. guanyangensis*	NA	GX0173	MT373108	MW548426
20	*S. guilinensis*	NA	GX0073-L17-2	MT373104	MW548427
21	*S. guishanensis*	Guishan, Shilin County, Yunnan	XH5401	AY854722	AY854779
22	*S. guiyang*	Guiyang City, Guizhou, China*	NA	PV007879	PV007880
23	*S. huangtianensis*	NA	GX0175	MT373109	MW548428
24	*S. huaningensis*	Huaning County, Yunnan	XH3701	AY854718	AY854775
25	*S. huanjiangensis*	NA	GX0124	MT373103	MW548429
26	*S. hugeibarbus*	Xiaoqikong Town, Libo County, Guizhou*	GZNU20150120005	MW014319	MW014319
27	*S. huizeensis*	Leye Town, Huize County, Yunnan	hrfri2018046	MH982229	MH982229
28	*S. hyalinus*	Alugudong, Luxi County, Yunnan	XH4701	AY854721	AY854778
29	*S. jii*	Gongcheng County, Guangxi	YNUSJ201308060038	MF100765	MF100765
30	*S. jiuxuensis*	Jiuxu Town, Hechi City, Guangxi	XH8501	AY854736	AY854793
31	*S. lateristriatus*	Maojiachong, Zhanyi County, Yunnan	XH1102	AY854703	AY854760
32	*S. lingyunensis*	Shadong, Lingyun County, Guangxi	XH0502	AY854691	AY854748
33	*S. longibarbatus*	Dongtang Township, Libo County, Guizhou*	GZNU20150809004	MW024372	MW024372
34	*S. longicornus*	Hongguo Town, Panzhou City, Guizhou*	GZNU20210503016	MZ634123	MZ634125
35	*S. lunanensis*	Shilin County, Yunnan	XH0302	AY854686	AY854743
36	*S. macrocephalus*	Heilongtan, Shilin County, Yunnan	XH0103	AY854683	AY854740
37	*S. macrolepis*	Nandan County, Guangxi	XH8201	AY854729	AY854786
38	*S. macrophthalmus*	Xiaao, Duan County, Guangxi	XH8401	AY854733	AY854790
39	*S. maculatus*	Yiliang, Yunnan	IHB:2006632	EU366193	EU366183
40	*S. maitianheensis*	Jiuxiang, Yiliang County, Yunnan	XH2301	AY854710	AY854767
41	*S. malacopterus*	Wulonghe, Shizong County, Yunnan	XH0901	AY854697	AY854754
42	*S. mashanensis*	NA	GX0026-L18-12	MT373107	MW548430
43	*S. microphthalmus*	Lingyun County, Guangxi	NNNU201712001	MN145877	MN145877
44	*S. multipunctatus*	Huishui County, Guizhou	NA	MG026730	MG026730
45	*S. oxycephalus*	Heilongtan, Shilin County, Yunnan	XH0201	AY854685	AY854742
46	*S. punctatus*	Dongtang Township, Libo County, Guizhou	GZNU20150811002	NC_058003	NC_058003
47	*S. purpureus*	Luoping County, Yunnan	IHB:2006638	EU366189	EU366178
48	*S. qiubeiensis*	Songming, Yunnan	IHB:2006624	EU366188	EU366182
49	*S. qujingensis*	Huize County, Yunnan	hrfri2018044	MH937706	MH937706

ID	Species	Locality (* type localities)	Voucher number	Cyt *b*	ND4
50	*S. rhinocerous*	Luoping County, Yunnan	NA	KR069119	KR069119
51	*S. ronganensis*	Rong'an County, Guangxi	NA	KX778473	KX778473
52	*S. sanxiaensis*	Guojiaba Town, Zigui County, Hubei*	KNHM 2019000001	MN106258	NA
53	*S. tianlinensis*	NA	GX0087-L17-16	MT373102	MW548431
54	*S. tingi*	Fuxian Lake, Yunnan	YNUST201406180002	MG323567	MG323567
55	*S. wumengshanensis*	Xuanwei County, Yunnan	YNUSM20160817008	MG021442	MG021442
56	*S. xiejiahuai*	Hongguo Town, Panzhou City, Guizhou*	S46	PQ165088	PQ165088
57	*S. xunlensis*	Huanjiang, Guangxi	IHB:04050268	EU366187	EU366184
58	*S. yangzongensis*	Yangzonghai Lake, Yunnan	XH6101	AY854725	AY854782
59	*S. yimenensis*	Yimen, Yunnan	IHB:2006646	EU366191	EU366180
60	*S. yishanensis*	Liujiang County, Guangxi	NA	MK387704	MK387704
61	*S. zhenfengensis*	Zhexiang Town, Zhenfeng County, Guizhou*	GZNU20150112021	MW014317	MW014317
62	*Carassius auratus*	NA	NA	AB111951	AB111951
63	*Cyprinus carpio*	NA	NA	JN105357	JN105357
64	*Garra orientalis*	NA	NA	JX290078	JX290078
65	*Neolissochilus hexagonolepis*	NA	NA	KU380329	KU380329
66	*Schizothorax yunnanensis*	NA	NA	KR780749	KR780749
67	*Barbus barbus*	NA	NA	AB238965	AB238965
68	*Onychostoma simum*	NA	NA	KF021233	KF021233
69	*Pethia ticto*	NA	NA	AB238969	AB238969
70	*Myxocyprinus asiaticus*	NA	NA	AY526869	AY526869
71	*Danio rerio*	NA	NA	KM244705	KM244705

Sinocyclocheilus xingrenensis sp. nov. can be distinguished from the 21 species belonging to the *S. angularis* group by the absence of horn-like structures and indistinct elevation at the head-dorsal junction (vs. presence) and tip of pectoral fins not reaching the pelvic-fin origin (vs. reaching the or beyond the pelvic-fin origin); from the three species in the *S. microphthalmus* group by an indistinct elevation at the head-dorsal junction (vs. distinct elevation); from the five species within the *S. jii* group with serrations along the posterior margin of the last unbranched fin of the dorsal fin (vs. absent); and from the 20 species in the *S. cyphotergous* group by an indistinct elevation at the head-dorsal junction (vs. distinct elevation) and tip of pectoral fins not reaching the pelvic-fin origin (vs. usually reaching the pelvic-fin origin) (Zhao and Zhang 2009).

For the 27 species of the *S. tingi* group, the new species can be distinguished by a series of morphological characters. By having irregular markings on the body lateral, the new species can be distinguished from *S. anophthalmus*, *S. longifinus*, *S. macrocephalus*, *S. qujingensis*, *S. xiejiahuai*, and *S. yangzongensis* (vs. presence). *Sinocyclocheilus xingrenensis* sp. nov. differs from *S. aluensis*, *S. bannaensis*, *S. grahami*, *S. guishanensis*, *S. huaningensis*, *S. huizeensis*, *S. lateristriatus*, *S. maitianheensis*, *S. malacopterus*, *S. macroscalus*, *S. purpureus*, *S. qiubeiensis*, *S. tingi*, *S. wenshanensis*, *S. wumengshanensis*, *S. xichouensis*, and *S. yimenensis* by body scaleless (vs. body covered with scales); from *S. maculatus* by lateral-line pores 65–76 (vs. 81–88), six gill rakers on first gill arch (vs. 14–17), irregular black markings mainly scattered above the lateral line (vs. irregular markings densely distributed on the body lateral) (Zhao and Zhang 2009); and from *S. oxycephalus* by body length 4.4–5.0 times body height (vs. 3.3–4.1 times), head length greater than body height (vs. head length equal to body height), head length 3.4–3.9 times mouth width (vs. 4.3–5.1 times), and tip of maxillary barbel reaching the anterior margin of the operculum (vs. reaching the posterior margin of the operculum) (Li 1985; Zhao and Zhang 2009).

The new species are morphologically close to *S. angustiporus* and *S. robustus* and were found to remain easily distinguishable by examining their type specimens. The new species can distinguish *S. angustiporus* by three unbranched dorsal-fin rays (vs. four), body scaleless (vs. body covered with tiny scales), six rakers on the first gill arch (vs. 7–9), tip of maxillary barbel reaching the anterior margin of the operculum (vs. reaching the posterior margin of the eye), larger body size (92.6 ± 15.0 mm vs. 59.2 ± 25.5 mm, $p = 0.017$), bigger eyes (4.7 ± 0.3 mm vs. 3.7 ± 0.9 mm, $p = 0.020$), longer head (25.0 ± 3.1 mm vs. 15.8 ± 6.4 mm, $p = 0.008$), and longer fins (all p-values were less than 0.05) (Table 4), and it is distributed in the Beipanjiang River basin (vs. the Nanpanjiang River basin). The new species can distinguish *S. robustus* by smaller body size (standard length 92.6 mm vs. standard length 162.7), three unbranched dorsal-fin rays (vs. four), eight branched pelvic-fin rays (vs. six), six rakers on the first gill arch (vs. 9), indistinct elevation at the head-dorsal junction (vs. distinct elevation) (Figs 4, 6), dorsal-fin origin opposite to the pelvic-fin origin (vs. dorsal-fin origin anterior to the

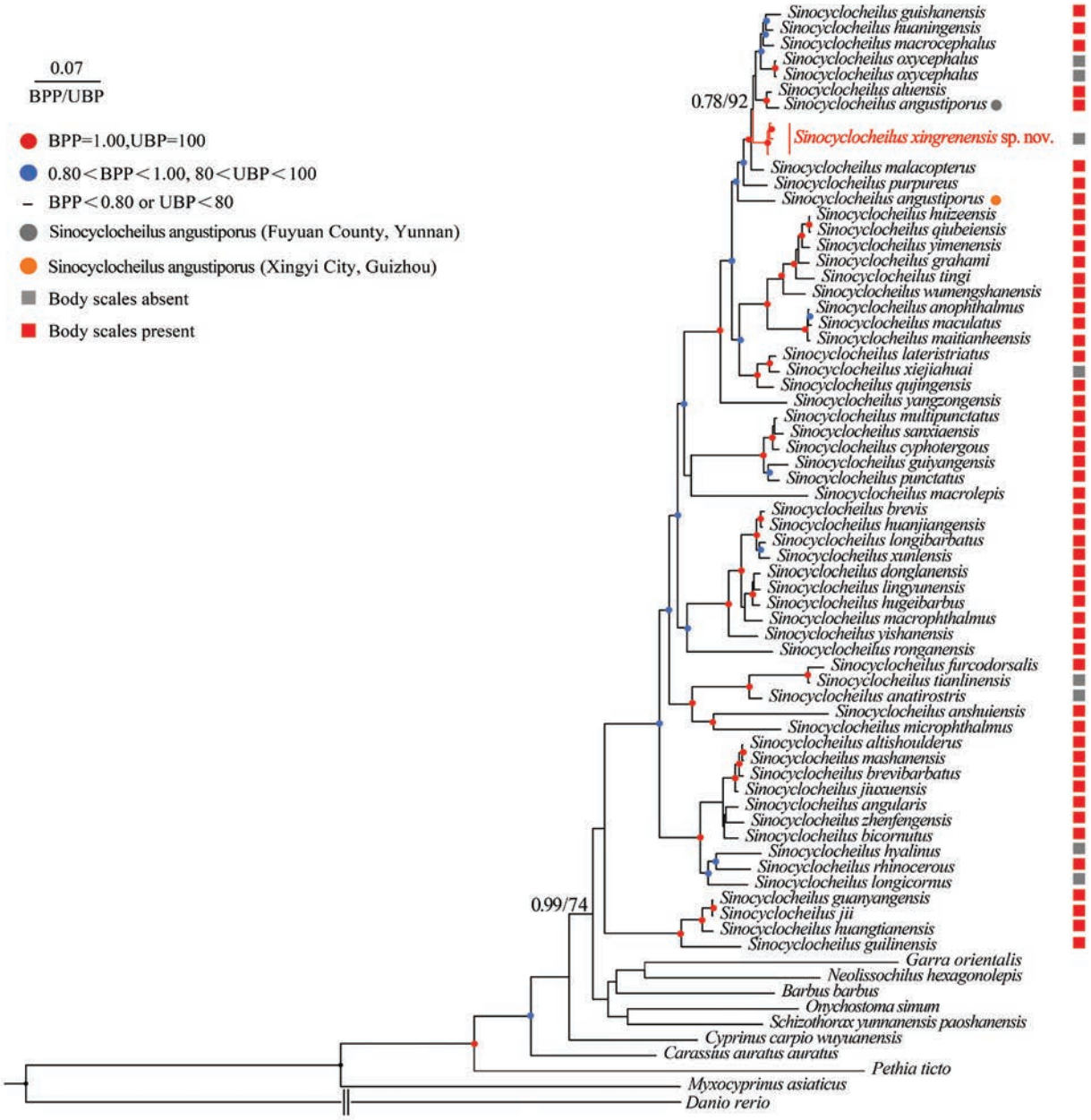

Figure 2. Phylogenetic tree based on mitochondrial Cyt *b* + ND4 genes. In this phylogenetic tree, ultra-fast bootstrap supports (UBP) from ML analyses/Bayesian posterior probabilities (BPP) from BI analyses were noted beside nodes. The scale bar represents 0.07 nucleotide substitutions per site. In addition to the nodes, different-colored rectangles indicate the presence or absence of scales for species in the genus *Sinocyclocheilus*.

pelvic-fin origin), and distributed in the Beipanjiang river basin (vs. Nanpanjiang river basin).

For the four species not placed in any species group, the new species differs from *S. pingshanensis*, *S. gracilis*, and *S. wui* by having irregular markings on the lateral body and body scaleless (vs. lacking irregular markings and body covered with tiny scales). The new species differs from *S. luolouensis* by eye normal (vs. eyes reduced), body scaleless (vs. body covered with tiny scales), lateral-line pores 65–77 (vs. 40–49), and tip of pectoral fin not reaching the pelvic-fin origin (vs. reaching the pelvic-fin origin).

Taxonomic account

Sinocyclocheilus xingrenensis Luo, Xiao, Zhou, Xiao & Zhou, sp. nov.

https://zoobank.org/53D64357-99FA-4E10-9590-002AFA9A39EE

Fig. 4, Table 4

Chresonymy. *Sinocyclocheilus gaowuensis*: Liu 2018 (Xingren City, Guizhou Province, China).

Material examined. *Holotype.* • GZNU20190508001, total length 149.4 mm (TL), standard length 123.5 mm (SL), collected by Jia-Jun-Zhou on May 8, 2019, in Yangsitun Vil-

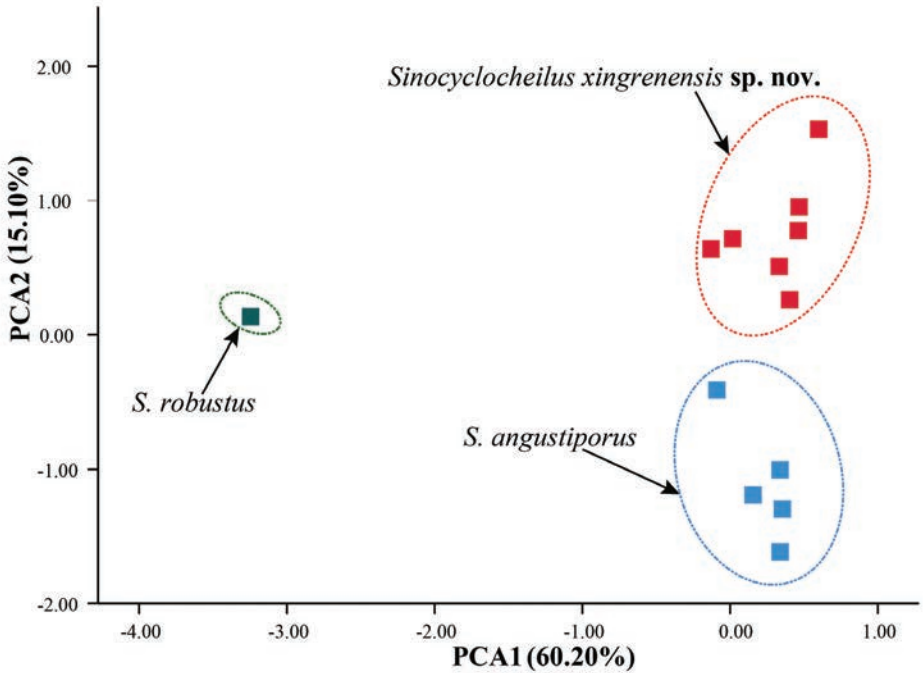

Figure 3. Scatter plots of the 1st and 2nd principal components for *S. robustus*, *S. angustiporus*, and *Sinocyclocheilus xingrenensis* sp. nov.

lage, Tianba Community, Xingren City, Guizhou Province, China (25.41255686°N, 105.21536082°E; ca. 1323 m a.s.l.).

Paratypes. • Six specimens from the same locality as the holotype: GZNU20190508002–GZNU20190508007, 79.7–123.5 mm SL, collected by Jia-Jun-Zhou on May 8, 2019; GZNU201250907001, 69.5 mm SL, collected by Tao Liu on September 7, 2012, in Gaowu Village, Xiashan Town, Xingren City, Guizhou Province, China (25.52536100°N, 105.20758400°E; ca. 1415 m a.s.l.).

Diagnosis. *Sinocyclocheilus xingrenensis* sp. nov. can be distinguished from its congeners by a combination of the following characteristics: (1) absence of horn-like structures and indistinct elevation at the head-dorsal junction; (2) body scaleless, with irregular black markings scattered above the lateral line; (3) eyes large, diameter 16–21% of head length; (4) dorsal-fin rays, iii, 6–7, last unbranched ray serrate along posterior margin; (5) tip of the pectoral fin not reaching the pelvic fin origin; (6) pelvic fin rays, i, 8, tip not reaching the anus; (7) lateral line complete and curved, with pores 65–77; (8) tip of maxillary barbel reaching the anterior margin of the operculum; (9) six rakers on the first gill arch. The major diagnostic characters for new species and related species are summarized in Table 3.

Description. Body fusiform, moderately elongated and compressed. Dorsal profile convex from nape to dorsal fin; body maximum depth positioned at insertion of dorsal fin; ventral profile slightly concave, tapering gradually toward the caudal fin.

Head short, length, 26–29% of SL, slightly compressed, head length greater than width. Eyes large, eye diameter 16–21% of HL, interorbital distance greater than distance between posterior nostrils. Snout short, U-shaped, and projecting beyond lower jaw in dorsal view, less than half HL. Mouth subinferior and arched, with slightly projecting lower jaw. Two pairs of nostrils, anterior nostril close to posterior nostril, nares at about 1/3 between snout tip and anterior margin of eye; anterior nostril short tubular, posterior margin of short tube with posterior flap, forward to cover mouth of tube; posterior nostril subcircular, open. Two pairs of barbels; rostral barbels not reaching the anterior margin of operculum when extended backward; maxillary barbel slightly shorter compared with rostral barbel, tips beyond the eye but reaching anterior margin of operculum when extended backward. Gill opening moderate, opercular membranes connected at isthmus. Six outer rakers on first gill arch. Pharyngeal teeth in three rows with counts of 2, 3, 4–4, 3, 2; pharyngeal teeth strong and well developed, with curved and pointed tips.

Dorsal-fin rays iii, 6–7; pectoral-fin rays i, 12–16; pelvic-fin rays i, 8; anal-fin rays iii, 5; and 15–18 branched caudal-fin rays. Dorsal fin short, 19–24% of SL, less than head length, 67–88% of HL; distal margin truncated, origin opposite to pelvic-fin origin, situated slightly anterior to midpoint between snout tip and caudal-fin base; last unbranched ray strong, softening toward tip, with serrations along posterior margin; first branched ray longest, shorter than HL, tip beyond the vertical of the anus. Pectoral fin short, distal margin truncated, length slightly smaller than HL, 18–22% of SL, tips beyond 3/4 of the distance between pectoral-fin origin and pelvic-fin origin, tips not reaching the pelvic-fin origin. Pelvic fin moderately developed, distal margin rounded, length 14–17% of SL, and tips not reaching the anus. Anal fin short, 14–17% of SL, distal margin rounded, origin close to the anus, a short

Table 3. Comparison of the diagnostic characters of the new species described here with those selected for the 27 species of the *S. tingi* group and the four unassigned species (the last four) within the genus *Sinocyclocheilus*. Grey shading indicates a clear difference in characters compared to that of *Sinocyclocheilus xingrenensis* sp. nov.

Species	Body lateral markings	Dorsal-fin rays	Pectoral-fin rays	Anal-fin rays	Pelvic-fin rays	Caudal -fin rays	Lateral-line scales/ pores	Body scales	Tip of pectoral fin reaching to pelvic-fin	Tip of pelvic-fin rays reaching to anus	Source
S. xingrenensis sp. nov.	Present	iii, 6–7	i, 12–16	iii, 5	i, 8	15–18	65–77	No	No	No	This study
S. aluensis	Present	iii, 7	i, 13–16	ii, 5	i, 7–9	15–17	71–75	Yes	No	No	Li et al. 2005
S. angustiporus	Present	iv, 7	i, 14	iii, 5	i, 8	16–17	70–74	Yes	No	No	Wu et al. 1989; This study
S. anophthalmus	Absent	iv, 8	i, 15–16	iii, 5	i, 8	16	52–56	Yes	Yes	No	Chen et al. 1988a
S. grahami	Present	iii, 7	i, 15–17	iii, 5	i, 8–9	16	61–69	Yes	No	No	Zhao and Zhang 2009
S. guishanensis	Present	iii, 7	i, 13–16	iii, 5	i, 7–8	15–16	73–80	Yes	No	No	Li et al. 2003a
S. huaningensis	Present	iii, 7	i, 16	iii, 5	i, 8	16	59–67	Yes	No	Yes	Li et al. 1998
S. huizeensis	Present	iii, 7	i, 15–16	iii, 5	i, 10	18	70–73	Yes	No	No	Cheng et al. 2015
S. xiejiahuai	Absent	iii, 6½	i, 13	iii, 5	i, 7	17	74	No	No	No	Fan et al. 2024
S. bannaensis	Present	iii, 8	i, 9	ii, 5	i, 9	16	47	Yes	Yes	No	Li et al. 2019
S. maculatus	Present	iii, 7	i, 14–15	iii, 5	i, 7-8	16	81–88	Yes	No	No	Zhao and Zhang 2009
S. maitianheensis	Present	iii, 7	i, 14–15	iii, 5	i, 9	18	70–82	Yes	No	Yes	Li 1992
S. malacopterus	Present	iii, 7	i, 14–18	iii, 5	i, 9	15–16	67–81	Yes	No	No	Chu and Cui 1985
S. longifinus	Absent	iii, 7	i, 16	ii, 5	i, 8	17	70–72	No	Yes	Yes	Li et al. 1998
S. macroscalus	Present	iv, 7	i, 15–16	iii, 5	i, 8	NA	70–79	Yes	No	No	Li 1992
S. macrocephalus	Absent	iv, 7	i, 15–17	iii, 5	i, 8	16	72–78	Yes	No	No	Li 1985
S. lateristritus	Present	iv, 7	i, 15–16	iii, 5	i, 8	17	75–91	Yes	No	No	Li 1992
S. purpureus	Present	iv, 6–7	i, 16	iii, 5	i, 8	NA	63–67	Yes	No	No	Li 1985
S. qiubeiensis	Present	iii, 7	i, 14–17	iii, 5	i, 8–9	16	67–81	Yes	No	No	Li et al. 2002b
S. qujingensis	Absent	iii, 7	i, 16	iii, 5	i, 8	16	70–79	Yes	No	No	Li et al. 2002c
S. robustus	Present	iv,7	i,13	iii, 5	i, 6	16	72	No	No	No	Chen et al. 1988b; This study
S. wumengshanensis	Present	iii, 7	16	ii, 5	i, 8	16	67–76	Yes	Yes	Yes	Li et al. 2003a
S. xichouensis	Present	iii, 6–7	i, 14–16	iii, 5	i, 8–9	NA	74–88	Yes	Yes	No	Pan et al. 2013
S. tingi	Present	iv, 7	i, 14–16	iii, 5	i, 6–8	16	62–73	Yes	No	No	Zhao and Zhang 2009
S. yangzongensis	Absent	iii, 7	i, 16	iii, 5	i, 9	16	71–81	Yes	No	No	Zhao and Zhang 2009
S. yimenensis	Present	iii, 7	i, 14–15	ii, 5	i, 8	16-17	70–79	Yes	No	No	Li et al. 2005
S. oxycephalus	Present	iii, 7	i, 15–16	iii, 5	i, 8–9	17	62–75	No	No	No	Li 1985; Zhao and Zhang 2009
S. wenshanensis	Present	iii, 7	i, 13–15	ii, 5	i, 7–8	14–15	67–72	Yes	No	Yes	Yang et al. 2018
S. gracilis	Absent	NA	NA	NA	NA	NA	NA	Yes	NA	NA	Li and Li 2014
S. pingshanensis	Absent	iii, 7	i, 13–15	ii, 5	i, 7–8	16	75–78	Yes	Yes	No	Wu et al. 2018
S. luolouensis	Present	iii, 7	i, 13–14	iii, 5	i, 7–8	16–17	40–49	Yes	Yes	Yes	Lan et al. 2013
S. wui	Absent	iii, 7	i, 14–15	ii, 5	i, 7–8	14–15	79–81	Yes	No	No	Li and An 2013

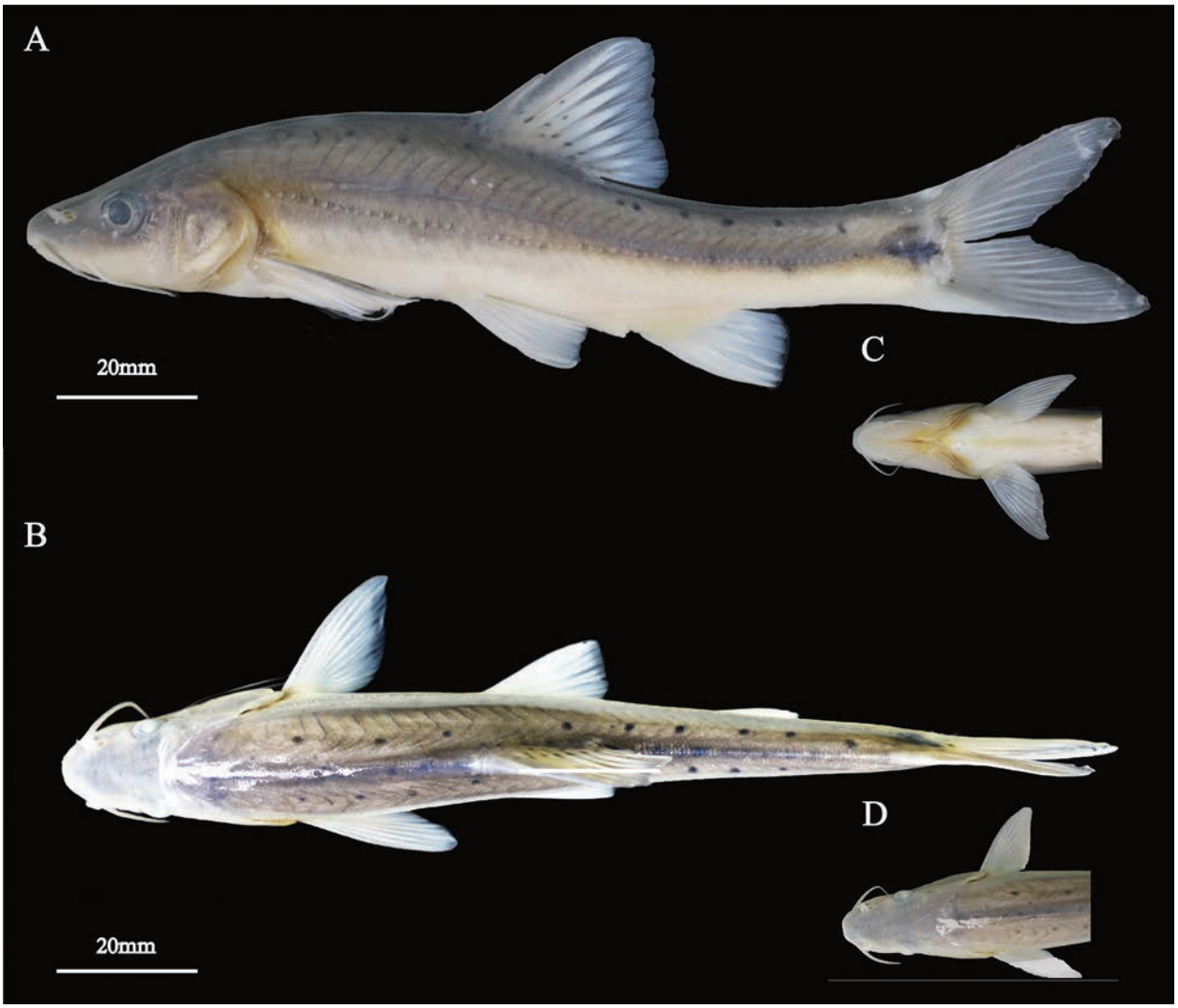

Figure 4. View of adult holotype GZNU20190508001 of *Sinocyclocheilus xingrenensis* sp. nov. in preservative. **A.** Lateral view; **B.** Dosal view; **C.** Ventral view of the head; **D.** Dosal view of the head.

distance between the origin and the anus, tips not reaching the caudal fin base. Caudal peduncle length 18–23% of SL, depth 47–67% of body depth. Caudal fin forked, upper lobe equal in length to the lower one, tips truncated.

Body scaleless. Lateral line complete and slightly curved, with pores 65–77, originating from upper margin of operculum and extending to end of caudal peduncle. With about 30 to 58 irregular black markings scattered above the lateral line, almost in a straight line, and a large black spot in the center of the end of the caudal peduncle.

Coloration and variation. In life, the body is golden yellow overall, with white pectoral fins and a slightly translucent white dorsal fin; the gills are blackish, with numerous black markings on the back and a relatively large black spot at the caudal fin base (Fig. 5). In 7% formalin solution, the specimens are dark gray above the lateral line and white below the lateral line, with each fin yellowish white (Fig. 4). Most specimens are consistent in their morphological characteristics, except for specimen GZNU20190508004, where the lateral line separates backward into two from the upper pectoral fin and converges at the base of the caudal fin.

Distribution. *Sinocyclocheilus xingrenensis* sp. nov. is found only in caves near Xingren City, Guizhou, China, including the type locality and from Gaowu Village, Xiashan Town, Xingren City. Much ecological information about the new species is currently unknown. The discovery site belongs to the Beipanjiang River basin.

Etymology. The specific epithet "*xingrenensis*" refers to the type locality of the new species: Xingren City, Guizhou Province, China. We propose the common English name "Xingren Golden-lined Fish" and the Chinese name "Xīng Rén Jīn Xiàn Bā (兴仁金线鲃)".

Discussion

This new species, named *Sinocyclocheilus gaowuensis,* was described by Liu (2018a) on the basis of single-numbered specimens and genetic information. However, this work

Table 4. Morphological characterization and statistical analysis of new species and *S. angustiporus*. Abbreviations: *Sx, S. xingrenensis* sp. nov., and *Sa*, *S. angustiporus.*

Character	*S. xingrenensis* sp. nov.			*S. angustiporus*		*P*-value from ANOVA
	Holotype	Range	Mean ± SD	Range	Mean ± SD	*Sx* vs. *Sa*
Dorsal fin rays	iii, 7	iii, 6–7	NA	iv, 7	NA	NA
Pectoral fin rays	i, 15	i, 12–16	NA	i, 14	NA	NA
Pelvic fin rays	i, 8	i, 8	NA	i, 8	NA	NA
Anal fin rays	iii, 5	iii, 5	NA	iii, 5	NA	NA
Caudal fin rays	15	15–18	NA	16–17	NA	NA
Lateral line pores	65	65–76	NA	NA	NA	NA
Total length	149.4	99.0–149.4	114.5 ± 17.2	55.40–128.08	73.9 ± 30.4	0.014
Standard length	123.5	79.7–123.5	92.6 ± 15.0	43.03–104.35	59.2 ± 25.5	0.017
Body depth	24.6	16.7–24.6	19.3 ± 2.5	10.24–24.59	14.6 ± 5.7	0.077
Head length	31.9	22.8–31.9	25.0 ± 3.1	12.08–27.19	15.8 ± 6.4	0.008
Head depth	21.5	14.3–21.5	15.9 ± 2.6	7.36–19.46	10.3 ± 5.1	0.032
Head width	16.2	11.5–16.2	13.3 ± 1.5	5.05–12.54	7.4 ± 3.0	0.001
Inter-Pre-Nasal Distance	5.1	4.8–6.2	5.4 ± 0.5	1.84–4.59	2.5 ± 1.2	0.000
Posterior Nasal Distance	6.9	4.2–6.9	5.2 ± 0.9	2.23–5.10	3.1 ± 1.2	0.005
Upper jaw length	9.4	5.0–9.4	6.2 ± 1.6	2.76–6.56	3.8 ± 1.6	0.029
Lower jaw length	7.9	4.8–7.9	5.6 ± 1.2	2.36–6.35	3.5 ± 1.6	0.028
Mouth width	8.2	6.2–8.2	6.9 ± 0.6	2.50–5.29	3.3 ± 1.1	0.000
Eye diameter	5.0	4.1–5.0	4.7 ± 0.3	3.09–5.32	3.7 ± 0.9	0.020
Interorbital distance	9.0	7.5–9.0	8.3 ± 0.5	3.32–7.61	4.7 ± 1.7	0.000
Dorsal-fin base length	17.4	10.7–17.4	12.5 ± 2.3	6.07–15.22	8.3 ± 3.9	0.039
Dorsal-fin length	24.7	15.3–24.7	19.9 ± 3.1	10.10–22.62	13.1 ± 5.4	0.019
Pectoral-fin length	23.2	14.1–23.2	17.9 ± 2.9	8.35–17.54	10.5 ± 4.0	0.004
Pectoral-fin base length	4.1	2.8–4.1	3.4 ± 0.4	1.97–3.78	2.5 ± 0.7	0.023
Prepectoral length	32.9	21.7–32.9	25.0 ± 3.7	12.67–28.45	16.5 ± 6.7	0.018
Pelvic-fin length	18.5	11.3–18.5	14.6 ± 2.4	6.73–14.53	8.8 ± 3.3	0.006
Pelvic-fin base length	7.7	4.0–7.7	4.9 ± 1.3	1.62–4.37	2.4 ± 1.1	0.005
Prepelvic length	59.1	39.2–59.1	45.6 ± 6.6	21.90–55.21	29.9 ± 14.2	0.027
Anal-fin length	17.8	12.4–17.8	14.6 ± 1.9	7.84–13.40	9.5 ± 2.3	0.002
Anal-fin base length	11.1	6.4–11.1	8.0 ± 1.5	3.92–9.70	5.4 ± 2.4	0.044
Preanal length	82.7	55.7–82.7	62.5 ± 9.5	30.68–75.53	41.8 ± 18.9	0.031
Caudal peduncle length	22.3	16.4–22.3	18.5 ± 2.2	9.01–18.11	12.3 ± 3.4	0.003
Caudal peduncle depth	13.1	8.7–13.1	10.5 ± 1.8	4.90–12.49	7.3 ± 3.0	0.040
Maxillary barbel length	10.4	7.7–13.5	10.3 ± 2.1	3.20–8.05	4.5 ± 2.0	0.001
Rostral barbel length	13.2	9.8–13.2	11.5 ± 1.4	3.17–10.07	5.0 ± 2.9	0.000

Figure 5. Live paratype of *Sinocyclocheilus xingrenensis* sp. nov.

Figure 6. Holotype specimens from *Sinocyclocheilus angustiporus* (IHB12209016-81X2001, **A–C**) and *Sinocyclocheilus robustus* (IHB12209038-8001091, **D–F**). **A, D.** Lateral view; **B, E.** Dosal view; and **C, F.** Ventral view.

Figure 7. Habitat of *Sinocyclocheilus xingrenensis* sp. nov.

was not widely accepted because it was an unpublished master's thesis, and the sequences were not deposited online. In this study, we formally describe *Sinocyclocheilus xingrenensis* sp. nov. based on multiple specimens and genetic data. The new species is morphologically (see above) and genetically distinguishable from other species of the genus *Sinocyclocheilus*.

Multiple lines of evidence suggest that the new species did not exhibit strict cave adaptations as young burrowers. Compared to strictly cave-dwelling species, such as *S. longicornus* (eye diameter 0.0–6.1% of HL) (Xu et al. 2023) and *S. sanxiaensis* (eye diameter 7.3% of SL) (Jing et al. 2019), the new species exhibit significantly larger eyes (eye diameter 16–21% of HL). This is related to the habitat, where the new species can be connected to surface streams through cave windows (Fig. 7), and their life rhythms may be closely related to photoperiods. Within the genus *Sinocyclocheilus*, we also mapped the distribution of scales in the phylogenetic tree, which showed that scale loss occurs in only a few species. Using the time of divergence of *S. xiejiahuai* as a reference (Fan et al. 2024), the loss of these scales occurred centrally after the Pleistocene (~2.58 million years ago). This suggests that scale degeneration may not be very ancient, ranging from early to late Pleistocene (Policarpo et al. 2021). This is similar to the degeneration or loss of eyes of species within the genus *Sinocyclocheilus* during the Pleistocene (Mao et al. 2021). This further suggests that most cave fishes may not have lived in cave ecosystems for more than a few million years. Thus, together with the eyes and scales, we hypothesize that the new species may be undergoing a gradual evolutionary process towards caves.

Although the population of this new species is not extremely small, its habitat is located in the center of the village, making it more susceptible to anthropogenic disturbance. Moreover, with the potential for future urbanization in the village, there is a significant risk of habitat degradation and destruction in the near future. On 5 February 2021, the Chinese government designated all species of *Sinocyclocheilus* endemic to China as second-class national protected animals (National Forestry and Grassland Administration & National Park Administration, 2021). Consequently, this species will also require appropriate conservation measures to mitigate the potential threats posed by future anthropogenic disturbances.

Author contributions

Jiang Zhou and Ming-Yuan Xiao conceived and designed the research; Ming-Yuan Xiao, Jia-Jia Wang, Tao Luo, and Jia-Jun Zhou conducted field surveys and collected samples; Tao Luo and Jia-Jia Wang performed molecular work; Ming-Yuan Xiao, Jia-Jia Wang, and Ning Xiao processed the English language of the manuscript; Jiang Zhou provided financial support. All authors read and approved the final version of the manuscript.

Funding

This research was supported by the programs of the Diversity and Distribution Survey of Chiroptera species in China (2021FY100302) and the Guizhou Normal University Academic Emerging Talent Fund Project (Qianshi Xin Miao [2021] 20).

Acknowledgments

We thank Mr. Hong-Fu Yang for providing specimens of some species for measurement. We thank Prof. E. Zhang and Dr. Man Wang for their help during specimen examination. We thank LetPub (www.letpub.com) for its linguistic assistance during the preparation of this manuscript.

References

Chen JX, Lan JH (1992) Description of a new genus and three new species of fishes from Guangxi, China (Cypriniformes, Cyprinidae, Cobitidae). Acta Zootaxonomica Sinica 17(1): 104–109. [In Chinese]

Chen YR, Chu XL, Luo ZY, Wu JY (1988a) A new blind Cyprinid fish from Yunnan, China with a reference to the evolution of its characters. Acta Zootaxonomica Sinica 34(1): 64–70. [In Chinese]

Chen JX, Zhao ZF, Zheng JZ, Li DJ (1988b) Description of three new barbine species from Guizhou, China (Cypriniformes, Cyprinides). Acta Academiae Medicinae Zunyi 11(1): 1–4(92–93). [In Chinese]

Chen YR, Yang JX, Zhu CG (1994) A new fish of the genus *Sinocyclocheilus* from Yunnan with comments on its characteristic adaptation (Cypriniformes, Cyprinidae). Dong Wu Fen Lei Xue Bao 19(2): 246–252. [In Chinese]

Chen YR, Yang JX, Lan JH (1997) One new species of blind cavefish from Guangxi with comments on its phyogenetic status (Cypriniformes, Cyprinidae, Barbinae). Acta Zootaxonomica Sinica 22(2): 219–223. [In Chinese]

Chen YQ, Peng CL, Zhang E (2016) *Sinocyclocheilus guanyangensis*, a new species of cavefish from the Li-Jiang basin of Guangxi, China (Teleostei, Cyprinidae). Ichthyological Exploration of Freshwaters 27(1): 1–8. [In Chinese]

Cheng C, Pan XF, Chen XY, Li JY, Ma L, Yang JX (2015) A new species of the genus *Sinocyclocheilus* (Teleostei, Cypriniformes), from Jinshajiang Drainage, Yunnan, China. Cave Research 2(4): 1–4.

Chu XL, Cui GH (1985) A revision of Chinese cyprinid genus Sinocyclocheilus with reference to the interspecific relationships. Acta Zootaxonomica Sinica. 10 (4): 435–441. [In Chinese]

Edgar RC (2004) MUSCLE: Multiple sequence alignment with high accuracy and high throughput. Nucleic Acids Research 32(5): 1792–1797. https://doi.org/10.1093/nar/gkh340

Fang PW (1936) Sinocyclocheilus tingi, a new genus and species of Chinese barbid fishes from Yunnan. Sinensia 7: 588–593.

Fan C, Wang M, Wang JJ, Luo T, Zhou JJ, Xiao N, Zhou J (2024) *Sinocyclocheilus xiejiahuai* (Cypriniformes, Cyprinidae), a new cave fish with extremely small population size from western Guizhou, China. ZooKeys 1214: 119–141. https://doi.org/10.3897/zookeys.1214.12762

Gan X, Wu TJ, Wei ML, Yang J (2013) A new blind barbine species, *Sinocyclocheilus anshuiensis* sp. nov. (Cypriniformes, Cyprinidae) from Guangxi, China. Zoological Research 34(5): 459–463. https://doi.org/10.11813/j.issn.0254-5853.2013.5.0459

Huang J, Gluesenkamp A, Fenolio D, Wu Z, Zhao Y (2017) Neotype designation and redescription of *Sinocyclocheilus cyphotergous* (Dai) 1988, a rare and bizarre cavefish species distributed in China (Cypriniformes, Cyprinidae). Environmental Biology of Fishes 100(11): 1483–1488. https://doi.org/10.1007/s10641-017-0658-2

Jiang WS, Li J, Lei XZ, Wen ZR, Han YZ, Yang JX, Chang JB (2019) *Sinocyclocheilus sanxiaensis*, a new blind fish from the Three Gorges of Yangtze River provides insights into speciation of Chinese cavefish. Zoological Research 40(6): 552–557. https://doi.org/10.24272/j.issn.2095-8137.2019.065

Kumar S, Stecher G, Tamura K (2016) MEGA7: Molecular evolutionary genetics analysis version 7.0 for bigger datasets. Molecular Biology and Evolution 33(7): 1870–1874. https://doi.org/10.1093/molbev/msw054

Lan JH, Zhang CG, Zhao YH (2004) A new speces of the genus *Sinocyclocheilus* from China (Cyprinformes, Cyprinidae, Barbinae). Acta Zootaxonomica Sinica29(2): 377–380. [In Chinese]

Lan JH, Gan X, Wu TJ, Yang J (2013) Cave Fishes of Guangxi, China. Science Press, Beijing. [In Chinese]

Lan YB, Qin XC, Lan JH, Xiu LH, Yang J (2017) A new species of the genus *Sinocyclocheilus* (Cypriniformes, Cyprinidae) from Guangxi, China. Journal of Xinyang Normal University (Natural Science Edition) 30(1): 97–101. https://doi.org/10.3969/j.issn.1003-0972.2017.01.021

Lanfear R, Frandsen PB, Wright AM, Senfeld T, Calcott B (2017) PartitionFinder 2: New methods for selecting partitioned models of evolution for molecular and morphological phylogenetic analyses. Molecular Biology and Evolution 34(3): 772–773. https://doi.org/10.1093/molbev/msw260

Li WX (1985) Four species of *Sinocyclocheilus* from Yunnan. Zoological Research 6(4): 423–427. [In Chinese]

Li GL (1989) On a new fish of the genus *Sincyclocheilus* from Guangxi China (Cypriniformes, Cyprinidae, Barbinae). Acta Zootaxonomica Sinica 14(1): 123–126. [In Chinese]

Li WX (1992) Description on three species of *Sinocyclocheilus* from Yunnan, China. Shui Sheng Sheng Wu Hsueh Bao 16(1): 57–61. [In Chinese]

Li WX, An L (2013) A new species of Sinocyclocheilus from Kunming, Yunnan – *Sinocyclocheilus wui* sp. nov. Journal of Jishou University 34(1): 82–84. https://doi.org/10.3969/j.isn.1007-2985.2013.01.019 [Natural Science Edition] [In Chinese]

Li WX, Lan JH (1992) A new genus and three new species of Cyprinidae from Guangxi, China. Journal of Zhanjiang Fisheries College 12(2): 46–51.

Li J, Li XH (2014) *Sinocyclocheilus gracilis*, a new species of hypogean fish from Guangxi, South China (Teleostei: Cypriniformes: Cyprinidae). Ichthyological Exploration of Freshwaters 24(3): 249–256.

Li WX, Tao JN (1994) A new species of Cyprinidae from Yunnan – *Sinocyclocheilus rhinocerous*, sp. nov. Joumal of Zhanjiang Fisheries College 14(1): 1–3. [In Chinese]

Li WX, Wu DF, Chen AL (1998) Two new species of *Sinocyclocheilus* from Yunnan, China. (Cypriniformes, Cyprinidae). Journal of Zhanjiang Ocean University 18(4): 1–5.[In Chinese]

Li WX, Zong ZG, Nong RB, Zhao CH (2000a) A new species of *Sinocyclocheilus* from Yunnan – *Sinocylocheilus maculatus* Li, sp. nov. Journal of Yunnan University 22(1): 79–80. [In Chinese]

Li WX, Xiao H, Zan RG, Luo ZF, Li HM (2000b) A new species of *Sinocyclocheilus* from Guangxi, China. Zoological Research 21(2): 155–157. [In Chinese]

Li WX, Mao WN, Lu ZM, Tao JN (2002a) Two new species of Cyprinidae from Yunnan. Journal of Yunnan University 24(5): 385–387. [In Chinese]

Li WX, Liao YP, Yang HF (2002b) Two new species of *Sinocyclocheilus* from Eastern Yunnan, China. Journal of Yunnan Agricultural University 17(2): 161–163. [In Chinese]

Li WX, Mao WL, Lu ZM (2002c) A new species of *Sinocyclocheilus* from Yunnan' China. Journal of Zhanjiang Ocean University 22(3): 1–2. [In Chinese]

Li WX, Mao WN, Lu ZM, Yan WZ (2003a) The two new species of *Sinocyclocheilus* from Yunnan, China. Journal of Jishou University 24(2): 63–65. [Natural Science Edition] [In Chinese]

Li WX, Ran JC, Chen HM (2003b) A new species of cave *Sinocyclocheilus* in Guizhou and its adaptation comment. Journal of Jishou University 24(4): 61–63. [Natural Sciences Edition] [In Chinese]

Li WX, Lan JC, Chen XY (2003c) A new species of cave *Sinocyclocheilus* from Guangxi – *Sinocyclocheilus jiuxuensis* Li et Ran, sp. nov. Journal of Guangxi Normal University 21(4): 83–85. [In Chinese]

Li WX, Xiao H, Zan RG, Luo ZY, Ban CH, Fen JB (2003d) A new species of *Sinocyclocheilus* from caves in Guangxi. Journal of Guangxi Normal University 21(3): 80–81. [In Chinese]

Li WX, Xiao H, Jin XL, Wu DJ (2005) A new species of *Sinocyclocheilus* from Yunnan, China. Xi Nan Nong Ye Xue Bao 18(1): 90–91. [In Chinese]

Li WX, Yang HF, Han F, Tao CP, Hong Y, Chen H (2007) A new species in cave of blind *Sinocyclocheilus* from Yunnan, China (Cypriniformes, Cyprinidae). Journal of Guangdong Ocean University 27(4): 1–3.

Li J, Li XH, Mayden RL (2014) *Sinocyclocheilus brevifinus* (Teleostei, Cyprinidae), a new species of cavefish from Guangxi, China. Zootaxa 3873(1): 37–48. https://doi.org/10.11646/zootaxa.3873.1.3

Li GH, Wu JJ, Leng Y, Zhou R, Pan XF, Han F, Li SY, Liang X (2018) A new species S*inocyclocheilus longshanensis* sp. nov. from Yunnan. Zhongguo Nongxue Tongbao 34(5): 153–158. [In Chinese]

Li WX, Li QQ, Chen HY (2019) A new species of *Sinocyclocheilus* from Yunnan, China: *Sinocyclocheilus bannaensis*. Journal of Jishou University (Natural Science Edition) 40(1): 61−63. [In Chinese]

Li WX, Mao WN (2007) A new species of the genus *Sinocyclocheilus* living in cave from Shilin, Yunnan, China (Cypriniformes, Cyprinidae). Acta Zootaxonomica Sinica 32(1): 226–229

Lin RD, Luo ZF (1986) A new blind barbid fish (Pisces, Cyprinidae) from subteeranean water in Guangxi, China. Shui Sheng Sheng Wu Hsueh Bao 10(4): 380–382. [In Chinese]

Liu T (2018a) Molecular Phylogenetic Relationships among 30 *Sinocyclocheilus* species Based on RAD-seq Technology. Yunnan University. Master Thesis.

Liu T, Deng HQ, Ma L, Xiao N, Zhou J (2018b) *Sinocyclocheilus zhenfengensis*, a new cyprinid species (Pisces, Teleostei) from Guizhou Province, Southwest China. Journal of Applied Ichthyology 34(4): 945–953. https://doi.org/10.1111/jai.13629

Luo FG, Huang J, Liu X, Luo T, Wen YH (2016) *Sinocyclocheilus ronganensis* Luo, Huang et Wen sp. nov., a new species belonging to *Sinocyclocheilus* Fang from Guangxi (Cypriniformes, Cyprinidae). Nanfang Nongye Xuebao 47(4): 650–655. https://doi.org/10.3969/j:issn.2095-1191.2016.04.650 [In Chinese]

Luo Q, Tang Q, Deng L, Duan Q, Zhang R (2023) A new cavefish of *Sinocyclocheilus* (Teleostei: Cypriniformes: Cyprinidae) from the Nanpanjiang River in Guizhou, China. Journal of Fish Biology 104(2): 1–23. https://doi.org/10.1111/jfb.15490

Mao WN, Lu ZM, Li WX, Ma HB, Huang G (2003) A new species of *Sinocyclocheilus* (Cyprinidae) from cave of Yunnan, China. Journal of Zhanjiang Ocean University 23(3): 1–2.

Mao TR, Liu YW, Meegaskumbura M, Yang J, Ellepola G, Senevirathne G, Fu CH, Gross JB, Pie MR (2021). Evolution in Sinocyclocheilus cavefish is marked by rate shifts, reversals, and origin of novel traits. BMC Ecology and Evolution 21: 1–14. https://doi.org/10.1186/s12862-021-01776-y

National Forestry and Grassland Administration, National Park Administration (2021) Announcement of the State Forestry and Grassland Administration and the Ministry of Agriculture and Rural Development (No. 3, 2021) (List of Wildlife under State Key Protection) [2021-02-05] https://www.forestry.gov.cn/main/5461/20210205/122418860831352.html

Nguyen LT, Schmidt HA, Von HA, Minh BQ (2015) IQ-TREE: A fast and effective stochastic algorithm for estimating maximum-likelihood phylogenies. Molecular Biology and Evolution 32(1): 268–274. https://doi.org/10.1093/molbev/msu300

Pan XF, Li L, Yang JX, Chen XY (2013) *Sinocyclocheilus xichouensis,* a new species of golden-line fish from the Red River drainage in Yunnan, China (Teleostei, Cypriniformes). Zoological Research 34(4): 368–373. https://doi.org/10.11813/j.issn.0254-5853.2013.4.0368

Policarpo M, Fumey J, Lafargeas P, Naquin D, Thermes C, Naville M, Dechaud C, Volff J-N, Cabau C, Klopp C, Møller PR, Bernatchez L, García-Machado E, Rétaux S, Casane D (2021) Contrasting gene decay in subterranean vertebrates: insights from cavefishes and fossorial mammals. Molecular biology and evolution 38(2): 589–605. https://doi.org/10.1093/molbev/msaa249

Ronquist F, Teslenko M, Van DMP, Ayres DL, Darling A, Höhna S, Larget B, Liu L, Suchard MA, Huelsenbeck JP (2012) MrBayes 3.2: Efficient Bayesian phylogenetic inference and model choicem across a large model space. Systematic Biology 61(3): 539–542. https://doi.org/10.1093/sysbio/sys029

Rambaut A, Drummond AJ, Xie D, Baele G, Suchard MA (2018) Posterior Summariza-tion in Bayesian Phylogenetics Using Tracer 1.7. Systematic Biology 67(5): 901–904. https://doi.org/10.1093/sysbio/syy032

Shao WH, Cheng GY, Lu XL, Zhou JJ, Zeng ZC (2024) Description of a new troglobitic Sinocyclocheilus (Pisces, Cyprinidae) species from the upper Yangtze River Basin in Guizhou, South China. Zoosystematics and Evolution 100(2): 515–529. https://doi.org/10.3897/zse.100.119520

Wang DZ, Chen YY (1989) Ddscriptions of three new species of Cyprinidae from Guizhou Province, China (Cypriniformes: Cyprinidae). Academiae Medicinae Zunyi 12(4): 29–34. [In Chinese]

Wang DZ, Liao JW (1997) A new species of *Sinocyclocheilus* from Guizhou, China (Cypriniformes, Cyprinidae, Barbinae). Acta Academiae Medicinae Zunyi 20(2/3): 1–3. [In Chinese]

Wang D, Zhao YH, Yang JX, Zhang CG (2014) A new cavefish species from Southwest China, *Sinocyclocheilus gracilicaudatus* sp. nov. (Teleostei, Cypriniformes, Cyprinidae). Zootaxa 3768(5): 583–590. https://doi.org/10.11646/zootaxa.3768.5.5

Wen H, Luo T, Wang Y, Wang S, Liu T, Xiao N, Zhou J (2022) Molecular phylogeny and historical biogeography of the cave fish genus *Sinocyclocheilus* (Cypriniformes, Cyprinidae) in southwest China. Integrative Zoology 17(2): 311–325. https://doi.org/10.1111/1749-4877.12624

Wu L, Li DJ, Zhao ZF, Zheng JZ, Ze Q, Xie JH, Lv KQ, Li GY (1989) The Fish Book of Guizhou. Guizhou People's Publishing House, Guiyang. [In Chinese]

Wu TJ, Liao ZP, Gan X, Li WX (2010) Two new species of *Sinocyclocheilus* in Guangxi, China (Cypriniformes, Cyprinidae). Journal of Guangxi Normal University (Natural Science Edition) 28(4): 116–120. https://doi.org/10.16088/j.issn.1001-6600.2010.04.008 [In Chinese]

Wu ZL, Li CQ, Lan C, Li WX (2018) Two new species of *Sinocyclocheilus* from Guangxi, China. Journal of Jishou University 39(3): 55–59. https://doi.org/10.13438/j.cnki.jdzk.2018.03.012 [Natural Science Edition] [In Chinese]

Wu L, Fan C, Lan C, Yu J, Wen H, Yang Q, Xiao N, Zhou J (2023) A long-ignored unique ecosystem of cavefishes in the southern karst: Achievements, challenges, and prospects. Environmental Science and Pollution Research 30(39): 90489–90499. https://doi.org/10.1007/s11356-023-28806-0

Xiao H, Chen SY, Liu ZM, Zhang RD, Li WX, Zan RG, Zhang YP (2005) Molecular phylogeny of Sinocyclocheilus (Cypriniformes, Cyprinidae) inferred from mitochondrial DNA sequences. Molecular Phylogenetics and Evolution 36(1): 67–77. https://doi.org/10.1016/j.ympev.2004.12.007

Xu C, Luo T, Zhou J-J, Wu L, Zhao X-R, Yang H-F, Xiao N, Zhou J (2023) *Sinocyclocheilus longicornus* (Cypriniformes, Cyprinidae), a new species of microphthalmic hypogean fish from Guizhou, Southwest China. ZooKeys 1141: 1–28. https://doi.org/10.3897/zookeys.1141.91501

Yang HF, Li QQ, Li WX (2017) A new species cave blind fish of the *Sinocyclocheilus* from Yunnan Province: *Sinocyclocheilus convexiforeheadus*. Journal of Jishou University 38(2): 58–60. [Natural Science Edition] [In Chinese]

Yang HF, Li CQ, Chen YY, Li WX (2018) A new species of *Sinocyclocheilus* from Yunnan: Sinocyclocheilus wenshanensis. Journal of Yunnan University (Natural Science Edition) 39(3): 507–512. [In Chinese]

Zhang CG, Dai DY (1992) A new species of the *Sinocyclocheilus* from Guangxi, China (Cypriniformes, Cyprinidae). Acta Zootaxonomica Sinica17(3): 377–380. [In Chinese]

Zhang CG, Zhao YH (2001) A new fish of *Sinocyclocheilus* from Guangxi, China with a comment on its some biological adaptation (Cypriniformes, Cyprinidae). Acta Zootaxonomica Sinica 26(1): 102–107. [In Chinese]

Zhao YH, Zhang CG (2009) Endemic fishes of *Sinocyclocheilus* (Cypriniformes, Cyprinidae) in China species diversity, cave adaptation, systematics and zoogeography. Science Press, Beijing. [In Chinese]

Zhao YH, Watanabe K, Zhang CG (2006) *Sinocyclocheilus donglanensis*, a new cavefish (Teleostei, Cypriniformes) from Guangxi, China. Ichthyological Research 53(2): 121–128. https://doi.org/10.1007/s10228-005-0317-z

Zhao YH, Lan JH, Zhang CG (2009) A new cavefish species, *Sinocyclocheilus brevibarbatus* (Teleostei, Cypriniformes, Cyprinidae),

from Guangxi, China. Environmental Biology of Fishes 86(1): 203–209. https://doi.org/10.1007/s10641-008-9338-6

Zheng JZ, Wang J (1990) Description of a new species of the genus *Sinocyclocheilus* from China (Cypriniformes, Cyprinidae). Acta Zootaxonomica Sinica 15(2): 251–254. [In Chinese]

Zheng CY, Xie JH (1985) One new carp of the genus *Sinocyclocheilus* (Barbinae, Cyprinidae) from Guizhou Province, China. Transactions of the Chinese Ichthyological Society 4: 123–126.

Zhou J, Zhang CG, He AY (2004) A new species of the genus *Sinocyclocheilus* from Guangxi, China (Cypriniformes, Cyprinidae). Acta Zootaxonomica Sinica 29(3): 591–594. [In Chinese]

Zhou J, Li XZ, Hou XF, Sun ZL, Gao L, Zhao T (2009) A new species of *Sinocyclocheilus* in Guizhou, China. Sichuan Journal of Zoology 28(3): 321–323. [In Chinese]

Zhou J, Liu Q, Wang HX, Yang LJ, Zhao DC, Zhang TH, Hou XF (2011) Description on a new species of *Sinocyclocheilus* in Guizhou. Sichuan. Journal of Zoology 30(3): 387–389. [In Chinese]

Zhu DG, Zhu Y (2012) A new species of the genus *Sinocyclocheilus* (Cypriniformes, Cyprinidae) from Guangxi, China. Acta Zootaxonomica Sinica 37(1): 222–226. [In Chinese]

Zhu DG, Zhu Y, Lan JH (2011) Description of a new species of Barbinae, *Sinocyclocheilus huangtianensis* from China (Teleostei, Cyprinidae). Zoological Research 32(2): 204–207.

Appendix 1

For specimen information examined by the *S. tingi* group (18 species).

Sinocyclocheilus aluensis (N = 2): China: Yunnan Province: Luxi County: Yipu Village (type locality). Currently these specimens are stored by Hong-Fu Yang at the fisheries workstation in Qubei County, Yunnan Province, China.

Sinocyclocheilus angustiporus (N = 5): China: Guizhou Province: Xinyi City (type locality): IHB12209016-81X2001, IHB12209016-81X2004, IHB12209016-81X2009, IHB12209016-81X2010, IHB12209016-81X2011. These specimens are stored at the Institute of Hydrobiology, Chinese Academy of Sciences, China.

Sinocyclocheilus robustus (N = 1): China: Guizhou Province: Xinyi City (type locality): IHB12209038-8001091. Currently preserved in the Institute of Hydrobiology, Chinese Academy of Sciences, China.

Sinocyclocheilus anophthalmus (N = 1): China: Yunnan Province: Yiliang County: Jiuxiang Township (type locality): KIZ1986003899. Currently preserved in the Kunming Institute of Zoology, Chinese Academy of Sciences, China.

Sinocyclocheilus grahami (N = 1): China: Yunnan Province: Kunming City: Dianchi Lake (type locality): KIZ2007003941. Currently preserved in the Kunming Institute of Zoology, Chinese Academy of Sciences, China.

Sinocyclocheilus huaningensis (N = 1): China: Yunnan Province: Huaning County (type locality): GZNU20221108001. Currently preserved in Guizhou Normal University, Guiyang City, Guizhou Province, China.

Sinocyclocheilus huizeensis (N = 2): China: Yunnan Province: Huize County: Wuxing Village (type locality): GZNU20160313001. Currently preserved in Guizhou Normal University, Guiyang City, Guizhou Province, China; China: Yunnan Province: Huize County: Dalong Spring (type locality): KIZ2013001246 (holotype). Currently preserved in the Kunming Institute of Zoology, Chinese Academy of Sciences, China.

Sinocyclocheilus lateristriatus (N = 6): China: Yunnan Province: Luliang County (type locality): GZNU20230825003–0825008. Currently preserved in Guizhou Normal University, Guiyang City, Guizhou Province, China.

Sinocyclocheilus macrocephalus (N = 1): China: Yunnan Province: Luliang County (type locality): GZNU20230501004. Currently preserved in Guizhou Normal University, Guiyang City, Guizhou Province, China.

Sinocyclocheilus maitianheensis (N = 3): China: Yunnan Province: Yiliangjiu Village (type locality): GZNU20230824001, GZNU20240105001–0105002. Currently preserved in Guizhou Normal University, Guiyang City, Guizhou Province, China.

Sinocyclocheilus malacopterus (N = 5): China: Yunnan Province: Luoping County: KIZ1980001282. Currently preserved in the Kunming Institute of Zoology, Chinese Academy of Sciences, China;China: Yunnan Province: Shizong County: Wulong Village (type locality): FWOQB 20180916001–0916004, collected by Hongfu Yang on 20 March 2018. Currently these specimens are stored by Hong-Fu Yang at the fisheries workstation in Qubei County, Yunnan Province, China.

Sinocyclocheilus oxycephalus (N = 3): China: Yunnan Province: Shilin County (type locality): GZNU20230501001–0501003. Currently preserved in Guizhou Normal University, Guiyang City, Guizhou Province, China.

Sinocyclocheilus purpureus (N = 1): China: Yunnan Province: Kaiyuan City: Zhongheying Town: Qiaotou Village (type locality): GZNU20200912001. Currently preserved in Guizhou Normal University, Guiyang City, Guizhou Province, China.

Sinocyclocheilus qiubeiensis (N = 1): China: Yunnan Province: Qiubei County (type locality): GZNU20210728001. Currently preserved in Guizhou Normal University, Guiyang City, Guizhou Province, China.

Sinocyclocheilus qujingensis (N = 2): China: Yunnan Province: Qujing County (type locality): GZNU20230825001–0825002. Currently preserved in Guizhou Normal University, Guiyang City, Guizhou Province, China.

Sinocyclocheilus tingi (N = 3): China: Yunnan Province: Yuxi City: Jiangchuan District (type locality): GZNU20230404001–0404003. Currently preserved in Guizhou Normal University, Guiyang City, Guizhou Province, China.

Sinocyclocheilus wenshanensis (N = 1): China: Yunnan Province: Wenshan City: Dehou Town (type locality): GZNU20200625001. Currently preserved in Guizhou Normal University, Guiyang City, Guizhou Province, China.

Sinocyclocheilus xichouensis (N = 1): China: Yunnan Province: Xichou County: Xingjie Town (type locality): GZNU20210730001. Currently preserved in Guizhou Normal University, Guiyang City, Guizhou Province, China.

Sinocyclocheilus xiejiahuai (N = 1): China: Guizhou Province: Panzhou City: Hongguo Town (type locality): GZNU20230304001. Currently preserved in Guizhou Normal University, Guiyang City, Guizhou Province, China.

Supplementary material 1

Uncorrected *p*-distance (%) between 24 species of the genus *Sinocyclocheilus* based on mitochondrial Cyt *b*.

Authors: Ming-Yuan Xiao, Jia-Jia Wang, Tao Luo, Jia-Jun Zhou, Ning Xiao, Jiang Zhou

Data type: xls

Link: https://doi.org/10.3897/zse.101.141444.suppl1

Supplementary material 2

Uncorrected *p*-distance (%) between 22 species of the genus *Sinocyclocheilus* based on mitochondrial ND4.

Authors: Ming-Yuan Xiao, Jia-Jia Wang, Tao Luo, Jia-Jun Zhou, Ning Xiao, Jiang Zhou

Data type: xls

Link: https://doi.org/10.3897/zse.101.141444.suppl2

Supplementary material 3

PCA loadings of the five principal components extracted from 29 morphometric data for *S. robustus*, *Sinocyclocheilus xingrenensis* sp. nov., and *S. angustiporus*

Authors: Ming-Yuan Xiao, Jia-Jia Wang, Tao Luo, Jia-Jun Zhou, Ning Xiao, Jiang Zhou

Data type: xlsx

Link: https://doi.org/10.3897/zse.101.141444.suppl3

Zoosyst. Evol. 101 (2) 2025, 437–447 | DOI 10.3897/zse.101.142297

PENSOFT

für Natur MUSEUM FÜR NATURKUNDE BERLIN

A new species of *Rhacophorus* (Anura, Rhacophoridae) from Xizang, China, with a revision of the distribution of *R. bipunctatus*

Shiyang Weng[1*], Xiaolong Liu[2,3*], Jianchuan Li[4], Guohua Yu[5,6], Junkai Huang[3]

1 *Institute of Plateau Biology of Xizang, Lhasa, 850030, China*
2 *Integrative Science Center of Germplasm Creation in Western China (CHONGQING) Science City, Biological Science Research Center, Southwest University, Chongqing, 400715, China*
3 *Key Laboratory of Freshwater Fish Reproduction and Development (Ministry of Education), School of Life Sciences, Southwest University, Chongqing, 400715, China*
4 *Xizang Museum of Natural Science, Lhasa, 850011, China*
5 *Key Laboratory of Ecology of Rare and Endangered Species and Environmental Protection (Guangxi Normal University), Ministry of Education, Guilin, 541004, China*
6 *Guangxi Key Laboratory of Rare and Endangered Animal Ecology, College of Life Science, Guangxi Normal University, Guilin, 541004, China*

https://zoobank.org/F7C7A5DF-0BBA-4EE1-B3F8-336F62197FAB

Corresponding authors: Junkai Huang (1198094210@qq.com); Guohua Yu (yugh2018@126.com)

Academic editor: Umilaela Arifin ♦ **Received** 20 November 2024 ♦ **Accepted** 29 January 2025 ♦ **Published** 24 February 2025

Abstract

A new species of *Rhacophorus* (Anura, Rhacophoridae), *Rhacophorus medogensis* **sp. nov.**, is described from Medog, Xizang Tibetan Autonomous Region, China. The new taxon can be distinguished from all phylogenetically closely related taxa (*R. rhodopus* and *R. bipunctatus* complexes) by the following combination of features: 1) body size medium (adult males SVL 31.6–38.7 mm, n = 17; adult females SVL 50.1–55.7 mm, n = 2); 2) pineal ocellus obvious; 3) toe webbing formula: I1–1II1–1.5III1–1IV1–1V; 4) irregularly shaped large black spots, white pattern in black spots on flanks; 5) snout pointed with appendage on tip; 6) tongue pyriform, with a deep notch at posterior tip; 7) tibiotarsal articulation reaching eye. In addition, we also discuss the distribution of *R. bipunctatus*, which is limited to northern India and central-western Myanmar, rather than the traditionally presumed range across South and Southeast Asia.

Key Words

Biodiversity, cryptic species, *Rhacophorus medogensis* sp. nov., taxonomy

Introduction

The genus *Rhacophorus* Kuhl & Van Hasselt, 1822, currently includes 46 species and is widely distributed across the tropical and subtropical regions of southern Asia, from India to China and Southeast Asia (AmphibiaChina 2024; AmphibiaWeb 2024; Frost 2024). *Rhacophorus bipunctatus*, commonly known as the Himalaya Flying Frog, was first described from the Khasi Hills in northern India (Bordoloi et al. 2007). The species has been reported from a broad distribution across South and Southeast Asia, including Bangladesh, Cambodia, China, Laos, Malaysia, Myanmar, Thailand, and Vietnam (Frost 2024). However, the taxonomic relationship between *R. bipunctatus* and *R. rhodopus* has been a topic of considerable debate over recent decades (Inger et al. 1999; Frost et al. 2006; Bordoloi et al. 2007; Chan et al. 2018).

* These authors contributed equally to this work.

Recent phylogenetic analyses have revealed the complexity in the relationships between *Rhacophorus bipunctatus* and *R. rhodopus*. Chan et al. (2018) suggested that they belong to distinct species complexes, indicating potential cryptic diversity. The phylogenetic analyses of Che et al. (2020) showed that the "*R. rhodopus*" population from Medog, Xizang, is distantly related to the type locality of *R. rhodopus* and is morphologically more similar to *R. bipunctatus* (Mathew & Sen, 2010), classifying it as *R. bipunctatus*. However, Li et al. (2022) and Tang et al. (2024) showed that the "*R. bipunctatus*" from Medog is distantly related to *R. bipunctatus* from northern India; four species (*R. rhodopus*, *R. napoensis*, *R. qiongica*, and *R. kio*) in China belong to the *R. rhodopus* and *R. bipunctatus* complexes. However, these studies did not include molecular and morphological data from the type locality of *R. bipunctatus*, leaving uncertainties regarding the true distribution and diversity within this complex. To address these gaps, this study incorporated sequences from near the type locality of *R. bipunctatus* (Mawblang, Cherapunji, Southern Khasi Hills, northern India) to reconstruct the phylogenetic relationships within the *R. rhodopus* and *R. bipunctatus* complexes. Based on both morphological and molecular evidence, we also describe a new species of *Rhacophorus* from Medog, Xizang.

Materials and methods sampling

Fieldwork was conducted at Medog, Xizang Tibetan Autonomous Region, China. Eight specimens were collected in May 2024. The specimens were collected by hand and subsequently euthanized with a low concentration of clove oil solution following standard euthanasia protocols for amphibians (Leary et al. 2020). Liver or muscle tissues were taken from the specimens and preserved in 95% ethanol. While the specimens were fixed in 75% ethanol. Voucher specimens SWU 0008599, SWU 0008600, SWU 0008601, SWU 0008602, SWU 0008603, SWU 0008604, SWU 0008699, and SWU 0008701 were deposited at Southwest University (SWU).

Morphology and morphometrics

We measured all the voucher specimens. All the measurements were made with slide calipers to the nearest 0.1 mm. Morphological terminology followed Fei (1999) and Fei et al. (2009) and is listed in Table 1; the webbing formula followed Myers and Duellman (1982). Morphological measurements of all specimens are listed in Table 2. Comparative morphological data of the new species and congeneric species were obtained from published literatures (Liu and Hu 1960; Ohler and Delorme 2006; Bordoloi et al. 2007; Fei et al. 2009, 2012; Chan and Grismer 2010; Rowley et al. 2012; Matsui et al. 2013; Li et al. 2022; Tang et al. 2024; Che et al. 2020). Sex of the specimens was determined by the presence of nuptial pads and vocal sac openings.

Table 1. Morphological characters used for adult individuals.

Abbreviation	Morphology
SVL	Snout-vent length
HL	Head length
HW	Head width
SL	Snout length
IND	Internarial distance
IOD	Interorbital distance
UEW	Width of upper eyelid
ED	Diameter of eye
TD	Diameter of tympanum
DNE	Distance from nostril to eye
FHL	Length of forearm and hand
TL	Tibia length
TFL	Length of foot and tarsus
FL	Foot length

DNA sequencing and molecular analyses

To construct a phylogeny for *Rhacophorus rhodopus* and *R. bipunctatus* complexes, we extracted total DNA from liver or muscle tissue using the Animal Tissue DNA Isolation Kit provided by Thermo Fisher Scientific. In this study, we chose five specimens (SWU 0008599, SWU 0008600, SWU 0008601, SWU 0008603, and SWU 0008699) to sequence three consecutive mitochondrial gene segments: partial 12S rRNA, $tRNA^{val}$, and partial 16S rRNA. The primers used for polymerase chain reaction (PCR) amplification are detailed in Table 3. The PCR amplification process was carried out in a 50-μL reaction volume, following the reaction cycling settings below: an initial denaturing step at 95 °C for 4 min; 35 cycles of denaturing at 94 °C for 60 s, annealing at 51 °C for 60 s, and extending at 72 °C for 60 s; and a final extending step of 72 °C for 10 min. Sequencing was conducted using the corresponding PCR primers and an internal primer (Rhint: 5'-GACAGTGTAACCCTCGTGAT-3') (Yu et al. 2019), and all sequences have been uploaded to GenBank (Table 4). Based on Tang et al. (2024), we selected species from the genera *Rhacophorus*, *Buergeria*, *Nyctixalus*, *Chiromantis*, *Theloderma*, *Kurixalus*, *Zhangixalus*, and *Leptomantis* as outgroups to reconstruct the phylogenetic relationships of the *R. rhodopus* and *R. bipunctatus* complexes; all GenBank accession numbers are listed in Table 4.

Sequences were aligned using the MUSCLE option in MEGA v. 7, and due to the absence of 12S rRNA and $tRNA^{val}$ sequences in some species, uncorrected pairwise distances (p-distances) were calculated only for 16S rRNA sequences (500 bp) between species (Kumar et al. 2016). Prior to phylogenetic reconstruction, the best substitution model was selected using the Akaike Information Criterion (AIC) in jMODELTEST v. 2.1.10 (Darriba et al. 2012). Bayesian inference (BI) was performed using MrBayes v.3.2.6 (Ronquist et al. 2012), with two runs performed simultaneously, each consisting of four Markov chains starting from a random tree. The chain was run for 6,000,000 generations, with sampling every

Table 2. Measurements (mm) of adult specimens in the type series of *R. medogensis* sp. nov.

NO	SWU 0008699	SWU 0008599	SWU 0008600	SWU 0008601	SWU 0008602	SWU 0008603	SWU 0008604	SWU 0008701
SEX	Adult male	Adult male	Adult male	Adult male	Adult male	Adult male	Adult male	Subadult
SVL	33.5	36.2	34.1	35.4	33.5	34.0	34.6	27.4
HL	12.1	13.4	11.8	13.1	12.0	12.3	12.7	10.8
HW	11.1	12.2	11.5	12.4	11.2	11.6	12.0	10.4
SL	5.0	5.4	5.3	5.4	5.3	5.2	5.3	4.7
IND	3.2	3.7	3.1	3.5	3.5	3.4	3.3	2.7
IOD	4.6	4.5	4.6	4.6	4.8	4.5	4.7	3.6
UEW	2.5	2.7	2.9	2.8	2.7	2.5	2.7	2.2
ED	4.2	4.6	4.3	4.4	4.4	4.2	4.4	3.6
TD	2.2	2.3	2.1	2.2	2.2	1.9	2.1	1.9
DNE	2.6	2.7	2.4	2.4	2.4	2.6	2.5	2.2
FHL	16.3	16.5	16.5	17.1	16.8	16.9	18.3	13.9
TL	16.6	17.9	16.3	17.7	16.2	17.6	17.6	14.5
TFL	22.4	23.0	21.9	23.5	22.7	23.3	23.3	18.4
FL	14.0	14.8	13.2	14.9	14.5	15.2	15.1	11.9

Table 3. Primer pairs for PCR amplification used in this study.

Gene	Primer	Source
12S rRNA, $tRNA^{val}$, and partial 16S rRNA	L1091 (5′–AAAAAGCTTCAAACTGGGATTAGATACCCCACTAT–3′)	Kocher et al. 1989
	16H1 (5′–CTCCGGTCTGAACTCAGATCACGTAGG–3′)	Hedges 1994

1,000 generations. When the average standard deviation of the split frequency was less than 0.01, the first 25% of the sampled trees were discarded as burn-in, and the remaining trees were used to create a consensus tree and estimate the Bayesian posterior probabilities. Maximum likelihood (ML) analyses were performed using RAxML v7.0.3 (Stamatakis 2014) under the GTRGAMMA model with 1000 bootstrap replicates.

Results

Phylogenetic analyses

The obtained sequence alignment was 1936 bp long. The phylogenetic trees inferred from BI and ML methods are generally consistent (Fig. 1). The phylogenetic results of this study show differences in the placement of certain species compared to Tang et al. (2024) but consistently indicate that the *Rhacophorus bipunctatus* complex is nested within the *R. rhodopus* complex. The *R. rhodopus* and *R. bipunctatus* complexes comprise 10 known species and 1 undescribed lineage (*R. medogensis* sp. nov., *R. rhodopus, R. napoensis, R. qiongica, R. borneensis, R. norhayatiae, R. reinwardtii, R. bipunctatus, R. kio, R. helenae,* and *R.* sp.). The sequence of *R. bipunctatus* from the near-type locality clusters together with those from northeastern India and central-western Myanmar, representing the "true" *R. bipunctatus*. The new species *R. medogensis* sp. nov. clusters within the *R. rhodopus* and *R. bipunctatus* complexes and represents the sister group to *R. borneensis, R. norhayatiae,* and *R. reinwardtii* with strong support (BPP = 0.98, BS = 77). The undescribed lineage (*R.* sp.) represents the sister group to *R. rhodopus* with strong support (BPP = 0.99, BS = 95). P-distances of 16S rRNA between the sequences of *R. medogensis* sp. nov. and the other species of *R. rhodopus* and *R. bipunctatus* complexes varied from 7.5% to 11.6%, while the p-distances of 16S rRNA between *R.* sp. and *R. rhodopus* is 7% (Table 5).

Taxonomic account

Rhacophorus medogensis sp. nov.

https://zoobank.org/4C0CEFC4-09D5-4229-B2A9-C0655D43E452

Figs 3, 4, Table 2

Chresonymy. *Rhacophorus rhodopus*—Hu 1987; Fei et al. 2004; Fei et al. 2009; Li et al. 2011; Fei et al. 2012; Li et al. 2022.

Rhacophorus bipunctatus—Che et al. 2020; Tang et al. 2024

Holotype. SWU 0008699, adult male, collected in May 2024 by Xiaolong Liu, Renda Ai, and Xianqi Li from Didong Village, Medog, Xizang Tibetan Autonomous Region, China (29.2205°N, 95.1293°E, elevation 771 m; Fig. 2A).

Paratypes. Six adult males (SWU 0008599, SWU 0008600, SWU 0008601, SWU 0008602, SWU 0008603, and SWU 0008604) were collected at Buqun (Xigong) Lake, Medog, Xizang Tibetan Autonomous Region, China (29.25241°N, 95.225759°E, elevation 1361 m). One subadult (SWU 0008701) was collected at the same locality as the holotype in May 2024 by Xiaolong Liu, Renda Ai, and Xianqi Li.

Table 4. Species used in phylogenetic analyses of this study.

No.	Species	Voucher	Locality	Accession No
1	*R. medogensis* sp. nov.	KIZ016380	Medog, Xizang, China	MW111517
2	*R. medogensis* sp. nov.	YPX40427	Medog, Xizang, China	MW111518
3	*R. medogensis* sp. nov.	L06245	Medog, Xizang, China	JX219441
4	*R. medogensis* sp. nov.	L062456	Medog, Xizang, China	JX219442
5	*R. medogensis* sp. nov.	SWU 0008599	Medog, Xizang, China	PQ963460
6	*R. medogensis* sp. nov.	SWU 0008600	Medog, Xizang, China	PQ963459
7	*R. medogensis* sp. nov.	SWU 0008601	Medog, Xizang, China	PQ963458
8	*R. medogensis* sp. nov.	SWU 0008603	Medog, Xizang, China	PQ963457
9	*R. medogensis* sp. nov.	SWU 0008699	Medog, Xizang, China	PQ963456
10	*R. bipunctatus*	CAS229913	Nagmung Township, Putao District, Kachin State, Myanmar	JX219445
11	*R. bipunctatus*	CAS235303	Mindat Township, Mindat District, Chin State, Myanmar	JX219444
12	*R. bipunctatus*	PUCZM/IX/SL360	Mizoram, Inida	MH087073
13	*R. bipunctatus*	PUCZM/IX/SL612	Mizoram, Inida	MH087076
14	*R. bipunctatus*	/	Mawblang, Cherapunji, Southern Khasi Hills, India*	OL988889
15	*R. napoensis*	GXNU YU000171	Napo, Guangxi, China	ON217796
16	*R. napoensis*	GXNU YU000173	Napo, Guangxi, China	ON217798
17	*R. napoensis*	VNMN:4118	Yen Tu, Bac Giang, Vietnam	LC010605
18	*R. napoensis*	VNMN:4120	Pu Huong, Nghe An, Vietnam	LC010609
19	*R. napoensis*	VNMN:4121	Thanh Hoa, Vietnam	LC010608
20	*R. napoensis*	AMNH-A 161418	Huon Son Reserve, Ha Tinh, Vietnam	AY843750
21	*R. qiongica*	SN 030035	Hainan, China	EU215529
22	*R. qiongica*	VNMN:4117	K' Bang, Gia Lai, Vietnam	LC010604
23	*R. qiongica*	FMNH253114	Ankhe Dist, Gia Lai, Vietnam	GQ204716
24	*R. rhodopus*	clone 5	Mengyang, Yunnan, China	EF646366
25	*R. rhodopus*	SCUM 060692L	Mengyang, Yunnan, China	EU215531
26	*R. rhodopus*	KIZ060821229	Lvchun, Yunnan, China	EF564574
27	*R. rhodopus*	2004.0409	Long Nai Khao, Phongsali, Laos	KR828049
28	*R. rhodopus*	2006.2519	Ban Vang Thong, Louangphrabang, Laos	KR828069
29	*R. rhodopus*	K3046	Doi Chiang Dao, Chiang Mai, Thailand	KR828066
30	*R. rhodopus*	K3085_1	Mae Lao-Mae Sae Wildlife Sanctuary, Chiang Mai, Thailand	KR828067
31	*R.* sp	clone 4	Jingdong, Yunnan, China	EF646365
32	*R.* sp	KIZ060821248	Jingdong, Yunnan, China	EF564575
33	*R.* sp	KIZ060821175	Yongde, Yunnan, China	EF564573
34	*R.* sp	clone 2	Yongde, Yunnan, China	EF646363
35	*R.* sp	KIZ587	Longling, Yunnan, China	EF564577
36	*R.* sp	KIZ589	Longling, Yunnan, China	EF564578
37	*R.* sp	USNM:Herp:587063	Kandawgyi National Gardens, Mandalay, Myanmar	MG935991
38	*R.* sp	0937Y4	Kui Buri NP, Prachuap Khiri Khan, Thailand	KR828058
39	*R.* sp	KUHE:53375	Genting, Pahang, Malaysia	LC010569
40	*R. borneensis*	NMBE 1056517	Batang Ai NP, Sarawak, Malaysia	JN377366
41	*R. borneensis*	BORN 22411	Sabah, Maliau Basin, Malaysia	AB781694
42	*R. helenae*	UNS 00451	Binh Thuan, Vietnam	JQ288090
43	*R. kio*	KUHE 55165	Xuan Lien, Than Hoa, Vietnam	AB781695
44	*R. lateralis*	/	Mudigere, India	AB530548
45	*R. norhayatiae*	Rao081205	Malaysia	JX219443
46	*R. norhayatiae*	NNRn	Johor, Endau Rompin, Malaysia	AB728191
47	*R. nigropalmatus*	Rao081204	Malaysia	JX219437
48	*R. reinwardtii*	ENS 16179 (UTA)	Java, Patuha, Indonesia	KY886328
49	*Buergeria buergeri*	TTU-R-11759	Japan	AF458122
50	*Chiromantis rufescens*	CAS 207601	Bioko Norte Province, Equatorial Guinea	AF458126
51	*Kurixalus idiootocus*	CAS 211366	Taipei, Taiwan, China	AF458129
52	*Leptomantis gauni*	FMNH 273928	Bintulu, Sarawak, Malaysia	JX219456
53	*Nyctixalus pictus*	FMNH 231094	Lahad Datu, Sabah, Malaysia	AF458135
54	*Theloderma albopunctatum*	ROM 30246	Vietnam	AF458148
55	*Zhangixalus smaragdinus*	HM05292	Xima, Yingjiang, Yunnan, China	MN613221

Etymology. The specific epithet "*medogensis*" is named after the type locality, Medog, Xizang, China. We suggest "Xizang flying frog" as its English common name and "Mò Tuō Shù Wā" (墨脱树蛙) as its Chinese common name.

Diagnosis. The genus *Rhacophorus*, also known as flying frogs, is characterized by the following features: 1) body size relatively moderate or large (SVL 30–100 mm, above 40 mm in most species); 2) presence of intercalary cartilage between terminal and penultimate phalanges of digits; 3)

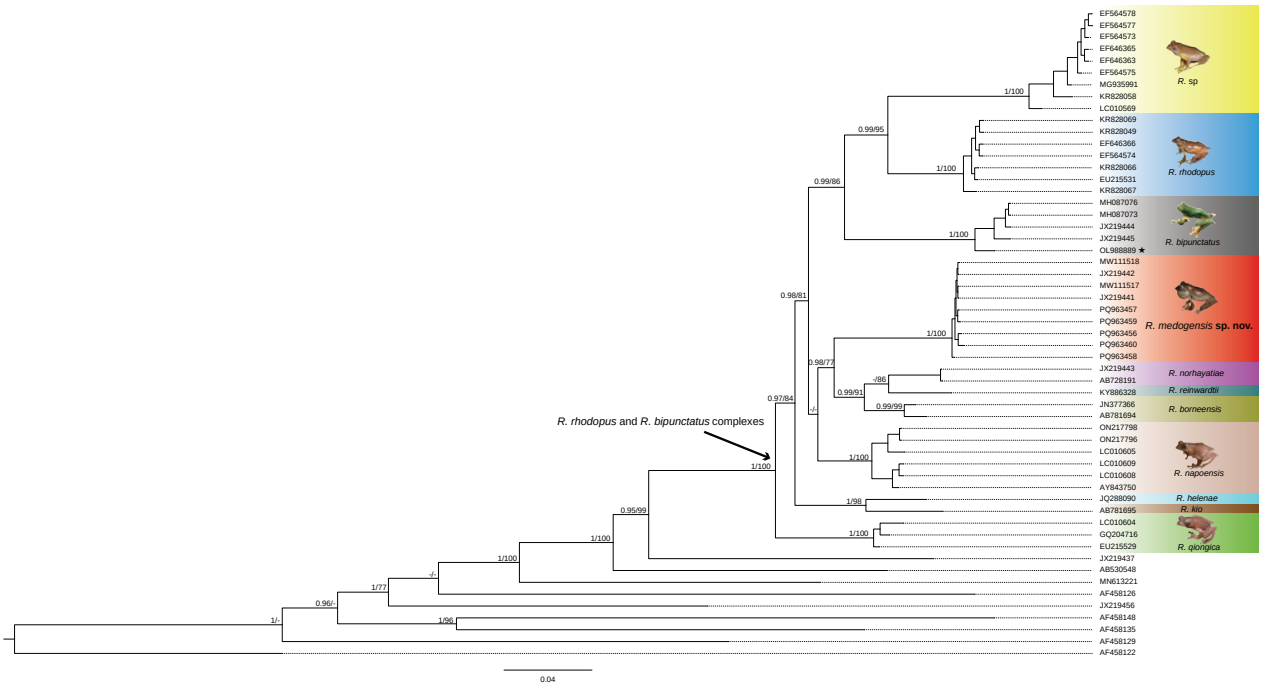

Figure 1. Bayesian phylogenetic tree of *R. rhodopus* and *R. bipunctatus* complexes and related species inferred from 12S rRNA, tRNA-^{Val}, and 16S rRNA genes. The numbers above and below the branches are Bayesian posterior probabilities (BPP) and maximum likelihood bootstrap values (BS), "-" denotes a BPP < 0.95 and BS < 70. The scale bar represents 0.04 nucleotide substitutions per site. The "black star" means this sequence from from near type locality of *R. bipunctatus*, *R. medogensis* sp. nov., *R. rhodopus* and *R.* sp photoed by Xiaolong Liu, *R. bipunctatus* from Bordoloi et al. (2007), *R. qiongica* photoed by Chenxi Liao, *R. napoensis* by Junkai Huang.

Table 5. Mean uncorrected pairwise distances (%) between clades of *R. rhodopus* and *R. bipunctatus* complexes and related species based on 16S rRNA sequences.

No	Species	1	2	3	4	5	6	7	8	9	10	11
1	*R. medogensis* sp. nov.											
2	*R. bipunctatus*	10.3										
3	*R. napoensis*	8.4	8.8									
4	*R.* sp	9.7	9.7	10.4								
5	*R. qiongica*	9.1	13.1	10.7	13.9							
6	*R. reinwardtii*	8.6	9.2	7.3	9.3	12.2						
7	*R. rhodopus*	11.6	10.1	11.3	7.0	12.3	10.3					
8	*R. norhayatiae*	8.6	9.5	8.1	9.3	13.5	5.8	11.1				
9	*R. helenae*	10.3	10.1	9.9	10.4	12.4	8.9	13.2	10.1			
10	*R. borneensis*	7.5	8.7	6.7	8.6	10.1	6.4	11.7	5.7	6.7		
11	*R. kio*	10.4	11.1	9.5	11.3	13.5	11.2	14.0	9.3	6.8	7.8	

terminal phalanges of fingers and toes Y-shaped; 4) tips of the digits expanded into large disks bearing circummarginal grooves; 5) webbed fingers; 6) skin not co-ossified to the skull; 7) upper eyelid projections absent, tarsal projections present in most species; 8) dermal folds along the forearm or tarsus present; 9) pupil horizontal; 10) iris without "X"-shaped marking; 11) white foam nests or jelly-encapsulated eggs produced by breeding pairs; and (12) distributed mainly in Indochina (Jiang et al. 2019). *Rhacophorus medogensis* sp. nov. is placed in the genus *Rhacophorus* due to the combination of the following features: 1) body size relatively moderate (adult males SVL 31.6–38.7 mm, n = 17; adult females SVL 50.1–55.7 mm, n = 2); 2) presence of intercalary cartilage between terminal and penultimate phalanges of digits; 3) terminal phalanges of fingers and toes Y-shaped; 4) tips of the digits expanded into large disks bearing circummarginal grooves; 5) webbed fingers; 6) tarsal projections present; 7) pupil horizontal; 8) iris without "X"-shaped marking. *Rhacophorus medogensis* sp. nov. can be distinguished from other species in the *R. rhodopus* and *R. bipunctatus* complexes by the following combination of features: 1) medium adult males body size (adult males SVL 31.6–38.7 mm); 2) dorsal surface reddish brown, light green, light brown, or grayish green in life; 3) pineal ocellus obvious; 4) toe webbing formula: I1–1II1–1.5III1–1IV1–1V; 5) irregularly shaped large black spots, white pattern in black spots on flanks; 6) snout pointed with an appendage on the tip; 7) tongue pyriform, with a deep notch at the posterior tip; 8) throat rough; 9) palm rough with small tubercles; 10) tibiotarsal articulation reaching the eye.

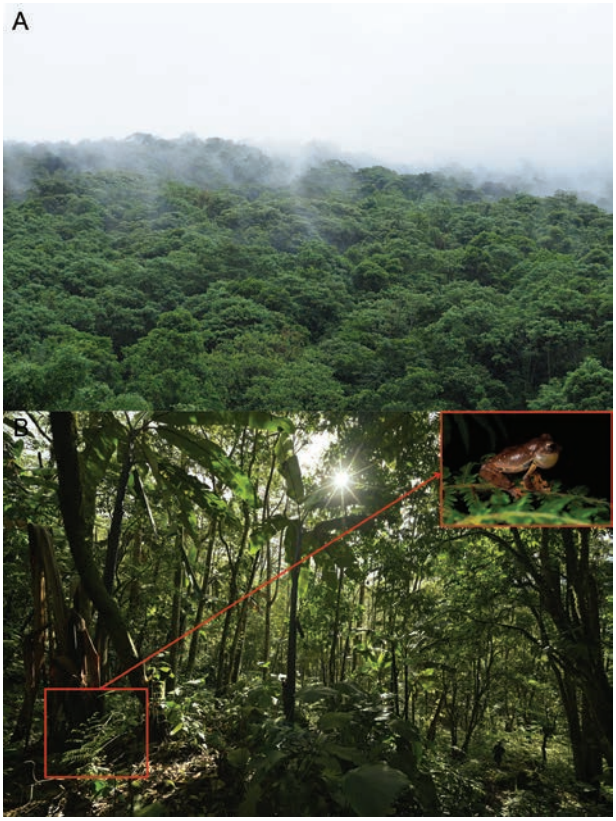

Figure 2. (A) Large habitat at the type locality of *R. medogensis* sp. nov., Didong Village, Medog County, Xizang Tibetan Autonomous Region, China (29.2205°N, 95.1293°E, elevation 771 m); (B) macrohabitat of *R. medogensis* sp. nov. (SWU 0008601), Buqun (Xigong) Lake, Medog County, Xizang Tibetan Autonomous Region, China (29.25241°N, 95.225759°E, elevation 1361 m).

Description of holotype. Adult male, medium body size (SVL 33.5 mm); head length (HL 12.1 mm) longer than head width (HW 11.1 mm); snout pointed with an appendage on tip, sloping in profile, and protruding beyond the margin of lower jaw in ventral view; snout length (SL 5.0 mm) is longer than the diameter of the eye (ED 4.2 mm); the canthus rostralis is distinct and curved; loreal region oblique, concave; nostrils oval, lateral, slightly protuberant, and slightly closer to the tip of snout than the eye; the internarial space (IND 3.2 mm) is slightly smaller than the interorbital distance (IOD 4.6 mm) and larger than the width of the upper eyelid (UEW 2.5 mm); the pupil is horizontal; pineal ocellus obvious; tympanum distinct (TD 2.2 mm), rounded, and nearly about half of eye diameter (ED 4.2 mm); the supratympanic fold is narrow and flat; tongue pyriform, with a deep notch at the posterior tip; choanae oval; vomerine teeth present in two series; with an internal single subgular vocal sac; a vocal sac opening on the floor of the mouth at each corner (Fig. 3).

Forelimbs strong, length of forearm and hand (FHL 16.3 mm); relative length of fingers I < II < IV < III; tips of all fingers expand into discs with circummarginal and transverse ventral grooves, disc of finger I smaller than discs of other fingers; entire web between fingers, webbing formula: I2–2II1–1.5III1–1IV; subarticular tubercles rounded and prominent, formula 1, 3, 4, 4; inner metacarpal tubercle single, oval, and prominent (Fig. 3C).

Hindlimbs slender and long, heels overlapping when legs at a right angle to the body, tibiotarsal articulation reaching the eye; tibia length (TL 16.6 mm) nearly equal to the length of forearm and hand (FHL 16.3 mm), longer than foot length (FL 14.0 mm), and shorter than the length of tarsus and foot (TFL 22.4 mm); relative length of toes I < II < III < V < IV, with the third and fifth toes being nearly equal in length; tips of all toes expanded into discs with circummarginal and transverse ventral grooves; entire web between toes, webbing formula: I1–1II1–1.5III1–1IV1–1V; subarticular tubercles rounded and prominent, formula 1, 1, 2, 3, 2; supernumerary tubercles absent; single inner metatarsal tubercle, oval, outer metatarsal tubercle absent; tibiotarsal joint with a small triangular fold of skin (Fig. 3D).

Dorsal skin smooth with very fine granules; throat rough, covered with small warts, and ventral surface of forelimbs smooth; palm rough with small tubercles; chest, belly, and ventral surface of small warts (Fig. 3A, B); dermal folds on forearm, tarsus, heels, and vent present.

Coloration of holotype in life. For coloration of the holotype in life (see Fig. 4). Dorsal surface reddish brown with a dark brown X-shaped marking; dark brown patches between the eyes; the dorsal surface of the body and limbs covered with small black dots; the supratympanic fold reddish brown; iris orange brown; the dorsal surface of limbs has distinct dark brown bands; a larger black spot present between the axillary and inguinal regions, as well as several smaller black spots located between the two larger spots, some white patterns in the black spots on flanks; ventral surface creamy white; throat pale yellow; ventral surface of the limbs orange; finger webbing yellow and toe webbing reddish orange; both the finger and toe discs are yellow.

Coloration of the holotype in preservative. After preservation in alcohol, the color faded, but the general pattern did not change. Dorsal color changed to grey-brown with a dark X-shaped marking and some small black dots; the ventral surface faded to white; the white pattern in the large black spots on the flanks has disappeared (Fig. 3A, B).

Sexual dimorphism. Males are smaller than females (Che et al. 2020); the forearms are slightly more robust, with a milky-white nuptial pad on the inner side of the first finger base; they possess a single internal subgular vocal sac, with oval-shaped openings that are relatively large.

Variation. The coloration in living individuals is variable. The dorsal surface typically displays a reddish-brown coloration, characterized by irregular dark brown or chestnut spots. Some individuals present light green, light yellow, or light brown coloration. The dorsal coloration can change in response to variations in environmental colors and the individual's condition. The black spots on the flanks exhibit three morphological forms: 1) a larger black spot typically present in the axillary and inguinal regions (SWU 0008602); 2) several smaller black spots located between the two larger spots (SWU 0008599,

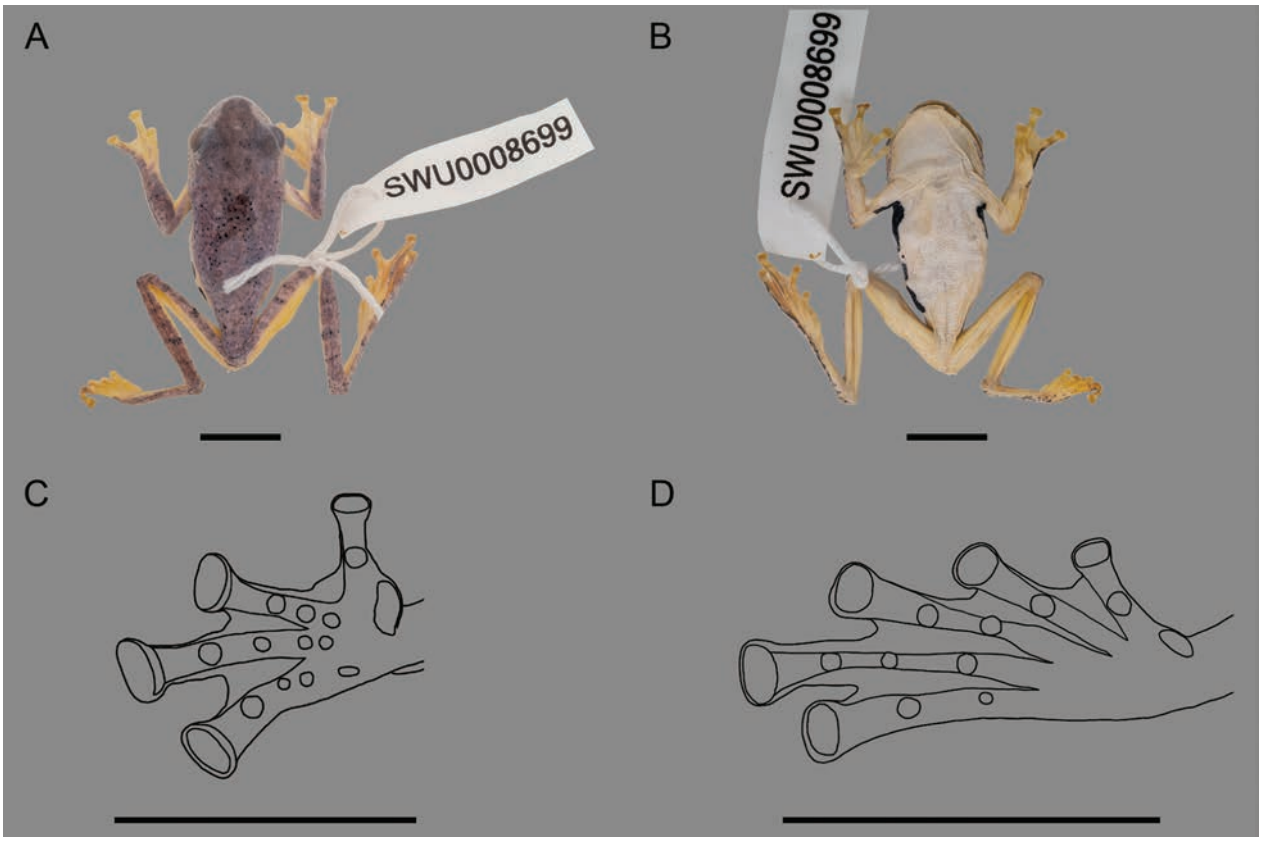

Figure 3. Holotype **(**SWU 0008699**)** of *R. medogensis* sp. nov. in preservative, showing (A) dorsal view, (B) ventral view, (C) Line drawing of the ventral view of hand, and (D) line drawing of the ventral view of foot. Scale bars: 10 mm.

SWU 0008600, SWU 0008601, and SWU 0008699); 3) the presence of a single axillary spot without an inguinal spot (SWU 0008604 and SWU 0008701).

Distribution and ecology. This species is currently known to be distributed only in Medog (Fig. 5). It inhabits humid shrublands, marshes, puddles, or slow-flowing ditches at elevations of 500–1700 m (Fig. 2B). Some individuals were found during the day in bamboo tubes with *R. tuberculatus*. Females are less common, and none were observed during surveys conducted in May.

Comparisons. Rather than comparing the new species to all known *Rhacophorus*, we focus on our morphological comparison with phylogenetically closely related taxa (*R. rhodopus* and *R. bipunctatus* complexes) (Table 6). *Rhacophorus medogensis* sp. nov. can be easily distinguished from *R. helenae, R. kio, R. borneensis, R. norhayatiae,* and *R. reinwardtii* by the dorsal surface being reddish brown (vs. green) and the web between toes being red with no black pigmentation (vs. black pigmentation present).

Rhacophorus medogensis sp. nov. differs from *R. bipunctatus* by 1) smaller body size (adult male SVL 31.6–38.7 mm, n = 17 vs. 37.8–50.4 mm, n = 28; Table 6); 2) dorsal surface reddish brown, light green, light brown, or grayish green in life (vs. dorsal surface green in life); 3) dorsal surface reddish brown, light green, light brown, or grayish green in life (vs. dorsal surface green in life); 4) white pattern in black spots on flanks (vs. blue pattern in black spots on flanks); 5) snout pointed with appendage on tip (vs. snout pointed without appendage on tip); 6) distinct bands on limbs (vs. indistinct bands on limbs); 7) palm rough with small tubercles (vs. palm smooth without small tubercles); 8) tibiotarsal articulation reaching eye (vs. tibiotarsal articulation reaching beyond eye); 9) tongue pyriform (vs. tongue rounded); 10) pineal ocellus obvious (vs. pineal ocellus absent).

Figure 4. Holotype (SWU 0008699) of *R. medogensis* sp. nov. in situ.

Rhacophorus medogensis sp. nov. differs from *R. napoensis* by 1) tibiotarsal articulation reaching eye (vs. tibiotarsal articulation reaching beyond eye); 2) tongue pyriform (vs. tongue cordiform); 3) pineal ocellus obvious (vs. pineal ocellus absent).

Table 6. Comparison of *R. medogensis* sp. nov. with species in *R. rhodopus* and *R. bipunctatus* complexes, "/" means unknown.

Species	*R. medogensis* sp. nov.	*R. bipunctatus*	*R. napoensis*	*R. qiongica*	*R. rhodopus*
Adult male	31.6–38.7 mm, n = 17	37.8–50.4 mm, n = 28	39.7–44.2 mm, n = 5	35.1–38.2 mm, n = 8	33.1–38.7 mm, n = 6
Adult female	50.1–55.7 mm, n = 2	37.3–59.1 mm, n = 8	/	49.3 mm, n = 1	50.2 mm, n = 1
Dorsal surface	Red brown, light green, light brown, or grayish green	Green	Red brown	Red brown	Red brown or yellow brown
Black spots on flanks	Two large spots in the axillary and inguinal regions	Two large spots	Two small spots	A series of small spots	One small spot in the axillary region
Pattern in black spots	White	Blue	/	Absent	/
Snout pointed	With appendage	Without appendage	With appendage	Without appendage	Without appendage
Bands on limbs	Distinct	Indistinct	Distinct	Distinct	Distinct
Throat	Rough	Rough	Rough	Smooth	Smooth
Palm	Rough	Smooth	Rough	Smooth	Rough
Tibiotarsal articulation	Reaching eye	Reaching beyond eye	Reaching beyond eye	Reaching beyond eye	Reaching eye
Tongue	Tongue pyriform	Tongue rounded	Tongue cordiform	Tongue cordiform	Tongue narrow and long
Pineal ocellus	Obvious	Absent	Absent	Absent	Absent
Toe webbing formula	I1–1II1–1.5III1–1IV1–1V	/	/	I1–1II1–1III1–1IV1–1V	/
Species	***R. kio***	***R. helenae***	***R. borneensis***	***R. norhayatiae***	***R. reinwardtii***
Adult male	58–79.1 mm, n = 10	72.3–85.5 mm, n = 3	50.9 mm, n = 1	60.6–64.7 mm, n = 5	41.7–49.8 mm, n = 6
Adult female	/	89.4–90.7 mm, n = 2	62.0 mm, n = 1	75.7–83 mm, n = 4	66.6–74.8 mm, n = 2
Dorsal surface	Green	Green	Green	Green	Green
Black spots on flanks	One large spot in the axillary region	One large spot in the axillary region	Irregular and mainly concentrated in the axillary region	Irregular in the axillary and inguinal regions	One spot in the axillary region
Pattern in black spots	Absent	Absent	Dark blue	Blue	Orange or yellow
Snout pointed	Without appendage	Without appendage	Without appendage	Without appendage	Without appendage
Bands on limbs	Distinct	Indistinct	Absent	Absent	Absent
Throat	Smooth	Smooth	/	/	/
Palm	Rough	/	/	/	/
Tibiotarsal articulation	Reaching beyond eye	/	Reaching point between eye and nostril	Not extend beyond snout	/
Tongue	Tongue moderate and oval	/	/	Tongue oval	/
Pineal ocellus	Absent	Absent	Absent	/	/
Toe webbing formula	I1–1II1–1III1–1IV1–1V	I1–1II1–1III1–1IV1–1V	I1–1II1–1III1–1IV1–1V	I1–1II1–1III1–1IV1–1V	I1–1II1–1III1–1IV1–1V

Rhacophorus medogensis sp. nov. differs from *R. qiongica* by 1) usually two large spots in the axillary and inguinal regions (vs. a series of small black spots on flanks); 2) white pattern in black spots on flanks (vs. no pattern in black spots on flanks); 3) snout pointed with appendage on tip (vs. snout pointed without appendage on tip); 4) throat rough (vs. throat smooth); 5) palm rough with small tubercles (vs. palm smooth without small tubercles); 6) tibiotarsal articulation reaching eye (vs. tibiotarsal articulation reaching beyond eye); 7) tongue pyriform (vs. tongue cordiform); 8) pineal ocellus obvious (vs. pineal ocellus absent); 9) toe webbing formula: I1–1II1–1.5III1–1IV1–1V (vs. toe webbing formula: I1–1II1–1III1–1IV1–1V).

Rhacophorus medogensis sp. nov. differs from its sister species *R. rhodopus* by 1) usually two large black spots in the axillary and inguinal regions (vs. one small black spot in the axillary region); 2) snout pointed with appendage on tip (vs. snout pointed without appendage on tip); 3) throat rough (vs. throat smooth); 4) tongue pyriform (vs. tongue narrow and long); 5) pineal ocellus obvious (vs. pineal ocellus absent).

Discussion

In this study, we reconstructed the phylogenetic relationships within the *Rhacophorus rhodopus* and *R. bipunctatus* complexes by including sequences from near the type locality of *R. bipunctatus* (Mawblang, Cherapunji, Southern Khasi Hills, northern India). Our results support previous studies indicating that *R. bipunctatus* and *R. rhodopus* are not monophyletic and likely represent multiple cryptic lineages (Chan et al. 2018; Che et al. 2020; Tang et al. 2024). The inclusion of samples from near the type locality allowed us to

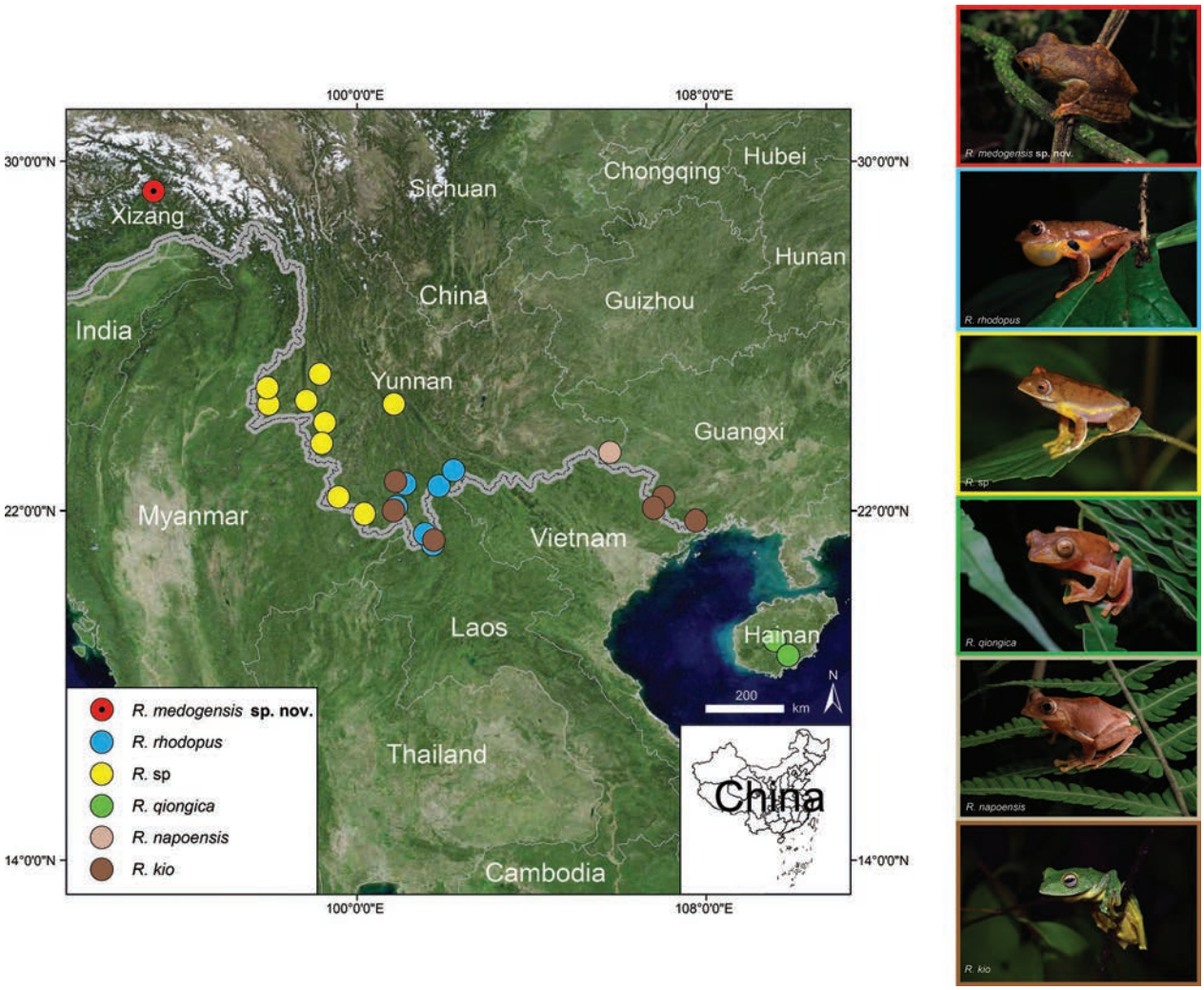

Figure 5. Map showing the distribution pattern of *R. rhodopus* complex species in China. Distribution sites accessed from Tang et al. (2024) and our data, *R. medogensis* sp. nov., *R. rhodopus* and *R.* sp photoed by Xiaolong Liu, *R. qiongica* photoed by Chenxi Liao, *R. napoensis* and *R. kio* photoed by Junkai Huang.

refine the distribution range of *R. bipunctatus*. Our phylogenetic analysis reveals that *R. bipunctatus* samples from near the type locality only cluster with those from central-western Myanmar, supporting the conclusion of Tang et al. (2024) that *R. bipunctatus* is limited to northern India and central-western Myanmar, rather than the traditionally presumed range across South and Southeast Asia (Frost 2024). In addition, our phylogenetic analysis identified a distinct cryptic species within the *R. rhodopus* complex distributed across western Yunnan, Myanmar, Thailand, and Malaysia. This lineage has historically been misidentified as *R. rhodopus* or *R. bipunctatus*. Due to a lack of available specimens, we provisionally refer to this lineage as *R.* sp. and recommend further investigation to clarify its taxonomic status.

The taxonomic ambiguity surrounding the populations in Medog, Xizang, also emerged as a key issue. Historically, researchers have referred to the Medog population as either *Rhacophorus rhodopus* or *R. bipunctatus* (Hu 1987; Fei et al. 2004, 2009, 2012; Li et al. 2011; Che et al. 2020). However, our results suggest that this population does not form a monophyletic group with either *R. rhodopus* from Yunnan or *R. bipunctatus* from India. Consequently, we describe this population as a new species, *R. medogensis*, to reflect its distinct evolutionary lineage and unique morphology.

Our findings also prompt a re-evaluation of the distribution records for species of *Rhacophorus rhodopus* and *R. bipunctatus* complexes in China. Fei et al. (2004) suggested that *R. rhodopus* was distributed in northern Medog and "true" *R. bipunctatus* in the south (Rotung area), but Che et al. (2020) suggested that only *R. bipunctatus* is distributed in Medog. Due to the lack of confirmed specimens of *R. bipunctatus* from southern Medog, we recommend that *R. bipunctatus* be excluded from distribution records in China until further specimen-based evidence is available. Currently, there are five known species of the *R. rhodopus* and *R. bipunctatus* complexes along with one undescribed species (*R. medogensis* sp. nov., *R. rhodopus*, *R. napoensis*, *R. qiongica*, *R. kio*, and *R.* sp) distributed across Xizang, Yunnan, Hainan, and Guangxi (Fig. 5).

Medog, located south of the Himalayas in Xizang, is recognized as a biodiversity hotspot (Myers et al. 2000). Recent infrastructure development, including road construction, has facilitated increased field surveys and led to the discovery of new species (Che et al. 2020; Yu et al. 2024; Shi et al. 2020). However, such development also poses potential threats to biodiversity in this region. It is therefore critical to conduct further comprehensive surveys to gain a deeper understanding of species diversity and implement conservation measures that address these emerging threats.

Acknowledgements

We thank Renda Ai and Xianqi Li for their fieldwork, Zhiyong Yuan for his assistance with the manuscript writing, and Jing Cao for her help in the molecular experiments. This work was supported by grants from the Science and Technology Major Project of Xizang (Program No. XZ2025) and the Key Research and Development Projects of Xizang (Program No. XZ202301ZY0036G).

References

AmphibiaChina (2024) The database of Chinese amphibians. Kunming Institute of Zoology (CAS), Kunming, Yunnan, China. http://www.amphibiachina.org/ [Accessed 17 October 2024]

AmphibiaWeb (2024) AmphibiaWeb. University of California, Berkeley, CA, USA. http://amphibiaweb.org/ [Accessed 17 October 2024]

Bordoloi S, Bortamuli T, Ohler A (2007) Systematics of the genus *Rhacophorus* (Amphibia, Anura): identity of red-webbed forms and description of a new species from Assam. Zootaxa 1653: 1–20. https://doi.org/10.11646/zootaxa.1653.1.1

Chan KO, Grismer LL (2010) Re-assessment of the Reinwardt's Gliding Frog, *Rhacophorus reinwardtii* (Schlegel 1840) (Anura, Rhacophoridae) in Southern Thailand and Peninsular Malaysia and its re-description as a new species. Zootaxa 2505(1): 40–50. https://doi.org/10.11646/zootaxa.2505.1.2

Chan KO, Grismer LL, Brown RM (2018) Comprehensive multi-locus phylogeny of Old World tree frogs (Anura, Rhacophoridae) reveals taxonomic uncertainties and potential cases of over- and underestimation of species diversity. Molecular Phylogenetics and Evolution 127: 1010–1019. https://doi.org/10.1016/j.ympev.2018.07.005

Che J, Jiang K, Yan F, Zhang YP (2020) Amphibians and Reptiles in Tibet-Diversity and Evolution. Science Press, Beijing, 803 pp. [in Chinese]

Darriba D, Taboada GL, Doallo R, Posada D (2012) jModelTest 2: More models, new heuristics and parallel computing. Nature Methods 9(8): 772. https://doi.org/10.1038/nmeth.2109

Fei L (1999) Atlas of Amphibians of China. Henan Science and Technology Press, Zhengzhou. [In Chinese]

Fei L, Ye CY, Jiang JP, Xie F (2004) An illustrated Key to Chinese Amphibians. Sichuan Science and Technology Publishing House, Chengdu. [In Chinese]

Fei L, Hu SQ, Ye CY, Huang YZ (2009) Fauna Sinica. Amphibia Vol. 2 Anura. Science Press, Beijing, 957 pp. [In Chinese]

Fei L, Ye CY, Jiang JP (2012) Colored Atlas of Chinese Amphibians and Their Distributions. Sichuan Science and Technology Publishing House, Chengdu. [In Chinese]

Frost DR (2024) Amphibian Species of the World: and Online Reference. Version 6.1. American Museum of Natural History, New York, USA. https://amphibiansoftheworld.amnh.org/ [Accessed 17 October 2024]

Frost DR, Grant T, Faivovich J, Bain RH, Haas A, Haddad CFB, De Sa RA, Channing A, Wilkinson M, Donnellan SC, Raxworthy CJ, Campbell JA, Blotto BL, Moler P, Drewes RC, Nussbaum RA, Lynch JD, Green DM, Wheeler WC (2006) The amphibian tree of life. Bulletin of the American Museum of Natural History 297: 1–370. https://doi.org/10.1206/0003-0090(2006)297[0001:TATOL]2.0.CO;2

Hedges SB (1994) Molecular evidence for the origin of birds. Proceedings of the National Academy of Sciences of the United States of America 91(7): 2621–2624. https://doi.org/10.1073/pnas.91.7.2621

Hu SQ (1987) Amphibians and Reptiles in Tibet. Science Press, Beijing. [in Chinese]

Inger RF, Orlov NL, Darevsky IS (1999) Frogs of Vietnam: A report on new collections. Fieldiana Zoology 92: 1–46. https://doi.org/10.5962/bhl.title.3478

Jiang DC, Jiang K, Ren JL, Wu J, Li JT (2019) Resurrection of the genus *Leptomantis*, with description of a new genus to the family Rhacophoridae (Amphibia: Anura). Asian Herpetological Research 10(1): 1–12. https://doi.org/10.16373/j.cnki.ahr.180058

Kocher TD, Thomas WK, Meyer A, Edwards SV, Pääbo S, Villablanca FX, Wilson AC (1989) Dynamics of mitochondrial DNA evolution in animals: Amplification and sequencing with conserved primers. Proceedings of the National Academy of Sciences of the United States of America 86(16): 6196–6200. https://doi.org/10.1073/pnas.86.16.6196

Kumar S, Stecher G, Tamura K (2016) MEGA7: Molecular Evolutionary Genetics Analysis Version 7.0 for Bigger Datasets. Molecular Biology and Evolution 33(7): 1870–1874. https://doi.org/10.1093/molbev/msw054

Leary S, Underwood W, Anthony R, Cartner S, Grandin T, Greenacre C, Gwaltney-Brant S, McCrackin M A, Meyer R, Miller D, Shearer J, Turner T, Yanong R, Johnson C L, Patterson-Kane E (2020) AVMA Guidelines for the euthanasia of animals: 2020. American Veterinary Medical Association, Schaumburg.

Li JT, Chen YY, Li SQ, Lv K, Wang YZ (2011) Catalogue of the type specimens of amphibians and reptiles in the herpetological museum of Chengdu Institute of Biology, Chinese Academy of Sciences: I. Rhacophoridae (Anura, Amphibia). Asian Herpetological Research Serial 2, 2: 129–141. https://doi.org/10.3724/SP.J.1245.2011.00129

Li J, Liu S, Yu GH, Sun T (2022) A new species of *Rhacophorus* (Anura, Rhacophoridae) from Guangxi, China. ZooKeys 1117: 123–138. https://doi.org/10.3897/zookeys.1117.85787

Liu CC, Hu SQ (1960) Preliminary report of Amphibia from southern Yunnan. Dong Wu Xue Bao 11(4): 509–538.

Mathew R, Sen N (2010) Pictorial Guide to Amphibians of North East India. Zoological Survey of India, Kolkata.

Matsui M, Shimada T, Sudin A (2013) A New Gliding Frog of the Genus *Rhacophorus* from Borneo. Current Herpetology 32(2): 112–124. https://doi.org/10.5358/hsj.32.112

Myers CW, Duellman WE (1982) A new species of *Hyla* from Cerro Colorado, and other tree frog records and geographical notes from western Panama. American Museum Noviates 2752: 1–25.

Myers N, Mittermeier RA, Mittermeier CA, da Fonseca GAB, Krnt J (2000) Biodiversity hotspots for conservation priorities. Nature 403: 853–858. https://doi.org/10.1038/35002501

Ohler A, Delorme M (2006) Well known does not mean well studied: Morphological and molecular support for existence of sibling species in the Javanese gliding frog *Rhacophorus reinwardtii* (Amphibia, Anura). Comptes Rendus Biologies 329(2): 86–97. https://doi.org/10.1016/j.crvi.2005.11.001

Ronquist F, Teslenko M, van der Mark P, Ayres DL, Darling A, Höhna S, Larget B, Liu L, Suchard MA, Huelsenbeck JP (2012) MrBayes 3.2: Efficient Bayesian Phylogenetic Inference and Model Choice Across a Large Model Space. Systematic Biology 61(3): 539–542. https://doi.org/10.1093/sysbio/sys029

Rowley JJL, Tran DTA, Hoang HD, Le DTT (2012) A new species of large flying frog (Rhacophoridae, *Rhacophorus*) from Lowland forests in Southern Vietnam. Journal of Herpetology 46(4): 480–487. https://doi.org/10.1670/11-261

Shi SC, Zhang MH, Xie F, Jiang JP, Liu WL, Ding L, Li L, Wang B (2020) Multiple data revealed two new species of the Asian horned toad *Megophrys* Kuhl & Van Hasselt, 1822 (Anura, Megophryidae) from the eastern corner of the Himalayas. ZooKeys 977: 101–161. https://doi.org/10.3897/zookeys.977.55693

Stamatakis A (2014) RAxML version 8: A tool for phylogenetic analysis and post-analysis of large phylogenies. Bioinformatics (Oxford, England) 30(9): 1312–1313. https://doi.org/10.1093/bioinformatics/btu033

Tang SJ, Xiao FR, Liu S, Wang LJ, Yu GH, Du LN (2024) Underestimated species diversity within the *Rhacophorus rhodopus* and *Rhacophorus bipunctatus* complexes (Anura, Rhacophoridae), with a description of a new species from Hainan, China. Zoosystematics and Evolution 100(2): 625–643. https://doi.org/10.3897/zse.100.118879

Yu GH, Hui H, Hou M, Wu ZJ, Rao DQ, Yang JX (2019) A new species of *Zhangixalus* (Anura, Rhacophoridae), previously confused with *Zhangixalus smaragdinus* (Blyth, 1852). Zootaxa 4711(2): 275–292. https://doi.org/10.11646/zootaxa.4711.2.3

Yu HQ, Lin YH, Wang YX, Zheng PY, Shi SC, Wang B, Jiang JP, Song ZB, Xie F (2024) A New Species of the Genus *Liurana* (Anura: Ceratobatrachidae) from Medog, China. Asian Herpetological Research 15(3): 131–139. https://doi.org/10.3724/ahr.2095-0357.2024.0008

Zoosyst. Evol. 101 (2) 2025, 449–463 | DOI 10.3897/zse.101.135560

PENSOFT

MUSEUM FÜR NATURKUNDE BERLIN

Morphological and molecular evidence for a new species of the genus *Leptobrachella* (Anura, Megophryidae) from Gaoligong Mountain Range, Yunnan, China

Yun-He Wu[1,2*], Zhong-Bin Yu[1,2*], Shen-Pin Yang[3], Zheng-Pan Duan[4], An-Ru Zuo[4], Ding-Can Zhang[4], Felista Kasyoka Kilunda[1,5], Robert W. Murphy[1,6], Jing Che[1,2]

1 *Key Laboratory of Genetic Evolution and Animal Models, and Yunnan Key Laboratory of Biodiversity and Ecological Conservation of Gaoligong Mountain, Kunming Institute of Zoology, Chinese Academy of Sciences, 650223, Kunming, Yunnan, China*
2 *Southeast Asia Biodiversity Research Institute, Chinese Academy of Sciences, 05282, Yezin, Nay Pyi Taw, Myanmar*
3 *Yunnan Gaoligongshan National Nature Reserve (Tengchong Bureau), 679100, Baoshan, Yunnan, China*
4 *Administrative Bureau of Tongbiguan Provincial Nature Reserve, 679300, Dehong, Yunnan, China*
5 *Kunming College of Life Science, University of the Chinese Academy of Sciences, 650204, Kunming, Yunnan, China*
6 *Centre for Biodiversity and Conservation Biology, Royal Ontario Museum, Toronto, Ontario M5S 2C6, Canada*

https://zoobank.org/781F9104-575C-464C-9802-A62CD195EB5B

Corresponding authors: Jing Che (chej@mail.kiz.ac.cn); Yun-He Wu (yunhe2009@163.com)

Academic editor: Umilaela Arifin ♦ **Received** 26 August 2024 ♦ **Accepted** 18 January 2025 ♦ **Published** 26 February 2025

Abstract

The Gaoligong Mountain Range in Yunnan Province, China, is characterized by its large variation in elevation and topography, together with its wide latitudinal range, resulting in extremely high levels of biodiversity. Studies show that the amphibian diversity of the Gaoligong Mountain Range is largely underestimated, especially in the south. During herpetological surveys in 2023 and 2024, three specimens of *Leptobrachella* were collected from the mountain at Tongbiguan Provincial Nature Reserve. Subsequent morphological comparisons and a phylogenetic reconstruction revealed that these specimens belonged to a previously unknown and morphologically distinct lineage of *Leptobrachella*, which we formally describe. Our discovery brings the number of species in the genus to 108, 44 of which occur in China, and seven on Gaoligong Mountain Range. This result confirms the underestimated amphibian diversity of the Gaoligong Mountain Range, especially in Tongbiguan Provincial Nature Reserve, where multiple sympatric congeneric species occur, including four species of *Leptobrachella*, five species and a putative new species of *Xenophrys*, and three species of *Polypedates*. These findings also highlight the need for future research to investigate the mechanisms of sympatric and syntopic coexistence.

Key Words

Asian Leaf Litter Toad, frog, *Leptobrachella albomarginata* sp. nov., sympatric distribution, Tongbiguan Provincial Nature Reserve

Introduction

The Asian leaf litter toad genus *Leptobrachella* Smith, 1925 (Megophryidae; Leptobrachiinae) occurs widely in the mountain forests of southern China, mainland Indochina, peninsular Malaysia, and the island of Borneo (Frost 2024). The genus is characterized by having a relatively small body size, vomerine teeth absent, the presence of an inner metacarpal tubercle, rounded fingertips, and macro-glands on the supra-axillary and femoral glands

* These authors contributed equally to this work.

(Dubois 1980; Ohler et al. 2011; Rowley et al. 2013). Given their small body size, conserved morphology and high degree of sympatry, the species diversity of *Leptobrachella* is likely underestimated (e.g. Chen et al. 2018, 2020; Wu et al. 2022). More than half of the recognized species were described in the past decade by utilizing morphological, molecular, and bioacoustic data (e.g. Lin et al. 2022; Luo et al. 2022; Liu et al. 2023; Luong et al. 2023; Matsui et al. 2023; Shi et al. 2023; Chen et al. 2024; Frost 2024; Li et al. 2024). Currently, the genus contains 107 recognized species, of which 43 have been recorded from China, and 23 were described in the past five years, mostly from southwestern China (AmphibiaChina 2024; Frost 2024).

Gaoligong Mountain Range is a sub-range located in the western part of China's Yunnan Province adjoining northern Myanmar, spanning approximately 600 km. It is drained by the Salween River on the east and the Irrawaddy River on the west, and characterized by its rugged terrain of deep valleys and high mountains, with elevations ranging from 210 m to 5128 m a.s.l. The unique geographic location and extreme topographic relief, together with its wide altitudinal and latitudinal range, have produced extreme differences in climate. The diverse climate and topography of the mountain has resulted in extremely high levels of biodiversity, forming a crossroad of three global biodiversity hotspots (i.e., Indo-Burma, Himalaya, and mountains of Southwest China) (Myers et al. 2000; Mittermeier et al. 2011). The range is one of the biologically richest places on Earth (Mittermeier et al. 2005; Chan et al. 2019). Several cryptic and novel herpetological species have been discovered and described in recent years (e.g. Lee et al. 2024; Yu et al. 2024; Wu et al. 2023, 2024a,b), indicating that amphibian diversity in the region may still be largely underestimated.

In recent years, we carried out a series of biodiversity surveys in Yingjiang County, from 2023 to 2024 and collected three specimens of *Leptobrachella*, which differed from known species in the genus by both morphological and molecular characteristics. Herein, we describe them as a new species.

Materials and methods

Sampling

During herpetological surveys at Tongbiguan Town, Yingjiang County, Yunnan, China conducted between 2023–2024 (Fig. 1), two adult specimens (one male and one female) of *Leptobrachella* were collected and photographed. In addition, one larvae was collected. After taking photographs, the adult frogs were euthanized using benzocaine. Liver tissues were taken from the specimens and preserved in 95% ethanol at -80 °C for DNA extraction. The specimens were then fixed in 10% formalin and after 24 hours stored in 75% ethanol. The procedures for tissue sampling and specimen fixation follow the protocols detailed in Chen et al. (2021). The larvae was directly stored as a whole in 75% alcohol for molecular experiments. All the newly collected specimens were deposited in the herpetological collection of the Museum of the Kunming Institute of Zoology (KIZ), Chinese Academy of Sciences (CAS). Research protocols were approved by the Ethics Committee of the Kunming Institute of Zoology, Chinese Academy of Science (IACUC no.: IACUC-OE-2021-07-001).

Morphological characters

Morphological characters were obtained for both adult specimens. All measurements were recorded with digital calipers to the nearest 0.1 mm. Morphological terminology and methods adhered to the guidelines of Fei et al. (2009). Measurements included the following: snout–vent length (SVL): measured from tip of snout to vent; head length (HDL): measured from tip of snout to rear of jaw; maximum head width (HDW): measured width of head at its widest point; snout length (SNT): measured from tip of snout to anterior corner of ocular aperture; eye diameter (ED): diameter of exposed portion of eyeball; width of upper eyelid (UEW): (maximum width of upper eyelid); tympanum diameter (TD): measured as maximal diameter of tympanum; distance from nostril to eye (DNE): distance from the front of the eye to the center of the nostril; distance from the center of the nostril to the tip of the snout (SN); internarial distance (IND): distance between nares; distance from anterior edge of tympanum to posterior corner of eye (TEY); interorbital distance (IOD): measured at narrowest point between eyes on top of the head; forearm length (FAL): measured from the elbow to the wrist; diameter of lower arm (LAD); forearm and hand length (FHL): distance from elbow to the tip of the third finger; hand length (HL): distance from the posterior end of the inner metacarpal tubercle to tip of third finger; hindlimb length (HLL); foot length (FL): distance from the proximal end of inner metatarsal tubercle to the tip of fourth toe; thigh length (THL): from the cloaca to the knee; tarsus length (TAL): measured as the distance from knee to heel; first to fourth finger length (FLI-IV): from the tip of the finger to its base where it joins the adjacent finger; IMTL (inner metatarsal tubercle length); PEC (maximum diameter of pectoral gland); FEM (maximum diameter of femoral gland); and SUP (maximum diameter of supra-axillary gland). Adult males and females were distinguished by the presence of vocal sacs (males), or eggs or enlarged oviducts (females).

DNA extraction, PCR and sequencing

Genomic DNA was extracted from the collected tissue samples using standard phenol-chloroform protocols (Sambrook et al. 1989). We amplified and sequenced a partial fragment of the mitochondrial ribosomal RNA gene (16S rRNA) using the primers 16SAR (Forward) and 16SBR (Reverse) (Kocher et al. 1989). The PCR amplification process was carried out in a 20-μl reaction volume. Polymerase Chain Reaction (PCR) condition followed was

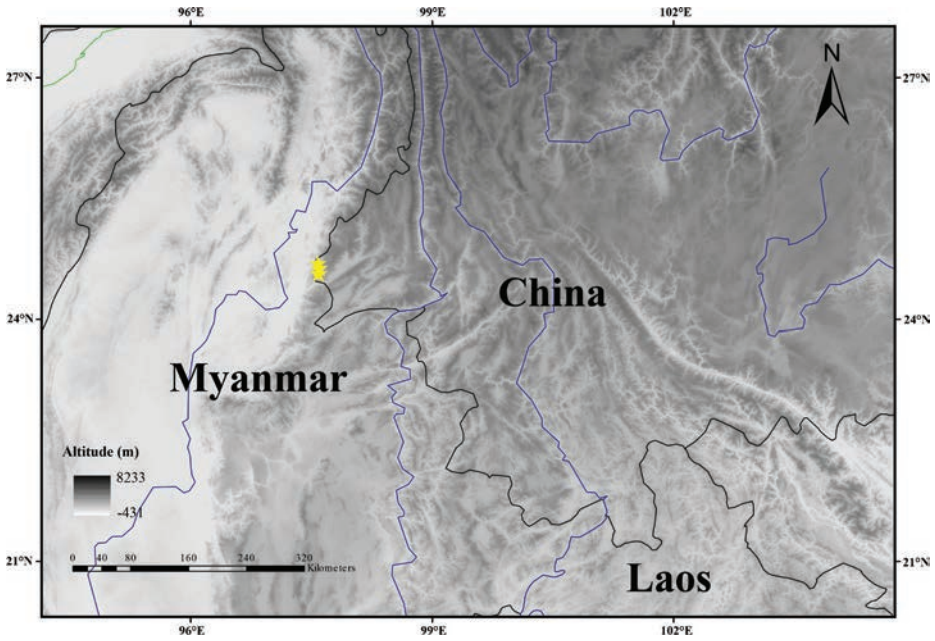

Figure 1. Collection localities (yellow stars) of *Leptobrachella albomarginata* sp. nov. specimens from Tongbiguan Provincial Nature Reserve, Yunnan, China used in this study.

initial denaturation at 95 °C for 4 minutes, followed by 35 cycles of denaturation at 94 °C for 45 seconds, annealing at 55 °C for 45 seconds and extension at 72 °C for 1 minute, and a final extending step of 72 °C for 10 minutes. Sequencing was conducted using an ABI 3730xl DNA automated sequencer (Applied Biosystems, UK). All sequences were assembled from forward and reverse reads and edited manually using AutoSeqMan (Sun 2018). New sequences were deposited in the GenBank (Suppl. material 1).

To construct a phylogeny for *Leptobrachella*, trees were inferred using Maximum Likelihood (ML) and Bayesian Inference (BI) based on 16S rRNA. Since the new species belong to Clade A of Chen et al. (2018), we included all species from Clade A along with all species described after the publication of Chen et al. (2018). The homologous sequences of related species in the genus *Leptobrachella*, and those of the outgroups *Leptobrachium huashen* and *Megophrys montana*, were downloaded from GenBank (Suppl. material 1). Sequences were aligned using the default parameters implemented in MEGA v6.0.6 (Tamura et al. 2013). Alignments were visually checked by eye for accuracy and trimmed to minimize missing characters in MEGA v.6.0.6 (Tamura et al. 2013). Uncorrected pairwise distances (*p*) of 16S rRNA were calculated using MEGA v6.0.6 with complete deletion of missing data and gaps (Tamura et al. 2013). For BI analyses, JMODELTEST v2.1.7 (Darriba et al. 2012) was used to select an appropriate nucleotide substitution model. Based on the Bayesian Information Criterion (BIC; Posada 2008), the GTR+I+G model was chosen as the optimal nucleotide substitution model. BI analysis was implemented by the CIPRES web server (Miller et al. 2010), with Markov Chain Monte Carlo (MCMC) for 10,000,000 generations. Trees were sampled every 1000 generations and the initial 25% of trees were discarded as burn-in. Convergence was assessed by the average standard deviation of split frequencies (less than 0.01) and the ESS values (greater than or equal to 200) in Tracer v.1.5 (Rambaut and Drummond 2009). ML analysis was performed using RAxML-HPC BlackBox v.8.2.10 with the GTRGAMMA model of molecular evolution, implemented by the CIPRES web server (Miller et al. 2010).

Results

The aligned sequence matrix of the 16S rRNA gene contained 91 individuals with 516 base pairs (bps) (including outgroups). Amongst the 516 sites, 253 were established as conserved sites and 257 were considered variable sites, of which 211 were found to be potentially parsimony-informative sites (including outgroups).

ML and BI analyses yielded near-identical topologies, with relatively high nodal support values for most terminal nodes. The monophyly of *Leptobrachella* was strongly supported (BPP = 1, BS = 97), forming three major clades (clades A–C, Fig. 2). Our new samples from Tongbiguan Provincial Nature Reserve nested in Clade A, which strongly clustered into a lineage (BI = 1, ML = 100; Fig. 2) and clustered with *L. tamdil*, *L. khasiorum*, and *L. yingjiangensis* with good support (BI = 1, ML = 78; Fig. 2).

The new population showed obvious genetic divergence from its congeners. The minimum uncorrected genetic distance was 9.1% between our species and *L. tamdil*, *L. khasiorum*, and *L. graminicola* (Suppl. material 2). These levels of pairwise divergence of the 16S rRNA gene far exceeded the threshold of 3.0% previously proposed by Vences et al. (2005) as a reliable indicator for identifying candidate new species in frogs.

Moreover, morphologically these specimens were distinguished from all other species of *Leptobrachella* by a series of taxonomically important diagnostic characters. Thus, we describe these specimens as a new species of *Leptobrachella*.

Figure 2. Phylogram of *Leptobrachella* derived from analyses of 16S rRNA mitochondrial gene. Nodal support values with Bayesian posterior probability (BPP) > 0.95 / ML inferences (ML-BS) > 70 are shown near the respective nodes. A "-" denotes a Bayesian posterior probability < 0.95 and bootstrap support < 70. Nodes without any numbers or symbols represent low support values (BS < 75% and BPP < 0.95). New samples for the present study are indicated in red bold font.

Taxonomic account

Leptobrachella albomarginata Wu, Yu, Kilunda, Murphy & Che, sp. nov.

https://zoobank.org/630BA976-31C1-4D96-AD45-4F6DAF801B07

Figs 3–5, Table 1

Type material. ***Holotype***: • KIZ 050905, an adult female from Tongbiguan Provincial Nature Reserve, Yingjiang County, Yunnan, China (24.56355°N, 97.58719°E, 1,634 m a.s.l.), collected on 20 April 2023 by Zhong-Bin Yu, Dong An, Yu-Xuan Wu, and Xian-Kun Huang.

Paratype: • KIZ 056551, an adult male from Tongbiguan Provincial Nature Reserve, Yingjiang County, Yunnan, China (24.63669°N, 97.59515°E, 1,318 m a.s.l.), collected on 30 April 2024 by Zhong-Bin Yu, Peng Yang, Dong An, and Xian-Rong Wu.

Etymology. The name refers to reverse-triangle markings and ∧-shaped marking with a white lining on dorsum of the new species: the specific epithet "*albus*" is a Latin

adjective which means "white", and "*marginis*" is Latin adjective for "border, lining". We propose the English common name "White-lined Leaf Litter Toad" and the Chinese common name "Bái Yuán Zhǎng Tū Chán (白缘掌突蟾)".

Diagnosis. *Leptobrachella albomarginata* sp. nov. can be distinguished from its congeners by the following combination of morphological characters: (1) body size small (SVL 26.5 mm in one adult male, 32.5 mm in one female); (2) tibiotarsal articulation reaches the middle eye; (3) tongue with a shallow notch at the posterior tip; (4) heels meeting; (5) toes with rudimentary webbing and narrow lateral fringes; (6) relative finger lengths: I ≈ II < IV < III; (7) reverse-triangle markings and a ∧-shaped marking with a white lining in dorsal view; (8) black and bluish-white marbling all over ventral surfaces of throat, chest and belly; (9) flanks with distinct irregular black spots; (10) iris bicolored, upper 1/3 of the iris being coppery, lower 2/3 silvery gray.

Description of the holotype (measurements in Table 1). KIZ 050905, adult female, body size small (SVL 32.5 mm), head longer (HDL 12.7 mm) than wide (HDW 11.8 mm); head triangular in dorsal view; snout short (SNT/HDL 37.0%), snout bluntly rounded in profile and obtusely pointed in dorsal view, projecting slightly beyond margin of the lower jaw; oval-shaped nostril dorsolaterally positioned, situated slightly below canthus, closer to tip of snout (SN 1.8 mm) than to anterior margin of eye (DNE 2.8 mm); loreal region oblique and slightly concave; canthus rostralis distinct; eyes large (ED/HDL 18.9%), eye diameter smaller than snout length (ED/SNT 51.1%); pupil vertical; eye diameter (ED 2.4 mm) less than snout length (SNT 4.7 mm); tympanum distinct, round; tympanic rim distinctly elevated relative to skin of temporal region; upper margin of tympanum in contact with supratympanic ridge; interorbital space (IOD 2.8 mm) flat, less than internarial distance (IND 3.5 mm) and width of upper eyelid (UEW 3.6 mm); vomerine teeth absent; tongue with shallow notch at posterior tip; supratympanic ridge distinct, extending from posterior corner of eye to supra-axillary gland (Fig. 3).

Forelimbs thin, slender; forearm shorter than hand, not enlarged (FAL 6.5 mm, HL 7.9 mm); fingertips round, slightly swollen, almost equal to phalange width; relative finger lengths: I ≈ II < IV < III; subarticular tubercles absent on fingers; supernumerary tubercles absent; finger webbing absent; lateral fringes absent; a large, round inner metacarpal tubercle, distinctly separated from small, laterally compressed outer metacarpal tubercle (Figs 3, 4).

Hindlimbs long, tibia slightly shorter than half of the snout-vent length (TAL/SVL ratio 44.9%); tibiotarsal articulation reaches the middle eye when hindlimb is stretched along the side of the body; heels meeting when hind limbs are flexed and held perpendicular to body; tips of toes rounded, slightly swollen; relative length of toes: IV > III > V > II > I; subarticular tubercles indistinct under the base of II and III toe; narrow lateral fringes present on all toes; rudimentary webbing between toes; inner metatarsal tubercle distinct and prolonged (IMTL 0.9 mm, 2.8% SVL), outer metatarsal tubercle absent (Figs 3, 4).

Table 1. Measurements (in mm) of type series of *Leptobrachella*. Bold font and an asterisk (*) indicate the holotype.

	KIZ 050905*	**KIZ 056551**
Sex	♀	♂
SVL	32.5	26.5
HDL	12.7	10.1
HDW	11.8	9.1
SNT	4.7	4.1
SNT/HDL	37.0%	40.6%
ED	4.2	3.6
IOD	2.8	3.2
UEW	3.6	2.6
IND	3.5	3.0
DNE	2.8	2.2
SN	1.8	1.5
ED	2.4	1.6
ED/HDL	18.9%	15.8%
ED/SNT	51.1%	39.0%
TEY	1.3	1.1
FHL	16.5	13.5
HL	7.9	7.1
LAD	2.1	1.7
FAL	6.5	6.8
HLL	47.3	40.2
THL	12.7	11.8
TAL	14.6	12.1
TAL/SVL	44.9%	45.7%
FL	13.1	10.8
IMTL	0.9	1.2
PEC	0.8	0.9
FEM	0.8	1.0
SUP	0.6	1.3

Skin on dorsum shagreened, lacking enlarged tubercles or warts; the back and surfaces of limbs scattered with fine tubercles and short longitudinal folds; upper arms and upper eyelid covered by small tubercles; tiny reddish warts on flanks; ventral skin smooth; pectoral gland laterally compressed, indistinct, not easy to find, about 0.8 mm in diameter; femoral glands small, oval, about 0.8 mm in diameter, located on posteroventral surfaces of thighs, closer to knee than to vent; supra-axillary gland raised, about 0.6 mm in diameter; ventrolateral glands present, dorsolaterally compressed forming an incomplete line (Fig. 3).

***Color of the holotype in life*.** Dorsum brown backgrounding, with small, distinct darker brown markings and spots; large reverse-triangle dark brown markings with white lining between anterior corner of eyes, connected to the ∧-shaped marking with white lining between axillae; a dark ∧-shaped stripe with white lining on rear part of dorsal surface; upper lip with dark brown vertical bars; supratympanic ridge reddish and large black marking under supratympanic ridge from posterior corner of eye to supra-axillary glands; most of tympanum black; transverse dark brown bars on dorsal surface of fingers and toes, lower arms, tarsus, thighs and tibia; supra-axillary gland coppery orange; three distinct dark blotches and several small black spots on flanks from groin to axilla;

Figure 3. Holotype of *Leptobrachella albomarginata* sp. nov. (KIZ 050905) in life. **A.** Lateral view; **B.** Lateral view of head; **C.** Dorsal view; **D.** Ventral view. Photos by Zhong-Bin Yu.

ventral surface of throat, chest, and belly creamy white; black and bluish-white marbling all over ventral surfaces of throat, chest and belly; ventral surfaces of limbs black, covered with bluish-white marbling; ventrolateral glands, pectoral glands and femoral glands white; iris bicolored, upper 1/3 of the iris being coppery, lower 2/3 silvery gray, with black reticulations throughout (Fig. 3).

***Color of holotype in preservative*.** After one year of storage in 75% alcohol, dorsum of the body and limbs fade to dark brown; transverse bars on limbs still distinct; three distinct dark blotches and several small black spots on flanks still clear; dark-brown, inverse reverse-triangle marking, connected to the ∧-shaped marking and a dark ∧-shaped stripe with a white lining on the rear part of the dorsal surface distinctly visible; elbow to upper arm distinctly creamy white in color on the dorsum; ventral surfaces of throat, chest and belly dull white with well-discernable marbling; inner metatarsal tubercle, inner metatarsal tubercle, supra-axillary, femoral and pectoral glands fading to gray (Fig. 4).

Description of the paratype (measurements in Table 1). KIZ 056551, adult male, body size small (SVL 26.5 mm), head longer (HDL 10.1 mm) than wide (HDW 9.1 mm); head triangular in dorsal view; snout short (SNT/HDL 40.6%), snout bluntly rounded in profile and obtusely pointed in dorsal view, projecting slightly beyond margin of the lower jaw; oval-shaped nostril dorsolaterally positioned, situated slightly below canthus, closer to tip of snout (SN 1.5 mm) than to anterior margin of eye (DNE 2.2 mm); loreal region oblique and slightly concave; canthus rostralis indistinct; eyes large (ED/HDL 15.8%), eye diameter slightly smaller than snout length (ED/SNT 39.0%); pupil vertical; eye diameter (ED 1.6 mm) less than snout length (SNT 4.1 mm); tympanum distinct, round; tympanic rim distinctly elevated relative to skin of temporal region; upper margin of tympanum in contact with supratympanic ridge; interorbital space (IOD 3.2 mm) flat, slightly larger than internarial distance (IND 3.0 mm) and width of upper eyelid (UEW 2.6 mm); vomerine teeth absent; tongue with shallow notch at posterior tip; supratympanic ridge distinct, extending from posterior corner of eye to supra-axillary gland; male with internal subgular vocal sacs, vocal sac openings slit-like, small, paired, located posteriolaterally on mouth floor (Fig. 5).

Forelimbs thin, slender; forearm shorter than hand, not enlarged (FAL 6.8 mm, HL 7.1 mm); fingertips round, slightly swollen, almost equal to phalange width; nuptial pad absent; relative finger lengths: I ≈ II < IV < III; subarticular tubercles absent on fingers; supernumerary tubercles absent; finger webbing absent; lateral fringes absent; a large, round inner metacarpal tubercle, distinctly separated from small, laterally compressed outer metacarpal tubercle (Fig. 5).

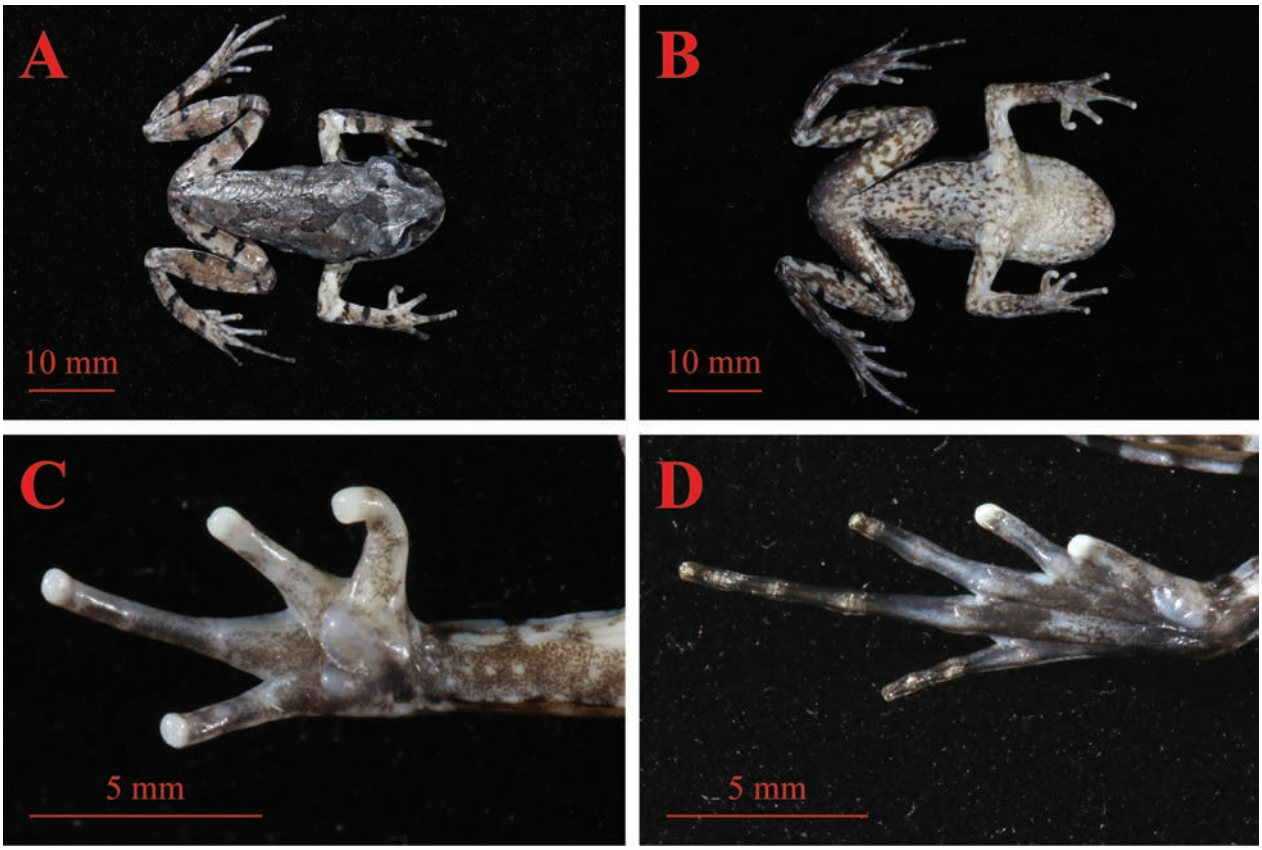

Figure 4. Holotype of *Leptobrachella albomarginata* sp. nov. (KIZ 050905) in preservative. **A.** Dorsal view; **B.** Ventral view; **C.** Ventral view of hand; **D.** Ventral view of toe. Photos by Zhong-Bin Yu.

Hindlimbs long, tibia slightly shorter than half of the snout-vent length (TAL/SVL ratio 45.7%); tibiotarsal articulation reaches the middle eye when hindlimb is stretched along the side of the body; heels meeting when hind limbs are flexed and held perpendicular to body; tips of toes rounded, slightly swollen; relative length of toes: IV > III > V > II > I; subarticular tubercles absent; narrow lateral fringes present on all toes; rudimentary webbing between toes; inner metatarsal tubercle distinct and prolonged (IMTL 1.2 mm, 4.5% SVL), outer metatarsal tubercle absent (Fig. 5).

Skin on dorsum shagreened; the back and surfaces of limbs scattered with fine tubercles and short longitudinal folds; upper arms and upper eyelid covered by small tubercles; tiny reddish warts on flanks; ventral skin smooth; pectoral gland laterally compressed, indistinct, not easy to find, about 0.9 mm in diameter; femoral glands small, oval, about 1.0 mm in diameter, located on posteroventral surfaces of thighs, closer to knee than to vent; supra-axillary gland raised, about 1.3 mm in diameter; ventrolateral glands present, dorsolaterally compressed forming an incomplete line (Fig. 5).

Color of the paratype in life. Dorsum brown backgrounding; large reverse-triangle dark brown markings with a white lining between anterior corner of eyes, connected to the ∧-shaped marking with a white lining between axillae; a dark 人-shaped stripe with a white lining on the rear part of dorsal surface; upper lip with dark brown vertical bars; supratympanic ridge reddish and large black marking under supratympanic ridge from posterior corner of eye to supra-axillary glands; most of tympanum black; transverse dark brown bars on dorsal surface of fingers and toes, lower arms, tarsus, thighs and tibia; supra-axillary gland coppery orange; one distinct dark blotch and several small black spots on flanks from groin to axilla (Fig. 5A).

Color of paratype in preservative. After six months of storage in 75% alcohol, dorsum of the body and limbs fade to dark brown; transverse bars on limbs still distinct; one distinct dark blotch and several small black spots on flanks still clear; dark-brown, inverse reverse-triangle marking, connected to the ∧-shaped marking and a dark 人-shaped stripe with white lining on the rear part of dorsal surface distinctly visible; elbow to upper arm distinctly creamy white on the dorsum; ventral surfaces of throat, chest and belly dull white with well-discernable marbling; inner metatarsal tubercle, supra-axillary, femoral and pectoral glands fading to gray (Fig. 5B–F).

Morphological variation. The paratype matches the overall characters of the holotype (see Table 1). The female specimen is relatively larger than the male (SVL 32.5 mm in a single adult female and 26.5 mm in a single adult male). Male with internal subgular vocal sacs, vocal sac

Figure 5. Paratype of *Leptobrachella albomarginata* sp. nov. (KIZ 056551). **A.** Laterodorsal view in life; **B.** Dorsal view in preservative; **C.** Ventral view in preservative; **D.** Ventral view of head in preservative; **E.** Ventral view of hand in preservative; **F.** Ventral view of toe in preservative. Photos by Zhong-Bin Yu.

openings slit-like, small, paired, located posteriolaterally on mouth floor. The size of the dark blotches on flanks is variable: KIZ 050905 has three distinct dark blotches and several small black spots on flanks; KIZ 056551 has a relatively small blotch and several small black spots on flanks.

Description of the larvae. KIZ 051631, an early metamorph at stages 44–46 was collected on 28 April 2023 (Gosner 1960). A young froglet with a relatively elongate body, bluntly rounded snout, and slender limbs with thin, delicate digits. After one year of storage in 75% alcohol, the ground dorsal coloration of the body and limbs now dark brown; dorsal parts of limbs with transverse dark brown bars; ventral surfaces of throat, chest and limbs creamy white (Suppl. material 3).

Distribution and ecology. *Leptobrachella albomarginata* sp. nov. is only known from Tongbiguan Provincial Nature Reserve, Tongbiguan Town, Yingjiang County, Yunnan, China. The new species inhabits montane streams surrounded by shrubland at elevations of approximately 1300–1600 m (Fig. 6). The breeding season of this species is likely in April as the female collected during this month was gravid. This species occurs sympatrically, if not syntopically with congeners *L. purpurus*, *L. yingjiangensis*, and *L. ventripunctata*. In addition, other frog species also found at the site include *Nanorana aenea*, *Limnonectes longchuanensis*, and *Jingophrys feii*.

Comparisons. Phylogenetically, the matrilineal genealogy assigns *Leptobrachella albomarginata*

Figure 6. Habitat at the type locality of *Leptobrachella albomarginata* sp. nov. at Tongbiguan Provincial Nature Reserve, Yingjiang County, Yunnan, China. (Photo by Zhong-Bin Yu).

sp. nov. to clade A. Thus, we compared *Leptobrachella albomarginata* sp. nov. to all other recognized species of clade A (Fei et al. 1990; Lathrop et al. 1998; Ohler et al. 2000, 2011; Das et al. 2010; Sengupta et al. 2010; Rowley et al. 2010, 2012, 2015, 2017; Jiang et al. 2013; Sung et al. 2014; Yang et al. 2016, 2018; Yuan et al. 2017; Hou et al. 2018; Wang et al. 2018, 2019, 2020, 2022; Chung et al. 2019; Chen et al. 2019, 2020, 2021a,b,c, 2023, 2024; Luo et al. 2020; Lyu et al. 2020; Qian et al. 2020; Li et al. 2020, 2024; Cheng et al. 2021; Nguyen et al. 2021; Wu et al. 2021; Shi et al. 2021, 2023; Lin et al. 2022; Luo et al. 2022; Luong et al. 2023; Liu et al. 2023; Matsui et al. 2023; Suppl. material 2).

Leptobrachella albomarginata sp. nov. differs from *L. bijie* by relative finger lengths: I ≈ II < IV < III (vs. relative finger lengths: I = II = IV < III), reverse-triangle markings and ∧-shaped marking with white lining (vs. lack of white lining); from *L. jinyunensis* by iris bicolored, upper 1/3 of the iris being coppery, lower 2/3 silvery gray (vs. iris gold above, gradually silver bellow), reverse-triangle markings and ∧-shaped marking with white lining (vs. lack of white lining); from *L. chishuiensis* by relative finger lengths: I ≈ II < IV < III (vs. relative finger lengths: II < IV < I < III), tibiotarsal articulation reaches the middle eye (vs. reaches the tympanum), reverse-triangle markings and ∧-shaped marking with white lining (vs. lack of white lining); from *L. jinshaensis* by reverse-triangle markings and ∧-shaped marking with white lining (vs. lack of white lining), black and bluish-white marbling all over ventral surfaces of throat, chest and belly (vs. absent); from *L. suiyangensis* by reverse-triangle markings and ∧-shaped marking with white lining (vs. lack of white lining), black and bluish-white marbling all over ventral surfaces of throat, chest and belly (vs. ventral part with distinct or indistinct light brown speckling); from *L. purpuraventra* by ventral surface of throat, chest, and belly creamy white (vs. ventral surface gray purple), relative finger lengths: I ≈ II < IV < III (vs. relative finger lengths: I = II = IV < III), reverse-triangle markings and ∧-shaped marking with white lining (vs. lack of white lining); from *L. bourreti* by a smaller body size, SVL 32.5 mm in one female (vs. 42.0–45.0 mm in adult females), nostrils closer to tip of snout than to anterior margin of eye (vs. nostrils closer to eye than to tip of snout); from *L. dong* by reverse-triangle markings and ∧-shaped marking with white lining (vs. lack of white lining), eye diameter smaller than snout length (vs. eye diameter longer than snout length); from *L. dushanensis* by tibiotarsal articulation reaches the middle eye (vs. reaches the interior corner of the eye), reverse-triangle markings and ∧-shaped marking with white lining (vs. lack of white lining); from *L. graminicola* by tibiotarsal articulation reaches the middle eye (vs. reaches the anterior edge of eye), narrow lateral fringes present on all toes (vs. wide lateral fringes), reverse-triangle markings and ∧-shaped marking with white lining (vs. lack of white lining); from *L. wulingensis* by iris bicolored, upper 1/3 of the iris being coppery, lower 2/3 silvery gray (vs. iris bicolored with bright orange or golden upper half, fades to silver in lower half), reverse-triangle markings and ∧-shaped marking with white lining (vs. lack of white lining); from *L. dorsospina* by a larger body size, SVL 32.5 mm in one female (vs. 25.0–26.4 mm in three adult females), relative finger lengths: I ≈ II < IV < III (vs. relative finger lengths: I < IV < II < III), reverse-triangle markings and ∧-shaped marking with white lining (vs. lack of white lining); from *L. niveimontis* by a larger body size, SVL 32.5 mm in one female (vs. 28.5–28.7 mm in three adult females), reverse-triangle markings and ∧-shaped marking with white lining (vs. lack of white lining), tibiotarsal articulation reaches the middle eye (vs. reaches beyond eye); from *L. yeae* by reverse-triangle markings and ∧-shaped marking with white lining (vs. lack of white lining), heels just meeting (vs. heels partially overlapped); from *L. yunyangensis* by relative finger lengths: I ≈ II < IV < III (vs. relative finger lengths: I < II = IV < III), heels just meeting (vs. heels overlapped), tibiotarsal articulation reaches the middle eye (vs. reaches beyond the anterior corner of the eye); from *L. alpina* by tibiotarsal articulation reaches the middle eye (vs. reaches anterior corner of the eye), reverse-triangle markings and ∧-shaped marking with white lining (vs. lack of white lining), ventrolateral glands forming a discontinuous line (vs. continuous); from *L. purpurus* by iris bicolored, upper 1/3 of the iris being coppery, lower 2/3 silvery gray (vs. upper half orange yellow, lower half sliver white), relative finger lengths: I ≈ II < IV < III (vs. relative finger lengths: I = II = IV < III), reverse-triangle markings and ∧-shaped marking with white lining (vs. lack of white lining), narrow lateral fringes present on all toes (vs. wide lateral fringes); from *L. eos* by a smaller body size, SVL 32.5 mm in one female (vs. 40.7 mm in one adult female), nostril closer to tip of snout than to anterior margin of eye (vs. nostril closer to eye than to tip of snout), narrow lateral fringes present on all toes (vs. wide lateral fringes); from *L. oshanensis* by toes with

rudimentary webbing and narrow lateral fringes (vs. absent), relative finger lengths: I ≈ II < IV < III (vs. relative finger lengths: I < II = IV < III); from *L. korifi* by tibiotarsal articulation reaches the middle eye (vs. reaches beyond the anterior corner of the eye), heels just meeting (vs. heels overlapped), subarticular tubercles indistinct under the base of II and III toe (vs. subarticular tubercles at base of each toe); from *L. sinorensis* by heels just meeting (vs. heels overlapped), reverse-triangle markings and ∧-shaped marking with white lining (vs. lack of white lining), tibiotarsal articulation reaches the middle eye (vs. reaches beyond the anterior corner of the eye); from *L. murphyi* by iris bicolored, upper 1/3 of the iris being coppery, lower 2/3 silvery gray (vs. upper half orange, lower half sliver white), tibiotarsal articulation reaches the middle eye (vs. reaches beyond eye), black and bluish-white marbling all over ventral surfaces of throat, chest and belly (vs. ventral surface of belly creamy white with small spots on the margin); from *L. tengchongensis* by iris bicolored, upper 1/3 of the iris being coppery, lower 2/3 silvery gray (vs. iris not bicolored, uniformly dark brown and scattered with minute, coppery reticulations throughout), a larger body size, SVL 32.5 mm in one female (vs. 28.8–28.9 mm in two adult females), reverse-triangle markings and ∧-shaped marking with white lining (vs. lack of white lining); from *L. tamdil* by relative finger lengths: I ≈ II < IV < III (vs. relative finger lengths: IV < I < II < III), head longer than wide (vs. head wider than long), iris bicolored, upper 1/3 of the iris being coppery, lower 2/3 silvery gray (vs. top third of iris bright orange, rest of iris grayish-cream), narrow lateral fringes present on all toes (vs. wide lateral fringes); from *L. khasiorum* by head longer than wide (vs. head wider than long), relative finger lengths: I ≈ II < IV < III (vs. relative finger lengths: IV < I < II < III), heels just meeting (vs. heels widely separated), iris bicolored, upper 1/3 of the iris being coppery, lower 2/3 silvery gray (vs. top third of iris bright orange, rest of iris yellowish-cream), narrow lateral fringes present on all toes (vs. wide lateral fringes); from *L. yingjiangensis* by dermal fringes in fingers absent (vs. narrow to moderate dermal fringes present on 2nd to 4th fingers), narrow lateral fringes present on all toes (vs. wide lateral fringes), iris bicolored, upper 1/3 of the iris being coppery, lower 2/3 silvery gray (vs. iris bicolored, upper half orange yellow, lower half sliver white), tibiotarsal articulation reaches the middle eye (vs. reaches anterior corner of the eye); from *L. namdongensis* by relative finger lengths: I ≈ II < IV < III (vs. relative finger lengths: I < II = IV < III), reverse-triangle markings and ∧-shaped marking with white lining (vs. lack of white lining); from *L. petrops* by toes with rudimentary webbing (vs. toes lacking webbing), tibiotarsal articulation reaches the middle eye (vs. reaches anterior edge of eye), reverse-triangle markings and ∧-shaped marking with white lining (vs. lack of white lining), iris bicolored, upper 1/3 of the iris being coppery, lower 2/3 silvery gray (vs. iris gold in lower half and copper in upper half); from *L. puhoatensis* by tibiotarsal articulation reaches the middle eye (vs. reaches anterior edge of eye), black and bluish-white marbling all over ventral surfaces of throat, chest and belly (vs. ventral surfaces deep reddish brown, faint white speckling on chest and belly); from *L. liui* by black and bluish-white marbling all over ventral surfaces of throat, chest and belly (vs. absent), reverse-triangle markings and ∧-shaped marking with white lining (vs. lack of white lining), narrow lateral fringes present on all toes (vs. wide lateral fringes); from *L. mangshanensis* by iris bicolored, upper 1/3 of the iris being coppery, lower 2/3 silvery gray (vs. iris bicolored, bright orange upper, grayish cream below), tibiotarsal articulation reaches the middle eye (vs. reaches anterior margin of snout); from *L. verrucosa* by heels just meeting (vs. heels not meeting), tibiotarsal articulation reaches the middle eye (vs. reaches anterior corner of eye); from *L. yunkaiensis* by black and bluish-white marbling all over ventral surfaces of throat, chest and belly (vs. surface of throat creamy white and scattered with small whitish dots, belly pinkish and scattered with small brown speckling), reverse-triangle markings and ∧-shaped marking with white lining (vs. lack of white lining), narrow lateral fringes present on all toes (vs. wide lateral fringes); from *L. shimentaina* by black and bluish-white marbling all over ventral surfaces of throat, chest and belly (vs. ventral surface grayish pink, with distinct hazy brown speckling on chest and ventrolateral flanks), reverse-triangle markings and ∧-shaped marking with white lining (vs. lack of white lining); from *L. maoershanensis* by tibiotarsal articulation reaches the middle eye (vs. reaches snout), relative finger lengths: I ≈ II < IV < III (vs. relative finger lengths: II < I < IV < III), reverse-triangle markings and ∧-shaped marking with white lining (vs. lack of white lining); from *L. bashaensis* by tibiotarsal articulation reaches the middle eye (vs. reaches snout), reverse-triangle markings and ∧-shaped marking with white lining (vs. lack of white lining); from *L. laui* by relative finger lengths: I ≈ II < IV < III (vs. relative finger lengths: I < IV < II < III), tibiotarsal articulation reaches the middle eye (vs. reaches anterior margin of eye), narrow lateral fringes present on all toes (vs. wide lateral fringes), iris bicolored, upper 1/3 of the iris being coppery, lower 2/3 silvery gray (vs. iris uniformly coppery orange), black and bluish-white marbling all over ventral surfaces of throat, chest and belly (vs. ventral surface of chest and belly opaque cream white with little brown dusting along the margins of ventrolateral glands); from *L. phiaoacensis* by black and bluish-white marbling all over ventral surfaces of throat, chest and belly (vs. throat, chest and belly pinkish white with dark brown specking), reverse-triangle markings and ∧-shaped marking with white lining (vs. lack of white lining); from *L. flaviglandulosa* by tibiotarsal articulation reaches the middle eye (vs. reaches beyond eye), reverse-triangle markings and ∧-shaped marking with white lining (vs. lack of white lining), iris bicolored, upper 1/3 of the iris being coppery, lower 2/3 silvery gray (vs. iris distinctly bicolored, typically golden-orange in upper half, fading to whitish gray in lower half); from *L. aerea* by narrow

lateral fringes present on all toes (vs. very weak lateral fringes), tibiotarsal articulation reaches the middle eye (vs. reaches to tip of snout), iris bicolored, upper 1/3 of the iris being coppery, lower 2/3 silvery gray (vs. iris bronze), reverse-triangle markings and ∧-shaped marking with white lining (vs. lack of white lining); from *L. pelodytoides* by narrow lateral fringes present on all toes (vs. very weak lateral fringes), rudimentary webbing between toes (vs. 1/3 toe webbing); from *L. minima* by narrow lateral fringes present on all toes (vs. absent), iris bicolored, upper 1/3 of the iris being coppery, lower 2/3 silvery gray (vs. iris dark golden in upper part, gray in lower part); from *L. feii* by tibiotarsal articulation reaches the middle eye (vs. reaches beyond eye), black and bluish-white marbling all over ventral surfaces of throat, chest and belly (vs. throat, chest and belly pinkish white with dark brown specking on belly periphery), reverse-triangle markings and ∧-shaped marking with white lining (vs. lack of white lining); from *L. aspera* by narrow lateral fringes present on all toes (vs. very weak lateral fringes), reverse-triangle markings and ∧-shaped marking with white lining (vs. lack of white lining); from *L. ventripunctata* by reverse-triangle markings and ∧-shaped marking with white lining (vs. lack of white lining), ventrolateral glands forming a discontinuous line (vs. continuous); from *L. guinanensis* by a smaller body size, SVL 32.5 mm in one female (vs. 38.7–41.8 mm in adult females), rudimentary webbing between toes (vs. 1/3 toe webbing), heels just meeting (vs. heels not meeting), black and bluish-white marbling all over ventral surfaces of throat, chest and belly (vs. ventral surface creamy white without dark brown spots); from *L. shiwandashanensis* by heels just meeting (vs. heels not meeting), tibiotarsal articulation reaches the middle eye in female (vs. reaches the shoulder in females), toes with narrow lateral fringes and rudimentary webbing (vs. without webbing and lateral fringes on toes); from *L. wuhuangmontis* by tongue with shallow notch at posterior tip (vs. tongue deeply notched behind), black and bluish-white marbling all over ventral surfaces of throat, chest and belly (vs. ventral surface grayish-white mixed with tiny white and black dots); from *L. wumingensis* by toes with narrow lateral fringes and rudimentary webbing (vs. absence of toe webbing and lateral fringes), tongue with shallow notch at posterior tip (vs. tongue with a deep notch at posterior tip), black and bluish-white marbling all over ventral surfaces of throat, chest and belly (vs. belly with tiny creamy white spots, throat creamy white with tiny light brown spots); from *L. phiadenensis* by head longer than wide (vs. head wider than long), black and bluish-white marbling all over ventral surfaces of throat, chest and belly (vs. throat, chest and belly white with dark specking on outer margins); from *L. shangsiensis* by narrow lateral fringes present on all toes (vs. very weak lateral fringes), head longer than wide (vs. head wider than long); from *L. nyx* by a smaller body size, SVL 32.5 mm in one female (vs. 37.0–41.0 mm in adult females), narrow lateral fringes present on all toes (vs. absent), flanks with distinct irregular black spots (vs. poorly distinct spots on flanks); from *L. damingshanensis* by narrow lateral fringes present on all toes (vs. very weak lateral fringes), relative finger lengths: I ≈ II < IV < III (vs. relative finger lengths: I < II < IV < III), black and bluish-white marbling all over ventral surfaces of throat, chest and belly (vs. absent); from *L. nahangensis* by a smaller body size, SVL 26.5 mm in one adult male (vs. 40.8 mm in one adult male), narrow lateral fringes present on all toes (vs. absent), tongue with shallow notch at posterior tip (vs. tongue deeply notched), iris bicolored, upper 1/3 of the iris being coppery, lower 2/3 silvery gray (vs. iris gold uniformly distributed with minute black, reticulations); from *L. pluvialis* by tibiotarsal articulation reaches the middle eye (vs. reaches nostril), relative finger lengths: I ≈ II < IV < III (vs. relative finger lengths: I < II = IV < III), narrow lateral fringes present on all toes (vs. absent); from *L. zhangyapingi* by a smaller body size, SVL 26.5 mm in one male (vs. 45.8–52.5 mm in seven adult males), heels just meeting (vs. heels widely separated), flanks with distinct irregular black spots (vs. absent), narrow lateral fringes present on all toes (vs. wide lateral fringes); from *L. sungi* by a smaller body size, SVL 26.5 mm in one male (vs. 48.3–52.7 mm in adult males), three distinct dark blotches and several small black spots on flanks (vs. absent or small); from *L. firthi* by three distinct dark blotches and several small black spots on flanks (vs. absent), narrow lateral fringes present on all toes in female (vs. absent in females); and from *L. isos* by three distinct dark blotches and several small black spots on flanks (vs. absent), tibiotarsal articulation reaches the middle eye (vs. reaches to nostril), narrow lateral fringes present on all toes in male (vs. wide in males).

Discussion

The amphibian diversity of Tongbiguan Provincial Nature Reserve is underestimated. In recent years, a series of new record genera, species, and new species records of amphibians have been reported from there, such as the genus *Nasutixalus* (Yang and Chan 2018), *L. yingjiangensis* (Yang et al. 2018), *Xenophrys dehongensis* (Lyu et al. 2023), *Xenophrys yingjiangensis* (Wu et al. 2024a), and *Polypedates teraiensis* (Yu et al. 2024). In addition, some studies have shown that cryptic species exist in this region (e.g. Chen et al. 2017, 2018; Wu et al. 2024a). These instances highlight that the true amphibian diversity of the reserve is substantially underestimated. Our new finding of *L. albomarginata* sp. nov. further confirms this view. Thus, intensifying field surveys with increased research efforts in this region will likely result in further discoveries of yet unknown lineages and new amphibian species. Our study reveals that species diversity within *Leptobrachella* remains largely underexplored. The discovery of *L. albomarginata* sp. nov. results in 108 species of *Leptobrachella*, 44 of which occur in China, and now seven on the Gaoligong Mountain Range.

The occurrence of co-distributed species may also be one of the reasons for the underestimation of species diversity in this region. Currently, multiple co-distributed species occur in the reserve. During our field work, four adult species of *Leptobrachella* (*L. purpurus*, *L. yingjiangensis*, *L. ventripunctata*, and *L. albomarginata* sp. nov.) were found syntopically at the same site and same time. A similar sympatric distribution pattern has also been reported, including four species and a putative new species of *Xenophrys* (*X. dehongensis*, *X. glandulosa*, *X. periosa*, *X. yingjiangensis*, and *X.* sp.; Wu et al. 2024a) and three species of *Polypedates* (*P. braueri*, *P. impresus*, and *P. teraiensis*; Yu et al. 2024). Future explorations and investigations need to treat species identifications with caution. Furthermore, studies should integrate life history data (e.g., advertisement call and breeding season) with genomic data to explore the drivers and mechanisms of sympatric coexistence and understand how these sympatric species interact and adapt to their respective niches.

Acknowledgments

This work was supported by the National Key R & D Program of China (2022YFC2602500), Science and Technology Basic Resources Investigation Program of China (Grant No. 2021FY100200); National Natural Science Foundation of China (NSFC 32100371); Yunnan Applied Basic Research Projects (No. 202301AT070312, 202301AT070431); Yunnan Revitalization Talent Support Program Yunling Scholar Project, China's Biodiversity Observation Network (Sino-BON), and the Animal Branch of the Germplasm Bank of Wild Species, CAS (Large Research Infrastructure Funding). We thank Dong An, Peng Yang, Xian-Kun Huang, and Xian-Rong Wu for their help in the field. We thank the Tongbiguan Provincial Nature Reserve for their support in undertaking field surveys and specimen collections.

References

AmphibiaChina (2024) The Database of Chinese Amphibians. Kunming Institute of Zoology (CAS), Kunming, Yunnan, China. Electronic Database. http://www.amphibiachina.org [accessed 31 December 2024]

Chan BPL, Bi Z, Duan SZ (2019) Introduction to a four-year biodiversity survey of Tengchong Section of Gaoligongshan National Nature Reserve, in the footsteps of pioneering naturalists in western Yunnan, China. Journal of Threatened Taxa 11(11): 14391−14401. https://doi.org/10.11609/jott.4438.11.11.14391-14401

Chen JM, Zhou WW, Poyarkov Jr NA, Stuart BL, Brown RM, Lathrop A, Wang YY, Yuan ZY, Jiang K, Hou M, Chen HM, Suwannapoom C, Nguyen SN, Duong TV, Papenfuss TJ, Murphy RW, Zhang YP, Che J (2017) A novel multilocus phylogenetic estimation reveals unrecognized diversity in Asian horned toads, genus *Megophrys sensu lato* (Anura: Megophryidae). Molecular Phylogenetics and Evolution 106: 28–43. https://doi.org/10.1016/j.ympev.2016.09.004

Chen JM, Poyarkov NA, Suwannapoom C, Lathrop A, Wu YH, Zhou WW, Yuan ZY, Jin JQ, Chen HM, Liu HQ, Nguyen TQ, Nguyen SN, Duong TV, Eto K, Nishikawa K, Matsui M, Orlov NL, Stuart BL, Brown RM, Rowley JJ, Murphy RW, Wang YY, Che J (2018) Large scale phylogenetic analyses provide insights into unrecognized diversity and historical biogeography of Asian leaf-litter frogs, genus *Leptolalax* (Anura: Megophryidae). Molecular Phylogenetics and Evolution 124: 162–171. https://doi.org/10.1016/j.ympev.2018.02.020

Chen WC, Liao X, Zhou SC, Mo YM (2019) A new species of *Leptobrachella* (Anura: Megophryidae) from southern Guangxi, China. Zootaxa 4563: 67–82. https://doi.org/10.11646/zootaxa.4563.1.3

Chen JM, Xu K, Poyarkov NA, Wang K, Yuan ZY, Hou M, Suwannapoom C, Wang J, Che J (2020) How little is known about "the little brown frogs": description of three new species of the genus *Leptobrachella* (Anura: Megophryidae) from Yunnan Province, China. Zoological Research 41(3): 292–313. https://doi.org/10.24272/j.issn.2095-8137.2020.036

Chen JM, Suwannapoom C, Wu YH, Poyarkov NA, Xu K, Pawangkhanant P, Che J (2021a) Integrative taxonomy reveals a new species of *Leptobrachella* (Anura: Megophryidae) from the mountains of northern Thailand. Zootaxa 5052(2): 41–64. https://doi.org/10.11646/zootaxa.5052.2.2

Chen WC, Peng W, Pan W, Liao N, Liu Y, Huang Y (2021b) A new species of *Leptobrachella* Smith 1925 (Anura: Megophryidae) from southern Guangxi, China. Zootaxa 5020: 581–596. https://doi.org/10.11646/zootaxa.5020.3.8

Chen WC, Yu GD, Cheng ZY, Meng T, Wei H, Zhou GY, Lu YW (2021c) A new species of *Leptobrachella* (Anura: Megophryidae) from central Guangxi, China. Zoological Research 42: 783–788. https://doi.org/10.24272/j.issn.2095-8137.2021.179

Chen WC, Peng WX, Li P, Yu GD (2023) A new species of the genus *Leptobrachella* Smith 1925 (Amphibia, Anura, Megophryidae) from Guangxi, China. ZooKeys 1178: 1–16. https://doi.org/10.3897/zookeys.1178.106038

Chen WC, Li P, Peng WX, Liu YJ, Huang Y (2024) The fourth species of *Leptobrachella* (Anura, Megophryidae) found at Shiwandashan National Nature Reserve, Guangxi, China. ZooKeys 1192: 257–279. https://doi.org/10.3897/zookeys.1192.98352

Cheng YL, Shi SC, Li J, Liu J, Li SZ, Wang B (2021) A new species of the Asian leaf litter toad genus *Leptobrachella* Smith, 1925 (Anura, Megophryidae) from northwest Guizhou Province, China. ZooKeys 1021: 81–107. https://doi.org/10.3897/zookeys.1021.60729

Chung HV, Tao NT, Vinh LQ, Truong NQ, Jiang J (2019) A new species of *Leptobrachella* Smith 1925 (Anura: Megophryidae) from Thanh Hoa Province, Vietnam. Raffles Bulletin of Zoology 67: 536–556. https://doi.org/10.26107/RBZ-2019-0042

Darriba D, Taboada GL, Doallo R, Posada D (2012) jModelTest 2: More models, new heuristics and parallel computing. Nature Methods 9(8): 772–772. https://doi.org/10.1038/nmeth.2109

Das I, Tron RKL, Rangad D, Hooroo RN (2010) A new species of *Leptolalax* (Anura: Megophryidae) from the sacred groves of Mawphlang, Meghalaya, north-eastern India. Zootaxa 2339(1): 44–56. https://doi.org/10.11646/zootaxa.2339.1.2

Dubois A (1980) Notes sur la systématique et la répartition des amphibiens anoures de Chine et des régions avoisinantes. IV. Classification générique et subgénérique des Pelobatidae Megophryinae. Bulletin

Mensuel de la Société Linnéenne de Lyon 49: 469–482. https://doi.org/10.3406/linly.1980.10444

Fei L, Hu SQ, Ye CY, Huang YZ (2009) Fauna Sinica. Amphibia Anura. Beijing: Science Press, 957 pp. [in Chinese]

Frost DR (2024) Amphibian Species of the World: An Online Reference. Version 6.1. https://amphibiansoftheworld.amnh.org/ [accessed 31 December 2024]

Gosner KL (1960) A simplified table for staging anuran embryos and larvae with notes on identification. Herpetologica 16(3): 183–190.

Hou Y, Zhang M, Hu F, Li S, Shi S, Chen J, Mo X, Wang B (2018) A new species of the genus *Leptolalax* (Anura, Megophryidae) from Hunan, China. Zootaxa 4444(3): 247–266. https://doi.org/10.11646/zootaxa.4444.3.2

Jiang K, Yan F, Suwannapoom C, Chomdej S, Che J (2013) A new species of the genus *Leptolalax* (Anura: Megophryidae) from northern Thailand. Asian Herpetological Research 4(2): 100–108. https://doi.org/10.3724/SP.J.1245.2013.00100

Kocher TD, Thomas WK, Meyer A, Edwards SV, Pääbo S, Villablanca FX, Wilson AC (1989) Dynamics of mitochondrial DNA evolution in animals: amplification and sequencing with conserved primers. Proceedings of the National Academy of Sciences of the USA 86(16): 6196–6200. https://doi.org/10.1073/pnas.86.16.6196

Lathrop A, Murphy RW, Orlov NL, Ho CT (1998) Two new species of *Leptolalax* (Anura: Megophryidae) from northern Vietnam. Amphibia-Reptilia 19: 253–267. https://doi.org/10.1163/156853898X00160

Lee PS, Liu B, Ouyang M, Ai RD, Liu XL, He YH, Huang PQ, Li YC, Naveen RS, Yuan ZY, Chen JM (2024) Hidden in the bamboo: A new parachuting frog (Rhacophoridae, *Rhacophorus*) from the borderlands of western China, with comments on the taxonomy of *R. rhodopus*. Zoosystematics and Evolution 100(3): 851–862. https://doi.org/10.3897/zse.100.120224

Li SZ, Liu J, Wei G, Wang B (2020) A new species of the Asian leaf litter toad genus *Leptobrachella* (Amphibia, Anura, Megophryidae) from southwest China. ZooKeys 943: 91–118. https://doi.org/10.3897/zookeys.943.51572

Li S, Li W, Cheng Y, Liu J, Wei G, Wang B (2024) Description of a new Asian Leaf Litter Toad of the genus *Leptobrachella* Smith, 1925 (Anura, Megophryidae) from southern Guizhou Province, China. Biodiversity Data Journal 12: e113427. https://doi.org/10.3897/BDJ.12.e113427

Lin SS, Li YH, Lu YH, Su HL, Wu SB, Zhang QQ, Mo MJ, Xiao XJ, Pan Z, Pan H, Zeng ZC, Wang J (2022) A new species of the genus *Leptobrachella* (Anura, Megophryidae) from northwestern Guangdong Province, China. Herpetozoa 35: 165–178. https://doi.org/10.3897/herpetozoa.35.e89981

Liu J, Shi S, Li S, Zhang M, Xiang S, Gang W, Wang B (2023) A new Asian leaf litter toad of the genus *Leptobrachella* (Amphibia, Anura, Megophryidae) from central south China. ZooKeys 1149: 103–134. https://doi.org/10.3897/zookeys.1149.85895

Luo T, Xiao N, Gao K, Zhou J (2020) A new species of *Leptobrachella* (Anura, Megophryidae) from Guizhou Province, China. ZooKeys 923: 115–140. https://doi.org/10.3897/zookeys.923.47172

Luo T, Wang W, Peng D, Lei B, Deng H, Ji S, Huang H, Zhou J (2022) A new species of the Asian Leaf Litter Toad genus *Leptobrachella* (Amphibia, Anura, Megophryidae) from Chongqing City, Southwest China. Asian Herpetological Research 13(2): 75–95. https://doi.org/10.16373/j.cnki.ahr.210052

Luong AM, Van Hoang C, Ziegler T, Nguyen TQ (2023) Two new species of *Leptobrachella* Smith 1925 (Amphibia: Megophryidae) from Cao Bang Province, Vietnam. Zootaxa 5369(3): 301–335. https://doi.org/10.11646/zootaxa.5369.3.1

Lyu JC, Dai LL, Wei PF, He YH, Yuan ZY, Shi WL, Zhou SL, Ran SY, Kuang ZF, Guo X, Wei G, Yuan G (2020) A new species of the genus *Leptobrachella* Smith, 1925 (Anura, Megophryidae) from Guizhou, China. 1008: 139–157. https://doi.org/10.3897/zookeys.1008.56412

Lyu ZT, Qi S, Wang J, Zhang SY, Zhao J, Zeng ZC, Wan H, Yang J, Mo Y, Wang Y (2023) Generic classification of Asian Horned Toads (Anura: Megophryidae: Megophryinae) and monograph of Chinese species. Zoological Research 44: 380–450. https://doi.org/10.24272/j.issn.2095-8137.2022.372

Miller MA, Pfeiffer W, Schwartz T (2010) Creating the CIPRES Science Gateway for inference of large phylogenetic trees. Gateway Computing Environments Workshop (GCE), 2010: 1–8. https://doi.org/10.1109/GCE.2010.5676129

Matsui M, Panha S, Eto K (2023) Two New Species of *Leptobrachella* from Northern Thailand (Amphibia, Anura, Megophryidae). Current Herpetology 42(1): 83–97. https://doi.org/10.5358/hsj.42.83

Mittermeier RA, Gil PR, Hoffmann M, Pilgrim J, Brooks T, Mittermeier CG, Lamoreux J, da Fonseca GAB (2005) Hotspots Revisited: Earth's Biologically Richest and Most Endangered Terrestrial Ecoregions. Mexico City: Conservation International, 392 pp.

Mittermeier RA, Turner WR, Larsen FW, Brooks TM, Gascon C (2011) Global biodiversity conservation: the critical role of hotspots. In: Zachos FE, Habel JC. Biodiversity Hotspots: Distribution and Protection of Conservation Priority Areas. Berlin: Springer, 3–22. https://doi.org/10.1007/978-3-642-20992-5_1

Myers N, Mittermeier RA, Mittermeier CG, Da Fonseca GA, Kent J (2000) Biodiversity hotspots for conservation priorities. Nature 403(6772): 853−858. https://doi.org/10.1038/35002501

Nguyen LT, Tapley B, Nguyen CT, Van Luong H, Rowley JJ (2021) A new species of *Leptobrachella* (Anura, Megophryidae) from Mount Pu Ta Leng, northwest Vietnam. Zootaxa 5016(3): 301–332. https://doi.org/10.11646/zootaxa.5016.3.1

Ohler A, Marquis O, Swan SR, Grosjean S (2000) Amphibian biodiversity of Hoang Lien Nature Reserve (Lao Cai Province, northern Vietnam) with description of two new species. Herpetozoa 13: 71–87.

Ohler A, Wollenberg KC, Grosjean S, Hendrix R, Vences M, Ziegler T, Dubois A (2011) Sorting out Lalos: description of new species and additional taxonomic data on megophryid frogs from northern Indochina (genus *Leptobrachella*, Megophryidae, Anura). Zootaxa 3147: 1–83. https://doi.org/10.11646/zootaxa.3147.1.1.

Posada D (2008) jModelTest: Phylogenetic model averaging. Molecular Biology and Evolution 25(7): 1253–1256. https://doi.org/10.1093/molbev/msn083

Qian TY, Xia X, Cao Y, Xiao NW, Yang DD (2020) A new species of *Leptobrachella* (Anura: Megophryidae) Smith, 1925 from Wuling Mountains in Hunan Province, China. Zootaxa 4816(4): 491–526. https://doi.org/10.11646/zootaxa.4816.4.4

Rambaut A, Drummond AJ (2009) Tracer. Version 1.5. http://tree.bio.ed.ac.uk/software/tracer/ [accessed 25 January 2021]

Rowley JJ, Dau VQ, Cao TT (2017) A new species of *Leptolalax* (Anura: Megophryidae) from Vietnam. Zootaxa 4273(1): 61–79. https://doi.org/10.11646/zootaxa.4273.1.5

Rowley JJL, Stuart BL, Richards SJ, Phimmachak S, Sivongxay N (2010) A new species of *Leptolalax* (Anura: Megophryidae) from Laos. Zootaxa 2681: 35–46. https://doi.org/10.11646/zootaxa.2681.1.3

Rowley JJL, Hoang HD, Dau VQ, Le DTT, Cao TT (2012) A new species of *Leptolalax* (Anura: Megophryidae) from central Vietnam. Zootaxa 3321: 56–68. https://doi.org/10.11646/zootaxa.3321.1.4

Rowley JJL, Dau QV, Nguyen TT (2013) A new species of *Leptobrachella* (Anura: Megophryidae) from the highest mountain in Indochina. Zootaxa 3737(4): 415–428. https://doi.org/10.11646/zootaxa.3737.4.5

Rowley JJL, Stuart BL, Neang T, Hoang HD, Dau VQ, Nguyen TT, Emmett DA (2015) A new species of *Leptolalax* (Anura: Megophryidae) from Vietnam and Cambodia. Zootaxa 4039: 401–417. https://doi.org/10.11646/zootaxa.4039.3.1

Sambrook J, Fritsch EF, Maniatis T (1989) Molecular Cloning: A Laboratory Manual. 2nd edn. Cold Spring Harbor Laboratory Press, Cold Spring Habor, NY.

Sengupta S, Sailo S, Lalremsanga HT, Das A, Das I (2010) A new species of *Leptolalax* (Anura: Megophryidae) from Mizoram, north-eastern India. Zootaxa 2406(1): 56–68. https://doi.org/10.11646/zootaxa.2406.1.3

Shi S, Hou Y, Song Z, Jiang J, Wang B (2021) A new leaf litter toad of *Leptobrachella* Smith, 1925 (Anura, Megophryidae) from Sichuan Province, China with supplementary description of *L. oshanensis*. Asian Herpetological Research 12(2): 143–166. https://doi.org/10.16373/j.cnki.ahr.200118

Shi S, Shen T, Wang X, Jiang J, Wang B (2023) Multiple data sources reveal a new Asian leaf litter toad of *Leptobrachella* Smith, 1925 (Anura, Megophryidae) from southwestern China. Asian Herpetological Research 14(1): 65–94. https://doi.org/10.16373/j.cnki.ahr.220065

Sun YB (2018) FasParser2: a graphical platform for batch manipulation of tremendous amount of sequence data. Bioinformatics 34(14): 2493–2495. https://doi.org/10.1093/bioinformatics/bty126

Sung YH, Yang J, Wang Y (2014) A new species of *Leptolalax* (Anura: Megophryidae) from southern China. Asian Herpetological Research 5(2): 80–90. https://doi.org/10.3724/SP.J.1245.2014.00080

Tamura K, Stecher G, Peterson D, Filipski A, Kumar S (2013) MEGA6: Molecular evolutionary genetics analysis version 6.0. Molecular Biology and Evolution 30(12): 2725–2729. https://doi.org/10.1093/molbev/mst197

Vences M, Thomas M, Van der Meijden A, Chiari Y, Vieites DR (2005) Comparative performance of the 16S rRNA gene in DNA barcoding of amphibians. Frontiers in Zoology 2(1): 1–12. https://doi.org/10.1186/1742-9994-2-5

Wang J, Yang J, Li Y, Lyu Z, Zeng Z, Liu Z, Ye Y, Wang Y (2018) Morphology and molecular genetics reveal two new *Leptobrachella* species in southern China (Anura, Megophryidae). ZooKeys (776): 105–137. https://doi.org/10.3897/zookeys.776.22925

Wang J, Li YL, Li Y, Chen HH, Zeng YJ, Shen JM, Wang YY (2019) Morphology, molecular genetics, and acoustics reveal two new species of the genus *Leptobrachella* from northwestern Guizhou Province, China (Anura, Megophryidae). ZooKeys 848: 119–154. https://doi.org/10.3897/zookeys.848.29181

Wang J, Lyu ZT, Qi S, Zeng ZC, Zhang WX, Lu LS, Wang YY (2020) Two new *Leptobrachella* species (Anura, Megophryidae) from the Yunnan-Guizhou Plateau, southwestern China. ZooKeys 995: 97–125. https://doi.org/10.3897/zookeys.995.55939

Wang J, Qi S, Dai KY, Lyu ZT, Zeng ZC, Chen HH, Li YQ, Zhao YY, Wang YZ, Wang YY (2022) A new *Leptobrachella* species (Anura, Megophryidae) from South China, with comments on the taxonomic status of *L. chishuiensis* and *L. purpurus*. Zoosystematics and Evolution 98(1): 165–180. https://doi.org/10.3897/zse.98.73162

Wu YH, Pawangkhanant P, Chen JM, Gao W, Suwannapoom C, Che J (2021) Confirmation of *Leptobrachella ventripunctata* (Fei, Ye & Li, 1990), based on molecular and morphological evidence in Thailand. Biodiversity Data Journal 9: e74097. https://doi.org/10.3897/BDJ.9.e74097

Wu YH, Chen JM, Pawangkhanant P, Yothawut C, Karuno AP, Suwannapoom C, Che J (2022) Distribution extension of *Leptobrachella eos* (Ohler, Wollenberg, Grosjean, Hendrix, Vences, Ziegler & Dubois, 2011): first record from Thailand. Herpetozoa 35: 25–32. https://doi.org/10.3897/herpetozoa.35.e78627

Wu YH, Hou SB, Yuan ZY, Jiang K, Huang RY, Wang K, Liu Q, Yu ZB, Zhao HP, Zhang BL, Chen JM, Wang LJ, Stuart BL, Chambers EA, Wang YF, Gao W, Zou DH, Yan F, Zhao GG, Fu ZX, Wang SN, Jiang M, Zhang L, Ren JL, Wu YY, Zhang LY, Yang DC, Jin JQ, Yin TT, Li JT, Zhao WG, Murphy RW, Huang S, Guo P, Zhang YP, Che J (2023) DNA barcoding of Chinese snakes reveals hidden diversity and conservation needs. Molecular Ecology Resources 23(5): 1124–1141. https://doi.org/10.1111/1755-0998.13784

Wu YH, Yu ZB, Chen JM, Kilunda FK, Zhang DC, Zuo CS, Zuo AR, Duan ZP, Che J (2024a) A field survey on the genus *Xenophrys* (Amphibia, Megophryidae) confirms underestimated diversity in the Gaoligong Mountains, with the description of a new species. Zoosystematics and Evolution 100(3): 1041–1052. https://doi.org/10.3897/zse.100.127635

Wu YH, Yu ZB, Lu CQ, Zhang YP, Dong WJ, Liu XL., Kilunda FK, Xiong Y, Jiang YF, Ouyang H, Fu ZX, He YB, Yuan ZY, Che J (2024b) A new species of the genus *Amolops* (Amphibia: Ranidae) and the first national record of *Amolops vitreus* from China. Vertebrate Zoology 74: 343–357. https://doi.org/10.3897/vz.74.e108013

Yang J, Chan BPL (2018) A new phytotelm-breeding treefrog of the genus *Nasutixalus* (Rhacophoridae) from western Yunnan of China. Zootaxa 4388: 191–206. https://doi.org/10.11646/zootaxa.4388.2.3

Yang JH, Wang YY, Chen GL, Rao DQ (2016) A new species of the genus *Leptolalax* (Anura: Megophryidae) from Mt. Gaoligongshan of western Yunnan Province, China. Zootaxa 4088(3): 379–394. https://doi.org/10.11646/zootaxa.4088.3.4

Yang J, Zeng ZC, Wang Y (2018) Description of two new sympatric species of the genus *Leptolalax* (Anura: Megophryidae) from western Yunnan of China. PeerJ 6(e4586): 1–32. https://doi.org/10.7717/peerj.4586

Yu ZB, Kilunda FK, Wang K, Cao YY, Wu CL, Duan ZP, Zuo CS, Zhang DC, Wu YH, Che J (2024) The first discovery of *Polypedates teraiensis* (Dubois, 1987) (Rhacophoridae, Anura) in China. Biodiversity Data Journal 12: e127029. https://doi.org/10.3897/BDJ.12.e127029

Yuan Z, Sun R, Chen J, Rowley JJL, Wu Z, Hou S, Wang S, Che J (2017) A new species of the genus *Leptolalax* (Anura: Megophryidae) from Guangxi, China. Zootaxa 4300(4): 551–570. https://doi.org/10.11646/zootaxa.4300.4.5

Supplementary material 1

Localities and voucher data for all specimens used in this study

Authors: Yun-He Wu, Zhong-Bin Yu, Shen-Pin Yang, Zheng-Pan Duan, An-Ru Zuo, Ding-Can Zhang, Robert W. Murphy, Jing Che

Data type: xlsx

Link: https://doi.org/10.3897/zse.101.135560.suppl1

Supplementary material 2

Average uncorrected p-distances (percentage) among *Leptobrachella* species

Authors: Yun-He Wu, Zhong-Bin Yu, Shen-Pin Yang, Zheng-Pan Duan, An-Ru Zuo, Ding-Can Zhang, Robert W. Murphy, Jing Che

Data type: xlsx

Explanation note: Average uncorrected p-distances (percentage) among *Leptobrachella* species calculated from 16S rRNA gene sequences (below the diagonal) and standard error estimates (above the diagonal). The ingroup mean uncorrected p-distances are shown on the diagonal.

Link: https://doi.org/10.3897/zse.101.135560.suppl2

Supplementary material 3

Larvae of *Leptobrachella albomarginata* sp. nov. (KIZ 051631) in preservative

Authors: Yun-He Wu, Zhong-Bin Yu, Shen-Pin Yang, Zheng-Pan Duan, An-Ru Zuo, Ding-Can Zhang, Robert W. Murphy, Jing Che

Data type: jpg

Link: https://doi.org/10.3897/zse.101.135560.suppl3

Zoosyst. Evol. 101 (2) 2025, 465–471 | DOI 10.3897/zse.101.136965

PENSOFT

MUSEUM FÜR NATURKUNDE BERLIN

Description of a new loach species, *Yunnanilus triangulus* sp. nov. (Cypriniformes, Nemacheilidae), from Yunnan, China

Mei Liu[1,2*], Jian-Bing Lyu[3*], Li-Na Du[1,2], Xiao-Yong Chen[3]

1 *Key Laboratory of Ecology of Rare and Endangered Species and Environmental Protection, Guangxi Normal University, Ministry of Education, Guilin, Guangxi 541004, China*

2 *Guangxi Key Laboratory of Rare and Endangered Animal Ecology, College of Life Sciences, Guangxi Normal University, Guilin, Guangxi 541004, China*

3 *Kunming Natural History Museum of Zoology, Kunming Institute of Zoology, Chinese Academy of Sciences, Kunming, Yunnan, 650223, China*

https://zoobank.org/0D26F007-FE9F-47B8-A7F2-6DF23B3FA812

Corresponding authors: Li-Na Du (dulina@mailbox.gxnu.edu.cn); Xiao-Yong Chen (chenxy@mail.kiz.ac.cn)

Academic editor: Nicolas Hubert ♦ **Received** 12 September 2024 ♦ **Accepted** 16 January 2025 ♦ **Published** 26 February 2025

Abstract

A new species of the genus *Yunnanilus*, designated *Yunnanilus triangulus* **sp. nov.**, is described from the Nanpan River in Yunnan Province, southwestern China. Nuptial males of this species are distinguished by the presence of tubercles on the caudal peduncle during the reproductive period, a feature not observed in other members of the genus. The new species is further characterized by the following unique combination of morphological characters: body scaled, smaller eyes than interorbital width, nine inner gill rakers on first gill arch, lateral head length 27.1%–30.9% SL, head width 14.3%–17.2% SL, eye diameter 19.6%–23.8% of lateral head length, and caudal peduncle depth 94.0%–130.6% of its length. Morphological and molecular evidence support the validity of this species, despite its geographic proximity to *Y. polylepis*. These findings underscore the ecological specialization that exists within the genus *Yunnanilus* and highlight the urgent need for species-specific conservation strategies, given their restricted distributions and dependence on specific habitats.

Key Words

Caudal peduncle with tubercles, freshwater fish, morphological characters, sexual dimorphism

Introduction

Nichols (1925) designated *Nemacheilus pleurotaenia* Regan, 1904, as the type species of the nemacheilid loach subgenus *Yunnanilus*, with the following defining characters: short and compressed body, small scales, incomplete lateral line, slightly forked caudal fin, nostrils separated by greater distance than between posterior nostril and eye, and anterior nostril forming flap-like tube. Subsequently, Kottelat and Chu (1988) elevated *Yunnanilus* to the rank of genus, while Yang and Chen (1995) later categorized *Yunnanilus* species into two major assemblages, *Y. nigromaculatus* and *Y. pleurotaenia* species groups, based on the presence or absence of lateral and cephalic lateral line pores. Du et al. (2021) retained the *Y. pleurotaenia* group within *Yunnanilus* but reassigned the *Y. nigromaculatus* group to the revalidated genus *Eonemachilus* Berg, 1938. A more recent phylogenetic analysis of Chinese nemacheilids with tube-shaped anterior nostrils by Du et al. (2023) confirmed the generic status of *Yunnanilus* and refined its diagnostic characters to mouth inferior; anterior and posterior nostrils separated, anterior nostrils tube-like, without elongated barbel-like structure; cheeks scaleless; lips with furrows; and lateral line and cephalic lateral line pores present (Du et al. 2021, 2023).

* These authors contributed equally to this work.

Currently, *Yunnanilus* comprises 20 valid species, all restricted to lakes, marshes, and slow-flowing waters within Yunnan and Sichuan Provinces of southwestern China (Qin et al. 2024). Among these, six species are distributed in the Yangtze River system, including *Y. discoloris* Zhou & He, 1989, *Y. longibulla* Yang, 1990, *Y. pleurotaenia* (Regan, 1904), and *Y. spanisbripes* An, Liu & Li, 2009 in the Jinsha River; *Y. sichuanensis* Ding, 1995 in the Yalong River; and *Y. jiuchiensis* Du, Hou, Chen & Yang, 2018 in the Tuo River; and 13 species are distributed in the Pearl River basin, including *Y. beipanjiangensis* Li, Mao & Sun, 1994 in the Beipan River; *Y. analis* Yang, 1990; *Y. chui* Yang, 1991; *Y. elakatis* Cao & Zhu, 1989; *Y. forkicaudalis* Li, 1999; *Y. macrogaster* Kottelat & Chu, 1988; *Y. macrolepis* Li, Tao & Mao, 2000; *Y. macrositanus* Li, 1999; *Y. nanpanjiangensis* Li, Tao & Lu, 1994; *Y. paludosus* Kottelat & Chu, 1988; *Y. parvus* Kottelat & Chu, 1988; *Y. polylepis* Qin, Shao, Du & Wang, 2024; and *Y. yangi* He et al., 2024 in the Nanpan River, and one species, *Y. chuanheensis* Jiang, Zhao, Du & Wang, 2021 in the Red River (Lixian River) (Du et al. 2021; Qin et al. 2024).

In April 2018, eight specimens of *Yunnanilus* were collected from a tributary of the Nanpan River in Huaning County, Yuxi City, Yunnan Province, China. Morphological and molecular analyses confirmed that these specimens represent a previously undescribed member of the genus, which is herein described and compared with all known congeners.

Materials and methods

All care and handling of experimental animals complied with the relevant laws of the Chinese Laboratory of Animal Welfare and Ethics (GB/T 35892-2018). Upon their collection, all specimens were rapidly euthanized by an overdose of anesthetic clove oil. The right-side pelvic fins of five individuals were removed and preserved in 99% ethanol for molecular analyses, and eight individuals were stored in 10% formalin for morphological comparisons. The specimens were deposited in the Kunming Natural History Museum of Zoology, Kunming Institute of Zoology (KIZ), Chinese Academy of Sciences (CAS).

All counts and measurements followed the methodology described by Kottelat (1990). Initial data processing and preliminary statistical analyses were performed using Excel software. Genomic DNA was extracted from ethanol-preserved fin tissue, and partial sequences of the mitochondrial cytochrome c oxidase subunit I (COI) and cytochrome *b* (Cyt *b*) were sequenced by Tsingke Biotechnology Co., Ltd. (China). All sequences were assembled using SeqMan within the DNAStar package and aligned using MEGA v11.0 (Tamura et al. 2021). Sequences were submitted to GenBank (Accession Nos. PQ300642–PQ300646 for COI, PQ306053–PQ306057 for Cyt *b*). The phylogenetic position of *Yunnanilus triangulus* sp. nov. was determined using maximum-likelihood (ML) and Bayesian inference (BI) methods via the CIPRES Science Gateway (Miller et al. 2010). The ML tree was constructed using RAxML-HPC v8 (Stamatakis 2014) with a rapid bootstrapping configuration and 1000 bootstrap iterations. The BI tree was constructed using MrBayes in XSEDE v3.2.7a (Ronquist et al. 2012), with two simultaneous runs of four Markov chains starting from a random tree. The chains were run for five million generations and sampled every 100 generations. The first 25% of sampled trees were discarded as burn-in, and the remaining trees were used to generate a consensus tree and estimate Bayesian posterior probabilities (BPPs). The resulting phylogenetic trees were viewed and edited using Figtree v1.4.4.

Results

***Yunnanilus triangulus* sp. nov.**

https://zoobank.org/228876CA-206D-4960-BC2E-4B1692267979

Holotype. • KIZ2018002410 female, 51.8 mm standard length (SL), Dalongtan Spring, Wangma Village, Huaning County, Yuxi City, Yunnan, P.R. China; Nanpan River, 24.1716°N, 102.9182°E, 1619 m a.s.l., X.Y. Chen, L.L. Xu, and H.D. Lyu, collected April 2018.

Paratypes. • Seven specimens. Female: KIZ2018002404, 2406–2407, 2409, 2411, 38.9–54.6 mm SL; Male: KIZ2018002405, KIZ2018002408, 37.1–39.1 mm SL; same as holotype.

Etymology. The specific name *triangulus* is derived from the unique presence of a tubercle on the caudal peduncle in nuptial males, a character not previously recorded in the genus *Yunnanilus*. We suggest the Chinese vernacular name "三角云南鳅" and the English vernacular name "triangle Yunnan loach." Gender: masculine.

Diagnosis. The new species can be distinguished from all other members of the genus by the presence of a unique triangular tubercle on the male caudal peduncle. It shares a body covered by scales, except on head and thorax, with *Y. chuanheensis*, *Y. jiuchiensis*, *Y. longibulla*, *Y. macrogaster*, *Y. macrolepis*, *Y. parvus*, *Y. pleurotaenia*, *Y. polylepis*, and *Y. spanisbripes*. However, the new species can be readily differentiated from these congeners by the following combination of characters: eye diameter shorter than interorbital width (vs. longer in *Y. jiuchiensis* and *Y. longibulla*), outer gill raker absent (vs. present in *Y. macrolepis* and *Y. spanisbripes*), processus dentiformis absent (vs. present in *Y. macrogaster*, *Y. parvus*, and *Y. pleurotaenia*), six branched pelvic-fin rays (vs. seven or eight in *Y. chuanheensis*), eight branched dorsal-fin rays (vs. nine in *Y. polylepis*), and specific metric characters.

Description. All morphometric and meristic data are given in Table 1. Greatest body depth anterior to dorsal fin origin, posterior portion gradually compressed from dorsal fin to caudal fin base. Lateral head longer than deep, deeper than wide. Snout slightly blunt, shorter than postorbital length of head. Eye diameter smaller than interorbital width; posterior nostril closer to anterior margin of eye than to tip of snout; anterior and posterior nostrils separated by distance greater than diameter of posterior nostril; base of anterior nostril tube-shaped, not elongated to barbel-like structure.

Table 1. Morphometric and meristic data of *Yunnanilus triangulus* sp. nov.

Characters	Holotype	Paratypes (mean ± SD)	
		Females (N = 5)	Males (N = 2)
Total length (mm)	51.8	49.6–67.3 (55.6 ± 7.0)	47.8–49.3 (48.6 ± 1.1)
Standard length (mm)	40.8	38.9–54.6 (44.1 ± 6.1)	37.1–39.1 (38.1 ± 1.4)
Percent of standard length (%)			
Deepest body depth	20.4	21.6–23.1 (22.1 ± 0.6)	20.9–21.2 (21.1 ± 0.2)
Head width	15.5	15.0–17.2 (15.7 ± 0.9)	14.3–14.4 (14.3 ± 0.0)
Lateral head length	27.7	27.1–29.0 (28.3 ± 0.8)	29.9–30.9 (30.4 ± 0.7)
Predorsal length	54.9	51.3–55.4 (53.8 ± 1.8)	53.6–54.8 (54.2 ± 0.8)
Prepelvic length	55.8	55.8–59.9 (58.1 ± 1.5)	56.9–57.7 (57.3 ± 0.5)
Preanal length	78.7	80.4–82.0 (81.4 ± 0.7)	80.2–81.7 (80.9 ± 1.1)
Preanus length	75.5	77.0–78.4 (77.5 ± 0.6)	77.1–77.2 (77.1 ± 0.1)
Caudal-peduncle length	13.0	9.4–12.1 (10.7 ± 1.0)	10.9–11.8 (11.3 ± 0.6)
Caudal-peduncle depth	12.2	11.5–12.8 (12.1 ± 0.5)	11.4–12.1 (11.8 ± 0.5)
Percent of Lateral head length (%)			
Head width	56.1	53.2–59.3 (55.5 ± 2.5)	46.2–48.0 (47.1 ± 1.2)
Head depth	60.0	55.1–60.9 (57.4 ± 2.2)	49.6–56.9 (53.2 ± 5.2)
Eye diameter	22.8	19.6–23.8 (21.0 ± 1.6)	21.3–21.4 (21.4 ± 0.0)
Interorbital width	23.9	21.3–27.4 (24.0 ± 2.2)	22.7–23.0 (22.8 ± 0.2)
Snout length	31.5	31.7–38.1 (35.1 ± 2.4)	31.2–35.2 (33.2 ± 2.8)
Percent of Caudal-peduncle length (%)			
Caudal-peduncle depth	94.0	105.9–130.6 (113.1 ± 10.2)	102.5–104.9 (103.7 ± 1.7)
Percent of distance between pectoral-fin origin and pelvic-fin origin			
Pectoral-fin length	73.8	56.9–76.5 (66.9 ± 8.0)	89.0–92.0 (90.5 ± 2.1)
Percent of distance between pelvic-fin origin and anal-fin origin			
Pelvic-fin length	69.1	53.2–66.1 (61.5 ± 5.5)	74.1–76.6 (75.4 ± 1.8)
Dorsal-fin rays	3, 8	3, 8	3, 8
Pectoral-fin rays	1, 10	1, 10–11	1, 10–11
Pelvic-fin rays	1, 6	1, 6	1, 6
Anal-fin rays	2, 5	2, 5	2, 5
Branched caudal-fin rays	16	15–17	16

Body densely scaled, except head and thorax; scales more numerous and larger in males from pectoral to pelvic-fin insertion. Three pairs of barbels, two rostral pairs and one maxillary pair, length of inner rostral barbel one half of outer rostral barbel, reaching anterior nostril; outer rostral barbel reaching posterior nostril, and maxillary barbel reaching posterior margin of eye. Processus dentiformis on upper jaw absent.

Dorsal fin with three unbranched and eight branched rays, origin closer to caudal-fin base than to snout tip, predorsal length 51.3–55.4% SL. Pectoral fin with one unbranched and 10–11 branched rays. Pelvic fin with one unbranched and six branched rays, origin posterior to dorsal fin origin, tips of adpressed fin not reaching anus, longer in males than females (74.1%–76.6% of distance between pelvic-fin insertion and anal-fin origin vs. 53.2%–69.1% in females). Anal fin with two unbranched and five branched rays, origin closer to anus and distant from caudal fin. Caudal fin with two unbranched and 15–17 branched rays (mostly 16). Series of temporal tubercles present on caudal peduncle in nuptial males. Lateral line incomplete, terminating between tip of pectoral fin and dorsal fin origin. 9–11 inner gill rakers on first gill arch. Cephalic lateral system with 12–15+3 infraorbital canal pores, 7–9 supraorbital canal pores, 6–8 supratemporal canal pores, and 6–10 preoperculomandibular canal pores.

Stomach U-shaped (Fig. 2B); intestine long and straight. Swim bladder divided into two chambers; anterior chamber covered by dumbbell-shaped bony capsule, and posterior chamber well developed, connected to anterior chamber by a slender tube, approximately half posterior chamber in length (Fig. 2A).

Coloration. In life, head and trunk with light golden background color. Ventral head and abdomen surface without color pattern. In females, trunk with 15–17 long and twisted dark brown saddles, connected together on dorsal. Some bars bifurcated (Fig. 1H). In males, body with black longitudinal stripe on both sides (Fig. 1D). Fin rays with dark pigments, fin membrane hyaline. In formalin-fixed specimens, lateral stripes and blotches somewhat faded, body generally light yellow.

Sexual dimorphism. Series of temporal tubercles present on caudal peduncle in nuptial male individuals (Fig. 2C), absent in females. Pelvic fin longer in males than females. Males without color patterns except for longitudinal stripes on body sides, females with long and twisted bars on trunks. Tubercles triangular, semi-translucent, angle to the body approximately 30 degrees, yellowish when preserved in formalin.

Distribution and habitat. *Yunnanilus triangulus* sp. nov. is currently only known from Dalongtan Spring, Wangma Village, Huaning County, Yuxi City, Yunnan, China; Nanpan

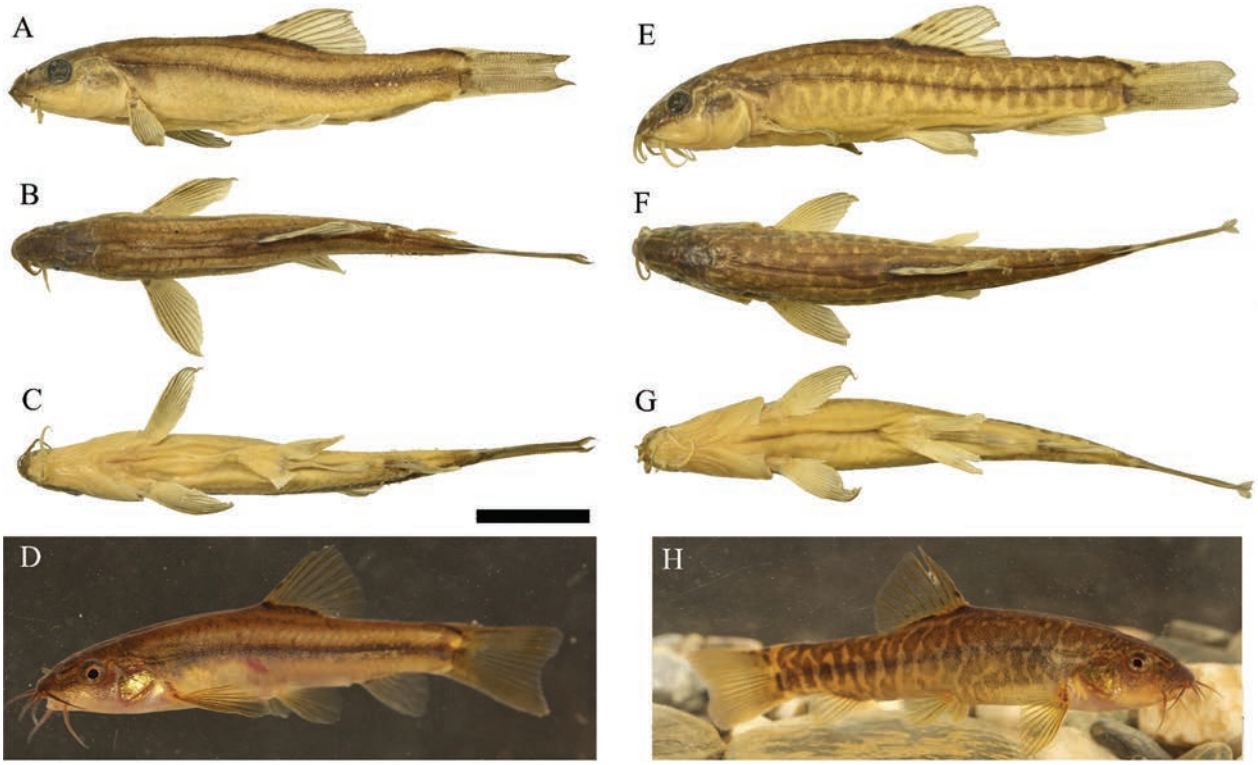

Figure 1. Morphometric characters of *Yunnanilus triangulus* sp. nov. **A–D.** Lateral, dorsal, and ventral views, as well as a living photo of male, paratype KIZ2018002405; **E–H.** Lateral, dorsal, ventral, and living photo of female, holotype KIZ2018002410. Scale bar: 1 cm.

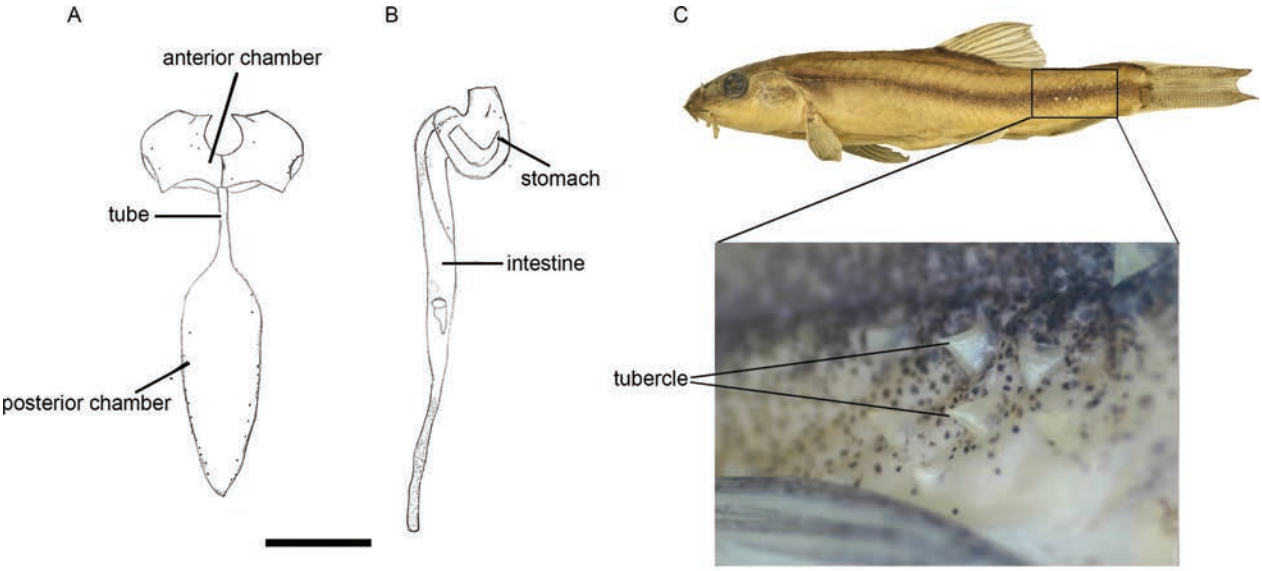

Figure 2. Air bladder (**A**), stomach and intestine (**B**) (KIZ2018002404), and male tubercles on caudal peduncle (**C**) (KIZ2018002405) in *Yunnanilus triangulus* sp. nov.

River (24.1716°N, 102.9182°E, 1619 m a.s.l.). The habitat comprises a deep pool, approximately 3 m in depth and characterized by abundant macrophytes (Fig. 3). Sympatric fish species at the time of collection included *Discogobio yunnanensis*, *Pseudorasbora parva*, and *Carassius auratus*.

Genetic comparisons. In total, 1746 base pairs (670 bp for COI and 1 076 bp for Cyt *b*) from *Yunnanilus triangulus* sp. nov. were amplified and analyzed in this study. These sequences were used for molecular phylogenetic analysis together with 37 complete mitochondrial genomes, 25 Cyt *b* sequences, and 21 COI sequences from GenBank. *Parabotia fasciata* Dabry de Thiersant, 1872, and *Leptobotia elongata* (Bleeker, 1870), two botiid species, served as the outgroups. Given that the BI and ML analyses produced nearly identical topologies, only the BI tree with BPPs and

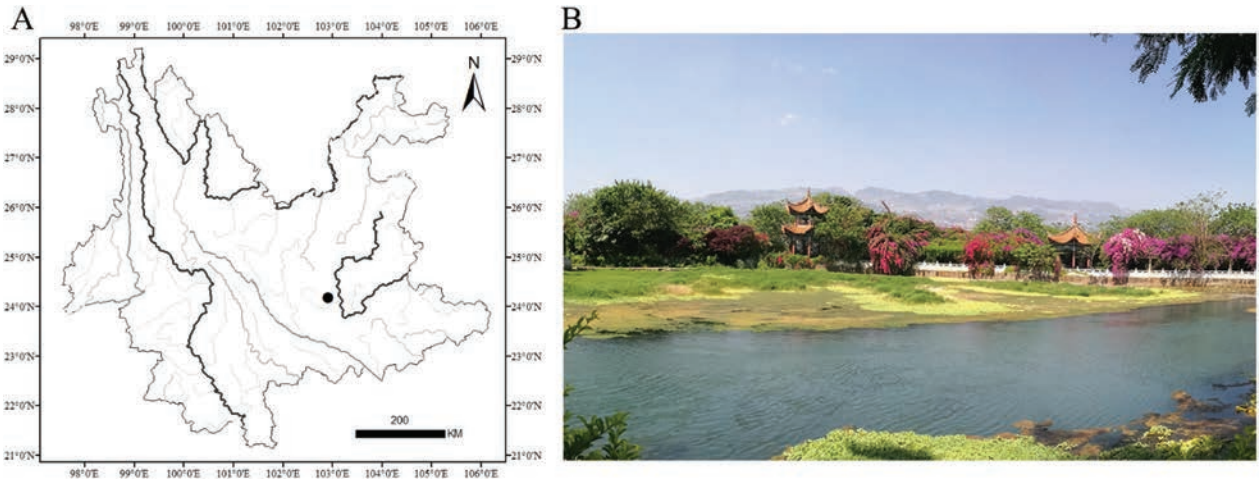

Figure 3. Type locality of *Yunnanilus triangulus* sp. nov. **A.** Distribution map; **B.** Habitat photo of type locality at time of collection.

bootstrap support (BS) values is presented (Fig. 4). The phylogenetic tree strongly supported the placement of *Yunnanilus triangulus* sp. nov. within *Yunnanilus*. The new species also formed a monophyly with *Y. analis*, *Y. chuanheensis*, and *Y. pleurotaenia* (BPP = 1; BS = 99) and exhibited a sister relationship to *Y. jiuchiensis* and *Y. polylepis*. However, the molecular phylogenies did not support the monophyly of *Yunnanilus* itself. In particular, *Yunnanilus yangi* was weakly supported as a sister group to *Eonemachilus* (BPP = 59; BS = 71), forming a clade with other species of *Yunnanilus* (Fig. 4).

The uncorrected *p*-distances of the Cyt *b* and COI genes between *Yunnanilus triangulus* sp. nov. and the other six species ranged from 1.19% to 7.5% (average 3.13%). The maximum and minimum uncorrected *p*-distances were found between *Y. yangi* and *Y. polylepis* and between *Y. analis* and *Y. pleurotaenia*, respectively (Table 2).

Discussion

Molecular analysis unequivocally placed *Yunnanilus triangulus* sp. nov. within the genus *Yunnanilus*. This placement was further corroborated by several morphological features characteristic of the genus, including mouth inferior, lateral and cephalic lateral line pores present, anterior and posterior nostrils separated, an anterior nostril tube-shaped, and a tip not elongated into a barbel-like structure (Du et al. 2023; Qin et al. 2024).

The description of this new species increases the total number of *Yunnanilus* species native to the Yangtze, Pearl, and Red River basins to 21. Notably, *Yunnanilus triangulus* sp. nov. can be distinguished based on a combination of morphological characteristics related to the presence of scales, relative sizes of the eye diameter and interorbital width, absence of a processus dentiformis, lack of an outer gill raker on the first gill arch, and the specific number of branched caudal fin rays. The genus *Yunnanilus* can be broadly divided into two morphological groups based on the presence or absence of body scales. The 'scaleless' group contains *Y. analis*, *Y. beipanjiangensis*, *Y. chui*, *Y. discoloris*, *Y. forkicaudalis*, *Y. paludosus*, and *Y. yangi*, while the 'scaled' group includes the new species together with *Y. chuanheensis*, *Y. elakatis*, *Y. jiuchiensis*, *Y. longibulla*, *Y. macrogaster*, *Y. macrolepis*, *Y. macrositanus*, *Y. nanpanjiangensis*, *Y. parvus*, *Y. pleurotaenia*, *Y. polylepis*, *Y. sichuanensis*, and *Y. spanisbripes*. However, *Yunnanilus triangulus* sp. nov. can be distinguished from *Y. elakatis*, *Y. macrositanus*, *Y. nanpanjiangensis*, and *Y. sichuanensis* by whole body covered by scales, except head and thorax (vs. scales present only on caudal peduncle), from *Y. longibulla* and *Y. jiuchiensis* by eye diameter shorter than interorbital width (vs. longer), from *Y. parvus*, *Y. macrogaster*, *Y. pleurotaenia*, *Y. macrolepis*, *Y. spanisbripes*, and *Y. longibulla* by

Table 2. Uncorrected p-distances (%) between nine species in the genus *Eonemachilus* and *Yunnanilus* based on mitochondrial COI and Cyt *b* genes.

		1	2	3	4	5	6	7	8
1	*Eonemachilus niger*								
2	*E. longidorsalis*	8.14							
3	*Yunnanilus yangi*	9.64	12.08						
4	*Y. polylepis*	9.17	10.64	9.44					
5	*Y. triangulus*	**8.53**	**9.79**	**7.54**	**4.34**				
6	*Y. jiuchiensis*	6.76	7.88	7.29	3.88	**1.89**			
7	*Y. chuanheensis*	9.99	11.33	6.66	5.89	**2.43**	2.77		
8	*Y. pleurotaenia*	8.55	10.20	7.42	4.18	**1.19**	1.86	2.03	
9	*Y. analis*	6.89	7.82	7.46	4.35	**1.37**	2.26	2.32	0.05

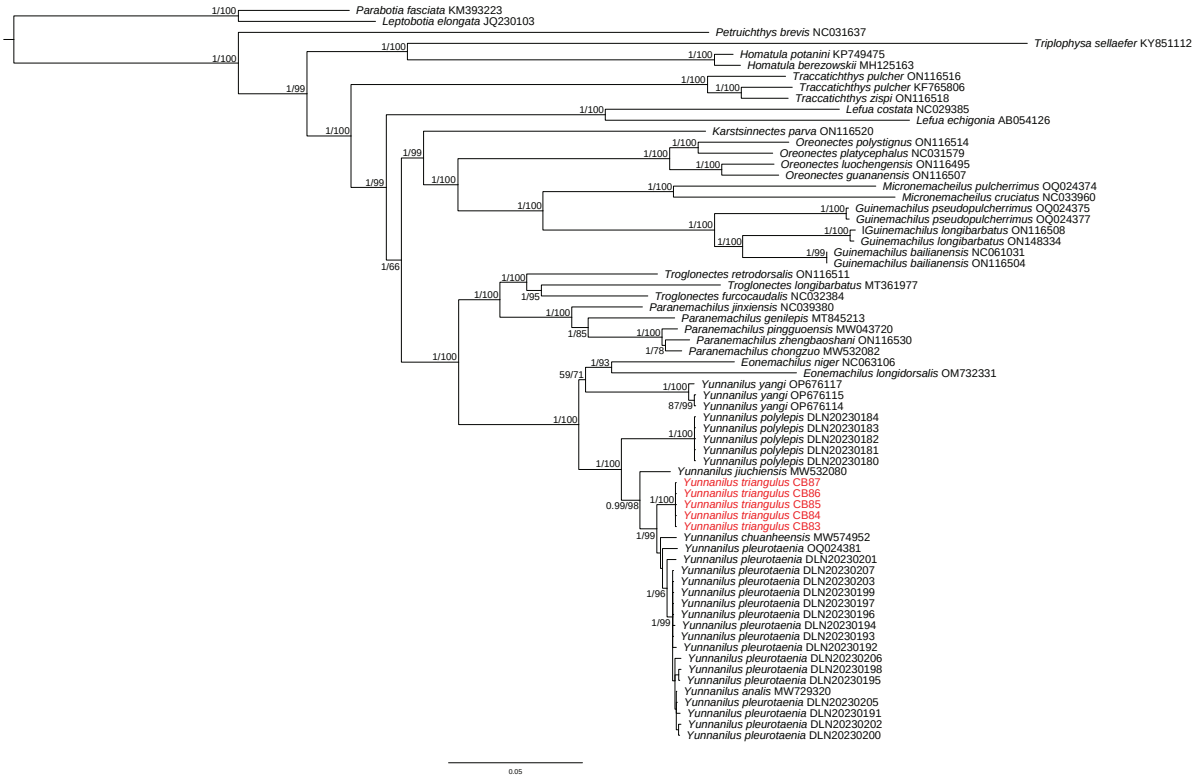

Figure 4. Bayesian phylogram of *Yunnanilus* based on a concatenated dataset of mitochondrial cytochrome c oxidase subunit I (COI) and cytochrome b (Cyt *b*) sequences. Numbers on branches represent BPPs from BI and bootstrap supports from ML.

processus dentiformis absent (vs. present), from *Y. macrolepis* and *Y. spanisbripes* by outer gill raker on first gill arch absent (vs. present), and from *Y. polylepis* by body depth 20.0%–23.0% SL (vs. 15.0%–20.0%) and caudal peduncle depth 94.0%–131.0% of its length (vs. 73.0%–89.0%).

Sexual dimorphism is a common characteristic in members of the family Nemacheilidae. For example, males of the genus *Oreonectes* develop genital papillae posterior to the anus (Du et al. 2008); those of the genera *Triplophysa* and *Barbatula* exhibit thickened and widened outer branched pectoral-fin rays, accompanied by a slender pad of tubercles located anteroventral to the orbit (Zhu 1989). In *Yunnanilus*, sexual dimorphism is often expressed through color pattern variations. Although Qin et al. (2024) documented the presence of small tubercles on the body in nuptial males of *Y. polylepis*, with the presence of triangular tubercles on the caudal peduncle in nuptial males not previously reported. Zhang and Shen (1999) suggested that nuptial tubercles typically occur in areas of the body in contact during courtship or male-male competition, potentially serving to facilitate close physical interaction. Hence, we hypothesize that the caudal peduncle tubercles observed in *Yunnanilus triangulus* sp. nov. play a role in stimulating ovulation in females. However, further studies are necessary to validate this proposition.

Species of *Yunnanilus* are typically confined to small water bodies rich in submerged macrophytes, environments highly vulnerable to anthropogenic impacts and pollution. In September 2024, a survey of the type locality of *Yunnanilus triangulus* sp. nov. revealed that the species had disappeared in the pond, likely due to the rapid decline of submerged macrophytes and the introduction of large numbers of carp into the habitat. The sensitivity of *Yunnanilus* to water pollution, invasive species, and predation has led to consistent population declines across its range. These findings underscore the urgent need for targeted conservation strategies to safeguard *Yunnanilus* species and other freshwater fish in this ecologically significant karst region. It is hoped that this report will stimulate further research and conservation initiatives to address the growing threats faced by freshwater ecosystems in southwestern China.

Nomenclatural acts registration

The electronic version of this article in portable document format represents a published work according to the International Commission on Zoological Nomenclature (ICZN); hence the new name contained in the electronic version is effectively published under the Code from the electronic edition alone (see Articles 8.5–8.6 of the Code). This published work and the nomenclatural acts it contains have been registered in ZooBank LSIDs (Life Science Identifiers) and can be resolved and the associated information can be viewed through any standard web browser by appending the LSID to the prefix http://zoobank.org/.

Authors' Contributions

M.L. and L.-N.D. measured the specimens, analyzed the data, conceived and designed the study, and prepared the manuscript, J.-B.L. analyzed the molecular data and constructed the phylogenetic tree. X.-Y.C. provided conceptualization and funding acquisition for the field survey and resources. All authors read and approved the final version of the manuscript.

Acknowledgments

This study was funded by the Project of the Innovation Team of Survey and Assessment of the Pearl River Fishery Resources (2023TD-10), Guangxi Natural Science Foundation Project (2022GXNSFAA035563), Key Laboratory of Ecology of Rare and Endangered Species and Environmental Protection (Guangxi Normal University), Ministry of Education, China (ERESEP2022Z05), and the Position of Bioclassonomist of Chinese Academy of Sciences (CAS-TAX-24-054). We are grateful to L.L. Xu and H.D. Lyu for collecting specimens. We thank C. Watts for English corrections and suggestions. We thank C.Y. Lei for providing topotype specimens of *Yunnanilus yangi*. We especially thank help and supports from Bureau of Parks and Woods of Yuxi City throughout the field survey.

References

Du LN, Chen XY, Yang JX (2008) A review of the Nemacheilinae genus *Oreonectes* Günther with descriptions of two new species (Teleostei, Balitoridae). Zootaxa 1729: 23–36. https://doi.org/10.11646/zootaxa.1729.1.3

Du LN, Yang J, Min R, Chen XY, Yang JX (2021) A review of the Cypriniform tribe Yunnanilini Prokofiev, 2010 from China, with an emphasis on five genera based on morphologies and complete mitochondrial genomes of some species. Zoological Research 42: 310–334. https://doi.org/10.24272/j.issn.2095-8137.2020.229

Du LN, Li SJ, Xu F, Luo T, Luo FG, Yu GH, Zhou J (2023) Clarification of Phylogenetic Relationships among Chinese Nemacheilids with Tube-Shaped Anterior Nostrils, with a Description of a New Genus and Two New Species. Journal of Zoological Systematics and Evolutionary Research 2023: 3600085. [11 pp] https://doi.org/10.1155/2023/3600085

Kottelat M (1990) Indochinese nemacheilines: A revision of nemacheiline loaches (Pisces: Cypriniformes) of Thailand, Burma, Laos, Cambodia and southern Viet -nam. Druckerei braunstein, München. Indochinese Nemacheilines, 262 pp.

Kottelat M, Chu XL (1988) Revision of *Yunnanilus* with descriptions of a miniature species flock and six new species from China (Cypriniformes, Homalopteridae). Environmental Biology of Fishes 23: 65–93. https://doi.org/10.1007/BF00000739

Miller MA, Pfeiffer W, Schwartz T (2010) "Creating the CIPRES Science Gateway for inference of large phylogenetic trees" in proceedings of the Gateway Computing Environments Workshop (GCE), 14 Nov. 2010, New Orleans, LA, 1–8. https://doi.org/10.1109/GCE.2010.5676129

Nichols JT (1925) Nemacheilus and related loaches in China. American Museum Novitates 171: 1.

Qin ZX, Shao WH, Du LN, Wang ZX (2024) A new species of *Yunnanilus* (Cypriniformes, Nemacheilidae) from Yunnan, southwest China. Zoosystematics and Evolution 100(2): 747–754. https://doi.org/10.3897/zse.100.122962

Ronquist F, Teslenko M, van der Mark P, Ayres DL, Darling A, Höhna S, Larget B, Liu L, Suchard MA, Huelsenbeck JP (2012) MrBayes 3.2: Efficient Bayesian phylogenetic inference and model choice across a large model space. Systematic Biology 61(3): 539–542. https://doi.org/10.1093/sysbio/sys029

Stamatakis A (2014) RAxML Version 8: A tool for phylogenetic analysis and post-analysis of large phylogenies. Bioinformatics 30(9): 1312–1313. https://doi.org/10.1093/bioinformatics/btu033

Tamura K, Stecher G, Kumar S (2021) Mega11: Molecular evolutionary genetics analysis version 11. Molecular Biology and Evolution 38(7): 3022–3027. https://doi.org/10.1093/molbev/msab120

Yang JX, Chen YR (1995) The biology and resource utilization of the fishes of Fuxian Lake, Yunnan. Yunnan Science and Technology Press, Kunming, China, 224 pp

Zhang E, Shen JZ (1999) Horny derivative of bone-fish skin—multicellular horny tubercle. Chinese Journal of Zoology 34(3): 52–56.

Zhu SQ (1989) The Loaches of the Subfamily Nemacheilinae in China (Cypriniformes, Cobitidae). Jiangsu Science & Technology Publishing House, Nanjing, China, 1–150.

Zoosyst. Evol. 101 (2) 2025, 473–483 | DOI 10.3897/zse.101.144042

PENSOFT

MUSEUM FÜR NATURKUNDE BERLIN

A new Pacific Ocean species of *Typhlonida* Macpherson & Baba, 2022 (Crustacea, Decapoda, Munididae) from the flank of the emergent seamount Isla del Coco (Costa Rica) with notes on the phylogeny of the genus

Dong Dong[1], Charlotte A. Seid[2], Xinzheng Li[1,3,4], Greg W. Rouse[2]

1 *Department of Marine Organism Taxonomy & Phylogeny, Qingdao Key Laboratory of Marine Biodiversity and Conservation, Institute of Oceanology, Chinese Academy of Sciences, Qingdao 266071, China*

2 *Scripps Institution of Oceanography, University of California San Diego, La Jolla, CA 92093, USA*

3 *University of Chinese Academy of Sciences, Beijing, China*

4 *Laoshan Lab, Qingdao 266237, China*

https://zoobank.org/C4CA66D7-90F7-4E69-A2BE-F692D9B39BA5

Corresponding authors: Greg W. Rouse (grouse@ucsd.edu); Xinzheng Li (lixzh@qdio.ac.cn)

Academic editor: M. Christodoulou ♦ **Received** 10 December 2024 ♦ **Accepted** 6 February 2025 ♦ **Published** 26 February 2025

Abstract

The genus *Typhlonida* Macpherson & Baba in Machordom et al. 2022 is a group of munidid squat lobsters typically found in deep waters. This study describes and illustrates a new species, *Typhlonida cocoensis* **sp. nov.**, from a seamount area in the eastern Pacific. *Typhlonida cocoensis* **sp. nov.** is closely related to *T. sanctipauli* (Henderson, 1885) but can be readily distinguished from the latter by its relatively small eyes, narrow anterior margin of the thoracic sternite 4, lack of granules on the lateral surfaces of sternite 7, and unarmed anterior branchial regions dorsally. In addition to morphological comparisons, genetic distance and phylogenetic analyses were used to support the recognition of this new species. The phylogenetic positions of the *Typhlonida* and *Antillimunida* species from the eastern Pacific are discussed.

Key Words

Eastern Pacific, phylogeny, squat lobsters, taxonomy, *Typhlonida*

Introduction

Munididae is a family of squat lobsters typically living in the deep waters of the continental shelf and slope (Baba et al. 2008). It is one of the most diverse groups of marine invertebrates in the world, currently containing 497 species worldwide (Machordom et al. 2022). *Munida* Leach, 1820, was once the largest genus in the Munididae, until it was divided into 11 genera by Machordom et al. (2022) based on morphological, molecular, and biogeographic analyses. Species with minor morphological differences have been shown to have significant genetic divergence (e.g., Macpherson et al. 2024). Given the complex interspecific variation and morphological similarity among some of these genera, molecular analysis is becoming necessary in the taxonomic determination of munidid species.

Despite the high species richness around the world, munidids show remarkably low biodiversity in the eastern Pacific, i.e., off the Pacific coast of the American continents. Only 22 species in seven genera have so far been reported from this vast area (Hendrickx 2003; Baba et al. 2008; Hendrickx and Ayón-Parente 2010; Liu et al. 2020; Gallardo Salamanca et al. 2021; Machordom et al. 2022): *Antillimunida bapensis* (Hendrickx, 2000), *A. gracilipes* (Faxon, 1893), *A. hispida* (Benedict, 1902), *Babamunida obesa* (Faxon, 1893), *Dactylonida mexicana* (Benedict,

1902), *Grimothea curvipes* (Benedict, 1902), *G. debilis* (Benedict, 1902), *G. gregaria* (Fabricius, 1793), *G. johni* (Porter, 1903), *G. lipkeholthuisi* (Hendrickx & Ayón-Parente, 2010), *G. macrobrachia* (Hendrickx, 2003), *G. monodon* (H. Milne Edwards, 1837), *G. montemaris* (Bahamonde & López, 1962), *G. planipes* (Stimpson, 1860), *G. quadrispina* (Benedict, 1902), *Iridonida refulgens* (Faxon, 1893), *I. tenella* (Benedict, 1902), *I. williamsi* (Hendrickx, 2000), *Trapezionida diritas* (Gallardo Salamanca & Macpherson, 2021), *Typhlonida perlata* (Benedict, 1902), *T. propinqua* (Faxon, 1893), *T. alba* (Liu, Li & Lin, 2020). *Typhlonida microphthalma* (A. Milne-Edwards, 1880) was once reported from Cocos Island (Faxon, 1893, 1895), but the record was questionable (Hendrickx 2000; Baba et al. 2008).

Unlike in other regions, some species of Munididae in the eastern Pacific, such as *G. monodon* and *G. johni*, can aggregate into large populations and are therefore of high commercial value, so the genetic diversity and evolutionary history of those species are well documented (e.g., Haye et al. 2010). In contrast, most species are still seldom reported due to their restricted distribution, deep-sea habitat, or low abundance, and therefore remain poorly studied at the genetic level (Hendrickx 2000, 2021). Genetic data are available for only nine species in the eastern Pacific for phylogenetic studies.

In January 2019, a research expedition was organized to investigate the biodiversity of deep-sea seamounts off the Pacific margin of Costa Rica, during which several munidid specimens were collected. A new species of *Typhlonida* Macpherson & Baba in Machordom et al. 2022 was recognized after morphological examination and molecular analyses. The phylogenetic relationships of species within the genus *Typhlonida* were investigated through a phylogenetic reconstruction including the new species and other newly sequenced species from the eastern Pacific. The new species is hereby described and illustrated, contributing to the species and genetic biodiversity of the munidid fauna in the eastern Pacific.

Materials and methods

Sample collection and morphological examination

The material for this study was collected during the Schmidt Ocean Institute research cruise FK190106 in the seamount area of Cocos Canyon, off the Pacific coast of Costa Rica. The specimen was collected using the remotely operated vehicle (ROV) *SuBastian* deployed from the research vessel *Falkor*. The collected specimen was photographed alive and fixed in 95% ethanol. Specimen collection and field operations in Costa Rica were performed under permits INCOPESCA-CPI-003-12-2018 and R-070-2018-OT-CONAGEBIO, issued by the Government of Costa Rica. DNA sequencing for this project was authorized by the contract for the grant of prior informed consent between MINAE-SINAC-ACMC and Jorge Cortés Núñez for the basic research project: "FK190106 – Cuantificación de los vínculos biológicos, químicos y físicos entre las comunidades quimiosintéticas con el mar profundo circundante."

The size of the specimen is given as the postorbital carapace length (pcl), which refers to the carapace length excluding the rostrum. The terminology used mainly follows Machordom et al. (2022). The specimen collected during the expedition was deposited in El Museo de Zoología de la Universidad de Costa Rica (MZUCR), and a tissue sample was deposited in the Scripps Institution of Oceanography Benthic Invertebrate Collection (SIO-BIC). The abbreviations used in the text are as follows: P1, pereiopod 1 (chelipeds); P2–4, pereiopods 2 to 4 (first to third walking legs).

DNA extraction, amplification, and sequencing

To explore the relationships of the new species with other munidid species from the eastern Pacific, we included *T. propinqua* and *A. bapensis*, which are deposited at SIO-BIC, and the holotype of *T. alba* (with the help of Dr. Liu Xinming, currently deposited at the Marine Biology Museum, Chinese Academy of Sciences), in the phylogenetic study (Suppl. material 1). These three species, together with the new species, were selected for gene marker sequencing in this study.

Total genomic DNA was extracted from pereiopods and abdominal muscle tissue using the Zymo Research DNA-Tissue Miniprep Kit (Irvine, California, USA) and EasyPure Marine Animal Genomic DNA Kit (TransGen). Partial sequences of two mitochondrial genes, cytochrome c oxidase subunit I (COI) and 16S rRNA (16S), and one nuclear gene, histone 3 (H3), were amplified via polymerase chain reaction (PCR). The primers used for COI amplification were HCO2198 and LCO1490 (Folmer et al. 1994). The primers used for 16S amplification were 16Sar and 16S1472 (Simon et al. 1994; Crandall and Fitzpatrick 1996). The primers used for H3 amplification were AF and AR (Colgan et al. 1998). Reactions were carried out following the original procedures with minor modifications. PCR products were purified using the ExoSAP-IT protocol (USB Affymetrix, Ohio, USA), and Sanger sequencing was performed in both directions by Eurofins Genomics (Louisville, Kentucky, USA) and Tsingke Biotech Co., Ltd. (Beijing, China). Sequences were checked and assembled based on the contigs using the DNASTAR LASERGENE software package (DNASTAR, Inc., Madison, WI, USA). New sequences obtained in this study were deposited in GenBank (PQ599895–PQ599898, PQ604650–PQ604652, PQ621049–PQ621051).

Genetic distances and phylogenetic analyses

A total of 124 sequences (including three genes) of 46 species in Munididae were downloaded from NCBI GenBank for genetic distances and phylogenetic analyses

(Suppl. material 1). These species cover all 11 genera newly established or revised by Machordom et al. (2022) from *Munida sensu lato*, and another two genera, *Babamunida* Cabezas, Macpherson & Machordom, 2008, and *Garymunida* Macpherson & Baba in Machordom et al. 2022, to represent all four major lineages of Munididae recovered in Machordom et al. (2022). To verify the systematic status of the new species, we included all the available genetic data for the genus *Typhlonida* (species with at least a COI sequence), as well as all species of Munididae from the eastern Pacific in the phylogenetic study (Suppl. material 1). *Munidopsis kexueae* Dong, Gan & Li, 2021 was chosen as the outgroup.

The sequences of each gene were aligned using the software MAFFT (Katoh and Standley 2013) and then manually trimmed. The average genetic distances between the new species and closely related species, based on COI sequences, were estimated under the Kimura 2-parameter model (Kimura 1980) in MEGA 6 (Tamura et al. 2013).

The two mitochondrial genes were combined to generate a "mito-dataset," which includes 51 species (including the new species and outgroup, similarly hereinafter). All three genes were concatenated to generate an "all-dataset" (including 39 species with the H3 gene and at least one mitochondrial gene). Both datasets were partitioned by genes and codons, and the best nucleotide base substitution models were estimated using PARTITIONFINDER 2 (Lanfear et al. 2017). Phylogenetic relationships were inferred from both datasets using maximum likelihood (ML) by IQ-TREE (Nguyen et al. 2015) and Bayesian inference by MRBAYES (Ronquist et al. 2012). Nodal supports of ML trees were evaluated in two approaches: SH-aLRT branch test (Guindon et al. 2010) using 1000 replicates and ultrafast bootstrap (UFBoot) with 5000 replicates (Minh et al. 2013). Bayesian inferences were run for at least 3 million generations, and the nodal support was assessed with posterior probabilities (PP). The first 25% of the initial trees were discarded as burn-in. The implementation of MAFFT, PARTITIONFINDER2, IQ-TREE, and MRBAYES was pipelined in the program PHYLOSUITE (Zhang et al. 2020).

Result

Phylogenetics

Ten new sequences were obtained in this study: four of COI, three of 16S, and three of H3. The final alignment length of each gene was as follows: COI (639 bp), 16S (506 bp), and H3 (328 bp).

The phylogenetic trees generated from the mito-dataset (Fig. 1) and all-dataset (Suppl. material 2) were mostly congruent. Similarly, the topologies of the ML and Bayesian trees were consistent on the relationships of the main clades. According to the trees derived from the mito-dataset, the new species was paired with *T. sanctipauli* (Henderson, 1885), but this relationship was only supported by the UFBoot value (= 100). All the species of *Typhlonida* formed a clade, which roughly contained two subclades. One subclade (subclade I) included only species from the eastern Pacific and Atlantic Oceans, with high support in the mito-dataset trees (SH-aLRT = 89.4, PP = 0.99), while in the all-dataset-derived trees, it was only supported by the PP value (=0.99). It is noteworthy that *Antillimunida bapensis* was recovered within this subclade, rather than clustering with other *Antillimunida* species. A second subclade (subclade II), which mainly consists of Indo-West Pacific species, was highly supported by all inference methods.

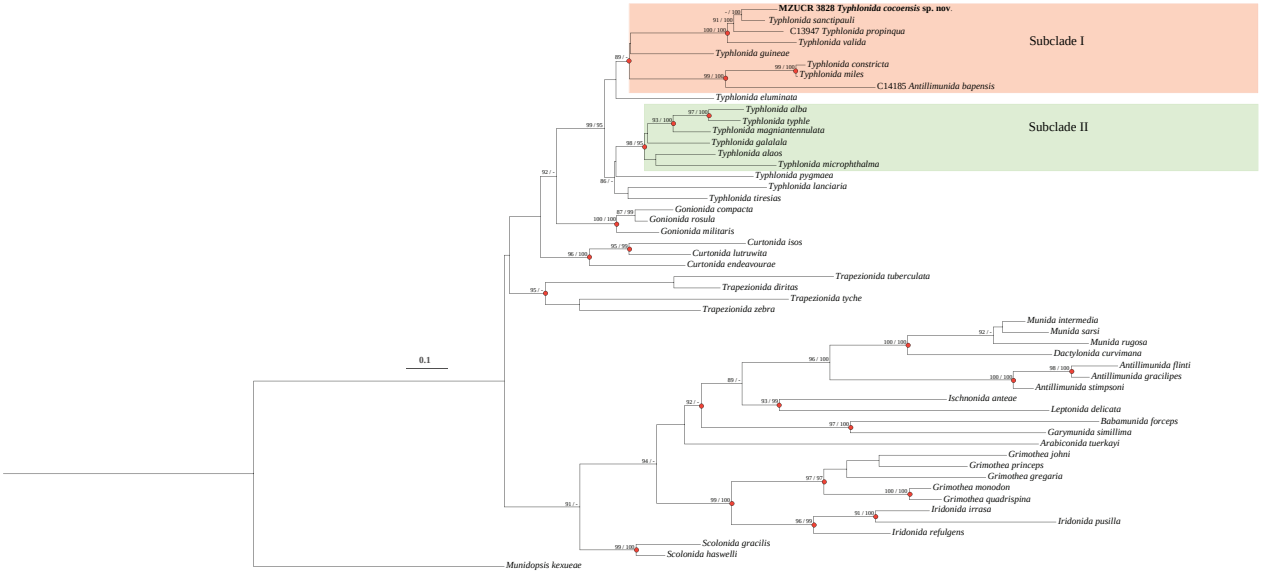

Figure 1. Phylogenetic tree obtained after the maximum likelihood analysis based on the mito-dataset. SH-aLRT value (percentage, left) and UFBoot value (right) are indicated adjacent to each node. Only values of SH-aLRT ≥ 85% and UFBoot ≥ 95% are shown. Nodes with PP support above 0.95 are marked with red circles.

Systematics

Superfamily Galatheoidea Samouelle, 1819

Family Munididae Ahyong, Baba, Macpherson & Poore, 2010

Genus *Typhlonida* Macpherson & Baba in Machordom et al., 2022

***Typhlonida cocoensis* sp. nov.**

https://zoobank.org/6D7B968B-78B4-4FD8-B5CB-FA58E9B00AFB

Figs 2–5

Material examined. ***Holotype*** • MZUCR 3828 (tissue sample SIO-BIC C13940), female (pcl 10.7 mm), Cocos Canyon, Isla del Coco, Costa Rica, eastern Pacific, 5.5821°N, 87.0657°W, 831.5 m, coll. Greg Rouse and Avery Hiley, using ROV *SuBastian* on R/V *Falkor*, dive S0223, event S8, cruise FK190106, 18 January 2019.

Diagnosis. Carapace slightly longer than broad (excluding rostrum); branchial margins with 5 spines; posterior margin unarmed. Sternite 3 posterior margin contacting sternite 4 on median 0.3 part; sternite 4 triangular; lateral surfaces of sternite 7 smooth. Pleonal tergites 2 with 9 spines on anterior ridge. Eyes moderately large; diameter of cornea approximately twice wider than sinus between rostral spine and supraocular spine. Basal article of antennular peduncle with distolateral spine more than twice longer than distomesial spine. Merus of third maxilliped with three spines on flexor margin. Lateral margin of P1 fixed finger with small paired subterminal spines followed by row of spines; mesial margin of P1 dactylus only with basal spine.

Description. Carapace: Slightly longer than broad (excluding rostrum), approximately 1.3 times longer than broad. Frontal margin oblique. Lateral margins slightly convergent posteriorly; anterolateral spines strong, tip falling short of base of supraocular spine; hepatic margin convex, with acute spine and additional small spines; branchial margin armed with 5 spines; posterior branchial margin with oblique ridges; posterior margin unarmed. Dorsal surface gently convex transversely; cervical grooves clear; main transverse ridges present on gastric, cardiac, intestinal, and posterior branchial regions bearing fine setae anteriorly; short scale-like rugae present among main ridges and on epigastric, hepatic, and anterior branchial regions; postcervical spines well developed; gastric region elevated, with pairs of strong epigastric spines posterior to supraorbital spines and each flanked by relatively short mesial and posterolateral spines; additional pair of minute epigastric spines present laterally. Rostral spine spiniform, dorsally carinate, approximately 0.4 times remaining carapace length, horizontal in lateral view; supraocular spines spiniform and subparallel, smoothly carinate, approximately 0.4 times of rostral spine length, slightly overreaching distal end of cornea. Pterygostomial flaps with transverse or oblique ridges on lateral surface, anterior part with shallow groove near dorsal margin; anterior end with acute small spine.

Sternal plastron: longer than broad; posterior margin distinctly concave. Sternite 3 approximately 3.6 times as broad as long, anterior margin bilobate and faintly denticulate; posterior margin contacting sternite 4 on median 0.3 part; lateral parts slightly bent ventrally. Sternite 4 triangular, anterolateral margins straight; ventral surface excavated, bearing several scale-like rugae. Sternite 5 and 6 with transverse, interrupted ridges and shallowly grooved along midline. Sternite 7 smooth on lateral parts, with oblique ridges posteriorly and deep cavity medially.

Pleon: Tergite 2 with 9 spines evenly along anterior ridge. Dorsal surfaces of tergites 2–5 each with 2 transverse ridges interspaced by shallow groove; lateral part of each segment with scale-like rugae.

Telson: Broader than long; divided into 8 plates. Dorsal surface with scale-like rugae.

Eyes: Moderately large. Cornea dilated, hemispheric, slightly wider than eyestalk, diameter approximately twice wider than sinus between rostral spine and supraocular spine, and third of distance between bases of anterolateral spines. Distal margin of cornea reaching proximal third of rostral spine; eyelash dense.

Antennular peduncle: Basal article (excluding distal spines) approximately 2.3 times longer than broad, reaching distal 0.4 of rostral spine. Distolateral spine more than twice longer than distomesial spine. Lateral margin with 2 median spines. Ventral surface with scale-like rugae.

Antennal peduncle: Reaching distal cornea margin. Article 1 immovable, with strong distomesial spine hardly reaching distal end of article 2. Article 2 armed with strong distomesial spine reaching distal end of article 3, and distolateral spine falling short of distal end of article 3; mesial margins with small median tubercles. Article 3 subrectangular, unarmed. Article 4 short and unarmed.

Third maxilliped: Ischium slightly longer than merus, with weak distoflexor and disto-extensor spines; ventral surface with row of short rugae on midline. Merus with three spines on flexor margin: proximal and distal spines strong, median spine minute; extensor margin strongly rugose, with small distal spine; ventral surface scattered with short rugae. Carpus, propodus, and dactylus unarmed.

P1: Subequal, 1.8 times pcl; each segment covered with thick, long, and non-iridescent setae, bearing numerous scale-like rugae on surfaces and margins. Merus approximately 0.7 times PCL, 3.9 times as long as broad; distal margin with strong dorsal, dorsomesial, ventromesial, and lateral spines; distal dorsal spine followed by row of 7 spines or acute tubercles decreasing in size proximally extending to proximal end of merus; distal dorsomesial spine followed by 2 dorsal spines and another prominent ventral spine. Carpus subcylinderical, approximately half of merus length, 2.0 times longer than broad; distal margin with distinct dorsal, dorsomesial, and small ventrolateral spines; distal dorsal spine followed by row of 4 spines on dorsal midline, distal dorsomesial spine followed by row of 4 spines (distal second and third spines most prominent), 2 spines along dorsolateral margin, 2 spines on ventral midline, several tubercle-like spines on lateral margin,

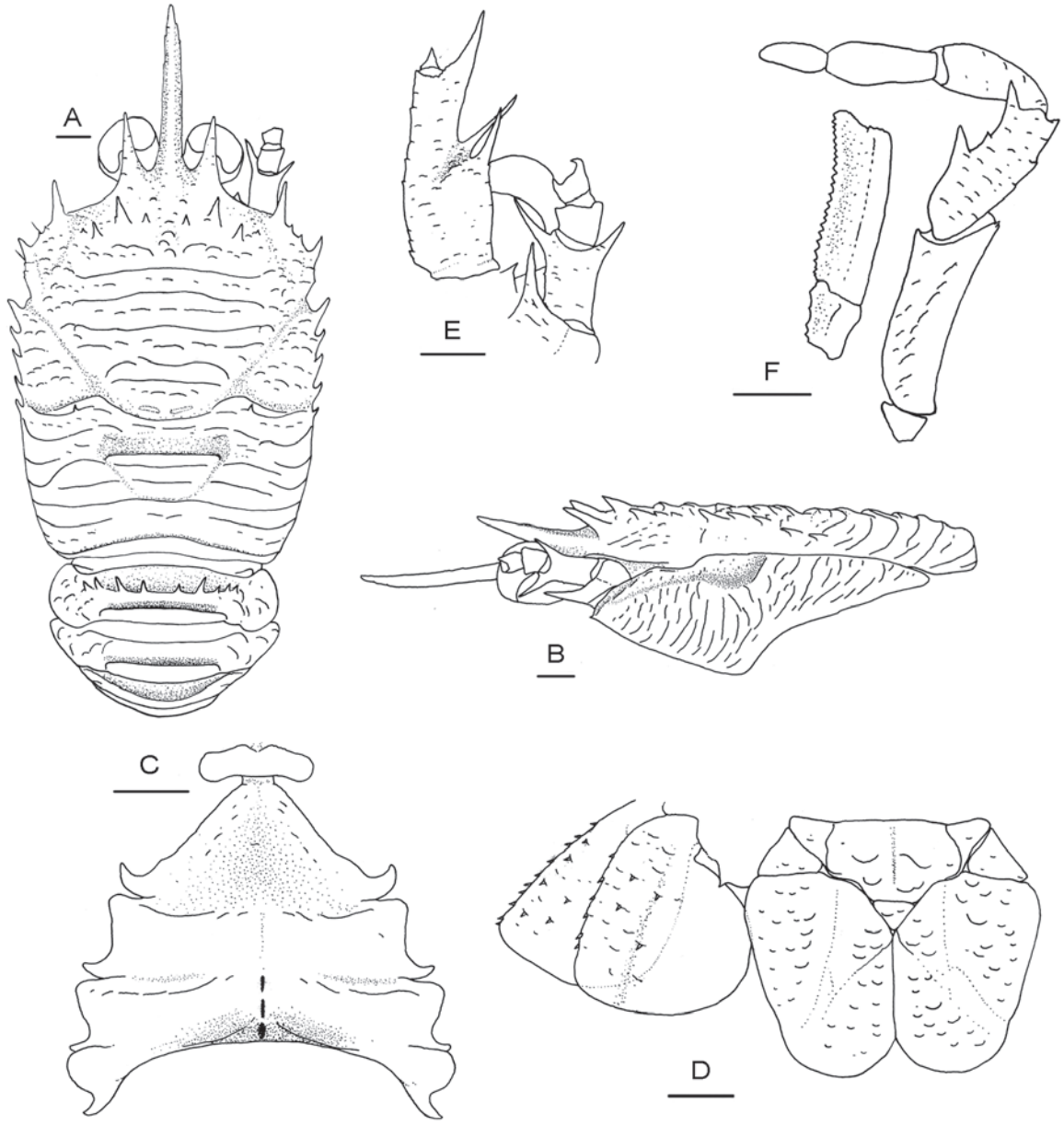

Figure 2. *Typhlonida cocoensis* sp. nov., MZUCR 3828, holotype, female. **A.** Carapace and pleonal tergite 1–4, dorsal view; **B.** Carapace and left pterygostomian flap, lateral view; **C.** Sternal plastron, ventral view; **D.** Telson and left uropod; **E.** Left antennular and antennal peduncles, ventral view; **F.** Left third maxilliped, ventral view. Scale bars: equal 1.0 mm.

and 2 or 3 small spines near distoventral margin. Palm relatively compressed, 0.6 times merus length, 2.7 times longer than broad; dorsal surface with small distal spine adjacent to base of dactylus and row of 3 spines along midline, dorsomesial margin with row of 5 spines, dorsolateral margin with row of 17 spines of different sizes extending from proximal end of palm to subdistal end of fixed finger, ventromesial margin with row of 5 spines (distalmost spines much prominent). Fingers approximately 0.9 times palm length, tips hooked; occlusal margins nearly straight, denticulate; lateral margin of fixed finger with small paired subterminal spines followed by row of spines mentioned above; mesial margin of movable finger with single strong basal spine and acute tubercles proximally.

P2 and P4 (P3 missing): Surfaces of merus, carpus, and propodus with fine rugae; extensor margins bearing dense setae; P2 approximately 1.6 times pcl, reaching midlength of P1 palm. Meri compressed; P2 merus approximately 0.6 times pcl, P4 merus 0.7 times P2 merus length; length-width ratio: P2 and P4 meri being 5.2 and 4.3, respectively; extensor margin with row of slender spines (disto-extensor spine strongest) on P2, and scattered minute spines on P4; flexor margin with row of spines (decreasing in size proximally) on entire length of P2, and only single strong distal spine followed by row of elevated scale-like rugae on P4. Carpi subequal in length and width on P2 and P4, approximately 0.3 times P2 merus length; extensor margin with 2 longitudinal ridges, mesial ridge with 4 spines

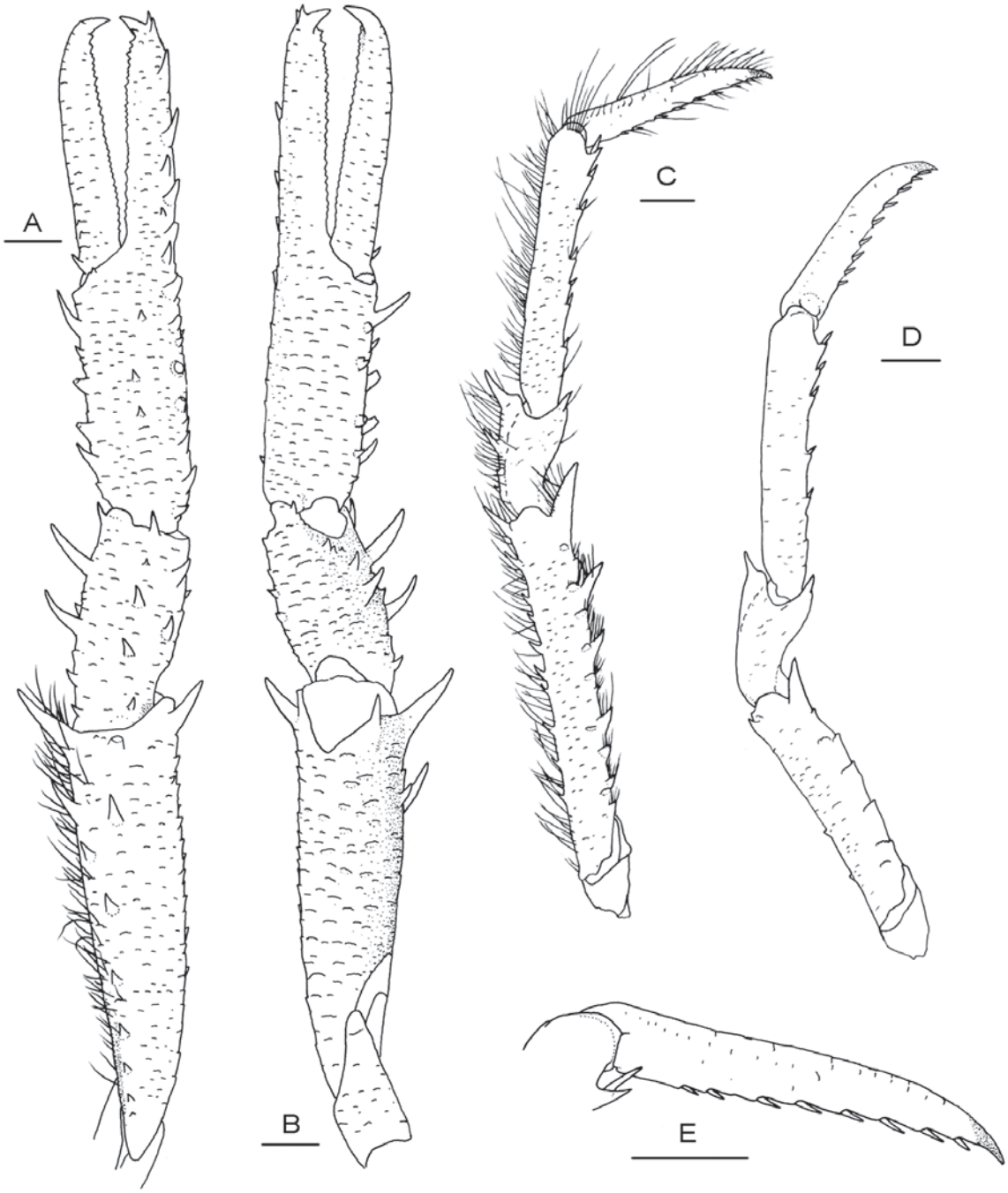

Figure 3. *Typhlonida cocoensis* sp. nov., MZUCR 3828, holotype, female. **A.** Right P1, setae illustrated only on mesial margin of merus, dorsal view; **B.** Right P1, ventral view; **C.** Right P2, lateral view; **D.** Right P4, lateral view; **E.** Dactylus of right P2, lateral view. Setae omitted on **B, D**, and **E**. Scale bars: equal 1.0 mm.

(distal two much prominent) on P2 and only single distal spine on P4, lateral ridge low and unarmed; flexor margin with prominent distoflexor spine. Propodi slender, subequal in width; P4 propodus 0.9 times P2 propodus length; length-width ratio: P2 and P4 propodus being 7.2 and 6.3, respectively; extensor margin straight; flexor margin with 5–7 corneous spines, distalmost spine based on acute tooth paired with small mesial spine. Dactyli subequal in length, P2 dactylus approximately 0.6 times of P2 propodus length, 5.7 times longer than broad; extensor margin straight, with feeble rugae; flexor margin straight, armed with 8 or 9 movable corneous spines on entire length.

Coloration. Dorsal surfaces of carapace and pleon generally light orange; anterior part of carapace, including rostral spine, supraocular spines, anterolateral spines, and epigastric spines, red-orange. Pereiopods whitish.

Habitat. Submarine canyon on the flank of Isla del Coco, Costa Rica.

Distribution. Only known from the type locality, depth 831.5 m.

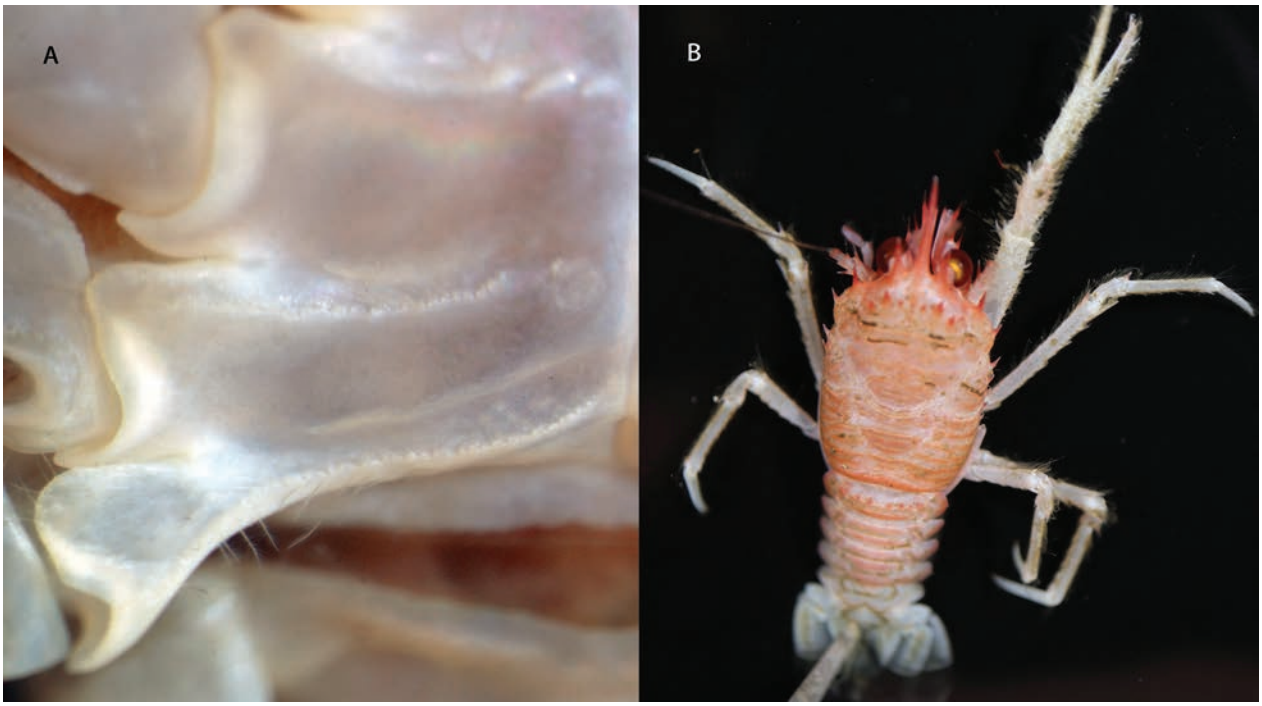

Figure 4. *Typhlonida cocoensis* sp. nov., MZUCR 3828, holotype, female. **A.** Sternite 5–7 on the right side, ventral view; **B.** color in life, dorsal view.

Etymology. Named in honor of the type locality off Isla del Coco (Cocos Island), an oceanic island protected within Parque Nacional Isla del Coco and designated as a UNESCO World Heritage Site for its rich biodiversity. We thank Jorge Cortés Núñez, Universidad de Costa Rica, for proposing this name and for his contributions to deep-sea research and biodiversity studies of Isla del Coco (Cortés 2012).

Remarks. The new species is characterized by the moderately dilated cornea, distomesial spine of antennular article 1 less than half length of distolateral spine, short distomesial spines of basal and second antennal articles, 5 branchial marginal spines, and triangular and narrow thoracic sternite 4. These morphological features link the new species to the genus *Typhlonida* (Machordom et al. 2022). The new species has flat and smooth lateral surfaces of the thoracic sternite 7, with the transverse ridges of sternite 7 extending posterior to rather than onto the lateral surface. This character distinguishes the new species from other congeners in *Typhlonida*. This character assimilates the new species to a group of species with lateral surfaces of sternite 7 granulated. For the new species, however, no granulation was observed on the lateral surfaces (Fig. 4A).

The new species is morphologically close to *T. sanctipauli*, which is distributed in the East and West Atlantic Ocean (Baba et al. 2008). Both species have a row of spines only on the anterior ridge of pleonal tergite 2, 2 flexor spines on the merus of the third maxilliped, and the P2 meri with row of spines on the flexor margin. The new species differs from *T. sanctipauli* in the following characters: The eyes are relatively small with the cornea width approximately a third of the distance between bases of the anterolateral spines; anterior margin of the thoracic sternite 4 is very narrow, contacting median 0.3 of the posterior margin of sternite 3; the lateral surfaces of sternite 7 are smooth; and the anterior branchial regions are unarmed. In *T. sanctipauli*, the eyes are comparatively large with the cornea width more than 0.4 times the distance between the bases of the anterolateral spines; anterior margin of the sternite 4 broad, contacting at least half length of the posterior margin of sternite 3; the lateral surfaces of sternite 7 are granulated; and the anterior branchial region has one dorsal spine (de Saint Laurent and Macpherson 1988; de Melo-Filho and de Melo 1992).

Among the munidid species distributed in the eastern Pacific, the new species is morphologically similar to *Grimothea curvipes*, which is known only from the deep sea (1890–2743 m) off southern Chile (Retamal et al. 2020). Both species have five branchial marginal spines, a moderately dilated cornea, a narrow anterior margin of sternite 4, a row of spines on the anterior ridge of pleonal tergite 2, two flexor spines on the merus of the third maxilliped, and a row of spines on the flexor margin of P2 meri. The genus *Grimothea* Leach, 1820, is characterized by article 1 of the antennal peduncle being fused with the lateral margin of the epistome. By contrast, *Typhlonida* and other munidid genera (except *Iridonida*) have this article clearly separated from the epistome. This feature, however, is still unclear on *G. curvipes* based on the previous descriptions of the holotype (Benedict 1902; Hendrickx 2003); therefore, the taxonomic position of *G. curvipes* remained dubious and temporarily assigned to *Grimothea* (Machordom et al. 2022). Besides the difference in generic characters, the new species readily differs from *G. curvipes* in having

Figure 5. *Typhlonida cocoensis* sp. nov. in habitat; depth 831.5 m, Cocos Canyon; image credit ROV SuBastian/Schmidt Ocean Institute.

flat and smooth lateral surfaces of sternite 7, a short distomesial spine of antennular article 1, unarmed articles 3 and 4 of the antennal peduncle, a weak distoflexor spine of the third maxilliped ischium, and a row of spines on the entire lateral margin of the P1 fixed finger. In *G. curvipes*, the transverse ridges of sternite 7 extend onto the lateral surfaces; the distomesial and distolateral spines of antennular article 1 are subequal (distolateral spine slightly longer); articles 3 and 4 of the antennal peduncle each have small distolateral spines; the ischium of the third maxilliped has a strong distoflexor spine; and the P1 fixed finger only has distal and basal spines (Hendrickx 2003).

Only three *Typhlonida* species have been previously reported in the eastern Pacific: *T. alba*, *T. perlata*, and *T. propinqua*. Due to the lack of molecular data, all these species were assigned to *Typhlonida* based on morphology (Machordom et al. 2022). The new species resembles *T. perlata*, which occurs in the deep sea from the Gulf of California to the Galápagos Islands (Baba et al. 2008). Besides the structure of the sternite 7, *T. perlata* is different from the new species in having a relatively small cornea of the eyes with the diameter approximately as wide as the sinus between the rostral spine and supraocular spine (instead of more than two times wider), the flexor margin of the third maxilliped merus with a single spine (instead of two spines), and the dactylus of the P1 unarmed on the mesial margin (instead of with a strong basal spine) (Hendrickx 2000).

Faxon (1893, 1895) once reported *Munida microphthalma* (= *T. microphthalma*) from Cocos Island based on a single ovigerous female, but the identity of the specimen was in doubt (Hendrickx 2000; Baba et al. 2008). *Typhlonida microphthalma* differs from the new species in having the granulated lateral surfaces of sternite 7, the much-reduced cornea, and the antennal article 3 armed with a distomesial spine (Hendrickx 2000). Faxon (1893, 1895) noted that the Cocos specimen had no spines on the P1 dactylus and the dorsal surface of the palm, and only two spines on the pleonal tergite 2; these characters are also inconsistent with those of the new species.

The smallest genetic distance based on COI was observed between the new species and *T. sanctipauli*, at 5.8%, showing a moderate genetic divergence commensurate with other interspecific distances in Munididae (Macpherson et al. 2024). The GenBank accession numbers of sequences obtained in this study are provided in Suppl. material 1.

Discussion

The phylogenetic trees recovered in this study are congruent with those of Machordom et al. (2022) regarding the monophyly of each genus. The *Typhlonida* clade can essentially be divided into two subclades, which is also

consistent with the results of Machordom et al. (2022), based on the concatenated genes and COI sequence, respectively (figs 7 and S2 in Machordom et al. 2022).

The new species, together with *T. propinqua* and *T. alba*, was placed within the *Typhlonida* clade in both trees derived from the mito-dataset (Fig. 1) and all-dataset (Suppl. material 2). The new species was sister to *T. sanctipauli*, supported by a robust ultrafast bootstrap value (from the mito-dataset), demonstrating an agreement of the phylogenetic and morphological analyses on the relationship between the two species. In subclade I, the new species and two other eastern Pacific species (*T. propinqua* and *A. bapensis*) were grouped with five species from the Atlantic Ocean. *Typhlonida* is characterized by having small corneas (Machordom et al. 2022). However, these eight species have relatively large or moderate-sized eyes with the cornea markedly dilated, resulting in the projection of the supraocular spine on the median or mesial part of the cornea. In contrast, *Typhlonida* species in subclade II have much-reduced small corneas, with most parts of the eyestalk and cornea located between the supraocular spine and the rostral spine. It is interesting to note that subclade II includes species from the West Pacific, eastern Pacific, and Atlantic Oceans, suggesting that the members of this phenotype are globally distributed. The phylogenetic status of other *Typhlonida* species, however, remains still unclear, as they do not belong to any subclade with significant support according to the results of both ML and BI analyses.

It is noteworthy that *A. bapensis* was within the *Typhlonida* clade, which was supported by each inference method. Molecular data of the *Antillimunida* species from the eastern Pacific were lacking in previous studies. *Antillimunida* morphologically differs from *Typhlonida* mainly in having a spinose posterior margin of the carapace, a longer P4 merus distally reaching to the anterior margin of the carapace, and a single spine on the flexor margin of the third maxilliped merus (Machordom et al. 2022). Re-examination of the specimens of *A. bapensis* and *A. hispida* from SIO-BIC shows that both species have a short P4 merus and at least two flexor spines on the third maxilliped merus. However, the spine patterns on the carapace can still link the two species to other congeners.

Machordom et al. (2022) inferred that the ancestral range for most of the munidid lineages was in the West Pacific region; nevertheless, for *Typhlonida*, the eastern Pacific specimens were absent in that biogeographic analysis. It is necessary to include more species and sufficient genetic data, particularly from type localities, in the future to clarify the true systematic status of the two genera *Typhlonida* and *Antillimunida*, as well as their evolutionary history and dispersal route around the world.

Acknowledgements

We thank the captain and crew of R/V *Falkor* cruise FK190106, the pilots and technicians of ROV *SuBastian*, chief scientist Erik Cordes, collaborator Jorge Cortés Núñez at the University of Costa Rica, and the cruise science participants for their crucial assistance with specimen collection. We are grateful to Zihui Shen for providing valuable post-preservation photos of the specimen. Operations at sea were funded by the Schmidt Ocean Institute. The study was also supported by the National Natural Science Foundation of China (No. 42176114) and the Biological Resources Programme, Chinese Academy of Sciences (CAS-TAX-24-029).

References

Ahyong ST, Baba K, Macpherson E, Poore GCB (2010) A new classification of the Galatheoidea (Crustacea: Decapoda: Anomura). Zootaxa 2676: 57–68. https://doi.org/10.11646/zootaxa.2676.1.4

Baba K, Macpherson E, Poore GCB, Ahyong ST, Bermudez A, Cabezas P, Lin C-W, Nizinski M, Rodrigues C, Schnabel KE (2008) Catalogue of squat lobsters of the world (Crustacea: Decapoda: Anomura – families Chirostylidae, Galatheidae and Kiwaidae). Zootaxa 1905: 1–220. https://doi.org/10.11646/zootaxa.1905.1.1

Bahamonde N, López MT (1962) Un galatheido nuevo para Chile. *Munida montemaris* n. sp. (Crustacea Decapoda, Anomura). Revista Chilena de Historia Natural 55: 85–91. https://rchn.biologiachile.cl/pdfs/1960-1963/1/Bahamonde_&_Lopez_1962.pdf

Benedict JE (1902) Description of a new genus and forty six new species of crustaceans of the family Galatheidae with a list of the known marine species. Proceedings of the Biological Society of Washington 26: 243–334. https://doi.org/10.5479/si.00963801.26-1311.243

Cabezas P, Macpherson E, Machordom A (2008) A new genus of squat lobster (Decapoda: Anomura: Galatheidae) from the South West Pacific and Indian Ocean inferred from morphological and molecular evidence. Journal of Crustacean Biology 28: 68–75. https://doi.org/10.1651/07-2823R.1

Colgan DJ, McLauchlan A, Wilson GDF, Livingston SP, Edgecombe GD, Macaranas J, Cassis G, Gray MR (1998) Histone H3 and U2 snRNA DNA sequences and arthropod molecular evolution. Australian Journal of Zoology 46: 419–437. https://doi.org/10.1071/ZO98048

Cortés J (2012) Marine biodiversity of an Eastern Tropical Pacific oceanic island, Isla del Coco, Costa Rica. Revista de Biología Tropical 60 (Supplement 3): 131–185. https://doi.org/10.15517/rbt.v60i3.28356

Crandall KA, Fitzpatrick Jr JF (1996) Crayfish molecular systematics: using a combination of procedures to estimate phylogeny. Systematic Biology 45: 1–26. https://doi.org/10.1093/sysbio/45.1.1

de Melo-Filho GAS, de Melo GAS (1992) Reexamination of the material of *Munida* Leach (Crustacea: Anomura: Galatheidae) collected by the H.M.S. Challenger (1872–1876) along the Brazilian Coast. Proceedings of the Biological Society of Washington 105: 760–774. https://decapoda.nhm.org/pdfs/29511

de Saint Laurent M, Macpherson E (1988) *Munida benguela*, espèce nouvelle d'Afrique du Sud. Comparaison avec *Munida sanctipauli* Henderson, 1885 (Crustacea: Decapoda: Galatheidae). Bulletin du Muséum National d'Histoire Naturelle 4: 105–115. https://doi.org/10.5962/p.287498

Dong D, Gan Z, Li X (2021) Descriptions of eleven new species of squat lobsters (Crustacea: Anomura) from seamounts around the Yap and Mariana Trenches with notes on DNA barcodes and phylogeny. Zoological Journal of the Linnean Society 192: 306–355. https://doi.org/10.1093/zoolinnean/zlab003

Fabricius JC (1793) Entomologia systematica emendata et aucta. Secundum classes, ordines, genera, species adjectis synonymis, locis; observatiosnibus, descriptionibus. Hafniae, 519 pp. https://doi.org/10.5962/bhl.title.125869

Faxon W (1893) Reports on the dredging operations off the west coast of Central America to the Galapagos, to the west coast of Mexico, and in the Gulf of California, in charge of Alexander Agassiz, carried on by the U.S. Fish Commission Steamer "Albatross", during 1891 ... VI. Preliminary descriptions of new species of Crustacea. Bulletin of the Museum of Comparative Zoology at Harvard College 24: 149–220.

Faxon W (1895) Reports on an exploration off the west coasts of Mexico, Central and South America, and off the Galapagos Islands, in charge of Alexander Agassiz, by the U.S. Fish Commission steamer "Albatross," during 1891, Lieut.-Commander Z.L. Tanner, U.S.N. commanding. XV. The stalk-eyed Crustacea. Memoirs of the Museum of Comparative Zoology at Harvard College 18: 1–292.

Folmer O, Black M, Hoeh W, Lutz R, Vrijenhoek R (1994) DNA primers for amplification of mitochondrial cytochrome c oxidase subunit I from diverse metazoan invertebrates. Molecular Marine Biology and Biotechnology 3: 294–299. https://api.semanticscholar.org/CorpusID:13287260

Gallardo Salamanca MA, Macpherson E, Tapia Guerra JM, Asorey CM, Sellanes J (2021) A new species of *Munida* Leach, 1820 (Crustacea: Decapoda: Anomura: Munididae) from seamounts of the Nazca-Desventuradas Marine Park. PeerJ 9: e10531. https://doi.org/10.7717/peerj.10531

Guindon S, Dufayard JF, Lefort V, Anisimova M, Hordijk W, Gascuel O (2010). New algorithms and methods to estimate maximum-likelihood phylogenies: assessing the performance of PhyML 3.0. Systematic Biology 59: 307–321. https://doi.org/10.1093/sysbio/syq010

Haye PA, Salinas P, Acuña E, Poulin E (2010) Heterochronic phenotypic plasticity with lack of genetic differentiation in the southeastern Pacific squat lobster *Pleuroncodes monodon*. Evolution & Development 12: 628–634. https://doi.org/10.1111/j.1525-142X.2010.00447.x

Henderson JR (1885) XXXIX. – Diagnoses of the new species of Galatheidea collected during the 'Challenger' expedition. Annals and Magazine of Natural History 16: 407–421. https://doi.org/10.1080/00222938509459908

Hendrickx, ME (2000) The genus *Munida* Leach (Crustacea, Decapoda, Galatheidae) in the eastern tropical Pacific, with description of two new species. Bulletin de l'Institut Royal des Sciences Naturelles de Belgique 70: 163–192. https://research.nhm.org/pdfs/29679

Hendrickx ME (2003) The temperate species of the genus *Munida* Leach (Crustacea, Decapoda, Galatheidae) in the east Pacific, with the description of a new species and additional records for tropical-subtropical species. Bulletin de l'Institut Royal des Sciences Naturelles de Belgique 73: 115–136. https://research.nhm.org/pdfs/29681

Hendrickx ME (2021) Squat lobsters (Crustacea: Decapoda: Anomura: Galatheoidea) from off the northwestern coast of the Baja California Peninsula, Mexico. Zootaxa 4965: 375–384. https://doi.org/10.11646/zootaxa.4965.2.10

Hendrickx ME, Ayón-Parente M (2010) A new species of *Munida* Leach (Decapoda, Galatheidae) from off the West Coast of Baja California, Mexico. In: Fransen, CHJM, De Grave S, Ng PKL (Eds) Studies on Malacostraca: Lipke Bijdeley Holthuis Memorial Volume. Crustaceana Monographs 14: 305–314. https://doi.org/10.1163/9789047427759_020

Katoh K, Standley DM (2013) MAFFT multiple sequence alignment software version 7: improvements in performance and usability. Molecular Biology and Evolution 30: 772–780. https://doi.org/10.1093/molbev/mst010

Kimura M (1980) A simple method for estimating evolutionary rates of base substitutions through comparative studies of nucleotide-sequences. Journal of Molecular Evolution 16: 111–120. https://doi.org/10.1007/BF01731581

Lanfear R, Frandsen PB, Wright AM, Senfeld T, Calcott B (2017) PartitionFinder 2: new methods for selecting partitioned models of evolution formolecular and morphological phylogenetic analyses. Molecular biology and evolution 34: 772–773. https://doi.org/10.1093/molbev/msw260

Leach WE (1820) Galatéadées. In: Dictionnaire des Sciences Naturelles. F. G. Levreault, Paris, 49–56. https://doi.org/10.5962/bhl.title.42219

Liu X, Li X, Lin R (2020) A new squat lobster species of the genus *Munida* Leach, 1820 (Crustacea: Anomura: Galatheoidea: Munididae) from hydrothermal vents on the Eastern Pacific Rise. Zootaxa. 4743(1): 131–136. https://doi.org/10.11646/zootaxa.4743.1.12

Machordom A, Ahyong ST, Andreakis N, Baba K, Buckley D, Garcia-Jimenez R, Mccallum AW, Rodriguez-Flores PC, Macpherson E (2022) Deconstructing the crustacean squat lobster genus *Munida* to reconstruct the evolutionary history and systematics of the family Munididae (Decapoda, Anomura, Galatheoidea). Invertebrate Systematics 36: 926–970. https://doi.org/10.1071/IS22013

Macpherson E, Rodríguez-Flores PC, Machordom A (2024) DNA barcoding and morphology revealed the existence of seven new species of squat lobsters in the family Munididae (Decapoda, Galatheoidea) in the southwestern Pacific. ZooKeys 1188: 91–123. https://doi.org/10.3897/zookeys.1188.114984

Milne Edwards H (1837) Histoire naturelle des crustacés, comprenant l'anatomie, la physiologie et la classification de ces animaux. Librairie Encyclopédique de Roret, Paris, 532 pp.

Milne-Edwards A (1880). Reports on the results of dredging under the supervision of Alexander Agassiz, in the Gulf of Mexico and in the Caribbean Sea, 1877, '78, '79, by the U.S. Coast Survey Steamer "Blake", Lieut.-Commander C.D. Sigsbee, U.S.N., and Commander J.R. Bartlett, U.S.N. commanding. VIII. Études préliminaires sur les Crustacés. Bulletin of the Museum of Comparative Zoology at Harvard College. 8: 1–68.

Minh BQ, Nguyen MA, von Haeseler A (2013) Ultrafast approximation for phylogenetic bootstrap. Molecular Biology and Evolution 30: 1188–1195. https://doi.org/10.1093/molbev/mst024

Nguyen LT, Schmidt HA, von Haeseler A, Minh BQ (2015) IQ-TREE: a fast and effective stochastic algorithm for estimating maximum-likelihood phylogenies. Molecular Biology and Evolution 32: 268–274. https://doi.org/10.1093/molbev/msu300

Porter CE (1903) Carcinología Chilena. Descriptíon de un nuevo galatéido. Revista Chilena de Historia Natural 7: 274–277. https://www.marinespecies.org/aphia.php?p=sourcedetails&id=130236

Retamal MA, Guzmán G, De los Ríos-Escalante P (2020) An annotated checklist and bibliography of deep-water isopods and decapod crus-

taceans from Chile, including the Submarine Ridge Salas y Gomez and Nazca Plates. In: Hendrickx ME (Ed.) Deep-sea pycnogonids and crustaceans of the Americas. Springer, Cham, 585–602. https://doi.org/10.1007/978-3-030-58410-8_22

Ronquist F, Teslenko M, van der Mark P, Ayres DL, Darling A, Höhna S, Larget B, Liu L, Suchard MA, Huelsenbeck JP (2012) MrBayes 3.2: efficient Bayesian phylogenetic inference and model choice across a large model space. Systematic Biology 61: 539–542. https://doi.org/10.1093/sysbio/sys029

Samouelle, G (1819). The entomologists' useful compendium; or an introduction to the knowledge of British Insects, comprising the best means of obtaining and preserving them, and a description of the apparatus generally used; together with the genera of Linné, and modern methods of arranging the Classes Crustacea, Myriapoda, spiders, mites and insects, from their affinities and structure, according to the views of Dr. Leach. Also an explanation of the terms used in entomology; a calendar of the times of appearance and usual situations of near 3,000 species of British Insects; with instructions for collecting and fitting up objects for the microscope. Thomas Boys, London, 496 pp. [412 pls.] https://doi.org/10.5962/bhl.title.34177

Simon C, Frati F, Beckenbach A, Crespi B, Liu H, Flook P. (1994) Evolution, weighting, and phylogenetic utility of mitochondrial gene-sequences and a compilation of conserved polymerase chain-reaction primers. Annals of the Entomological Society of America 87: 651–701. https://doi.org/10.1093/aesa/87.6.651.

Stimpson W (1860) Notes on North American Crustacea, in the Museum of the Smithsonian Institution, No. II. Annals of the Lyceum of Natural History of New York 7: 177–246. https://doi.org/10.1111/j.1749-6632.1862.tb00153.x

Tamura K, Stecher G, Peterson D, Filipski A, Kumar S (2013) MEGA6: molecular evolutionary genetics analysis version 6.0. Molecular Biology and Evolution 30: 2725–2729. https://doi.org/10.1093/molbev/mst197

Zhang D, Gao F, Jakovlić I, Zou H, Zhang J, Li WX, Wang GT (2020) PhyloSuite: An integrated and scalable desktop platform for streamlined molecular sequence data management and evolutionary phylogenetics studies. Molecular Ecology Resources 20(1): 348–355. https://doi.org/10.1111/1755-0998.13096

Supplementary material 1

Species and GenBank accesion numbers of sequences included in present study

Authors: Dong Dong, Charlotte A. Seid, Xinzheng Li, Greg W. Rouse

Data type: docx

Link: https://doi.org/10.3897/zse.101.144042.suppl1

Supplementary material 2

Phylogenetic tree obtained by the maximum likelihood analysis based on the all-dataset

Authors: Dong Dong, Charlotte A. Seid, Xinzheng Li, Greg W. Rouse

Data type: pdf

Explanation note: SH-aLRT value (percentage, left) and UFBoot value (right) are indicated adjacent to each node. Only values of SH-aLRT ≥ 85% and UFBoot ≥ 95% are shown. Nodes with PP support above 0.95 are marked with red circles.

Link: https://doi.org/10.3897/zse.101.144042.suppl2

Zoosyst. Evol. 101 (2) 2025, 485–507 | DOI 10.3897/zse.101.144060

PENSOFT

MUSEUM FÜR NATURKUNDE BERLIN

Underestimated species diversity in *Zhangixalus* (Anura, Rhacophoridae) with a description of two cryptic species from southern China

Yuanqiang Pan[1,2], Shuo Liu[3], Ju Chen[1,2], Guohua Yu[1,2]

1 *Key Laboratory of Ecology of Rare and Endangered Species and Environmental Protection (Guangxi Normal University), Ministry of Education, Guilin 541004, China*

2 *Guangxi Key Laboratory of Rare and Endangered Animal Ecology, College of Life Science, Guangxi Normal University, Guilin 541004, China*

3 *Kunming Natural History Museum of Zoology, Kunming Institute of Zoology, Chinese Academy of Sciences, Kunming 650223, China*

https://zoobank.org/B0739698-F0E0-435F-977E-EF73CE9EB2DB

Corresponding author: Guohua Yu (yugh2018@126.com)

Academic editor: Umilaela Arifin ♦ **Received** 10 December 2024 ♦ **Accepted** 6 February 2025 ♦ **Published** 26 February 2025

Abstract

It has been shown that species diversity of tree frogs in the genus *Zhangixalus* might have been underestimated. In this study, based on previously published data and newly collected samples from China, we constructed a phylogeny of the genus *Zhangixalus* using mitochondrial 12S rRNA-tRNA^{Val}-16S rRNA genes and revealed two novel lineages of *Zhangixalus* from southern China, one containing newly collected samples from Pingbian, Yunnan, and one containing samples from Chengbu, Hunan. Combining evidence from morphological comparison and species delimitation, we described these two lineages as two new species. *Zhangixalus daweishanensis* **sp. nov.** from Mt. Dawei, Pingbian is sister to *Z. dorsoviridis*, and it can be distinguished from congeners by body size medium (SVL 30.0–33.5 mm in males and 43.7–50.7 mm in females); heels not meeting when legs positioned at right angle to body; internal vocal sac; dorsum uniformly green; black blotches in axilla, groin, and posterior part of thigh; and throat yolk yellow. *Zhangixalus nanshanensis* **sp. nov.** from Nanshan National Park, Chengbu, Hunan, which has been confused with *Z. nigropunctatus*, is sister to the clade of *Z. lishuiensis* and *Z. zhoukaiyae* and is distinguishable from congeners by body size medium (SVL 28.1–36.7 mm in males and 45.2 mm in a female); dorsum uniformly green; vocal sac external; throat yellow with greyish brown blotches; outer metatarsal tubercle absent; heels not meeting when legs positioned at right angle to body; and black blotches in axilla, groin, and posterior part of thigh. In addition, we considered the samples of nominal *Z. dorsoviridis* from Son La, Vietnam represent a cryptic species, and more studies are required to unravel the taxonomy and distribution of *Z. dorsoviridis* and *Z. nigropunctatus* complexes, as the taxonomic status of some records of these two species in China also remains unclear. We supported that *Z. duboisi* and *Z. omeimontis* are distinct from each other and considered that *Z. zhoukaiyae* and *Z. lishuiensis* are two separate species.

Key Words

Cryptic species, phylogeny, species delimitation, *Zhangixalus dorsoviridis*, *Zhangixalus nigropunctatus*

Introduction

The genus *Zhangixalus* Li, Jiang, Ren & Jiang, 2019, which uses *Zhangixalus dugritei* (David, 1872) as the type species, was split from *Rhacophorus* Kuhl & Van Hasselt, 1822 *sensu lato*. It is characterized by medium-to-large body size, absence of dermal folds along limbs, absence of tarsal projections, terminal phalanges of fingers and toes Y-shaped, and usual green dorsal coloration (Jiang et al. 2019). The genus is distributed widely in eastern Asia and northern Indochina and currently contains 44 species (Frost 2024), of which 30 have been recorded in China (AmphibiaChina 2024).

Studies in recent years have demonstrated that species diversity of *Zhangixalus* had been severely underestimated in the past owing to morphological conservation, and new species have been constantly discovered with the use of molecular data (e.g., Yu et al. 2019a; Nguyen et al. 2020, 2024; Ninh et al. 2020; Brakels et al. 2023; Gonggoli et al. 2024; Nguyen et al. 2024; Pan et al. 2024). Among those new species discovered recently, a few of them were newly discovered with narrow distribution (e.g., Nguyen et al. 2020; Ninh et al. 2020; Brakels et al. 2023), and most were split from species previously considered to be distributed widely or were confused with known species, which mainly involves the taxonomic changes in the *Z. nigropunctatus* (Liu, Hu & Yang, 1962) and *Z. dorsoviridis* (Bourret, 1937) complexes. *Zhangixalus nigropunctatus* was originally described from Weining, western Guizhou, China (Liu et al. 1962) and was once recorded widely from Yunnan, Guizhou, Hunan, and Anhui with discontinuous distribution in China (Fei 1999; Fei et al. 2012). However, the samples of nominal *Z. nigropunctatus* from Anhui were recovered as sister to *Z. dorsoviridis* and described as *Z. zhoukaiyae* (Pan, Zhang & Zhang, 2017) by Pan et al. (2017), the samples of nominal *Z. nigropunctatus* from Pingbian and Jinping of Yunnan did not cluster together with topotypes of *Z. nigropunctatus* (Yu et al. 2009; Li et al. 2012a) and were moved into *Z. dorsoviridis* (Li et al. 2012a), and the samples of nominal *Z. nigropunctatus* from Xinping and Longling of Yunnan represent a cryptic species (*Z. yunnanensis* Pan, Hou, Yu & Liu, 2024; Pan et al. 2024), implying that taxonomic status of other records of this species (e.g. Hunan) also needs further investigation (Pan et al. 2024).

Moreover, it has been revealed that some species with similar external morphology occurred sympatrically, which could easily lead to misidentification and therefore underestimation of species diversity. For example, the specimen ROM 38011 was collected from the type locality of *Z. dorsoviridis* (Sa Pa, Vietnam) and was originally identified as *Z. dorsoviridis* (Orlov et al. 2001). However, this specimen differs from *Z. dorsoviridis* by having a dark throat, and phylogenetically it is not related to true *Z. dorsoviridis* (Li et al. 2012a; Mo et al. 2016; Liu et al. 2017; Pan et al. 2024). Although it was once moved to *Z. nigropunctatus* by Li et al. (2012a), it is actually neither *Z. dorsoviridis* nor *Z. nigropunctatus* (Pan et al. 2024), but belongs to *Z. thaoae* Nguyen, Nguyen, Ninh, Le, Bui, Orlov, Hoang & Ziegler, 2024, a new species described recently by Nguyen et al. (2024). In addition, based on Pan et al. (2024), the taxonomic status of the sample of nominal *Z. dorsoviridis* from Son La, Vietnam (VNMN 4099) is also unclear. Therefore, the actual diversity of *Zhangixalus* probably remains underestimated due to the common occurrence of endemism and narrow-ranged species (Dufresnes and Litvinchuk 2022).

During our recent field surveys in southern Yunnan and southwestern Hunan, China (Fig. 1), some *Zhangixalus* specimens resembling *Z. dorsoviridis*, *Z. nigropunctatus*, and *Z. thaoae* were collected from Pingbian and Chengbu Counties. Considering the underestimated species diversity of *Zhangixalus* and the taxonomic history of *Z. dorsoviridis* and *Z. nigropunctatus*, we sequenced these newly collected treefrogs to confirm their identity. Our phylogenetic analyses revealed that these specimens form two distinct lineages, one containing specimens

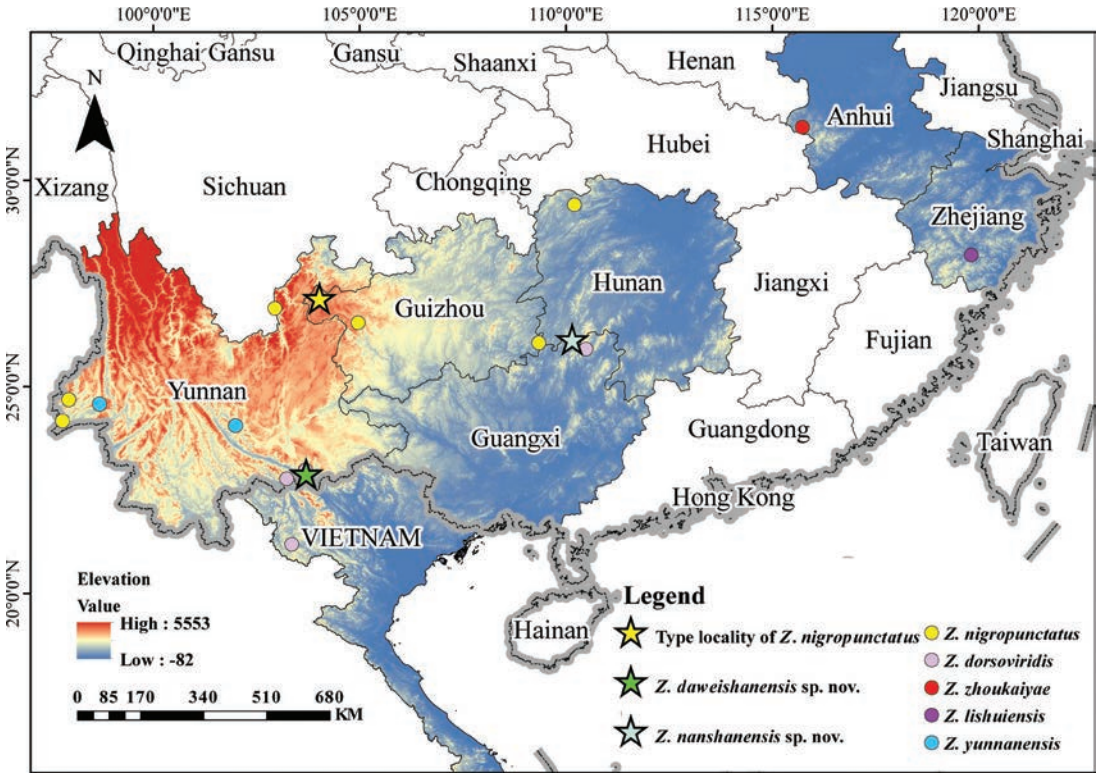

Figure 1. Known distribution sites of *Z. daweishanensis* sp. nov. and *Z. nanshanensis* sp. nov. and related species. The stars represent the type localities of the two new species and *Z. nigropunctatus*. The map was generated using ArcMap v.10.2 (ESRI Inc.).

newly collected from Pingbian, Yunnan, and one containing specimens from Chengbu, Hunan. Furthermore, our morphological examination suggested that these two lineages differ from known members of *Zhangixalus* by a series of characters. Herein, we officially describe them as two new species of *Zhangixalus*.

Materials and methods

Sampling

This study was carried out in accordance with the ethical guidelines issued by the Ethics Committee of Guangxi Normal University. In Yunnan, China, field surveys were conducted on 9 March and 3 May 2021 at Pingbian County, and a total of seven treefrog specimens of *Zhangixalus* were collected during the surveys. In Hunan, China, field surveys were conducted on 5 April 2024 at Chengbu County, and a total of eight treefrog specimens of *Zhangixalus* were collected during the surveys. Specimens were photographed, euthanized, fixed, and then stored in 75% ethanol. Liver tissues were preserved in 99% ethanol. Specimens were deposited at Guangxi Normal University (GXNU).

Phylogenetic analysis and species delimitation

Total genomic DNA was extracted from liver tissue samples that were stored in 99% ethanol. A fragment encoding mitochondrial 12S rRNA, $tRNA^{val}$, and 16S rRNA genes was amplified and sequenced using the primers and protocols of Yu et al. (2019a). 12 samples (seven from Pingbian and five from Chengbu) were newly sequenced, and all new sequences have been deposited in GenBank under Accession PV010194–PV010202 and PQ998508–PQ998510 (Table 1). Additionally, 53 homologous sequences of other *Zhangixalus* species and outgroups were obtained from GenBank (Table 1). *Theloderma albopunctatum* (Liu & Hu, 1962), *Rhacophorus rhodopus* (Liu & Hu, 1960), and *Leptomantis gauni* (Inger, 1966) were included in the data as outgroups.

Sequences were aligned using MUSCLE with default parameters in MEGA v.XI (Tamura et al. 2021). Uncorrected genetic *p*-distances (using 16S rRNA sequences) between species were calculated in MEGA v.XI. The best substitution model was selected using the corrected Akaike Information Criterion (AICc) in jModelTest v.2.1.10 (Darriba et al. 2012). Bayesian Inference was performed in MrBayes v.3.2.7 (Ronquist et al. 2012) under the selected substitution model (GTR + I + G). Two runs were performed simultaneously with four Markov chains starting from a random tree. The chains were run for 5,000,000 generations and sampled every 100 generations. The first 25% of the sampled tree was discarded as burn-in after the standard deviation of split frequencies of the two runs was less than 0.01. The remaining trees were then used to create a consensus tree and to estimate Bayesian posterior probabilities (BPPs). In addition, a Maximum Likelihood (ML) analysis was conducted in RaxmlGUI v. 8.2 (Stamatakis 2014) with 1000 rapid bootstrap replicates. The node was considered strongly supported with BPP ≥ 0.95 and bootstrap value ≥ 70 (Leaché and Reeder 2002).

We used Assemble Species by Automatic Partitioning (ASAP) for species delimitation. For this method, we used the simple distance (*p*-distance) model, and the partition with the lowest ASAP P-score was the best partition (Puillandre et al. 2021).

Morphology

Morphometric data were taken using electronic digital calipers to the nearest 0.1 mm. Morphological terminology followed (Yu et al. 2019a). Measurements included: snout-vent length (SVL, from tip of snout to vent); head length (HL, from tip of snout to rear of jaws); head width (HW, width of head at its widest point); snout length (SL, from tip of snout to anterior corner of eye); internarial distance (IND, distance between nares); interorbital distance (IOD, minimum distance between upper eyelids); upper eyelid width (UEW, maximum width of upper eyelid); eye diameter (ED, diameter of exposed portion of eyeball); distance between nostril and eye (DNE, from nostril to anterior border of eye); tympanum diameter (TD, the greater of tympanum vertical and horizontal diameters); forearm and hand length (FHL, from elbow to tip of third finger); tibia length (TL, distance from knee to heel); foot length (FL, from proximal end of inner metatarsal tubercle to tip of fourth toe); and length of foot and tarsus (TFL, from tibiotarsal joint to tip of fourth toe). Webbing formula followed (Myers and Duellman 1982). Comparative morphological data of other *Zhangixalus* species were taken from their original descriptions or re-descriptions (Boulenger 1892; Stejneger 1907; Smith 1924a; Inger 1947; Liu et al. 1962; Inger 1966; Lue et al. 1994, 1995; He 1999; Orlov et al. 2001; Ohler et al. 2000; Harvey et al. 2002; Matsui and Panha 2006; Rao et al. 2006; Bordoloi et al. 2007; Chou et al. 2007; Fei et al. 2009, 2010; Jiang et al. 2016; Zhang et al. 2011; Fei et al. 2012; Li et al. 2012b; Mo et al. 2016; Liu et al. 2017; Pan et al. 2017; Chen et al. 2018; Yu et al. 2019a; Nguyen et al. 2020; Ninh et al. 2020; Brakels et al. 2023; Gonggoli et al. 2024; Lue et al. 2024; Nguyen et al. 2024; Pan et al. 2024). Multivariate principal component analysis (PCA) was conducted in SPSS v.17.0 (SPSS Inc.), based on the correlation matrix of size-standardized measurements (all measurements divided by SVL) of adult males. Scatter plots of the scores of the first three factors of PCA were used to examine the differentiation between the new species and its closest relatives revealed by phylogenetic analyses. Differences in quantitative characters of adult males between these three species were also evaluated with t-tests in SPSS. In these analyses, Levene's test was also performed for each character to test for equality of variances.

Table 1. Species used for phylogenetic analyses in this study.

Species	Voucher No.	Locality	Accession No.
Leptomantis gauni	FMNH273928	Sarawak, Malaysia	JX219456
Rhacophorus rhodopus	SCUM 060692L	Mengyang, Yunnan, China	EU215531
Theloderma albopunctatum	ROM 30246	Vietnam	AF458148
Zhangixalus arboreus	TTU–R–11748	Japan	AF458142
Z. burmanus	SCUM 060614L	Mt. Gaoligong, Yunnan, China	EU215537
Z. chenfui	SCUM 060404L	Mt. Omei, Sichuan, China	EU215534
Z. daweishanensis sp. nov.	GXNU YU000392	Pingbian, Yunnan, China	PQ998508
Z. daweishanensis sp. nov.	GXNU YU000393	Pingbian, Yunnan, China	PV010195
Z. daweishanensis sp. nov.	GXNU YU000394	Pingbian, Yunnan, China	PV010196
Z. daweishanensis sp. nov.	GXNU YU000395	Pingbian, Yunnan, China	PQ998507
Z. daweishanensis sp. nov.	GXNU YU000396	Pingbian, Yunnan, China	PV010197
Z. daweishanensis sp. nov.	KIZL040279	Pingbian, Yunnan, China	PQ998510
Z. daweishanensis sp. nov.	KIZL040278	Pingbian, Yunnan, China	PQ998509
Z. dennysi	ROM 30249	Vietnam	AF458139
Z. dorsoviridis	ROM 38015	Sa Pa, Lao Cai, Vietnam	JX219423
Z. dorsoviridis	Rao060821200	Jinping, Yunnan, China	JX219424
Z. dorsoviridis	YN080446	Pingbian, Yunnan, China	JX219425
Z. dorsoviridis	Rao060821199	Pingbian, Yunnan, China	JX219426
Z. dorsoviridis	KIZ060821287	Jinping, Yunnan, China	EF564563
Z. dorsoviridis	KIZ060821287	Jinping, Yunnan, China	EF564491
Z. duboisi	VNMN:4103	Lao Cai, Vietnam	LC010581
Z. duboisi	VNMN:4104	Lao Cai, Vietnam	LC010582
Z. dugritei	SCUM 051001L	Baoxing, Sichuan, China	EU215541
Z. dulitensis	BORNEENSIS09087	Borneo, Malaysia	AB847123
Z. feae	SCUM 050642W	Hekou, Yunnan, China	EU215544
Z. franki	VNMN 011687	Ha Giang, Vietnam	LC548746
Z. hongchibaensis	CIB 097687	Wuxi, Chongqing, China	JN688883
Z. hui	Li01	Zhaojue, Sichuan, China	JN688878
Z. hungfuensis	SCUM 060425L	Wenchuan, Sichuan, China	EU215538
Z. jodiae	VNMN 07122	Vietnam	LC545595
Z. lishuiensis	YPX47792	Lishui, Zhejiang, China	KY653720
Z. lishuiensis	GXNU YU000510	Lishui, Zhejiang, China	PQ901907
Z. lishuiensis	GXNU YU000509	Lishui, Zhejiang, China	PQ901906
Z. melanoleucus	BEI 01010	Phou Samsoum Mt., Xiengkhoang, Laos	OQ305233
Z. melanoleucus	ZMMU A–7781	Phou Samsoum Mt., Xiengkhoang, Laos	OQ305234
Z. melanoleucus	BEI 01011	Phou Samsoum Mt., Xiengkhoang, Laos	OQ305235
Z. melanoleucus	AUP 02507	Phou Samsoum Mt., Xiengkhoang, Laos	OQ305236
Z. minimus	KIZ 061214YP	Mt. Dayao, Guangxi, China	EU215539
Z. moltrechti	SCUM 061106L	Lianhuachi, Taiwan, China	EU215543
Z. nanshanensis sp. nov.	GXNU YU000771	Chengbu, Hunan, China	PV010198
Z. nanshanensis sp. nov.	GXNU YU000772	Chengbu, Hunan, China	PV010199
Z. nanshanensis sp. nov.	GXNU YU000773	Chengbu, Hunan, China	PV010200
Z. nanshanensis sp. nov.	GXNU YU000774	Chengbu, Hunan, China	PV010201
Z. nanshanensis sp. nov.	GXNU YU000776	Chengbu, Hunan, China	PV010202
Z. nigropunctatus	EU924623	Weining, Guizhou, China	EU924623
Z. nigropunctatus	GZ070658	Weining, Guizhou, China	JX219430
Z. nigropunctatus	SCUM 070657L	Weining, Guizhou, China	EU215533
Z. nigropunctatus	GXNU YU000361	Weining, Guizhou, China	PP187265
Z. nigropunctatus	GXNU YU000362	Weining, Guizhou, China	PP187266
Z. nigropunctatus	GXNU YU000363	Weining, Guizhou, China	PP187267
Z. omeimontis	SCUM 061104L	Pingbian, Yunnan, China	EU215536
Z. omeimontis	SCUM 0606137L	Pengxian, Sichuan, China	EU215535
Z. pachyproctus	KIZ090148	Puer, Yunnan, China	MN613222
Z. pinglongensis	NHMG201002011	Shiwandashan, Guangxi, China	KU170684
Z. puerensis	SCUM 060649L	Puer, Yunnan, China	EU215542
Z. schlegelii	–	Hiroshima, Japan	AB202078
Z. smaragdinus	KIZ 20160298	Yingjiang, Yunnan, China	MN613219
Z. thaoae	IEBR A 5136	Lao Cai, Vietnam	LC762092
Z. thaoae	IEBR A 5137	Lao Cai, Vietnam	LC762093
Z. thaoae	IEBR A 5138	Lao Cai, Vietnam	LC762094
Z. thaoae	ROM 38011	Sa Pa, Lao Cai, Vietnam	JX219427
Z. yaoshanensis	NHMG150408	Jinxiu, Guangxi, China	MG322122
Z. yunnanensis	GXNU YU20160269	Xinping, Yunnan, China	PV010194
Z. yunnanensis	GXNU YU20160268	Xinping, Yunnan, China	PP187269
Z. yunnanensis	GXNU YU20160267	Xinping, Yunnan, China	PP187270
Z. zhoukaiyae	AHU–RhaDB–120428	Jinzhai, Anhui, China	KU601502
Z. zhoukaiyae	GXNU YU05293	Jinzhai, Anhui, China	PQ901908
Zhangixalus sp.	VNMN:4099	Ta Xua, Son La, Vietnam	LC010577

Results

Phylogenetic relationship

The obtained sequence alignment was 1972 bp. Phylogenetic analyses revealed that the specimens newly collected from Mt. Dawei, Pingbian, Yunnan (GXNU YU000392–396, KIZL040278–279) form a novel clade. This clade was recovered as sister to the clade consisting of *Z. dorsoviridis* from the type locality (Sa Pa, Vietnam), Jinping, and Pingbian with strong support (100% for BI and 93% for ML) (Fig. 2), meaning that there is a cryptic lineage living in sympatry with *Z. dorsoviridis* at Mt. Dawei, Pingbian, Yunnan, China. In addition, the specimens collected from Nanshan National Park, Chengbu, Hunan (GXNU YU000771–774, YU000776) also formed a novel clade, and it was sister to the clade of *Z. lishuiensis* (Liu, Wang & Jiang, 2017) and *Z. zhoukaiyae*; then the three together were sister to the clade formed by *Z. dorsoviridis* and the cryptic lineage in Pingbian with strong support (100% for BI and ML) (Fig. 2).

The average genetic distance within the genus *Zhangixalus* ranges from 0.58% between *Z. hui* (Liu, 1945) and *Z. dugritei* (David, 1872) to 15.67% between *Z. jodiae* Nguyen, Ninh, Orlov, Nguyen & Ziegler, 2020, and *Z. dulitensis* (Boulenger, 1892). The 16S *p*-distances between the novel clade consisting of Pingbian specimens and the other *Zhangixalus* lineages included in this study ranged from 2.02% (vs. *Z. dorsoviridis*) to 10.25% (vs. *Z. dulitensis*), and the genetic distances between the novel lineage from Chengbu, Hunan, and other *Zhangixalus* species ranged from 1.93% (vs. *Z. lishuiensis*) to 12.07% (vs. *Z. dulitensis*) in 16S rRNA sequences (Suppl. material 2).

The best partition (score = 2.0) obtained by the ASAP analysis assigned all *Zhangixalus* samples used in this study into 31 species, two of which correspond to the clade of samples from Chengbu, Hunan, and the clade of the newly collected samples from Pingbian, Yunnan, respectively. *Zhangixalus dugritei* and *Z. hui* were assigned into one; the sample of nominal *Z. dorsoviridis* from Son La, Vietnam (VNMN 4099) was assigned into one with *Z. jodiae*, and other candidate species completely correspond to other known species used in this study (Fig. 3).

Morphometric analysis

Morphometric data are summarized in Suppl. material 1. The novel lineage from Mt. Dawei can be distinguished from *Z. dorsoviridis* by a smaller internarial distance and tympanum (Tables 2, 3), ventral surface of the thigh that is orange-yellow during the breeding season (vs. bright orange-red), heels not meeting when legs positioned at right angle to body (vs. overlapping), and other characters (see diagnosis below).

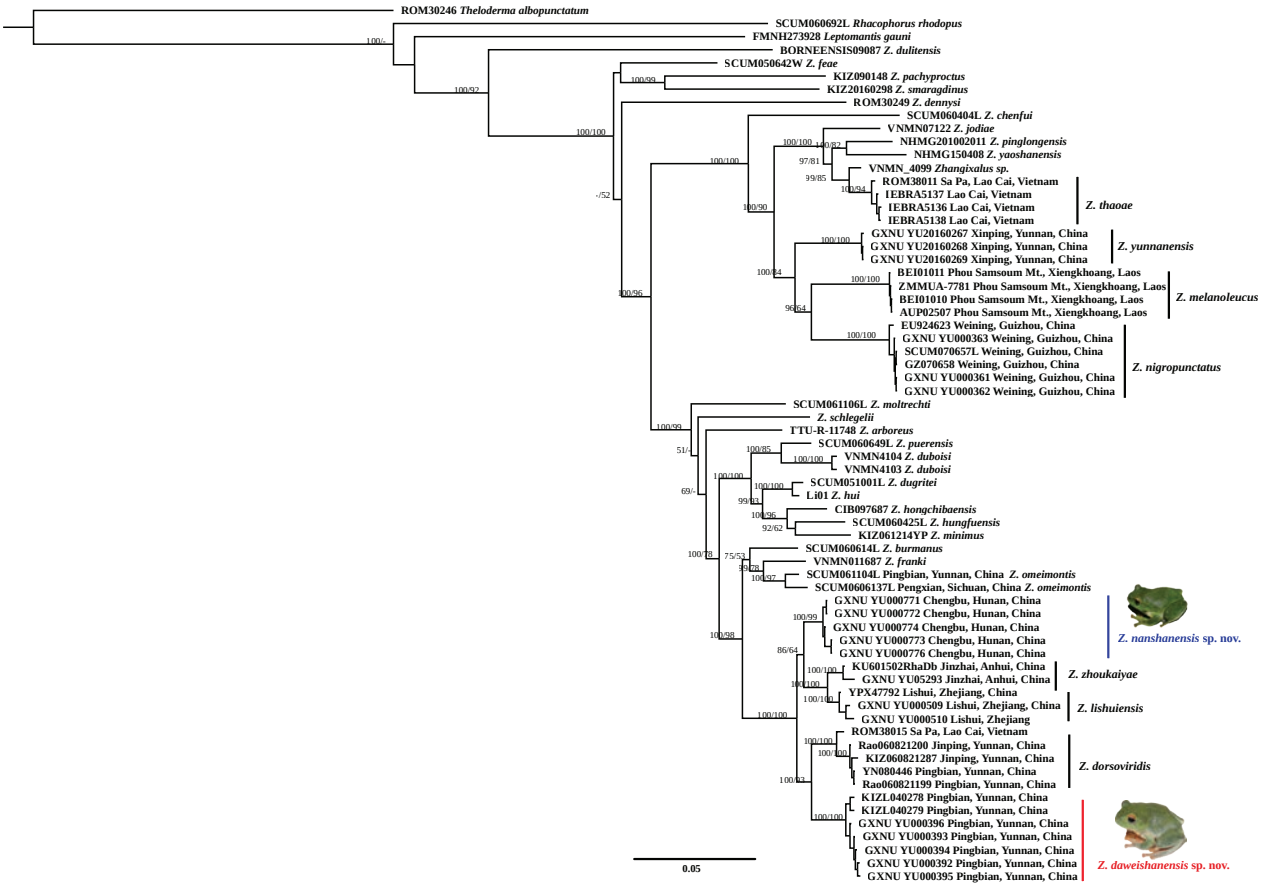

Figure 2. Bayesian phylogram of *Zhangixalus* inferred from mitochondrial 12S–tRNA^{Val}–16S sequences. Numbers above and below branches are Bayesian posterior probabilities and ML bootstrap values (only values above 50% are shown), respectively.

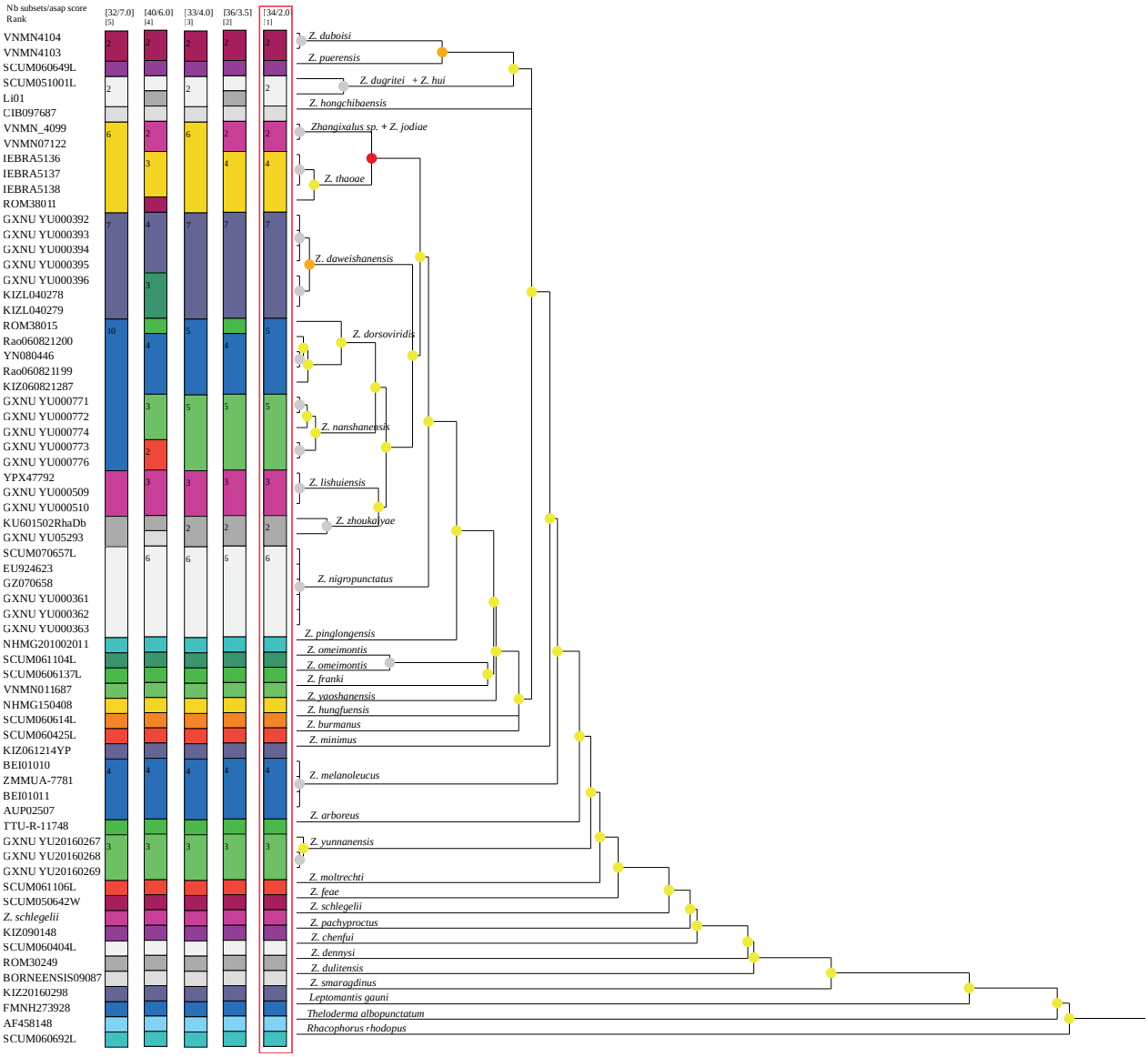

Figure 3. ASAP species delimitation based on 16S rRNA sequences. The best partition with the lowest score is highlighted with a red frame.

Table 2. Measurements (mm) of *Z. daweishanensis* sp. nov. (n = 7) and *Z. dorsoviridis* (n = 11; from Orlov et al. 2001).

Character	*Z. daweishanensis* sp. nov.				*Z. dorsoviridis*			
	male (n = 3)		female (n = 4)		male (n = 9)		female (n = 2)	
	range	Mean ± S.D	range	Mean ± S.D	range	Mean ± S.D	range	Mean ± S.D
SVL	32.0–33.5	32.5 ± 0.8	43.7–50.7	46.0 ± 3.2	31.37–42.43	37.18 ± 3.91	37.91–42.83	40.19 ± 3.73
HL	11.3–11.7	11.5 ± 0.2	14.4–15.6	14.8 ± 0.5	11.24–15.71	13.22 ± 1.51	12.51–14.14	13.13 ± 1.20
HW	12.3–12.8	12.5 ± 0.3	15.9–17.3	16.3 ± 0.6	11.05–15.29	13.51 ± 1.51	14.53–15.06	14.78 ± 1.22
SL	5.4–5.9	5.7 ± 0.2	7.0–8.1	7.6 ± 0.4				
IND	4.1	4.1 ± 0.0	5.2–5.7	5.4 ± 0.2				
IOD	4.3–4.5	4.4 ± 0.1	4.8–5.6	5.3 ± 0.4	6.88–9.05	7.67 ± 0.80	8.80–9.58	9.16 ± 1.46
UEW	2.2–2.5	2.4 ± 0.2	2.9–3.3	3.1 ± 0.3				
ED	4.1–4.4	4.3 ± 0.1	4.3–5.3	4.9 ± 0.4	3.40–4.66	4.05 ± 0.42	3.90–4.64	4.27 ± 0.52
TD	2.0–2.2	2.1 ± 0.1	2.6–3.3	3.1 ± 0.3	1.69–3.15	2.30 ± 0.51	2.37–2.40	2.39 ± 0.02
DNE	2.2–2.3	2.2 ± 0.1	3.1–3.5	3.4 ± 0.2				
FHL	16.6–17.1	16.8 ± 0.3	21.9–24.1	23.3 ± 1.0				
TL	14.2–20.6	18.3 ± 3.5	13.6–20.8	16.9 ± 3.3	10.85–19.12	15.66 ± 2.66	13.70–17.96	15.83 ± 3.00
TFL	21.7–31.8	27.8 ± 5.4	21.8–32.1	26.4 ± 5.0				
FL	14.7–21.4	18.8 ± 3.5	14.2–21.7	17.6 ± 3.6	12.63–17.43	15.41 ± 1.83	17.20–19.50	18.34 ± 1.68

Table 3. Summary statistics of male specimens (mean ± standard deviation) and results of the *t*–test between the *Z. daweishanensis* sp. nov. (n = 3) and *Z. dorsoviridis* (n = 5) from Pingbian, Yunnan. The *t*–test was performed on the size–adjusted data, except SVL. * = $p < 0.05$, ** = $p < 0.01$.

Character	Mean ± SD(n = 3)	Mean ± SD(n = 5)	Levene's test		t–test	
	Z. daweishanensis	*Z. dorsoviridis*	F	P–value	t	P–value
SVL	32.57 ± 0.823	37.04 ± 2.625	1.541	0.261	-2.788	0.0320*
HL	0.353 ± 0.013	0.372 ± 0.017	0.792	0.408	-1.603	0.1600
HW	0.385 ± 0.018	0.386 ± 0.008	2.382	0.174	-0.136	0.8960
SL	0.174 ± 0.006	0.176 ± 0.010	1.827	0.225	-0.252	0.8100
IND	0.126 ± 0.004	0.143 ± 0.007	4.913	0.069	-3.78	0.0090**
IOD	0.137 ± 0.007	0.138 ± 0.008	0.192	0.677	-0.252	0.8090
ED	0.131 ± 0.007	0.121 ± 0.011	1.007	0.354	1.441	0.2000
TD	0.066 ± 0.004	0.081 ± 0.003	0.566	0.48	-5.62	0.0010**
FHL	0.516 ± 0.020	0.517 ± 0.029	0.584	0.474	-0.05	0.9620
TL	0.561 ± 0.100	0.422 ± 0.031	9.512	0.022	2.346	0.1300
TFL	0.853 ± 0.151	0.781 ± 0.236	5.873	0.052	0.466	0.6570
FL	0.575 ± 0.099	0.437 ± 0.013	12.224	0.013	2.344	0.1320

We retained the first two principal components that accounted for 74.32% of the total variance (Table 4). Loadings for PC1, which accounted for 40.48% of the total variance, were most heavily loaded on internarial distance (IND), and Loadings for PC2, which accounted for 33.84%, were most heavily loaded on snout length (SL). Differentiation was found along the PC1 axis between the newly collected specimens from Pingbian and *Z. dorsoviridis* (Fig. 4).

For the cryptic lineage from Nanshan National Park, the measurement DNE was not included in PCA analysis because it was not available for *Z. lishuiensis* and *Z. zhoukaiyae*. We retained the three principal components that accounted for 75.25% of the total variance (Table 5). Loadings for PC1, which accounted for 36.71% of the total variance, were most heavily loaded on foot length (FL). Loadings for PC2, which accounted for 21.63% of the total variance, were most heavily loaded on forearm and hand length (FHL), and Loadings for PC3, which accounted for 16.91%, were most heavily loaded on head length (HL). Differentiation was found along both the PC1 and PC3 axes between the specimens from Nanshan National Park and *Z. lishuiensis* from the type locality, and differentiation was also found along the PC3 axis between the specimens from Nanshan National Park and *Z. zhoukaiyae*. The results of PCA analysis revealed distinct morphometric differences in head length between the specimens from Nanshan National Park and *Z. lishuiensis*, as well as in head length between the specimens from Nanshan National Park and *Z. zhoukaiyae* (Fig. 5). Moreover, the t-tests demonstrated that male specimens from Nanshan National Park differed significantly ($p < 0.05$) from male topotypes of *Z. zhoukaiyae* in HW, IOD, UEW, and TD (Table 6) and differed significantly ($p < 0.05$) from *Z. nigropunctatus* in HW, UEW, ED, TD, TL, and TFL (Suppl. material 4: table S4). Additionally, the new lineage is distinguishable from its congeners by body size and the combination of texture and coloration pattern.

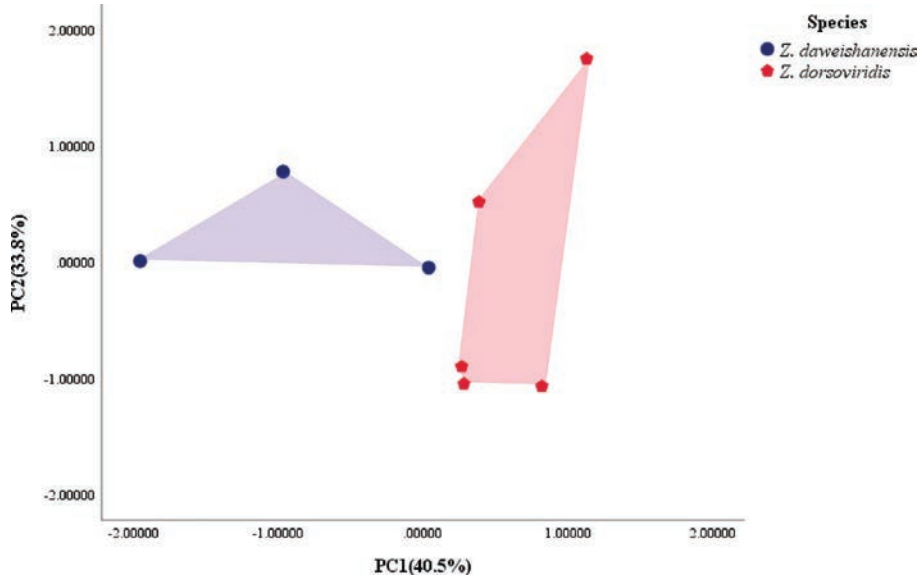

Figure 4. Scatterplot of principal components 1 and 2 of size–adjusted male morphometric data of *Z. daweishanensis* sp. nov. and *Z. dorsoviridis* from Pingbian, Yunnan, China.

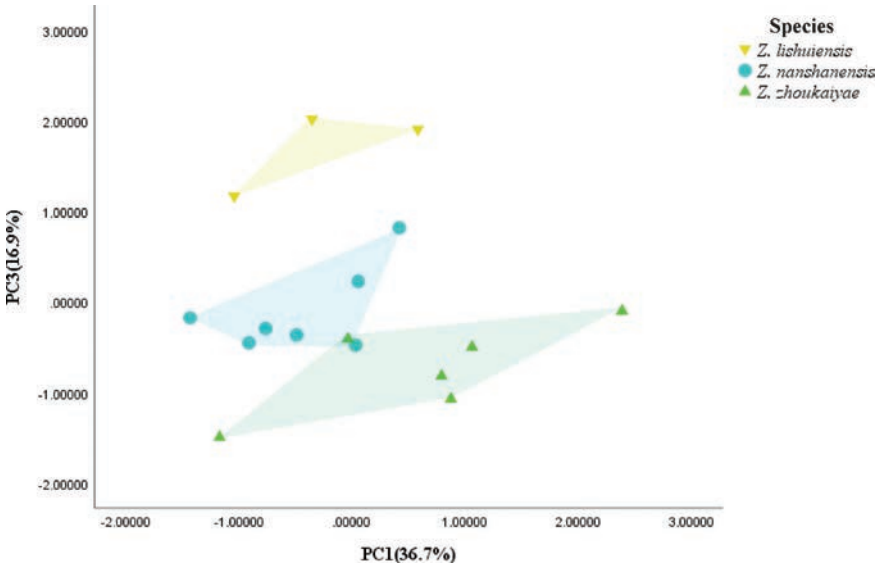

Figure 5. Scatterplot of principal components 1 and 3 of size–adjusted male morphometric data of *Z. nanshanensis* sp. nov., *Z. lishuiensis*, and *Z. zhoukaiyae*.

Table 4. Factor loadings of the first two principal components of 11 size–adjusted male morphometric characteristics of *Z. daweishanensis* sp. nov. and *Z. dorsoviridis* from Pingbian, Yunnan.

Character	PC1	PC2
Eigenvalue	4.453	3.722
% variation	40.482	33.838
HL	0.813	0.364
HW	0.630	0.397
SL	0.052	**-0.958**
IND	**0.915**	0.015
IOD	0.432	0.623
ED	-0.320	-0.416
TD	0.776	-0.343
FHL	0.414	0.788
TL	-0.831	0.463
TFL	-0.227	0.898
FL	-0.868	0.441

Table 5. Factor loadings of the first three principal components of 12 size–adjusted male morphometric characteristics of *Z. nanshanensis* sp. nov., *Z. lishuiensis*, and *Z. zhoukaiyae*.

Character	PC1	PC2	PC3
Eigenvalue	4.405	2.595	2.029
% variation	36.710	21.627	16.910
HL	-0.083	-0.285	**0.906**
HW	0.733	-0.423	0.308
SL	0.058	0.645	0.368
IND	0.513	-0.405	0.456
IOD	0.705	-0.395	-0.465
UEW	0.594	-0.568	-0.456
ED	0.636	0.413	0.327
TD	0.381	-0.510	0.328
FHL	0.318	**0.722**	0.057
TL	0.851	0.297	0.094
TFL	0.755	0.432	-0.345
FL	**0.895**	0.219	0.026

Therefore, on the basis of the above molecular and morphological evidence, we officially describe these two cryptic lineages as two new species.

Taxonomic account

Zhangixalus daweishanensis sp. nov.

https://zoobank.org/F65518E3-F6C4-4FFF-9832-0BB28FF88B00

Figs 6–9

Daweishan tree frog/Dà Weī Shān Shù wā (大围山树蛙)

Holotype. GXNU YU000396, adult male, collected on 3 May 2021 by Guohua Yu from Dawei Mountain, Pingbian County, Yunnan Province, China (22°54'6.32"N, 103°41'33.25"E, 1740 m a.s.l.).

Paratypes. GXNU YU000392–000395, four adult females, collected on 3 May 2021 from the type locality by Guohua Yu; KIZL040278–040279, two adult males, collected on 9 March 2021 by Shuo Liu from the type locality.

Etymology. The species epithet is named for Dawei Mountain, Pingbian County, Yunnan, China, where the species was collected. We suggest the English common name "Daweishan tree frog" and the Chinese common name "Dà Weī Shān Shù wā (大围山树蛙)".

Diagnosis. The new treefrog species is assigned to *Zhangixalus* by the presence of intercalary cartilage between terminal and penultimate phalanges of digits, Y-shaped distal end of terminal phalanx, tips of digits expanded into large discs bearing circum-marginal grooves, and vomerine teeth present, dermal folds along limbs not significant, tarsal projections absent, green dorsal colouration and medium body size (Jiang et al. 2019). Phylogenetically, the new species is nested within the genus *Zhangixalus* with strong support (100% for BI and ML).

Zhangixalus daweishanensis sp. nov. can be distinguished from its congeners by a combination of the following characters: 1) body size medium (SVL 30.0–33.5 mm in males and 43.7–50.7 mm in females); 2) head wider than long; 3) upper half of iris orange and lower half yellow-brown; 4) heels not meeting when legs positioned at right angle to body, tibiotarsal articulation reaching posterior corner of eye; 5) IND/SVL 12.2%–13.0%

Table 6. Summary statistics of male specimens (mean ± standard deviation) and results of the *t*–test between the *Z. nanshanensis* sp. nov. (n = 7) and *Z. zhoukaiyae* (n = 6). The *t*–test was performed on the size–adjusted data, except SVL. * = $p < 0.05$, ** = $p < 0.01$.

Character	Mean ± SD (n = 7)	Mean ± SD (n = 6)	Levene's test		t–test	
	Z. nanshanensis	*Z. zhoukaiyae*	F	P–value	t	P–value
SVL	33.3 ± 2.57	34.0 ± 3.40	0.639	0.441	-0.387	0.706
HL	0.349 ± 0.010	0.338 ± 0.020	1.128	0.311	1.195	0.257
HW	0.368 ± 0.007	0.395 ± 0.025	7.052	0.022	-2.586	0.044*
SL	0.191 ± 0.069	0.147 ± 0.015	2.44	0.147	1.519	0.157
IND	0.105 ± 0.011	0.115 ± 0.009	0.137	0.719	-1.907	0.083
IOD	0.123 ± 0.008	0.154 ± 0.015	1.677	0.222	-4.497	0.001**
UEW	0.071 ± 0.002	0.154 ± 0.015	6.947	0.023	-12.971	0.000**
ED	0.124 ± 0.009	0.124 ± 0.012	0.477	0.504	0.003	0.998
TD	0.061 ± 0.003	0.069 ± 0.006	6.361	0.028	-2.937	0.022*
FHL	0.530 ± 0.025	0.523 ± 0.032	0.447	0.518	1.555	0.148
TL	0.441 ± 0.026	0.442 ± 0.025	0.082	0.78	-0.122	0.905
TFL	0.679 ± 0.028	0.682 ± 0.024	3.457	0.09	-0.133	0.896
FL	0.429 ± 0.024	0.437 ± 0.032	0.878	0.369	-0.547	0.595

Figure 6. Dorsal (**a**), ventral (**b**), lateral (**c**), and rear (**d**) views of the holotype of *Z. daweishanensis* sp. nov. (GXNU YU000396) in preservative. Photos by Yuanqiang Pan.

in males; 6) dorsum uniformly green; 7) black blotches in axilla, groin, and posterior part of thigh; 8) vocal sac internal; 9) webbing greyish in female and yellow in male; 10) fingers webbed one third, webbing formula I2–2II1½–2⅔III2–2IV, and toes webbed half, webbing formula I1–1½II1–2III1–2½IV2½–1V; 11) throat, chest, venter, and ventral surface of limbs yolk yellow in male.

Description of holotype. Adult male, body robust, size small (SVL 33.5 mm); HL (11.3 mm) 91.9% of HW (12.3 mm); snout bluntly rounded; possesses canthus rostralis; the tip of the snout slightly protrudes beyond the edge of the lower jaw in ventral view; snout (SL 5.9 mm) longer than eye (ED 4.2 mm); nostril oval, slightly protuberant, located at the one-third between snout tip and

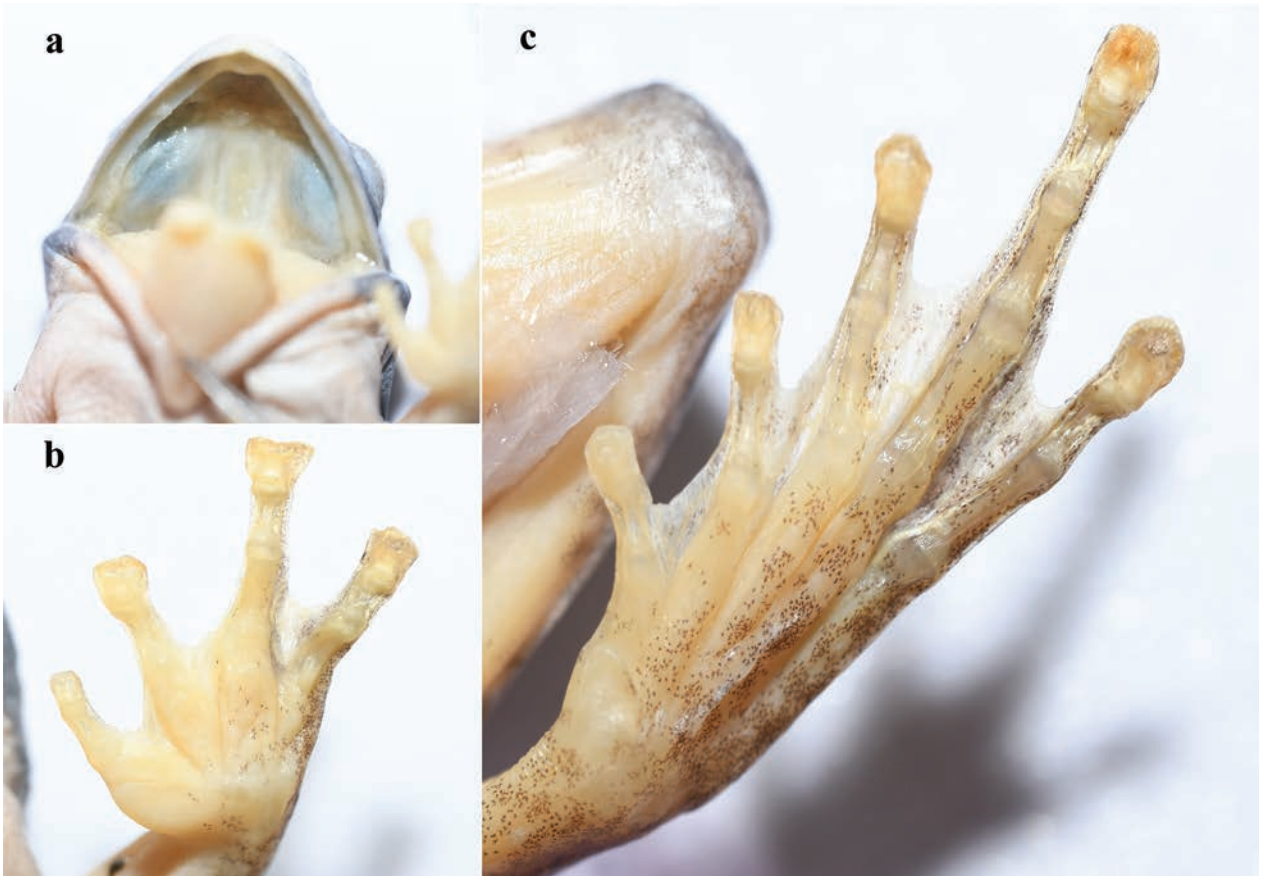

Figure 7. Views of vomerine teeth (**a**), hand (**b**), and foot (**c**) of the holotype of *Z. daweishanensis* sp. nov. (GXNU YU000396). Photos by Yuanqiang Pan.

eye; IND (4.1 mm) equal to IOD (4.3 mm) and wider than UEW (2.5 mm); pineal spot absent; pupil oval, horizontal; tympanum distinct (TD 2.0 mm), rounded, slightly smaller than half of ED (4.2 mm), nearly equal to the distance between eye and nostril (DNE 2.2 mm); supratympanic fold distinct, curves from posterior edge of eye to insertion of arm; vomerine teeth distinct; choanae oval, horizontal; tongue attached anteriorly and notched posteriorly; single internal vocal sac, with a sac slit opening on floor of mouth at each corner.

Relative length of fingers I < II < IV < III; tips of all fingers expanded into discs with circum-marginal grooves; nuptial pad present on first finger; fingers webbed one third, webbing formula I2–2II1½–2⅔III2–2IV; lateral fringe on free edge of all fingers; subarticular tubercles prominent and rounded, formula 1, 1, 2, 2; supernumerary tubercles present; inner metacarpal tubercle large, ovoid, outer metacarpal tubercle smaller in size, flattened; dermal fringe along outer edge of forearm present, not well developed.

Hind limbs moderate long, heels not meeting when legs positioned at right angle to body; tibiotarsal articulation reaching posterior margin of eye; relative length of toes I < II < V < III < IV; tibia (TL 20.6 mm) 61.5% of body size, shorter than foot (FL 21.4 mm); tips of toes expanded into discs with circum-marginal grooves, smaller than finger discs; toes webbed half, webbing formula I1–1½II1–2III1–2½IV2½–1V; subarticular tubercles prominent and rounded, formula 1, 1, 2, 3, 2; supernumerary tubercles present; inner metatarsal tubercle oval, prominent; outer metatarsal tubercle absent; dermal fringe along outer edge of tibia, tarsus, and fifth toe.

Dorsal surface of body and head smooth; dorsolateral folds absent; throat fine granular; chest, belly, and ventral surface of limbs granular.

Coloration in life. the upper half of iris orange, and the lower half yellow-brown; dorsal surface grass green; side of head and tympanic region green; lower part of flanks cream mottled with saffron yellow; throat, chest, and venter yolk yellow; limbs dorsally green and ventrally yolk yellow; anterior and posterior of thigh orange-yellow; large black blotches in axilla, groin, and posterior and anterior part of thigh; white fringes along outer edge from elbow to the fourth finger and from tibiotarsal articulation to the fifth toe; ventral surface of hand yolk yellow; webbing between fingers and toes light yellow (Fig. 8).

Coloration in preservative. Dorsal surface fades to dark blue; lower part of flanks, ventral surface of body and limbs, and posterior and anterior parts of thigh light yellow (Fig. 6).

Sexual dimorphism. The new species is sexually dimorphic, with females being distinctly larger than males and having no vocal sac and nuptial pad. Males have

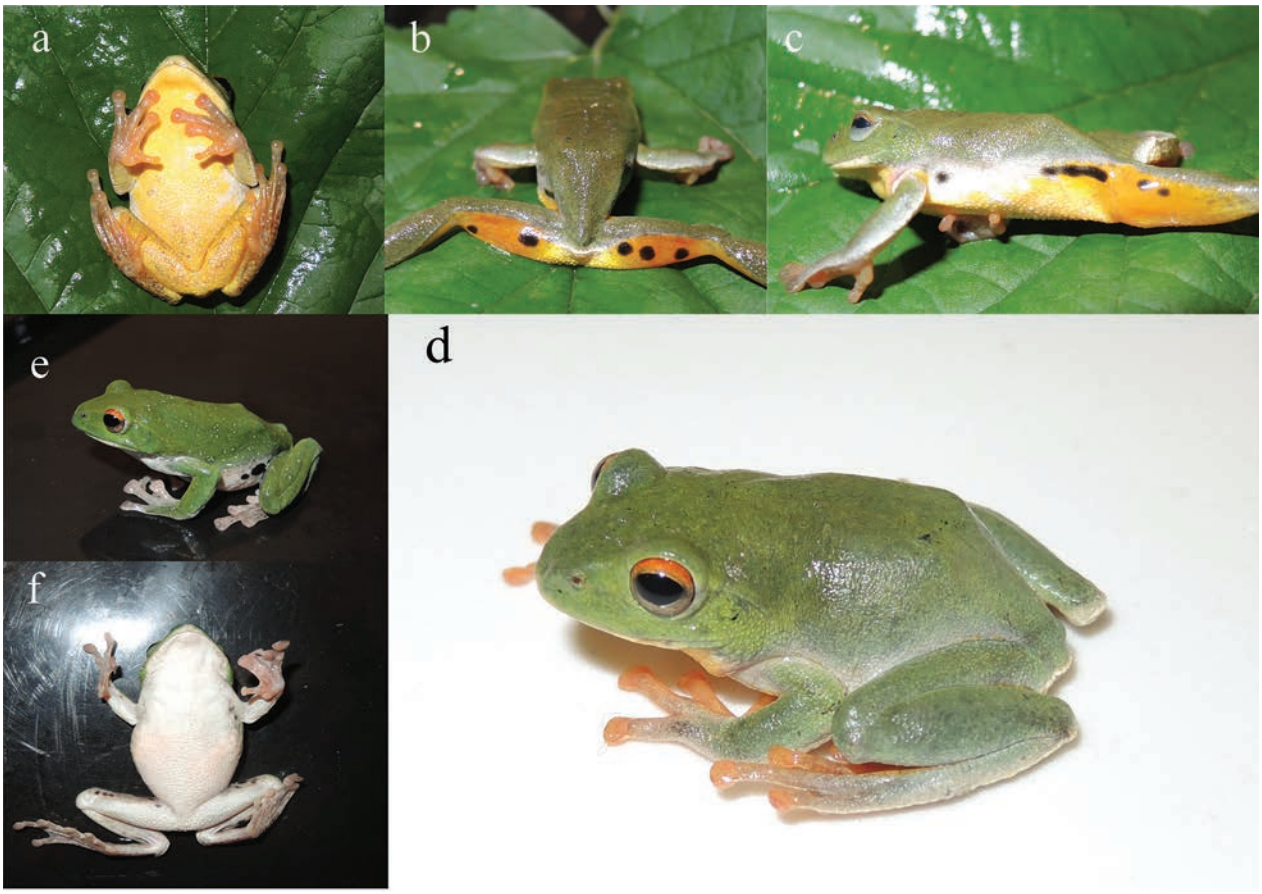

Figure 8. Views of the adult male holotype of *Z. daweishanensis* sp. nov. (GXNU YU000396; **a–d**) and adult female paratype of *Z. daweishanensis* sp. nov. (GXNU YU000393; **e, f**) in life. Photos by Guohua Yu.

internal single subgular vocal sac and orange-yellow nuptial pad on base of finger I during the breeding season. Ventral surface and anterior yolk yellow and posterior parts of thigh orange-yellow in males during breeding season.

Morphological variation. The colour pattern varied amongst individuals. Dorsal surfaces are nearly uniform green, with exceptions of paratypes GXNU YU000392 and GXNU YU000393, which have yellowish-green spots scattered on dorsal surface (Figs 8, 9). The paratypes GXNU YU000395 and KIZL040279 have no black blotch in axilla (Fig. 9). All specimens have black blotches on anterior part of thigh with the exception of the paratype KIZL040278. Moreover, number and distribution pattern of black blotches varied among specimens, as generally the black blotches in females are larger than those in males, and black blotches on thighs in males are discrete (vs. merged in females).

Distribution and ecology. The new species is currently only known from the type locality (Dawei Mountain, Pingbian County, Yunnan). During the surveys, the species was found on branches or leaves of roadside bushes near a small pond formed by a cutoff stream at the type locality (Fig. 10), and calls of this species were heard. *Feihyla palpebralis* (Smith, 1924) (Smith 1924b), *Gracixalus yunnanensis* Yu, Hui, Wang, Rao, Wu & Yang, 2019 (Yu et al. 2019b), and *Zhangixalus omeimontis* (Stejneger, 1924) were also found at the same site during the surveys.

Comparison. Phylogenetically, the new species is closely related to *Z. dorsoviridis*. *Zhangixalus daweishanensis* sp. nov. can be distinguished from *Z. dorsoviridis*, with which the new species has previously been confused, by narrower internarial distance (mean IND/SVL in males 0.126 ± 0.004 [0.122–0.130, n = 3] vs. 0.143 ± 0.007 [0.136–0.151, n = 5]), narrower tympanum (mean TD/SVL in males 0.066 ± 0.004 [0.060–0.069, n = 3] vs. 0.081 ± 0.003 [0.075–0.083, n = 5]) (Table 3), ventral, anterior, and posterior surface of thigh orange-yellow and dorsomedial surface of tibia and tarsus yolk yellow in males (vs. orange-red) (Suppl. material 4: fig. S1), webbing between fingers and toes light yellow (vs. gray or yellow-greenish) (Ostroshabov et al. 2013), nuptial pad present (vs. absent), and heels not meeting when legs positioned at right angle to body (vs. overlap) (Orlov et al. 2001).

The newly collected specimens are also morphologically similar to *Z. thaoae*, which was confused with *Z. dorsoviridis* in Vietnam. *Zhangixalus daweishanensis* sp. nov. can be distinguished from *Z. thaoae* by the upper half of the iris is orange and the lower half is yellow-brown (vs. iris red-bronze), webbing light yellow (vs. orange with some gray pattern); internal single subgular vocal sac (vs. external single subgular vocal sac), nuptial pad orange-yellow (vs. grey), heels not meeting when legs positioned at right angle to body (vs. overlapping), and ventral surface of limbs granular (vs. smooth) (Table 7).

Table 7. Morphological comparisons of *Z. daweishanensis* sp. nov., *Z. nanshanensis* sp. nov., *Z. dorsoviridis*, *Z. nigropunctatus*, *Z. lishuiensis*, *Z. thaoae*, *Z. yunnanensis*, and *Z. zhoukaiyae*.

Species	*Z. daweishanensis* sp. nov.	*Z. nanshanensis* sp. nov.	*Z. dorsoviridis*	*Z. nigropunctatus*	*Z. zhoukaiyae*	*Z. lishuiensis*	*Z. yunnanensis*	*Z. thaoae*
Color of iris	The upper half of the iris is orange, and the lower half is yellow–brown	Yellowish–brown	Orange red or The upper half of the iris is orange, and the lower half is yellow–brown	Yellowish gold	Golden–yellow	Yellow	Yellowish–brown	Red–bronze
Finger webbing	Webbed one third	Webbed one third	Webbed one third	Rudimentary	Webbed half	Webbed one third	Webbed one third	Webbed one third
Toe webbing	Webbed half	Webbed half	Webbed half	Webbed half	Webbed 2/3	Webbed half	Webbed half	Webbed half
Webbing color	Light yellow	Webbing between inner three fingers and toes light yellow and webbing between fingers III and IV and between outer three toes greyish in males	Gray or greenish yellow	Grayish	Grayish	Golden yellow	Grayish	Ventral side of webbing orange with some gray pattern
Coloration of dorsum	Green	Uniformly green or green with some irregularly indigo blue patch	Green or green with small yellow spots scattered on the dorsal surface	Green or green with small yellow spots scattered on the dorsal surface	The dorsal and lateral sides/surfaces of the body are bright green without spots	Uniformly green or green with with sparse light blue–green specks	Green or green with small yellow spots scattered on the dorsal surface	Dorsal surface of the head and body green without spots
Coloration of belly	Yolk yellow	Bright yellow	White or yellow	Grayish–white	Yellowish–white	Golden yellow	Cream white mottled with yolk yellow	Light yellow
Colorations of flanks	Cream mottled with saffron yellow	Yellow with faint small black mottled shadows	Grayish–white or orange red	Yellow	Cream bellow with small brow spots	Golden yellow	Cream mottled with greyish–brown	Cream with a black blotch
Colorations of thighs	Orange–yellow	Bright yellow	Bright orange–red	Yellow or grayish	Yellowish with grayish blotching	Golden yellow	Light yellow	Orange
Black blotches in axilla, groin and posteriorpart of thigh	Unmarked or with large and conspicuous black spots.	Unmarked or densely covered with small specks	Large and conspicuous	Large	decorated with irregular grayish blotching	Unmarked or with small light gray spots	Large	Anterior part of thigh and ventral surface of tibia orange without spots; posterior parts of thigh orange with a large black blotch
Coloration of throat	Yolk yellow	White mottled with pale yellow and faint small black spots	White or yellow	The edge of the lower lip along the throat is dark gray	Yellowish–white	White	Black	Lower jaw cream, with grey marbling, and throat region white
Vocal sac	Internal	External	Internal	External	External	Internal	External	External
Source	this study	this study	Orlov et al. 2001; Zhang et al. 2011; Ostroshabov et al. 2013	Liu et al. 1962; Fei et al. 2012	Pan et al. 2017	Liu et al. 2017	Pan et al. 2024	Nguyen et al. 2024

Compared to other species with relatively similar body size, the new species can be easily distinguished from *Z. achantharrhena* (Lue, Lai & Chen, 1994), *Z. dulitensis*, *Z. faritsalhadii* Gonggoli, Munir, Kaprawi, Kirschey & Hamidy, 2024, *Z. jarujini* (Matsui & Panha, 2006), *Z. puerensis* (He, 1999) and *Z. wui* (Li, Liu, Chen, Wu, Murphy, Zhao, Wang & Zhang, 2012) by dorsum uniformly green (vs. green with black and white spots in *Z. achantharrhena*, yellowish-green with a few purplish dots on head and back and a purplish line round snout in *Z. dulitensis*, yellowish-green in *Z. faritsalhadii*, brownish with dark marking in *Z. jarujini*, green with many reddish-brown blotches edged with dark brown in *Z. puerensis* and dark yellowish-brown to light green with

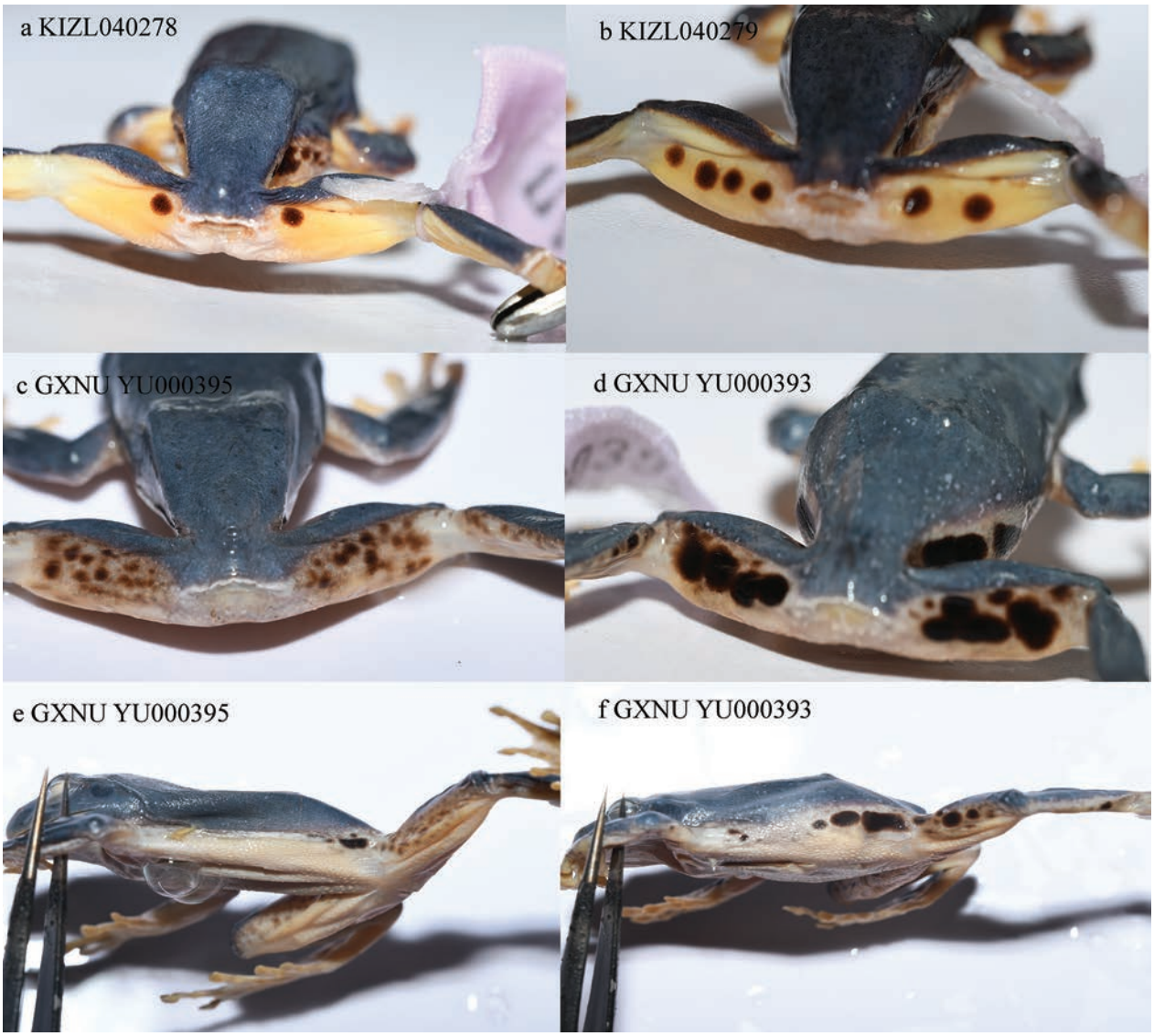

Figure 9. Morphological variation in color pattern of *Z. daweishanensis* sp. nov. in preservative. Photos by Yuanqiang Pan.

numerous light-brown spots in *Z. wui*); from *Z. chenfui* (Liu, 1945), *Z. hungfuensis* (Liu & Hu, 1961), *Z. leucofasciatus* (Liu & Hu, 1962), *Z. lishuiensis*, *Z. minimus* (Rao, Wilkinson & Liu, 2006), *Z. suffry* (Bordoloi, Bortamuli & Ohler, 2007), *Z. taipeianus* (Liang & Wang, 1978) and *Z. yaoshanensis* (Liu & Hu, 1962) by having black blotches in axilla, groin and posterior part of thigh (vs. absent); from *Z. jodiae*, *Z. melanoleucus* Brakels, Nguyen, Pawangkhanant, Idiiatullina, Lorphengsy, Suwannapoom & Poyarkov, 2023, *Z. moltrechti* (Boulenger, 1908), *Z. nigropunctatus*, *Z. pinglongensis* (Mo, Chen, Liao & Zhou, 2016), *Z. yunnanensis*, and *Z. zhoukaiyae* by vocal sac internal (vs. external); and from *Z. schlegelii* by throat yolk yellow (vs. throat faintly mottled with brown) (Suppl. material 3).

The new species is distinguishable from *Z. amamiensis* (Inger, 1947), *Z. arboreus* (Okada & Kawano, 1924), *Z. arvalis* (Lue, Lai & Chen, 1995), *Z. aurantiventris* (Lue, Lai & Chen, 1994), *Z. burmanus* (Andersson, 1939), *Z. dennysi* (Blanford, 1881), *Z. duboisi* (Ohler, Marquis, Swan & Grosjean, 2000), *Z. dugritei*, *Z. feae* (Boulenger, 1893), *Z. franki* Ninh, Nguyen, Orlov, Nguyen & Ziegler, 2020, *Z. hongchibaensis* (Li, Liu, Chen, Wu, Murphy, Zhao, Wang & Zhang, 2012), *Z. hui*, *Z. omeimontis*, *Z. owstoni* (Stejneger, 1907), *Z. pachyproctus* Yu, Hui, Hou, Wu, Rao & Yang, 2019, *Z. prasinatus* (Mou, Risch & Lue, 1983), *Z. prominanus* (Smith, 1924), *Z. smaragdinus* (Blyth, 1852), *Z. viridis* (Hallowell, 1861), and *Z. yinggelingensis* (Chou, Lau & Chan, 2007) by smaller body size (SVL 32.0–33.5 mm) (vs. SVL > 50 mm in the following species) and a combination of the following characters: dorsal surface uniformly green and no brown stripe along canthus rostralis and supratympanic fold (vs. dorsal surface green with brown blotches and a brown stripe along canthus rostralis in *Z. burmanus*, *Z. duboisi*, *Z. hongchibaensis*, *Z. hui*, and *Z. omeimontis*, green or dark brown with irregularly brown spots in *Z. dugritei*); the upper half of iris orange and the lower half yellow-brown (vs. greenish in *Z. amamiensis*, *Z. burmanus*, *Z. arboreus*, reddish in

Figure 10. Habitat of *Z. daweishanensis* sp. nov. at the type locality. Photo by Guohua Yu.

Z. prominanus, yellow in *Z. arvalis*, pale yellow in *Z. aurantiventris*, yellowish-gold in *Z. dennysi*, *Z. omeimontis*, *Z. prasinatus*, and *Z. smaragdinus*, dark gold in *Z. duboisi*, yellowish-brown in *Z. dugritei*, *Z. hongchibaensis*, reddish brown in *Z. hui*, yellowish gold mottled with silver in *Z. owstoni*, silver in *Z. yinggelingensis*); internal vocal sac (vs. external vocal sac in *Z. arvalis*, *Z. dugritei*, *Z. hui*, and *Z. prasinatus*); and black blotches in axilla, groin and anterior and posterior part of thighs (vs. absent *Z. arvalis*, *Z. aurantiventris*, *Z. dennysi*, *Z. feae*, *Z. franki*, *Z. pachyproctus*, *Z. prominanus* and *Z. smaragdinus*) (Suppl. material 3).

Zhangixalus nanshanensis sp. nov.

https://zoobank.org/68E0B4AE-3831-43BA-B5AD-EB5D5B39DBE8

Figs 11–13

Nanshan tree frog/Nān Shān Shù wā (南山树蛙)

Holotype. GXNU YU000771, adult male, collected on 5 April 2024 by Guohua Yu, Shangjing Tang, and Ju Chen from Nanshan National Park, Chengbu County, Hunan Province, China (26°8'50.17"N, 110°8'4.31"E, 1785 m a.s.l.).

Paratypes. Six adult males (GXNU YU000772–YU000776, GXNU YU000778) and an adult female (GXNU YU000777) were collected on 5 April 2024 by Guohua Yu, Shangjing Tang, and Ju Chen from the type locality.

Etymology. The species epithet is named for Nanshan National Park, Chengbu County, Hunan, China, where the species was collected. We suggest the English common name "Nanshan tree frog" and the Chinese common name "Nān Shān Shù wā (南山树蛙)".

Diagnosis. The new treefrog species is assigned to *Zhangixalus* by the presence of intercalary cartilage between terminal and penultimate phalanges of digits, Y-shaped distal end of terminal phalanx, tips of digits expanded into large discs bearing circum-marginal grooves, and vomerine teeth present, dermal folds along limbs not significant, tarsal projections absent, green dorsal colouration and medium body size (Jiang et al. 2019). Phylogenetically, the new species is nested within the genus *Zhangixalus* with strong support (100% for BI and 99% for ML).

Zhangixalus nanshanensis sp. nov. can be distinguished from its congeners by a combination of the following characters: 1) body size medium (SVL 28.1–36.7 mm in males); 2) head width less wider than long; 3) iris yellowish-brown; 4) heels not meeting when legs positioned at right angle to body, tibiotarsal articulation reaching posterior corner of eye; 5) dorsum uniformly green or green with some irregularly indigo blue patch; 6) posterior part of thigh yellow with small black blotches; 7) ventral side of hand and foot bright yellow with irregular gray-brown spots; 8) flanks cream mottled with saffron yellow and have faint small black mottled shadows; 9) vocal sac external; 10) throat pale saffron yellow with faint small black spots; 11) webbing between fingers and toes greyish in females, and webbing between inner three fingers and toes light yellow, and webbing between fingers III and IV and between outer three toes greyish in males; 12) fingers webbed one third, webbing formula I2–2⅓II1½–3III2⅓–2IV, and toes webbed half, webbing formula I1–2II1–2III1–2½IV3–1V.

Description of holotype. Adult male, body robust, size small (SVL 33.7 mm); head length slightly less than the head width, HL (12.0 mm) 99.2% of HW (12.1 mm); snout bluntly rounded, possesses canthus rostralis, the tip of the snout slightly protrudes beyond the edge of the lower jaw in ventral view; snout (SL 5.2 mm) longer than eye (ED 4.6 mm); nostril oval, slightly protuberant, located at the one-third between snout tip and eye; IND (3.9 mm) shorter than IOD (4.2 mm) and wider than UEW (2.4 mm); pineal spot absent; pupil oval, horizontal; tympanum small (TD 2.1 mm), rounded, smaller than ED (4.6 mm), nearly equal to the distance between eye and nostril (DNE 2.2 mm); supratympanic fold distinct, curves from posterior edge of eye to insertion of arm; vomerine teeth distinct; choanae oval, horizontal; tongue attached anteriorly and notched posteriorly; single external vocal sac, with a sac slit opening on floor of mouth at each corner.

Relative length of fingers I < II < IV < III; tips of all fingers expanded into discs with circum-marginal grooves; nuptial pad present on first finger; fingers webbed one third, webbing formula I2–2⅓II1½–3III2⅓–2IV; lateral fringe on free edge of all fingers; subarticular tubercles prominent and rounded, formula 1, 1, 2, 2; supernumerary tubercles present; inner metacarpal tubercle large, ovoid, outer metacarpal tubercle small, flattened, and divided into two; dermal fringe along outer edge of forearm present, not well developed.

Hind limbs moderate long, heels not meeting when legs positioned at right angle to body; tibiotarsal articulation reaching posterior margin of eye; relative length of toes I < II < V < III < IV; tibia (TL 15.0 mm) 44.5% of body size, longer than foot (FL 14.6 mm); tips of toes expanded into discs with circum-marginal grooves, smaller than finger discs; toes webbed half, webbing formula I1–2II1–2III1–2½IV3–1V; subarticular tubercles prominent and rounded, formula 1, 1, 2, 3, 2; supernumerary tubercles present; inner metatarsal tubercle oval, prominent; outer metatarsal tubercle absent.

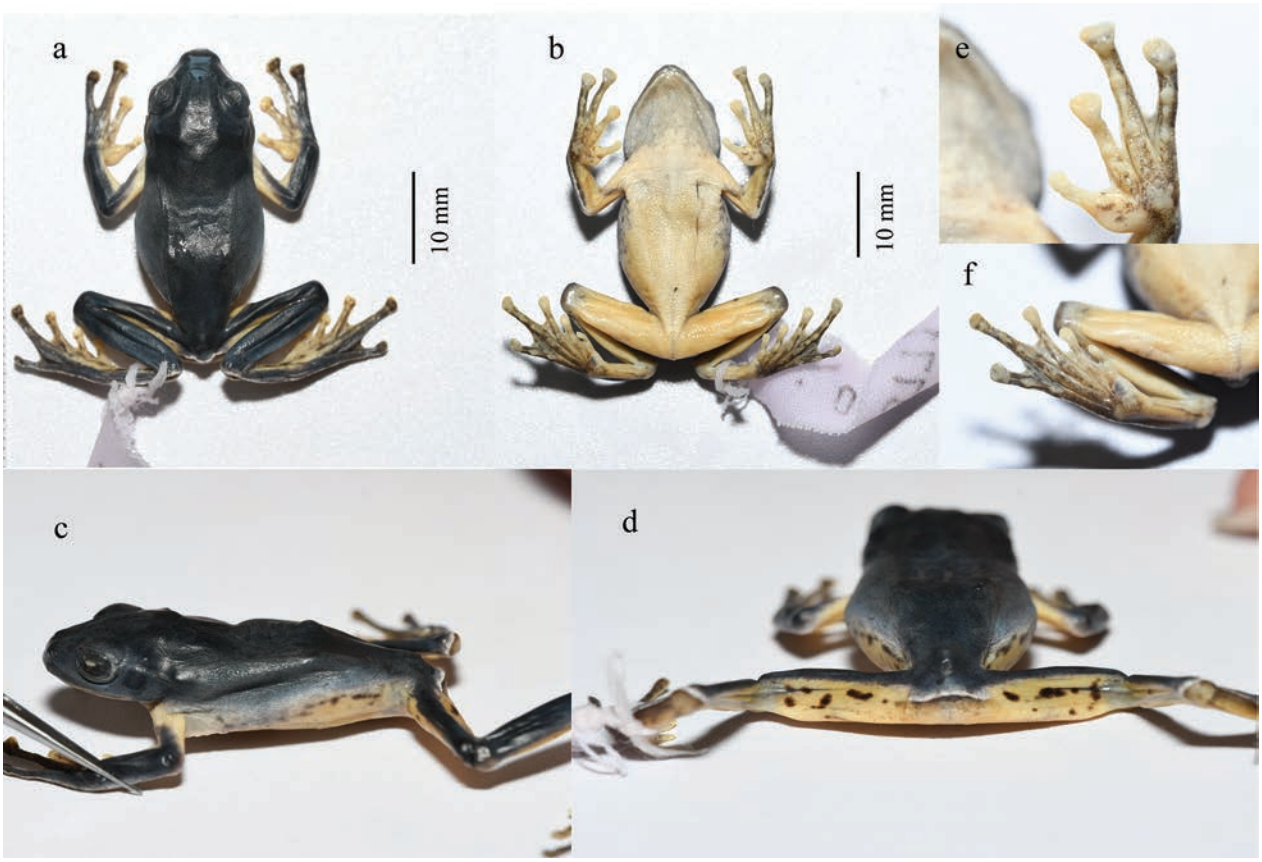

Figure 11. Views of the adult male holotype of *Z. nanshanensis* sp. nov. (GXNU YU000771) in preservative. Photos by Yuanqiang Pan.

Dorsal surface of body and head smooth; dorsolateral folds absent; throat granular; chest, belly, and ventral surface of limbs granular.

Coloration in life. Iris yellowish-brown; dorsal surface grass green; side of head and tympanic region green; body of flanks green mottled with yellow; throat white mottled with pale yellow and faint small black spots; chest, abdomen, ventral surface of limbs, and dorsomedial surface of tibia and tarsus bright yellow; anterior and posterior parts of thigh yellow with small black blotches; faint small black mottled shadows on flank and groin; white fringes along outer edge from tibiotarsal articulation to the fifth toe; ventral surface of hand and foot yellow with greyish-brown spots; webbing between inner three fingers and toes light yellow and webbing between fingers III and IV and between outer three toes greyish; dorsal side of discs of fingers I and II and discs of toes I–III light yellow and dorsal side of discs of fingers III and IV and dorsal side of discs of toes IV and V greyish-brown (Fig. 12).

Coloration in preservative. Dorsal surface dark blue; lower part of flanks and ventral surface of body and limbs cream, throat milky white covered with greyish pattern; ventral surface of hand and foot cream with irregular gray-brown spots.

Sexual dimorphism. The new species is sexually dimorphic, with females being distinctly larger than males and having no vocal sac and nuptial pad. Males have external single subgular vocal sac and light-yellow nuptial pad on base of finger I. Ventral surface and anterior and posterior parts of thigh yolk yellow in males (vs. cream white in females) during breeding season.

Morphological variation. The colour pattern varied amongst individuals. The paratype GXNU YU000772 has only a few irregularly black spots on posterior surface of thigh, the paratype GXNU YU000775 has no large black spots on the posterior surface of thigh, and these two paratypes have no large black blotches on flank (Fig. 13). Throat of the female paratype GXNU YU000777 is white mottled with a few irregular dark blotches (Fig. 12). The paratypes GXNU YU000777 and GXNU YU000773 have some irregularly indigo blue patches on dorsum (Fig. 12). In addition, coloration of the new species in life can vary as day period and microhabitat change; dorsum is lighter nocturnally than during the day, with dorsal surfaces appearing light to dark green and even dark brown.

Distribution and ecology. The new species is currently known from the type locality (Nanshan National Park, Chengbu County, Hunan, China). During the surveys, the species was found calling in wet meadows nearby a pond at the type locality (Fig. 14). *Zhangixalus minimus* was also found at the same site during the surveys.

Comparison. Phylogenetically, the new species is closely related to *Z. lishuiensis* and *Z. zhoukaiyae*. *Zhangixalus nanshanensis* sp. nov. can be distinguished from *Z. lishuiensis* by vocal sac external (vs. internal), throat light yellow mottled with black spots in males (vs. white), shorter head (Fig. 15), outer metacarpal tubercle present (vs. absent), and

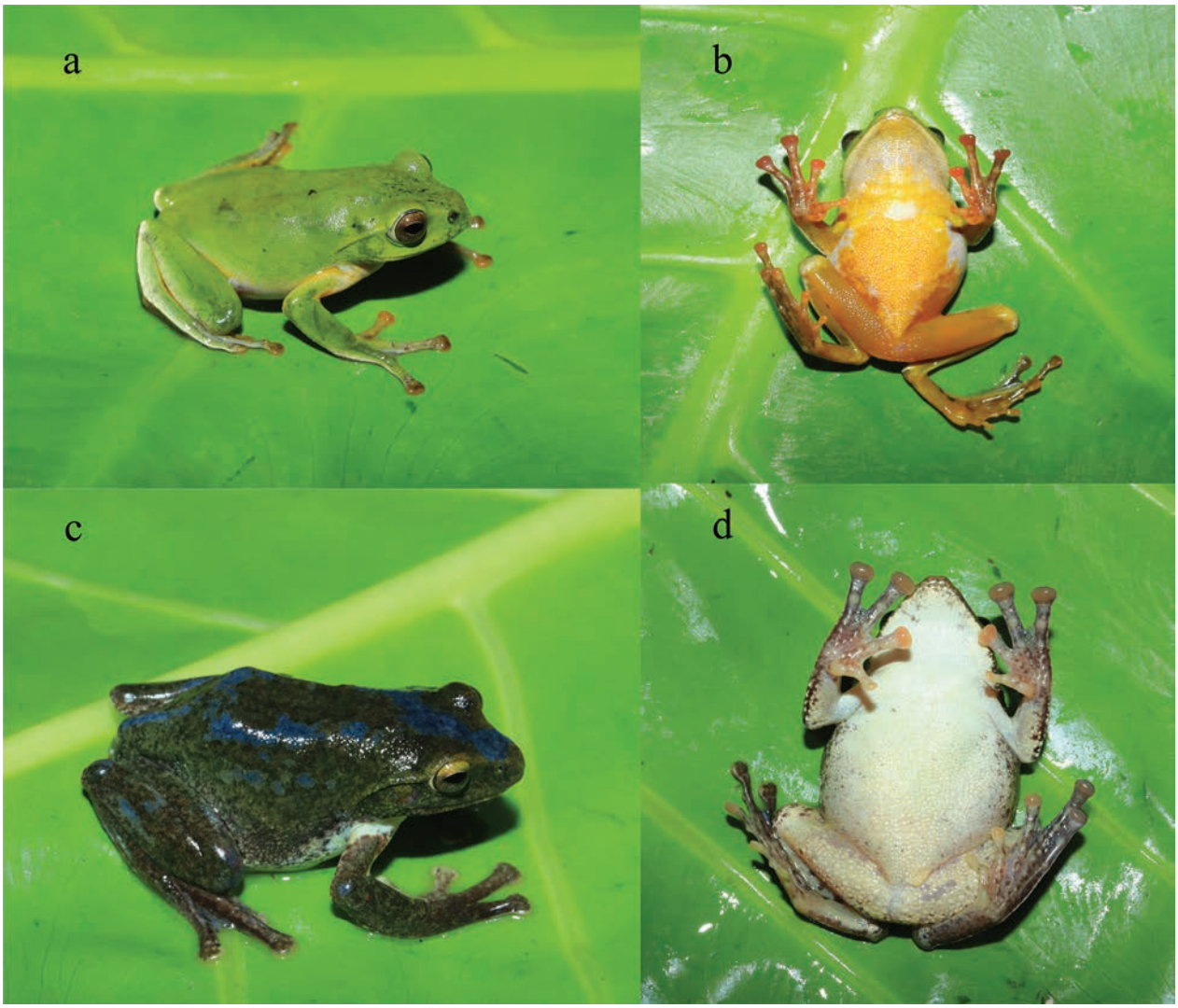

Figure 12. Views of the adult male holotype of *Z. nanshanensis* sp. nov. (GXNU YU000771; **a, b**) and adult female paratype of *Z. nanshanensis* sp. nov. (GXNU YU000777; **c, d**) in life. Photos by Guohua Yu

flanks cream mottled with saffron yellow and having faint small black mottled shadows (vs. flanks yellow). *Zhangixalus nanshanensis* sp. nov. can be distinguished from *Z. zhoukaiyae* by throat yellow with greyish brown blotches (vs. pure paler yellowish without black), outer metatarsal tubercle absent (vs. present), upper eyelid width smaller than interorbital distance (vs. upper eyelid width approximately equal to interorbital distance), and outer fingers webbed one third and outer toes webbed half (vs. fingers webbed half and outer toes webbed two thirds) (Tables 6, 7).

Zhangixalus nanshanensis sp. nov. can be distinguished from *Z. nigropunctatus*, with which the new species has previously been confused, by fingers webbed one third (vs. finger web rudimentary or 1/4 webbed), tibiotarsal articulation reaching posterior margin of eye (vs. reaching posterior margin of tympanum), ventral surface yellow in males (vs. greyish white), outer metatarsal tubercle absent (vs. present), snout steeper in profile (Fig. 15), and wider head, narrower upper eyelid, smaller tympanum, longer tibia, and longer foot and tarsus (Suppl. material 4: table S4).

Zhangixalus nanshanensis sp. nov. can be distinguished from *Z. yunnanensis* by throat light yellow mottled with greyish (vs. throat dark black), snout steeper in profile (Fig. 15), and fingers webbed nearly half (vs. rudimentary) (Table 7).

Zhangixalus nanshanensis sp. nov. can be distinguished from *Z. dorsoviridis* by iris yellowish-brown (vs. the upper half of iris orange and the lower half yellow-brown), external single subgular vocal sac (vs. internal single subgular vocal sac), throat yellow mottled with faint small black spots (vs. lacking dark spots on throat), ventral, anterior, and posterior surface of thigh and dorsomedial surface of tibia and tarsus yolk yellow in males (vs. orange-red; Suppl. material 4: fig. S1), and heels not meeting when legs positioned at right angle to body (vs. overlap) (Table 7).

Zhangixalus nanshanensis sp. nov. can be distinguished from *Z. thaoae* by iris yellowish-brown (vs. red-bronze), webbing between inner three fingers and toes light yellow, and webbing between fingers III and IV and between outer three toes greyish in males (vs. orange

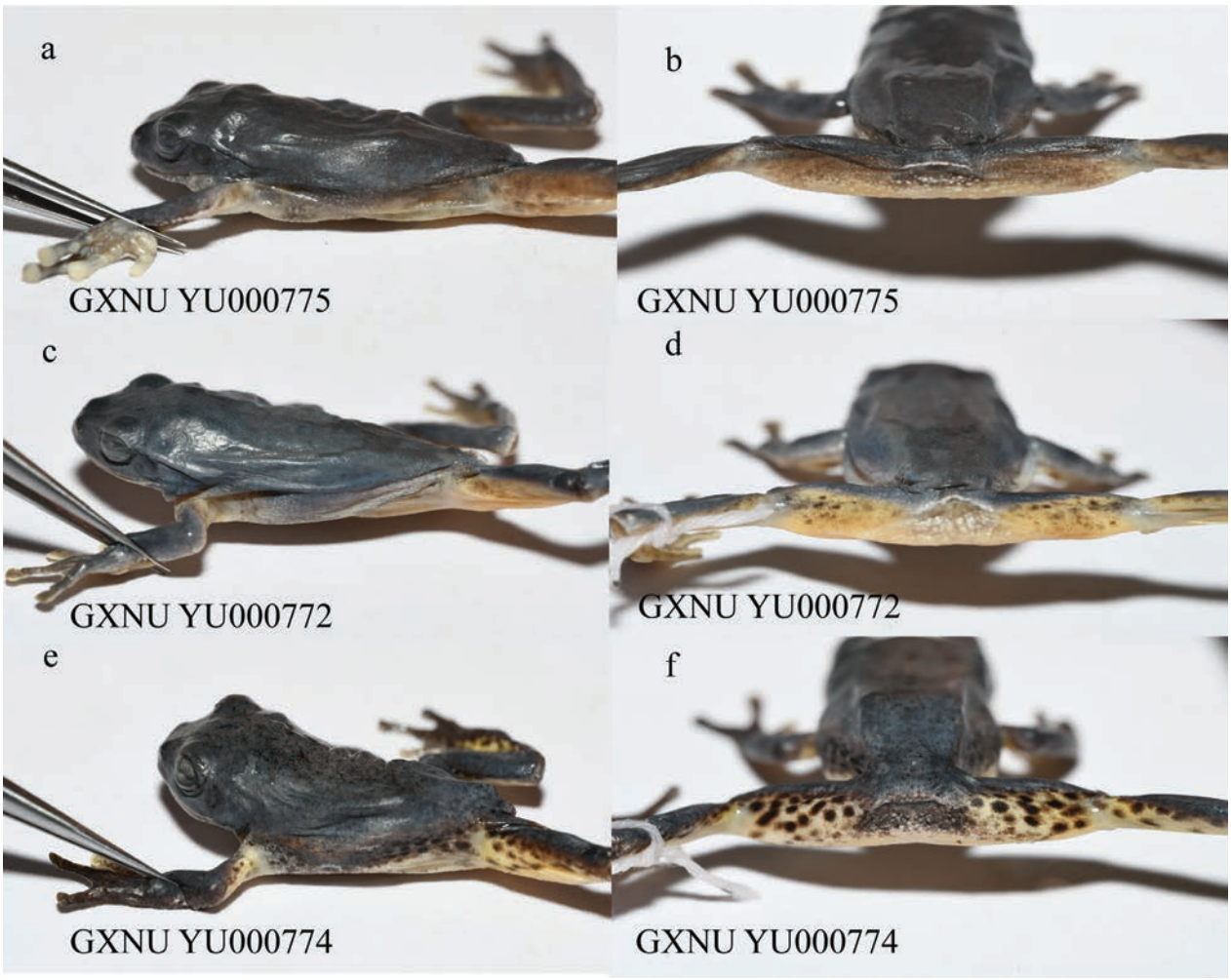

Figure 13. Morphological variation in color pattern of *Z. nanshanensis* sp. nov. in preservative. Photos by Yuanqiang Pan.

with some gray pattern), and heels not meeting when legs positioned at right angle to body (vs. overlap) (Table 7).

Zhangixalus nanshanensis sp. nov. can be distinguished from *Z. daweishanensis* sp. nov. by iris yellowish-brown (vs. the upper half of iris orange and the lower half yellow-brown; Suppl. material 4: fig. S1), external single subgular vocal sac (vs. internal single subgular vocal sac), throat yellow mottled with faint small black spots in males (vs. yellow with no black spots), and webbing between outer two fingers and webbing between outer three toes greyish in males (vs. yellow) (Table 7).

In body size, besides *Z. dorsoviridis*, *Z. lishuiensis*, *Z. nigropunctatus*, *Z. daweishanensis* sp. nov., *Z. thaoae*, *Z. yunnanensis*, and *Z. zhoukaiyae*, the new species is relatively similar to *Z. achantharrhena*, *Z. chenfui*, *Z. dulitensis*, *Z. hungfuensis*, *Z. faritsalhadii*, *Z. jarujini*, *Z. jodiae*, *Z. leucofasciatus*, *Z. melanoleucus*, *Z. minimus*, *Z. moltrechti*, *Z. pinglongensis*, *Z. puerensis*, *Z. schlegelii*, *Z. suffry*, *Z. taipeianus*, *Z. wui*, and *Z. yaoshanensis*. The new species can be easily distinguished from *Z. achantharrhena*, *Z. dulitensis*, *Z. faritsalhadii*, *Z. jarujini*, *Z. puerensis* and *Z. wui* by dorsum uniformly green (vs. green with black and white spots in *Z. achantharrhena*, yellowish-green with a few purplish dots on head and dorsum and a purplish line round snout in *Z. dulitensis*, yellowish-green with numerous dark spot and irregular blotches cream in *Z. faritsalhadii*, brownish with dark marking in *Z. jarujini*, green with many reddish-brown blotches edged with dark brown in *Z. puerensis* and dark yellowish-brown to light green with numerous light-brown spots in *Z. wui*); from *Z. chenfui*, *Z. hungfuensis*, *Z. leucofasciatus*, *Z. minimus*, *Z. suffry*, *Z. taipeianus* and

Figure 14. Habitat of the *Z. nanshanensis* sp. nov. at the type locality. Photo by Guohua Yu

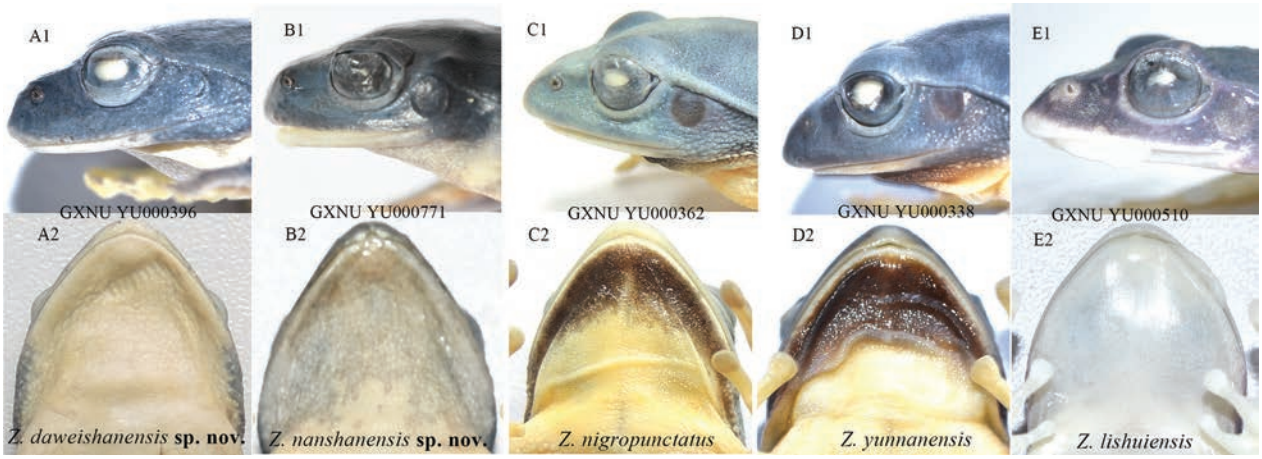

Figure 15. Lateral views of the head and throat of *Z. daweishanensis* sp. nov., *Z. nanshanensis* sp. nov., *Z. nigropunctatus*, *Z. yunnanensis*, and *Z. lishuiensis*. Photo by Guohua Yu.

Z. yaoshanensis by having black blotches in axilla, groin and posterior part of thigh (vs. absent); from *Z. schlegelii* by vocal sac external (vs. internal); from *Z. jodiae*, *Z. moltrechti*, and *Z. pinglongensis* by throat saffron yellow mottled with faint small black spots (vs. greyish in *Z. jodiae*, white in *Z. moltrechti*, and white with slightly gray background in *Z. pinglongensis*); and from *Z. melanoleucus* by webbing between inner three fingers and toes light yellow and webbing between fingers III and IV and between outer three toes greyish (vs. mottled with black blotches in *Z. melanoleucus*) (Suppl. material 3).

The new species is distinguishable from *Z. amamiensis*, *Z. arboreus*, *Z. arvalis*, *Z. aurantiventris*, *Z. burmanus*, *Z. dennysi*, *Z. duboisi*, *Z. dugritei*, *Z. feae*, *Z. franki*, *Z. hongchibaensis*, *Z. hui*, *Z. omeimontis*, *Z. owstoni*, *Z. pachyproctus*, *Z. prasinatus*, *Z. prominanus*, *Z. smaragdinus*, *Z. viridis*, and *Z. yinggelingensis* by smaller body size and a combination of the following characters: 1) dorsal surface uniformly green and no brown stripe along canthus rostralis and supratympanic fold (vs. dorsal surface green with brown blotches and a brown stripe along canthus rostralis in *Z. burmanus*, *Z. duboisi*, *Z. hongchibaensis*, *Z. hui*, and *Z. omeimontis*, green or dark brown with irregularly brown spots in *Z. dugritei*); 2) iris is yellowish-brown (vs. greenish in *Z. amamiensis*, *Z. burmanus* and *Z. arboreus*, reddish in *Z. prominanus*, yellow in *Z. arvalis*, pale yellow in *Z. aurantiventris*, yellowish-gold in *Z. dennysi*, *Z. omeimontis*, *Z. prasinatus*, and *Z. smaragdinus*, dark gold in *Z. duboisi*, reddish brown in *Z. hui*, yellowish gold mottled with silver in *Z. owstoni*, and silver in *Z. yinggelingensis*); 3) external vocal sac (vs. internal vocal sac in *Z. amamiensis*, *Z. arboreus*, *Z. aurantiventris*, *Z. burmanus*, *Z. dennysi*, *Z. feae*, *Z. hongchibaensis*, *Z. omeimontis*, *Z. owstoni*, *Z. pachyproctus*, *Z. smaragdinus*, *Z. viridis* and *Z. yinggelingensis*; and 4) black blotches in axilla, groin and anterior and posterior part of thighs (vs. absent in *Z. arvalis*, *Z. aurantiventris*, *Z. dennysi*, *Z. feae*, *Z. franki*, *Z. pachyproctus*, *Z. prominanus* and *Z. smaragdinus*) (Suppl. material 3).

Discussion

It has been revealed that *Z. nigropunctatus*, which was once recorded widely in central and south-western China (Fei et al. 2012) and north-western Vietnam (Poyarkov et al. 2021), actually involves multiple misidentified populations (Yu et al. 2019a; Li et al. 2012a; Mo et al. 2016; Pan et al. 2017; Pan et al. 2024; Nguyen et al. 2024), some of which were moved into other known species (e.g., Li et al. 2012a) and some of which were described as new species (e.g., Pan et al. 2017; Pan et al. 2024; Nguyen et al. 2024). In Hunan, China, *Z. nigropunctatus* was recorded from Chengbu and Sangzhi Counties (Fei et al. 2012; AmphibiaChina 2024). In this study, based on molecular and morphological evidence, we revealed that the Chengbu population in southwestern Hunan represents an independent species of *Zhangixalus*. This result further improves our understanding of the taxonomy of the *Z. nigropunctatus* complex and implies that the taxonomy of the Sangzhi population of *Z. nigropunctatus* also needs further investigation. In addition, *Z. nigropunctatus* is also recorded from southeastern Guizhou (Leishan County; AmphibiaChina 2024), which is adjacent to southwestern Hunan. It is possible that the Leishan population belongs to *Z. nanshanensis* sp. nov. pending additional data. Similarly, it could be expected that this new species would be found in adjacent northeastern Guangxi (Fig. 1).

It is a little surprise that there is a novel lineage of *Zhangixalus* (*Z. daweishanensis* sp. nov.) allied to *Z. dorsoviridis* at Mt. Dawei, Pingbian, Yunnan. Yu et al. (2009) and Li et al. (2012a) found that *Z. nigropunctatus* from Pingbian and Jinping did not group together with topotypes of this species, and Li et al. (2012a) placed these two populations into *Z. dorsoviridis* as they are closely related to *Z. dorsoviridis* with low genetic divergence. Around the same time, Zhang et al. (2011) reported the first record of *Z. dorsoviridis* from China based on samples collected from Mt. Dawei, Pingbian. In this study, we found the newly collected specimens from Mt. Dawei, Pingbian, form a distinct clade, being sister to *Z. dorsoviridis*,

and morphologically can be distinguished from *Z. dorsoviridis* by a series of characters. It is interesting that there are two sibling species living in sympatry at Mt. Dawei, Pingbian, and additional studies are required to investigate the mechanism of speciation of these two species.

In addition, more studies are required to unravel the taxonomy and distribution of *Z. dorsoviridis*, which is exactly known from northern Vietnam (Sa Pa) and southern Yunnan (Jinping and Pingbian) based on the present and previous phylogenetic analyses (Li et al. 2012a; Pan et al. 2024). Hou et al. (2017) recorded this species from Maoershan National Nature Reserve, Guilin, Guangxi. Geographically, this site is far away from northern Vietnam and southern Yunnan, and morphologically, the Maoershan population differs from *Z. dorsoviridis* from northern Vietnam and southern Yunnan in color pattern (Fig. 16) and nuptial pad, which is absent in *Z. dorsoviridis* according to Orlov et al. (2001) but present on the base of finger I in the Maoershan population (Hou et al. 2017). Therefore, we consider that the taxonomy of nominal *Z. dorsoviridis* from Maoershan National Nature Reserve remains unclear. Additionally, the specimen VNMN 4099, which was collected from Son La, Vietnam, and was identified as *Z. dorsoviridis* (Nguyen et al. 2014), was recovered as sister to *Z. thaoae*, indicating that the taxonomic status of this specimen remains undetermined and probably represents a cryptic species. Being inconsistent with the phylogenetic analyses, the ASAP analysis assigned *Z. jodiae* (voucher number: VNMN 07122) and VNMN 4099 into one taxon, and the genetic distance between them was estimated to be zero. This is due to the fact that the sequence of VNMN 4099 (LC010577, 461 bp) overlapped only partially with the sequence of *Z. jodiae* (LC545595, 725 bp), and the overlapping region has no mutation. Furthermore, we found that the male specimen TBUPAE525 of nominal *Z. dorsoviridis* from near Nong Vai Village, Son La Province, Vietnam (Pham et al. 2017) is distinguishable from *Z. dorsoviridis* by iris yellow (vs. upper of iris bright orange; Fig. 16) and larger body size (54.1 mm vs. maximum length 43.2 mm for adult male of *Z. dorsoviridis* from the type locality), implying that this specimen from Son La Province, Vietnam, may also be a misidentification.

Recently, Dufresnes and Litvinchuk (2022) considered *Z. hui* as a synonym of *Z. dugritei*, noted that *Z. lishuiensis* is likely conspecific with *Z. zhoukaiyae*, and *Z. duboisi* is likely conspecific with *Z. omeimontis* (Dufresnes and Litvinchuk 2022). However, we consider that the taxonomic rearrangements of Dufresnes and Litvinchuk (2022) should be treated with caution. Dufresnes and Litvinchuk (2022) estimated the divergence between *Z. duboisi* and *Z. omeimontis* to be 1.5% using a sample of nominal *Z. duboisi* from Pingbian, Yunnan (voucher YN080484, GenBank accession: JX219418). However, *Z. duboisi* from Pingbian actually belongs to *Z. omeimontis* (Shui et al. 2023) and we recovered that *Z. duboisi* is sister to *Z. puerensis* and *Z. omeimontis* is sister to *Z. franki* (Fig. 2). The divergence between *Z. duboisi* and *Z. omeimontis* in 16S rRNA is estimated to be 5.1%. These results support that *Z. duboisi* and *Z. omeimontis* are distinctive from each other.

Owing to the fact that *Z. zhoukaiyae* and *Z. lishuiensis* were morphologically similar and the genetic divergence between them is relatively low, the taxonomic status of

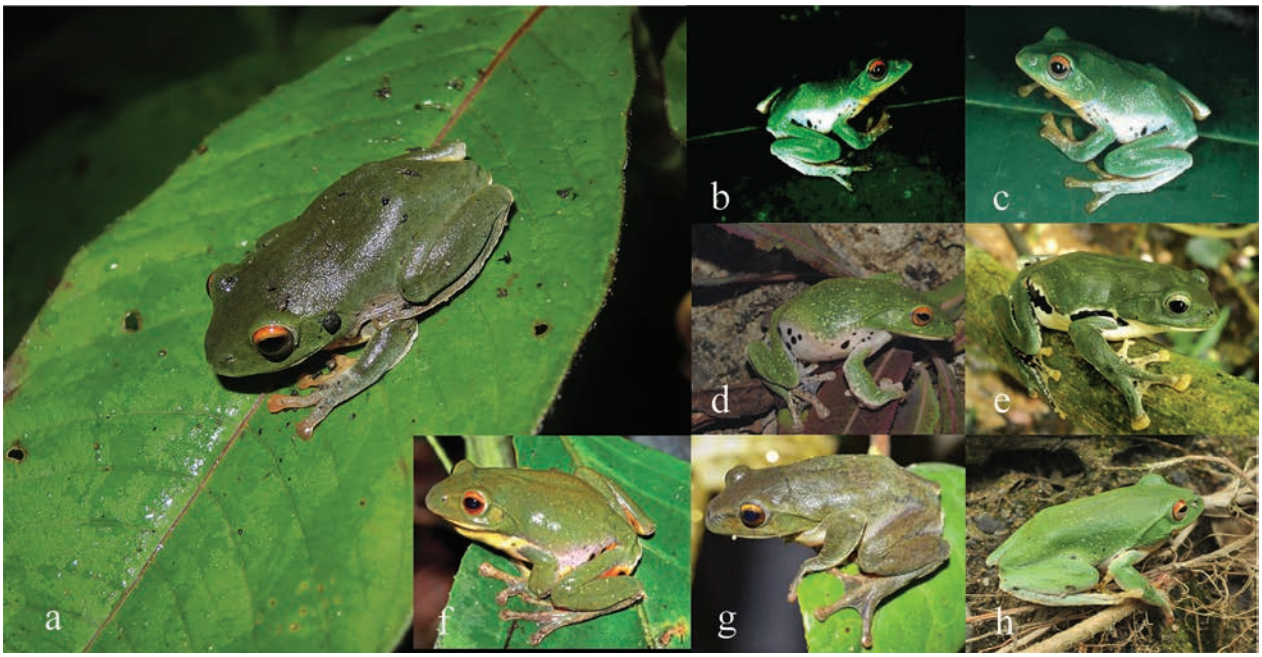

Figure 16. Views of *Z. daweishanensis* sp. nov. from the type locality (**a**; photo by Guohua Yu) and *Z. dorsoviridis* from Sa Pa, Vietnam (type locality; **b–d**), Copia NR, Vietnam (**e**; TBU PAE 525), Pingbian, Yunnan, China (**f, h**), and Mao'er Mountain, Guangxi, China (**g**). The images in **b–h** were reproduced from Orlov et al. (2001), Orlov et al. (2008), Mo et al. (2016), Pham et al. (2017), Zhang et al. (2011), Hou et al. (2017), and Pan et al. (2017), respectively.

these two species was questioned (Dufresnes and Litvinchuk 2022; Brakels et al. 2023; Hong et al. 2024). In this study, we revealed that *Z. lishuiensis* can be distinguished from *Z. zhoukaiyae* by a longer head (Fig. 5), and they were assigned into different taxa by both analyses of species delimitation. Therefore, combining the morphological distinctions outlined in the original descriptions, e.g., *Z. zhoukaiyae* has an external vocal sac (Pan et al. 2017), whereas *Z. lishuiensis* has an internal vocal sac (Liu et al. 2017) (Table 7 and Suppl. material 4: table S6), we agree with Pan et al. (2024) that *Z. zhoukaiyae* and *Z. lishuiensis* are two separate species. Additionally, although the genetic divergence between *Z. hui* and *Z. dugritei* is low, they differ from each other in karyotype structure and snout color (yellow-brown in *Z. hui* and green in *Z. dugritei*; Li et al. 2012b). So, we temporarily regard the *Z. hui* and *Z. dugritei* as two separate species, as other genetic factors (gene introgression or incomplete lineage sorting) may have led to their extremely low genetic distance.

In summary, we revealed that the species diversity in *Zhangixalus* was underestimated and described two cryptic species of this genus. Moreover, our results indicated the *Z. nigropunctatus* and *Z. dorsoviridis* complexes involve other cryptic species and misidentifications. Therefore, additional studies are required to resolve these taxonomic confusions and clarify the species diversity of the genus *Zhangixalus* based on multiple lines of evidence.

Acknowledgements

We thank Shangjing Tang for her assistance with sample collection. Thanks also go to Xiangjian Wu for his help in collecting distribution data. This work was supported by grants from the National Natural Science Foundation of China (32060114, 32460128), Guangxi Natural Science Foundation Project (2022GXNSFAA035526), and Key Laboratory of Ecology of Rare and Endangered Species and Environmental Protection (Guangxi Normal University), Ministry of Education (ERESEP2022Z04).

References

AmphibiaChina (2024) The database of Chinese amphibians. Kunming Institute of Zoology (CAS), Kunming, Yunnan, China. https://www.Amphibiachina.org [Accessed 4 May 2024]

Andersson LG (1939) [1938] Batrachians from Burma collected by Dr. R. Malaise, and from Bolivia and Ecuador collected by Dr. C. Hammarlund. Arkiv för Zoologi. Stockholm 30(23): 1–24.

Blanford WT (1881) On a collection of reptiles and frogs chiefly from Singapore. Proceedings of the Zoological Society of London 1881(1): 215–226. https://doi.org/10.1111/j.1096-3642.1881.tb01281.x

Blyth E (1852) Report of Curator, Zoological Department. Journal of the Asiatic Society of Bengal 21: 341–358.

Bordoloi S, Bortamuli T, Ohler A (2007) Systematics of the genus *Rhacophorus* (Amphibia, Anura): identity of red-webbed forms and description of a new species from Assam. Zootaxa 1653: 1–20. https://doi.org/10.11646/zootaxa.1653.1.1

Boulenger GA (1892) An account of the reptiles and batrachians collected by Mr. C. Hose on Mt. Dulit, Borneo. Proceedings of the Zoological Society of London 1892: 505–508.

Boulenger GA (1893) Concluding report on the reptiles and batrachians obtained in Burma by Signor L. Fea dealing with the collection made in Pegu and the Karin Hills in 1887–88. Annali del Museo Civico di Storia Naturale di Genova (Serie 2) 13: 304–347.

Boulenger GA (1908) Descriptions of a new frog and a new snake from Formosa. Annals and Magazine of Natural History (Series 8) 2: 221. https://doi.org/10.1080/00222930808692472

Bourret R (1937) Notes herpétologiques sur l'Indochine française. XIV. Les batraciens de la collection du Laboratoire des Sciences Naturelles de l'Université. Descriptions de quinze especes ou variétés nouvelles. Annexe au Bulletin Général de l'Instruction Publique Hanoi 1937: 5–56.

Brakels P, Nguyen TV, Pawangkhanant P, Idiiatullina S, Suwannapoom C, Poyarkov NA (2023) Mountain jade: A new high–elevation microendemic species of the genus *Zhangixalus* (Amphibia: Anura: Rhacophoridae) from Laos. Zoological Research 44: 374–379. https://doi.org/10.24272/j.issn.2095-8137.2022.382

Chen WC, Liao XW, Zhou SC, Mo YM, Huang Y (2018) Rediscovery of *Rhacophors yaoshanensis* and *Theloderma kwangsiensis* at their type localities after five decades. Zootaxa 4379(4): 484–496. https://doi.org/10.11646/zootaxa.4379.4.2

Chou WH, Lau MW, Chan BPL (2007) A new treefrog of the genus *Rhacophorus* (Anura: Rhacophoridae) from Hainan Island, China. Raffles Bulletin of Zoology Singapore 55: 157–165.

Darriba D, Taboada GL, Doallo R, Posada D (2012) jModelTest 2: more models, new heuristics and parallel computing. Nature Methods 9: 772. https://doi.org/10.1038/nmeth.2109

David A (1872) [1871] Rapport adressé a MM. les Professeurs–Administráteurs du Museum d'histoire naturelle. Nouvelles Archives du Muséum d'Histoire Naturelle Paris 7: 75–100.

Dufresnes C, Litvinchuk SN (2022) Diversity, distribution and molecular species delimitation in frogs and toads from the Eastern Palaearctic. Zoological Journal of the Linnean Society 195: 695–760. https://doi.org/10.1093/zoolinnean/zlab083

Fei L (1999) Atlas of Amphibians of China., Henan Publishing House of Science and Technology, Zhengzhou.

Fei L, Hu SQ, Ye CY, Huang YZ (2009) Fauna Sinica. Amphibia. Volume 3. Anura Ranidae. Science Press, Beijing.

Fei L, Ye CY, Jiang JP (2010) Colored Atlas of Chinese Amphibians.: Sichuan Publishing House of Science and Technology, Chengdu.

Fei L, Ye YC, Jiang JP (2012) Colored Atlas of Chinese Amphibians and Their Distributions. Sichuan Publishing House of Science and Technology, Chengdu.

Frost DR (2024) Amphibian Species of the World: an Online Reference. Version 6.2. American Museum of Natural History, New York. https://amphibiansoftheworld.amnh.org/index.php [Accessed 15 Oct 2024]

Gonggoli AD, Munir M, Kaprawi F, Kirschey T, Hamidy A (2024) A new species of tree frog (Amphibia, Anura, Rhacophoridae) from Central Java, Indonesia. Raffles Bulletin of Zoology Singapore 72: 219–234. https://doi.org/10.26107/RBZ–2024–0019

Hallowell E (1861) [1860] Report upon the Reptilia of the North Pacific Exploring Expedition, under command of Capt. John Rogers, U.S. N. Proceedings. Academy of Natural Sciences of Philadelphia 12: 480–510.

Harvey MB, Pemberton AJ, Smith EN (2002) New and poorly known parachuting frogs (Rhacophoridae: *Rhacophorus*) from Sumatra and Java. Herpetological Monographs 16: 46–92. https://doi.org/10.1655/0733-1347(2002)016[0046:NAPKPF]2.0.CO;2

He XR (1999) A new species of the family Rhacophoridae from Yunnan—*Polypedates puerensis*. Sichuan Journal of Zoology 18: 99–100.

Hong F, Yu L, Han J, Fang J (2024) Discussion on the Attribution of Species of the Genus *Zhangixalus* at the Junction of Zhejiang and Anhui, China. Chinese Journal of Zoology 59: 225–232. https://doi.org/10.13859/j.cjz.202422288

Hou SB, Yuan ZY, Jiang K, Zhao LS, Wang SN, Wu ZJ, Che J (2017) *Rhacophorus dorsoviridis* Bourret, a new record of amphibians in Guangxi and comparison with morphologically similar species. Sichuan Journal of Zoology 36: 59–60.

Inger RF (1947) Preliminary survey of the amphibians of the Riukiu islands. Fieldiana Zoology 32: 297–352. https://doi.org/10.5962/bhl.title.2991

Inger RF (1966) The systematics and zoogeography of the Amphibia of Borneo. Fieldiana Zoology 52: 1–402. https://doi.org/10.5962/bhl.title.3147

Jiang K, Wang K, Yang JX, Jin J, Dahu Z, Yan F, Pan H, Che J (2016) Two new records of Amphibia from Tibet, China, with description of *Rhacophorus burmanus*. Sichuan Journal of Zoology 35(2): 210–216.

Jiang D, Jiang K, Ren J, Wu J, Li J (2019) Resurrection of the genus *Leptomantis*, with description of a new genus to the family Rhacophoridae (Amphibia: Anura). Asian Herpetological Research 10: 1–12. https://doi.org/10.16373/j.cnki.ahr.180058

Leache AD, Reeder TW (2002) Molecular systematics of the Eastern Fence Lizard (*Sceloporus undulatus*): a comparison of Parsimony, Likelihood, and Bayesian approaches. Systematic Biology 51: 44–68. https://doi.org/10.1080/106351502753475871

Li JT, Li Y, Murphy RW, Rao DQ, Zhang YP (2012a) Phylogenetic resolution and systematics of the Asian tree frogs, *Rhacophorus* (Rhacophoridae, Amphibia). Zoologica Scripta 41: 557–570. https://doi.org/10.1111/j.1463-6409.2012.00557.x

Li JT, Liu J, Chen YY, Wu JW, Murphy RW, Zhao EM, Wang YZ, Zhang YP (2012b) Molecular phylogeny of treefrogs in the *Rhacophorus dugritei* species complex (Anura: Rhacophoridae), with descriptions of two new species. Zoological Journal of the Linnean Society 165: 143–162. https://doi.org/10.1111/j.1096-3642.2011.00790.x

Liang YS, Wang CS (1978) A new tree frog *Rhacophorus taipeianus* (Anura: Rhacophoridae) from Taiwan (Formosa). Quarterly Journal of the Taiwan Museum 31: 185–202.

Liu CC (1945) New frogs from West China. Journal of the West China Border Research Society, Series B 15: 28–44.

Liu CC, Hu SQ (1960) [1959] Preliminary report of Amphibia from southern Yunnan. Acta Zoologica Sinica: 11: 508–538.

Liu CC, Hu SQ (1961) Tailless Amphibians of China. Science Press, Beijing.

Liu CC, Hu SQ (1962) A herpetological report of Kwangsi. Acta Zoologica Sinica, 73–104.

Liu C, Hu S, Yang FH (1962) Preliminary report of Amphibia from western Kweichow. Acta Zoologica Sinica 14: 381–392.

Liu BQ, Wang YF, Jiang K, Chen HM, Zhou JJ, Xu JN, Wu CH. (2017) A new treefrog species of the genus *Rhacophorus* Found in Zhejiang, China (Anura: Rhacophoridae). Chinese Journal of Zoology 52: 361–372.

Lue KY, Lai JS, Chen SL (1994) A new species of *Rhacophorus* (Anura: Rhacophoridae) from Taiwan. Herpetological 50: 303–308.

Lue KY, Lai JS, Chen SL (1995) A new species of *Rhacophorus* (Anura: Rhacophoridae) from Taiwan. Journal of Herpetology 29: 338–345. https://doi.org/10.2307/1564982

Lue BQ, Huang JK, Zhou JQ, Lu WZ, Zhou JJ, Wang YF, Zhou LM, Chen LH (2024) New subspecies of *Zhangixalus* (Amphibia, Anura, Rhacophoridae) —— *Zhangixalus taipeianus jingningensis*. Chinese Journal of Wildlife 45(04): 912–920. https://link.cnki.net/urlid/23.1587.s.20240506.1529.002

Matsui M, Panha S (2006) A new species of *Rhacophorus* from eastern Thailand (Anura: Rhacophoridae). Zoological Science 23(5): 477–481. https://doi.org/10.2108/zsj.23.477

Mo YM, Chen WC, Liao X, Zhou SC (2016) A new species of the genus *Rhacophorus* (Anura: Rhacophoridae) from southern China. Asian Herpetological Research 7: 139–150. https://doi.org/10.16373/j.cnki.ahr.150070

Mou YP, Risch JP, Lue KY (1983) *Rhacophorus prasinatus*, a new tree frog from Taiwan, China (Amphibia, Anura, Rhacophoridae). Alytes 2: 154–162.

Myers CW, Duellman WE (1982) A new species of Hyla from Cerro Colorado, and other tree frog records and geographical notes from western Panama. American Museum Novitates 2752: 1–32.

Nguyen TT, Matsui M, Eto K, Orlov NL (2014) A preliminary study of phylogenetic relationships and taxonomic problems of Vietnamese *Rhacophorus* (Anura: Rhacophoridae). Russian Journal of Herpetology 21(4): 274–280.

Nguyen TT, Ninh HT, Orlov N, Nguyen TQ, Ziegler T (2020) A new species of the genus *Zhangixalus* (Amphibia: Rhacophoridae) from Vietnam. Journal of Natural History 54: 257–273. https://doi.org/10.1080/00222933.2020.1754484

Nguyen TT, Nguyen HH, Ninh HT, Le LTH, Bui HT, Orlov N, Hoang CV, Ziegler T (2024) *Zhangixalus thaoae* sp. nov., a new green treefrog species from Vietnam (Anura, Rhacophoridae). ZooKeys 1197: 93–113. https://doi.org/10.3897/zookeys.1197.104851

Ninh HT, Nguyen TT, Orlov N, Nguyen TQ, Ziegler T (2020) A new species of the genus *Zhangixalus* (Amphibia: Rhacophoridae) from Vietnam. European Journal of Taxonomy 688(688): 1–8. https://doi.org/10.5852/ejt.2020.688

Ohler A, Marquis O, Swan SR, Grosjean S (2000) Amphibian biodiversity of Hoang Lien Nature Reserve (Lao Cai Province, northern Vietnam) with description of two new species. Herpetozoa Wien 13: 71–87.

Okada Y, Kawano U (1924) On the ecological distribution of two new varieties of *Rhacophorus* in Japan. Zoological Magazine 36: 104–109. [144–153]

Orlov NL, Lathrop A, Murphy RW, Ho CT (2001) Frogs of the family Rhacophoridae (Anura: Amphibia) in the northern Hoang Lien Mountains (Mount Fan Si Pan, Sa Pa District, Lao Cai Province), Vietnam. Russian Journal of Herpetology 8: 17–44.

Orlov NL, Nguyen N, Cuc HT (2008) Description of a new species and new records of *Rhacophorus* genus (Amphibia: Anura: Rhacophoridae) with the review of amphibians and reptiles diversity of Ghu Yang Sin National Park (Dac Lac Province, Vietnam). Russian Journal of Herpetology 15: 67–84.

Ostroshabov AA, Orlov NT, Nguyen TT (2013) Taxonomy of Frogs of Genus *Rhacophorus* of "hoanglienensis orlovi" Complex. Russian Journal of Herpetology 20: 301–324.

Pan T, Zhang Y, Wang H, Wu J, Kang X, Qian L, Li K, Zhang Y, Chen J, Rao D, Jiang JP, Zhang B (2017) A New Species of the Genus *Rhacophorus* (Anura: Rhacophoridae) from Dabie Mountains in East China. Asian Herpetological Research 8: 1–13.

Pan YQ, Hou M, Yu GH, Liu S (2024) A new species of *Zhangixalus* (Anura, Rhacophoridae) from Yunnan, China. Zoosystematics and Evolution 100: 183–197. https://doi.org/10.3897/zse.100.113850

Pham AV, Nguyen T, Ziegler T, Nguyen TT (2017) New records of tree frogs (Anura: Rhacophoridae: *Rhacophorus*) from Son La Province, Vietnam. Herpetology Notes 10: 379–386.

Poyarkov NA, Nguyen TV, Popov ES, Geissler P, Pawangkhanant P, Suwannapoom TNC, Orlov NL (2021) Recent progress in taxonomic studies, biogeographic analysis, and revised checklist of amphibians of Indochina. Russian Journal of Herpetology 28 (3A): 1–110. https://doi.org/10.30906/1026-2296-2021-28-3A-1-110

Puillandre N, Brouillet S, Achaz G (2021) ASAP: assemble species by automatic partitioning. Molecular Ecology Resources 21: 609–620. https://doi.org/10.1111/1755-0998.13281

Rao DQ, Wilkinson JA, Liu HN (2006) A new species of *Rhacophorus* (Anura: Rhacophoridae) from Guangxi Province, China. Zootaxa 1258: 17–31. https://doi.org/10.11646/zootaxa.1258.1.2

Ronquist F, Teslenko M, van der Mark P, Ayres DL, Darling A, Hohna S, Larget B, Liu L, Suchard MA, Huelsenbeck JP (2012) MrBayes 3.2: efficient Bayesian phylogenetic inference and model choice across a large model space. Systematic Biology 61: 539–542. https://doi.org/10.1093/sysbio/sys029

Shui KC, Zhang SY, Liu ZF, Zhu YH, Gong YN, Zhao J (2023) Classification of *Zhangixalus* species in Nanling National Nature Reserve, Guangdong two new provincial records were recorded. Sichuan Journal of Zoology 42: 75–84. https://doi.org/10.11984/j.issn.1000-7083.20220257

Smith MA (1924a) Two lizards and a new tree frog from the Malay Peninsula. Journal of the Federated Malay States Museums 11: 183–186.

Smith MA (1924b) New tree-frogs from Indo-China and the Malay Peninsula. Proceedings of the Zoological Society of London 1924: 225–234. https://doi.org/10.1111/j.1096-3642.1924.tb01499.x

Stamatakis A (2014) RAxML version 8: a tool for phylogenetic analysis and post–analysis of large phylogenies. Bioinformatics 30: 1312–1313. https://doi.org/10.1093/bioinformatics/btu033

Stejneger L (1907) Herpetology of Japan and adjacent territory. Bulletin of the United States National Museum 58: 1–577. https://doi.org/10.5479/si.03629236.58.i

Stejneger L (1924) Herpetological novelties from China. Occasional Papers of the Boston Society of Natural History 5: 119–121.

Tamura K, Stecher G, Kumar S (2021) MEGA11: Molecular Evolutionary Genetics Analysis Version 11. Molecular Biology and Evolution 38: 3022–3027. https://doi.org/10.1093/molbev/msab120

Yu GH, Rao DQ, Zhang MW, Yang JX (2009) Re–examination of the phylogeny of Rhacophoridae (Anura) based on mitochondrial and nuclear DNA. Molecular Phylogenetics and Evolution 50: 571–579. https://doi.org/10.1016/j.ympev.2008.11.023

Yu GH, Hui H, Hou M, Wu ZJ, Rao DQ, Yang JX (2019a) A new species of *Zhangixalus* (Anura: Rhacophoridae), previously confused with *Zhangixalus smaragdinus* (Blyth, 1852). Zootaxa 4711(2): 275–292. https://doi.org/10.11646/zootaxa.4711.2.3

Yu GH, Hong H, Wang J, Rao DQ, Wu ZJ, Yang JX. (2019b). A new species of *Gracixalus* (Anura, Rhacophoridae) from Yunnan, China. ZooKeys 851: 91–111. https://doi.org/10.3897/zookeys.851.32157

Zhang J, Jiang K, Hou M (2011) *Rhacophorus dorsoviridis* Bourret, a new record of family Rhacophoridae to China. Acta Zootaxonomica Sinica 36: 986–989.

Supplementary material 1

Measurements of *Z. daweishanensis* sp. nov., *Z. nanshanensis* sp. nov., *Z. dorsoviridis*, *Z. nigropunctatus*, *Z. lishuiensis*, *Z. yunnanensis* and *Z. zhoukaiyae*

Authors: Yuanqiang Pan, Shuo Liu, Ju Chen, Guohua Yu
Data type: xlsx

Link: https://doi.org/10.3897/zse.101.144060.suppl1

Supplementary material 2

Mean uncorrected pairwise distances (%) between clades of *Z. daweishanensis* sp. nov. and *Z. nanshanensis* sp. nov. and related species based on 16S rRNA sequences

Authors: Yuanqiang Pan, Shuo Liu, Ju Chen, Guohua Yu
Data type: xls

Link: https://doi.org/10.3897/zse.101.144060.suppl2

Supplementary material 3

Morphological comparison between the new species and congeners of *Zhangixalus*

Authors: Yuanqiang Pan, Shuo Liu, Ju Chen, Guohua Yu
Data type: xlsx

Link: https://doi.org/10.3897/zse.101.144060.suppl3

Supplementary material 4

Additional tables and figures

Authors: Yuanqiang Pan, Shuo Liu, Ju Chen, Guohua Yu
Data type: docx
Explanation note: **table S4.** Summary statistics of male specimens (mean ± standard deviation) and results of the t-test between the *Z. nanshanensis* sp. nov. (n = 7) and *Z. nigropunctatus* (n = 6). The t-test was performed on the size-adjusted data, except SVL. * = $p < 0.05$, ** = $p < 0.01$. **table S5.** Summary statistics of male specimens (mean ± standard deviation) and results of the t-test between the *Z. nanshanensis* sp. nov. (n = 7) and *Z. yunnanensis* (n = 7). The t-test was performed on the size-adjusted data, except SVL. * = $p < 0.05$, ** = $p < 0.01$. **table S6.** Summary statistics of male specimens (mean ± standard deviation) and results of the t-test between the *Z. lishuiensis* (n = 3) and *Z. zhoukaiyae* (n = 6). The t-test was performed on the size-adjusted data, except SVL. * = $p < 0.05$, ** = $p < 0.01$. **fig. S1.** Views of *Z. zhoukaiyae* (A & a), *Z. nigropunctatus* (B & b; photos by Guohua Yu), *Z. dorsoviridis* (C & c), *Z. lishuiensis* (D & d; photos by Guohua Yu), *Z. nanshanensis* sp. nov. (E & e; photos by Guohua Yu), and *Z. daweishanensis* sp. nov. (F & f; photos by Guohua Yu) in life. A & a were reproduced from Pan et al. (2017), C was reproduced from Mo et al. (2016), and c was reproduced from Zhang et al. (2011).

Link: https://doi.org/10.3897/zse.101.144060.suppl4

Zoosyst. Evol. 101 (2) 2025, 509–532 | DOI 10.3897/zse.101.144277

PENSOFT

für Natur MUSEUM FÜR NATURKUNDE BERLIN

Three new species of the millipede genus *Enghoffosoma* Golovatch, 1993 from Thailand (Diplopoda, Polydesmida, Paradoxosomatidae)

Theemaporn Benchapong[1], Henrik Enghoff[2], Natdanai Likhitrakarn[3], Ratmanee Chanabun[4,5], Anuwat Aoonkum[4,5], Ruttapon Srisonchai[1,5]

1 *Department of Biology, Faculty of Science, Khon Kaen University, Khon Kaen, 40002 Thailand*
2 *Natural History Museum of Denmark, University of Copenhagen, Universitetsparken 15, DK-2100 København Ø, Denmark*
3 *Program of Agriculture, Faculty of Agricultural Production, Maejo University, Chiang Mai 50290, Thailand*
4 *Program in Animal Science, Faculty of Agricultural Technology, Sakon Nakhon Rajabhat University, Sakon Nakhon 47000, Thailand*
5 *Biodiversity and Utilization Research Unit, Center of Excellence in Modern Agriculture, Sakon Nakhon Rajabhat University, Sakon Nakhon 47000, Thailand*

https://zoobank.org/878BA02C-D70D-4B43-9F6D-0FAD25979917

Corresponding author: Ruttapon Srisonchai (ruttasr@kku.ac.th)

Academic editor: Luiz Felipe Iniesta ♦ **Received** 12 December 2024 ♦ **Accepted** 25 January 2025 ♦ **Published** 26 February 2025

Abstract

An examination of newly collected material from northeastern Thailand revealed three new millipede species in the genus *Enghoffosoma* Golovatch, 1993: *E. furca* **sp. nov.**, *E. parvispina* **sp. nov.**, and *E. rubellum* **sp. nov.** We utilized morphological evidence together with genetic analysis of the COI gene to validate species identification. Each of the new species has unique characteristics, particularly in the structure of the gonopodal solenophore, that easily distinguish them from other species in the genus. The interspecific *p*-distances calculated from 658-bp barcoding sequences between the new species and their congeners show ranges of 18.56% to 22.78% for *E. furca* **sp. nov.**, 15.09% to 21.25% for *E. parvispina* **sp. nov.**, and 15.09% to 22.37% for *E. rubellum* **sp. nov.**, supporting the morphological distinctions. Preliminary phylogenetic trees using Bayesian inference (BI) and maximum likelihood (ML) indicate that the genus *Enghoffosoma* is monophyletic, with two of the newly described species forming distinct clades. Our findings increase the total number of *Enghoffosoma* species to 16 (including six in Thailand) and underscore a greater diversity within the genus than previously known. Morphological illustrations of the new species, derived from SEM micrographs, and a distribution map of all known species are included.

Key Words

Biodiversity, identification, phylogeny, South-East Asia, taxonomy

Introduction

Currently, Thailand stands out as a significant hotspot for millipede diversity with a total of 282 species identified across various habitats. Notably, approximately 84% of these species are endemic, highlighting the unique biodiversity in the country's ecosystems. Among the families of millipede in the class Diplopoda, the family Paradoxosomatidae Daday, 1889 has long been recognized as the most species-rich group not only globally (1,600 species) but also in Thailand, comprising 106 out of the total 267 described species (Likhitrakarn et al. 2023).

Research on the systematics of several groups of millipedes has progressed rapidly in Thailand in recent years (Pimvichai et al. 2009, 2014; Likhitrakarn et al. 2010, 2011; Srisonchai et al. 2018, 2024). However, only a few genera of Paradoxosomatidae, such as *Desmoxytes* Chamberlin, 1923, *Gigaxytes* Srisonchai, Enghoff & Panha, 2018, *Nagaxytes* Srisonchai, Enghoff & Panha, 2018, *Siamaxytes* Srisonchai & Panha, 2024, and *Spinaxytes* Srisonchai et al., 2018,

have been analyzed integratively (Srisonchai et al. 2024). Additionally, some paradoxosomatid genera occurring in the country (viz., *Orthomorpha* Bollman, 1893, *Antheromorpha* Jeekel, 1968, *Tylopus* Jeekel, 1968 and *Enghoffosoma* Golovatch, 1993), which exhibit a diverse range of morphological characteristics are lacking genetic analysis and still require systematic revision (Likhitrakarn et al. 2011).

The millipede genus *Enghoffosoma* Golovatch, 1993 is probably one of the most taxonomically diverse genera of Paradoxosomatidae in Asia, especially in South-East Asia (Likhitrakarn et al. 2014). The members of the genus are primarily distinguished based on gonopod characters in combination with other somatic features. To date, 13 species of *Enghoffosoma* have been described worldwide: one species in China, two species in Laos, one species in Myanmar, 6 species in Vietnam, and 3 species in Thailand (*E. bispinum* Likhitrakarn, Golovatch & Panha, 2014; *E. funda* Likhitrakarn, Golovatch & Panha, 2014; and *E. zebra* Likhitrakarn, Golovatch & Panha, 2014) (Golovatch 1993, 2011, 2016; Golovatch et al. 2016; Golovatch and Semenyuk 2018; Likhitrakarn et al. 2014; Nguyen and Golovatch 2016).

In the present study, we examined recently collected specimens of *Enghoffosoma* from the northeastern region of Thailand. These specimens appear to be geographically isolated from other species. Morphological evidence obtained from scanning electron micrographs and molecular data support the identification of three distinct morphotypes, which are described here as new species.

Materials and methods

Specimen collections and preservation

The specimens were collected by hand from the northeastern region of Thailand. Live animals were photographed in the field using a Canon EOS 90D digital camera equipped with a Canon EF-S 60 mm f/2.8 Macro USM lens. All specimens were placed in 10% ethanol for proper euthanization based on the procedure of the American Veterinary Medical Association (American Veterinary Medical Association 2020), and subsequently preserved in 70% ethanol for morphological examination, and 95% ethyl alcohol for DNA analysis.

The collecting sites (latitude, longitude, and elevation) were recorded by a Garmin GPSMAP 60CSx, and all exact coordinates were double-checked with Google Earth. The background image for the distribution map was taken from the website Elastic Terrain Map (http://elastic-terrain.xyz/) and altered with Adobe Photoshop CC2024.

This work was conducted under the approval of the Khon Kaen University's Animal Care and Use Committee (Protocol Reviews No. IACUC-KKU-70/67) and with permission to conduct research in protected areas (Department of National Parks, Wildlife and Plant Conservation; Protocols No. 23103 and 23104).

Morphological study

All specimens were studied under a Nikon SMZ445 stereo microscope and were measured with a TIGA 6x1/128 in a vernier caliper. For scanning electron micrographs, dissected body parts were mounted on aluminum stubs, air-dried, coated with gold at 30 mAmp for 240 seconds, and then studied under a JEOL, JSM-5410 LV microscope. After imaging, all specimens were removed from the stubs and preserved in ethanol in Eppendorf tubes for long-term preservation. The images were processed and edited with Adobe Photoshop CC2024 and line drawings were sketched in Adobe Illustrator 2018.

The species identification and morphological descriptions followed Golovatch (1993, 2011, 2016), Likhitrakarn et al. (2014), Golovatch and Semenyuk (2018), Nguyen and Golovatch (2016), and Srisonchai et al. (2023, 2024).

Abbreviations of somatic characters

cl claw of leg,
cx coxa of leg,
ep epiproct,
fe femur of leg,
hy hypoproct,
oz ozopore,
pfe prefemur of leg,
pk pleurosternal keel,
pof postfemur of leg,
pp paraproct,
sc sensory cones,
ta tarsus of leg,
ti tibia of leg,
vb ventral brushes.

Abbreviations of gonopod characters

a process a on solenophore,
ca cannula of gonopod,
cox coxa of gonopod,
fm femur,
ls lateral sulcus,
p process p on femur,
prf prefemur of gonopod,
sg seminal groove of gonopod,
sl solenomere of gonopod,
sp spatula-like process,
sph solenophore of gonopod,
sph-l small process located on base of solenophore, clearly seen in lateral view,
sph-m small process located on base of solenophore, clearly seen in mesal view.

Institutional abbreviations

CUMZ Chulalongkorn University Museum of Zoology, Bangkok, Thailand
MZKKU Khon Kaen University Museum of Zoology, Thailand (invertebrate collections)
NHM Natural History Museum, London, United Kingdom
NHMW Natural History Museum, Vienna, Austria
NHMD Natural History Museum of Denmark, University of Copenhagen, Denmark
ZFMK Zoological Research Museum A. Koenig, Leibniz Institute for Animal Biodiversity, Bonn, Germany

DNA extraction, amplification, sequencing and phylogenetic reconstruction

A total of 24 sequences were used for phylogenetic study, comprising 17 sequences from this study and 7 sequences available from GenBank (Suppl. material 1). Outgroups were selected based on the recent phylogenetic studied including *Antheromorpha festiva* (Brölemann, 1916), *Desmoxytes planata* (Pocock, 1895), *Orthomorpha setosa* (Attems, 1937), *Oxidus gracilis* (C.L. Koch, 1847) and *Tylopus roseiparaterga* Nguyen, 2012 (Nguyen et al. 2018; Likhitrakarn et al. 2019; Srisonchai et al. 2024). The new sequences have been submitted to GenBank, and their accession numbers are shown in Suppl. material 1 (PV031917–PV031933).

Genomic DNA was extracted from body rings and leg tissues using the NucleoSpin Tissue Kit. The COI gene was amplified via polymerase chain reactions (PCR) using the universal primers LCO1490 and HCO2198 — LCO-1490 (5′-GGT CAA CAA ATC ATA AAG ATA TTG G-3′) and HCO-2198 (5′-TAA ACT TCA GGG TGA CCA AAA AAT CA-3′) (Folmer et al. 1994). The PCR reaction was performed in a total volume of 40.0 µL, consisting of EmeraldAmp GT PCR Master Mix (16 µL), ddH_2O (12 µL), 8 µL primers (4 µL each), and 4.0 µL of DNA template. The annealing step was carried out at 43 °C for 1 minute, followed by an extension step at 72 °C for 2 minutes. PCR products were screened for successful amplification of COI fragments using 1% agarose gel electrophoresis with TBE 1X and were observed under UV trans-illumination. The resulting amplified products were sent for commercial sequencing at Bioneer Corporation, South Korea.

The DNA sequences were checked for errors by putting them into the same reading frame, translating into proteins, and all sequences were aligned using MEGA 11 (Tamura et al. 2021). The aligned data were subsequently analyzed with JModelTest2 on XSEDE (Darriba et al. 2012) through the CIPRES Gateway (Miller et al. 2010) to assess nucleotide evolution models and identify the best-fit substitution model.

The phylogenetic trees were reconstructed using, Bayesian inference (BI) and maximum likelihood (ML), through the online CIPRES Science Gateway (Miller et al. 2010). For the BI analysis, data were executed with KAKUSAN 4.0 (Tanabe 2011) to generate the original file, adjusting for the best-fit model (GTR+I+G). The analysis was then conducted in MrBayes on XSEDE 3.2.7a (Ronquist et al. 2012), using a Markov chain Monte Carlo (MCMC) approach for 30 million generations, running with 4 chains of MCMC and sampling every 1,000 generations. For ML analysis, an optimal tree was conducted by using IQ-Tree on XSEDE 2.3.2 (Minh et al. 2020) with the GTR+I+G substitution model and branch support was estimated using 1,000 bootstrap (BS) replicates. The visualizations of the ML and BI trees were accomplished in FigTree v. 1.4.4 (Rambaut 2018), and visually processed in Adobe Illustrator 2018. The evaluation of node robustness involves considering maximum likelihood bootstrap support values (BS) > 70% and Bayesian inference posterior probabilities (PP) > 0.95% as strong support (Hillis and Bull 1993; Huelsenbeck and Rannala 2004).

Uncorrected pairwise genetic distances (*p*-distances) were also calculated in MEGA 11.

Results

DNA sequences and phylogenetic tree

The COI sequence alignments consisted of 658 base pairs with 243 variable sites, 415 conserved sites, and 187 parsimony-informative sites. The range of percentual distances between outgroups (*A. festiva, D. planata, O. setosa, O. gracilis,* and *T. roseiparaterga*) and *Enghoffosoma* species was 17.82–30.85%. The range of interspecific distances within the genus *Enghoffosoma* was 15.09–22.78%. The interspecific distances between other *Enghoffosoma* species (vs the three new species) were 18.56–22.78% for *E. furca* sp. nov., 15.09–21.25% for *E. parvispina* sp. nov. and 15.09–22.37% for *E. rubellum* sp. nov. The largest intraspecific distance was found in *E. parvispina* with 1.88%. Additional information for genetic distances is provided in Suppl. material 2.

The Bayesian inference and maximum likelihood analyses based on the COI gene fragment resulted in the same topology for the ingroup (Fig. 1). The genus *Enghoffosoma* is monophyletic with high support (PP = 0.99, BS = 79). However, some deep nodes on trees had low statistical support which questions the reliability of the calculated relationships within the genus. The new species are recovered as monophyletic with strong support, with *E. parvispina* sp. nov. nested together with *E. rubellum* sp. nov. (PP = 1, BS = 67), while *E. furca* sp. nov., represented by only one terminal, was grouped together with *E. bispinum* (PP = 1.00, BS = 73).

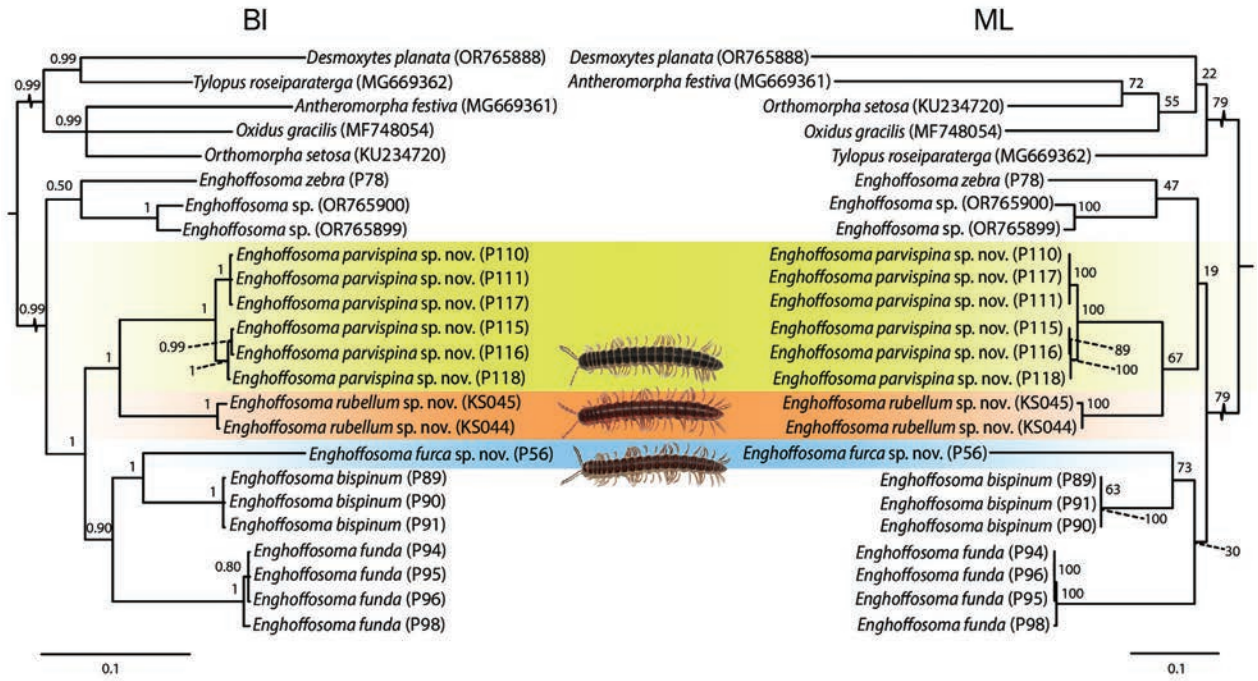

Figure 1. Phylogenetic tree of COI gene fragment based on Bayesian Inference (BI) and maximum likelihood (ML). Nodal numbers refer to Bayesian posterior probabilities (PP) from BI and bootstrap support (BS) from ML. Different colors represent three new species (*Enghoffosoma furca* sp. nov., *Enghoffosoma parvispina* sp. nov. and *Enghoffosoma rubellum* sp. nov.), corresponding to the live photographs. Scale bar indicates substitutions per site.

Systematics

Class Diplopoda de Blainville in Gervais, 1844
Order Polydesmida Pocock, 1887
Family Paradoxosomatidae Daday, 1889
Subfamily Paradoxosomatinae Daday, 1889
Tribe Paradoxosomatini Daday, 1889

Genus *Enghoffosoma* Golovatch, 1993

Enghoffosoma Golovatch, 1993: 8.

Enghoffosoma — Golovatch, 2011: 262; Nguyen and Sierwald 2013: 1258; Likhitrakarn et al., 2014: 492; Nguyen and Golovatch 2016: 152; Golovatch and Semenyuk 2018: 7; Likhitrakarn et al. 2023: 74.

Diagnosis. *Enghoffosoma* can be differentiated from the other seven genera within the tribe Paradoxosomatini by the following combination of characteristics: paraterga conspicuous as short keels; pleurosternal keel present on rings 2–17; gonopod telopodite suberect, typically branched, with a very long and slender solenophore; solenomere also very long; femur often bearing a distal process; a distinct demarcation between the femur and the postfemoral portion; solenophore frequently featuring process(es) or lobe(s) near its base.

Enghoffosoma is distinguished from *Ciliciosoma* Verhoeff, 1940, *Strongylosoma* Brandt, 1883, and *Substrongylosoma* Golovatch, 1984 by the presence of a conspicuous demarcation between the femur and the postfemoral part of the gonopod. The gonopod telopodite in *Enghoffosoma* is branched, which contrasts with *Haplogonomorpha* Mršić, 1996, whose species lack an apical branch. *Enghoffosoma* is separated from *Lohmanderodesmus* Schubart, 1934 and *Stosatea* Gray, 1843 by the typically long and slender solenophore in *Enghoffosoma* compared to the stout lobe in *Lohmanderodesmus* and the broad lamella in *Stosatea*. *Enghoffosoma* differs from *Tetrarthrosoma* Verhoeff, 1898 in having a distal process on the femur and a solenophore that branches into 2 or 3 processes.

Type-species. *Sundanina spinipleura* Carl, 1941.

List of Enghoffosoma species in Thailand. 1) *E. bispinum* Likhitrakarn, Golovatch & Panha, 2014. 2) *E. funda* Likhitrakarn, Golovatch & Panha, 2014. 3) *E. furca* sp. nov. 4) *E. parvispina* sp. nov. 5) *E. rubellum* sp. nov. 6) *E. zebra* Likhitrakarn, Golovatch & Panha, 2014.

Enghoffosoma bispinum Likhitrakarn, Golovatch & Panha, 2014

Enghoffosoma bispinum Likhitrakarn, Golovatch & Panha, 2014 in Likhitrakarn et al. 2014: 508.

Enghoffosoma bispinum — Nguyen & Golovatch, 2016: 151; Likhitrakarn et al. 2023: 74; Srisonchai et al. 2024: 4.

Material examined. Thailand • 3 ♂ 2 ♀ (MZKKU); Rayong Province, Mueang Rayong District, Khao Yai Chum Temple; 12°39'23.7"N, 101°26'47.8"E; 21 July 2024; R. Srisonchai and T. Benchapong leg.

Distribution and habitat. *E. bispinum* is currently known from only two locations in Rayong Province, situated just 10 km apart. All newly collected specimens were observed walking on the ground, with some found on thin layers of leaf litter.

Enghoffosoma funda Likhitrakarn, Golovatch & Panha, 2014

Enghoffosoma funda Likhitrakarn, Golovatch & Panha, 2014 in Likhitrakarn et al. 2014: 505.

Enghoffosoma funda — Nguyen & Golovatch, 2016: 151; Likhitrakarn et al. 2023: 74.

Material examined. Thailand • 15 ♂ 8 ♀ (MZKKU); Sisaket Province, Kantharalak District, Sisaket Nature Resources Environment Office # 6; 14°39'19.4"N, 104°37'34.4"E; 5 October 2024; T. Benchapong leg. • 25 ♂ 23 ♀ (MZKKU); Sisaket Province, Kantharalak District, Ban Kae Monastery; 14°41'13.8"N, 104°37'10.1"E; 5 October 2024; T. Benchapong leg.

Distribution and habitat. This species is restricted to a small area within the dry deciduous forests of Sisaket Province. The type locality and its surrounding area are characterized by sandstone habitats. A recent visit to the type locality confirmed the presence of several topotypic specimens, observed on humid ground covered with a thin layer of leaf litter.

Enghoffosoma furca Benchapong & Srisonchai, sp. nov.

https://zoobank.org/8EDBCF72-F232-4FAB-91BD-AE721F6987BD

Figs 2–5

Material examined. ***Holotype*:** Thailand • ♂ (MZKKU-MYR0007); Chaiyaphum Province, Phakdee Chumphon District, Thum Kaeo Monastery, on forest floor; 405 m a.s.l.; 15°58'27.2"N, 101°24'36.5"E; 3 September 2023; R. Srisonchai and T. Benchapong leg.

***Paratypes*:** Thailand • 7 ♂♂, 5 ♀♀ (MZKKU-MYR0008); same data as holotype • ♂ (CUMZ-MYR0034); same data as for holotype • ♂ (NHM); same data as for holotype • ♂ (NHMD); same data as for holotype • ♂ (NHMW), same data as for holotype • ♂ (ZFMK-MYR14168); same data as for holotype.

Other materials. Thailand • ♂ broken specimen (MZKKU); same data as holotype.

Etymology. The specific name is a Latin noun in apposition and refers to the two-pronged fork solenomere.

Diagnosis. Distal region of femoral part of gonopod without process, and tip of solenomere forklike (Fig. 5A–E, J–H). Similar in these respects to *E. triangulare* Nguyen & Golovatch, 2016 (Fig. 15G), but the new species differs from it by having tip of largest process *in situ* directed posteriad (vs mesad) (Figs 5D, 14D, G, 15D, G). Genetically distant from the other *Enghoffosoma* species by 18.56–22.78% of COI sequences.

Description. Holotype: length 30.4 mm, height of midbody 3.5 mm, width of midbody prozonum and metazonum 3.0 and 3.5 mm, respectively. Males: length 27.5–29.4 mm, height of midbody 3.3–3.5 mm, width of midbody prozona and metazona 3.1–3.2 and 3.6–3.7 mm, respectively. Females: length 28.8–32.9 mm, height of midbody 3.5 mm, width of midbody prozona and metazona 3.5–3.6 and 4.0–4.1 mm, respectively. Width of head < collum = ring 2 = 3= 4 < 5–13 (male); head < ring 2 = 3 < 4 < collum < 5–13 (female), thereafter gradually tapering towards telson.

Coloration (Fig. 2A–C): Color of specimens in life predominantly dark brown to blackish brown. Head, antenna, collum, metaterga and epiproct dark brown to blackish brown (except pale brown tip of epiproct). Anterior part of collum and intermediate part of metaterga with pale brown patches. Paraterga and sterna yellowish white. Surface below paraterga and legs brown. A few basal podomeres of leg pale brown. Coloration in alcohol after one year of preservation faded to dark brown.

Head and clypeolabral region (Figs 3K, 4A, C): Vertex bare; with a shallow and conspicuous epicranial suture. Frons sparsely setose. Clypeus and labrum normal.

Antennae (Figs 3G, K, 4A, B): Short; covered by long and dense setae; reaching backward to ring 3 (♂) or 2 (♀). In length, antennomeres 6>2=3=4=5>1=7. Antennomeres 5–7 slightly clavate; each with a group of sensilla basiconica distally. With four apical cones.

Collum (Fig. 3A, D): Broad and wide. With two transverse rows of inconspicuous setae; 2+2 in anterior position and 1+1 ca. at midlength of collum. Paraterga of collum poorly developed (= obtuse tip).

Tegument (Figs 3A–F, H, 4K, H): With microspinulation, velvetlike. Prozona, metazona, paraterga and surface below paraterga microspinulate. Prozona on lateral side of body finely shagreened.

Metaterga (Figs 3H, I, 4L): Metatergum 2 with one transverse row of setae (mostly inconspicuous and broken off), 2+2 in anterior position. Metaterga 3–19 with one transverse row of setae, 1+1 in anterior position. Stricture between prozona and metazona striolate, shallow and narrow. Axial line and transverse sulcus missing.

Limbus (Fig. 4J): Limbus of midbody ring conspicuous; with rows of very long filaments, fused, arranged anteroposteriorly; margin finely spiculate; surface in front of limbus with a low ridge.

Paraterga (Figs 3H, I, 4G): Quite short, stout and small. Paraterga 2–4 short and thin. Paraterga 5–17 stouter and larger than others. The following paraterga slightly reduced in size and gradually tapering toward telson. Lateral margin without incision. Posterior corner rounded, directed caudad. Ozopores conspicuous, small, oval; present on rings 5, 7, 9, 10, 12, 13, 15–19; visible in lateral view; located near tip of paraterga.

Pleurosternal keels (Figs 3D–F, 4D): Well-developed, conspicuous; slightly curved. Keels on rings 2–4 small; rings 2–8 crestlike, with a sharp caudal tooth posteriorly; gradually reduced to small caudal tooth in rings 9–17; absent in rings 18 and 19.

Telson (Fig. 3J, L, M, N): Preanal ring (epiproct) quite slender; coniform in dorsal view; lateral setiferous tubercles and apical tubercles inconspicuous; tip truncate; with four spinnerets arranged at the corner, each located inside a shallow depression and surrounded by a crownlike collar. Paraprocts simple, slightly convex. Hypoproct subtriangular; with inconspicuous setiferous tubercles.

Sterna (Fig. 4E, F): Sparsely setose; cross-impressions shallow; posteriorly with a small tubercle near each

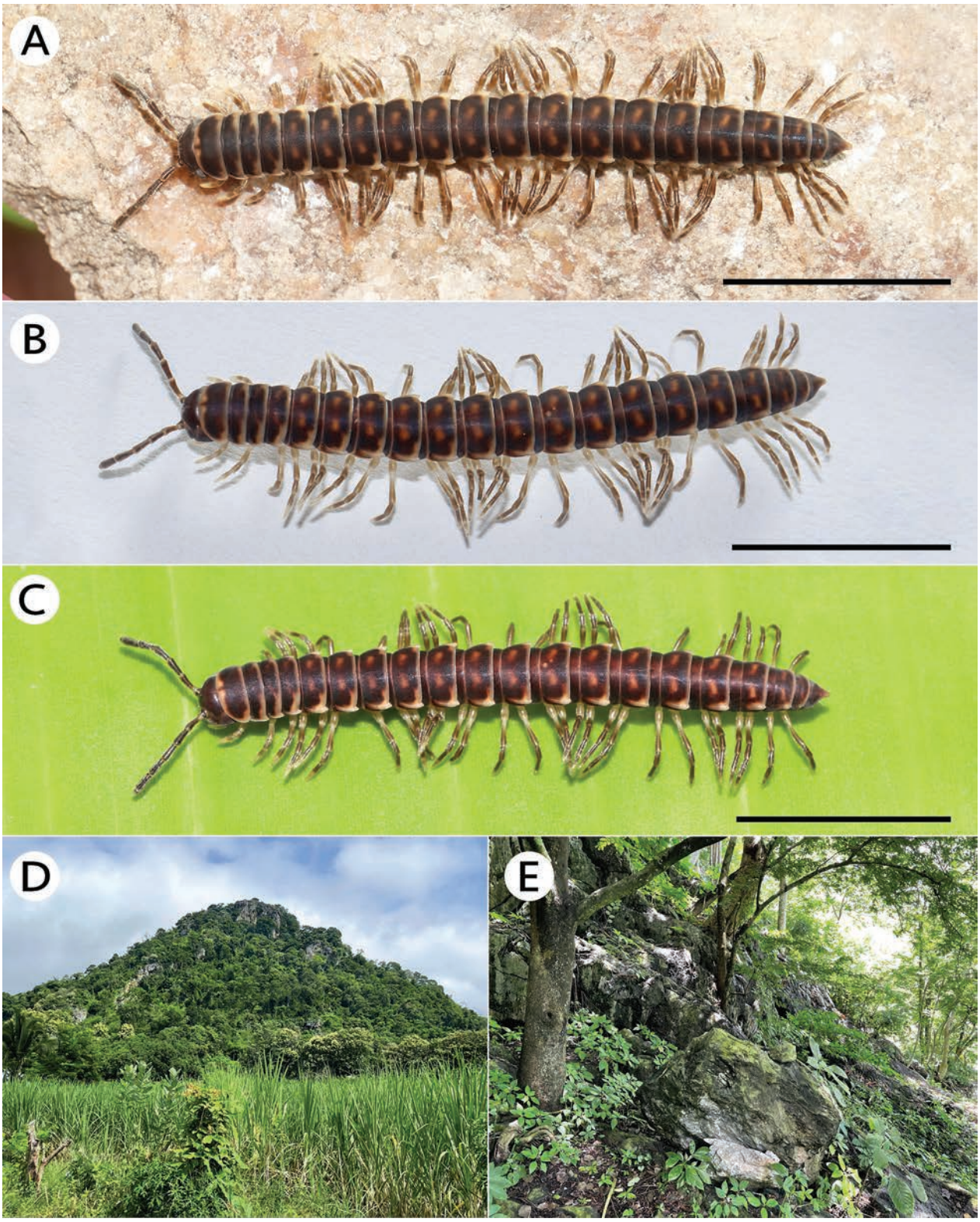

Figure 2. Live photographs of *Enghoffosoma furca* sp. nov. and habitat. **A–C.** Male paratype from type locality; **D, E.** Limestone habitat. Scale bars: 10 mm.

coxa. Sternal lobe between male coxae 4, large, subtrapeziform; tip truncate; with two pores.

Legs (Fig. 4M–O): Moderately long, slender, densely setose; length of midbody leg ca. 3.9–4.6 mm in both sexes; about 1.3–1.4 times (♂) or 1.1 times (♀) as long as midbody height. Prefemur slightly swollen basally. In length, femur > tibia > postfemur = prefemur > tarsus > coxa (♂). Distoventral part of tibia and tarsus of legs 1–10 in male with ventral brushes. Claw quite long, slender, pointed. Adenostyles in male absent.

Gonopods (Fig. 5): Coxa (cox) large; with a distoanterior group of setae. Cannula (ca) long and slender. Te-

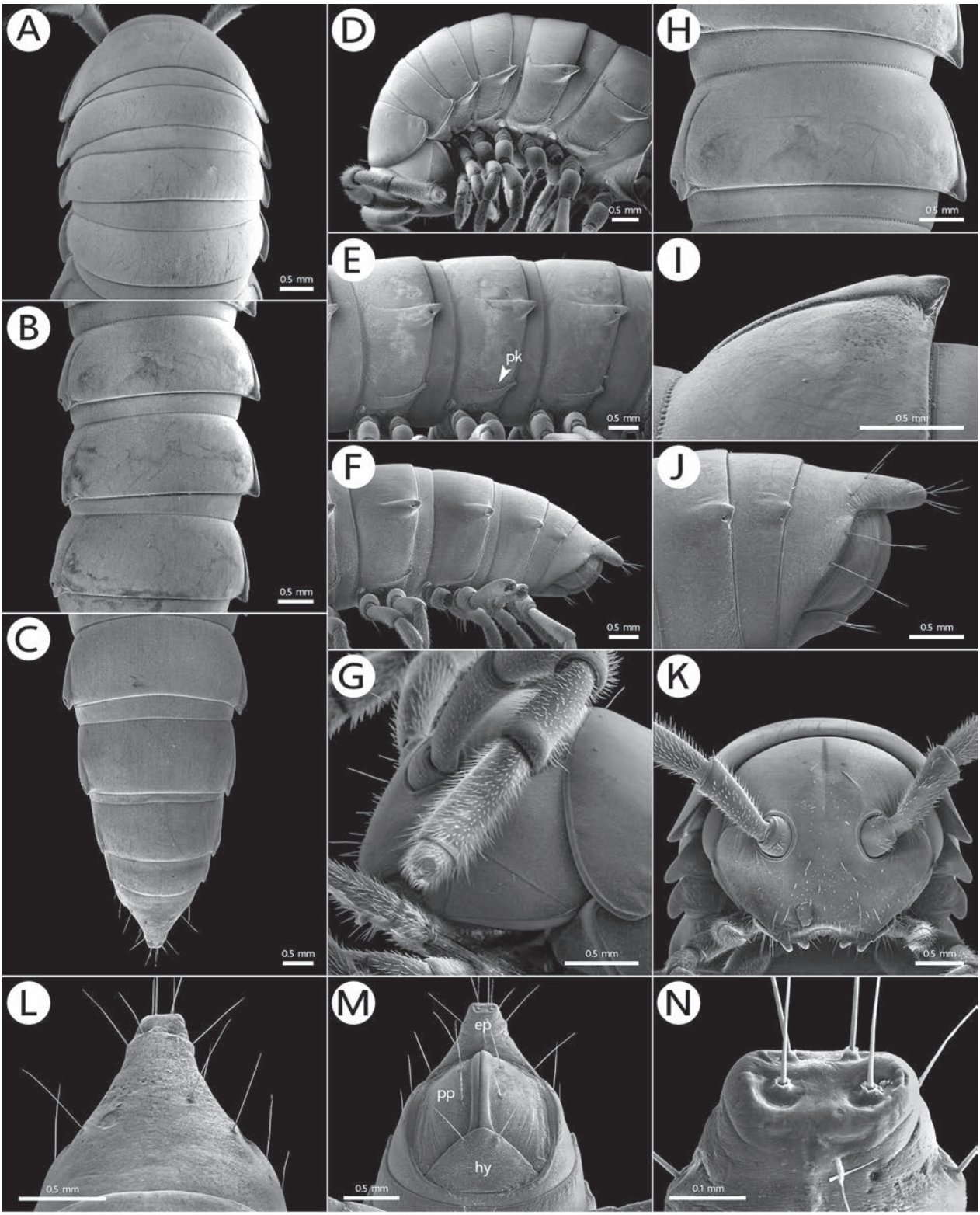

Figure 3. Scanning electron micrographs of *Enghoffosoma furca* sp. nov., male paratype (MZKKU-MYR0008). **A, D.** Anterior body part; **B, E.** Body rings 8–10; **C, F.** Posteriormost body rings and telson; **G.** Head and antenna; **H.** Body ring 10; **I.** Paraterga of ring 10; **J.** Telson; **K.** Head; **L–N.** Telson. **A–C, H, I, L.** Dorsal view; **D–F, G, J.** Lateral view. Abbreviations: ep = epiproct; hy = hypoproct; pk = pleurosternal keel; pp = paraproct.

lopodite long and slender; forming a 90° angle with coxa. Prefemur (prf) densely setose; about 1/2 as long as femur. Femur (fm) quite long and slender; without process distally. Seminal groove (sg) running entirely on mesal surface of femur. Lateral sulcus (ls) deep and conspicuous (Fig. 5B). Mesal sulcus inconspicuous. Postfemoral part inconspicuous. Solenophore (sph) well-developed; slightly broad; partly wrapped around solenomere; basomesally

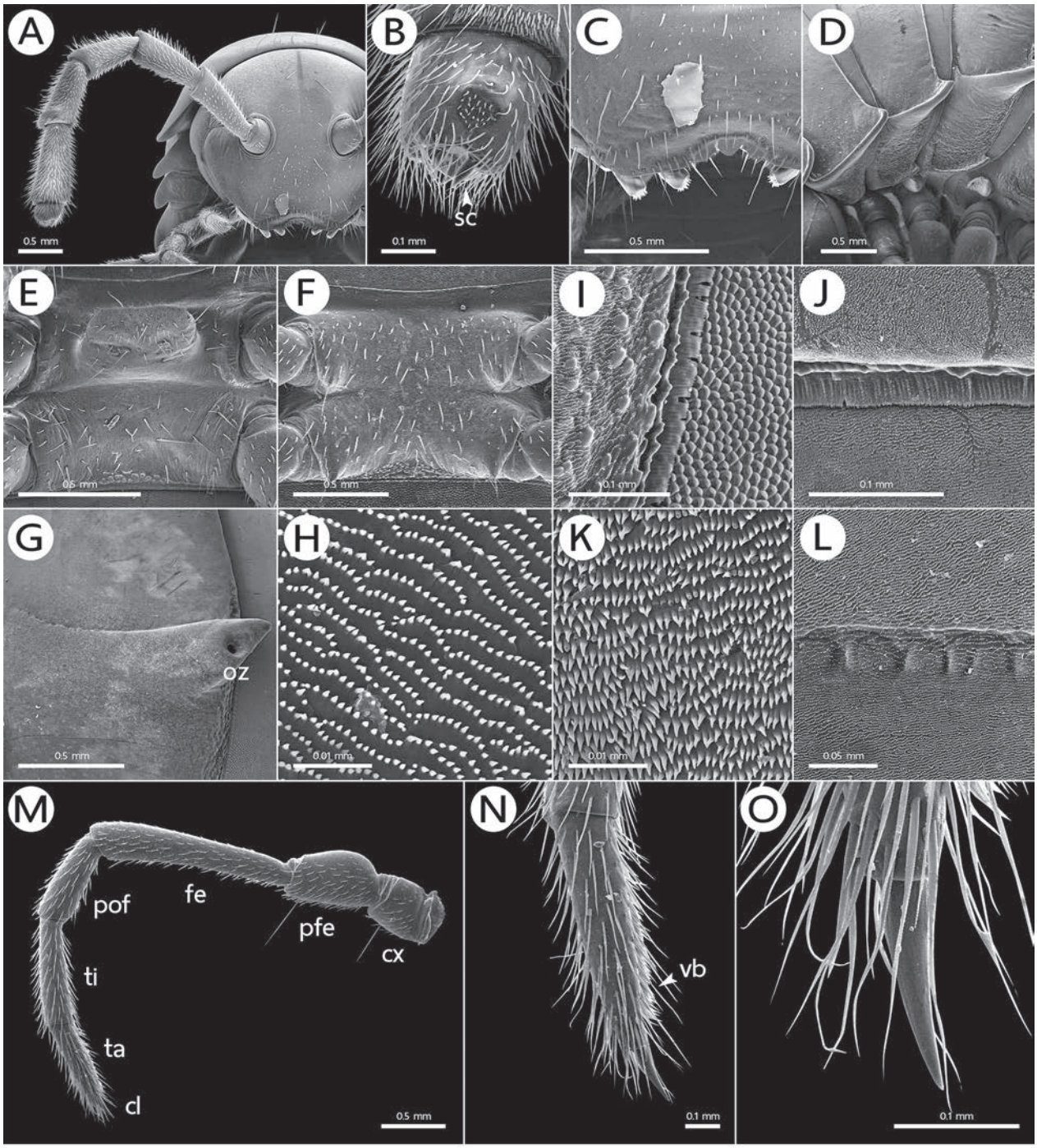

Figure 4. Scanning electron micrographs of *Enghoffosoma furca* sp. nov., male paratype (MZKKU-MYR0008). **A.** Head and antenna; **B.** Antennomeres 7 and 8; **C.** Clypeus, labrum and tip of gnathochilarium; **D.** Pleurosternal keels on rings 2–4; **E.** Sternal lobe between male coxae 4; **F.** Sternum of ring 10; **G.** Ozopore on paraterga of ring 10; **H.** Surface below paraterga of ring 10; **I, J.** Surface and limbus between rings 10 and 11, lateral and dorsal views; **K.** Surface of prozona of ring 10; **L.** Stricture between prozona and metazona of ring 10; **M.** Male right leg of ring 10; **N.** Ventral brushes on male tarsus; **O.** Claw. Abbreviations: cx = coxa; cl = claw; fe = femur; oz = ozopore; pfe = prefemur; pof = postfemur; sc = sensory cones; ta = tarsus; ti = tibia; vb = ventral brushes.

with three processes (two small and one large), tip of the large one *in situ* directed posteriad (Fig. 5D). Solenomere (sl) long; twisted; distally forklike, branching into two processes of the same length, with only the axial one having seminal groove running along it.

Distribution and habitat (Fig. 2D, E). Known only from the type locality in Chaiyaphum Province. All individuals were found walking on the ground among leaf litter in limestone forest habitat.

Remarks. In general appearance, *E. furca* sp. nov. is morphologically similar to *E. anchoriforme* Likhitrakarn et al., 2014 and *E. lanceolatum* Likhitrakarn et al., 2014 by showing dark brown color and with a small pale brown patch on each side of metaterga in both sexes (Fig. 2A–C).

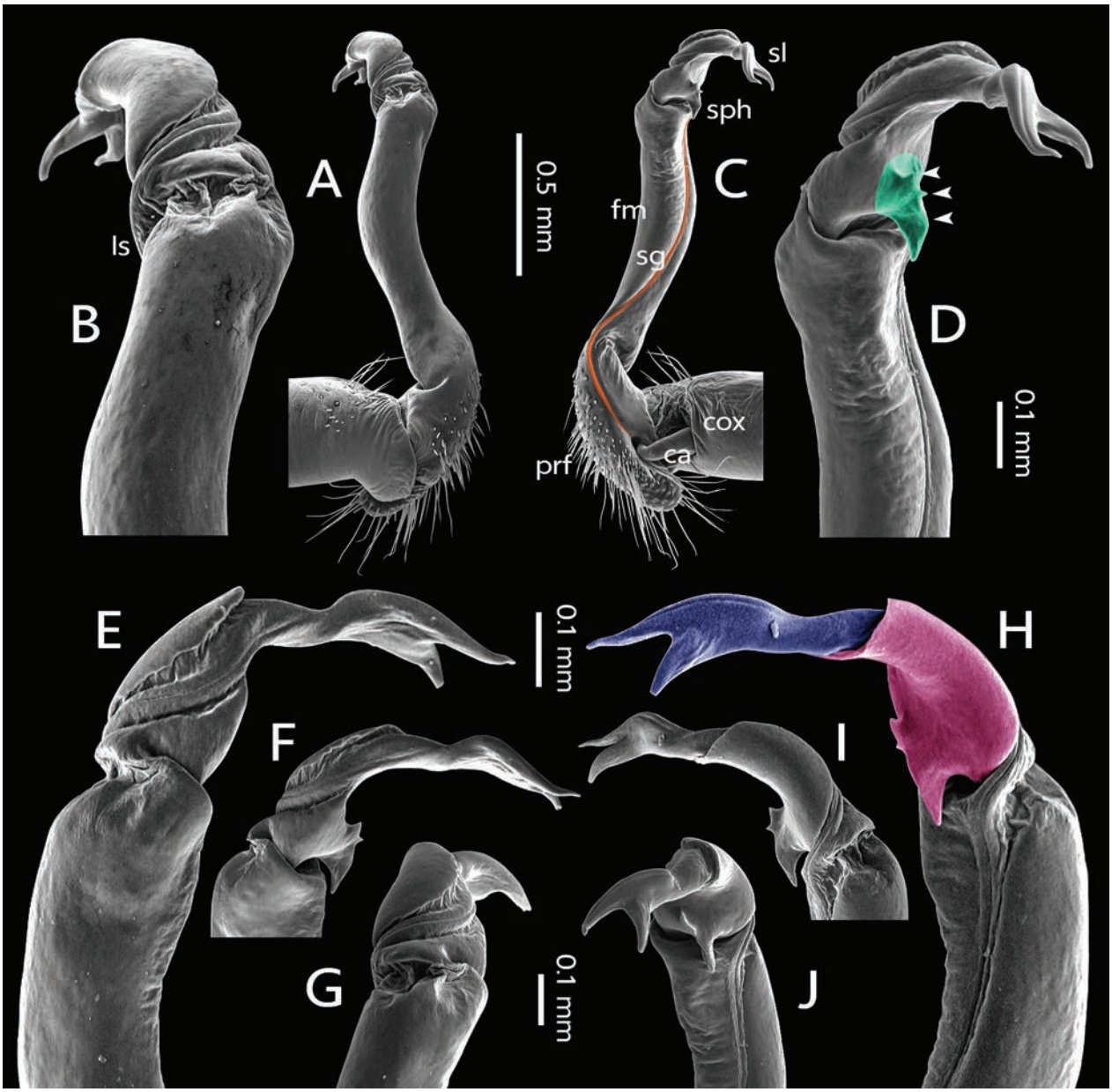

Figure 5. Scanning electron micrographs of *Enghoffosoma furca* sp. nov., right gonopod, male paratype (MZKKU-MYR0008). **A, B.** Lateral view; **C, D.** Mesal view (white arrows point to processes); **E.** Ventral view; **F, G.** Subventral view; **H.** Dorsal view; **I, J.** Subdorsal views. Colors: orange = seminal groove (sg); navy blue = solenomere (sl); pink = solenophore (sph); cyan = three processes. Abbreviations: cox = coxa; ca = cannula; fm = femur; ls = lateral sulcus; prf = prefemur; sg = seminal groove; sl = solenomere; sph = solenophore.

Enghoffosoma parvispina Benchapong & Srisonchai, sp. nov.

https://zoobank.org/D81AF0FC-7232-4766-9469-2F5BD78FEB6C

Figs 6–9

Material examined. ***Holotype*:** Thailand • ♂ (MZKKU-MYR0009); Ubon Ratchathani Province, Khong Chiam District, Tham Heo Sin Chai Temple, on forest floor; 130 m a.s.l.; 15°18'31.2"N, 105°29'07.6"E; 23 June 2024; R. Srisonchai and T. Benchapong leg.

***Paratypes*:** Thailand • 15 ♂♂, 15 ♀♀ (MZKKU-MYR0010); same data as for holotype • ♂, ♀ (CUMZ-MYR0035); same data as for holotype • ♂, ♀ (NHM); same data as for holotype • ♂, ♀ (NHMD); same data as for holotype • ♂, ♀ (NHMW), same data as for holotype • ♂ (ZFMK-MYR14170) ♀ (ZFMK-MYR14169); same data as for holotype.

Other materials. Thailand • 56 ♂♂, 4 ♀♀; same data as for holotype • ♂ (MZKKU); Ubon Ratchathani Province, Khong Chiam District, Thung Na Muang Waterfall, on forest floor; 130 m a.s.l.; 15°31'58"N, 105°35'48"E; 2 Jun. 2022; R. Srisonchai and T. Benchapong leg. • 8 ♂♂, 8 ♀♀ (MZKKU); Ubon Ratchathani Province, Khong Chiam District, Soi Sawan Waterfall, on forest floor; 240 m a.s.l.; 15°27'40"N, 105°34'39"E; 15 Jun. 2022; R. Srisonchai and T. Benchapong leg.; MZKKU • 15 ♂♂, 13 ♀♀ (MZKKU); Ubon Ratchathani Province, Khong Chiam District, Pha Taem National Park, on forest floor;

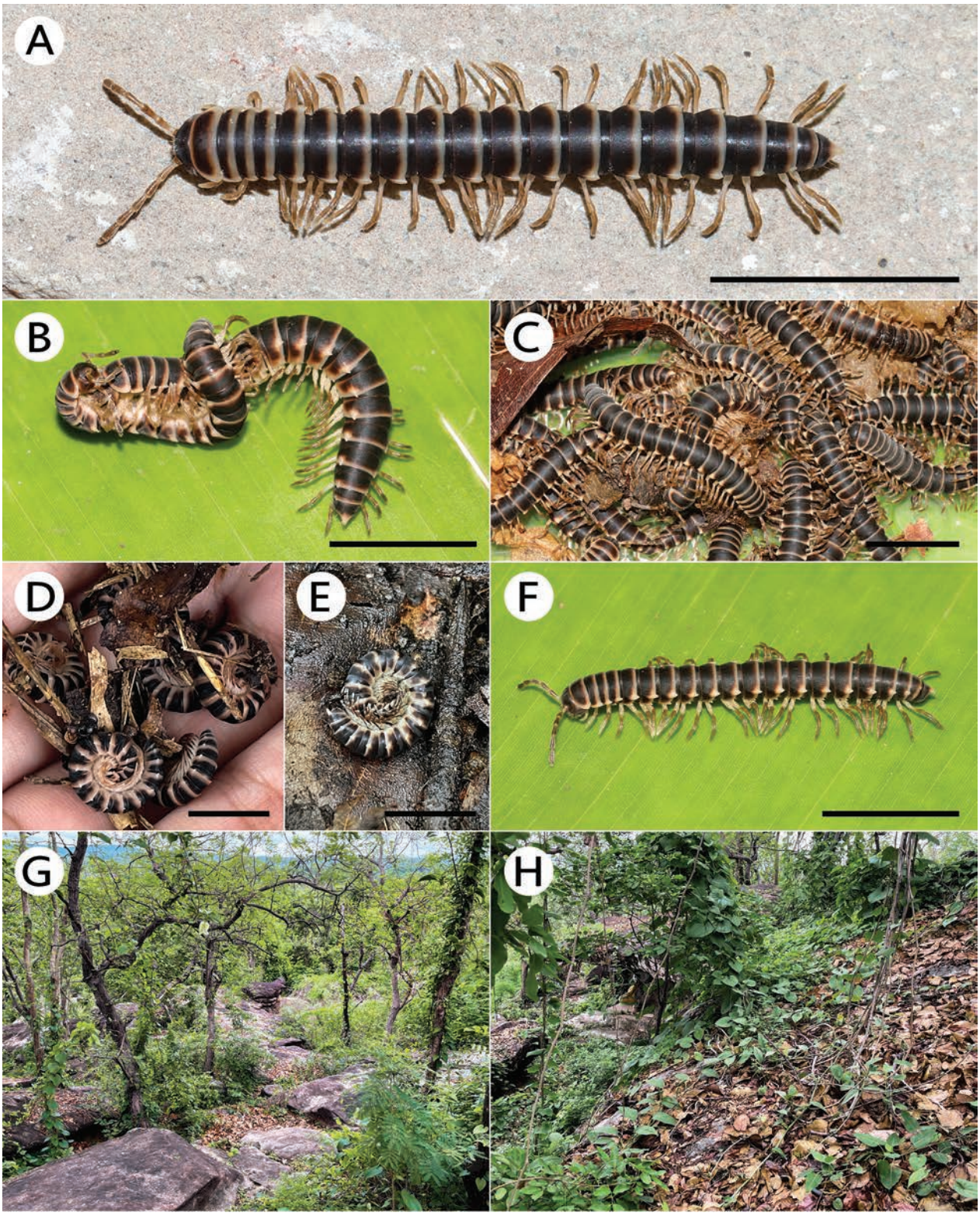

Figure 6. Live photographs of *Enghoffosoma parvispina* sp. nov. and habitat. **A–F, D.** Paratypes; **G, H.** Sandstone habitat. Scale bars: 10 mm.

200 m a.s.l.; 15°23'56.8"N, 105°30'29.8"E; 24 May. 2022; N. Likhitrakarn and R. Srisonchai leg. • 4 ♂♂, ♀ (MZKKU); Ubon Ratchathani Province, Khong Chiam District, Pha Taem National Park, on forest floor; 200 m a.s.l.; 15°23'56.8"N, 105°30'29.8"E; 23 June 2024; R. Srisonchai and T. Benchapong leg. • 2 ♀♀ (MZKKU); Ubon Ratchathani Province, Khong Chiam District, Khong Chiam Police Station, on forest floor; 90 m a.s.l.; 15°23'56.8"N, 105°30'29.8"E; 24 May 2022; N. Likhitrakarn and R. Srisonchai leg. • 4 ♂♂, 3 ♀♀ (MZKKU); Ubon Ratchathani Province, Khong Chiam District, Peerada Hug Moon, on forest floor; 100 m a.s.l.; 15°18'53.7"N, 105°29'59.1"E; 24 June 2024; R. Srisonchai and T. Benchapong leg.

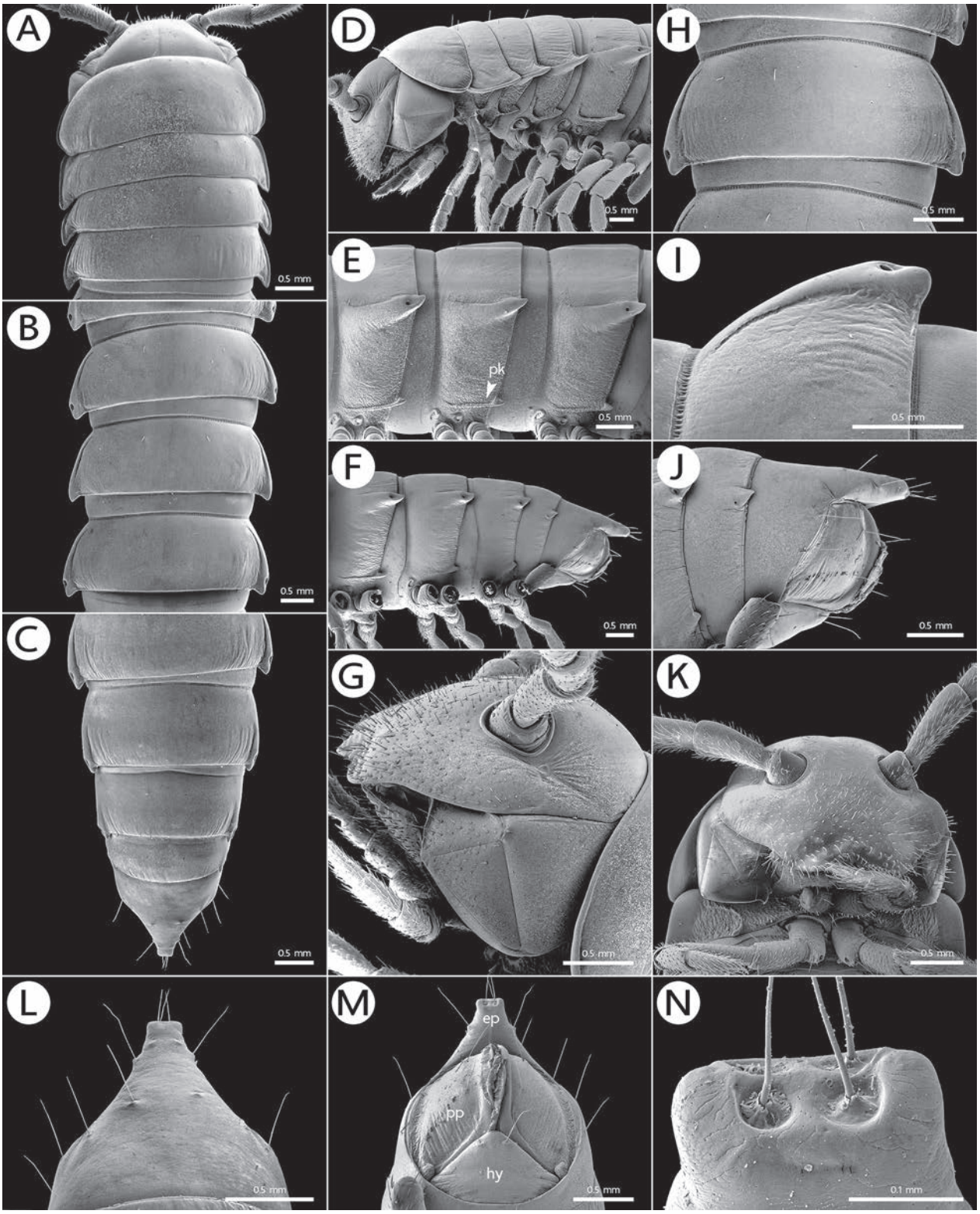

Figure 7. Scanning electron micrographs of *Enghoffosoma parvispina* sp. nov., male paratype (MZKKU-MYR0010). **A, D.** Anterior body part; **B, E.** Body rings 8–10; **C, F.** Posteriormost body rings and telson; **G.** Head and antenna; **H.** Body ring 10; **I.** Paraterga of ring 10; **J.** Telson; **K.** Head; **L–N.** Telson. **A–C, H, I, L.** Dorsal view; **D–F, G, J.** Lateral view. Abbreviations: ep = epiproct; hy = hypoproct; pk = pleurosternal keel; pp = paraproct.

Etymology. The specific name is a noun in apposition referring to a small process on the lateral base of the solenophore.

Diagnosis. Femoral part of gonopod with a long process (p) distally (Fig. 9D–G, I, J) and solenophore with two major lobes/processes (Fig. 9E). Similar in these

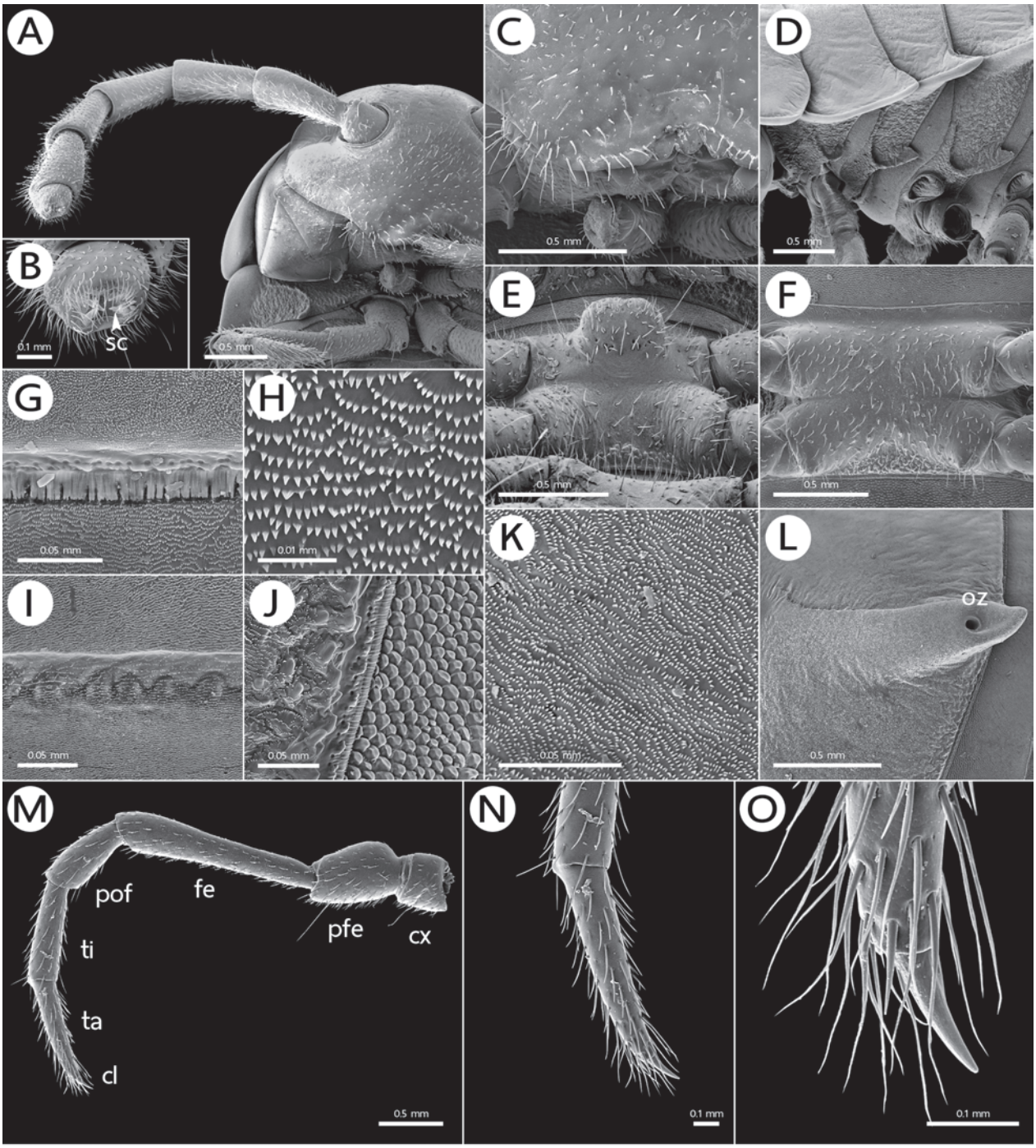

Figure 8. Scanning electron micrographs of *Enghoffosoma parvispina* sp. nov., male paratype (MZKKU-MYR0010). **A.** Head and antenna; **B.** Antennomeres 7 and 8; **C.** Clypeus, labrum and tip of gnathochilarium; **D.** Pleurosternal keels on rings 2–4; **E.** Sternal lobe between male coxae 4; **F.** Sternum of ring 10; **G, J.** Surface and limbus between rings 10 and 11, dorsal and lateral views; **H.** Surface of prozona of ring 10; **I.** Stricture between prozona and metazona of ring 10; **K.** Surface below paraterga of ring 10; **L.** Ozopore on paraterga of ring 10; **M.** Male right leg of ring 10; **N.** Tarsus; **O.** Claw. Abbreviations: cx = coxa; cl = claw; fe = femur; oz = ozopore; pfe = prefemur; pof = postfemur; sc = sensory cones; ta = tarsus; ti = tibia.

respects to *E. extraspinosum* Golovatch & Semenyuk, 2018 (Fig. 14B) and *E. rubellum* sp. nov. (Fig. 13). Differs from them by the presence of a small process (sph-l) at base of solenophore (Fig. 9B, E, I) and without ventral brushes on male legs 1–10. Genetically distant from other *Enghoffosoma* species by 15.09–21.25% of COI sequences.

Description. Holotype: length 28.5 mm, height of midbody 3.1 mm, width of midbody prozonum and metazonum 3.0 and 3.5 mm, respectively. Males: length 26.5–28.9 mm, height of midbody 2.7–3.2 mm, width of midbody prozona and metazona 2.7–3.1 and 3.3–3.6 mm, respectively. Females: length 28.1–30.6 mm, height of midbody 3.4–3.7 mm, width of midbody prozona and metazona 3.3–3.6 and

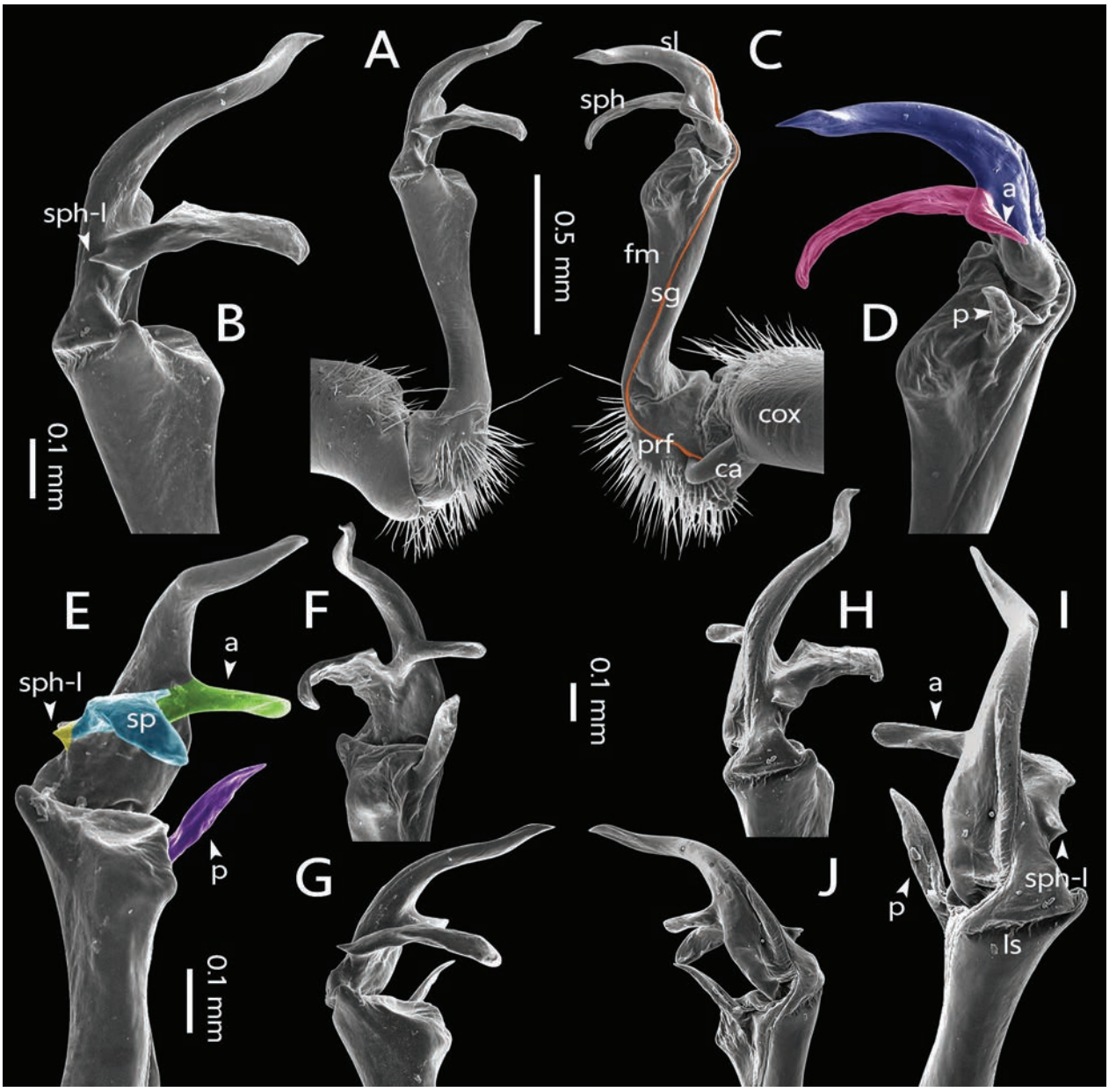

Figure 9. Scanning electron micrographs of *Enghoffosoma parvispina* sp. nov., holotype, right gonopod male paratype (MZK-KU-MYR0010). **A, B.** Lateral view; **C, D.** Mesal view; **E.** Ventral view; **F, G.** Subventral view; **H.** Dorsal view; **I, J.** Subdorsal view. Colors: green = process a (a); purple = process on femur (p); orange = seminal groove (sg); navy blue = solenomere (sl); pink = solenophore (sph); sky blue = spatula-like process (sp); yellow = lateral process on solenophore (sph-l). Abbreviations: a = process a; cox = coxa; ca = cannula; fm = femur; ls = lateral sulcus; p = process on femur; pfm = postfemur; prf = prefemur; sg = seminal groove; sl = solenomere; sph = solenophore; sph-l = lateral process on solenophore.

3.6–3.7 mm, respectively. Width of head < collum < ring 4 < 2 = 3 < 5–13 (male); head < ring 2 = 3 = 4 < collum < 5–15 (female), thereafter gradually tapering towards telson.

Coloration (Fig. 6A–F): Specimens in life brownish black or black. Head black. Antenna light brown. Collum, metaterga and surface below paraterga brownish black. Epiproct except the whitish tip, posterior part of collum and of metaterga brownish white. Paraterga, sterna and lower part of surface below paraterga and tip of epiproct white. Antenna and legs light brown; except a few basal podomeres whitish brown. Coloration in alcohol after two years of preservation changed to brownish black.

Head and clypeolabral region (Figs 7G, K, 8A, C): Vertex almost bare; epicranial suture conspicuous, shallow. Frons with sparse setae. Clypeus and labrum simple and normal.

Antennae (Fig. 8A, B): Quite short; densely setose; reaching backward to ring 4 (♂) or 3 (♀). In length, antennomeres 6>2=3=4=5>1=7. Antennomeres 5–7 clavate; each with a group of sensilla basiconica distally. With four apical cones.

Collum (Fig. 7A, D): Broad and wide. With two transverse rows of inconspicuous setae: 3+3 in anterior position and 1+1 in ca. at midlength of collum. Paraterga of collum poorly developed (= round tip).

Tegument (Figs 7A–F, H, 8H, K): With microspinulation. Prozona, metazona, paraterga and surface below paraterga microspinulate. Prozona on lateral side of body finely shagreened. Stricture between prozona and metazona striolate, quite deep and narrow.

Metaterga (Figs 9H, I, 8I): Metaterga 2–6 with one transverse row of setae (mostly inconspicuous and broken off), 3+3 in anterior position. Metaterga 7–19 with one transverse row of setae, 1+1 ca. at midlength of metaterga. Stricture between prozona and metazona striolate, shallow and narrow. Axial line and transverse sulcus missing.

Limbus (Fig. 8G): Limbus of midbody ring conspicuous; with rows of very long filaments, fused, arranged anteroposteriorly; margin finely spiculate; surface in front of limbus with a low ridge.

Paraterga (Figs 7H, I, 8L): Short, stout and small. Paraterga 2–4 short and thin. Paraterga 5–16 stouter and larger than others. The following paraterga slightly reduced in size and gradually tapering toward telson. No incision on lateral margin. Posterior corner obtuse, directed caudad. Ozopores conspicuous, small, oval; present on rings 5, 7, 9, 10, 12, 13, 15–19; visible in lateral view; located near tip of paraterga.

Pleurosternal keels (Figs 7D–F, 8D): Conspicuous. Rings 2–4 with small ridges; rings 2–8 crestlike, with a sharp caudal tooth posteriorly; increasingly reduced to small caudal tooth in rings 9–17; absent in rings 18 and 19.

Telson (Fig. 7J, L–N): Preanal ring (epiproct) quite slender, slightly attenuate near tip; lateral setiferous tubercles inconspicuous; apical tubercles a little swollen; tip truncate, sometimes concave; with four spinnerets arranged at the corner, each located inside a deep depression and surrounded by a crownlike collar. Paraprocts simple, slightly convex. Hypoproct subtriangular; with inconspicuous setiferous tubercles.

Sterna (Fig. 8E, F): Sparsely setose; cross-impressions shallow; posteriorly with a small tubercle near each coxa. Sternal lobe between male coxae 4, large, subtrapeziform; tip round; with two pores.

Legs (Fig. 8M–O): Moderately long, slender, densely setose; length of midbody leg ca. 4.1–4.6 mm in both sexes; about 1.4–1.5 times (♂) or 1.2–1.3 times (♀) as long as midbody height. Prefemur slightly swollen basally. In length, femur > tarsus > tibia > postfemur = prefemur > coxa (♂). Ventral brushes absent. Claw quite long, slender, pointed. Adenostyles in male absent.

Gonopods (Fig. 9): Coxa (cox) quite short and stout; with a distoanterior group of setae. Cannula (ca) long and slender. Telopodite long and slender; forming a 90° angle with coxa. Prefemur (prf) densely setose; about 1/2 as long as femur. Femur (fm) quite long and slender; distally with a long and sharp process (p), directed anteromesad. Seminal groove (sg) running entirely on mesal surface of femur. Lateral sulcus (ls) conspicuous, deep and wide. Mesal sulcus inconspicuous (Fig. 9L). Postfemoral part inconspicuous. Solenophore (sph) well-developed; consisting of three processes (two major and one small) (Fig. 9B, D). First process (sp) large and very long, spatula-like (Fig. 9D, E, I). Second process (a) smaller and shorter than the first one; located basomesally; tip *in situ* directed mesad (Fig. 9D, E, I). Third process (sph-l) smallest; spinelike; located at base of the first one; tip *in situ* directed ventrad (Fig. 9B, E, I). Solenomere (sl) very long and slender; slightly twisted.

Distribution and habitat (Fig. 6G, H). Based on extensive field surveys, this species inhabits sandstone habitats along the Mekong River in Ubon Ratchathani Province and, due to the proximity of the type locality near the Thai-Laos border, it may also occur in Laos and Cambodia.

Remarks. Based on gonopod solely, this species is very similar to *E. rubellum* sp. nov. It can be distinguished by the lateral small spine at base of solenophore (sph-l) (Fig. 9B, E, I).

Enghoffosoma rubellum Benchapong & Srisonchai, sp. nov.

https://zoobank.org/13D8D4AB-286A-490D-BD7F-90BBD677FC3D
Figs 10–13

Material examined. ***Holotype*****:** Thailand • ♂ (MZKKU-MYR0011); Sakon Nakhon Province, Phu Phan District, Tham Si Kaeo Temple, on forest floor; 315 m a.s.l.; 16°55'18.5"N, 103°53'48.5"E; 22 August 2020; R. Chanabun, A. Aoonkum, R. Srisonchai and T. Benchapong leg.

Paratypes**:** Thailand • ♂ (MZKKU-MYR0012); same data as for holotype • ♂ 4 ♀♀ (MZKKU-MYR00012); same data as for holotype; 13 Aug. 2022. • ♂ (CUMZ-MYR0036); same data as for holotype; 13 Aug. 2022 • ♂ (NHM); same data as for holotype; 13 Aug. 2022 • ♂ (NHMD); same data as for holotype; 13 Aug. 2022 • ♂ (NHMW), same data as for holotype; 13 Aug. 2022 • ♂ (ZFMK-MYR14171); same data as for holotype; 13 Aug. 2022.

Other materials. Thailand • 2 ♂♂, 3 ♀♀ (MZKKU); same data as for holotype • 9 broken ♂♂, 4 broken ♀♀ (MZKKU); same data as for holotype • ♂ (MZKKU); Sakon Nakhon Province, Phu Phan District, Tham Phrong Temple, on forest floor; 320 m a.s.l.; 16°49'18.3"N, 103°58'25.4"E; 22 August 2020; R. Srisonchai and T. Benchapong leg. • ♂ (MZKKU); Sakon Nakhon Province, Phu Phan District, Wiwekkaram Temple, on forest floor; 330 m a.s.l.; 16°51'03.0"N, 103°55'27.7"E; 22 August 2021; R. Srisonchai and T. Benchapong leg. • ♂ (MZKKU); Sakon Nakhon Province, Phu Phan District, Wiwekkaram Temple, on forest floor; 330 m a.s.l.; 16°51'03.0"N, 103°55'27.7"E; 13 August 2022.

Etymology. The specific name is an adjective and refers to the remarkable reddish brown body color of living specimens.

Diagnosis. Femoral part of gonopod with a long process (p) distally (Fig. 13D–I) and solenophore with two major lobes/processes (Fig. 13E). Similar in these respects to *E. extraspinosum* (Fig. 14B) and *E. parvispina* sp. nov. (Fig. 7). Differs from them by the presence of

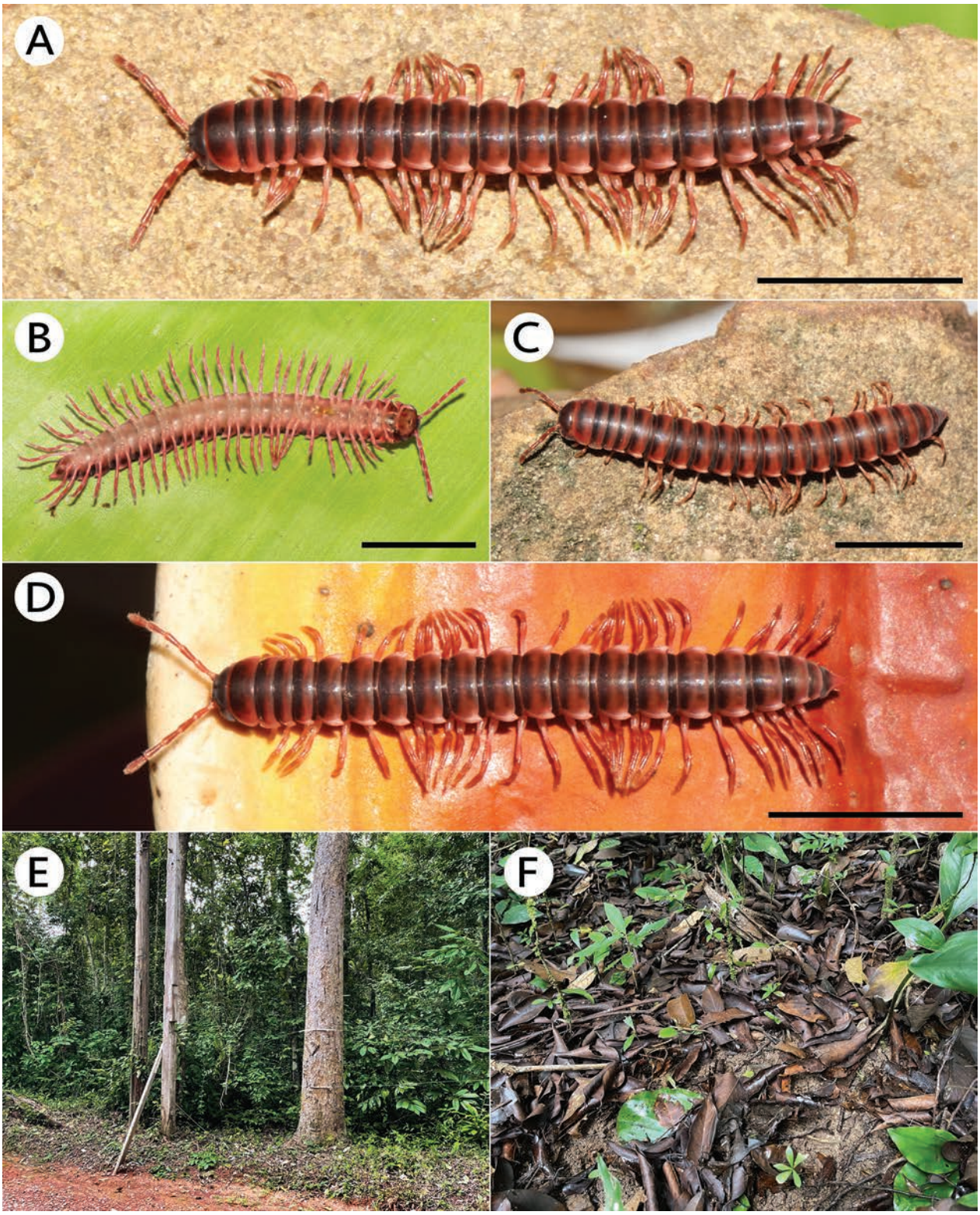

Figure 10. Live photographs of *Enghoffosoma rubellum* sp. nov. and habitat. **A–D.** Paratypes; **E, F.** Sandstone habitat. Scale bars: 10 mm.

a small process (process sph-m) at base of solenophore (Fig. 13C–F, H, I) and by having ventral brushes on male legs 1–10 (Fig. 12M). Genetically distant from other *Enghoffosoma* species by 15.09–22.37% of COI sequences.

Description. Holotype: length 25.7 mm, height of midbody 3.2 mm, width of midbody prozonum and metazonum 2.9 and 3.7 mm, respectively. Males: length 25.7–27.1 mm, height of midbody 3.2–3.6 mm, width of midbody prozona and metazona 2.7–3.1 and 3.3–3.6 mm, respectively. Females: length 28–35.4 mm, height of midbody 3.6–4.3 mm, width of midbody prozona and metazona 3.6–4.1 and 4.0–4.7 mm, respectively. Width of head < collum < ring 3 = 4 < 2 < 5–15 (male), head < collum < ring 2 = 3 = 4 < 5–15 (female), thereafter gently tapering towards telson.

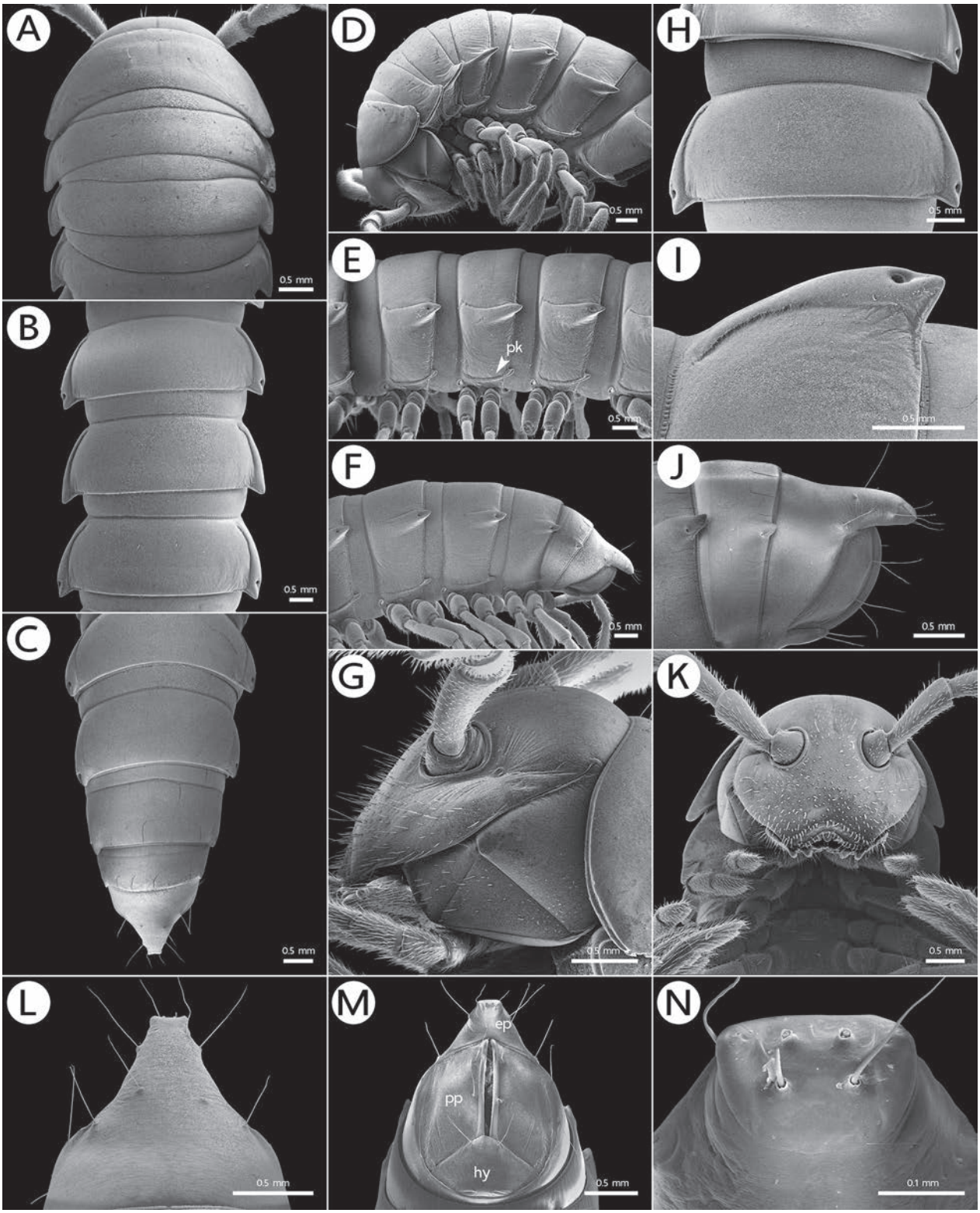

Figure 11. Scanning electron micrographs of *Enghoffosoma rubellum* sp. nov., male paratype (MZKKU-MYR0012). **A, D.** Anterior body part; **B, E.** Body rings 8–10; **C, F.** Posteriormost body rings and telson; **G.** Head and antenna; **H.** Body ring 10; **I.** Paraterga of ring 10; **J.** Telson; **K.** Head; **L–N.** Telson. **A–C, H, I, L.** Dorsal view; **D–F, G, J.** Lateral view. Abbreviations: ep = epiproct; hy = hypoproct; pk = pleurosternal keel; pp = paraproct.

Coloration (Fig. 10A–D): Live specimens brownish red or crimson red. Head and anterior part of metaterga dark brown to brown. Antenna brownish red. Collum, metaterga and epiproct brownish red to crimson red. Paraterga, sternа, surface below paraterga whitish pink; except the middle part of surface below paraterga dark brown. Legs and a few basal podomeres light brown. Coloration in alcohol after two years reddish brown to brown.

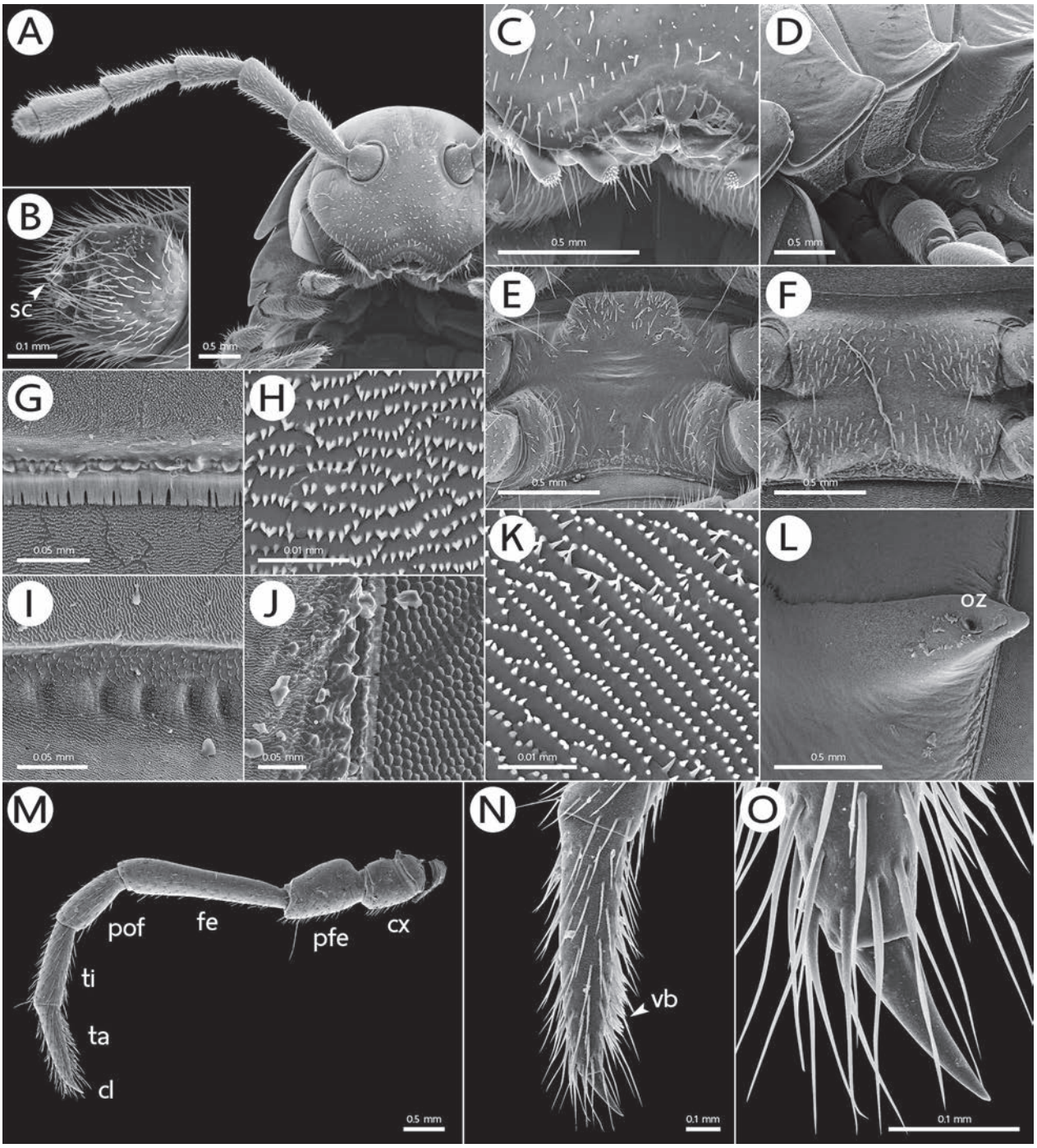

Figure 12. Scanning electron micrographs of *Enghoffosoma rubellum* sp. nov., male paratype (MZKKU-MYR0012). **A.** Head and antenna; **B.** Antennomere 7 and 8; **C.** Clypeus, labrum and tip of gnathochilarium; **D.** Pleurosternal keels on rings 2–4; **E.** Sternal lobe between male coxae 4; **F.** Sternum of ring 10; **G, J.** Surface and limbus between rings 10 and 11, dorsal and lateral views; **H.** Surface of prozona of ring 10; **I.** Stricture between prozona and metazona of ring 10; **K.** Surface below paraterga of ring 10; **L.** Ozopore on paraterga of ring 10; **M.** Male right leg of ring 10; **N.** Ventral brushes on male tarsus; **O.** Claw. Abbreviations: cx = coxa; cl = claw; fe = femur; oz = ozopore; pfe = prefemur; pof = postfemur; sc = sensory cones; ta = tarsus; ti = tibia; vb = ventral brushes.

Head and clypeolabral region (Figs 11K, 12A, C): Vertex entirely bare; epicranial suture conspicuous. Frons sparsely setose. Clypeus and labrum normal.

Antennae (Fig. 12A, B): Short; densely setose; reaching backward to ring 3 (♂) or 2 (♀). In length, antennomeres 2=3>4=6>1>7. Antennomeres 5–7 slightly clavate; each with a group of small sensilla basiconica distally. With four apical cones.

Collum (Fig. 11A, D): Broad and wide. With two transverse rows of inconspicuous setae: 3+3 in anterior position and 1+1 ca. at midlength of collum. Paraterga of collum poorly developed (= obtuse tip).

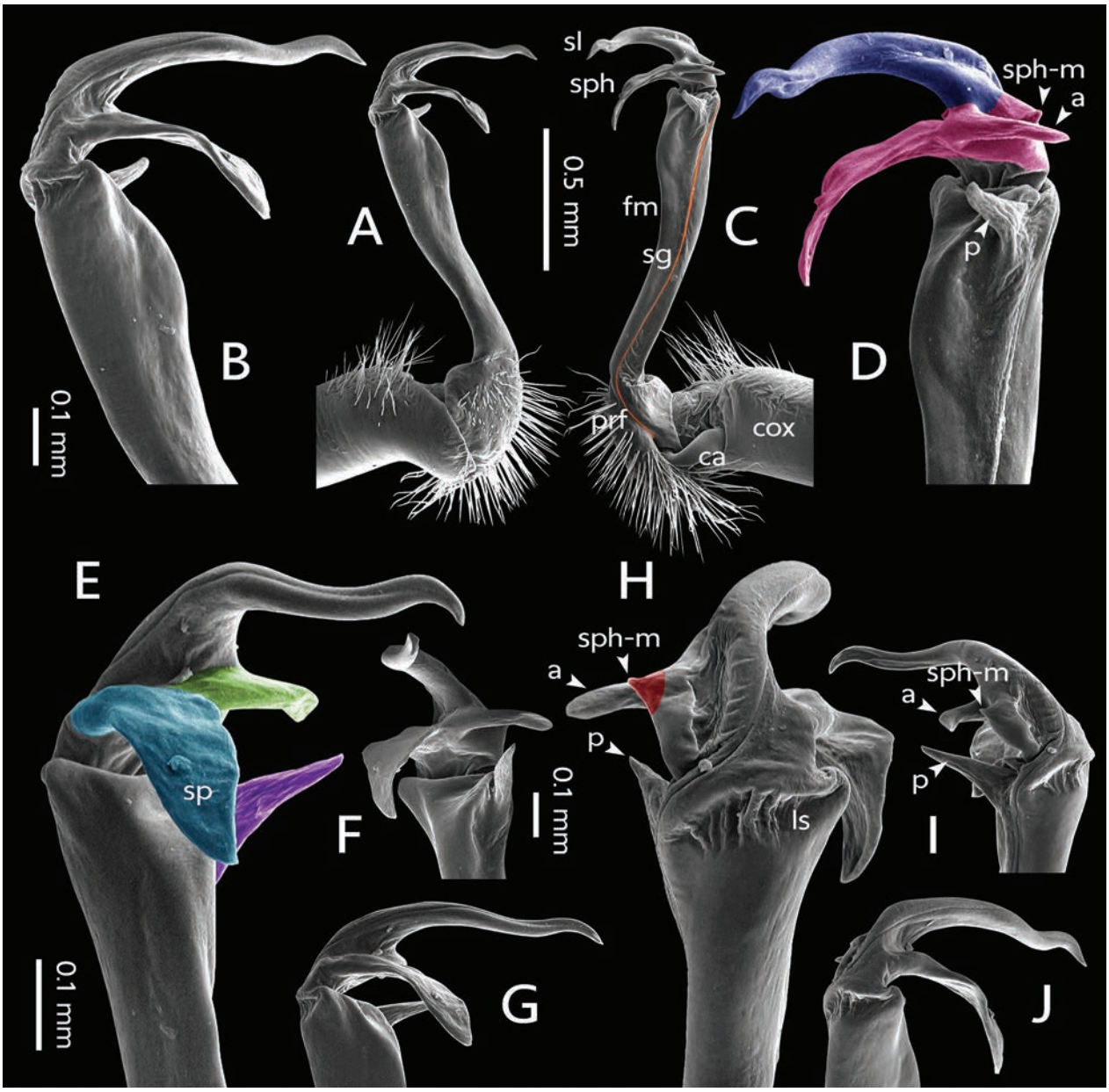

Figure 13. Scanning electron micrographs of *Enghoffosoma rubellum* sp. nov., right gonopod, male paratype (MZKKU-MYR0012). **A, B.** Lateral view; **C, D.** Mesal view; **E.** Ventral view; **F, G.** Subventral view; **H.** Dorsal view; **I, J.** Subdorsal view. Colors: green = process a (a); purple = process on femur (p); orange = seminal groove (sg); navy blue = solenomere (sl); pink = solenophore (sph); sky blue = spatula-like process (sp); red = mesal process on solenophore (sph-m). Abbreviations: a = process; cox = coxa; ca = cannula; fm = femur; ls = lateral sulcus; p = process on femur; pfm = postfemur; prf = prefemur; sg = seminal groove; sl = solenomere; sph = solenophore; sph-m = mesal process on solenophore.

Tegument (Figs 11–F, H, 12K, L): With microspinulation, velvetlike. Prozona, metazona, paraterga and surface below paraterga microspinulate. Prozona on lateral side of body finely shagreened. Stricture between prozona and metazona striolate, quite deep and narrow.

Metaterga (Figs 11H, I, 12I): Metatergum 2–4 with one transverse row of setae (mostly inconspicuous and broken off), 3+3 in anterior position. Metaterga 5–8 with one transverse row of setae, 2+2 in anterior position. Metaterga 9–19 with one transverse row of setae, 1+1 in anterior position. Stricture between prozona and metazona striolate, shallow and narrow. Axial line and transverse sulcus missing.

Limbus (Fig. 12G): Limbus of midbody ring conspicuous; with rows of very long filaments, hairlike, arranged anteroposteriorly; margin finely spiculate; surface in front of limbus with a low and irregular ridge.

Paraterga (Figs 11H, I, 12L): Quite short, stout and small. Paraterga 2–4 short and thin. Paraterga 5–16 stouter and larger than the others. The following paraterga slightly reduced in size and gradually tapering toward telson. No indentation on lateral margin. Posterior corner obtuse, directed caudad. Ozopores small but conspicuous,

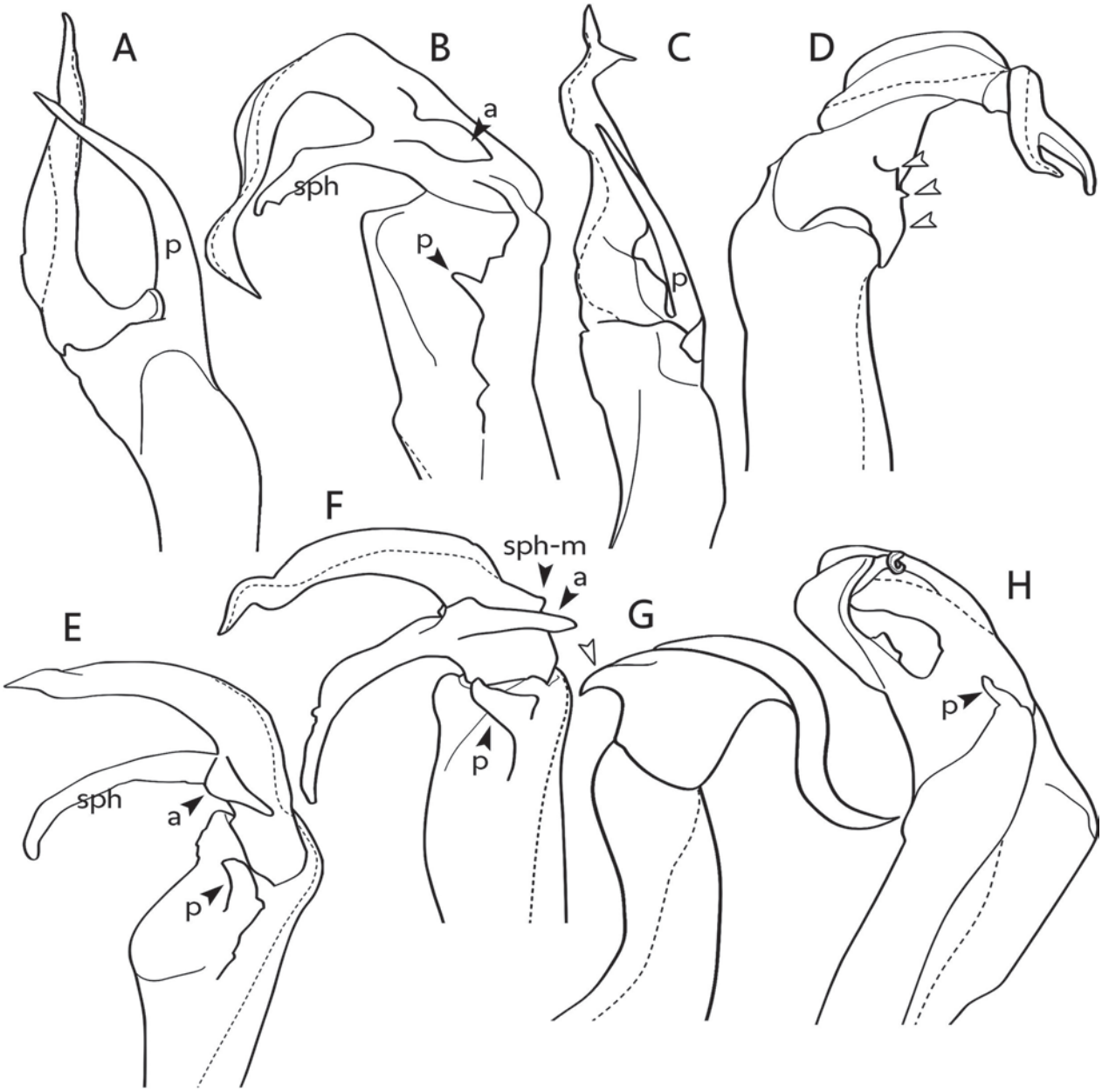

Figure 14. Outline of gonopod telopodite of some *Enghoffosoma* species that show similar conformation in the distal part, all in mesal view. **A.** *E. bispinum* Likhitrakarn et al., 2014; **B.** *E. extraspinosum* Nguyen & Golovatch, 2016; **C.** *E. funda* Likhitrakarn et al., 2014; **D.** *E. furca* sp. nov.; **E.** *E. parvispina* sp. nov.; **F.** *E. rubellum* sp. nov.; **G.** *E. triangulare* Nguyen & Golovatch, 2016; **H.** *E. zebra* Likhitrakarn et al., 2014. Abbreviations: a = process a; p = process p on femur; sph-m = mesal process on solenophore.

oval; present on rings 5, 7, 9, 10, 12, 13, 15–19; visible in lateral view; located near tip of paraterga.

Pleurosternal keels (Figs 11D–F, 12D): Rather well-developed, conspicuous; slightly curved. Keels on rings 2–4 small; rings 2–8 crestlike, with a sharp caudal tooth posteriorly; increasingly reduced to small caudal tooth in rings 9–17; absent in rings 18 and 19.

Telson (Fig. 11J, L, M, N): Preanal ring (epiproct) quite slender, coniform in dorsal view; lateral setiferous tubercles inconspicuous; apical tubercles a little swollen; tip concave; with four spinnerets arranged at the corner without depression. Paraprocts simple, convex. Hypoproct subtriangular; with inconspicuous setiferous tubercles.

Sterna (Fig. 12E, F): Sparsely setose; cross-impressions shallow; posteriorly with a small tubercle near each coxa. Sternal lobe between male coxae 4, broad and large, trapeziform; tip round; with two inconspicuous pores.

Legs (Fig. 12M–O): Moderately long, slender, densely setose; length of midbody leg ca. 4.0–5.1 mm in both sexes; about 1.3 times (♂) or 1.1–1.2 times (♀) as long as midbody height. Prefemur slightly swollen basally. In length, femur > tarsus = tibia = prefemur > postfemur > coxa (♂). Tarsus of legs 1–10 in male with ventral brushes. Claw quite long, slender, pointed. Adenostyles in male absent.

Gonopods (Fig. 13): Coxa (cox) short and stout; with a distoanterior group of setae. Cannula (ca) long and slen-

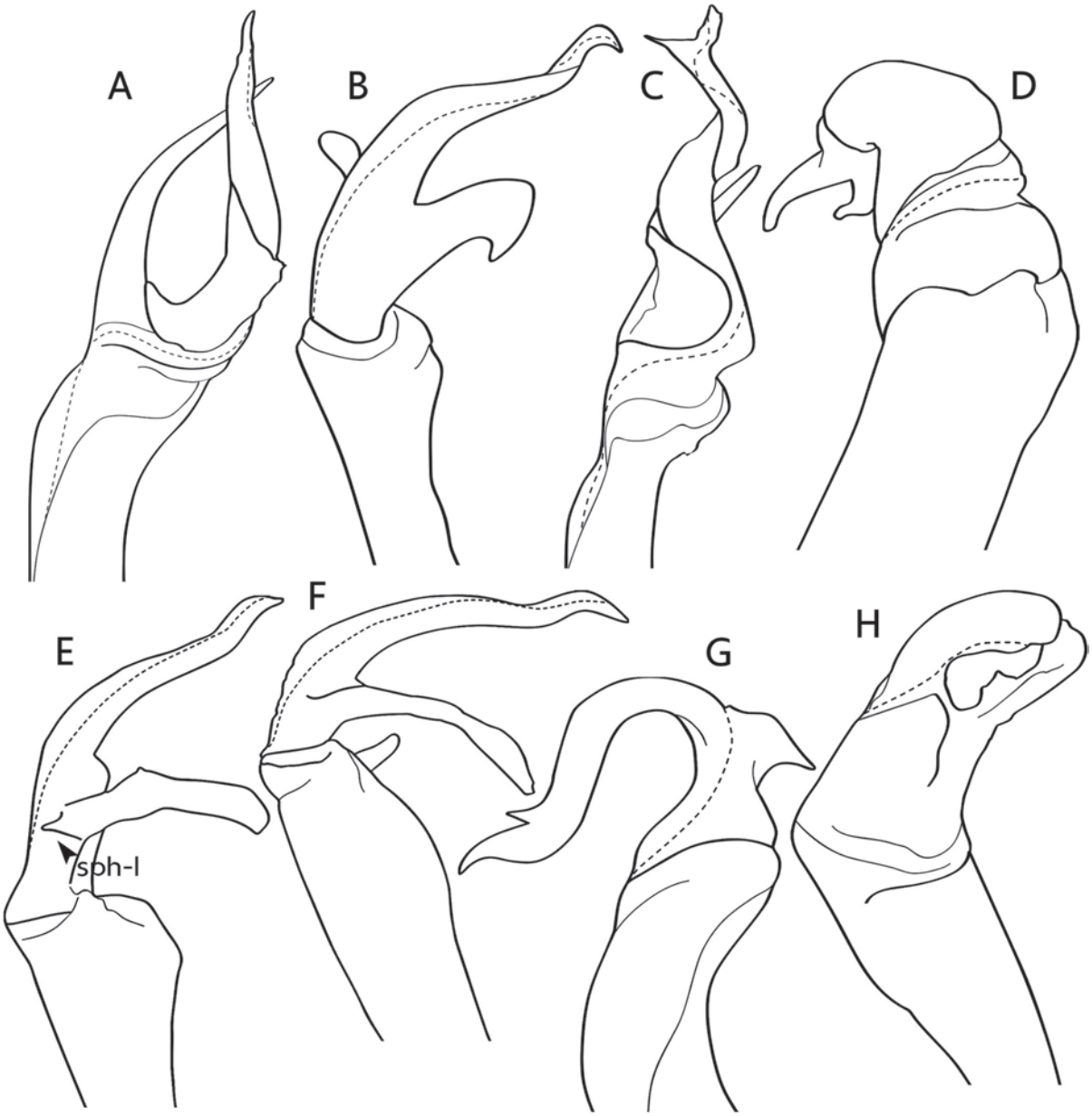

Figure 15. Outline of gonopod telopodite of some *Enghoffosoma* species that show similar conformation in the distal part, all in lateral view **A.** *E. bispinum* Likhitrakarn et al., 2014; **B.** *E. extraspinosum* Nguyen & Golovatch, 2016; **C.** *E. funda* Likhitrakarn et al., 2014; **D.** *E. furca* sp. nov.; **E.** *E. parvispina* sp. nov.; **F.** *E. rubellum* sp. nov.; **G.** *E. triangulare* Nguyen & Golovatch, 2016; **H.** *E. zebra* Likhitrakarn et al., 2014. Abbreviation: sph-l = lateral process on solenophore.

der. Telopodite long and slender; forming a 90° angle with coxa. Prefemur (prf) with dense and long seta; shorter than femur; about 1/3 as long as femur. Femur (fm) very long and slenderer; distally with a long and sharp process (p), digitiform, directed mesad. Seminal groove (sg) running entirely on mesal surface of femur. Lateral sulcus (ls) conspicuous, deep and wide; with 4–5 transverse ridges inside sulcus (Fig. 13H). Mesal sulcus inconspicuous. Postfemoral part (pfm) inconspicuous. Solenophore (sph) well-developed; consisting of three processes. First process (sp) large and very long, spatula-like; tip obtuse, directed posteriad (Fig. 13D, E). Second process (a) smaller and shorter than the first one; slender; located basomesally; tip *in situ* directed dorsolaterad (Fig. 13D, E, H, I). Third process (sph-m) smallest; spinelike; located at base of the second one, clearly seen in dorsal view; tip *in situ* directed mesad (Fig. 13D, H, I). Solenomere (sl) very long and slender; slightly twisted near tip.

Distribution and habitat (Fig. 10E, F). The new species is distributed along the Phu Phan mountain range in Sakon Nakhon Province. All specimens were seen walking and curling their bodies on moist leaf litter in sandstone forest habitat.

Remarks. Among all recorded *Enghoffosoma* species, *E. rubellum* sp. nov. shows such vivid brownish red/red body color that it is easily distinguished from all congeners.

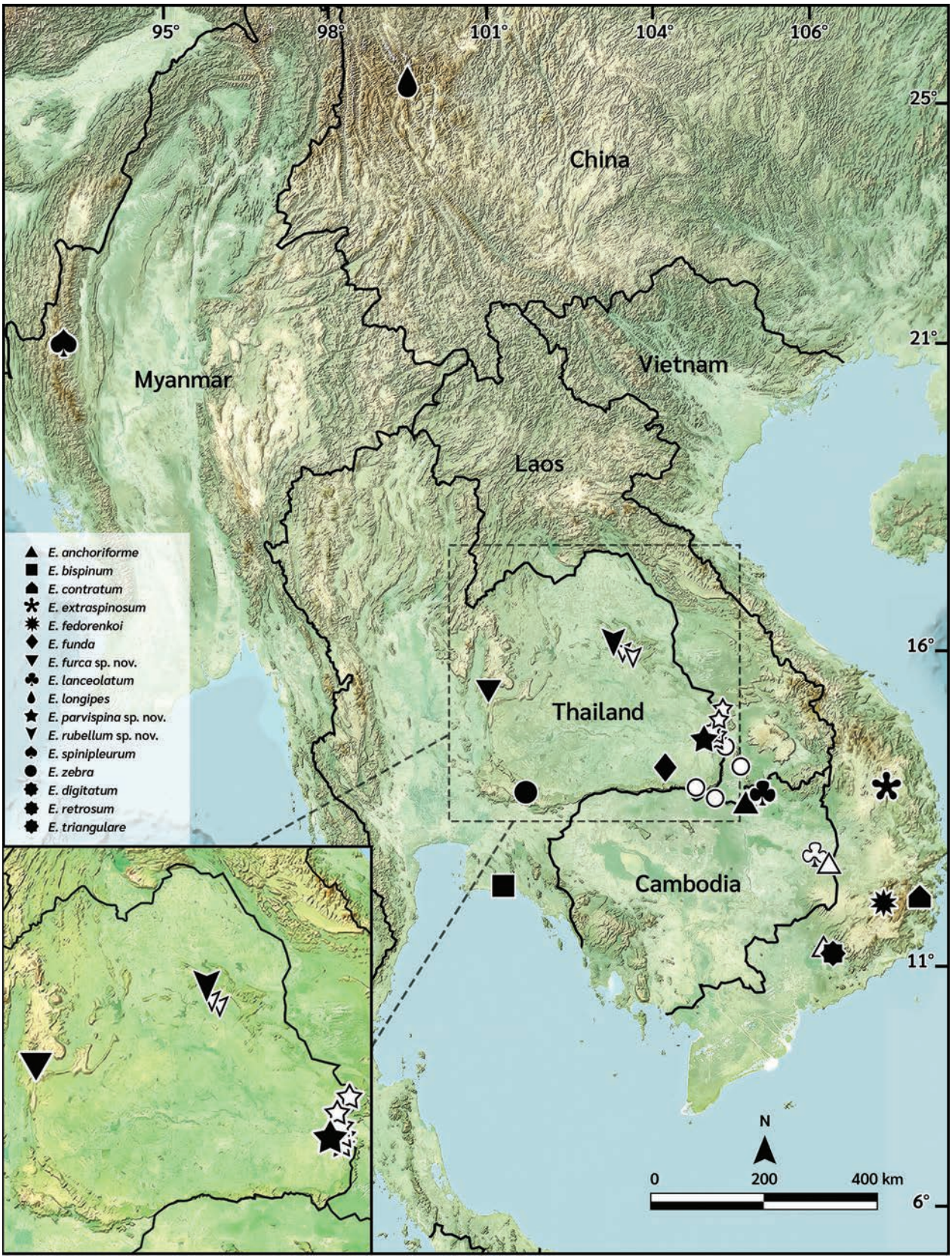

Figure 16. Distribution of all *Enghoffosoma* species. Color of symbol: black = type locality, white = other localities. Inset photo indicates locations of three new species. Type localities of *E. digitatum* Nguyen & Golovatch, 2016, *E. retrosum* Nguyen & Golovatch, 2016 and *E. triangulare* Nguyen & Golovatch, 2016 are in the same location and indicated by the same symbol.

***Enghoffosoma zebra* Likhitrakarn, Golovatch & Panha, 2014**

Enghoffosoma zebra Likhitrakarn, Golovatch & Panha, 2014 in Likhitrakarn et al. 2014: 493.

Enghoffosoma zebra—Nguyen & Golovatch, 2016: 151; Likhitrakarn et al. 2023: 74.

Distribution. Thailand (Nakhon Ratchasima and Ubon Ratchathani provinces) and Laos (Champasak Province).

Remarks. Likhitrakarn et al. (2014) observed variation in the femur of gonopod; some specimens bear a short process (referred to as process p) (Fig. 14H), while others have a longer one.

Discussion

This is the first treatment of the genus *Enghoffosoma* that integrates morphological characteristics and molecular data. It is important to note that the details of the gonopod telopodite clearly differentiate all species from each other. *E. furca* sp. nov. differs from the other species by the presence of three short processes, while *E. parvispina* sp. nov. and *E. rubellum* sp. nov. can be distinguished by the presence of small spinelike processes sph-l and sph-m, at the base of the solenophore, respectively. This aligns with the results of previous studies on paradoxosomatids and xystodesmids, where the integration of morphological and molecular approaches provided sufficient data for accurate species identification (Means et al. 2021; Srisonchai et al. 2024). Other morphological traits such as the color pattern, the sternal lobe on the male coxae 4 and the male tarsal brush can also be used for reliable discrimination. The use of SEM in this study provided deep detail of some informative characters, especially the apical part of the gonopod telopodite. *E. parvispina* sp. nov. and *E. rubellum* sp. nov. both have small spinule-like processes (sph-l and sph-m, respectively) at the base of the solenophore, though these processes arise from different positions: lateral and mesal, respectively. Additionally, *E. extraspinosum* also exhibits a similar process, located midway on a small lobe of the solenophore (Golovatch and Semenyuk 2018).

The interspecific genetic distances of the barcoding COI gene seem to agree with the morphological evidence: the three new species differ significantly from the others, showing high genetic distances of over 15.09% (18.56–22.78% for *E. furca* sp. nov., 15.09–21.25% for *E. parvispina* sp. nov. and 15.09–22.37% for *E. rubellum* sp. nov.). These values closely match the interspecific distances observed in other Paradoxosomatidae, which typically range from 11.4% to above 25% (Decker 2016; Nguyen et al. 2017; Srisonchai et al. 2024). Our phylogenetic tree places *E. parvispina* and *E. rubellum* as separate clades, and *E. furca*, represented by a single terminal, as part of a different lineage, further reinforces the usefulness of gonopod characteristics in distinguishing these species. A discussion of the phylogeny of *Enghoffosoma*, however, is beyond the scope of our current work. To elucidate phylogenetic relationships within *Enghoffosoma* and with their closely related genera, further investigations incorporating additional genetic markers and more taxa is necessary.

The number of described *Enghoffosoma* species found exclusively in Thailand has now reached six. Of these, five species inhabit sandstone environments, while only one is known to occur in limestone habitats. Field surveys conducted between 2020 and 2024 have revealed a greater diversity of *Enghoffosoma* in Thailand than previously thought. These findings indicate that northeastern Thailand is an important area for millipede biodiversity (Fig. 16). It is expected that further exploration in other areas of Thailand, as well as in other countries in the region, like Laos, Cambodia, Myanmar and China, will reveal even more diversity within this genus.

Acknowledgements

The funding for this work was obtained from the National Science, Research and Innovation Fund through the Fundamental Fund of Khon Kaen University (2568), and partly supported by the Office of the Permanent Secretary, Ministry of Higher Education, Science, Research and Innovation (OPS MHESI), Thailand Science Research and Innovation (TSRI) (Grant No. RGNS65-056). The research capability enhancement program through graduate student scholarship (TB), Faculty of Science, Khon Kaen University, is gratefully acknowledged. Thanks are due to staff members of the Department of National Parks, Wildlife and Plant Conservation in Thailand who supported all available surveys in protected areas. We give special gratitude to ASRU and MZKKU colleagues for their assistance in the fieldwork. Special thanks also go to D.J. Anderson for grammar checking and comments. The editor (Luiz Iniesta) and referees (Sergei Golovatch and Dragan Antić) are acknowledged for valuable comments that enormously improved the manuscript. The copy editor (Gabriel Hershman and Bilyana Nikolova) kindly corrected a final version of the manuscript and the CIPRES Science Gateway V 3.3 provided access to computational analysis.

References

American Veterinary Medical Association (2020) AVMA Guidelines for the Euthanasia of Animals: 2020 edn. https://www.avma.org/sites/default/files/2020-02/Guidelines-on-Euthanasia-2020.pdf

Darriba D, Taboada GL, Doallo R, Posada D (2012) jModelTest 2: more models, new heuristics and parallel computing. Nature Methods 9: 772. https://doi.org/10.1038/nmeth.2109

Decker P (2016) Integrative taxonomic revision of the polymorphic flat-millipede genera *Oncocladosoma* and *Somethus* in South Australia (Diplopoda: Polydesmida: Paradoxosomatidae). Invertebrate Systematics 30(3): 201–218. https://doi.org/10.1071/IS15047

Folmer O, Black M, Hoeh W, Lutz R, Vrijenhoek R (1994) DNA primers for amplification of mitochondrial cytochrome c oxidase subunit

I from diverse metazoan invertebrates. Molecular Marine Biology and Biotechnology 3: 294–299.

Golovatch SI (1993) On several new or poorly-known Oriental Paradoxosomatidae (Diplopoda Polydesmida). Arthropoda Selecta 2(1): 3–14. https://doi.org/10.15298/arthsel.30.1.01

Golovatch SI (2011) On several new or poorly-known Oriental Paradoxosomatidae (Diplopoda: Polydesmida), XI. Arthropoda Selecta 20(1): 259–266. https://doi.org/10.15298/arthsel.20.4.02

Golovatch SI (2016) On several new or poorly-known Oriental Paradoxosomatidae (Diplopoda: Polydesmida), XIX. Arthropoda Select 25(2): 131–152. https://doi.org/10.15298/arthsel.25.2.01

Golovatch SI, Semenyuk I (2018) On several new or poorly-known oriental paradoxosomatidae (Diplopoda: Polydesmida), XXIII. Arthropoda Selecta 27(1): 1–21. https://doi.org/10.15298/arthsel.27.1.01

Golovatch SI, VandenSpiegel D, Semenyuk II (2016) On several new or poorly-known Oriental Paradoxosomatidae (Diplopoda: Polydesmida), XXI. Arthropoda Selecta 25(4): 335–354. https://doi.org/10.15298/arthsel.25.4.01

Hillis DM, Bull JJ (1993) An empirical test of bootstrapping as a method for assessing confidence in phylogenetic analysis. Systematic Biology 42(2): 182–192. https://doi.org/10.1093/sysbio/42.2.182

Huelsenbeck JP, Rannala B (2004) Frequentist properties of Bayesian posterior probabilities of phylogenetic trees under simple and complex substitution models. Systematic Biology 53(6): 904–913. https://doi.org/10.1080/10635150490522629

Likhitrakarn N, Golovatch SI, Prateepasen R, Panha S (2010) Review of the genus *Tylopus* Jeekel, 1968, with descriptions of five new species from Thailand (Diplopoda, Polydesmida, Paradoxosomatidae). ZooKeys 72: 23–68. https://doi.org/10.3897/zookeys.72.744

Likhitrakarn N, Golovatch SI, Panha S (2011) Revision of the Southeast Asian millipede genus *Orthomorpha* Bollman, 1893, with the proposal of a new genus (Diplopoda, Polydesmida, Paradoxosomatidae). ZooKeys 131: 1–161. https://doi.org/10.3897/zookeys.131.1921

Likhitrakarn K, Golovatch SI, Panha S (2014) Review of the Southeast Asian millipede genus *Enghoffosoma* Golovatch, 1993 (Diplopoda, Polydesmida, Paradoxosomatidae), with descriptions of new species. Zootaxa 3811(4): 491–514. https://doi.org/10.11646/zootaxa.3811.4.4

Likhitrakarn N, Golovatch SI, Semenyuk I, Efeykin BD, Panha S (2019) Review of the millipede genus *Orthomorpha* Bollman, 1893 (Diplopoda, Polydesmida, Paradoxosomatidae) in Vietnam, with several new records and descriptions of two new species. ZooKeys 898: 121–158. https://doi.org/10.3897/zookeys.898.39265

Likhitrakarn N, Srisonchai R, Golovatch SI (2023) An updated catalogue of the millipedes (Diplopoda) of Thailand. Tropical Natural History 7: 51–92. https://li01.tcithaijo.org/index.php/tnh/article/view/258815

Means JC, Hennen DA, Marek PE (2021) A revision of the minor species group in the millipede genus *Nannaria* Chamberlin, 1918 (Diplopoda, Polydesmida, Xystodesmidae). ZooKeys 1030(1): 1–180. https://doi.org/10.3897/zookeys.1030.62544

Miller MA, Pfeiffer W, Schwartz T (2010) Creating the CIPRES Science Gateway for inference of large phylogenetic trees. In 'Proceedings of the Gateway Computing Environments Workshop (GCE)', 14 November 2010, New Orleans, LA, USA. INSPEC 11705685, 1–8. https://doi.org/10.1109/GCE.2010.5676129

Minh BQ, Schmidt HA, Chernomor O, Schrempf D, Woodhams MD, von Haeseler A, Lanfear R (2020) IQ-TREE 2: New models and efficient methods for phylogenetic inference in the genomic era. Molecular Biology and Evolution 37: 1530–1534. https://doi.org/10.1093/molbev/msaa015

Nguyen AD, Golovatch SI (2016) The millipede genus *Enghoffosoma* Golovatch, 1993 recorded in Vietnam for the first time, with descriptions of three new species (Diplopoda, Polydesmida, Paradoxosomatidae). Zootaxa 4139(2): 151–166. https://doi.org/10.11646/zootaxa.4139.2.1

Nguyen AD, Sierwald, P. (2013) A worldwide catalog of the family Paradoxosomatidae Daday, 1889 (Diplopoda: Polydesmida). CheckList 9(6): 1132–1353. https://doi.org/10.15560/9.6.1132

Nguyen AD, Korsós Z, Jang KH, Hwang UW (2017) A revision and phylogenetic analysis of the millipede genus *Oxidus* Cook, 1911 (Polydesmida, Paradoxosomatidae). European Journal of Taxonomy 293: 1–22. https://doi.org/10.5852/ejt.2017.293

Nguyen AD, Nguyen SG, Le SX (2018) On the millipede genus *Antheromorpha* Jeekel, 1968 (Diplopoda: Polydesmida: Paradoxosomatidae) from Vietnam, with a description of a new species. Raffles Bulletin of Zoology 66: 96–109.

Pimvichai P, Enghoff H, Panha S (2009) A revision of the *Thyropygus allevatus* group. Part 1: the *T. opinatus* subgroup (Diplopoda: Spirostreptida: Harpagophoridae). Zootaxa 2016(1): 17–50. https://doi.org/10.11646/zootaxa.2016.1.2

Pimvichai P, Enghoff H, Panha S (2014) Molecular phylogeny of the *Thyropygus allevatus* group of giant millipedes and some closely related groups. Molecular Phylogenetics and Evolution 71: 170–183. https://doi.org/10.1016/j.ympev.2013.11.006

Rambaut A (2018) Figtree ver 1.4.4. Institute of Evolutionary Biology, University of Edinburgh, Edinburgh. http://tree.bio.rd.ac.uk/software/figtree [Accessed at 27 December 2023]

Ronquist F, Teslenko M, van der Mark P, Ayres DL, Darling A, Höhna S, Larget B, Liu L, Suchard MA, Huelsenbeck JP (2012) MrBayes 3.2: Efficient Bayesian phylogenetic inference and model choice across a large model space. Systematic Biology 61: 539–542. https://doi.org/10.1093/sysbio/sys029

Srisonchai R, Enghoff H, Likhitrakarn N, Panha S (2018) A revision of dragon millipedes I: genus *Desmoxytes* Chamberlin, 1923, with the description of eight new species (Diplopoda, Polydesmida, Paradoxosomatidae). ZooKeys 761: 1–177. https://doi.org/10.3897/zookeys.761.24214

Srisonchai R, Inkhavilay K, Ngor PB, Sutcharit C, Likhitrakarn N (2023) Uncovering endemism in high montane forests: Two new species of millipede genus *Tylopus* Jeekel, 1968 (Diplopoda: Polydesmida: Paradoxosomatidae) from Cambodia and Laos.Tropical Natural History 1(7): 151–164.

Srisonchai R, Enghoff H, Likhitrakarn N, Jeratthitikul E, Jirapatrasilp P, Panha S, Sutcharit C (2024) Molecular phylogeny of dragon millipedes (Diplopoda: Polydesmida: Paradoxosomatidae) from mainland South-East Asia, with description of a new genus and species. Zoological Journal of the Linnean Society 202(1): zlad164. https://doi.org/10.1093/zoolinnean/zlad164

Tamura K, Stecher G, Kumar S (2021) MEGA11: molecular evolutionary genetics analysis version 11. Molecular Biology and Evolution 38(7): 3022–3027. https://doi.org/10.1093/molbev/msab120

Tanabe AS (2011) Kakusan4 and Aminosan: two programs for comparing nonpartitioned, proportional and separate models for combined molecular phylogenetic analyses of multilocus sequence data. Molecular Ecology Resources 11: 914–921. https://doi.org/10.1111/j.1755-0998.2011.03021.x

Supplementary material 1

List of species names used in this study and their COI accession numbers

Authors: Theemaporn Benchapong, Henrik Enghoff, Natdanai Likhitrakarn, Ratmanee Chanabun, Anuwat Aoonkum, Ruttapon Srisonchai

Data type: docx

Link: https://doi.org/10.3897/zse.101.144277.suppl1

Supplementary material 2

Uncorrected *p*-distances of cytochrome c oxidase subunit I (COI) sequence divergences in the genus *Enghoffosoma*

Authors: Theemaporn Benchapong, Henrik Enghoff, Natdanai Likhitrakarn, Ratmanee Chanabun, Anuwat Aoonkum, Ruttapon Srisonchai

Data type: xlsx

Link: https://doi.org/10.3897/zse.101.144277.suppl2

Zoosyst. Evol. 101 (2) 2025, 533–550 | DOI 10.3897/zse.101.141741

PENSOFT

für Natur MUSEUM FÜR NATURKUNDE BERLIN

New species of *Tygarrup* centipedes from Xizang, China (Geophilomorpha, Mecistocephalidae)

Chao Jiang[1], Jiabo Fan[1,2], Chunxue You[2], Weichun Li[3], Luqi Huang[1]

1 *State Key Laboratory for Quality Ensurance and Sustainable Use of Dao-di Herbs, National Resource Center for Chinese Materia Medica, China Academy of Chinese Medical Sciences, Beijing 100700, China*

2 *Tianjin Key Laboratory of Agricultural Animal Breeding and Healthy Husbandry, College of Animal Science and Veterinary Medicine, Tianjin Agricultural University, Tianjin 300392, China*

3 *College of Agronomy, Jiangxi Agricultural University, Nanchang 330045, China*

https://zoobank.org/41DEF99E-4563-48E3-B7BB-59F8D3B19439

Corresponding authors: Chao Jiang (jiangchao0411@126.com); Luqi Huang (huangluqi01@126.com)

Academic editor: Martin Husemann ♦ **Received** 13 November 2024 ♦ **Accepted** 21 January 2025 ♦ **Published** 26 February 2025

Abstract

Prior to this study, the genus *Tygarrup* Chamberlin, 1914, is known to contain only two species in Xizang, China. New records derived from multiple collections allow for the distribution ranges of six species to be refined: *Tygarrup tridentatus* Jiang & Huang, **sp. nov.**, *Tygarrup cerrus* Jiang & Huang, **sp. nov.**, *Tygarrup multiporus* Jiang & Huang, **sp. nov.**, and *Tygarrup fimbriatus* Jiang & Huang, **sp. nov.** are described as new. *Tygarrup muminabadicus* Titova, 1965, was first reported in the fauna of Xizang. *Tygarrup poriger* (Verhoeff, 1942) is rediscovered and redescribed, and *Tygarrup nepalensis* Shinohara, 1965 is synonymized with *T. poriger*. Remarks are provided for all encountered species, and a key to all *Tygarrup* species in China is presented.

Key Words

Biodiversity, key, new record, taxonomy

Introduction

Xizang, the second largest provincial administrative unit of China, is located in the western and southern parts of the Tibetan Plateau. This region, known as the "third pole of the earth," is the highest place in the world. Its southern region, the Himalaya, exhibits a pronounced vertical stratification of ecosystems and is recognized as a biodiversity hotspot for the study of animal taxonomy as well as biological evolution (Cai et al. 2018; Li et al. 2022). A century ago, seventeen centipede species have been documented in Xizang, comprising eight species of Scolopendromorpha and seven species of Lithobiomorpha (Lewis 2010; Song et al. 2010; Ma et al. 2014; Qiao et al. 2019; Niu et al. 2021; Chen et al. 2023). However, understanding of the soil centipede species diversity in Xizang remains quite limited. To date, only two species of Geophilomorpha have been described from the region, both of which belong to the genus *Tygarrup* Chamberlin, 1914 (Silvestri 1919; Verhoeff 1942). This includes the incompletely described species *T. diversidens* (Silvestri, 1919) from the Himalayas and *T. poriger* (Verhoeff, 1942) from "the middle Himalaya," near Shigatse. The objective of the present study is to enhance our knowledge of the species diversity within Geophilomorpha in Xizang, with a focus on the discovery and description of new species of *Tygarrup* centipedes.

The genus *Tygarrup*, characterized by its elongated head capsule, clypeus with an entire plagula, spiculum absent, clypeal pleurite without setae, coxosternum of the first maxillae divided, whereas that of the second maxillae is undivided, and the sternal typically with pores present in males (Uliana et al. 2007). It is the second largest genus in the family Mecistocephalidae Bollman, 1893, and comprises 15 known species (Uliana et al. 2007; Bonato et al. 2011; Chao et al. 2020). This genus is mainly distributed

in the tropical and subtropical regions of East Asia and Southeast Asia and can adapt to a variety of climates ranging from tropical rainforests to cold high mountains (Silvestri 1919; Verhoeff 1939, 1942; Paik 1961; Uliana et al. 2007; Bonato et al. 2011; Chao et al. 2020). Before this study, only three species of *Tygarrup* had been documented in China, with two species being restricted to Xizang (Silvestri 1919; Verhoeff 1942; Chao et al. 2020).

During our examination of *Tygarrup* specimens from Xizang, we identified six species within the genus, including four new species. In this study, we describe these species, with a particular focus on the new species.

Materials and methods

Specimens were collected by tweezers and preserved in 75% ethanol. The type materials are deposited in the National Resource Center for Chinese Materia Medica, China Academy of Chinese Medical Sciences, Beijing, China (CMMI).

Specimens were dissected, and their cephalic capsules, forcipular segments, mandibles, maxillary complexes, and remaining bodies were mounted on temporary slides using 75% ethanol or lactic acid. Taxonomic characters were examined and photographed (Figs 1, 2) using a Leica M205 FCA stereomicroscope (7.8–160×) and an Olympus BX51 microscope (100–400×). Photos were converted into hand-drawn illustrations using Sketchbook 6.0.6. Localities were mapped with ArcMap 10.7.1. The terminology of morphology follows Bonato et al. (2010a).

Results

Taxonomy

Order Geophilomorpha Pocock, 1895
Family Mecistocephalidae Bollman, 1893

Genus *Tygarrup* Chamberlin, 1914

Type species. *Tygarrup intermedius* Chamberlin, 1914, by original designation.

Diagnosis. See Uliana et al. (2007).

Tygarrup tridentatus Jiang & Huang, sp. nov.

https://zoobank.org/4201B13D-F951-465C-894D-450027BCB860
Figs 1A–C, 3

Material examined. ***Holotype*.** • ♀ (CMMI 20240725001D), China, Xizang Autonomous Regions, Yadong County, Xiasima town (27.4788°N, 88.9063°E), 2960 m asl., 25.vii.2024, leg. Chao Jiang.

***Paratypes*.** • 4♀♀ 3♂♂ 3 juveniles (CMMI 20230720002D, CMMI 20230725002D, -003D), same as holotype but collected at 20–25.vii.2024.

Other materials. • 2♀♀ 1♂ 1 juvenile (CMMI 20240721001D, 20240724001D), China, Xizang Autonomous Regions, Yadong County, Pangda village, 2100–2400 m asl., 21–24.vii.2024, leg. Chao Jiang & Qing Li, 3♀♀ (CMMI 20240720001D), Upper Yadong village, G562 National Road (27.5481°N, 88.9998°E), 3460 m asl., 20.vii.2024, leg. Chao Jiang & Qing Li; • 1♀ 2♂♂ 5 juveniles (CMMI 20240715001D–005D), Cuona County, Lei Menba ethnic village, Lei Hydroelectric-power station (27.8196°N, 91.7462°E), 2490 m asl., 15.vii.2024, leg. Chao Jiang & Qing Li, 2♀♀ 4♂♂ (CMMI 20240714001D), Entrance of leibugou valley (27.9240°N, 91.8381°E), 3840 m asl., 14.vii.2024, leg. Chao Jiang; • 1♀ 1♂ (CMMI 20240714301D), Gongri Menba ethnic village, Mengyu Sanshenghu Lake (27.9267°N, 91.8728°E), 4410 m asl., 14.vii.2024, leg. Chao Jiang & Qing Li.

Diagnosis. A *Tygarrup* species with 45 leg-bearing segments. Body length of adult reaches 2.5 cm. Transverse suture curved. Clypeal setae 9–12 pairs. Forcipular trochanteroprefemur, tibia, and tarsungulum, each with a well-developed tooth, article II without teeth. Sternal pores present in males only.

Description. Maximum length of male 2.5 cm and female 2.3 cm.

Color (of preserved specimens in alcohol) morph 1: head and forcipular segment reddish-brown, trunk and legs homogeneously yellow, without dark patches (Fig. 1A–C, in Yadong populations); morph 2: head and forcipular segment dark red, trunk and legs yellow, with dark patches along the trunk, sternal sulci darker (in Cuona populations).

Cephalic plate 1.6 × longer than the widest. Transverse suture rounded. Lateral margins sinuous to straight, convergent backwards slightly, anterior margin convex, with a median incision, posterior margin slightly rounded (Fig. 3A).

Clypeus 1.9 × wider than long (Fig. 3B). Clypeus with an entire plagula covering most of the clypeus, areolation only present along the anterior margin of the head; clypeal setae as follows: 1 pair on the areolate part; 7–10 pairs along the anterior margin of the clypeal plagula, 1 pair on the central part of plagula (Fig. 3C).

Labrum (Fig. 3C): Mid-piece ca. 2 × longer than wide, posteriorly pointed and well sclerotized. Anterior ala triangular, and medial margin reduced to a vertex; posterior margin of each side-piece sinuous.

Cephalic pleurite without spiculum or setae; areolate part present along anterior margin and paraclypeal suture; stilus well-developed, nearly straight, with an anterior incision on each side (Fig. 3B).

First maxillae (Fig. 3D): Coxosternite 2 × wider than long, divided by mid-longitudinal suture, anterior corners of coxosternum not projecting. Medial projection about 1.5 × wider than long, internal margin with several setae, distal lobe curved inward; telopodite about 4 × longer than wide, curved inward.

Second maxillae (Fig. 3D): Coxosternite undivided, ca. 1.5 × wider than long; anterior and posterior margins concave, lateral margins concave medially, posterior corners only slightly projecting externally; areolation on medial part,

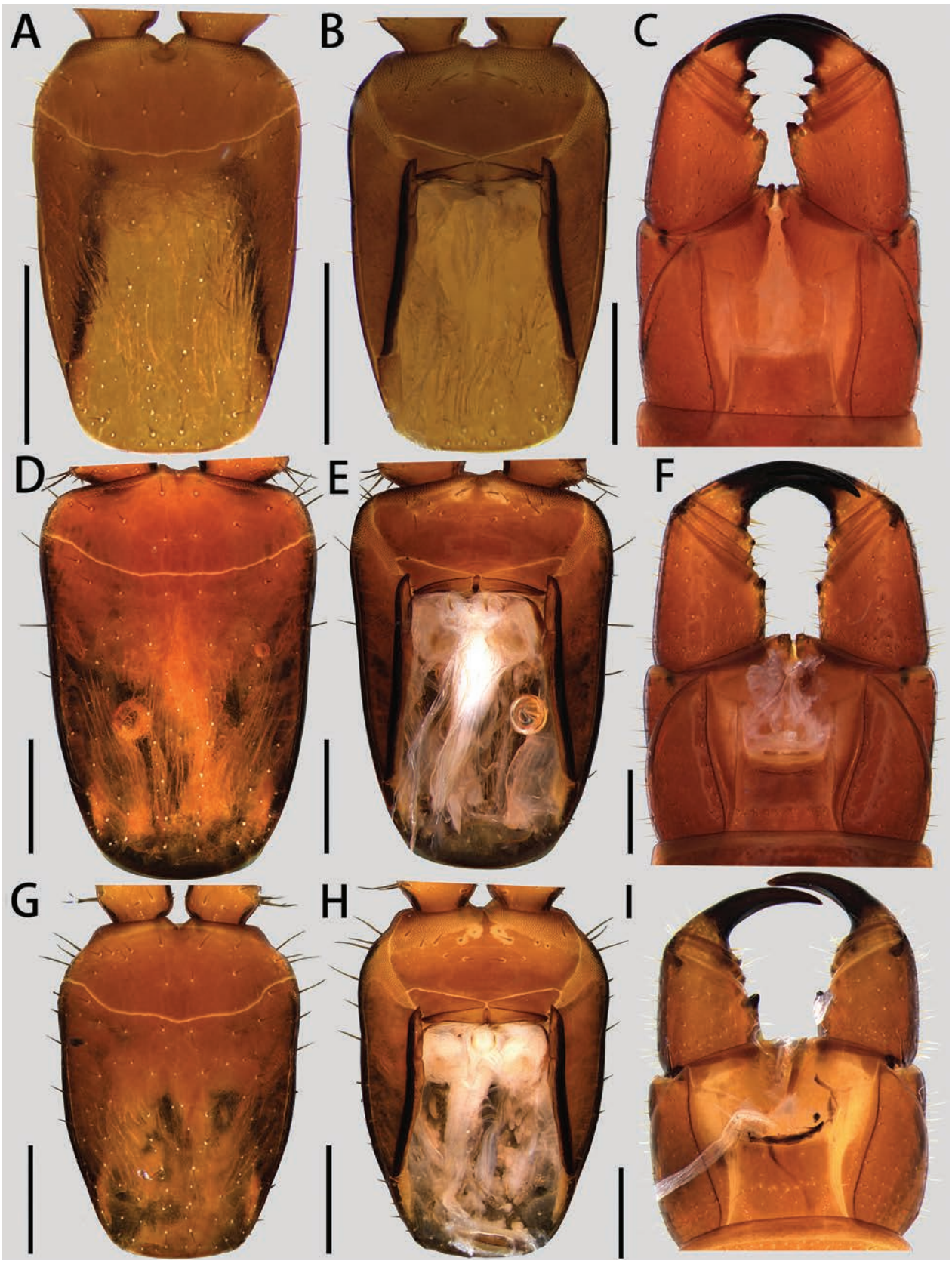

Figure 1. Cephalic plate and forcipular segments. **A, D, G.** Cephalic plates, dorsal; **B, E, H.** Cephalic plates, ventral; **C, F, I.** Forcipular segments, dorsal. **A–C.** *Tygarrup tridentatus* sp. nov., holotype; **D–F.** *Tygarrup cerrus* sp. nov., holotype; **G–I.** *Tygarrup multiporus* sp. nov., holotype. Scale bar: 500 μm.

with pores along the lateral margins, setae present along the posterior part. Foraminal process surrounding the metameric pore separated from lateral margin of coxosternite. Telopodites of the second maxillae well developed, surpassing those of the first maxillae; article 1 of telopodite ca. 4.7 × longer than wide, curved outward, with distal setae on

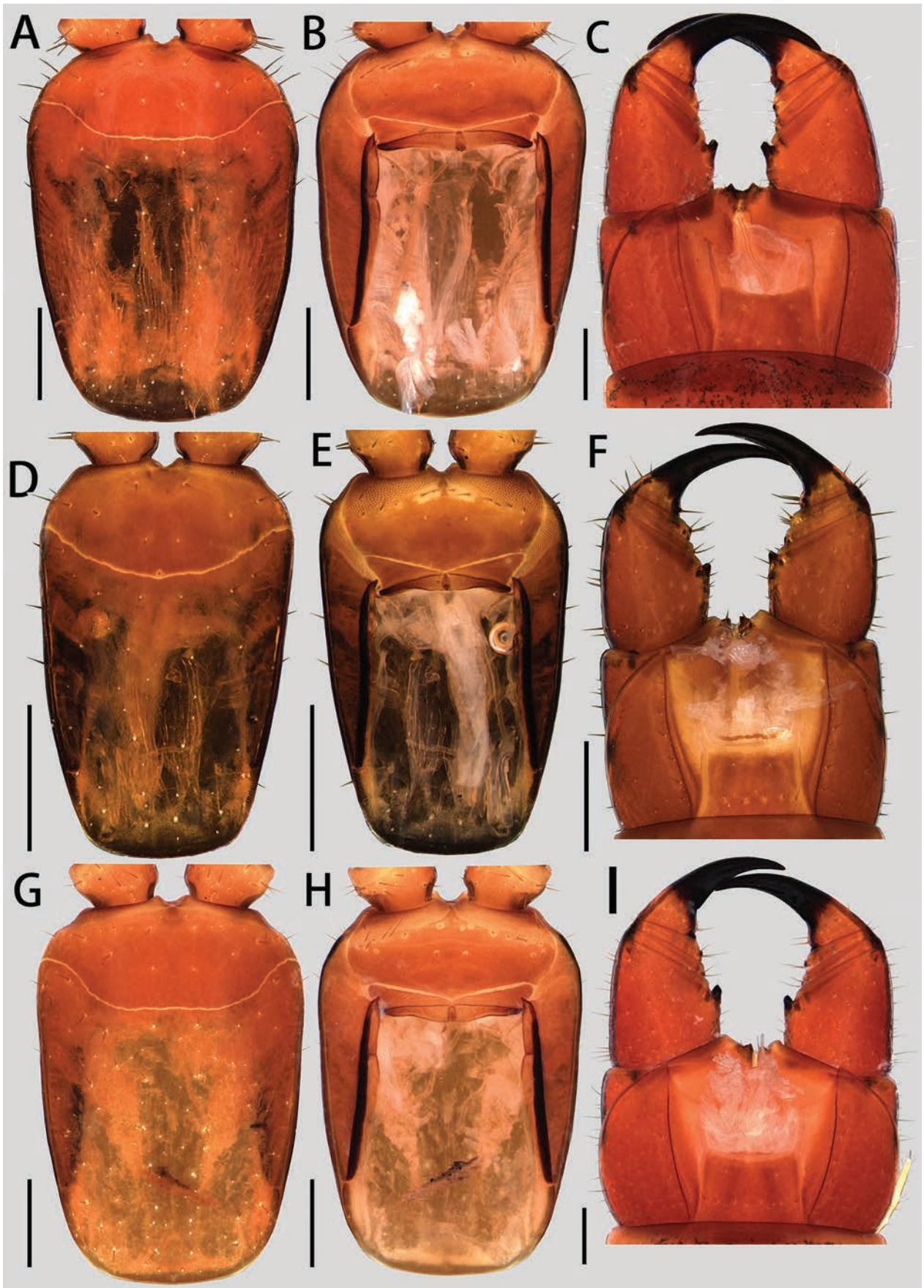

Figure 2. Cephalic plate and forcipular segments. **A, D, G.** Cephalic plates, dorsal; **B, E, H.** Cephalic plates, ventral; **C, F, I.** Forcipular segments, dorsal. **A–C.** *Tygarrup fimbriatus* sp. nov., holotype; **D–F.** *Tygarrup poriger* (Verhoeff, 1942) (spm. CMMI 20240309001D); **G–I.** *Tygarrup muminabadicus* Titova, 1965 (spm. CMMI 20240310001D). Scale bar: 500 μm.

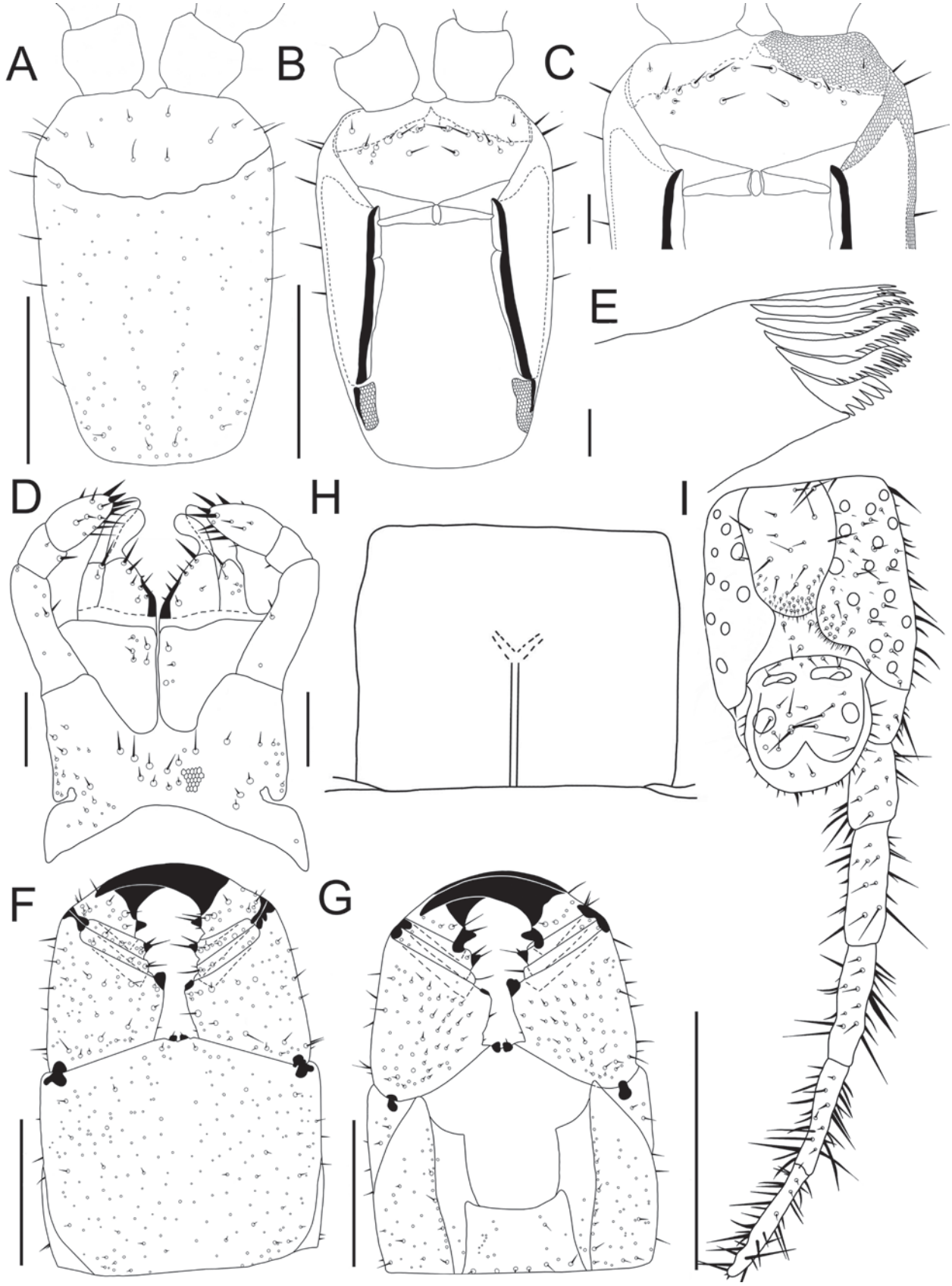

Figure 3. *Tygarrup tridentatus* sp. nov., holotype. **A.** Cephalic plate, dorsal; **B.** Cephalic plate, ventral (maxillary complex removed); **C.** Clypeus, ventral (maxillary complex removed); **D.** Maxillary complex, ventral; **E.** Mandible, ventral; **F.** Forcipular segment, ventral; **G.** Forcipular segment, dorsal; **H.** Seventh sternum of leg-bearing segment, ventral; **I.** Ultimate leg-bearing segment and left leg, ventral. Scale bars: 500 µm (**A, B, F, G, I**); 100 µm (**C, D, H**); 25 µm (**E**).

the internal surface; article 2 of telopodite 1.3 × longer than wide, with distal setae on the internal side; article 3 ca. 2.2 × longer than wide, with distal end densely covered with setae; apical claw large and simple.

Mandible with ca. 5 well-developed and ca. 2 rudimentary pectinate lamellae; first lamella with 3 teeth, similar in size; intermediate lamellae with 6–7 teeth (Fig. 3E).

***Forcipular segment*:** Coxosternite 1.2 × wider than long, anterior margin with a pair of small teeth (Fig. 3F); scapular points of pleura surpass the anterior margin of coxosternite. Forcipular trochanteroprefemur about 1.3 × longer than wide, with a prominent distal tooth, femur without teeth, tibia and tarsungulum each with a well-developed tooth (Fig. 3G).

***Leg-bearing segments*:** A total of 45 leg-bearing segments. Sternal sulcus bifurcate, faintly impressed, with an acute angle (Fig. 3H); sternal pores present on males, absent on females.

Ultimate leg-bearing segment densely setose. Tergite sub-rectangular, 1.6 × longer than wide. Coxopleuron about 1.1 × longer than wide and 1.7 × longer than ultimate sternite. Ca. 13–22 coxal pores on ventral and lateral sides of each coxopleuron, the innermost two or three pores usually larger than others (Fig. 3I). The ultimate leg telopodite not swollen, with scattered setae, without pretarsus.

Postpedal segments densely setose in both sexes. Male gonopods bi-articulate, narrow, and separated by a conical projection. Female gonopods inconspicuous bi-articulate, subtriangular (Fig. 3I). Anal pores present on each ventro-lateral side of postpedal segments.

Etymology. Latin: *tridentatus* = trident. The new species name refers to its forcipular trochanteroprefemur, tibia, and tarsungulum, each with a well-developed tooth. We suggest the Chinese common name as "三齿地蜈蚣".

Distribution. China (Xizang).

Remarks. This new species resembles *Tygarrup poriger* (Verhoeff, 1942) in possessing a tooth on the dorsal base of the forcipular tarsungulum. However, it is distinct from *T. poriger* by the presence of a well-developed tooth on the forcipular femur (Figs 1C, 3F).

Tygarrup cerrus Jiang & Huang, sp. nov.

https://zoobank.org/35956858-705E-46F1-A5D5-34D5477FD794

Figs 1D–F, 4

Material examined. ***Holotype*.** •♀ (CMMI 20240307017D), China, Xizang Autonomous Regions, Bomi County, Qingduo town (30.0946°N, 95.7031°E), 2850 m asl., 7.iii.2024, leg. Chao Jiang.

***Paratypes*.** •6♀♀ 7♂♂ (CMMI 20240307011D–016D, 018D–024D), same as holotype.

Diagnosis. A *Tygarrup* species with 45 leg-bearing segments. Body length of adult reaches 3.6 cm. Transverse suture curved. Clypeal setae 9–12 pairs. Forcipular trochanteroprefemur and tibia, each with a small tubercle. Cerrus present as two lateral groups of setae. Sternal pores present in males only.

Description. Maximum length of male 3.6 cm and female 3.4 cm.

Color (of preserved specimens in alcohol): head and forcipular segment dark red, trunk and legs yellow, with dark patches along the trunk (Fig. 1D–F).

Cephalic plate 1.5 × longer than the widest. Transverse suture rounded. Lateral margins nearly straight and convergent backwards, anterior margin convex, with a median incision, posterior margin rounded. Setae arranged nearly symmetrically (Fig. 4A).

Clypeus 2.1 × wider than long (Fig. 4B). Clypeus with an entire plagula covering most of the clypeus, areolation only present along the anterior margin of the head; clypeal setae as follows: 1 pair on the areolate part, 7–10 pairs along to the anterior margin of the clypeal plagula, 1 pair on the central part of plagula (Fig. 4C).

Labrum (Fig. 4C): Mid-piece ca. 2.4 × longer than wide, posteriorly pointed and well sclerotized. Anterior ala triangular, medial margin reduced to a vertex; posterior margin of each side-piece sinuous.

Cephalic pleurite without spiculum or setae; areolate part present along anterior margin and paraclypeal suture; stilus well developed, nearly straight, with an anterior incision on each side (Fig. 4B).

First maxillae (Fig. 4D): Coxosternite 1.7 × wider than long, divided by mid-longitudinal suture, the anterior corners of coxosternum not projecting. Medial projection about 1.3 × wider than long, internal margin with several setae, distal lobe curved inward; telopodite about 3 × longer than wide, curved inward.

Second maxillae (Fig. 4D): Coxosternite undivided, ca. 1.2 × wider than long; both the anterior and posterior margins concave, lateral margins concave medially, posterior corners only slightly projecting externally; areolation on medial part, setae present along the posterior part; the foraminal process surrounding the metameric pore separated from lateral margin of coxosternite. Telopodites of the second maxillae well developed, surpassing those of the first maxillae; article 1 of the telopodite 2.8–3.2 × longer than wide, curved outward; article 2 of the telopodite ca. 1.1 × longer than wide; article 3 ca. 1.8 × longer than wide, with distal end densely covered with setae; apical claw large and simple.

Mandible with ca. 6 well-developed and ca. 2 rudimentary pectinate lamellae; the first lamella with 5 teeth, similar in size; intermediate lamellae with 11–15 teeth (Fig. 4E).

Forcipular segment: Coxosternite 1.4 × wider than long, anterior margin with a pair of truncated teeth (Fig. 4F); scapular points of pleura not reaching the anterior margin of coxosternite (Fig. 4G). Cerrus present as two lateral groups of setae (Fig. 4H). Forcipular trochanteroprefemur about 1.4 × longer than wide and has a small distal tubercle, femur with or without tubercle, tibia with a small pointed tubercle, tarsungulum without tubercle (Fig. 4G).

***Leg-bearing segments*.** A total of 45 leg-bearing segments. Sternal sulcus bifurcate, faintly impressed, with an acute angle (Fig. 4I); sternal pores present on males, absent on females.

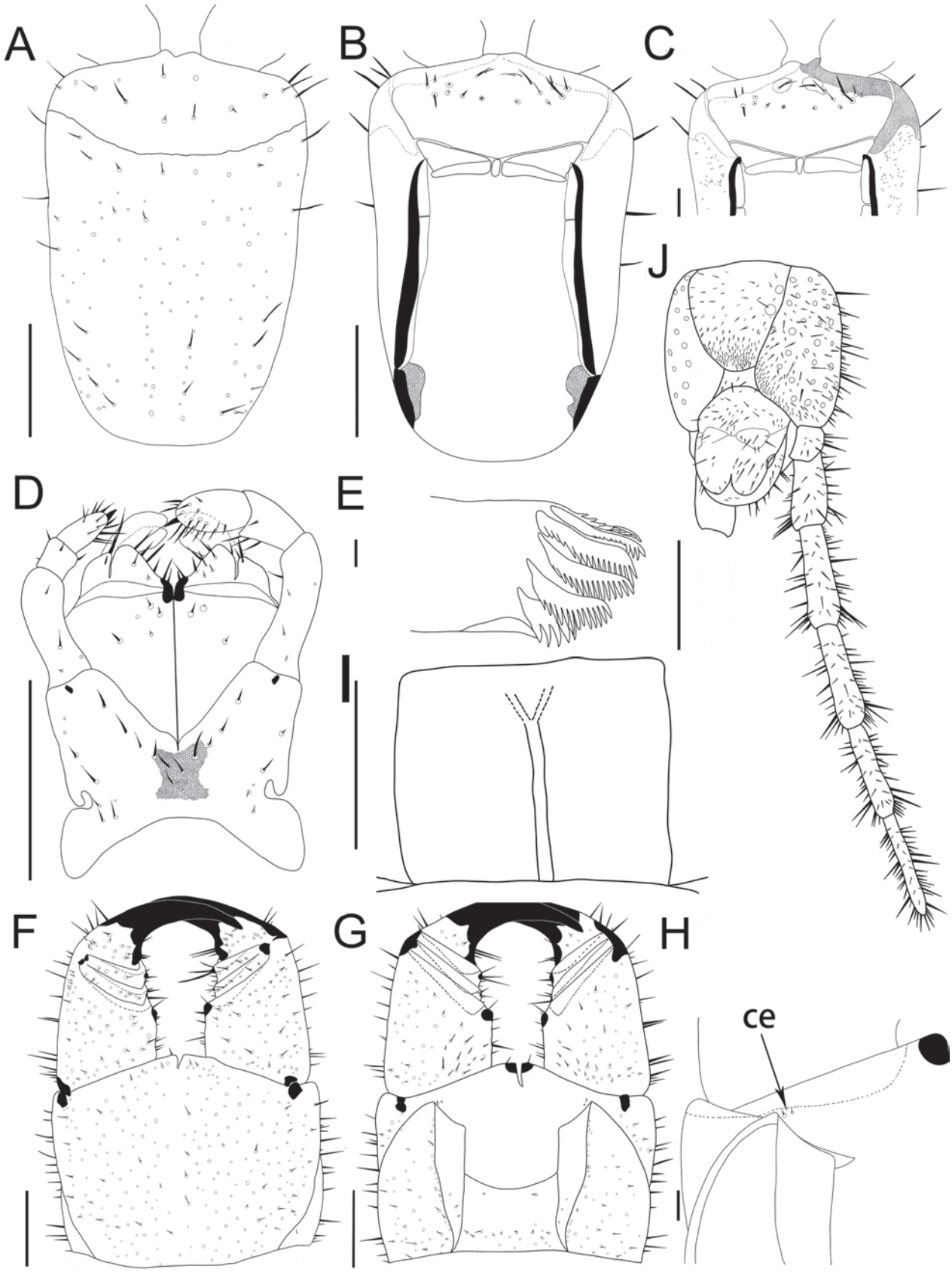

Figure 4. *Tygarrup cerrus* sp. nov., holotype. **A.** Cephalic plate, dorsal; **B.** Cephalic plate, ventral (maxillary complex removed); **C.** Clypeus, ventral (maxillary complex removed); **D.** Maxillary complex, ventral; **E.** Mandible, ventral; **F.** Forcipular segment, ventral; **G.** Forcipular segment, dorsal; **H.** Part of forcipular segment, dorsal; **I.** Seventh sternum of leg-bearing segment, ventral; **J.** Ultimate leg-bearing segment and left leg, ventral. Abbreviations: ce – cerrus. Scale bars: 500 μm (**A, B, D, F, G, I, J**); 100 μm (**C, H**); 25 μm (**E**).

Ultimate leg-bearing segment densely setose. Tergite sub-rectangular, 1.4 × longer than wide. Coxopleuron about 0.9 × longer than wide and 1.5 × longer than ultimate sternite. Ca. 30–60 coxal pores on ventral and lateral sides of each coxopleuron, the innermost two or three pores usually larger than others (Fig. 4J). The ultimate leg telopodite not swollen, with scattered setae, without pretarsus.

Postpedal segments densely setose for both sexes. Male gonopods bi-articulate, narrow, and separated by a conical projection. Female gonopods simple, subtriangular, and touching each other at their bases (Fig. 4J). Anal pores present on each ventro-lateral side of postpedal segments.

Etymology. The new species name refers to the presence of a paired lateral group of setae on the dorsal side of the forcipular coxosternite, termed 'cerrus' by Crabill (1970). We suggest the Chinese common name as "织地蜈蚣".

Distribution. China (Xizang).

Remarks. In mecistocephalids, the presence of a cerrus is a consistent character observed in several species, particularly within the genera *Dicellophilus* Cook, 1896, *Takashimaia* Miyosi, 1955, *Proterotaiwanella* Bonato, Foddai & Minelli, 2002, *Krateraspis* Lignau, 1929, and some species of *Mecistocephalus* Newport, 1843 (Bonato et al. 2002, 2003, 2010b; Uliana et al. 2007; Dyachkov and Bonato 2022; Pan et al. 2024). However, there have been no reports of the presence of a cerrus in any species of *Tygarrup* to date. The discovery of cerrus in the newly described species *T. cerrus* sp. nov. offers a further understanding of the evolutionary development of this structure within the Mecistocephalidae as well as phylogenetic relationships among the mecistocephalid genera.

Tygarrup multiporus Jiang & Huang, sp. nov.

https://zoobank.org/5A9F733C-5880-4647-A377-706428584E8D

Figs 1G–I, 5

Material examined. ***Holotype*.** • ♀ (CMMI 20240312003D), China, Xizang Autonomous Regions, Medog County, near Deergong village (29.1810°N, 95.1439°E), 1710 m asl., 12.iii.2024, leg. Chao Jiang.

***Paratypes*.** • 2♀♀ (CMMI 20240309012D, 20240311003D), China, Xizang Autonomous Regions, Medog County, near Renqingbensi Temple (29.3075°N, 95.3573°E), 1920 m asl., 9–11.iii.2024, leg. Chao Jiang.

Diagnosis. A *Tygarrup* species with 45 leg-bearing segments. Body length of adult reaches 3.4 cm. Cephalic frontal plate postero-lateral corner bears 10–20 pore-like sensilla. Clypeal plagula with 6 pairs of setae on antero-medial and several pore-like sensilla on antero-lateral corners. Forcipular trochanteroprefemur and tibia, each with a tubercle, femur and tarsungulum without tubercles. Sternal pores present in males only.

Description. Maximum length 3.4 cm.

Color (of preserved specimens in alcohol): Head and forcipular segment reddish-brown, trunk and legs homogeneously yellow, without dark patches (Fig. 1G–I).

Cephalic plate (Fig. 5A) 1.5 × longer than the widest. Transverse suture curved, forms a backward-directed angle medially. Lateral margins sinuous, convergent backwards strongly, anterior margin convex, with a median incision, posterior margin rounded. Frontal plate postero-lateral corner bears 10–20 pore-like sensilla. Setae arranged nearly symmetrically.

Clypeus 2 × wider than long. Clypeus with an entire plagula covering most of the clypeus, areolation only present along the anterior margin of the head; clypeal setae as follows: 1 pair on the areolate part, 2 pairs along the anterior margin of the clypeal plagula, 2 pairs on the antero-medial part inside a large insula, 1 pair on the central part of plagula. Five to eight pore-like sensilla on each antero-lateral corner (Fig. 5B).

***Labrum*:** Mid-piece ca. 2.1 × longer than wide, posteriorly pointed and well sclerotized. Anterior ala triangular, medial margin reduced, distinct shorter than lateral margin; posterior margin of each side-piece sinuous (Fig. 5B).

Cephalic pleurite without spiculum or setae; areolate part present along anterior margin and paraclypeal suture; stilus well developed, nearly straight, with an anterior incision on each side (Fig. 5B).

First maxillae (Fig. 5C): Coxosternite 1.9 × wider than long, divided by mid-longitudinal suture, anterior corners of coxosternum not projecting. Medial projection about 1.3 × wider than long, internal margin with several setae, distal lobe curved inward; telopodite about 2.3 × longer than wide, curved inward.

Second maxillae (Fig. 5C): Coxosternite undivided, ca. 1.4 × wider than long; both the anterior and posterior margins concave, lateral margins concave medially, posterior corners only slightly projecting externally; areolation on medial part, setae present along the posterior part; the foraminal process surrounding the metameric pore separated from lateral margin of coxosternite. Telopodites of the second maxillae well developed, surpassing those of the first maxillae; article 1 of the telopodite 2.9–3.5 × longer than wide, curved outward; article 2 of the telopodite ca. 1.4 × longer than wide; article 3 ca. 2.3 × longer than wide, with distal end densely covered with setae; apical claw large and simple.

Mandible with ca. 6–7 well-developed and ca. 2 rudimentary pectinate lamellae; the first lamella with 4 teeth, similar in size; intermediate lamellae with 9–13 teeth (Fig. 5D).

***Forcipular segment*:** Coxosternite 1.4 × wider than long, anterior margin with a pair of truncated teeth (Fig. 5E); scapular points of pleura not reaching the anterior margin of coxosternite (Fig. 5F). Forcipular trochanteroprefemur about 1.3 × longer than wide and has a conical distal tooth, intermediate articles each with a small tooth, tarsungulum without tooth.

***Leg-bearing segments*.** A total of 45 leg-bearing segments. Sternal sulcus bifurcate faintly impressed, with an acute angle (Fig. 5G); sternal pores present on males, absent on females.

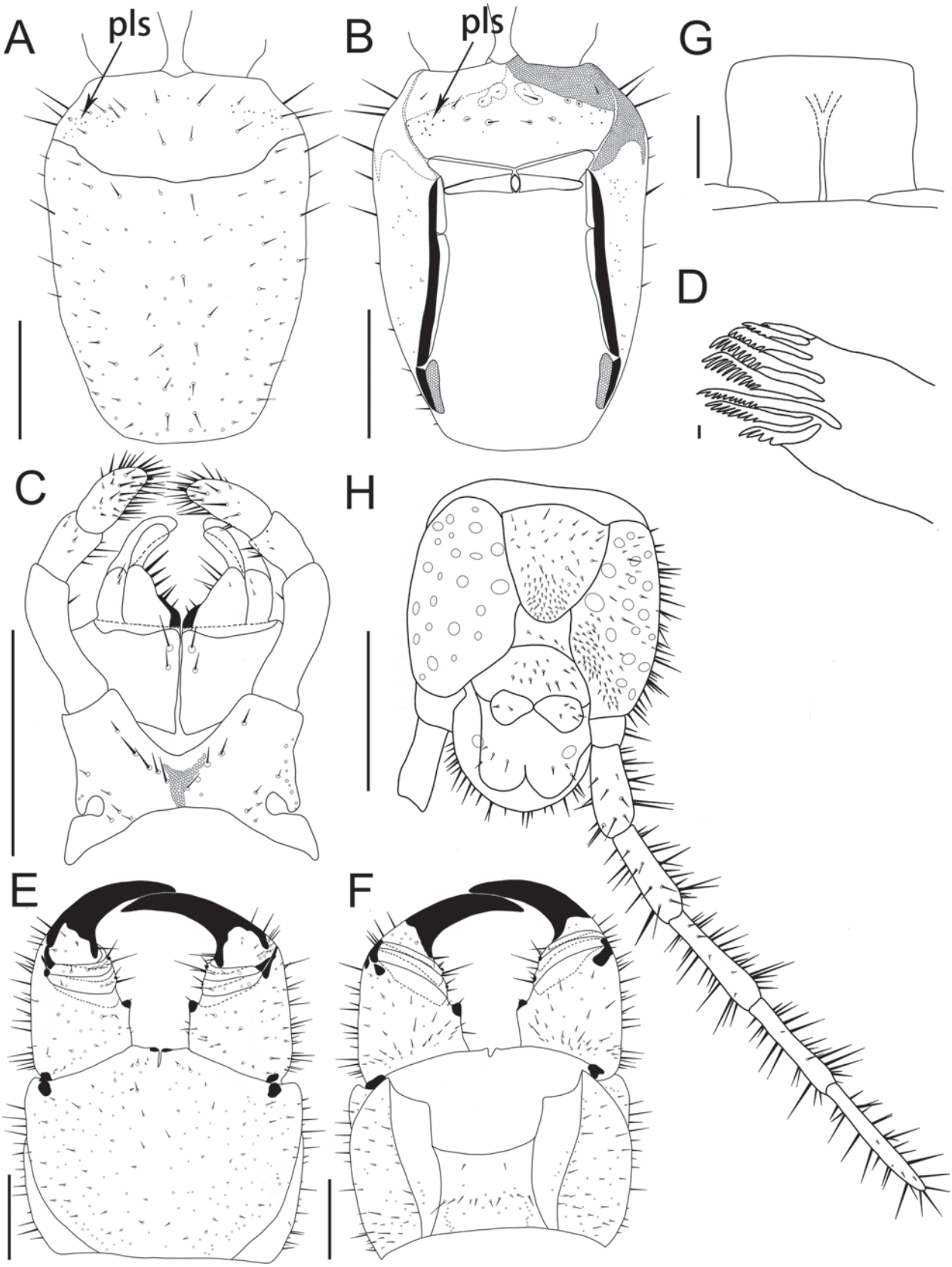

Figure 5. *Tygarrup multiporus* sp. nov., holotype. **A.** Cephalic plate, dorsal; **B.** Cephalic plate, ventral (maxillary complex removed); **C.** Maxillary complex, ventral; **D.** Mandible, ventral; **E.** Forcipular segment, ventral; **F.** Forcipular segment, dorsal; **G.** Seventh sternum of leg-bearing segment, ventral; **H.** Ultimate leg-bearing segment and left leg, ventral. Abbreviations: pls – pore-like sensilla. Scale bars: 500 μm (**A–C, E–H**); 25 μm (**D**).

Ultimate leg-bearing segment densely setose. Tergite sub-rectangular, 1.1 × longer than wide. Coxopleuron about 0.8 × longer than wide and 1.7 × longer than ultimate sternite. Ca. 20–28 coxal pores on ventral and lateral sides of each coxopleuron, the innermost two pores usually larger than others (Fig. 5H). The ultimate leg telopodite not swollen, with scattered setae, without pretarsus.

Postpedal segments densely setose for both sexes. Male gonopods bi-articulate, narrow, and separated by a conic projection. Female gonopods simple, subtriangular, and touching each other at their bases (Fig. 5H). Anal pores present on each ventro-lateral side of postpedal segments.

Etymology. The new species name refers to the presence of many pore-like sensilla on cephalic capsule and clypeus plagula. We suggest the Chinese common name as "多孔地蜈蚣".

Distribution. China (Xizang).

Remarks. This new species is distinguished from all the hitherto known *Tygarrup* species by the presence of pore-like sensilla on its clypeal plagula and cephalic plate, a character not previously documented in this genus. However, when Titova (1983) described *T. crassignathus* Titova, 1983, and *T. singaporiensis* Verhoeff, 1937, the illustrations of the clypeal plagula (Titova 1983: figs 5, 10) showed numerous dense small spots, which are inferred herein to possibly be pore-like sensilla.

The new species is further distinguished from *T. crassignathus* by the absence of an incrassate forcipular trochanteroprefemurand a large distal tooth, features present in the latter (Titova 1983: fig. 7). Instead, the new species possesses a forcipular trochanteroprefemurtooth of typical dimensions. The new species can also be distinguished from *T. singaporiensis* by the number of clypeus plagula pore-like sensilla (more than 5–10 on each side, confined to the antero-lateral corner vs. more than 50 on each side, extending from the antero-lateral corner to the paramedian setae) and the clypeus setae (2 lateral and 6 paramedian setae vs. 10 or 11 lateral and 6 or fewer paramedian setae) (Titova 1983: fig. 9).

Tygarrup fimbriatus Jiang & Huang, sp. nov.

https://zoobank.org/60EDCB5D-4A74-4810-9394-601036025430

Figs 2A–C, 6

Material examined. ***Holotype*****.** • ♀ (CMMI 20240311004D), China, Xizang Autonomous Regions, Medog County, Hanmi (29.3619°N, 95.1337°E), 2000 m asl., 11.iii.2024, leg. Chao Jiang.

Paratypes**.** • 3♀♀ 4♂♂, (CMMI 20240311005D–007D, 009D–012D), same as holotype.

Other materials. • 1♀ (CMMI 20240311013D), China, Xizang Autonomous Regions, Medog County, Beibeng village (29.2488°N, 95.1901°E), 920 m asl., 11.iii.2024, leg. Chao Jiang, 1♀ (CMMI 20240313011D), Damu village (29.4864°N, 95.4547°E), 1350 m asl., 8.iii.2024, leg. Chao Jiang; • 9♀♀ 4♂♂, (CMMI 20240307001D–009D, 20240313001D–004D), Bomi County, Yigong village, near Tongmai Bridge (30.0989°N, 95.0673°E), 2050 m asl., 7–13.iii.2024, leg. Chao Jiang, 1♀ (CMMI 20240308004D), Gu village, G319 National Road (29.9973°N, 95.3092°E), 2405 m asl., 13.iii.2024, leg. Chao Jiang.

Diagnosis. A *Tygarrup* species with 45 leg-bearing segments. Body length of adult reaches 5.5 cm. Cephalic frontal plate postero-lateral corner bears 10–20 pore-like sensilla. Clypeal plagula with 9–12 pairs of setae along the anterior margin and several pore-like sensilla on antero-lateral corners. Labral posterior alae fringed with hair-like projections along the posterior margins. Forcipular trochanteroprefemur with a tooth, tarsungulum without tubercle. Sternal pores present in males only.

Description. Maximum length of male 4.1 cm, and of females, 5.5 cm.

Color (of preserved specimens in alcohol): Head and forcipular segment reddish-brown, trunk and legs homogeneously yellow, without dark patches (Fig. 2A–C).

Cephalic plate (Fig. 6A) 1.4 × longer than the widest. Transverse suture rounded. Lateral margins sinuous, convergent backwards, anterior margin convex, with a median incision, posterior margin rounded. Frontal plate postero-lateral corner bears 10–20 pore-like sensilla. Setae arranged nearly symmetrically.

Clypeus (Fig. 6B) 2.1 × wider than long. Clypeus with an entire plagula covering most of the clypeus, areolation only present along the anterior margin of the head; clypeal setae as follows: 1 pair on the areolate part, 4 (considered as damaged and repaired in left side of holotype)–10 pairs along the anterior margin of the clypeal plagula, 1 pair on the central part of plagula. Six to twelve pore-like sensilla on each antero-lateral corner.

Labrum**:** Mid-piece ca. 1.8 × longer than wide, posteriorly pointed and well sclerotized. Anterior ala triangular; medial margin reduced, distinct shorter than lateral margin; posterior margin of each side-piece sinuous (Fig. 6B); posterior alae fringed with hair-like projections along the posterior margins (Fig. 6C).

Cephalic pleurite without spiculum or setae; areolate part present along anterior margin and paraclypeal suture; stilus well developed, nearly straight, with an anterior incision on each side (Fig. 6B).

First maxillae (Fig. 6D): Coxosternite 1.7 × wider than long, divided by mid-longitudinal suture, anterior corners of coxosternum not projecting. Medial projection about 1.4 × wider than long, internal margin with several setae, distal lobe curved inward; telopodite about 2.3 × longer than wide, curved inward.

Second maxillae (Fig. 6D): Coxosternite undivided, ca. 1.4 × wider than long; both the anterior and posterior margins concave, lateral margins concave medially, posterior corners only slightly projecting externally; areolation on medial part, setae present along the posterior part; the foraminal process surrounding the metameric pore separated from lateral margin of coxosternite. Telopodites of the second maxillae well developed, surpassing those of the first maxillae;

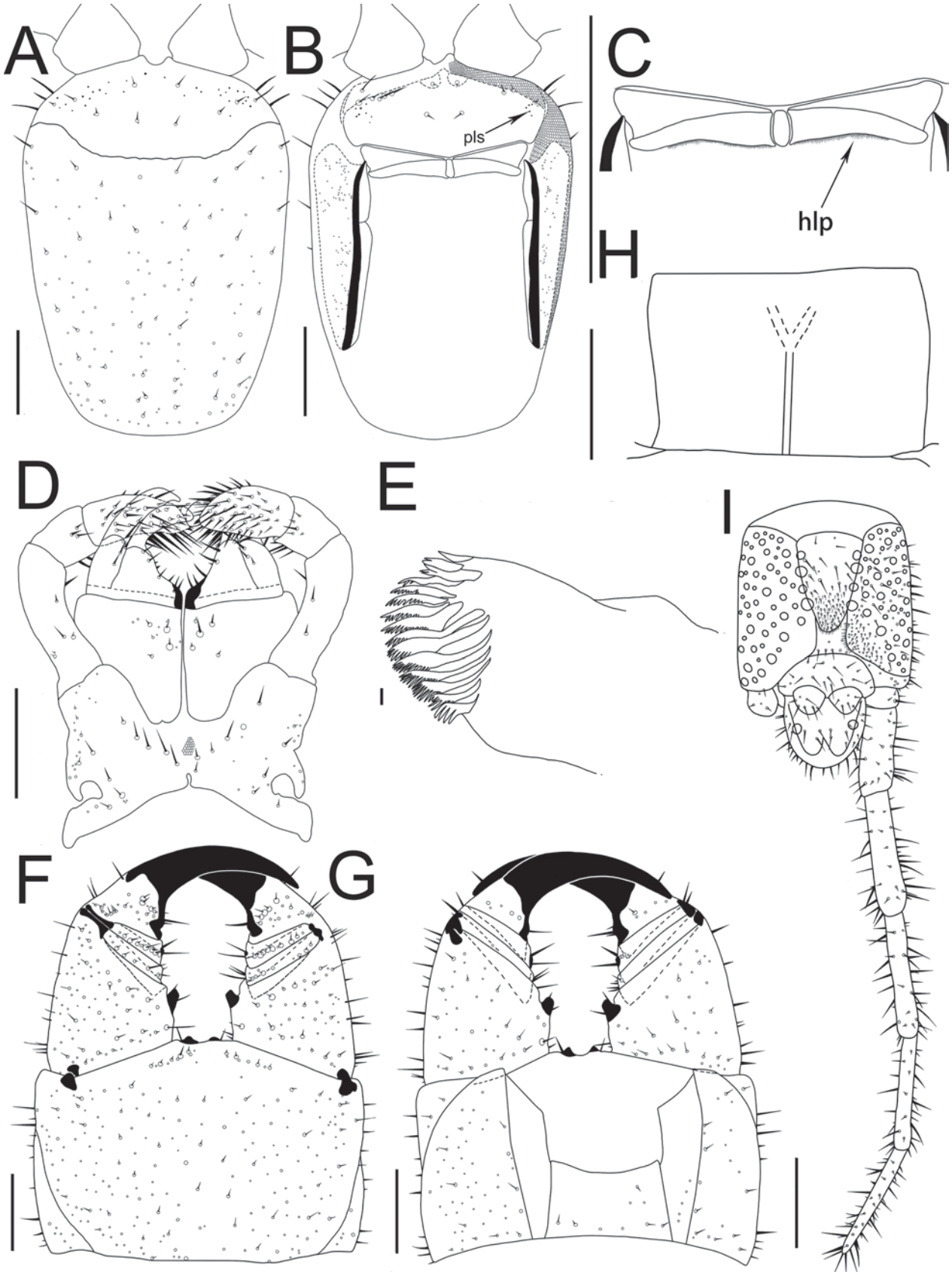

Figure 6. *Tygarrup fimbriatus* sp. nov., holotype. **A.** Cephalic plate, dorsal; **B.** Cephalic plate, ventral (maxillary complex removed); **C.** Labrum, dorsal; **D.** Maxillary complex, ventral; **E.** Mandible, ventral; **F.** Forcipular segment, ventral; **G.** Forcipular segment, dorsal; **H.** Seventh sternum of leg-bearing segment, ventral; **I.** Ultimate leg-bearing segment and left leg, ventral. Abbreviations: pls – pore-like sensilla, hlp – hair-like projections. Scale bars: 500 μm (**A, B, D, F–I**); 250 μm (**C**); 25 μm (**E**).

article 1 of the telopodite 3–3.3 × longer than wide, curved outward; article 2 of the telopodite ca. 1.1 × longer than wide; article 3 ca. 1.8 × longer than wide, with distal end densely covered with setae; apical claw simple.

Mandible with ca. 10–12 well-developed and ca. 2 rudimentary pectinate lamellae; the first lamella with 4–5 teeth, similar in size; intermediate lamellae with 9–12 teeth (Fig. 6E).

***Forcipular segment*:** Coxosternite 1.4 × wider than long, anterior margin with a pair of truncated teeth (Fig. 6F); scapular points of pleura reaching the anterior margin of coxosternite (Fig. 6G). Forcipular trochanteroprefemur about 1.4 × longer than wide and has a conical distal tooth (Bomi population) or a truncated distal tooth (Medog populations), intermediate articles with or without tubercle, tarsungulum without tubercle.

***Leg-bearing segments*:** A total of 45 leg-bearing segments. Sternal sulcus bifurcate faintly impressed, with an acute angle (Fig. 6H); sternal pores present on males, absent on females.

Ultimate leg-bearing segment densely setose. Tergite sub-rectangular, 1.1 × longer than wide. Coxopleuron as long as wide and 1.7 × longer than sternite. Ca. 50–80 coxal pores on ventral and lateral sides of each coxopleuron, the innermost two to four pores usually larger than others (Fig. 6I). The ultimate leg telopodite not swollen, with scattered setae, without pretarsus.

Postpedal segments densely setose for both sexes. Male gonopods bi-articulate, narrow, and separated by a conical projection. Female gonopods simple, subtriangular, and touching each other at their bases (Fig. 6I). Anal pores present on each ventro-lateral side of postpedal segments.

Etymology. Latin *fimbr* = fiber; the new species name refers to the presence of hair-like projections along the posterior margins of the labral posterior alae. We suggest the Chinese common name as "流苏地蜈蚣".

Distribution. China (Xizang).

Remarks. This new species resembles *T. multiporus* sp. nov., especially in the presence of pore-like sensilla on the clypeal plagula and cephalic plate. However, it can be distinguished from the latter by several distinct features: it possesses 9–12 pairs of setae along the anterior margin of the clypeal plagula, has hair-like projections along the posterior margins of the labral posterior alae, trunk along with dark patches, and exhibits a larger body size and elevated coxopleural pore numbers. In contrast, *T. multiporus* sp. nov. has only 3–4 pairs of setae along the anterior margin of the clypeal plagula, smooth posterior margins on the labral posterior alae, and a homogeneously yellow trunk without dark patches.

The presence of hair-like projections along the posterior margins of the labral posterior alae, a character typically associated with the genus *Dicellophilus* Cook, 1896, is reported in the genus *Tygarrup* for the first time. These projections are clearly shorter in *Tygarrup* than in *Dicellophilus* (Bonato et al. 2010b; Tsukamoto and Eguchi 2024). This distinction highlights the unique adaptation of the new species within the *Tygarrup* genus.

Tygarrup poriger (Verhoeff, 1942)

Figs 2D–F, 7

Brahmaputrus poriger Verhoeff, 1942: 51–52, figs 15–21.
Tygarrup poriger: Crabill 1968: 286–287.
Tygarrup nepalensis Shinohara, 1965: 303–306, figs 1–11. syn. nov.

Material examined. • 12 spms (CMMI 20240309001D, -003D, -005D, -008D, -013D, -014D, -016D, -018D–020D, 20240311001D, 20240311002D), China, Xizang Autonomous Regions, Medog County, near Renqingbensi Temple (29.3075°N, 95.3573°E), 1920 m asl., 9–11.iii.2024, leg. Chao Jiang, • 10 spms (CMMI 20240310002D, -006D–009D, -011D, -014D, 20240312005D, -007D, -013D) near Deergong village (29.1810°N, 95.1439°E), 1710 m asl., 10–12.iii.2024, leg. Chao Jiang, • 3 spms (CMMI 20240310016D, -017D, -019D), Shuwang Forestry (29.1946°N, 95.1920°E), 1780 m asl., 10.iii.2024, leg. Chao Jiang.

Diagnosis. A *Tygarrup* species with 45 leg-bearing segments. Clypeal setae 7–9 pairs. Forcipular trochanteroprefemur and tibia, each with a tooth, femur without, tarsungulum with a triangular tooth on the dorsal base. Sternal pores present in males only.

Re-description. Maximum length of male 3.6 cm and female 3.3 cm.

Color (of preserved specimens in alcohol): head and forcipular segment dark red, trunk and legs yellow, with dark patches along the trunk (Fig. 2D–F).

Cephalic plate (Fig. 7A) 1.5 × longer than the widest. Transverse suture rounded. Lateral margins nearly straight and convergent backwards, anterior margin convex, with a median incision, posterior margin rounded. Setae arranged nearly symmetrically.

Clypeus 2 × wider than long (Fig. 7B). Clypeus with an entire plagula covering most of the clypeus, areolation only present along the anterior margin of the head; clypeal setae as follows: 1 pair on the areolate part, 3–5 pairs along the anterior margin of the clypeal plagula, 2 pairs on the antero-medial part inside a large insula, and 1 pair on the central part of plagula (Fig. 7C).

Labrum (Fig. 7C): Mid-piece ca. 1.7 × longer than wide, posteriorly pointed and well sclerotized. anterior ala triangular, medial margin reduced to a vertex; posterior margin of each side-piece sinuous.

Cephalic pleurite without spiculum or setae; areolate part present along anterior margin and paraclypeal suture; stilus well developed, nearly straight, with an anterior incision on each side (Fig. 7B).

First maxillae (Fig. 7D): Coxosternite 1.8 × wider than long, divided by mid-longitudinal suture, anterior corners of coxosternum not projecting. Medial projection about 1.2 × wider than long, internal margin with several setae, distal lobe curved inward; telopodite about 2.1 × longer than wide, curved inward.

Second maxillae (Fig. 7D): Coxosternite undivided, ca. 1.4 × wider than long; both the anterior and posterior margins concave, lateral margins concave medially, posterior corners only slightly projecting externally;

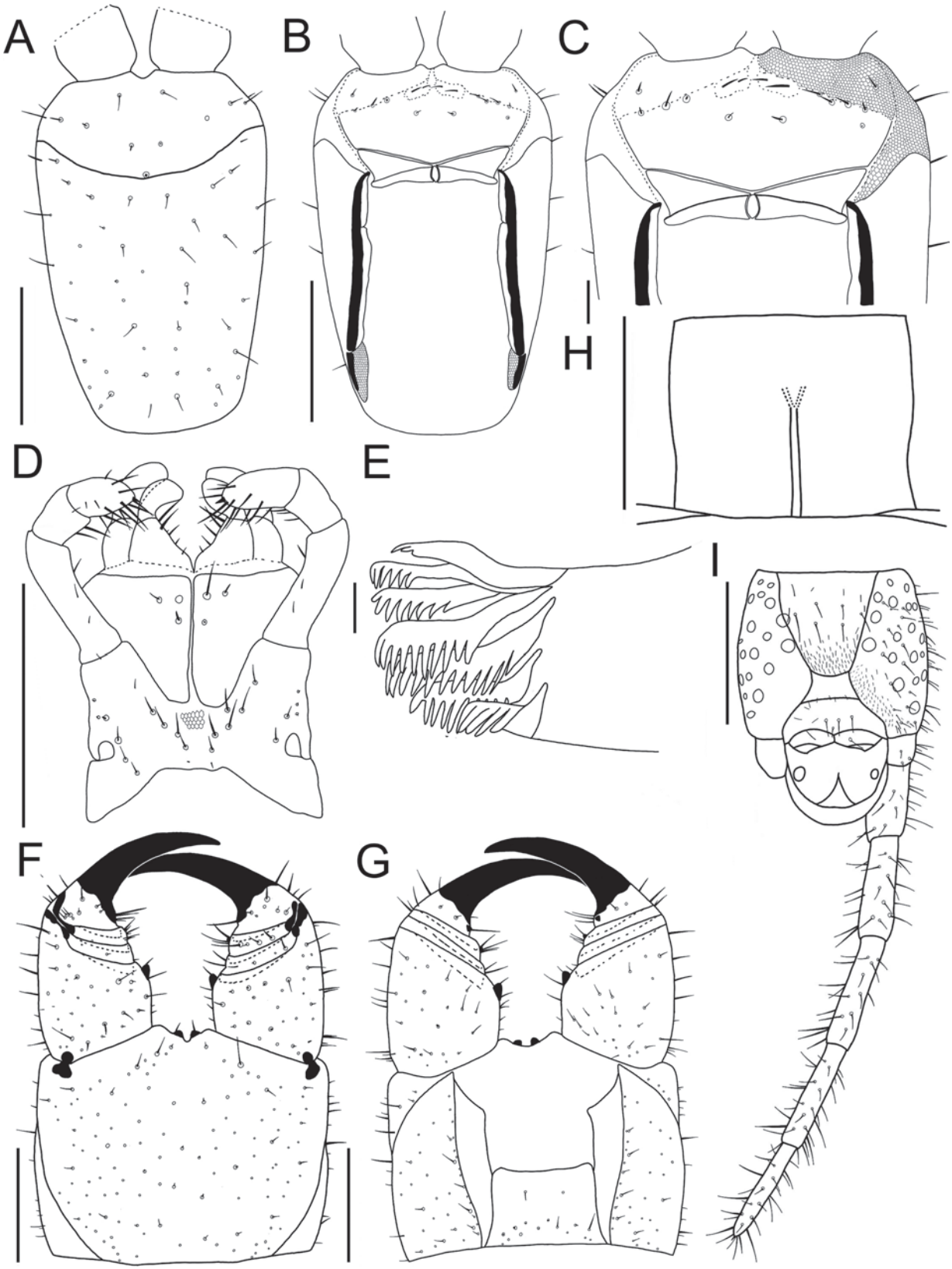

Figure 7. *Tygarrup poriger* (Verhoeff, 1942) (spm. CMMI 20240309001D). **A.** Cephalic plate, dorsal; **B.** Cephalic plate, ventral (maxillary complex removed); **C.** Clypeus, ventral (maxillary complex removed); **D.** Maxillary complex, ventral; **E.** Mandible, ventral; **F.** Forcipular segment, ventral; **G.** Forcipular segment, dorsal; **H.** Seventh sternum of leg-bearing segment, ventral; **I.** Ultimate leg-bearing segment and left leg, ventral. Scale bars: 500 µm (**A, B, D, F–I**); 100 µm (**C**); 25 µm (**E**).

areolation on medial part, setae present along the posterior part; the foraminal process surrounding the metameric pore separated from lateral margin of coxosternite. Telopodites of the second maxillae developed, surpassing those of the first maxillae when stretched; article 1 of the telopodite ca. 3.1 × longer than wide, curved outward;

article 2 of the telopodite ca. 1.6 × longer than wide; article 3 ca. 2.2 × longer than wide, with distal end densely covered with setae; apical claw large and simple.

Mandible with ca. 7 well-developed and ca. 2 rudimentary pectinate lamellae; the first lamella with 5 teeth, similar in size; intermediate lamellae with 9–12 teeth (Fig. 7E).

***Forcipular segment*:** Coxosternite 1.3 × wider than long, anterior margin with a pair of truncated teeth (Fig. 7F); scapular points of pleura reaching the anterior margin of coxosternite (Fig. 7G). Forcipular trochanteroprefemur about 1.3 × longer than wide and has a prominent distal tooth, femur with or without tubercle, tibia with a small pointed tubercle, tarsungulum with a triangular tooth on dorsal base.

***Leg-bearing segments*:** A total of 45 leg-bearing segments. Sternal sulcus bifurcate faintly impressed, with an acute angle (Fig. 7H); sternal pores present on males, absent on females.

Ultimate leg-bearing segment densely setose. Tergite sub-rectangular, 1.1 × longer than wide. Coxopleuron about 0.9 × longer than wide and 1.6 × longer than sternite. Ca. 20–35 coxal pores on ventral and lateral sides of each coxopleuron, the innermost two pores usually larger than others (Fig. 7I). The ultimate leg telopoditenot swollen, with scattered setae, without pretarsus.

Postpedal segments densely setose for both sexes. Male gonopods bi-articulate, narrow, and separated by a conical projection. Female gonopods inconspicuous bi-articulate, subtriangular, and touching each other at their bases (Fig. 7I). Anal pores present on each ventro-lateral side of postpedal segments.

Distribution. China (Xizang), Nepal.

Remarks. Verhoeff (1942) originally described a new genus, *Brahmaputrus*, and type species, *B. poriger,* from Shigatse, Xizang, of China, with 45 leg-bearing segments and males with sternal pores. Crabill (1968) considered the genus *Brahmaputrus* Verhoeff, 1942, as a synonym of *Tygarrup* Chamberlin, 1914. This species differs from other *Tygarrup* species for its forcipular trochanteroprefemur with a tooth, femur without, and tarsungulum with a tooth on dorsal base.

Shinohara (1965) originally described a *Tygarrup* species, *T. nepalensis*, based on 28 specimens from Ralwaling Himal, East Nepal. However, illustrations given by Shinohara (1965: figs 5–11) show minor variation with *T. poriger* sensu Verhoeff (1942: figs 15–21) and the present study (Fig. 7) in the clypeal setae, forcipular articles, maxillae, shape of the ultimate leg-bearing segment, and coxal pore numbers, particularly the dorsal tooth on the forcipular tarsungulum. Therefore, *Tygarrup nepalensis* Shinohara, 1965, is treated as a junior synonym of *Tygarrup poriger* (Verhoeff, 1942).

Tygarrup muminabadicus Titova, 1965

Figs 2G–I, 8

Tygarrup muminabadicus Titova, 1965: 871–876, figs 1, 2; Bonato et al. 2003: figs 8C, 9E, 10A, 13B; Dyachkov 2020: 80, 2022:75, figs 5–11.

Material examined. • 3 spms, (CMMI 20220525124, -126, -128), China, Xizang Autonomous Regions, Jilong County, near Rukaer (28.4481°N, 85.2467°E), 2970 m asl., 25.v.2022, leg. Xiaoxia Tian; • 2 spms (CMMI 20210705142, CMMI 20210705144), Luozha County, Lakang town, (28.1125°N, 91.1251°E), 3230 m asl., 5.vii.2022, leg. Chao Jiang; • 1 spms (CMMI 20210708102), Jiacha County, Anrao town (29.1420°N, 92.5829°E), 3240 m asl., 8.vii.2021, leg. Chao Jiang; 1 spm (CMMI 20220620103), Linzhi, Bayi district, Sejilashan Mt. (29.6213°N, 94.6514°E), 20.vi.2022, leg. Xiaoxia Tian, • 5 spms (CMMI 20201013119D–123D), Fuqing Road, 13.x.2020, leg. Chao Jiang, • 2 spms (CMMI 20201013137, CMMI 20201013142), Birishenshan Mt., 13.x.2020, leg. Chao Jiang; 1 spm (CMMI 20240310018D), Medog County, Shuwang Forestry (29.1946°N, 95.1920°E), 1780 m asl., 10.iii.2024, leg. Chao Jiang, • 7 spms (CMMI 20240310001D, -003D, -004D, -015D, CMMI 20240312001D, -008D, -009D), near Deergong village (29.1810°N, 95.1439°E), 1710 m asl., 10–12.iii.2024, leg. Chao Jiang.

Diagnosis. A *Tygarrup* species with 45 leg-bearing segments. Body length of adult reaches 5 cm. Clypeal plagula with 6–9 pairs of setae along the anterior margin; plagula without pore-like sensilla. Labral posterior alae posterior margins smooth, without hair-like projection. Forcipular trochanteroprefemur with a tooth, femur, and tarsungulum without tooth. Sternal pores present in males only. Coxopleuron with ca. 40–70 coxal pores. Female gonopods unarticulated.

Distribution. China (Xizang), Tajikistan, Kashmir.

Remarks. Specimens from Xizang could be assigned only tentatively to *T. muminabadicus*, as they are largely consistent with the original description (Titova 1965) and topotypes (Dyachkov 2022) of this species, only differing for a more inward-curved first maxillary telopodite (clavate in the original illustration) and for the elevated number of coxal pores on coxopleuron. This species has been previously documented in Tajikistan (Titova 1965; Dyachkov 2020, 2022) and Kashmir (Bonato et al. 2003) and is now reported for the first time in the Chinese fauna. The morphological characters of Chinese specimens are delineated through the accompanying illustrations (Figs 2G–I, 8).

T. diversidens, a Himalayan species that was originally described by Silvestri (1919) as *Lamnonyx diversidens*. This description was based on numerous specimens across a wide area of the Himalayas, extending from Assam in the east to Kashmir in the west. These distributions also include two localities in Xizang (Rotung and Renging) and are considered Xizang's *Tygarrup* species. The species also has the inwardly curved first maxillary telopodite (Silvestri 1919: fig. XX5) but is distinguished from *T. muminabadicus* by having bi-articulate female gonopods (Silvestri 1919: fig. XX8). However, the original description of *T. diversidens* is very inadequate, leaving the taxonomic relationship of this nominal species with other *Tygarrup* species from the Himalayas undetermined, necessitating further investigation (Bonato and Minelli 2004).

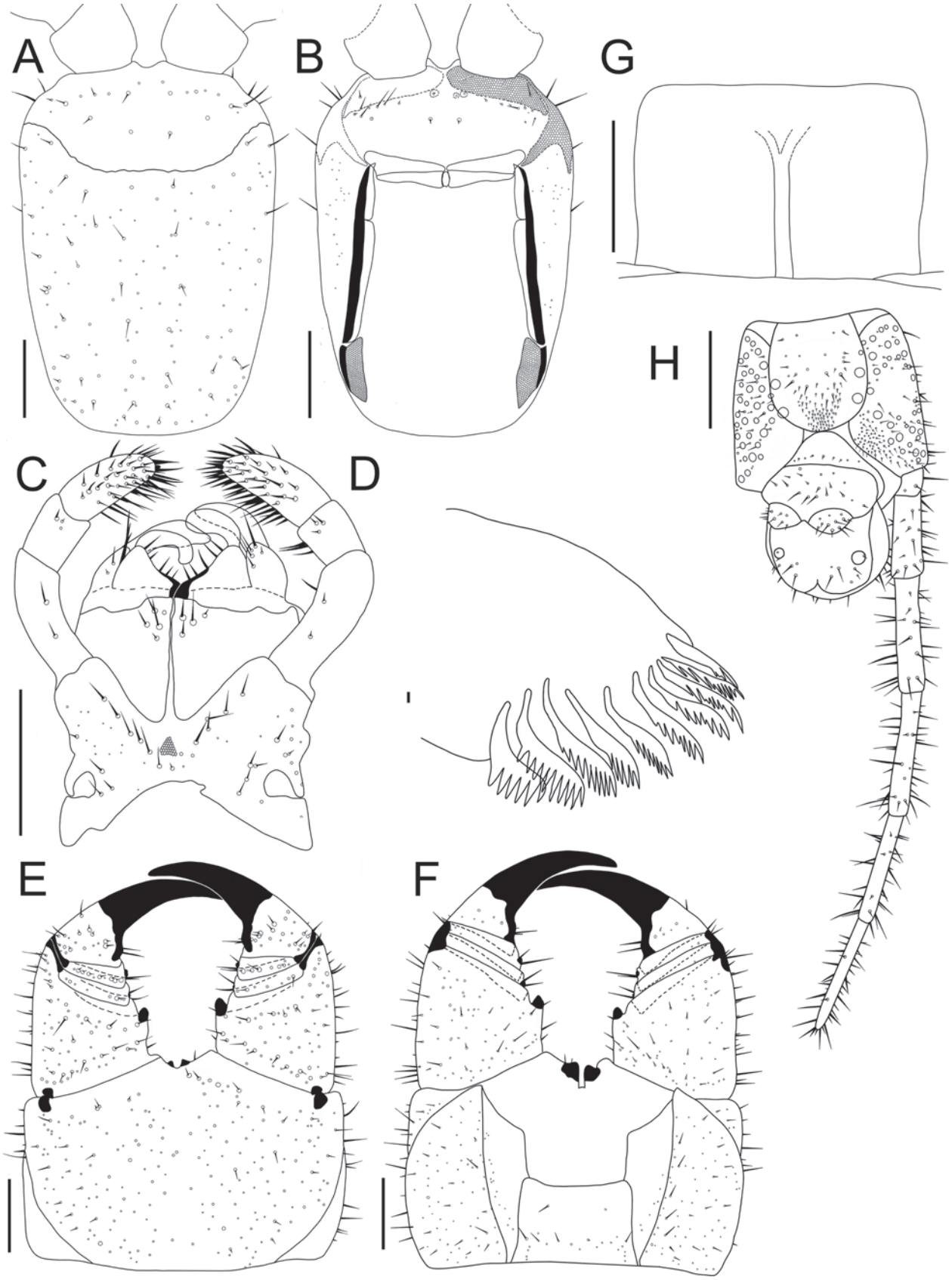

Figure 8. *Tygarrup muminabadicus* Titova, 1965 (spm. CMMI 20240310001D). **A.** Cephalic plate, dorsal; **B.** Cephalic plate, ventral (maxillary complex removed); **C.** Maxillary complex, ventral; **D.** Mandible, ventral; **E.** Forcipular segment, ventral; **F.** Forcipular segment, dorsal; **G.** Seventh sternum of leg-bearing segment, ventral; **H.** Ultimate leg-bearing segment and left leg, ventral. Scale bars: 500 μm (**A–C, E–H**); 25 μm (**D**).

Discussion

In the present study, we investigated the genus *Tygarrup* from Xizang and identified six species within the genus (Fig. 9). Certain morphological characters, such as pore-like sensilla, cerrus, and the hair-like projections along the posterior margins of the labral posterior alae, were discovered for the first time to be effective in distinguishing species within the *Tygarrup* genus for the first time. The introduction of these new morphological characters allows for a more accurate differentiation of *Tygarrup* species in Xizang, contributing to a better understanding of the diversity of soil centipede species in this region.

Tygarrup species from Xizang dwell in both tropical dry forests and alpine environments. The lowest recorded altitude for their habitat is 920 meters (*T. fimbriatus* sp. nov.), while the highest extends up to 4400 meters (*T. tridentatus* sp. nov.). Among them, *T. tridentatus* sp. nov. and *T. poriger* can inhabit both cold mountain regions and low-altitude warmer forests. In contrast, *T. cerrus* sp. nov. is found exclusively in high mountain coniferous forests at around 3000 meters in altitude. Based on our available specimens and historical records (Verhoeff 1942; Shinohara 1965), most *Tygarrup* species in Xizang live at altitudes above 1700 meters, while *Tygarrup* species in other regions predominantly inhabit forests or greenhouses below 1500 meters (Silvestri 1919; Attems 1929; Titova 1983; Bonato et al. 2004; Uliana et al. 2007; Bonato and Minelli 2010; Dyachkov 2020, 2022). Historical literatures and our results also show that the number of *Tygarrup* species in the Himalayan mountainous regions within the same scale is higher than in the northern Qinghai-Tibet Plateau region as well as in the southern tropical rainforests and Gangetic Plains (Silvestri 1919). The complexity of mountains is usually tightly associated with high biodiversity (Perrigo et al. 2020). In multiple animal and plant groups, the uplift of the Himalayas has promoted biological diversification (Xia et al. 2022; Liu et al. 2024). Therefore, the Himalayas, with their complete tropical monsoon mountain vertical natural zones ranging from lowland tropical monsoon rainforests to alpine snow zones, may have facilitated the diversification of the *Tygarrup* species in Xizang. Considering the diversity of the Himalayan ecosystem, the sampled regions available are still only fragmentary and insufficient for the diversity research of *Tygarrup*. Therefore, the faunal diversity in this region is likely still underestimated.

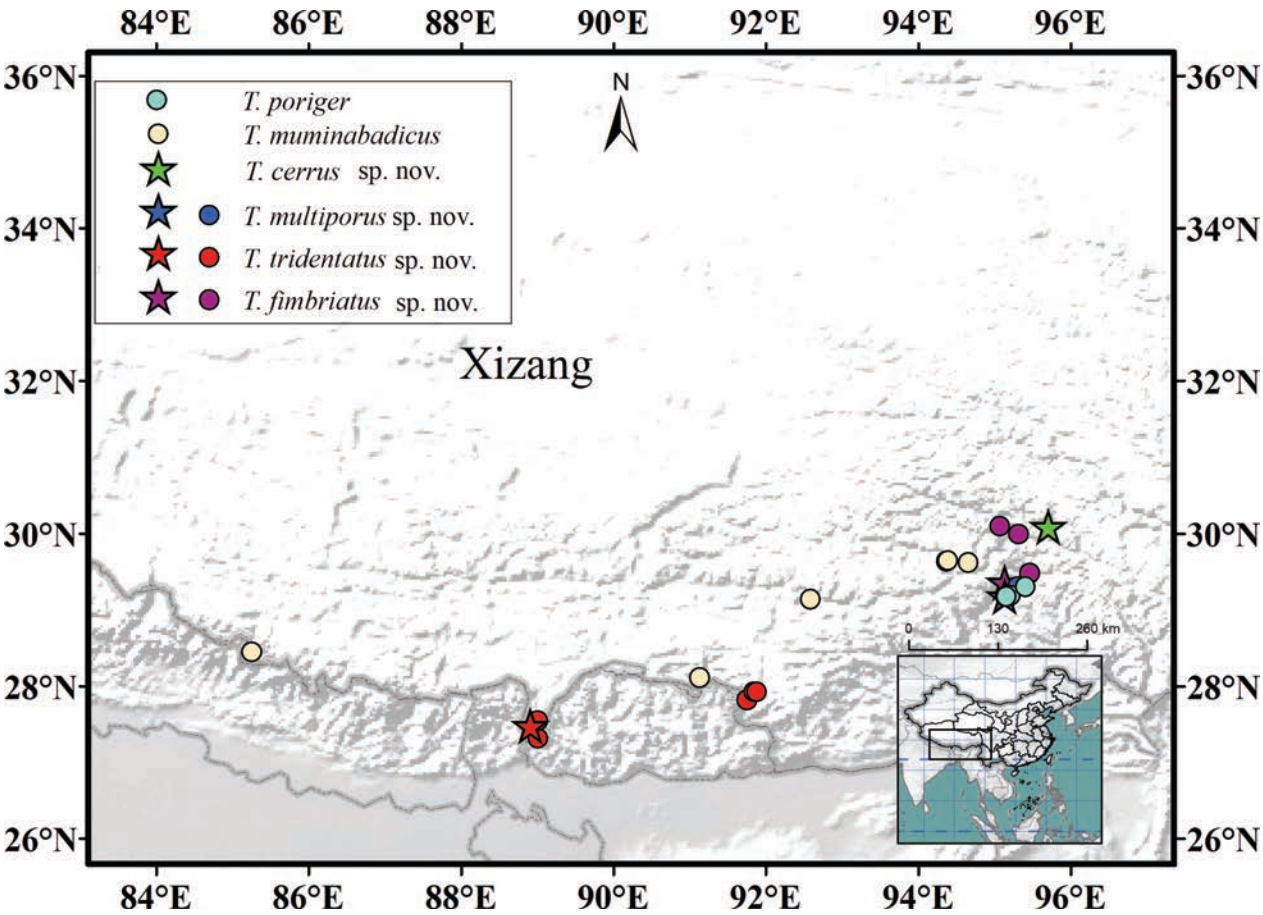

Figure 9. Collected localities of species of *Tygarrup* in Xizang of China. Stars represent type localities.

Key to the six confined *Tygarrup* species of China

1 Cerrus composed of two lateral groups of setae (Fig. 4H)..... *T. cerrus* sp. nov.
– Cerrus absent 2
2 Antero-lateral corners of plagula evidently bear pore-like sensilla..... 3
– Antero-lateral corners of plagula absent pore-like sensilla..... 4
3 Posterior margins of labral posterior alae bear hair-like projections (Fig. 6C) ..... *T. fimbriatus* sp. nov.
– Posterior margins of labral posterior alae absent hair-like projection (Fig. 5B)..... *T. multiporus* sp. nov.
4 Central part of plagula with ca. 15 paired setae arranged in three irregular rows (Chao et al. 2020: fig. 3)... *T. daliensis*
– Central part of plagula with 6–11 paired setae arranged in two irregular rows..... 5
5 Forcipular tarsungulum with a tooth 6
– Forcipular tarsungulum without tooth (Fig. 8F)..... *T. muminabadicus*
6 Forcipular article III and tarsungulum with a prominent pointed tooth (Fig. 3F, G)..... *T. tridentatus* sp. nov.
– Forcipular article III with a small tubercle, tarsungulum with a triangular tooth on dorsal base (Fig. 7G)..... *T. poriger*

Acknowledgements

We are grateful to Dr. Huiqin Ma (Hengshui University, China) for providing important literature. We wish to thank Ms. Jiaxin Dong and Ms. Yaru Zhang for their assistance in preparing the line drawings of the new species. We sincerely thank Dr. Huiqin Ma and the anonymous reviewer for providing valuable comments that significantly improved this paper.

The research was supported by the Key Project at Central Government Level: the Ability Establishment of Sustainable Use for Valuable Chinese Medicine Resources (nos. 2060302), the CACMS Innovation Fund (nos. CI2023E002), and the Survey of Wildlife Resources in Key Areas of Xizang (Phase II) (nos. ZL202303601).

References

Attems CG (1929) Das Tierreich. 52 Myriapoda. I. Geophilomorpha. De Gruyter & Co., Berlin-Leipzig, 388 pp. https://doi.org/10.1515/9783111430638

Bonato L, Minelli A (2004) The centipede genus *Mecistocephalus* Newport 1843 in the Indian peninsula (Chilopoda, Geophilomorpha, Mecistocephalidae). Tropical Zoology 17(1): 15–63. https://doi.org/10.1080/03946975.2004.10531198

Bonato L, Minelli A (2010) The geophilomorph centipedes of the Seychelles (Chilopoda, Geophilomorpha). Phelsuma 18: 9–38.

Bonato L, Foddai D, Minelli A (2002) A new mecistocephalid centipede from Ryukyu Islands and a revisitation of '*Taiwanella*' (Chilopoda, Geophilomorpha, Mecistocephalidae). Zootaxa 86: 1–12. https://doi.org/10.11646/zootaxa.86.1.1

Bonato L, Foddai D, Minelli A (2003) Evolutionary trends and patterns in centipede segment number based on a cladistic analysis of Mecistocephalidae (Chilopoda, Geophilomorpha). Systematic Entomology 28(4): 539–579. https://doi.org/10.1046/j.1365-3113.2003.00217.x

Bonato L, Foddai D, Minelli A, Shelley R (2004) The centipede order Geophilomorpha in the Hawaiian islands (Chilopoda). Bishop Museum Occasional Papers 78: 13–32.

Bonato L, Edgecombe GD, Lewis JG, Minelli A, Pereira LA, Shelley RM, Zapparoli M (2010a) A common terminology for the external anatomy of centipedes (Chilopoda). ZooKeys 69: 17–51. https://doi.org/10.3897/zookeys.69.737

Bonato L, Dányi L, Minelli A (2010b) Morphology and phylogeny of *Dicellophilus*, a centipede genus with a highly disjunct distribution (Chilopoda, Mecistocephalidae). Zoological Journal of the Linnean Society 158(3): 501–532. https://doi.org/10.1111/j.1096-3642.2009.00557.x

Bonato L, Edgecombe GD, M Zapparoli, Minelli A (2011) Chilopoda – Taxonomic overview: Geophilomorpha. Treatise on Zoology – Anatomy, Taxonomy, Biology. The Myriapoda Volume 1: 407–443. https://doi.org/10.1163/9789004188266_020

Cai T, Fjeldså J, Wu Y, Shao S, Chen Y, Quan Q, Li X, Song G, Qu Y, Qiao G, Lei F (2018) What makes the Sino-Himalayan mountains the major diversity hotspots for pheasants?. Journal of Biogeography 45(3): 640–651. https://doi.org/10.1111/jbi.13156

Chao JL, Lee KS, Yang ZZ, Chang HW (2020) Two new species of centipedes, *Tygarrup daliensis* sp. nov. (Mecistocephalidae) and *Australobius cangshanensis* sp. nov. (Lithobiidae), from Southwestern China. Opuscula Zoologica (Budapest) 51(S2): 57–67. https://doi.org/10.18348/opzool.2020.S2.57

Chen TY, Jiang C, Huang LQ (2023) A new species of *Otostigmus* (Chilopoda, Scolopendromorpha, Scolopendridae) from China, with remarks on the phylogenetic relationships of *Otostigmus politus* Karsch, 1881. ZooKeys 1168: 161–178. https://doi.org/10.3897/zookeys.1168.82750

Crabill RE (1968) A bizzare case of sexual dimorphism in a centipede with consequent submergence of a genus (Chilopoda, Geophilomorpha, Mecistocephalidae). Entomological News 79: 286–287.

Crabill RE (1970) Concerning mecistocephalid morphology and the true identity of the type-species of *Mecistocephalus*. Journal of Natural History 4: 231–237. https://doi.org/10.1080/00222937000770221

Dyachkov YuV (2020) New data on the centipede (Chilopoda) fauna from Tajikistan. Ecologica Montenegrina 36: 78–86. https://doi.org/10.37828/em.2020.36.6

Dyachkov YuV (2022) On new records of Geophilomorpha (Chilopoda) from Middle Asia. Ecologica Montenegrina 60: 70–79. https://doi.org/10.37828/em.2022.60.11

Dyachkov YuV, Bonato L (2022) Morphology and distribution of the Middle Asian centipede genus *Krateraspis* Lignau, 1929

(Chilopoda, Geophilomorpha, Mecistocephalidae). ZooKeys 1095: 143–164. https://doi.org/10.3897/zookeys.1095.80806

Lewis JGE (2010) A revision of the rugulosus group of Otostigmussubgenus-sOtostigmus Porat, 1876 (Chilopoda, Scolopendromorpha, Scolopendridae). Zootaxa 2579: 1–29. https://doi.org/10.11646/zootaxa.2579.1.1

Li L, Xu X, Qian H, Huang X, Liu P, Landis JB, Fu Q, Sun L, Wang H, Deng T (2022) Elevational patterns of phylogenetic structure of angiosperms in a biodiversity hotspot in eastern Himalaya. Diversity and Distributions 28(12): 2534–2548. https://doi.org/10.1111/ddi.13513

Liu R, Wang WJ, Wang H, Ree RH, Li DZ, Yu W B (2024) Plant species diversification in the Himalaya–Hengduan Mountains region: an example from an endemic lineage of *Pedicularis* (Orobanchaceae) in the role of floral specializations and rapid range expansions. Cladistics 40(6): 636–652. https://doi.org/10.1111/cla.12596

Ma H, Pei S, Hou X, Zhu T, Wu D, Gai Y (2014) An annotated checklist of Lithobiomorpha of China. Zootaxa 3847(3): 333–358. https://doi.org/10.11646/zootaxa.3847.3.2

Niu M, Li Y, Di Z (2021) *Otostigmus* (*Otostigmus*) *xizangensis* n. sp., from China and a case of sexual dimorphism in the subgenus *Otostigmus* (*Otostigmus*) Porat, 1876 (Chilopoda, Scolopendromorpha, Scolopendridae). Zootaxa 5081(2): 295–300. https://doi.org/10.11646/zootaxa.5081.2.8

Paik KY (1961) The myriapods fauna of Quelpart Island, Korea. Theses collection of Kyungpook University 5: 75–88.

Pan YY, Fan JB, You CX, Jiang C (2024) Identification of two new species of *Mecistocephalus* (Chilopoda, Geophilomorpha, Mecistocephalidae) from southern China and the re-description of *Mecistocephalus smithii* Pocock, 1895. ZooKeys 1218: 1–23. https://doi.org/10.3897/zookeys.1218.130709

Perrigo A, Hoorn C, Antonelli A (2020) Why mountains matter for biodiversity. Journal of Biogeography 47(2): 315–325. https://doi.org/10.1111/jbi.13731

Qiao P, Qin W, Ma H, Zhang T (2019) Two new species of lithobiid centipedes and the first record of *Lamyctes africanus* Porath (Chilopoda, Lithobiomorpha) in China. Journal of Natural History 53(15–16): 897–921. https://doi.org/10.1080/00222933.2019.1606355

Shinohara K (1965) A new species of Chilopoda from Himalaya. Journal of the College of Arts and Science, Chiba University, Natural Science Series 4(3): 303–306.

Silvestri FH (1919) Contributions to a knowledge of the Chilopoda Geophilomorpha of India. Record of the Indian Museum 16: 45–107. https://doi.org/10.5962/bhl.part.25916

Song Z, Zhu M, Liang A (2010) The genus *Cryptops* Leach (Scolopendromorpha, Cryptopidae, Cryptopinae) in China, with description of a new species and a new recorded species. Acta Zootaxonomica Sinica 35(02): 376–380. https://www.researchgate.net/publication/316643879

Titova LP (1965) A new chilopod (*Tygarrup muminabadicus* Titova sp. n.; Mecistocephalidae Chilopoda) from South Tajikistan. Zoologichesckii Zhurnal 44: 871–876. [In Russian]

Titova LP (1983) Two new *Tygarrup* Chamb. (Chilopoda, Geophilida, Mecistocephalidae) from Indochina. Annalen des Naturhistorischen Museums 85B: 147–156.

Tsukamoto S, Eguchi K (2024) Integrative taxonomy of *Dicellophilus* Cook, 1896 (Chilopoda, Geophilomorpha, Mecistocephalidae) in Japan, with a description of a new species. Zoosystematics and Evolution 100(3): 821–840. https://doi.org/10.3897/zse.100.121512

Uliana M, Bonato L, Minelli A (2007) The Mecistocephalidae of the Japanese and Taiwanese islands (Chilopoda, Geophilomorpha). Zootaxa 1396(1): 1–84. https://doi.org/10.11646/zootaxa.1396.1.1

Verhoeff KW (1939) Chilopoden der Insel Mauritius. Zoologische Jahrbücher, Abteilung für Systematik 72: 71–89.

Verhoeff KW (1942) Chilopoden aus innerasiatischen Hochgebirgen. Zoologischer Anzeiger 137: 35–52.

Xia XM, Yang MQ, Li CL, Huang SX, Jin WT, Shen TT, Wang F, Li XH, Yoichi W, Zhang LH, Zheng YR Wang XQ (2022) Spatiotemporal evolution of the global species diversity of Rhododendron. Molecular Biology and Evolution 39(1): msab314. https://doi.org/10.1093/molbev/msab314

Zoosyst. Evol. 101 (2) 2025, 551–570 | DOI 10.3897/zse.101.133434

PENSOFT

für Natur MUSEUM FÜR NATURKUNDE BERLIN

An illustrated type catalogue of *Diplommatina* Benson, 1849 from mainland China, with description of a new species, *Diplommatina yipingica* (Gastropoda, Cyclophoroidea)

Guang-Long Xie[1*], Guoyi Zhang[2,3*], Kaibaryer Meng[4], Frank Köhler[3]

1 *School of Life Sciences, Qufu Normal University, Qufu, Shandong, China*

2 *Evolution & Ecology Research Centre, School of Biological, Earth and Environmental Sciences, University of New South Wales, Sydney 2052, Australia*

3 *Australian Museum Research Institute, Australian Museum, 1 William St, Sydney 2000, Australia*

4 *National Zoological Museum of China, Institute of Zoology, Chinese Academy of Sciences, Beijing, China*

https://zoobank.org/BD2439F8-5ADE-4B33-8CEB-D151068C7AB1

Corresponding authors: Guang-Long Xie (gxie@hotmail.com); Guoyi Zhang (starsareitherose@gmail.com)

Academic editor: Thomas von Rintelen ♦ **Received** 30 July 2024 ♦ **Accepted** 21 December 2024 ♦ **Published** 28 February 2025

Abstract

We document type material of 41 nominal species from mainland China that were originally assigned to *Diplommatina*. This catalogue is based on inspection of the Heude Type collection in the National Zoological Museum of China, Beijing and complemented with information on types held by other international museums from a comprehensive literature review. We designate lectotypes of five nominal species, *Diplommatina abbreviata* Heude, 1890, *D. confusa* Heude, 1885, *D. intermedia* Heude, 1890, *D. minuscula* Heude, 1890, *D. pupinella* Heude, 1885 and *D. pyra* Heude, 1885.

In addition, a new species, *Diplommatina yipingica* Zhang, **sp. nov.**, is described from Qingdao City, Shandong Province. A new name, *D. yunnanensis*, is introduced for *Diplommatina minuscula* Chen & Zhang, 1998, which is a junior homonym of *D. minuscula* Heude, 1890.

Key Words

Diplommatinidae, nomenclature, Shandong Province, *Sinica*, type material

Introduction

Diplommatina Benson, 1849 is a speciose genus containing species from Asia and the Pacific (Webster et al. 2012). With its evolutionary origins estimated to date back to the early or mid-Cretaceous, the genus is of considerable evolutionary antiquity (e.g., Köhler 2023). Several species from mainland China were described by early European malacologists, such as Gredler (1881, 1884, 1885, 1886, 1887a, 1887b), Möllendorff (1882, 1885a, 1885b, 1886) and Heude (1885), while comparatively few contemporary studies have since complemented our knowledge of the Chinese fauna. Indeed, a comprehensive taxonomic review of the Chinese diplommatinids that goes beyond the appraisal of shell features is long overdue. Type specimens are critical to any such revision. As the bearers of taxonomic names, they will facilitate future assessments of the validity of taxa (Winston 1999). Relevant types for many Chinese species are scattered across museums in China, North America and Europe. This means that a compilation of the known type repositories will be a valuable resource for future revisions. We found that the following museums have

* These authors contributed equally to this work.

important type collections of Chinese diplommatinids: the National Zoological Museum of China, Institute of Zoology, Chinese Academy of Sciences (IZCAS) (containing significant parts of the Heude collection), the Museum of Comparative Zoology, Harvard University, Cambridge, USA (MCZ) (containing part of the Heude collection); the Naturmuseum Senckenberg, Frankfurt (SMF) (for types by Möllendorff and Yen); Academy of Natural Sciences of Drexel University, Philadelphia (ANSP) (containing the Pilsbry Collection), the Sammlung des Franziskaner-Gymnasiums, Bozen (containing the Gredler Collection; Zilch (1974)) and the Smithsonian National Museum of Natural History, Washington (UNSM).

Before the mid-20th century, taxa were generally described by European authors, such as Gredler (1881, 1884, 1885, 1886, 1887a, 1887b), Möllendorff (1882, 1885a, 1885b, 1886), Heude (1885, 1890), Schmacker and Boettger (1890), and Yen (1939). In addition, Pilsbry and Hirase (1908) described species based on specimens received from mainland China. Based on these works, Zilch (1953, 1974) compiled a checklist of *Diplommatina* from mainland China. Since then, six works by Chinese authors have been published adding to the documentation of *Diplommatina* species in China (Chen et al. 1994; Ran et al. 1999; Chen et al. 2001; Chen et al. 2002; Hu et al. 2003; Zhou et al. 2005; Luo et al. 2008). However, in many of the works, the internal shell sculpture, which is taxonomically relevant, has not been adequately documented. Overall, more than 30 species and subspecies of *Diplommatina*, have been described from mainland China, with most of them occurring in southern China. Luo et al. (2008) suggested that the genus is narrowly distributed in southern China with the highest taxonomic diversity found in Hunan and Hubei Provinces and Chongqing City (Fig. 1). This statement requires confirmation by future research.

All diplommatinid genera are presently delimited using certain shell characters, such as coiling direction, shell shape, size and external and internal sculpture (Möllendorff 1885b; Schmacker and Boettger 1890; Kobelt 1902; Thiele 1929; Wenz 1939; Luo et al. 2008; Hwang et al. 2009; Egorov 2013; Liew et al. 2014; Neubert and Bouchet 2015; Budha et al. 2017; Greke 2017;Nurinsiyah and Hausdorf 2017), as well as operculum morphology (Kobelt 1902; Yamazaki et al. 2013; Budha et al. 2017) and radula (Yamazaki et al. 2013). All Chinese species known at the time were placed in the subgenus *Sinica* by Kobelt (1902: 455) based on the configuration of internal plicae. However, more comprehensive molecular studies are required to confirm the diagnostic value of these features in diplommatinid systematics (Webster et al. 2012). Molecular phylogenetic studies have shown that most genera of Diplommatinidae are monophyletic and have associated mapped morphological traits, but the phylogenetic relationships of some genera remain unclear, such as *Diplommatina* (Webster et al. 2012; Köhler 2023). The present study provides molecular data for one species as well as a detailed description of its morphology.

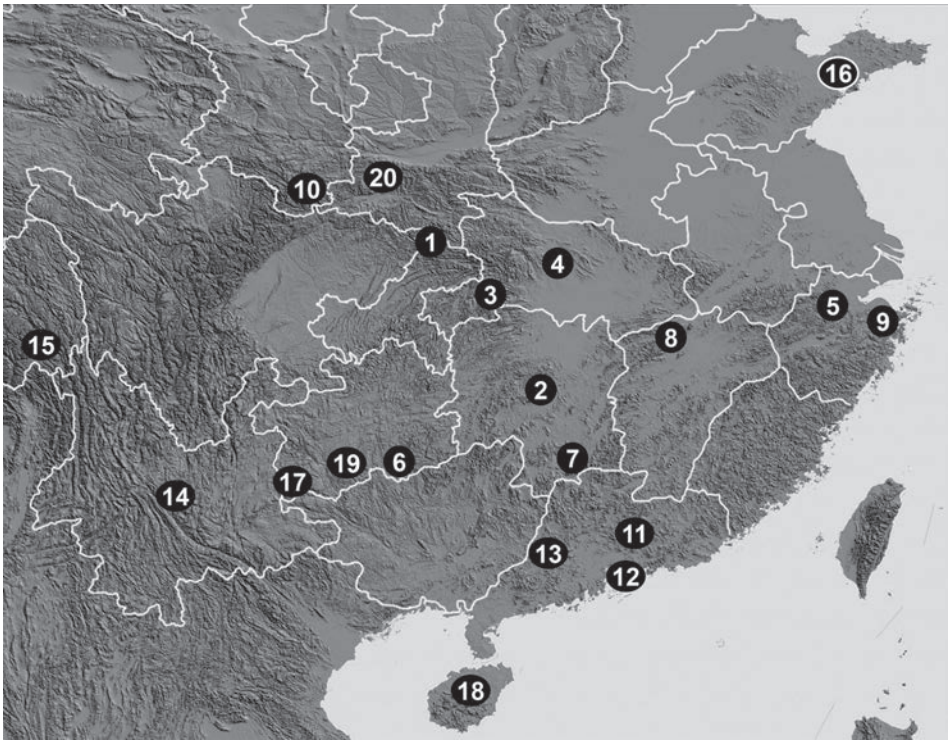

Figure 1. Type localities of *Diplommatina* species. 1. Chengkou, Chongqing City; 2. Hunan Province; 3. Badong, Hubei Province; 4. Hubei Province; 5. Hangzhou City, Zhejiang Province; 6. Libo, Guizhou; 7. Mangshan Hunan; 8. Lushan, Jiujiang City, Jiangxi Province; 9. Dalanshan, Ningbo City, Zhejiang Province; 10. Kangxian County, Longnan City, Gansu Province; 11. Luofushan, Huizhou City, Guangdong Province; 12. Dapengwan, HongKong City; 13. Zhaoqing City, Guangdong Province; 14. Yünnan Province; 15. Xizang Autonomous Region; 16. Laoshan, Qingdao City; 17. Xingyi City, Guizhou Province; 18 . Hainan Province; 19. Luodian County, Guizhou; 20. Longxian County, Shaanxi Province.

Material and methods

Abbreviations used

ANSP– Academy of Natural Sciences of Drexel University, Philadelphia, USA; **FMB**– Franziskanermuseum Bozen, Italy; **HMT** - Heude Museum Type Collection, IZCAS, China; **MCZ** – Museum of Comparative Zoology, Harvard University, Cambridge, Mass., USA; **IZCAS** – National Zoological Museum of China, Institute of Zoology, Chinese Academy of Sciences, Beijing, China; **SMF** – Naturmuseum Senckenberg, Frankfurt/Main, Germany; **USNM** – United States National Museum, Smithsonian Institution, Washington D.C., USA.

Methods

Our terminology for shell features follows Budha et al. (2017). Map of all type localities is shown in Fig. 1. The shell photographs, showcasing both the apertural and lateral views, were captured using a Keyence VHX-1000C Large depth-of-field 3D Digital Microscope.

We used morphometrics and molecular phylogenetics to determine the similarities and differences between the proposed new species *Diplommatina yipingica* and all other examined type specimens of congeners. Shell morphological variation was assessed using geometric morphology methods (GMM): Landmarks and semi-landmarks were defined along the contour of the shell in apertural view and analysed by using tpsUtil32 software (Rohlf 2004), tpsDig32 (Rohlf 2005) and MorphoJ version 1.07a (Klingenberg 2011) (Fig. 2). The following landmarks ("LM") were used: LM 1: Apex of shell; LM 2 & LM 7: Right and left terminal points on penultimate suture, respectively; LM 3 & LM 6: Right and left terminal points on last suture, respectively; LM 4 & LM 5: Crossing of peristome and left and right profile of body whorl. Semi-landmarks: Eight equidistant semi-landmarks (LM 8 – LM 15) between LM 2 and LM 3; eight equidistant semi-landmarks (LM 16 – LM 23) between LM 3 and LM 4; eighteen equidistant semi-landmarks (LM 24 – LM 41) between LM 4 and LM 5; eight semi-landmarks (M 42 – LM 49) between LM 5 and LM 6; eight semi-landmarks (LM 50 – LM 57) between LM 6 and LM 7. Shape was assessed using principal component analysis (PCA) across all specimens and all landmarks. Discriminant analysis used cross-validation and 1,000 permutations amongst groups based on the phylogenetic groups. In addition, a canonical variance analysis (CVA) is used, which simplifies descriptions of variation according to the phylogenetic groups.

Whole genomic DNA (for SDNU specimens) was extracted from a piece of the foot muscle following the instructions of the manual (Tiangen DP316). PCRs were conducted in volumes of 25 µl each containing 12.5 µl of cwbio 2× Es Taq MasterMix Dye, 9.5 µl of ddH_2O, 1 µl of template DNA and each 1 µl of PCR primers (10 µM). Reactions were performed in a SimpliAmpTM Thermal Cycler using the following thermal cycling profile: Initial denaturation for 30 s at 94 °C, 40 cycles of each 10 s at 94 °C, 50 s at 45 °C and 50 s at 72 °C and a final extension at 72 °C for 10 min (for 16Sar and 16Sbr; Palumbi et al. (1991)). PCR amplicons were inspected on a 1% agarose gel for quality and fragment size, then were purified and sequenced on an automated sequencer.

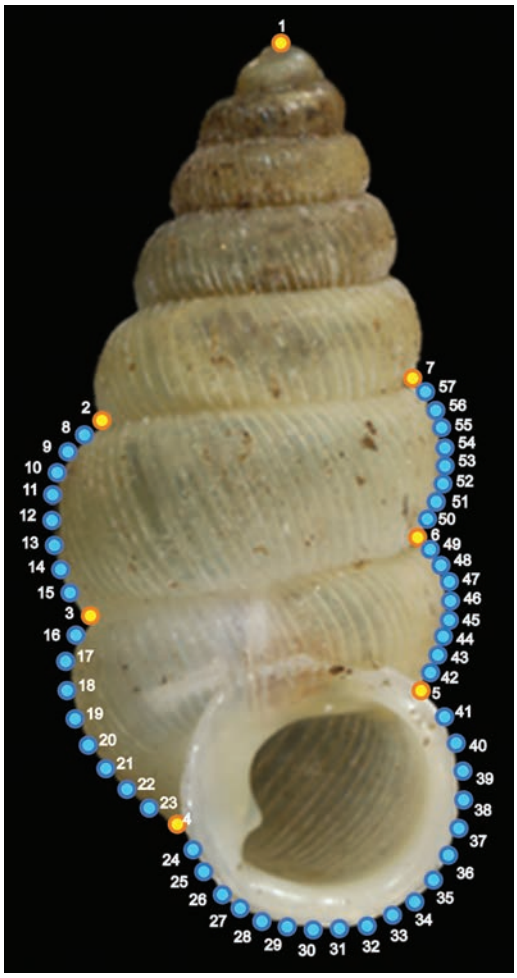

Figure 2. Shell photo showing landmarks used in this study.

The chromatographs and sequences were assembled in pregap4 1.6 and gap4 4.11.2 (Staden et al. 2003) with visualisation by trev 1.9 (Bonfield et al. 2002). DNA sequences were aligned using MAFFT 7.526 (Nakamura et al. 2018). We used Gblocks 0.91b (Castresana 2000) to remove ambiguously aligned parts of the multiple sequence alignment. The best-fit model of sequence evolution was selected by using ModelTest-ng (Kozlov et al. 2019) based on the Bayesian Information Criterion (BIC). Bayesian Inference was performed using MrBayes version 3.2.7 (Ronquist et al. 2012). We performed two Markov Chain Monte Carlo run-seach of them containing four chains (3 heated and 1 cold) for a total of 400,000 generations. Sampling rate was 100 generations. The temperature was set as 0.1. The first 50% of trees were discarded as burn-in.

Results

Morphological examinations of shell

Principal Component Analysis (PCA) of all individuals and all landmarks showed that 70.6% of observed morphological variance was explained by the first two principal components (PC1:60.8%; PC2:9.8%). The PCA plot showed that *Diplommatina yipingica* is similar to *D. pupinella*, *D. futilis*, *D. intermedia*, *D. paxillus longipalatalis*, *D. paxillus hunanensis*, *D. yunannensis* and *D. schmackeriana* in terms of general shell shape. The Canonical Variate Analysis (CVA) identified 41% of observed morphological variance and was explained by the first two major axes of variance to account for a relevant proportion of variance (CV1:23.3%; CV2:17.7%). In contrast, the CVA plot showed *D. yipingica* cluster together, separated with remaining species (Fig. 3).

Molecular phylogenetic analyses

Sequences from 20 individuals of *Diplommatina* spp. and two individuals from the outgroup genus *Palaina* were used for phylogenetic reconstruction. The final concatenated dataset of the alignment of 16S sequences had a total length of 424 bp (76% of the original 556 positions). Based on the phylogenetic tree presented herein (Fig. 4), *Diplommatina* is a monophyletic group with maximal nodal support (Bayesian posterior probability = 1). *Diplommatina* forms a polytomy of three main lineages. This topology is consistent with a phylogenetic tree published by Boonmachai et al. (2023). *Diplommatina yipingica*, Zhang, sp. nov. belongs to the *Diplommatina* group (Clade A) known from China, Borneo, Malaysia and Thailand first identified by Webster et al. (2012).

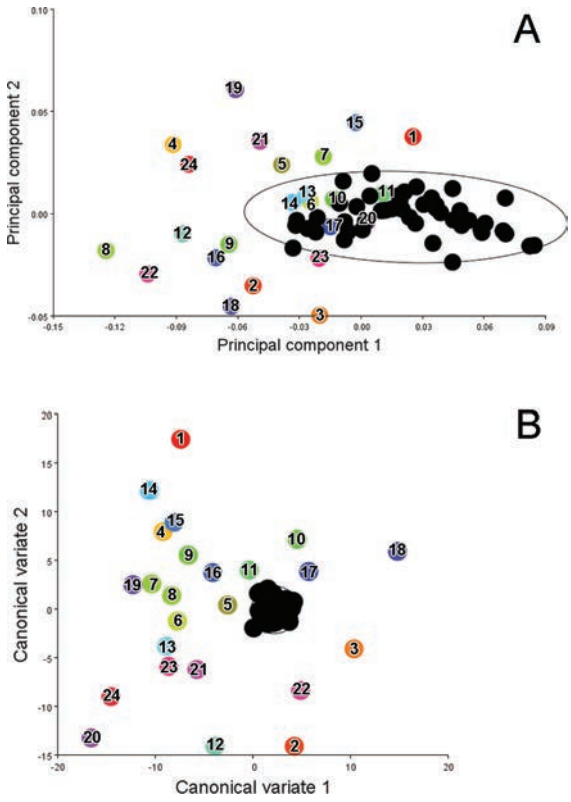

Figure 3. Scatter plots of GMM analysis. **A.** Scatter plots of PCA scores based on the data from apertural views of the *Diplommatina* species; **B.** Scatter plot of CVA of the geometric data. 1 *D. abbreviata*; 2 *D. confusa*; 3 *D. conica*; 4 *D. contracta*; 5 *D. cristata*; 6 *D. futilis*; 7 *D. hangchowensis hangchowensis*; 8 *D. hangchowensis granum*; 9 *D. inermis*; 10 *D. intermedia*; 11 *D. hunanensis*; 12 *D. paxillus* var. *robusta*; 13 *D. longipalatalis*; 14 *D. minuscula*; 15 *D. mucronata*; 16 *D. paxillus*; 17 *D. pupinella*; 18 *D. pyra*; 19 *D. rufa*; 20 *D. schmackeriana*; 21 *D. sculptilis*; 22 *D. setchuanensis*; 23 *D. subcylindrica*; 24 *D. triangulata*. Black dot is *D. yipingica*.

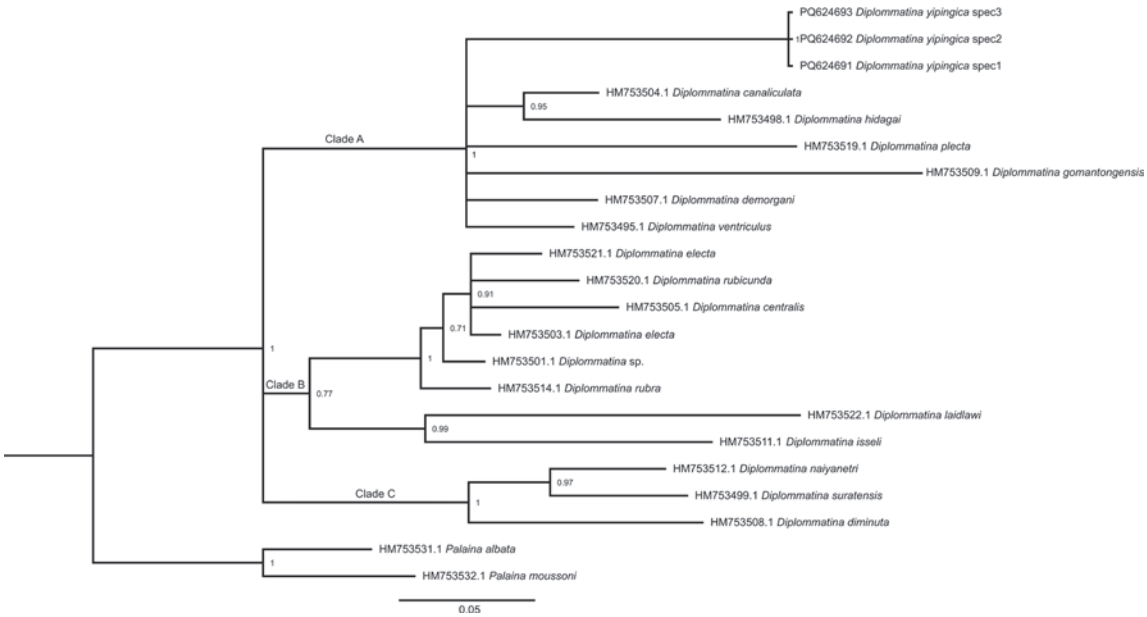

Figure 4. Bayesian Inference tree inferred from 16S gene sequences of *Diplommatina* and related genera.

Taxonomic part

Diplommatina abbreviata Heude, 1890

Diplommatina abbreviata Heude, 1890: 131, pl. 36, fig. 21. – Yen, 1939: 32, pl. 2, fig. 51.

Type material. ***Lectotype***, HMT 232a (Figs 5A, 12A), designated herein; six paralectotypes HMT 232b, paralectotype USNM 472301, 5 paralectotypes MCZ 167234.

Type locality. "Tchen-kou, Szechwan" [Chengkou, Chongqing City].

Brief description. Shell dextral, with about 6 whorls. Protoconch smooth. Penultimate whorl slightly expanded, body whorls nearly as wide. Constriction at slight right of parietal wall. No spiral striation visible. Teleoconch with thin, widely-spaced, radial ribs; with ca. 6 ribs per 0.5 mm on penultimate whorl and ca. 5 ribs per 0.5 mm on body whorls. Dorsal fold absent. Umbilicus closed. No double lip. Columellar tooth present. One long horizontal palatalis just above columella. One short vertical palatalis.

Remarks. The lectotype is designated herein in accordance with Art. 74 of the Code (ICZN 1999) for the stabilisation of the name. Johnson (1973) listed 'paratypes' housed in USNM and MZC.

Diplommatina (*Sinica*) *apicina* (Gredler, 1885)

Moussonia apicina Gredler, 1885: 229–231.

Diplommatina (*Sinica*) *apicina* – Kobelt & Möllendorff, 1898: 139; Kobelt, 1902: 455; Zilch, 1953: 25.

Diplommatina apicina – Yen 1939: 31, pl. 2, fig. 40.

Type material. Not seen.

Other material. Eight non-type specimens SMF 39624 (Figs 5B, 12B).

Type locality. "Ta-hung-tung, Thien-heu-san, Kueitschen" [Hunan Province], the current name of the locality cannot be confirmed.

Brief description. Shell dextral. 7 Whorls. Penultimate and body whorls nearly equal in width. Teleoconch with thin, widely spaced, radial ribs; with ca. 7 ribs per 0.5 mm on penultimate whorl and ca. 5 ribs per 0.5 mm on body whorls. Double lip present. Columellar tooth present. One horizontal palatalis above columella. No vertical palatalis visible.

Remarks. Kobelt and Möllendorff (1898) assigned this species to the subgenus *Sinica*. Yen (1939) and Zilch (1953) listed probable syntypes in the SMF; one figured by Yen (1939: pl. 2, fig. 40), However, discrepancies in the collection locality and collector in relation to the original description suggest that these specimens are non-type specimens. Further type specimens are likely kept in the Gredler collection in the Franziskanermuseum Bozen (see Zilch (1974)).

Diplommatina (*Sinica*) *confusa* Heude, 1885

Diplommatina confusa Heude, 1885: 97, pl. 24, figs 12, 12a. – Yen, 1948: 75.

Diplommatina (*Sinica*) *confusa* –Kobelt & Möllendorff, 1898: 140; Kobelt, 1902: 460.

Type material. ***Lectotype*** HMT 229a (Figs 5C, 12C), designated herein; 33 paralectotypes HMT 229b, paralectotype USNM 472304, nine paralectotypes MCZ 167034.

Type locality. "Tchen-K'eou" [Chengkou, Chongqing City].

Brief description. Shell dextral, with about 6 whorls. Protoconch smooth. Penultimate whorl slightly expanded, body whorls nearly as wide. Constriction at slightly right of parietal wall. No spiral striation visible. Teleoconch with thin, widely spaced, radial ribs, ca. 7 ribs per 0.5 mm on penultimate whorl, ca. 5 ribs per 0.5 mm on body whorl. Dorsal fold absent. Umbilicus closed. Double lip present. Columellar tooth present. One short horizontal palatalis just above columella. One vertical palatalis.

Remarks. The lectotype is designated herein in accordance with Art. 74 of the Code (ICZN 1999) for the stabilisation of the name. Johnson (1973) listed 'paratypes' housed in USNM and MZC. Kobelt and Möllendorff (1898) assigned this species to the subgenus *Sinica*. For HMT specimens, 33 specimens moved to *D.* (*S.*) *setchuanensis* by Dr. C.-C. Hwang, one specimen has been separated by Dr. C.-C. Hwang as form A (Figs 5D, 12D), another specimen as form B (Figs 5E, 12E). Both forms alleged to be distinct from *D. confusa*.

Diplommatina (*Sinica*) *conica* Möllendorff, 1885

Diplommatina conica Möllendorff, 1885: 163–164. – Yen, 1939: 31, pl. 2, fig. 43.

Diplommatina (*Sinica*) *conica* – Kobelt & Möllendorff, 1898: 140; Kobelt, 1902: 460; Zilch, 1953: 28.

Type material. ***Lectotype*** SMF 39646 (Figs 5F, 12F); six paralectotypes SMF 39647, three paralectotypes SMF 39658.

Type locality. "Patung, Hupei" [Badong, Hubei Province].

Brief description. Shell dextral, with about 7 whorls. Penultimate whorl slightly expanded, body whorl nearly as wide. Constriction at middle of parietal wall. No spiral striation visible. Teleoconch with strong, dense, radial ribs; ca. 7 ribs per 0.5 mm on both penultimate and body whorls. Dorsal fold absent. Umbilicus absent. Double lip present. Columellar tooth present. One short horizontal palatalis just above columella. One vertical palatalis.

Remarks. Yen (1939) designated and figured the lectotype (SMF 39646). Kobelt and Möllendorff (1898) assigned this species to the subgenus *Sinica*.

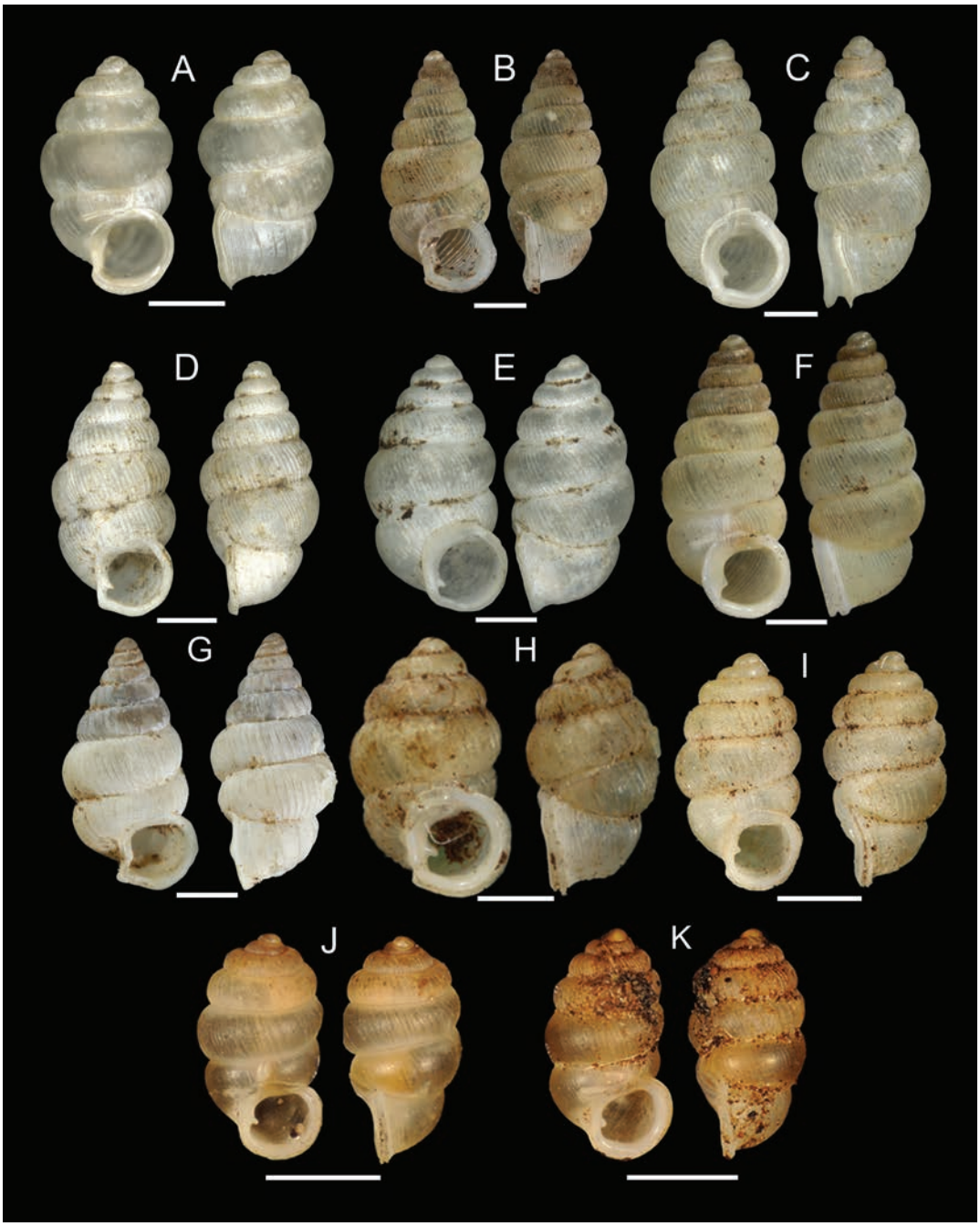

Figure 5. A. Lectotype of *D.* (*Sinica*) *abbreviata* HMT 232a; **B.** Non-type specimen of *D.* (*Sinica*) *apicina* SMF 39624; **C.** Lectotype of *D.* (*Sinica*) *confusa* HMT 229a; **D.** Paralectotype of *D.* (*Sinica*) *confusa* HMT 229, non-*confusa* "form A"; **E.** Paralectotype of *D.* (*Sinica*) *confusa* HMT 229, non-*confusa* "form B"; **F.** Lectotype of *D. conica*, SMF39646; **G.** Non-type specimen of *D. consularis* SMF 39625; **H.** *D.* (*Sinica*) *contracta*, SMF 39649; **I.** Paratype of *D.* (*Sinica*) *futilis*, SMF 39627; **J.** *D.* (*Sinica*) *hangchowensis* ANSP94748; **K.** Holotype of *D. hangchowensis granum*, ANSP94747. Scale bar: 1 mm.

Diplommatina (*Sinica*) *consularis* Gredler, 1886

Diplommatina consularis Gredler, 1886: 13–15. – Yen, 1939: 31, pl. 2, fig. 41.
Diplommatina (*Sinica*) *consularis* – Kobelt & Möllendorff, 1898: 140; Kobelt, 1902: 461; Zilch, 1953: 28.

Type material. 12 syntypes FMB37

Other material. Three non-type specimens SMF 39625 **(**Figs 5G, 12G**)**.

Type locality. "Peshang, Hunan" [Hunan Province]; the current name of the locality cannot be confirmed.

Brief description. Shell dextral, with about 7 whorls. Penultimate whorl slightly expanded, body whorl nearly as wide. Teleoconch with thin, widely spaced, radial ribs; with ca. 6 ribs per 0.5 mm on penultimate whorl and ca. 5 ribs per 0.5 mm on body whorls. No double lip. Columellar tooth present. One short horizontal palatalis above columella. No vertical palatalis visible.

Remarks. Zilch (1953) listed syntypes in the SMF, one of which was figured earlier by Yen (1939). Nevertheless, discrepancies in the collection locality in relation to the original description suggest that these specimens are

non-type specimens. Further type specimens are likely kept in the Gredler collection in the Franziskanermuseum Bozen (see Zilch (1974)). Kobelt and Möllendorff (1898) assigned this species to the subgenus *Sinica*.

Diplommatina (*Sinica*) *contracta* Möllendorff, 1886

Diplommatina contracta Möllendorff, 1886: 173–175. – Yen, 1939: 32, pl. 2, fig. 53.
Diplommatina (*Sinica*) *contracta* – Kobelt & Möllendorff, 1898: 140; Kobelt, 1902: 461; Zilch, 1953: 28.

Type material. ***Lectotype*** SMF 39649 (Figs 5H, 12H); three paralectotypes SMF 39650.

Type locality. "Patung, Hupei" [Badong, Hubei Province].

Brief description. Shell dextral, with about 6 whorls. Penultimate whorl slightly expanded, body whorl nearly as wide. No spiral striation visible. Teleoconch with strong, widely-spaced, radial ribs; ca. 5 ribs per 0.5 mm on penultimate whorl, ca. 3 ribs per 0.5 mm on body whorl. Dorsal fold absent. Umbilicus unknown. Double lip present. Columellar tooth present. No horizontal nor vertical palatalis visible.

Remarks. Yen (1939) designated and depicted the lectotype. Kobelt and Möllendorff (1898) assigned this species to the subgenus *Sinica*.

Diplommatina (*Sinica*) *cristata* Gredler, 1887

Diplommatina cristata Gredler, 1887: 367–368.
Diplommatina (*Sinica*) *cristata* – Kobelt & Möllendorff, 1898: 140; Kobelt, 1902: 461.

Type material. Five syntypes FMB39.

Type locality. "Hupé" [Hubei Province].

Remarks. Kobelt and Möllendorff (1898) assigned this species to the subgenus *Sinica*. We did not examine the types, hence, no diagnosis is provided.

Diplommatina (*Sinica*) *futilis* Gredler, 1887

Diplommatina futilis Gredler, 1887: 368–369. – Yen, 1939: 32, pl. 2, fig. 52.
Diplommatina (*Sinica*) *futilis* – Kobelt & Möllendorff, 1898: 140; Kobelt, 1902: 464.

Type material. Four syntypes SMF 39627 (Figs 5I, 12I). 16 syntypes FMB 65.

Type locality. "Hupé" [Hubei Province].

Brief description. Shell dextral, with about 6 whorls. Penultimate whorl slightly expanded; body whorl nearly as wide. No spiral striation visible. Teleoconch with weak, densely-spaced, radial ribs; ca. 8 ribs per 0.5 mm on penultimate whorl. Dorsal fold absent. Umbilicus unknown. Double lip present. Columellar tooth present. One horizontal palatalis above columella. No vertical palatalis visible.

Remarks. Yen (1939) listed four 'paratypes' in the SMF and figured one; referred to as 'cotypes' by Zilch (1953). Sixteen type specimens are kept in the Gredler collection in the Franziskanermuseum Bozen (see Zilch (1974)). Kobelt and Möllendorff (1898) assigned this species to the subgenus *Sinica*.

Diplommatina hangchowensis hangchowensis Pilsbry & Hirase, 1908

Diplommatina hangochowensis Pilsbry & Hirase, 1908: 37–38, fig. 1.

Type material. ***Lectotype*** ANSP 94748 (Figs 5J, 12J), 1 paralectotype ANSP 360072.

Type locality. "Hangchow, Che-kiang" [Hangzhou City, Zhejiang Province].

Brief description. Shell dextral, with about 6 whorls. Penultimate whorl slightly expanded; body whorl nearly as wide. Constriction at the middle of the parietal wall. Teleoconch with weak, widely-spaced, radial ribs; ca. 7–9 ribs per 0.5 mm on penultimate whorl. Dorsal fold absent. Umbilicus unknown. Double lip present. Columellar tooth present. One horizontal palatalis just above the columella. One vertical palatalis.

Remarks. The lectotype was designated by Baker (1964: 164) by reference to a single type specimen (Art. 74.5 of the Code). We treat *Diplommatina hangochowensis granum* as the junior synonym.

Diplommatina hangchowensis granum Pilsbry & Hirase, 1908

Diplommatina hangochowensis granum Pilsbry & Hirase, 1908: 37–38

Type material. ***Lectotype*** ANSP 94747 (Figs 5K, 12K).

Type locality. "Hangchow" [Hangzhou City, Zhejiang Province].

Remarks. The lectotype was designated by Baker (1964: 164) by reference to a single type specimen (Art. 74.5 of the Code). This taxon is a junior homonym of *Diplommatina granum* Bavay & Dautzenberg, 1904 and, therefore, permanently invalid. We consider it to be a junior synonym of *D. hangochowensis* described from the same type locality. Therefore, we refrain from introducing a replacement name.

Diplommatina (*Sinica*) *inermis* Gredler, 1887

Diplommatina inermis Gredler, 1887: 336.
Diplommatina (*Sinica*) *inermis* – Kobelt & Möllendorff, 1898: 140; Kobelt, 1902: 465.

Type material. Five syntypes FMB 92.

Type locality. "Pa-tong" [Badong, Hubei Province].

Remarks. The type collection of Gredler is in the Franziskanermuseum in Bozen (Zilch 1974). Kobelt and Möllendorff (1898) assigned this species to the subgenus *Sinica*. We did not examine the types, hence, no diagnosis is provided.

Diplommatina intermedia Heude, 1890

Diplommatina intermedia Heude, 1890: 131, pl. 36, fig. 22.

Type material. ***Lectotype*** HMT 233a (Figs 6A, 12L), designated herein; 11 paralectotypes HMT 233b; two paralectotypes MCZ 167031.

Type locality. "Tchen-kou, Szechwan" [Chengkou, Chongqing City].

Brief description. Shell dextral, with about 6 whorls. Protoconch smooth. Penultimate whorl slightly expanded; body whorl nearly as wide. Constriction at slightly left of parietal wall. No spiral striation visible. Teleoconch with thin, dense, radial ribs; ca. 6 ribs per 0.5 mm on penultimate whorl, ca. 4 ribs per 0.5 mm on body whorl. Dorsal fold absent. Umbilicus open, shallow. Double lip present. Columellar tooth present. One short horizontal palatalis above columella. One vertical palatalis.

Remarks. The lectotype is designated herein in accordance with Art. 74 of the Code (ICZN 1999) for the stabilisation of the name. *Diplommatina intermedia* Nicolas, 1891 and *D. balansai* var. *intermedia* Bavay & Dautzenberg, 1904 are both junior homonyms.

Diplommatina liboensis Ran, Chen & Zhang, 1999

Diplommatina liboensis Ran, Chen & Zhang, 1999: 281, fig. 1.

Type material. ***Holotype*** IZCAS TM136833 (Figs 6B, 12M), 72 paratypes IZCAS TM101985-102056.

Other material. Non-type specimens IZCAS TM136834-136926.

Type locality. Libo County, Guizhou Province.

Brief description. Shell dextral, with about 7.5 whorls. Protoconch smooth. Penultimate whorl slightly expanded; body whorl nearly as wide. Teleoconch with thin, dense, radial ribs; ca. 5 ribs per 0.5 mm on penultimate whorl, ca. 4 ribs per 0.5 mm on body whorl. Double lip present. Columellar tooth absent. No horizontal palatalis nor vertical palatalis visible.

Remarks. The specimens TM136834-136926, the date of collection and the number of specimens, inconsistent with the original description, are confirmed as non-type specimens.

Diplommatina longxianensis Chen, Liu, Xu &Yan, 1994

Diplommatina longxianensis Chen, Liu, Xu &Yan, 1994:44, fig. 1.

Type material. ***Holotype*** IZCAS TM010064 (Figs 6C, 12N), 29 paratypes IZCASTM010065-010093.

Type locality. Longxian County, Shaanxi Province.

Brief description. Shell dextral, with about 6.5 whorls. Protoconch smooth. Penultimate whorl slightly expanded; body whorl nearly as wide. Teleoconch with thin, dense, radial ribs; ca. 7 ribs per 0.5 mm on penultimate whorl, ca. 6 ribs per 0.5 mm on body whorl. No double lip. Columellar tooth present. No horizontal palatalis nor vertical palatalis visible.

Remarks. The original literature mentions 26 paratypes (Chen et al. 1994). Nonetheless, 29 specimens were deposited together that correspond to the collection's locality and time mentioned in literature, indicating that the correct number of paratypes should be 29 (ICZN Art 72.4.1).

Diplommatina mangshanensis Hu, Yin & Chen, 2003

Diplommatina mangshanensis Hu, Yin & Chen, 2003: 232–234, figs 1, 2.

Type material. ***Holotype*** IZCAS CT-001 (Figs 6D, 12O), two paratypes CT-002, five paratypes CT-003.

Type locality. Mangshan, Hunan Province.

Brief description. Shell dextral, with about 5.5 whorls. Protoconch smooth. Penultimate whorl slightly expanded, body whorls nearly as wide. Teleoconch with thin, widely spaced, radial ribs; with ca. 8 ribs per 0.5 mm on penultimate whorl and ca. 7 ribs per 0.5 mm on body whorls. Double lip present. Columellar tooth present. One long horizontal palatalis just above columella. One short vertical palatalis.

Remarks. Five paratypes (CT-003) are juveniles.

Diplommatina minuscula Heude, 1890

Diplommatina minuscula Heude, 1890: 131, pl. 36, fig. 20.

Type material. ***Lectotype***, HMT 234a (Figs 6E 12P), designated herein; two paralectotypes HMT 234b, two paralectotypes MCZ 167032.

Type locality. "Tchen-kou, Szechwan" [Chengkou, Chongqing City].

Brief description. Shell dextral, with about 6–6.5 whorls. Protoconch smooth. Penultimate whorl slightly expanded; body whorl nearly equal in width. Constriction at middle of parietal wall. No spiral striation visible. Teleoconch with strong, widely-spaced, radial ribs; ca. 6–8 ribs per 0.5 mm on both penultimate and body whorls. Dorsal fold absent. Umbilicus closed. Double lip present. Columellar tooth present. One short horizontal palatalis just above columella. One short vertical palatalis.

Remarks. The lectotype is designated herein in accordance with Art. 74 of the Code (ICZN 1999) for the stabilisation of the name. Johnson listed 'paratypes' housed in the MCZ. *Diplommatina minuscula* Chen & Zhang, 1998 is a junior homonym and, therefore, the name is permanently invalid. A replacement name *Diplommatina yunnanensis* is proposed below (ICZN Art 34.2).

Diplommatina (*Sinica*) *paxillus paxillus* (Gredler, 1881)

Moussonia paxillus Gredler, 1881: 29–31, pl. 1, fig. 7.

Diplommatina (*Sinica*) *paxillus* – Schmacker & Boettger, 1890: 121; Kobelt & Möllendorff, 1898: 141; Kobelt, 1902: 469; Zilch, 1953: 34.

Diplommatina paxillus paxillus – Yen, 1939: 31, pl. 2, fig. 46.

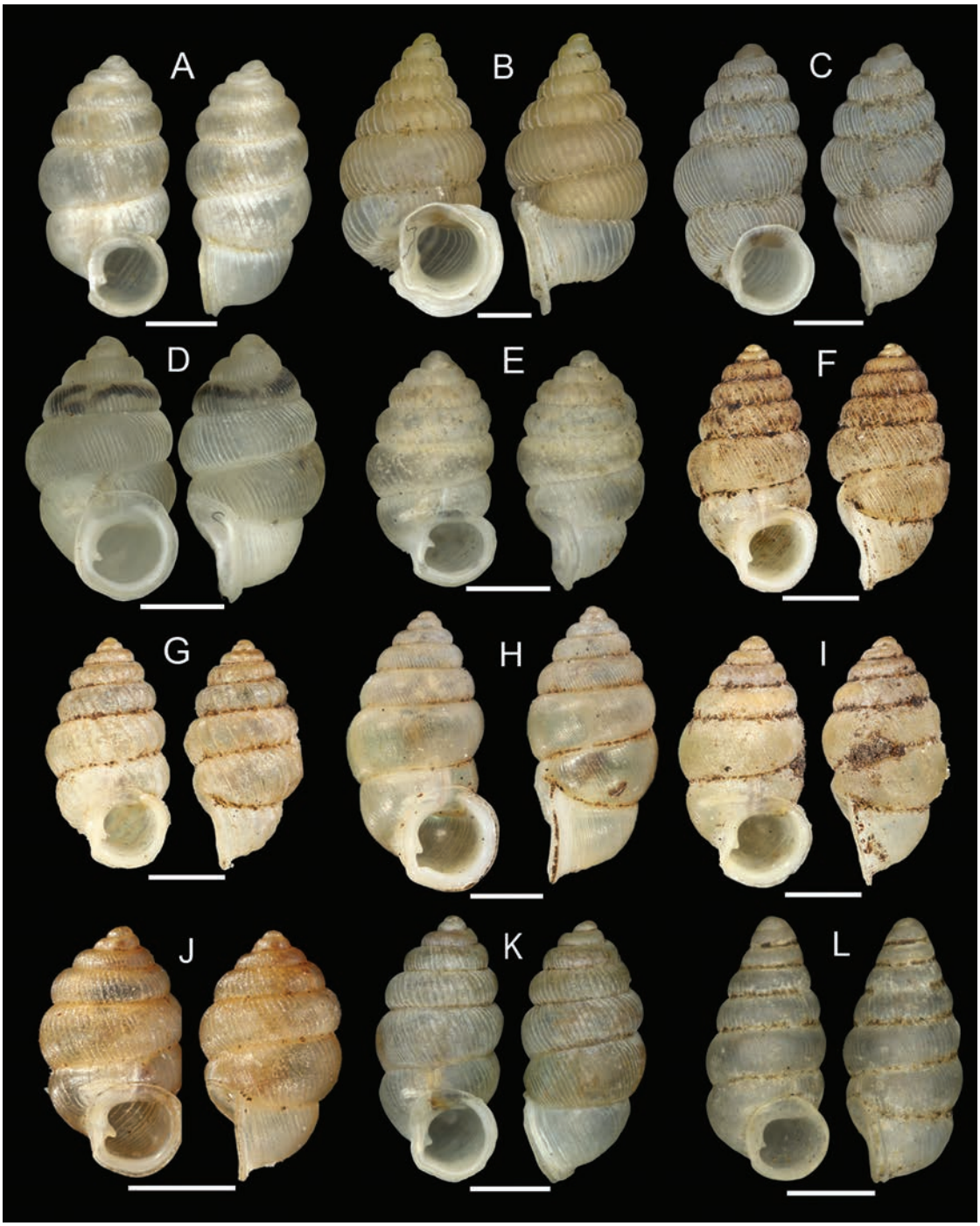

Figure 6. A. Lectotype of *D.* (*Sinica*) *intermedia* HMT 233a; **B.** Holotype of *D. liboensis* IZCAS TM136833; **C.** Holotype of *D. longxianensis* IZCAS TM010064; **D.** Holotype of *D. mangshanensis* IZCAS CT-001; **E.** Lectotype of *D.* (*Sinica*) *minuscula* HMT 234a; **F.** Paratype of *D. paxillus*, SMF39629; **G.** Paratype of *D. paxillus hunanensis*, SMF39641; **H.** Lectotype of *D. paxillis robusta* SMF39642; **I.** Lectotype of *D. paxillus longipalatalis*, SMF39639; **J.** Lectotype of *D. mucronata*, SMF39662; **K.** Paratype of *D.* (*Sinica*) *pupinella*, HMT 231a; **L.** Lectotype of *D.* (*Sinica*) *pyra* HMT 230a. Scale bar: 1 mm.

Type material. Seven syntypes SMF 39629 (Figs 6F, 12Q). Two syntypes FMB 142.

Type locality. "Yün-tscheu-fu" [Hunan Province]; the current name of the locality cannot be confirmed.

Brief description. Shell dextral, with about 7 whorls. Protoconch smooth. Penultimate whorl wider than body whorl. Constriction at middle of parietal wall. Teleoconch with weak, dense, radial ribs; ca. 10 ribs per 0.5 mm on penultimate whorl, ca. 7 ribs per 0.5 mm on body whorl. Dorsal fold absent. Umbilicus unknown. Double lip present. Columellar tooth present. One strong horizontal palatalis just above columella. One short vertical palatalis.

Remarks. Yen (1939) listed 'paratypes' in the SMF and figured one; referred to as 'cotypes' by Zilch (1953). Two type specimens are kept in the Gredler collection in the Franziskanermuseum Bozen (see Zilch (1974)). Kobelt and Möllendorff (1898) assigned this species to the subgenus *Sinica*.

Diplommatina (*Sinica*) *paxillus hunanensis* Zilch, 1953

Diplommatina paxillus var. *latecostata* Gredler, 1887: 157.
Diplommatina (*Sinica*) *paxillus* var. *latecostata* – Kobelt & Möllendorff, 1898: 141; Kobelt, 1902: 469.
Diplommatina paxillus latecostata – Yen, 1939: 32, pl. 2, fig. 49.
Diplommatina (*Sinica*) *paxillus hunanensis* Zilch, 1953: 34.

Type material. Seven syntypes SMF 39641(Figs 6G, 12R).

Type locality. "Hunan" [Hunan Province].

Brief description. Shell dextral, with about 6 whorls. Protoconch smooth. Penultimate whorl wider than body whorl. Constriction at middle of parietal wall. Teleoconch with strong, widely spaced, radial ribs; about 3 ribs per 0.5 mm on both penultimate and body whorl. Dorsal fold absent. Umbilicus unknown. Double lip present. Columellar tooth present. One vertical palatalis. No horizontal visible.

Remarks. Yen (1939) listed and figured one 'paratype' in the SMF. Zilch (1953) listed seven 'cotypes'. Further type specimens are likely kept in the Gredler collection in the Franziskanermuseum Bozen (see Zilch (1974)). The original name is an objective junior synonym of *Diplommatina latecostata* Mousson, 1870 and, therefore, permanently invalid. Zilch (1953) introduced *Diplommatina paxillus* var. *hunanensis* as a replacement name.

Diplommatina (*Sinica*) *paxillus lissa* (Gredler, 1884)

Moussonia paxillus var. *lissa* Gredler, 1884: 260.
Diplommatina paxillus var. *lissa* – Gredler, 1887: 157.
Diplommatina (*Sinica*) *paxillus* var. *lissa* – Kobelt & Möllendorff, 1898: 141; Kobelt, 1902: 470.
Diplommiatina paxillus lissa – Yen, 1939: 31, pl. 2, fig. 47.

Type material. Four syntypes FMB 110.

Type locality. "Shang-in Hisen" [Southern than Heng-Zhou Fu, Hunan Province].

Brief description. Shell dextral. Protoconch smooth, about 7 whorls. Penultimate whorl wider than the body whorl. Constriction at the centre-right of the parietal wall. Teleoconch with weak, dense, radial ribs. Dorsal fold absent. Umbilicus unknown. Double lips present. Columellar tooth presents. One nipple-formed tooth at the bottom of peristome. One horizontal palatalis just above the columella. No vertical palatalis visible.

Remarks. Yen (1939) listed several non-type lots housed in the SMF. *Diplommatina paxillus* var. *robusta* is a junior synonym (Yen 1939; Zilch 1953).

Diplommatina (*Sinica*) *paxillus robusta* Möllendorff, 1886

Diplommatina paxillus var. *robusta* Möllendorff, 1886: 174.

Type material. ***Lectotype*** SMF 39642 (Figs 6H, 12S); six paralectotypes SMF 39643 (from "Heng-shan-hsian and Heng-dshou-fu").

Typelocality. "Shang-in-shien, Hunan" [Hunan Province].

Remarks. Yen (1939) designated the lectotype and synonymised *D. paxillus* var. *robusta* with *D. paxillus* var. *lissa*. This treatment was followed by Zilch (1953) and is maintained herein.

Diplommatina (*Sinica*) *paxillus longipalatalis* Schmacker & Boettger, 1890

Diplommatina (*Sinica*) *paxillus* var. *longipalatalis* Schmacker & Boettger, 1890: 123. – Kobelt & Möllendorff, 1898: 141; Kobelt, 1902: 470; Zilch, 1953: 34.
Diplommatina paxillus longipalatalis – Yen, 1939: 32, pl. 2, fig. 48.

Type material. ***Lectotype*** SMF 39639 (Figs 6I, 12T); 4 paralectotypes SMF 39640.

Type locality. "Lüshan-Gebirge bei Kiukiang" [Lushan, Jiujiang City, Jiangxi Province].

Brief description. Shell dextral, with about 7 whorls. Protoconch smooth. Penultimate whorl wider than body whorl. Constriction at middle of parietal wall. Teleoconch with weak, dense, radial ribs. Dorsal fold absent. Umbilicus unknown. Double lip present. Columellar tooth present. One long, strong horizontal palatalis above columella. One short vertical palatalis.

Remarks. Yen (1939) designated and figured the lectotype.

Diplommatina (*Sinica*) *paxillus mucronata* Schmacker & Boettger, 1890

Diplommatina (*Sinica*) *paxillus* var. *mucronata* Schmacker & Boettger, 1890: 122. – Kobelt & Möllendorff, 1898: 141; Kobelt, 1902: 470; Zilch, 1953: 35.
Diplommatina paxillus mucronata – Yen, 1939: 32, pl. 2, fig. 50.

Type material. ***Lectotype*** SMF 39662 (Figs 6J, 12U); two paralectotypes SMF 39663.

Type locality. "Dalanshan-Gebirge bei Ningpo" [Dalanshan, Ningbo City].

Brief description. Shell dextral, with about 6 whorls. Protoconch smooth. Penultimate whorl wider than body whorl. Constriction at right of parietal wall. Teleoconch with weak, dense, radial ribs; ca. 8 ribs per 0.5 mm on penultimate whorl. Dorsal fold absent. Umbilicus unknown. Double lip absent. Columellar tooth present. One long, strong horizontal palatalis just above columella. One vertical palatalis.

Remarks. Yen (1939) designated and figured the lectotype.

Diplommatina (*Sinica*) *pupinella* Heude, 1885

Diplommatina pupinella Heude, 1885: 97, pl. 24, fig. 13.
Diplommatina (*Sinica*) *pupinella* – Kobelt & Möllendorff, 1898: 141; Kobelt, 1902: 470.

Type material. Lectotype, HMT 231a (Figs 6K, 12V), designated herein; seven paralectotypes HMT 231b, paralectotype USNM 472300, four paralectotypes MCZ 167030.

Type locality. "Tchen-k'eou" [Chengkou, Chongqing City].

Brief description. Shell dextral, with about 7 whorls. Protoconch smooth. Penultimate slightly expanded; body whorl nearly as wide. Constriction at slightly left of parietal wall. No spiral striation visible. Teleoconch with strong, dense, radial ribs; ca. 7 ribs per 0.5 mm on both penultimate and body whorls. Dorsal fold absent. Umbilicus open, shallow. Double lip present. Columellar tooth present. One short horizontal palatalis just above columella. One vertical palatalis.

Remarks. The lectotype is designated herein in accordance with Art. 74 of the Code (ICZN 1999) for the stabilisation of the name. Johnson (1973) listed 'paratypes' in USNM and MCZ. Kobelt and Möllendorff (1898) assigned this species to the subgenus *Sinica*.

Diplommatina (*Sinica*) *pyra* Heude, 1885

Diplommatina pyra Heude, 1885: 98, pl. 24, fig. 14.

Diplommatina (*Sinica*) *pyra* – Kobelt & Möllendorff, 1898: 141; Kobelt, 1902: 471.

Type material. Lectotype, HMT 230a (Figs 6L, 12W), designated herein; paralectotype MCZ 167219.

Type locality. "Tchen Keou tin" [Chengkou, Chongqing City].

Brief description. Shell dextral, with about 7 whorls. Protoconch smooth. Penultimate slightly expanded; body whorl nearly as wide. Constriction at middle of parietal wall. No spiral striation visible. Teleoconch with strong, dense, radial ribs; ca. 7 ribs per 0.5 mm on penultimate whorl, ca. 8 ribs per 0.5 mm on body whorl. Dorsal fold absent. Umbilicus open, shallow. Double lip present. Columellar tooth absent. One short horizontal palatalis just above columella. No vertical palatalis visible.

Remarks. The lectotype is designated herein in accordance with Art. 74 of the Code (ICZN 1999) for the stabilisation of the name. Johnson (1973) listed one 'paratype' in the MCZ. Kobelt and Möllendorff (1898) assigned this species to the subgenus *Sinica*.

Diplommatina qinghensis Chen, Zhang & Wang, 2002

Diplommatina qinghensis Chen, Zhang & Wang, 2002: 221–224, figs 3, 4.

Type material. ***Holotype*** IZCAS CT-014 (Figs 7A, 13A), four paratypes IZCAS CT-015, nine paratypes IZCAS CT-016.

Type locality. Kangxian, Longnan City, Gansu Province.

Brief description. Shell dextral, with about 5.5 whorls. Protoconch smooth. Penultimate whorl slightly expanded; body whorl nearly as wide. Teleoconch with thin, dense, radial ribs; ca. 10 ribs per 0.5 mm on penultimate whorl, ca. 8 ribs per 0.5 mm on body whorl. No double lip. Columellar tooth absent. No horizontal palatalis nor vertical palatalis visible.

Remarks. The holotype corresponds to the figure in the original description; however, the shell size is larger than that described in the original literature.

Diplommatina (*Sinica*) *rufa* Möllendorff, 1882

Diplommatina rufa Möllendorff, 1882: 350, pl. 10, fig. 8. – Yen, 1939: 32, pl. 2, fig. 54.

Diplommatina (*Sinica*) *rufa* Kobelt & Möllendorff, 1898: 141; Kobelt, 1902: 471; Zilch, 1953: 35.

Type material. ***Lectotype*** SMF 39665 (Figs 7B, 13B); four paralectotypes SMF 39666, three paralectotypes SMF 39667.

Type locality. "Lo-fou-shan, Kwangtung" [Luofushan, Huizhou City, Guangdong Province].

Brief description. Shell dextral, with about 5 whorls. Protoconch smooth. Penultimate whorl slightly wider than body whorl. Constriction at slightly right of parietal wall. Teleoconch smooth. Dorsal fold absent. Umbilicus unknown. Double lip present. Columellar tooth present. One horizontal palatalis just above columella. One vertical palatalis.

Remarks. Yen (1939) designated and depicted the lectoptype. Kobelt and Möllendorff (1898) assigned this species to the subgenus *Sinica*.

Diplommatina schmackeriana Yen, 1939

Diplommatina schmackeriana Yen, 1939: 33, pl. 2, fig. 55.

Type material. ***Lectotype*** SMF 40281(Figs 7C, 13C); two paratypes SMF 40282, paratype SMF 40283.

Type locality. "Mirsbay, Kwangtung" [Dapengwan, Hong Kong].

Brief description. Shell dextral, with about 6 whorls. Protoconch smooth. Penultimate whorl slightly wider than body whorl. Constriction at slightly left of parietal wall. Penultimate whorl and body whorl smooth. Dorsal fold absent. Umbilicus unknown. Double lip present. Columellar tooth present. One strong horizontal palatalis just above columella. One short vertical palatalis.

Remarks. The holotype has been figured by Yen (1939).

Diplommatina (*Sinica*) *sculptilis* Möllendorff, 1885

Diplommatina sculptilis Möllendorff, 1885: 368–370, pl. 9, fig. 5. – Yen, 1939: 31, pl. 2, fig. 44.

Diplommatina (*Sinica*) *sculptilis* – Kobelt & Möllendorff, 1898: 141; Kobelt, 1902: 472; Zilch, 1953: 36.

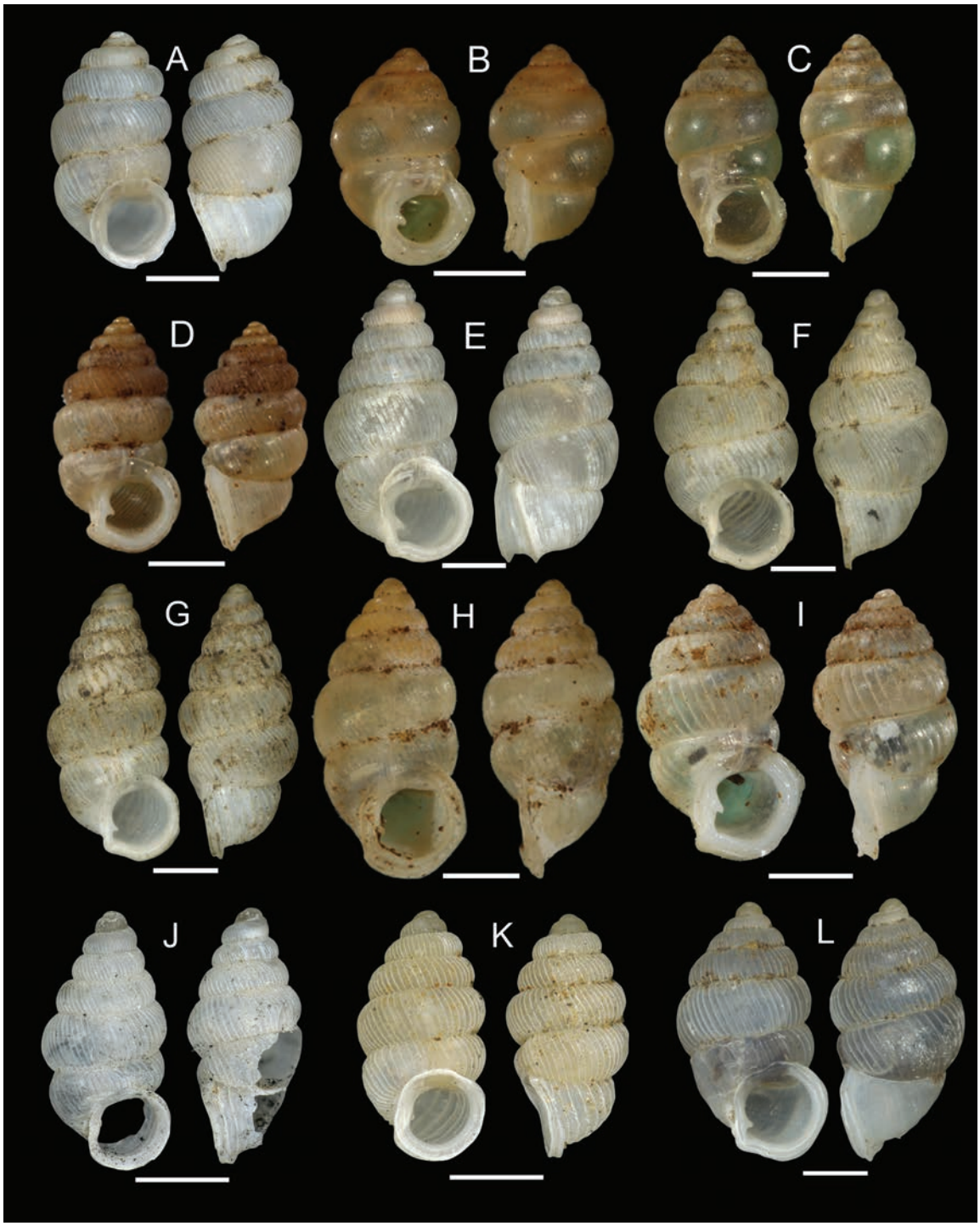

Figure 7. A. Holotype of *D. qinghensis* IZCAS CT-014; **B.** Lectotype of *D. rufa*, SMF39665; **C.** Holotype of *D. schmackeriana,* SMF40281; **D.** Lectotype of *D.* (*Sinica*) *sculptilis*, SMF 39655; **E.** Lectotype of *D.* (*Sinica*) *setchuanensis* HMT 228a; **F.** Paralectotype of *D.* (*Sinica*) *setchuanensis* HMT 228, non-*setchuanensis* form A; **G.** Paralectotype of *D.* (*Sinica*) *setchuanensis* HMT 228, non-*setchuanensis* form B; **H.** Holotype of *D. subcylindrica*, SMF39661; **I.** Holotype of *D. triangulata*, SMF39672; **J.** Holotype of *D. xiazayuensis* IZCAS TM1010000; **K.** Paratypes of *D. xiazayuensis* IZCAS TM010045 ; **L.** Holotype of *D. xingyinensis* IZCAS CT-022. Scale bar: 1 mm.

Type material. ***Lectotype*** SMF 39655 (Figs 7D, 13D); paralectotypes SMF 39656-39660, paralectotype ANSP 212197.

Type locality. "Shiu-hing, Guang-dung" [Zhaoqing City, Guangdong Province].

Brief description. Shell dextral, with about 7 whorls. Protoconch smooth. Penultimate whorl slightly wider than body whorl. Constriction at middle of parietal wall. Teleoconch with weak, dense, radial ribs; ca. 6 ribs per 0.5 mm on both penultimate and body whorls. Dorsal fold absent. Umbilicus unknown. Double lip present. Columellar tooth present. One strong horizontal palatalis just above columella. One short vertical palatalis.

Remarks. Yen (1939) designated and figured the lectotype. Kobelt and Möllendorff (1898) assigned this species to the subgenus *Sinica*.

Diplommatina (*Sinica*) *setchuanensis* Heude, 1885

Diplommatina setchuanensis Heude, 1885: 97, pl. 24, figs 10 and 10a-b.
Diplommatina (*Sinica*) *setchuanensis* – Kobelt & Möllendorff, 1898: 141; Kobelt, 1902: 471.

Type material. ***Lectotype*** HMT 228a (Figs 7E, 13E), designated herein; five paralectotypes HMT 228b, lot "A", 4 paralectotypes (see Remarks below) (Figs 7F, 13F), lot "B", 16 paralectotypes (see Remarks below) (Figs 7G, 13G); paralectotype USNM 472302, five paralectotypes MCZ 167226.

Typelocality. "Tchen-k'eou" [Chenkou, Chongqing City].

Brief description. Shell dextral, with about 7 whorls. Protoconch smooth. Penultimate whorl slightly expanded; body whorl nearly as wide. Constriction at slightly right of parietal wall. No spiral striation visible. Teleoconch with strong, dense, radial ribs; ca. 6 ribs per 0.5 mm on penultimate whorl, ca. 7 ribs per 0.5 mm on body whorl. Dorsal fold absent. Umbilicus closed. Double lip present. Columellar tooth present. No horizontal palatalis nor vertical palatalis visible.

Remarks. The lectotype is designated herein in accordance with Art. 74 of the Code (ICZN 1999) for the stabilisation of the name. Johnson listed 'paratypes' in USNM and MCZ. C.-C. Hwang studied the type series and separated two specimen lots A and B (see above) as representing different species.

Diplommatina szechuanensis Pilsbry, 1934

Diplommatina szechuanensis Pilsbry, 1934: 25, pl. 6, figs 1 and 1a.

Type material. ***Holotype*** ANSP 159705, paratypes ANSP 464794.

Typelocality. "Chengwai, Szechwan" [Sichuan Province].

Brief description. Shell dextral, with about 7 whorls. Protoconch smooth. Teleoconch with strong, dense, radial ribs, apart on the front of the penult whorl, 6 ribs per 0.5 mm on body whorl. The last whorl consists of a slightly oblique palatal rib at the constriction, a rather strong parietal lamella and the inward continuation of the columellar lamella.

Remarks. The holotype was originally designated by Pilsbry (1934) in the legend of plate 6 (p. 28). The types have been listed in the catalogue of Baker (1964: 165).

Diplommatina (*Sinica*) *subcylindrica* Möllendorff, 1882

Diplommatina subcylindrica Möllendorff, 1882: 349–350. – Yen, 1939: 31, pl. 2, fig. 42.
Diplommatina (*Sinica*) *subcylindrica* – Kobelt & Möllendorff, 1898: 142; Kobelt, 1902: 473; Zilch, 1953: 36.

Type material. ***Lectotype*** SMF 39661 (Figs 7H, 13H), designated by Yen (1939).

Type locality. Yang-hu, Fudshien. The current name of the locality cannot be confirmed.

Brief description. Shell dextral, with about 7 whorls. Protoconch smooth. Penultimate whorl slightly wider than body whorl. Constriction at middle of parietal wall. Teleoconch with weak, dense, radial ribs. Dorsal fold absent. Umbilicus unknown. Double lip present. Columellar tooth weak. One strong horizontal palatalis just above columella. One short vertical palatalis.

Remarks. A single type specimen is known to exist. It has been referred to as the holotype and was figured by Yen (1939). However, the original description does not contain a type designation nor does it specify the number of specimens on which it is based. Therefore, Yen's (1939) reference to the holotype is herein considered to constitute a lectotype designation in accordance with Art. 74.6 of the Code (ICZN 1999). Kobelt and Möllendorff (1898) assigned this species to the subgenus *Sinica*.

Diplommatina (*Sinica*) *tantilla* (Gould, 1859)

Paxillus tantillus Gould, 1859: 138.
Diplommatina (*Sinica*) *tantilla* – Kobelt & Möllendorff, 1898: 142; Kobelt, 1902: 475.
Diplommatina tantilla – Yen, 1939: 33, pl. 2, fig. 57.

Type material. Whereabouts unknown.

Type locality. Hong-Kong [China].

Remarks. Kobelt and Möllendorff (1898) assigned this species to the subgenus *Sinica*. Yen (1939) listed and figured non-type material in the SMF. We did not examine the types; hence, no diagnosis is provided.

Diplommatina triangulata Yen, 1939

Diplommatina triangulata Yen, 1939: 33, pl. 2, fig. 56.

Type material. ***Holotype*** SMF 39672 (Figs 7I, 13I).

Type locality. "Mang-hao, Yünnan" [Manghao, Yunnan Province].

Brief description. Shell dextral, with about 7 whorls. Protoconch smooth. Penultimate whorl expanded. Constriction at slightly right of parietal wall. Teleoconch with strong, widely-spaced, radial ribs; ca. 4 ribs per 0.5 mm on both penultimate and body whorls. Dorsal fold absent. Umbilicus unknown. Double lip present. Columellar tooth present. One strong horizontal palatalis just above columella. One short vertical palatalis.

Remarks. The holotype was figured by Yen (1939).

Diplommatina (*Sinica*) *xiazayuensis* Chen & Guo, 2001

Diplommatina xiazayuensis Chen & Guo, 2001:166–169, figs 4, 5.

Type locality. Zayu, Xizang Autonomous Region.

Type material. ***Holotype*** IZCAS TM1010000 (Figs 7J, 13J), 53 paratypes IZCAS TM010001-010053.

Brief description. Shell dextral, with about 6.5 whorls. Protoconch smooth. Penultimate whorl slightly expanded, body whorls nearly as wide. Teleoconch with thin, widely spaced, radial ribs; with ca. 8 ribs per 0.5 mm on penultimate whorl and ca. 7 ribs per 0.5 mm on body whorls. Double lip present. Columellar tooth present. No horizontal palatalis nor vertical palatalis visible.

Remarks. The holotype is broken; therefore, the paratype IZCAS TM010045 (Fig. 7K) was also photographed. In the original literature, there are a total of 37 paratypes. However, 53 specimens match the collection locality and time in the literature and were deposited together, suggesting that the paratypes should be 53. (ICZN Art 72.4.1).

Diplommatina xingyinensis Zhou, Chen & Li, 2005

Diplommatina xingyinensis Zhou, Chen & Li, 2005: 725–727, figs 1–4.

Type material. ***Holotype*** IZCAS CT-022 (Figs 7L, 13K), 31 paratypes IZCAS CT-019, six paratypes IZCAS CT-020, 13 paratypes IZCAS CT-021,one paratype IZCAS CT-019a.

Type locality. Xingyi City, Guizhou Province.

Brief description. Shell dextral, with about 6.5 whorls. Protoconch smooth. Penultimate whorl slightly expanded, body whorls nearly as wide. Teleoconch with thin, widely-spaced, radial ribs; with ca. 7 ribs per 0.5 mm on penultimate whorl and ca. 6 ribs per 0.5 mm on body whorls. Double lip present. Columellar tooth present. No horizontal palatalis nor vertical palatalis visible.

Remarks. The holotype was originally designated by Zhou, Chen & Li.

Diplommatina yunnanensis Zhang, Xie & Köhler, nom. nov.

Diplommatina minuscula Chen & Zhang, 1998: Vol 23, No 4, 347. fig. 2
Diplommatina yunnanensis Zhang, Xie & Köhler, nom. nov.

Type material. ***Holotype*** IZCAS TM009566 (Figs 8A, 13L), 24 paratypes IZCAS TM009547-009570, one paratype IZCAS 156036, one paratype IZCAS 155985, 138 paratypes IZCAS TM048307-048444.

Type locality. Mengla County, Yunnan

Brief description. Shell dextral, with about 7.5 whorls. Protoconch smooth. Penultimate whorl slightly expanded, body whorls nearly as wide. Teleoconch with strong, widely spaced, radial ribs; with ca. 6 ribs per 0.5 mm on penultimate whorl and ca. 5 ribs per 0.5 mm on body whorls. Double lip present. Columellar tooth absent. No horizontal palatalis nor vertical palatalis visible.

Remarks. The original spelling of the species name "*minusculus*" is incorrect. The name is an adjective and needs to be in the same gender as the genus name (ICZN Art 31.2). The correct name is '*minuscula*", which renders this taxon a junior homonym of *D. minuscula* Heude, 1890. Here, *D. yunnanensis* is introduced as a replacement name in accordance with Art 34.2 of the Code (ICZN 1999). The type material has been deposited with the NCMZ (Chen and Zhang 1998). The type locality is Xishaungbanna in Yunnan Province. In the original literature, there are a total of 138 paratypes. However, 164 specimens were deposited together and the collection locality and time in the literature were matched, suggesting that the paratypes should total 164 (ICZN Art 72.4.1).

Diplommatina yipingica Zhang, sp. nov.

https://zoobank.org/09B25CA7-C670-4A5E-BE86-20E33C4DA1BF

Material examined. ***Holotype*** SDNU.Gas.0337.01.001 (Figs 9, 13O); paratypes SDNU.Gas.0337.02 (Fig. 10) (coll. G. Zhang, 11 July 2018).

Type locality. Beijiushui, Laoshan, Qingdao City, Shandong Province, 36.205°N, 120.591°E, altitude 413 m a.s.l.

Description. Shell dextral, with about 5.5 whorls. Protoconch smooth, completely covered with small pits. Penultimate slightly expanded, body whorl nearly equal in width. Constriction at middle of parietal wall. No spiral striation visible. Teleoconch with strong, widely spaced, radial ribs; about 8–12 (9.8 ± 1.8) ribs per 0.5 mm on penultimate whorl, 5–9 (7.3 ± 1.9) ribs per 0.5 mm on body whorl. Dorsal fold absent. Umbilicus closed. Double lip absent. Columellar tooth present. Columellaris strong. One short horizontal palatalis just above columella. No vertical palatalis present. Shell with one palatalis and two parietalis; Prt1 shorter than Prt 2.

Diagnosis. Penultimate slightly expanded, body whorl nearly equal in width. Shell with one palatalis and three parietalis. Prt1 shorter than Prt 2.

Etymology. The name is derived from the Chinese word yiping [= yishengpingan], which means a fully peaceful and safe life.

Distribution. Known from type locality only.

Ecology. Lives in leaf litter. May climb up on plants after rain (Fig. 11).

Remarks. *Diplommatina yipingica* is similar to *Diplommatina pupinella*, *D. futilis*, *D. intermedia*, *D. paxillus longipalatalis*, *D. paxillus hunanensis*, *D. yunannensis* and *D. schmackeriana* in terms of general shell shape. (Fig. 3). *Diplommatina schmackeriana* differs in having a smooth shell. *Diplommatina paxillus hunanensis* has more widely-spaced ribs. *Diplommatina paxillus longipalatalis* has weaker ribs. Lip morphology differs from species with a double lip, such as *D. futilis*.

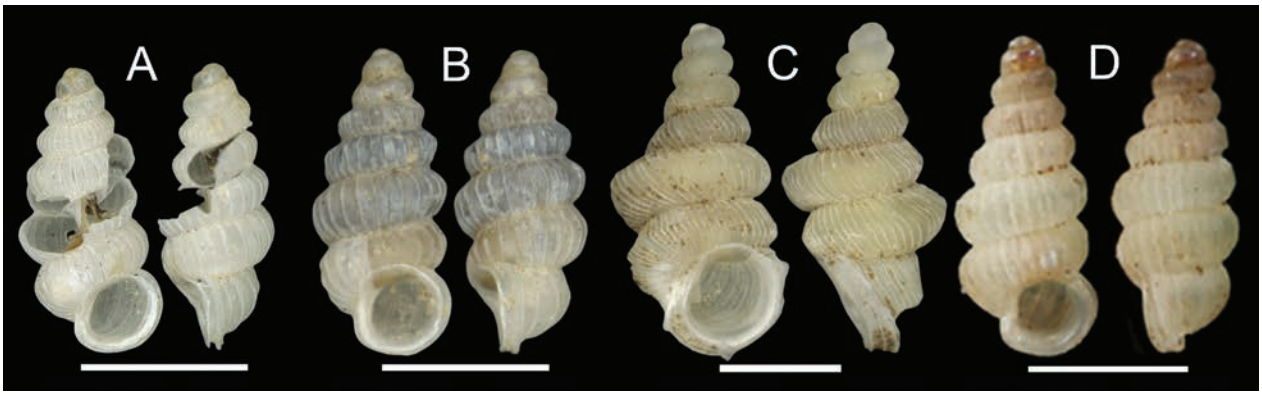

Figure 8. A. Holotype of *D. yunnanensis* IZCAS TM009566; **B.** Paratype of *D. yunnanensis* IZCAS TM009567; **C.** Holotype of *D. elbowforis* IZCAS TM008914; **D.** Lectotype of *D. herziana*, SMF39652. Scale bar = 1 mm.

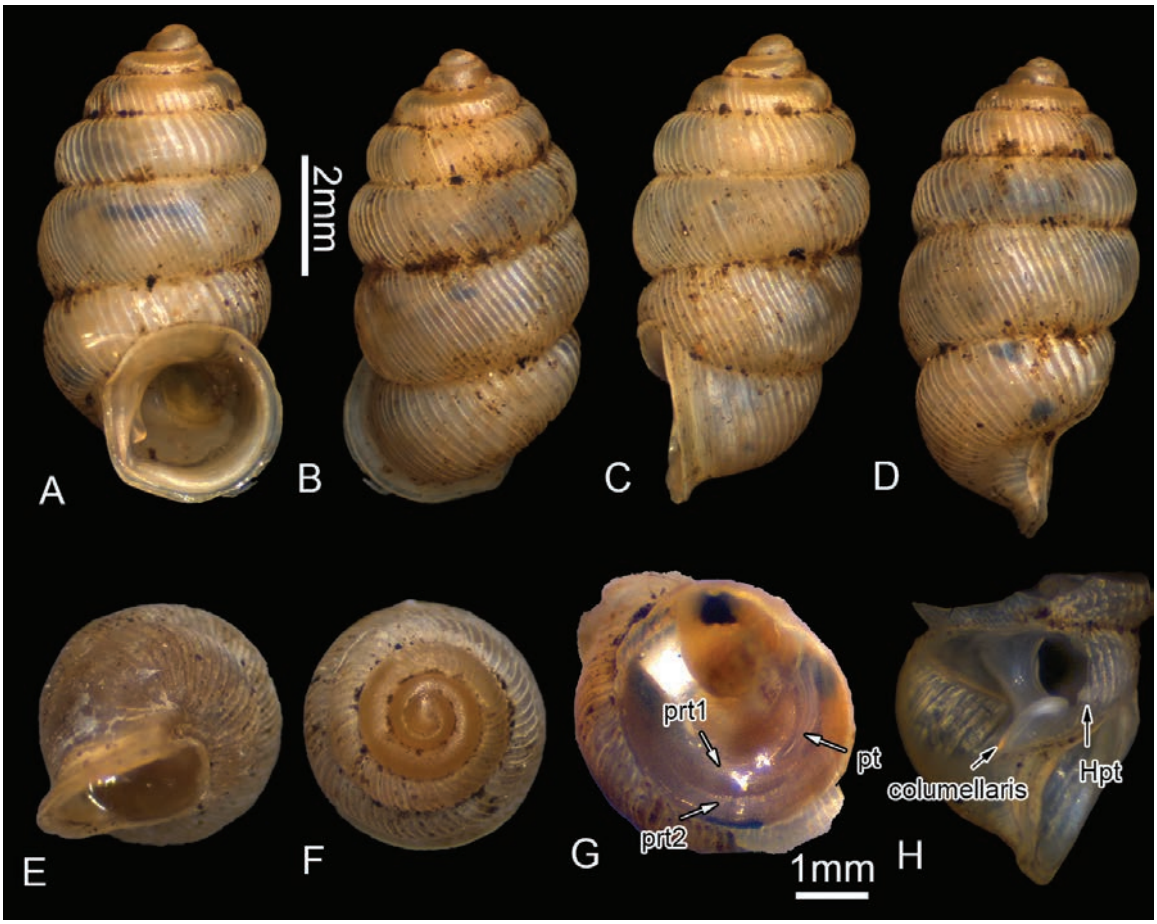

Figure 9. Type material of *Diplommatina yipingica* Zhang, sp. nov. **A–F.** Holotype of *D. yipingica* in apex, umbilicus, lateral, aperture and dorsal views. **G.** Palatalis and parietalis of new species; **F.** Columellaris of new species.

Additionally, the occurrence of *Diplommatina yipingica* is isolated far away from the known distributions of other congeners in China. The shell sizes of *D. kyobuntoensis* and *D. typosenica* from the Korean Peninsula are significantly smaller compared to the new species. In both of these species, the penultimate whorl is broader than the body whorl (Kuroda and Miyanaga 1939). Similarly, the Korean species *D. changensis* and *D. chejuensis* also exhibit a wider penultimate whorl compared to the body whorl and have more whorls than new species (Kwon & Lee, 1991).

Species with questionable genus assignment

Diplommatina (?) *elbowforis* Chen &Zhang, 1998

Diplommatina elbowforis Chen & Zhang, 1998: 348. fig. 3

Type material. ***Holotype*** IZCAS TM008914 (Figs 8C, 13M), 86 paratypes IZCAS TM008915-00900, 160 paratypes IZCAS 009001-009160, nine paratypes IZCAS 155987-155995.

Type locality. Mengla, Yunnan.

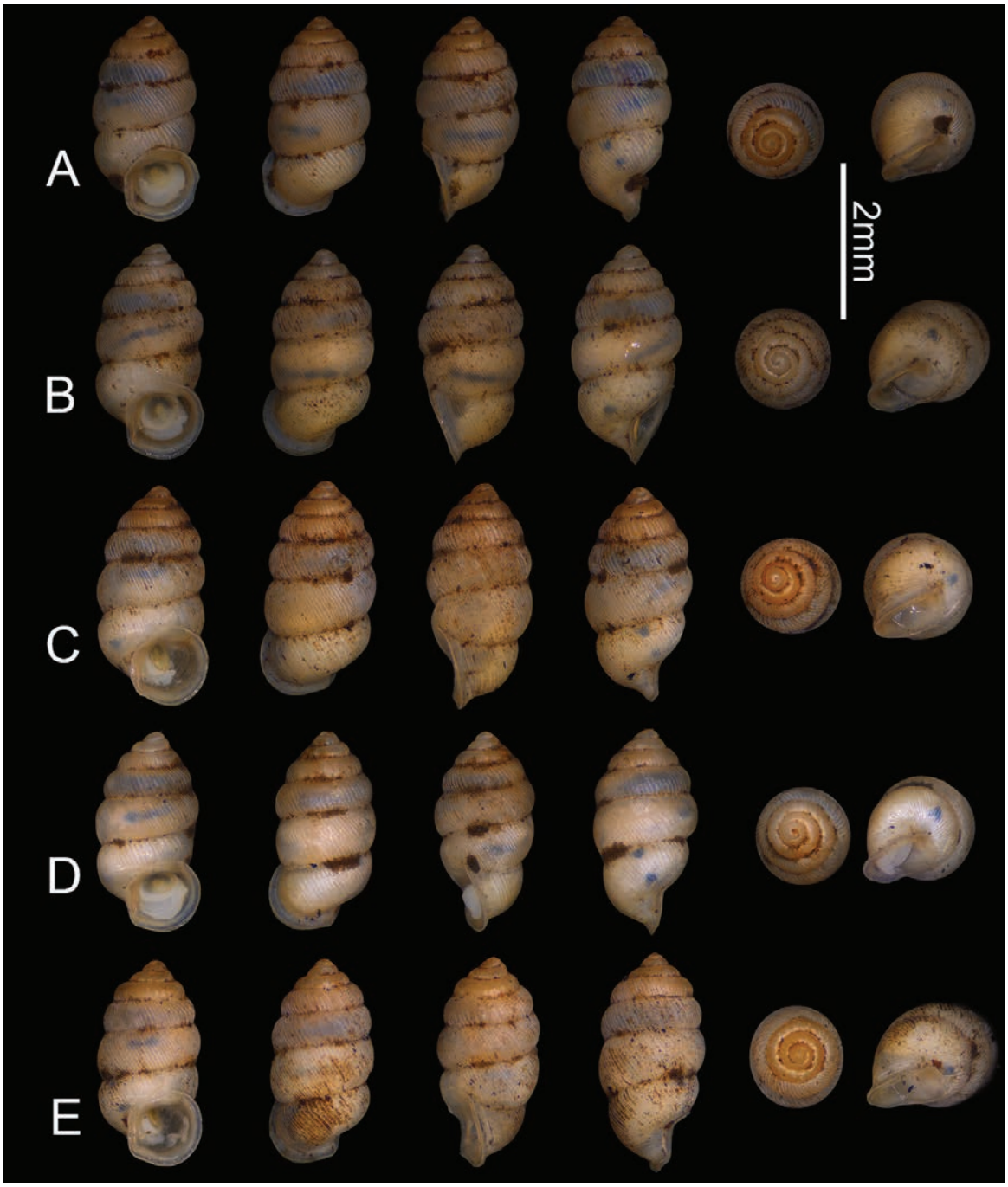

Figure 10. Paratypes of *Diplommatina yipingica* Zhang, sp. nov.

Brief description. Shell dextral, with about 7–7.5 whorls. Protoconch smooth. Penultimate whorl significantly expanded, slightly wider than body whorl. Teleoconch with strong, widely-spaced, radial ribs; with ca. 6 ribs per 0.5 mm on penultimate whorl and ca. 5 ribs per 0.5 mm on body whorls. Double lip present. Columellar tooth present. No horizontal palatalis nor vertical palatalis visible.

Remarks. In the original literature, 251 paratypes are mentioned. However, 255 specimens were deposited together and matched the collection locality and time in the literature, suggesting that the amount of the paratypes should be 255. (ICZN Art 72.4.1).

Figure 11. Living specimens of *Diplommatina yipingica.*

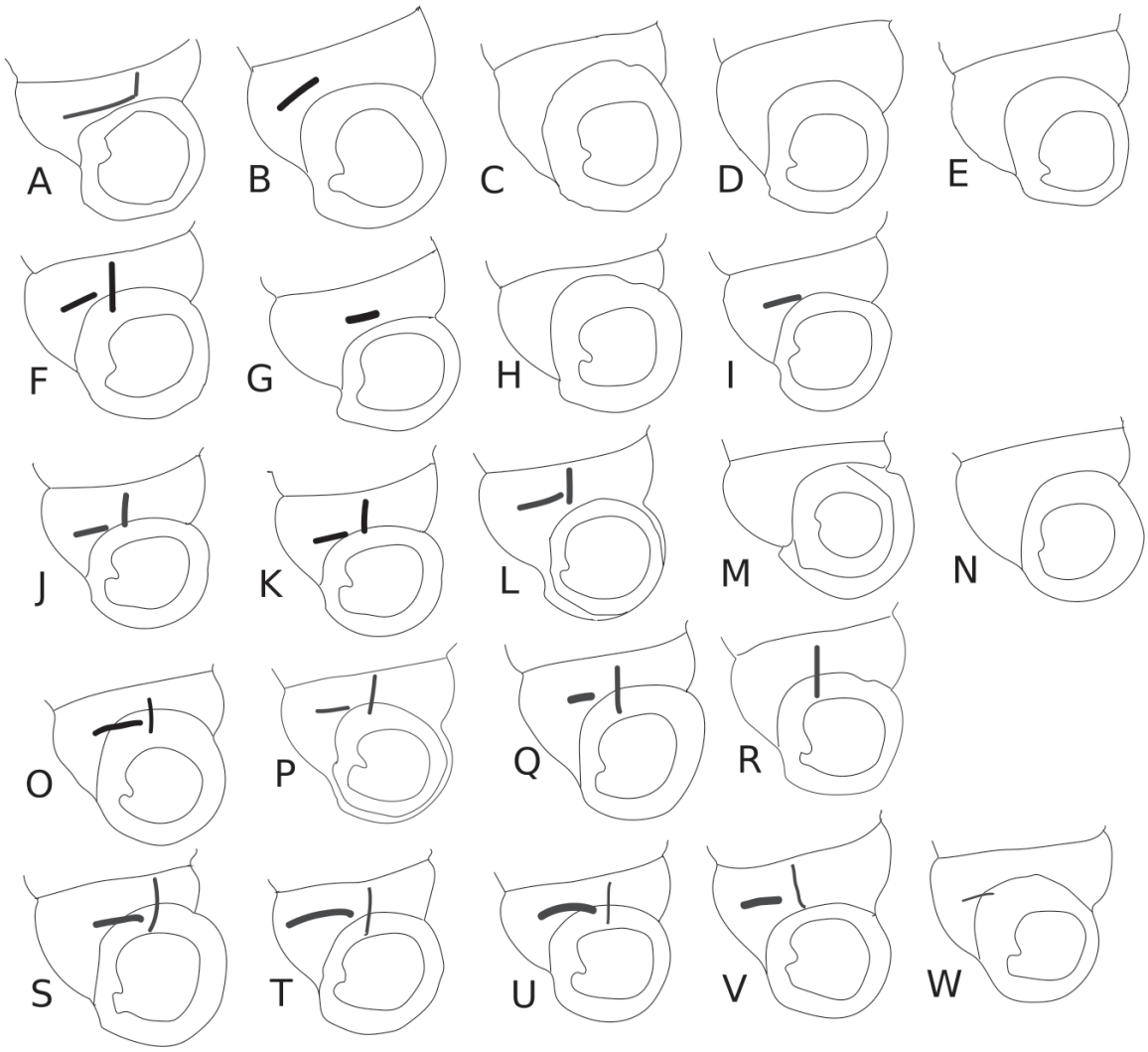

Figure 12. Parietalis of species of *Diplommatina*. **A.** *D.* (*Sinica*) *abbreviata*; **B.** *D.* (*Sinica*) *apicina*; **C.** *D.* (*Sinica*) *confusa*; **D.** *D.* (*Sinica*) *confusa*, not "form A"; **E.** *D.* (*Sinica*) *confusa*, not "form B"; **F.** Lectotype of *D. conica*; **G.** *D. consularis*; **H.** *D.* (*Sinica*) *contracta*; **I.** Paratype of *D.* (*Sinica*) *futilis*; **J.** *D.* (*Sinica*) *hangchowensis*; **K.** *D. hangchowensis granum*; **L.** *D.* (*Sinica*) *intermedia*; **M.** *D. liboensis*; **N.** *D. longxianensis*; **O.** *D. mangshanensis*; **P.** *D.* (*Sinica*) *minuscula*; **Q.** *D. paxillus*; **R.** *D. paxillus hunanensis*; **S.** *D. paxillis robusta*; **T.** *D. paxillus longipalatalis*; **U.** *D. mucronata*; **V.** *D.* (*Sinica*) *pupinella*; **W.** *D.* (*Sinica*) *pyra*.

Diplommatina (?) *herziana* Möllendorff, 1886

Diplommatina herziana Möllendorff, 1886: 176–177. – Yen, 1939: 31, pl. 2, fig. 45.

Diplommatina (*Eudiplommatina*) *herziana* – Kobelt & Möllendorff, 1898: 137.

Dipommatina (*Diplommatina*) *herziana* – Zilch, 1953: 20, pl. 8, fig. 127.

Type material. ***Lectotype*** SMF 39652 (Figs 8D, 13N); 30 paralectotypes SMF 39653, 38 paralectotypes SMF 39654.

Type locality. "Hainan" [Hainan Province].

Brief description. Shell dextral, with about 7 whorls. Penultimate and body whorls nearly equal in width. Constriction not visible. Teleoconch with strong, widely spaced, radial ribs; ca. 7 ribs per 0.5 mm on penultimate whorl, ca. 8 ribs per 0.5 mm on body whorl. Dorsal fold absent. Umbilicus unknown. Double lips present. Columellar tooth indistinct. No horizontal palatalis nor vertical palatalis visible.

Remarks. Yen (1939) designated and figured the lectotype (SMF 39652). Zilch (1953) placed this species in *Diplommatina* proper. This species probably is not a member of *Diplommatina*. The character descriptions are based on the original description of the species.

Diplommatina (?) *luodianensis* Luo, Chen & Zhou, 2008

Diplommatina luodianensis Luo, Chen & Zhou, 2008: 233–235, figs 1, 2.

Type material. Guizhou Normal University, not seen.

Type locality. Luodian, Dajin, Guizhou Province.

Brief description. Shell. Dextral. Protoconch smooth, about 7 whorls. Penultimate and body whorls nearly equal in width. Teleoconch with strong, widely-spaced radial ribs. Dorsal fold absent. Umbilicus small. Double lips present. Columellar tooth presents.

Remarks. No inner structures of *Diplommatina* can be seen. This species probably is not a member of

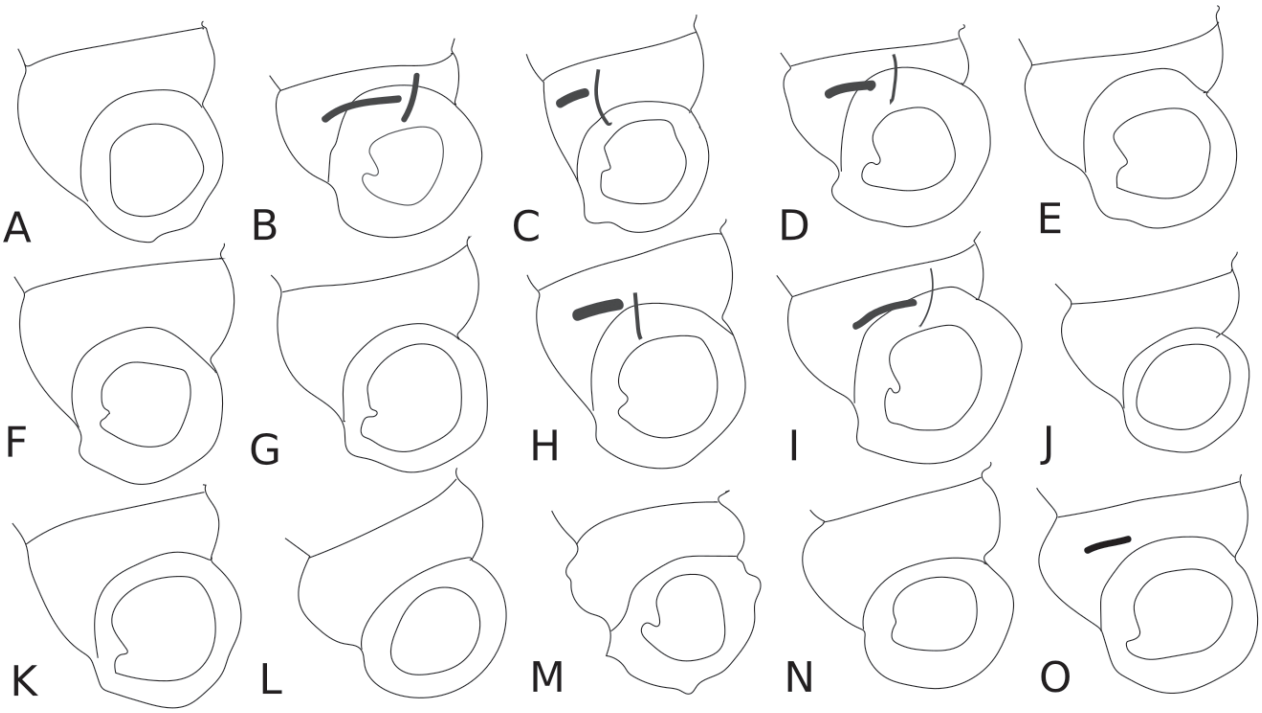

Figure 13. Parietalis of species of *Diplommatina*. **A.** *D. qinghensis*; **B.** *D. rufa*; **C.** *D. schmackeriana*; **D.** *D.* (*Sinica*) *sculptilis*; **E.** (*Sinica*) *setchuanensis*; **F.** *D.* (*Sinica*) *setchuanensis* HMT 228, not "form A"; **G.** *D.* (*Sinica*) *setchuanensis* HMT 228, not "form B"; **H.** *D. subcylindrica*; **I.** *D. triangulata*; **J.** *D. xiazayuensis*; **K.** *D. xingyinensis*; **L.** *D. yunnanensis*; **M.** *D. elbowforis*; **N.** *D. herziana*; **O.** *D. yipingica*.

Diplommatina. The character descriptions are based on the original literature for the species. The type specimens deposition in the main text, as stated in Guizhou Normal University, conflicts with the abstract that asserts this species was deposited at Guizhou Normal University and IZCAS.

Diplommatina (?) *xiaoqikongensis* Ran, Chen & Zhang, 1999

Diplommatina xiaoqikongensis Ran, Chen & Zhang, 1999: 282, fig. 2.

Type material. IZCAS, not seen.

Type locality. Libo County, Guizhou.

Remarks. The genus assignment remains tentative for the insufficient information provided in the original description.

Discussion

Both morphological and molecular evidence support the recognition of the new species *Diplommatina yipingica* in our sample set. However, this geometric morphometric analysis is based on only one individual per species, except for *Diplommatina yipingica*, which leads to insufficient statistical significance. Geometric morphometric methods are effective for analysing shell variation from a phenetic perspective and can improve the application of shell morphology in taxonomy. However, this approach requires substantial prior knowledge, because CVA can distinguish groups that PCA may not be able to (Dowle et al. 2015; Zhang and Wade. 2023). Previous studies on *Diplommatina* in China primarily rely on morphological characteristics and there are no molecular data available (Ran et al. 1999; Chen et al. 2001; Chen et al. 2002; Hu et al. 2003; Zhou et al. 2005; Luo et al. 2008). Subsequent studies should focus on more extensive sampling and utilise morphological and molecular evidence to revise *Diplommatina* in China. This can be done by integrating phylogenetics with morphology, verify traditional taxonomic characteristics and determining whether those characters are homoplasic or synapomorphic.

Acknowledgements

This study was funded by the National Natural Science Foundation of China (No. 32100349), National Students' innovation and entrepreneurship training programme (201910445019), Key project of Science-technology basic condition platform from the Ministry of Science and Technology of the People's Republic of China (No. 2005DKA21402). Special gratitude is due to Ronald Janssen, Julia Sigwart and Sigrid Hof (SMF), Paul Callomon (ANSP) and Daniel Lorenz (FMB) for help in obtaining information and photographs from type specimens under their care. We thank Junjie Qi and Xuyun Qiu for their assistance with collecting specimens.

References

Baker B (1964) Type land snails in the Academy of Natural Sciences of Philadelphia, Part III. Limnophile and thalassophile Pulmonata. Part IV. Land and fresh-water Prosobranchia. Proceedings of the Academy of Natural Sciences of Philadelphia 116: 149–193.

Bonfield JK, Beal KF, Betts MJ, Staden R (2002) Trev: a DNA trace editor and viewer Bioinformatics 18(1): 194–195. https://doi.org/10.1093/bioinformatics/18.1.194

Boonmachai T, Bergey EA, Nantarat N (2023) First record and description of three new species in the land snail genus *Diplommatina* Benson, 1849 (Caenogastropoda, Diplommatinidae) from Satun Province, Thailand. Zoosystematics and Evolution 99(1): 195–207. https://doi.org/10.3897/zse.99.99030

Budha PB, Naggs F, Backeljau T (2017) The genus *Diplommatina* Benson, 1849 (Gastropoda: Caenogastropoda: Diplommatinidae) in Nepal, with the description of seven new species. European Journal of Taxonomy 337: 1–30. https://doi.org/10.5852/ejt.2017.337

Castresana J (2000) Selection of conserved blocks from multiple alignments for their use in phylogenetic analysis. Molecular Biology and Evolution 17(4): 540–552. https://doi.org/10.1093/oxfordjournals.molbev.a026334

Chen D-N, Liu Y-H, Xu W-X, Yan Y-G (1994) Two new species of land snails from China (Prosobrachia; Mesogastropoda; Cyclophoridae). Sinzoologia 11: 43–46.

Chen D-N, Zhang G-Q (1998) Description on new species and zoogeographical analysis of the land mollusks from xishuangbanna and neighboring area, Yunnan province (Gastropoda: Prosobranchia: Archaeogastropda, Mesogastropod). Acta Zootaxonomica Sinica 23(4): 346–356.

Chen D-N, Zhang G-Q, Liu X-Y (2001) Two new species of land snails in Xizang Autonomous Region, China (Prosobranchia: Mesogastropoda: Cyclophoridae). Acta Zootaxonomica Sinica 26(2): 166–169.

Chen D-N, Zhang G-Q, Wang H-J. (2002) Two new species of land snails from Gansu Province, China (Prosobrachia; Mesogastropoda; Cyclophoridae). Acta Zootaxonomica Sinica 27(2): 221–224.

Dowle EJ, Morgan-Richards M, Brescia F, Trewick, SA (2015). Correlation between shell phenotype and local environment suggests a role for natural selection in the evolution of *Placostylus* snails. Molecular Ecology 24(16): 4205–4221. https://doi.org/10.1111/mec.13302

Egorov R (2013) Treasure of Russian shells Supplement 3. A review of the genera of the terrestrial pectinibranch molluscs Part III. Littoriniformes. Liareidae, Pupinidae, Diplommatinidae, Alycaeidae, Cochlostomidae. Colus Publications, Moscow, 61 pp.

Gould AA (1859) Descriptions of new species of shells brought home by the North Pacific Exploring Expedition. Proceedings of the Boston Society of Natural History 7: 138–142. https://doi.org/10.5962/bhl.part.4821

Gredler V (1881) Zur Conchylienfauna von China. II. Stück. Jahrbücher der Deutschen Malakozoologischen Gesellschaft 8: 10–33.

Gredler V (1884) Zur Conchylien-Fauna von China. VI. Stück. Archiv für Naturgeschichte 50: 257–280.

Gredler V (1885) Zur Conchylien-Fauna von China. VII. Stück. Jahrbücher der Deutschen Malakozoologischen Gesellschaft 12: 219–235.

Gredler V (1886) Zur Conchylien-Fauna von China. IX. Stück. Malakozoologische Blätter 9: 1–20.

Gredler V (1887a) Zur Conchylien-Fauna von China. X. Stück. Malakozoologische Blätter 9: 121–163.

Gredler V (1887b) Zur Conchylien-Fauna von China. XIII. Stück. Jahrbücher der Deutschen Malakozoologischen. Gesellschaft 14: 343–373.

Greke K (2017) Taxonomic review of Diplommatinidae (Caenogastropoda) from Wallacea and the Papuan region. In: Telnov D (Ed.) Biodiversity, biogeography and nature conservation in Wallacea and New Guinea. Vol. 3, 151–316. [pls 119–147]

Heude PM (1885) Notes sur les mollusques terrestres de la vallée du Fleuve Bleu. Mémoires concernant l'Histoire Naturelle de l'Empire Chinois 3: 88–132.

Heude PM (1890) Notes sur les mollusques terrestres de la vallée du Fleuve Bleu. Mémoires concernant l'Histoire Naturelle de l'Empire Chinois 4: 125–188.

Hu Z-Q, Yin H-Q, Chen D-N (2003) A new species of land snails from Mangshan, Hunan Province, China (Prosobranchia, Mesogastropoda, Cyclophoridae). Acta Zootaxonomica Sinica 28(2): 232–234.

Hwang C-C, Chang K-M, Tada A (2009) Two new species of the land snail genus *Diplommatina* (*Benigoma*) Kuroda, 1928 (Gastropoda: Diplommatinidae) from Taiwan. Bulletin of Malacology 33: 21–36.

International Commission on Zoological Nomenclature (1999) International Code of Zoological Nomenclature, 4th edn. International Trust for Zoological Nomenclature, London, xxix + 306 pp.

Johnson RI (1973) Heude's molluscan types of Asian land and fresh-water mollusks, mostly from the People's Republic of China, described by P.M. Heude. Special Occasional Publication No. 1 (MCZ Harvard University Cambridge Mass.), 111 pp. https://doi.org/10.5962/bhl.title.141074

Klingenberg CP (2011) MorphoJ: an integrated software package for geometric morphometrics. Molecular Ecology Resources 11: 353–357. https://doi.org/10.1111/j.1755-0998.2010.02924.x

Kobelt W (1902) Das Tierreich. Eine Zusammenstellung und Kennzeichnung der rezenten Tierformen. 16. Lieferung. Mollusca. Cyclophoridae. Das Tierreich, Berlin (R. Friedländer), 662 pp. [34 pls + 1 map]

Kobelt W, Möllendorff OF (1898) Katalog der gegenwärtig lebend bekannten Pneumonopomen. Nachrichtsblatt der Deutschen Malakozoologischen Gesellschaft 30: 129–160. https://doi.org/10.5962/bhl.title.14877

Köhler F (2023) Peeking back in time: Novel insights into the evolutionary relationships of diplommatinids (Caenogastropoda, Cyclophoroidea) from around Australia. Zoologica Scripta 53: 78–86. https://doi.org/10.1111/zsc.12629

Kozlov AM, Darriba D, Flouri T, Morel B, Stamatakis A (2019) RAxML-NG: a fast, scalable and user-friendly tool for maximum likelihood phylogenetic inference. Bioinformatics 35(21): 4453–4455. https://doi.org/10.1093/bioinformatics/btz305

Kuroda T, Miyanaga M (1939) New Land Shells from Norther Tyosen (Korea). Venus 9(2): 66–85.

Kwon OK, Lee JS (1991) New Land Snails in Korea. Korean Journal of Malacology7(1): 1–11.

Liew T, Vermeulen J, Marzuki M, Schilthuizen M (2014) A cybertaxonomic revision of the micro-landsnail genus *Plectostoma* Adam (Mollusca, Caenogastropoda, Diplommatinidae), from Peninsular Malaysia, Sumatra and Indochina. ZooKeys 393: 1–107. https://doi.org/10.3897/zookeys.393.6717

Luo T-C, Chen D-N, Zhou W-C (2008) A new species of the genus *Diplommatina* Benson, 1849 form China (Prosobranchia, Mesogastropoda, Diplommatinidae). Acta Zootaxonomica Sinica 33(2): 233–235.

Möllendorff OF (1882) Materialien zur Fauna von China. Jahrbücher der Deutschen Malakozoologischen Gesellschaft 9: 337–356.

Möllendorff OF (1885a) Diagnoses specierum novarum sinensium. Nachrichtsblatt der Deutschen Malakozoologischen Cesellschaft 17: 161–192.

Möllendorff OF (1885b) Materialien zur Fauna von China. Jahrbücher der Deutschen Malakozoologischen Gesellschaft 12: 349–411.

Möllendorff OF (1886) Materialien zur Fauna von China. Jahrbücher der Deutschen Malakozoologischen Gesellschaft 13: 156–210.

Nakamura T, Yamada K, Tomii K, Katoh K (2018) Parallelization of MAFFT for large-scale multiple sequence alignments. Bioinformatics 34(14): 2490–2492. https://doi.org/10.1093/bioinformatics/bty121

Neubert E, Bouchet P (2015) The Diplommatinidae of Fiji–a hotspot of Pacific land snail biodiversity (Caenogastropoda, Cyclophoroidea). ZooKeys 487: 1–85. https://doi.org/10.3897/zookeys.487.8463

Nurinsiyah AS, Hausdorf B (2017) Revision of the Diplommatinidae (Gastropoda: Cyclophoroidea) from Java. Zootaxa 4312(2): 201–245. https://doi.org/10.11646/zootaxa.4312.2.1

Palumbi S, Martin A, Romano S, Mcmillan WO, Stice L, Grabowski G (1991) The Simple Fool's Guide to PCR. Department of Zoology, University of Hawaii, Honolulu, 1–45.

Pilsbry HA (1934) Zoological Results of the Dolan West China Expedition of 1931. Part II. Mollusks. Proceedings of the Academy of Natural Sciences of Philadelphia 86: 5–28.

Pilsbry HA, Hirase Y (1908) New land shells of the Chinese Empire: I. Proceedings of the Academy of Natural Sciences of Philadelphia 60: 37–43.

Ran J-C, Chen D-N, Zhang G-Q (1999) Two new species of land snails from China (Prosobranchia: Mesogastropoda: Cyclophoridae). Acta Zootaxonomica Sinica 24(3): 281–284.

Rohlf FJ (2004) tpsUtil, file utility program, version 1.26. Department of Ecology and Evolution, State University of New York at Stony Brook. https://life2.bio.sunysb.edu/ee/rohlf/software.html

Rohlf FJ (2005) tpsDig, digitize landmarks and outlines, version 2.05. Department of Ecology and Evolution, State University of New York at Stony Brook.

Ronquist F, Teslenko M, Van Der Mark P, Ayres DL, Darling A, Höhna S, Larget B, Liu L, Suchard MA, Huelsenbeck JP (2012) MrBayes 3.2: efficient Bayesian phylogenetic inference and model choice across a large model space. Systematic Biology 61(3): 539–542. https://doi.org/10.1093/sysbio/sys029

Schmacker B, Boettger O (1890) Neue Materialien zur Charakteristik und geographischen Verbreitiung chinesischer und japanischer Binnenmollusken 1. Nachrichtsblatt der Deutschen Malakozoologischen Gesellschaft 22: 113–144.

Staden R, Judge DP, Bonfield JK (2003) Managing sequencing projects in the GAP4 Environment. Introduction to bioinformatics. In: Krawetz SA, Womble DD (Eds) Introduction to Bioinformatics. Human Press, Totawa, 327–344. https://doi.org/10.1007/978-1-59259-335-4_20

Thiele J (1929) Handbuch der systematischen Weichtierkunde (Teil 1), part 1. Gustav Fischer Verlag, Jena, 778 pp.

Webster NB, Van Dooren T, Schilthuizen M. (2012) Phylogenetic reconstruction and shell evolution of the Diplommatinidae (Gastropoda: Caenogastropoda). Molecular Phylogenetics and Evolution 63(3): 625–638. https://doi.org/10.1016/j.ympev.2012.02.004

Wenz W (1939) Gastropoda. Teil I: Allgemeiner Teil und Prosobranchia. In: Schindewolf OH (Ed.) Handbuch derPaläozoologie. Vol. 6. Borntraeger, Berlin, 241–480 (issue 2, 1938) + 481–720 (issue 3, 1939).

Winston JE (1999) Describing species: practical taxonomic procedure for biologists. Columbia University Press, 512 pp.

Yamazaki K, Yamazaki M, Ueshima R (2013) Systematic review of diplommatinid land snails (Caenogastropoda, Diplommatinidae) endemic to the Palau Islands. (1) Generic classification and revision of Hungerfordia species with highly developed axial ribs. Zootaxa 3743(1): 1–71. https://doi.org/10.11646/zootaxa.3743.1

Yen T-C (1939) Die chinesischen Land- und Süßwasser-Gastropoden des Natur-Museums Senckenberg. Abhandlungen der Senckenbergischen Naturforschenden Gesellschaft 444: 30–33.

Zhang G, Wade CM (2023) Molecular phylogeny and morphological evolution of the Chinese land snail *Cathaica* Möllendorff, 1884 (Eupulmonata: Camaenidae) in Shandong Province, China. Biological Journal of the Linnean Society 140(4): 556–577. https://doi.org/10.1093/biolinnean/blad067

Zhou W-C, Chen D-N, Li Y (2005) A new species of the genus *Diplommatina* Benson, 1849 form China (Prosobranchia, Mesogastropoda, Cyclophoridae). Acta Zootaxonomica Sinica 30(4): 725–727.

Zilch A (1953) Die Typen und Typoide des Natur-Museums Senckenberg, 9: Mollusca, Cyclophoridae, Diplommatininae. Archiv für Molluskenkunde 82(1–3): 1–85.

Zilch A (1974) Vinzenz Gredler und die Erforschung der Weichtiere Chinas durch Franziskaner aus Tirol. Archiv für Molluskenkunde 104(4–6): 171–228.

Zoosyst. Evol. 101 (2) 2025, 571–581 | DOI 10.3897/zse.101.144719

PENSOFT

für Natur MUSEUM FÜR NATURKUNDE BERLIN

Retrieval of the genus *Capitellus* Siddiqi, 1983, with description of *C. caramborum* sp. nov. (Dorylaimida, Belondiridae) associated with Andalusian (Spain) olive groves

Miriam García-Ruiz[1], Joaquín Abolafia[1], Reyes Peña-Santiago[2]

1 *Departamento de Biología Animal, Biología Vegetal y Ecología, Universidad de Jaén, Jaén, Spain*

2 *Retired Professor, Universidad de Jaén, Jaén, Spain*

https://zoobank.org/2F62AE4E-8CBC-452E-A01F-23ECC9DD1BCB

Corresponding author: Miriam García-Ruiz (migarcir@ujaen.es)

Academic editor:A. Schmidt-Rhaesa ♦ **Received** 17 December 2024 ♦ **Accepted** 9 January 2025 ♦ **Published** 28 February 2025

Abstract

A new species of belondirid nematode, collected in olive groves of the southern Iberian Peninsula, is described, including SEM observations and molecular (LSU, SSU) study. *Capitellus caramborum* **sp. nov.** is characterized by its 0.82–1.09 mm long body, lip region offset by constriction and 6.0–6.5 µm wide with a distinct perioral refractive disc 4.0–4.5 µm wide, odontostyle 6.0–6.5 µm long, odontophore bearing basal flanges and 1.8–2.0 times the odontostyle long, neck 223–296 µm long, pharyngeal expansion occupying 53–59% of the total neck length, female genital system diovarian, uterus simple and 27–38 µm or 1.4–1.9 body diameters long, vulva (*V* = 53–56) longitudinal, tail convex conoid to subcylindrical (24–34 µm, *c* = 31–38, *c'* = 1.8–2.1), spicules strongly curved ventrad and 23–25 µm long, and four ventromedian supplements. Morphological and molecular data support the retrieval of *Capitellus* as a valid genus, its taxonomy being updated, including the transference of *Dorylaimellus neocapitatus* to it.

Key Words

Description, dorylaims, LSU, morphology, nematodes, new combination, phylogeny, SSU, taxonomy

Introduction

In his revision of the subfamily Dorylaimellinae Jairajpuri, 1964, Siddiqi (1983) proposed the new genus *Capitellus* to transfer *Dorylaimellus capitatus* Siddiqi, 1964, as its only and type species. Siddiqi (*op. cit.*) also stated that *Capitellus* was (p. 4) unique among the Dorylaimellinae in having a continuous lip region and an angular, "refractive perioral disc," thus putting especial emphasis on the relevance of this peculiar feature as its most recognizable diagnostic trait. Besides, *Capitellus* was characterized by its indistinct perioral sclerotized pieces, diovarian female genital system, and subcylindrical tail. Jairajpuri and Ahmad (1992) admitted *Capitellus* as a valid taxon but lowered its category to a subgeneric level under the genus *Dorylaimellus* Cobb, 1913; meanwhile, Andrássy (2009) considered both taxa to be identical.

Available information about the type and only species, *C. capitatus* (Siddiqi, 1964) Siddiqi 1983, is limited to a rather simple original description and illustrations based on eleven females collected from soil around roots of mango at Kareli, Madhya Pradesh, India. Moreover, Siddiqi (1983) reported its presence in other territories and habitats: Pakistan, lucerne soil in Tanzania, and banana soil in Trinidad; nevertheless, the author did not provide further data about these populations.

Peralta and Peña-Santiago 2000 (see also Jiménez-Guirado et al. 2007) described *Dorylaimellus neocapitatus* from several locations of the southern Iberian Peninsula, Spain, associated with Mediterranean brushwood (*Ulex parviflorus* Pourr., *Echinospartum boissieri* (Sapch) Rothm., *Retama* sp., *Chamaerops humilis* L., *Pistacia lentiscus* L., *Foeniculum vulgare* Mill., and *Lavandula stoechas* Lam.), but also with almond groves

and a wheat field. This species shared with *C. capitatus* the presence of a refractive perioral disc and other features of their general morphology, but it was easily separable from this in several relevant morphometrics.

Two populations of a Dorylaimellinae taxon were collected in the course of a nematological survey conducted to study the free-living fauna inhabiting olive soils in the framework of the project *Soil O-Live* (EU Horizon Program grant No 101091255). Its morphological and molecular study revealed that it belonged to an unknown form very similar to *C. capitatus* and *D. neocapitatus*. Thus, this contribution aims to describe it, to obtain its molecular characterization, and to discuss its evolutionary relationships. The results are presented in the following.

Materials and methods

Nematodes and their morphological and morphometrical study

A total of 20 specimens found in soils of olive groves were available to study. Nematodes were extracted by centrifugation (CDFA 2015, based on Jenkins 1964) and/or with Baermann's funnels following the protocol by Flegg (1967); somewhat modified, killed by heat, fixed in 4% formaldehyde, preserved in anhydrous glycerin according to Siddiqi's (1964b) method, mounted on permanent glass slides that were sealed with paraffin, and measured and photographed using an Eclipse 80i microscope (Nikon) equipped with differential interference contrast optics, a drawing tube (*camera lucida*), and a DS digital camera. Morphometrics include Demanian indices (de Man, 1880) and other measurements and ratios, some of them presented in a separate table, while others form part of the literal description of species. Two specimens preserved in glycerin were selected for observation with a SEM according to Abolafia (2015). The nematodes were hydrated in distilled water, dehydrated in a graded ethanol−acetone series, critical point dried, coated with gold, and observed with a Zeiss Merlin microscope (5 kV).

Molecular study

For molecular analyses, single specimens were temporarily mounted in a drop of 1 M sodium chloride containing glass beads. This was followed by DNA extraction from single individuals as described by Archidona-Yuste et al. (2016). The D2–D3 domains were amplified using the D2A (5′−ACAAGTACCGTGAGGGAAAGTTG−3′) and D3B (5′−TCGGAAGGAACCAGCTACTA−3′) primers (Nunn, 1992; De Ley et al., 1999). The portion of 18S rRNA was amplified using primers 988F (5′−CTCAAAGATTAAGCCATGC−3′), 1912R (5′−TTTACGGTCAGAACTAGGG−3′), 1813F (5′−CTGCGTGAGAGGTGAAAT−3′), and 2646R (5′−GCTACCTTGTTACGACTTTT−3′) (Holterman et al. 2006). All polymerase chain reaction (PCR) assays were done according to the conditions described by Archidona-Yuste et al. (op. cit.). The amplified PCR products were purified using ExoSAP-IT (Affimetrix, USB products) and used for direct sequencing on a DNA multicapillary sequencer (Model 3130XL genetic analyzer; Applied Biosystems, Foster City, CA, USA), using the BigDye Terminator Sequencing Kit V.3.1 (Applied Biosystems, Foster City, CA, USA), at the StabVida sequencing facilities (Caparica, Portugal) according to the Sanger et al. (1977) method. The newly obtained sequences were submitted to the GenBank database under the accession numbers indicated on the phylogenetic trees.

Phylogenetic analyses

For phylogenetic relationships, analysis was based on 18S and 28S rDNA fragments. The obtained sequences were manually edited using Chromas 2.6.6 (Technelysium) and aligned with other rDNA sequences available in GenBank using the ClustalW alignment tool implemented in MEGA7 (Kumar et al. 2016). Poorly aligned regions at extremes were removed from the alignments using MEGA7. The best-fit model of nucleotide substitution used for the phylogenetic analysis was statistically selected using jModelTest 2.1.10 (Darriba et al. 2012). The phylogenetic tree was generated with the Bayesian inference method using MrBayes 3.2.6 (Ronquist et al. 2012). *Romanomermis culicivorax* Ross & Smith, 1976 (DQ418791 and EF417153, for the 18S and 28S rDNA trees, respectively) was chosen as an outgroup. The analysis under the General Time Reversible plus Invariant sites plus Gamma distribution (GTR + I + G) model was initiated with a random starting tree and run with the Markov chain Monte Carlo (MCMC) (Larget and Simon 1999) for 1×10^6 generations. A total of 25% of samples was discarded as burn-in. The tree was visualized and saved with FigTree 1.4.4 (Rambaut 2018).

Results

***Capitellus caramborum* sp. nov.**

https://zoobank.org/4B2DFECC-F1DC-490A-AF08-47C3CDB1C121

Figs 1–4

Material examined. Fourteen females and six males from two locations, in variable states of preservation.

Morphometrics. See Table 1.

Description. Baena (type) population:

Adult. Slender (*a* = 40–49) nematodes of small to medium size, 0.82–1.04 mm long. Body cylindrical, tapering towards both extremities. Upon fixation, habitus regularly curved ventrad, often adopting an open C shape. Cuticle dorylaimid, two-layered, thin, *ca* 1 µm thick throughout the entire body, outer layer bearing very fine transverse striation, better observable with SEM.

Table 1. Main morphometrics of *Capitellus* species. Measurements in µm except L in mm, and in the form: average ± sd (range).

Species	*C. caramborum* sp. nov.				*C. capitatus*	*C. neocapitatus*
Population	Baena			Antequera	Type	Several
Country	Spain			Spain	India	Spain
	Holotype	Paratypes				
n	♀	7♀♀	6♂♂	6♀♀	11♀♀	23♀♀
Character						
L	0.98	0.94 ± 0.05 (0.88–1.04)	0.88 ± 0.05 (0.82–0.94)	1.04 ± 0.50 (0.97–1.09)	0.58–0.65	0.75–0.99
a	47	45.3 ± 3.1 (40–49)	45.3 ± 3.1 (40–49)	48.7 ± 2.3 (44–51)	30–37	35–42
b	3.6	3.7 ± 0.2 (3.5–4.1)	3.7 ± 0.2 (3.5–4.1)	3.7 ± 0.1 (3.6–3.9)	2.7–3.3	2.7–3.7
c	34	35.0 ± 2.3 (31–38)	35.0 ± 2.3 (31–38)	34.0 ± 2.0 (32–36)	21–25	28–39
V	54	54 ± 1.0 (53–56)	–	54.0 ± 1.0 (53–56)	54–56	52–59
c'	2.0	1.9 ± 0.1 (1.8–2.0)	2.1 ± 0.1 (2.0–2.1)	2.1 ± 0.1 (1.9–2.1)	2.2[1]	1.3–1.7
Lip region diameter	6.5	6.3 ± 0.2 (6.0–6.5)	6.3 ± 0.3 (6.0–6.5)	6.3 ± 0.3 (6.0–6.5)	?	6.5–7.5
Odontostyle length	6.0	6.1 ± 0.2 (6.0–6.5)	6.1 ± 0.2 (6.0–6.5)	6.3 ± 0.3 (6.0–6.5)	4.5	5.0–5.5
Odontophore length	12	11.9 ± 0.4 (11.5–12.5)	12.1 ± 0.3 (12–12.5)	12.1 ± 0.5 (11.5–12.5)	13–14	10–12
Neck length	268	253 ± 14 (225–268)	248 ± 25 (223–283)	282 ± 17 (252–296)	217[1]	221–278
Pharyngeal expansion length	143	137 ± 14 (106–155)	134 ± 16 (111–158)	153 ± 19 (118–174)	113[1]	131–159
Body diameter at neck base	21	21.0 ± 0.9 (20–23)	20.1 ± 0.8 (19–21)	21.6 ± 1.1 (20–23)	?	20–26
mid-body	21	20.9 ± 1.0 (20–23)	19.9 ± 0.7 (19–21)	21.3 ± 0.8 (20–22)	20[1]	21–28
anus/cloaca	14	14.9 ± 0.7 (14–16)	15.9 ± 0.5 (15–17)	14.9 ± 0.6 (14–16)	12[1]	15–18
Distance vulva – anterior end	529	512 ± 34 (464–574)	–	562 ± 27 (522–595)	354[1]	420–533
Prerectum length	90	94.5 ± 3.0 (90–96)	72.4 ± 9.9 (58–79)	94.6 ± 3.1 (92–98)	?	62–98
Rectum/cloaca length	19	18.7 ± 1.3 (17–20)	?	19.4 ± 0.2 (19–20)	?	12–18
Tail length	29	27.0 ± 1.7 (24–29)	33.0 ± 1.0 (32–34)	30.6 ± 1.0 (29–32)	26	23–28
Spicules length	–	–	24.3 ± 0.8 (23–25)	–	–	–
Ventromedian supplements	–	–	4	–	–	–

Lateral chord 6.0–6.5 µm wide, occupying less than one-third (26–31%) of mid-body diameter, bearing abundant granular gland bodies. Body pores abundant, appearing as (SEM observations, Fig. 4J) short longitudinal slits. Lip region cap-like, offset by constriction, 1.7–2.0 times as wide as high and up to one-third (28–33%) of body diameter at neck base, with a well-differentiated, refractive perioral disc; SEM observations: lips amalgamated, their inner region visibly offset and somewhat expanded, forming a small sucker-like perioral disc 4.0–4.5 µm wide and divided into six triangular sectors by the existence of six radial, interlabial incisures running from the oral aperture to the margin of the disc, labial and cephalic papillae low, but comparatively large and distinct, button-like, with a coarse pore at their center. Amphid fovea cup-like, its opening 6.0–6.5 µm wide, occupying the entire diameter of lip region. Cheilostom 6.0–6.5 µm long, almost cylindrical, thin-walled, with circumoral sclerotized pieces at its anterior end. Odontostyle typical dorylaimid but small, almost equal (0.9–1.0 times) to lip region diameter long, occupying 0.56–0.66% of body length, *ca* 5.0 times as long as wide, with short aperture *ca* one-fifth of its length. Guiding ring simple, often inconspicuous. Odontophore visibly flanged, 1.8–2.0 times the odontostyle. Pharynx consisting of a slender and weakly muscular anterior region suddenly enlarging into the basal expansion 10–16 times as long as wide, 5.3–8.1 times longer than body diameter at neck base, occupying more than half (53–59%) of the total neck length, and surrounded by a distinct spiral muscular sheath, its gland nuclei and outlets obscure in the specimens examined, some specimens bearing a few refractive globules at its anterior end. Cardia small and rounded, 9–11 µm long.

Female. Genital system diovarian, with both branches equally and variably developed, the anterior 74–122 µm or 8–12% of the total body length, the posterior 87–108 µm or 9–11%. Ovaries comparatively small, often not reaching the oviduct-uterus junction, 31–61 µm the anterior and 36–48 µm the posterior, with oocytes first arranged in two or more rows and then in one single one. Oviduct 42–65 µm or 2.1–3.3 body diameters long, consisting of a long and slender distal region made of prismatic cells and a developed proximal *pars dilatata* with visible lumen. A distinct sphincter present between oviduct and uterus. Uterus a simple tube-like structure 27–38 µm or 1.4–1.9 body diameters long. Vagina extending inwards 8.0–9.5 µm, to less than one-half (38–45%) of body diameter: *pars proximalis* 5.0–6.0 × 6.0–6.5, with almost straight to somewhat convergent walls that are encircled by weak musculature, *pars distalis* 3.0 µm long. Vulva a longitudinal slit *ca* 2 µm long. Prerectum 6.2–6.6, rectum 1.2–1.3 anal body diameters long. Tail convex conoid to slightly subcylindrical.

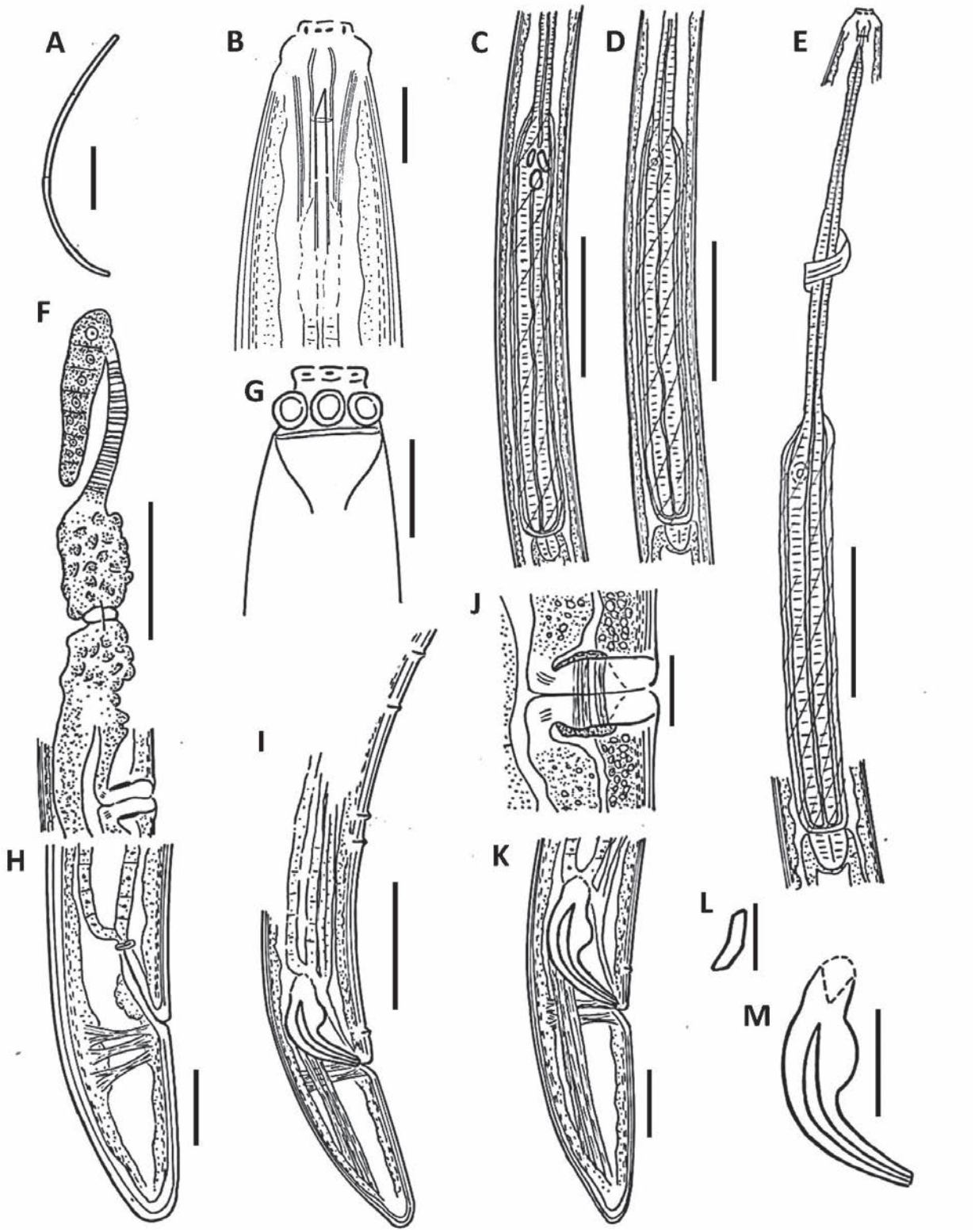

Figure 1. *Capitellus caramborum* sp. nov. **A–H, J.** Female; **I, K–M**. Male; **A.** Entire; **B.** Anterior region, lateral median view; **C.** Pharyngeal expansion with globules; **D.** Pharyngeal expansion without globules; **E.** Neck region; **F.** Anterior genital branch; **G.** Anterior region, lateral surface view; **H, K.** Caudal region; **I.** Posterior body region with ventromedian supplements; **L.** Lateral guiding piece; **M.** Spicule. Scale bars: 200 μm (**A**); 5 μm (**B, G, J, L**); 50 μm (**C–E**); 25 μm (**F, I**); 10 μm (**H, K, M**).

Male. Genital system diorchic, with opposite testes. In addition to the adcloacal pair, situated at 4–5 μm from the cloacal aperture, there invariably are four very simple (non-mammiform but a low pore-like structure, Fig. 4I) ventromedian supplements arranged in a more posterior pair located at 38–41 μm from the ad-cloacal pair and two more anterior and spaced ones at 23–25 μm from the posterior pair. Spicules dorylaimid, strongly curved ventrad,

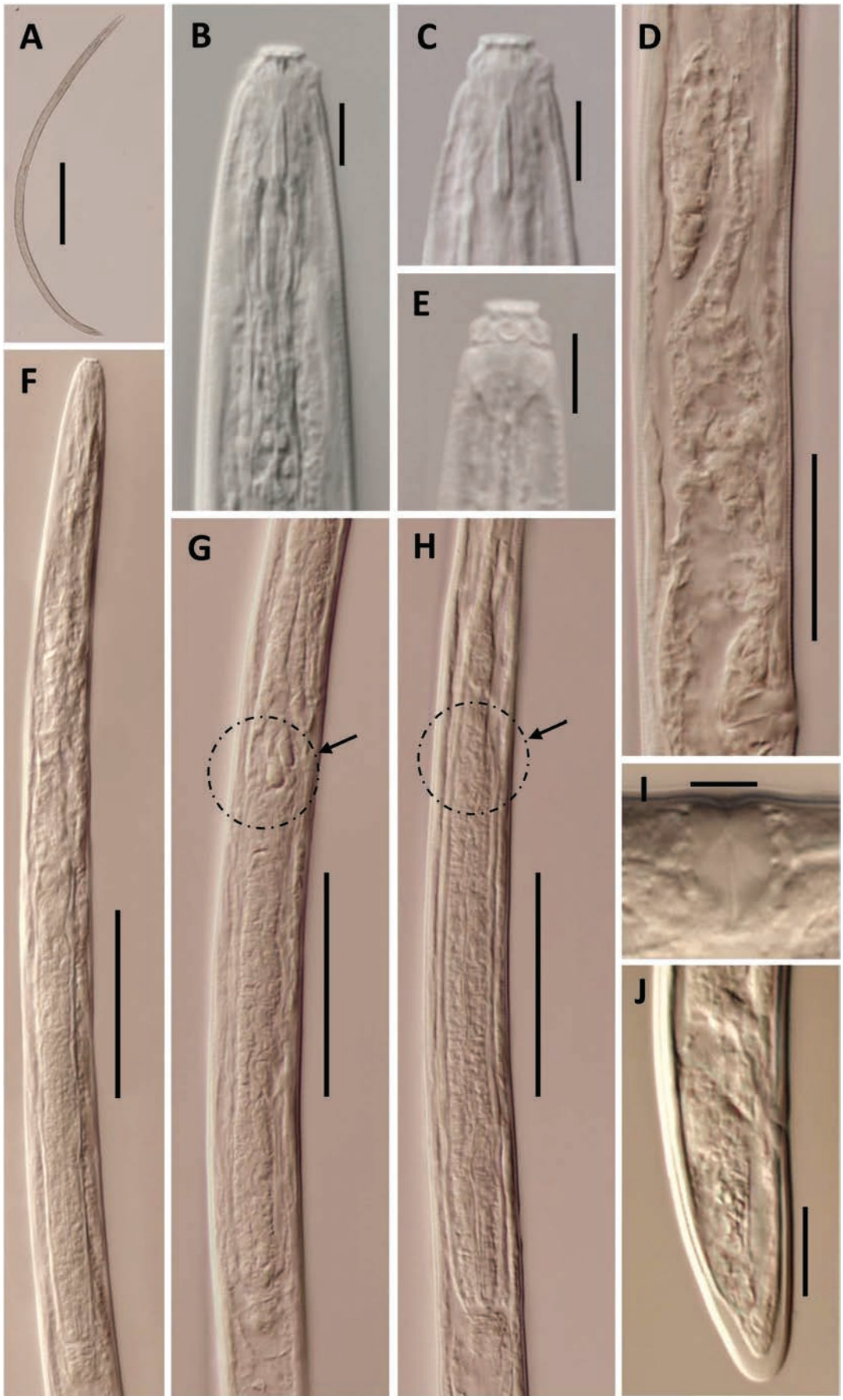

Figure 2. *Capitellus caramborum* sp. nov. (Female, LM). **A.** Entire; **B, C.** Anterior body region, lateral median view; **D.** Anterior genital branch; **E.** Anterior region, lateral surface view; **F.** Neck region; **G.** Pharyngeal expansion with globules; **H.** Pharyngeal expansion without globules; **I.** Vagina region; **J.** Caudal region. Scale bars: 200 µm (**A**); 5 µm (**B, C, E, I**); 25 µm (**D**); 50 µm (**F, G, H**); 10 µm (**J**).

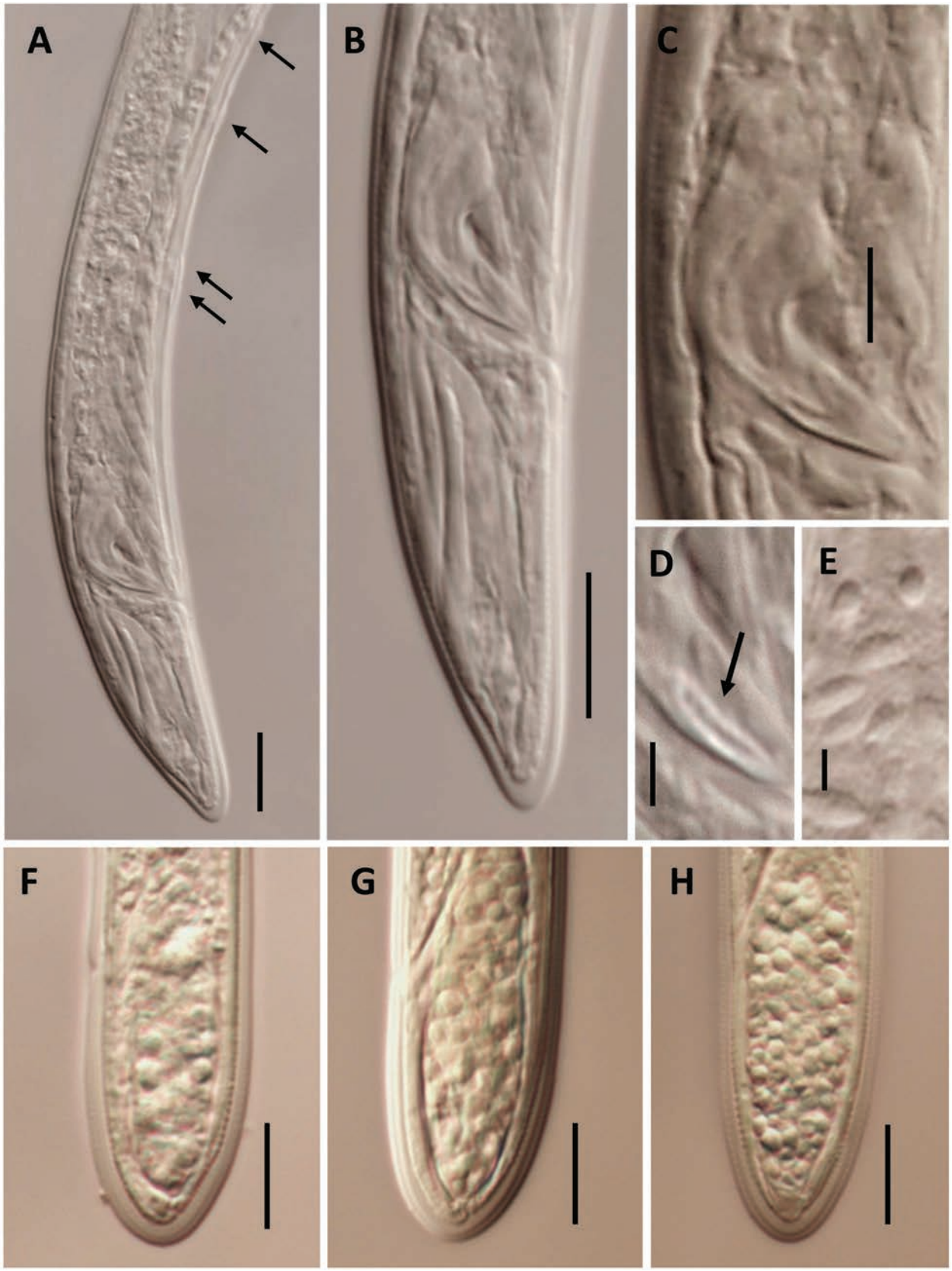

Figure 3. A–E. *Capitellus caramborum* sp. nov. (Male, LM). **A.** Posterior body region, with arrowheads pointing at ventromedian supplements; **B.** Caudal region; **C.** Spicule; **D.** Lateral guiding piece; **E.** Sperm cells; **F–H.** *Capitellus neocapitatus* (Peralta & Peña-Santiago, 2000), comb. nov.; **F–H.** Female tail. Scale bars: 10 µm (**A, B, F–H**); 5 µm (**C**); 2 µm (**D, E**).

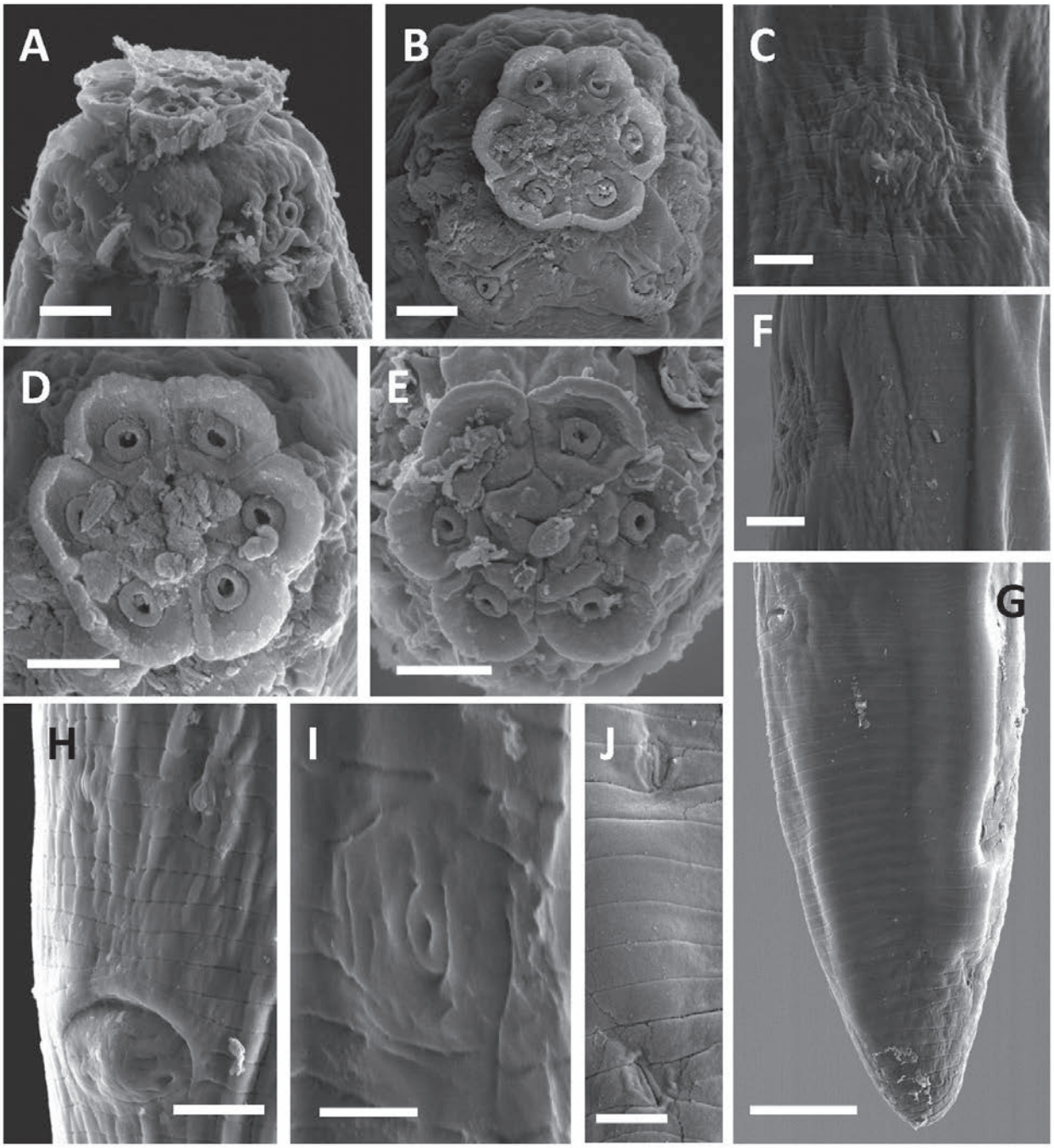

Figure 4. *Capitellus caramborum* sp. nov. (SEM). **A.** Lip region, lateral view; **B.** Lip region, in face view; **C.** Vulva, ventral view; **D, E.** Perioral disc, in face view; **F.** Vulva region, lateral view; **G.** Female caudal region, subventral view; **H.** Cloacal aperture and ad-cloacal genital papillae; **I.** Detail of ventromedian supplement; **J.** Caudal pores of female tail. Scale bars: 1 µm (**A, B, D, E, I, J**); 2 µm (**C, F, H**); 5 µm (**G**).

3.7–4.1 times as long as wide and 1.4–1.7 times longer than body diameter: head 3.0–3.5 µm long, up to one-sixth (13–15%) of spicule length, and almost as long as wide; median piece occupying less than one-third (15–31%) of maximum width; ventral hump and hollow very prominent, the former located at 7.5–9.0 µm from the anterior end; curvature 127–128°. Lateral guiding piece simple, 6 µm long. Tail somewhat less convex conoid than that of female.

Antequera population. Females are morphologically identical and morphometrically very similar to those of the type population, as the ranges of their more relevant measurements and ratios are coincident or widely overlap. No male found.

Molecular characterization. After sequencing and editing, four sequences were obtained for phylogenetic analyses. Two 18S rDNA sequences, 1719 bp in length (acc. PQ877190–PQ877191), showed 98.14% identity to a sequence (AY552969) assigned to *Dorylaimellus virginianus* Cobb, 1913 (Jairajpuri & Ahmad, 1980) and 97.85%, 97.62%, and 98.02% identity to sequences assigned to *D.*

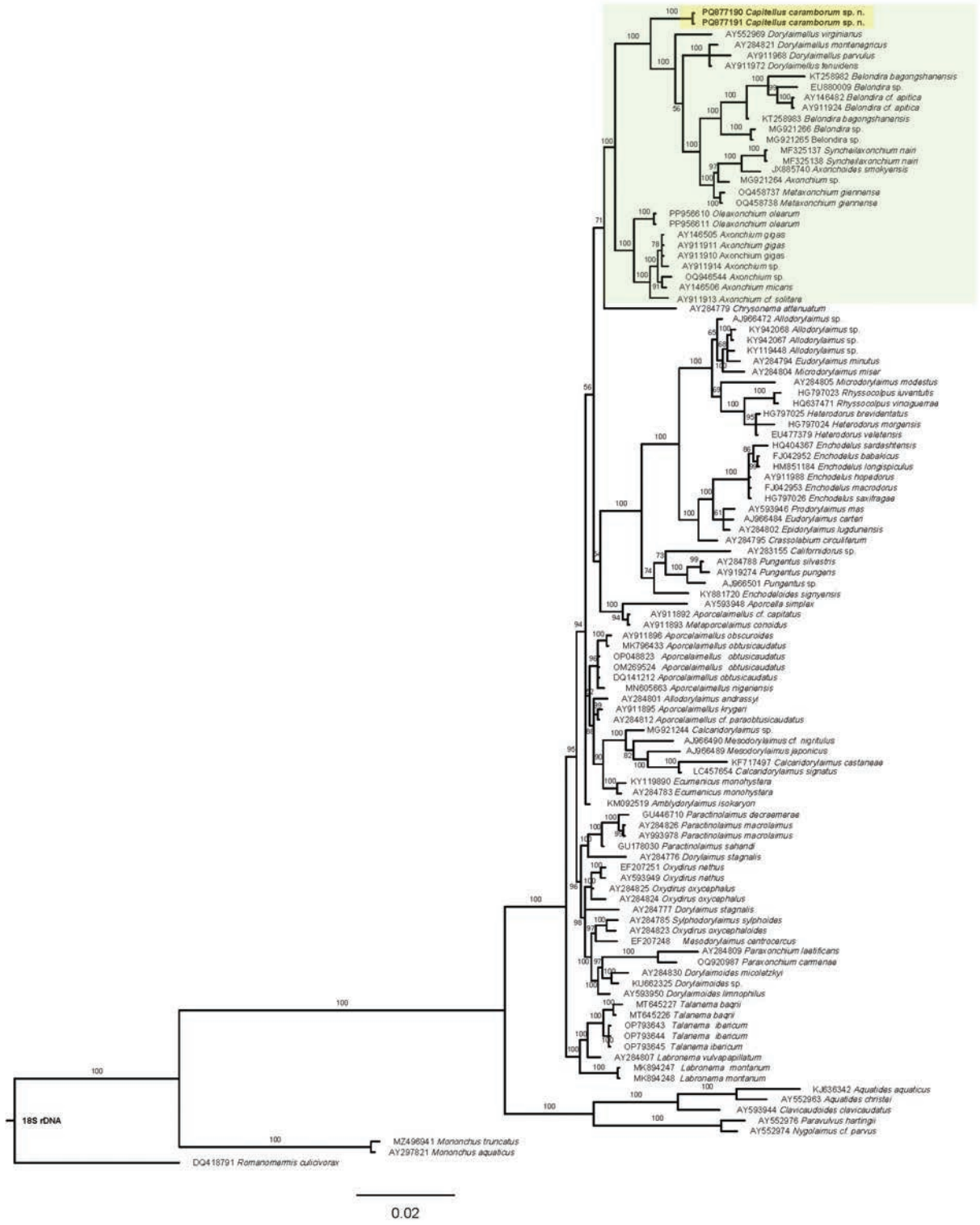

Figure 5. Bayesian inference tree from the newly sequenced *Capitellus caramborum* sp. nov. based on sequences of the 18S rDNA region. Bayesian posterior probabilities (%) are given for each clade. The scale bar shows the number of substitutions per site.

montenegricus Andrássy, 1959 (Jairajpuri & Ahmad, 1980), *D. parvulus* Thorne, 1939 (Jairajpuri & Ahmad, 1980), and *D. tenuidens* Thorne, 1939, respectively (AY284821, AY911968, and AY911972).

Two 28S rDNA sequences, 793 bp in length (acc. PQ877192–PQ877193), showed 83.61% identity to two sequences (KT258984, KT25985) assigned to *Belondira bagongshanensis* Wu, Huang, Xie, Wang & Xu, 2017, 91.14% to those of *Belondira* sp. (MG921267, MG921268), and 80.71% identity to *B. coomansi* Golhasan, Heydari, Miraeiz, Abolafia & Peña-Santiago, 2018 (MF363124).

Diagnosis. The new species is characterized by its 0.82–1.09 mm long body, lip region offset by constric-

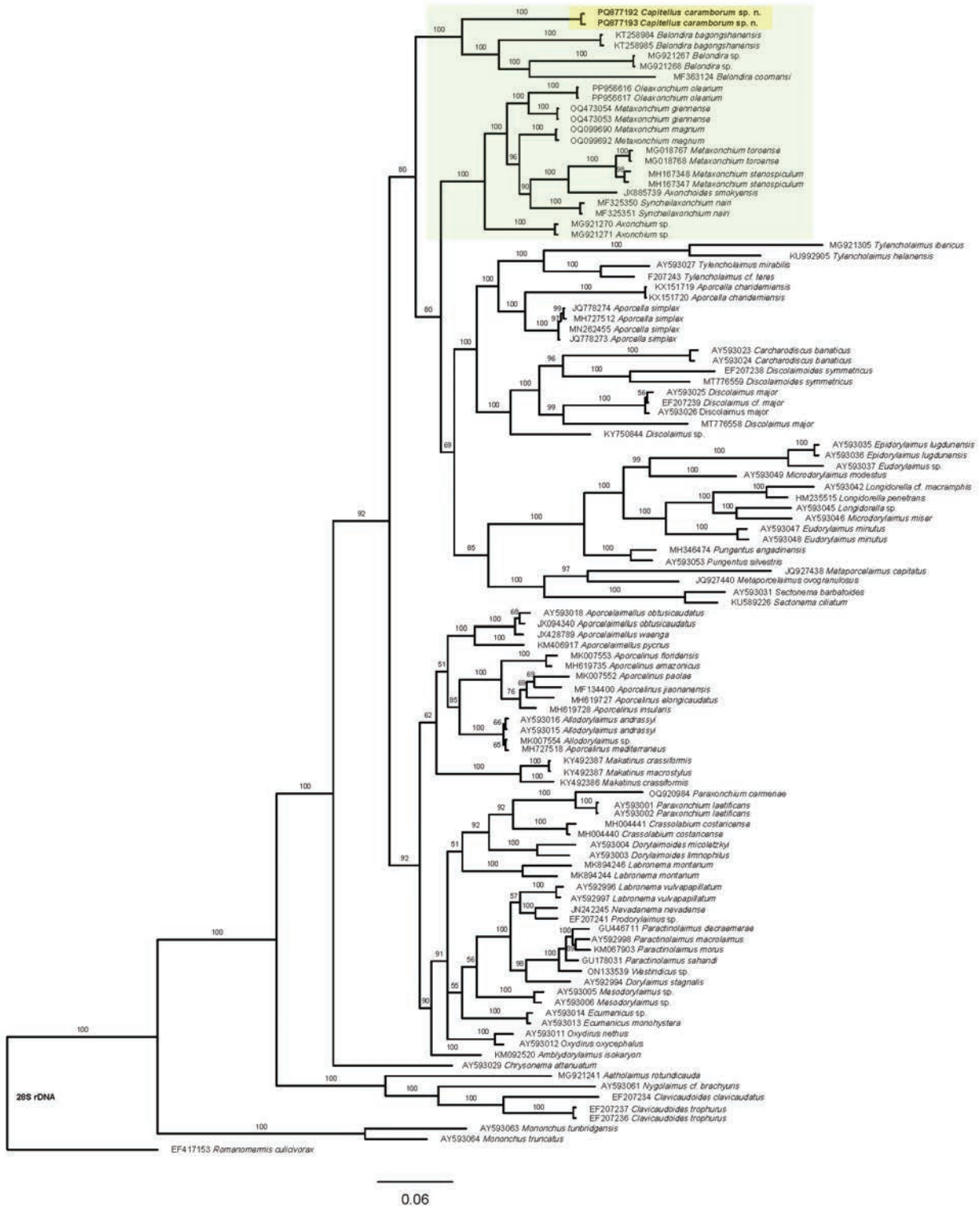

Figure 6. Bayesian inference tree from the newly sequenced *Capitellus caramborum* sp. nov. based on sequences of the 28S rDNA region. Bayesian posterior probabilities (%) are given for each clade. The scale bar shows the number of substitutions per site.

tion, and 6.0–6.5 µm wide with a distinct perioral refractive disc 4.0–4.5 µm wide, odontostyle 6.0–6.5 µm long, odontophore bearing basal flanges and 1.8–2.0 times the odontostyle long, neck 223–296 µm long, pharyngeal expansion occupying 53–59% of the total neck length, female genital system diovarian, uterus simple and 27–38 µm or 1.4–1.9 body diameters long, vulva (V = 53–56) longitudinal, tail convex conoid to subcylindrical (24–34 µm, c = 31–38, c' = 1.8–2.1), spicules strongly curved ventrad and 23–25 µm long, and four ventromedian supplements.

Separation from its relatives. The new species is similar to *C. capitatus* and *D. neocapitatus*. It differs from *C. capitatus*, a mainly pantropical taxon, in its lon-

ger (0.82–1.09 *vs.* 0.58–0.65 mm) and slender (*a* = 44–51 *vs. a* = 30–37 in females) body, lip region offset by constriction (*vs.* almost continuous), larger odontostyle (5.5–6.5 *vs.* 4.5 µm), comparatively shorter tail (*c* = 31–38 *vs. c* = 21–25), and male present (*vs.* absent). From *D. neocapitatus*, a very close taxon, in its narrower lip region (6.0–6.5 *vs.* 6.5–7.5 µm wide, n = 21), longer odontostyle (6.0–6.5 *vs.* 5.0–5.5 µm) – it means that the odontostyle is almost equal *vs.* appreciably shorter than lip region diameter –, relatively shorter pharyngeal expansion (53–59 *vs.* 59–63% of the total neck length), more conoid (*vs.* more subcylindrical, Fig. 3F–H), and comparatively longer female tail (*c'* = 1.8–2.1 *vs. c'* = 1.3–1.7), and male present (*vs.* absent).

Type locality and habitat. Southern peninsular Spain, the Andalusia region, Córdoba province, Baena municipality, "El Valle" farm (37.799704, -4.310439, elevation 351 m), where the new species was found in the rhizosphere of an olive grove.

Other locality and habitat. Southern peninsular Spain, the Andalusia region, Málaga province, Antequera municipality, "La Capilla" farm (37.198283, -4.543868, elevation 491 m), where the new species was found in the rhizosphere of an olive grove.

Etymology. The specific name refers to the "Carambos," the familiar nickname of the first author's mother.

General discussion

Morphologically, *C. caramborum* sp. nov. forms a recognizable group of species together with *C. capitatus* and *D. neocapitatus*, all of them easily distinguishable by having a distinct perioral disc visibly refractive, which should be regarded as a very relevant synapomorphy (if not autapomorphy) in Dorylaimellinae. Besides, the general morphology of the three species is nearly identical, and their morphometrics (Table 1) are rather similar too.

Unfortunately, molecular studies of Dorylaimellinae representatives for comparison are limited to a few 18S-rDNA and no 28S-rDNA sequences. Thus, the evolutionary relationships of the new species as derived from the analyses whose results are presented in trees of Fig. 5 (18S-rDNA) & 6 (28S-rDNA) only confirm its belonging to maximally supported (100%) clades constituted by members of Belondiridae Thorne, 1939 (highlighted in green in both trees), excepting *Oxydirus* Thorne, 1939 sequences. Nevertheless, this clade includes all Belondiridae representatives in the 18S tree, while the 28S tree only contains *Belondira* sequences.

Present findings support the idea that *Capitellus* is a valid taxon. On the one hand, the new species now described is the third one displaying a very unusual (?unique) feature within Dorylaimellinae, and it forms a recognizable group with two previously known forms. On the other hand, the 18S tree shows that the two sequences of the new species form a clade that is separated from that including other *Dorylaimellus* species, which form part of another clade together with several belondiriid taxa. Thus, *Capitellus* is provisionally recovered as a valid genus, and, consequently, *D. neocapitatus* is transferred to it.

Updated taxonomy of *Capitellus*

Diagnosis

Small-sized nematodes, 0.58–1.09 mm long. Cuticle dorylaimid. Lip region continuous with the adjoining body or offset by weak constriction, with fused lips displaying a conspicuous, perioral, refractive disc. Amphid fovea cup-like, with large aperture. Cheilostom with variably perceptible perioral sclerotized pieces. Odontostyle dorylaimid, up to as long as lip region diameter. Guiding ring simple. Odontophore bearing flanged base. Pharyngeal expansion occupying one-half to two-thirds of the total neck length. Female genital system di-ovarian, with longitudinal vulva. Female tail conoid to subcylindrical. Spicules dorylaimid. Four variably spaced ventromedian supplements with hiatus.

Type species:
C. capitatus (Siddiqi, 1964) Siddiqi, 1983
= *Dorylaimellus capitatus* Siddiqi, 1964
= *Dorylaimellus* (*Dorylaimellus*) *capitatus* Siddiqi, 1964 (Jairajpuri & Ahmad, 1980)
= *Dorylaimellus* (*Capitellus*) *capitatus* Siddiqi, 1964 (Jairajpuri & Ahmad, 1992)

Other species:
C. caramborum sp. nov.
C. neocapitatus (Peralta & Peña-Santiago, 2000), comb. nov.
= *Dorylaimellus neocapitatus* Peralta & Peña-Santiago, 2000

Acknowledgements

This contribution derives from the project *Soil O-Live*. This project has received funding from the European Union's Horizon Europe research and innovation programme under grant agreement No. 101091255 (Soil Deal for Europe – HORIZON-MISS-2021-SOIL-02-03). The authors thank Dr. Pablo Castillo (IAS, Córdoba, Spain) for his collaboration in molecular analyses and are grateful for the SEM pictures obtained with the assistance of technical staff (Amparo Martínez-Morales) and equipment belonging to the Centro de Instrumentación Científico-Técnica (CICT) of the University of Jaén.

References

Abolafia J (2015) A low-cost technique to manufacture a container to process meiofauna for scanning electron microscopy. Microscopy Research & Technique 78: 771−776. https://doi.org/10.1002/jemt.22538

Andrássy (1959) Neue und wenig bekannte Nematoden aus Jugoslawien. Annales Nistorico-Naturales Museum Nationalis Hungarici 51: 271−272.

Andrássy I (2009) Free-living nematodes of Hungary III (*Nematoda errantia*). Pedozoologica Hungarica No. 5 (Series Csuzdi C. and Mahunka S). Hungarian Natural History Museum and Systematic Zoology Research Group of the Hungarian Academy of Sciences, Budapest, Hungary, 608 pp.

Archidona-Yuste A, Navas-Cortés JA, Cantalapiedra-Navarrete C, Palomares-Rius JE, Castillo P (2016) Unravelling the biodiversity and molecular phylogeny of needle nematodes of the genus *Longidorus* (Nematoda, Longidoridae) in olive and a description of six new species. PLoS ONE 11: e0147689. https://doi.org/10.1371/journal.pone.0147689

CDFA (2015) Protocol for extraction of plant parasitic nematodes from samples. https://www.cdfa.ca.gov/plant/ppd/nematode_extraction.html

Cobb NA (1913) New nematode genera found inhabiting fresh water and non-brackish soils. Journal of the Washington Academy of Sciences 3: 432−444. https://doi.org/10.5962/bhl.part.20323

Darriba D, Taboada GL, Doallo R, Posada D (2012) jModelTest 2: more models, new heuristics and parallel computing. Nature Methods 9: 772. https://doi.org/10.1038/nmeth.2109

De Ley P, Felix AM, Frisse LM, Nadler SA, Sternberg PW, Thomas WK (1999) Molecular and morphological characterization of two reproductively isolated species with mirror−image anatomy (Nematoda, Cephalobidae). Nematology 1: 591−612. https://doi.org/10.1163/156854199508559

Flegg JJM (1967) Extraction of *Xiphinema* and *Longidorus* species from soil by a modification of Cobb's decanting and sieving technique. Annals of Applied Biology 60: 423−437. https://doi.org/10.1111/j.1744-7348.1967.tb04497.x

Golhasan B, Heydari R, Miraeiz E, Abolafia J, Peña-Santiago R (2018) Molecular and morphological characterization of *Belondira coomansi* n. sp. (Nematoda, Dorylaimida, Belondiridae) from Iran. Journal of Helminthology 92: 630−636. https://doi.org/10.1017/S0022149X17000840

Holterman M, van derWurff A, van den Elsen S, vanMegen H, Bongers T, Holovachov O, Bakker J, Helder J (2006) Phylum-wide analysis of SSU rDNA reveals Deep phylogenetic relationships among nematodes and accelerated evolution toward crown clades. Molecular Biology and Evolution 23: 1792−1800. https://doi.org/10.1093/molbev/msl044

Jairajpuri, MS (1964) Studies on Nygellidae n. fam. and Belondiridae Thorne, 1939 (Nematoda, Dorylaimoidea) with description of ten new species from India. Proceedings of the Helminthological Society of Washington 31: 173−187.

Jairajpuri MS, Ahmad M (1980) Revised classification on the superfamily Belondiroidea Thorne, 1964 with notes on the systematics of *Dorylaimellus* Cobb, 1913 (Nematoda, Dorylaimida). Indian Journal of Nematology 10: 9−22.

Jairajpuri MS, Ahmad W (1992) Dorylaimida. Free-living, predaceous and plant-parasitic Nematodes. Oxford & IBH Publishing Co. Pvt. Ltd. New Delhi, India, 458 pp. https://doi.org/10.1163/9789004630475

Jenkins WR (1964) A rapid centrifugal-flotation technique for separating nematodes from soil. Plant Disease Reporter 48: 692.

Jiménez-Guirado D, Peralta M, Peña-Santiago R (2007) Nematoda, Mononchida, Dorylaimida I. In: Ramos MA, et al. (Eds) Fauna Ibérica, 30. Museo Nacional de Ciencias Naturales, CSIC, Madrid, 325 pp.

Kumar S, Stecher G, Tamura K (2016) MEGA7: molecular evolutionary genetics analysis version 7.0 for bigger datasets. Molecular Biology and Evolution 33: 1870−1874. https://doi.org/10.1093/molbev/msw054

Larget B, Simon DL (1999) Markov chain Monte Carlo algorithms for the Bayesian analysis of phylogenetic trees. Molecular Biology and Evolution 16: 750−759. https://doi.org/10.1093/oxfordjournals.molbev.a026160

Man JG de (1880) Die Einheimischen, frei in der reinen Erde und im süssen Wasser lebende Nematoden monographisch bearbeitet. Vorläufiger Bericht und descriptive-systematischer Theil. Tijdschrift van de Nederlandse Dierkundige Vereeniging 5 (1881): 1−104.

Nunn GB (1992) Nematode molecular evolution. An investigation of evolutionary patterns among nematodes based upon DNA sequences. Ph.D. dissertation, University of Nottingham, UK, 228 pp.

Peralta M, Peña-Santiago R (2000) Nematodes of the order Dorylaimida from Andalucía Oriental, Spain. The genus *Dorylaimellus* Cobb, 1913. Part I. Journal of Nematode Morphology and Systematics 2 (1999): 121−136.

Rambaut A (2018) Figtree, a graphical viewer of phylogenetic trees. Available online at https://github.com/rambaut/figtree/releases/tag/v1.4.4

Ronquist F, Teslenko M, van der Mark P, Ayres DL, Darling A, Höhna S, Larget B, Liu L, Suchard MA, Huelsenbeck JP (2012) MrBayes 3.2: efficient Bayesian phylogenetic inference and model choice across a large model space. Systematic Biology 61: 539−542. https://doi.org/10.1093/sysbio/sys029

Ross JR, Smith SM (1976) A review of the mermithid parasites (Nematode, Mermithid) described from North America mosquitoes (Diptera, Culicidae) with description of three new species. Canadian Journal of Zoology 54: 1084−1102. https://doi.org/10.1139/z76-124

Sanger F, Nicklen S, Coulson AR (1977) DNA sequencing with chain-terminating inhibitors. Proceedings of the National Academy of Sciences USA 74: 5463−5467. https://doi.org/10.1073/pnas.74.12.5463

Siddiqi MR (1964a) Six new nematode species in the superfamily Dorylaimoidea from India. Labdev Journal of Science and Technology 2: 136−144.

Siddiqi MR (1964b) Studies on *Discolaimus* spp. (Nematoda, Dorylaimidae) from India. Zeitschrift für Zoologische Systematik und Evolutionsforschung 2: 174−184. https://doi.org/10.1111/j.1439-0469.1964.tb00720.x

Siddiqi MR (1983) Taxonomy of the subfamily Dorylaimellinae (Nematoda, Dorylaimida). Pakistan Journal of Nematology 1: 1−38.

Thorne G (1939) A monograph of the nematodes of the superfamily Dorylaimoidea. Capita Zoologica 8: 1−261.

Wu WJ, Huang X, Xie H, Wang K, Xu CL (2017) Morphometrics and molecular analysis of the free-living nematode, *Belondira bagongshanensis* n. sp. (Dorylaimida, Belondiridae), from China. Journal of Helminthology 91: 7−13. https://doi.org/10.1017/S0022149X15001091

Zoosyst. Evol. 101 (2) 2025, 583–596 | DOI 10.3897/zse.101.144271

PENSOFT

MUSEUM FÜR NATURKUNDE BERLIN

Vastnema crassicutaneum gen. et sp. nov. (Nematoda, Dorylaimida, Dorylaimidae), an interesting new taxon from natural areas of Vietnam

Tam T. T. Vu[1,2], Joaquín Abolafia[3], Anh D. Nguyen[1,2], Thi Mai Linh Le[1,2], Reyes Peña-Santiago[4]

1 *Institute of Ecology and Biological Resources, Vietnam Academy of Science and Technology, 18 Hoang Quoc Viet, Cau Giay, Hanoi, Vietnam*

2 *Graduate University of Science and Technology, Vietnam Academy of Science and Technology. 18 Hoang Quoc Viet, Cau Giay, Hanoi, Vietnam*

3 *Departamento de Biología Animal, Biología Vegetal y Ecología, Universidad de Jaén, Campus "Las Lagunillas" s/n, Edificio B3, 23071- Jaén, Spain*

4 *Universidad de Jaén, Jaén, Spain*

https://zoobank.org/B9E64763-486C-429E-AC47-F78ED360333F

Corresponding author: Tam T. T. Vu (vtam7572@gmail.com)

Academic editor: A. Schmidt-Rhaesa ♦ **Received** 12 December 2024 ♦ **Accepted** 24 January 2025 ♦ **Published** 28 February 2025

Abstract

A new dorylaimid taxon, *Vastnema crassicutaneum* gen. et sp. nov., collected in natural habitats of Vietnam, is characterized, including morphological description, morphometrics, SEM observations, and molecular (18S-, 28S-rDNA) analyses. *Vastnema* gen. nov. is distinguished and separated from its relatives by a combination of key traits: large size (body 4.79–6.35 mm long), lip region tapering and continuous with the adjoining body, very short neck (*b*-ratio 6.3–8.7), presence of a peculiar uterine differentiation, pre-equatorial (V = 38–44) vulva, and 45–58 stomata-like ventromedian supplements. The new species is characterized by its three-layered cuticle, 12.5–15.5 µm thick at the anterior region; lip region 26–31 µm wide; odontostyle 49–60 µm long, or 1.8–2.0 times the lip region diameter; neck 627–888 µm long; pharyngeal expansion occupying 46–49% of the total neck length; uterus complex and 571–804 µm, or 3.2–4.3 body diameters long; longitudinal vulva; tail short and rounded in both sexes (39–56 µm, c = 98–140, c' = 0.5–0.7); and spicules 138–160 µm long. Both morphological and molecular data support a close relationship of the new taxon with some Labronematinae representatives but also reveal that internal and external relationships of Dorylaimidae might be more complex than traditionally assumed.

Key Words

Labronematinae, LSU, morphometrics, phylogeny, SEM, SSU, taxonomy

Introduction

Dorylaims, the members of the order Dorylaimida, are probably the most diverse nematode taxon, being present everywhere on the six continents and in all kinds of continental habitats, either freshwater sediments and/or arable and pristine soils (Peña-Santiago 2021). Traditionally, the study of dorylaimid fauna of Vietnam did not receive too much attention. Actually, Nguyen et al. (2014) compiled previous records of only 25 species and 15 genera. Nevertheless, the inventory of species significantly increased throughout the last decade by, among other contributions, Álvarez-Ortega et al. (2015, 2016), Nguyen et al. (2016, 2017), Nguyen and Peña-Santiago (2018, 2020), Hoang et al. (2019), and Vu et al. (2024).

Several populations of an interesting dorylaimid form were collected in the course of a nematological survey conducted to explore the nematode fauna of Vietnam. Its study revealed that it was distinguished by a unique combination of features and that it was not comparable to any known genus. Thus, this contribution aims to characterize the new taxon and to discuss its evolutionary relationships. The results are presented in the following.

Materials and methods

Sampling, extraction, and processing of nematodes

A total of 26 adult specimens, collected in soil samples from three natural areas of Vietnam, were studied. Nematodes were extracted using a modified Baermann funnel technique, heat killed, and fixed in TAF solution (Southey 1986) for morphological observations or in a DESS mixture (Yoder et al. 2006) for molecular analyses. Then, specimens were transferred to anhydrous glycerol (Seinhorst 1959, 1962), mounted on glass slides for their observation with light microscopy, and measured and photographed using an Eclipse 80i microscope (Nikon, Tokyo, Japan) equipped with differential interference contrast optics, a drawing tube (camera lucida), and a DS digital camera. Line drawings were made from taken photomicrographs and/or sketches obtained by means of camera lucida. Morphometrics include Demanian indices and other measurements and ratios, some of them presented in a separate table, while others form part of the literal description of species. All measurements were recorded in µm, except body length in mm. After filming and taking pictures, selected specimens were submitted to molecular studies.

DNA extraction, polymerase chain reaction (PCR), and sequencing

Nematode DNA was extracted from a single individual as described by Holterman et al. (2006), and DNA extracts were stored at –20 °C until used as PCR templates. The D2, D3 expansion segment of 28S rDNA and 18S was amplified using the forward D2A (5′–ACAAGTACCGTGGGGAAAGTTG–3′) and reverse D3B (5′–TCGG AAGGAACCAGCTACTA–3′) primers (Subbotin et al. 2006), and the 18S rDNA fragment was amplified using the primers 18S (18F: 5′-TCTAGAGCTAATACATGCAC-3′/18R: 5′-TACGGAAACCTTGTTACGAC-3′) (Floyd et al. 2005). All PCR reactions contained 12.5 µl of Hot-Start Green PCR Master Mix (2x) (Promega, USA), 1 µl of the forward and reverse primer (10 µM each), the 3 µl DNA template, and sterile Milli-Q water to 25 µl of the total volume. All PCR reactions were performed in a SimpliAmp thermal cycler (Thermo Fisher Scientific) as follows: an initial denaturation step at 95 °C for 4 min, followed by 40 cycles at 95 °C for 30 s, 54 °C for 30 s, and 72 °C for 60 s with a final incubation for 5 min at 72 °C. Amplicons were visualized under UV illumination after simple safe gel staining and gel electrophoresis. Purified PCR products were sent to Apical Scientific Company for sequencing (Selangor, Malaysia). After sequencing, the obtained rDNA sequence fragments were deposited in GenBank.

Phylogenetic analyses

For exploring phylogenetic relationships, analyses were based on 18S and 28S rDNA. The newly obtained sequences were manually edited using Chromas 2.6.6 (Technelysium, Queensland, 110 Australia) and aligned with other sequences available in GenBank using the ClustalW alignment tool implemented in MEGA11 (Kumar et al. 2021). Poorly aligned regions at extremes were removed from the alignments using MEGA11. The best-fit model of nucleotide substitution used for the phylogenetic analysis was statistically selected using jModelTest 2.1.10 (Darriba et al. 2012). The phylogenetic tree was generated with the Bayesian inference method using MrBayes 3.2.6 (Ronquist et al. 2012). The analysis under the generalized time reversible and invariant sites and gamma distribution (GTR + I + G) model was initiated with a random starting tree and run with the Markov chain Monte Carlo (Larget and Simon 1999) for 1×10^6 generations. The tree was visualized and saved with FigTree 1.4.4 (Rambaut 2018).

Results and discussion

Taxonomy and systematics

Family: Dorylaimidae de Man, 1876
Subfamily: Labronematinae Peña-Santiago & Álvarez-Ortega, 2014

***Vastnema* Vu, Abolafia & Peña-Santiago, gen. nov.**
https://zoobank.org/D80ECAAF-2697-4B75-9521-5EAAD6CB72CC

Type and only species. *Vastnema crassicutaneum* sp. nov.

Etymology. The genus name derives from VAST (Vietnam Academy of Science and Technology) and "*nema*".

Diagnosis. Dorylaimidae. Labronematinae. Large to very large-sized nematodes. Cuticle dorylaimid, very thick, three-layered. Lip region tapering, continuous with the adjoining body, with totally fused lips and very small cephalic papillae. Amphid aperture less than one-half of lip region diameter. Odontostyle strong, up to twice the lip region diameter, with wide aperture. Guiding ring, delicate, double. Odontophore rod-like, simple. Pharynx unusually short, entirely muscular, very gradually enlarging, with basal expansion occupying less than half of the total neck length. Female genital system di-ovarian with a peculiar uterine differentiation, well-developed *pars refringens vaginae*, and pre-equatorial longitudinal vulva. Tail similar in both sexes, short and rounded. Spicules dorylaimid, slender. Ventromedian supplements 45–58 in number, very shortly spaced, small, not typically mammiform, with hiatus.

Morphological separation from its closest genera

The general appearance of the new genus (large size, strong odontostyle, double guiding ring, rounded tail in both sexes) resembles the morphological pattern observed in some members of Labronematinae Peña-Santiago & Álvarez-Ortega, 2014, especially *Labronema* Thorne, 1939, and *Nevadanema* Álvarez-Ortega & Peña-Santiago, 2012. It differs from *Labronema*, a very heterogeneous genus (needing a good revision, *cf.* Andrássy 2009, 2011) in its larger size (body 4.79–6.35 mm *vs.* very occasionally exceeding 4.5 mm long), lip region tapering, with rounded anterior margin and continuous with the adjoining body (*vs.* not tapering, with truncate or even somewhat sunken anterior margin and often offset by deep constriction), very short neck (b = 6.3–8.7 *vs.* b-ratio always less than 6.3 and very sporadically more than 5.0), presence (*vs.* absence) of a peculiar uterine differentiation, pre-equatorial (V = 38–44 *vs.* equatorial or post-equatorial vulva, V-ratio never under 44 and very often *ca* 50 or more), and much more ventromedian supplements (45–58 *vs.* a maximum of 31) with different shape (very low and resembling stomata of tree leaves *vs.* typically mammiform). [See also the detailed separation of type species from some atypical members of *Labronema*.] The new genus is easily distinguishable from *Nevadanema* by its much larger general size (*vs.* body length 2.36–3.40 mm), lip region shape (*vs.* cap-like and offset by constriction), larger odontostyle aperture (more than one-third *vs.* less than one-fifth of total length), comparatively much shorter neck (*vs.* b = 3.6–4.5), pre-equatorial vulva (*vs.* V = 49–56), complex (*vs.* simple) uterus, and male as frequent as female (*vs.* male absent).

Descriptions of species

***Vastnema crassicutaneum* sp. nov.**

https://zoobank.org/2BDC6FBA-31AA-4079-A389-CE3CC740BFB9

Figs 1–6

Material examined. Sixteen females and eight males from three locations, in good state of preservation, some specimens probably slightly flattened due to their large body, including wide diameter at mid-body.

Morphometrics. See Table 1.

Type population. (Nature Reserve Nam Xuan Lac, Cho Don district, Bac Can province) 11 females and seven males.

Holotype. Female adult, Northern Vietnam, Bac Can province, Cho Don district, Nam Xuan Lac nature reserve, December 2021 (coordinates 22°17'30"N, 105°31'06"E, elevation 800 m), soil from a wild forest.

Paratypes. Eleven females and seven males with the same collection details as the holotype.

Other material. All in Northern Vietnam. i) Ha Giang province, Bac Me district, Du Gia nature reserve, October 2023 (coordinates 22°43'13"N, 105°11'32"E, elevation 300 m); ii) Ninh Binh province, Cuc Phuong National Park, August 2019 (coordinates 20°21'06"N, 105°35'22"E, elevation 430 m), soil from a wild forest.

Description. Adult. Moderately slender to slender (a = 25–34) nematodes of large to very large size, 4.79–6.35 mm long. Body cylindrical, clearly narrowing towards the anterior end, much less towards the posterior extremity, as the tail is short and rounded. Upon fixation, habitus almost straight. Cuticle smooth (but a very fine transverse striation is appreciable with SEM), three-layered, consisting of thin outer and inner layers and much thicker intermediate layer, especially conspicuous at level of anterior region and tail, 12.5–15.5 µm thick at anterior region, 9–15 µm in midbody, and 14–20 µm on tail. Lateral chord 12–29 µm wide, occupying up to one-sixth (8–16%) of midbody diameter, lacking any differentiation. Body pores very small, the lateral ones arranged in a single row throughout the body length, a few dorsal and ventral pores are present at cervical region. Lip region rounded, occasionally slightly asymmetrical, visibly tapering, less than one-fourth (18–24%) of body diameter at neck base, 2.2–2.5 times as wide as high, continuous with the adjoining body or hardly offset by a very shallow depression. SEM observations: lips totally amalgamated, oral field wide as inner and outer labial papillae are quite close, perioral area not differentiated, labial papillae button-like, cephalic papillae appearing as very small pores (Fig. 6A–C). Amphidial fovea cup-like, its aperture 10.5–13.5 µm wide, occupying less than one-half (33–48%) of lip region diameter, appearing as a wide transverse slit visibly occluded at its middle. Cheilostom almost cylindrical, 32–40 µm long, with moderately thick walls, but lacking any other specialization. Odontostyle strong, 1.7–2.0 times longer than lip region diameter, 8.3–11.8 times as long as wide, 0.89–1.13% of body length, its aperture 19–27 µm long or less than one-half (36–48%) of the total length. Guiding ring, double, but very delicate and difficult to visualize in some specimens. Odontophore simple, rod-like, 1.3–1.6 times the odontostyle. A mucro 2.5–8.5 × 1.5–3 µm is present in several specimens at level of odontophore base (Fig. 2A, B, K). Pharynx comparatively very short (b = 6.3–8.7), strongly muscular, very gradually enlarging into the basal expansion that is 3.4–6.1 times as long as wide, 1.9–3.0 times longer than body diameter at neck base, and occupies up to one-half (46–49%) of the total neck length; pharyngeal gland nuclei located as follows: DO = 52–56, DN = 53–58, S_1N_1 = 67–69, S_1N_2 = 74–79, S_2N = 83–88. Nerve ring located at 228–308 µm or 33–36% of the total neck length from the anterior end. Pharyngo-intestinal junction consisting of a conical to somewhat cylindroid cardia 41–84 × 17–32 µm almost entirely enveloped by intestinal tissue, and a weak, ring-like structure around the junction of cardia to pharyngeal base.

Female. Genital system diovarian, with both branches equally and well-developed, the anterior 823–1250 µm long, or 16–24% of body length, the posterior 835–1153 µm long, or 15–21% of body length. Ovaries variable in length, 221–704 µm the anterior, 185–619 µm the posterior, often reaching and surpassing the sphincter level, with oocytes arranged first in several rows and then in a single one. Oviduct variably long too, 157–349 µm or 0.8–2.0 body diameters,

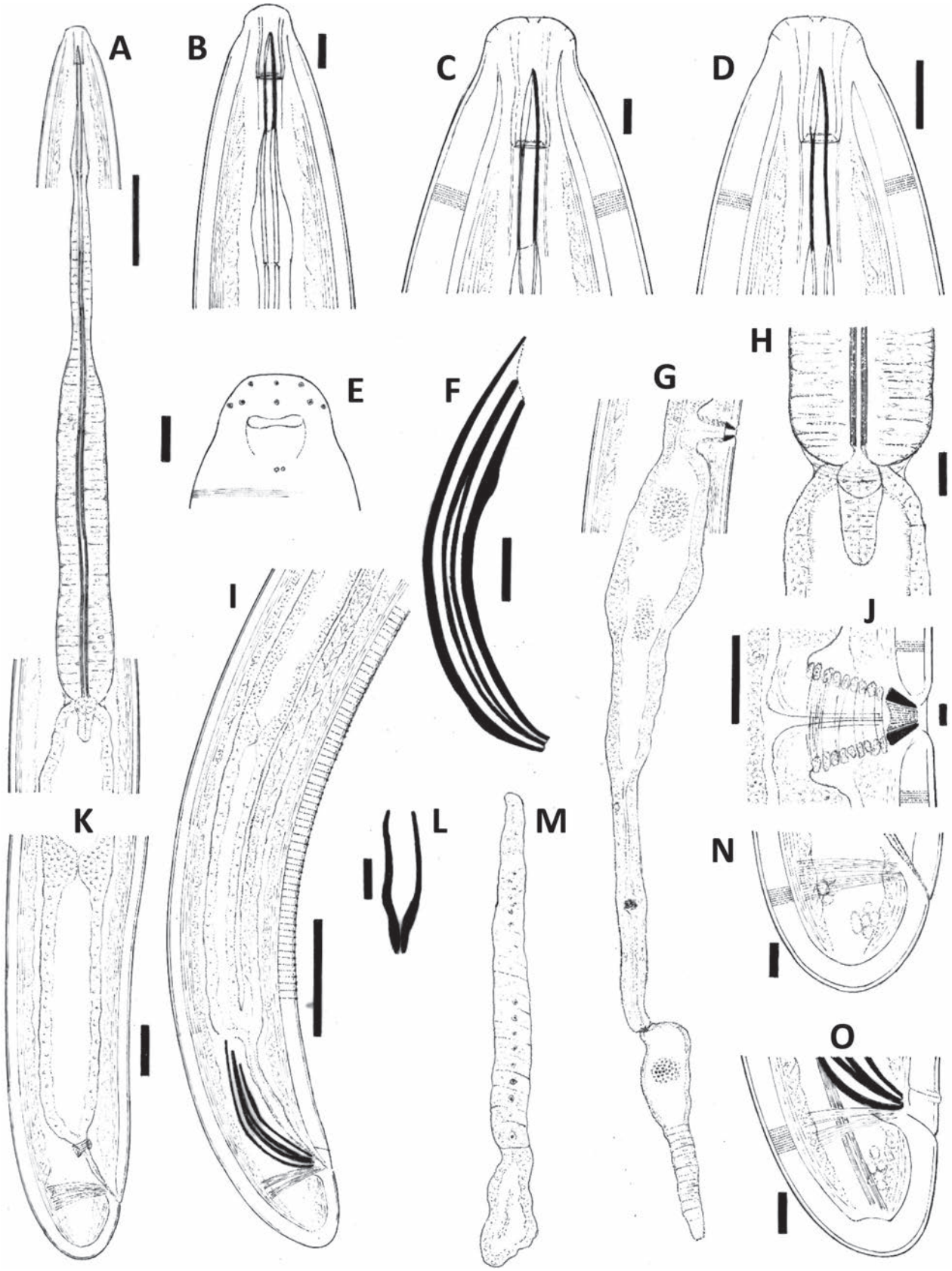

Figure 1. *Vastnema crassicutaneum* gen. et sp. nov. from Vietnam. **A.** Neck region; **B–D.** Anterior region, lateral median view; **E.** Anterior region, lateral surface view; **F.** Spicule; **G.** Female, posterior genital branch; **H.** Pharyngo-intestinal junction; **I.** Male, posterior body region; **J.** Vagina; **K.** Female, posterior body region; **L.** Lateral guiding piece; **M.** Posterior ovary; **N.** Female, caudal region; **O.** Male, caudal region. Scale bars: 100 µm (**A, G, I, M**); 20 µm (**B, D, F, H, N, O**); 10 µm (**C, E, J, L**); 50 µm (**K**).

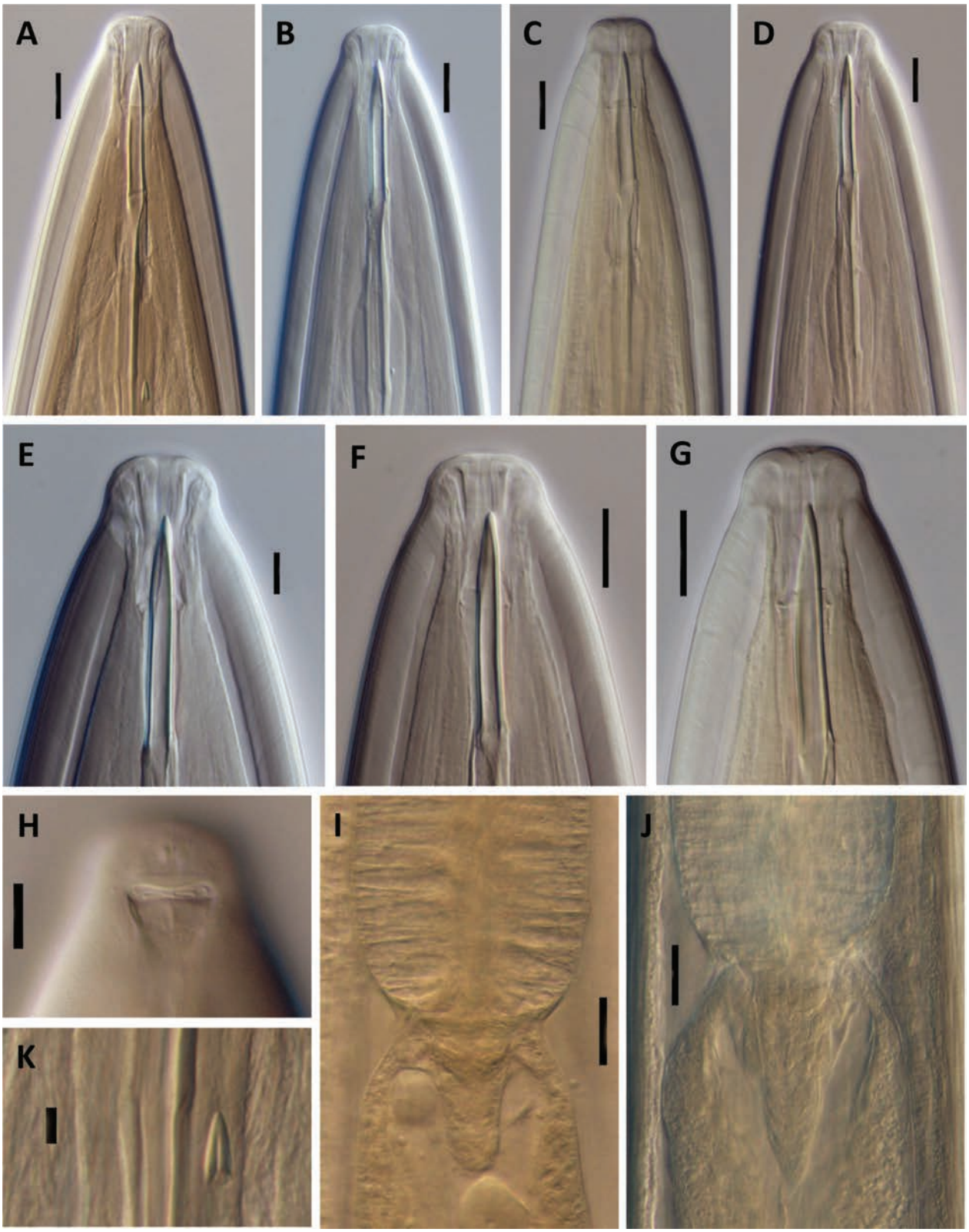

Figure 2. *Vastnema crassicutaneum* gen. et sp. nov. from Vietnam (LM). **A–G.** Anterior region, lateral median view; **H.** Anterior region, lateral surface view; **I, J.** Pharyngo-intestinal junction; **K.** Mucro located at odontophore base. Scale bars: 20 µm (**A–D, F, G, I, J**); 10 µm (**E, H**); 5 µm (**K**).

consisting of two sections almost equal in length: distal part made of prismatic cells and proximal one an elongated ***pars dilatata*** always with wide lumen inside and containing abundant sperm cells, therefore functioning as spermatheca. A weak sphincter separates the oviduct from the uterus. Uterus 571–804 µm or 3.2–4.3 body diameters long, bipartite, consisting of distal, longer, and slender region with narrow lumen and a proximal, shorter, and wider region with

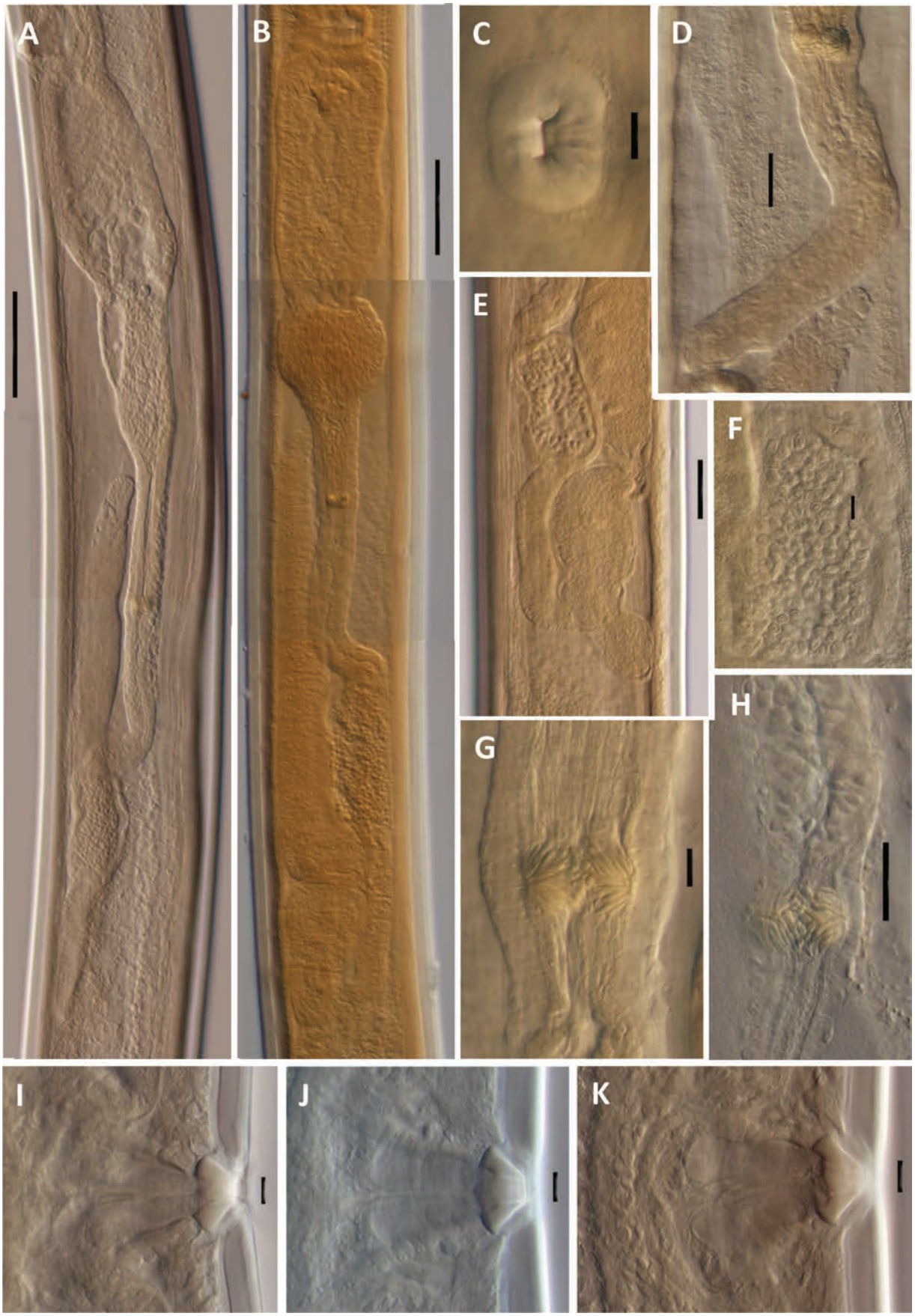

Figure 3. *Vastnema crassicutaneum* gen. et sp. nov. from Vietnam (LM, female genital system); **A, B.** Posterior branch; **C.** Vulva, ventral view; **D.** Oviduct-uterus junction; **E.** Oviduct; **F.** Sperm cells inside *pars dilatata oviductus*; **G, H.** Uterus differentiation; **I–K.** Vagina, lateral view. Scale bars: 100 µm (**A**); 10 µm (**C, F, G, I–K**); 20 µm (**D, H**); 50 µm (**E**).

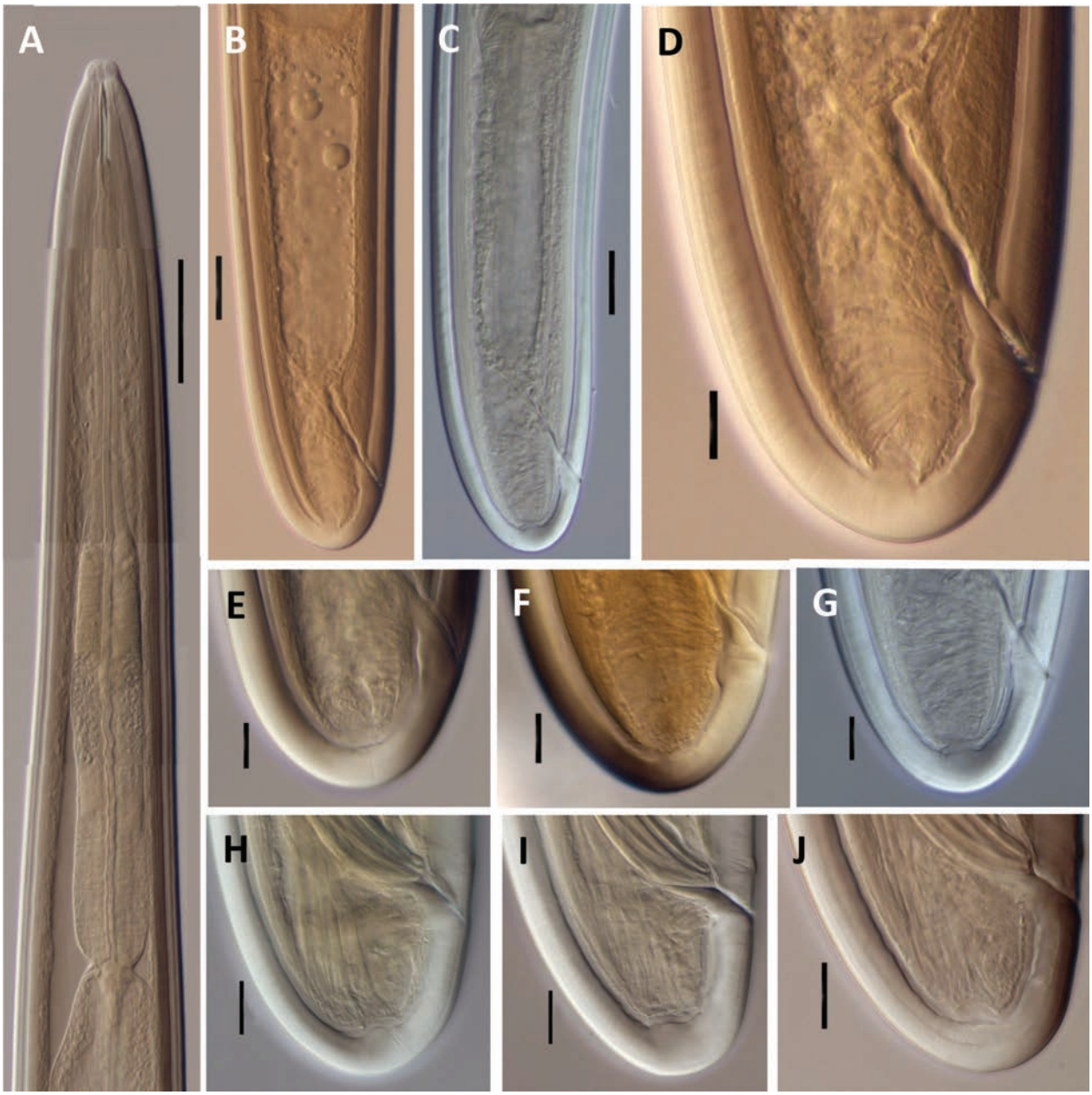

Figure 4. *Vastnema crassicutaneum* gen. et sp. nov. from Vietnam (LM, neck and posterior region); **A.** Neck region; **B, C.** Female, posterior body region; **D.** Female, rectum and caudal region; **E–G.** Female, caudal region; **H–J.** Male, caudal region. Scale bars: 100 µm (**A**); 50 µm (**B, C**); 20 µm (**D–J**).

broad lumen and often containing abundant sperm cells inside; distal region always bearing a very special differentiation, resembling the Z-like structure of some dorylaims, with a concentration of many small spindle-shaped elements visibly refringent that adopt a peculiar arrangement (Fig. 3A, B, G, H), all together measuring 13–18 × 22–26 µm. Vagina 54–73 µm long, to *ca* one-third (31–36%) of body diameter: ***pars proximalis*** 39–51 × 26–37 µm, with divergent walls surrounded by moderately developed circular musculature; ***pars refringens***, consisting of (lateral view) two separated triangular pieces 12–16 × 6–10 µm and with a combined width of 26–32 µm; ***pars distalis*** 5–10 µm long. Vulva longitudinal, slightly elliptical, 8–11 µm long. Prerectum 2.2–3.3, rectum 0.8–1.3 body diameters long. Anus a weakly arched transverse slit *ca* 15 µm long. Tail short and rounded, inner core 17–22 µm long, occupying less than half (37–48%) of tail length, caudal pores two pairs, at the middle of tail, one sublateral, another subdorsal.

Male. Prerectum 3.4–5.5, cloaca 1.3–1.5 times longer than body diameter at level of the cloacal aperture. Genital system diorchic with opposite testes. Sperm cells elliptical, 8 × 4.5 µm. In addition to the pre-cloacal pair, situated at 16–24 µm from the cloacal aperture, there is a series of 47–58, shortly spaced (7–14, exceptionally reaching 19 µm in between), very low, ventromedian supplements, the most posterior of them located at 101–154 µm from the adcloacal pair, thus with a perceptible hiatus. As seen with SEM, the ventromedian supplements are not mammiform

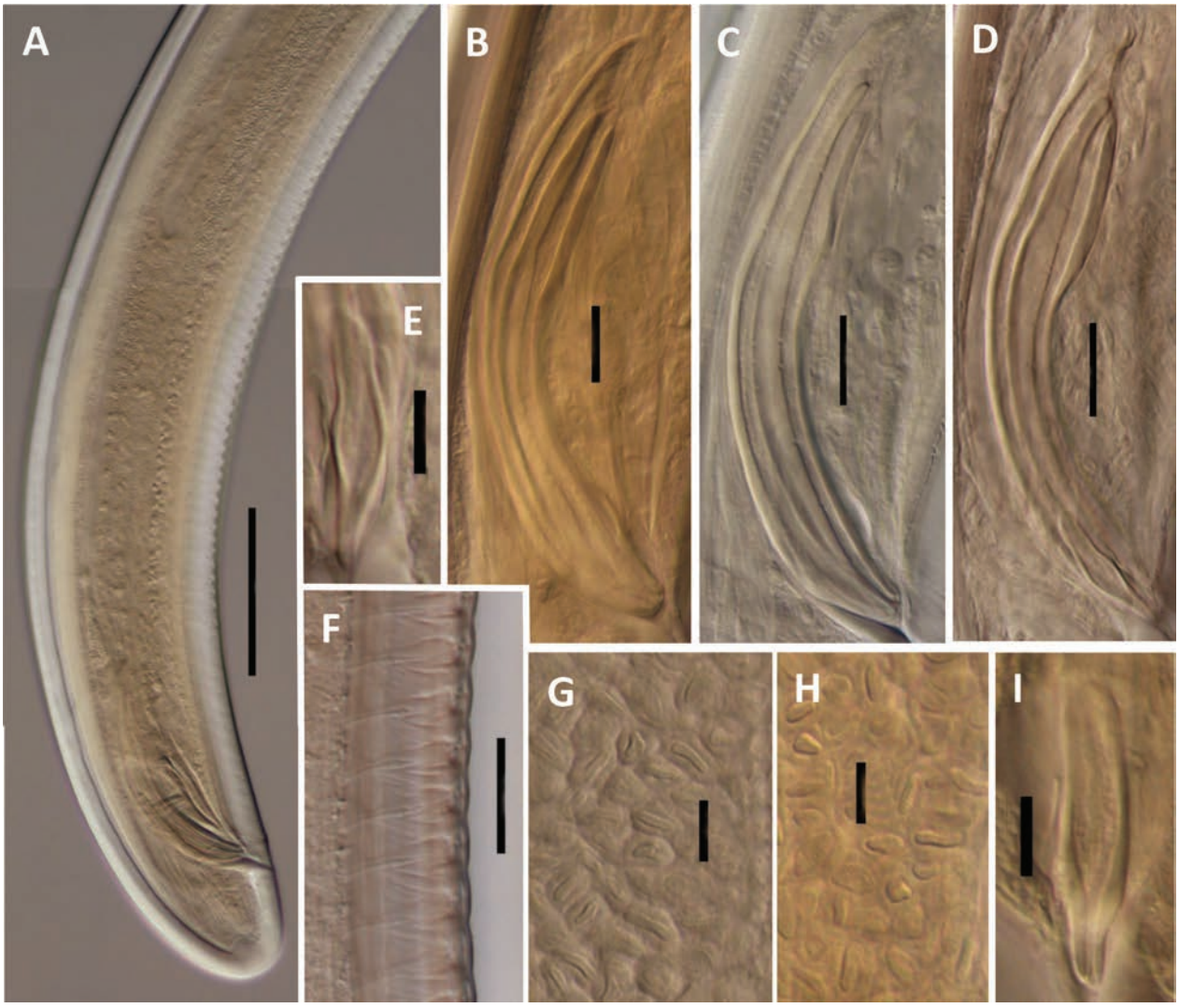

Figure 5. *Vastnema crassicutaneum* gen. et sp. nov. from Vietnam (LM, male traits); **A.** Posterior body region; **B–D.** Spicule, arrowheads pointing at the ventral hump; **E, I.** Lateral guiding piece; **F.** Ventromedian supplements. Scale bars: 100 µm (**A**); 20 µm (**B–D, F**); 10 µm (**E, G–I**).

as so usual in dorylaims but appear as short longitudinal slits that resemble the stomata of plant leaves (Fig. 6K–M). Spicules dorylaimid, relatively slender, 6.9–9.1 times longer than wide, 1.8–2.0 times longer than body diameter at level of the cloacal aperture: head 12–25 µm long, occupying up to one-sixth (8–16%) of spicule length, 1.2–1.8 times as long as wide, with its dorsal side visibly longer than the ventral one; median piece 6.5–8.5 µm wide, occupying 32–44% of spicule maximum width; posterior tip 5–9 µm wide; ventral hump and hollow little marked in general, the hump situated at 49–70 µm or 33–47% of spicule length; curvature 118–135°. Lateral guiding pieces 16–24 µm long, 4.0–4.8 times wider than long, almost cylindrical but visibly tapering at its posterior third. Tail similar to that of female, maybe slightly more conoid.

Other populations. (six females and one male from two locations): Morphologically identical to type material. Morphometrically very similar too, with totally coincident or widely overlapping ranges of main measurements and ratios, although a few minor differences are also noted; for instance, prerectum length is appreciably longer in Ha Giang specimens: 324–390 *vs.* 206–321 µm in females and 473 *vs.* 324–390 µm in males.

Molecular characterization. After sequencing and editing, six (three 18S and three 28S) rDNA sequences were obtained of type material for phylogenetic analyses. The three 28S sequences were 798, 679, and 651 bp long, with 511 bp in common, and a Blast search showed that the longest of them was 96.9% similar to that of *Labronema porosum* Vu, Elshishka, Nguyen, Le, Mladenov & Peneva, 2024 (acc. PP060468), 96.3% to that of *L. bidoupense* Vu, Elshishka, Nguyen, Le, Mladenov & Peneva, 2024 (acc. PP060469), 92.0% to that of *Labronema vulvapapillatum* (Meyl, 1954) Loof & Grootaert, 1981 (acc. AY592997), 91.5% to that of *L. vulvapapillatum* (acc. AY592996), 91.3% to that of *Labronema* sp., and 90.8% to that of *Nevadanema nevadense* Álvarez-Ortega & Peña-Santiago, 2012 (acc. JN242245), all of them rounded-tailed representatives of Dorylaimidae de Man, 1876, Labronematinae Peña-Santiago & Álvarez-Ortega, 2014.

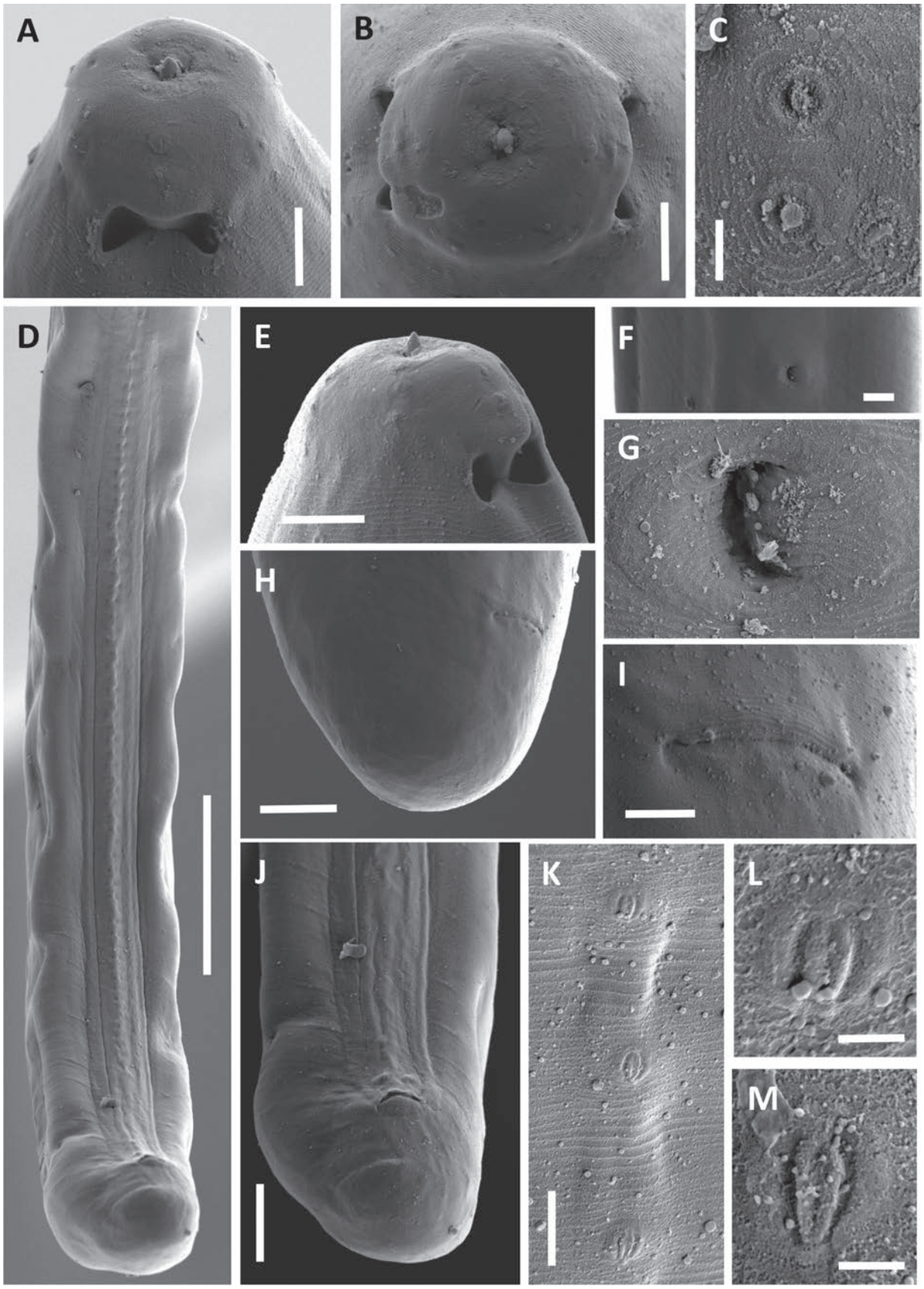

Figure 6. *Vastnema crassicutaneum* gen. et sp. nov. from Vietnam (SEM); **A.** Lip region, lateral view; **B.** Lip region, in face view; **C.** Labial papillae; **D.** Male, posterior body region, ventral view; **E.** Lip region, subventral view; **F, G.** Vulva, ventral view; **H.** Female, subventral view; **I.** Anus; **J.** Male, caudal region; **K–M.** Detail of ventromedian supplements. Scale bars: 5 µm (**A, B, E, I**); 1 µm (**C**); 100 µm (**D**); 10 µm (**F**); 4 µm (**G**); 20 µm (**H, J**); 3 µm (**K**); 1 µm (**L, M**).

Table 1. Main morphometrics of *Vastnema crassicutaneum* gen. et sp. nov. from Vietnam. Measurements in µm except L in mm, in the form: average ± sd (range).

Population		Nam Xuan Lac, Bac Can			Du Gia, Ha Giang		Cuc Phuong, Ninh Binh
		Holotype	Paratypes	Paratypes			
Character	n	♀	11♀♀	7♂♂	4♀♀	♂	2♀♀
L		6.19	5.51 ± 0.47 (5.00–6.35)	5.18 ± 0.26 (4.79–5.48)	5.80 ± 0.37 (5.26–6.09)	5.66	5.25, 5.63
a		31	29.4 ± 2.7 (25–34)	31.1 ± 2.4 (27–34)	32.2 ± 1.8 (30–34)	33	29, 40
b		7.7	7.1 ± 0.7 (6.3–8.4)	7.2 ± 0.8 (6.3–8.7)	7.3 ± 0.1 (7.2–7.5)	7.6	7.0, 6.3
c		129	113 ± 11 (98–131)	107 ± 17 (94–140)	116 ± 22 (101–142)	107	103, 106
V		41	41.8 ± 1.6 (39–44)	-	39.0 ± 1.2 (38–41)	-	?, 44
c'		0.5	0.5 ± 0.0 (0.5–0.6)	0.6 ± 0.0 (0.5–0.7)	0.5 ± 0.1 (0.5–0.6)	0.7	0.5, 0.5
Lip region diameter		31	29.3 ± 1.4 (27–31)	28.1 ± 1.3 (26–30)	27.0 ± 1.2 (26–28)	28	31, 31
Odontostyle length		55	55.2 ± 2.7 (51–60)	53.4 ± 2.6 (49–57)	55.3 ± 2.8 (52–58)	55	51, 70
Odontophore length		80	77.7 ± 4.0 (72–84)	75.9 ± 3.8 (70–79)	73–0 ± 2.4 (70–76)	77	73, 82
Neck length		803	777 ± 54 (627–821)	720 ± 44 (631–755)	794 ± 59 (706–837)	746	746, 888
Pharyngeal expansion length		386	370 ± 29 (292–390)	341 ± 22 (299–364)	386 ± 42 (338–418)	357	357, 449
Body diameter at neck base		167	148 ± 10 (133–167)	136 ± 12 (122–156)	148 ± 4.9 (145–154)	138	142, 137
mid-body		200	188 ± 11 (172–210)	168 ± 20 (144–194)	180 ± 4.3 (175–185)	170	179, 141
anus		96	94.1 ± 4.0 (88–102)	79.0 ± 3.9 (71–84)	94.3 ± 1.5 (93–96)	76	99, 99
Distance vulva – anterior end		2564	2300 ± 193 (2035–2585)	-	2256 ± 91 (2143–2344)	-	?, 2491
Prerectum length		321	259 ± 39 (206–321)	339 ± 57 (265–412)	361 ± 30 (324–390)	473	319, 228
Rectum/cloaca length		121	89.9 ± 11.8 (79–121)	108 ± 7 (96–117)	74 ± 5.6 (68–79)	98	97, 90
Tail length		48	48.8 ± 3.1 (45–56)	49.0 ± 5.1 (39–54)	50.3 ± 6.7 (43–56)	53	51, 53
Spicules length		-	-	149 ± 7 (139–160)	-	138	-
Ventromedian supplements		-	-	47–58	-	45	-

The three 18S sequences were 1698, 1690, and 1689 bp long, with 1684 bp in common, and a Blast search showed that the longest of them was 97.2% similar to that of *Aporcelaimellus* sp. (acc. JX674034), 97.2% to that of *L. ferox* Thorne, 1939 (acc. AY552972), 97.2% to that of *Aporcelaimellus* sp. (acc. PP099686), 97.1% to that of *Prodorylaimus* sp. (EF207246), and 97.0% to that of *Mesodorylaimus* sp. (acc. MG921256).

Diagnosis. The new species is characterized by its 4.79–6.35 mm long body, cuticle three-layered and 12.5–15.5 µm thick at anterior region, lip region continuous with the adjoining body and 26–31 µm wide, odontostyle 49–60 µm long or 1.8–2.0 times the lip region diameter, neck 627–888 µm long, pharyngeal expansion occupying 46–49% of the total neck length, female genital system diovarian, uterus complex and 571–804 µm or 3.2–4.3 body diameters long, pre-equatorial (V = 38–44) and longitudinal vulva, tail short and rounded in both sexes (39–56 µm, c = 98–140, c' = 0.5–0.7), spicules 138–160 µm long, and 45–58 small ventromedian supplements with hiatus.

Separation from some resembling species. The new species resembles a few *Labronema* species. In having large size, it compares to *L. magnum* Altherr, 1972, a freshwater species known to occur in Nepal, Russia, and Sweden (see taxonomic revision by Peña-Santiago, 2022), but it differs from this in its much thicker cuticle (*vs.* for instance, 4–5 µm at anterior region), lip region with different shape (*vs.* anterior region truncate, offset by weak constriction, and one-third as wide as body diameter at neck base), comparatively much shorter neck (*vs.* b = 4.1–6.3), more anterior vulva (*vs.* V = 44–53), longer spicules (*vs.* 118–135 µm), and more numerous (*vs.* 21–31) ventromedian supplements with different aspect (*vs.* typically mammiform).

In having continuous lip region, it also resembles several atypical *Labronema* representatives, including *L. hyalinum* (Thorne & Swanger, 1936), Thorne, 1939, *L. neopacificum* Rahman, Jairajpuri, Ahmad & Ahmad, 1987, *L. orientale* Andrássy, 2011, *L. singhalense* Andrássy, 2011, *L. stechlinense* Altherr, 1968, and *L. thornei* Ferris, 1968, but all of them show smaller general size (body length up to 3.73 mm long, odontostyle up to 48 µm long), comparatively longer neck (b-ratio up to 5.2), more posterior vulva (V = 45–55), shorter spicules (up to 120 µm long), and much less ventromedian supplements (up to 29) with different shapes.

Type material. Female holotype, seven female and three male paratypes, and one male paratype deposited at the Department of Nematology, Institute of Ecology and Biological Resources, VAST, Hanoi, Vietnam. Four (two female and two male) paratypes at the Nematode Collection of the University of Jaén, Spain. Four (two female and two male) paratypes at USDANC, Beltsville, Maryland, USA.

Etymology. The species epithet derives from the Latin terms *crassus* = thick and *cutaneum* = skin, cuticle, and refers to this peculiar trait of the new taxon.

Evolutionary relationships of the new taxon

Morphologically, *Vastnema crassicutaneum* gen. et sp. nov. is characterized by a unique combination of very unusual traits within the family Dorylaimidae de Man, 1876, and even the order Dorylaimida. First, its very thick, three-layered cuticle is only observed in some very large dorylaims and should be regarded, with a cladistic approach, as a relevant apomorphy. Second, its comparatively short pharynx/neck, with b-ratio always exceeding 6.0 and very often appreciably more, probably is an

autapomorphy of the new taxon, especially if its rounded-tailed condition is considered. Third, the presence of an exclusive uterine specialization, resembling those known as Z-like structures but significantly different from them in its nature, is another recognizable autapomorphic feature too. Fourth, the high number and, in particular, the shape of male ventromedian supplements, appearing as plant leaf stomata rather than button-like or mammiform structures, certainly is (at least) an infrequent apomorphy. Other interesting traits (lip region continuous and with totally fused lips, double guiding ring, pre-equatorial vulva, rounded-tailed sexes) are more usual apomorphic features within dorylaims. As mentioned, the new taxon shares several traits (strong odontostyle, double guiding ring, rounded tail in both sexes) with members of the subfamily Labronematinae, in particular *Nevadanema* and some *Labronema* representatives, supporting a close relationship between them.

As derived from the molecular analyses of obtained sequences, whose results are presented in Figs 7 (18S tree), 8 (28S tree), the evolutionary relationships of the new taxon basically agree with those deduced from morphological observations. Thus, and in both trees, *Vastnema* gen. nov. sequences form part of a maximally (100%) supported clade also including sequences of *Labronema* representatives. Moreover, the 28S tree, which provides better general resolution, shows that the (*Vastnema* gen. nov. + *Labronema* spp.) clade belongs to a much larger (highlighted in yellow, and also maximally supported) clade containing sequences of Dorylaimidae and Actinolaimidae Thorne, 1939 taxa. It is remarkable that this large subclade is divided into two subclades,

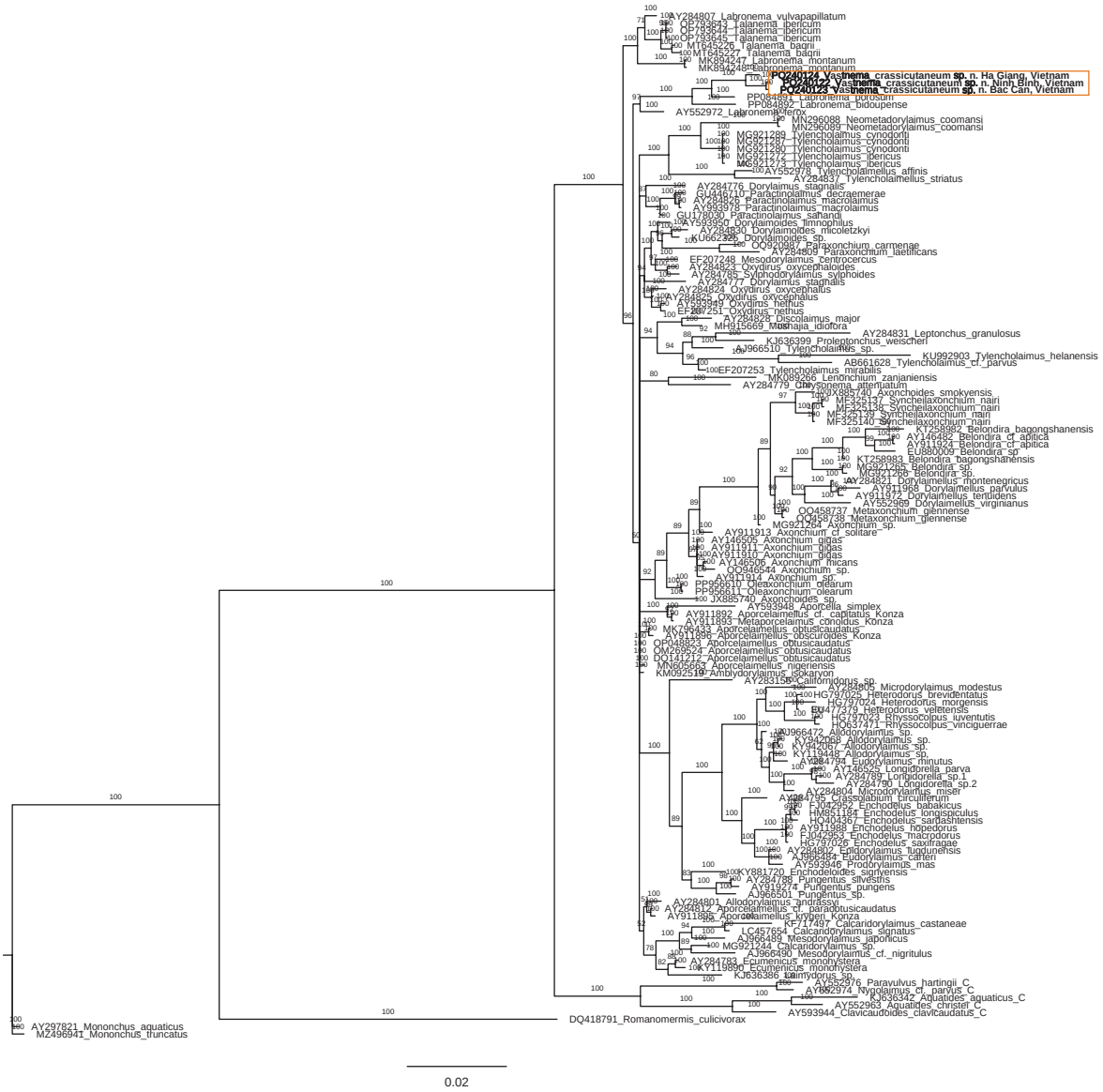

Figure 7. Bayesian inference tree from the newly sequenced *Vastnema crassicutaneum* gen. et sp. nov. based on sequences of the 18S rDNA region. Bayesian posterior probabilities (%) are given for each clade. The scale bar shows the number of substitutions per site.

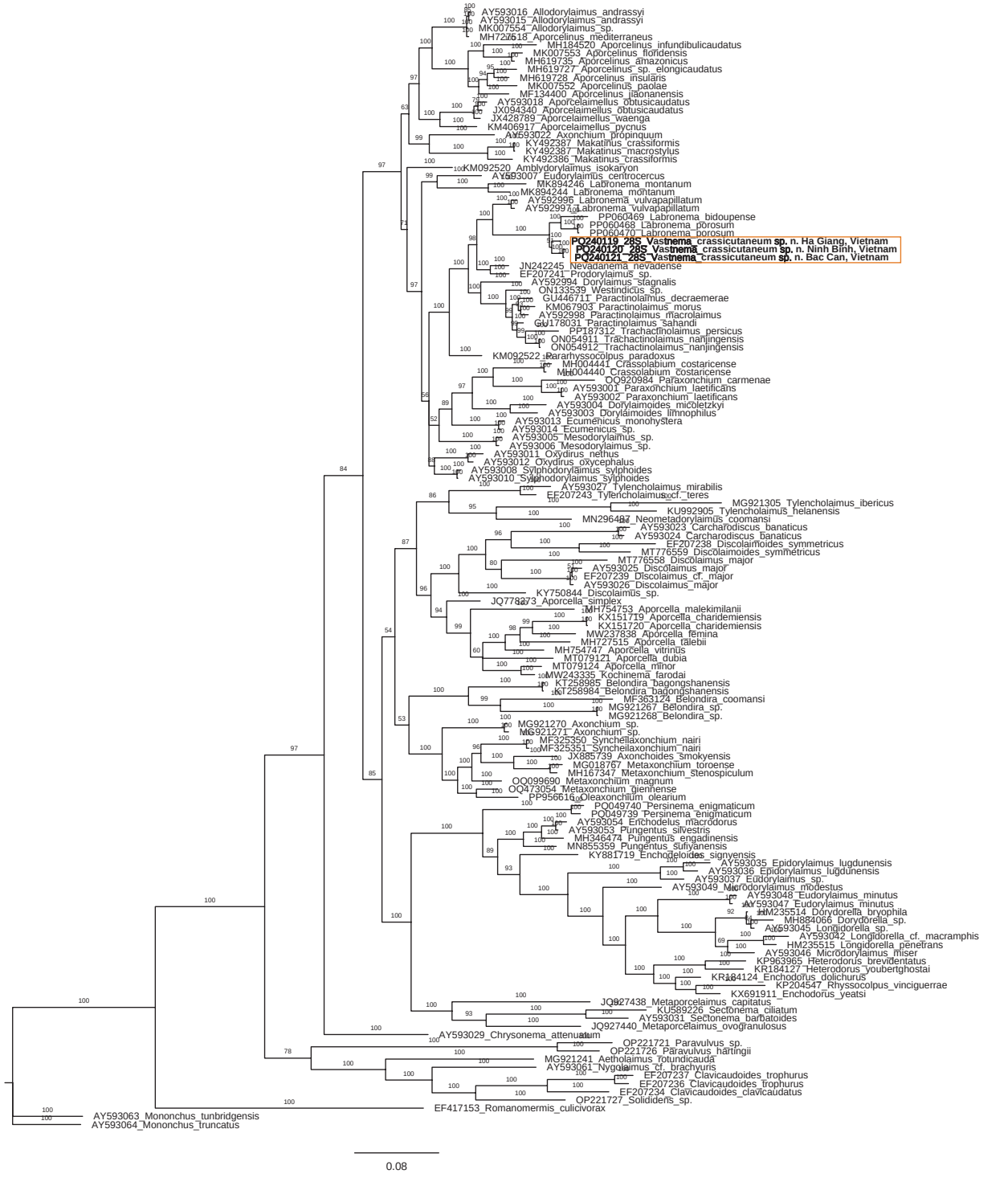

Figure 8. Bayesian inference tree from the newly sequenced *Vastnema crassicutaneum* gen. et sp. nov. based on sequences of the 28S rDNA region. Bayesian posterior probabilities (%) are given for each clade. The scale bar shows the number of substitutions per site.

one including sequences of *Vastnema* gen. nov., *Labronema*, *Nevadanema*, and *Prodorylaimus* sp., and another consisting of sequences of *Dorylaimus stagnalis* Dujardin, 1845, plus several actinolaims.

An integrative approach to the subject, combining morphological and molecular information, supports a very close relationship of the new taxon with Labronematinae representatives, but also that internal and external relationships of Dorylaimidae might be more complex than traditionally assumed, a question that will require much further research before its elucidation.

Acknowledgements

The senior author (RPS) deeply appreciates the invitation, support, and reception of the Department of Nematology, Institute of Ecology and Biological Resources

(IEBR), Vietnamese Academy of Sciences and Technology (VAST), Hanoi, Vietnam, to visit its lab and to participate in the project NCXS01.04/23-25. The Spanish authors (JA, RPS) thank the staff (Amparo Martínez-Morales), and this study used the facilities of the equipment of "Centro de Instrumentación Científico-Técnica (CICT)," University of Jaén, for assistance to obtain SEM pictures.

The work is supported by the Vietnam Academy of Science and Technology (VAST) under the project NCXS01.04/23-25 "Developing the first-class research team on the discovery of diversity and application potential of hymenopterans, myriapods, and soil nematodes in the limestone mountains of northeastern Vietnam."

References

Altherr E (1968) Nématodes de la nappe phréatique du réseau fluvial de la Saale (Thuringe) et psammniques du Lac Stechlin (Brandebourg dur nord). Limnologica 6: 247–320.

Altherr E (1972) Contribution à la connaissance des Nématodes rithrostygopsammiques et rithrostygopséphiques de Suède. Revue Suisse de Zoologie 79: 881–902. https://doi.org/10.5962/bhl.part.97141

Álvarez-Ortega S, Peña-Santiago R (2012) Nematodes of the order Dorylaimida from Andalucía Oriental, Spain. *Nevadanema nevadense* gen. n., sp. n. (Qudsianematidae) from Sierra Nevada National Park. Nematology 14: 249–264. https://doi.org/10.1163/138855411X589309

Álvarez-Ortega S, Nguyen, TAD, Abolafia J, Vu TTT, Peña-Santiago R (2015) Three new species of the genus *Aporcelaimoides* Heyns, 1965 from Vietnam (Nematoda, Dorylaimida, Aporcelaimidae), with an updated taxonomy of the genus. Zookeys 516: 1–26. https://doi.org/10.3897/zookeys.516.10087

Álvarez-Ortega S, Nguyen TAD, Abolafia J, Vu TTT, Bonkowski M, Peña-Santiago R (2016) Three new species of *Sectonema* Thorne, 1930 (Dorylaimida, Aporcelaimidae) from Vietnam. Nematology 18: 517–536. https://doi.org/10.1163/15685411-00002974

Andrássy I (2009) Free-living nematodes of Hungary. III. Pedozoologica Hungarica n° 5. Hungarian Natural History Museum. Budapest, Hungary, 608 pp.

Andrássy I (2011) Three new bisexual species of *Labronema* Thorne, 1939 (Nematoda, Qudsianematidae). Opuscula Zoologica Budapestinensis 43: 107–120. https://www.oalib.com/research/2072275

Darriba D, Taboada GL, Doallo R, Posada D (2012) jModelTest 2: more models, new heuristics and parallel computing. Nature Methods 9: 772. https://doi.org/10.1038/nmeth.2109

Dujardin F (1845) Histoire naturelle des helminthes ou vers intestinaux. Librairie Encyclopédique de Roret, Paris, 654 pp.

Ferris VR (1968) Biometric analyses in the genus *Labronema* (Nematoda, Dorylaimida) with a description of *L. thornei* n. sp. Nematologica 14: 276–284. https://doi.org/10.1163/187529268X00480

Floyd RM, Rogers AD, Lambshead PJD, Smith CR (2005) Nematode-specific PCR primers for the 18S small subunit rRNA gene. Molecular Ecology Notes 5(3): 611–612. https://doi.org/10.1111/j.1471-8286.2005.01009.x

Hoang H, Chu HH, Nguyen TAD, Trinh QP, Abolafia J, Peña-Santiago R (2019) Morphological and molecular characterisation of *Chitwoodius coffeae* sp. n. (Dorylaimida, Tylencholaimidae) from Vietnam, with a revised taxonomy of the genus. Nematology 21: 509–521. https://doi.org/10.1163/15685411-00003231

Holterman M, Wurff A, Elsen S, Megen H, Bongers T, Holovachov O, Bakker J, Helder J (2006) Phylum-wide analysis of SSU rDNA reveals deep phylogenetic relationships among nematodes and accelerated evolution toward crown clades. Molecular Biology and Evolution 23: 1792–1800. https://doi.org/10.1093/molbev/msl044

Kumar S, Stecher G, Tamura K (2021) MEGA 11: Molecular Evolutionary Genetics Analysis version 11.0. Molecular Biology and Evolution 38: 3022–3027. https://doi.org/10.1093/molbev/msab120

Larget B, Simon DL (1999) Markov Chain Monte Carlo Algorithms for the Bayesian Analysis of Phylogenetic Trees. Molecular Biology and Evolution 16: 750–759. https://doi.org/10.1093/oxfordjournals.molbev.a026160

Loof PAA, Grootaert P (1981) Redescription of *Labronema vulvapapillatum* Meyl, (1954) nov. comb. (Dorylaimoidea). Nematologica 27: 139–145. https://doi.org/10.1163/187529281X00197

Man J G de (1876) Onderzoekingen over vrij in de aarde levende Nematoden. Tijdschrift Nederlandsche dierkundige Vereeniging 2: 78–196.

Meyl AH (1954) Die bisher in Italien gefundenen freilebenden Erd und Süsswasser-Nematoden. Archivio Zoologico Italiano, Torino 39: 161–264.

Nguyen TAD, Peña-Santiago R (2018) Two new species of the genus *Metaxonchium* Coomans & Nair, 1975 (Nematoda, Dorylaimida, Belondiridae) from Vietnam. Zootaxa 4415: 150–160. https://doi.org/10.11646/zootaxa.4415.1.7

Nguyen TAD, Peña-Santiago R (2020) Morphological and molecular characterization of *Epidorylaimus procerus* sp. n. (Dorylaimida, Qudsianematidae) from Vietnam. Journal of Nematology 52: e2020–112 [8 pp]. https://doi.org/10.21307/jofnem-2020-112

Nguyen TAD, Vu TTT, Bonkowski M, Peña-Santiago R (2014) New data of three rare belondirid species (Nematoda, Dorylaimida, Belondiridae) from Vietnam, with the first record and description of the male of *Oxybelondira paraperplexa* Ahmad & Jairajpuri, 1979. Biodiversity Data Journal 2: e1156. https://doi.org/10.3897/BDJ.2.e1156

Nguyen TAD, Abolafia J, Bonkowski M, Peña-Santiago R (2016) Two new species of the genus *Aporcelinus* Andrássy, 2009 (Nematoda, Dorylaimida, Aporcelaimidae) from Vietnam. Zootaxa 4103: 550–560. https://doi.org/10.11646/zootaxa.4103.6.5

Nguyen TAD, Abolafia J, Dumack K, Bonkowski M, Peña-Santiago R (2017) Two known species of *Aporcelinus* Andrássy, 2009 (Dorylaimida, Aporcelaimidae) from Vietnam, with the first molecular study of the genus. Nematology 19: 853–868. https://doi.org/10.1163/15685411-00003092

Peña-Santiago R (2021) Morphology and bionomics of dorylaims (Nematoda: Dorylaimida). Nematology Monographs and Perspectives 13 (Series Editors: Cook, R. & Hunt, D.J.). Brill. Leiden, The Netherlands, 278 pp. https://doi.org/10.1163/9789004447851

Peña-Santiago R (2022) New synonyms in the genus *Labronema* Thorne, 1939 (Nematoda, Dorylaimida, Dorylaimidae). Nematology 24: 953–957. https://doi.org/10.1163/15685411-bja10175

Peña-Santiago R, Álvarez-Ortega S (2014) An integrative approach to assess the phylogeny and the systematics of rounded-tailed genera of the subfamily Qudsianematinae (Nematoda, Dorylaimida). Zoologica Scripta 43: 418–428. https://doi.org/10.1111/zsc.12058

Rahman MF, Jairajpuri MS, Ahmad I, Ahmad W (1987) Two new species of *Labronema* Thorne, 1939 (Nematoda, Dorylaimida) from India. Nematologica 32(1986): 367–373. https://doi.org/10.1163/187529286X00264

Rambaut A (2018) Figtree, a graphical viewer of phylogenetic trees. https://github.com/rambaut/figtree/releases/tag/v1.4.4

Ronquist F, Teslenko M, van der Mark P, Ayres DL, Darling A, Höhna S, Larget B, Liu L, Suchard MA, Huelsenbeck JP (2012). MrBayes 3.2: Efficient Bayesian phylogenetic inference and model choice across a large model space. Systematic Biology 61(3): 539–542. https://doi.org/10.1093/sysbio/sys029

Seinhorst JW (1959) A rapid method for the transfer of nematodes from fixative to anhydrous glycerine. Nematologica 4: 67–69. https://doi.org/10.1163/187529259X00381

Seinhorst JW (1962) On the killing, fixation and transferring to glycerine of nematodes. Nematologica 8: 29–32. https://doi.org/10.1163/187529262X00981

Southey JF (1986) Laboratory methods for work with plant and soil nematodes. London: Her Majesty' Stationery Office, 202 pp.

Subbotin SA, Sturhan D, Chizhov VN, Vovlas N, Baldwin JG (2006) Phylogenetic analysis of Tylenchida Thorne, 1949 as inferred from D2 and D3 expansion fragments of the 28S rDNA gen sequences. Nematology 8: 455–74. https://doi.org/10.1163/156854106778493420

Thorne G (1939) A monograph of the nematodes of the superfamily Dorylaimoidea. Capita Zoologica 8: 1–261.

Thorne G, Swanger HH (1936) A monograph of the nematode genera *Dorylaimus* Dujardin, *Aporcelaimus* n. gen., *Dorylaimoides* n. gen., and *Pungentus* n. gen. Capita Zoologica 6: 1–223.

Vu TTT, Elshishka M, Nguyen AD, Le TML, Mladenov A, Peneva V (2024) Two new species of genus *Labronema* Thorne, 1939 (Nematoda, Dorylaimidae) from natural parks of Vietnam with an identification key to the species with a medium-sized odontostyle. Zookeys 1215: 1–26. https://doi.org/10.3897/zookeys.1215.128183

Yoder M, De Ley I T, King I, Mundo-Ocampo M, Mann J, Blaxter M, Poiras L, De Ley P (2006) DESS: a versatile solution for preserving morphology and extractable DNA of nematodes. Nematology 8: 367–376. https://doi.org/10.1163/156854106778493448

Zoosyst. Evol. 101 (2) 2025, 597–608 | DOI 10.3897/zse.101.133734

PENSOFT

MUSEUM FÜR NATURKUNDE BERLIN

Molecular phylogeny and taxonomy of the genus *Eozapus* (Mammalia, Rodentia, Zapodidae) with the description of a new species

Siyu Yang[1], Fei Xie[1], Chengxin Zhou[1], Zongyun Zhang[1], Xuming Wang[2], Shaoying Liu[2], Shunde Chen[1]

1 *School of Life Sciences, Sichuan Normal University, Chengdu, Sichuan, 610101, China*

2 *Sichuan Academy of Forestry, Chengdu, Sichuan, 610081, China*

https://zoobank.org/FC6276C1-4634-4400-8567-CB843C5809CE

Corresponding authors: Shaoying Liu (shaoyliu@163.com); Shunde Chen (csd111@126.com)

Academic editor: Melissa T. R. Hawkins ♦ **Received** 2 August 2024 ♦ **Accepted** 4 December 2024 ♦ **Published** 10 March 2025

Abstract

Eozapus is a monotypic genus in the family Zapodidae, with a single species and two subspecies: *Eozapus setchuanus setchuanus* and *Eozapus setchuanus vicinus* in the mountains of southwestern China. *Eozapus setchuanus* is one of the oldest and rarest species. The molecular phylogenetic and evolutionary history of this species has not yet been explored because of its small size and difficulty in capturing it. In this study, we collected 51 specimens, sequenced one mitochondrial gene and two nuclear genes, and conducted morphological analyses to clarify the phylogenetic relationship and evolutionary history of this genus. Both molecular and morphological analyses supported the classification of these three species within the genus *Eozapus*. We describe a new species, *Eozapus wanglangensis* **sp. nov.**, and propose elevating *E. s. vicinus*, previously considered a subspecies of *Eozapus setchuanus*, to the status of an independent species. Furthermore, the uplift of the Qinghai-Tibetan Plateau, the complex topography of sky islands, and climate change promoted the speciation and diversity of the genus *Eozapus*.

Key Words

Eozapus, jumping mouse, new species, phylogenetic

Introduction

The mountains of southwestern China, which are known as “sky islands” (He and Jiang 2014), have been considered key biodiversity hotspots (Myers et al. 2000). The complex topography of the sky islands and diversified climate conditions may have led to the evolution of a unique fauna of endemic species and the emergence of new lineages (Wei et al. 2018). Previous phylogenetic and phylogeographic studies in this region have revealed cryptic new species of small mammals in the region, such as *Niviventer* (Zhang et al. 2016), *Crocidura* (Chen et al. 2020), the long-tailed mole (He et al. 2019), *Ochotona* (Koju et al. 2017), and Asian shrew-like moles (Wan et al. 2018).

The family Zapodidae is widespread, containing three genera, *Eozapus, Zapus,* and *Napaeozapus*, with only 11 species: *E. setchuanus, Z. hudsonius, Z. trtinotatus, Z. princeps, Z. luteus, Z. montanus, Z. oregonus, Z. pacificus, Z. saltator, N. abietorum, and N. insignis.* (Wilson and Mittermeier 2018; Mammal Diversity Database 2022). Fan et al. (2009) formerly presented molecular evidence confirming the validity of these three genera. Based on the discovery of an early Miocene fossilized tooth of the genus *Eozapus* in Inner Mongolia, researchers believe that this supports the hypothesis that Zapodidae originated in Asia (Smith and Xie 2008; Wilson and Mittermeier 2018).

Eozapus is one monotypic genus in Zapodidae, with an endemic species in the mountains of southwestern China and two subspecies, *Eozapus setchuanus setchuanus* (Pousargues, 1896) and *Eozapus setchuanus vicinus* (Thomas, 1912). However, there are differing opinions among researchers regarding the taxonomy of *Eozapus setchuanus*. Specifically, Fan et al. (2009) reported that the two subspecies of *Eozapus setchuanus* did not form reciprocally monophyletic taxa in the molecular phylogenetic tree,

casting doubt on the traditional bifurcation of *E. setchuanus* into two subspecies. The other researchers agree with this taxonomic view (Cheng et al. 2021; Sui et al. 2022; Wei et al. 2022;). The molecular evolutionary history and the genetic differentiation of the two subspecies of this species have not yet been investigated in detail. Whether *E. s. vicinus* can be considered a separate and valid species has not yet been systematically analyzed from a molecular perspective (Michaux and Shenbrot 2017; Liu and Wu 2019; Cheng et al. 2021; Sui et al. 2022).

Due to the rarity of species within the genus *Eozapus*, capturing individuals is challenging. Consequently, the distribution of the two subspecies of *Eozapus setchuanus* remains poorly described in many regions. In this study, we collected 51 specimens of the genus *Eozapus* from southwestern China, which greatly improved the problem of under-sampling in previous studies (Fan et al. 2009). Morphological characteristics, principal component analysis of skulls, and mitochondrial and nuclear genes were analyzed to clarify the phylogenetic relationships within the genus *Eozapus*, determine the status of *E. s. vicinus* as a distinct species, and explore its evolutionary history.

Materials and methods

Sampling and DNA sequencing

In this study, 51 *Eozapus* specimens were collected from the Sichuan, Shaanxi, Gansu, and Ningxia provinces of China (Fig. 1, Table 1). Specimens were collected primarily using the snap trap method. Field surveys and collections of specimens both follow relevant laws and regulations in China. The field-collected samples were numbered, and morphological data (including body weight, tail length, ear height, and hindfoot length) were measured (Suppl. material 1: table S1). Liver and muscle tissues were obtained and preserved in analytically pure alcohol (99%). Upon return to the laboratory, tissues were stored in a -80 °C freezer for subsequent molecular analyses, while specimens were prepared as the study skins for morphological studies. All tissues and specimens used in this study were archived at the Sichuan Academy of Forestry (SAF) and the College of Life Sciences of Sichuan Normal University (SCNU) (Table 1).

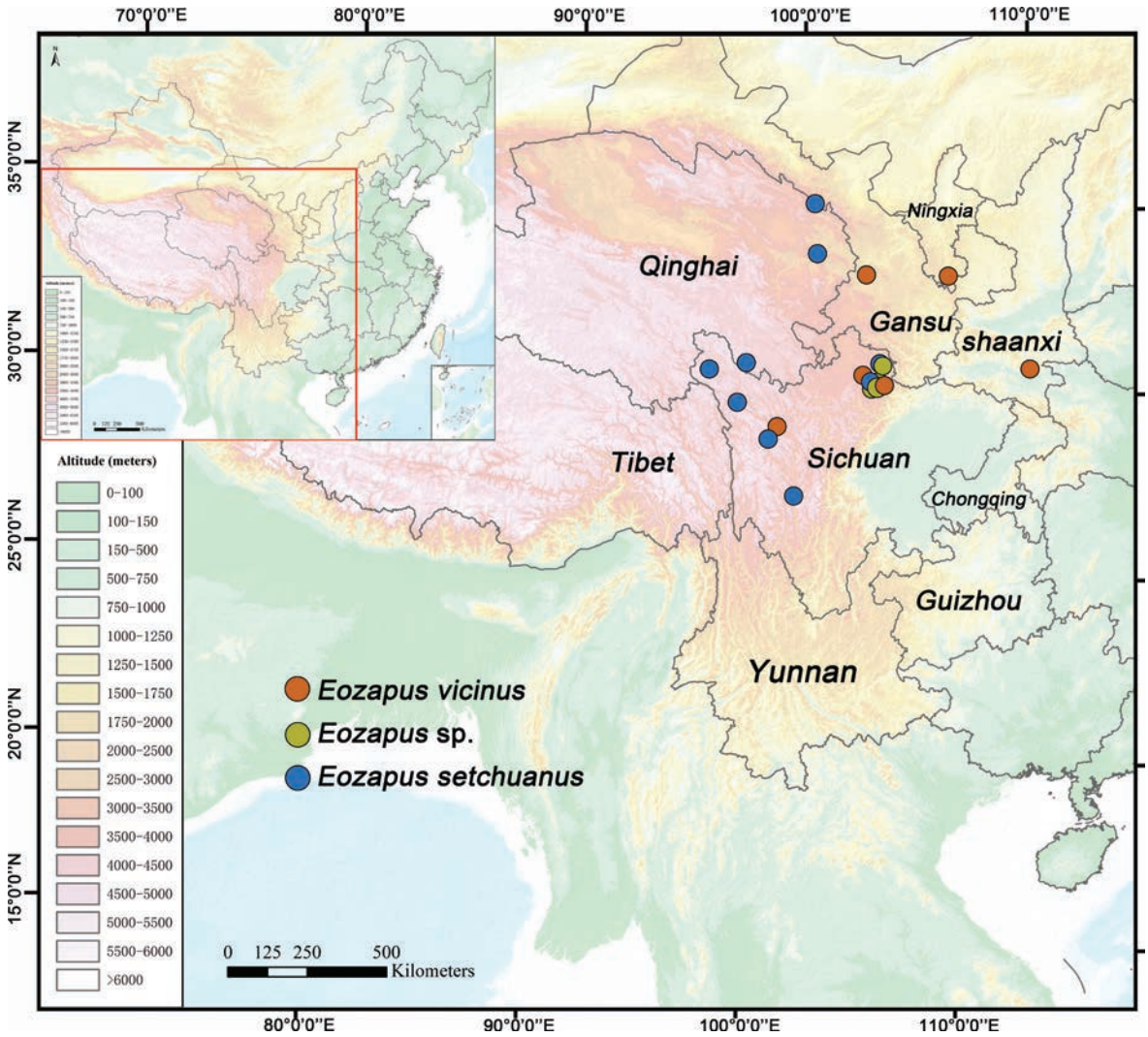

Figure 1. Map of the collection sites of the genus *Eozapus* in this study.

Table 1. Information on the collection sites of *Eozapus* specimens in this study (* represents topotype of *Eozapus* sp. and *E. setchuanus*).

Species	Field ID	Museum number	Genbank number			Locality	Longitude, Latitude	Elevation(m)
			CYT B	GHR	IRBP			
E. vicinus	csd2795	SAF13456	PQ723106	PQ752861	PQ752872	Hanzhong, Shaanxi, China	107.6301°E, 33.7101°N	2422
	csd2798	SAF11120	PQ723107	PQ752862	PQ752873	Guyuan, Ningxia, China	106.2746°E, 35.3905°N	2200
	csd2799	SAF11121	PQ723108	PQ752863	PQ752874	Guyuan, Ningxia, China	106.2746°E, 35.3905°N	2200
	csd2800	SAF11128	PQ723109	PQ752864	PQ752875	Guyuan, Ningxia, China	106.2936°E, 35.3781°N	2040
	csd2801	SAF11134	PQ723110	PQ752865	PQ752876	Guyuan, Ningxia, China	106.3279°E, 35.3676°N	2100
	csd2802	SAF11137	PQ723111	PQ752866	PQ752877	Guyuan, Ningxia, China	106.2746°E, 35.3905°N	2200
	csd2803	SAF11163	PQ723112	PQ752867	PQ752878	Guyuan, Ningxia, China	106.3279°E, 35.3676°N	2000
	csd2804	SAF11724	PQ723113	PQ752868	PQ752879	Songpan, Sichuan, China	103.562°E, 32.85°N	3110
	csd2965	SAF181316	PQ723114	PQ752869	PQ752880	Wanglang, Sichuan, China	104.0923°E, 32.9709°N	2600
	csd2967	SAF181367	PQ723115	-	-	Wanglang, Sichuan, China	104.7907°E, 32.0786°N	3000
	csd3532		PQ723116	-	-	Jiuzhaigou, Sichuan, China	103.9291°E, 33.0414°N	3037
	csd3576	SAF06319	PQ723117	PQ752870	PQ752881	Wanglang, Sichuan, China	104.0982°E, 32.9705°N	2614
	csd3577	SAF06352	PQ723118	-	-	Wanglang, Sichuan, China	104.7907°E, 32.0786°N	2614
	csd3581	SAF07345	PQ723119	PQ752871	PQ752882	Gannan, Gansu, China	103.5857°E, 34.9024°N	2780
Eozapus sp.	csd2808	SAF03225	PQ752960	-	-	Jiuzhaigou, Sichuan, China	103.8474°E, 33.0619°N	3100
	csd2814	*SAF181406	PQ752961	PQ752966	PQ752969	Wanglang, Sichuan, China	104.1571°E, 32.9526°N	\
	csd2970	*SAF191428	PQ752962	PQ752967	PQ752970	Wanglang, Sichuan, China	103.9919°E, 32.9308°N	3200
	csd2976	*SAF181458	PQ752963	PQ752968	PQ752971	Wanglang, Sichuan, China	103.9824°E, 32.9144°N	\
	csd2977	*SAF181457	PQ752964	-	-	Wanglang, Sichuan, China	103.9824°E, 32.9144°N	\
	csd5014	*SAF191248	PQ752965	-	-	Wanglang, Sichuan, China	104.0221°E, 32.0069°N	2931
E. setchuanus	csd1710	*SCNU03078	PQ752883	PQ752914	PQ752937	Kangding, Sichuan, China	101.5789°E, 29.788°N	3681
	csd1711	*SCNU03079	PQ752884	-	-	Kangding, Sichuan, China	101.5789°E, 29.788°N	3681
	csd1712	*SCNU03080	PQ752885	-	-	Kangding, Sichuan, China	101.5789°E, 29.788°N	3681
	csd2793	SAF13404	PQ752886	PQ752915	PQ752938	Guoluo, Qinghai, China	99.8186°E, 34.7792°N	3526
	csd2796	SAF12192	PQ752887	PQ752916	PQ752939	Shiqu, Sichuan, China	97.562°E, 32.854°N	3939
	csd2797	SAF12451	PQ752888	PQ752917	PQ752940	Haibei, Qinghai, China	99.8695°E, 38.2803°N	3150
	csd2806	SAF04507	PQ752889	PQ752918	PQ752941	Litang, Sichuan, China	99.8253°E, 29.5655°N	3450
	csd2962	SAF13391	PQ752890	-	-	Guoluo, Qinghai, China	100.5531°E, 33.4533°N	4152
	csd2973	SAF181425	PQ752891	PQ752919	PQ752942	Wanglang, Sichuan, China	104.0117°E, 32.9921°N	3526
	csd3532	SAF20721	PQ752892	-	-	Jiuzhaigou, Sichuan, China	103.9292°E, 33.0414°N	3037
	csd3545	*SAF11707	PQ752893	PQ752920	PQ752943	Kangding, Sichuan, China	101.831°E, 30.381°N	3870
	csd3547	*SAF11633	PQ752894	PQ752921	PQ752944	Kangding, Sichuan, China	101.84°E, 30.403°N	3490
	csd3548	*SAF11705	PQ752895	PQ752922	PQ752945	Kangding, Sichuan, China	101.831°E, 30.381°N	3870
	csd3549	*SAF11711	PQ752896	PQ752923	PQ752946	Kangding, Sichuan, China	101.831°E, 30.381°N	3870
	csd3550	*SAF11716	PQ752897	PQ752924	PQ752947	Kangding, Sichuan, China	101.831°E, 30.381°N	3870
	csd3551	*SAF11710	PQ752898	PQ752925	PQ752948	Kangding, Sichuan, China	101.831°E, 30.381°N	3870
	csd3552	*SAF11718	PQ752899	PQ752926	PQ752949	Kangding, Sichuan, China	101.831°E, 30.381°N	3870
	csd3553	*SAF11706	PQ752900	PQ752927	PQ752950	Kangding, Sichuan, China	101.832°E, 30.382°N	3871
	csd3554	*SAF11698	PQ752901	-	-	Kangding, Sichuan, China	101.84°E, 30.403°N	3840
	csd3555	*SAF11717	PQ752902	PQ752928	PQ752951	Kangding, Sichuan, China	101.831°E, 30.381°N	3870
	csd3556	*SAF11704	PQ752903	PQ752929	PQ752952	Kangding, Sichuan, China	101.831°E, 30.381°N	3871
	csd3557	*SAF12427	PQ752904	PQ752930	PQ752953	Kangding, Sichuan, China	99.594°E, 38.417°N	3275
	csd3558	*SAF11708	PQ752905	PQ752931	PQ752954	Kangding, Sichuan, China	99.8695°E, 38.2803°N	3870
	csd3559	*SAF11715	PQ752906	PQ752932	PQ752955	Kangding, Sichuan, China	101.831°E, 30.381°N	3870
	csd3560	*SAF11709	PQ752907	PQ752933	PQ752956	Kangding, Sichuan, China	101.831°E, 30.381°N	3870
	csd3579	SAF071043	PQ752908	PQ752934	PQ752957	Dege, Sichuan, China	104.0982°E, 32.9705°N	4145
	csd3583	SAF071076	PQ752909	-	-	Dege, Sichuan, China	103.9292°E, 33.0414°N	4150
	csd3584	SAF071021	PQ752910	-	-	Dege, Sichuan, China	107.6301°E, 33.7101°N	4010
	csd3585	SAF071080	PQ752911	PQ752935	PQ752959	Dege, Sichuan, China	106.2746°E, 35.3905°N	4010
	csd3587	SAF071063	PQ752912	PQ752936	PQ752958	Dege, Sichuan, China	99.1561°E, 31.8753°N	4020

The extraction of total DNA was carried out following the manufacturer's protocols for the animal liver or muscle tissue DNA extraction kit (Chengdu Fukuji Biological Co.). In this study, three genes were amplified for molecular phylogenetic and related analyses: one mitochondrial gene (CYT B, 1059 bp) and two nuclear genes (growth hormone receptor [GHR, 569 bp] and inverted repeat-binding protein [IRBP, 590 bp]). PCR amplifications were performed in a reaction volume mixture of 25 µl, containing 3 mM $MgCl_2$, 0.2 U rTaq polymerase (Takara, Dalian, China), 1 × reaction buffer, 0.2 mM of each dNTP, 0.4 mM of each primer, and approximately 100–500 ng of genomic DNA. The primers used for PCR amplification are listed in Suppl. material 1: table S1. PCR amplification was performed with an initial denaturation step at 94 °C for 5 min, followed by 35 cycles of denaturation at 94 °C for 45 s, annealing at 49–60 °C for 45 s, extension at 72 °C for 90 s, and a final extension step at 72 °C for 10 min. PCR products were identified using 1% agarose gel electrophoresis and then sent to QingKe Biological Co., Ltd. for purification and bidirectional Sanger sequencing.

Sequencing results were aligned preliminarily using MEGA v5 (Tamura et al. 2013). All sequences were manual corrections edited to ensure the proper translation, thereby avoiding potential impacts on subsequent analyses. CYT B, IRBP, and GHR sequences from the selected *Eozapus* species and the outgroup *Stylodipus sungorus*, *Stylodipus andrewsi*, and *Stylodipus telum* were downloaded from GenBank (Suppl. material 1: table S2).

Phylogenetic analyses

Three datasets were created for phylogenetic analysis: 1) a mitochondrial dataset (CYT B), 2) a nuclear gene dataset (nuDNA), and 3) an all-gene combined dataset (CYT B + nuDNA). The optimal base substitution model for each dataset was determined using jModelTest 2.1.7 (Posada 2008), and the Akaike information criterion (AIC) was used to assess the fitness of each model (Luo et al. 2010). The optimal substitution models for each gene and dataset are listed in Suppl. material 1: table S3.

Phylogenetic trees were constructed using Bayesian inference (BI) based on the three established datasets. The MrBayes 3 program was used to reconstruct the BI tree (Ronquist and Huelsenbeck 2003). Parameter settings for the BI tree were based on those described by Chen et al. (2012). Posterior distributions were obtained using the Markov chain Monte Carlo (MCMC) method with one cold chain and three heated chains for 100 million generations at a sampling interval of 10,000. The first 2,000 generations were treated as burn-ins. The Markov chain MCMC runs were repeated twice to confirm a consistent approximation of the posterior parameter distributions. Figtree v1.4.3 was used to visualize the BI tree output, and a posterior probability (PP) > 0.95 was considered strong support (Huelsenbeck and Rannala 2004).

Genetic distance and species delimitation

Genetic distances between clades were calculated based on the CYT B gene using the Kimura 2-parameter model in MEGA v5.05 (Tamura et al. 2011).

BPP v3.0 was used to test the hypothesis of independent evolutionary lineages represented by populations (Yang and Rannala 2010; Yang et al. 2012; Yu et al. 2013). To verify the genetic differentiation detected in the genus *Eozapus*, the gene tree constructed in the previous step was used as a guide tree, and the validity of our assignment of the three putative species was tested in BPP v3.1. The analysis of Chen et al. (2022) was followed, which was defined using Algorithm 0 and Algorithm 1, with τ representing the root age of the species tree and θ representing the size parameter of the population. These two important parameters significantly affect the posterior probability of the BPP (Yang and Rannala 2010; Pan et al. 2019; Chen et al. 2022). Twelve analyses were conducted using three different prior combinations of τ and θ: (1) τ = G (2, 2000), θ = G (2, 2000); (2) τ = G (1, 10), θ = G (2, 2000); and (3) τ = G (1, 10), θ = G (1, 10) (Leaché and Fujita 2010). Each rjMCMC was run for 100,000 generations, with samples collected every 100 generations after discarding 10,000 generations as preburn-in. When the posterior probability exceeded 0.95, the analysis supports that each evolutionary branch is a separate species.

Divergence time

Since mitochondrial genes may lead to an earlier estimated differentiation time (Phillips 2009; Zheng et al. 2011), the nuclear gene dataset was used for estimation in this study. The time of differentiation of the genus *Eozapus* was analyzed and imputed using BEAST v1.7.5 (Drummond et al. 2012) based on the nuDNA dataset. Four fossil calibration points were used in this study, as described by Shenbrot et al. (2017). (1) *Stylodipus* and *Chimaerodipus* originated within the Dipodinae at approximately 3.84–5.49 Ma (mean = 4.85, standard deviation = 0.61, upper 95% = 3.84–5.85 Ma). (2) *Eremodipus* and *Jaculus* originated within the Dipodidae at approximately 3.75–5.74 Ma (mean = 4.73, standard deviation = 0.61, upper 95% = 3.73–5.73 Ma). (3) Differentiation of *Jaculus* occurs at approximately 1.18–2.31 Ma (mean = 1.73, standard deviation = 0.354, upper 95% = 1.15–2.31 Ma). (4) Dipodinae originated at approximately 9.46–11.47 Ma (mean = 10.53, standard deviation = 0.65, upper 95% = 9.46–11.60 Ma). The remaining parameters were set as described by Chen et al. (2022).

Morphological data and analyses

A total of 17 complete skull specimens of intact adult individuals were obtained and measured using digital Vernier calipers, with an accuracy of 0.01 mm, as described previously (Liu et al. 2007, 2012; Patton and Conroy 2017). The measurement metrics included body weight (BW), head-body length (HBL), tail length (TL), hindfoot length (HFL), ear length (EL), profile length (PL), skull basal length (SBL), median palatal length (MPL), zygomatic breadth (ZB), least breadth between the orbits (LBO), brainstem breadth (BB), height of the braincase (HB), auditory bulla length (ABL), upper toothrow length (UTRL), length of the upper molars (LUM), upper molar row breadth (UMRB), mandibular length (ML), lower toothrow length (LTRL), and length of the lower molar row (LLMR). Because external measurement data may display differences between different measurers, they were not used for the morphological analysis. SPSS v17.0 was used to analyze the measurement values of the indicators. When the data satisfied a normal distribution, principal component analysis (PCA) was used to evaluate the overall similarity between species, and discriminant analysis (DA) was used to determine whether the classification was correct.

Results

Phylogenetic analyses

We obtained 51 CYT B sequences of 1059 bp and 37 nuclear gene sequences of 1159 bp (GHR: 569 bp; IRBP: 590 bp). The new sequences were deposited in GenBank (Accession Numbers PQ723106–PQ723119, PQ75286–PQ752971, Table 1). MrBayes was used to reconstruct phylogenetic relationships based on the three datasets, and all three topological structures obtained were largely consistent (Fig. 2). BI results based on three different datasets supported the division of the genus *Eozapus* into three clades. *E. vicinus* was monophyletic and was consistently positioned as the most basal lineage across all three datasets (CYT B: PP = 1.00, nuDNA = 0.38, and CYT B + nuDNA = 1.00). *Eozapus* sp. was identified as a sister group of *E. setchuanus*. In the CYT B phylogenetic tree, evolutionary relationships within this taxon were highly supported. The CYT B + nuDNA gene tree was identical and well supported (PP = 1.00) by the topology of this taxon in the CYT B gene tree (Fig. 2).

Genetic distances and species delimitation

The K2P genetic distances between the three clades of *Eozapus* based on the CYT B gene are shown in Table 2. The results revealed that the genetic distance values ranged from 10.9% to 17.8%. The genetic distance value between *E. vicinus* and *Eozapus* sp. was at 17.8%, followed by 16.6% between *E. vicinus* and *E. setchuanus*, and 10.9% between *Eozapus* sp. and *E. setchuanus* was the smallest. Genetic distances among all species showed good species-level variation.

Table 2. Kimura two-parameters (K2P) genetic distances in the genus *Eozapus* based on the CYT B gene.

	E. vicinus	***Eozapus* sp.**
E. vicinus		
Eozapus sp.	0.178	
E. setchuanus	0.166	0.109

The results from BPP based on the CYT B + nuDNA and nuDNA datasets produced 36 results, all of which strongly supported the division of *Eozapus* into three clades (PP = 1.00; Suppl. material 1: table S4).

Molecular divergence estimation

The results indicated that the most recent common ancestor of *Eozapus* dates back to the Miocene (8.15 Ma, 95% CI = 5.23–10.62), marking the divergence of *E. vicinus* from the other two species. The divergence time of *Eozapus* sp. and *E. setchuanus* (6.12 Ma, 95% CI = 3.41–9.16) occurs in the Miocene (Fig. 3).

Morphological analysis

A total of 14 craniodental and 5 external indicators were measured (Suppl. material 1: table S5). External indicators were excluded from the morphological analysis because of potential interobserver variation in measurements (Jiang et al. 2003). Additionally, owing to damage to the zygomatic bones of several specimens during handling, ZB measurements were excluded from the analysis, leaving 13 skull measurements for morphological analysis (Table 3).

The results of the PCA based on 13 cranial measurements revealed that the two principal components explained

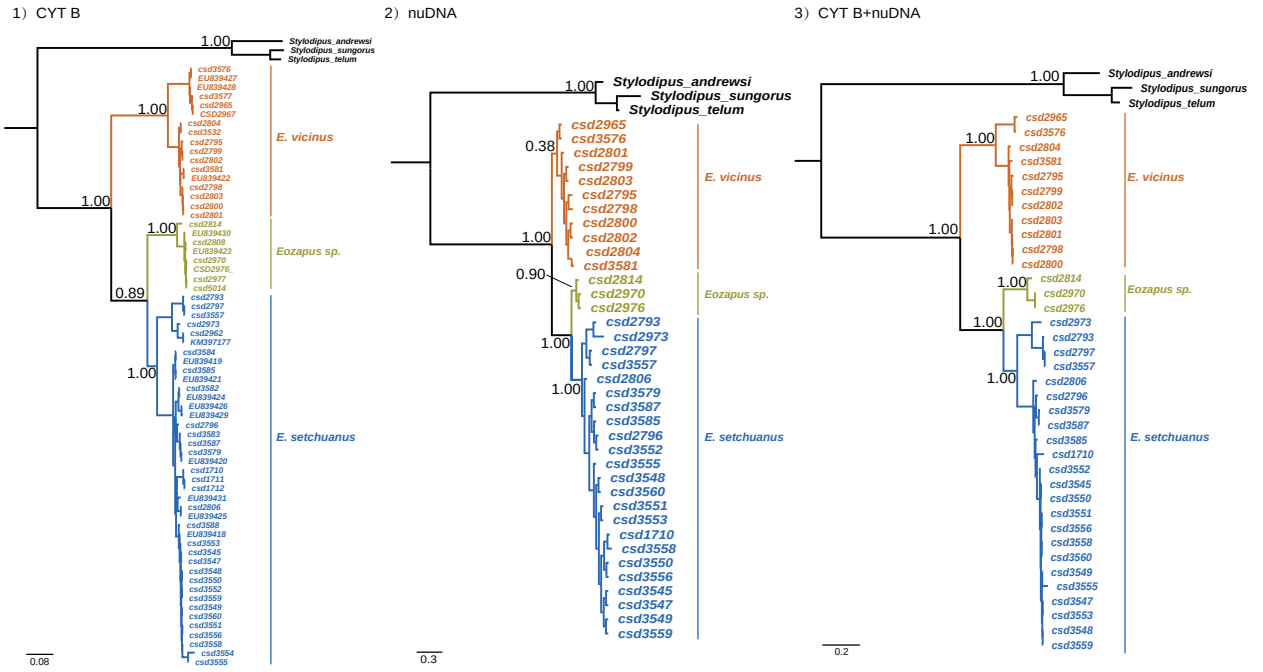

Figure 2. Bayesian phylogenetic analyses based on the CYT B dataset, the nuDNA dataset, and the CYT B+nuDNA dataset. The numbers above the branches refer to Bayesian posterior probabilities (PP).

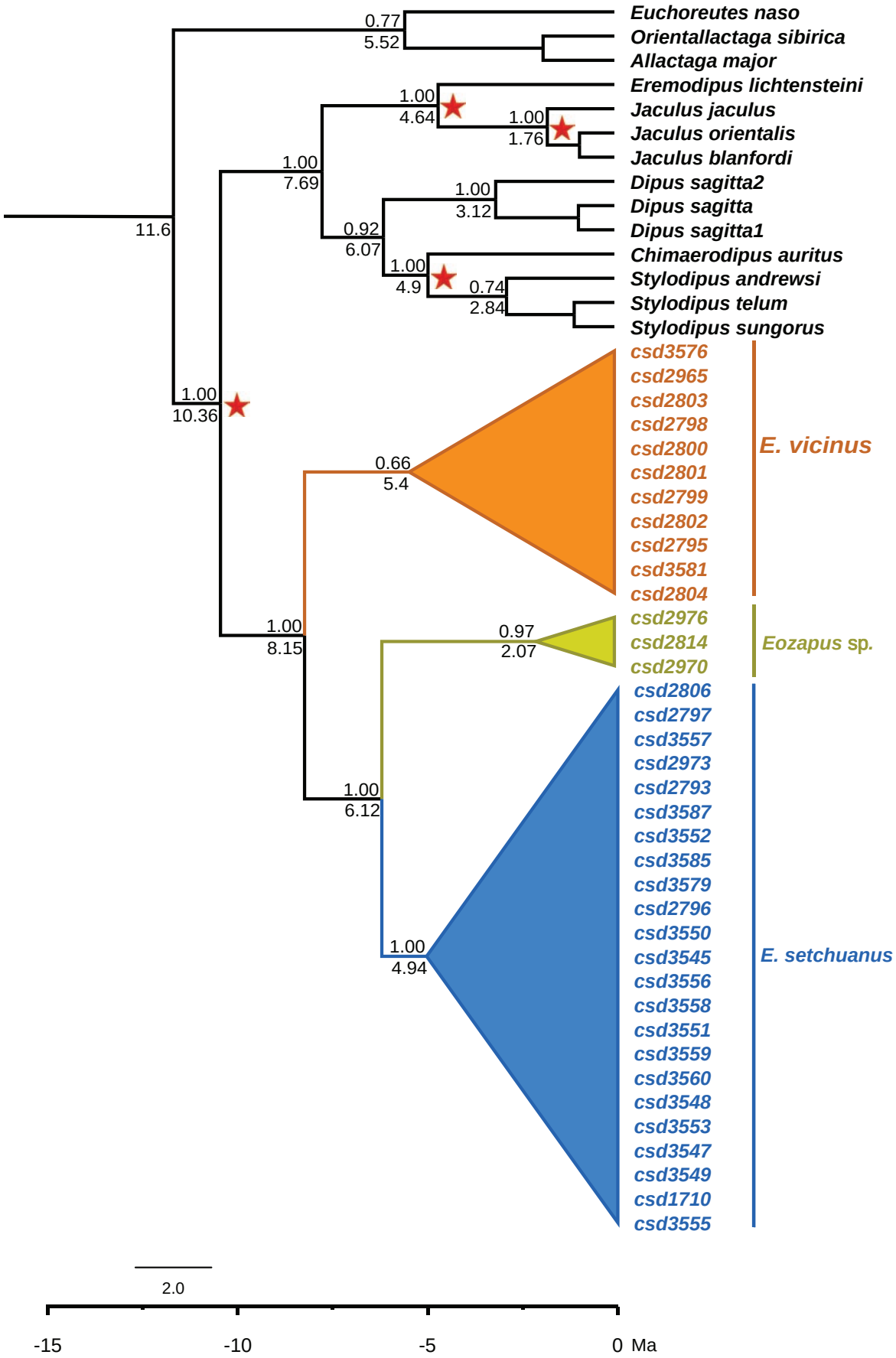

Figure 3. Divergence times estimated using BEAST based on the nuDNA dataset. Branch lengths represent time. Numbers above the nodes indicate posterior probabilities (PP). Numbers below the nodes represent the median divergence time. The four asterisks indicate fossil-calibrated nodes.

Table 3. The average and standard deviation of the measurement data of the skull morphology of the specimens of the genus *Eozapus* used in this study.

Measurements	*E. vicinus* n = 7	*Eozapus* sp. n = 3	*E. setchuanus* n = 7
PL	22.12 ± 1.06	21.58 ± 0.67	22.16 ± 1.15
	20.37–24.09	20.83–22.12	20.20–23.73
SBL	16.58 ± 1.12	16.22 ± 0.65	16.87 ± 0.89
	14.25–18.10	15.50–16.77	15.75–18.22
MPL	9.77 ± 0.52	9.62 ± 0.41	9.96 ± 0.47
	8.69–10.48	9.17–9.97	9.12–10.48
LBO	3.94 ± 0.13	3.76 ± 0.20	3.95 ± 0.17
	3.69–4.15	3.63–3.99	3.79–4.30
BB	10.16 ± 0.44	10.24 ± 0.27	10.51 ± 0.40
	9.20–10.71	9.98–10.52	9.72–10.96
HB	8.19 ± 0.11	8.11 ± 0.14	8.42 ± 0.48
	8.03–8.40	8.02–8.27	7.86–9.38
ABL	5.81 ± 0.11	5.84 ± 0.12	6.05 ± 0.22
	5.56–5.95	5.71–5.92	5.88–6.52
UTRL	9.83 ± 0.57	9.51 ± 0.12	10.26 ± 0.48
	8.54–10.44	9.37–9.61	9.35–10.89
LUM	3.72 ± 0.29	3.87 ± 0.14	4.02 ± 0.08
	3.00–3.92	3.71–3.98	3.95–4.14
UMRB	4.87 ± 0.11	4.80 ± 0.10	5.01 ± 0.11
	4.70–5.03	4.74–4.91	4.78–5.11
ML	13.01 ± 0.63	12.49 ± 0.23	13.21 ± 0.70
	11.82–14.07	12.24–12.69	12.12–14.05
LTRL	8.46 ± 0.51	8.01 ± 0.06	8.65 ± 0.46
	7.28–9.07	7.96–8.07	8.08–9.31
LLMR	3.47 ± 0.39	3.62 ± 0.05	3.86 ± 0.10
	2.51–3.65	3.57–3.66	3.75–4.03

Notes: PL: profile length; SBL: skull basal length; MPL: median palatal length; LBO: least breadth between the orbits; BB: braincase breadth; HB: height of the braincase; ABL: auditory bulla length; UTRL: upper toothrow length; LUM: length of upper molars; UMRB: upper molar row breadth; ML: mandibular length; LTRL: lower toothrow length; LLMR: length of lower molar row.

77.049% of the variance (Table 4). The first principal component (PC1) accounted for 59.533% of the variance and showed positive factor loadings. PL, SBL, and MPL had factor loadings > 0.9, indicating a strong correlation with PC1, Factor loadings > 0.8 included UTR, ML, and LTRL. The second principal component (PC2) explained 17.516% of the variance and had mostly negative factor loadings, with LUM and LLMR being the largest loading, correlating strongly with PC2. It also was negatively correlated with LBO (loadings < - 0.2) (Table 4). The PCA results indicated that most individuals were effectively classified into three species with minimal overlap (Fig. 4).

Table 4. Percent variance explained on the two components of PCA of cranial measurements of *Eozapus*.

Variables	PC1	PC2
PL	0.949	0.049
SBL	0.924	0.163
MPL	0.930	0.124
LBO	0.514	-0.236
BB	0.597	0.168
BH	0.629	0.578
ABL	0.250	0.878
UTR	0.835	0.459
LUM	0.088	0.945
UMR	0.786	0.402
ML	0.839	0.343
LTRL	0.810	0.378
LLMR	0.111	0.929
Eigenvalue	7.739	2.277
Explained(%)	59.533	17.516

Discriminant analysis (DA) showed that the three specimens within *Eozapus* were accurately classified (Fig. 4). Correct taxonomic determination was obtained for 100.0% of the original grouped samples, and cross-validation results indicated that 100% of the samples were correctly classified.

The skull of *Eozapus* sp. is the smallest (average PL = 21.58 mm), while that of *E. setchuanus* is 22.16 mm and *E. vicinus* is 22.37 mm. In fact, the average skull measurement of *Eozapus* sp. was less than that of the other two species. The SBL (average = 16.22 mm), UTRL (average = 9.51 mm), ML (average = 12.49 mm), and LTRL (average = 8.01 mm) of *Eozapus* sp. were the shortest, whereas the UTRL (average = 10.26 mm), ML (average = 13.21 mm), and LTRL (average = 8.65 mm) of *E. setchuanus* are the longest (Table 3). The tooth formula of this genus is 1.0.1.3/1.0.0.3. Depression of the occlusal surface of the upper molars in the genus *Eozapus* is variable; *E. vicinus* is slightly concave, *Eozapus* sp. is moderate, while *E. setchuanus* is severely concave (Fig. 5a2, b2, c2, a6, b6, c6). The lengths of the first and second lower molars are nearly equal, and the third lower molar (m_3)

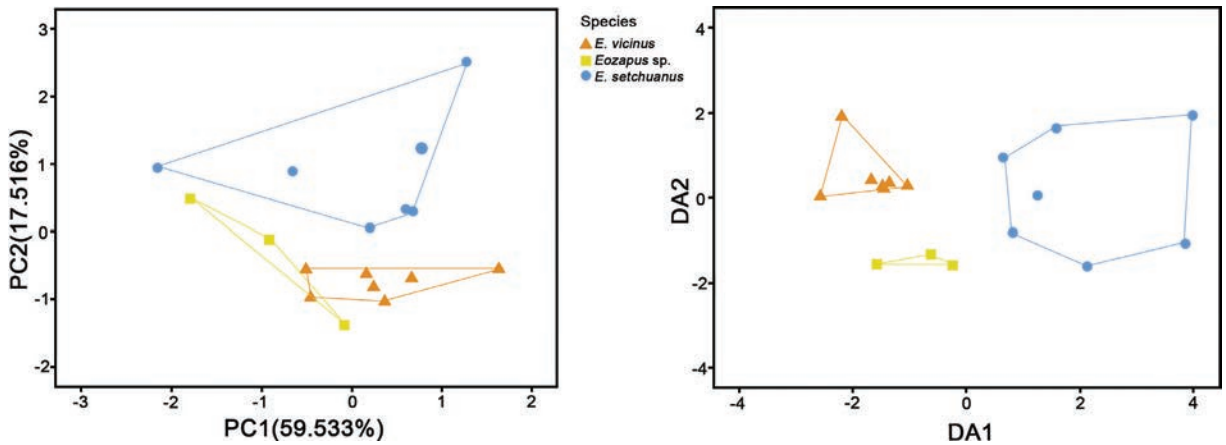

Figure 4. Result of the principal component analysis (PCA) and the discriminant analysis (DA) based on skull measurement data of the genus *Eozapus*.

is reduced (approximately 30%). On the second lower molar (m_2), the metalophid of *E. vicinus* penetrated the entire surface of the second lower molar (m_2) from the middle, whereas for *Eozapus* sp. and *E. setchuanus*, the metalophid of the m_2 is discontinuous and concave inward medially (Fig. 5a6, b6, c6). In addition, *Eozapus* sp. has a distinctly depressed longitudinal groove in the middle of the third lower molar (m_3) and towards the lingual side (Fig. 5b6); the m_3 of *E. vicinus* is flat in the middle (Fig. 5a6), and *E. setchuanus* also has a depressed longitudinal groove in the middle of the third lower molar (m_3), but differs from *E. vicinus* in that it is directed to the buccal side (Fig. 5c6).

Hair characteristics of the genus *Eozapus* are as follows (Fig. 6d). The color of the dorsal and notal hairs was the same in all three species, brownish yellow, but *E. vicinus* was slightly lighter than *Eozapus* sp., while in *E. setchuanus* the extent of the yellow wash on the individual hairs extended further towards the root (Fig. 6). (1) *E. vicinus* exhibits pure white at the base and tip of hair in its abdomen. (2) *Eozapus* sp. has no brownish-yellow longitudinal stripes on its chest, and its hair base is white with yellow tips on its abdomen. (3) *E. setchuanus* has a brownish-yellow longitudinal stripe on its chest. The hair at the base was purely white with yellowish tips on its abdomen.

Based on the distinct morphological characteristics and deep genetic divergence described in the preceding sections, we recognized the jumping mouse from the Wanglang National Nature Reserve as a distinct, undescribed species within *Eozapus* and formally described it as follows.

Eozapus wanglangensis Yang, Liu & Chen, sp. nov.

https://zoobank.org/B9AA3CF7-0465-4415-B65E-0BC65D58C665

Suggested common name in English: Wanglang jumping mouse

Suggested common name in Chinese: 王朗林跳鼠 [Wang Lang Lin Tiao Shu]

Type material. ***Holotypes*:** • An adult female (SAF191248) captured by Rui Liao and Xuming Wang in September 2019 from the Wanglang National Nature Reserve, Pingwu, Sichuan Province, China (32.0069°N, 104.0221°E; 2931 m a.s.l.). The study skin and skull specimens have been deposited at the Sichuan Academy of Forestry (SAF).

Paratypes (n = 5): • Three specimens (SAF181406♂, SAF181457♀, and SAF181458♀) were collected by Rui Liao, Xuming Wang, and Haijun Jiang in September 2018 from the type locality at elevations ranging from 2900 to 3200 m. • One specimen of unknown sex (SAF06364) was collected by Shaoying Liu in 2006 from the type locality. • One female specimen (SAF03225♀) was collected by Zhiyu Sun in June 2003 from Jiuzhaigou, Sichuan Province, China (33.0619°N, 103.8474°E; 3100 ma. s.l.).

Measurements of holotype (mm). BW = 27 g; HBL = 78.00; TL = 120.00; HFL = 28.00; EL = 13.00; PL = 21.78; SBL = 16.39; MPL = 9.97; LBO = 3.66; BB = 9.98; HB = 8.02; ABL = 5.90; UTRL = 9.61; LUM = 3.91; UMRB = 4.74; ML = 12.96; LTRL = 8.07; LLMR = 3.64; ZB = 10.09.

Etymology. The special name "Wanglang" refers to the Wanglang National Nature Reserve, the type locality of the new species, known for its rich biodiversity. We suggest "Wanglang jumping mouse" as the English common name and "王朗林跳鼠 (Wang lang Lin tiao shu)" as the Chinese common name.

Diagnosis. Slender body, longer hindfoot, adapted for jumping. The head-body length (HBL) averages approximately half as long as the total length (TL) and is slightly shorter or longer than half the TL. The skull is smaller than that of the other two species of *Eozapus*. Physical characteristics include a brownish-yellow body on the back. The tail is slender and covered with sparse, short, tan hairs, and the scales are conspicuous. It is distinguished from other species based on the following features: (1) Abdominal hair coloration differs from that of the other two species of *Eozapus*. Compared to the pure white abdominal hairs of *E. vicinu*s, the abdominal hairs of this species are white at the base and yellow at the tips. *E. setchuanus* has a brownish-yellow longitudinal stripe on the abdomen, which is absent in this species.; (2) The second lower molar (m_2) has a longitudinal deep groove, and the metalopaid is concave inward medially; (3) a distinctly depressed longitudinal groove in the middle of the third lower molar (m_3) and towards the lingual side

Description. Small jumping mouse with a head-body length of 65–78 mm (average 71 mm) and tail length of 120–132 mm (average 126 mm), featuring a distinctly bicolored (grayish to brown) tail above and white below (HBL/TL = 0.56). Hind foot length ranges from 28 to 30 mm (average 29 mm), with ear height measuring 12–15 mm (average 13 mm). The muzzle was light brown with a tan ring above the nasal pads. The dorsum of the body is bright rusty brown with a longitudinal brown stripe from the forehead through the eyes to below the eyes and between the ears and the base of the tail. Abdominal hair has a white base and a light-yellow tip, clearly distinguishing the coloration between the back and abdomen. The tail was slender and covered with sparse, short, yellowish-brown hairs. All four feet are beige, with shorter forefeet and elongated hind limbs and hind feet.

The skull of *E. wanglangensis* sp. nov. is the smallest in the genus *Eozapus*, measuring 21.58 ± 0.67 mm. It features a curved cranial surface with the highest point at the junction of the frontal and parietal bones. The muzzle is slender, with the anterior end of the nasal bone much longer than the anterior end of the maxillary incisors. The skull has a well-developed and pronounced sagittal crest, a wider interorbital region, slender and curved zygomatic bones, nearly parallel zygomatic arches on both sides, and small auditory bullae. Compared to other *Eozapus* species, the skull length (SBL) of *E. wanglangensis* sp. nov. is the smallest, averaging 16.22 mm.

The maxillary incisors of *E. wanglangensis* sp. nov. are orange-red and vertically oriented, with pronounced longitudinal grooves on their anterior margins. The premolars are small and round. The first upper molar (M^1) is larger than the second, featuring four small, equal cusps on its occlusal surface with deep concave folds on both the buccal and lingual sides. The third upper molars (M^3)

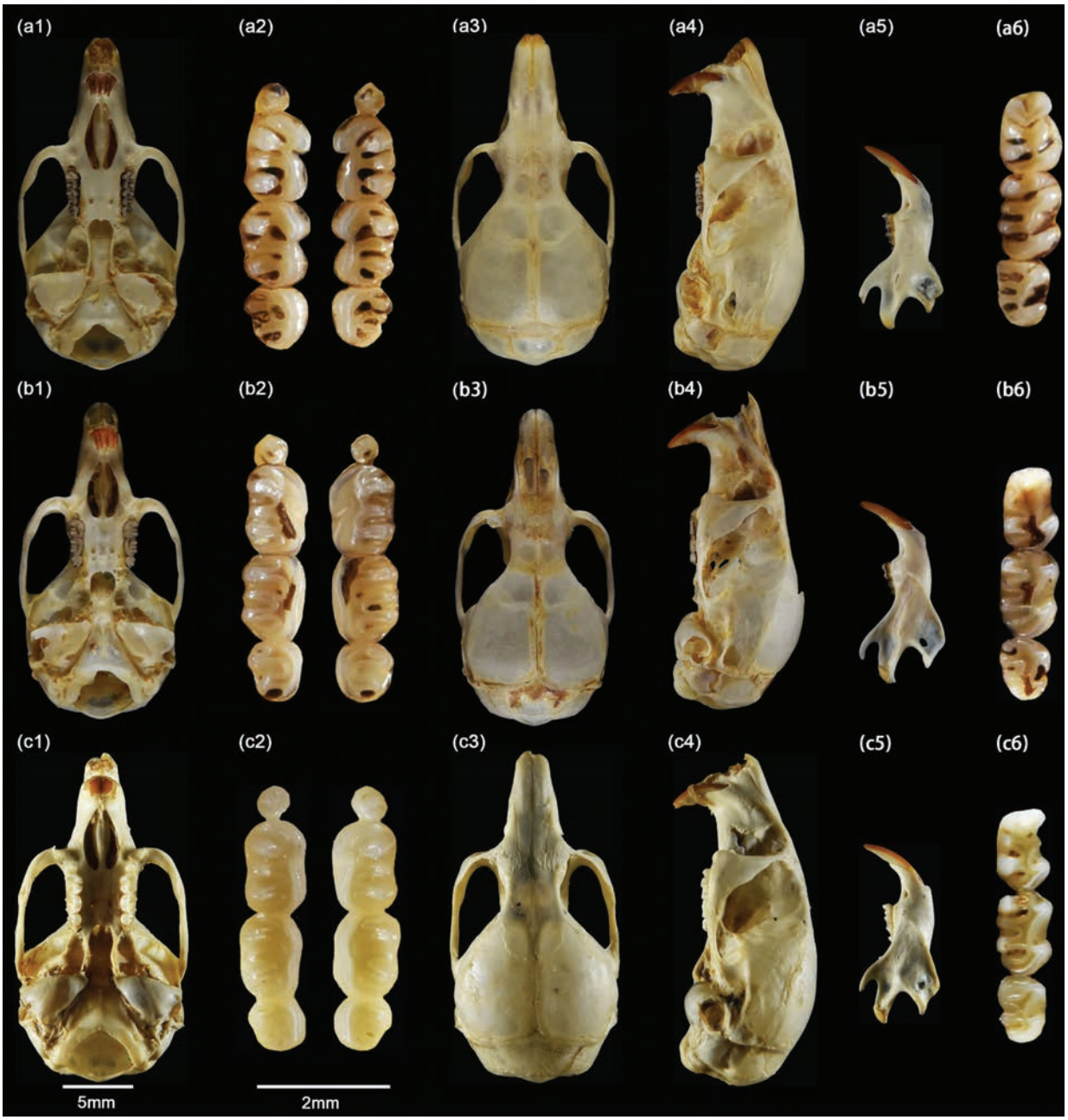

Figure 5. Skulls and tooth comparison among species of the genus *Eozapus*. **a.** *E. vicinus* **a1–a6**; **b.** *Eozapus* sp. **b1–b6**; **c.** *E. setchuanus* c1-c6 holotype; (1) ventral view; (2) upper tooth row; (3) dorsal view; (4) lateral view; (5) lower jaws; (6) lower tooth row; The red arrow indicates the position of the dental variation.

are the smallest. The anterior third of the anterior margin of the first upper molar (M^1) exhibits a concave fold that divides the tooth into an anterior inner lobe, with five prominent small transverse lobes on the outer side. The second and fourth lobes are taller than the other lobes. However, the second upper molar (M^2) lacks an anterior inner lobe (Fig. 5b2). The lower molars all have four distinct medial lobe-like projections. The first lower molar (m_1) is almost the same size as the second lower molar (m_2), with one concave fold on the anterior margin and two folds on the lateral side. The second and third lower molars each have one medial concave fold. There is a distinctly depressed longitudinal groove in the middle of the third lower molar (m_3) (Fig. 5b6).

Distribution and ecology. *E. wanglangensis* sp. nov. is primarily found in the Wanglang National Nature Reserve and central Jiuzhaigou County, Sichuan Province. This species inhabits forests and forest-edge grasslands at altitudes ranging from 1800 to 3100m, preferring forests with denser shrubs and streams.

Comparisons. *E. wanglangensis* sp. nov. is the smallest species of *Eozapus*, with a head-body length-to-total length ratio (HBL/TL) of 0.56. In comparison, *E. setchuanus* has an HBL/TL ratio of 0.65, whereas *E. vicinus* has an HBL/TL ratio of 0.61. Compared to *E. setchuanus* (UTRL = 10.26 ± 0.48 mm; UMRB = 5.01 ± 0.11 mm) and *E. vicinus* (UTRL = 9.83 ± 0.57 mm; UMRB = 4.87 ± 0.11 mm), *E. wanglangensis* sp. nov. exhibits smaller values for

Figure 6. Pelage comparisons among species of the genus *Eozapus*: **a.** *Eozapus vicinus* (museum number SAF11163); **b.** *Eozapus* sp. (museum number SAF191248); **c.** *Eozapus setchuanus* (museum number SAF11706); **d.** Hair variation (below chest to hindfoot); (1) dorsal view; (2) ventral view; (3) lateral view.

UTRL (9.51 ± 0.12 mm) and UMRB (4.80 ± 0.10 mm). *Eozapus wanglangensis* sp. nov. has no brownish-yellow longitudinal stripes on its chest, and its hair base is white with yellow tips on its abdomen. This species differs in that the second lower molar (m_2) is discontinuous on the mesofossette and has a longitudinal groove medially, and there is a distinctly depressed longitudinal groove in the middle of the third lower molar (m_3) and towards the lingual side.

Discussion

Geological formations and climate change have been closely linked to the evolution of small mammals (Li et al. 2022). The complex topography and geographic history of the "sky islands," along with diversified climate conditions, may have led to the evolution of the endemic *Eozapus* species and the emergence of new species. Our study reveals that the origin of species within the genus *Eozapus* dates to the Miocene. We hypothesize that climate change during the Miocene facilitated the expansion and divergence of *Eozapus* species. The speciation and evolution of this genus were closely associated with the uplift of the Qinghai-Tibetan Plateau (QTP). Previous studies have suggested that the QTP uplifted several times, one of which was 6–8 Ma ago (Molnar et al. 1993; Molnar 2005; Song et al. 2007). This geological movement has altered the climate and topographic structure of the region, creating isolation between mountain ranges and promoting the allopatric speciation, dispersal, and divergence of species, thereby providing a foundation for biodiversity. The divergence times observed within the genus *Eozapus* closely coincided with the uplift time of the QTP.

It is worth noting that the species within *Eozapus* are quite genetically distinct and have been isolated/separate for a long evolutionary time but appear similar from external morphology. It is possible that each mountain in the 'sky islands' has acted as refugia and provided the only continuously suitable habitats for *Eozapus* since the Miocene. After long-term isolation, populations in each refugium likely became isolated in situ, resulting in allopatric speciation. Previous phylogenetic and phylogeographic investigations have revealed cryptic species of small mammals in this "sky islands" region (Koju et al. 2017; Wan et al. 2018; He et al. 2019; Chen et al. 2020).

A previous study by Fan et al. (2009) revealed that *Eozapus setchuanus* and *E. vicinus*, previously considered as two subspecies of *E. setchuanus*, did not form reciprocally monophyletic lineages. We hypothesize that this conclusion may be attributed to several factors, including the single origin of the samples, the limited sample size, and the authors' morphological judgment based primarily on geographic distribution. Notably, the three *Eozapus* species are known to be distributed in the Wanglang Nature Reserve of Sichuan Province (Table 1). In this study, we addressed these issues and established the independence of the three species of the genus *Eozapus* from comprehensive molecular and morphological analyses.

Conclusion

In this study, we reorganized the phylogenetic relationships of the genus *Eozapus* through molecular and morphological analyses and reassessed the species diversity of this genus. These results indicated that the *Eozapus* species are quite genetically distinct and have a long evolutionary history in the sky islands of southwestern China, but they appear quite similar in convergent external morphology. We describe a new species, *Eozapus wanglangensis* sp. nov., and suggest elevating *E. s. vicinus*, previously considered a subspecies of *E. setchuanus*, as a distinct species, *E. vicinus*. Furthermore, the uplift of the Qinghai-Tibetan Plateau, the complex topography of sky islands, and climate change promoted the speciation and diversity of the genus *Eozapus*.

Acknowledgments

The study is supported by the National Natural Science Foundation of China (32070424) to Shunde Chen; the National Natural Science Foundation of China (32370496) to Shaoying Liu; the Natural Science Foundation of Sichuan Province (25NSFSC0983) to Shunde Chen; and the Experimental Technology Project of Sichuan Normal University (SYJS2023018).

References

Chen SD, Qing J, Liu Z, Liu Y, Tang MK, Murphy RW, Pu YT, Wang XM, Tang KY, Guo KJ, Jiang XL, Liu SY (2020) Multilocus phylogeny and cryptic diversity of white-toothed shrews (Mammalia, Eulipotyphla, *Crocidura*) in China. BMC Evolutionary Biology 20: 29. https://doi.org/10.1186/s12862-020-1588-8

Chen SD, Tang KY, Wang XM, Li FJ, Fu CK, Liu Y, Abu ul Hassan Faiz, Jiang XL, Liu SY (2022) Multi-locus phylogeny and species delimitations of the striped-back shrew group (Eulipotyphla, Soricidae): Implications for cryptic diversity, taxonomy and multiple speciation patterns. Molecular phylogenetics and evolution 177: 107619. https://doi.org/10.1016/j.ympev.2022.107619

Cheng JL, Xia L, Wen ZX, Zhang Q, Ge DY, Yang QS (2021) Review on the systematic taxonomy of Dipodoidea in China. Acta Theriologica Sinica 41(3): 275–283. https://doi.org/10.16829/j.slxb.150531

Drummond AJ, Suchard MA, Xie D, Rambaut A (2012) Bayesian phylogenetics with BEAUti and the BEAST 1.7. Molecular biology and evolution 29(8): 1969–1973. https://doi.org/10.1093/molbev/mss075

Fan ZX, Liu SY, Liu Y, Zeng B Guo C, Yue B (2009) Molecular phylogeny and taxonomic reconsideration of the subfamily Zapodinae (Rodentia, Dipodidae), with an emphasis on Chinese species. Molecular Phylogenetics and Evolution 51(3): 447–453. https://doi.org/10.1016/j.ympev.2009.03.005

He K, Eliécer E, Gutiérrez, Heming NM, Koepfli K, Wan T, He S, Jin W, Liu SY, Jiang XL (2019) Cryptic phylogeographic history sheds light on the generation of species diversity in sky-island mountains. Journal of Biogeography 46: 2232–2247. https://doi.org/10.1111/jbi.13664

He K, Jiang XL (2014) Sky islands of southwest China. I: An overview of phylogeographic patterns. Chinese Science Bulletin 59: 585–597. https://doi.org/10.1007/s11434-013-0089-1

Huelsenbeck J, Rannala B (2004) Frequentist properties of Bayesian posterior probabilities of phylogenetic trees under simple and complex substitution models. Systematic biology 53(6): 904–913. https://doi.org/10.1080/10635150490522629

Jiang XL, Wang YX, Hoffmann RS (2003) A review of the systematics and distribution of Asiatic short-tailed shrews, genus Blarinella (Mammalia, Soricidae). Mammalian Biology 68(4): 193–204. https://doi.org/10.1078/1616-5047-00085

Koju NP, He K, Chalise MK, Ray C, Chen ZZ, Zhang B, Jiang XL (2017) Multilocus approaches reveal underestimated species diversity and inter-specific gene flow in pikas (Ochotona) from southwest-ernChina. Molecular Phylogenetics and Evolution 107: 239–245. https://doi.org/10.1016/j.ympev.2016.11.005

Leaché AD, Fujita MK (2010) Bayesian species delimitation in West African forest geckos (Hemidactylus fasciatus). Proceedings. Biological sciences 277(1697): 3071–3077. https://doi.org/10.1098/rspb.2010.0662

Li Q, Li Q, Xu RC, Wang YQ (2022) Rodent faunas, their paleogeographic pattern, and responses to climate changes from the early Eocene to the early Oligocene in Asia. Frontiers in Ecology and Evolution 10: 955779. https://doi.org/10.3389/fevo.2022.955779

Liu SY, Wu Y (2019) Handbook of the mammals of China. Strait Book Company.

Liu SY, Sun ZY, Zeng ZY, Zhao EM (2007) A new species (*Proedomys*: Aricolinae: Murida) from the Liangshan Mountains of Sichuan Province, China. Journal of Mammalogy 5: 1170–1178. https://doi.org/10.1644/06-MAMM-A-141R2.1

Liu SY, Liu Y, Guo P, Sun ZY, Murphy RW, Fan ZX, Fu JR, Zhang YP (2012) Phylogeny of oriental voles (Rodentia, Muridae, Arvicolinae): Molecular and morphological evidence. Zoological Science 9: 610–622. https://doi.org/10.2108/zsj.29.610

Luo A, Qiao H, Zhang Y, Shi W, Ho SY, Xu W, Zhang A, Zhu C (2010) Performance of criteria for selecting evolutionary models in phylogenetics: a comprehensive study based on simulated datasets. BMC evolutionary biology 10: 242. https://doi.org/10.1186/1471-2148-10-242

Mammal Diversity Database (2022) Mammal Diversity Database (Version 1.9.1). Zenodo. https://doi.org/10.5281/zenodo.4139818

Michaux J, Shenbrot G (2017) Family Dipodidae (Jerboas). Handbook of the mammals of the world, 7. Rodents II. Barselonain: Lynx Edicionsin in association with Conservation International and IUCN.

Molnar P (2005) Mio-pliocene growth of the Tibetan Plateau and evolution of East Asian climate. Palaeontologia Electronica 8(2A): 23P.

Molnar P, England P, Martinod J, (1993) Mantle Dynamics, Uplift of the Tibetan Plateau, and the Indian Monsoon. Reviews of Geophysics 31: 357–396. https://doi.org/10.1029/93RG02030

Myers N, Mittermeier RA, Mittermeier CG, Fonseca GABD, Kent J (2000) Biodiversity hotspots for conservation priorities. Nature 403: 853–858. https://doi.org/10.1038/35002501

Pan T, Sun Z, Lai XL, Orozcoterwengel P, Yan P, Wu G, Wang H, Zhu W, Wu X-B, Zhang B-W (2019) Hidden species diversity in Pachyhynobius: A multiple approaches species delimitation with mitogenomes. Molecular phylogenetics and evolution 137: 138–145. https://doi.org/10.1016/j.ympev.2019.05.005

Patton JL, Conroy CJ (2017) The conundrum of subspecies: Morphological diversity among desert populations of the California vole (Microtus californicus, Cricetidae). Journal of Mammalogy 98: 1010–1026. https://doi.org/10.1093/jmammal/gyx074

Phillips MJ (2009) Branch-length estimation bias misleads molecular dating for a vertebrate mitochondrial phylogeny. Gene 441(1–2): 132–140. https://doi.org/10.1016/j.gene.2008.08.017

Posada D (2008) jModelTest: phylogenetic model averaging. Molecular biology and evolution 25(7): 1253–1256. https://doi.org/10.1093/molbev/msn083

Pousargues E (1896) Note sur une espéce asiatique du genre *Zapus* (Coues). Annales des Sciences Naturelles 8(1): 220.

Ronquist F, Huelsenbeck JP (2003) MrBayes 3: Bayesian phylogenetic inference under mixed models. Bioinformatics 19(12): 1572–1574. https://doi.org/10.1093/bioinformatics/btg180

Shenbrot G, Bannikova A, Giraudoux P, Quere J, Raoul F, Lebedev V (2017) A new recent genus and species of three-toed jerboas (Rodentia, Dipodinae) from China: A living fossil?. Journal of Zoological Systematics and Evolutionary Research 55(4): 356–368. https://doi.org/10.1111/jzs.12182

Smith AT, Xie Y (2008) A guide to the mammals of China. Princeton University Press. Princeton, New Jersey, 135–144.

Song YG, Fang XM, Torii M, Ishikawa N, Li JJ, An ZS (2007) Late Neogene rock magnetic record of climatic variation from Chinese eolian sediments related to uplift of the Tibetan Plateau. Journal of Asian Earth Sciences 30: 324–332. https://doi.org/10.1016/j.jseaes.2006.10.004

Sui LL, Cheng JL, Xia L, Yang QS (2022) Phylogeny and distribution patterns of Dipodoidea in China. Acta Theriologica Sinica 42(2): 131–143. https://doi.org/10.16829/j.slxb.150616

Tamura K, Peterson D, Peterson N, Stecher G, Nei M, Kumar S (2011) MEGA5: molecular evolutionary genetics analysis using maximum likelihood, evolutionary distance, and maximum parsimony methods. Molecular biology and evolution 28(10): 2731–2739. https://doi.org/10.1093/molbev/msr121

Tamura K, Stecher G, Peterson D, Filipski A, Kumar S (2013) MEGA6: Molecular Evolutionary Genetics Analysis version 6.0. Molecular biology and evolution 30(12): 2725–2729. https://doi.org/10.1093/molbev/mst197

Thomas O (1912) On a collection of small mammals from the Tsin-ling Mountains, Central China, presentedby Mr. G. Fenwick Owen to the National Museum. The Annals and Magazine of Natural History 8.10(58): 402. https://doi.org/10.1080/00222931208693252

Wan T, He K, Jin W, Liu SY, Chen ZZ, Zhang B, Jiang, XL (2018) Climate niche conservatism and complex topography illuminate the cryptic diversification of Asian shrew-like moles. Journal of Biogeography 45: 2400–2414. https://doi.org/10.1111/jbi.13401

Wei F, Costanza R, Dai Q, Stoeckl N, Gu X, Farber S, Zhang W (2018) The value of ecosystem services from Giant Panda reserves. Current Biology 28: 2174–2180 [e7]. https://doi.org/10.1016/j.cub.2018.05.046

Wei FW, Yang QS, Wu Y, Jiang XL, Liu SY (2022) Taxonomy and distribution of Mammals in China. Science Press.

Wilson DE, Mittermeier RA (2018) Handbook of the Mammals of the World: True Mice and Rats Gerbils and Relatives. Barcelona: Lynx Edicions.

Yang Z, Rannala B (2010) Bayesian species delimitation using multilocus sequence data. Proceedings of the National Academy of Sciences of the United States of America 107(20): 9264–9269. https://doi.org/10.1073/pnas.0913022107

Yang FS, Qin AL, Li YF, Wang XQ (2012) Great genetic differentiation among populations of Meconopsis integrifolia and its implication for plant speciation in the Qinghai-Tibetan Plateau. PLoS ONE 7(5): e37196. https://doi.org/10.1371/journal.pone.0037196

Yu G, Zhang M, Rao D, Yang J (2013) Effect of Pleistocene climatic oscillations on the phylogeography and demography of red knobby newt (Tylototriton shanjing) from southwestern China. PLoS ONE8(2): e56066. https://doi.org/10.1371/journal.pone.0056066

Zhang B, He K, Wan T, Chen P, Sun G, Liu SY, Nguyen TS, Lin LK, Jiang XL (2016) Multi-locus phylogeny using topotype specimens sheds light on the systematics of Niviventer (Rodentia, Muridae) in China. BMC Evolutionary Biology 16: 261. https://doi.org/10.1186/s12862-016-0832-8

Zheng Y, Rui P, Masaki KO, Zeng X (2011) Exploring patterns and extent of bias in estimating divergence time from mitochondrial DNA sequence data in a particular lineage: A case study of salamanders (order Caudata). Molecular Biology and Evolution 28(9): 2521–2535. https://doi.org/10.1093/molbev/msr072

Supplementary material 1

Supplementary file

Authors: Siyu Yang, Fei Xie, Chengxin Zhou, Zongyun Zhang, Xuming Wang, Shaoying Liu, Shunde Chen

Data type: docx

Explanation note: **table S1.** Primers used for PCR and sequencing used in this study; **table S2.** Sampling information including localities and GenBank accession numbers from GenBank in this study; **table S3.** The best molecular evolution model used in phylogenetic reconstructions based on jModeltest; **table S4.** Result of BPP species delimitation based on CYT B+nuDNA and nuDNA dataset; **table S5.** Cranial measurements of the genus *Eozapus* used in this study.

Link: https://doi.org/10.3897/zse.101.133734.suppl1

Zoosyst. Evol. 101 (2) 2025, 609–625 | DOI 10.3897/zse.101.145722

PENSOFT

MUSEUM FÜR NATURKUNDE BERLIN

On the commercial shrimps of the "*Parapenaeopsis cornuta* (Kishinouye, 1900)" species group (Crustacea, Decapoda, Penaeidae)

Tin-Yam Chan[1], Chien-Hui Yang[1], Appukttannair Biju Kumar[2], Amirah Hurzaid[3]

1 *Institute of Marine Biology and Center of Excellence for the Oceans, National Taiwan Ocean University, Keelung 202301, Taiwan*

2 *Department of Aquatic Biology & Fisheries, University of Kerala, Thiruvananthapuram 695581, Kerala, India*

3 *Biological Sciences Department, School of Distance Education and School of Biological Sciences, University Sains Malaysia, 11800 Minden, Penang, Malaysia*

https://zoobank.org/370E684B-7400-4D34-AD7B-E63425B02860

Corresponding authors: Chien-Hui Yang (chyang@ntou.edu.tw); Amirah Hurzaid (amirahhurzaid@usm.my)

Academic editor: M. Christodoulou ♦ **Received** 1 January 2025 ♦ **Accepted** 17 February 2025 ♦ **Published** 14 March 2025

Abstract

Penaeid shrimps belonging to the *Parapenaeopsis cornuta* (Kishinouye, 1900) species group hold significant commercial value in the Indo-West Pacific, but their taxonomy has been problematic. A taxonomic revision of this group, supported by molecular genetic analysis using the barcoding gene COI, confirmed the validity of all four species within the group. Their distinguishing characteristics are redefined and illustrated, and a key for identifying the four species in the "*P. cornuta*" group is provided.

Key Words

DNA barcode, marine, molecular, revision, taxonomy

Introduction

The moderate small penaeid shrimp (body length excluding rostrum about 10 cm), *Parapenaeopsis cornuta* (Kishinouye, 1900), is generally considered to be widely distributed in the Indo-West Pacific (Japan to India and Australia) and fished commercially in some areas (Chan 1998; Holthuis 1980; 1984; Liu and Zhong 1988; Yu and Chan 1986). This species, however, has a lot of taxonomic ambiguities (also see Hsu and Chan 2023). A very similar species, *P. maxillipedo* Alcock, 1906, was described from India and also considered to be widely distributed in the Indo-West Pacific, but with a more southern distribution from India to the Philippines and Australia (Chan 1998; Holthuis 1980; 1984; Pérez Farfante and Kensley 1997). Alcock (1906), in his original description of *P. maxillipedo*, suspected that this species may belong to the same species as *P. cornuta*. Some later workers had synonymized these two names or treated them as subspecies (e.g., Dall and Rothlisberg 1990; Racek and Dall 1965; Racek and Yaldwyn 1971). Liu and Wang (1987) split the Chinese material of *P. cornuta* into three species with the erections of *P. sinica* Liu & Wang, 1987, and *P. incisa* Wang & Liu in Liu and Wang 1987 from southern China, without knowing that V. C. Nguyên (1971) had already named their *P. sinica* as *P. amicus* from Vietnam. Nevertheless, some workers (e.g., Dall and Rothlisberg 1990; Hayashi 1992) commented that the distinguishing characters proposed for *P. amicus* and *P. incisa* are too subtle and considered both names to be junior synonyms of *P. cornuta*. On the other hand, Sakai and Shinomiya (2011) erected a genus, *Kishinouyepenaeopsis*, for these four very similar species, namely *P. cornuta*, *P. maxillipedo*, *P. amicus*, and *P. incisa*. Recent molecular analysis by Hurzaid et al. (2020) even suggested that there may be more than eight species in *Kishinouyepenaeopsis*.

As commented in Hsu and Chan (2023), splitting of *Parapenaeopsis* Alcock, 1901 s. l. is not adopted because there are still many controversies on the status and nomenclature in separating *Parapenaeopsis* s. l. like the separation of the genus *Penaeus* Fabricius, 1798 (see Yang et al. 2023). For example, Sakai and Shinomiya

(2011) used only the differences of the petasma to split *Parapenaeopsis* into seven genera. Chanda (2016a, b) disagreed with such classification but created two more generic names in *Parapenaeopsis* s. l. Until there are better supports for those genera created by Sakai and Shinomiya (2011), the genus *Kishinouyepenaeopsis* is not recognized and treated as a junior synonym of *Parapenaeopsis*. The term "*P. cornuta*" species group is hence used to refer to these four closely related species.

Of the four species in the "*P. cornuta*" species group, *P. amicus* is quite different and rather easy to recognize (see Hsu and Chan 2023). This work, with the aid of DNA barcoding data, compared *P. cornuta, P. maxillipedo,* and *P. incisa* material from different areas, including their topotypic localities, as well as abundant specimens of *P. amicus* from Taiwan. The results showed that the four currently recognized names in the "*P. cornuta*" species group are all valid. The distinguishing characteristics of these four named species are redefined in order to facilitate the taxonomy of this species group if more taxa will be discovered later.

Materials and methods

Specimens examined are deposited in the National Taiwan Ocean University, Keelung (**NTOU**), Universiti Sains Malaysia, Penang (**USM**), Natural History Museum and Institute, Chiba, Japan (**CBM**), Marine Biological Museum of the Chinese Academy of Sciences, Qingdao (**MBM**). As members of the "*P. cornuta*" species group are widely distributed in the Indo-West Pacific and fished commercially in many areas, there are a lot of reports on them with abundant material deposited at many institutions worldwide. Nevertheless, most previous publications on this group did not state or illustrate explicitly the distinguishing characters used in this work and rendered their identities indeterminable. It was considered too major a task to examine all the material of this group around the world and to verify the identification of all previous records. The synonymy given, therefore, is restricted to important taxonomic literature of the species. To facilitate their identification by shrimp workers, a key as well as a table of distinguishing characters for the species of this group are herein provided. The measurements provided are carapace length (cl), which is measured dorsally from the posteriormost orbital margin to the posterior margin of the carapace (Fig. 2a). The length and width ratio of the anterior plate of the thelycum is measured as width = widest part, length = from widest part to most distal (or anteriormost) point (Fig. 5a). The terminology used mainly follows Chan (1998) with Hsu and Chan (2023). As there are a lot of specimens of *P. cornuta* and *P. amicus* deposited in NTOU (see Hsu and Chan 2023), the counts and measurements given in the "Diagnosis" and "Remarks" were randomly selected from five and 10 specimens of each sex of these two species for the Taiwanese material, respectively. All specimens from other localities were included for comparisons amongst species.

DNA barcodes (mitochondrial cytochrome c oxidase I gene, mtCOI, Hebert et al. 2003) were employed to determine the taxonomic status of *P. cornuta, P. maxillipedo, P. amicus,* and *P. incisa*. Specimens sequenced in this work are shown in Table 1. Crude genomic DNA was extracted from the fifth pleopod or the muscles of the abdomen using the DNeasy® Blood and Tissue Kit (Qiagen, Hilden, Germany) following the protocol of the manufacturer. The universal primer, LCO1490/HCO2198 (~657 bp, Folmer et al. 1994), was used for the sequence amplification. PCR reactions, cycling profiles (annealing temperature 47.8 °C for mtCOI gene), product checking, and sequencing procedures followed Yang et al. (2015). Output sequences were edited for contig assembly by SeqMan Pro™ (Lasergene®; DNASTAR, Madison, WI, USA) before being blasted on GenBank (National Center for Biotechnology Information, NCBI) to check if any potential contamination. EditSeq (Lasergene®; DNASTAR) was used to translate into the corresponding amino acid sequences to avoid the inclusion of pseudogenes for the COI dataset (Song et al. 2008). All mtCOI sequences from the "*P. cornuta*" species group reported by Hurzaid et al. (2020) were included in the analyses. Sequence alignment was performed by the MAFFT v. 7 online service (Katoh et al. 2019), and a nucleotide length of 615 bp was used in the final analyzed dataset. The two Taiwanese specimens of *P. cornuta* [NTOU M02358] did not achieve this nucleotide length and only had 612 and 470 bp. The gaps in these two shorter sequences were filled by the fifth nucleotide "N". Corrected pairwise distance was calculated based on the Kimura 2-parameter model (K2P; Kimura 1980) by MEGA v.11 (Tamura et al. 2021). A maximum-likelihood (ML) tree was constructed using the IQ-TREE web server (Trifinopoulos et al.

Table 1. Pairwise distance (%) based on the Kimura-2-parameter (K2P) model of partial mitochondrial COI sequences (615 bp) among four species of the "*Parapenaeopsis cornuta*" group in a dataset of sequences generated in this work plus three sequences of *P. amicus* from Taiwan in Hurzaid et al. (2020) with their specimens re-examined. Numbers in parentheses are sample sizes. GenBank numbers, see Fig. 8.

	P. cornuta (6- **J**, T, C)	***P. maxillipedo*** (7- **I**, M)	***P. amicus*** (3- T)	***P. incisa*** (2- **C**)
P. cornuta (6- **J**, T, C)	0.0–0.7			
P. maxillipedo (7- **I**, M)	13.5–16.0	0.0–0.7		
P. amicus (3- T)	14.2–17.5	19.7–20.6	0.2–0.5	
P. incisa (2- **C**)	15.0–17.5	19.3–20.7	20.4–20.9	0.0

J: Japan, T: Taiwan, C: Southern China, I: India, M: Malaysia.
Bold: type-locality of the species.

2016) with 1000 bootstrap replicates based on the model of "TIM2+G4+F" and with the congeneric species *P. hardwickii* (Miers, 1878) used as an outgroup.

Systematic account

Family Penaeidae Rafinesque, 1815
Genus *Parapenaeopsis* Alcock, 1901

Parapenaeopsis cornuta (Kishinouye, 1900)

Figs 1a, 2a, 3a, 4a, 5a, 6a, 7a, b

Penaeus cornutus Kishinouye 1900: 23, unnumbered text fig., p1. 7-figs 9, 9A (type locality: Ariake, Japan).

Parapenaeopsis cornutus – Kubo 1949: 374 (? in part–Taiwanese material), figs 7Z, 10B, 22I, 32C, D, 47N, 63A, B, 75F, L, 78L, 135C, 136A, B.

Parapenaeopsis cornuta – Hayashi 1986: 67, fig. 26; 1992: 105, fig. 57a-c; Liu and Wang 1987: 524, fig. 2; Liu and Zhong 1988: 208, fig. 129, pl. 6: 5; Hsu and Chan 2023: 224, figs 2, 6b.

Kishinouyepenaeopsis cornuta – Sakai and Shinomiya 2011: 499, figs 3A, B, 4F; De Grave and Fransen 2011: 216.

Material examined. **Japan** • [CBM ZC3280]: Tosa Bay, Katsura-hama Beach, commercial trawler, 10–20 m, 28 Nov. 1996, 3♂♂, cl 15.6–17.4 mm, 1 ♀, cl 19.0 mm • [NTOU M02640]: Aichi, Minami-Chita, Toyohama fishing port, commercial trawler, 18 m, 31 Oct. 2024, 1♂, cl 20.7 mm • [NTOU M02641]: Aichi, Nishio, Isshiki fishing port, commercial trawler, 22.5 m, 14 Dec. 2024, 1♂, cl 14.3 mm, 3♀♀, cl 21.5–24.6 mm.

Taiwan • [NTOU M02355]: Yilan County, Dasi fishing port, commercial trawler, 10 Mar. 1985, 2♂♂, cl 14.5–18.4 mm • [NTOU M02356]: Yilan County, Dasi fishing port, commercial trawler, 5 Aug. 1982, 1♂, cl 22.9 mm, 1♀, cl 28.9 mm • [NTOU M02357]: Keelung City, commercial trawler, 12 Oct. 1990, 1♂, cl 14.5 mm • [NTOU M02358]: Changhua County, Wenzi fishing port, commercial trawler, 5 Aug. 2021, 3♂♂, cl 16.6–17.4 mm, 39♀♀, cl 17.2–22.0 mm • [NTOU M02359]: Chiayi County, Budai fishing port, commercial trawler, 26 May 1974, 2♀♀, cl 18.0–18.7 mm • [NTOU M02360]: Chiayi County, Budai fishing port, commercial trawler, 20 Jan. 1995, 1♀, cl 18.2 mm • [NTOU M02485]: Chiayi County, Budai fishing port, commercial trawler, 2 Jul. 2002, 1♀, cl 13.6 mm • [NTOU M02361]: Kaohsiung City, Singda fishing port, commercial trawler, 24 Jul. 1984, 2♀♀, cl 16.1–17.0 mm • [NTOU M02362]: Kaohsiung City, Kaohsiung port, station 4, 1 Mar. 1994, 2♂♂, both cl 18.1 mm • [NTOU M02363]: Kaohsiung City, Cijin, 25 Mar. 1996, 4♂♂, cl 18.6–19.5 mm, 7♀♀, cl 19.1–23.1 mm • [NTOU M02364]: Pingtung County, Donggang fishing port, commercial trawler, 28 Jul. 1985, 2♂♂, cl 15.1–16.8 mm, 2♀♀, cl 19.2–19.3 mm • [NTOU M02419]: No specific data, 2♀♀, cl 21.1–21.2 mm • [NTOU M02486]: No specific data, 2♂♂, cl 19.0–19.2 mm, 2♀♀, cl 23.1–23.4 mm • [NTOU M02487]: No specific data, 1♂, cl 18.3 mm, 3♀♀, cl 16.2–22.8 mm.

Southern China • [MBM 155050]: Fujian, Xiamen fish market, 05F-16, 3 Sep. 2005, 2♂♂, cl 18.1–18.7 mm, 2♀♀, cl 19.4–22.3 mm • [MBM 155083]: Guangdong, Yangjiang, Zhapo, Dajiao hill, 54-K187B, 18 Nov. 1954, 2♂♂, cl. 14.3–17.7 mm, 2 ♀♀, cl 15.7–16.8 mm • [MBM 155080]: Hainan, Boao, stn 3, 8 Nov. 1990, 2♀♀, cl 12.0–16.3 mm • [MBM 155074]: Hainan, Sanya bay, stn 3, CJ97C-164, 3–4 m, Nov. 1997, 1♀, cl 18.1 mm.

Diagnosis. Rostrum more or less horizontal, straight, extending to distal segment of antennular peduncle and often reaching tip of antennular peduncle, armed with 6–8 (avg. 7.0, n = 27) dorsal teeth (excluding epigastric tooth), tip devoid of tooth and slightly curved upwards. Postrostral carina generally having a weak median pit and with posterior 1/4 broadened and obscure, extending posteriorly to 0.72–0.92 (avg. 0.85, n = 30) of carapace length. Longitudinal suture short and extending to about level of epigastric tooth. Pereiopods I and II with basial spines and epipods. Pereiopod III generally lacking basial spine, rarely a minute to small basial spine present only in males. Abdominal somites I and II lacking dorsal carina. Telson without lateral movable spinules. Males with endopod of pleopod II strongly modified into boot-like shape, distal margin straight or more often distinctly concave medially, anterodistal part bearing tuft of dense long stiff setae extending beyond distal margin; petasma lacking distomedian projection but with distolateral projections strongly elongated and horn-like, tip of horn distinctly protruded at outer side. Female thelycum with anterior plate mostly semi-quadrate to sometimes semi-circular and 0.74–0.95 (avg. 0.85, n = 16) as long as wide, anterior margin with median part occasionally slightly protruded, surface slightly sunken and rarely with median longitudinal furrow; posterior plate with weak median ovate boss, lateral parts as large semicircular process; tuft of setae behind posterior plate long and thick.

Coloration. (Fig. 7a, b) Body generally greenish to bluish gray and densely covered with dark green dots. Antennal flagellae and abdomen slightly banded. Tip of rostrum dark brown to reddish brown. Eyes black gray. Uropods of tail fan dark green to dark red and with yellowish margins. Thoracic appendages pinkish white. Pleopods with rami reddish. Tuft of long setae behind thelycum bluish. Color photographs verified belonging to this species are provided by Hayashi (1986: fig. 26) and Hsu and Chan (2023: fig. 6b).

Distribution. Known with certainty from Japan to Taiwan and southern China, intertidal to 32 m deep (Liu and Zhong 1988). Perhaps more widely distributed west to India and south to northern Australia (see Remarks).

Remarks. For those distinguishing characters found in this study to be useful in separating the species of the "*P. cornuta*" group (Figs 1–6, Table 2), topotypic material of *P. cornuta* from Japan has the pereiopod III generally lacking a basial spine; postrostral carina with the posterior part faded and extending to a position with a distinct distance from the posterior margin of the carapace; male pleopod II with endopod boot-like and having the distal margin straight or medially concave; petasma with tip of horn distinctly protruded only at the outer side; thelycum

with anterior plate generally semi-quadrate and slightly shorter than width; posterior plate bearing a weak median ovate boss and a tuft of long setae behind it. Specimens with the above characteristics from Japan [CBM ZC3280, NTOU M02641], Taiwan [NTOU M02358], and southern China [MBM 155074] have 99.3–100% similarity in the barcoding mtCOI gene (615 bp, Table 1) and can be safely considered as belonging to the same species. Of the 100 specimens (including 27 males) examined, only two males from Japan [CBM ZC3280] and Taiwan [NTOU M02356] have their pereiopods III bearing small basial spines (on both sides). As the median boss at the posterior plate of the thelycum is weak in this species, this boss is sometimes rather rudimentary in small females.

Although *P. cornuta* can be readily separated from the other species of the "*P. cornuta*" species group by a combination of characters (Table 2), it does not have a unique and conspicuous distinguishing character. Its number of rostral teeth, shape of the postrostral carina, pereiopod III lacking an basial spine and even body coloration are nearly identical with *P. amicus* and *P. incisa* (exact coloration still unknown). The petasma and boot-like endopod of the pleopod II in males, as well as the shape of the anterior plate of the thelycum and the tuft of hairs (including color of hairs) behind the thelycum, are almost the same between *P. cornuta* and *P. maxillipedo* (Figs 3a, b, 4a, b, 5a, b). Only the median boss at the posterior plate of the thelycum is relatively lower (Fig. 5a) than that of *P. maxillipedo* (Fig. 5b), while the median part of the posterior plate is flattened or sunken in *P. incisa* (Fig. 5d) and *P. amicus* (Fig. 5c), respectively. Nevertheless, the characteristic shape of the thelycum is generally underdeveloped in small females of penaeids. Therefore, the posterior plate of the thelycum is very similar amongst small females of *P. cornuta*, *P. maxillipedo,* and *P. incisa*.

The lack of a unique, conspicuous character to distinguish *P. cornuta* from the other species of the "*P. cornuta*" group renders the verification of the distribution records of this species very difficult. The original description of *P. cornuta* (Kishinouye 1900) also has not mentioned nor illustrated clearly the present distinguishing characters used for separating the species of the "*P. cornuta*" group. The whereabouts of the type of *P. cornuta* is not known, and it is not in the National Museum of Nature and Science, Tokyo (personal communication from Tohru Naruse) or the University of Tokyo (where Kishinouye studied, personal communication from Tomoyuki Komai). Nevertheless, there is no report nor evidence that there is more than one species of the "*P. cornuta*" group present in Japan (see Hayashi 1986, 1992; Kubo 1949). Thus, the Japanese specimens examined in this work can be treated as typical *P. cornuta*.

It has been considered that *P. cornuta* is widely distributed in the Indo-West Pacific from Japan to India and tropical Australia (see Chan 1998; Holthuis 1980, 1984; Pérez Farfante and Kensley 1997). Other than its records from Taiwan and southern China confirmed by the present material examined, reports of this species from other areas need verification. For example, there is the possibility that the photographs assigned to "*P. cornuta*" from Thailand (Chaitiamvong and Supongpan 1992: pl. 44) and Australia (Grey et al. 1983: fig. 39) may actually represent *P. amicus* or *P. incisa* as some molecular analyses (Hurzaid et al. 2020; Fakhruddin et al. 2024) have already suggested that *P. incisa* is likely at least ranging to the Strait of Malacca or even to Bangladesh (see "Discussion" below).

Parapenaeopsis maxillipedo Alcock, 1906

Figs 1b, 2b, 3b, 4b, 5b, 6b, 7c

Parapenaeopsis maxillipedo Alcock 1906: 40, pl. VIII–fig. 24, 24a–b (type-locality: Bombay and Madras, India and Arakan, Myanmar); Holthuis 1984: PEN Para 8, 4 unnumbered figs; De Bruin et al. 1995: 32, 3 unnumbered figs; Chan 1998: 944, 3 unnumbered figs.

Parapenaeopsis (*Kishinouyepenaeopsis*) *maxillipedo* – Psomadakis et al. 2019: 39, 4 unnumbered figs.

Kishinouyepenaeopsis maxillipedo – De Grave and Fransen 2011: 216.

Material examined. **India** • [NTOU M02625]: Tamil Nadu, Tuticorin fishing harbor, commercial trawler, 18 Mar. 2017, 2♂♂, cl 14.4–16.0 mm, 3♀♀, cl 11.4–22.3 mm • [NTOU M02626]: Tamil Nadu, Tuticorin fishing harbor, commercial trawler, 22 Mar. 2017, 1♂, cl 11.9 mm, 1♀, cl 19.0 mm • [NTOU M02627]: Tamil Nadu, Tuticorin fishing harbor, commercial trawler, 22 Mar. 2017, 1♂, cl 12.1 mm, 1♀, cl 15.4 mm • [NTOU M02628]: Muttom, Jeppiaar fishing harbor, commercial trawler, Sep. 2018, 2♂♂, cl 13.9–14.0 mm. **Malaysia** • [USM_INV1006]: Strait of Malacca, Pantai Remis, Perak, 10 Aug. 2023, 1♂, cl 18.6 mm • [USM_INV1009]: Strait of Malacca, Pantai Remis, Perak, 10 Aug. 2023, 1♂, cl 22.5 mm • [USM_INV1010]: Strait of Malacca, Pantai Remis, Perak, 10 Aug. 2023, 1♂, cl 18.9 mm • [USM_INV1011]: Strait of Malacca, Pantai Remis, Perak, 10 Aug. 2023, 1♀, cl 26.8 mm • [USM_INV1012]: Strait of Malacca, Pantai Remis, Perak, 10 Aug. 2023, 1♀, cl 25.7 mm.

Diagnosis. Rostrum generally straight and horizontal, reaching between base and middle of distal antennular peduncle segment, bearing 8–10 (avg. 8.9, n = 15) dorsal teeth (excluding epigastric tooth), tip without tooth, and slightly curved upwards. Postrostral carina distinct and similar width along entire length but often with a weak median pit, almost reaching posterior margin of carapace and being 0.91–0.97 (avg. 0.96, n = 16) of carapace length. Longitudinal suture short and extending to about level of epigastric tooth. Pereiopods I and II bearing basial spines and epipods. Pereiopod III generally armed with distinct basial spine. Abdominal somites I and II without dorsal carina. Telson without movable lateral spinules. Males with endopod of pleopod II strongly modified into boot-like shape, distal margin straight or slightly concave medially, median part of distal margin concealed by tuft of dense long stiff setae arose from anterodistal part of endopod; petasma horn-like with distolateral projections strongly elongated, tip of horn bearing distinct protuberance only at outer side. Female thelycum, anterior plate generally semi-quadrate or sometimes semi-circular, 0.79–1.03 (avg. 0.91, n = 7) as

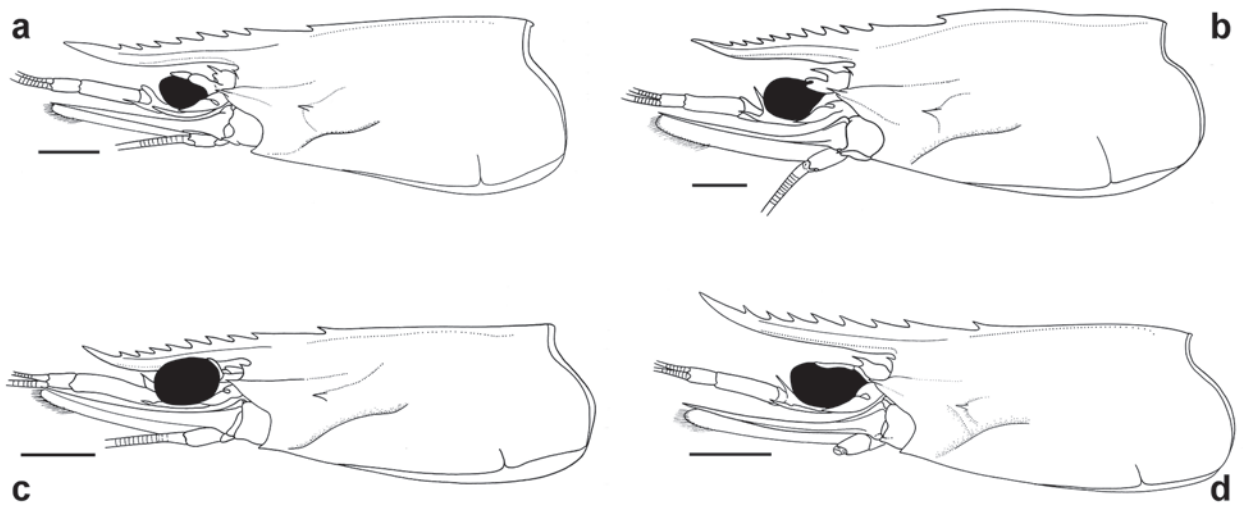

Figure 1. Carapace and anterior appendages, lateral view. **a.** *Parapenaeopsis cornuta* (Kishinouye, 1900), Cijin, Kaohsiung City, Taiwan, female cl 22.4 mm (NTOU M02363). **b.** *P. maxillipedo* Alcock, 1906, Strait of Malacca, Pantai Remis, Perak, Malaysia, female cl 26.8 mm (USM_INV 1011). **c.** *P. amicus* V. C. Nguyên, 1971, Budi fishing port, Chiayi County, Taiwan, female cl 27.3 mm (NTOU M02372). **d.** *P. incisa* Wang & Liu in Liu and Wang 1987, Sanya, Hainan, Southern China, females cl 17.6 mm (MBM 155044). Scale bars: 5 mm.

long as wide, surface slightly sunken and lacking median longitudinal furrow; posterior plate with distinct and often high median ovate boss, lateral parts semicircular; tuft of setae behind posterior plate long and thick.

Coloration. (Fig. 7b) Body greenish yellow and covered with dense yellowish to dark green dots. Eyes black gray. Antennal flagellae pinkish to yellowish and alternated with dark bands. Rostrum with tip reddish to dark reddish brown, bases of rostral teeth sometimes black and continuous as thick black line. Thoracic appendages whitish to pinkish white and greenish yellow. Abdomen with dense dark green dots arranged as distinct transverse bands, last somite (or somite VI) bearing a large black or brown posterolateral spot anteriorly accompanied with thick white margin. Uropods of tailfan reddish to dark red and with yellowish green margins or distal parts yellowish green. Pleopods pale white to pale yellow or reddish, outer parts of peduncles sometimes whitish. Tuft of long setae behind thelycum bluish. Color photograph belonging to this species given in Chaitiamvong and Supongpan (1992: pl. 43).

Distribution. Known with certainties from India to Thailand and Strait of Malacca, shallow water less than 30 m deep (Chan 1998). Perhaps more widely distributed eastwards to the Philippines and northern Australia (see Remarks).

Remarks. The relationships between *P. maxillipedo* and *P. cornuta* are extremely confusing in literature. *Parapenaeopsis maxillipedo* was suspected to belong to the same species as *P. cornuta* in the original description (Alcock 1906), and some authors also suspected or considered these two names to be synonyms (e.g., Dall 1957; Dall and Rothlisberg 1990; De Man 1911; Hall 1961). Other workers, however, considered that *P. maxillipedo* is a distinct species or subspecies (e.g., Chaitiamvong and Supongpan 1992; Chan 1998; Chanda 2016b; Holthuis 1980, 1984; Kubo 1949; Liu and Wang 1987; Liu and Zhong 1988; Motoh and Buri 1984; Muthu 1968; Racek and Dall 1965; Racek and Yaldwyn 1971) and proposed many characters to separate it from *P. cornuta*. Careful comparisons and molecular analyses of materials assigned to *P. maxillipedo* and *P. cornuta* in this work reveal that there are large nucleotide divergences (13.5–16.0%, Table 1) between these two species and they can be separated by the following characters.

As commented on by many workers (Chan 1998; Chanda 2016b; Dall 1957; De Man 1911; Hall 1961; Holthuis 1984; Kubo 1949; Liu and Wang 1987; Liu and Zhong 1988; Motoh and Buri 1984; Muthu 1968; Racek and Dall 1965; Racek and Yaldwyn 1971), the pereiopod III generally bears a distinct basial spine in *P. maxillipedo* (Fig. 6b) but lacks a basial spine in *P. cornuta* (Fig. 6a). Nevertheless, as pointed out by Kubo (1949) as well as Racek and Dall (1965), there are variations in this character. Of the 16 specimens (including nine males and seven females) of *P. maxillipedo* examined in this work, a male [NTOU M02625] and a female [NTOU M02627] from India lack a basial spine at the pereiopod III on both sides. Another female [NTOU M02625], also from India, only has a small basial spine at the pereiopod III. On the other hand, only two (both males) of the 100 specimens (including 27 males) examined in *P. cornuta* have small ischial spines present on the pereiopods III. The rostrum is generally shorter (maximum extending to the middle of the distal antennular segment) but armed with more teeth (8–10, avg. 8.9) in *P. maxillipedo* (Fig. 1b). The rostrum of *P. cornuta* (Fig. 1a) is relatively longer (maximum reaching tip of antennular peduncle) and bears fewer teeth (6–8, avg. 7.0). The postrostral carina is distinct along the entire length and almost reaches the posterior margin of

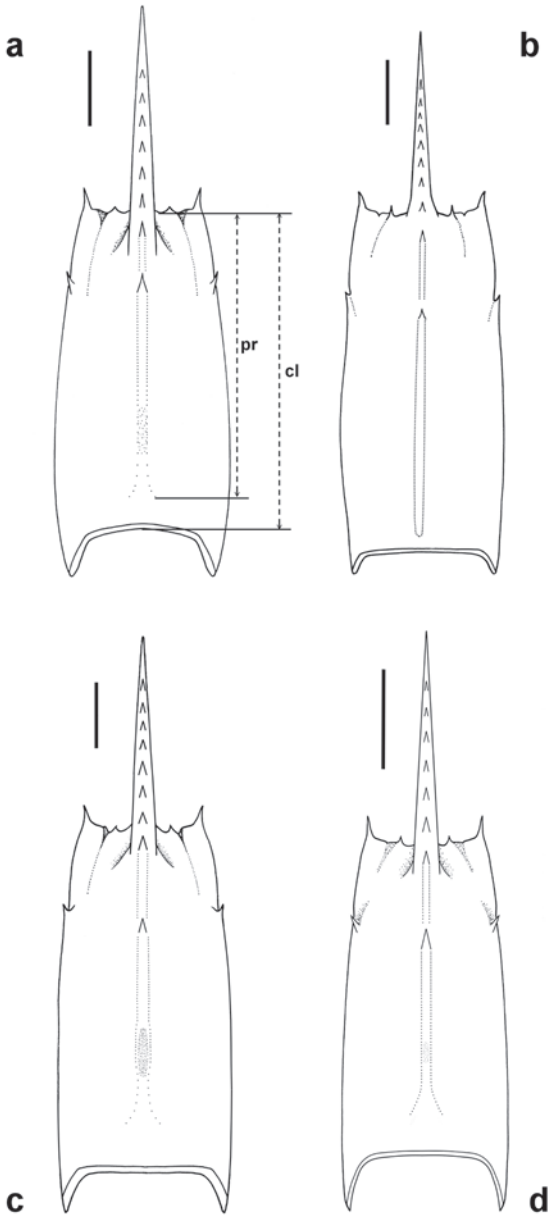

Figure 2. Carapace, dorsal view. **a.** *Parapenaeopsis cornuta* (Kishinouye, 1900), Cijin, Kaohsiung City, Taiwan, female cl 22.4 mm (NTOU M02363). **b.** *P. maxillipedo* Alcock, 1906, Strait of Malacca, Pantai Remis, Perak, Malaysia, female cl 26.8 mm (USM_INV 1011). **c.** *P. amicus* V. C. Nguyên, 1971, Budi fishing port, Chiayi County, Taiwan, female cl 27.3 mm (NTOU M02372). **d.** *P. incisa* Wang & Liu in Liu and Wang 1987, Sanya, Hainan, Southern China, females cl 17.6 mm (MBM 155044). pr: postrostral carina length; cl: carapace length. Scale bars: 5 mm.

the carapace (postrostral carina/cl: 0.91–0.97, avg. 0.96) in *P. maxillipedo* (Figs 1b, 2b), but it is faded and broadened at posterior 1/4 and terminates with a distinct distance from the posterior carapace (postrostral carina/cl: 0.72–0.92, avg. 0.85) in *P. cornuta* (Figs 1a, 2a). The median boss at the posterior plate of the thelycum is strongly elevated in *P. maxillipedo* (Fig. 5b) but weak in *P. cornuta* (Fig. 5a). However, as the development of the thelycum is related to size, the median bosses in some juveniles of *P. maxillipedo* are sometimes low and rather similar to that of *P. cornuta*. The most distinct difference between *P. maxillipedo* and *P. cornuta* is body coloration. Some of the Indian specimens and all Malaysian specimens of *P. maxillipedo* examined in this study are accompanied by color photographs showing the same color pattern. The abdomen is distinctly banded and bears a large dark spot with an anterior thick white margin on the lateral surfaces of the last somite in *P. maxillipedo* (Fig. 7c). In *P. cornuta*, the bandings on the abdomen are obscure, and there is no large spot on the last abdominal somite (Figs 7a, b; see also Hayashi 1986; Hsu and Chan 2023).

Although *P. cornuta* has been reported from India (Chanda 2016b; Muthu 1968), the original description of *P. maxillipedo* described from India and Myanmar clearly mentioned that this species has more rostral teeth (8–10 excluding epigastric tooth), a postrostral carina as "… continued right up to the posterior border of the carapace, is sharp and particularly prominent….," the pereiopod III bearing a big basial spine, and the middle of the posterior plate of the thelycum with "…a globous tubercle…" (Alcock 1906). The present Indian specimens with characteristics described in the previous paragraph fit well with the original description of *P. maxillipedo* and can be considered as typical of this species. As the basial spine is occasionally absent or small at the pereiopod III in *P. maxillipedo*, the records of *P. cornuta* from India based only on males (Chanda 2016b; Muthu 1968) become doubtful. Even those Indian records of *P. cornuta* represent a species different from *P. maxillipedo*; there are possibilities that they may be *P. amicus* or *P. incisa* because these two species also lack a basial spine at the pereiopod III, and the latter species has recently been suggested to occur off Bangladesh (Fakhruddin et al. 2024).

Actually, most of the characters used in separating *P. maxillipedo* from *P. cornuta* can also be applied to distinguish it from *P. amicus* or *P. incisa* (Table 2). *Parapenaeopsis maxillipedo* is unique in the "*P. cornuta*" species group as it has the postrostral carina distinct along the entire length (Fig. 2b) and likely also in its coloration (Fig. 7c, *P. incisa* still without information on coloration but probably similar to *P. cornuta* and *P. amicus*). Moreover, *P. maxillipedo* differs from the other species of the "*P. cornuta*" group by generally having more rostral teeth (Fig. 1b), longer postrostral carina (Figs 1b, 2b), bearing a large basial spine at the pereiopod III (Fig. 6b), and posterior plate of thelycum having a high median boss (Fig. 5b). Nevertheless, the petasma and endopod of pleopod II in males are almost identical between *P. maxillipedo* and *P. cornuta* (Figs 3a, b, 4a, b). The thelycum of these two species is also rather similar, but with the median boss at the posterior plate more developed and the anterior plate somewhat more elongated (0.79–1.03, avg. 0.91 as long as wide) in *P. maxillipedo* (Fig. 5b; vs. 0.74–0.95, avg. 0.85 as long as wide in *P. cornuta*, Fig. 5a).

Although *P. maxillipedo* has been reported from India to the Philippines and tropical Australia (see Chan

Table 2. Distinguishing characters amongst the species of the "*Parapenaeopsis cornuta*" group. Those in bold are unique characteristics for that species, while those in red are rather subtle and more difficult to perceive.

	P. cornuta	*P. maxillipedo*	*P. amicus*	*P. incisa*
Rostrum extending to	distal antennular segment and often reaching tip of antennular peduncle	base and middle of distal segment of antennular peduncle	around tip of second segment of antennular peduncle	distal antennular segment or just overreaching antennular peduncle
Dorsal teeth (excluding epigastric tooth)	6–8, avg. 7.0	8–10, avg. 8.9	7–9, avg. 7.8	6–8, avg. 7.0
Postrostral carina	0.72–0.92, avg. 0.85 carapace length, posterior 1/4 broadened and obscure	**0.91–0.97, avg. 0.96 carapace length, entire length similar width, and distinct**	0.77–0.89, avg. 0.85 carapace length, posterior 1/4 broadened and obscure	0.77–0.89, avg. 0.84 carapace length posterior 1/4 broadened and obscure
Pereiopod III basial spine	usually absent, rarely present only in males	**usually present**	always absent	always absent
Male pleopod II endopod	greatly modified and boot-like, distal margin medially straight or concave	greatly modified and boot-like, distal margin medially straight or concave	**normal, sword-like**	greatly modified and boot-like, **distal margin medially protruded and convex**
Petasma, tip of horn-like distolateral projection	with distinct protuberance only at outer side	with distinct protuberance only at outer side	**distinctly protruded at both sides and hammer-like**	**bifurcate, no lateral protuberance**
Thelycum anterior plate	semi-quadrate, 0.74–0.95, avg. 0.85 as long as wide, rarely with median longitudinal furrow	semi-quadrate, 0.79–1.03, avg. 0.91 as long as wide, median longitudinal furrow absent	**semicircular, 0.59–0.73, avg. 0.65 as long as wide, with median longitudinal furrow**	**rectangular with lateral margins concave, 0.99–1.17, avg. 1.09 as long as wide,** median longitudinal furrow absent
Thelycum posterior plate median part	**weakly elevated into a weak median ovate boss**	**highly elevated into a distinct median ovate boss**	**surface sunken**	**surface flattened**
Tuft of hairs behind thelycum	thick and long, bluish in color	thick and long, bluish in color	**thin and short, colorless**	thick and long, color unknown
Coloration	abdomen slightly banded, last somite without special markings	**abdomen distinctly banded, last somite bearing large dark posterolateral spot with anterior thick white margin**	abdomen slightly banded, last somite without special markings	color unknown

1998; Holthuis 1980, 1984; Pérez Farfante and Kensley 1997), the present study is only able to verify its distribution in India, Thailand, and Malaysia. Materials of this species from India and Malaysia are here examined. The color photograph of *P. maxillipedo* from Thailand given by Chaitiamvong and Supongpan (1992: pl. 43) shows the characteristic large back spot on the last abdominal somite of this species. The drawings of *P. maxillipedo* in the FAO species identification guides for the Western Indian Ocean (Holthuis 1984), Sri Lanka (De Bruin et al. 1995), Myanmar (Psomadakis et al. 2019), Western Central Pacific (Chan 1998) also showed clearly the characteristic large dark spot with an anterior thick white margin on the last abdominal somite. On the other hand, the Philippine material reported as "*P. maxillipedo*" by Motoh and Buri (1984) was described as the basial spine at the pereiopod III sometimes small in females and the bands on the abdomen wider, but the characteristic large dark spot at the last abdominal somite was absent in their illustrated line-drawing (Motoh and Buri 1984: fig. 71). The Australian material reported as "*P. cornuta maxillipedo*" by Racek and Dall (1965) was also described as having the basial spine at the pereiopod III much reduced, like in some females from New Guinea (see also Racek and Yaldwyn 1971). Re-examination of the Philippines, New Guinea, and Australian material will be necessary to understand the exact eastern geographical range of *P. maxillipedo*.

Parapenaeopsis amicus V. C. Nguyên, 1971

Figs 1c, 2c, 3c, 4c, 5c, 7d

Parapenaeopsis amicus V. C. Nguyên 1971: 46, fig. 1 (type locality: West Tonkin Gulf); Hsu and Chan 2023: 222, figs 1, 6a.

Parapenaeopsis sinica Liu and Wang 1986: 214 (nomen nudum), 1987: 527, fig. 4. (type locality: Wailuo, Guangdong, China); Liu and Zhong 1988: 212, fig. 131, pl. 3: 4, 5: 6.

Kishinouyepenaeopsis amicus – De Grave and Fransen 2011: 215.

Material examined. Taiwan • [NTOU M02365]: Yilan County, Dasi fishing port, commercial trawler, 17 Jul. 1984, 1♀, cl 26.6 mm • [NTOU M02366]: Hsinchu City, Nanliao fishing port, commercial trawler, 4 Jul. 1984, 1♀, cl 31.1 mm

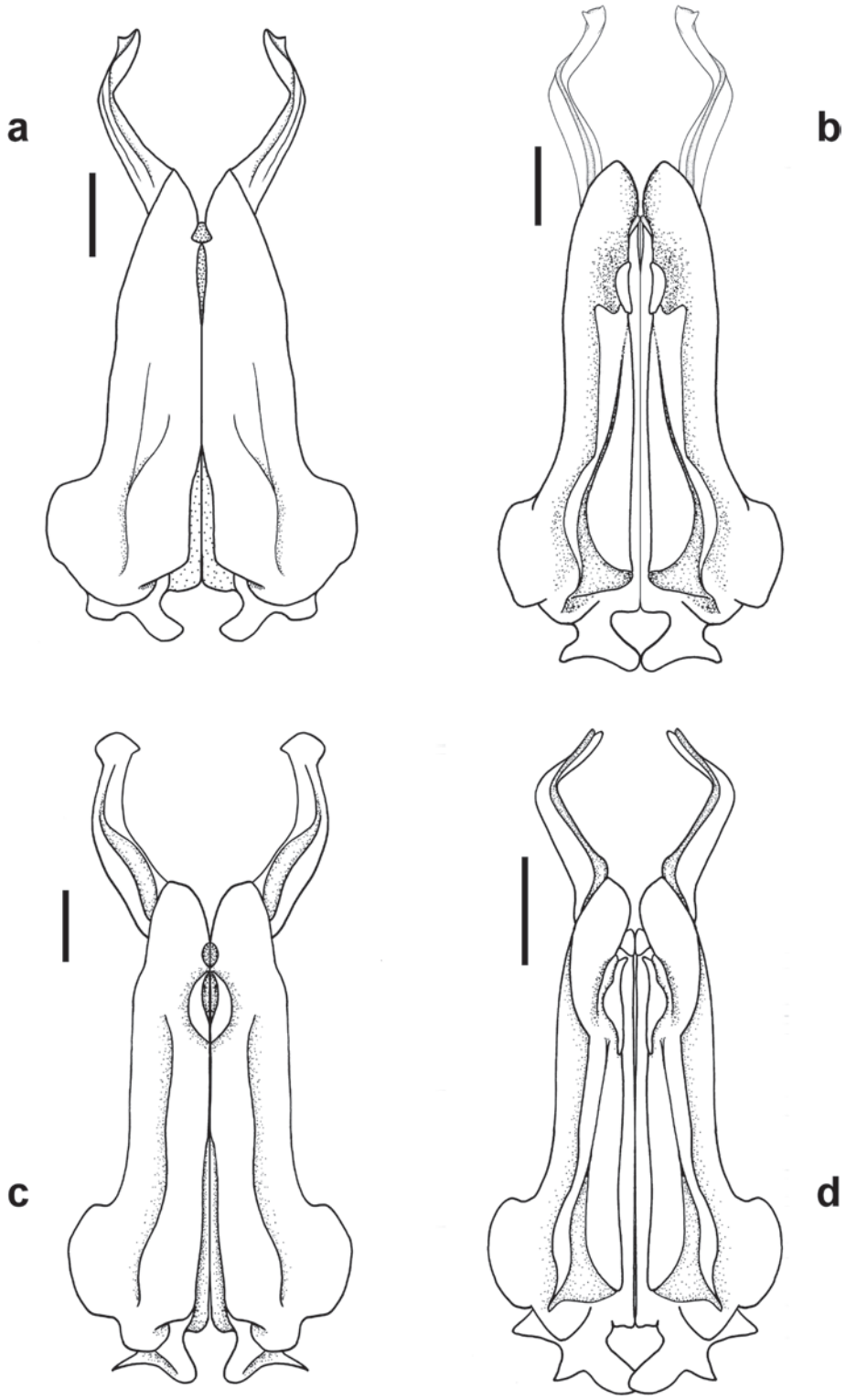

Figure 3. Petasma, ventral view. **a.** *Parapenaeopsis cornuta* (Kishinouye, 1900), Cijin, Kaohsiung City, Taiwan, male cl 18.8 mm (NTOU M02363). **b.** *P. maxillipedo* Alcock, 1906, Strait of Malacca, Pantai Remis, Perak, Malaysia, male cl 22.5 mm (USM_INV 1009). **c.** *P. amicus* V. C. Nguyên, 1971, Budi fishing port, Chiayi County, Taiwan, male cl 26.0 mm (NTOU M02372), modified from Hsu & Chan, 2023. **d.** *P. incisa* Wang & Liu in Liu and Wang 1987, Sanya, Hainan, Southern China, males cl 14.9 mm (MBM 155044). Scale bars: 1 mm.

• [NTOU M02367]: Changhua County, Wenzi fishing port, commercial trawler, 5 Aug. 2021, 16♂♂, cl 17.5–22.3 mm, 18♀♀, cl 18.4–25.0 mm • [NTOU M02368]: Yunlin County, Mailiao, Jul. 2009, 12♂♂, cl 11.4–17.6 mm, 18♀♀, cl 13.0–22.5 mm • [NTOU M02369]: Yunlin County, Mailiao, 18 May 2010, 2♂♂, cl 23.0–24.3 mm, 1♀, cl 28.4 mm • [NTOU M02418]: Chiayi County, Budai fishing port, commercial trawler, 26 May 1974, 3♂♂, cl 15.6–26.9 mm, 1♀, cl 30.5 mm • [NTOU M02370]: Chiayi County, Budai fishing port, commercial trawler, 20 Jan. 1995, 4♂♂, cl 18.1–21.5 mm, 2♀♀, cl 18.4–20.1 mm • [NTOU M02371]: Chiayi County, Budai fishing port, commercial trawler, 5 Feb.

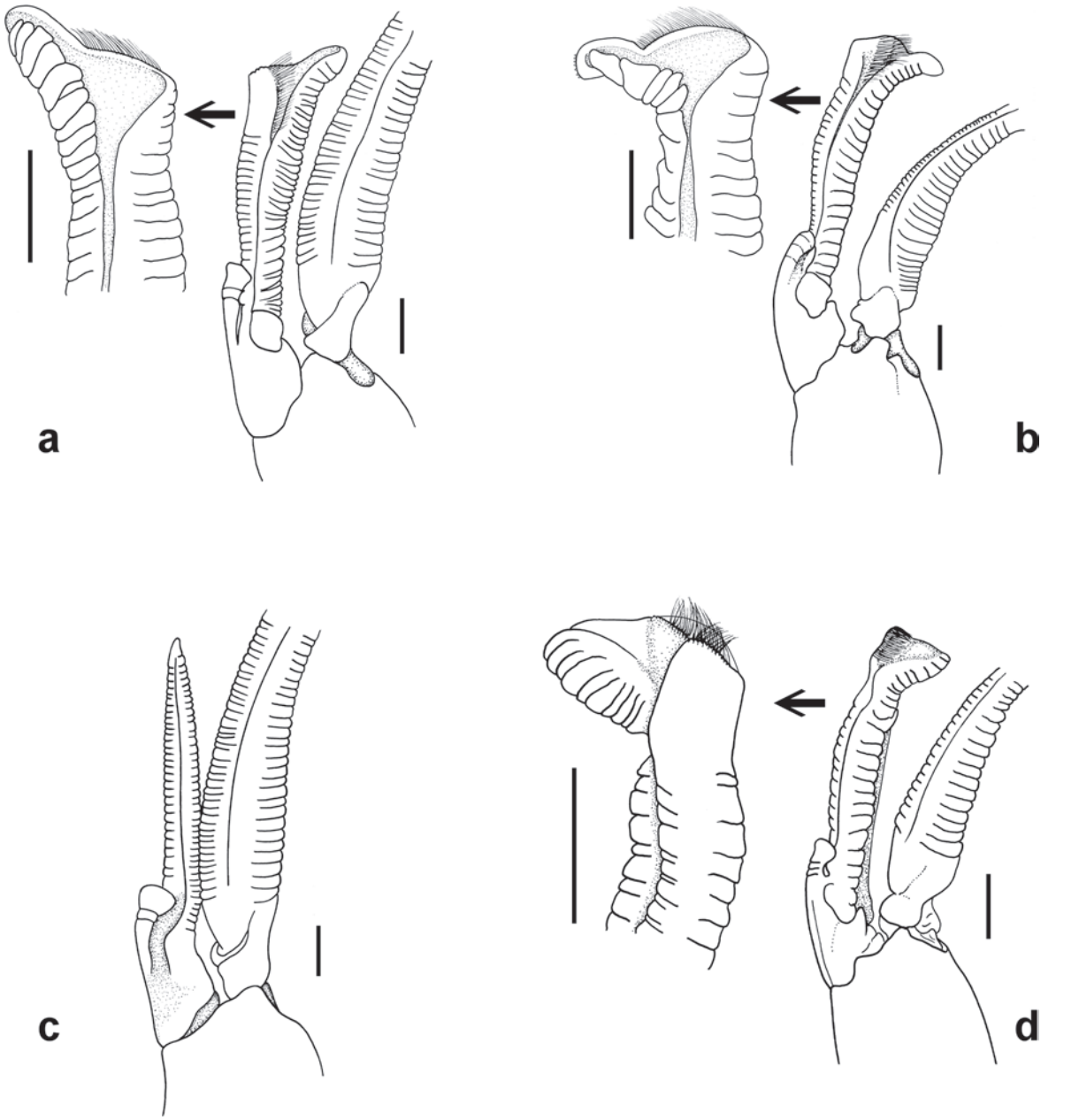

Figure 4. Right pleopod II endopod and basal part of exopod, dorsal view, and only thick, stiff setae shown. Magnified distal part of endopod in **a**, **b**, **d** in ventral view. **a.** *Parapenaeopsis cornuta* (Kishinouye, 1900), Cijin, Kaohsiung City, Taiwan, male cl 18.8 mm (NTOU M02363). **b.** *P. maxillipedo* Alcock, 1906, Strait of Malacca, Pantai Remis, Perak, Malaysia, male cl 22.5 mm (USM_INV 1009). **c.** *P. amicus* V. C. Nguyên, 1971, Budi fishing port, Chiayi County, Taiwan, male cl 26.0 mm (NTOU M02372), modified from Hsu & Chan, 2023. **d.** *P. incisa* Wang & Liu in Liu and Wang 1987, Sanya, Hainan, Southern China, males cl 14.9 mm (MBM 155044). Scale bars: 1 mm.

2000, 20♂♂, cl 15.1–22.7 mm, 20♀♀, cl 15.3–23.4 mm • [NTOU M00762]: Chiayi County, Budai fishing port, commercial trawler, 2 Jul. 2002, 8♂♂, cl 26.5–29.2 mm, 10♀♀, cl 22.5–33.2 mm • [NTOU M02372]: Chiayi County, Budai fishing port, commercial trawler, 8 Feb. 2021, 21♂♂, cl 22.2–26.0 mm, 21♀♀, cl 23.1–31.1 mm • [NTOU M02417]: Chiayi County, Budai fishing port, commercial trawler, 12 Dec. 2021, 2♀♀, cl 26.3–29.5 mm • [NTOU M02373]: Kaohsiung City; 10 Mar. 1975, 1♂, cl 24.4 mm, 1♀, cl 29.2 mm • [NTOU M02374]: Pingtung County, Donggang fishing port, commercial trawler, 5 Mar. 2021, 2♂♂, cl 24.5–25.0 mm, 1♀, cl 28.4 mm • [NTOU M02375]: Penghu County, Third fishing port, commercial trawler, Jun.–Aug. 2013, 3♀♀, cl 24.1–36.6 mm.

Diagnosis. Rostrum horizontal straight with tip recurved upwards, armed with 7–9 (avg. 7.8, n = 20, excluding epigastric tooth) teeth along dorsal border except near tip, extending to around tip of second segment of antennular peduncle. Postrostral carina with posterior 1/4 broadened and obscure, often with weak median pit, extending posteriorly to 0.77–0.89 (avg. 0.85, n = 20) of carapace length. Longitudinal suture short, extending posteriorly to about level of epigastric tooth. Pereiopods I and II bearing basial spines and epipods, pereiopod III lacking basial

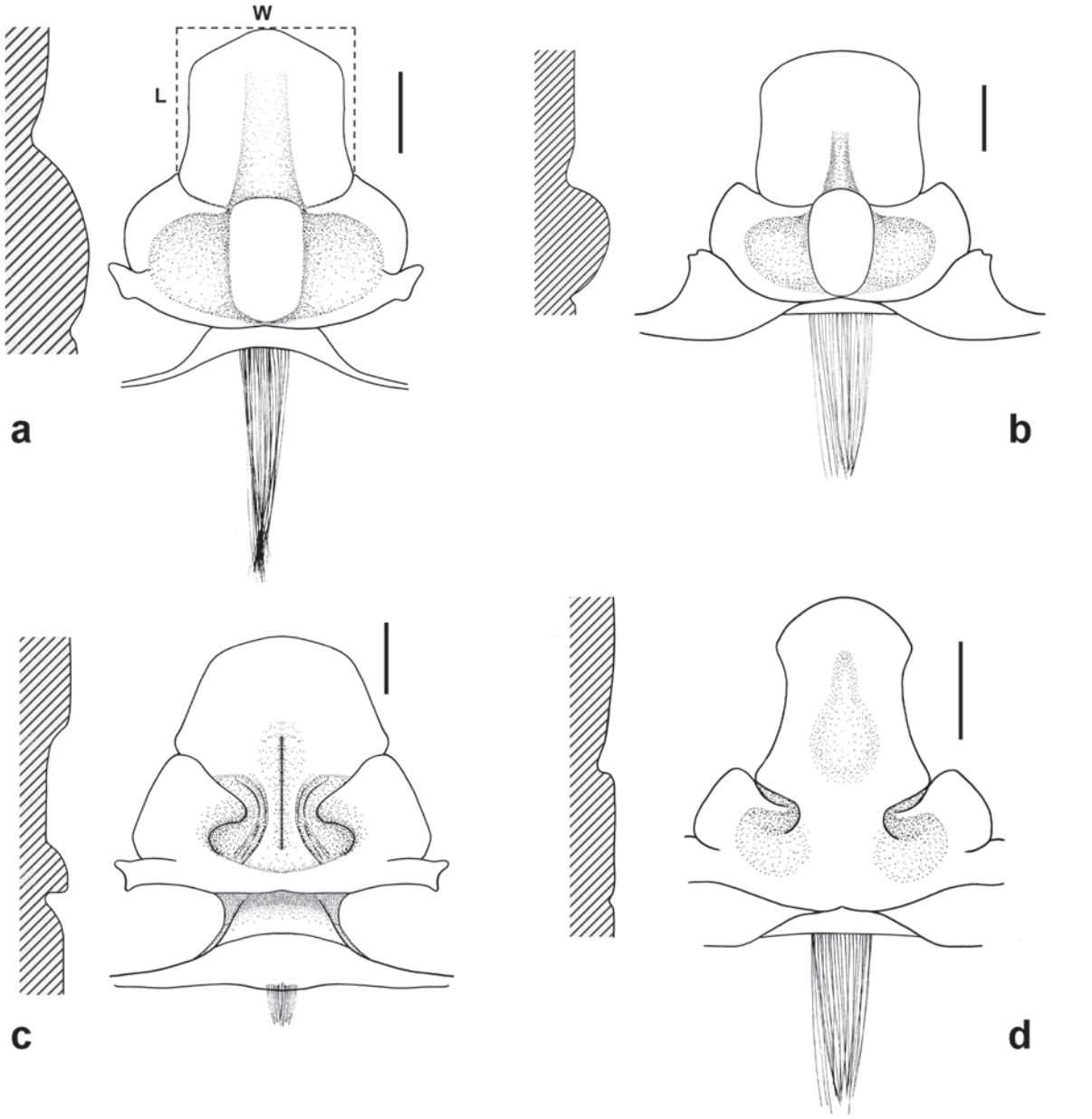

Figure 5. Thelycum, ventral view. Adjacent shading figure representing lateral cross-section along midline. **a.** *Parapenaeopsis cornuta* (Kishinuoue, 1900), Cijin, Kaohsiung City, Taiwan, female cl 22.4 mm (NTOU M02363). **b.** *P. maxillipedo* Alcock, 1906, Strait of Malacca, Pantai Remis, Perak, Malaysia, female cl 26.8 mm (USM_INV 1011). **c.** *P. amicus* V. C. Nguyên, 1971, Budi fishing port, Chiayi County, Taiwan, female cl 27.3 mm (NTOU M02372). **d.** *P. incisa* Wang & Liu in Liu and Wang 1987, Sanya, Hainan, Southern China, females cl 17.6 mm (MBM 155044). L: anterior plate length; W: anterior plate width. Scale bars: 1 mm.

spine. Abdominal somites I and II without dorsal carina. Telson lacking movable lateral spinules. Males with endopod of pleopod II normal in shape, sword-like as exopod; petasma with distolateral projections elongated and horn-like, tip of horn distinctly protruded on both sides (outer protrusion often larger) and hammer-like. Female thelycum with anterior plate shovel-like to semicircular (more often), 0.59–0.73 (avg. 0.65, n = 10) as long as wide, surface sunken with distinct median longitudinal furrow extending to posterior plate; posterior plate with median part also sunken, lateral parts as 2 large semicircular processes; tuft of setae behind posterior plate short and thin.

Coloration. (Fig. 7c) Similar to *P. cornuta* except tuft of short setae behind thelycum colorless. Color photograph of this species given in Hsu and Chan (2023).

Distribution. Known with certainty from Vietnam to southern China and Taiwan, intertidal to about 50 m deep (Liu and Wang 1987; Liu and Zhong 1988).

Remarks. Although the general appearance of *P. amicus* is very similar to the other members of the "*P. cornuta*" species group, it can be readily distinguished by the shape of genitalia. For males, *P. amicus* is unique in having a normal pleopod II endopod (Fig. 4c; v.s. greatly modified and boot-like, Figs 4a, b, d). In females, the tuft

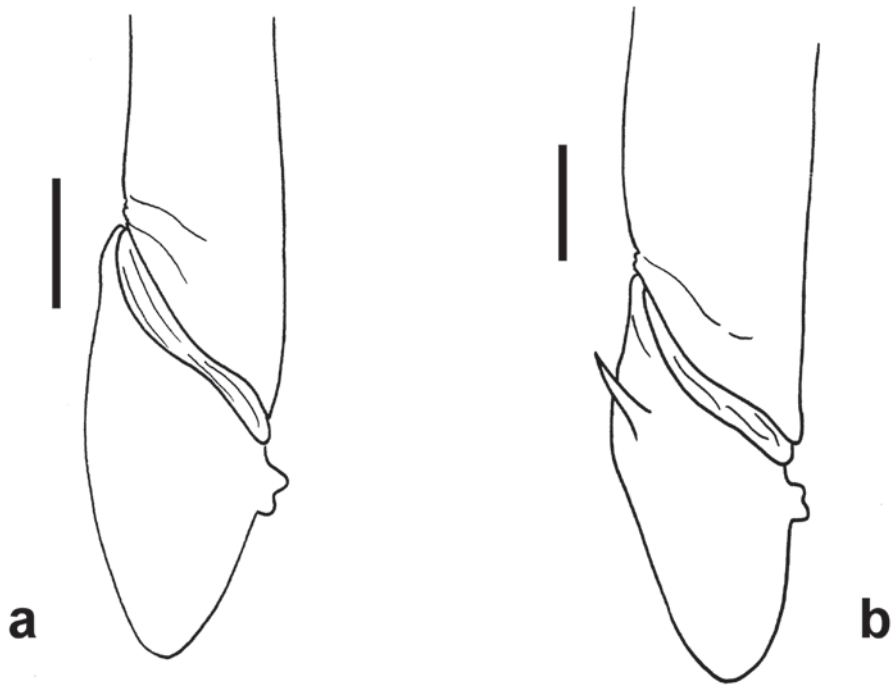

Figure 6. Left pereiopod III basis and proximal part of ischium, lateral view. **a.** *Parapenaeopsis cornuta* (Kishinouye, 1900), Cijin, Kaohsiung City, Taiwan, female cl 22.4 mm (NTOU M02363). **b.** *P. maxillipedo* Alcock, 1906, Strait of Malacca, Pantai Remis, Perak, Malaysia, female cl 26.8 mm (USM_INV 1011). Scale bars: 1 mm.

Figure 7. a. *Parapenaeopsis cornuta* (Kishinouye, 1900), Keelung City, Taiwan, male cl 14.5 mm (NTOU M02357), from Hsu & Chan, 2023 (reproduced with permission from the copyright holder). **b.** Fishery catch mainly composed of *P. cornuta*, Toyohama fish market, Aichi Prefecture, Japan (photographed by T. Nakano). **c.** *P. maxillipedo* Alcock, 1906, Tuticorin fishing harbor, Tamil Nadu, India, female cl 19.0 mm (NTOU M02626). **d.** *P. amicus* V. C. Nguyên, 1971, Budi fishing port, Chiayi County, Taiwan, female cl 29.5 mm (NTOU M02417), from Hsu & Chan, 2023 (reproduced with permission from the copyright holder).

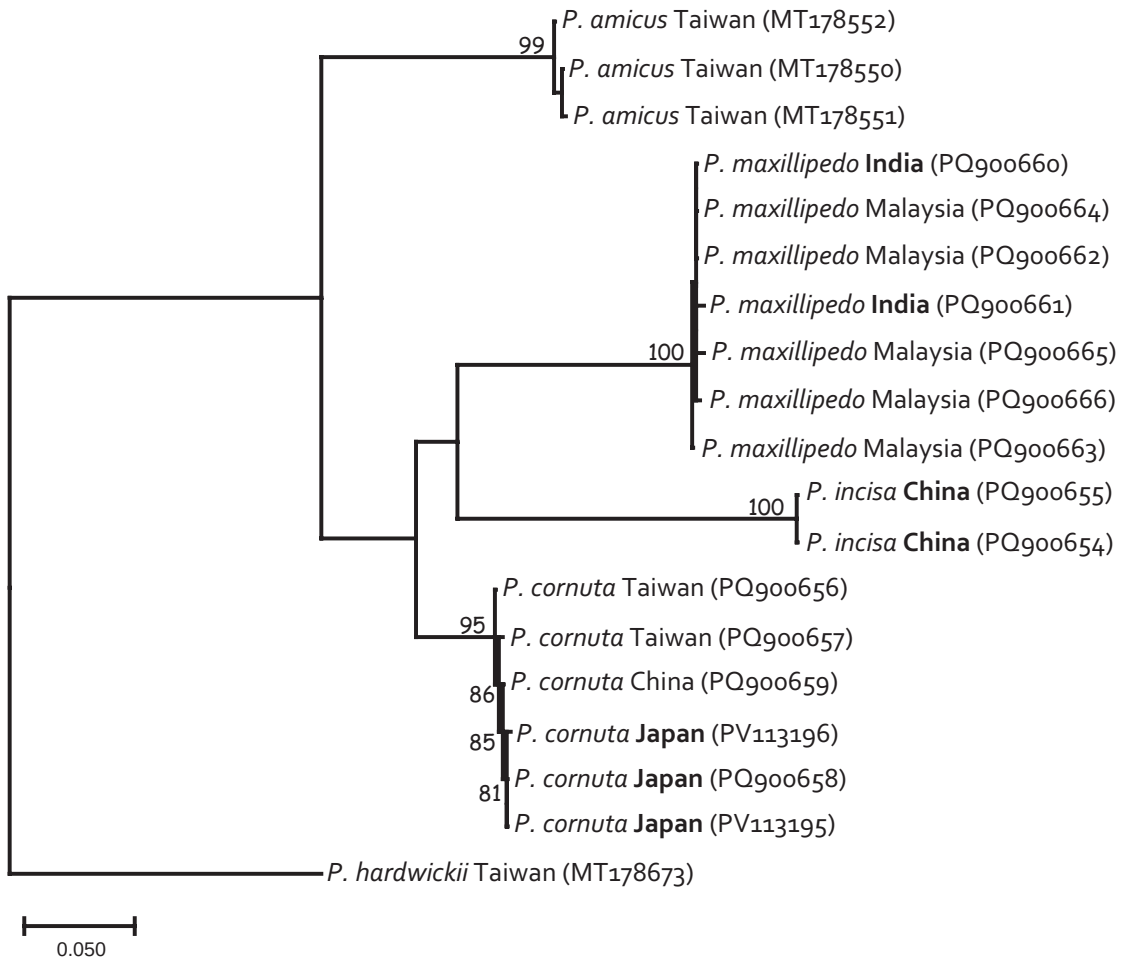

Figure 8. Maximum-likelihood tree (TIM2+G4+F model) amongst the species of the "*Parapenaeopsis cornuta*" group based on the DNA barcode gene mtCOI (615 bp) sequences generated from this work plus three sequences of *P. amicus* from Taiwan used in Hurzaid et al. (2020) and with specimens re-examined. *Parapenaeopsis hardwickii* was used as an outgroup. Numbers at nodes represent bootstrap support; values below 80 are not shown. Bold: type-locality.

of setae behind the thelycum is thin and short (Fig. 5c; v.s. thick and long, Figs 5 a, b, d). Efforts to locate the types of *P. amicus* were unsuccessful (personal communication from Tran Anh Duc). As both *P. amicus*, described from Vietnam (V. C. Nguyên 1971: fig. 1B), and *P. sinica* Liu & Wang, 1987, described from southern China (Liu and Wang 1987: fig. 4e; Liu and Zhong 1988: fig. 131–5), have the characteristic short and thin setae behind the thelycum, they are determined to be synonyms.

Besides the pleopod II endopod in males and tuft of setae behind the thelycum in females, *P. amicus* can also be separated from the other species of the group by some subtle differences in the genitalia (Table 2). The tip of the horn-like petasma has both sides distinctly protruded and hammer-like in *P. amicus* (Fig. 3c), but only with the outer side protruded in *P. cornuta* (Fig. 3a) and *P. maxillipedo* (Fig. 3b) or both sides not protruded in *P. incisa* (Fig. 3d). In *P. amicus*, the thelycum has a median longitudinal furrow, the anterior plate is relatively short (0.59–0.73, avg. 0.65 as long as wide), and the posterior plate medially sunken (Fig. 5c). For the other species of the "*P. cornuta*" group, the thelycum (Figs 5a, b, d) generally lacks a median longitudinal furrow (but is occasionally present in *P. cornuta*), the anterior plates are usually longer (0.74–1.17 as long as wide), and the median parts of the posterior plates are flattened (in *P. incisa*, Fig. 5d) to more or less protruding into a boss [low in *P. cornuta* (Fig. 5a) and high in *P. maxillipedo* (Fig. 5b)]. However, the characteristic shape of the genitalia is generally less developed in juveniles and young specimens. These subtle differences in genitalia are hence sometimes not useful to separate small individuals of this species group.

It is also found that the rostrum is relatively shorter, not reaching the tip of the antennular peduncle, in *P. amicus* (Fig. 1c) and *P. maxillipedo* (fig. 1b). In *P. cornuta* (Fig. 1a) and *P. incisa* (Fig. 1d), the rostrum is often extending to or even overreaching the tip of the antennular peduncle. Other differences previously proposed to distinguish *P. amicus* from the other species of the "*P. cornuta*" group [such as the number of rostral teeth, postrostral carina length, the presence of a median pit on postrostral carina, and setae on the branchiocardiac groove (Liu and Wang 1987; Liu and Zhong 1988; V. C. Nguyên 1971)] are found to be rather variable, with many overlappings.

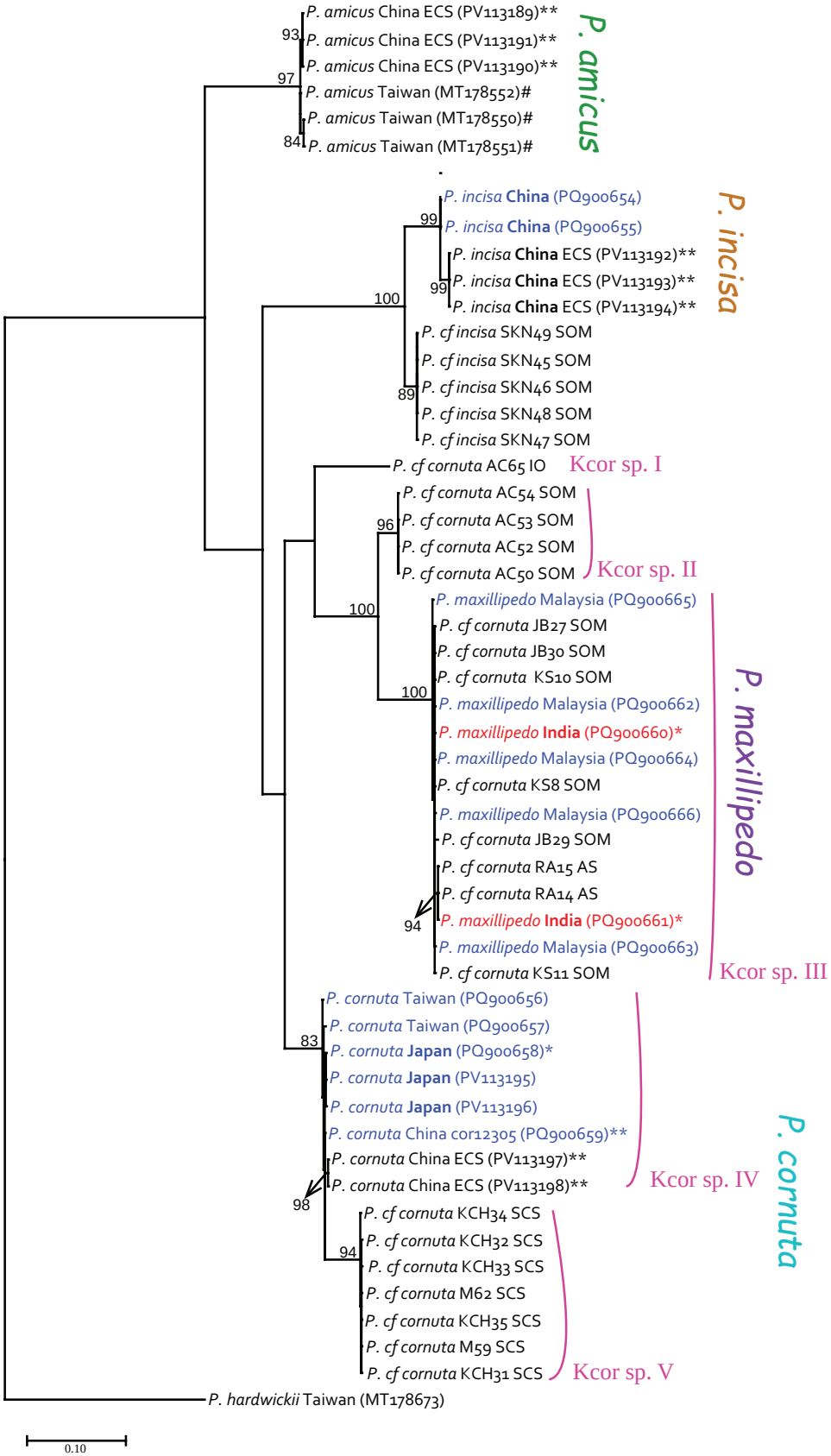

Figure 9. Maximum-likelihood tree (TIM2+G4+F model) amongst the species of the "*Parapenaeopsis cornuta*" group based on the DNA barcode gene mtCOI (615 bp) dataset in Hurzaid et al., 2020: fig. 3 plus the sequences generated in this work. *Parapenaeopsis hardwickii* was used as an outgroup. Numbers at nodes represent bootstrap support; values below 80 are not shown. Bold: type-locality; blue: sequences generated from this work; red: same specimens sequenced in Hurzaid et al. (2020) and the present work, but with different sequences and clade assignments. *Sequences generated from this work are from the same specimens used in Hurzaid et al. (2020). **Sequences used in Li et al. (2014). # Specimens re-examined in this work.

Molecular analysis also indicates that *P. amicus* is more distant from the other species of the "*P. cornuta*" group (Figs 8, 9, Table 1). However, the body color of *P. amicus* (Fig. 7d) is very similar to *P. cornuta* (Figs 7a, b) and very likely also with *P. incisa* (see Hsu and Chan 2023; Liu and Zhong 1988), rendering it difficult to determine its exact distribution from literature. At present, it can only be confirmed that *P. amicus* is distributed from Vietnam to eastern Guangdong in southern China and Taiwan (Hsu and Chan 2023; Liu and Wang 1987; Liu and Zhong 1988). Whether *P. amicus* has a wider geographical distribution will need re-examination of the material reported as "*P. cornuta*" in the various localities from India to Australia. For example, a recent study found that *P. amicus* is actually much more abundant than *P. cornuta* in Taiwan (Hsu and Chan 2023).

Parapenaeopsis incisa Wang & Liu in Liu & Wang, 1987

Figs 1d, 2d, 3d, 4d, 5d

Parapenaeopsis incisa Liu and Wang 1986: 214 (nomen nudum); 1987: 525, fig. 3. (type locality: Wailuo, Guangdong, China); Liu and Zhong 1988: 210, fig. 130.

Kishinouyepenaeopsis incisa – De Grave and Fransen 2011: 216.

Material examined. Southern China • [MBM 155054]: Guangdong, Zhanjiang, Naozhou Island, 29 Jul. 1976, 1♀, cl 14.6 mm • [MBM 155041]: Hainan, Yinngehai, 55-K444, 7 Dec. 1955, 3♂♂, cl 14.5–14.8 mm, 3♀♀, cl 16.3–18.2 mm • [MBM 155057]: Hainan, Yinngehai, 57-K275, 26 Jun. 1957, 2♂♂, cl 12.9–14.4 mm, 2♀♀, cl 16.5–17.6 mm • [MBM 155044]: Hainan, Sanya, fish market, 90C-324, 25 Nov. 1990, 3♂♂, cl 13.2–14.9 mm, 3♀♀, cl 14.9–17.6 mm.

Diagnosis. Rostrum more or less horizontal, straight, and with tip recurved upwards, bearing 6–8 (avg. 7.0, n = 14, excluding epigastric tooth) teeth along dorsal border except near tip, extending to distal antennular segment or just overreaching antennular peduncle. Postrostral carina with posterior 1/4 broadened and obscure, sometimes with weak median pit, extending posteriorly to 0.77–0.89 (avg. 0.84, n = 17) of carapace length. Longitudinal suture short, extending posteriorly to about level of epigastric tooth. Pereiopods I and II with basial spines and epipods, pereiopod III without basial spine. Abdominal somites I and II with dorsal carina absent. Telson lacking movable lateral spinules. Males with endopod of pleopod II strongly modified and boot-like; medial part of distal margin protruded and convex, but concealed by tuft of dense long stiff setae arising from anterodistal part of endopod; petasma horn-like with distolateral projections strongly elongated, tip of horn more or less bifurcated and without lateral protuberances on both sides. Female thelycum with anterior plate elongated rectangular and lateral margins more or less concave, 0.99–1.17 (avg. 1.09, n = 9) as long as wide, surface slightly sunken; posterior plate with median part completely flattened, lateral parts semicircular; tuft of setae behind posterior plate long and thick.

Coloration. Not known, but likely similar to *P. cornuta* and *P. amicus*. The photograph of a fresh specimen from the Strait of Malacca, Malaysia, probably belongs to *P. incisa* (Fakhruddin et al. 2024: fig. 1; see Discussion); it has a color pattern very similar to *P. cornuta* and *P. amicus*, except with the body having more yellowish and greenish taints.

Distribution. Known with certainty from around Hainan Island in the South China Sea, intertidal to about 30 m deep (Liu and Wang 1987; Liu and Zhong 1988). Probably also distributed to the Strait of Malacca off Malaysia and Bangladesh (Fakhruddin et al. 2024; see Discussion).

Remarks. *Parapenaeopsis incisa* closely resembles *P. cornuta* and mainly differs in the shape of the genitalia. In males, the boot-like endopod of pleopod II has the median part of the distal margin protruded in *P. incisa* (Fig. 4d) but is straight or concave in *P. cornuta* (Fig. 4a). The tip of the horn-like petasma lacks a lateral protrusion in *P. incisa* (Fig. 3d) but is distinctly protruded on the outer side in *P. cornuta* (Fig. 3a). The thelycum of *P. incisa* has the anterior plate more or less rectangular and relatively long (0.99–1.17, avg. 1.09 as long as wide), while the median part of the posterior plate is completely flattened without any sign of elevation (Fig. 5d). In *P. cornuta*, the thelycum has the anterior plate semi-quadrate and relatively short (0.74–0.95, avg. 0.85 as long as wide), and the posterior plate bears a weak median ovate boss (Fig. 5a). These unique shapes of the genitalia are also useful in separating *P. incisa* from the other two species of the "*P. cornuta*" group (Table 2, Figs 3–5). Similar to the situation in *P. amicus*, other differences previously proposed to separate *P. incisa* from the other species of the "*P. cornuta*" group (Liu and Wang 1987; Liu and Zhong 1988) actually have many overlaps.

Although morphologically *P. incisa* is most similar to *P. cornuta*, the high genetic differences (COI sequence divergence 15.0–17.5%, Table 1) of *P. incisa* from the other species of the "*P. cornuta*" group well support its specific status. As *P. incisa* can only be satisfactorily distinguished from the other species of the "*P. cornuta*" group mainly by subtle differences in genitalia (Table 2), careful examination of the material reported as "*P. cornuta*" from various localities is necessary to determine the exact distribution of *P. incisa*.

Discussion

Of the four species in the "*P. cornuta*" species group, *P. cornuta* and *P. maxillipedo* are generally considered to have wide overlapping Indo-West Pacific distributions from India to the Philippines and Australia (see Chan 1998; Holthuis 1980; Pérez Farfante and Kensley 1997). The two other species, *P. amicus* and *P. incisa*, are thought to have rather restricted geographical ranges, with the former known from Vietnam to southern China and Taiwan (Hsu and Chan 2023), while the latter is found only in southern China (Liu and Zhong 1988). However, *P. incisa*

has recently been reported from Malaysia and Bangladesh (Fakhruddin et al. 2024). Although the present morphological and molecular comparisons validate the four nominal taxa in the "*P. cornuta"* species group (Fig. 8), the molecular genetic analysis of Hurzaid et al. (2020) indicated that there may be at least eight species in this group. Some specimens used for molecular analyses from Japan [CBM ZC3280], India [NTOU M02625] and *P. amicus* from Taiwan [NTOU M00762] are the same in the present analysis as in Hurzaid et al. (2020). A specimen [MBM 155074] of *P. cornuta* from southern China used in molecular analyses is also the same amongst Li et al. (2014), Hurzaid et al. (2020), and this work. However, the sequenced specimens from India [NTOU M02625] were assigned to *P. cornuta* by Hurzaid et al. (2020) but were determined to be *P. maxillipedo* in the present study. As such, there was a mistake in Hurzaid et al. (2020) in considering that both the Indian and Japanese materials belong to the same species and genetic clade (i.e., "Kcor sp. IV" in Hurzaid et al. 2020). The present Indian material actually belongs to the clade "Kcor sp. III" of Hurzaid et al. (2020). With this correction, the genetic analysis of Hurzaid et al. (2020) suggested the following (Fig. 9): there may be another species similar to *P. incisa* from the Strait of Malacca, or *P. incisa* has a wider distribution from southern China to at least the Strait of Malacca. *Parapenaeopsis cornuta* is at least distributed down to the southern part of the South China Sea off Malaysia (i.e., Mersing, Johor, and Kuching), with "Kcor sp. V" in Hurzaid et al. (2020) highly likely not representing a different species. On the other hand, *P. maxillipedo* is at least distributed from India to the Andaman Sea sides of Thailand (Ranong) and Indonesia (Lambeso, Aceh Jaya) as well as westward to the Strait of Malacca, or may need to be split into three species.

Another recent molecular analysis also suggested that *P. incisa* occurs in the Strait of Malacca and Bangladesh (Fakhruddin et al. 2024). However, the COI analyses by Fakhruddin et al. (2024: fig. 2) and Hurzaid et al. (2020: fig. 3) have different conclusions even though they are based on similar datasets. The Chinese and Strait of Malacca clades of "*P. incisa*" were determined to be separate and represented different species in Hurzaid et al. (2020). In contrast, the "*P. incisa*" materials from the Strait of Malacca and China were grouped in the same clade and mentioned as belonging to the same species with only "…a genetic distance of 0.5%..." between them in Fakhruddin et al. (2024). Re-analysis of the genetic distance between the single "Chinese" specimen (KR349256) and the abundant material (22 specimens) from the Strait of Malacca in Fakhruddin et al. (2024) reveals that there is actually a 4.94–5.34% sequence divergence in the COI gene (600–615 bp) between the specimens from these two localities. Moreover, this single "Chinese" COI sequence used in Fakhruddin et al. (2024) is from unpublished data on GenBank with its locality not specified and with a 1.38% difference from the sequences of the three Chinese specimens analyzed in Hurzaid et al. (2020; same sequences in Li et al. 2014). On the other hand, the result of 16S analysis in Fakhruddin et al. (2024: fig. 3) showing materials of "*P. incisa*" from different localities represented different genetic clades is more in collaboration with the conclusion of Hurzaid et al. (2020). Their "Chinese" 16S sequence (KR781021) is also based on unpublished data with its locality not specified on GenBank as well as their 16S sequence from Bangladesh (ON264685). Re-analysis of the 16S data in Fakhruddin et al. (2024) shows a sequence divergence as high as 2.57–3.07% (475 bp) amongst the material from China, the Strait of Malacca, and Bangladesh, suggesting that these populations may each represent a separate species. Examination of more material of the "*P. cornuta"* species group from various Indo-West Pacific localities using the following key and distinguishing characters defined in this work (Table 2) is necessary to fully understand the diversity and geographical distribution of each species in this group of commercial shrimp.

Key to the species of the "*Parapenaeopsis cornuta*" group

1 Postrostral carina distinct and of similar width along entire length, posterior end less than 1/10 carapace length from posterior margin of carapace; pereiopod III usually armed with basial spine; abdomen distinctly banded and with last somite bearing large white margined dark posterolateral spot ..... *P. maxillipedo*

– Postrostral carina with posterior 1/4 broadened and obscure, posterior end more than 1/10 carapace length from posterior margin of carapace; pereiopod III usually lacking basial spine; abdomen not distinctly banded and last somite without special markings* 2

2 Males with endopod of pleopod II normal and sword-like; females with tuft of hairs behind thelycum short and colorless, thelycum bearing median longitudinal furrow and with posterior plate medially sunken ..... *P. amicus*

– Males with endopod of pleopod II greatly modified and boot-like; females with tuft of hairs behind thelycum long and bluish*, thelycum usually lacking longitudinal furrow and with posterior plate medially flattened or elevated 3

3 Males with distal margin of endopod of pleopod II medially convex, tip of petasma lacking lateral protuberance; female thelycum with anterior plate 0.99–1.17 times as long as wide and lateral margins concave, posterior plate medially flattened ..... *P. incisa*

– Males with distal margin of endopod of pleopod II medially straight or concave, tip of petasma bearing distinct outer protuberance; female thelycum with anterior plate 0.74–0.95 times as long as wide and lateral margins not distinctly concave, posterior plate having a weak median ovate boss ..... *P. cornuta*

* Exact coloration of *P. incisa* still unknown.

Acknowledgements

Sincerely thanks are extended to T. Komai of the Natural History Museum and Institute, Chiba for information on the material studied by Kishinouye and sending us on loan Japanese specimens; T. Naruse of the University of the Ryukyus, Okinawa for information on the specimens of *P. cornuta* deposited at the National Museum of Nature and Science, Tokyo; X. Li of the Chinese Academy of Sciences, Qingdao for sending us on loan Chinese material of *P. cornuta, P. amicus* and *P. incisa* as well as the sequence data used in his 2014 paper; K. Araki and T. Nakano of the Aichi Fisheries Research Institute, H. Sakaji and H. Nishida of the Fisheries Research Institute, Japan Fisheries Research and Education Agency, Yokohama for providing specimens and photographs of Japanese *P. cornuta* for this work; T.A. Duc of the Hanoi University of Science for translating the original description of *P. amicus* and information of the types of this species; C.C. Lin of the National Taiwan Ocean University, Keelung for preparing the line drawings. This work was supported by grants from the National Science and Technology Council, Taiwan, R.O.C., and the Center of Excellence for the Oceans (National Taiwan Ocean University), which is financially supported by the Featured Areas Research Center Program within the framework of the Higher Education Sprout Project by the Ministry of Education (MOE) in Taiwan, R.O.C.

References

Alcock A (1906) Catalogue of the Indian decapod Crustacea in the Collections of the Indian Museum. Part III. Macrura. Fasciculus I. The Prawns of the *Penaeus* group. Trustees of the Indian Museum, Calcutta, 57 pp. [9 pls.]

Chaitiamvong S, Supongpan M (1992) A Guide to Penaeoid Shrimps Found in Thai Waters. Australian Institute of Marine Science, Townsville, 77 pp.

Chan TY (1998) Shrimps and prawns. In: Carpenter KE, Niem VH (Eds) FAO Species Identification Guide for Fishery Purposes. The Living Marine Resources of the Western Central Pacific. Vol. 2 Cephalopods, Crustaceans, Holothurians and Sharks, Rome, FAO: 851–971.

Chanda A (2016a) Diagnosis of Genera found in India under Family Penaeidae. Lap Lambart Academic Publishing, Germany, 80 pp.

Chanda A (2016b) A study on newly described genera *Alcockpenaeopsis, Batepenaeopsis, Helleropenaeopsis, Kishinouyepenaeopsis* and *Parapenaeopsis* from Indian water. Poultry, Fisheries & Wildlife Sciences 4(1): 1–12. https://doi.org/10.4172/2375-446X.1000147

Dall W (1957) A revision of the Australian species of Penaeinae (Crustacea Decapoda: Penaeidae). Australian Journal of Marine and Freshwater Research 8(2): 136–232. https://doi.org/10.1071/MF9570136

Dall W, Rothlisberg PC (1990) Taxonomy. In: Dall W, Hill BJ, Rothlisberg PC, Sharples DJ (Eds) The Biology of the Penaeidae. Advances in Marine Biology, Academic Press, London, Vol. 27: 55–126. https://doi.org/10.1016/S0065-2881(08)60169-8

De Bruin GHP, Russell BC, Bogusch A (1995) FAO Species Identification Field Guide for Fishery Purposes. The Marine Fishery Resources of Sri Lanka. FAO, Rome, 400 pp. [plates I–XXXII]

De Grave S, Fransen CHJM (2011) Carideorum catalogus: the recent species of the dendrobranchiate, stenopodidean, procaridideanand caridean shrimps (Crustacea: Decapoda). Zoologische Mededelingen 85(9): 195–589.

De Man JG (1911) The Decapoda of the Siboga Expedition. Part I. Family Penaeidae. Siboga expeditie 39a: 1–131.

Fabricius JC (1798) Supplementum Entomologiae Systematicae. Proft et Storch, Hafniae, 572 pp. https://doi.org/10.5962/bhl.title.65803

Fakhruddin NF, Nor SAM, Hurzaid A (2024) Integrative taxonomy analysis reveals the first record of the shrimp *Kishinouyepenaeopsis incisa* (Wang & Liu in Liu & Wang, 1987) (Decapoda, Penaeidae). Check List 20(5): 1142–1148. https://doi.org/10.15560/20.5.1142

Folmer O, Black M, Hoeh W, Lutz R, Vrijenhoek R (1994) DNA primers for amplification of mitochondrial cytochrome c oxidase subunit I from diverse metazoan invertebrates. Molecular Marine Biology and Biotechnology 3: 294–299.

Grey DL, Dall W, Baker A (1983) A Guide to the Australian Penaeid Prawns. Darwin: Department of Primary Production of the Northern Territory, 140 pp.

Hall DNF (1961) The Malayan Penaeidae (Crustacea, Decapoda). Part II. Further taxonomic notes on the Malayan species. Bulletin of the Raffles Museum 26: 76–119.

Hayashi K (1986) Dendrobranchiata and Caridea. In: Baba K, Hayashi K, Toriyama M (Eds) Decapod Crustaceans from Continental Shelf and Slope around Japan, Japan Fisheries Resource Conservation Association, Tokyo: 38–149, 232–279.

Hayashi K (1992) Dendrobranchiata Crustaceans from Japanese Waters. Seibutsu Kenkyusha, Tokyo, 300 pp. [In Japanese]

Hebert PDN, Cywinska A, Ball SL, deWaard JR (2003) Biological identifications through DNA barcodes. Proceedings of the Royal Society of London B Biological Sciences 270: 313–321. https://doi.org/10.1098/rspb.2002.2218

Holthuis LB (1980) FAO species catalogue, Vol. 1. Shrimps and prawns of the world. An annotated catalogue of species of interest to fisheries. FAO Fisheries Synopsis 125(1): 1–261.

Holthuis LB (1984) Lobsters. FAO Species Identification Sheets, Western Indian Ocean, Fishing Area 51. FAO of the United Nations Publisher, Rome, 190 pp.

Hsu YC, Chan TY (2023) On the Penaeid shrimps of the genus *Parapenaeopsis* Alcock, 1901 (Crustacea, Decapoda) from Taiwan. Zootaxa 5361: 221–236. https://doi.org/10.11646/zootaxa.5361.2.4

Hurzaid A, Chan TY, Mohd Nor SA, Muchlisin ZA, Chen WJ (2020) Molecular phylogeny and diversity of penaeid shrimps (Crustacea: Decapoda) from South-East Asian waters. Zoologica Scripta 49: 596–613. https://doi.org/10.1111/zsc.12428

Katoh K, Rozewicki J, Yamada KD (2019) MAFFT online service: multiple sequence alignment, interactive sequence choice and visualization. Briefings in Bioinformatics 20(4): 1160–1166. https://doi.org/10.1093/bib/bbx108

Kimura M (1980) A simple method for estimating evolutionary rate of base substitutions through comparative studies of nucleotide sequences. Journal of Molecular and Evolution 16: 111–120. https://doi.org/10.1007/BF01731581

Kishinouye K (1900) Japanese species of the genus *Penaeus*. Journal of Fisheries Bureau, Tokyo 8,1–29 + 1–34. [pls. 1–8] https://doi.org/10.5962/bhl.title.53711

Kubo I (1949) Studies on penaeids of Japanese and its adjacent waters. Journal of the Tokyo College of Fisheries 36: 1–467.

Li X, Xu Y, Kou Q (2014) Molecular phylogeny of *Parapenaeopsis* Alcock, 1901 (Decapoda: Penaeidae) based on Chinese materials and 16S rDNA and COI sequences. Journal of Ocean University of China 13(1): 104–114. https://doi.org/10.1007/s11802-014-2272-7

Liu R, Wang Y (1986) Studies on *Parapenaeopsis* (Crustacea, Decapoda, Penaeidae) of Chinese waters. Transactions of the Chinese Crustacean Society 1: 214–215.

Liu R, Wang Y (1987) Studies on Chinese species of the genus *Parapenaeopsis* (Decapoda, Crustacea). Oceanologia et Limnologia Sinica 6: 523–539.

Liu R, Zhong Z (1988) Penaeoid Shrimps of the South China Sea. Agricultural Publishing House, Beijing China, 278 pp. [in Chinese]

Miers EJ (1878) Notes on the Penaeidae in the collection of the British Museum, with descriptions of some new species. Proceedings of the Zoological Society of London 46: 298–310. https://doi.org/10.1111/j.1469-7998.1878.tb07959.x

Motoh H, Buri P (1984) Studies on the penaeoid prawns of the Philippines. Researches on Crustacea 13–14: 1–120. https://doi.org/10.18353/rcustacea.13.14.0_1

Muthu MS (1968) On some new records of penaeid prawns from the east coast of India. Indian Journal of Fisheries 15: 145–154.

Nguyên VC (1971) A study on Penaeidae from Tonkin Gulf. Nội San Nghiên cứu biển 4: 41–60.

Pérez Farfante I, Kensley B (1997) Penaeoid and sergestoid shrimps and prawns of the world. Keys and diagnoses for the families and genera. Mémoires du Muséum National d'Histoire Naturelle 175: 1–233.

Psomadakis PN, Htun T, Russell BC, Mya TT (2019) Field identification guide to the living marine resources of Myanmar. FAO Species Identification Guide for Fishery Purposes. Rome, FAO and MOALI.

Racek AA, Dall W (1965) Littoral Penaeinae (Crustacea Decapoda) from northern Australia, New Guinea, and adjacent waters. Verhandelingen der Koninklijke Nederlandse Akademie van Wetenschappen, afdeeling Natuurkunde 56(3): 1–119.

Racek AA, Yaldwyn JC (1971) Notes on littoral Penaeinae (Crustacea: Decapoda) from the New Guinea area. Proceedings of the Linnean Society of New South Wales 95(3): 209–214.

Sakai K, Shinomiya S (2011) Preliminary report on eight new genera formerly attributed to *Parapenaeopsis* Alcock, 1901, sensu lato (Decapoda, Penaeidae). Crustaceana 84(4): 491–504. https://doi.org/10.1163/001121611X557037

Song H, Buhay JE, Whiting MF, Crandall KA (2008) Many species in one: DNA barcoding overestimates the number of species when nuclear mitochondrial pseudogenes are coamplified. Proceedings of the National Academy of Sciences of the United States of America 105: 13486–13491. https://doi.org/10.1073/pnas.0803076105

Tamura K, Stecher G, Kumar S (2021) MEGA 11: Molecular Evolutionary Genetics Analysis version 11. Molecular Biology and Evolution 38: 3022–3027. https://doi.org/10.1093/molbev/msab120

Trifinopoulos J, Nguyen LT, von Haeseler A, Minh BQ (2016) W-IQ-TREE: a fast online phylogenetic tool for maximum likelihood analysis. Nucleic Acids Research 44: W232–W235. https://doi.org/10.1093/nar/gkw256

Yang C-H, Sha Z, Chan TY, Liu R (2015) Molecular phylogeny of the deep-sea penaeid shrimp genus *Parapenaeus* (Crustacea: Decapoda: Dendrobranchiata). Zoologica Scripta 44(3): 312–323. https://doi.org/10.1111/zsc.12097

Yang C-H, Ma KY, Chu KH, Chan TY (2023) Making sense of the taxonomy of the most commercially important shrimps *Penaeus* Fabricius, 1798. s. l. (Crustacea: Decapoda: Penaeidae), a way forward. Aquaculture 563: 1–10. https://doi.org/10.1016/j.aquaculture.2022.738955

Yu HP, Chan TY (1986) The Illustrated Penaeoid Prawns of Taiwan. Southern Materials Center, Taipei, 183 pp.

Zoosyst. Evol. 101 (2) 2025, 627–641 | DOI 10.3897/zse.101.146587

PENSOFT

für Natur MUSEUM FÜR NATURKUNDE BERLIN

A new species of the *Drawida ghilarovi* species complex (Oligochaeta, Moniligastridae) in Changbai Mountain, Northeast China

Min Liu[1,2], Jiangni Li[2], Yufeng Zhang[2], Nonillon M. Aspe[3], Donghui Wu[4], Huifeng Zhao[2,4], Guo Zheng[1]

1 *College of Life Science, Shenyang Normal University, Shenyang 110034, Liaoning, China*

2 *Hebei Key Laboratory of Animal Diversity, College of Life Science, Langfang Normal University, Langfang 065000, China*

3 *College of Fisheries and Marine Sciences, Mindanao State University at Naawan, Naawan 9023, Misamis Oriental, Philippines*

4 *Key Laboratory of Wetland Ecology and Environment, Northeast Institute of Geography and Agroecology, Chinese Academy of Sciences, Changchun 130102, China*

https://zoobank.org/E029530F-FC0F-4156-9CF5-FAF7A61D37B4

Corresponding authors: Huifeng Zhao (zhaohf@lfnu.edu.cn); Guo Zheng (zhengguo@synu.edu.cn)

Academic editor: Pavel Stoev ♦ **Received** 13 January 2025 ♦ **Accepted** 6 March 2025 ♦ **Published** 21 March 2025

Abstract

The earthworm genus *Drawida* Michaelsen, 1900, has remained taxonomically and biogeographically unclear in China, with only one species described, *D. ganini* Zhang & Wu, 2021, which belongs to the *D. ghilarovi* Gates, 1969 species complex. Here, a new species, *D. yanbianensis* Liu & Zhao, **sp. nov.**, is described from Northeast China based on both morphological characters and molecular data. The new species is characterized by having a single pair of female pore slits on segment XII, a clitellum spanning five segments (X−XIV), a short body length (45.8–78 mm), having large and oval-shaped spermathecal ampulla with long coiled ducts, and having ovisacs from the ovary chamber on XI extending to XV. The new species status is supported with molecular data using the mitochondrial COI gene and four nuclear genes. The phylogenetic analysis shows that the new species is clustered with *D. ghilarovi* with a COI K2P genetic distance from the other species ranging from 12.4% to 20.9%. This study contributes to a deeper understanding of the evolution and distribution of the *D. ghilarovi* species complex and expands the known diversity within the genus *Drawida*.

Key Words

DNA barcoding, earthworm, Far East, Moniligastridae, taxonomy

Introduction

Earthworms are large soil animals that play an extremely important role in soil ecosystems, as well as in biological monitoring (Edwards 2004). However, the taxonomic work, particularly on the family Moniligastridae Claus, 1880, in contrast to other earthworm families, has been limited. The taxonomy of earthworms is somewhat limited by the simplicity of invertebrate structures, as they lack complex appendages or highly specialized copulatory organs (Pérez-Losada et al. 2009). Additionally, because earthworms are soft-bodied animals, their fossil record is extremely scarce (Piearce et al. 1990), making it challenging to trace their ancestors and evolutionary characteristics. The identification of earthworms primarily relies on the adult specimens with careful examination on the type of prostomium, arrangement of setae, position and morphology of the clitellum, male pores, spermathecal pores, and internal organs like testis sacs, spermathecae, ovisac, and gizzards. However, these morphological characteristics are variable, and different taxa may exhibit overlapping variability within the same character (Pop et al. 2003). Due to the limited availability of reliable taxonomic features, many morphologically similar

species are either grouped as a single species with various morphological types or classified as species complexes. These complexes often encompass diverse taxonomic groups with uncertain taxonomic categories (Gates 1972; Sims and Gerard 1985; Briones 1993).

The earthworms in the family of Moniligastridae mainly occur in Asia, with possible origin in "east or near Myanmar" (Gates 1972, 1982; Jamieson 1977). Moniligastridae is essentially an Oriental family with some species distributed in the eastern Palearctic region (Stephenson 1923; Gates 1972). To date, Moniligastridae has 204 species belonging to five genera, with *Drawida* Michaelsen, 1900, being the most speciose with 147 species (Misirlioğlu et al. 2023). *Drawida* is widely distributed in India, Sri Lanka, Southeast Asia, China, the Korean Peninsula, Japan, and Far East Russia (Gates 1969; Blakemore et al. 2010; Narayanan et al. 2017, 2024; Zhang et al. 2020; Zhao et al. 2022).

Around 23 *Drawida* valid species and subspecies have been recorded in Northeast Asia (Zhang et al. 2021), with *D. ghilarovi* Gates, 1969, being the first species described in mountainous forests in Far East Russia (Gates 1969). The detailed description of the morph and distribution of *D. ghilarovi* was provided by Ganin et al. (2013, 2014), with three colorful morphs (black, brown, and grey) found among different individuals that occurred near the border of China and the Korean Peninsula.

Blakemore et al. (2014) firstly defined the *D. ghilarovi* species complex based on its wide distribution and similar regional congeners. *D. ghilarovi* shares certain similarities with several closely related regional congeners, such as *D. csuzdii* Blakemore, 2014; *D. guryeensis* Hong, 2002; *D. jeombongsan* Blakemore, 2014; and *D. tairaensis* Ohfuchi, 1938, with four gizzards in XIII−XVI, but these species exhibit distinct differences in morphological and genetic characteristics. The species complex includes six species: *D. csuzdii, D. ganini* Zhang & Wu, 2021, *D. ghilarovi, D. guryeensis, D. jeombongsan,* and *D. tairaensis*, and distributed in the Far East Russia, Northeast China, and the Korean Peninsula. In Northeast China, there is still a lack of taxonomic research on the morphological delimitation of the *D. ghilarovi* species complex. Existing studies have mainly focused on the analysis of the genetic differentiation of the complex, mainly based on mitochondrial data. Blakemore et al. (2010) first definitively associated a *Drawida* type specimen to its COI barcode. Atopkin and Ganin (2015) found significant genetic differentiation between two ecotypes of *D. ghilarovi* through the analysis of cytochrome c oxidase subunit I (COI) and 16S ribosomal RNA gene; Ganin and Atopkin (2018) first conducted the intraspecific molecular differentiation of *D. ghilarovi*, demonstrating that different ecotypes of *D. ghilarovi* possess distinct population structures; Zhang et al. (2021) described *D. ganini* based on the COI evidence and the pigmentation of black.

Shekhovtsov et al. (2022) revealed that *D. ghilarovi* in Far East Russia includes three genetic clades through the analysis of transcriptomic datasets. Clade I is only composed of grey morphs; clade II consists of both grey and brown morphs and contains the type location specimen of *D. ghilarovi* (GenBank accession HG970204); clade III not only contains the grey and brown morphs but also the black morphs of *D. ganini*. Shekhovtsov et al. (2022) concluded that pigmentation is not an important character for species delimitation of earthworms. However, except for the difference in pigmentation, *D. ganini* is distinguished from *D. ghilarovi* by having inconspicuous female pores, a smaller ovary chamber, a less coiled spermathecae duct, and the position of the clitellum in X−XV (vs. IX−XV) and the gizzard in XII−XV (vs. XIII−XVI). *D. ganini* in clade III should be a valid species, and the other lineages of clade III should be unsolved taxa.

A comprehensive collection of earthworms was done on the Changbai Mountains in Northeast China, where individuals of the *D. ghilarovi* species complex were observed to possess distinguishing morphological features. Here, we verify the phylogenetic relationship of members of the *D. ghilarovi* species complex using the mitochondrial and nuclear data with the establishment of a new species, *D. yanbianensis* Liu & Zhao sp. nov.

Materials and methods

Sampling

Earthworm specimens were collected during the summer of 2023, around the month of July, in Helong County (42.5717°N, 128.7817°E) and Antu County (42.5361°N, 128.2777°E), Yanbian Prefecture, Jilin Province, Northeast China. Sampling was done by digging and hand sorting. Collected samples were fixed in 100% ethanol for subsequent morphological and molecular analyses.

Morphological examination

External and internal characteristics of 15 clitellates (518R0_03, 518R0_05–10, 520R0_01–04, 520R0_06, and 520R0_08–10) were examined using a stereomicroscope (ZEISS) and ZEN 3.3. pro software for image capturing. Body length and width were measured; the features of the prostomium, the male and female pores, and the spermathecal pore, as well as the internal structures such as the spermathecae, testis sacs, and gizzards, were examined and documented.

DNA extraction, amplification, and sequencing

Total genomic DNA was extracted from the posterior part of 34 earthworm specimens of *Drawida* using the TIANamp Genomic DNA Kit (Beijing, China) following the manufacturer's instructions. Fragment of the mitochondrial gene of the cytochrome c oxidase subunit I (COI) and two nuclear genes, 28S rRNA (28S) and

internal transcribed spacer 2 (ITS2), were amplified using the polymerase chain reaction (PCR). Two other nuclear genes, A-kinase anchor protein 17A (AKAP17) and flavin adenine dinucleotide synthetase 1 (FLAD1), were amplified using nested PCR. The primers used are shown in Table 1. The mixture (total volume 25 µl) contained 1 µl of template DNA and 17.25 µl of sterile ddH_2O, 2.0 µl of dNTPs, 2.5 µl of Easy Taq-Buffer, 0.25 µl of TransGen Easy Taq Polymerase, and 1 µl of each primer [forward and reverse primers, 10 uM]. The PCR protocol for COI was as follows: denaturation for 30 sec at 95 °C, annealing for 30 sec at 51 °C, and extension for 45 sec at 72 °C for 35 cycles with an initial denaturation step for 5 min at 95 °C and a final extension step for 5 min at 72 °C. For 28S and ITS2, the annealing temperature was 54 °C, while for AKAP17 and FLAD1, the annealing temperature was 48 °C. The PCR products were examined by electrophoresis in a 1% agarose gel and sent to Tianyi Huiyuan Biotechnology Co., Ltd. (Beijing, China) for sequencing using Sanger sequencing with an ABI 3730 automated sequencer. Sequences were aligned and edited using MEGA5 software (Tamura et al. 2011). All sequences and annotation information of the species were submitted to GenBank and shown in Table 2.

Molecular species delimitation analyses

Preliminary inference of species hypotheses through the distance matrix method of Assemble Species by Automatic Partitioning (ASAP) and the phylogenetic method of Generalized Mixed Yule Coalescent (GMYC) were applied for COI and 28S. ASAP is an automated species delimitation method based on COI and is designed to identify unique barcode gaps, that is, thresholds of genetic distance, thereby determining whether two individuals belong to the same species (Puillandre et al. 2021). ASAP is less prone to mismatches, has a short computation time, and is performed online (https://bioinfo.mnhn.fr/abi/public/asap).

GMYC is a species delimitation method based on speciation models (Fujisawa and Barraclough 2013) by fitting within and between species branching models to reconstruct gene trees. A bifurcated, rooted, ultrametric tree inferred by the BEAST package v1.7.5 (Drummond et al. 2012) and single-locus data as input files were provided to GMYC analysis performed in R 3.6.2 based on the splits v1.0–19 package.

Bayesian Phylogenetics and Phylogeography (BPP) is a Bayesian multispecies coalescent method that simulates explicitly the evolution of multi-gene data (Yang 2015; Flouri et al. 2018; Luo et al. 2018). BPP analyses were performed based on the five loci (COI, 28S, ITS2, AKAP17, and FLAD1) to confirm putative species. BPP v4.7 was used to estimate the species divergence times (τ) and population size parameters (θ) under the multispecies coalescent model on a fixed species phylogeny (A00). The population size parameters (θs) were assigned the inverse-gamma prior IG (3, 0.005), with a mean of 0.005/(3 – 1) = 0.0025. The divergence time at the root of the species tree (τ0) was assigned the IG prior (3, 0.005), with a mean of 0.0025, while the other divergence time parameters were specified by the uniform Dirichlet distribution (Yang and Rannala 2010). Species delimitation was performed using a fixed guide tree A10 in the within-model parameter posterior generated by running A00. The calculation of genetic distances using the Kimura-two-parameter (K2P) (Kimura 1980) model is shown in Table 3.

Phylogenetic analysis

Mitochondrial, nuclear, and the combined datasets were used to infer the phylogenetic relationship of the species in the *D. ghilarovi* complex, respectively. *Drawida cf. japonica* (Michaelsen, 1892) was set as outgroups. Maximum likelihood (ML) and Bayesian inference (BI) approaches were used to construct phylogenetic trees. ML analysis was performed in RAxML 8.0 (Stamatakis 2014) with the default rapid hill-climbing algorithm and the GTRGAMMA model to search for the best tree; the clade support value was

Table 1. Primers used for PCR and sequencing in this study.

Marker	Primer	Sequence (5'–3')	Round	Source
COI	LCO1490	GGTCAACAAATCATAAAGATATTGG		Folmer et al. 1994
	HCO2198	TAAACTTCAGGGTGACCAAAAAATCA		
	COIE	TATACTTCTGGGTGTCCGAAGAATCA		Bely and Wray 2004
28S	28sF1	GAGTACGTGAAACCGTCTAG		Pérez-Losada et al. 2009
	28sR1	CGTTTCGTCCCCAAGGCCTC		
ITS2	E58S-F1	ATCACTGGGTTCGTGCGT		Shekhovtsov et al. 2013
	E28S-2	CCKCTTCACTCGCCGTTA		
AKAP17	AKAP17-F1	AAYTGGGARGTNATGGARAA	Round 1	This study
	AKAP17-R1	TCYTTRAACATNARYTTCAT		
	AKAP17-F2	AARATGATHAARCCNGAYCARTT	Round 2	
	AKAP17-R2	GCYTTNACRAANCCCATRTAYTC		
FLAD1	FLAD1-F1	GGNCCNACNCAYGAYGAYAT	Round 1	This study
	FLAD1-R1	TTNGGRTGNGTRTTYTCCAT		
	FLAD1-F2	TGYAARGCNTTYTTYGGNACNGA	Round 2	
	FLAD1-R2	TTNACNCKCATRAAYTCNGGCCA		

Table 2. List of *Drawida* species incorporated in the analysis.

Specimen ID	Species	Location	Latitude, Longitude	Accession Number				
				COI	28S	ITS2	AKAP17	FLAD1
518R0_01	*D. yanbianensis*	China: Jilin: Yanbian: Helong	42.5717°N, 128.7817°E	-	PQ415138	PQ415160	-	-
518R0_03	*D. yanbianensis*	China: Jilin: Yanbian: Helong	42.5717°N, 128.7817°E	-	PQ415140	PQ415168	-	-
518R0_04	*D. yanbianensis*	China: Jilin: Yanbian: Helong	42.5717°N, 128.7817°E	-	PQ415141	PQ415167	-	-
518R0_05	*D. yanbianensis*	China: Jilin: Yanbian: Helong	42.5717°N, 128.7817°E	-	PQ415142	PQ415165	-	-
518R0_06	*D. yanbianensis*	China: Jilin: Yanbian: Helong	42.5717°N, 128.7817°E	PQ411138	PQ415139	PQ415166	PQ423888	PQ427083
518R0_07	*D. yanbianensis*	China: Jilin: Yanbian: Helong	42.5717°N, 128.7817°E	PQ411139	PQ415134	PQ415164	PQ423889	PQ427082
518R0_08	*D. yanbianensis*	China: Jilin: Yanbian: Helong	42.5717°N, 128.7817°E	PQ411140	PQ415135	PQ415163	-	-
518R0_09	*D. yanbianensis*	China: Jilin: Yanbian: Helong	42.5717°N, 128.7817°E	PQ411141	PQ415136	PQ415162	-	-
518R0_10	*D. yanbianensis*	China: Jilin: Yanbian: Helong	42.5717°N, 128.7817°E	PQ411142	PQ415137	PQ415161	-	-
520R0_01	*D. yanbianensis*	China: Jilin: Yanbian: Antu	42.5361°N, 128.2777°E	PQ411143	PQ415147	PQ415159	-	-
520R0_02	*D. yanbianensis* (Paratype)	China: Jilin: Yanbian: Antu	42.5361°N, 128.2777°E	PQ411144	-	PQ415158	-	-
520R0_03	*D. yanbianensis*	China: Jilin: Yanbian: Antu	42.5361°N, 128.2777°E	PQ411145	-	PQ415157	-	-
520R0_04	*D. yanbianensis*	China: Jilin: Yanbian: Antu	42.5361°N, 128.2777°E	-	-	PQ415156	-	-
520R0_05	*D. yanbianensis*	China: Jilin: Yanbian: Antu	42.5361°N, 128.2777°E	PQ411146	-	-	-	-
520R0_06	*D. yanbianensis* (Holotype)	China: Jilin: Yanbian: Antu	42.5361°N, 128.2777°E	PQ411147	PQ415148	PQ415155	-	-
520R0_07	*D. yanbianensis*	China: Jilin: Yanbian: Antu	42.5361°N, 128.2777°E	PQ411148	PQ415144	PQ415154	PQ423891	PQ427084
520R0_08	*D. yanbianensis* (Paratype)	China: Jilin: Yanbian: Antu	42.5361°N, 128.2777°E	PQ411149	PQ415143	PQ415153	PQ423890	-
520R0_09	*D. yanbianensis*	China: Jilin: Yanbian: Antu	42.5361°N, 128.2777°E	PQ411150	PQ415145	PQ415152	-	-
520R0_10	*D. yanbianensis*	China: Jilin: Yanbian: Antu	42.5361°N, 128.2777°E	PQ411151	PQ415146	PQ415151	-	-
425DFH1	*D. ganini*	China: Heilongjiang: Muling River	46.049°N, 132.5939°E	-	PQ415125	PQ415171	-	-
425DFH2	*D. ganini*	China: Heilongjiang: Muling River	46.049°N, 132.5939°E	PQ411152	PQ415129	PQ415170	-	-
425DFH3	*D. ganini*	China: Heilongjiang: Muling River	46.049°N, 132.5939°E	PQ411153	PQ415130	PQ415172	-	-
425DFH4	*D. ganini*	China: Heilongjiang: Muling River	46.049°N, 132.5939°E	PQ411154	PQ415131	PQ415173	-	-
425DFH5	*D. ganini*	China: Heilongjiang: Muling River	46.049°N, 132.5939°E	PQ411155	PQ415132	PQ415169	PQ423895	PQ427088
425DFH6	*D. ganini*	China: Heilongjiang: Muling River	46.049°N, 132.5939°E	-	PQ415133	-	PQ423894	PQ427087
425DFH7	*D. ganini*	China: Heilongjiang: Muling River	46.049°N, 132.5939°E	PQ411156	PQ415126	PQ415174	-	-
425DFH8	*D. ganini*	China: Heilongjiang: Muling River	46.049°N, 132.5939°E	PQ411157	PQ415127	PQ415175	-	-
425DFH9	*D. ganini*	China: Heilongjiang: Muling River	46.049°N, 132.5939°E	-	PQ415128	PQ415176	-	-
425DFH10	*D. ganini*	China: Heilongjiang: Muling River	46.049°N, 132.5939°E	PQ411158	-	-	-	-
425DFH11	*D. ganini*	China: Heilongjiang: Muling River	46.049°N, 132.5939°E	PQ411159	-	-	-	-
425DFH12	*D. ganini*	China: Heilongjiang: Muling River	46.049°N, 132.5939°E	PQ411160	-	-	-	-
-	*D. ganini*	Russia: Jewish Autonomous Region(Bch): Bastak Reserve	48.5930°N, 135.0324°E	HG970192–HG970193	-	-	-	-
-	*D. ganini*	Russia: Khabarovsk Territory(Chch): Chirki River	48.0939°N, 135.0859°E	HG970194–HG970196	-	-	-	-
-	*D. ganini*	Russia: Khabarovsk Territory(Nch): Nanaian Region	49.2716°N, 136.4625°E	HG970197–HG970199	-	-	-	-

Specimen ID	Species	Location	Latitude, Longitude	Accession Number				
				COI	28S	ITS2	AKAP17	FLAD1
-	*D. ganini*	Russia: Primorye Territory(Pch): Razdol'naja River	43.3345°N, 131.5440°E	HG970200–HG970202	-	-	-	-
-	*D. ganini*	Russia: Primorye Territory(Khch): ike Khanka Reserv	44.38°N, 132.49°E	KY711475	-	-	-	-
-	*D. ganini*	Russia: Jewish Autonomous Region (Sch):v. Stolbowoe	47.54°N, 131.06°E	KY711476–KY711477	-	-	-	-
-	Group unsolved	Russia: Primorye Territory (SK): Sikhote-Alin Reserve	45.13°N, 136.29°E	KY711492	-	-	-	-
-	Group unsolved	Russia: Primorye Territory (Ss): Sikhote-Alin Reserve	44.59°N, 136.31°E	KY711493	-	-	-	-
-	Group unsolved	Russia: Primorye Territory (SsK): Sikhote-Alin Reserve	45.13°N, 136.29°E	KY711494–KY711495	-	-	-	-
-	Group unsolved	Russia: Southern Sikhote-Alin (ShK): Shivki Mountain	47.00°N, 134.22°E	KY711496–KY711498	-	-	-	-
-	Group unsolved	Russia: Kahabarovsk Territory: Southern Sikhote-Alin (ShS)	47.00°N, 134.22°E	KY711499–KY711501	-	-	-	-
-	Group unsolved	Russia: Primorye Territory (Lkd): Lazovsky Ridge	43.30°N, 133.35°E	KY711507	-	-	-	-
-	Group unsolved	Russia: Primorye Territory (Lkk): Lazovsky Ridge	43.30°N, 133.35°E	KY711508	-	-	-	-
-	Group unsolved	Russia: Primorye Territory (Vkd): Marine Biological Station "Vostok"	42.53°N, 132.44°E	KY711509–KY711510	-	-	-	-
-	Group unsolved	Russia: Primorye Territory (Vkk): Marine Biological Station "Vostok"	43.41°N, 132.09°E	KY711512–KY711514	-	-	-	-
-	*D. ghilarovi*	Russia: Primorye Territory: Kedrovaja Pad' Reserve (Ps)	42.2619°N, 130.3735°E	HG970204	-	-	-	-
-	*D. ghilarovi*	Russia: Primorye Territory (Uz): Ussurijskij Reserve	43.3325°N, 132.2118°E	HG970205	-	-	-	-
-	*D. ghilarovi*	Russia: Primorye Territory(GK): Biological Station "Gornotayozhnaya"	43.41°N, 132.09°E	KY711481	-	-	-	-
-	*D. ghilarovi*	Russia: Primorye Territory (Gs): Biological Station "Gornotayozhnaya"	43.41°N, 132.09°E	KY711483–KY711484	-	-	-	-
-	*D. ghilarovi*	Russia: Primorye Territory (Lk): Lazovsky Reserve	43.00°N, 133.44°E	KY711485–KY711487	-	-	-	-
-	*D. ghilarovi*	Russia: Primorye Territory(Uz): Ussurijskij Reserve	43.33°N, 132.21°E	KY711503–KY711506	-	-	-	-
-	*D. ghilarovi*	Russia: Primorye Territory (Ps): Kedrovaja Pad' Researve	42.26°N, 130.37°E	KY711516	-	-	-	-
-	Group6	Russia: Primorye Territory (Ps): Kedrovaja Pad' Researve	42.26°N, 130.37°E	KY711515	-	-	-	-
519R1_36	*D. ghilarovi*	China: Jilin: Yanbian: Wangqing	43.3257°N, 129.4149°E	PQ411161	PQ415150	-	-	-
519R1_38	*D. ghilarovi*	China: Jilin: Yanbian: Wangqing	43.3257°N, 129.4149°E	PQ411162	-	-	PQ423893	PQ427085
519R1_40	*D. ghilarovi*	China: Jilin: Yanbian: Wangqing	43.3257°N, 129.4149°E	PQ411163	PQ415149	-	PQ423892	PQ427086
R101	Group4	(Shekhovtsov et al. 2022)	-	OL785715	-	-	-	-
R123	Group unsolved	(Shekhovtsov et al. 2022)	-	OL785716	-	-	-	-

Specimen ID	Species	Location	Latitude, Longitude	Accession Number				
				COI	28S	ITS2	AKAP17	FLAD1
R108	Group6	(Shekhovtsov et al. 2022)	-	OL785717				
HN-LN-GR-I3_01	*D. cf. japonica*	China: Henan: Luoyang: Luoning	34.4364°N, 111.6368°E	PQ288577	PQ432447	-	PQ452810	PQ452826
HN-LN-GR-I3_02	*D. cf. japonica*	China: Henan: Luoyang: Luoning	34.4364°N, 111.6368°E	PQ288578	PQ432448	-	PQ452809	PQ452827
-	*D. angiang*	Vietnam: An Giang: Tinh Bien District	10.5882°N, 104.9506°E	ON303834	-	-	-	-
-	*D. cochinchina*	Vietnam: Dong Nai: Xuan Loc District	10.7931°N, 107.5257°E	ON303833	-	-	-	-
-	*D. cochinchina*	Vietnam: Dong Nai: Xuan Loc District	10.7931°N, 107.5257°E	ON303831	-	-	-	-
-	*D. gracilis*	(Ganin and Atopkin 2018)	-	JN887887	-	-	-	-
-	*D. gracilis*	(Ganin and Atopkin 2018)	-	JN793516	-	-	-	-
-	*D. bullata*	(Ganin and Atopkin 2018)	-	JN793527	-	-	-	-
-	*D. bullata*	(Ganin and Atopkin 2018)	-	JN887894	-	-	-	-
-	*D. nepalensis*	(Nguyen et al. 2022)	-	ON303830	-	-	-	-
-	*D. nepalensis*	(Nguyen et al. 2022)	-	MT472588	-	-	-	-
-	*D. japonica japonica*	(Nguyen et al. 2022)	-	EF077597	-	-	-	-
-	*D. gisti gisti*	(Nguyen et al. 2022)	-	JQ405262	-	-	-	-
-	*D. hattamimizu* (neotype)	Japan: Ishikawa: Kanazawa: Hatta	136.39°E, 36.34 °N	GQ500899	-	-	-	-
-	*D. hattamimizu*	Japan: Ishikawa: Kanazawa: Hatta	36.38°N, 136.41°E	AB543205	-	-	-	-
-	*D. nepalensis*	(Nguyen et al. 2022)	-	MH845467	-	-	-	-
-	*D. koreana*	(Nguyen et al. 2022)	-	KR047039	-	-	-	-
-	*D. koreana*	(Nguyen et al. 2022)	-	MH845538	-	-	-	-
IEW435-17	*D. ghatensis*	(Thakur 2021)	-	-	-	-	-	-
IEW434-17	*D. ghatensis*	(Thakur 2021)	-	-	-	-	-	-
IEW388-17	*D. brunnea*	(Thakur 2021)	-	-	-	-	-	-
IEW391-17	*D. impertusa*	(Thakur 2021)	-	-	-	-	-	-
IEW393-17	*D. impertusa*	(Thakur 2021)	-	-	-	-	-	-
IEW420-17	*D. circumpapillata*	(Thakur 2021)	-	-	-	-	-	-
IEW425-17	*D. travancorense*	(Thakur 2021)	-	-	-	-	-	-
IEW444-17	*D. robusta*	(Thakur 2021)	-	-	-	-	-	-
IEW445-17	*D. robusta*	(Thakur 2021)	-	-	-	-	-	-
IEW451-17	*D. scandens*	(Thakur 2021)	-	-	-	-	-	-
IEW459-17	*D. nilam*	(Thakur 2021)	-	-	-	-	-	-
HY-10	*D. jeombongsan*	(Blakemore et al. 2014)	-	-	-	-	-	-

Table 3. Percentage of K2P distances of COI of *D. yanbianensis* sp. nov. and the other species of the *D. ghilarovi* species complex. Values in parentheses showed intragroup distance (values in %).

	Species	1	2	3	4	5	6	7
1	Group1 (*D. yanbianensis*)	(0–9.1)						
2	Group2 (*D. ghilarovi*)	12.4–15.4	(0.2–7.1)					
3	Group3 (*D. jeombongsan*)	16.7–17.8	16.7–19.2	(0)				
4	Group4 (R101)	13.0–15.4	10.4–13.5	16.2	(0)			
5	*D. ganini*	16.9–20.9	16.3–20.3	19.2–21.2	16.9–19.0	(0–12.1)		
6	Group unsolved	16.9–19.4	13.6–18.8	18.1–20.7	14.1–17.0	8.1–16.2	(0.2–15.6)	
7	Group6 (R108)	17.1–18.8	15.6–19.9	17.4–18.5	16.5–19.5	16.5–21.0	16.7–21.3	(5.8)

assessed using 1000 rapid bootstrap replicates. BI was done in MrBayes v.3.2.6 (Ronquist et al. 2012) and ran in two million generations to ensure the average standard deviation of split frequencies is less than 0.01. The best nucleotide substitute models were chosen using jModelTest 2.1 (Darriba et al. 2012) based on the Akaike Information Criterion, which are TPM3uf+I+G for COI and SYM+I+G for the remaining three nuclear markers. The results of p files of BI were examined in Tracer v.1.7.2 (Rambaut et al. 2018), and the ESS larger than 200 were evaluated for convergence and to ensure sufficient burn-in for the trees. Both ML and BI trees were visualized and edited using FigTree v1.4.4 (Rambaut 2018).

Table 4. Comparison of key morphological characteristics of the *Drawida ghilarovi* species complex and related taxa (NA: not available).

Character	*D. yanbianensis*	*D. ganini*	*D. ghilarovi*	*D. csuzdii*	*D. guryeensis*	*D. jeombongsan*	*D. tairaensis*	*D. hattamimizu*	*D. nemora*	*D. ofunatoensis*
Color	Gray	Black	Brown or gray	Unpigmented in alcohol	Light pinkish or bluish	Light blue	Flesh coloured or pinkish and transparent	Dark blue-black	Dark blue	Yellowish
Length (mm)	45.8–78	66–121	100–142	120	62–83	60+	60–93	Averaging 246	65–185	228–283
Width (mm)	4.5–7.5	4.9–5.6	6	NA	2.3–2.5	NA	up to 2.7	9–10	Up to 6.5	Up to 6.5
Genital markings	6–12; irregular	6–10; irregular	5–13; irregular	Unilateral; irregular	8–10; paired	7/8/11/12; paired	Absent	6–9 or 10 or 11–12,13, paired	6–13; irregular	7–13; variously paired
Clitellum	10–14; greyish white	10–15; greyish white	9–15	$^{1}/_{2}$ 9–15; reddish	10–13; pinkish	Unclear	10–13	9/10–15/16; ash-grey	9/10–13/14; yellowish gray alive	10–13
Spermathecae	Ampulla large; duct long coiled	Ampulla medium; duct less coiled	Duct long coiled	Spherical ampulla; duct convoluted	Ampulla medium; duct long twisted	NA	Duct convoluted	Ampulla as sacs; duct long coiled	Duct convoluted	Duct convoluted
Spermathecal atrium	Absent	Absent	Absent	Absent	Present; 7/8	Absent	Present; 7/8	Absent	Absent	Absent
Ovisacs	11–15, palm shaped	11–12, palm shaped	11, long egg sacs	10/11/12, long, as far back as 14	12, extending to 16	NA	12–16	12 or 12/13/14, large paired	10/11/12 as far back as 14	11/12, short
Male pore	10/11; ventral bc lines, no penis	10/11; ventral bc lines, no penis	10/11; mediolateral in bc lines, no penis	10/11; mid-bc lines, no penis	10/11; two pairs, short and bla de-shape penis	10/11; no penis	10/11; no penis	10/11; ventral cd lines, no penis	10/11; penis small	10/11; small disc-shaped penis
Female pore	12; paired	Inconspicuous	11/12; paired	12 near 11/12; paired	11/12; paired	12; paired	12 near 11/12; paired	12; paired	12 near 11/12; paired	11/12; paired
Gizzard segments	Four; 12–17	Four; 12–15	Four; 13–16	Four; 13–16	Four; 13–16	Four; 13–16	Four; 13–19	Six; 13–18	Five; 12/13–15/16	Four; 12–17/18
Testis sacs	Ivory-white and large; IX–X(XI, XII)	IX–X	Hemispherical; IX–X	Spherical; IX–X	IX–X, mostly in X	X–XI	Spherical; X–XI (IX–X?)	IX–X	Spherical; IX–X	X–XI (IX–X?)
Vas deferens	Long coiled	Coiled	Long coiled	Slightly coiled	Long coiled	NA	Coiled	Long and convoluted	Slightly coiled	Coiled

Estimating divergence times

Divergence dates within the *D. ghilarovi* complex were estimated using a dataset of 74 COI sequences. Calibration was achieved by applying an earthworm mitochondrial COI clock rate of 0.024 substitutions per site per million years, as previously established by Chang and James (2011). The analysis was conducted using the BEAST v1.7.5 package, employing a strict clock model and a Yule speciation model. Two independent runs, each comprising 10,000,000 generations, were performed with sampling every 1,000 generations. The maximum clade credibility tree was subsequently generated using TreeAnnotator, summarizing node ages and posterior probabilities.

Abbreviations used in morphological figures

ag accessory gland;
amp ampulla;
fp female pore;
mp male pore;
sp spermathecal pore;
cl clitellum;
vd vas deferens;
ts testis sac;
gm genital markings;
os ovisac;
prg prostate gland;
p prostomium.

Results

Morphological characterization

Family Moniligastridae Claus, 1880

Genus *Drawida* Michaelsen, 1900

Generic diagnosis. Body size, small to giant [e.g., *D. japonica* (28~ mm); *D. hattamimizu* (~1000 mm)]. Prostomium prolobous. Clitellum is commonly in X−XIII, usually extending forward or backward [e.g., *D. nemora*

(IX, X−XIII, XIV)], or inconspicuous. Setae four pairs, lumbricine. Dorsal pores more usually absent or intermittently present [e.g., *D. companio* Blakemore, 2014 (15/16, 19/20/21, 25/26/27)]. Male pores in or near 10/11. Female pores usually paired in 11/12, or XII, or inconspicuous. Spermathecal pores paired in 7/8, or inconspicuous. A pair of testis sacs typically located in IX−X. A pair of ovisacs extends backward from ovary chamber (typically in XI). Spermathecae paired in VII−VIII. Two to six gizzards within segments XI–XVIII [or especially up to nine in *D. hattamimizu* extending to XX or XXI; five or six in *D. nilamburensis* Bourne, 1894 in XXVII–XXXIV]. Oesophageal gizzards, calciferous glands, and intestinal caeca absent.

Drawida yanbianensis Liu & Zhao, sp. nov.

https://zoobank.org/17775E03-10D2-4E7E-8003-274875BDBAFE

Fig. 4

Material examined. ***Holotype*:** • one clitellate (520R0_06) (COI accession number: PQ411147), Antu County (42.5361°N, 128.2777°E, 604 m elev.), Yanbian Prefecture, Jilin Province, 2023-07-21, coll. Huifeng Zhao. ***Paratypes***: • two clitellates [520R0_02 (COI accession number: PQ411144), 520R0_08 (COI accession number: PQ411149)], same data as of holotype.

Other specimens. 12 clitellates (518R0_03, 518R0_05 −10, 520R0_01, 520R0_03 −04, 520R0_09 −10), Helong County (42.5717°N, 128.7817°E, 42.6 m elev.), Yanbian Prefecture, Jilin Province, 2023-07-21, coll. Huifeng Zhao. All the specimens of the new species have been deposited in the Hebei Key Laboratory of Animal Diversity, Langfang Normal University, Hebei, China (C-HLU).

Etymology. The specific name of the species refers to the distribution area in Northeast China.

Diagnosis. Body grey, length 45.8–78.0 mm, diameter 2.3–2.6 mm, number of segments 91–144. Prostomium prolobous. Clitellum in X−XIV, ring-shaped. Setae: lumbricine, four pairs, existing in each segment. Spermathecal pores: one pair in 7/8, approximately on the setae cd line, ventro-laterally positioned, and spermathecal atrium absent. Dorsal pores absent. Genital markings: paired or unpaired, existing irregularly in segments VI−XII. Male pores: one pair, in intersegmental furrow 10/11, between setae b and c, near b, lip-shaped. Penis absent. Female pores: one pair slits on setae ab line of XII, near the 11/12 interval. Gizzards four in XII−XVII segments. Testis sacs: one pair, ivory-white present on IX−X, or elongate to XI or XII; vas deferens long coiled in IX−X, with one pair of elliptical prostate gland in X. Ovisac paired in XI−XV, palm-shaped. Four pairs of hearts in VI−IX. Spermathecae: one pair, hanging on the septum on 7/8, ampulla large in VIII, slightly yellowish, oval-shaped, with long coiled duct, spermathecal atrium absent.

Description. ***External characters*:** Length 45.8–78.0 mm, diameter 2.3–2.6 mm, 91–144 segments, body grey. Prostomium prolobous. Dorsal pores absent. Setae lumbricine, 4 pairs, small dots that exist in every segment except the first, about ab = cd, aa = 1.5 bc. Clitellum within X−XIV, greyish white and ring-shaped. Genital markings either paired or unpaired irregularly in VI−XII, or absent. Spermathecal pores, paired in 7/8, ventral, approximately on the setae cd line. Male pores, paired in 10/11, between setae b and c, near b, about 0.17 body circumference apart, lip-shaped, superficial without a copulatory organ, penis absent. Female pores, paired on setae ab line of XII, near the 11/12 interval.

***Internal characters*:** Hearts four pairs in VI−IX. Septa 7/8/9 relatively thick and muscular. Four gizzards in XII−XVII segments, milk-white. Testis sacs paired, ivory-white and large, each present on IX−X, or elongate to XI or XII, vas deferens long coiled in IX−X, with one pair elliptical prostate gland in X. Male atrium absent. Ovarian chamber complete, ovisacs paired, palm-shaped in XI−XV. Spermathecae paired in VII−VIII, ampulla large in VIII, slightly yellowish, oval-shaped, with long coiled duct, atrium absent. Accessory glands grape-like, stalkless, in correspondence with external genital markings.

Distribution. Helong County (42.5717°N, 128.7817°E) and Antu County (42.5361°N, 128.2777°E), Yanbian Prefecture, Jilin Province, Northeast China.

Habitat. Litter or subsoil geophage in forest soils.

Remarks. The new species is morphologically similar to *D. ghilarovi* and *D. ganini*, which are distributed in the Russian Far East and Northeast China (Gates 1969; Ganin et al. 2013; Zhang et al. 2021). They are similar in the position and number of male pores, spermathecal pores and spermathecae, prostomium, dorsal pores, and the absence of a penis. However, *D. yanbianensis* sp. nov. is distinguished from *D. ganini* and *D. ghilarovi* by having female pores on XII and the clitellum spanning five segments in X−XIV. The female pores of *D. ganini* are inconspicuous, while those of *D. ghilarovi* are located in the internode of 11/12; the position of the clitellum of *D. ganini* is located in X−XV, while that of *D. ghilarovi* is located in IX−XV. In addition, the new species (45.8–78 mm) is shorter than *D. ganini* (66–121 mm) and *D. ghilarovi* (100–142 mm) in body length. The new species have four gizzards in XII−XVII, but the position differs from that of *D. ganini*, which is in XII−XV, and that of *D. ghilarovi*, which is in XIII−XVI. The spermathecae of *D. yanbianensis* sp. nov. are oval-shaped with a large ampulla and a long coiled duct, while the ampulla of *D. ganini* is medium in size and has a less coiled duct.

The new species exhibits distinct morphological differences from the other species within the *D. ghilarovi* complex. *Drawida yanbianensis* sp. nov. lacks a penis in contrast to *D. nemora*, *D. guryeensis*, and *D. ofunatoensis* (Hong 2002; Blakemore et al. 2014). *Drawida hattamimizu* has six gizzards in XIII−XVIII, with an average length of 246 mm and a width ranging from 9 to 10 mm (Blakemore et al. 2010), which is much larger than that of the new species. Additionally, *D. yanbianensis* sp. nov. is approximately the same size as *D. csuzdii*, *D. jeombongsan*, and *D. tairaensis*, but the new species is gray in color with grayish-white clitellum, while *D. csuzdii* is unpigmented with reddish clitellum and *D. jeombongsan* is light blue with unclear clitellum (Blakemore et al. 2014). Moreover, the new species is characterized by its

grey coloration and a width ranging from 4.5 to 7.5 mm. In contrast, *D. tairaensis* exhibits flesh or pinkish coloration (Blakemore et al. 2014) and has a narrower (up to 2.7 mm) width than the new species.

Phylogenetic relationships and species delimitation

With the combined available data online, a total of 76 COI sequences revealed new phylogenetic relationships within the *D. ghilarovi* complex based on COI, with some individuals of our specimens scattered between clades II and III (Fig. 1). Based on the phylogenetic analysis and morphological characters, the *D. ghilarovi* complex is divided into seven groups. Different approaches support the identical topology of those groups, although the most support values are low (Fig. 1). The *D. ghilarovi* complex is shown to be a monophyletic group with a posterior probability (PP) of 100% and a bootstrap value (BV) of 71%.

The phylogenetic tree generated from the analysis of the multiple loci dataset, including COI, 28S, ITS2, AKAP17, and FLAD1, using both maximum likelihood (ML) and Bayesian inference (BI) methods (Fig. 2),

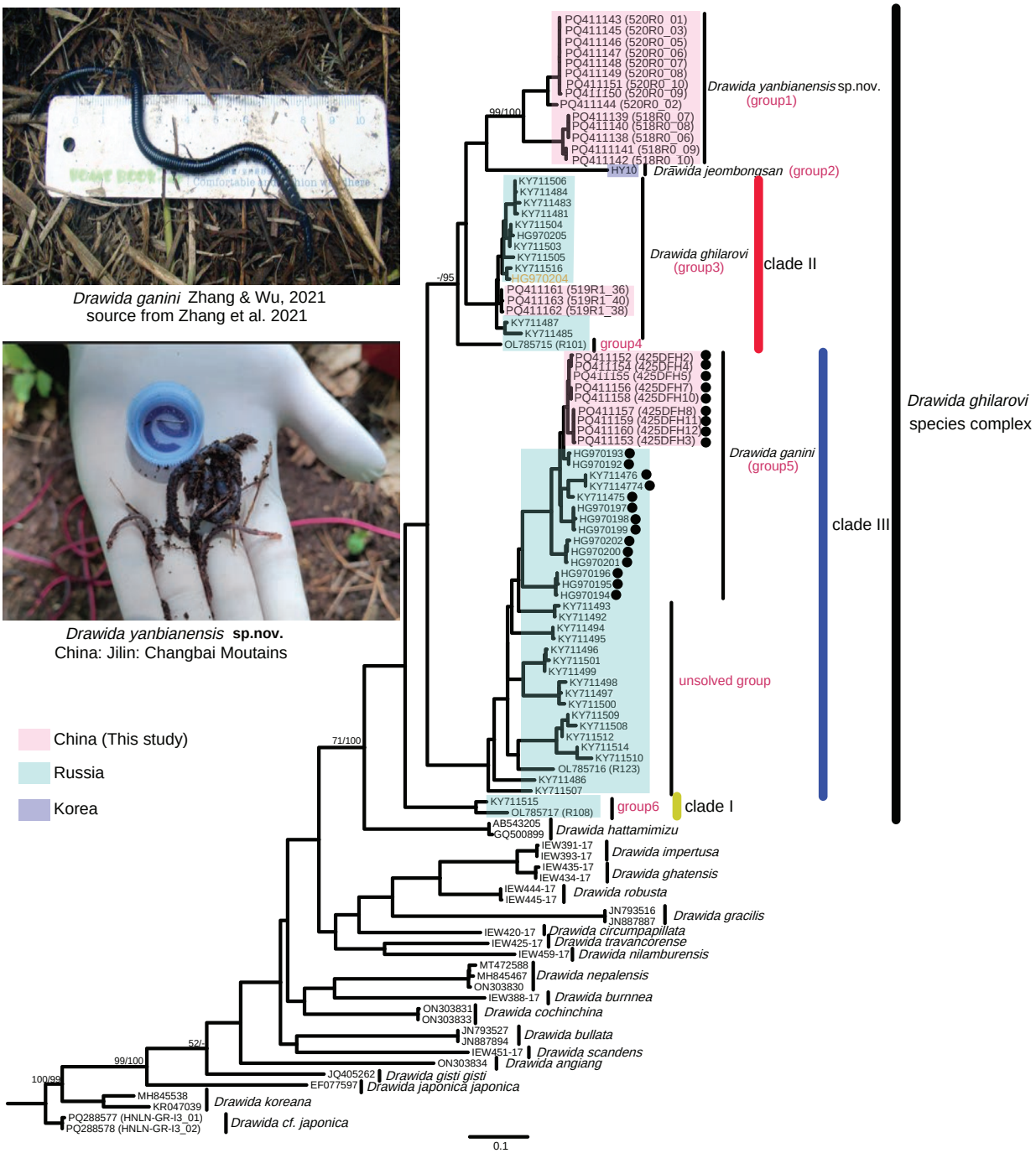

Figure 1. The phylogenetic tree based on COI using the maximum likelihood method. Numbers near branches indicate the maximum likelihood bootstrap support/Bayesian posterior probabilities. Posterior probability values lower than 80% and bootstrap values lower than 50% indicate weak support and are not shown.

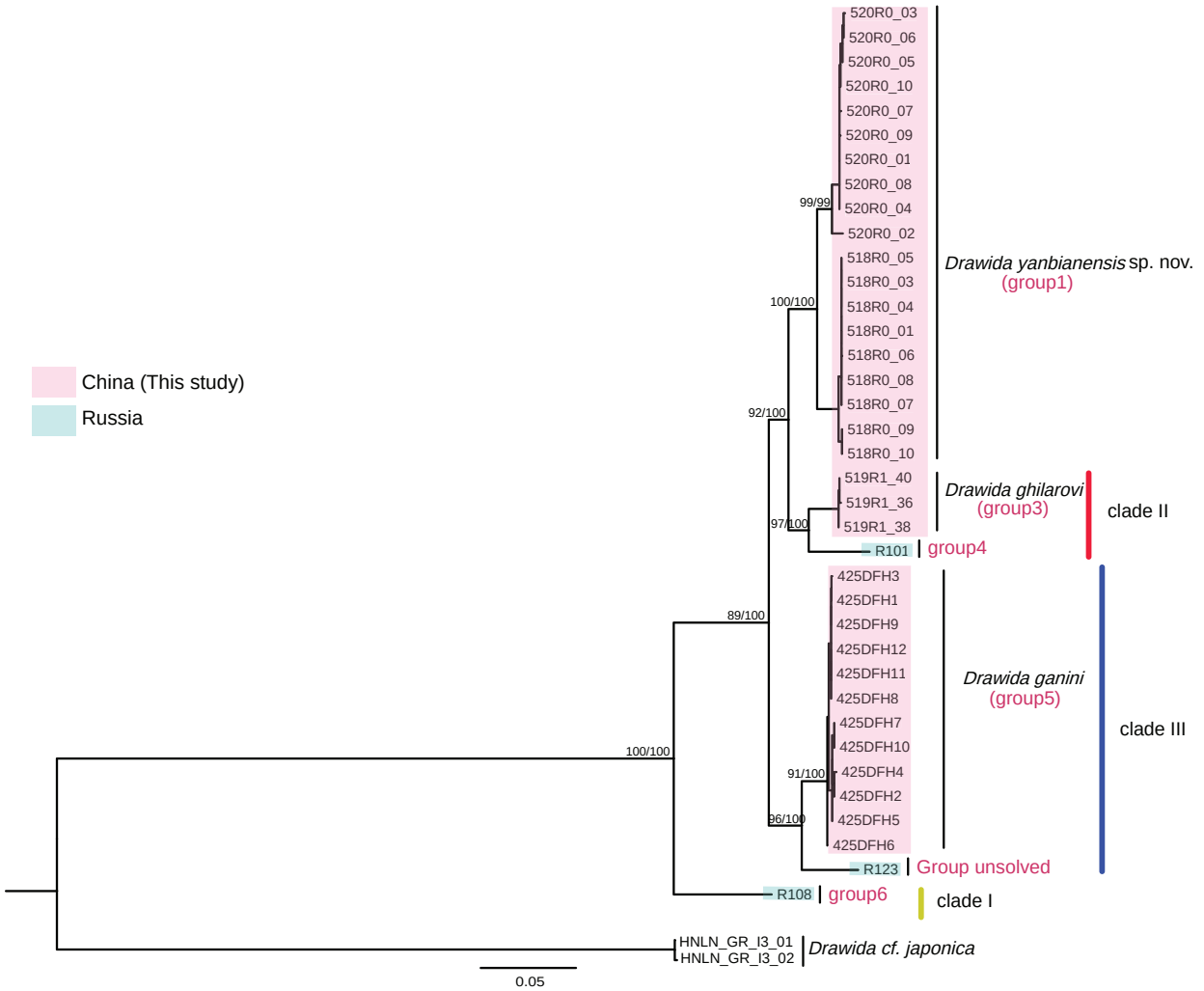

Figure 2. An ML concatenated tree of five genetic markers (COI, 28S, ITS2, FADL1, and AKAP17). Nodes with ML bootstraps > 70% are considered well-supported. Numbers near branches indicate the maximum likelihood bootstrap support/Bayesian posterior probabilities. The scale bar indicates the branch length.

exhibits a topological structure that is remarkably similar to the ML tree constructed solely with COI data (Fig. 1). In this tree, the clade corresponding to the *D. ghilarovi* complex is robustly supported, with both PP and BV being 100%. Additionally, the close relationship between the new species and *D. ghilarovi* is strongly corroborated, with a BV of 92% and a PP of 100%. In the concatenated phylogenetic tree of the *D. ghilarovi* complex (Fig. 2), the clades identified by Shekhovtsov et al. (2022) are as follows: Clade I, which comprises group 6, is strongly supported by high PP (100%) and BV (100%); Clade II, a well-supported clade with a BV of 97% and a PP of 100%, consists of members from groups 3 and 4; and Clade III, supported with a PP of 96% and a BV of 100%, is composed of members from groups 5 and 6.

The species delimitation by BPP into three Molecular Operational Taxonomic Units (MOTUs) is identical to the morphological classification (Fig. 3). ASAP also divides into three MOTUs using the 28S, consistent with BPP and morphological delimitation; however, it splits the new species into two MOTUs using COI. GMYC, on the other hand, delineates only one MOTU for all three species using 28S, while it splits the new species into two MOTUs and lumps *D. ganini* and *D. ghilarovi* using COI (Fig. 3). BPP is recognized as an accurate method for species delimitation because it incorporates multi-locus histories, which align with the multiple characters used in morphological approaches. In contrast, ASAP and GMYC consider only single-locus evolutionary histories. Here, ASAP demonstrated better performance compared to GMYC, a finding corroborated by another molecular species delimitation study on earthworms by Goulpeau et al. (2022).

Results of K2P analysis of COI show that the intraspecific sequence divergence for the new species ranged from 0–9.1% (Table 3, Suppl. material 1), and *D. yanbianensis* sp. nov. differs from the other species or group of *D. ghilarovi* complex ranging from 12.4%−20.9% (Table 3). The ancestor of the *D. ghilarovi* complex emerged around 9.0 million years ago (Ma; 95% credible range of 11.2–7.2 Ma) during the Late Miocene (Suppl. material 2). Most groups within the *D. ghilarovi* complex diverged between approximately 8.2 and 3.7 Ma. The two subclades of *D. yanbianensis* sp. nov. split around 2.8 Ma, coinciding with the onset of the Quaternary Period (Suppl. material 2).

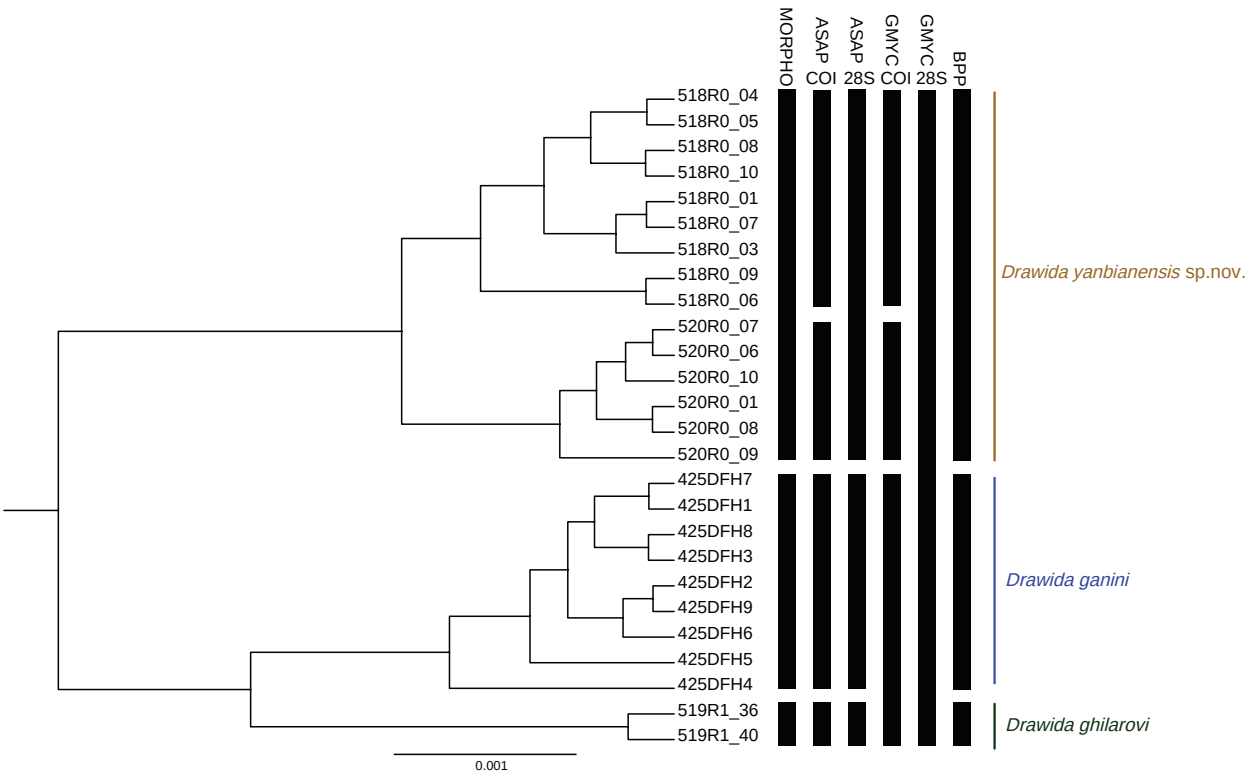

Figure 3. Species delimitation of the *Drawida ghilarovi* species complex. ASAP, automated barcode gap discovery; GMYC, generalized mixed Yule coalescent model; BPP, Bayesian phylogenetics and phylogeography.

Discussion

The earthworms of Moniligastridae mainly occur in Asia, with their probable origin inferred to be in the 'east or near Myanmar' (Gates 1972, 1982; Jamieson 1977; Narayanan et al. 2024). This inference is based on the fact that four out of the five known genera of Moniligastridae are naturally distributed in the eastern or nearby areas of Myanmar. The widespread distribution of Moniligastridae is largely attributed to the dispersal of *Drawida* species. *Drawida* was described by Stephenson (1923: 118, 124) as "one of the large Indian genera"; its headquarters appear to be in Sri Lanka, southern India, eastern Himalayas, and Myanmar (Blakemore 2009). The historical migration patterns of *Drawida* across Asia, especially East Asia, where the *D. ghilarovi* complex occurs, are unknown until Gates (1972). A more comprehensive sampling strategy that covers the entire distribution area of the genus for elucidating the phylogeographic patterns and evolutionary history of *Drawida* is essential in the future.

Temperature and food resources are the primary variables restricting the growth and productivity of earthworms (Fayolle et al. 1997). The mountains in northeastern Asia are well-preserved alpine ecosystems in high-altitude regions (Yang and Xu 2003). Earthworms inhabiting these areas are exposed to significant temperature fluctuations and are cold-tolerant, such as the members of the *D. ghilarovi* complex (−16 °C in worms to −20 °C for cocoons) (Berman et al. 2010), and many lumbricid species, such as *Eisenia nordenskioldi* (Eisen, 1879), *Aporrectodea tuberculata* (Eisen, 1874), *A. trapezoides* (Dugès, 1828), *etc*., also occur in this region (Shekhovtsov et al. 2018, 2020, 2023; Zhao et al. 2022). Pheretimoid is the advantaged earthworm group in most habitats around the world, but they are intolerant to the cold environment as the cocoons are killed below 5 °C (Richardson et al. 2009; Görres et al. 2018). However, few *Pheretimoid* species are found in the alpine forests of East Asia, with only one exception thus far (Dong et al. 2024), presumably due to their intolerance of cold habitats. Therefore, the *D. ghilarovi* complex and some lumbricid species share the cold and fertilized mountain niche. The gut microbiota may provide multiple physiological benefits to their hosts, especially in adapting to temperature and food resources (Yang et al. 2023). A study by Hoek et al. (2016) showed that the cooperation of gut bacterial communities can enhance the tolerance of *E. nordenskioldi* to harsh environmental conditions in high-latitude cold regions. Thus, with the advancement of earthworm genomics research, especially studies based on whole genomes, the mechanisms of cold tolerance in alpine earthworms will be further elucidated.

The geographic isolation of the mountainous region in Northeast Asia is a primary driver of speciation within the *D. ghilarovi* complex. Through molecular and morphological analyses, the delimitation of the *D. ghilarovi* complex has been performed, with the description of a new endemic species likely resulting from allopatric speciation. In this study, two distinct lineages identified within the species *D. yanbianensis* sp. nov. in Helong (518R0) and Antu (520R0) counties exhibit a significant population genetic divergence, as evidenced by a 9.1% K2P distance.

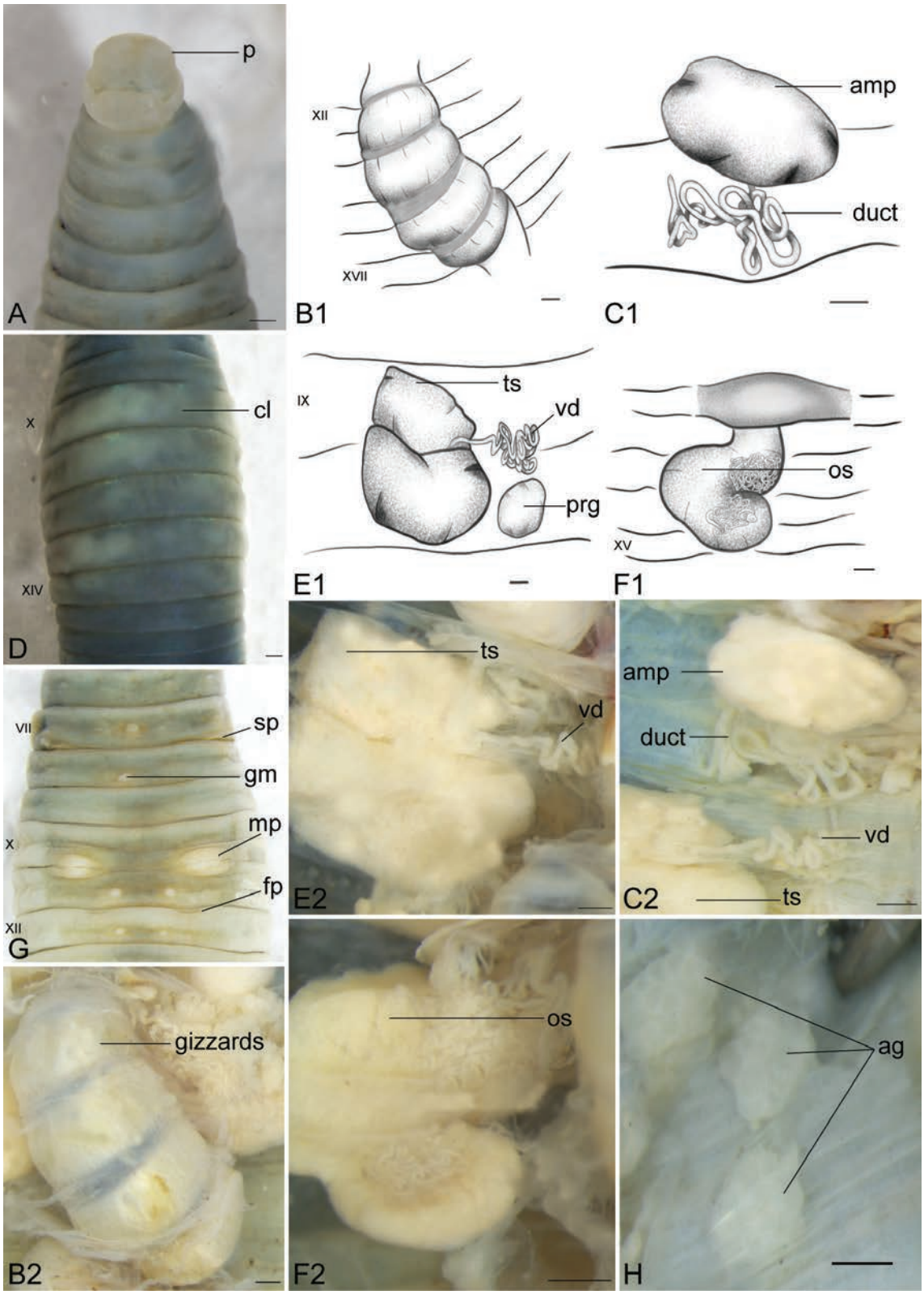

Figure 4. *Drawida yanbianensis* sp. nov.**,** holotype (520R0_06). **A.** Ventral view of the prostomium; **B1, B2.** Ventral view of gizzards; **C1, C2.** Left spermathecae; **D.** Dorsal view of clitellum region; **E1, E2.** Left testis sac and prostate gland; **F1, F2.** Left ovisac; **G.** Ventral view of genital markings and the spermathecal pores, male pores, female pores; **H.** Ventral view of right accessory glands. Scale bars: 0.5 mm.

This genetic differentiation suggests that these populations are likely undergoing the process of allopatric speciation (Shekhovtsov et al. 2022). An in-depth study of this complex in the future can help us better understand the evolutionary history of montane species in Northeast Asia.

It is widely acknowledged that the *D. ghilarovi* complex exhibits morphological conservatism, as referred to in the review by Narayanan et al. (2024). Consequently, the utilization of molecular data is deemed essential for the accurate delimitation of species within this complex.

The findings of this study indicate that the COI gene alone may potentially lead to an overestimation of species boundaries. In contrast, a multi-locus coalescence-based species delimitation approach, particularly when incorporating nuclear markers, demonstrates a significantly enhanced accuracy in the assignment and delineation of species (Fig. 3). This study exhibits additional potential species diversity in the *D. ghilarovi* complex in Northeast Asia, exemplified by the unresolved group as depicted in Fig. 1. This underscores the necessity for further taxonomic scrutiny of the complex. The subsequent step should involve integrative taxonomic analyses encompassing morphological, genetic, ecological, and behavioral data for the *D. ghilarovi* complex. Additionally, current phylogenetic and phylogeographic studies of the *D. ghilarovi* complex are notably deficient in molecular data from related species such as *D. csuzdii*, *D. guryeensis*, and *D. tairaensis*. This gap highlights the imperative for future research to address this shortfall and provide a more comprehensive understanding of the complex.

Conclusion

In this study, an integrative taxonomic approach, incorporating both morphological and molecular data, has been employed to delimit a new species, *D. yanbianensis* sp. nov., within the *D. ghilarovi* complex. This delimitation approach significantly augments taxonomic precision, thereby holding immense significance for the field of earthworm taxonomy. Furthermore, it contributes to the enrichment of the biodiversity of the Changbai Mountains region in Northeast China. This discovery is instrumental in deepening our understanding of the complexity and stability of the local ecosystem and offers valuable data and research opportunities for the conservation of biodiversity.

Acknowledgments

We thank Duc-Anh Nguyen for improving the manuscript. This study was supported by the Science and Technology Project of Hebei Education Department (BJ2025152), and by the Program of Central Guidance Fund for Local Science and Technology Development (246Z2907G), and by the Liaoning Province International Science and Technology Cooperation Program (2024JH2/101900024).

References

Atopkin DM, Ganin GN (2015) Genetic differentiation of black and grey colored forms of the earthworm *Drawida ghilarovi* Gates, 1969 (Moniligastridae, Oligochaeta) on Russian Far East. European Journal of Soil Biology 67: 12–16. https://doi.org/10.1016/j.ejsobi.2014.12.003

Bely AE, Wray GA (2004) Molecular phylogeny of naidid worms (Annelida: Clitellata) based on cytochrome oxidase I. Molecular Phylogenetics and Evolution 30: 50–63. https://doi.org/10.1016/S1055-7903(03)00180-5

Berman DI, Mescheryakova EN, Leirikh AN, Kurenshchikov DK (2010) Geographic range and cold hardiness of the earthworm *Drawida ghilarovi* (Oligochaeta, Moniligastridae). Biology Bulletin 37: 895–904. https://doi.org/10.1134/S1062359010090049.

Blakemore RJ (2009) Cosmopolitan Earthworms–A Global and Historical Perspective. In: Shain DH (Ed.) Annelids in Modern Biology. Wiley and Blackwell, New Jersy, 257–283. https://doi.org/10.1002/9780470455203.ch14

Blakemore RJ, Kupriyanova E, Grygier MJ (2010) Neotypification of *Drawida hattamimizu* Hatai, 1930 (Annelida, Oligochaeta, Megadrili, Moniligastridae) as a model linking mtDNA (COI) sequences to an earthworm type, with a response to the 'Can of Worms' theory of cryptic species. ZooKeys 41: 1–29. https://doi.org/10.3897/zookeys.41.374

Blakemore RJ, Lee S, Seo H-y (2014) Reports of *Drawida* (Oligochaeta: Moniligastridae) from far East Asia. Journal of Species Research 3: 127–166. https://doi.org/10.12651/JSR.2014.3.2.127

Briones MJI (1993) Two ecotypes in *Allolobophora caliginosa* (Oligochaeta, Lumbricidae). Acta Oecologica-international Journal of Ecology 14: 317–325.

Chang C-H, James S (2011) A critique of earthworm molecular phylogenetics. Pedobiologia 54: S3–S9. https://doi.org/10.1016/j.pedobi.2011.07.015

Darriba D, Taboada GL, Doallo R, Posada D (2012) jModelTest 2: more models, new heuristics and parallel computing. Nature Methods 9: 772. https://doi.org/10.1038/nmeth.2109

Dong Y, Jiang J, Zhang J, Shen Z, Sun J (2024) Three New Earthworm Species of the Genus *Metaphire* (Oligochaeta:Megascolecidae) From Eastern and Southern China. Chinese Journal of Zoology 59: 397–407. https://doi.org/10.13859/j.cjz.202423079

Drummond AJ, Suchard MA, Xie D, Rambaut A (2012) Bayesian phylogenetics with BEAUti and the BEAST 1.7. Molecular Biology and Evolution 29: 1969–1973. https://doi.org/10.1093/molbev/mss075

Edwards C (2004) The Importance of Earthworms as Key Representatives of the Soil Fauna. Earthworm Ecology, 3–11. https://doi.org/10.1201/9781420039719.pt1

Fayolle L, Michaud H, Cluzeau D, Stawiecki J (1997) Influence of temperature and food source on the life cycle of the earthworm *Dendrobaena Veneta* (Oligochaeta). Soil Biology and Biochemstry 29(3–4): 747–750. https://doi.org/10.1016/S0038-0717(96)00023-5

Flouri T, Jiao X, Rannala B, Yang Z (2018) Species Tree Inference with BPP Using Genomic Sequences and the Multispecies Coalescent. Molecular Biology and Evolution 35: 2585–2593. https://doi.org/10.1093/molbev/msy147

Folmer O, Black M, Hoeh W, Lutz R, Vrijenhoek R (1994) DNA primers for amplification of mitochondrial cytochrome c oxidase subunit I from diverse metazoan invertebrates. Molecular Marine Biology and Biotechnology 3: 294–299.

Fujisawa T, Barraclough TG (2013) Delimiting species using single-locus data and the Generalized Mixed Yule Coalescent approach: a revised method and evaluation on simulated data sets. Systematic Biology 62: 707–724. https://doi.org/10.1093/sysbio/syt033

Ganin GN, Atopkin DM (2018) Molecular differentiation of epigeic and anceic forms of *Drawida ghilarovi* Gates, 1969 (Moniligastridae, Clitellata) in the Russian Far East: Sequence data of two mitochondrial genes. European Journal of Soil Biology 86: 1–7. https://doi.org/10.1016/j.ejsobi.2018.02.004

Ganin GN, Anisimov AP, Roslik GY, Atopkin DM (2013) Earthworms *Drawida ghilarovi* Gates, 1969 (Oligochaeta, Moniligastridae): Polimorphism, geographic range, ecology specifics. Amurian Zoological Journal 4: 401–404. https://doi.org/10.13140/rg.2.1.2289.1041

Ganin GN, Anisimov AP, Roslik GY, Atopkin DM, Sokolova EN (2014) The Russian Far East endemic (*Drawida ghilarovi*, Oligochaeta, Moniligastridae): Polymorphism, ecology specifics and karyotype. Zoologicheskii Zhurnal 93: 1070–1079.

Gates GE (1969) On a new species of the moniligastrid earthworm genus *Drawida* Michaelsen, 1900. Zoologiceskij Zurnal 48: 674–676.

Gates GE (1972) Burmese earthworms. An introduction to the systematics and biology of megadrile oligochaetes with special reference to Southeast Asia. Transactions of the American Philosophical Society 62: 1–326. https://doi.org/10.2307/1006214

Gates GE (1982) Farewell to north American megadriles. Megadrilogica 4(1–2): 12–77.

Görres JH, Connolly ST, Chang C-H, Carpenter NR, Keller EL, Nouri-Aiin M, Schall JJ (2018) Winter hatching in New England populations of invasive pheretimoid earthworms *Amynthas agrestis* and *Amynthas tokioensis*: a limit on population growth, or aid in peripheral expansion? Biological Invasions 20: 1651–1655. https://doi.org/10.1007/s10530-018-1663-x

Goulpeau A, Penel B, Maggia ME, Marchán DF, Steinke D, Hedde M, Decaëns T (2022) OTU delimitation with earthworm DNA barcodes: A comparison of methods. Diversity 14(10): 866. https://doi.org/10.3390/d14100866

Hoek TA, Axelrod K, Biancalani T, Yurtsev EA, Liu J, Gore J (2016) Resource availability modulates the cooperative and competitive nature of a microbial crossfeeding mutualism. PLOS Biology 15(6): e1002606. https://doi.org/10.1371/journal.pbio.1002540

Hong Y (2002) New earthworms of the genus *Drawida* Michaelsen, 1900 (Oligochaeta: Moniligastridae) from Korea. Revue Suisse De Zoologie 109: 475–482. https://doi.org/10.5962/bhl.part.79602

Jamieson BGM (1977) On the phylogeny of the Moniligastridae, with description of new species of *Moniligaster* (Oligochaeta, Annelida). Evolutionary Theory 2: 95–114.

Kimura M (1980) A simple method for estimating evolutionary rates of base substitutions through comparative studies of nucleotide sequences. Joural of Molecular Evolution 16: 111–120. https://doi.org/10.1007/BF01731581

Luo A, Ling C, Ho SYW, Zhu C (2018) Comparison of Methods for Molecular Species Delimitation Across a Range of Speciation Scenarios. Systematic Biology 67: 830–846. https://doi.org/10.1093/sysbio/syy011

Misirlioğlu M, Reynolds JW, Stojanović M, Trakić T, Sekulić J, James SW, Csuzdi C, Decaëns T, Lapied E, Phillips HRP, Cameron EK, Brown GG (2023) Earthworms (Clitellata, Megadrili) of the world: an updated checklist of valid species and families, with notes on their distribution. Zootaxa 5255: 417–438. https://doi.org/10.11646/zootaxa.5255.1.33

Narayanan SP, Sathrumithra S, Christopher G, Julka JM (2017) New species and new records of earthworms of the genus *Drawida* from Kerala part of the Western Ghats biodiversity hotspot, India (Oligochaeta, Moniligastridae). ZooKeys 691: 1–18. https://doi.org/10.3897/zookeys.691.13174

Narayanan SP, Paliwal R, Thomas AP, Julka JM (2024) Catalogue of the moniligastrid earthworms (Clitellata, Moniligastrida, Moniligastridae) of the world. Zootaxa 5416: 1–66. https://doi.org/10.11646/zootaxa.5416.1.1

Nguyen TT, Lam DH, Tran BTT, Nguyen AD (2022) Two new *Drawida* (Oligochaeta, Moniligastridae) earthworms from Vietnam. ZooKeys 1099: 41–56. https://doi.org/10.3897/zookeys.1099.72112

Pérez-Losada M, Ricoy M, Marshall JC, Domínguez J (2009) Phylogenetic assessment of the earthworm *Aporrectodea caliginosa* species complex (Oligochaeta: Lumbricidae) based on mitochondrial and nuclear DNA sequences. Molecular Phylogenetics and Evolution 52: 293–302. https://doi.org/10.1016/j.ympev.2009.04.003

Piearce TG, Oates K, Carruthers WJ (1990) A fossil earthworm embryo (Oligochaeta) from beneath a Late Bronze Age midden at Potterne, Wiltshire, UK. Journal of Zoology 220: 537–542. https://doi.org/10.1111/j.1469-7998.1990.tb04732.x

Pop AA, Wink M, Pop VV (2003) Use of 18S, 16S rDNA and cytochrome c oxidase sequences in earthworm taxonomy (Oligochaeta, Lumbricidae). Pedobiologia 47: 428–433. https://doi.org/10.1078/0031-4056-00208

Puillandre N, Lambert A, Brouillet S, Achaz G (2021) ASAP: assemble species by automatic partitioning. Molecular Ecology Resources 21: 609–620. https://doi.org/10.1111/1755-0998.13281

Rambaut A (2018) Figtree 1.4.4. http://tree.bio.ed.ac.uk/software/figtree/ [accessed 25 November.2018]

Rambaut A, Drummond AJ, Xie D, Baele G, Suchard MA (2018) Posterior Summarization in Bayesian Phylogenetics Using Tracer 1.7. Systematic Biology 67: 901–904. https://doi.org/10.1093/sysbio/syy032

Richardson DR, Bruce AS, Paul FH (2009) Soil Moisture and Temperature: Tolerances and Optima for a Non-Native Earthworm Species, *Amynthas agrestis* (Oligochaeta: Opisthopora: Megascolecidae). Southeastern Naturalist 8: 325–334. https://doi.org/10.1656/058.008.0211

Ronquist F, Teslenko M, van der Mark P, Ayres DL, Darling A, Hohna S, Larget B, Liu L, Suchard MA, Huelsenbeck JP (2012) MrBayes 3.2: efficient Bayesian phylogenetic inference and model choice across a large model space. Systematic Biology 61: 539–542. https://doi.org/10.1093/sysbio/sys029

Shekhovtsov SV, Golovanova EV, Peltek SE (2013) Cryptic diversity within the Nordenskiold's earthworm, *Eisenia nordenskioldi* subsp. *nordenskioldi* (Lumbricidae, Annelida). European Journal of Soil Biology 58: 13–18. https://doi.org/10.1016/j.ejsobi.2013.05.004

Shekhovtsov SV, Berman DI, Bulakhova NA, Makarova OL, Peltek SE (2018) Phylogeography of earthworms from high latitudes of Eurasia. Acta Zoologica Academiae Scientiarum Hungaricae 64: 369–382 https://doi.org/10.17109/AZH.64.4.369.2018

Shekhovtsov SV, Golovanova EV, Ershov NI, Poluboyarova TV, Berman DI, Bulakhova NA, Szederjesi T, Peltek SE (2020) Phylogeny of the *Eisenia nordenskioldi* complex based on mitochondrial genomes. European Journal of Soil Biology 96: 103137. https://doi.org/10.1016/j.ejsobi.2019.103137

Shekhovtsov SV, Shipova AA, Bulakhova NA, Berman DI (2022) Differentiation within the *Drawida ghilarovi* complex (Moniligastridae: Annelida) revealed by multigene transcriptomic dataset analysis. European Journal of Soil Biology 111: 103411. https://doi.org/10.1016/j.ejsobi.2022.103411

Shekhovtsov SV, Vasiliev G, Latif R, Poluboyarova TV, Peltek SE, Rapoport I (2023) The mitochondrial genome of *Dendrobaena tellermanica* Perel, 1966 (Annelida: Lumbricidae) and its phylogenetic position. Vavilov Journal of Genetics and Breeding 27: 146–152. https://doi.org/10.18699/VJGB-23-20

Sims RW, Gerard BM (1985) Earthworms: keys and notes for the identification and study of the species. Linnean Society of London and the Estuarine and Brackish-Water Sciences Association, London, 31 pp. https://doi.org/10.1163/9789004611405

Stamatakis A (2014) RAxML version 8: a tool for phylogenetic analysis and post-analysis of large phylogenies. Bioinformatics 30: 1312–1313. https://doi.org/10.1093/bioinformatics/btu033

Stephenson J. (1923) The Fauna of British India, including Ceylon and Burma—Oligochaeta. Taylor and Francis, London, 117–182.

Tamura K, Peterson D, Peterson N, Stecher G, Nei M, Kumar S (2011) MEGA5: molecular evolutionary genetics analysis using maximum likelihood, evolutionary distance, and maximum parsimony methods. Molecular Biology and Evolution 28: 2731–2739. https://doi.org/10.1093/molbev/msr121

Thakur SS, Lone AR, Tiwari N, Jain SK, James SW, Yadav S (2021) A contribution to the earthworm diversity (Clitellata, Moniligastridae) of Kerala, a component of the Western Ghats biodiversity hotspot, India, using integrated taxonomy. Animal Biodiversity and Conservation 44: 117–137. https://doi.org/10.32800/abc.2021.44.0117

Yang Z (2015) The BPP program for species tree estimation and species delimitation. Current Zoology 61: 854–865 https://doi.org/10.1093/czoolo/61.5.854

Yang Z, Rannala B (2010) Bayesian species delimitation using multilocus sequence data. Proc Natl Acad Sci USA 107: 9264. Proceedings of the National Academy of Sciences of the United States of America 107: 9264–9269. https://doi.org/10.1073/pnas.0913022107

Yang X, Xu M (2003) Biodiversity conservation in Changbai Mountain Biosphere Reserve, northeastern China: status, problem, and strategy. Biodiversity and Conservation 12: 883–903. https://doi.org/10.1023/A:1022841107685

Yang Y, Callaham MA, Wu X, Zhang Y, Wu D, Wang D (2023) Gut microbial communities and their potential roles in cellulose digestion and thermal adaptation of earthworms. Science of The Total Environment. 903(4): 166666. https://doi.org/10.1016/j.scitotenv.2023.166666.

Zhang Y, Ganin GN, Atopkin DM, Wu D (2020) Earthworm *Drawida* (Moniligastridae) Molecular phylogeny and diversity in Far East Russia and Northeast China. The European Zoological Journal 87: 180–191. https://doi.org/10.1080/24750263.2020.1741705

Zhang Y, Atopkin DM, Wang L, Wu D (2021) Description of a new earthworm species of the genus *Drawida* (Oligochaeta: Moniligastridae) from Northeast China and Far East Russia. Journal of Asia-Pacific Biodiversity 14: 425–429. https://doi.org/10.1016/j.japb.2021.03.006

Zhao H, Fan S, Aspe NM, Feng L, Zhang Y (2022) Characterization of 15 Earthworm Mitogenomes from Northeast China and Its Phylogenetic Implication (Oligochaeta: Lumbricidae, Moniligastridae). Diversity-Basel 14: 714. https://doi.org/10.3390/d14090714

Supplementary material 1

The intraspecific K2P distances of COI of *D. yanbianensis* sp. nov.

Authors: Min Liu, Jiangni Li, Yufeng Zhang, Nonillon M. Aspe, Donghui Wu, Huifeng Zhao, Guo Zheng

Data type: docx

Link: https://doi.org/10.3897/zse.101.146587.suppl1

Supplementary material 2

The time framework of the *Drawida ghilarovi* species complex was calibrated using a nucleotide substitution rate of 2.4% per site per million years for the COI gene

Authors: Min Liu, Jiangni Li, Yufeng Zhang, Nonillon M. Aspe, Donghui Wu, Huifeng Zhao, Guo Zheng

Data type: ai

Link: https://doi.org/10.3897/zse.101.146587.suppl2

Zoosyst. Evol. 101 (2) 2025, 643–660 | DOI 10.3897/zse.101.143936

PENSOFT

für Natur MUSEUM FÜR NATURKUNDE BERLIN

A revision of Bithyniidae (Mollusca, Gastropoda) from the Inle Lake Basin, Myanmar

Le-Jia Zhang[1,2,3], Shu-Sen Shu[1,2,3], Xin-Yuan Song[1,2,3], Nay Htet Naing[1,2,3], Thaung Naing Oo[4], Xiao-Yong Chen[1,2,3]

1 *Southeast Asia Biodiversity Research Institute, Chinese Academy of Sciences, Yezin, Nay Pyi Taw, 05282, Myanmar*

2 *Yunnan Key Laboratory of Biodiversity and Ecological Conservation of Gaoligong Mountain, Kunming Institute of Zoology, Chinese Academy of Sciences, Kunming 650023, China*

3 *Yunnan International Joint Laboratory of Southeast Asia Biodiversity Conservation, Mengla 666303, China*

4 *Forest Department, Ministry of Natural Resources and Environmental Conservation, Nay Pyi Taw 15015, Myanmar*

https://zoobank.org/C0F8018F-646D-491E-A749-715896CBF713

Corresponding author: Xiao-Yong Chen (chenxy@mail.kiz.ac.cn)

Academic editor: Frank Köhler ♦ **Received** 9 December 2024 ♦ **Accepted** 11 February 2025 ♦ **Published** 24 March 2025

Abstract

Inle Lake, located on the Shan Plateau of Myanmar, is the only ancient lake on the Indochinese Peninsula and a biodiversity hotspot of freshwater fauna with high diversity and endemism, including molluscs. However, recent research on its biodiversity remains limited. Based on morphological, anatomical, and molecular studies, we systematically revise the freshwater snails of the family Bithyniidae from the Inle Lake basin. We provide an updated re-description of four bithyniid species within three genera from the Inle Lake basin, including one new record, *Digoniostoma iravadica* **comb. nov.** The endemic genus *Parabithynia* **syn. nov.** with one endemic species of Inle Lake, *Hydrobioides physcus* **comb. rev.**, is considered a synonym of *Hydrobioides*. *Gabbia nana* **comb. nov.** is assigned to *Gabbia* based on shell morphology and molecular phylogeny. *Hydrobioides dautzenbergi* **stat. rev.** from Thailand is recognised as a valid species rather than a synonym of *Hydrobioides nassa*, which is endemic to Shan State of Myanmar. There are altogether seven bithyniid species recorded from the Inle Lake basin and surrounding area, including four endemic species.

Key Words

Ancient lake, bithyniid snail, phylogeny, radula, Shan State, taxonomy

Introduction

Inle Lake, located on the southern Shan Plateau, is the second largest lake in Myanmar and the only ancient lake on the Indochinese Peninsula, which was formed around 1.5 million years ago; despite its relatively small size (covering about 116 square kilometres) and shallow depth (averaging only two meters), Inle Lake supports remarkable freshwater biodiversity and endemism, similar to other ancient lakes such as Baikal, Tanganyika, and Biwa (Hampton et al. 2018). There are 13 families and 28 genera of fish native to the Inle Lake basin, including 15 endemic species (Kano et al. 2016); 36 species of freshwater molluscs, including 18 endemic species, have been recorded from the Inle Lake basin (Annandale 1918; Annandale and Rao 1925).

Bithyniidae is one of the most common families of freshwater snails in the Inle Lake basin. This diverse and common family of freshwater snails is widely distributed across Africa, Eurasia, and Australia, inhabiting rivers, wetlands, ponds, and lakes. It also includes *Helicostoa*, the only known group of obligate sessile freshwater snails (Zhang et al. 2024a). Annandale (1918) recorded and described altogether six bithyniid species from the Inle Lake basin and surrounding areas: *Hydrobioides turrita* (Blanford, 1869) (subfossils from Heho), *Hydrobioides nassa*

(Theobald, 1866), *Parabithynia physcus* (Annandale, 1918), *Hydrobioides avarix* Annandale, 1918, *Hydrobioides nana* Annandale, 1918, and *Gabbia alticola* (Annandale, 1918). Of these, four species (*P. physcus, H. avarix, H. nana, G. alticola*) and one genus, *Parabithynia* Pilsbry, 1928, were considered endemic to the Inle Lake basin. Sawada (2022) revisited Annandale's historical malacological collection from Inle Lake, kept in the Kyoto University Museum, including the dry-shell specimens of three bithyniid species (*H. nassa, P. physcus, G. alticola*). However, since the works of Annandale and Rao (Annandale and Rao 1925; Rao 1928), there have been almost no published modern studies and collected records of freshwater snails from the Inle Lake basin or even Shan State.

In July 2024, we conducted comprehensive fieldwork for freshwater fauna in the Inle Lake basin, collecting a diverse assemblage of freshwater molluscs, including bithyniid snails. The present study aims to provide a systematic revision and re-description of bithyniid snails from the Inle Lake basin based on shell morphology, anatomy, and molecular study, after a nearly century-long gap in research on this biodiversity hotspot of freshwater fauna.

Materials and methods

Materials

Seven type specimens of three species (one for *Hydrobioides nassa*, three for *Hydrobioides physcus*, three for *Hydrobioides avarix*) were examined from the Natural History Museum, London (**NHMUK**). Fieldwork was conducted in the Inle Lake basin from 1 Jul. 2024 to 11 Jul. 2024. The samples of bithyniid snails were collected in five localities (Fig. 1B); the types of habitats included lake, rice field, shallow pond, wetland, and river (details see in Systematic Descriptions). The samples were fixed using 75% ethanol and then preserved in analytical pure ethanol. Additional materials for comparison were collected in Mandalay Region and mountains of Kalaw Township (Shan State) (details see in Systematic descriptions: *Hydrobioides nassa, Digoniostoma iravadica*). The newly collected specimens are deposited in the Kunming Institute of Zoology, Chinese Academy of Sciences, Kunming (**KIZ**), and the Southeast Asia Biodiversity Research Institute, Chinese Academy of Sciences, Yezin, Nay Pyi Taw (**SEABRI**).

Examination of morphology

The shell height (H) and width (W) were measured with a calliper to a precision of 0.01 mm. The specimens were photographed in a consistent orientation using focus stacking methods with a Nikon® Z5 camera and a Nikon® Nikkor Z MC 105mm f/2.8 VR lens. S. Zerene Stacker 1.04 software was used to do focus stacking. Radulae were extracted through dissection; radulae were cleaned by boiling in 1% NaOH solution for half an hour and rinsed with distilled water. Radulae and operculum were coated with gold before scanning electron microscopy with a Zeiss® Sigma 300 scanning electronic microscope. The male genital structure of the snail was examined during dissection and photographed under a stereomicroscope. The terms used for describing the operculum are according to Zhang and von Rintelen (2021). The newly collected specimens were identified based on the description of shell, radula, male genitalia, and collecting locality provided by Annandale (1918), Rao (1989), and comparisons to type specimens. Abbreviations of radula: **ct**–central teeth; **lt**–lateral teeth; **imt**–inner marginal teeth; **omt**–outer marginal teeth.

Molecular methods

DNA was extracted from 10–20 mg of foot tissue of each snail using a mollusc-specific CTAB/chloroform 112 extraction protocol (Winnepenninckx et al. 1993). A fragment of the mitochondrial 16S gene was amplified through polymerase chain reaction (PCR) with the following primer pairs: LCO1490, 5′-GGTCAACAAATCATAAAGATATTGG-3′, and COX-B7R, 5′-ACCACCAGCTGGATCAAAAA-3′ (Schultheiß et al. 2011) for COI; 16Sar-L, 5′-CGCCTGTTTATCAAAAACAT-3′, and 16Sbr-H, 5′-CCGGTCTGAACTCAGATCACGT-3′ (Palumbi et al. 2002). PCR amplifications were conducted in volumes of 30 μL under the following cycling conditions: an initial denaturing step at 94 °C for 10 min, followed by 35 cycles of 94 °C for 1 min, 50 °C for 1 min (COI) or 52 °C for 30 s (for 16S), and 72 °C for 1 min, with a final extension step of 10 min at 72 °C. The purification and sequencing were conducted by Sangon Biotech.

Sequence and phylogenetic analyses

New sequences of four species have been uploaded to GenBank; 46 sequences of 25 bithyniid species were included in the present study (Suppl. material 1). *Amnicola dalli* (AY622435) of family Amnicolidae was selected as the outgroup based on Zhang et al. (2024b). Sequences were aligned using MUSCLE as implemented in Geneious (https://www.geneious.com). Genetic distances were calculated using MEGA X (Kumar et al. 2018). GTR+G was suggested as the best-fit model of sequence evolution for our dataset by means of the Akaike and Bayesian information criteria in MEGA X. A Bayesian inference (BI) analysis was performed with MrBayes 3.2.6 (Ronquist et al. 2012) as implemented in Geneious with four independent chains for 5,000,000 generations, sample freq = 1,000, burnin = 25%, and it was confirmed that convergence was reached based on the trace plots generated in Geneious Prime 2020. A maximum likelihood (ML) analysis was conducted with RAxML as implemented in Geneious, with support estimated by 1,000 bootstrap replicates (Kozlov et al. 2019).

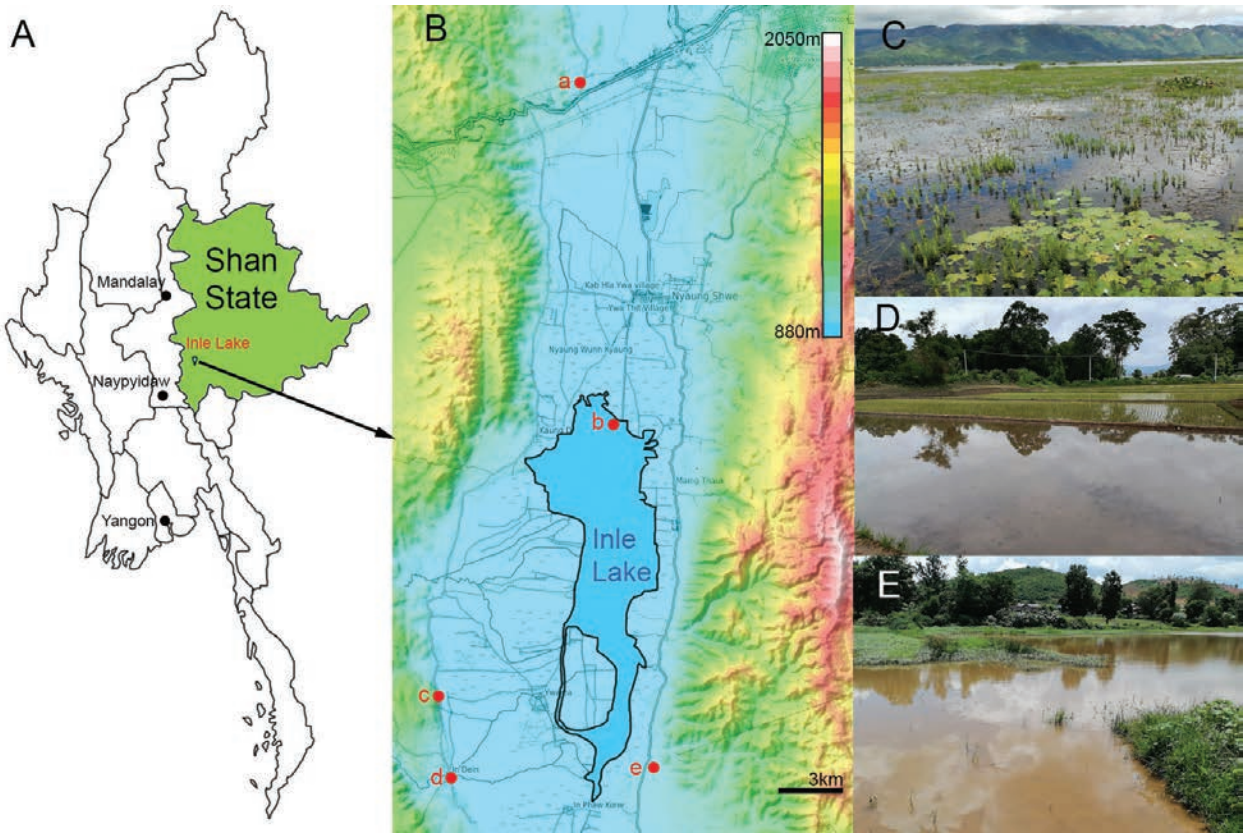

Figure 1. Collecting sites of bithyniid snails in the Inle Lake basin. **A.** A map of Myanmar showing the location of Shan State and Inle Lake; **B.** A red dot (site a to e) showing the collecting sites in the Inle Lake basin, an altitude map modified based on the resources from https://topographic-map.com (license offered by the website builder Guillaume VK); **C.** Habitat at the site b, Inle Lake; **D.** Habitat at the site e, rice field; **E.** Habitat at the site a, shallow pond.

Results

Molecular phylogeny

The molecular tree (Fig. 2) reveals that *Hydrobioides* is not a monophyletic group. *Hydrobioides dautzenbergi* is the sister group of a clade including species of *Hydrobioides*, *Gabbia*, and *Digoniostoma*. *Hydrobioides nassa* is the sister species of *Hydrobioides physcus*. *Gabbia nana* is a distinct species, clustered with *Gabbia pygmaea*. *Digoniostoma* is a highly supported monophyletic group, which is sister to genus *Gabbia*. *Digoniostoma iravadica* is a distinct species clustered with the clade including *Digoniostoma funiculata*, *Digoniostoma siamensis siamensis*, and *Digoniostoma siamensis goniomphalos*. Four subfamilies of Bithyniidae (Parafossarulinae, Bithyninae, Helicostoinae, Mysorellinae) are generally supported by the tree. All the species from the Inle Lake basin belong to the subfamily Mysorellinae.

Systematic descriptions

Class Gastropoda Cuvier, 1795
Order Littorinimorpha Golikov & Starobogatov, 1975
Family Bithyniidae Gray, 1857

Subfamily Mysorellinae Annandale, 1920

***Hydrobioides* Nevill, 1885**

Hydrobioides Nevill, 1885: 42.
Paranerita Annandale, 1920: 4.
Parabithynia Pilsbry, 1928, syn. nov.: 108.
Bithynia (*Parabithynia*) – Popova et al. 1970: 95.

Type species. *Fairbankia turrita* Blanford, 1869 (original designation; Myanmar, Irrawaddy River, "Kyoukpong").

Diagnosis. Shell medium for the family, solid, aperture lip thickened, outer lip outward extended; penial appendix located in the central of penis, penial appendix slightly shorter than distal part of penis.

Remarks. According to Molluscabase (2024a), there are six extant valid species assigned to this genus; five species are described from Myanmar, and one species is described from Laos. The type species of this genus is *Hydrobioides turrita* (Blanford, 1869) with high spiral whorls and an extremely outward extended outer lip (Fig. 3P); its type locality is "Kyoukpong" near the Irrawaddy River in Myanmar (probably referring to Kyouk Pon near Bagan in the Mandalay Region), and it was also collected from Heho near the Inle Lake basin as subfos-

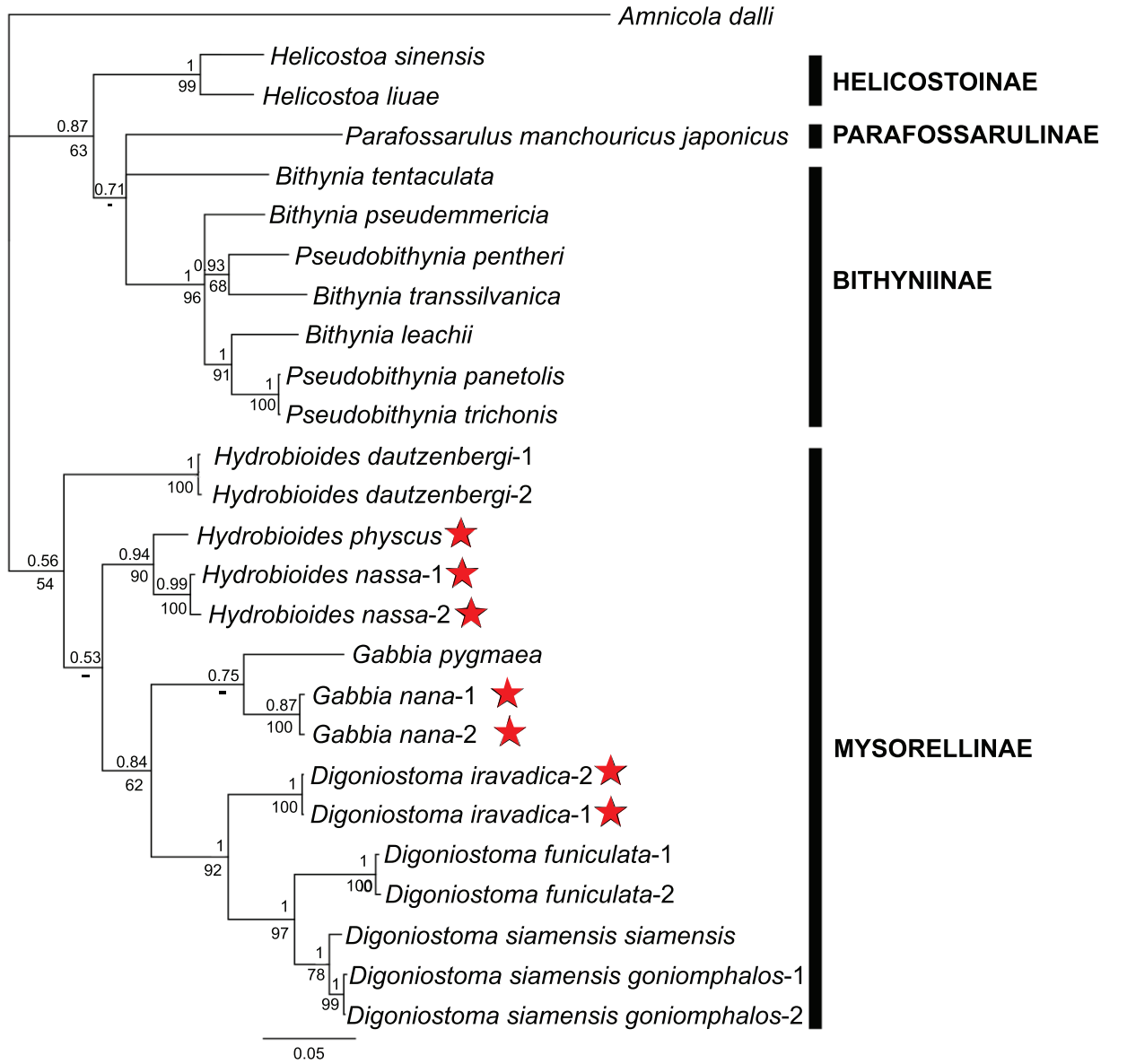

Figure 2. Bayesian inference phylogram based on partial COI and 16S sequences of the selected bithyniid snails, with an emphasis on species from the Inle Lake basin (red star). Numbers above branches are BI posterior probabilities, and numbers underneath branches are ML bootstrap values.

sils (Annandale 1918). However, this species has never been collected again since Annandale (1918). Based on shell characters of *Hydrobioides turrita*, we consider that the outward extended outer lip is the most important morphological diagnosis character for this genus. *Hydrobioides nassa* is always considered widely distributed in north to central Thailand, but we consider that the Thai population should be another species (see in remarks of *Hydrobioides nassa*). We consider that *Parabithynia* Pilsbry, 1928, should be a synonym of *Hydrobioides* (see in remarks of *Hydrobioides physcus*). The molecular study based on 16S and COI does not support *Hydrobioides* as a monophyletic group (Fig. 2). The taxonomy of this genus needs systematic revision.

Hydrobioides nassa (Theobald, 1866)

Bithinia nassa Theobald, 1866: 275 (Myanmar, Shan State).

Hydrobioides nassa – Annandale, 1918: 118–120, pl. 13, figs 1–7, pl. 14, figs 4, 4a.

Hydrobioides nassa distoma Annandale, 1918 †: 120, pl. 13, fig. 1 (Myanmar, Shan States, Heho plain).

Hydrobioides nassa lacustris Annandale, 1918: 119, pl. 13, figs 4, 4a, 5, 5a, 7 (Myanmar, Shan States, Inle Lake).

Hydrobioides nassa rivicola Annandale, 1918: 119–120, pl. 13, figs 6, 6a (Myanmar, Shan States, small streams at Thamakan).

Diagnosis. Shell medium, high spiral whorls, a varix near outer lip, outer lip outward extended.

Material examined. • 1 ***syntype*** (preserved dry), Upper Salwin River, Purchase of W. Theobald, NHMUK.1888.12.4.845; 3 specimens (preserved in ethanol), Shan State, Taunggyi District, Taungpoetgyi, near Tone Lae, river near spring (Fig. 1B. c), 20°29'48.9"N, 96°50'17.5"E, 2 Jul. 2024, Le-Jia Zhang leg., KIZ.2400054–2400056 • 2 specimens (preserved in ethanol), Shan State, Taunggyi District, Nyaungshwe, Inle Lake, floating islands near Intha (Fig. 1B. b), 20°36'33.4"N, 96°54'53.8"E, 3 Jul. 2024, Le-Jia Zhang leg., KIZ.2400057–2400058 • 2 specimens (preserved in ethanol), Shan State, Taunggyi District, Kalaw, river near Nanthe' Cafe Garden, 20°36'30.6"N, 96°33'55.3"E, 11 Jul. 2024, Le-Jia Zhang leg., KIZ.2400059–2400060.

Description. Shell (Fig. 3) medium for the family (Table 1), thin but solid, conical, bright yellow or olive grey, with five whorls at adulthood; teleoconch relatively high, smooth, without shoulder, a weak to strong varix structure on the body whorl, close to or directly connected to the outer lip; aperture ovate, lip thickened, nearly half of shell in height, outer lip outward extended; umbilicus covered by inner lip completely.

Operculum (Fig. 3E, 4A) calcium, ovate, thin, slightly smaller than aperture, transparent grey; exterior surface smooth, nucleus close to the inner opercular margin; interior surface with wide concentric veins on inner opercular region, nuclear region relatively small, with irregular veins.

Penis (Fig. 5A) with a grey penial appendix located in the central of penis, penial appendix slightly shorter than distal part of penis.

Radula (Fig. 6) taenioglossate (2 + 1 + 1 + 1 + 2); central tooth upper margin with one broad triangle central cusp and two to three small sharp cusps on either side, lateral margin each with two to three small sharp cusps; lateral tooth with one broad tongue-shape central cusp and three to four small sharp cusps; inner marginal tooth with 14 to 15 small cusps; outer marginal tooth with eight to nine small cusps.

Remarks. This species can be easily distinguished from other bithyniid snails based on the varix structure near the outer lip. The location of varix can be relatively far from the outer lip (Fig. 3I–M), viz. "*Hydrobioides nassa lacustris*" (Fig. 3N), mostly found in Inle Lake; the varix also can be directly connected to the outer lip (Fig. 3E–H), viz. "*Hydrobioides nassa rivicola*" (Fig. 3O), mostly found in rivers. However, there is no clear boundary between these two morphotypes. The syntype is quite similar to the "*lacustris* "type but much bigger than the newly collected specimens (Fig. 3A–D). This species was considered widely distributed in north to central Thailand. However, "*Hydrobioides nassa*" from Thailand does not have an obvious varix and an extended outward outer lip, and the molecular analysis has confirmed that the Thailand species is distinct from *Hydrobioides nassa* from the type locality, Shan State of Myanmar (Fig. 2). Therefore, we consider that *Hydrobioides dautzenbergi* Walker, 1927, stat. rev. (type locality: Thailand, Chieng Mai) should be a valid species name for the "*Hydrobioides nassa*" from Thailand. *Hydrobioides nassa* is probably endemic to Shan State, Myanmar.

Habitat and distribution. Rivers, ponds, wetlands, and lakes of Shan State, Myanmar.

Values are arithmetic means, standard deviations, maximum and minimum values (in brackets) of shell height (H), shell width (W), and aperture height (AH) of *n* measured specimens.

Hydrobioides physcus Annandale, 1918, comb. rev.

Hydrobioides physcus Annandale, 1918: 121–122, pl. 13, figs 8, 8a, 9, pl. 14, figs 5, 5a (Myanmar, Shan State, Inle Lake).
Hydrobioides (*Paranerita*) *physcus*–Annandale, 1920: 45.
Paranerita physcus – Annandale & Rao, 1925: 115.
Parabithynia physcus – Pilsbry, 1928: 108
Gabbia physcus – Subba Rao, 1989: 78, figs 127–129.

Diagnosis. Shell medium, low spiral whorls, weak keel on shoulder, outer lip outward extended.

Material examined. • 3 probable ***paratypes*** (preserved dry), Inle Lake, South Shan, Burma. "Ex. India Museum", NHMUK.20060144; 2 specimens (preserved in ethanol), Shan State, Taunggyi District, Inn Paw Hkon, Inthein, riverbank under Inthein Bridge (Fig. 1B. d), 20°27'35.9"N, 96°50'32.6"E, 1 Jul. 2024, Le-Jia Zhang leg., KIZ.2400061–2400062 • 2 specimens (preserved in ethanol), Shan State, Taunggyi District, Nyaungshwe, Inle Lake, floating islands near Intha (Fig. 1B. c), 20°36'33.4"N, 96°54'53.8"E, 3 Jul. 2024, Le-Jia Zhang leg., KIZ.2400063–2400064.

Description. Shell (Fig. 7) medium for the family (Table 1), relatively thick, solid, subglobose to globose, white or bright yellow to orange yellow, with four whorls at adulthood; teleoconch low, with a keel on shoulder, forming weak nodules on shoulder with vertical growth lines, two weak additional keels on body whorl; aperture ovate, lip thickened, always more than half of shell in height, outer lip outward extended; umbilicus covered by inner lip completely.

Operculum (Figs 7A, 4B) calcium, ovate, thin, slightly smaller than aperture, transparent grey; exterior surface smooth, nucleus close to the central of operculum; interior surface with relatively thin outer opercular region, narrow weak concentric veins on the margin of inner opercular region, nuclear region relatively large, with irregular veins and grains.

Penis (Fig. 5B) with a white penial appendix located in the central of penis, penial appendix slightly shorter than distal part of penis.

Radula (Fig. 8) taenioglossate; central tooth upper margin with one broad triangle central cusp and two to three small sharp cusps on either side, lateral margin each with two to three small sharp cusps; lateral tooth with one broad tongue-shape central cusp and two to three small sharp cusps; inner marginal tooth with 10 to 11 small cusps; outer marginal tooth with six small cusps.

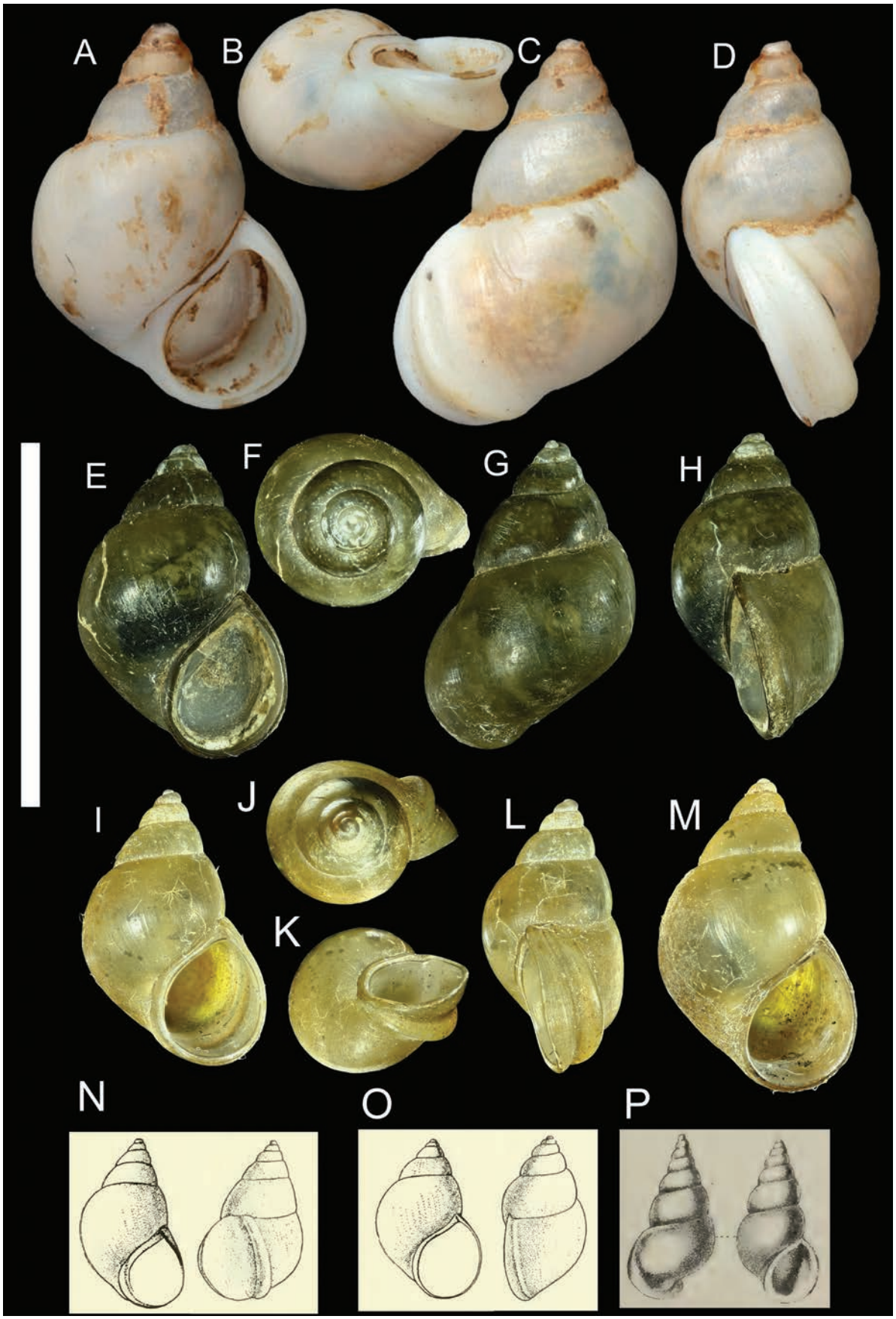

Figure 3. Shell of *Hydrobioides nassa* (**A–O**) and *Hydrobioides turrita* (P). **A–D**. NHMUK.1888.12.4.845, Syntype of *Bithinia nassa*, from Natural History Museum (2014); **E–H.** KIZ.2400057, Kalaw; I–M, KIZ.2400054 (I–L), 2400055 (M), Inle Lake; **N.** "*Hydrobioides nassa lacustris*" from Annandale, 1918; **O.** "*Hydrobioides nassa rivicola*" from Annandale, 1918; **P.** "Bythinea(?) trrita" from Nevill (1881). Scale bars: 1 cm (**A–I**).

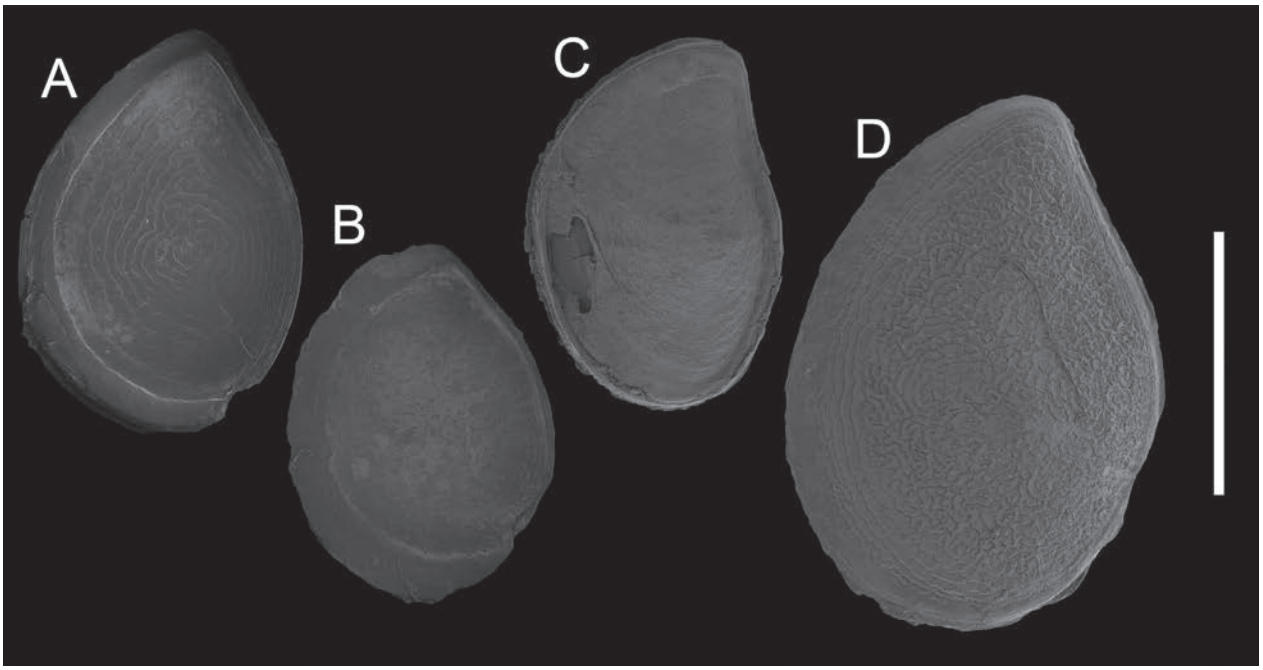

Figure 4. SEM photo of the opercular inner surface of bithyniid snails from the Inle Lake basin. **A.** *Hydrobioides nassa*; **B.** *Hydrobioides physcus*; **C.** *Gabbia nana*; **D.** *Digoniostoma iravadica*. Scale bars: 1 mm.

Table 1. Shell measurements of bithyniid snails from the Inle Lake basin.

Species	*n*	H	W	AH	W/H	AH/H
Hydrobioides nassa	6	7.97 ± 0.76 (6.57–8.87)	5.23 ± 0.49 (4.3–5.69)	4.23 ± 0.35 (3.67–4.57)	0.66 ± 0.01 (0.64–0.69)	0.53 ± 0.03 (0.5–0.57)
Hydrobioides physcus	4	5.94 ± 0.27 (5.52–6.18)	5.19 ± 0.11 (5.08–5.36)	4.02 ± 0.20 (3.75–4.29)	0.88 ± 0.03 (0.84–0.92)	0.68 ± 0.03 (0.64–0.7)
Hydrobioides avarix	2	(6.57–6.7)	(4.43–4.48)	(3.42–3.48)	(0.67)	(0.52)
Gabbia nana	9	4.54 ± 0.38 (3.74–5.15)	3.44 ± 0.27 (2.87–3.77)	2.64 ± 0.20 (2.23–2.92)	0.76 ± 0.02 (0.73–0.79)	0.58 ± 0.02 (0.57–0.62)
Digoniostoma iravadica	6	12.06 ± 0.42 (11.42–12.65)	6.91 ± 0.22 (6.55–7.28)	6.22 ± 0.29 (5.82–6.65)	0.57 ± 0.02 (0.55–0.61)	0.52 ± 0.02 (0.48–0.53)

Remarks. This species can be easily distinguished from other bithyniid snails based on the thick subglobose to globose shell with keels and shoulder. It also can be distinguished from *H. nassa* based on opercular characters and less small cusps on inner and outer marginal teeth. This species is the type species and only extant species of genus *Parabithynia* Pilsbry, 1928, which is now endemic to Inle Lake. Several fossil species of this genus were reported from China and Russia (Popova 1981; Yu et al. 1978), but the assignment needs a revision. Our molecular study confirms that this species is the sister species of *H. nassa*, with a close genetic relationship (p distance of 16S: 4.3–4.5%). The similarity in shell (especially the extended outer lip), operculum, and male genital structure also supports that these two species should be placed in one genus. Therefore, we consider that *Parabithynia* is a synonym of *Hydrobioides*. *Hydrobioides physcus* comb. rev. should be re-assigned to its original genus.

Habitat and distribution. Inle Lake and the big rivers connected to Inle Lake; swamps in Heho, Shan State, Myanmar.

Hydrobioides avarix Annandale, 1918

Hydrobioides avarix Annandale, 1918: pl. 14, figs 1, 2, 2a, 2b, 2c (Myanmar, Shan State, NW shore of Inle Lake, a stream near Fort Stedman, now Maing Thauk).

Material examined. • 3 probable ***syntypes*** (preserved dry), Inle Lake, South Shan, Burma. "Ex. India Museum", NHMUK.20060143.

Remarks. We did not discover this species during our fieldwork and only examined three probable syntypes. The detailed descriptions of shell, operculum, radula, and male genitalia of this species have been given by Annandale (1918). This species can be distinguished from *Hydrobioides nassa* by more inflated whorls and a simple outer lip without the varix structure nearby. It can be distinguished from *Gabbia nana* comb. nov. based on a larger and thinner shell with less inflated whorls and an operculum, which is much smaller than the aperture. The validity and genus assignment of this species need further study based on fresh specimens.

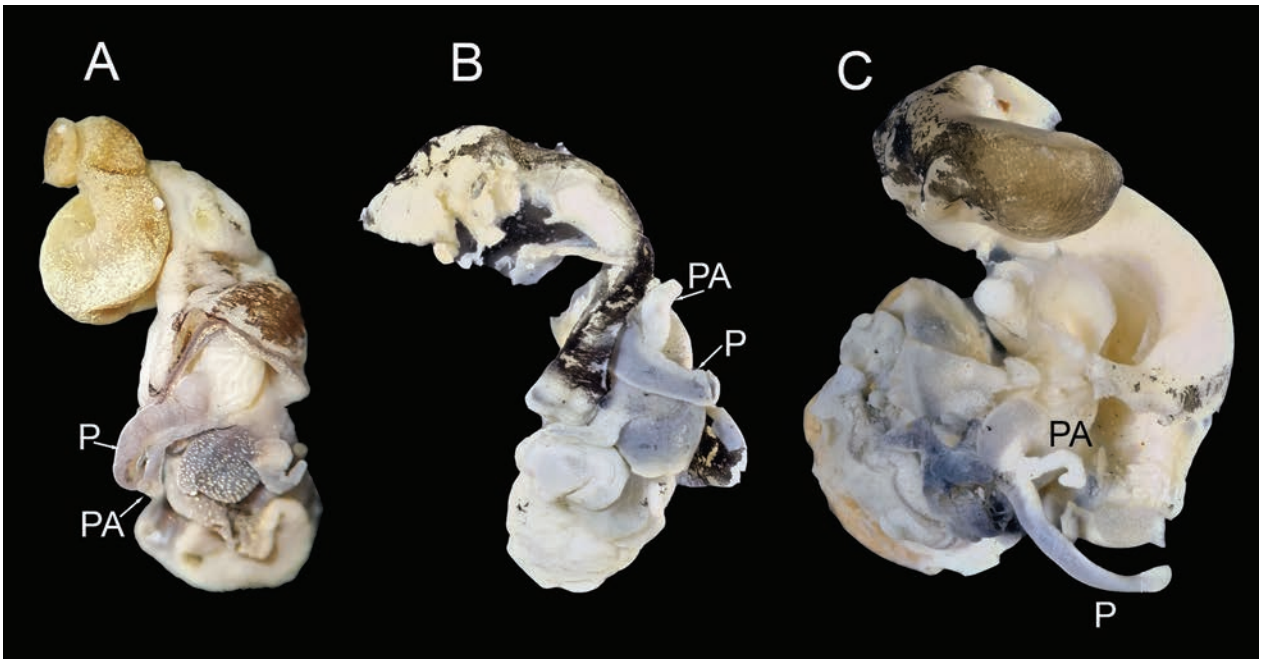

Figure 5. Male genitalia of bithyniid snails from the Inle Lake basin. **A.** *Hydrobioides nassa*; **B.** *Hydrobioides physcus*; **C.** *Digoniostoma iravadica*. P refers to penis; PA refers to penial appendix.

Gabbia Tryon, 1865

Type species. *Gabbia australis* Tryon, 1865 accepted as *Gabbia vertiginosa* (Frauenfeld, 1862) (type by monotypy; Australia, New South Wales).

Remarks. This genus is a highly diverse genus with nearly 50 species. Most species were assigned to this genus only based on the morphology of a small globose shell with an inflated body whorl. The taxonomy of this genus needs a systematic revision using molecular methods, especially a large number of species from Australia (including the type species *Gabbia vertiginosa*).

Gabbia nana (Annandale 1918), comb. nov.

Hydrobioides nana Annandale, 1918: pl. 14, fig. 3 (Myanmar, Shan State, NW shore of Inle Lake, Fort Stedman, now Maing Thauk).

Diagnosis. Shell small, transparent white to pale yellow, high spiral whorls, inflated body whorl.

Material examined. • 10 specimens (preserved in ethanol), Shan State, Taunggyi District, Nampan, water in rice field (Fig. 1B. e), 20°28'02.6"N, 96°55'58.1"E, 5 Jul. 2024, Le-Jia Zhang leg., KIZ.2400065–2400075.

Description. Shell (Fig. 9) small for the family (Table 1), thin but solid, subglobose, transparent white to pale yellow, with four to 4.5 whorls at adulthood; teleoconch relatively high, smooth, without shoulder, body whorl inflated; aperture ovate, lip slightly thickened, always more than half of shell in height; umbilicus covered by inner lip or with narrow slit.

Operculum (Figs 9A, F, 4C) calcium, ovate, thin, slightly bigger than aperture, transparent grey; exterior surface smooth, nucleus close to inner opercular margin; interior surface with weak concentric growth lines and small grains on inner opercular region.

No fresh male specimen discovered.

Radula (Fig. 10) taenioglossate; central tooth upper margin with one long triangle central cusp and three small sharp cusps on either side, lateral margin each with three small sharp cusps; lateral tooth with one long triangle central cusp and four small sharp cusps; inner marginal tooth with 16 to 17 small cusps; outer marginal tooth with nine small cusps.

Remarks. This species is assigned to *Gabbia* based on its morphology of a small globose shell with an inflated body whorl and its close relationship with *Gabbia pygmaea* in the molecular phylogeny (Fig. 2). It cannot be assigned to *Hydrobioides* since this species lacks an outward extended outer lip. It can be distinguished from *Gabbia pygmaea* (Preston, 1908) (type locality: Myanmar, Thayet) based on its higher spiral whorls and white to pale yellow shell.

Habitat and distribution. Only known from the wetlands and small creeks in the Inle Lake basin.

Digoniostoma Annandale, 1920

Digoniostoma Annandale, 1920 in Annandale & Seymour Sewell (1920): 103–104; Starobogatov, 1970: 26; Izzatullaev, 1982: 336–340; Rao, 1989: 79–80; Ng & Tan, 2024: 154–155.

Bithynia (*Digoniostoma*) – Brandt, 1974: 58; Ramakrishna, 2007: 118–122; Glöer & Bössneck, 2013: 137–156.

Bithynia – Molluscabase, 2024b: synonym.

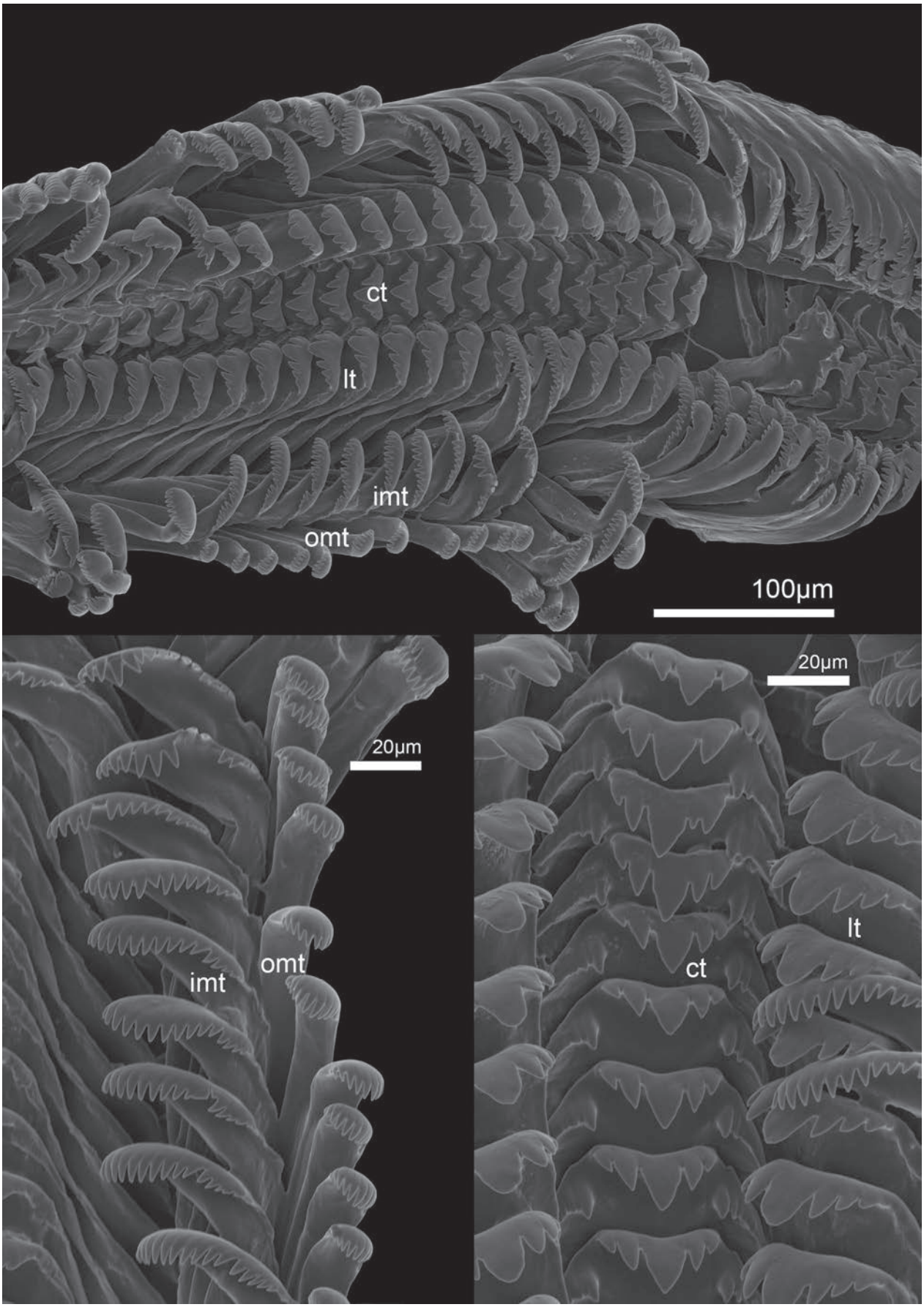

Figure 6. SEM photo of the radula of *Hydrobioides nassa*.

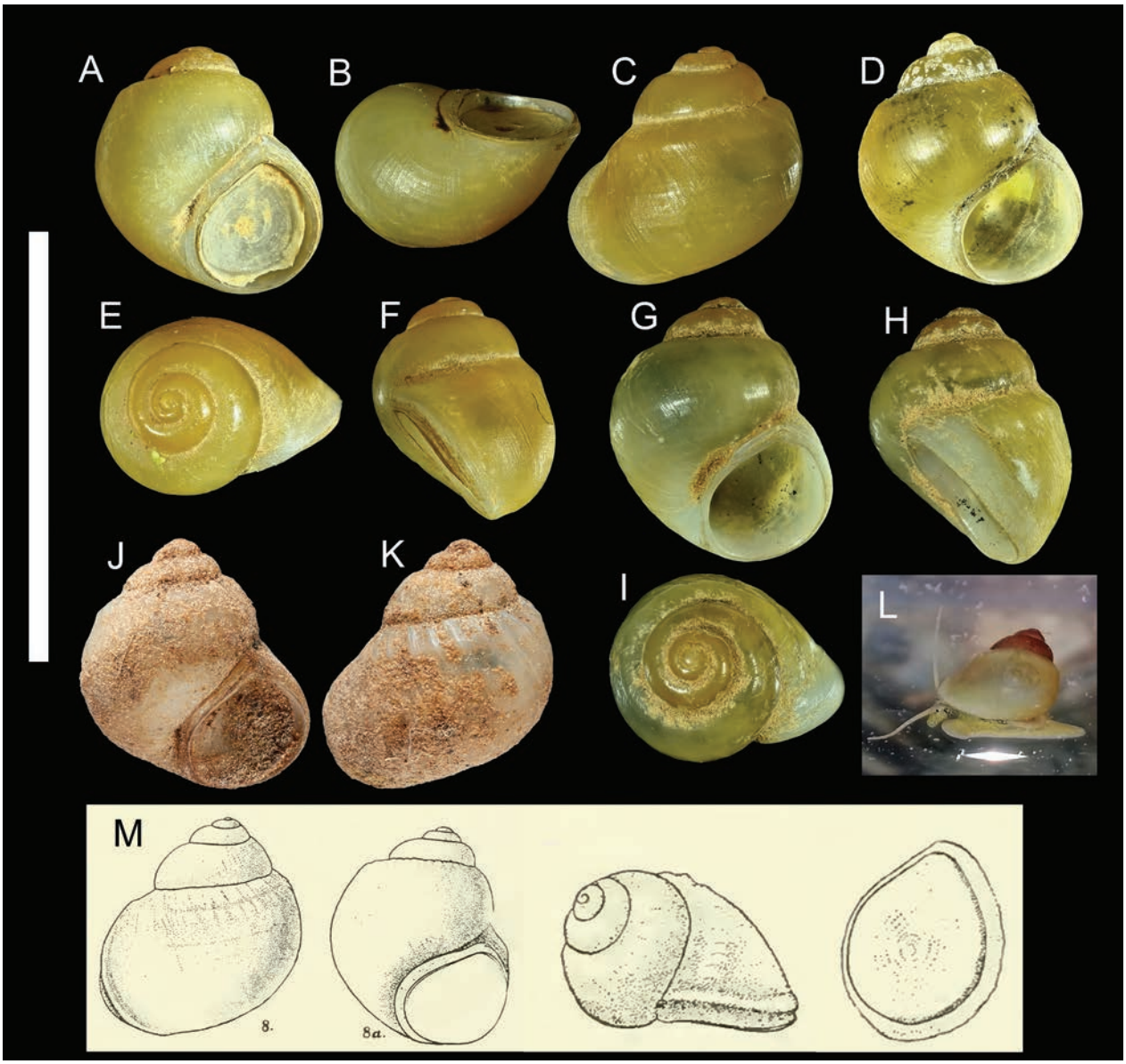

Figure 7. Shell of *Hydrobioides physcus*. **A–C.** KIZ.2400063, Inle Lake; **D.** KIZ.2400064, Inle Lake; **E–F.** KIZ.2400063, Inle Lake; **G–I.** KIZ.2400063, Inthein; **J–K.** Probable paratype, NHMUK.20060144, taken by Aimee McArdle, NHMUK Photographic Unit; **L.** Living animal in aquarium; **M.** Drawings of the type specimens from Annandale, 1918. Scale bars: 1 cm (**A–I**).

Type species. *Paludina cerameopoma* Benson, 1830 (original designation).

Diagnosis. Shell large for the family, thin and fragile, inner lip straight, base of peristome angled, umbilicus open, usually with a keel around; penial appendix located close to the base of penis, penial appendix much shorter than distal part of penis.

Remarks. This genus is always considered as a subgenus or even a synonym of *Bithynia* by some recent studies, e.g., Glöer and Bössneck (2013) and Molluscabase (2024b). However, the molecular study has confirmed that *Digoniostoma* from South and Southeast Asia is a distinct group and not closely related to *Bithynia*, mainly from Europe. Morphologically, this genus also can be easily distinguished from other bithyniid groups based on large shell with base of peristome angled and open umbilicus with a keel around. Molecular, morphological, and distributional evidence all support that *Digoniostoma* is a valid genus. There are 11 species and subspecies assigned to this genus based on molecular evidence and former morphological studies: *Digoniostoma cerameopoma* (Benson, 1830); *Digoniostoma funiculata* (Walker, 1927), stat. nov.; *Digoniostoma kashmirense* (G. Nevill, 1885); *Digoniostoma lithoglyphoides* Nesemann & Sharma, 2007; *Digoniostoma oxiana* Izzatullaev, 1982; *Digoniostoma pulchella* (Benson, 1836); *Digoniostoma iravadica* (Blanford, 1869); *Digoniostoma siamensis siamensis* (Lea, 1856), stat. nov.; *Digoniostoma siamensis goniomphalos* (Morelet, 1866) stat. nov.; *Digoniostoma textum* Annandale, 1921; *Digoniostoma truncatum* (Eydoux & Souleyet, 1852). The taxonomy of *Digoniostoma* species, especially the species from India, should be revised.

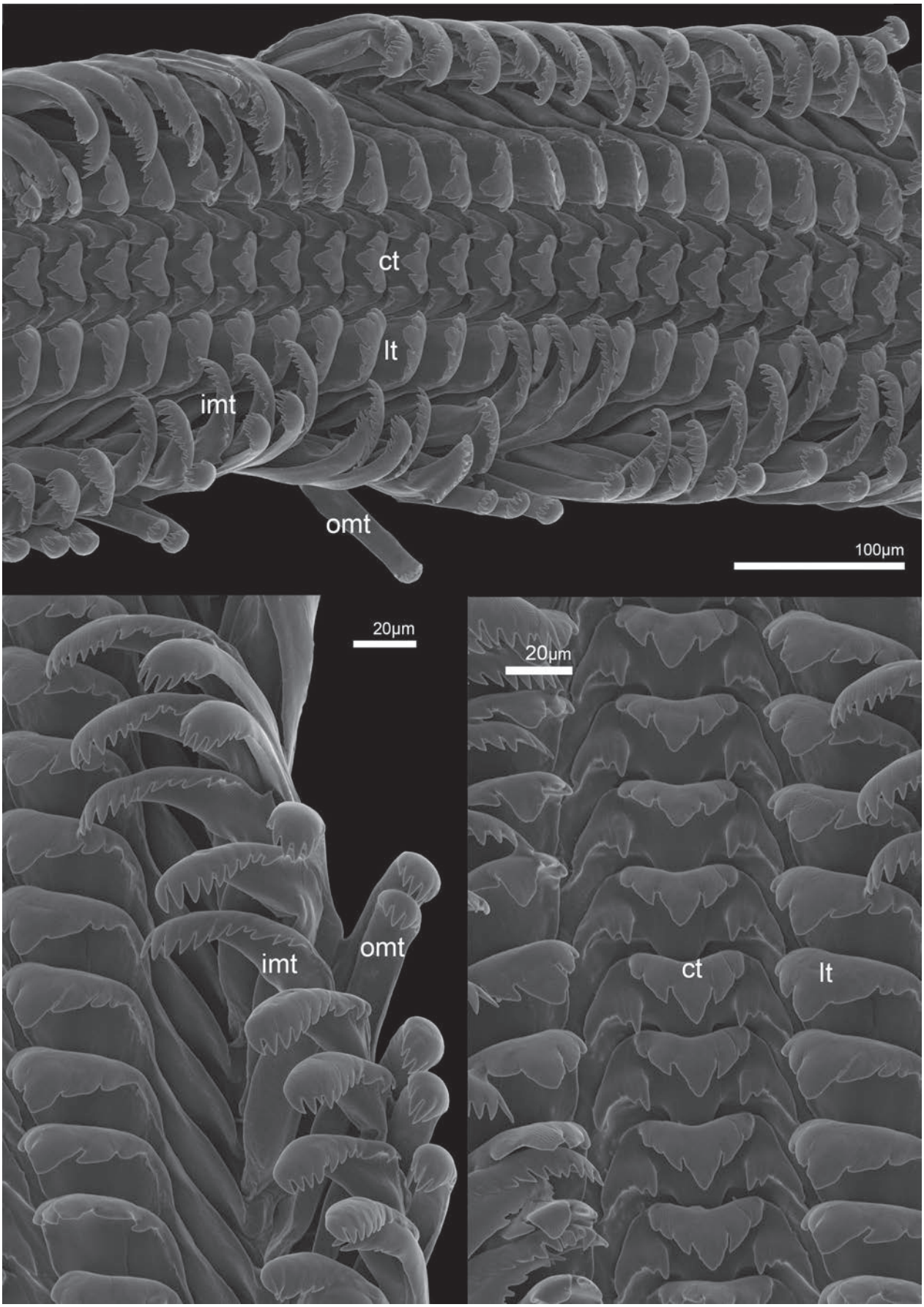

Figure 8. SEM photo of the radula of *Hydrobioides physcus*.

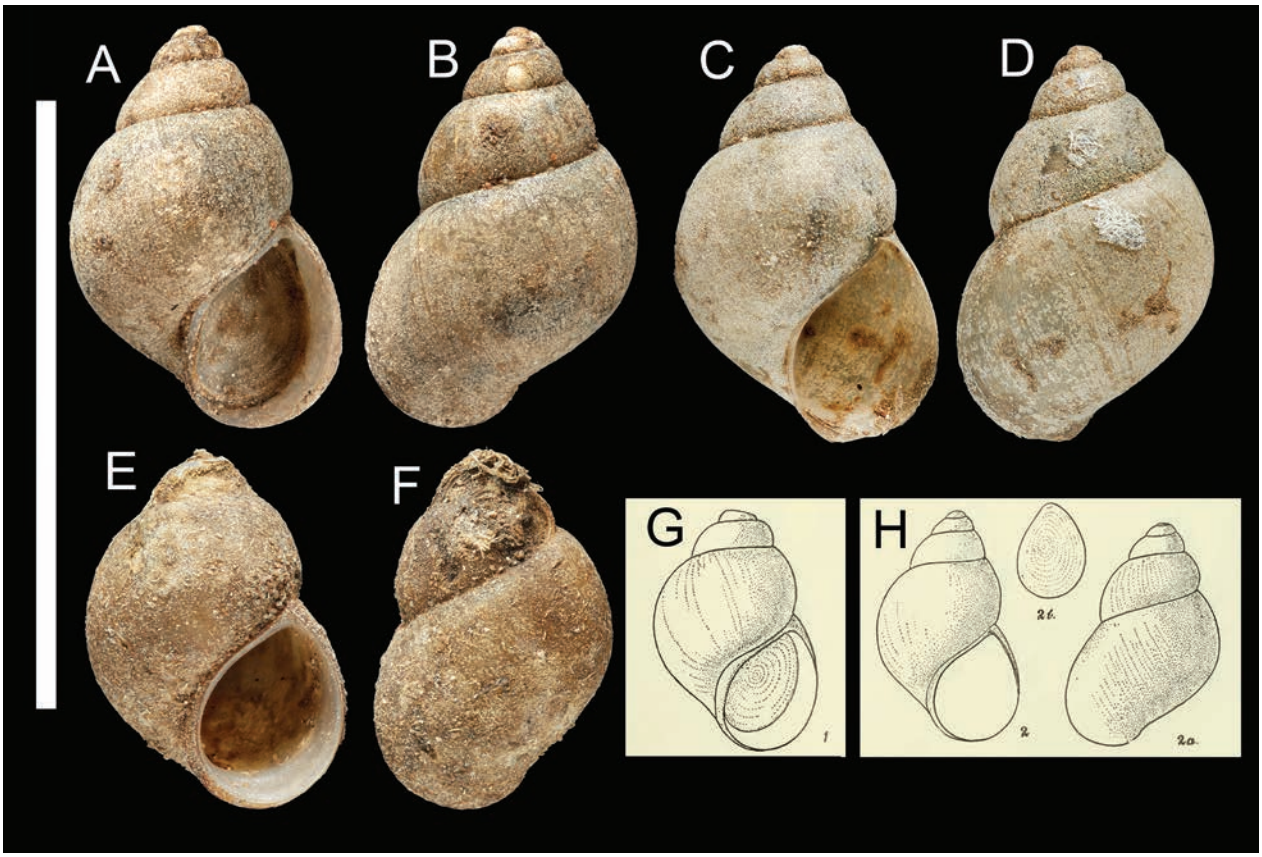

Figure 9. Shell of *Hydrobioides avarix*. **A–F.** Probable syntypes, NHMUK 20060143, taken by Aimee McArdle, NHMUK Photographic Unit; **G–H.** Drawing of the type specimens of *Hydrobioides avarix* from Annandale, 1918. Scale bars: 1 cm (**A–F**).

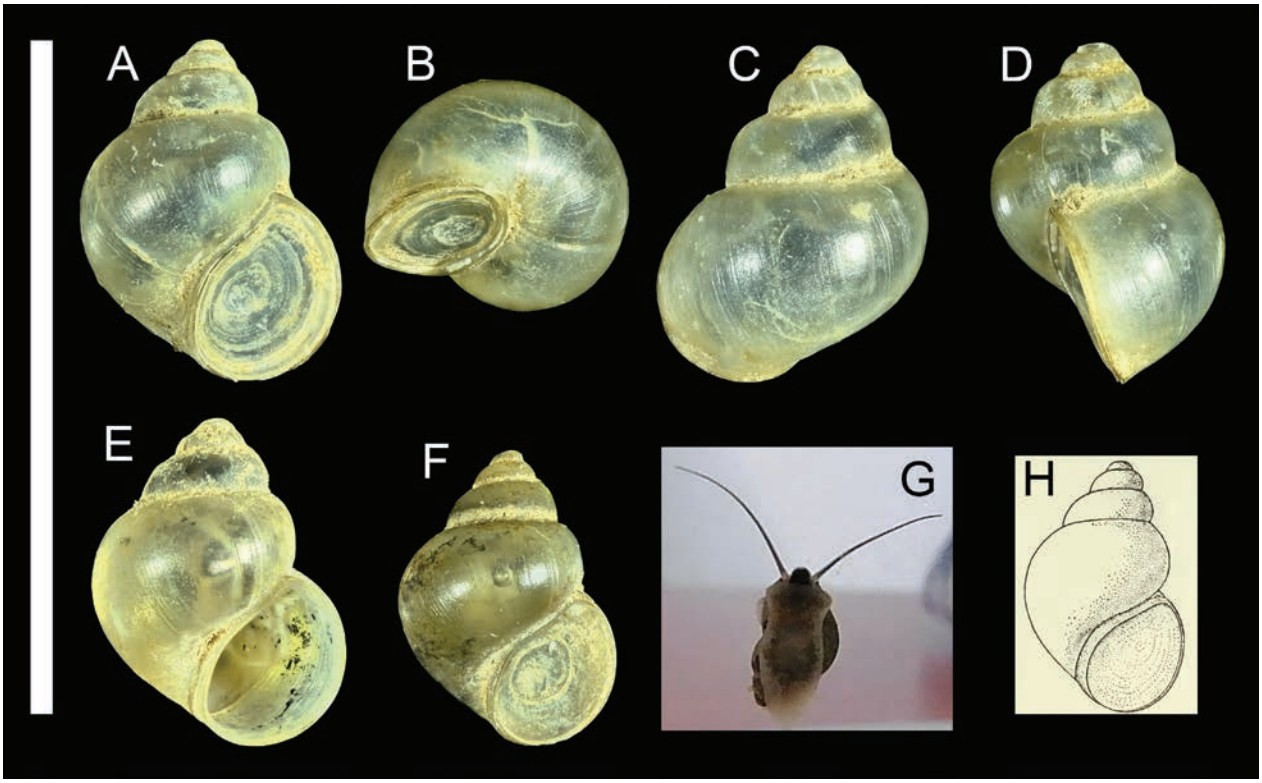

Figure 10. Shell of *Gabbia nana*. **A–D.** KIZ. 2400065, Nampan; **E.** KIZ. 2400066, Nampan; **F.** KIZ. 2400067, Nampan; **G.** Living animal in aquarium; **H.** Drawing of the type specimens of *Hydrobioides nana* from Annandale, 1918. Scale bars: 1 cm (**A–F**).

***Digoniostoma iravadica* (Blanford, 1869), comb. nov.**

Bithynia iravadica Blanford, 1869: 446 (Myanmar, Mandalay, Ava, swamp, and river); Molluscabase, 2021: taxon inquirendum.

D. iravadica – Rao, 1989: no description or remarks, only figures with ambiguous genus assignment and species name, figs 122–123.

Diagnosis. Shell big, thin, high spiral whorls, thin outer lip, base of peristome angled, umbilicus narrow and deep, penial appendix about one-third of distal part of penis in length.

Material examined. • 7 specimens preserved in ethanol, Shan State, Taunggyi District, Shwenyaung, Taung Lay Lone, a shallow pond in the north of town (Fig. 1B. a), 20°44'56.7"N, 96°53'59.4"E, 6 Jul. 2024, Le-Jia Zhang leg., KIZ.2400076–2400082 • 1 dry shell specimen, Mandalay Region, Meiktila, Wundwin, Seywa, dry pond near road, 21°14'15.2"N, 95°50'27.7"E, 29 Jun. 2024, Le-Jia Zhang leg., KIZ.2400083.

Description. Shell (Fig. 11) relatively large for the family (Table 1), thin and fragile, high conical, pale olive green to grey, with 5.5 whorls at adulthood; teleoconch high, relatively smooth but with very fine grid-like micro-structure, without shoulder; aperture ovate, nearly half of shell in height, outer lip thin, inner lip straight, base of peristome angled; umbilicus narrow and deep, always open obviously, with a keel around.

Operculum (Figs 11A, G, 4A) calcium, ovate, thin, slightly smaller than aperture, transparent grey; exterior surface smooth, with obviously concentric growth lines, nucleus close to the inner opercular margin; interior surface with many vermicular veins covering most parts of inner opercular region, and a few concentric veins on the margin of inner opercular region.

Penis (Fig. 5C) with a white penial appendix located close to the base of penis, penial appendix about one-third of distal part of penis in length.

Radula (Fig. 12) taenioglossate; central tooth upper margin with one long triangle central cusp and four small sharp cusps on either side, lateral margin each with three small sharp cusps; lateral tooth with one long triangle central cusp and four small sharp cusps; inner marginal tooth with 10 to 11 small cusps; outer marginal tooth with 10 small cusps.

Remarks. This species can be distinguished from other *Digoniostoma* species based on high spiral whorls, fine grid-like micro-structure shell surface, narrow umbilicus, and very long distal part of the penis. The molecular study also confirms the validity of this species. The radula of *Digoniostoma iravadica* has the central cusp with a different shape and a larger number of small sharp cusps on both the central tooth and the lateral tooth, compared to that of *Hydrobioides* species from Inle Lake.

Habitat and distribution. Rivers, swamps, and shallow ponds in central Myanmar (Mandalay, Meiktila, Taunggyi).

Discussion

Ancient lakes are widely recognised as important refuges and evolutionary centres for aquatic fauna. As the only ancient lake on the Indochinese Peninsula, Inle Lake supports a high diversity of bithyniid snails. The five bithyniid species examined in the present study are all endemic to Myanmar, with three species (*Hydrobioides physcus*, *Hydrobioides avarix*, and *Gabbia nana*) restricted to the Inle Lake basin and nearby region (Heho). We did not find two tiny bithyniid species endemic to the Inle Lake basin, viz. *Hydrobioides avarix* and *Gabbia alticola* (Annandale 1918). Based on the original description and the type specimens figured by Sawada (2022), we considered *Gabbia alticola* a valid endemic species. With altogether four endemic bithyniid species, the Inle Lake basin appears to have the highest known endemicity of Bithyniidae worldwide, surpassing Lake Skadar and Lake Trichonis of the Balkan Peninsula, each with three endemic bithyniid species (Glöer et al. 2007). In total, including the newly recorded *Digoniostoma iravadica*, seven bithyniid species have been recorded from the Inle Lake basin. Our study confirms the continued existence of four species and provides the first molecular-based revision of the bithyniid fauna from the Inle Lake basin.

Our multi-method study has significantly improved the taxonomy of bithyniid snails. *Hydrobioides nassa* has long been considered a common species in northern to central Thailand (Brandt 1974; Kulsantiwong et al. 2013; Bunchom et al. 2021). However, all previous studies did not compare the Thai population to the population from the type locality, Shan State of Myanmar. Our present study confirms that the true *Hydrobioides nassa* from Shan State can be clearly distinguished from the Thai "*Hydrobioides nassa*" based on shell morphology and molecular phylogeny. The molecular tree has revealed that the Thai "*Hydrobioides nassa*" is not even closely related to *Hydrobioides nassa*, and the sister species of *Hydrobioides nassa* is *Hydrobioides physcus*, endemic to Inle Lake. Therefore, we reintroduce the name *Hydrobioides dautzenbergi* for the Thai species, though its genus assignment requires further study due to the polyphyletic condition of *Hydrobioides* (Fig. 2). Genus *Parabithynia* with the type species *Hydrobioides physcus* is considered a synonym of *Hydrobioides* based on strong evidence of molecular study and morphology. *Digoniostoma* should be a valid genus based on molecular, morphological, and distributional evidence.

The present study on Bithyniidae represents the first part of our systematic survey and study of freshwater snails from the Inle Lake basin. As an important biodiversity hotspot of freshwater fauna, Inle Lake is increasingly threatened by human activities (Iwai et al. 2022). Further research on other freshwater snails from the Inle Lake region will enhance our understanding of the biodiversity and evolution of freshwater snails in this ancient plateau lake and provide valuable insights for the conservation of Inle Lake.

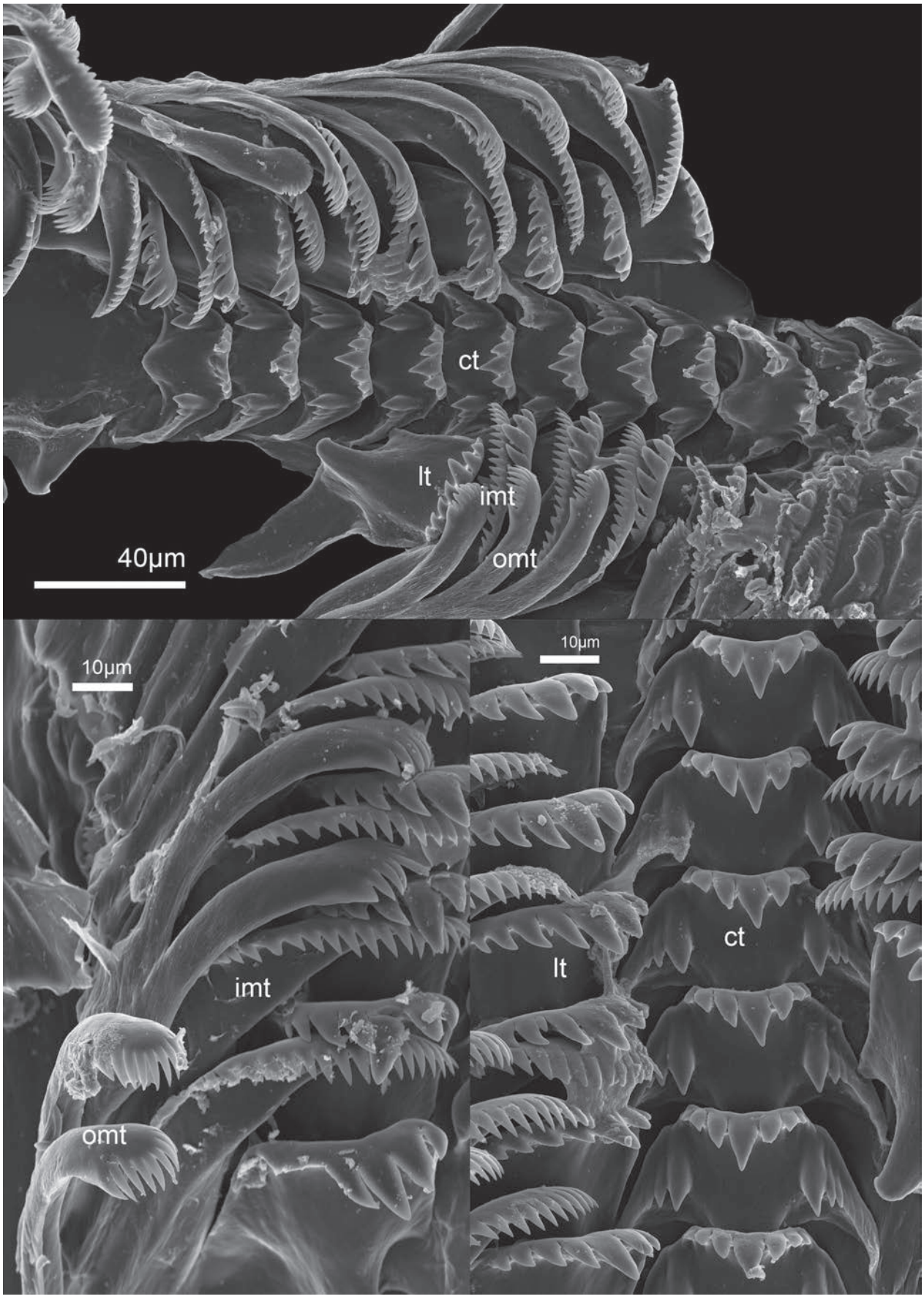

Figure 11. SEM photo of the radula of *Gabbia nana*.

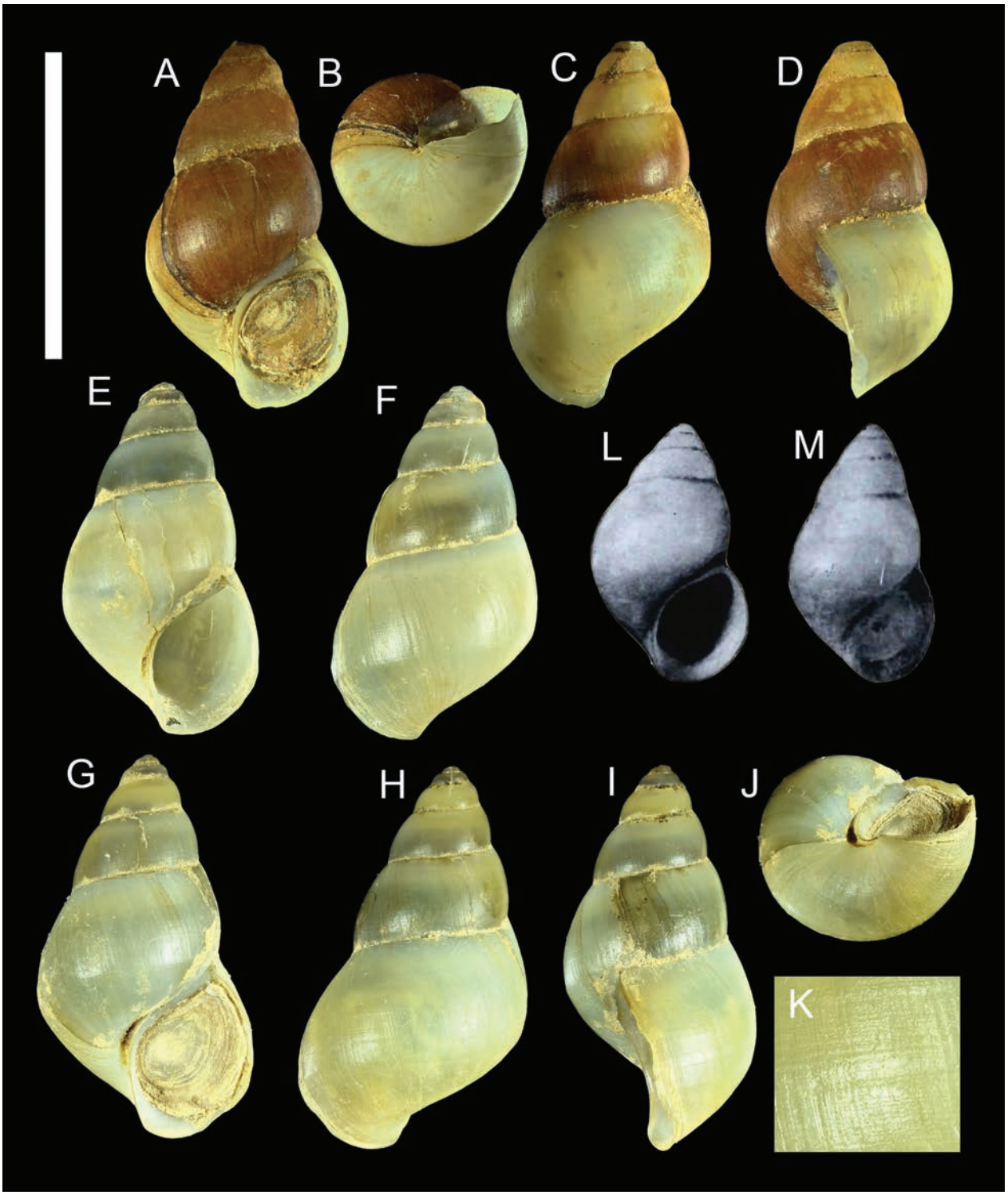

Figure 12. Shell of *Digoniostoma iravadica*. **A–D.** KIZ.2400076, Shwenyaung, dyed brown by the minerals; **E–F.** KIZ.2400077, Shwenyaung; **G–J.** KIZ.2400078, Shwenyaung; **K.** Micro-structure on shell surface; **L–M.** Figure from Rao (1989). Scale bars: 1 cm (**A–J**).

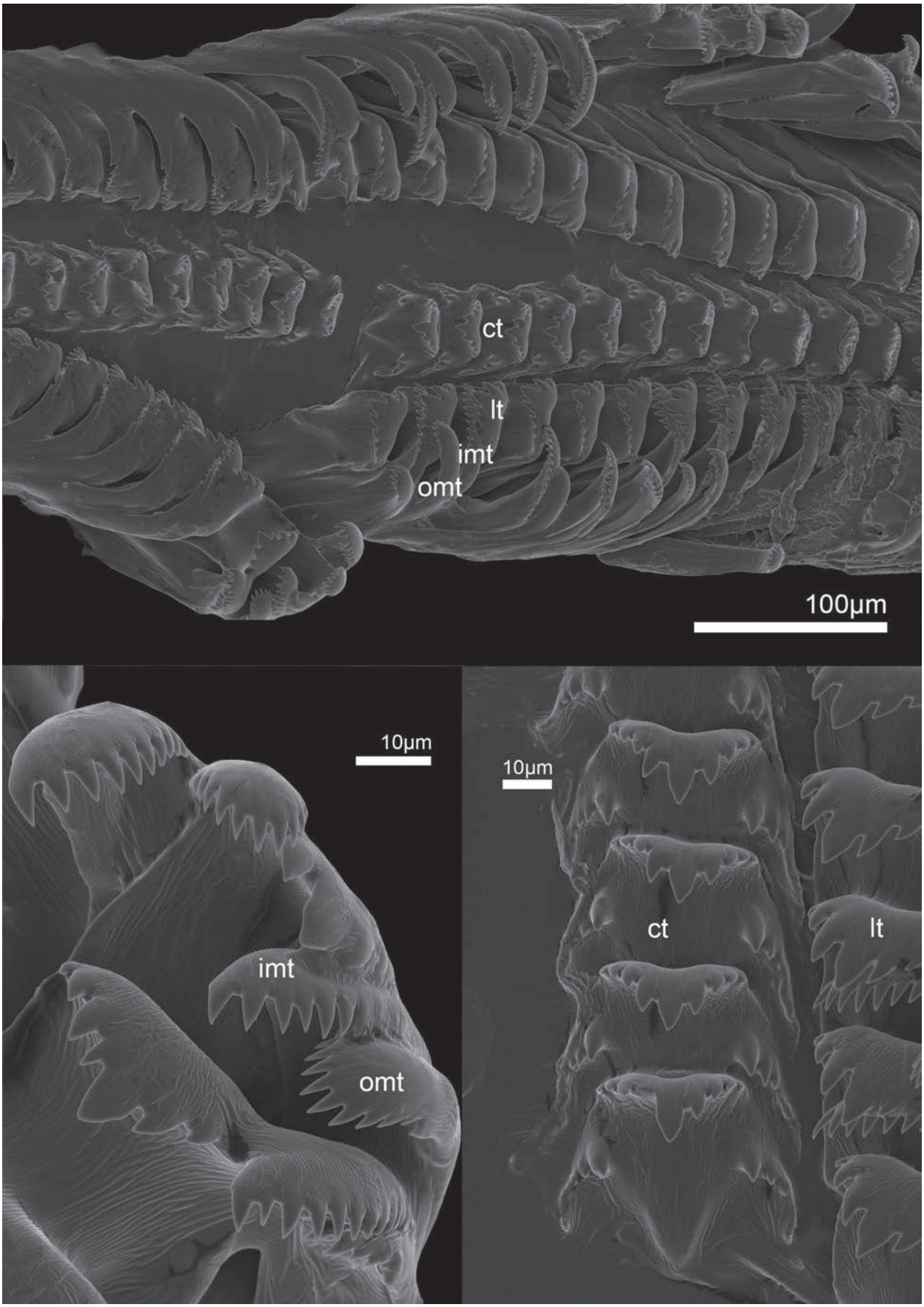

Figure 13. SEM photo of the radula of *Digoniostoma iravadica*.

Acknowledgements

We thank Daw Khin Pa Pa Shwe (Forestry Research Institute, Nay Pyi Taw, Myanmar), Thinnsu Tin (SEABRI), Phyo Htet Zaw (SEABRI), Nyein Chan Kyaw for their help in conducting fieldwork and collecting specimens, Cai-Xin Liu (SEABRI) for helping in taking photos, Jon Ablett (NHMUK), Andreia Salvador (NHMUK), and Aimee McArdle (NHMUK) for helping in examining and taking photos of the type specimen, and Guillaume VK for providing resources for the map. We thank Zhijia Gu (Platform for Plant Multi-dimensional Imaging and Diversity Analysis, Kunming Institute of Botany, CAS) for the SEM technical support. This work was funded by the Southeast Asia Biodiversity Research Institute, CAS (Grant No. Y4ZK111B01), Transboundary Cooperation on Biodiversity Research and Conservation in Gaoligong Mountains (Grant No. E1ZK251), and Yunnan Province Science and Technology Department (Grant No. 202203AP140007).

References

Annandale N (1918) Aquatic molluscs of the Inle Lake and connected waters. Records of the Indian Museum 14: 103–182. https://doi.org/10.5962/bhl.part.18607

Annandale N (1920) Materials for a generic revision of the freshwater gastropod molluscs of the Indian Empire. Part III. The Freshwater Genera of Hydrobiidae. Records of the Indian Museum 22: 1–6. https://doi.org/10.26515/rzsi/v22/i1/1921/163524

Annandale N, Rao HS (1925) Further observations on the aquatic gastropods of the Inlé watershed. Records of the Zoological Survey of India: 101–127. https://doi.org/10.26515/rzsi/v27/i2/1925/163462

Annandale N, Seymour Sewell RB (1920) Progress report on a Survey of the freshwater gastropod molluscs of the Indian Empire and of their trematode parasites. Indian Journal of Medical Research 8(1): 93–124.

Blanford WT (1869) Descriptions of new land and freshwater molluscan species collected by Dr. John Anderson in Upper Burma and Yunnan. Proceedings of the Zoological Society London 37(1): 444–450. https://doi.org/10.1111/j.1469-7998.1869.tb07354.x

Brandt RAM (1974) The non-marine aquatic Mollusca of Thailand. Archiv für Molluskenkunde 105: 1–423.

Bunchom N, Saijuntha W, Pilap W, Suksavate W, Vaisusuk K, Suganuma N, Agatsuma T, Petney TN, Tantrawatpan C (2021) Genetic variation of a freshwater snail *Hydrobioides nassa* (Gastropoda: Bithyniidae) in Thailand examined by mitochondrial DNA sequences. Hydrobiologia 848: 2965–2976. https://doi.org/10.1007/s10750-019-04013-2

Glöer P, Bössneck U (2013) Freshwater molluscs from Nepal and North India with the description of seven new species (Gastropoda: Bithyniidae, Lymnaeidae, Planorbidae). Archiv für Molluskenkunde 142(1): 137–156. https://doi.org/10.1127/arch.moll/1869-0963/142/137-156

Glöer P, Albrecht C, Wilke T (2007) Enigmatic distribution patterns of the Bithyniidae in the Balkan Region (Gastropoda: Rissooidea). Mollusca 25(1): 13–22.

Hampton SE, McGowan S, Ozersky T, Virdis SG, Vu TT, Spanbauer TL, Kraemer BM, Swann G, Mackay AW, Powers SM, Meyer MF, Labou SG, O'Reilly CM, DiCarlo M, Galloway AWE, Fritz SC (2018) Recent ecological change in ancient lakes. Limnology and Oceanography 63(5): 2277–2304. https://doi.org/10.1002/lno.10938

Iwai CB, Khaung T, Prasopsuk J, Ravindran B (2022) Environmental risk assessment of floating gardens in Inle Lake, Myanmar. Urban Climate 44: 101194. https://doi.org/10.1016/j.uclim.2022.101194

Izzatullaev Z (1982) Molluscs of the family Bithyniidae (Gastropoda, Pectinibranchia) in the Middle Asia. Zoologicheskiy Zhurnal 61(1): 336–340.

Kano Y, Musikasinthorn P, Iwata A, Tun S, Yun LKC, Win SS, Matsui S, Tabata R, Yamasaki T, Watanabe K (2016) A dataset of fishes in and around Inle Lake, an ancient lake of Myanmar, with DNA barcoding, photo images and CT/3D models. Biodiversity Data Journa 4: e10539. https://doi.org/10.3897/BDJ.4.e10539

Kozlov AM, Darriba D, Flouri T, Morel B, Stamatakis A (2019) RAxML-NG: a fast, scalable and 1495 user-friendly tool for maximum likelihood phylogenetic inference. Bioinformatics 35(21): 4453–4455. https://doi.org/10.1093/bioinformatics/btz305

Kulsantiwong J, Prasopdee S, Ruangsittichai J, Ruangjirachuporn W, Boonmars T, Viyanant V, Pierossi P, Hebert PDN, Tesana S (2013) DNA barcode identification of freshwater snails in the family Bithyniidae from Thailand. PLoS One 8(11): e79144. https://doi.org/10.1371/journal.pone.0079144

Kumar S, Stecher G, Li M, Knyaz C, Tamura K (2018) MEGA X: molecular evolutionary genetics analysis across computing platforms. Molecular biology and evolution 35(6): 1547. https://doi.org/10.1093/molbev/msy096

MolluscaBase eds (2021) MolluscaBase. Bithynia iravadica W. T. Blanford, 1869. https://www.molluscabase.org/aphia.php?p=taxdetails&id=1346994 [on 2024-10-21]

MolluscaBase [eds] (2024a) MolluscaBase. Hydrobioides G. Nevill, 1885. https://www.molluscabase.org/aphia.php?p=taxdetails&id=850522 [on 2024-10-21]

MolluscaBase [eds] (2024b) MolluscaBase. Digoniostoma Annandale, 1920. https://www.molluscabase.org/aphia.php?p=taxdetails&id=883875 [on 2024-10-21]

Natural History Museum (2014) Specimens (from Collection specimens) [Data set resource]. Natural History Museum. https://data.nhm.ac.uk/dataset/collection-specimens/resource/05ff2255-c38a-40c9-b657-4ccb55ab2feb [on 2024-10-29]

Nevill G (1881) New or little-known Mollusca of the Indo-Malayan fauna. Journal of the Asiatic Society of Bengal 50(2): 125–167.

Nevill G (1885) Hand List of Mollusca in the Indian Museum, Calcutta. Part II. Gastropoda. Prosobranchia-Neurobranchia (contd.). Office of Superintendent of Government Printing: Calcutta.

Ng TH, Tan SK (2024) The Family Bithyniidae Gray, 1857 (Gastropoda: Truncatelloidea) in Peninsular Malaysia and Singapore. Tropical Natural History 24: 153–163. https://doi.org/10.58837/tnh.24.1.262922

Palumbi SR, Martin A, Romano S, McMillan WO, Stice L, Grabowski G, MacMillan WO (2002) The Simple Fool's Guide to PCR. University of Hawaii Press, Honolulu.

Pilsbry HA (1928) *Paranerita* Annandale, 1920. The Nautilus 41(3): 108.

Popova SM (1981) Kaynozoyskaya kontinental'naya malakofauna yuga Sibiri i sopredel'nykh territoriy [The Cenozoic continental malacofauna of Southern Siberia and adjacent territories]. Nauka, Moskva.

Popova SM, Devyatkin YV, Starobogatov YI (1970) Mollyuski kyzylgirskoy svity Gornogo Altaya [Molluscs of the Kyzylgir Formation of the Altay Mountains]. Nauka, Moskva.

Ramakrishna AD (2007) Handbook on Indian Freshwater Molluscs. Zoological Survey of India, Pune.

Rao HS (1928) The aquatic and amphibious Mollusca of the northern Shan States, Burma. Records of the Zoological Survey of India 30(4): 399–468. https://doi.org/10.26515/rzsi/v30/i4/1928/162555

Rao S (1989. Handbook of Freshwater Molluscs of India. Zoological Survey of India: Calcutta.

Ronquist F, Teslenko M, Van Der Mark P, Ayres DL, Darling A, Höhna S, Larget B, Liu L, Suchard MA, Huelsenbeck JP (2012) MrBayes 3.2: efficient Bayesian phylogenetic inference and model choice across a large model space. Systematic Biology 61(3): 539–542. https://doi.org/10.1093/sysbio/sys029

Sawada N (2022) Revisiting the Annandale malacological collection from Inle Lake, Myanmar kept in the Kyoto University Museum. Molluscan Research 42(3): 212–220. https://doi.org/10.1080/13235818.2022.2097043

Schultheiß R, Wilke T, Jørgensen A, Albrecht C (2011) The birth of an endemic species flock: demographic history of the *Bellamya* group (Gastropoda, Viviparidae) in Lake Malawi. Biological Journal of the Linnean Society 102(1): 130–143. https://doi.org/10.1111/j.1095-8312.2010.01574.x

Starobogatov YI (1970) Molluscan fauna and zoogeographic zonation of continental freshwater bodies of the world. Nauka Publishers, Leningrad.

Theobald W (1866) Notes on a collection of land and freshwater shells from the Shan States. – Collected by F. Fedden, Esq., 1864–65. Journal of the Asiatic Society of Bengal 34(2): 273–279.

Winnepenninckx B, Backeljau T, De Wachter R (1993) Extraction of high molecular weight DNA from molluscs. Trends in Genetics 9: e407. https://doi.org/10.1016/0168-9525(93)90102-N

Yu W, Mao XL, Chen ZQ, Huang LS (1978) Early Tertiary gastropod fossils from the coastal region of Bohai. Paleontological and Geological Research Institute, Nanjing.

Zhang LJ, von Rintelen T (2021) The neglected operculum: a revision of the opercular characters in river snails (Caenogastropoda: Viviparidae). Journal of Molluscan Studies 87(2): eyab008. https://doi.org/10.1093/mollus/eyab008

Zhang LJ, Shi ZA, Chen ZY, von Rintelen T, Zhang W, Lou ZJ (2024a) Rediscovery and systematics of the enigmatic genus *Helicostoa* reveals a new species of sessile freshwater snail with remarkable sexual dimorphism. Proceedings of the Royal Society B 291: 20231557. https://doi.org/10.1098/rspb.2023.1557

Zhang L.J, Bernardes SC, Meng K, von Rintelen T (2024b) A new family of freshwater snails with Cretaceous origin from Yunnan, China. Zoological Journal of the Linnean Society 202(1): zlae117. https://doi.org/10.1093/zoolinnean/zlae117

Supplementary material 1

Supplementary data

Authors: Le-Jia Zhang, Shu-Sen Shu, Xin-Yuan Song, Nay Htet Naing, Thaung Naing Oo, Xiao-Yong Chen

Data type: xlsx

Link: https://doi.org/10.3897/zse.101.143936.suppl1

Zoosyst. Evol. 101 (2) 2025, 661–679 | DOI 10.3897/zse.101.144134

PENSOFT

für Natur MUSEUM FÜR NATURKUNDE BERLIN

Taxonomic revision on the *Gobio* group in the Yellow River drainage, with discussion on the validity of the genus *Acanthogobio* (Cypriniformes, Gobionidae)

Yutian Fang[1,2], Zhixian Sun[1,3], Yahui Zhao[1]

1 *State Key Laboratory of Animal Biodiversity Conservation and Integrated Pest Management, Institute of Zoology, Chinese Academy of Sciences, Beijing, 100101, China*

2 *University of Chinese Academy of Sciences, Beijing, China*

3 *Shanghai Universities Key Laboratory of Marine Animal Taxonomy and Evolution, Shanghai Ocean University, Shanghai, 201306, China*

https://zoobank.org/72D44F7D-13D3-4AFA-A57E-B11B2175A6F3

Corresponding author: Yahui Zhao (zhaoyh@ioz.ac.cn)

Academic editor: Nicolas Hubert ♦ **Received** 11 December 2024 ♦ **Accepted** 7 March 2025 ♦ **Published** 25 March 2025

Abstract

The Yellow River drainage is a biodiversity hotspot for the *Gobio* group, but no one has yet reviewed these species systematically. This study examined the type specimens of the species in the *Gobio* group and numerous newly captured specimens in the Yellow River drainage for an overall morphological comparison. A phylogenetic tree of those species based on mitochondrial cytochrome-*b* sequences was also constructed. Our results indicate the presence of four species, i.e., *Gobio guentheri* (this was described as *Acanthogobio guentheri*), *G. rivuloides*, *G. coriparoides*, and *G. huanghensis*. Morphological and molecular phylogenetic analyses indicated that *G. tchangi* is a junior synonym of *G. huanghensis*, while *G. meridionalis* is a junior synonym of *G. rivuloides*. Additionally, the phylogenetic analysis showed that the genus *Acanthogobio* is nested within *Gobio*. In order to maintain the monophyly of *Gobio*, this study suggests that the genus *Acanthogobio* should be a junior synonym of *Gobio*, and the type species *A. guentheri* should be treated as *Gobio guentheri*. Furthermore, the type specimens of *Romanogobio johntreadwelli* and *R. amplexilabris* were checked, and this study confirmed that these two species are junior synonyms of *G. rivuloides*. Therefore, the genus *Romanogobio* is not distributed in the Yellow River drainage. The *Gobio* species are primarily distributed in the upper and middle reaches of the Yellow River drainage, from Qushian Township, Qinghai Province, to Sanmenxia City, Henan Province, at an average elevation above 300 meters. A diagnostic key for four valid *Gobio* species in the Yellow River drainage is provided.

Key Words

East Asia, freshwater fish, morphology, phylogenetic analysis, taxonomy

Introduction

The Yellow River is the second longest river in East Asia; it is located between 35°N and 43°N latitude and 112°E and 120°E longitude. Originating from the Bayan Har Mountains on the Qinghai-Tibet Plateau, the Yellow River flows through nine provinces over 5,464 kilometers and eventually drains into the Bohai Sea, with a drainage area of 752,546 square kilometers (Song et al. 2022). Based on the characters of the riverscape and environment, this long river was divided into three sections: the upper reaches were defined from the origin to Hekou Township, Togtoh County, Inner Mongolia Autonomous Region; the middle reaches, from Togtoh County to Taohuayu, Zhengzhou City, Henan Province; and the lower reaches were defined as the section downstream of Taohuayu (Yellow River Conservancy Commission 2013). There are 147 native freshwater fishes recorded in this vast river drainage (Zhao et al. 2020).

The Yellow River drainage is a biodiversity hotspot for the *Gobio* group in East Asia. This monophyletic group

within the family Gobionidae includes the genera *Gobio, Acanthogobio, Romanogobio,* and *Mesogobio* (Yang et al. 2006), and three genera (i.e., *Gobio, Acanthogobio,* and *Romanogobio*) occur in the Yellow River drainage. The genus *Gobio* is a group of small-sized freshwater fish widely distributed across Eurasia (Chen 1998; Kottelat and Freyhof 2007). They are characterized by having one pair of barbels, mouth inferior, gill rakes rudimentary, thoracic region flattened and naked, possessing seven branched dorsal-fin rays and six branched anal-fin rays (Luo et al. 1977; Chen 1998). A total of 11 species inhabit East Asia (Wu et al. 2012; Li 2015), and five of them have been recorded in the Yellow River drainage (Li 2015). *Romanogobio* is distinguished by epithelial crests on scales on the dorsal half of the body, a depth of caudal peduncle 2.6–4.2 times in caudal peduncle length, and an anus closer to the pelvic-fin base than to the anal-fin origin (Naseka 1996; Kottelat and Freyhof 2007). This genus is mainly distributed in Europe, with only two species distributed in the Yellow River drainage (Naseka 1996; Kottelat and Freyhof 2007; Wu et al. 2012). *Acanthogobio* is a monotypic genus, and *A. guentheri* is the only species (Herzenstein 1892). It is restricted to the upper reaches of the Yellow River drainage and is characterized by several distinct features: barbel reaching between posterior preopercle margin and posterior opercular margin; ventral scaleless region extends beyond pelvic-fin; the absence of scales on the pre-dorsal region; anus positioned at the posterior one-third of the distance from pelvic-fin base end to anal-fin origin; and the second unbranched ray of the dorsal fin forms a stiff spine (Chen 1998).

Eight species within the *Gobio* group have been recorded from the Yellow River in the past centuries. They are *Acanthogobio guentheri* from the upper reaches; *Gobio rivuloides, G. huanghensis, G. tchangi, G. coriparoides, Romanogobio johntreadwelli, Romanogobio amplexilabris,* and *G. meridionalis* from the upper and middle reaches. Although numerous taxonomists have recorded those species from the *Gobio* group in the Yellow River drainage (Herzenstein 1892; Nichols 1925; Bănărescu and Nalbant 1973; Luo et al. 1977; Chen et al. 1987; Li 2015), no one has yet reviewed these species. Therefore, it is necessary to conduct an overall review of the *Gobio* group in the Yellow River drainage and provide an accurate diagnostic key to them. In this study, based on the specimens collected from the Yellow River drainage and the adjacent river system, and also the type materials of each species, we are able to compare the differences among these species and determine their validity.

Material and methods

Specimen collection, examination, and preservation

Most of the specimens were collected between 2022 and 2024 from the main stream and tributaries of the Yellow River drainage, including the Fenhe, Luohe, and Qinhe Rivers, and some small tributaries. Fish were collected using fish traps and hand nets. After collection, the specimens were fixed in 10% formaldehyde and stored in 70% ethanol, or directly fixed in 95% ethanol. Meanwhile, some *Gobio rivuloides* specimens collected from the Haihe River drainage were also used for comparison since the type locality of this species is Niang-tze Kwan (=Niangziguan Township, Pingding County, Yangquan City, Shanxi Province), which belongs to the Haihe River drainage.

The holotype of the *Gobio tchangi* is preserved at the Institute of Zoology, Chinese Academy of Sciences, Beijing, China (ASIZB, abbreviation follows Sabaj, 2020; 2023). The syntypes of *G. huanghensis* and paratypes of *G. meridionalis* are at the Institute of Hydrobiology, Chinese Academy of Sciences, Hubei, China (IHB), and holotypes of *G. rivuloides, G. coriparoides, Romanogobio johntreadwelli,* and *R. amplexilabris* are at the American Museum of Natural History, New York, the United States (AMNH).

Morphological study

Measurements were taken on the left side of the specimens using a digital caliper, which rounded to 0.01 mm; all measurements were made point to point, never by projection. Counts were also made on the left side of specimens. If the scales or fin rays were damaged from the left side, counts were made on the right side. Methods for counts and measurements followed Zhao and Sun (2021). The lateral line scales include the scales on the caudal-fin base. The last two rays in dorsal and anal fins based on a single pterygiophore were counted as one ray. Only adult specimens (larger than 60 mm standard length) were measured; juveniles and smaller, bent, or damaged specimens were not included in the measurements (Kottelat and Persat 2005). To determine the position of the anus, we define the distance from the posterior margin of the pelvic-fin base to the anterior edge of the anus as the pelvic fin-anus distance, and the distance from the anterior edge of the anus to the anal-fin as the anus-anal fin distance.

In order to get a general perception on external morphologic differences, nineteen measurable traits, $\log_{10}$–standardized to eliminate the allometries, were input into Past v4.17 (Hammer and Harper 2001) for principal component analysis (PCA).

Molecular phylogenetic analyses

Molecular studies were based on the mitochondrial Cytochrome-*b* (Cyt *b*) sequences. DNA was extracted from the pelvic fin on the right side of the fish. The Cyt *b* gene was amplified using primers L14724 (5'-GACTTGAAAAACCACCGTTG-3') and H15915 (5'-CTCCGATCTCCGGATTACAAGAC-3') following He and Chen (2009). Sequencing reactions were performed according to the operating instructions of BigDye Terminator v3.1 (BDT),

with 1 μL of primer (3.2 pmol/μL), 1 μL of template DNA, 2 μL of BigDye® Terminator v3.1, and 6 μL of double distilled water (dd H2O) for a total reaction volume of 10 μL. The thermo-cycling conditions were initial denaturation for 2 min at 96 °C, denaturation for 10 s at 96 °C, annealing for 10 s at 50 °C, and extension for 1 min at 60 °C. After 30 cycles, a final extension was performed at 60 °C for 3 min, and the polymerase chain reaction (PCR) products were preserved at 4 °C. Sequencing was carried out by Beijing TsingKe Biotech Co., Ltd. (China).

The sequencing results were assembled using SeqMan, and other sequences were acquired from the NCBI database. The voucher ID of each individual and GenBank accession number are given in Table 1. Twenty-six Cyt *b* sequences of *Gobio* species were included in the molecular phylogenetic analyses. *Hemibarbus labeo* was used as an outgroup. Nucleotide sequence alignment was conducted using MEGA 11 (Kumar et al. 2018) with ClustalW. ModelFinder (Kalyaanamoorthy et al. 2017) was used to select the best-fit model using Bayesian information criterion (BIC). The Bayesian inference (BI) phylogenies were inferred using MrBayes v3.2.6 (Ronquist et al. 2012) under the GTR model (two parallel runs, 2,000,000 generations), with the initial 25% of sampled data discarded as burn-in. The final phylogenetic trees were modified on the TVBOT: Tree Visualization By One Table (https://www.chiplot.online/tvbot.html, Xie et al. 2023). Each sequence was labeled with its own taxonomic nomenclature, and the evolutionary divergence of sequence pairs between and within groups (i.e., species) was estimated using the Kimura 2-parameter model (Kimura 1980).

Results

Based on morphological comparisons and molecular phylogenetic analyses, we conclude that there are four valid species distributed in the Yellow River drainage: *Gobio huanghensis* Lo, Yao & Chen, 1977; *G. rivuloides* Nichols, 1925; *G. coriparoides* Nichols, 1925; and *G. guentheri* Herzenstein, 1892. A diagnostic key to these species is given herein.

Table 1. Voucher codes, sampling localities and accession numbers of *Gobio* group species and outgroup for molecular phylogenetic analyses.

Voucher Code	Species	Locality	Drainage	Accession no.	Source
–	*Gobio huanghensis*	Hainan Tibetan Autonomous Prefecture, Qinghai Prov. China	Yellow River	FJ904648	Qi et al. from NCBI (Unpublished)
ASIZB 242021	*G. huanghensis*	Xing County, Shanxi Prov. China	Yellow River	–	This study
ASIZB 242022	*G. huanghensis*	Xing County, Shanxi Prov. China	Yellow River	–	This study
ASIZB 242025	*G. huanghensis*	Baode County, Shanxi Prov. China	Yellow River	–	This study
ASIZB 242026	*G. huanghensis*	Liulin County, Shanxi Prov. China	Yellow River	–	This study
ASIZB 242030	*G. huanghensis*	Hangjin Banner, Inner Mongolia Aut. Reg. China	Yellow River	–	This study
ASIZB 242040	*G. huanghensis*	Lin County, Shanxi Prov. China	Yellow River	–	This study
IHB 0411036	*G. coriparoides*	–	–	JN003326	Tang et al. 2011
–	*G. coriparoides*	Luonan County, Shaanxi Prov. China	Luohe R., Yellow River Drainage	EU934492	Liu et al. 2010
ASIZB 241456	*G. coriparoides*	Jingle County, Shanxi Prov. China	Fenhe R., Yellow River Drainage	–	This study
ASIZB 242015	*G. coriparoides*	Jingle County, Shanxi Prov. China	Fenhe R., Yellow River Drainage	–	This study
ASIZB 242033	*G. coriparoides*	Lan County, Shanxi Prov. China	Fenhe R., Yellow River Drainage	–	This study
ASIZB 242038	*G. guentheri*	Jishishan Bonan, Dongxiang and Salar Autonomous County, Gansu Prov. China	Yinchuan R., Yellow River Drainage	–	This study
ASIZB 242039	*G. guentheri*	Jishishan Bonan, Dongxiang and Salar Autonomous County, Gansu Prov. China	Yinchuan R., Yellow River Drainage	–	This study
ASIZB 242061	*G. guentheri*	Liulin County, Shanxi Prov. China	Yellow R.	–	This study
–	*G. rivuloides*	Yushe County, Shanxi Prov. China	Zhuozhanghe R., Haihe River drainage	OP354083	Ni et al. 2023
–	*G. rivuloides*	Yushe County, Shanxi Prov. China	Zhuozhanghe R., Haihe River drainage	OP354084	Ni et al. 2023
ASIZB 219283	*G. rivuloides*	Huguan County, Shanxi Prov. China	Xihe R., Haihe River Drainage	–	This study
ASIZB 239687	*G. rivuloides*	Shangyi County, Hebei Prov. China	Yanghe R., Haihe River Drainage	–	This study
ASIZB 241457	*G. rivuloides*	Pingshan County, Hebei Prov. China	Hutuohe R., Haihe River Drainage	–	This study
ASIZB 242027	*G. rivuloides*	Luonan County, Shaanxi Prov. China	Luohe R., Yellow River Drainage	–	This study
ASIZB 242028	*G. rivuloides*	Luonan County, Shaanxi Prov. China	Luohe R., Yellow River Drainage	–	This study
ASIZB 241459	*G. meridionalis*	Xing County, Shanxi Prov. China	Yellow R.	–	This study
ASIZB 242016	*G. meridionalis*	Bohaiwan County, Inner Mongolia Aut. Reg. China	Yellow R.	–	This study
ASIZB 242018	*G. meridionalis*	Bohaiwan County, Inner Mongolia Aut. Reg. China	Yellow R.	–	This study
ASIZB 242062	*G. meridionalis*	Daning County, Shanxi Prov. China	Yellow R.	–	This study
UAIC 14403.01	*Romanogobio ciscaucasicus*			JN003325	Tang et al. 2011
HDBI1292–773	*R. benacensis*	Kamenita Vrata, Croatia	Mirna R.	MG791924	Jelić et al. 2018
HDBI1323–771	*R. benacensis*	Kamenita Vrata, Croatia	Mirna R.	MG791926	Jelić et al. 2018
Outgroup					
–	*Hemibarbus labeo*	–	–	DQ267432	Lim et al. from NCBI (Unpublished)

Key to the species of genus *Gobio* in the Yellow River drainage

1 Anus centrally located between pelvic-fin base and anal-fin origin or closer to pelvic-fin base 2
– Anus positioned at posterior one-third of distance from pelvic-fin base end to anal-fin origin..... 3
2 Barbel reaching beyond posterior margin of preopercle, length 41.3%–58.2% of HL; scales above lateral line 6.5; scales below lateral line 4; circumpeduncular scales 16 ..... *Gobio huanghensis*
– Barbel reaching between vertical of posterior edge of orbit and posterior margin of preopercle, length 31.1–42.1% of HL; scales above lateral line 5.5; scales below lateral line 3; circumpeduncular scales 12–14 .....*Gobio rivuloides*
3 Barbel reaching between vertical of posterior edge of orbit and posterior margin of preopercle margin, length 30.4%–41.2% of HL; the second unbranched dorsal-fin ray soft, thin; scales on pre-dorsal region, ventral scaleless region extends to middle of pectoral-fin base end to pelvic-fin base or just extends to pectoral-fin base end .....*Gobio coriparoides*
– Barbel reaching between posterior margin of preopercle and posterior margin of opercular, length 53.3%–89.4% of HL; second unbranched dorsal-fin ray stiff, robust; no scales on pre-dorsal region, ventral scaleless region extends to posterior pelvic fin .....*Gobio guentheri*

Gobio huanghensis Lo, Yao & Chen, 1977

Figs 1–3, Table 2

Gobio huanghensis Lo, Yao & Chen, 1977: 496.
Gobio rivuloides: Institute of Zoology, Chinese Academy of Sciences (1959, not Nichols, 1925): 43.
Gobio tchangi: Li (2015): 178.

Material examined. • IHB 56–IX–004 (Syntype), 1 specimen, 121.9 mm SL, Lanzhou City, Gansu Province, China. ASIZB 56773–56778, 6 specimens, 115.6–157.6 mm SL; near Lanzhou City, Gansu Province, from the main stream of the Yellow River; collected by Sizhong Li; 1958. • ASIZB 232934, 1 specimen, 80.4 mm SL; Liulin County, Lvliang City, Shanxi Province, from the main stream of the Yellow River (37.3891°N, 110.6281°E, ca 630 m a.s.l.); collected by Xin Wang; 31 July 2022. • ASIZB 241489–241490, 241497, 3 specimens, 64.7–107.4 mm SL; Xing County, Lvliang City, Shanxi Province, from the main stream of the Yellow River (38.5196°N, 110.9076°E, ca 770 m a.s.l.); collected by Yutian Fang, 20 October 2023. • ASIZB 242021–242024, 4 specimens, 72.2–128.9 mm SL; Xing County, Lvliang City, Shanxi Province, from the main stream of the Yellow River (38.5193°N, 110.9072°E, ca 780 m a.s.l.); collected by Yutian Fang, 22 May 2024. • 1 ASIZB 242025, specimen, 99.5 mm SL; Baode County, Xinzhou City, Shanxi Province, from the main stream of the Yellow River (38.7821°N, 110.9691°E, ca 780 m a.s.l.); collected by Zhixian Sun, 21 May 2024. • ASIZB 242026, 1 specimen, 106.3 mm SL; Liulin County, Lvliang City, Shanxi Province, from the main stream of the Yellow River (37.3947°N, 110.6316°E, ca 630 m a.s.l.); collected by Yutian Fang, 26 May 2024. • ASIZB 242019–242020, 2 specimens, 118.6–124.6 mm SL; Baode County, Xinzhou City, Shanxi Province, from the main stream of the Yellow River (39.0212°N, 110.0596°E, ca 810 m a.s.l.); collected by Zhixian Sun, 6 July 2024. • ASIZB 242029, 1 specimen, 94.9 mm SL; Daning County, Linfen City, Shanxi Province, from the main stream of the Yellow River (36.4587°N, 110.4876°E, ca 600 m a.s.l.); collected by Zhixian Sun, 8 July 2024. • ASIZB 242030–242032, 3 specimens, 66.8–80.3 mm SL; Hangjin Banner, Ordos City, Inner Mongolia Autonomous Region, from the main stream of the Yellow River (40.6085°N, 107.2969°E, ca 1040 m a.s.l.); collected by Junyuan Hao, 28 June 2024. • ASIZB 242040, 1 specimen, 88.6 mm SL; Lin County, Lvliang City, Shanxi Province, from the main stream of the Yellow River (37.6423°N, 110.7796°E, ca 670 m a.s.l.); collected by Zhixian Sun, 8 July 2024.

Vouchers for molecular study. • ASIZB 242021–242022, 2 specimens, Xing County, Lvliang City, Shanxi Province, from the main stream of the Yellow River (38.5193°N, 110.9072°E, ca 780 m a.s.l.); collected by Yutian Fang, 22 May 2024. • ASIZB 242025, 1 specimen, Baode County, Xinzhou City, Shanxi Province, from the main stream of the Yellow River (38.7821°N, 110.9691°E, ca 780 m a.s.l.); collected by Zhixian Sun, 21 May 2024. • ASIZB 242026, 1 specimen, Liulin County, Lvliang City, Shanxi Province, from the main stream of the Yellow River (37.3947°N, 110.6316°E, ca 630 m a.s.l.); collected by Yutian Fang, 26 May 2024. • ASIZB 242030, 1 specimen, Hangjin Banner, Ordos City, Inner Mongolia Autonomous Region, from the main stream of the Yellow River (40.6085°N, 107.2969°E, ca 1040 m a.s.l.); collected by Junyuan Hao, 28 June 2024.

Diagnosis. This species can be distinguished from other *Gobio* species in the Yellow River drainage by following characteristics: barbel reaching beyond posterior preopercle margin (vs. reaching between vertical of posterior orbit and posterior preopercle margin in *G. rivuloides* and *G. coriparoides*); lateral-line scales 41–44 (mode 43, mean 42) (vs. mean 40 in *G. coriparoides*); circumpeduncular scales 14–16 (mode 16, mean 16) (vs. mean 12 in *G. rivuloides*, 18 in *G. coriparoides* and 20 in *G. guentheri*); longitudinal epithelial crests present on pre-dorsal scales (vs. absent in G. coriparoides and G. guentheri); anus centrally located between pelvic-fin base and anal-fin origin (vs. positioned at posterior one-third of distance from pelvic-fin base end to anal fin origin in *G. coriparoides* and *G. guentheri*).

Redescription. Body elongated, dorsal body profile rising from nostrils to dorsal-fin origin, dropping along dorsal-fin base, then gradually sloping to caudal-fin base.

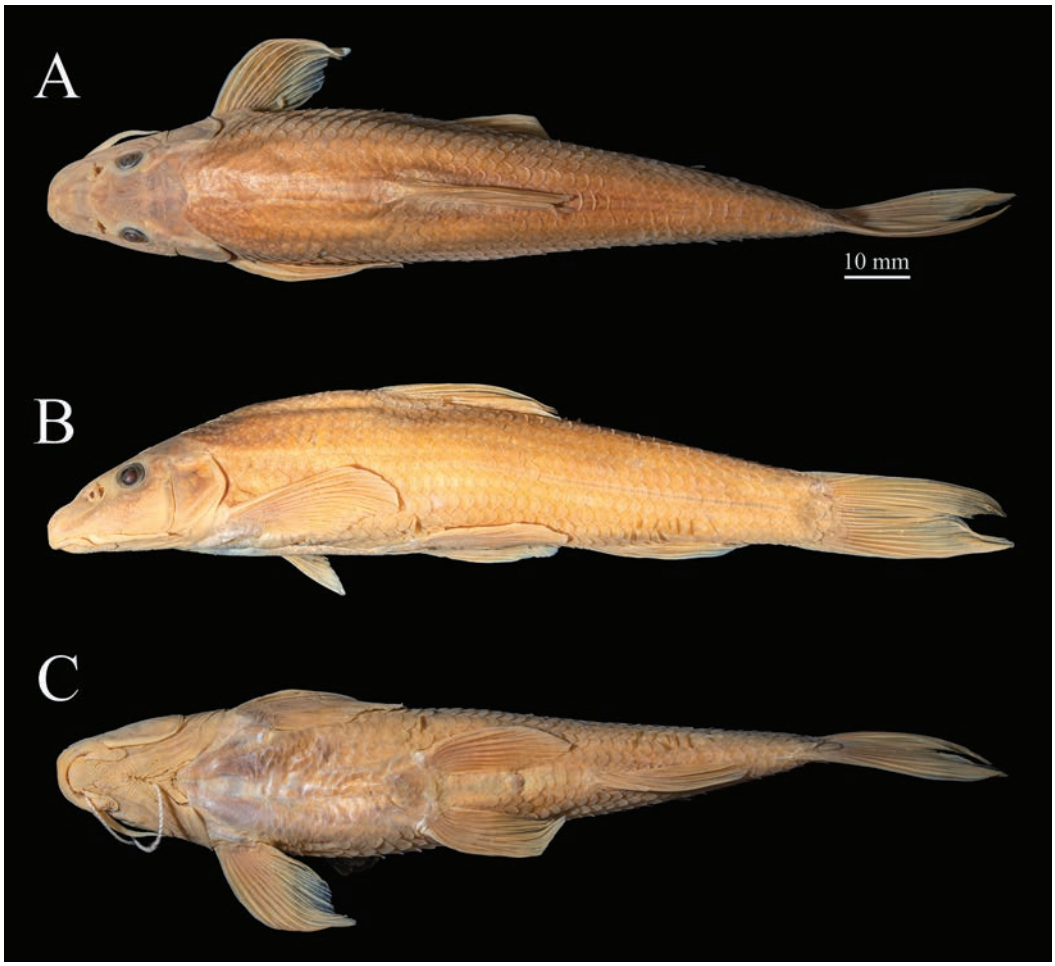

Figure 1. *Gobio huanghensis*, syntype, IHB 56–IX–004, 121.9 mm SL. **A.** Dorsal view; **B** Lateral view; **C** Ventral view; photographed by Yiyang Xu.

Maximum body depth at dorsal-fin origin. Head elongated, length larger than body depth; snout pointed and elongated, with moderate concavity on top of snout before nostrils. Mouth horseshoe-shaped and inferior, with one pair of maxillary barbels root at extremity of upper lip, barbel elongated, extending over posterior preopercle margin. Upper lip thin, lower lip fused with throat, lateral lobes of lower lip well developed, lips connected at mouth corner, tiny papillae on lips, lateral lobes, and chin (Fig. 3A). Eyes positioned on dorsal half of head; interorbital region flattened; width slightly larger than eye diameter. Thoracic region flattened, abdomen rounded, caudal peduncle robust, compressed laterally. Anus centrally located between pelvic-fin base and anal-fin origin.

Body covered with moderately large cycloid scales. Lateral line complete, almost straight in lateral center. Lateral line scales 41 (1 specimen), 42 (7), 43 (11), 44 (3); scales above lateral line 6 (2), 6.5 (19), 7.5 (1); scales below lateral line 3 (1), 4 (21); circumpeduncular scales 14 (2), 16 (20). Longitudinal epithelial crests present on pre-dorsal region scales (Fig. 3B); ventral scaleless region only before pectoral-fin base end.

Dorsal fin with three unbranched and seven (22 specimens) branched rays; distal margin concave, origin closer to snout than caudal-fin base. Pectoral fin with one unbranched and 13 (3), 14 (19) branched rays; tip of adpressed not reaching anterior margin of pelvic-fin insertion. Pelvic fin with one unbranched and seven (22) branched rays; tip of adpressed reaching to posterior anus. Anal fin with three unbranched and six (22) branched rays; origin closer to pelvic-fin insertion than to caudal-fin base. Caudal fin deeply forked, with nine branched rays on upper lobes and eight branched rays on lower lobes, lobes pointed, upper lobes slightly more pointed than lower lobes.

Total vertebrae 4+37–38. Gill rakers rudimentary. Pharyngeal teeth “3, 5–5, 3”.

Coloration in life. Dorsal side of head and body greyish brown, mid-lateral side shallow greyish yellow, and ventral side grayish white. Dorsal side of body with 5–6 black crossbars (first at posterior of head, second at dorsal-fin base origin, third at posterior of dorsal-fin base, fourth at vertical position above anal-fin base origin, fifth and sixth on caudal peduncle, respectively). Flank with 7–9 black blotches; margin of scales on back and flank slightly black pigmented. One slightly fluorescent yellowish-green stripe extends above lateral line. One distinct black stripe between anterior orbit and snout. Fins translucent, with slightly black pigments on dorsal fin, pectoral fin, and caudal fin rays; fins without black spots (Fig. 2B).

Figure 2. General view of *Gobio huanghensis*. **A.** Preserved specimen, ASIZB 242040, 88.6 mm SL; **B.** Freshly caught individual, uncatalogued, Fengjiachuan Township, Baode County, Xinzhou City, Shanxi Province, from the main stream of the Yellow River.

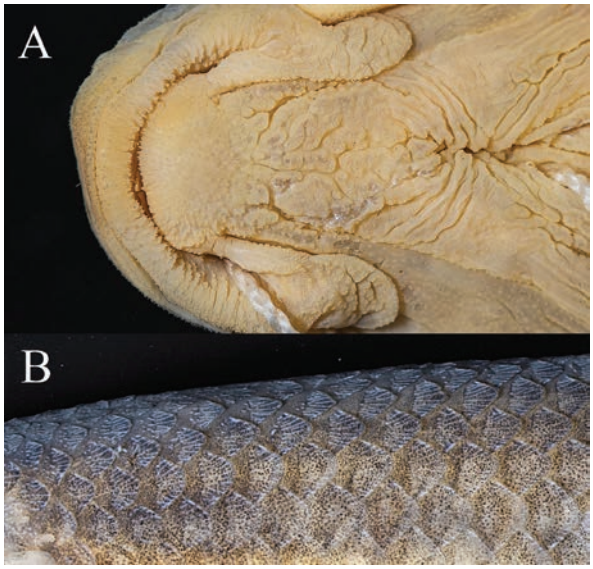

Figure 3. Mouth and pre-dorsal region of *Gobio huanghensis*. **A.** Tiny papillae on lips, lateral lobes, and chin; **B.** Epithelial crests on pre-dorsal region scales. Photographed by Yiyang Xu.

Coloration in preservation. Dorsal side of head and body yellowish grey, mid-lateral side shallow yellowish grey, and ventral side greyish white. Dorsal side of body with 5–6 black crossbars in same position as live individual. Flank with 7–9 dark grey blotches, first three or four blotches vague. Margin of scales on back and flank slightly black pigmented. The fluorescent yellowish-green stripe faded. One distinct black stripe between anterior orbit and snout. Fins pale, with slightly black pigments on dorsal fin, pectoral fin, and caudal fin rays; fins without black spots. The black pigments on fin rays faded after long-time preserve.

Sexual dimorphism. No sexual dimorphism observed.

Distribution. *Gobio huanghensis* is distributed in the main stream of the Yellow River drainage, from Lanzhou City, Gansu Province, to Yongji City, Yuncheng City, and Shanxi Province (Fig. 4A).

Habitat and biology. *Gobio huanghensis* inhabits the main stream of the Yellow River. It usually appears in fast-flowing water with sandy bottoms and high turbidity, which is caused by fine sediments. It feeds in sand on the bottom of the river.

Remarks. *Gobio tchangi* was originally described by Li (2015). In the original description, *G. tchangi* is said to resemble *G. huanghensis*, the only difference between the two species being the location of the anus (3.5 scales from anus to anal-fin base in *G. tchangi* vs. 5 scales in *G. huanghensis*). However, after carefully measuring specimens of both *G. tchangi* and *G. huanghensis*, the 3.5 scales from the anus to the anal-fin base in *G. tchangi* were found to be incorrect. The holotype of *G. tchangi* (ASIZB 56774, Fig. 5A) has 5 scales between the anus and anal-fin base, and other specimens of *G. tchangi* (ASIZB 56773, 56775–56778) also had 5–6 scales between the anus and the anal-fin base. Additionally, the scales between the anus and anal-fin base are not neatly aligned, making this an unreliable taxonomic trait. Therefore, we use the pelvic fin-anus distance and anus-anal fin distance to measure the position of the anus. The position of the anus did not differ between the two nominal species (pelvic fin-anus distance averaged 94.0% of anus-anal fin distance in *G. tchangi*, compared to 98.1% in *G. huanghensis*).

To further compare the morphological difference between *Gobio huanghensis* and *G. tchangi*, a PCA based on 22 specimens, including the holotype *of G. tchangi,* was generated. The first three components contributed 98.3% of the variance. Principal component 1 (PC 1) primarily represents the body size of the specimens, while PC 2 and PC 3 reflect their morphology. PCA loadings (Table 3) indicate that body depth, pelvic-fin base length, and anal-fin base length contribute most to PC 2. Even these characters have high loadings; *G. huanghensis* and *G. tchangi* were not separated in PC 2 or in PC 3 (Fig. 6).

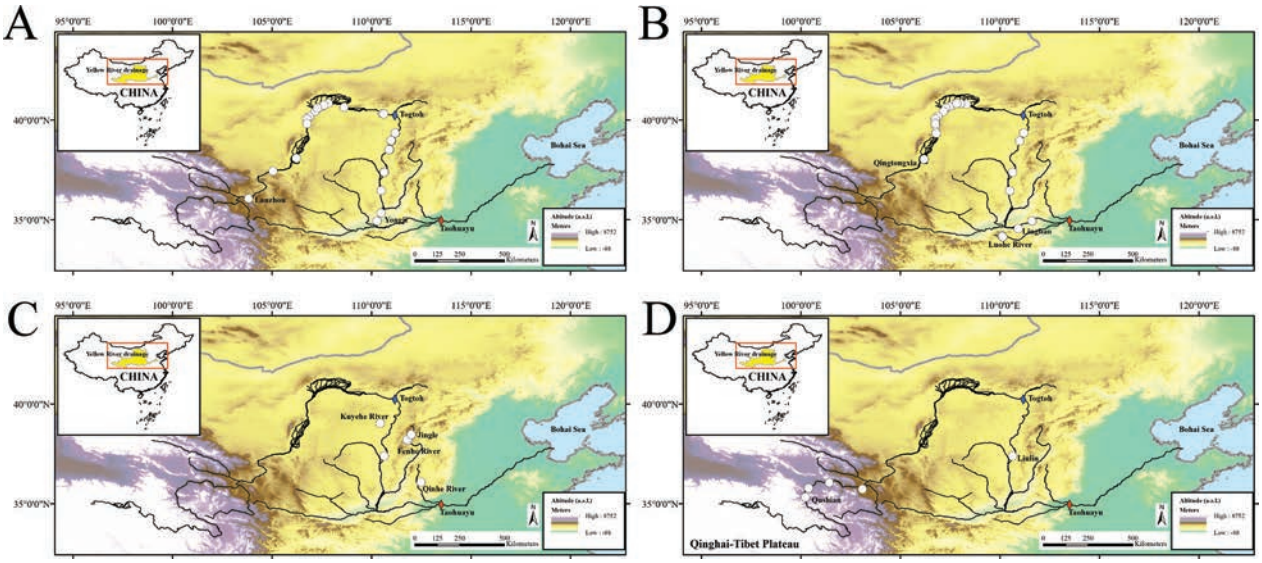

Figure 4. The distribution of the four *Gobio* species in the Yellow River drainage. **A.** *Gobio huanghensis*; **B.** *Gobio rivuloides*; **C.** *Gobio coriparoides*; **D.** *Gobio guentheri*.

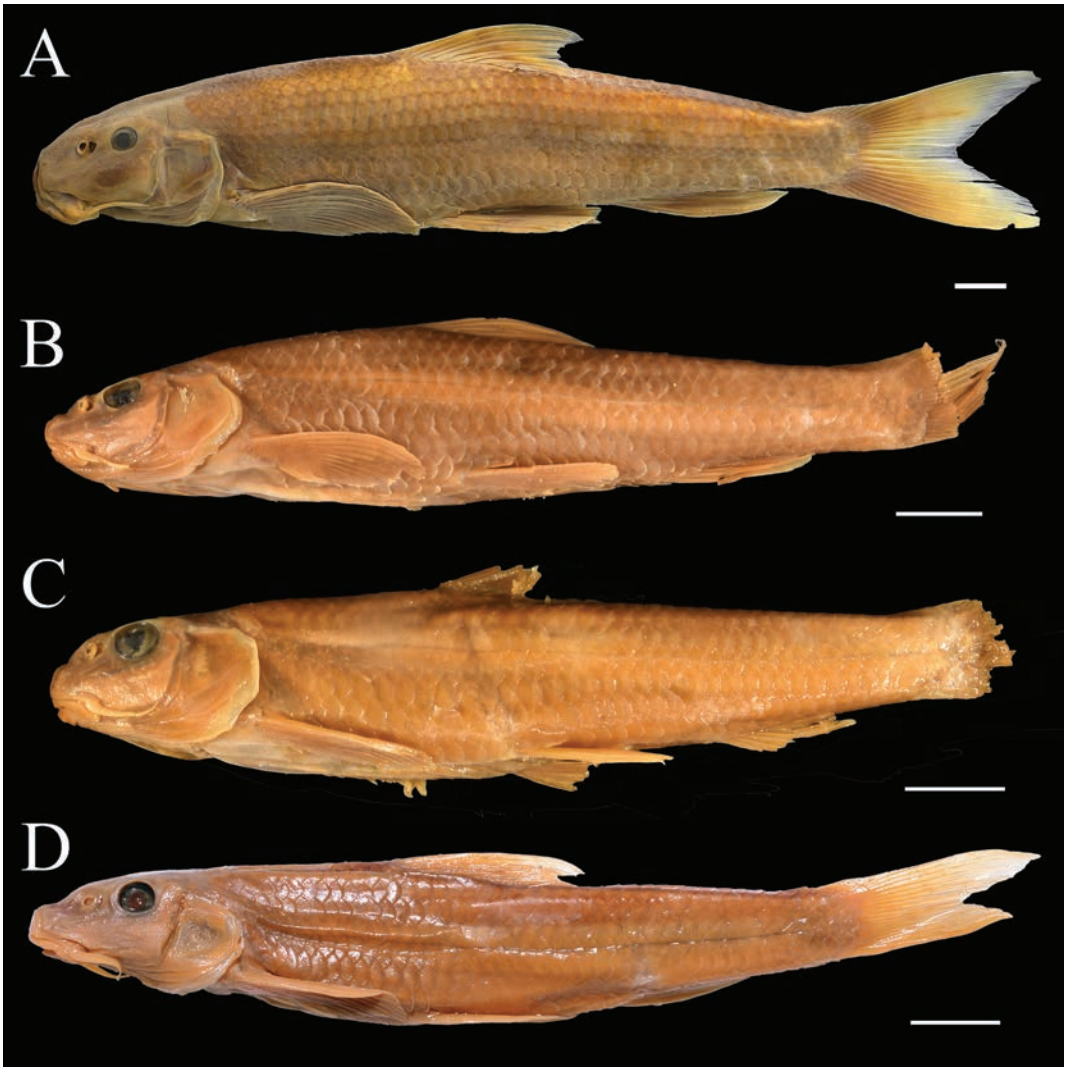

Figure 5. The type specimens of four invalid *Gobio* species in the Yellow River drainage. **A.** *Gobio tchangi* (= *G. huanghensis*), holotype, ASIZB 56774, 152.8 mm SL, photographed by Xueyuan Li; **B.** *Romanogobio johntreadwelli* (= *G. rivuloides*), holotype, AMNH 29694, 93.7 mm SL, photographed by Ryan J. Thoni; **C.** *Romanogobio amplexilabris* (= *G. rivuloides*), holotype, AMNH 29696, 80.6 mm SL, photographed by Ryan J. Thoni; **D.** *Gobio meridionalis* (= *G. rivuloides*), paratype, IHB 81–7–1997, 88.6 mm SL; photographed by Zhixian Sun.

Table 2. Morphometric measurements of *Gobio* species in the Yellow River drainage.

Characters	*Gobio huanghensis* (n = 17)			*Gobio tchangi* (n = 6)				*Gobio rivuloides* (n = 10)		
				Holotype	Holotype + Other Specimens					
	Range	Mean	SD		Range	Mean	SD	Range	Mean	SD
Dorsal-fin rays	7	7		7	7	7		7	7	
Anal-fin rays	6	6		6	6	6		6–7	6	
Pectoral-fin rays	13–14	14		14	13–14	14		13–14	14	
Pelvic-fin rays	7	7		7	7	7		7	7	
Lateral line scales	42–44	43		43	41–43	42		40–43	42	
Scales above lateral line	6–7.5	6.5		6.5	6–6.5	6.5		5.5–7.5	6	
Scales below lateral line	3–4	4		4	4	4		3–4	3	
Circumpeduncular scales	14–16	16		14	14–16	16		14–16	14	
SL (mm)	64.7–128.9			152.8	115.6–157.6			66.9–119.2		
In percent of SL										
Body depth	18.0–24.1	21.2	1.7	21.0	16.5–21.0	18.8	1.8	19.0–22.8	20.5	1.5
Dorsal-fin base length	13.0–15.7	14.3	0.7	13.9	13.8–15.2	14.4	0.6	13.5–15.1	14.5	0.5
Pectoral-fin base length	4.2–5.8	5.2	0.5	6.4	4.8–6.4	5.8	0.6	4.5–6.6	5.7	0.6
Pelvic-fin base length	3.9–5.7	4.7	0.6	5.1	4.4–5.1	4.7	0.3	3.9–5.6	4.8	0.6
Anal-fin base length	9.1–10.5	9.9	0.4	10.8	10.2–11.5	10.7	0.4	8.6–10.8	9.3	0.7
Pre-dorsal length	43.8–48.7	46.8	1.5	45.9	44.9–46.3	45.9	0.5	41.7–49.9	45.8	2.6
Pre-pectoral length	23.7–25.6	24.5	0.6	23.3	23.3–25.1	24.0	0.7	23.3–33.7	25.8	2.9
Pre-pelvic length	47.1–51.2	48.7	1.1	48.3	47.2–50.3	48.7	1.3	45.2–51.1	48.1	1.8
Pre-anal length	68.8–73.8	71.5	1.3	71.1	70.2–73.5	71.4	1.5	69.7–73.4	71.2	1.1
Post-dorsal length	52.7–58.5	56.8	1.3	56.4	55.8–58.8	57.0	1.0	54.1–62.0	57.7	2.8
Caudal peduncle length	18.8–22.1	20.0	0.8	19.0	18.3–19.6	19.1	0.5	22.3–17.8	20.2	1.5
Caudal peduncle depth	9.0–12.2	9.9	0.7	9.8	8.8–9.8	9.1	0.4	8.3–11.5	9.6	1.0
Head length (mm)	16.4–32.0			36.1	27.7–36.7			16.9–27.5		
In percent of HL										
Head depth	53.0–62.6	55.7	2.7	59.9	54.1–62.2	57.6	3.1	55.7–62.4	58.7	2.1
Head width	53.4–64.1	59.9	3.3	61.9	53.2–70.3	60.3	6.1	58.8–65.3	62.4	2.2
Eye diameter	20.8–27.0	23.3	1.8	20.4	19.8–22.3	21.1	0.9	24.7–32.1	27.6	2.1
Interorbital width	20.4–27.1	23.3	1.7	22.7	21.9–24.5	23.2	1.0	18.4–24.7	21.9	1.9
Snout length	34.8–46.6	41.2	3.2	43.6	39.4–43.6	42.1	1.4	33.4–39.4	35.6	1.7
Barbel length	41.3–57.1	47.3	4.7	45.3	45.3–58.2	51.5	4.3	31.8–39.9	36.3	2.9

	Gobio meridionalis (n = 24)						*Gobio coriparoides* (n = 15)			*Gobio guentheri* (n = 11)		
	Paratypes (n = 6)			Other specimens (n = 18)								
	Range	Mean	SD	Range	Mean	SD	Range	Mean	SD	Range	Mean	SD
Dorsal-fin rays	7	7		7	7		7	7		7	7	
Anal-fin rays	6	6		6	6		6	6		6	6	
Pectoral-fin rays	14–15	14		13–15	13		14–15	14		14–15	15	
Pelvic-fin rays	7	7		7	7		7	7		7	7	
Lateral line scales	40–42	42		41–43	42		39–41	40		40–43	42	
Scales above lateral line	5.5	5.5		5.5	5.5		6.5–7.5	6.5		5–8	7	
Scales below lateral line	3	3		2–3	3		4–5	4		4	4	
Circumpeduncular scales	12	12		12–14	12		16–18	18		20–24	20	
SL (mm)	60.0–88.6			72.1–109.1			60.0–81.8			69.0–143.4		
In percent of SL												
Body depth	17.7–21.8	19.4	1.5	18.6–22.5	20.6	1.1	22.6–26.8	25.5	1.2	21.4–30.1	26.5	2.6
Dorsal-fin base length	12.7–15.2	13.8	0.9	13.4–15.1	14.2	0.4	13.1–16.1	14.9	1.0	14.0–16.7	15.2	0.7
Pectoral-fin base length	5.2–6.9	6.2	0.7	4.9–6.3	5.6	0.4	4.8–6.9	5.7	0.6	5.5–7.1	6.2	0.5
Pelvic-fin base length	3.8–5.7	4.6	0.6	4.3–5.6	5.0	0.3	4.3–6.1	5.3	0.5	5.3–7.3	6.0	0.6
Anal-fin base length	8.1–9.7	8.9	0.7	8.6–9.9	9.3	0.4	9.1–11.2	10.1	0.6	9.3–11.3	10.3	0.6
Pre-dorsal length	42.5–46.3	44.5	1.2	42.8–46.7	44.1	0.9	44.8–48.6	46.7	1.2	45.7–49.6	47.8	1.1
Pre-pectoral length	23.8–27.1	25.6	1.2	22.0–25.3	23.7	0.8	24.3–27.3	25.7	0.9	24.3–27.4	25.6	0.9
Pre-pelvic length	47.4–50.9	49.3	1.2	47.4–50.6	49.1	1.0	45.8–48.7	47.3	0.8	47.2–50.5	48.9	1.2
Pre-anal length	68.7–74.9	72.1	2.4	69.3–73.8	72.0	1.3	68.5–72.6	70.2	1.2	70.9–76.6	73.3	1.9
Post-dorsal length	55.5–58.8	56.7	1.2	56.4–61.7	58.3	1.2	55.5–58.3	56.7	0.9	53.7–57.8	56.0	1.3
Caudal peduncle length	15.6–19.7	18.1	1.4	17.9–21.3	19.7	0.9	18.0–23.7	21.0	1.3	17.3–20.9	19.3	1.1
Caudal peduncle depth	9.1–10.0	9.8	0.3	8.8–10.3	9.5	0.6	11.4–13.5	12.3	0.6	10.7–13.9	12.8	1.1
Head length (mm)	14.6–23.6			17.6–24.8			14.9–20.8			16.3–34.3		
In percent of HL												
Head depth	50.8–60.4	55.8	3.8	52.7–65.6	58.0	2.8	61.0–69.4	65.2	2.1	54.6–64.5	60.6	3.3
Head width	47.1–60.5	53.2	4.6	53.2–74.8	62.4	5.2	63.2–72.4	66.9	2.7	55.1–65.9	61.4	3.8
Eye diameter	20.9–26.4	24.4	2.3	23.7–29.1	25.7	1.3	24.6–29.3	27.0	1.4	22.1–28.6	24.5	2.1
Interorbital width	24.4–29.6	27.2	2.0	23.5–29.3	26.1	1.4	24.0–32.6	29.9	2.2	24.9–30.4	27.3	2.2
Snout length	35.1–43.2	38.3	3.9	31.9–37.7	34.4	1.6	27.6–33.6	30.4	1.7	29.9–36.9	34.2	2.3
Barbel length				31.1–39.5	35.5	2.3	30.4–41.2	35.7	3.4	53.3–89.4	72.1	10.7

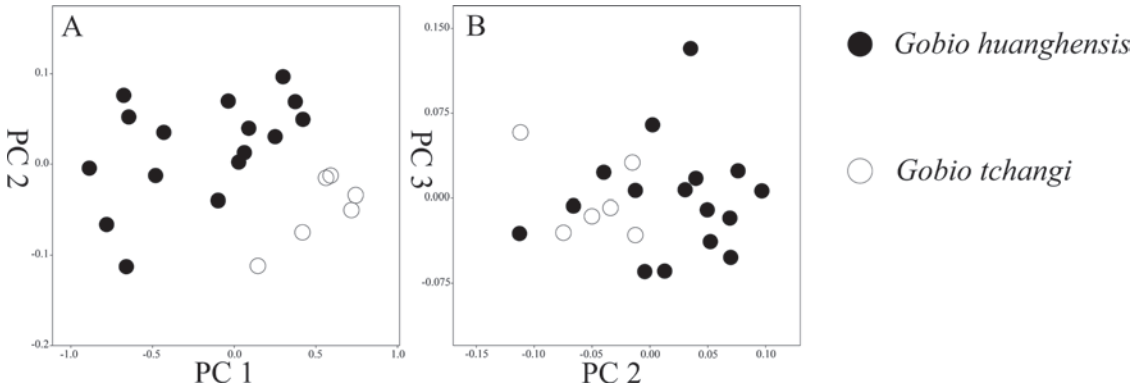

Figure 6. A. Scatterplot of PC1 against PC2 and **B.** PC2 against PC3 extracted from 19 morphometric data of *Gobio huanghensis* and *Gobio tchangi*.

Table 3. Loadings on the first three principal components extracted from morphometric data of *Gobio huanghensis* and *G. tchangi*.

Morphometric measurements	PC 1	PC 2	PC 3
Standard length	0.235	–0.046	–0.015
Body depth	0.222	0.579	0.100
Head length	0.217	0.037	–0.029
Head depth	0.226	0.160	0.128
Head width	0.235	0.235	–0.227
Dorsal-fin base length	0.223	–0.135	0.272
Pectoral-fin base length	0.278	–0.265	–0.710
Pelvic-fin base length	0.220	–0.571	0.327
Anal-fin base length	0.242	–0.294	0.208
Caudal peduncle length	0.218	–0.041	–0.102
Caudal peduncle depth	0.214	0.211	0.292
Eye diameter	0.155	0.071	–0.095
Interorbital width	0.234	0.121	0.180
Snout length	0.244	–0.001	–0.202
Pre-dorsal length	0.237	0.072	–0.099
Pre-pectoral length	0.228	0.028	0.023
Pre-pelvic length	0.237	–0.002	0.058
Pre-anal length	0.238	0.010	0.018
Post-dorsal distance	0.235	–0.078	0.036

Additionally, the type locality of *Gobio tchangi* is Lanzhou City, Gansu Province, which is the same as that of *G. huanghensis*. Based on the morphological comparisons and distribution, we treat *G. tchangi* as a junior synonym of *G. huanghensis*.

Gobio rivuloides Nichols, 1925

Figs 7, 8, Table 2

Gobio rivuloides Nichols, 1925: 5.
Gobio (*Romanogobio*) *johntreadwelli*: Bănărescu & Nalbant (1973): 145.
Gobio (*Romanogobio*) *amplexilabris*: Bănărescu & Nalbant (1973): 147.
Gobio meridionalis: Chen et al. (1987): 119.
Romanogobio johntreadwelli: Naseka (1996): 160.
Romanogobio amplexilabris: Naseka (1996): 160.
Romanogobio rivuloides: Naseka (1996): 160.

Material examined. • AMNH 8420 (Holotype), 1 specimen, 133.5 mm SL; Niang-tze-kwan, Shansi (=Niangziguan Township, Pingding County, Yangquan City, Shanxi Province), collected by C. H. Pope. AMNH 29694, 1 specimen, 93.7 mm SL; Linfen City, Shanxi Province, from the Qingshuihe River, a tributary of the Yellow River drainage. • AMNH 29696, 1 specimen, 80.6 mm SL; Linfen City, Shanxi Province, from the Qingshuihe River, a tributary of the Yellow River drainage. IHB 81–7–1981, 81–7–1983, 81–7–1984, 81–7–1985, 81–7–1987, 81–7–1997, 6 specimens, 60.0–88.6 mm SL; Lingbao City, Sanmenxia City, Henan Province, from the Hongnongjian River. • ASIZB 241458, 1 specimen, 109.1 mm SL; Hequ County, Xinzhou City, Shanxi Province, from the main stream of the Yellow River (39.3502°N, 111.1931°E, ca 840 m a.s.l.); collected by Yutian Fang, 17 October 2023. • ASIZB 241459, 1 specimen, 96.9 mm SL; Xing County, Lvliang City, Shanxi Province, from the main stream of the Yellow River (38.5145°N, 110.8782°E, ca 760 m a.s.l.); collected by Xin Wang, 2 March 2022. • ASIZB 242016–242018, 3 specimens, 84.5–100.2 mm SL, Wuhai City, Inner Mongolia Autonomous Region, from the main stream of the Yellow River (39.7124°N, 106.7635°E, ca 1060 m a.s.l.); collected by Junyuan Hao, 11 May 2024. • ASIZB 241457, 1 specimen, 82.5 mm SL; Pingshan County, Shijiazhuang City, Hebei Province, from the Hutuohe River (38.3994°N, 113.6947°E, ca 280 m a.s.l.); collected by Zhixian Sun, 6 July 2023. • ASIZB 215395, 1 specimen, 70.3 mm SL; Yangyuan County, Zhangjiakou City, Hebei Province, from the Sangganhe River (40.1735°N, 114.5267°E, ca 820 m a.s.l.); 20 October 2019. • ASIZB 239685–239687, 3 specimens, 73.7–98.9 mm SL; Shangyi County, Zhangjiakou City, Hebei Province, from the Yanghe River (40.8887°N, 114.2029°E, ca 1040 m a.s.l.); collected by Chen Tian, 2 October 2023. • ASIZB 242027–242028, 242042, 3 specimens, 66.9–77.9 mm SL; Luonan County, Shangluo City, Shaanxi Province, from the Luohe River, a tributary of the Yellow River drainage (34.1927°N, 110.0943°E, ca 1010 m a.s.l.); collected by Yutian Fang, 28 May 2024. • ASIZB 242043–242046, 4 specimens, 87.8–93.9 mm SL; Qingtongxia City, Wuzhong County, Ningxia Hui Autonomous Region, from the main stream of the Yellow River (38.0387°N, 106.1837°E, ca 1130 m a.s.l.); collected by Junyuan Hao, 4 August 2024. • ASIZB 242047–242051, 5 specimens, 72.1–92.0 mm SL; Hangjin Banner, Ordos City, Inner Mongolia Autonomous Region,

Figure 7. *Gobio rivuloides*, holotype, AMNH 8420, 133.5 mm SL. **A.** Dorsal view; **B.** Lateral view; **C.** Ventral view; photographed by Ryan J. Thoni.

from the main stream of the Yellow River (40.8379°N, 107.8308°E, ca 1030 m a.s.l.); collected by Junyuan Hao, 30 July 2024. • ASIZB 242052–242055, 4 specimens, 75.8–85.1 mm SL; Bohaiwan County, Wuhai City, Inner Mongolia Autonomous Region, from the main stream of the Yellow River (39.8317°N, 106.7551°E, ca 1070 m a.s.l.); collected by Junyuan Hao, 27 July 2024. • ASIZB 242056–242057, 2 specimens, 118.3–119.2 mm SL; Huailai County, Zhangjiakou City, Hebei Province, from the Yanghe River, a tributary of the Haihe River drainage (40.3804°N, 115.3630°E, ca 490 m a.s.l.); collected by Chen Tian, 28 July 2023.

Vouchers for molecular study. ASIZB 219283, 1 specimen, Huguan County, Changzhi City, Shanxi Province, from the Xihe River, a tributary of the Haihe River drainage (35.9271°N, 113.6309°E, ca 540 m a.s.l.); collected by Zhixian Sun, 2 September 2020. ASIZB 239687, 1 specimen, Shangyi County, Zhangjiakou City, Hebei Province, from the Yanghe River, a tributary of the Haihe River drainage (40.8887°N, 114.2029°E, ca 1040 m a.s.l.); collected by Chen Tian, 2 October 2023. ASIZB 241457, 1 specimen, Pingshan County, Shijiazhuang City, Hebei Province, from the Hutuohe River, a tributary of the Haihe River drainage (38.3994°N, 113.6947°E, ca 280 m a.s.l.); collected by Zhixian Sun, 6 July 2023. ASIZB 242027–242028, 2 specimens, Luonan County, Shangluo City, Shaanxi Province, form the Luohe River, a tributary of the Yellow River drainage (34.1927°N, 110.0943°E, ca 1010 m a.s.l.); collected by Yutian Fang, 28 May 2024. ASIZB 241459, 1 specimen, Xing County, Lvliang City, Shanxi Province, from the main stream of the Yellow River (38.5145°N, 110.8782°E, ca 760 m a.s.l.); collected by Xin Wang, 2 March 2022. ASIZB 242016, 242018, 2 specimens, Wuhai City, Inner Mongolia Autonomous Region, from the main stream of the Yellow River (39.7124°N, 106.7635°E, ca 1060 m a.s.l.); collected by Junyuan Hao, 11 May 2024. ASIZB 242062, 1 specimen, Daning County, Linfen City, Shanxi Province, from the main stream of the Yellow River (36.4587°N, 110.4876°E, ca 600 m a.s.l.); collected by Zhixian Sun, 8 July 2024.

Diagnosis. This species can be distinguished from other *Gobio* species in the Yellow River drainage by following characteristics: barbel reaching between vertical position of posterior orbit and posterior preopercle margin (vs. reaching beyond posterior preopercle margin in *G. huanghensis* and *G. guentheri*); lateral-line scales 40–43 (mode 42, mean 42) (vs. mean 40 in *G. coriparoides*); circumpeduncular scales 12–16 (mode 12, mean 12) (vs. more than 16 in *G. huanghensis*, *G. coriparoides*, and *G. guentheri*); longitudinal epithelial crests present on pre-dorsal scales (vs. absent in *G. coriparoides* and *G. guentheri*); anus centrally located between pelvic-fin base and anal-fin origin or closer to pelvic-fin base (vs. positioned at posterior one-third of distance from pelvic-fin base end to anal fin origin in *G. coriparoides* and *G. guentheri*).

Redescription. Body elongated, dorsal body profile rising from nostrils to dorsal-fin origin, dropping along dorsal-fin base, then gradually sloping to caudal-fin base. Maximum body depth at dorsal-fin origin. Head relative

Figure 8. General view of *Gobio rivuloides*. **A.** Preserved specimen, ASIZB 242042, 66.9 mm SL; **B.** Same individual in life.

elongated, length slightly larger than body depth; snout relative elongated. Mouth horseshoe-shaped and inferior, with one pair of maxillary barbels root at extremity of upper lip, barbel relative elongated, reaching from vertical position of posterior orbit to posterior preopercle margin. Lips thin, lower lip fused with throat; lips connected at mouth corner. Eyes positioned on dorsal half of head; interorbital region flattened; width almost equal to eye diameter. Thoracic region flattened, abdomen rounded, caudal peduncle robust, compressed laterally. Anus centrally located between pelvic-fin base and anal-fin origin or closer to pelvic-fin base.

Body covered with moderately large cycloid scales. Lateral line complete, almost straight in lateral center. Lateral line scales 40 (4 specimens), 41 (9), 42 (17), 43 (4); scales above lateral line 5.5 (27), 6 (3), 6.5 (3), 7.5 (1); scales below lateral line 2 (1), 3 (30), 4 (3); circumpeduncular scales 12 (23), 14 (9), 16 (2). Longitudinal epithelial crests present on pre-dorsal region scales; the ventral scaleless region extends to middle of pectoral-fin base and to pelvic-fin base.

Dorsal fin with three unbranched and seven (34 specimens) branched rays; distal margin concave, origin closer to snout than caudal-fin base. Pectoral fin with one unbranched and 13 (15), 14 (16), and 15 (3) branched rays; tip of adpressed not reaching anterior margin of pelvic-fin insertion. Pelvic fin with one unbranched and seven (34) branched rays; tip of adpressed reaching to posterior anus. Anal fin with three unbranched and six (33), seven (1) branched rays; origin closer to pelvic-fin insertion than to caudal-fin base. Caudal fin deeply forked, with nine branched rays on upper lobes and eight branched rays on lower lobes, lobes pointed, upper lobes slightly more pointed than lower lobes.

Total vertebrae 4+34–36. Gill rakers rudimentary. Pharyngeal teeth “3, 5–5, 3”.

Coloration in life. Dorsal side of head and body brownish yellow, mid-lateral side shallow brownish yellow, and ventral side grayish white. Dorsal side of body with 5–6 black crossbars (first at posterior of head, second at dorsal-fin base origin, third at posterior of dorsal-fin base, fourth at vertical position above anal-fin base origin, fifth and sixth on caudal peduncle, respectively). Flank with 7–10 black blotches; margin of scales on back and flank black pigmented. One slightly fluorescent yellowish-green stripe extends above lateral line. One distinct black stripe between anterior orbit and snout. Fins translucent, dorsal fin, pectoral fin, pelvic fin, and caudal fin with some black spots (Fig. 8B). The specimens collected in the main stream of the Yellow River have paler color and less black spots than those specimens that were collected from the tributaries. We assume that because the water from the main stream of the Yellow River is more turbid (caused by sand), the fish present lighter colors.

Coloration in preservation. Dorsal side of head and body greyish brown, mid-lateral side greyish yellow, and ventral side greyish white. Dorsal side of body with 5–6 black crossbars in same position as live individual. Flank with 7–10 dark grey blotches, first three or four blotches vague. Margin of scales on back and flank black pigmented. The fluorescent yellowish-green stripe faded. One distinct black stripe between anterior orbit and snout. Fins pale, dorsal fin, pectoral fin, pelvic fin, and caudal fin with some black spots. The color of specimens that were

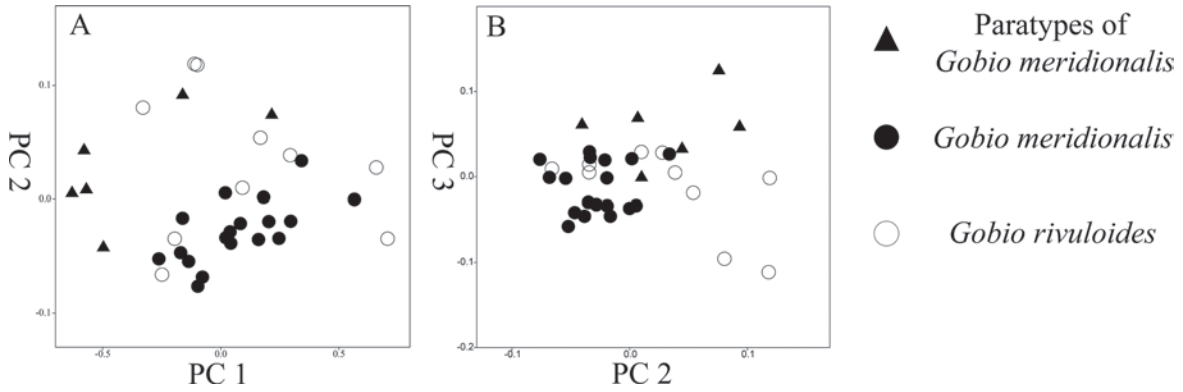

Figure 9. A. Scatterplot of PC1 against PC2 and **B.** PC2 against PC3 extracted from 19 morphometric data of *Gobio meridionalis* and *G. rivuloides*.

collected in mainstream of the Yellow River could be lighter, dorsal side of head and body shallow greyish yellow, mid-lateral and ventral sides greyish white. Dorsal side of body with 5–6 shallow black crossbars in same position as live individual. The blotches on flank vague, merge into a shallow dark stripe from posterior head to caudal peduncle end. Margin of scales on back and flank slightly black pigmented. The fluorescent yellowish-green stripe faded. One distinct black stripe between anterior orbit and snout. Fins pale, with slightly black pigments on dorsal fin, pectoral fin, and caudal fin rays; fins without black spots. The black pigments on fin rays faded after long-time preserve.

Sexual dimorphism. No sexual dimorphism observed.

Distribution. *Gobio rivuloides* is widely distributed in the Yellow River drainage and the Haihe River drainage. In the Yellow River drainage, this species is distributed in both the mainstream, from Qingtongxia City to Lingbao City, and the tributaries, such as the Luohe, Qijiahe, Qinhe, and Hongnongjian Rivers, etc. (Fig. 4B).

Habitat and biology. *Gobio rivuloides* inhabits both the main stream and the tributaries of the Yellow River. It usually appears in fast-flowing water with sandy bottoms with gravel and pebbles. It feeds on the bottom of the river.

Remarks. *Romanogobio johntreadwelli* and *R. amplexilabris* were originally described by Bănărescu and Nalbant (1973) in the subgenus *Romanogobio* under the genus *Gobio*. This subgenus was treated as a genus in the subsequent studies (e.g., Naseka 1996). Naseka (1996) put these species into the genus *Romanogobio*. The type locality of these species is the Qingshuihe River, a tributary of the Yellow River drainage in Shanxi Province. We tried to collect more topotypes of these two species, but unfortunately, the habitat of the type locality has been degraded and the river has dried up. We examined the holotype (Fig. 5B, C) and paratypes of both species. The specimens have 40–42 lateral line scales, scales above lateral line 5.5, scales below lateral line 3, circumpeduncular scales 12, the anus positioned at middle of the pelvic-fin base end to the anal-fin origin or closer to the pelvic-fin base, a total of vertebrae 4+35, and a barbel relative elongated, reaching from vertical position of posterior orbit to posterior preopercle margin. All of the characters described above agree with those of *Gobio rivuloides*. *Romanogobio johntreadwelli* and *R. amplexilabris* are junior synonyms of *G. rivuloides*.

Gobio meridionalis (Fig. 5D) was originally described by Xu in Chen et al. (1987). According to the original description, this species is similar to *G. rivuloides*, but it has 12 circumpeduncular scales (vs. 14 in *G. rivuloides*) and lacks black spots on its body. Following this original description, we identified some specimens as *G. meridionalis*. We measured a series of characters of *G. meridionalis* (including the paratypes) and *G. rivuloides* and then conducted PCA for a detailed comparison. The first three components contributed 94.6% of the variance. Principal component 1 (PC 1) primarily represents the body size of the specimens, while PC 2 and PC 3 reflect their morphology. The PCA loadings presented in Table 4 indicate that pelvic-fin base length, snout length, and pre-pectoral length contribute most to PC 2. Even these characters have high loadings; *G. meridionalis* and *G. rivuloides* could not be separated in PC 2, nor in PC 3. However, neither PC 1 versus PC 2 nor PC 2 versus PC 3 could separate these two species (Fig. 9). The difference in coloration should be related to water turbidity (Kottelat and Persat 2005); the high turbidity of water in the main stream causes the lighter color of *G. meridionalis*, while the low turbidity of water in the tributaries causes the darker coloration and black spots of *G. rivuloides*. The circumpeduncular scales with several traits were also reported in *G. lozanoi* and *G. occitaniae* (Kottelat and Persat 2005). This result indicates that the number of circumpeduncular scales is an unreliable taxonomic characteristic, and the difference between 12 and 14 circumpeduncular scales should not be used to differentiate *G. meridionalis* and *G. rivuloides*.

We sequenced the Cyt *b* gene and reconstructed a phylogenetic tree for species within the genus *Gobio* that inhabit the Yellow River drainage (Fig. 10). The phylogenetic tree shows that *G. meridionalis* is nested within *G. rivuloides*. To maintain the monophyly of *G. rivuloides*, we propose that *G. meridionalis* is a synonym of *G. rivuloides*. Additionally, we calculated the genetic distances for the Cyt *b* gene (Table 5). The genetic

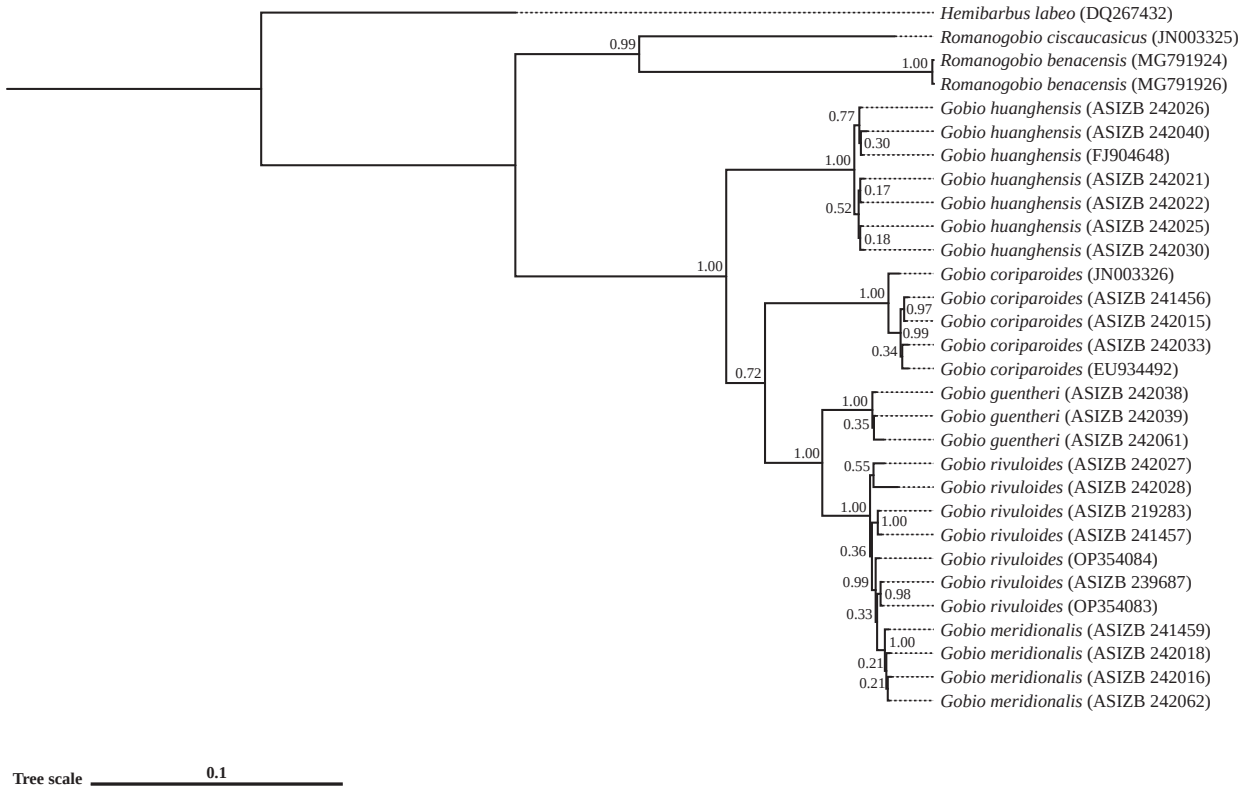

Figure 10. Molecular phylogenetic tree of *Gobio huanghensis*, *G. coriparoides*, *G. guentheri*, *G. rivuloides*, and *G. meridionalis* reconstructed by the Bayesian inference method based on the Cyt *b* sequence (1140 bp).

Table 4. Loadings on the first three principal components extracted from morphometric data of *Gobio meridionalis* and *G. rivuloides*.

Morphometric measurements	PC 1	PC 2	PC 3
Standard length	0.227	–0.059	–0.025
Body depth	0.238	–0.069	–0.147
Head length	0.201	0.205	–0.014
Head depth	0.213	0.201	–0.161
Head width	0.278	0.147	–0.415
Dorsal-fin base length	0.251	–0.051	–0.051
Pectoral-fin base length	0.223	–0.004	0.656
Pelvic-fin base length	0.278	–0.538	0.235
Anal-fin base length	0.258	–0.289	0.083
Caudal peduncle length	0.279	–0.080	–0.158
Caudal peduncle depth	0.216	0.117	0.090
Eye diameter	0.160	–0.105	–0.344
Interorbital width	0.204	0.056	0.142
Snout length	0.211	0.551	0.299
Pre-dorsal length	0.216	0.136	–0.108
Pre-pectoral length	0.192	0.326	0.050
Pre-pelvic length	0.210	–0.002	–0.091
Pre-anal length	0.221	–0.036	–0.023
Post-dorsal distance	0.246	–0.220	–0.004

distance between *G. rivuloides* and *G. meridionalis* is 0.0068, which is comparable to the intraspecific distance of *G. rivuloides* (0.0062). This result further supports *G. meridionalis* to be a junior synonym of *G. rivuloides*.

Naseka (1996) also placed *Gobio rivuloides* in the genus *Romanogobio*. However, phylogenetic analysis (Fig. 10) suggests that *G. rivuloides* should remain within the genus *Gobio*.

Gobio coriparoides Nichols, 1925

Figs 11, 12, Table 2

Gobio coriparoides Nichols, 1925: 4.

Material examined. • AMNH 8418 (Holotype), 1 specimen, 77.8 mm SL; the vicinity of Ningwu, Kolan, and Tsinglo, Shansi (=Ningwu, Kelan and Jingle County, Shanxi Province), collected by C. H. Pope. • ASIZB 232933, 1 specimen, 67.9 mm SL; Liulin County, Lvliang City, Shanxi Province, from the main stream of the Yellow River (37.3891°N, 110.6281°E); 31 July 2022. • ASIZB 241456 (Topotype), 1 specimen, 81.8 mm SL; Jingle County, Xinzhou City, Shanxi Province, from the Fenhe River (38.4726°N, 111.9957°E, ca 1250 m a.s.l.); collected by Dong Sheng, 14 September 2023. • ASIZB 242006–242008, 242009, 242011, 242016, and 242033–242037, 11 specimens, 60.0–73.0 mm SL; Lan County, Lvliang City, Shanxi Province, from the Fenhe River (38.2148°N, 111.7785°E, ca 1150 m a.s.l.); collected by Yutian Fang, 16 May 2024. • ASIZB 242015, 242041 (Topotype), 2 specimens, 68.3–70.7 mm SL, Jingle County, Xinzhou City, Shanxi Province; from the Fenhe River (38.4720°N, 111.9970°E, ca 1260 m a.s.l.); collected by Yutian Fang, 17 May 2024.

Vouchers for molecular study. • ASIZB 241456 (Topotype), 1 specimen, Jingle County, Xinzhou City, Shanxi Province, from the Fenhe River (38.4726°N, 111.9957°E, ca 1250 m a.s.l.); collected by Dong Sheng, 14 September 2023. • ASIZB 242015 (Topotype), 1 specimen, Jingle

Figure 11. *Gobio coriparoides*, holotype, AMNH 8420, 77.8 mm SL. **A.** Dorsal view; **B.** Lateral view; **C.** Ventral view; photographed by Ryan J. Thoni.

County, Xinzhou City, Shanxi Province; from the Fenhe River (38.4720°N, 111.9970°E, ca 1260 m a.s.l.); collected by Yutian Fang, 17 May 2024. • ASIZB 242033, 1 specimen, Lan County, Lvliang City, Shanxi Province, from the Fenhe River (38.2148°N, 111.7785°E, ca 1150 m a.s.l.); collected by Yutian Fang, 16 May 2024.

Diagnosis. This species can be distinguished from other *Gobio* species in East Asia by following characteristics: barbel reaching between vertical position of posterior orbit and posterior preopercle margin (vs. reaching beyond posterior preopercle margin in *G. huanghensis* and *G. guentheri*); lateral-line scales 39–41 (mode 40, mean 40) (vs. more than 40 in *G. huanghensis, G. rivuloides* and *G. guentheri*); circumpeduncular scales 16–20 (mode 18, mean 18) (vs. lesser than 16 in *G. rivuloides*); anus positioned at posterior one-third of distance from pelvic-fin base end to anal-fin origin (vs. anus centrally located between pelvic-fin base and anal-fin origin in *G. huanghensis* and *G. rivuloides*).

Redescription. Body relative abbreviated, dorsal body profile rising from nostrils to dorsal-fin origin, dropping along dorsal-fin base, then gradually sloping to caudal-fin base. Maximum body depth at dorsal-fin origin. Head relative abbreviated, length equal to body depth; snout obtuse. Mouth horseshoe-shaped and inferior, with one pair of maxillary barbels root at extremity of upper lip, barbel relative elongated, reaching from vertical position of posterior orbit to posterior preopercle margin. Lips thin, lower lip fused with throat; lips connected at mouth corner. Eyes positioned on dorsal half of head; interorbital region flattened; width larger than eye diameter. Thoracic region flattened, abdomen rounded, caudal peduncle robust, compressed laterally. Anus positioned at posterior one-third of distance from pelvic-fin base end to anal-fin origin.

Body covered with moderately large cycloid scales. Lateral line complete, almost straight in lateral center. Lateral line scales 39 (3 specimens), 40 (11), 41 (1); scales above lateral line 6 (4), 6.5 (8), 7 (2), 7.5 (1); scales below lateral line 4 (14), 5 (1); circumpeduncular scales 16 (6), 18 (8), 20 (1). Longitudinal epithelial crests absent on pre-dorsal region scales; the ventral scaleless region of most specimens (9) extends to middle of pectoral-fin base and to pelvic-fin base; other specimens (6) extend to pectoral-fin base.

Dorsal fin with three unbranched and seven (15 specimens) branched rays; distal margin concave, origin closer to snout than caudal-fin base. Pectoral fin with one unbranched and 14 (10), 15 (5) branched rays; tip of adpressed reaching anterior margin of pelvic-fin insertion. Pelvic fin with one unbranched and seven (15) branched rays; tip of adpressed reaching to posterior anus. Anal fin with three unbranched and six (15) branched rays; origin closer to pelvic-fin insertion than to caudal-fin base. Caudal fin deeply forked, with nine branched rays on upper lobes and eight branched rays on lower lobes, lobes rounded, upper lobes slightly more pointed than lower lobes.

Total vertebrae 4+35. Gill rakers rudimentary. Pharyngeal teeth “3, 5–5, 3”.

Figure 12. General view of *Gobio coriparoides*. **A.** Preserved specimen, ASIZB 242041, 68.3 mm SL; **B.** Live individual, uncatalogued, Duanjiazhai Township, Jingle County, Xinzhou City, Shanxi Province, from the Fenhe River.

Coloration in life. Dorsal side of head and body yellowish brown, mid-lateral side shallow yellowish grey, and ventral side grayish white. Dorsal side of body without black crossbars. Flank with 8–12 vague black blotches; margin of scales on back and flank slightly black pigmented. One slightly fluorescent yellowish-green stripe extends above lateral line. One distinct black stripe between anterior orbit and snout. Fins translucent, with slightly black pigments on dorsal fin, pectoral fin, and caudal fin rays; fins without black spots (Fig. 12B).

Coloration in preservation. Dorsal side of head and body brownish grey, mid-lateral side shallow brownish grey, and ventral side greyish white. Dorsal side of body with one dark stripe from posterior head to caudal peduncle end. Small blotches on flank vague, merge into a dark stripe. Margin of scales on back and flank slightly black pigmented. The fluorescent yellowish-green stripe faded. One distinct black stripe between anterior orbit and snout. Fins pale, with slightly black pigments on dorsal fin, pectoral fin, and caudal fin rays; fins without black spots. The black pigments on fin rays faded after long-time preserve.

Sexual dimorphism. No sexual dimorphism observed.

Distribution. *Gobio coriparoides* is mainly distributed in the tributaries of the Yellow River drainage, such as the Fenhe, Kuyehe, and Qinhe Rivers, etc. It is rarely found in the mainstream of the Yellow River (Fig. 4C).

Habitat and biology. *Gobio coriparoides* inhabits the tributaries of the Yellow River. It usually appears in fast-flowing water with sandy bottoms mixed with gravel and pebbles. It feeds on the bottom of the river.

Gobio guentheri (Herzenstein, 1892)

Fig. 13, Table 2

Acanthogobio guentheri Herzenstein, 1892: 228.
Gobio guentheri: Tang et al. (2011): 103.

Material examined. • ASIZB 78479–78487, 9 specimens, 104.7–143.4 mm SL, Guide County, Hainan Tibetan Autonomous Prefecture, Qinghai Province, from the main stream of the Yellow River, 1958. • ASIZB 242038–242039, 2 specimens, 69.0–81.3 mm SL; Jishishan Bonan, Dongxiang and Salar Autonomous County, Linxia Hui Autonomous Prefecture, Gansu Province, from the Yinchuanhe River, a tributary of the Yellow River drainage (35.7280°N, 103.0919°E, ca 1750 m a.s.l.), collected by Yutian Fang, 21 April 2024.

Vouchers for molecular study. • ASIZB 242038–242039, 2 specimens, Jishishan Bonan, Dongxiang and Salar Autonomous County, Linxia Hui Autonomous Prefecture, Gansu Province, from the Yinchuanhe River, a tributary of the Yellow River drainage (35.7280°N, 103.0919°E, ca 1750 m a.s.l.), collected by Yutian Fang, 21 April 2024. • ASIZB 242061, 1 specimen, Liulin County, Lvliang City, Shanxi Province, from the main stream of the Yellow River (37.3891°N, 110.6281°E); 31 July 2022.

Diagnosis. This species can be distinguished from other *Gobio* species in the Yellow River drainage by following characteristics: barbel reaching beyond posterior preopercle margin (vs. reaching between vertical position of posterior orbit and posterior preopercle

Figure 13. General view of *Gobio guentheri*. **A.** *Gobio guentheri*, ASIZB 78482, 136.9 mm SL, photographed by Xueyuan Li; **B.** Live individual, uncatalogued, Jishishan Bonan, Dongxiang and Salar Autonomous County, Linxia Hui Autonomous Prefecture, Gansu Province, from the Yinchuanhe River.

margin in *G. rivuloides* and *G. coriparoides*); lateral-line scales 40–43 (mode 42, mean 42) (vs. lesser than 40 in *G. coriparoides*); circumpeduncular scales 20–24 (mode 20, mean 20) (vs. lesser than 20 in *G. huanghensis* and *G. rivuloides*); anus positioned at posterior one-third of distance from pelvic-fin base end to anal-fin origin (vs. anus centrally located between pelvic-fin base and anal-fin origin in *G. huanghensis* and *G. rivuloides*). The second unbranched ray of the dorsal fin forms a stiff spine (vs. the second unbranched ray of the dorsal fin is soft in *G. huanghensis*, *G. rivuloides*, and *G. coriparoides*). No scales on pre-dorsal region (vs. present in *G. huanghensis*, *G. rivuloides*, and *G. coriparoides*), ventral scaleless region extends beyond pelvic-fin base (vs. not extending beyond pelvic-fin base in *G. huanghensis*, *G. rivuloides*, and *G. coriparoides*).

Redescription. Body relative abbreviated, dorsal body profile rising from nostrils to dorsal-fin origin, dropping along dorsal-fin base, then gradually sloping to caudal-fin base. Maximum body depth at dorsal-fin origin. Head elongated, length lesser than body depth; snout relative obtuse, with moderate concavity on top of snout before nostrils. Mouth horseshoe-shaped and inferior, with one pair of maxillary barbels root at extremity of upper lip, barbel elongated, extending over posterior preopercle margin to posterior opercular margin. Eyes positioned on dorsal half of head; interorbital region flattened; width larger than eye diameter. Thoracic region flattened, abdomen rounded, caudal peduncle robust, compressed laterally. Anus positioned at posterior one-third of distance from pelvic-fin base end to anal-fin origin.

Body covered with moderately large cycloid scales. Lateral line complete, almost straight in lateral center. Lateral line scales 40 (1 specimen), 41 (4), 42 (5), 43 (1); scales above lateral line 5 (1), 6 (4), 7 (3), 8 (3); scales below lateral line 4 (11); circumpeduncular scales 20 (7), 22 (3), 24 (1). No scales on pre-dorsal region, skin on pre-dorsal region tiny cortical protuberances. Ventral scaleless region extends beyond pelvic-fin base.

Dorsal fin with three unbranched and seven (11 specimens) branched rays, the second unbranched ray stiff, robust; distal margin concave, origin closer to snout than caudal-fin base. Pectoral fin with one unbranched and 14 (5), 15 (6) branched rays; tip of adpressed not reaching anterior margin of pelvic-fin insertion. Pelvic fin with one unbranched and seven (11) branched rays; tip of adpressed reaching to posterior anus. Anal fin with three unbranched and six (11) branched rays; origin closer to pelvic-fin insertion than to caudal-fin base. Caudal fin deeply forked, with nine branched rays on upper lobes and eight branched rays on lower lobes, lobes pointed, upper lobes slightly more pointed than lower lobes.

Total vertebrae 4+35–36. Gill rakers rudimentary. Pharyngeal teeth “3, 5–5, 3”.

Coloration in life. Dorsal side of head and body yellowish grey, mid-lateral side shallow yellowish grey, and ventral side grayish white. Flank with 6–8 vague black blotches; margin of scales on flank black pigmented. One slightly fluorescent yellowish-green stripe extends above lateral line. One distinct black stripe between anterior orbit and snout. Fins translucent, with slightly black pigments on fin rays; fins without black spots (Fig. 13B).

Coloration in preservation. Color of aged specimen preservation in formalin brownish yellow. A series of black dots on upper lateral side, flank with 6–8 vague blotches. Color of specimen preservation in 95% ethanol; dorsal side of head and body grey, mid-lateral side greyish yellow, and ventral side greyish white. A series of black dots on upper lateral side, flank with 6–8 vague blotches. One slightly silvery stripe extends above lateral line, margin of scales on flank black pigmented. Fins pale, without spots and pigmented.

Sexual dimorphism. No sexual dimorphism observed.

Distribution. *Gobio guentheri* is distributed in the upper reaches of the Yellow River drainage from Qushian Township to Liulin County (Fig. 4D).

Habitat and biology. *Gobio guentheri* usually appears in fast-flowing water with sandy bottoms. It feeds in sand on the bottom of the river.

Discussion

Romanogobio is not in the Yellow River drainage

The genus *Romanogobio* was established by Bănărescu (1961) as a subgenus of the genus *Gobio*. The type species of *Romanogobio* is *Gobio kesslerii* Dybowski, 1862, from Europe. This subgenus was treated as a genus in subsequent studies (e.g., Naseka 1996). The species belonging to this genus are characterized by a shallower body and slender caudal peduncle, epithelial crests on scales covering the dorsal half of the body, and an anteriorly positioned anus (Kottelat and Freyhof 2007). Naseka (1996) examined the vertebral column of Gobionidae, and he assigned *Gobio rivuloides*, *G.* (*R.*) *johntreadwelli*, and *G.* (*R.*) *amplexilabris* into the genus *Romanogobio* based on their anus position: the anus is closer to pelvic-fin base, which indicates an increased pre-anal vertebral column count.

Even though the anus position is closer to pelvic-fin base, phylogenetic analysis shows *Gobio rivuloides* remain within the genus *Gobio* (Fig. 10). Additionally, the presence of epithelial crests is also seen in *G. huanghensis* (Fig. 3B). In this situation, i.e., genus characteristics of *Romanogobio* also shown in some *Gobio* species, these characters are not reliable enough for differentiating *Romanogobio* and *Gobio*, especially in East Asia. Therefore, these characteristics should be reconsidered for the genus characteristics of *Romanogobio*.

According to Yang (2005), the divergence time between the genera *Romanogobio* and *Gobio* is estimated to be approximately 19 Mya, while the divergence time between *Gobio* species in East Asia and Europe occurred around 5 Mya. These results indicate that ancestral species dispersed into Europe following the retreat of the ancient Tethys Sea, ultimately giving rise to the modern genus *Romanogobio*. This genus should be a Europe-endemic genus, and East Asia is out of its distribution.

Acanthogobio, a junior synonym of genus *Gobio*

Acanthogobio guentheri was the first species described in the genus *Acanthogobio*. Subsequently, between 1904 and 1908, three other species were described as new within the same genus: *A. oxyrhynchus* (= *Hemibarbus labeo*, Luo et al. 1977), *A. paltschevskii* (= *Hemibarbus maculatus*, Luo et al. 1977), and *A. longirostris* (= *Hemibarbus longirostris*, Okada 1961). To date, the genus *Acanthogobio* remains a monotypic genus, with *A. guentheri* as its type species.

Based on mitochondrial Cytochrome-*b* (Cyt *b*) sequences, Yang et al. (2006) constructed a phylogenetic tree for the subfamily Gobioninae and found that the genus *Gobio* was not monophyletic; the genus *Acanthogobio* was nested within the phylogenetic tree of the genus *Gobio*. Tang et al. (2011) further explored the phylogeny of Gobioninae using a broader dataset that included Cytochrome-*b* (Cyt *b*), Cytochrome c Oxidase I (COI), Exon 3 of the recombination activating gene 1 (RAG 1), and Opsin (rhodopsin, Rh) sequences. It also showed that *A. guentheri* was nested within *Gobio*. In order to keep the monophyly of *Gobio*, they synonymized *Acanthogobio* as *Gobio* and recognized the species *A. guentheri* as *G. guentheri*.

The phylogenetic tree in this study shows that the *Acanthogobio guentheri* is nested within the genus *Gobio*, sistering to *G. rivuloides* (Fig. 10). The genetic distances between *A. guentheri* and *G. rivuloides* are even closer to the distance between *G. rivuloides* and *G. huanghensis* (0.0415 vs. 0.0890, Table 5). Our results support the conclusion that the genus *Acanthogobio* is a synonym of *Gobio*.

Gobio guentheri is a distinctive species within the genus *Gobio*. Its dorsal fin has a robust, stiff spine, the pre-dorsal region lacks scales, and the ventral scaleless region extends to the posterior pelvic fin. These characters, regarded as the secondary traits, might represent subsequent adaptations to the special habitat in the upper reaches.

Table 5. Genetic distances of the Cyt *b* gene computed by MEGA 11 amongst 5 analyzed species of *Gobio*, *Hemibarbus labeo* was used as the outgroup.

	Species	Intraspecific	1	2	3	4	5
1	*Gobio huanghensis*	0.0015					
2	*Gobio coriparoides*	0.0055	0.0996				
3	*Gobio guentheri*	0.0029	0.0946	0.0833			
4	*Gobio rivuloides*	0.0062	0.0890	0.0888	0.0415		
5	*Gobio meridionalis*	0.0013	0.0901	0.0912	0.0431	0.0068	
6	*Hemibarbus labeo* (Outgroup)	NA	0.1946	0.2173	0.1987	0.1940	0.1946

The distribution of the genus *Gobio* species in the Yellow River drainage

The Yellow River marks the southernmost distribution of the *Gobio* species. A total of ten species belong to the genus *Gobio* in East Asia (Chen 1998; Xie 2007), with four of them inhabiting the Yellow River drainage. Among these four species, *G. huanghensis*, *G. coriparoides*, and *G. guentheri* are endemic to the Yellow River drainage (Li 2015) and only distributed in the upper and middle reaches. This endemism is attributed to the relatively isolated environment of the upper and middle reaches of the Yellow River, formed by the uplift of the Tibetan Plateau (Lin et al. 2024). In contrast, other river systems in northern East Asia were more interconnected during the regression of the Bohai Sea, Yellow Sea, and East China Sea at the Last Glacial Maximum (Yoo et al. 2016), leading to a lack of endemic *Gobio* species in those regions (Xie 2007). Furthermore, *Gobio huanghensis* and *G. guentheri* inhabit only the mainstream, while *G. coriparoides* is primarily found in tributaries. *Gobio rivuloides* can be found in both mainstreams and tributaries.

Gobio species are found exclusively in the upper and middle reaches of the Yellow River basin. However, according to Li (2015), there is no distribution in the section of the Yellow River upstream of Longyang Gorge, nor do they inhabit the lower reaches of the river. They inhabit environments with an average elevation of above 300 meters. *Gobio guentheri* is distributed in the uppermost part of the Yellow River and can be found in Qushian Township, Qinghai Province, on the Qinghai-Tibet Plateau. The lowermost extent of *G. guentheri* distribution is Liulin County, Shanxi Province, but it is rare in this region, with only one specimen collected (Fig. 4D). *Gobio guentheri* is primarily distributed in high-altitude regions, with an average elevation of 630–2,700 meters. *Gobio huanghensis* is widely distributed in both the upper and middle reaches of the Yellow River mainstream (Fig. 4A). The uppermost part of its distribution is in Lanzhou City, Gansu Province, while the lowermost extent is in Yongji City, Shanxi Province. The average elevation of its distribution is 340–1,600 meters. The uppermost distribution of *G. rivuloides* in the mainstream is in Qingtongxia City, Ningxia Hui Autonomous Region, while the lowermost extent is in Sanmenxia City, Henan Province. It also inhabits tributaries such as the Hongnongjian River, the Qijiahe River, and the Luohe River (Fig. 4B). The average elevation of its distribution is 300–1,100 meters. *Gobio coriparoides* is only restricted to the tributaries; it can only be found in tributary habitats in the middle reaches of the Yellow River drainage (Fig. 4C). The average elevation of its distribution is 630–1,260 meters.

Acknowledgements

We thank Dr. Yingnan Wang and Xiaowei Meng from the National Animal Collection Resource Center, Institute of Zoology, Chinese Academy of Sciences, Beijing, China (ASIZB), for their help in checking specimens. We also thank Dong Sheng, Shuya Sun, Xin Wang, Chen Tian, Wuyang Liu, Ting Jiang, Junyuan Hao, Wanjing Zhang, Chongzhao Wang, and Xueyuan Li from the Institute of Zoology, Chinese Academy of Sciences, Beijing, China, for their help in collecting specimens. We thank Yiyang Xu and Haoyang Xie from the Institute of Hydrobiology, Chinese Academy of Sciences, Hubei, China (IHB), for their assistance in photographing the syntypes of *Gobio huanghensis*. Finally, we thank Dr. Ryan J. Thoni from the American Museum of Natural History, New York, United States (AMNH), for his help in photographing the type specimens.

This work was supported by the National Natural Science Foundation of China (NSFC32270464), the investigation project of the Ministry of Agriculture and Rural Affairs of the People's Republic of China: "Yellow River Fisheries Resources and Environmental Survey," and Sino BON—Inland Water Fish Diversity Observation Network.

References

Bănărescu PM (1961) Weitere systematische studien über die gattung Gobio (Pisces, Cyprinidae), insbesondere im Donaubecken. Věstnik Československé společnosti zoologické 25(4): 318–346.

Bănărescu PM, Nalbant TT (1973) Pisces, Teleostei: Cyprinidae (Gobioninae). de Gruyter, Berlin, 298 pp.

Chen YY (1998) Fauna Sinica Osteichthyes Cypriniformes II. Science Press, Beijing, China, 526 pp.

Chen JX, Xu QT, Wang XT, Fang SM, Song SL (1987) Fishes in Qinling Mountain area. Science Press, Beijing, 260 pp.

Hammer Ø, Harper DA (2001) Past: paleontological statistics software package for educaton and data anlysis. Palaeontologia Electronica 4: 1.

He DK, Chen YF (2009) Phylogeography of *Schizothorax o'connori* (Cyprinidae: Schizothoracinae) in the Yarlung Tsangpo River, Tibet. Hydrobiologia 635: 251–262. https://doi.org/10.1007/s10750-009-9918-2

Herzenstein vS (1892) Ichthyologische Bemerkungen aus dem Zoologischen Museum der Kaiserlichen Akademie der Wissenschaften. Mélanges biologiques tirés du Bulletin de l'Académie impériale des sciences de St Pétersbourg 13: 228.

Institute of Zoology Chinese Academy of Sciences (1959) Preliminary investigation report of piscatorial biological basis in the Yellow River. Science Press, Beijing.

Jelić D, Jelić M, Žutinić P, Šimunović I, Zupančič P, Naseka A (2018) Distribution of endangered Italian gudgeon Romanogobio benacensis (Cypriniformes, Cyprinidae, Gobioninae) with remarks on distinguishing morphological characters. Zookeys 729: 103–127. https://doi.org/10.3897/zookeys.729.20615

Kalyaanamoorthy S, Minh BQ, Wong TKF, von Haeseler A, Jermiin LS (2017) ModelFinder: fast model selection for accurate phylogenetic estimates. Nat Methods 14: 587–589. https://doi.org/10.1038/nmeth.4285

Kimura M (1980) A simple method for estimating evolutionary rates of base substitutions through comparative studies of nucleotide sequences. Journal of Molecular Evolution 16: 111–120. https://doi.org/10.1007/BF01731581

Kottelat M, Freyhof J (2007) Handbook of European freshwater fishes. Kottelat, Cornol, Switzerland and Freyhof, Berlin, Germany, 646 pp.

Kottelat M, Persat H (2005) The genus Gobio in France, with redescription of *G. gobio* and description of two new species (Teleostei: Cyprinidae). Cybium: Revue Internationale d'Ichtyologie 29: 211–234.

Kumar S, Stecher G, Li M, Knyaz C, Tamura K (2018) MEGA X: Molecular Evolutionary Genetics Analysis across Computing Platforms. Molecular Biology and Evolution 35: 1547–1549. https://doi.org/10.1093/molbev/msy096

Li SZ (2015) Fishes of the Yellow River. The Sueichan Press, Taiwan, 640 pp.

Lin X, Liu J, Liu HJ, Shang M (2024) When was the Yellow River Formed? Earth Science Online 49: 2158–2185. https://doi.org/10.3799/dqkx.2023.124

Liu HZ, Yang JQ, Tang QY (2010) Estimated evolutionary tempo of East Asian gobionid fishes (Teleostei: Cyprinidae) from mitochondrial DNA sequence data. Chinese Science Bulletin 55: 1501–1510. https://doi.org/10.1007/s11434-010-3159-7

Luo YL, Yue PQ, Chen YY (1977) Gobioninae. In: Wu XW (Ed.) The cyprinid fishes of China. Vol. 2, Shanghai Science and Technology Press, Shanghai, China, 439–549.

Naseka A (1996) Comparative study on the vertebral column in the Gobioninae (Cyprinidae, Pisces) with special reference to its systematics. Publicaciones Especiales Instituto Español de Oceanografía: 149–167.

Ni XM, Chen Y, Deng GM, Fu CZ (2023) Pleistocene Landscape Dynamics Drives Lineage Divergence of a Temperate Freshwater Fish *Gobio rivuloides* in Coastal Basins of Northern China. Genes 14: 2146. https://doi.org/10.3390/genes14122146

Nichols JT (1925) Some Chinese fresh-water fishes: V. Gudgeons Related to the European *Gobio gobio*. American Museum Novitates No. 181: 2–6.

Okada Y (1961) Studies on the Freshwater Fishes of Japan. Prefectural University of Mie: Tsu, Japan, 860 pp.

Ronquist F, Teslenko M, van der Mark P, Ayres DL, Darling A, Höhna S, Larget B, Liu L, Suchard MA, Huelsenbeck JP (2012) MrBayes 3.2: efficient Bayesian phylogenetic inference and model choice across a large model space. Systematic Biology 61: 539–542. https://doi.org/10.1093/sysbio/sys029

Sabaj MH (2020) Codes for Natural History Collections in Ichthyology and Herpetology. Copeia 108(3): 593–669. https://doi.org/10.1643/ASIHCODONS2020

Sabaj MH (2023) Codes for Natural History Collections in Ichthyology and Herpetology (online supplement). Version 9.5 (10 Nov 2023). American Society of Ichthyologists and Herpetologists, Washington, DC 108(3): 593–669. https://asih.org

Song ML, Wang YX, Shi YX (2022) Characteristics of water resources and water environment in different sections of the Yellow River basin and ecological protection paths. Water Resources Development and Management 8: 17–25. https://doi.org/10.16616/j.cnki.10-1326/TV.2022.06.04

Tang KL, Agnew MK, Chen WJ, Vincent Hirt M, Raley ME, Sado T, Schneider LM, Yang L, Bart HL, He SP, Liu HZ, Miya M, Saitoh K, Simons AM, Wood RM, Mayden RL (2011) Phylogeny of the gudgeons (Teleostei: Cyprinidae: Gobioninae). Molecular Phylogenetics and Evolution 61: 103–124. https://doi.org/10.1016/j.ympev.2011.05.022

Wu HL, Shao GZ, Lai CF, Zhuang LH, Lin PL (2012) Latin-Chinese Dictionary of Fish Names by Classification System. China Ocean University Press, Qingdao, Shandong, 602 pp.

Xie YH (2007) Freshwater Fishes in Northeast Region of China. Liaoning Science and Technology Publishing House, Shenyang, Liaoning, 600 pp.

Xie JM, Chen YR, Cai GJ, Cai RL, Hu Z, Wang H (2023) Tree Visualization by One Table (tvBOT): A web application for visualizing, modifying and annotating phylogenetic trees. Nucleic Acids Research 51: 587–592. https://doi.org/10.1093/nar/gkad359

Yang JQ (2005) Molecular phylogeny, evolutionary process and biogeography of the Gobioninae (Pisces: Cyprinidae). PhD Thesis, Institute of Hydrobiology, Chinese Academy of Science, Wuhan, China.

Yang JQ, He SP, Freyhof J, Witte K, Liu HZ (2006) The Phylogenetic Relationships of the Gobioninae (Teleostei: Cyprinidae) Inferred from Mitochondrial Cytochrome *b* Gene Sequences. Hydrobiologia 553: 255–266. https://doi.org/10.1007/s10750-005-1301-3

Yellow River Conservancy Commission (2013) Summary of the comprehensive planning of the Yellow River Basin (2012–2030). Yellow River News, 002 pp.

Yoo DG, Lee GS, Kim GY, Kang NK, Yi BY, Kim YJ, Chun JH, Kong GS (2016) Seismic stratigraphy and depositional history of late Quaternary deposits in a tide-dominated setting: An example from the eastern Yellow Sea. Marine and Petroleum Geology 73: 212–227. https://doi.org/10.1016/j.marpetgeo.2016.03.005

Zhao YH, Sun ZX (2021) Standard of Morphological Measurements and Description for Cyprinidae, Based on an Example of Gobionine Fishes (Teleostei: Cypriniformes). Bio-protocol: e1010622. https://doi.org/10.21769/BioProtoc.1010622

Zhao YH, Xing YC, Lü BB, Zhou CJ, Yang WB, Zhao K (2020) Species diversity and conservation of freshwater fishes in the Yellow River basin. Biodiversity Science 28: 1496. https://doi.org/10.17520/biods.2020191

Zoosyst. Evol. 101 (2) 2025, 681–695 | DOI 10.3897/zse.101.146469

PENSOFT

MUSEUM FÜR NATURKUNDE BERLIN

Description of a new cave-dwelling species of *Claea* (Teleostei, Cypriniformes, Nemacheilidae) from the Yangtze River basin in Sichuan, southern China

Hao-Tian Lei[1], Li He[2,3], Jun-Hao Huang[4], Jia-Jun Zhou[5,6], De-Kui He[4]

1 *College of Plant Protection, China Agricultural University, Beijing 100093, China*
2 *State Grid Tianfu New Area Electric Power Supply Company, Chengdu 610094, Sichuan, China*
3 *Sichuan Cave Exploration Team, No. 66, 5th Shuangcheng Road, Chenghua District, Chengdu 610051, Sichuan, China*
4 *The Museum of Aquatic Organisms, Institute of Hydrobiology, Chinese Academy of Sciences, Wuhan 430072, Hubei Province, China*
5 *Zhejiang Forest Resource Monitoring Center, Hangzhou 310020, Zhejiang, China*
6 *Zhejiang Forestry Survey Planning and Design Company Limited, Hangzhou 310020, Zhejiang, China*

https://zoobank.org/DA08B820-ACC8-4F3D-B098-E446674360C4

Corresponding authors: Jia-jun Zhou (cnwaters@foxmail.com); De-kui He (hedekui@ihb.ac.cn)

Academic editor: Nicolas Hubert ♦ **Received** 11 January 2025 ♦ **Accepted** 6 March 2025 ♦ **Published** 26 March 2025

Abstract

The first obligatory troglobitic *Claea* species, *Claea scet*, is described from a subterranean river in a cave connected to the Yangtze River in Hulu Town, Shawan District, Leshan City, Sichuan Province, southern China. *C. scet* differs from all congeners by the following combination of characters: Body pale without pigmentation; eye vestigial, diameter of eye 3.8–5.9% SL; short anal fin, anal fin height 7.0–8.4% SL. Molecular phylogenetic analysis supported the validity of the new species and revealed a close relationship between *Claea* and hypogean *Triplophysa* species.

Key Words

Cavefish, *Claea*, morphology, Nemacheilidae, phylogeny

Introduction

The genus *Claea*, a group featuring small benthic nemacheilid fishes adapted to torrential habitats, is characterized by the presence of a processus dentiformis on the median portion of the upper jaw, the absence of an adipose crest between the dorsal fin and caudal fin base, a scaleless body, the lack of a supra-pelvic flap, and the absence of marked sexual dimorphism. This genus is widely distributed in the upper Yangtze River basin in China (Kottelat 2012). The genus was first established by Sauvage (1874) based on the type species *Oreias dabryi* (now *C. dabryi*), described from a single specimen collected in Dengchigou, Baoxing County, Ya'an City, Sichuan Province, China (Kottelat 2012). The taxonomic validity of *Oreias* has been historically contentious due to insufficient original descriptions and ambiguous type locality information. Consequently, *O. dabryi* was subsequently reclassified into *Barbatula* and *Nemachilus* in later studies, reflecting uncertainties in key intergeneric diagnostic traits (Nichols 1944; Cao and Wu 1962). Bănărescu and Nalbant (1976) re-examined and redescribed the type specimen of *O. dabryi* and described two additional species, *O. furcatus* from Sichuan Province and *O. crassipedunculatus* from Yunnan Province, China, based on preserved specimens. Later, a new subspecies, *Oreias dabryi nanpanjiangensis*, was described from the Nanpanjiang River, a tributary of the Pearl River (Zhu and Cao 1988). Zhu (1989) proposed that *Oreias* was a junior synonym of *Schistura*, with *O. furcatus* and *O. crassipedunculatus* synonymized under *S. dabryi*.

However, Chu and Chen (1990) reinstated the validity of *Oreias* and reclassified *Oreias dabryi nanpanjiangensis* as a species of *Triplophysa*, citing the presence of sexual dimorphism and the absence of a prominent median upper jaw protrusion, which are diagnostic features of *Triplophysa*. Subsequent studies accepted the validity of *Oreias*, and two new species were described from the Yangtze River basin: *O. dabryi microphthalmus* (= *Claea microphthalmus*) and *O. niulanjiangensis* (Ding and Deng 1990; Wu and Wu 1992; Liao et al. 1997; Chen 1998; Chen et al. 2006; Zhang and Zhao 2016; Zhang et al. 2019; Du et al. 2021; Guo 2021). Outside of China, five species have been reported in Vietnamese literature (Nguyen 2005; Hoa et al. 2012), including two from the Lixiangjiang River, a tributary of the Red River (*O. sonlaensis* and *O. trilineatus*), and three from the Vietnamese Mekong (*O. hoai, O. lineatus,* and *O. punctatus*). The generic name *Oreias* Sauvage, 1874, was noted as a junior homonym of *Oreias* Kaup, 1829 (Aves) and *Oreias* Temminck, 1838 (Aves), prompting the proposal of *Claea* as a replacement name (Kottelat 2011). Kottelat (2012) further revised the genus, reclassifying *C. microphthalmus* into *Triplophysa* and assigning all Vietnamese species to *Schistura,* thereby restricting the genus *Claea* to the upper Yangtze River basin in China. Zhang et al. (2024) recently revised *Claea*, transferring *C. niulanjiangensis* to *Triplophysa* and reclassifying *T. wulongensis* from the Wujiang River as *C. wulongensis* based on the absence of secondary sexual characteristics and the presence of a prominent processus dentiformis. Additionally, they described a new species, *C. minibarba*, from the Shennongxi and Qingjiang River, tributaries of the upper Yangtze River in Hubei Province, China. Currently, *Claea* comprises three recognized species: *C. dabryi, C. minibarba,* and *C. wulongensis*.

The extensive karst mountain regions in southwestern China, characterized by numerous limestone caves and subterranean river systems, provide habitats for a diverse array of cave-adapted fish species, including members of the nemacheilid genera *Eoemacheilus, Guinemacheilus, Karstsinnectes, Oreonectes, Paranemacheilus, Triplophysa, Troglonectes,* and *Yunnanilus* (Lan et al. 2013; Liu et al. 2017; Wu et al. 2018; Ma et al. 2019; Du et al. 2023; Luo et al. 2023a). Many of these species exhibit obligate troglobitic adaptations, including reduced eyes, elongated fins, and depigmentation. However, members of *Claea* are typically epigean, with no prior records from subterranean environments except for *C. wulongensis*, which lacks definitive troglobitic features (Chen et al. 2021). In May 2023, during a cave survey in Taojin Cave, part of the Dadu River basin (a tributary of the upper Yangtze River) in Sichuan Province, China, specimens of an obligate troglobitic nemacheilid fish were collected. Comprehensive morphological and phylogenetic analyses confirmed these specimens as the first obligatory troglobitic species of *Claea*, herein described as *Claea scet* sp. nov.

Materials and methods

Sample collection

A total of 16 specimens were collected from Taojin Cave, located in Shiqianggou, Hulu Town, Shawan District, Leshan City, Sichuan Province, China, within the Dadu River basin, during May 2023 and June 2024. Specimens were captured using hand-nets and subsequently transferred to an aquarium for behavioral observation over several days. Following the observation period, individuals were euthanized using eugenol in accordance with ethical guidelines. Tissue samples from the right fin (n = 5) were excised and preserved in 95% ethanol for molecular analysis, with storage maintained at –20 °C to ensure DNA integrity. Whole specimens were fixed in 5% formaldehyde for 5–7 days and then transferred to 75% ethanol for long-term preservation. All collected specimens were cataloged and deposited in the Museum of Aquatic Organisms at the Institute of Hydrobiology, Chinese Academy of Sciences (IHB). The handling and experimental procedures involving these specimens adhered strictly to the ethical standards outlined in the Chinese Laboratory Animal Welfare and Ethics guidelines (GB/T 35892–2018).

Morphometric data acquiring

Morphometric data were collected using digital calipers interfaced directly with a computer, ensuring precision to the nearest 0.1 mm. Measurements and meristic counts (Table 2) were conducted on the left side of each specimen, following the standardized methodology outlined by Rainboth and Kottelat (1991). All linear measurements are expressed as proportions of either standard length (SL) or lateral head length (HL). The internostril width was defined as the linear distance between the anterior margins of the nostrils. Fin ray counts were performed under a ZEISS Stemi 508 stereomicroscope to ensure accuracy. For anatomical analysis, one specimen of each species was dissected to examine the morphology of the intestine and the structural configuration of the air bladder chambers. Vertebral counts (n = 1) were obtained from microcomputed tomography (CT) images acquired using a Siemens Somatom Definition X-ray machine, with three-dimensional reconstructions generated using CTvox software.

DNA extraction, amplification, sequencing, and phylogenetic analysis

Total genomic DNA was extracted from pelvic fin tissue using the rapid salt-extraction protocol (Aljanabi and Martinez 1997). The mitochondrial Cytochrome *b* gene (Cyt *b*) and Cytochrome oxidase subunit 1 (*CO*I) gene were amplified and sequenced for two individuals (IHB 202305300003 & IHB 202305300005), following the methodologies described by He and Chen

(2009). Electropherograms were manually inspected for quality using Chromas 2.22 (Technelysium Pty Ltd), and sequence alignments were performed using Clustal X 2.0 (Larkin et al. 2007).

A total of 145 complete mitochondrial genomes or sequences of the Cyt *b* and *CO*I genes from genera *Claea*, *Triplophysa*, *Troglonectes*, *Traccatichthys*, *Schistura*, *Oreonectes*, *Lefua*, *Karstsinnectes*, *Hedinichthys*, and *Barbatula* within the family Nemacheilidae were retrieved from the NCBI database. These sequences were utilized to reconstruct molecular phylogenetic relationships. Corresponding GenBank accession numbers are provided in Table 1.

Phylogenetic trees were constructed using both maximum likelihood (ML) and Bayesian inference (BI) methods. The concatenated dataset included the Cyt *b* and *CO*I genes, as well as complete mitochondrial genome sequences, excluding the D-loop region. Cyt *b* and *CO*I fragements were manually selected from complete mitochondrial genome sequences according to annotations from GenBank. Sequences were aligned in MAFFT v.7.245 (Katoh and Standley 2013) and manually examined in AliView (Larsson 2014) to ensure the correct reading frame. Thirty-four species from the family Cobitidae were designated as outgroups. The optimal nucleotide substitution model was determined using jModelTest 2.1.4 (Darriba et al. 2012), with the best-fit model (GTR + G + I) selected based on Akaike's Information Criterion (AIC) among 88 candidate models. ML analysis was conducted in RAxML 8.2.10 (Stamatakis 2014) under the GTRGAMMAIX model, with 2000 bootstrap replicates to assess node support. BI analysis was performed using MrBayes 3.2.6 (Ronquist et al. 2012), with two independent runs of two million generations each and four Markov chain Monte Carlo (MCMC) chains. Convergence of the BI analysis was evaluated based on the average standard deviation of split frequencies. Resulting phylogenetic trees were visualized and annotated using FigTree 1.4.4 (Rambaut 2018). Additionally, mean pairwise *p*-distances (number of substitutions per site) among haplotypes within the genus *Claea* were calculated based on the Cyt *b* gene using MEGA11 software (Tamura et al. 2021).

Table 1. GenBank accession numbers of loach species used in the phylogenetic analysis.

GenBank accession numbers	Species	Family	Genes
AB242161	*Acantopsis choirorhynchos*	Cobitidae	complete mitochondrial genome
NC_027663	*Cobitis biwae*	Cobitidae	complete mitochondrial genome
EU333980	*Cobitis choii*	Cobitidae	complete mitochondrial genome
EU656112	*Cobitis choii*	Cobitidae	complete mitochondrial genome
KF926686	*Cobitis elongatoides*	Cobitidae	complete mitochondrial genome
KF908768	*Cobitis granoei*	Cobitidae	complete mitochondrial genome
MZ339224	*Cobitis hankugensis*	Cobitidae	complete mitochondrial genome
MN841275	*Cobitis hankugensis*	Cobitidae	complete mitochondrial genome
MN756662	*Cobitis hugowolfeldi*	Cobitidae	complete mitochondrial genome
MT259034	*Cobitis macrostigma*	Cobitidae	complete mitochondrial genome
MK156771	*Cobitis macrostigma*	Cobitidae	complete mitochondrial genome
NC_029441	*Cobitis matsubarae*	Cobitidae	complete mitochondrial genome
MH349461	*Cobitis nalbanti*	Cobitidae	complete mitochondrial genome
MZ707538	*Cobitis nigrolinea*	Cobitidae	complete mitochondrial genome
AY526868	*Cobitis sinensis*	Cobitidae	complete mitochondrial genome
AP010782	*Cobitis striata*	Cobitidae	complete mitochondrial genome
AB054125	*Cobitis striata*	Cobitidae	complete mitochondrial genome
AP009306	*Cobitis takatsuensis*	Cobitidae	complete mitochondrial genome
OQ645452	*Cobitis tetralineata*	Cobitidae	complete mitochondrial genome
OP651767	*Lepidocephalichthys berdmorei*	Cobitidae	complete mitochondrial genome
DQ026434	*Misgurnus anguillicaudatus*	Cobitidae	complete mitochondrial genome
PP932689	*Misgurnus anguillicaudatus*	Cobitidae	complete mitochondrial genome
KF562047	*Misgurnus bipartitus*	Cobitidae	complete mitochondrial genome
MF579258	*Misgurnus mizolepis*	Cobitidae	complete mitochondrial genome
KF386025	*Misgurnus mohoity*	Cobitidae	complete mitochondrial genome
AB242171	*Misgurnus nikolskyi*	Cobitidae	complete mitochondrial genome
AB242168	*Pangio anguillaris*	Cobitidae	complete mitochondrial genome
NC_033958	*Paracanthocobitis botia*	Cobitidae	complete mitochondrial genome
NC_033959	*Paracanthocobitis zonalternans*	Cobitidae	complete mitochondrial genome
KJ027397	*Paramisgurnus dabryanus*	Cobitidae	complete mitochondrial genome
KF771003	*Paramisgurnus dabryanus*	Cobitidae	complete mitochondrial genome
ON116497	*Paranemachilus genilepis*	Cobitidae	complete mitochondrial genome
ON116499	*Paranemachilus jinxiensis*	Cobitidae	complete mitochondrial genome
ON116530	*Paranemachilus zhengbaoshani*	Cobitidae	complete mitochondrial genome
KT906089	*Claea dabryi*	Nemacheilidae	complete mitochondrial genome
MG238214/MG238118	*Claea dabryi*	Nemacheilidae	Cyt *b*, *CO*I
MG238216/MG238120	*Claea dabryi*	Nemacheilidae	Cyt *b*, *CO*I
PQ860813/PQ860770	*Claea scet* sp. nov.	Nemacheilidae	Cyt *b*, *CO*I
PQ860814/PQ860771	*Claea scet* sp. nov.	Nemacheilidae	Cyt *b*, *CO*I
OP750011	*Claea minibarba*	Nemacheilidae	Cyt *b*

GenBank accession numbers	Species	Family	Genes
OP750012	*Claea minibarba*	Nemacheilidae	Cyt *b*
OP750013	*Claea minibarba*	Nemacheilidae	Cyt *b*
OP750014	*Claea minibarba*	Nemacheilidae	Cyt *b*
OP750015	*Claea minibarba*	Nemacheilidae	Cyt *b*
KP715096	*Barbatula barbatula*	Nemacheilidae	complete mitochondrial genome
CM074126	*Barbatula barbatula*	Nemacheilidae	complete mitochondrial genome
PQ354418	*Barbatula barbatula*	Nemacheilidae	complete mitochondrial genome
KT192057	*Barbatula labiata*	Nemacheilidae	complete mitochondrial genome
KF574248	*Barbatula nuda*	Nemacheilidae	complete mitochondrial genome
MW288293	*Barbatula quignardi*	Nemacheilidae	complete mitochondrial genome
KT259193	*Barbatula* sp.	Nemacheilidae	complete mitochondrial genome
MK900633	*Barbatula toni*	Nemacheilidae	complete mitochondrial genome
AB242162	*Barbatula toni*	Nemacheilidae	complete mitochondrial genome
KM405199	*Barbatula toni*	Nemacheilidae	complete mitochondrial genome
KM017732	*Hedinichthys potanini*	Nemacheilidae	complete mitochondrial genome
JX144893	*Hedinichthys variegatus*	Nemacheilidae	complete mitochondrial genome
MN821008	*Hedinichthys yarkandensis*	Nemacheilidae	complete mitochondrial genome
KP050360	*Hedinichthys yarkandensis*	Nemacheilidae	complete mitochondrial genome
KT224367	*Hedinichthys yarkandensis*	Nemacheilidae	complete mitochondrial genome
KT192439	*Hedinichthys yarkandensis*	Nemacheilidae	complete mitochondrial genome
OP554813	*Hedinichthys yarkandensis*	Nemacheilidae	complete mitochondrial genome
KX447641	*Hedinichthys yarkandensis*	Nemacheilidae	complete mitochondrial genome
ON116515	*Karstsinnectes acridorsalis*	Nemacheilidae	complete mitochondrial genome
ON116506	*Karstsinnectes anophthalmus*	Nemacheilidae	complete mitochondrial genome
ON116531	*Karstsinnectes parvus*	Nemacheilidae	complete mitochondrial genome
ON116520	*Karstsinnectes parvus*	Nemacheilidae	complete mitochondrial genome
KT943751	*Lefua costata*	Nemacheilidae	complete mitochondrial genome
AB054126	*Lefua echigonia*	Nemacheilidae	complete mitochondrial genome
ON116504	*Micronemacheilus bailianensis*	Nemacheilidae	complete mitochondrial genome
NC_033960	*Micronemacheilus cruciatus*	Nemacheilidae	complete mitochondrial genome
ON116508	*Micronemacheilus longibarbatus*	Nemacheilidae	complete mitochondrial genome
MK387705	*Micronemacheilus pulcherrimus*	Nemacheilidae	complete mitochondrial genome
MZ853161	*Micronemacheilus pulcherrimus*	Nemacheilidae	complete mitochondrial genome
ON116507	*Oreonectes guananensis*	Nemacheilidae	complete mitochondrial genome
ON116495	*Oreonectes luochengensis*	Nemacheilidae	complete mitochondrial genome
ON116496	*Oreonectes platycephalus*	Nemacheilidae	complete mitochondrial genome
MW043722	*Oreonectes polystigmus*	Nemacheilidae	complete mitochondrial genome
AB242172	*Schistura balteata*	Nemacheilidae	complete mitochondrial genome
PP212943	*Schistura callichromu*	Nemacheilidae	complete mitochondrial genome
KY404236	*Schistura fasciolata*	Nemacheilidae	complete mitochondrial genome
MK361215	*Schistura incerta*	Nemacheilidae	complete mitochondrial genome
KU380330	*Schistura scaturigina*	Nemacheilidae	complete mitochondrial genome
PP114298	*Schistura yingjiangensis*	Nemacheilidae	complete mitochondrial genome
ON116516	*Traccatichthys pulcher*	Nemacheilidae	complete mitochondrial genome
ON116518	*Traccatichthys zispi*	Nemacheilidae	complete mitochondrial genome
KT213584	*Triplophysa aliensis*	Nemacheilidae	complete mitochondrial genome
KT213585	*Triplophysa alticeps*	Nemacheilidae	complete mitochondrial genome
MZ325251	*Triplophysa angeli*	Nemacheilidae	complete mitochondrial genome
KJ739868	*Triplophysa anterodorsalis*	Nemacheilidae	complete mitochondrial genome
MT992550	*Triplophysa baotianensis*	Nemacheilidae	complete mitochondrial genome
JQ686729	*Triplophysa bleekeri*	Nemacheilidae	complete mitochondrial genome
JX135578	*Triplophysa bleekeri*	Nemacheilidae	complete mitochondrial genome
MZ958819	*Triplophysa bombifrons*	Nemacheilidae	complete mitochondrial genome
KR052018	*Triplophysa bombifrons*	Nemacheilidae	complete mitochondrial genome
KT213588	*Triplophysa brevicauda*	Nemacheilidae	complete mitochondrial genome
KT213589	*Triplophysa chondrostoma*	Nemacheilidae	complete mitochondrial genome
KY945352	*Triplophysa cuneicephala*	Nemacheilidae	complete mitochondrial genome
OR857527	*Triplophysa dalaica*	Nemacheilidae	complete mitochondrial genome
KY945353	*Triplophysa dalaica*	Nemacheilidae	complete mitochondrial genome
KT213590	*Triplophysa dalaica*	Nemacheilidae	complete mitochondrial genome
OR857526	*Triplophysa dalaica*	Nemacheilidae	complete mitochondrial genome
OR857525	*Triplophysa dalaica*	Nemacheilidae	complete mitochondrial genome
OR857524	*Triplophysa dalaica*	Nemacheilidae	complete mitochondrial genome
OR857523	*Triplophysa dalaica*	Nemacheilidae	complete mitochondrial genome
KT213591	*Triplophysa dorsalis*	Nemacheilidae	complete mitochondrial genome
KT241024	*Triplophysa dorsalis*	Nemacheilidae	complete mitochondrial genome
PP455386	*Triplophysa erythraea*	Nemacheilidae	complete mitochondrial genome
PQ040451	*Triplophysa erythraea*	Nemacheilidae	complete mitochondrial genome
OQ998929	*Triplophysa fengshanensis*	Nemacheilidae	complete mitochondrial genome
PP114297	*Triplophysa grahami*	Nemacheilidae	complete mitochondrial genome
KT213592	*Triplophysa hsutschouensis*	Nemacheilidae	complete mitochondrial genome

GenBank accession numbers	Species	Family	Genes
OQ603602	*Triplophysa jianchuanensis*	Nemacheilidae	complete mitochondrial genome
ON116521	*Triplophysa langpingensis*	Nemacheilidae	complete mitochondrial genome
KT966735	*Triplophysa lixianensis*	Nemacheilidae	complete mitochondrial genome
OQ998928	*Triplophysa longipectoralis*	Nemacheilidae	complete mitochondrial genome
OQ998931	*Triplophysa longliensis*	Nemacheilidae	complete mitochondrial genome
KT213594	*Triplophysa markehenensis*	Nemacheilidae	complete mitochondrial genome
PP979136	*Triplophysa microphthalma*	Nemacheilidae	complete mitochondrial genome
KT213595	*Triplophysa microps*	Nemacheilidae	complete mitochondrial genome
KT213596	*Triplophysa minxianensis*	Nemacheilidae	complete mitochondrial genome
KT213597	*Triplophysa moquensis*	Nemacheilidae	complete mitochondrial genome
OQ998932	*Triplophysa nandanensis*	Nemacheilidae	complete mitochondrial genome
OQ274895	*Triplophysa nanpanjiangensis*	Nemacheilidae	complete mitochondrial genome
OQ992507	*Triplophysa nasobarbatula*	Nemacheilidae	complete mitochondrial genome
ON116529	*Triplophysa nasobarbatula*	Nemacheilidae	complete mitochondrial genome
MT361978	*Triplophysa nasobarbatula*	Nemacheilidae	complete mitochondrial genome
KT213598	*Triplophysa nujiangensa*	Nemacheilidae	complete mitochondrial genome
KT213599	*Triplophysa orientalis*	Nemacheilidae	complete mitochondrial genome
KJ631323	*Triplophysa orientalis*	Nemacheilidae	complete mitochondrial genome
KT213600	*Triplophysa pappenheimi*	Nemacheilidae	complete mitochondrial genome
KY419201	*Triplophysa pappenheimi*	Nemacheilidae	complete mitochondrial genome
KT213601	*Triplophysa pseudostenura*	Nemacheilidae	complete mitochondrial genome
KM396312	*Triplophysa robusta*	Nemacheilidae	complete mitochondrial genome
KM406486	*Triplophysa robusta*	Nemacheilidae	complete mitochondrial genome
JF268621	*Triplophysa rosa*	Nemacheilidae	complete mitochondrial genome
MW582822	*Triplophysa sanduensis*	Nemacheilidae	complete mitochondrial genome
KT213602	*Triplophysa scleroptera*	Nemacheilidae	complete mitochondrial genome
KY851112	*Triplophysa sellaefer*	Nemacheilidae	complete mitochondrial genome
KT213603	*Triplophysa siluroides*	Nemacheilidae	complete mitochondrial genome
KJ781206	*Triplophysa siluroides*	Nemacheilidae	complete mitochondrial genome
KT213587	*Triplophysa* sp.	Nemacheilidae	complete mitochondrial genome
KT259195	*Triplophysa* sp.	Nemacheilidae	complete mitochondrial genome
KT456271	*Triplophysa* sp.	Nemacheilidae	complete mitochondrial genome
KT213586	*Triplophysa* sp.	Nemacheilidae	complete mitochondrial genome
ON116519	*Triplophysa* sp.	Nemacheilidae	complete mitochondrial genome
KX376478	*Triplophysa* sp.	Nemacheilidae	complete mitochondrial genome
KX376479	*Triplophysa* sp.	Nemacheilidae	complete mitochondrial genome
KX354975	*Triplophysa stenura*	Nemacheilidae	complete mitochondrial genome
KT213604	*Triplophysa stenura*	Nemacheilidae	complete mitochondrial genome
KJ631324	*Triplophysa stewarti*	Nemacheilidae	complete mitochondrial genome
KT213605	*Triplophysa stewarti*	Nemacheilidae	complete mitochondrial genome
JQ663847	*Triplophysa stoliczkai*	Nemacheilidae	complete mitochondrial genome
KP979754	*Triplophysa strauchii*	Nemacheilidae	complete mitochondrial genome
KP297875	*Triplophysa strauchii*	Nemacheilidae	complete mitochondrial genome
KT224363	*Triplophysa tenuis*	Nemacheilidae	complete mitochondrial genome
KT122845	*Triplophysa tibetana*	Nemacheilidae	complete mitochondrial genome
KM212178	*Triplophysa tibetana*	Nemacheilidae	complete mitochondrial genome
KT224364	*Triplophysa tibetana*	Nemacheilidae	complete mitochondrial genome
KT259194	*Triplophysa ulacholica*	Nemacheilidae	complete mitochondrial genome
KT008666	*Triplophysa venusta*	Nemacheilidae	complete mitochondrial genome
PP203140	*Triplophysa weiheensis*	Nemacheilidae	complete mitochondrial genome
MW582823	*Claea wulongensis*	Nemacheilidae	Cyt *b*
OQ754129	*Claea wulongensis*	Nemacheilidae	Cyt *b*
KT224365	*Triplophysa wuweiensis*	Nemacheilidae	complete mitochondrial genome
KT751089	*Triplophysa xiangxiensis*	Nemacheilidae	complete mitochondrial genome
KT224366	*Triplophysa xichangensis*	Nemacheilidae	complete mitochondrial genome
OQ998934	*Triplophysa zhenfengensis*	Nemacheilidae	complete mitochondrial genome
MT992551	*Triplophysa zhenfengensis*	Nemacheilidae	complete mitochondrial genome
ON116501	*Troglonectes barbatus*	Nemacheilidae	complete mitochondrial genome
MG738689	*Troglonectes daqikongensis*	Nemacheilidae	complete mitochondrial genome
ON116505	*Troglonectes donglanensis*	Nemacheilidae	complete mitochondrial genome
ON116509	*Troglonectes duanensis*	Nemacheilidae	complete mitochondrial genome
ON116502	*Troglonectes elongatus*	Nemacheilidae	complete mitochondrial genome
ON116512	*Troglonectes furcocaudalis*	Nemacheilidae	complete mitochondrial genome
ON116523	*Troglonectes jiarongensis*	Nemacheilidae	complete mitochondrial genome
NC_058004	*Troglonectes longibarbatus*	Nemacheilidae	complete mitochondrial genome
ON116498	*Troglonectes macrolepis*	Nemacheilidae	complete mitochondrial genome
ON116494	*Troglonectes microphthalmus*	Nemacheilidae	complete mitochondrial genome
ON116511	*Troglonectes retrodorsalis*	Nemacheilidae	complete mitochondrial genome
ON116522	*Troglonectes shuilongensis*	Nemacheilidae	complete mitochondrial genome
ON116510	*Troglonectes translucens*	Nemacheilidae	complete mitochondrial genome

Table 2. Morphometric measurements for *Claea scet*, sp. nov, *C.dabryi*, *C.minibarba* and *C.wulongensis*.

Characteristics	*Claea scet* (n = 14)				*Claea dabryi* (n = 31)			*Claea minibarba* (n = 7) (Zhang et al. 2024)			*Claea wulongensis* (n = 8) (Guo et al. 2021)		
	Holotype	Range	Mean	S.D.	Range	Mean	S.D.	Range	Mean	S.D.	Range	Mean	S.D.
Scales		Absent		/	Absent		/	Absent		/	Absent		/
Lateral line		Complete		/	Complete		/	Complete		/	Complete		/
Dorsal fin rays		III,8–9	III,8	/	III,7–8	III,7	/	III,8	III,8	/	III,8	III,8	/
Anal fin rays		III,5–6	III,5	/	II,5	II,5	/	II,5	II,5	/	I,5	I,5	/
Pectoral fin rays		I,10	I,10	/	I,8–9	I,8	/	I,10	I,10	/	I,8–9	I,8–9	/
Pelvic fin rays		I,5–6	I,6	/	I,5–6	I,6	/	I,6	I,6	/	I,5–7	I,5–7	/
Caudal fin rays		2+16	2+16	/	2+15–17	2+16	/	2+16	2+16	/	2+16	2+16	/
Standard length (SL,mm)	51.3	34.2–58.9	50.9	4.7	37.6–88.5	60.5	14.4	48.8–69.9	62.6	6.6	49.0–67.2	55.7	6.2
In percentage of SL (%)													
Head Length	24.6	20.8–25.5	23.4	1.4	20.4–24.8	23.8	1.0	21.1–23.3	21.9	1.0	20.4–23.5	22.6	1.0
Body depth	13.5	10.1–13.6	11.7	1.1	9.6–15.0	12.5	1.4	14.7–17.6	15.9	1.0	9.3–13.6	12.1	1.3
Predorsal length	54.6	50.0–56.3	54.0	2.0	49.0–59.1	52.9	2.0	50.5–54.0	52.4	1.3	50.4–54.2	51.9	0.9
Prepelvic length	51.7	50.2–56.0	53.6	1.6	47.1–53.1	49.8	1.6	47.7–50.6	49.8	1.6	48.3–50.9	49.7	0.9
Preanal length	77.0	73.4–77.9	75.9	1.1	71.6–78.4	74.5	1.7	72.7–75.2	73.9	1.0	71.5–77.7	73.4	1.8
Dorsal-fin height	11.8	9.4–19.3	13.6	3.9	16.1–22.2	18.8	1.3	15.8–18.1	16.8	0.8	15.0–19.8	16.2	1.5
Dorsal-fin base length	12.0	8.4–12.5	11.1	1.0	9.4–13.3	11.3	1.0	10.8–12.3	11.6	0.6	10.7–13.4	12.4	0.9
Anal-fin height	8.0	7.0–8.4	7.7	0.4	13.8–20.0	16.4	1.4	13.6–15.7	14.8	0.7	12.4–16.5	14.5	1.3
Anal-fin base length	9.1	8.4–9.6	8.3	0.8	5.6–10.6	8.0	1.0	7.8–9.0	8.1	0.4	6.6–8.2	7.4	0.6
Pelvic-fin length	14.9	12.2–15.5	13.8	1.0	13.3–17.6	14.9	0.9	12.5–15.1	13.8	0.8	12.5–14.5	13.2	0.6
Pectoral-fin length	20.1	16.7–22.0	19.1	1.2	18.3–22.3	17.6	1.4	15.0–17.6	16.8	0.9	15.6–18.4	17.6	1.0
Caudal-fin length	17.8	15.7–20.5	17.9	1.7	17.4–23.4	20.0	1.4	15.2–18.1	17.2	1.0	15.9–20.8	18.1	1.3
Caudal-peduncle length (CPL)	16.1	14.4–18.9	15.9	1.2	15.4–22.3	17.9	1.4	18.0–20.5	19.2	1.0	14.2–20.7	16.6	1.2
Caudal-peduncle depth (CPD)	8.2	5.5–8.5	7.0	0.9	5.5–10.3	8.3	1.0	9.5–11.7	10.7	0.7	7.6–9.4	8.5	0.7
In percentage of HL (%)													
Head depth	44.4	40.4–56.1	45.6	4.4	39.6–52.0	44.9	3.0	55.5–59.4	57.5	1.6	45.3–54.2	50.6	2.9
Head width	60.3	51.6–77.0	59.8	7.2	45.9–59.7	53.4	3.6	61.5–68.0	64.0	2.1	55.7–65.8	62.4	3.5
Snout length	40.2	28.6–44.7	37.8	5.4	35.7–45.2	41.0	2.5	42.3–46.3	45.0	1.3	38.9–45.0	41.9	1.9
Eye diameter	5.6	3.8–5.9	5.1	0.9	13.7–23.3	17.8	2.6	15.8–18.4	16.9	0.9	11.1–19.1	17.0	2.1
Interorbital width	27.1	18.3–31.9	25.6	4.3	22.8–26.3	27.3	2.5	30.3–36.3	32.6	2.2	38.5–43.1	41.3	1.5
Maxillary barbel length	25.4	22.4–34.9	26.0	3.5	29.8–47.4	34.9	3.9	21.5–29.6	26.9	2.7	21.8–35.9	29.8	3.2
Inner rostral barbel length	17.1	11.5–20.4	16.3	2.5	15.6–24.7	20.2	2.4	16.0–21.7	18.8	2.5	16.5–23.4	21.6	1.2
Outer rostral barbel length	26.8	23.0–32.8	27.5	3.5	30.2–47.5	37.9	3.9	22.1–28.0	25.1	2.4	21.4–41.5	32.4	4.5
CPD/CPL (%)	51.2	34.4–52.8	44.2	5.7	33.7–53.4	46.5	4.3	50.8–61.2	55.6	3.7	44.3–57.4	51.2	4.5

Results

Taxonomic account

Family Nemacheilidae Regen, 1911
Genus *Claea* Sauvage, 1874

Claea scet sp. nov.

https://zoobank.org/AADDEC5A-A9BC-4F7D-976F-4FE0CDD79299

Holotype. • IHB 202305300005, 51.3 mm SL; a subterranean tributary of the Dadu River in the Yangtze River drainage in Taojin Cave, Shiqianggou, Hulu Town, Shawan District, Leshan City, Sichuan Province, China (29°17'47.0"N 103°38'13.0"E; 570 m elevation); collected by Li He & Ze-Yu Li, 28.V.2023.

Paratypes. • IHB 202305300001–202305300004, IHB 202305300006–202305300009, 8, 43.1–56.4 mm SL; other data same as holotype; • IHB 202305300010–202305300016, 7, 34.2–58.9 mm SL; same locality as holotype, collected by Yuan Li & Ze-Yu Li, VI-16-2024.

Diagnosis. *C. scet* resembles all known species of *Claea* in possessing a processus dentiformis at the medium of the upper jaw, absence of tubercle-bearing, elevated skin on the sides of the head and a thickened tuberculated pad on the dorsal surface of the thickened and widened rays of the pectoral fin in males, absence of adipose crest between dorsal fin and caudal fin base, body scaleless, and absence of supra-pelvic flap, all of which are diagnostic features of *Claea*. *C. scet* can be distinguished from *C. dabryi*, *C. minibarba* and *C. wulongensis* by the combination of the following characters (see Table 2): Processus dentiformis reduced, not covering lower jaw when mouth shut; eye vestigial, diameter of eye 3.8–5.9% SL; short anal fin, anal fin height 7.0–8.4% SL. *C. scet* is further distinguished from *C. dabryi* by shorter maxillary barbels (22.4–27.5% SL *vs.* 29.8–47.4% SL) and shorter outer rostral barbels (23.0–29.8% SL *vs.* 30.2–47.5% SL). *C. scet* is further distinguished from *C. minibarba* by a more depressed body (body depth 10.1–13.5% SL *vs.* 14.7–17.6% SL), a more posteriorly situated pelvic fin (prepelvic length 51.7–56.0% SL *vs.* 47.7–50.6% SL), a longer pectoral fin (17.6–20.2% SL *vs.* 15.0–17.6% SL), a shallower

caudal peduncle (5.5–8.5% SL *vs.* 9.5–11.7% SL) and a more elongated head (head depth 41.4–46.5% HL *vs.* 55.5–59.4% HL and head width 52.3–60.3% HL *vs.* 61.5–68.0% HL). *C. scet* is further distinguished from *C. wulongensis* by a more posteriorly situated pelvic fin (prepelvic length 51.7–56.0% SL *vs.* 48.3–50.9% SL), a longer anal fin base (8.4–9.6% SL *vs.* 6.6–8.2% SL), more closely situated eyes (interorbital length 23.5–31.9%HL *vs.* 38.5–43.1% HL).

Description. Morphometric data for 16 type specimens of *C. scet* are provided in Suppl. material 1. Juvenile individuals with a standard length (SL) of less than 40 mm were excluded from morphological comparisons with congeners (Table 2). The general body profile is illustrated in Fig. 1. The body is elongated, subcylindrical anteriorly, and laterally compressed posteriorly. The dorsal profile of the head is nearly straight, while the dorsal profile of the body is convex. The ventral profile is almost straight from the snout tip to the anal fin origin, with a slight concavity posterior to the anal fin origin. The greatest body depth occurs anterior to the dorsal fin origin, gradually decreasing toward the caudal fin base. The body is entirely scaleless and smooth, with a complete and straight lateral line. The cephalic lateral line system comprises 3 + 8 infraorbital, 6 supraorbital, 3 supratemporal, and 10 preopercular-mandibular pores (Fig. 2).

The head is moderately depressed, longer than wide, and wider than deep. The snout is pointed, with a snout length measuring 38.1–44.7% of the head length (HL). The eyes are reduced, with a diameter of 3.8–5.9% HL, and are positioned dorsolaterally on the head. Both anterior and posterior nostrils are closely situated; the anterior nostril is housed in a short tube with an elongated, tube-like tip that does not reach the anterior margin of the eye. The mouth is inferior and curved, with thin lips exhibiting shallow surface furrows. The upper lip is complete and connected to the lower lip at the corners of the mouth. The lower lip features a distinct V-shaped median incision. The upper and lower jaws are arched, with a weakly developed processus dentiformis on the upper jaw compared to congeners (Figs 2, 3), not covering the lower jaw when mouth is shut. Three pairs of barbels are present: two pairs of rostral barbels (the inner pair not reaching the corner of the mouth, and the outer pair slightly longer than the inner pair) and one pair of maxillary barbels, which extend to the posterior margin of the eye when fully extended (Fig. 2).

Figure 1. Morphological characters of holotype, IHB 202305300005 of *Claea scet* sp. nov. in preservative (10% formalin). **A.** Lateral view; **B.** Dorsal view; **C.** Ventral view

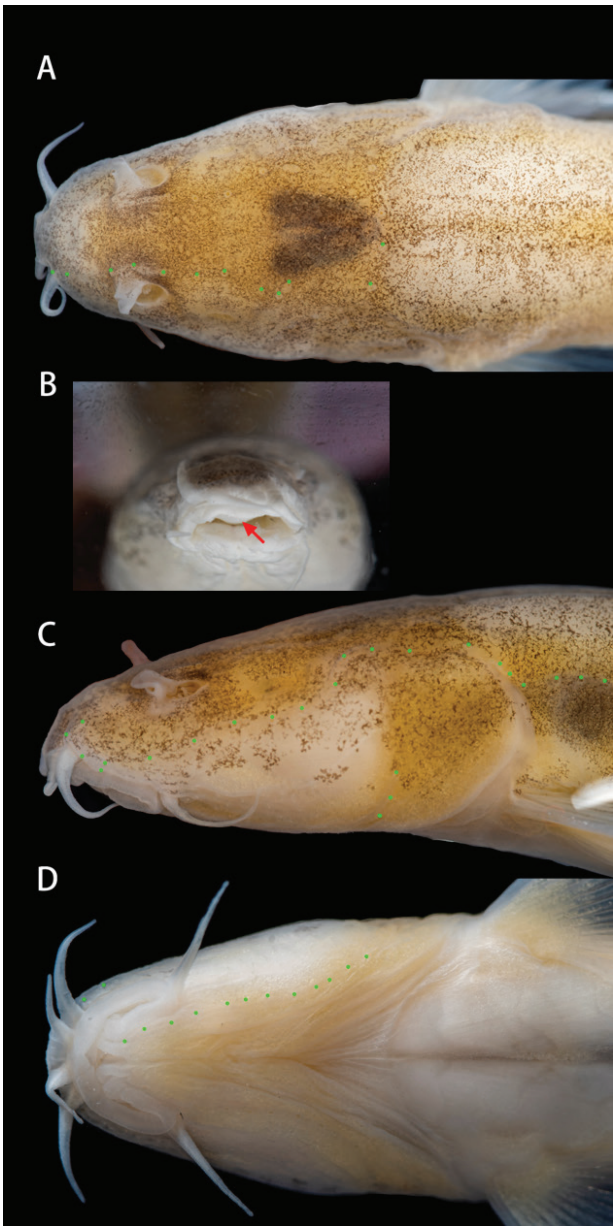

Figure 2. Detailed cephalic morphology of holotype, IHB 202305300005 of *Claea scet* sp. nov. **A.** Dorsal side view of head; **B.** Frontal view of head, processus dentiformis shown by a red arrow; **C.** Lateral sideview of head, and **D.** Ventral side view of head (Cephalic lateral line system highlighted as green dots).

Dorsal fin with 3 simple and 8 (n = 12) or 9 (n = 4) branched fin rays, origin behind mid-point between snout tip and caudal-fin base and posterior to the pelvic fin origin, distal margin truncate, length of dorsal fin greater than body depth. Pelvic fins with 1 simple and 5 (n = 1) or 6 (n = 15) branched fin rays, origin closer to anal fin origin than pectoral fin origin, tips of pelvic fins not reaching anus. Pectoral fins with 1 simple and 10 branched fin rays, extending beyond the halfway to pelvic-fin origin. Anal fin with 3 simple and 5 (n = 7) or 6 (n = 8) branched fin rays, origin closer to pelvic-fin insertion than to caudal fin base. Caudal fin forked, with 2 simple and 16 branched fin rays, the upper lobe slightly longer than the lower (Figs 1, 6).

Intestine short, without bend or loops immediately posterior to stomach. Bony capsule of the air bladder large and thin, dumbbell-shaped, (Fig. 5), posterior chamber of air bladder degenerated. Vertebrae 4 + 38 (Fig. 4).

Coloration. In their natural subterranean aquatic habitats, live specimens exhibit a general body coloration of light gray with a faint pinkish hue, accompanied by sparse pigmentation distributed laterally and dorsally. The ventral region is semi-transparent, while all fins appear hyaline. In specimens preserved in 10% formalin, the body coloration transitions to light gray with a moderate yellowish tint, and pigmentation is observed to fade in some individuals (Figs 1, 6).

Distribution. This species is presently only known from a subterranean tributary of the Dadu River in the upper Yangtze River in Taojin Cave, Shiqianggou, Hulu Town, Shawan District, Leshan City, Sichuan Province, China (Figs 7, 9).

Etymology. The specific name "scet" is in reference to the abbreviation of Sichuan Cave Exploration Team, a cave exploration team who collected the type specimens, in recognition of their contributions to the understanding of cave fishes of Sichuan Province. "川洞山鰍 (Pinyin: Chuan Dong Shan Qiu)" is proposed for the Chinese common name of this new species.

Field notes. The Taojin Dolomite Cave, situated adjacent to a backroad in Shiqianggou, is characterized as a shaft-type cave with a broad entrance. Access to the cave is restricted to the Single Rope Technique (SRT) for descent. During the rainy season, elevated water levels render the cave inaccessible, while at other times, the interior remains

Figure 3. Comparison of processus dentiformis of different *Claea*. spp. **A.** *C. scet*, 51.28 mm SL, IHB 202305300005; **B.** *C. dabryi* 98.35 mm SL, IHB 81VII2537; **C.** *C. minibarba*, 62.31 mm SL, IHB 202204288315.

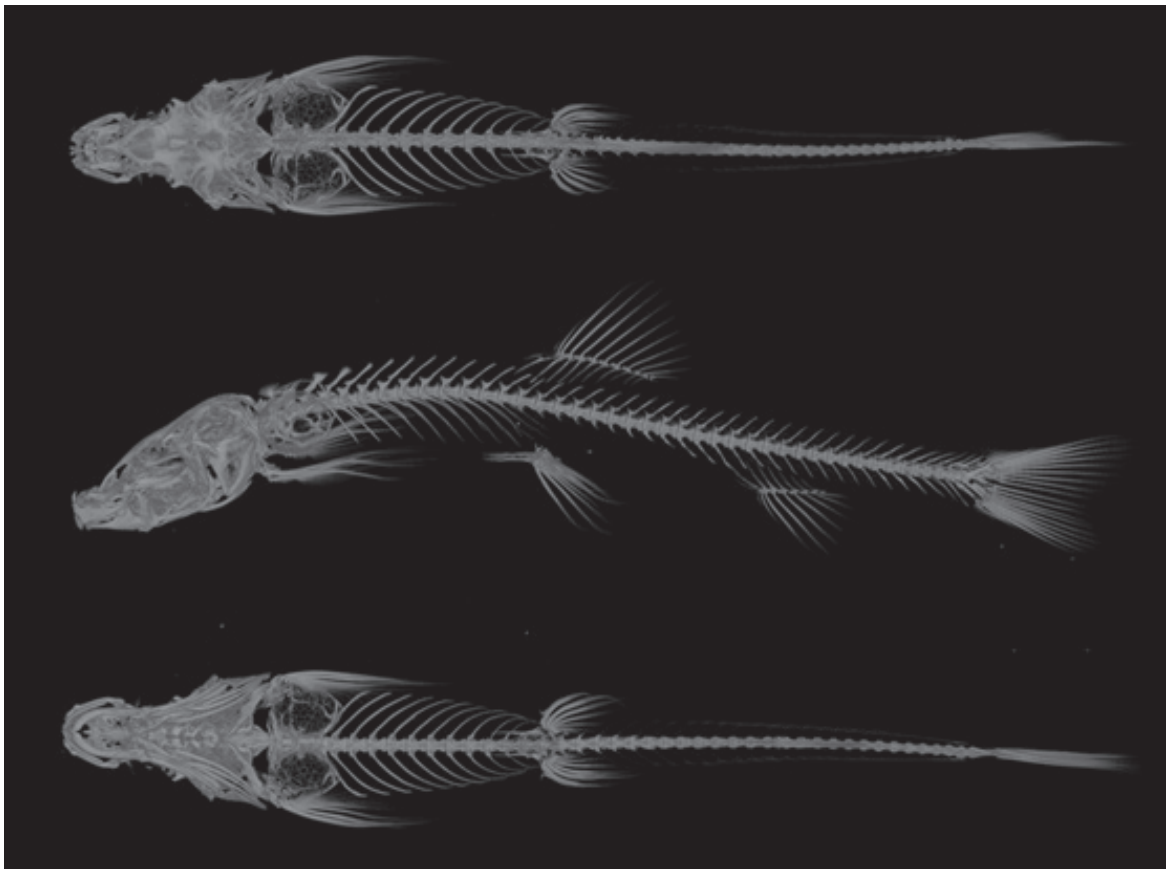

Figure 4. Dorsal, lateral and ventral views of the micro-CT graph of the skeleton of holotype IHB 202305300005 of *Claea scet* sp. nov.

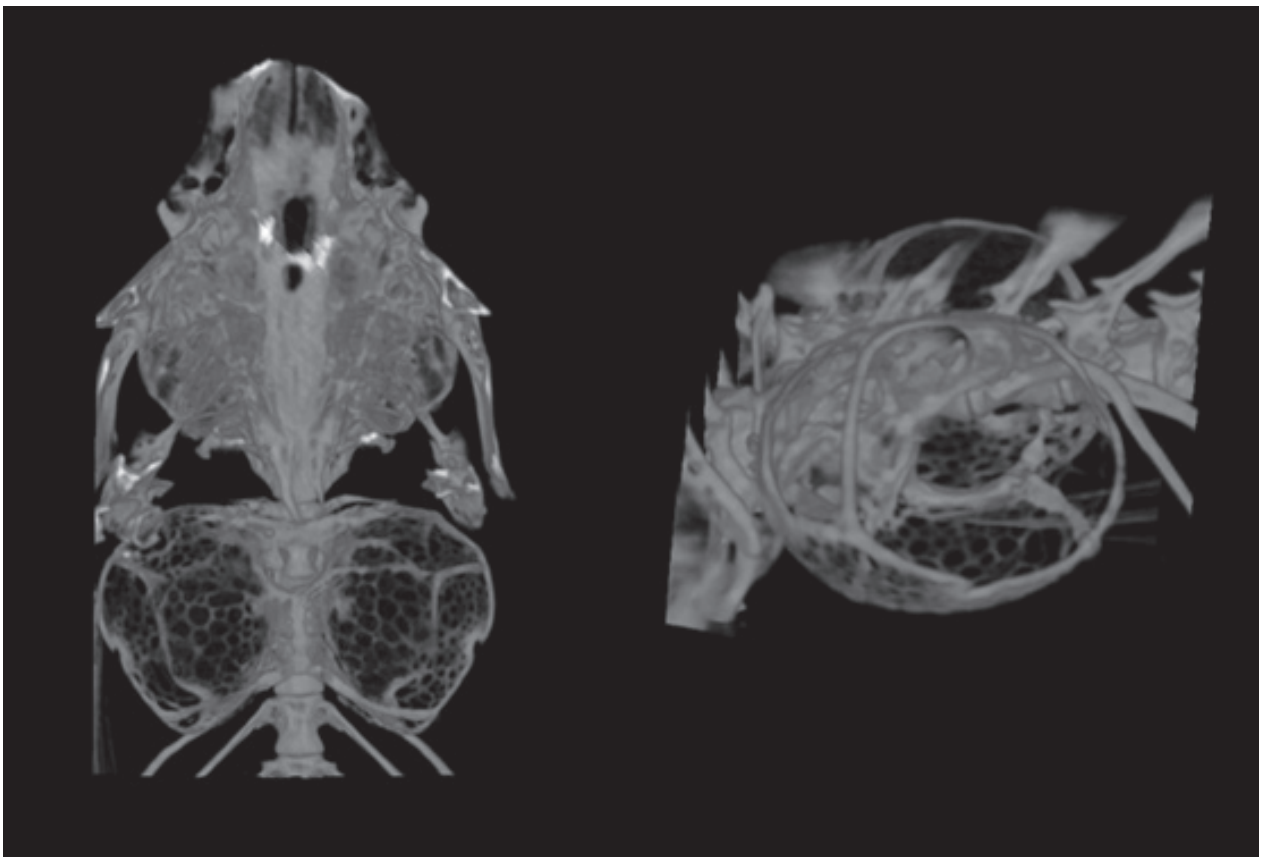

Figure 5. Dorsal and lateral profile of Bony capsule of the air bladder.

Figure 6. *Claea scet* sp.nov. in life, paratype IHB 202305300009. Photo from Jiajun Zhou.

humid with spacious tunnels. This species inhabits pools located within the deep dark zone of the cave, where environmental conditions during the survey period in May 2023 included an air temperature of 18–19 °C and a water temperature of 15 °C (Fig. 7). Other troglobites found inside the same cave were *Jujiroa duqianae* Tian & He, 2023 (Coleoptera, Carabidae), *Paratachys* sp. (Coleoptera, Carabidae), *Domene lizeyui* Wang & He, 2024 (Coleoptera, Staphylinidae), *Epanerchodus* sp. (Polydesmida, Polydesmidae), and *Chetoneura* sp. (Diptera, Keroplatidae).

Molecular phylogeny

Both phylogenetic methods (ML and BI) recovered a similar tree topology (Fig. 8) based on two mitochondrial gene fragments (Cyt *b*, *CO*I). All *Claea* species formed a monophyly (except for GenBank accession no. KT906089 of *C. dabryi*, collected from Gaoyanzi River in Pengzhou, Chengdu City, Sichuan Province, China (31°2'59.89"N, 104°0'58.55"E, which could be misidentified.) with strong support, and as the sister group to the hypogean *Triplophysa* species. Although the genus *Triplophysa* is non-monophyletic, all hypogean *Triplophysa* and non-cavefishes separate into monophyletic clades. The monophyly of the new species is strongly supported. Phylogenetic analyses supported the new species, *C. scet* being a closely related sister species of *C. dabryi* from the Jinsha River (the upper Yangtze River). The average genetic distance (*p*-distance) between the new species and other *Claea* species ranges from 1.95% (with *C. dabryi*) to 6.02% (*C. wulongensis*) for Cyt *b* (Table 3).

Key to the species of *Claea*

A key to four species of *Claea* is shown below.

1 Processus dentiformis reduced, not covering lower jaw when mouth shut ..... *C. scet*
– Processus dentiformis prominent, covering lower jaw when mouth shut 2
2 Interorbital length larger than 38% HL ..... *C. wulongensis*
– Interorbital length lesser than 38% HL 3
3 Maxillary barbels extending to the middle of eye ..... *C. minibarba*
– Maxillary barbels extending beyond posterior margin of eye ..... *C. dabryi*

Discussion

Discovery of the first troglobitic fish species from the karst regions north of the Yangtze River, China.

The limestone caves and subterranean water systems of southwestern China's extensive karst regions harbor more than 170 endemic cavefish species across two orders (Cypriniformes, Siluriformes) and five families (Balitoridae, Cyprinidae, Nemacheilidae, Cobitidae, Amblycipitidae) (Ma et al. 2019; Luo et al. 2023b). Notably, all documented Chinese cavefish species are confined to karstic zones south of the Yangtze River, particularly within the upper Pearl, upper Red, and upper Yangtze River basins. Of the 14 troglobitic fish species recorded from the Yangtze River system (Table 4), all originate from the mainstream or southern-bank tributaries, including *Sinocyclocheilus sanxiaensis* (Three Gorges Reservoir), *Claea wulongensis* (Wujiang River), and *Triplophysa xiangxiensis* (Yuanjiang River) (Yang et al. 1986; Jiang et al. 2019; Chen et al. 2021). The discovery

Figure 7. Taojin Cave, the type locality of *Claea scet* sp.nov. and individuals of *Claea scet* sp.nov. found in the cave. **A.** environs of the cave; **B.** Li He descending into the cave using SRT; **C.** Author collecting *Claea scet* sp.nov. with hand-net; **D.** Author filming live image of *Claea scet* sp. nov.; **E, F.** Individuals of *Claea scet* sp.nov. resting on gravelly bottom of the subterranean river in Taojin.

of *Claea scet*—the first cavefish recorded from northern tributaries of the Yangtze River—significantly expands the known biogeographic range of Chinese cavefishes (Fig. 9). Given the extensive limestone cave networks within the Sichuan Basin, Wushan Mountains, and Daba Mountains, systematic ichthyofaunal surveys in these regions are expected to yield critical insights into the diversity and evolution of Yangtze River cavefish assemblages.

Table 3. The average pairwise *p*-distances (the number of substitutions per site with pairwise) between species of *Claea* based on Cyt b gene sequences.

	C. minibarba	*C. dabryi*	*C. scet*	*C. wulongensis*
C. minibarba	/			
C. dabryi	0.0600	/		
C. scet	0.0591	0.0195	/	
C. wulongensis	0.0439	0.0584	0.0602	/

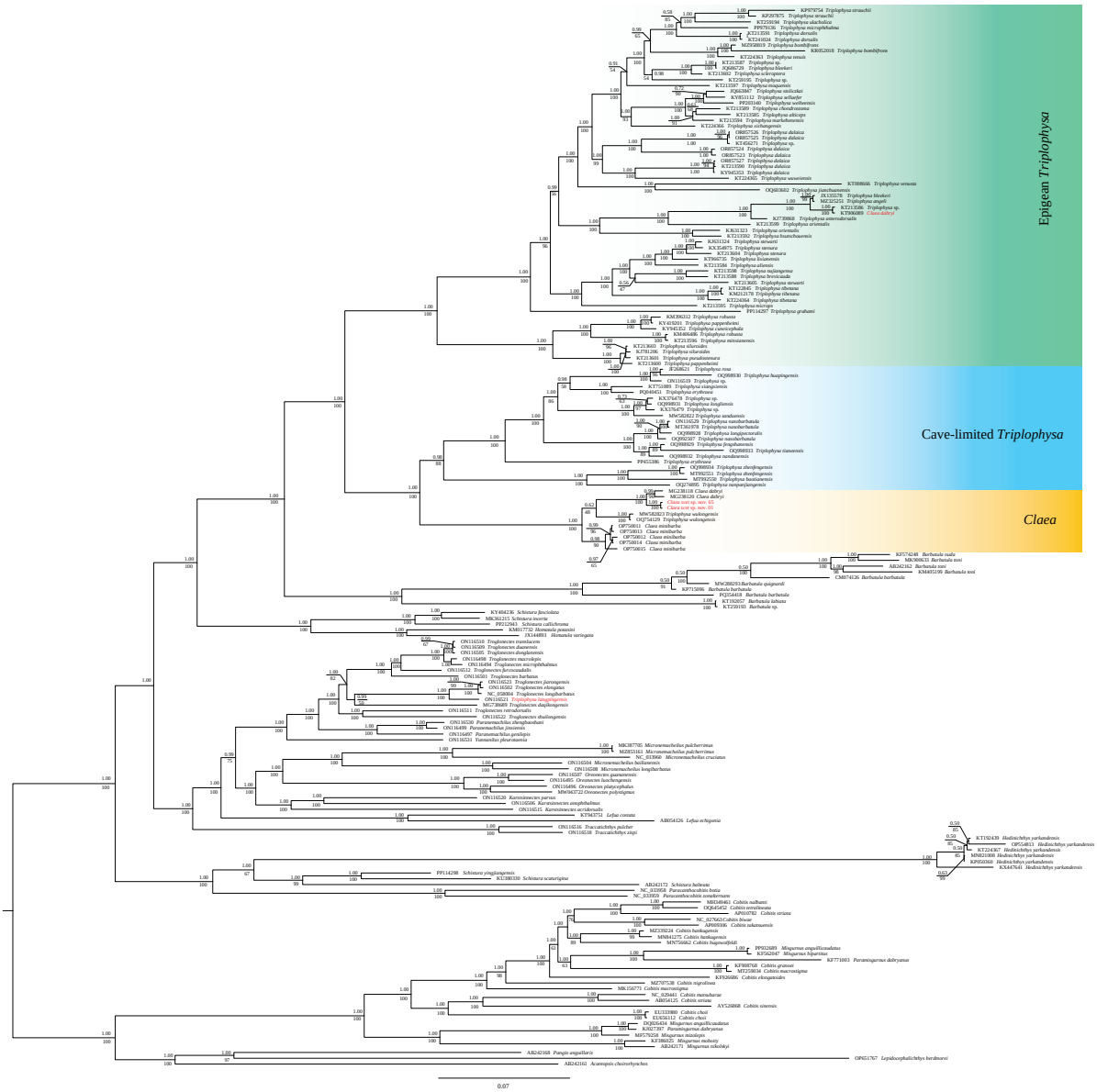

Figure 8. Phylogenetic tree of *Claea*, both epigean and hypogean *Triplophysa* and other closely related congeners reconstructed based on combined two mitochondrial (Cyt *b* and *COI*) gene fragments. Ultrafast bootstrap (UFB) supports from maximum likelihood (ML) analyses/Bayesian posterior probabilities (BPP) from Bayesian inference (BI) analyses are noted beside nodes. The scale bar represents 0.07 nucleotide substitutions per site.

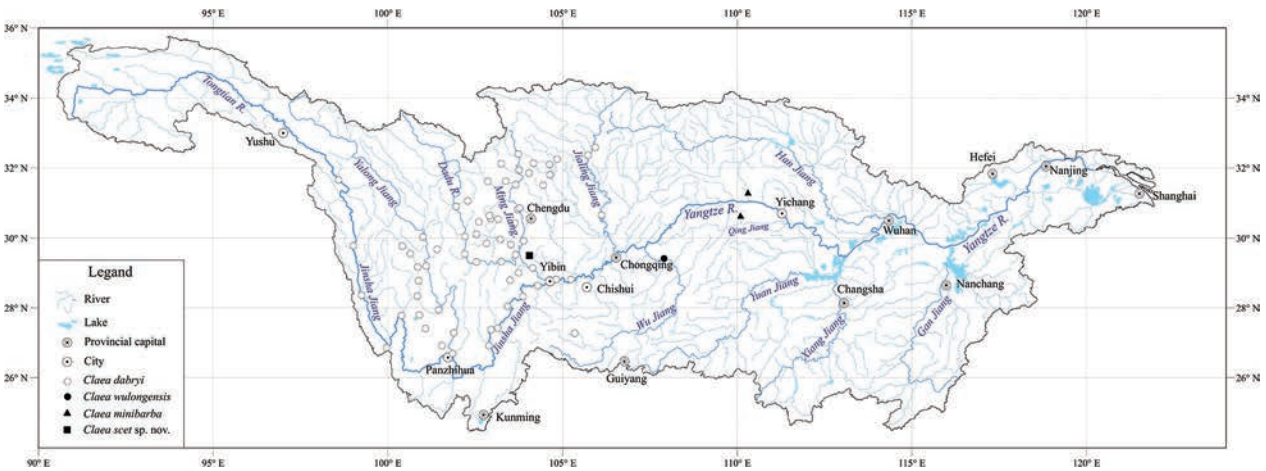

Figure 9. Distribution and hydrology of the type locality of *Claea scet* sp. nov. (square), *C. wulongensis* (black circle), *C. minibarba* (triangle) and known distribution of *C. dabryi* (white circle).

Table 4. List of locality information of known cavefish species from the Yangtze River basin.

Species	Familly	Type locality	Tributary	Reference
Claea scet	Nemacheilidae	Shawan District, Leshan City, Sichuan Province, China	Dadu River	This study
Claea wulongensis	Nemacheilidae	Wulong County, Chongqing City,China	Wujiang River	Chen et al. 2021
Sinocyclocheilus grahami	Cyprinidae	Dianchi Lake, Kunming City, Yunnan Province, China	Jinshajiang River	Zhao & Zhang, 2009
Sinocyclocheilus guiyang	Cyprinidae	Qingzhen County, Guiyang City, Guizhou Province, China	Wujiang River	Shao et al. 2024
Sinocyclocheilus huizeensis	Cyprinidae	Huize County, Qujing City, Yunnan Province, China	Niulanjiang River	Cheng et al. 2015
Sinocyclocheilus multipunctatus	Cyprinidae	Guizhou Province, China	Wujiang River	Zhao & Zhang, 2009
Sinocyclocheilus sanxiaensis	Cyprinidae	Zigui County, Hubei Province, China.	Mainstream of Yangtze River	Jiang et al. 2019
Sinocyclocheilus wumengshanensis	Cyprinidae	Xundian Hui and Yi Autonomous County, Kunming City, Yunnan Province, China	Niulanjiang River	Li et al. 2003
Triplophysa erythraea	Nemacheilidae	Huaren County, Xiangxi Tujia and Miao Autonomous Prefecture, Hunan province, China	Yuanjiang River	Huang et al. 2019
Triplophysa qingzhenensis	Nemacheilidae	Qingzhen County, Guiyang City, Guizhou Province, China	Wujiang River	Liu et al. 2022
Triplophysa qini	Nemacheilidae	Fengdu County, Chongqing City, China	Wujiang River	Deng et al. 2022
Triplophysa rosa	Nemacheilidae	Wulong County, Chongqing City, China	Wujiang River	Chen et al. 2005
Triplophysa xiangxiensis	Nemacheilidae	Longshan County, Xiangxi Tujia and Miao Autonomous Prefecture, Hunan province, China	Yuanjiang River	Yang et al. 1986
Triplophysa wudangensis	Nemacheilidae	Wudang Distinct, Guiyang City, Guizhou Province, China	Wujiang River	Liu et al. 2022

Historically, cavefish research in China has centered on Guangxi and Yunnan provinces, while studies of Sichuan's subterranean fauna have primarily focused on invertebrates (Hou et al. 2006; Deuve et al. 2020; Yang et al. 2023; Wang and He 2024). Prior to this study, no obligatory troglobitic fish had been documented in Sichuan. The discovery of *C. scet* as the province's first cavefish species underscores the potential for undiscovered troglobitic fish diversity within Sichuan's subterranean hydrological networks, warranting intensified exploration of these understudied ecosystems.

Discovery of the first obligatory troglobitic member of *Claea* provides potential novel perspective of evolution of nemacheilid cavefishes

The genus *Claea* comprises predominantly epigean species, with only two exceptions documented in subterranean environments: *C. wulongensis* and the newly described *C. scet*. Notably, *C. wulongensis* lacks definitive troglomorphic adaptations, rendering *C. scet* the sole obligatory troglobitic member of the genus. Phylogenetic reconstructions reveal a sister-group relationship between *Claea* and hypogean *Triplophysa* lineages, with both genera forming distinct monophyletic clusters that further group with epigean *Triplophysa* species. This topology aligns with prior molecular analyses (Xiong et al. 2017; Yan 2017; Chen et al. 2019; Guo 2021; Zhang et al. 2024). Contrasting with the monophyletic assemblage of hypogean *Triplophysa*, the two hypogean *Claea* species (*C. scet* and *C. wulongensis*) do not form a sister group (Fig. 7). Instead, *C. scet* demonstrates closer genetic affinity to the epigean *C. dabryi* from the Jinsha River drainage, suggesting independent evolutionary origins of troglomorphic traits within *Claea*. The minimal pairwise genetic divergence (*p*-distance = 1.95%) between *C. scet* and *C. dabryi* supports a recent speciation event (Fig. 8, Table 3).

While *Triplophysa*—the nemacheilid genus with the highest diversity of hypogean species—has been extensively studied for cave adaptation patterns (Shi et al. 2018; Zhang et al. 2024), persistent questions regarding its monophyly (as evidenced by phylogenetic analyses) highlight the significance of discovering a troglobitic *Claea* species as a novel model system for investigating subterranean adaptation mechanisms in Nemacheilidae.

Beyond canonical troglomorphic traits (e.g., reduced pigmentation and eyes), *C. scet* exhibits unique morphological features absent in congeners, including a reduced processus dentiformis (Fig. 3). Its fins and barbels, however, do not enlarge to serve as sensory organs as they are on many other cavefishes, with sizes that do not exhibit a prominent difference compared with epigean congeners. The functional significance of these morphological innovations warrants comprehensive investigation through integrated studies of physiology, ecological interactions, and behavioral ecology in this newly described taxon.

Acknowledgements

We would like to express our sincere gratitude to Ze-Yu Li (Panzhihua, China) and Yuan Li (Deyang, China) for providing the specimen of the new species and assistance during the cave surveys, to Prof. Ming-Yi Tian (SCAU), Cheng-Bin Wang (MYNU), Zhen Wang (Chengdu, China) and Chao Zhou (Chengdu, China) for their constant support, to Xin-Yang Zou (Chongqing, China) for helping us to take the aerial photos of the cave, to Hao Jin, Yue-Hai Yu, Xue-Fei Liu, Li-Fei Chen, Peng Yang, Long-Jue Hu, Can Tang, Jin-Xiong Duan, Song-Lun Xie, Cheng-Xing Zhu (all Sichuan Cave Exploration Team, Chengdu) for their help in the field collection, to Wen-chu Yan for her generous offer of comparative specimens and to Hao-yang Xie for his assistance in acquiring the morphological and molecular phylogeny data.

This study was financially supported by the National Key Research and Development Program of China (Grant no.2021YFC3200103) and the National Natural Science Foundation of China (Grant no. 32070436).

References

Aljanabi SM, Martinez I (1997) Universal and rapid salt-extraction of high-quality genomic DNA for PCR-based techniques. Nucleic Acids Research 25(22): 4692–4693. https://doi.org/10.1093/nar/25.22.4692

Bănărescu P, Nalbant TT (1976) The genus *Oreias* Sauvage, 1874 (Pisces, Cobitidae). Nymphaea 4: 185–193. [pls. 1–2]

Cao WX, Wu XW (1962) An investigation of the fish biology and fishery problems in Ganze-Apa region of western Szechuan Province [J]. Acta Zootaxonomica Sinica 2: 79–112. https://doi.org/10.3724/issn1000-3207-1962-2-79-4

Chen YY (1998) The fishes of the Hengduan Mountains Region. Science Press, Beijing. [In Chinese, English abstract]

Chen XY, Yang JX (2005) *Triplophysa rosa* sp. nov.: a new blind loach from China. Journal of Fish Biology 66: 599–608. https://doi.org/10.1111/j.0022-1112.2005.00622.x

Chen L, Lu ZM, Mao WN (2006) A new species of *Schistura* discovered in Yunnan, China. Guizhou Agricultural Sciences 34(5): 54–55. [In Chinese, English abstract]

Chen W, Yang J, Li Y, Li X (2019) Exploring taxonomic diversity and biogeography of the family Nemacheilinae (Cypriniformes). Ecology and Evolution 9(18): 10343–10353. https://doi.org/10.1002/ece3.5553

Chen S, Sheraliev B, Shu L, Peng Z (2021) *Triplophysa wulongensis*, a new species of cave-dwelling loach (Teleostei, Nemacheilidae) from Chongqing, Southwest China. ZooKeys 1026: 179–192. https://doi.org/10.3897/zookeys.1026.61570

Cheng C, Pan XF, Chen XY, Li JY, Ma L, Yang JX (2015) A new species of the genus *Sinocyclocheilus* (Teleostei:Cypriniformes), from Jinshajiang Drainage, Yunnan, China. Cave Research 2(4): 1–4.

Chu, XL Chen YR (1990) The fishes of Yunnan, China. Part II. Science Press, Beijing, 313 pp. [In Chinese]

Darriba D, Taboada GL, Doallo R, Posada D (2012) jModelTest 2: more models, new heuristics and parallel computing. Nature Methods 9(8): 772. https://doi.org/10.1038/nmeth.2109

Deng SQ, Wang XB, Zhang E (2022) *Triplophysa qini*, a new stygobitic species of loach (Teleostei: Nemacheilidae) from the upper Chang-Jiang Basin in Chongqing, Southwest China. Ichthyological Exploration of Freshwaters, IEF–1178, 1–11.

Deuve T, He L, Tian MY (2020) Descriptions of the first semi-aphenopsian troglobiotic Patrobini and of a new anophthalmic cave-dwelling Trechini from central Sichuan, China (Coleoptera: Caraboidea), Annales de la Société entomologique de France (N.S.) 56(2): 93–105. https://doi.org/10.1080/00379271.2020.1722748

Ding RH, Deng QX (1990) The Noemacheilinae Fishes From Sichuan,With Description of A New Species I. *Paracobitis, Nemacheilus* and *Oreias* (Cypriniformes: Cobitidae). Zoological Research 11(4): 285–287.

Du LN, Yang J, Min R, Chen XY, Yang JX (2021) A review of the Cypriniform tribe Yunnanilini Prokofiev, 2010 from China, with an emphasis on five genera based on morphologies and complete mitochondrial genomes of some species. Zoological Research 42(3): 310–334. https://doi.org/10.24272/j.issn.2095-8137.2020.229

Du LN, Li SJ, Xu F, Luo T, Yu GH, Zhou J (2023) Clarification of Phylogenetic Relationships among Chinese Nemacheilids with Tube-Shaped Anterior Nostrils, with a Description of a New Genus and Two New Species. Journal of Zoological Systematics and Evolutionary Research 2023(2): 1–11. https://doi.org/10.1155/2023/3600085

Guo YS (2021) Colored Atlas of Fishes in Sichuan, Vol II. 505–507. Science Press, Beijing. [In Chinese]

He DK, Chen YF (2009) Phylogeography of *Schizothorax o'connori* (Cyprinidae: Schizothoracinae) in the Yarlung Tsangpo River, Tibet. Hydrobiologia 635(1): 251–262. https://doi.org/10.1007/s10750-009-9918-2

Hoa NT, Hao NV, Thuong HT (2012) Two new species of *Oreias* Sauvage, 1874 discovered in Son La city, Vietnam. Academia Journal of Biology32(4): 45–53. https://doi.org/10.15625/0866-7160/v32n4.720

Hou Z, Platvoet D, Li S (2006) *Gammarus abstrusus* n. sp., a new cave-dwelling gammaridean amphipod from Sichuan, China (Amphipoda, Gammaridea). Crustaceana 79(10): 1209–1222. https://doi.org/10.1163/156854006778859605

Huang TF, Zhang PL, Huang XL, Wu T, Gong XY, Zhang YX, Peng QZ, Liu ZX (2019) A new cave-dwelling blind loach, *Triplophysa erythraea* sp. nov. (Cypriniformes: Nemacheilidae), from Hunan Province, China. Zoological Research 40(4): 331–336. https://doi.org/10.24272/j.issn.2095-8137.2019.049

Jiang WS, Li J, Lei XZ, Wen ZR, Han YZ, Yang JX, Chang JB (2019) S*inocyclocheilus sanxiaensis*, a new blind fish from the Three Gorges of Yangtze River provides insights into speciation of Chinese cavefish. Zoological Research 40(6): 552–557. https://doi.org/10.24272/j.issn.2095-8137.2019.065

Katoh K, Standley DM (2013) MAFFT multiple sequence alignment software version 7: improvements in performance and usability. Molecular Biology and Evolution 30(4): 772–780. https://doi.org/10.1093/molbev/mst010

Kottelat M (2011) *Claea*, a new replacement name for *Oreias* Sauvage, 1874 (Teleostei: Nemacheilidae). Ichthyological Exploration of Freshwaters 21(4): 384.

Kottelat M (2012) Conspectus cobitidum: an inventory of the loaches of the world (Teleostei: Cypriniformes: Cobitoidei). The Raffles Bulletin of Zoology 26: 1–199.

Lan JH, Gan X, Wu TJ, Yang J (2013) Cave Fishes of Guangxi, China. Science Press, Beijing, 266 pp. [In Chinese]

Larkin MA, Blackshields G, Brown NP, Chenna R, McGettigan PA, McWilliam H, Valentin F, Wallace IM, Wilm A, Lopez R, Thompson JD, Gibson TJ, Higgins DG (2007) Clustal W and Clustal X version 2.0. Bioinformatics (Oxford, England) 23(21): 2947–2948. https://doi.org/10.1093/bioinformatics/btm404

Larsson A (2014) AliView: a fast and lightweight alignment viewer and editor for large datasets. Bioinformatics (Oxford, England) 30(22): 3276–3278. https://doi.org/10.1093/bioinformatics/btu531

Li WX, Mao WN, Lu ZM, Yan WZ (2003) The two new species of *Sinocyclocheilus* from Yunnan, China. Journal of Jishou University 24(2): 63–65. [Natural Science Edition] [In Chinese, English abstract]

Liao JW, Wang DZ, Luo ZF (1997) A new species and a new subspecies of *Schistura* [sic] from Guangxi and Guizhou, China (Cypriniformes: Cobitidae: Nemacheilinae). Acta Academiae Medicinae Zunyi 20(2–3): 4–7. [In Chinese, English summary]

Liu SW, Pan XF, Yang JX, Chen XY (2017) A new cave-dwelling loach, *Triplophysa xichouensis* sp. nov. (Teleostei Nemacheilidae) from Yunnan, China. Journal of Fish Biology 90(3): 834–846. https://doi.org/10.1111/jfb.13201

Liu F, Zeng Z, Gong Z (2022) Two new hypogean species of *Triplophysa* (Cypriniformes: Nemacheilidae) from the River Yangtze drainage in Guizhou, China. Journal of Vertebrate Biology 71: 22062.1–14. https://doi.org/10.25225/jvb.22062

Luo T, Yang Q, Wu L, Wang YL, Zhou JJ, Deng HQ, Xiao N, Zhou J (2023a) Phylogenetic relationships of Nemacheilidae cavefish (*Heminoemacheilus, Oreonectes, Yunnanilus, Paranemachilus,* and *Troglonectes*) revealed by analysis of mitochondrial genome and seven nuclear genes. Zoological Research 44(4): 693–697. https://doi.org/10.24272/j.issn.2095-8137.2022.266

Luo T, Chen ZX, Zhao XR, Yu J, Lan CT, Zhou JJ, Xiao N, Zhou J (2023b) *Balitora anlongensis*, the first cavefish species of the genus *Balitora* (Teleostei, Balitoridae) from Guizhou Province, southwest China. ZooKeys 1185: 21–42. https://doi.org/10.3897/zookeys.1185.108545

Ma L, Zhao YH, Yang JX (2019) Cavefish of China. In: White WB, Culver DC, Pipan T (Eds) Encyclopedia of caves (3rd edn.). Academic Press, Pittsburgh, USA, 237–254. https://doi.org/10.1016/B978-0-12-814124-3.00027-3

Nguyen VH (2005) Freshwater fishes of Vietnam (Vol. II). Nha Xuat Ban Nong Nghiep, Hanoi, 760 pp. [In Vietnamese]

Nichols JT (1944) The Fresh-Water Fishes of China. Nature 154: 5. https://doi.org/10.1038/154005a0

Rainboth WJ, Kottelat M (1991) Indochinese nemacheilines: a revision of nemacheiline loaches (Pisces: Cypriniformes) of Thailand, Burma, Laos, Cambodia and southern Viet Nam. Copeia, 1991. https://doi.org/10.2307/1446613

Rambaut A (2018) Figtree ver 1.4.4. Institute of Evolutionary Biology, University of Edinburgh, Edinburgh.

Ronquist F Teslenko M, van der Mark P, Ayres DL, Darling A, Höhna S, Larget B, Liu L, Suchard MA, Huelsenbeck JP (2012) MrBayes 3.2: efficient Bayesian phylogenetic inference and model choice across a large model space. Systematic Biology 61(3): 539–542. https://doi.org/10.1093/sysbio/sys029

Sauvage HE (1874) Notices ichthyologiques. II. Sur un cyprin de genre nouveau provenant de Chine. Revue et Magasin de Zoologie 2(3): 332–340.

Shao WH, Cheng GY, Lu XL, Zhou JJ, Zeng ZX (2024) Description of a new troglobitic *Sinocyclocheilus* (Pisces, Cyprinidae) species from the upper Yangtze River Basin in Guizhou, South China. Zoosystematics and Evolution 100: 515–529. https://doi.org/10.3897/zse.100.119520

Shi C, Yao M, Lv X, Zhao Q, Peng Z, Luo Y (2018) Body and organ metabolic rates of a cave fish, *Triplophysa rosa*: influence of light and ontogenetic variation. Journal of comparative physiology. B, Biochemical, Systemic, and Environmental Physiology 188(6): 947–955. https://doi.org/10.1007/s00360-018-1178-x

Stamatakis A (2014) RAxML version 8: a tool for phylogenetic analysis and post-analysis of large phylogenies. Bioinformatics (Oxford, England) 30(9): 1312–1313. https://doi.org/10.1093/bioinformatics/btu033

Tamura K, Stecher G, Kumar S (2021) MEGA11: Molecular Evolutionary Genetics Analysis Version 11. Molecular Biology and Evolution 38(7): 3022–3027. https://doi.org/10.1093/molbev/msab120

Wang CB, He L (2024) First discovery of troglobitic Paederinae (Coleoptera, Staphylinidae) from China. ZooKeys 1216: 27–42. https://doi.org/10.3897/zookeys.1216.132155

Wu YF, Wu CZ (1992) The fishes of the Qinghai-Xizang Plateau. Sichuan Publishing House of Science and Technology, Chengdu, 599 pp. [In Chinese, English summary]

Wu TJ, Wei ML, Lan JH, Du LN (2018) *Triplophysa anshuiensis*, a new species of blind loach from the Xijiang River, China (Teleostei, Nemacheilidae). ZooKeys 744: 67–77. https://doi.org/10.3897/zookeys.744.21742

Xiong KY, Sun ZY, Guo YS (2017) Revision of *Homatula* and *Schistura* classification in Sichuan Province. Journal of China Southwest Normal University 38(1): 21–27. [Natural Sciences] [In Chinese, English abstract] https://link.cnki.net/doi/10.16246/j.issn.1673-5072.2017.01.004

Yan YL (2017) The origin and evolution of cave-dwelling group of *Triplophysa* fishes (Teleostei, Cypriniformes, Nemacheilidae). (Doctoral dissertation, Southwest University). [In Chinese, English abstract]

Yang GY, Yuan FX, Liao YM (1986) A new blind Cobitidae fish from the subterranean water in Xiangxi, China. Huazhong Nongye Daxue Xuebao 5(3): 219–223. [In Chinese]

Yang W, He L, Yu H, Lin Y (2023) A new cave-dwelling spider of the genus *Speleoticus* (Araneae, Nesticidae) from Sichuan, China. Biodiversity Data Journal 11: e107751. https://doi.org/10.3897/BDJ.11.e107751

Zhang CG, Zhao YH (2016) Species Diversity and Distribution of Inland Fishes in China. Science Press, Beijing, 127–151. [in Chinese]

Zhang CG, Zhao YH, Yang, JX (2019) Fishes in the Jinsha Jiang River Basin, the Upper Reaches of the Yangtze River, China [M]. Science Press, Beijing. [in Chinese]

Zhang CY, Luo P, Huang F, Zhang E (2024) Revision of the loach genus *Claea* Kottelat, 2010 (Teleostei: Nemacheilidae) in China, with a description of a new species from the Chang-Jiang basin. Zootaxa 5543(3): 404–422. https://doi.org/10.11646/zootaxa.5543.3.6

Zhang J, Shu L, Peng Z (2024) Adaptive evolution of mitochondrial genomes in *Triplophysa* cavefishes. Gene 893: 147947. https://doi.org/10.1016/j.gene.2023.147947

Zhao YH, Zhang CG (2009) Endemic fishes of *Sinocyclocheilus* (Cypriniformes: Cyprinidae) in China species diversity, cave adaptation, systematics and zoogeography. Science Press, Beijing. [In Chinese]

Zhu SQ (1989) The loaches of the subfamily Nemacheilinae in China (Cypriniformes: Cobitidae). Jiangsu Science and Technology Publishing House, Nanjing, 150 pp. [In Chinese, English summary].

Zhu SQ, Cao WX (1988) Descriptions of two new species and a new subspecies of Nemacheilinae from Yunnan Province (Cypriniformes: Cobitidae). Acta Zootaxonomica Sinica 13(1): 95–100. [In Chinese, English summary]

Supplementary material 1

Raw data of the type speciemens of *Claea scet*

Authors: Hao-Tian Lei, Li He, Jun-Hao Huang, Jia-Jun Zhou, De-Kui He

Data type: xlsx

Link: https://doi.org/10.3897/zse.101.146469.suppl1

Zoosyst. Evol. 101 (2) 2025, 697–710 | DOI 10.3897/zse.101.146027

PENSOFT

MUSEUM FÜR NATURKUNDE BERLIN

Two new species of the loach genus *Homatula* Nichols, 1925 (Pisces, Nemacheilidae) from the upper Chang-Jiang Basin in China

Liang Cao[1], Yi Liu[1,2], Zhixuan Zeng[3], Wenjing Yi[1], E Zhang[1]

1 *Institute of Hydrobiology, Chinese Academy of Sciences, Wuhan 430072, Hubei Province, China*

2 *University of Chinese Academy of Sciences, Beijing 100049, China*

3 *The Department of Endocrinology, Hubei Clinical Medical Research Center for Endocrinology and Metabolic Diseases, Branch of National Clinical Research Center for Metabolic Diseases, Tongji Hospital, Huazhong University of Science and Technology, Wuhan 430030, Hubei Province, China*

https://zoobank.org/B49514A4-5753-4411-8156-4C43D6788B8F

Corresponding author: E Zhang (zhange@ihb.c.cn)

Academic editor: Nicolas Hubert ♦ **Received** 14 January 2025 ♦ **Accepted** 6 March 2025 ♦ **Published** 26 March 2025

Abstract

Two new species of *Homatula* are herein described from the Wu-Jiang of the upper Chang-Jiang Basin in Guizhou Province, China. *Homatula xiangzhi* and *H. shexiang* are respectively assigned to the scaleless group and the partially scaled group of the genus. *Homatula xiangzhi* differs from all other species of the scaleless group in having a complete lateral line, an adipose crest along the dorsal mid-line of the caudal peduncle anteriorly terminating behind the middle of the anal-fin base, nine branched dorsal-fin rays, vertebrae 4+42-43 and no median notch on the lower jaw. *Homatula shexiang* is similar to *H. longidorsalis* in having nine branched dorsal-fin rays rather than seven or eight in all other species of the partially scaled group, but differs from it in having an adipose crest along the dorsal mid-line of the caudal peduncle anteriorly terminating behind the middle of the anal-fin base, a deeper head and a slender caudal peduncle. The validity of the two new species is further corroborated in a molecular phylogenetic analysis, based on the Cytb gene.

Key Words

Cypriniformes, molecular phylogeny, morphology, taxonomy, Wu-Jiang

Introduction

Within the family Nemacheilidae, the genus *Homatula* is characterised by possessing adipose crests along dorsal and ventral mid-lines of the caudal peduncle (Nichols and Pope 1925; Hu and Zhang 2010; Min et al. 2022). Currently, it comprises 28 species from southern China and central Vietnam (Li et al. 2022; Che et al. 2023). This genus has a concentrated distribution in the upper Chang-Jiang Basin where six species have been documented: *H. berezowskii* (Günther, 1896), *H. oxygnathra* (Regan,1908), *H. potanini* (Günther, 1896), *H. tigris* Che, Dao, Chen, Pan, Hua, Liang & Wang, 2023, *H. variegata* (Sauvage & Dabry de Thiersant, 1874) and *H. wujiangensis* (Ding & Deng, 1990) (Guo et al. 2021; Liu et al. 2022; Che et al. 2023). Amongst them, three species, misplaced in *Nemacheilus* or *Paracobitis*, were previously reported from the Wu-Jiang, the largest tributary on the southern bank of the upper Chang-Jiang mainstream: *H. potanini*, *H. variegata* and *H. wujiangensis* (Wu 1989; Ding 1994; Yang et al. 2022). However, their identification needs re-evaluation especially given the taxonomic revisions of some relevant congeneric species outside this river during the past decade or more. For example, *H. variegata*, previously recognised as a species widespread in the upper Zhu-Jiang (Nanpan-Jiang), the upper Chang-Jiang and Huang-He Basins (Zheng 1989; Zhu 1989; Yang et al. 1994; Guo et al. 2021), was the taxonomic subject of many works (Hu and Zhang 2010; Gu and Zhang 2012). It is widely thought that its type locality was in the upper Chang-Jiang Basin. Kottelat (2012), though, asserted that the type locality of *H. variegata* was

in the Huang-He Basin. This hypothesis has been recently corroborated on the basis of examination on the type and topotypical specimens (Liu et al. 2022); *H. variegata* is truly represented by the population of the Wei-He, a tributary of the middle Huang-He Basin (Liu et al. 2022). In this context, it is urgently needed to assess the taxonomic status of specimens under the name of *H. variegata* from the Wu-Jiang or even from the upper Chang-Jiang Basin.

Field survey of fishes, conducted by us into the Wu-Jiang, yielded many specimens referred to as *H. variegata*, following the identification of this species by Zheng (1989), Wu (1989) and Ding and Deng (1990). These specimens were scrutinised to represent two undescribed species under a reliable taxonomic framework integrating morphological and molecular evidence. The purport of the present study is to provide a formal description of the two undescribed species, here named as *H. xiangzhi* sp. nov. and *H. shexiang* sp. nov., respectively.

Materials and methods

Fishes, utilised for this study, were collected in accordance with the Chinese Laboratory Animal Welfare and Ethics animal welfare laws. Specimens were captured during fish surveys conducted in 2018 and 2020. After being anaesthetised, all caught individuals were killed by immersion in ethanol or formalin. Captured specimens were either stored in 95% ethanol for DNA extraction or initially fixed in 10% formalin and then transferred to 70% ethanol for morphological examination.

All morphometric measurements and meristic counts were made on the left side of each individual when possible, following the methods utilised by Kottelat (1990). Measurements were taken point to point with digital calipers directly linked to a data-recording computer and data recorded to the nearest 0.1 mm. Meristic counts were made utilising a bilocular Zeiss Stereo Discovery V6; the last two branched rays in dorsal and anal fins, closely approximated at the base, were counted as a single ray. Micro-CT imagines were used to observe skeletal structures including the count of vertebrae. The Weberian apparatus was regarded as including four vertebrae. All meristic counts and morphometric measurements were provided in Table 2.

Genomic DNA was extracted from alcohol-preserved fin clips using the TIANamp Genomic DNA Kit (Tiangen Biotech, Beijing). Mitochondrial Cytb gene was amplified using polymerase chain reaction (PCR) with primers L14724 (GACTTGAAAAACCA CCGTTG) and H15915 (CTCCGATCTCCGGATTACAAGAC) (Xiao et al. 2001). The following thermal cycling profiles were adopted: 95 °C pre-denaturing (5 min), 94 °C denaturing (50 s), 53 °C for Cytb annealing (90 s), 72 °C extension (10 min), for 34 cycles, and 72 °C final extension (10 min) and then the product was preserved at 4 °C. Amplified products were subsequently purified and utilised for direct cycle sequencing by the Aoke Dingsheng Sequencing Company.

Twelve samples of *H. xiangzhi* (five) and *H. shexiang* (seven) were amplified for the Cytb gene. Four samples of *H. berezowskii* captured from the Han-Jiang and two samples of *H. wujiangensis* from the Wu-Jiang in our other field surveys were determined for the same gene (Table 1). Sequence data were archived in the public domain database GenBank. These sequences were subject to phylogenetic analysis, along with 46 GenBank- retrieved sequences from 23 congeneric species of *Homatula*. Sequences from two species of *Schistura* (*S. fasciolata* and *S. longa*) and two species of *Triplophysa* (*T. stoliczkai* and *T. stenura*) were used as outgroups (Table 1). Multiple alignments were prepared with MEGA 7.0 software for all sequences (Kumar et al. 2016). The general time-reversible model with invariant sites and a gamma distribution variation across sites (GTR+F+G4) was selected as the best-fitting model for the Cytb gene in ModelFinder (Kalyaanamoorthy et al. 2017), based on Akaike's Information Criterion (Akaike 1974). MrBayes 3.2.6 (Ronquist et al. 2012) was used to calculate Bayesian Inference (BI) tree and IQ-TREE v.1.6.8 (Nguyen et al. 2015) was applied to generate the Maximum-Likelihood (ML) tree. Two independent parallel Markov Chain Monte Carlo runs were monitored with Tracer v.1.7.1 (Rambaut et al. 2018) and the first 25% samples were discarded as burn-in. The tree was rooted by outgroups and visualised via FigTree v.1.4.3 (http://tree.bio.ed.ac.uk/software/figtree/).

All specimens, utilised in this study, are archived in the ichthyological collection at the Institute of Hydrobiology (IHB), Chinese Academy of Sciences, Wuhan City, Hubei Province, China. Photographic examination was made for types of *H. disparizona*, *H. longidorsalis* and *H. nanpanjiangensis* that are so far housed in the Kunming Institute of Zoology (KIZ), Chinese Academy of Sciences, Kunming City, Yunnan Province, as well as *H. oxygnathra* and *H. variegata* which are respectively deposited in the British Museum of Nature and History (BMNH) and the Muséum National d'Histoire naturelle de Paris (MNHN).

Availability of data and material

The datasets used and/or analysed during the current study are available from the corresponding author on reasonable request.

Results

***Homatula xiangzhi* Cao, Liu, Zeng & Zhang, sp. nov.**

https://zoobank.org/B49514A4-5753-4411-8156-4C43D6788B8F

Figs 1, 2.

Nemachelius variegatus: Wu, 1987: 27 (Nanming-He of Wu-Jiang).

Paracobitis variegatus: Ding, 1994: 51 (Wulong County, Wu-Jiang).

Holotype. IHB 202006048865, 98.0 mm SL; China: Guizhou Province: Guiyang City: Wudang District: Baishui-He, a tributary of Qingshui-He discharging into Wu-Jiang, at Shanglongjiao Village (26°46'21"N, 106°55'02"E) of Xiangzhi-Gou; collected by Z. X. Zeng in June 2020.

Table 1. The detailed information of sequences used in this study with sampling location and GenBank accession number.

Species	Sampling locality (River basin)	GenBank accession numbers	References
H. acuticephala	Eryuan, Yunnan (Lancang-Jiang)	HM010503	Min et al. (2012)
H. anguillioides	Eryuan, Yunnan (Lancang-Jiang)	HM010546	Min et al. (2012)
H. anteridorsalis	Baoshan, Yunnan	OP779698	Li et al. (2022)
	(Nu-Jiang)	OP779701	Li et al. (2022)
H. berezowskii	Shennongjia, Hubei	OM640077	This study
	(Han-Jiang)	PQ816783	This study
	Shiyan, Hubei	PQ816781	This study
	(Han-Jiang)	PQ816782	This study
H. cryptoclathrata	Longling, Yunnan	HM010569	Min et al. (2012)
	(Nu-Jiang)	HM010566	Min et al. (2012)
H. disparizona	Wenshan, Yunnan	MG238217	Min et al. (2023)
	(Red-River)	MG238218	Min et al. (2023)
H. geminusclathrata	Jingdong, Yunnan (Lancang-Jiang)	OP779703	Li et al. (2022)
H. guanheensis	Hanzhong, Shaanxi	OL329831	Liu et al. (2022)
	Langao, Shaanxi	OL329833	Liu et al. (2022)
	Xixia, Henan	MT771714	Zhou et al. (2021)
	(Han-Jiang)	MT771715	Zhou et al. (2021)
H. laxiclathra	Zhouzhi, Shaanxi	OL329841	Liu et al. (2022)
	Taibai, Shaanxi	OL329846	Liu et al. (2022)
	(Wei-He)	OL329848	Liu et al. (2022)
H. longibarbata	Dali, Yunnan	OP779704	Li et al. (2022)
	(Lancang-Jiang)	OP779705	Li et al. (2022)
H. longidorsalis	Yiliang, Yunnan	HM010500	Min et al. (2012)
	(Nanpan-Jiang)	HM010568	Min et al. (2012)
H. microcephala	Dali, Yunnan	OP779710	Li et al. (2022)
	(Lancang-Jiang)	OP779709	Li et al. (2022)
H. nanpanjiangensis	Luoping, Yunnan	HM010574	Min et al. (2012)
	(Nanpan-Jiang)	HM010577	Min et al. (2012)
H. nigra	Baoshan, Yunnan	OP779715	Li et al. (2022)
	(Nu-jiang)	OP779716	Li et al. (2022)
H. oxygnathra	Yuanmou, Yunnan	OL329836	Liu et al. (2022)
	(Jinsha-Jiang)	OL329835	Liu et al. (2022)
	Yanbian, Sichuan	OL329839	Liu et al. (2022)
	(Yalong-Jiang)	OL329838	Liu et al. (2022)
H. potanini	Leshan, Sichuan	JF340385	Min et al. (2012)
	(Jinsha-Jiang)	JF340386	Min et al. (2012)
H. pycnolepis	Dali, Yunnan	OP779718	Li et al. (2022)
	(Lancang-Jiang)	OP779719	Li et al. (2022)
H. shexiang sp. nov.	Kaiyang, Guizhou	OM640080	This study
	(Wu-Jiang)	PQ816776	This study
		PQ816775	This study
		OM640081	This study
		OM640082	This study
	Xiuwen, Guizhou	OM640083	This study
	(Wu-Jiang)	OM640084	This study
H. tigris	Kunming, Yunnan	ON124934	Che et al. (2023)
	(Jinsha-Jiang)	ON124932	Che et al. (2023)
		ON124933	Che et al. (2023)
H. variegata	Xi'an, Shaanxi	OL329850	Liu et al. (2022)
	(Wei-He)	OL329851	Liu et al. (2021)
	Luoning, Henan	OL681884	Liu et al. (2022)
	(Huang-He)	OL681883	Liu et al. (2022)
H. wenshanensis	Wenshan, Yunnan (Red-River)	MW548261	NCBI
H. wujiangensis	Jinfoshan, Chongqing	PQ816777	This study
	(Wu-Jiang)	PQ816778	This study
H. wuliangensis	Pu'Er,Yunnan	HM010517	Min et al. (2012)
	(Lancang-Jiang)	HM010496	Min et al. (2012)
H. xiangzhi sp. nov.	Guiyang, Guizhou	OM640088	This study
	(Wu-Jiang)	OM640089	This study
		OM640090	This study
		PQ816779	This study
		PQ816780	This study
H. dotui	Vietnam	OK230030	Nguyen et al. (2021)
		OK230029	Nguyen et al. (2021)
Schistura fasciolata	Yunnan, China	KY404236	NCBI
Schistura longa	Unknown	JF340408	Min et al. (2012)
Triplophysa stenura	Yunnan, China	JN837657	Min et al. (2012)
Triplophysa stoliczkai	Unknown	JQ663847	Li et al. (2013)

Figure 1. *Homatula xiangzhi* sp. nov, IHB 202006048865, holotype, 98.0 mm SL; China: Guizhou Province: Guiyang City: Wudang District: Baishui-He. Lateral (upper), dorsal (middle) and ventral (lower) view.

Paratypes. IHB 202006048864, 202006049211–9212, three specimens, 53.7–133.4 mm SL; other date same as holotype. IHB 20180055996–5997, two specimens, 61.0–76.6 mm SL and IHB 202006048866–8867, two specimens, 60.5–73.1 mm SL; China: Guizhou Province: Guiyang City: Wudang District: Pudu-He, a stream tributary to Qingshui-He of Wu-Jiang, at Duzhai Village (26°41'52"N, 113°12'39"E); collected by L. Cao, C. T. An and Z. T. Wang in October 2018 and by D. M. Guo and W. H. Shao in June 2020.

Diagnosis. A member of the scaleless group of *Homatula*, defined by having no scales on the body or a small number of scales sparsely scattering over the caudal peduncle. It is distinct from other six species of the group in having a complete (vs. incomplete in *H. wujiangensis*) lateral line, an elongate (vs. stout) body with a uniform depth (vs. non-uniform, gradually decreasing towards the caudal-fin base in *H. wujiangensis* and *H. robusta*), an adipose crest along the dorsal mid-line of the caudal peduncle anteriorly terminating vertically away from the anal-fin origin, but beyond the posterior end of the anal-fin base (vs. above vertical of the posterior end of the anal-fin base in *H. wenshanensis*; above or beyond the anal-fin origin in *H. nanpanjiangensis*, *H. oligolepis*, *H. disparizona* and *H. robusta*), a slender (vs. stout) caudal peduncle with (depth 42.0–53.8% of its length vs. 70.5–78.5% in *H. robusta* and 100.0–120.0% in *H. wujiangensis*) of its length, vertebrae 4+42-43 (vs. 4+47–48 in *H. wenshanensis* and 4+35–41 in remaining species), more branched dorsal-fin rays (9 vs. 7–8 in *H. disparizona*, *H. robusta*, *H. wenshanensis* and *H. wujiangensis*), a truncate (vs. emarginate in *H. disparizona*, *H. nanpanjiangensis* and *H. robusta* and forked in *H. wenshanensis*) and no median notch on the lower jaw (vs. present in *H. nanpanjiangensis*, *H. oligolepis*, *H. robusta*, *H. wenshanensis* and *H. wujiangensis*).

Description. Morphometric measurements for type specimens given in Table 2 and general appearance of holotype shown in Fig. 1.

Body elongated, anteriorly cylindrical and posteriorly compressed laterally, with uniform depth from behind head to caudal peduncle. Ventral profile of head straight or slightly concave; ventral profile of body straight or slightly concaved from pectoral-fin insertion to anal-fin origin and slightly convex from anal-fin origin to caudal-fin base. Body nearly scaleless; only a few tiny scales scattered over caudal peduncle. Lateral line complete, with 80–90 pored scales, extending along mid-lateral body to caudal-fin base. Adipose crests along dorsal and ventral mid-lines of caudal peduncle supported by rudimentary rays; dorsal adipose crest anteriorly terminating vertically away from the anal-fin origin, but beyond the posterior end of the anal-fin base and ventral adipose crest anteriorly extending close to posterior end of anal-fin base. Head relatively long and slightly depressed, wider than deep. Snout blunt when viewed laterally, shorter than postorbital head and slightly pointed in dorsal view. Eye oval or elliptical with slightly convex interorbital space, placed

Figure 2. Freshly-captured individual of *H. xiangzhi* sp.nov., collected from China: Guizhou Province: Guiyang City: Wudang District: Baishui-He, a tributary of Qingshui-He discharging into Wu-Jiang, at Shanglongjiao Village.

Table 2. Morphometric measurements for two new species of *Homatula*.

Characteristic	*H. xiangzhi* sp.nov.			*H. shexiang* sp.nov.		
	Holotype	Paratypes (n = 7)		Holotype	Paratypes (n = 15)	
		Range	Mean ± SD		Range	Mean ± SD
Standard length (mm)	98.0	53.7–133.4	76 ± 24.8	100.2	71.0–132.5	99.7 ± 19.9
% of Standard length						
Body depth	11.0	10.6–13.4	11.9 ± 1.0	11.2	11.3–15.1	12.9 ± 1.1
Head length	18.2	18.2–22.6	21.0 ± 1.4	19.0	17.0–21.1	19.2 ± 1.2
Head depth	9.3	8.7–11.6	10.5 ± 1.0	11.2	9.6–12.6	11.0 ± 0.8
Head width	11.0	11.2–13.4	12.2 ± 0.7	12.2	11.2–13.4	12.2 ± 0.6
Snout length	8.4	8.0–10.0	9.1 ± 0.6	8.6	7.8–10.0	8.7 ± 0.6
Eye diameter	3.3	2.9–4.4	3.6 ± 0.5	2.7	2.1–3.1	2.6 ± 0.2
Interorbital width	4.9	3.9–6.1	5.1 ± 0.6	4.8	4.3–6.6	5.3 ± 0.7
Dorsal-fin length	10.7	9.1–13.6	11.4 ± 1.7	9.4	8.9–12.9	10.6 ± 1.4
Pectoral-fin length	10.9	9.2–15.6	13.6 ± 2.2	12.3	11.1–15.2	13.1 ± 1.3
Pelvical-fin length	10.0	8.2–13.0	11.3 ± 1.7	10.5	9.2–12.7	10.7 ± 1.0
Anal-fin length	10.8	9.5–12.7	10.9 ± 1.1	12.9	11.8–14.5	13.0 ± 0.7
Vent to caudal-fin origin	31.4	27.8–35.5	30.4 ± 2.4	32.1	30.0–35.4	32.6 ± 1.8
Prepectoral length	18.5	16.4–24.0	21.1 ± 2.3	17.2	16.2–19.6	17.8 ± 1.0
Predorsal length	43.7	42.3–49.3	46.7 ± 2.1	47.1	42.1–49.9	45.5 ± 1.8
Prepelvic length	45.7	44.7–52.4	48.6 ± 2.2	46.5	42.4–50.2	46.2 ± 2.4
Preanal length	70.9	70.5–75.2	73.0 ± 1.4	71.0	67.2–73.6	70.7 ± 1.7
Caudal-peduncle length	20.0	17.6–22.2	19.3 ± 1.5	21.0	17.9–22.9	20.5 ± 1.5
Caudal-peduncle depth	9.4	8.0–10.4	9.3 ± 1.0	9.7	9.0–11.0	10.0 ± 0.6
Caudal-fin length	12.3	11.8–15.9	14.6 ± 1.3	12.5	12.0–15.5	13.5 ± 1.2
% of Head length						
Head depth	51.0	47.1–53.3	49.8 ± 2.8	59.2	54.0–60.8	57.5 ± 2.2
Head width	60.4	53.5–61.4	58.2 ± 2.5	64.0	60.6–68.0	63.8 ± 2.0
Snout length	46.3	40.5–45.5	43.5 ± 2.0	45.3	41.8–50.2	45.7 ± 2.5
Eye diameter	18.1	14.4–19.4	16.9 ± 1.9	14.1	11.8–15.1	13.7 ± 0.9
Interorbital width	26.8	21.4–27.8	24.4 ± 2.2	25.4	24.0–32.0	27.7 ± 2.2
% of Interorbital width						
Eye diameter	67.8	58.2–78.0	68.4 ± 7.5	55.5	41.5–56.7	49.8 ± 4.2
% of caudal-peduncle length						
Caudal-peduncle depth	47.0	42.0–53.8	47.3 ± 4.5	46.2	40.4–55.2	49.1 ± 4.9
P	i, 10	i, 9–11		i, 10	i, 9–11	
D	iii, 9	iii, 9		iii, 9	iii, 9	
V	i, 7	i, 7–8		i, 7	i, 7–8	
A	iii, 5	iii, 5		iii, 5	iii, 5	
C	9+8	9+8		9+8	9+8	
Vertebrae	4+43	4+42–43 (n = 4)		4+42	4+42–43 (n = 4)	

dorsolaterally in upper half of head, not reaching dorsal profile, when viewed laterally; eye diameter less than interorbital width. Anterior and posterior nostrils set closely; anterior nostril situated at end of small and oblique tube. Mouth inferior; lips thick, slightly folded, smooth with small median incision in upper lip and marked median longitudinal groove on lower lip. Upper jaw with shallow processus dentiformis; lower jaw spoon-like, without median notch. Two pairs of rostral barbels; inner barbels extending close to rictus and outer barbels reaching rictus. Maxillary barbels rooted in corners of mouth, extending close to vertical through middle of eye.

Cephalic lateralis system with 8 supraorbital, 4+10 infraorbital, 9 pre-operculo-mandibular and 3 supratemporal pores. Gill opening large, with its upper extremity aligned with centre of orbit.

Fin rays flexible. Dorsal fin with 3 unbranched and 9 branched rays; longest ray shorter than dorsal-fin base; distal margin slightly convex; origin closer to snout tip than to caudal-fin base. Pectoral fin with one unbranched and 9–11 branched rays, tip of depressed fin not reaching mid-way between pectoral- and pelvic-fin insertion. Pelvic fin with one unbranched and 7–8 branched rays, reaching about half the distance between pelvic-fin insertion and anus; origin of pelvic fin at vertical of 1st or 2nd branched dorsal fin ray. Axillary lobe present on pelvic-fin base. Anus set closer to anal-fin origin than to pelvic-fin insertion; separated from anal-fin origin by distance 1.2–1.5 times greater than eye diameter. Anal fin with 3 unbranched and 5 branched rays, tip of depressed fin not reaching caudal-fin base; distal margin slightly convex. Caudal fin with 9+8 branched rays and truncate with slightly concave outer margin.

Vertebrae 4+42–43 (n = 5), including 20–21 abdominal and 22 caudal vertebrae. Gas bladder bipartite; anterior chamber invisible, fully enclosed in capsule; posterior chamber degenerative. Intestine with a distinct transverse bend not reaching posterior end of U-shaped stomach.

Colouration. In formalin-stored specimens (Fig. 1), ground colour of body yellowish, with light yellowish ventral surface. Head yellowish with vermiform marks; snout, lips and anterior nostril light white. Thirteen to fourteen brown vertical bars on flank; anterior six or seven bars oval and closely set, but six post-dorsal bars nearly oblong and deep. Four or five brown rounded bars along dorsal mid-line of predorsal body; last three bars merged into a brown band in some individuals; some brown bars of irregular shape inserted between rounded bars along dorsal mid-line and vertical bars on flank, less or more touched with these bars and sometimes merged to form discontinuous brown band. Some irregular brown bars present on dorsum from behind dorsal-fin origin to anterior end of adipose crest amongst dorsal mid-line of caudal peduncle. A brown lateral stripe extending along base of dorsal adipose crest. Melanin pigments on branched rays forming proximal and subdistal brownish bands across dorsal fin. Pectoral, pelvic and anal fins translucent white yellowish. Caudal fin greyish with some dark black spots and blackish distal edge. Caudal-fin base with dark brown vertical bar. In freshly-collected individuals (Fig. 2), overall body colouration very similar to that of formalin-preserved specimens, but a little bright. Caudal fins and dorsal adipose crest red, particularly in spawning season.

Distribution. The type specimens were collected from Qingshui-He, tributary to Wu-Jiang of upper Chang-Jiang Basin in Guizhou Province, China. The species is also known from upstream of Mengjiang, tributary to Zhu-Jiang Basin in Huaxi District of Guiyang City and Changshun County of Qiannan Prefecture, Guizhou Province, China (Fig. 3).

Etymology. The specific epithet, used as a noun, is named after 'Xiangzhi'. This Chinese word means fragrant paper. The type locality (Xiangzhi-Gou) is named after the local intangible cultural heritage, the fragrant paper manufacturing technique. A corresponding common Chinese name "香纸荷马条鳅" is proposed here for the new species.

Homatula shexiang Cao, Liu, Zeng & Zhang, sp. nov.

https://zoobank.org/398A7428-A3A6-450B-96A7-76818EE2E333

Figs 4, 5

Nemachelius variegatus: Wu, 1987: 27 (Wu-Jiang).

Paracobitis variegatus: Ding, 1994: 51 (Wu-Jiang).

Holotype. IHB 202006048998, 100.2 mm SL; China: Guizhou: Guiyang City: Xiuwen District: Maodong-He, a stream tributary to Maotiao-He, under Wugong Bridge (26°54'11"N,106°29'22"E); collected by D. M. Guo and W. H. Shao, June 2020.

Paratypes. IHB202006048993–8997, 202006048999–9002, 202006200601–0602, 11 specimens, 71.9–125.6 mm SL; other date same as holotype. IHB 202006048907–8911, five specimens, 71.0–132.5 mm SL; China: Guizhou: Guiyang City: Kaiyang District: Macha-He (27°7'14"N, 107°0'1"E), a stream tributary to Qingshui-He; collected by D. M. Guo and W. H. Shao, June 2020.

Diagnosis. A member of the partially scaled group of *Homatula* defined by having a sparsely scaled or unscaled predorsal body. It differs from all other eight species of this group, except *H. longidorsalis* in possessing 9 (vs. 7 or 8) branched dorsal-fin rays. *Homatula shexiang* differs from this species in having an adipose crest along the dorsal mid-line of the caudal peduncle anteriorly terminating vertically away from the anal-fin origin (vs. above the anal-fin origin), a deep (vs. shallow) head (depth 54.0–60.8% of its length vs. 46.46–48.65%) and a slender (vs. stout) caudal peduncle with (depth 40.4–55.2% vs. 57.2–61.5% of its length).

Description. Morphometric measurements for type specimens given in Table 2. General appearance of holotype shown in in Fig. 4.

Body elongated, anteriorly cylindrical and posteriorly compressed laterally, with uniform depth from behind head to caudal-fin base. Ventral profile of head straight or slightly concave; ventral profile of head and body almost straight or slightly concave from pectoral-fin insertion to anal-fin origin and slightly convex from anal-fin origin to caudal-fin base. Body partially scaled; no scales on predorsal body, but scales only present on body behind dorsal-fin origin. Lateral line complete, with 85–95 pored scales, extending along mid-lateral body to caudal-fin base. Adipose crests along dorsal and ventral mid-lines of caudal peduncle supported by rudimentary rays. Dorsal adipose crest anteriorly terminating beyond the posterior end of the anal-fin base, but away from anal-fin origin.

Head relatively long and slightly depressed, wider than deep. Snout blunt in lateral view, slightly shorter

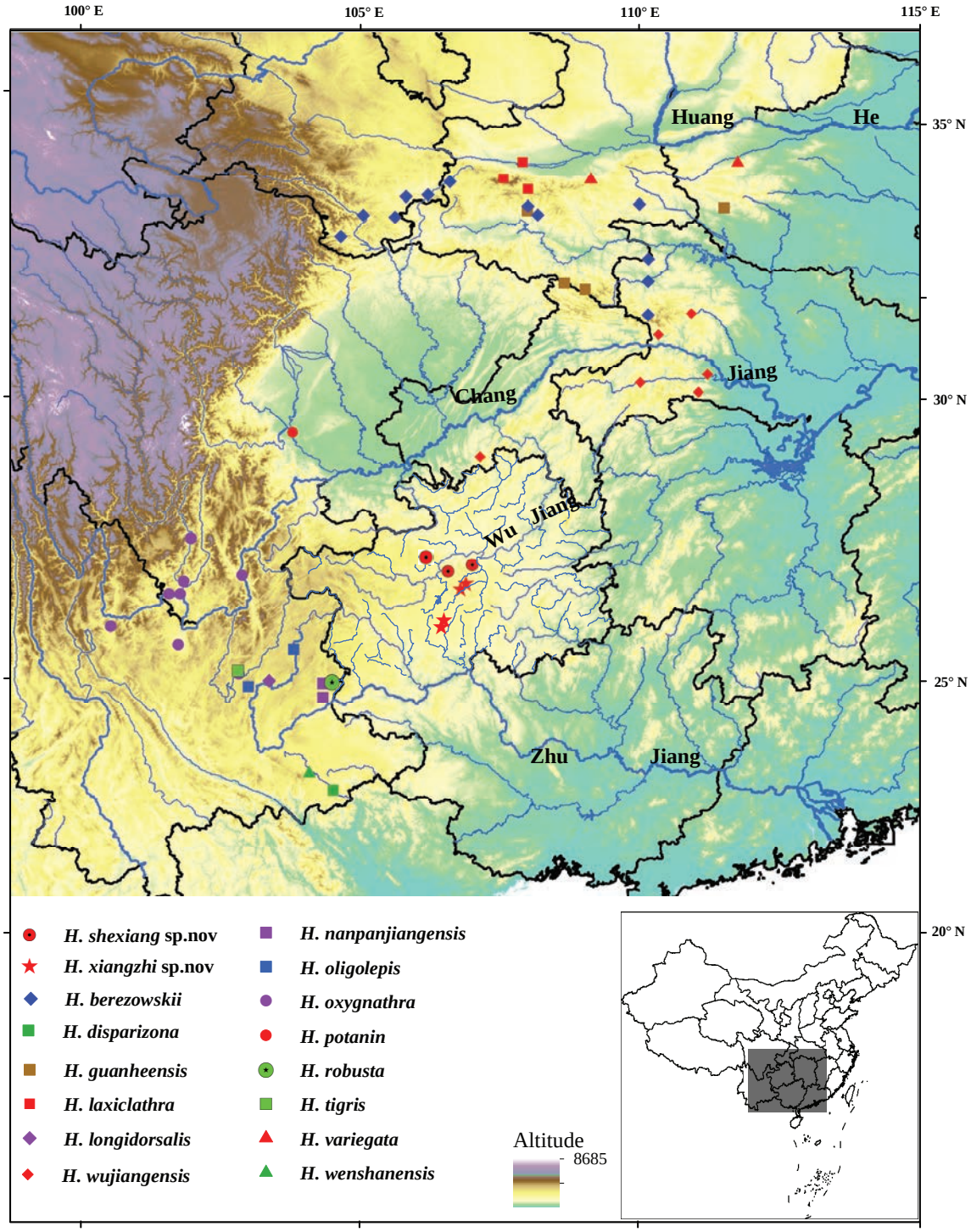

Figure 3. Distribution of the partially scaled and the scaleless group of *Homatula* in China.

than postorbital head. Eye oval with slightly convex interorbital space, positioned dorsolaterally in upper half of head, not reaching dorsal profile when viewed laterally; diameter less than interorbital width. Anterior and posterior nostrils set closely; anterior nostril situated at end of small and oblique tube. Mouth inferior; lips slightly thick, slightly folded and smooth with small median incision in upper lip and marked median longitudinal groove on lower lip. Upper jaw with shallow processus dentiformis and lower jaw spoon-like without median notch. Two pairs of rostral barbels; inner barbels extending to rictus and outer barbels reaching rictus. Maxillary barbels rooted in corners of mouth, extending close to vertical through middle of eye, but short of posterior margin of eye. Cephalic lateralis system with 8 supraorbital, 4+10 infraorbital, 9 preoperculo-mandibular and 3 supratemporal pores. Gill opening large, with its upper extremity aligned with centre of orbit.

Fin rays flexible. Dorsal fin with 3 unbranched and 9 branched rays; longest ray shorter than dorsal-fin base;

Table 3. Genetic distances of Cyt b amongst species of *Homatula*.

Species		1	2	3	4	5	6	7	8	9	10	11	12	13	14	15	16	17	18	19	20	21	22	23	24
***H. shexiang* sp.nov.**	1																								
***H. xiangzhi* sp.nov.**	2	3.6																							
H. tigris	3	6.7	7.9																						
H. variegata	4	7.8	7.8	8.5																					
H. berezowskii	5	7.7	8.0	8.0	3.2																				
H. guanhensis	6	7.6	7.7	8.4	1.4	3.0																			
H. laxiclathra	7	6.8	7.3	8.0	4.8	4.6	4.6																		
H. oxygnathra	8	7.8	7.7	8.1	5.3	4.9	5.1	2.1																	
H. longidorsalis	9	6.7	7.2	7.4	5.7	5.5	5.7	4.7	5.1																
H. nanpanjiangensis	10	7.4	7.1	6.7	5.1	5.1	5.2	4.4	4.8	4.5															
H. wujiangensis	11	8.5	8.9	10.0	9.3	8.9	9.3	8.9	9.3	8.7	8.2														
H. potanini	12	8.6	8.4	10.2	8.8	8.8	8.7	8.8	9.2	8.6	8.1	1.1													
H. anguillioides	13	8.2	8.7	8.2	9.7	9.4	9.5	9.1	9.3	8.4	7.8	9.7	9.5												
H. acuticephala	14	8.4	8.6	8.3	9.6	9.3	9.4	9.0	9.2	8.3	7.7	9.5	9.4	0.1											
H. anteridorsalis	15	10.3	10.1	10.8	11.0	11.1	10.6	10.5	10.4	9.9	9.1	11.2	10.9	4.1	4.0										
H. cryptoclathrata	16	9.8	9.8	10.4	10.6	10.5	10.1	9.7	9.7	9.5	8.8	10.6	10.5	3.8	3.7	1.8									
H. disparizona	17	8.1	8.6	9.0	9.8	9.4	10.0	8.4	8.8	8.2	7.5	9.7	9.8	8.5	8.6	10.0	9.3								
H. geminusclathrata	18	12.5	11.5	12.9	14.8	14.2	14.5	14.6	14.4	13.0	13.0	13.2	13.0	11.9	12.0	13.0	12.9	13.2							
H. longibarbata	19	8.8	8.3	9.6	10.5	9.9	10.1	9.5	9.2	9.2	8.3	9.3	9.1	4.2	4.1	4.2	4.3	9.8	11.6						
H. microcephala	20	10.2	10.3	10.0	11.0	10.8	11.1	11.0	10.9	9.8	9.6	10.3	10.3	4.5	4.5	4.2	4.1	9.5	11.6	4.9					
H. nigra	21	9.8	10.0	10.1	10.4	10.4	10.3	9.8	9.6	9.2	8.9	10.5	10.2	4.2	4.2	2.4	1.5	8.8	11.6	4.0	2.7				
H. pycnolepis	22	9.0	9.8	8.8	10.5	10.1	10.2	9.5	9.9	8.9	8.4	9.8	9.8	3.3	3.4	4.0	3.9	8.6	11.4	4.1	4.5	3.7			
H. wuliangensis	23	12.0	11.0	12.5	14.3	13.7	14.1	14.0	13.8	12.7	12.5	12.8	12.5	11.6	11.7	12.9	12.6	12.6	0.5	11.4	11.4	11.4	11.2		
H. wenshanensis	24	8.1	8.2	9.2	9.9	9.7	10.0	8.4	8.4	8.0	7.5	9.2	9.3	9.0	9.1	10.4	9.9	3.7	13.0	9.0	9.9	9.6	8.5	12.5	
H. dotui	25	14.1	14.7	14.7	14.8	14.2	14.7	14.3	13.5	13.0	13.1	13.3	13.3	13.8	13.7	14.6	15.2	13.7	16.6	13.4	14.7	15.0	13.9	16.0	12.9

Figure 4. *Homatula shexiang* sp. nov., IHB 202006048998, holotype, 100.2 mm SL; China: Guizhou: Guiyang City: Xiuwen District: Maodong-He, a stream tributary to Maotiao-He, under Wugong Bridge. Lateral (upper), dorsal (middle) and ventral (lower) view.

Figure 5. Freshly-captured individual of *Homatula shexiang* sp.nov. collected from China: Guizhou: Qianxi City:Wei-he.

distal margin slightly convex. Pectoral fin with one unbranched and 9–11 branched rays, tip of depressed fin not reaching mid-way between pectoral- and pelvic-fin insertion. Pelvic fin with one unbranched and 7–8 branched rays, reaching about mid-way between pelvic-fin insertion and anus; origin of pelvic fin at vertical of 1st or 2nd branched dorsal fin ray. Anus positioned closer to anal-fin origin than to pelvic-fin insertion; separated from anal-fin origin by distance 1.5–2 times greater than eye diameter. Anal fin with 3 unbranched and 5 branched rays, tip of depressed fin not reaching caudal-fin base; distal margin slightly convex. Caudal fin rounded; upper and lower lobes with 9 and 8 branched rays, respectively.

Vertebrae 4+42–43 (n = 4), including 20–21 abdominal and 22 caudal vertebrae. Gas bladder bipartite; anterior chamber invisible, fully enclosed in capsule; posterior chamber degenerative. Intestine with a distinct transverse bend not reaching posterior end of U-shaped stomach.

Colouration. In formalin-stored specimens (Fig. 4), ground colour of body yellowish. Dorsal and lateral head yellowish with vermiform brown marks; ventral head yellow, with white snout, lips and barbels. Eight or nine brown irregularly-shaped bars along dorsal mid-line of body from behind head to origin of dorsal adipose crest. Thirteen to fifteen brown vertical bars on flank; anterior nine bars usually confused with brown bars along dorsal mid-line of body and wider than interspace space; three or four brown vertical bars on caudal peduncle equal to interspace width. Ventral body surface white-yellow. Melanin pigments on branched rays to form proximal and subdistal brownish bands across dorsal fin. Pectoral, pelvic fins and anal fin translucent white-yellow. Caudal fin and adipose crest dusky, sometimes with some blackish spots. Caudal-fin base with a dark brown vertical bar. In freshly-collected specimens (Fig. 5), overall body colouration similar to that in formalin-stored specimens, but a little bright. Caudal fin and dorsal adipose crest reddish, particularly during spawning season.

Distribution. To date, known only from Wu-Jiang, tributary to upper Chang-Jiang in Guiyang and Qianxi, Guizhou Province, China (Fig. 3).

Etymology. The specific epithet, here used as a noun, is named after Mrs. She Xiang (奢香夫人), an outstanding female politician and the leader of the Yi nationality in Guizhou Province during the Min Dynasty. The Wugong Bridge, type locality of the new species, is one of stone bridges across the Maodong-He built by Mrs. She Xiang six hundred years ago. A corresponding common name "奢香荷马条鳅" in Chinese is proposed here for this new species.

Phylogenetic analysis and genetic distances

A total of 16 Cytb gene sequences with 1080 bp in length were amplified in this study. The molecular phylogenetic trees generated from the BI and ML analyses showed the same topologies, only the BI tree with Bayesian posterior probabilities (PP) and bootstrap support (BS) value being presented in Fig. 6. From the tree topologies, species of *Homatula* in China form a monophyletic clade with a high support. The two new species, *H. shexiang* sp. nov. and *H. xiangzhi* sp. nov., formed a highly-supported lineage itself and then constituted a well-supported clade which was sister to the species *H. tigris* with weak support. This group consisting of the three species was recovered as the sister to a well-supported clade formed by seven other species distributed in the Chang-Jiang, Huang-He and Nanpan-Jiang drainage areas.

The genetic distances between the *Homatula* species are provided in Table 3. Interspecific genetic distance between the two new species, *H. shexiang* and *H. xiangzhi* and other congeneric species ranged from 6.7% to 12.5% and 7.1% to 11.5% (Table 4), respectively. Interspecific genetic distance between the two new species was 3.6% and intraspecific genetic divergence was 0.61% and 0.06% for *H. shexiang* and *H. xiangzhi*, respectively. The molecular phylogenetic results supported *H. shexiang* and *H. xiangzhi* to be two distinct species.

Discussion

Body squamation is of taxonomic importance in species recognition of *Homatula*. All currently-recognised species of this genus can be divided into three groups: the scaled, the partially scaled and the scaleless (Li et al. 2019). *Homatula shexiang* and *H. xiangzhi* are respectively assigned

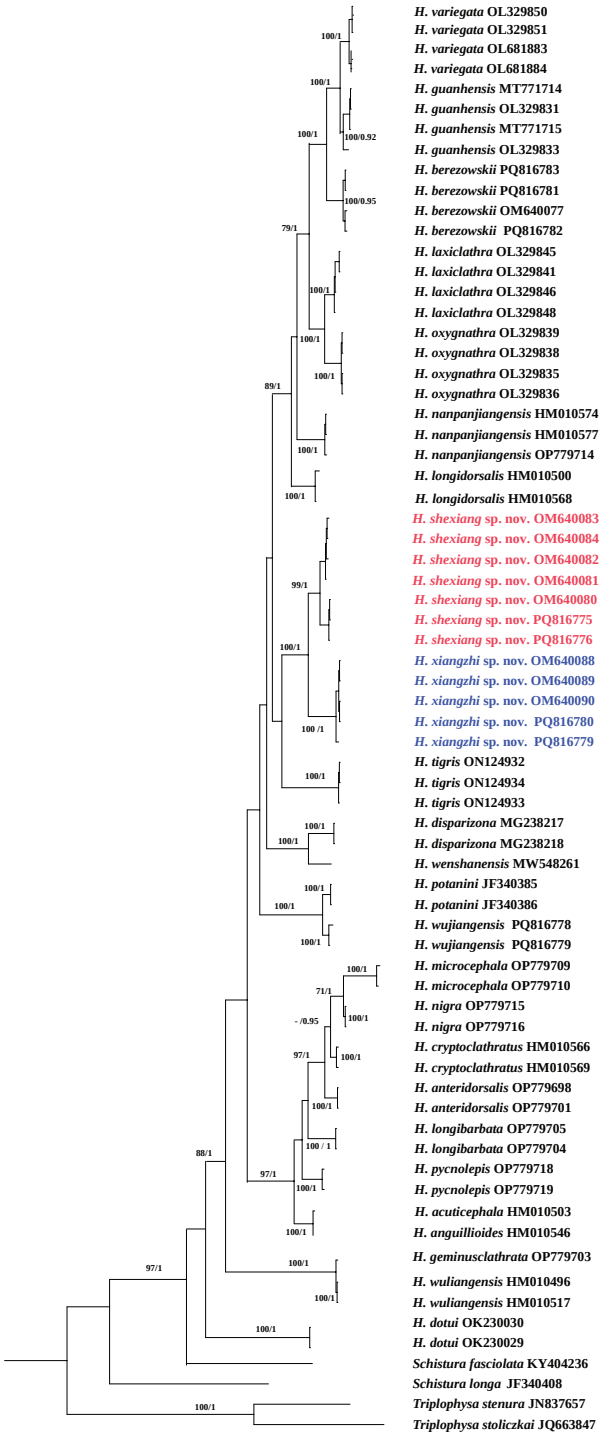

Figure 6. Bayesian Inference tree generated from the Cytb gene from species of *Homatula*. Nodal numbers indicate Bayesian posterior probabilities (> 0.9) and Maximum Likelihood bootstrap values (> 70%), respectively.

to the partially scaled group and the scaleless group. Each of both has remarkable morphological differences with all other members of the species group to which it is designated (Table 4). See the diagnosis and Table 4 for morphological variations between *H. xiangzhi* and other six species of the scaleless group, including *H. disparizona*, *H. nanpanjiangensis*, *H. oligolepis*, *H. robusta*, *H. wenshanensis* and *H. wujiangensis*. In the original description by Nguyen et al. (2021), *H. dotui* was referred to the scaleless group of this genus. Molecular analysis showed that *H. dotui* was distantly related to sampled Chinese congeneric species, indicating that it is not a member of this genus (Li et al. 2022). For this reason, this species is removed from *Homatula* in this study and its generic classification needs in-depth research. Likely, it belongs to its own genus.

Homatula shexiang has a sparsely scaled predorsal body, with its postdorsal portion fully covered with scales. It is thus assigned to the partially-scaled group of *Homatula*. Other eight congeneric species currently referred to this group are *H. berezowskii*, *H. guanheensis*, *H. laxiclathra*, *H. longidorsalis*, *H. oxygnathra*, *H. potanini*, *H. tigris* and *H. variegata*. Major diagnostic characters amongst these partially-scaled species are summarised in Table 4. *Homatula shexiang* has marked morphological variations with *H. longidorsalis* (see the diagnosis of this new species). Nine branched dorsal-fin rays can distinguish both from all other members of the partially-scaled group, with seven or eight rays. *Homatula shexiang* is further separated from these species by possessing a complete lateral line (vs. incomplete in *H. potanini*), an elongate (vs. robust) body with a uniform (vs. non-uniform, slightly declining towards the caudal-fin base in *H. potanini*) depth, no median notch on the lower jaw (vs. present in *H. variegata*, *H. berezowskii*, *H. guanheensis*, *H. laxiclathra* and *H. potanini*), a longer (vs. shorter) snout (length 41.8–50.2%, mean 45.7% of HL vs. 37.0–41.7% in *H. potanini* and 22.7–30.7%, mean 27.6% in *H. tigris*), a gill opening with the upper extremity aligning with the centre of orbit (vs. the lower edge of orbit in *H. berezowskii*, *H. guanheensis* and *H. oxygnathra*), pelvic-fin origin inserted vertically behind (vs. opposite in *H. variegata* and *H. laxiclathra*) dorsal fin origin, an adipose crest along the dorsal mid-line of the caudal peduncle anteriorly terminating beyond the posterior end of the anal-fin base, but beyond anal-fin origin (vs. above or beyond the anal-fin origin in *H. oxygnathra*, *H. potanini* and *H. tigris* or above the posterior end of the anal-fin base in *H. variegata*, *H. berezowskii*, *H. guanheensis* and *H. laxiclathra*) (see Table 4).

The validity of the two new species is each corroborated by its monophyletic nature recovered in the Cytb gene-based phylogenetic analysis (Fig. 6) and its distinct genetic divergence with all other sampled congeneric species (Table 3). Both were previously misidentified as *H. variegata* from the Wu-Jiang of the upper Chang-Jiang Basin (Wu 1989; Ding and Deng 1990). In the BI and ML trees, based on the Cytb gene (Fig. 6), both were sister to each other, but distantly allied to *H. variegata* s. str. from the Wei-He of the Huang-He Basin. Each of the two new species had an interspecific genetic distance of 6.7% to 12.5% and 7.1% to 11.5% with all other sampled congeneric species, respectively (Table 3). Their interspecific sequences divergence was 3.6%, greater than the threshold value 2%

Table 4. Major diagnostic characters for the partially scaled group and the scaleless group of *Homatula* in China.

Species	Characters								
	Body squamation	Caudal-peduncle depth (% of its length)	Median notch on lower jaw	Pelvic-fin origin	Dorsal fin branched rays	Anterior end of dorsal adipose crest of caudal peduncle	Caudal-fin shape	Lateral line	Vertebrae
H. variegata	Postdorsal body scaled, predorsal body scales sparse	36.4–46.6	Present	Opposite to dorsal fin insertion	8	Above the posterior end of the anal-fin base	Broadly rounded	Complete	4+42–44
H. laxiclathra		38.9–57.1	Present	Opposite to dorsal fin insertion	8	Above the posterior end of the anal-fin base	Obliquely truncate	Complete	4+43–44
H. berezowskii		33.9–63.4	Present	At vertical of 1st or 2nd branched dorsal fin ray	8	Above the posterior end of the anal-fin base	Truncate	Complete	4+42–44
H. guanheensis		46.1–65.0	Present	Opposite to dorsal fin insertion	7–8	Above the posterior end of the anal-fin base	Truncate	Complete	4+41–43
H. oxygnathra		45.1–56.0	Absent	At vertical of 1st or 2nd branched dorsal fin ray	8	Above the anal fin origin	Obliquely truncate	Complete	4+42–44
H. longidorsalis[a]		57.2–61.5	Absent	At vertical of 1st or 2nd branched dorsal fin ray	9	Above the anal fin origin	Obliquely truncate	Complete	4+42–44
H. potanini[b]		95.0–136.4	Present	At vertical of 1st or 2nd branched dorsal fin ray	8	Above the anal fin origin	Rounded or truncate	Incomplete	4+35–36
H. tigris[c]		43.1–55.3	Absent	At vertical of 1st or 2nd branched dorsal fin ray	8	Beyond anal-fin origin	slightly emarginate	Complete	4+40–41
***H. shexiang* sp.nov.**		42.0–53.8	Absent	At vertical of 1st or 2nd branched dorsal fin ray	9	Vertically away from the anal-fin origin but beyond the posterior end of the anal-fin base	Obliquely truncate	Complete	4+42–43
***H. xiangzhi* sp.nov.**	Body scaleless or only a few scales covering the caudal peduncle	42.0–57.8	Absent	At vertical of 1st or 2nd branched dorsal fin ray	9	Vertically away from the anal-fin origin, but beyond the posterior end of the anal-fin base	Obliquely truncate	Complete	4+42–43
H. oligolepis[d]		51.0–57.0	Present	At vertical of 1st or 2nd branched dorsal fin ray	9	Above the anal fin origin	Broadly rounded	Complete	4+39–41
H. nanpanjiangensis[d]		50.0–70.0	Present	At vertical of 1st or 2nd branched dorsal fin ray	8–9	Above the anal fin origin	Emarginated	Complete	4+36–38
H. disparizona[e]		47–62	Absent	Opposite to dorsal fin insertion	7–8	Beyond anal-fin origin	Emarginate	Complete	4+39–40
H. robusta[f]		70.5–78.5	Present	At vertical of 1st or 2nd branched dorsal fin ray	8	Beyond anal-fin origin	Emarginated	Complete	4+37–39
H. wujiangensis[b]		100–120	Present	At vertical of 1st or 2nd branched dorsal fin ray	8	Vertically away from the anal-fin origin but beyond the posterior end of the anal-fin base	Truncate	Incomplete	4+35–36
H. wenshanensis[g]		27.3–35. 0	Present	At vertical of 1st or 2nd branched dorsal fin ray	7	Above the posterior end of the anal-fin base	Furcate	Complete	4+47–48

a: morphometric measurements data used here is from Min and Yang (2021); b: morphometric measurements data used here is from Guo et al. (2021); c: the data used here is from Che et al. (2023); d: the data used here is from Min et al. (2010); e: the data used here is from Min et al. (2013); f: the data used here is from Min et al. (2022); g: the data used here is from Yang et al. (2017).

(Avise and Walker 1999) and the minimum value here detected between *H. variegata* and *H. guanheensis* (1.4%).

There are distinctive morphological differences between the two new species. Both differ from each other in head depth (47.1–53.3%, mean 49.8% of HL, vs. 54.0–60.8%, mean 57.5; see Fig. 7A); and eye size (diameter 58.2–78.0%, mean 68.4% of the interorbital width vs. 41.5–56.7%, mean 49.8%, see Fig. 7B) (Table 2). They also differ in body squamation; *H. shexiang* possesses a scaled post-dorsal body, but a scaleless body is found in *H. xiangzhi*. In addition, *H. xiangzhi*, based on Micro-CT scanned imagines, develops an inverted T-shaped supra-ethmoid-ethmoid complex with a vertical plate anteriorly bearing a more pronounced concavity when viewed laterally (Fig. 8). This contrasts with *H. shexiang* (5 specimens) that has a weakly-developed concavity

Comparative material examined

***H. berezowskii*.** China: Gansu Province: Jialing-Jiang of upper Chang-Jiang Basin in Hui County, IHB 82V2385–2386, two topotypes, 116.5–86.9 mm SL; in Feng County, IHB 82VI2418, 82V2290–2293, 73VI1044–1045, seven specimens, 58.2–122.5 mm SL; in Wen County, IHB 64VI0135–0139, 64VI0601–0603, 78V0484–0485, ten specimens, 74.6–128.0 mm SL; in Wudu County, IHB 92VI2749–2757, nine specimens, 97.9–129.7 mm SL; in Kang County, IHB 82VI2489, one specimen, 126.1 mm SL; and in Cheng County, IHB 82VI2547–2550, four specimens, 72.4–88.4 mm SL. China: Shaanxi Province, Jialing-Jiang of upper Chang-Jiang Basin in

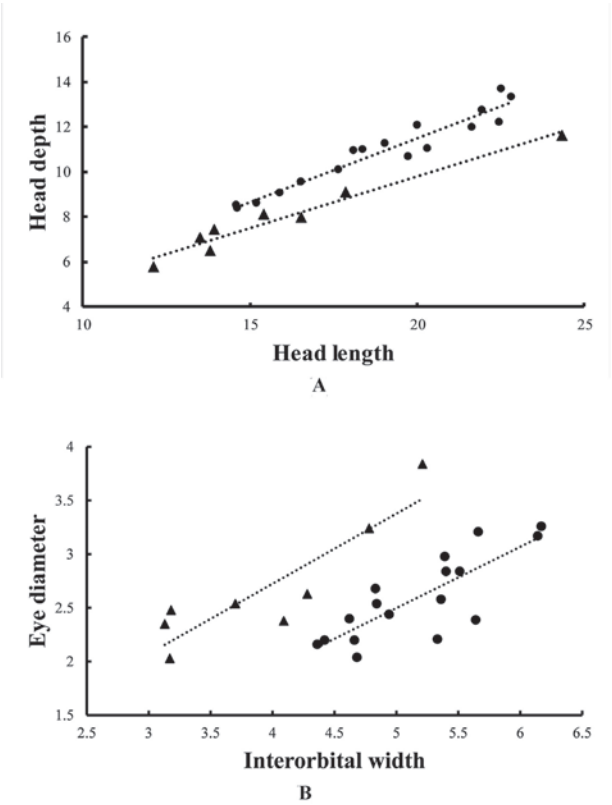

Figure 7. Comparisons of morphometric characters for two new species described in this study: *H. xiangzhi* sp.nov. (black triangle) and *H. shexiang* sp. nov. (black dot). **A.** Between head depth and its length (HL); **B.** Between eye diameter and interorbital width.

Fuoping County, IHB 80VI0869–0870, 80VI0874, 80VI0876–0881, nine specimens, 96.9–155.9 mm SL; in Ningshan County, IHB 80VI1032, one specimen, 89.7 mm SL; in Shanyang County, IHB 80VII1403, one specimen, 100.5 mm SL; in Jieyang County, IHB 73VI1191, 73VI1194, two specimens, 90.9–125.7 mm SL; in Baishu-Jiang, IHB 73VI1075, one specimen, 67.3 mm SL; and in Zhenba County, IHB 80VI1237–1241, 80VI1173–1174, 80VI1185, 80VI1176–1177, 80VI1181–1182, twelve specimens, 50.9–120.6 mm SL.

***H. disparizona*.** China: Yunnan Province: Red-He Basin, in Wenshan County, KIZ 2012000623, holotype, 76.0 mm SL (photograph examination). Data used in this study are from Min et al. (2013).

***H. guanheensis*.** China: Shaanxi Province: Han-Jiang of middle Chang-Jiang Basin, in Fuoping County: IHB 202106049918–9921, 202106055625–5627, seven specimens, 65.7–95.0 mm SL; in Langao County: IHB 202106049922–9923, 202106055640–5642, five specimens, 72.4 –135.9 mm SL.

***H. laxiclathra*.** China: Shaanxi Province: Wei-He of middle Huang-He Basin in Zhouzhi County, IHB 73V10738, 80VI0957, 82VI0103, 82VI0106–0108, 80VI0965–0968, 80VI0972, 11 type specimen, and IHB 202106049909–9912, 202106055611–5619, eight topotypes, 74.7–136.6 mm SL; in Taibai County, IHB 202106049899–9908, 10 specimens, 75.5–136.6 mm SL; and in Mei County, IHB 202106049888–9893, 202106049898, seven specimens, 65.6–131.3 mm SL.

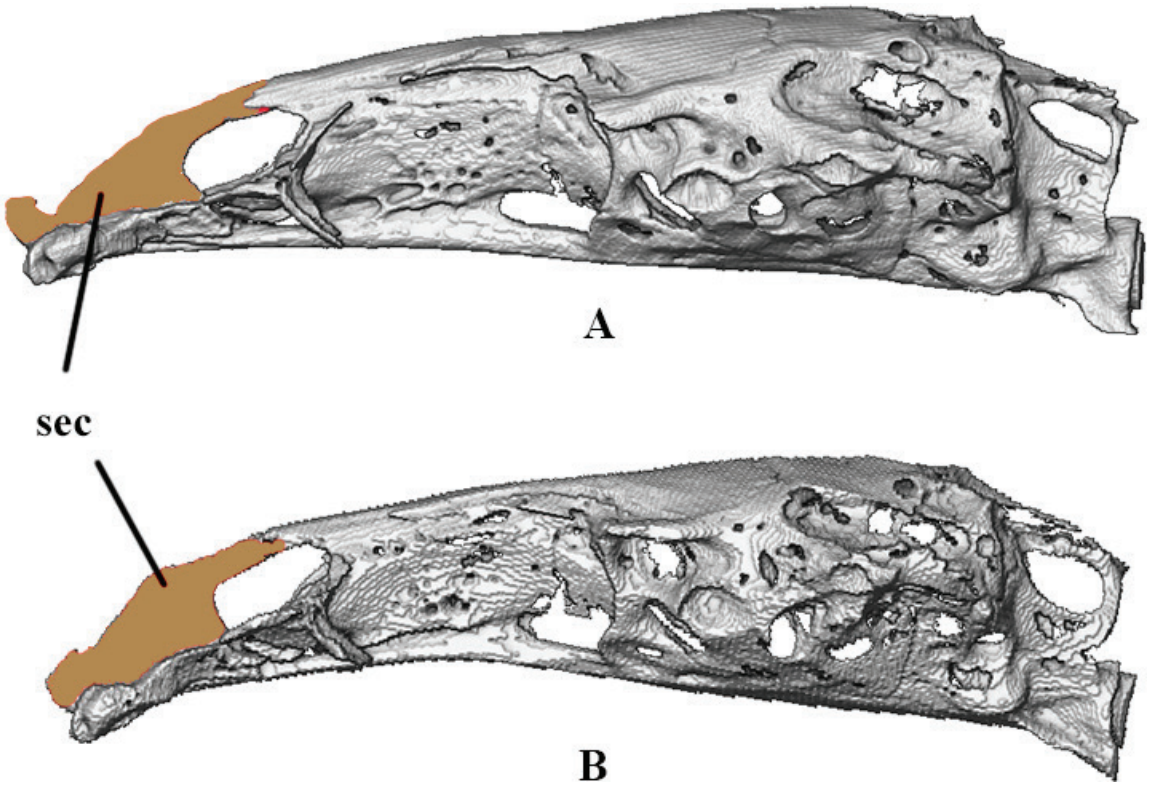

Figure 8. Lateral view of cranium of two new species described in this study. **A.** *H. xiangzhi* sp.nov. and **B.** *H. shexiang* sp.nov. sec: supraethmoid-ethmoid complex.

***H. longidorsalis*.** China: Yunnan Province: Nanpan-Jiang of Zhu-Jiang Basin in Yiliang County, KIZ 1987003989, holotype, 82.0 mm SL (photograph examination). China: Yunnan Province: Nanpan-Jiang of Zhu-Jiang Basin in Yiliang County, IHB 820093, one specimen, 155.9 mm SL. Morphometric measurements data used in this study are from Min and Yang (2021)

***H. nanpanjiangensis*.** China: Yunnan Province: Nanpan-Jiang of Zhu-Jiang Basin in Luoping County, KIZ 1994000023, holotype, 86.4 mm SL (photograph examination). Data from Min et al. (2010).

***H. oligolepis*.** China: Yunnan Province: Yangzong-Hai (= Lake) of Lancang-Jiang: IHB uncat, two type specimens, not in good condition. Morphometric measurements data from Zhu (1989) and Min et al. (2010).

***H. oxygnathra*.** China: Yunnan Province: upper Chang-Jiang Basin in Yuanmou County, BMNH-1908.2.27.23–24, lectotype and paralectotype, 86.7–113.3 mm SL, in Yunnan Fu (= Kunming City) (photograph examination); IHB 201909035461–5470, 10 specimens, 86.7–122.4 mm SL. China: Sichuan Province: upper Chang-Jiang Basin in Yanbian County, IHB 201909035805–5819, 15 specimens, 72.0–129.6 mm SL.

***H. potanini*.** China: Sichuan Province: Qingyi-Jiang of Chang-Jiang Basin in Emei City, IHB 42IX0661–2, 42IX0664, 42IX0666–7, 79IV0597–8, 79IV0600, 79IV0605, 79IV0609–10, 82V0301–4, 15 specimens, 68.6–83.3 mm SL. Morphometric measurements data used in this study are from Guo et al. (2021).

***H. variegata*.** China: Shaanxi Province: Wei-He of Huang-He Basin in Yenkiatsoun (= Baoji City), MNHN-IC-0000-7854, lectotype, and MNHN-B-2641, paralectotype, 96.8–103.5 mm SL; in Xi'an City, IHB 202106049914–9917, 202106055611–5614, topotypes, eight specimens, 65.9–122.4 mm SL.

***H. wujiangensis*.** China: Chongqing Province: Wu-Jinag of Chang-Jiang Basin in Jinfo Mountain, IHB 2017053707–3710, topotypes, four specimens, 40.5–76.3 mm SL.

Acknowledgements

Our sincere thanks go to D. M. Guo, X. Chen, W. H. Shao, Z. T. Wang and C.H. An (IHB) for their help with sampling in the field. We are also indebted to X. L. Lu and J. Y. Wang (Guiyang Qianren Ecological Conservation Center) for providing assistance in field survey. We would express our heartfelt gratitude to M. L. Wang (IHB) for assistance with taking Micro-CT imagines. This research work was funded by the National Sciences Foundation of China (NSFC No. 31801959).

References

Akaike HT (1974) A new look at the statistical model identification. Automatic Control IEEE Transactions on Automatic Control 19: 716–723. https://doi.org/10.1109/TAC.1974.1100705

Avise JC, Walker D (1999) Species realities and numbers in sexual vertebrates: perspectives from an asexually transmitted genome. Proceedings of the National Academy of Sciences 96: 992–995. https://doi.org/10.1073/pnas.96.3.992

Che XJ, Dao WD, Chen YC, Pan XF, Hua ZX, Liang X, Wang XA (2023) *Homatula tigris*, a new species of nemacheiline loach from the upper Yangtze River in Yunnan, China (Cypriniformes: Nemacheilidae). Ichthyological Exploration of Freshwaters 1187: 1–10. https://doi.org/10.23788/IEF-1187

Ding RH (1994) Fishes of Sichuan. Sichuan Science and Technology Press, Chengdu, China.

Ding RH, Deng QX (1990) The Noemacheilinae fishes from Sichuan, with description of a new species I. *Paracobitis, Nemacheilus* and *Oreias* (Cypriniformes: Cobitidae). Zoological Research 11: 285–290.

Gu JH, Zhang E (2012) *Homatula laxiclathra* (Teleostei: Balitoridae), a new species of nemacheiline loach from the Yellow River drainage in Shaanxi Province, northern china. Environmental Biology of Fishes 94: 591–599. https://doi.org/10.1007/s10641-011-9965-1

Guo YS, Sun ZY, He XH, Jin W, Chen YL (2021) Colored Atlas of Fishes in Sichuan. Science Press, Beijing, China.

Hu YT, Zhang E (2010) *Homatula pycnolepis*, a new species of nemacheiline loach from the upper Mekong drainage, South China (Teleostei: Balitoridae). Ichthyological Exploration of Freshwaters 21: 51–62. https://doi.org/10.2478/s11687-010-0010-2

Kalyaanamoorthy S, Minh BQ, Wong TK, Von Haeseler A, Jermiin LS (2017) ModelFinder: fast model selection for accurate phylogenetic estimates. Nature methods 14: 587–589. https://doi.org/10.1038/nmeth.4285

Kottelat M (1990) Indochinese namacheilines: A revieiion of nemacheiline loaches (Pisces: Cypriniformes) of Thailand, Burma, Laos, Cambodia and southern Viet Nam Pfeil, Mhnchen.

Kottelat M (2012) Conspectus cobitidum: an inventory of the loaches of the world (Teleostei: Cypriniformes: Cobitoidei). Raffles Bulletin of Zoology 16: 1–199.

Kumar S, Stecher G, Tamura K (2016) MEGA7: molecular evolutionary genetics analysis version 7.0 for bigger datasets. Molecular biology and evolution 33: 1870–1874. https://doi.org/10.1093/molbev/msw054

Li J, Si S, Guo R, Wang Y, Song Z (2013) Complete mitochondrial genome of the stone loach, *Triplophysa stoliczkai* (Teleostei: Cypriniformes: Balitoridae). Mitochondrial DNA 24: 8–10. https://doi.org/10.3109/19401736.2012.710225

Li X, Che X-J, Zhou W (2019) Loaches of *Homatula* (Teleostei: Nemacheilidae) from the upper Salween River in Yunnan, China with description of three new species. Zootaxa 4711: 330–348. https://doi.org/10.11646/zootaxa.4711.2.6

Li X, Yang B, Guo Y, Zhou W (2022) Three new species of *Homatula* (Teleostei: Nemacheilidae) from Yunnan, China, with comments on habitat conservation. PloS ONE 17: e0276846. https://doi.org/10.1371/journal.pone.0276846

Liu Y, Cao L, Zhang E (2022) Re-description of the loach species *Homatula variegata* (Dabry de Thiersant, 1874)(Pisces: Nemacheilidae) from the middle Huang-He basin in Shaanxi Province of Central China. Journal of Fish Biology 101: 154–167. https://doi.org/10.1111/jfb.15080

Min R, Yang JX (2021) A new species of *Homatula* (Teleostei: Cobitoidea: Nemacheilidae) from the Pearl River, China. ARPHA Preprints 2: e74357. https://doi.org/10.3897/arphapreprints.e74357

Min R, Chen X, Yang J (2010) *Paracobitis nanpanjiangensis*, a new loach (Balitoridae: Nemacheilinae) from Yunnan, China. Environmental Biology of Fishes 87: 199–204. https://doi.org/10.1007/s10641-010-9587-z

Min R, Chen XY, Yang JX, Winterbottom R, Mayden RL (2012) Phylogenetic Relationships of the Genus *Homatula* (Cypriniformes: Nemacheilidae), with Special Reference to the Biogeographic History around the Yunnan-Guizhou Plateau. Zootaxa 3586: 78–94. https://doi.org/10.11646/zootaxa.3586.1.9

Min R, Yang JX, Chen XY (2013) *Homatula disparizona*, a new species of loach from the Red River drainage in China (Teleostei: Nemacheilidae) from China. Ichthyological Exploration of Freshwaters 23: 351–355.

Min R, Zhao Y, Shi J, Yang J (2022) A new species of *Homatula* (Teleostei, Cobitoidea, Nemacheilidae) from the Pearl River drainage, Yunnan, China. ZooKeys 1089: 109–124. https://doi.org/10.3897/zookeys.1089.77203

Min R, Zhao Y-H, Kang B, Chen X-Y, Yang J-X (2023) Vicariance and monsoon as drivers of diversification of nemacheilid loaches (Teleostei: Cypriniformes) around the Hengduan Mountains of China. Zoological Research 44: 936–938. https://doi.org/10.24272/j.issn.2095-8137.2023.020

Nguyen LT, Schmidt HA, Von Haeseler A, Minh BQ (2015) IQ-TREE: a fast and effective stochastic algorithm for estimating maximum-likelihood phylogenies. Molecular Biology and Evolution 32: 268–274. https://doi.org/10.1093/molbev/msu300

Nguyen DT, Wu H, Cao L, Zhang E (2021) *Homatula dotui*, a new cave loach from Central Vietnam (Teleostei: Nemacheilidae). Ichthyological Exploration of Freshwaters 1142: 1–11. https://doi.org/10.23788/IEF-1142

Nichols JT, Pope CH (1925) Nemacheilus and related loaches in China. American Museum Novitates 171: 1–7.

Rambaut A, Drummond AJ, Xie D, Baele G, Suchard MA (2018) Posterior summarization in Bayesian phylogenetics using Tracer 1.7. Systematic biology 67: 901–904. https://doi.org/10.1093/sysbio/syy032

Ronquist F, Teslenko M, Van Der Mark P, Ayres DL, Darling A, Höhna S, Larget B, Liu L, Suchard MA, Huelsenbeck JP (2012) MrBayes 3.2: efficient Bayesian phylogenetic inference and model choice across a large model space. Systematic biology 61: 539–542. https://doi.org/10.1093/sysbio/sys029

Wu L (1989) The Fishes of Guizhou. Guizhou People's Publishing House, Guiyang, China.

Xiao WH, Zhang Y, Liu H (2001) Molecular systematics of Xenocyprinae (Teleostei: Cyprinidae): taxonomy, biogeography, and coevolution of a special group restricted in East Asia. Molecular phylogenetics and evolution 18: 163–173. https://doi.org/10.1006/mpev.2000.0879

Yang JX, Chen YR, Kottelat M (1994) Subspecific differentiation of Paracobit variegatus with comments on its zoogeography. Zoological Research 15: 58–67.

Yang HF, Li C, Liu T, Li W (2017) A report on a new species of *Homatula* from Yunnan (Cyprinifromes: Noemacheilidae). Journal of Yunnan Agricultural University 32: 1140–1144.

Yang X, Li JG, Wang YY (2022) The Fishes of Guizhou. Science Press, Beijing, China.

Zheng CY (1989) Fishes of the Pearl River. Science Press, Beijing, China.

Zhou CJ, Ma W, Wang X, Tang Y, Meng X, Nie G (2021) *Homatula guanheensis* sp. nov.(Teleostei: Nemacheilidae), a new species of loach from Henan Province, China. Biodiversity Data Journal 9: e65130. https://doi.org/10.3897/BDJ.9.e65130

Zhu SQ (1989) The loaches of the subfamily Nemacheilinae in China (Cypriniformes: Cobitidae). Jiangsu Science and Technology Publishing House, Nanjing, China.

Zoosyst. Evol. 101 (2) 2025, 711–734 | DOI 10.3897/zse.101.146895

PENSOFT

MUSEUM FÜR NATURKUNDE BERLIN

A survey of mimetid spiders (Araneae, Mimetidae) from Central Guizhou Province, China

Jianshuang Zhang[1], Haoshen Zhang[1], Jinxin Liu[2], Hao Yu[1], Xiang Xu[2]

1 *The State Key Laboratory of Southwest Karst Mountain Biodiversity Conservation of Forestry Administration, School of Life Sciences, Guizhou Normal University, Guiyang, Guizhou, China*

2 *College of Life Science, Hunan Normal University, Changsha Hunan, China*

https://zoobank.org/5077B2F5-571B-4836-8B15-D48CAC2D580A

Corresponding author: Xiang Xu (xux@hunnu.edu.cn)

Academic editor: Danilo Harms ♦ **Received** 16 January 2025 ♦ **Accepted** 28 February 2025 ♦ **Published** 28 March 2025

Abstract

A survey of the mimetids of Central Guizhou Province, China, is presented. A total of five species are addressed, raising the number of species of the genus *Mimetus* Hentz, 1832, known from this province from four to eight, making Guizhou the province with the most *Mimetus* species in China. Two of the taxa are new species: *M. guiyang* J. S. Zhang, Yu & Xu, **sp. nov.** and *M. lanmeiae* Liu, Yu & Xu, **sp. nov.**, both from Guiyang City, provincial capital of Guizhou. The other three known species include two new records from Guizhou, *M. caudatus* Wang, 1990, and *M. sinicus* Song & Zhu, 1993, as well as a species, *M. testaceus* Yaginuma, 1960, that was previously recorded from the province. The female of *M. caudatus* is described for the first time, based on the new material from Duyun City. Detailed descriptions, diagnoses, and photographs of the two new species and *M. caudatus*, as well as photographs of *M. sinicus* and *M. testaceus*, are provided. The DNA barcodes of *M. lanmeiae* **sp. nov.**, *M. sinicus*, and *M. testaceus* were obtained for species delimitation, matching of sexes, and future use.

Key Words

DNA barcoding, Guiyang City, morphology, new species, taxonomy

Introduction

Mimetidae is a small-sized spider family, comprising eight genera and 163 valid species distributed worldwide, often referred to as “pirate spiders” or “cannibal spiders”, are named for their araneophagic behaviors and predatory strategies (Harms and Harvey 2009a, b; Benavides et al. 2017; Benavides and Hormiga 2020; WSC 2025; see also Fig. 1A, B). Rather than constructing foraging webs, these spiders invade the webs of other spiders, where they simulate the vibrations of prey caught in the web or mimic the courtship signals of conspecific males. This sophisticated, deceptive, predatory tactic lures the resident spider into proximity, enabling the mimetid to ambush and feed on it, and is a well-documented example of aggressive mimicry (Cutler 1972; Jackson and Whitehouse 1986; Kloock 2001, 2012; see also Fig. 1C, D). Traditionally, mimetids were considered obligate araneophages, preying exclusively on other spiders. However, evidence from previous studies (Cutler 1972; Kloock 2001, 2012) and our own observations (Fig. 1E, F) indicates that these spiders are capable of consuming other arthropods. This may occur through kleptoparasitism, wherein mimetids exploit the webs of other spiders to acquire prey, or through active foraging behavior to locate alternative food sources.

Reflecting their highly specialized ecological niche, members of the family Mimetidae exhibit notable morphological adaptations, including prominent rows of raptorial spines on their anterior legs. These spines are strategically arranged to create a basket-like structure, effectively ensnaring prey during capture (Cutler 1972; Jackson and Whitehouse 1986; Harms and Harvey 2009a, b; Benavides et al. 2017; Benavides and Hormiga 2020; see also Figs 1A, F). Clearly, the biology of mimetid spiders is

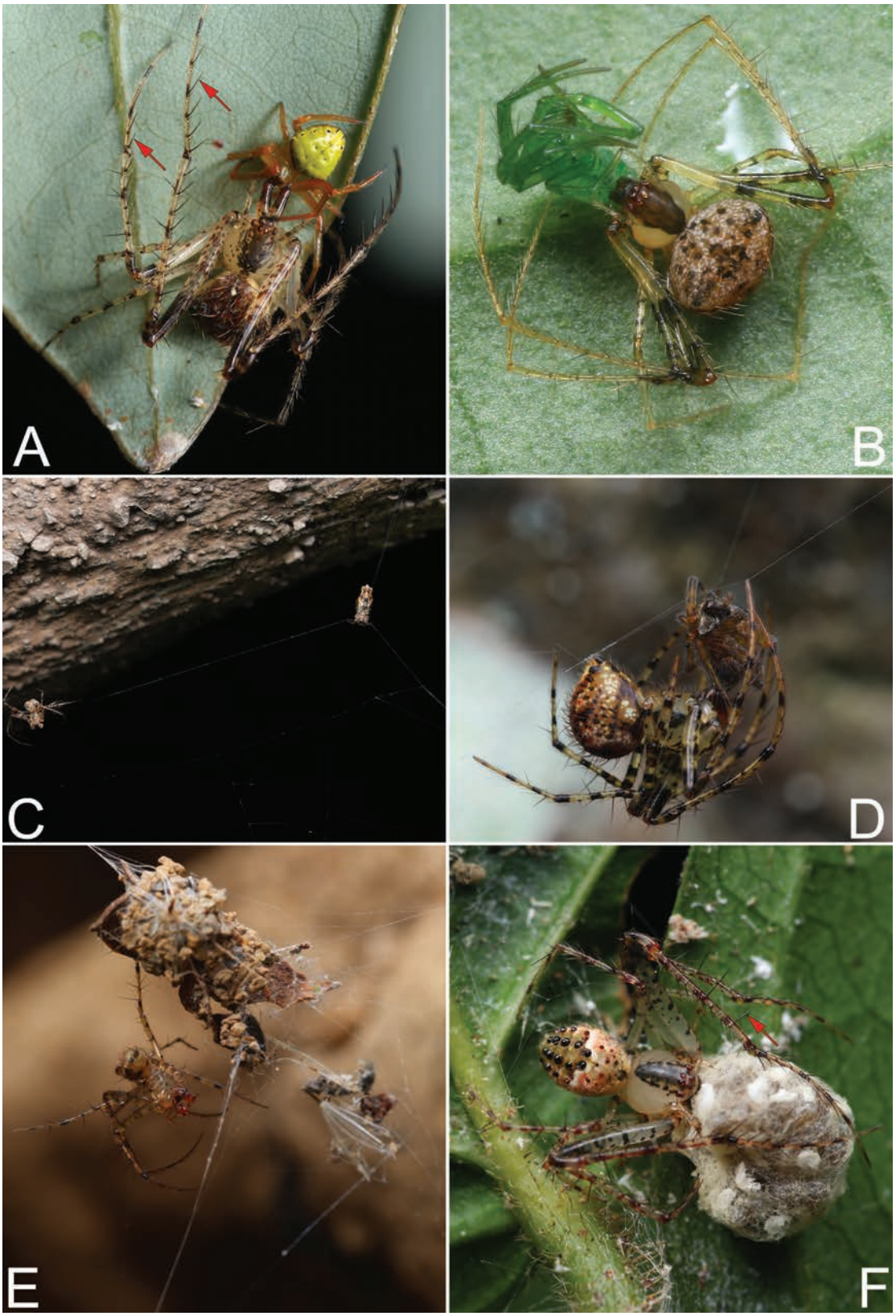

Figure 1. Araneophagic behaviors (**A, B**), predatory strategies (**C–F**), and rows of raptorial spines of mimetid spiders (**A, F**) **A.** *Mimetus* spp. has attacked and killed another spider of the family Araneidae; **B.** Mimetidae spp., feeding on an immature spider of an unknown family; **C.** Mimetidae spp. assaulting the web of a spider of genus *Cyclosa*; **D.** Mimetid at the end of a lunge toward and capture of a spider. Prey is held by a 'basket' formed by legs I–III of the mimetid. **E.** Mimetidae spp. had previously driven the resident from the web, thereby gaining exclusive access to the prey remaining on the web **F.** Mimetidae spp. wrapped up prey and scooped it up in a basket formed by legs I–III. Photographs by Q Lu (Shenzhen). **Note:** Red arrows in panel A and panel F point at raptorial spines on anterior legs.

unique, yet our understanding of them remains limited. Moreover, details of novel predatory strategies continue to emerge, highlighting the need for further investigation (Barrantes et al. 2025). However, the family Mimetidae serves as a typical example of how 'taxonomic ignorance of a group often discourages behavioral studies,' as highlighted by Jackson and Whitehouse (1986). Although the taxonomy of mimetid spiders has seen some groundbreaking advances in the new century, such as those by Harms and Harvey (2009a, b), Benavides and Hormiga (2016, 2020), and Benavides et al. (2017), there remains a substantial amount of work to be done. For alpha taxonomy, the diversity of Mimetidae remains insufficiently known, as a new genus and several new species have been described in recent years, and further new genera and species are expected to be established or discovered in the future (WSC 2025). For beta taxonomy, there is much dispute historically about the group's limits and its placement in the spider tree of life (Hormiga and Griswold 2014). Although the family has been revised regionally (Heimer 1986; Harms and Harvey 2009a, b; Benavides et al. 2017; Benavides and Hormiga 2016, 2020), the debate on the internal structure of this family remains open. Meanwhile, due to the lack of foundational data, particularly alpha-taxonomic information such as available specimens, molecular data, detailed descriptions, and high-quality diagnostic illustrations, phylogenetic studies on Mimetidae are somewhat biased both geopolitically and at the genus and species level, as the majority of studies have been carried out using Australian and Neotropical taxa (e.g., Heimer 1986; Harms and Harvey 2009a, b; Benavides et al. 2017; Benavides and Hormiga 2016, 2020), with only very few studies performed in Asia (Liu et al. 2021a, b), and some genera and most species from China were not included in the aforementioned phylogenetic revisions (Benavides and Hormiga 2020; Liu et al. 2021a, b).

Mimetus Hentz, 1832, is the type genus of the family and currently includes 70 extant species that are found worldwide except for the Polar Regions and Oceania, 20 of which are known to occur in China (WSC 2025; Table 1). As the most common genus of mimetids, *Mimetus* remains inadequately studied, and the species diversity is still insufficiently known. The possible reasons include, but are not limited to, the following: More than half of the species were only described based on a single sex (12 from males, 26 from females) (WSC 2025); most species documented in the 19th and 20th centuries were described based solely on somatic characters, with original descriptions being rather brief, illustrations either absent or inadequate, and lacking subsequent updates (Gan et al. 2019; Liu et al. 2021a, b; WSC 2025); types of some species do not exist (were not designated in original descriptions or are lost) or are difficult to locate or access (WSC 2025); *Mimetus* has been widely regarded as polyphyletic and will likely be split in the future (Benavides and Hormiga 2020; Liu et al. 2021a, b). In spite of these deficiencies, the majority of Chinese species have been described or redescribed in detail, alongside high-quality illustrations, to allow for easy recognition within this country (Zeng et al. 2016, 2019; Gan et al. 2019; Liu et al. 2021a, b; Wang et al. 2024).

Guizhou Province is recognized for its remarkable biodiversity, ranking among the top provinces in China and boasting the third-largest number of wildlife species nationally (Wang 2021; The People's Government of Guizhou Province 2022). The province is renowned for its diverse environments and complex topography, encompassing various habitats favored by mimetid spiders, such as subtropical evergreen broadleaf forests and karst landforms (Liu et al. 2021b; Zhao et al. 2021; Zhou et al. 2023). However, the genus *Mimetus* can be regarded as being poorly represented in Guizhou for a long time, with only two species recorded before 2019: *M. testaceus* Yaginuma, 1960, and *M. lamellaris* Zeng, Wang & Peng, 2016 (Wang 1990; Zeng et al. 2016). Until now, only four species have been recorded from Guizhou, including two new species that were described by Gan et al. (2019): *M. bucerus* Gan, Mi, Irfan, Peng, Ran & Zhan, 2019, and *M. yinae* Gan, Mi, Irfan, Peng, Ran & Zhan, 2019.

While examining spiders collected from Guiyang City (provincial capital of Guizhou) and adjacent areas (Fig. 2A), southwest China, we have found some *Mimetus* specimens that belong to five species: two species are new to science, one identified as *M. caudatus* Wang, 1990 (previously described based on male specimens only, new record for Guizhou) based on comparison with the type specimens, and the remaining two are identified as *M. sinicus* Song & Zhu, 1993 (new record for Guizhou) and *M. testaceus*, respectively. Thus, the total number of *Mimetus* species in Guizhou reaches eight, making Guizhou the province with the most *Mimetus* species in China (Fig. 2A, B; Table 1).

The goal of this paper is to describe the two new species; to redescribe *M. caudatus* and report the female for the first time; to provide color photographs of *M. sinicus* and *M. testaceus*; and to use DNA barcodes of *M. lanmeiae* sp. nov., *M. sinicus*, and *M. testaceus* for species delimitation, gender matching, and future use in molecular studies.

Materials and methods

Specimens in this study were collected by hand, pitfall trap, and beating vegetation. All examined specimens are deposited in the Museum of Guizhou Normal University, Guiyang, China (**MGNU**), except the holotype of *M. caudatus*, which is deposited in the College of Life Science, Hunan Normal University (**HNU**). Specimens were preserved in 75% or 95% alcohol and examined using an Olympus SZX7 stereomicroscope. Left male palps were examined and illustrated after dissection. Epigynes were removed and cleared in a warm 10% potassium hydroxide (KOH) solution. For *M. caudatus* and *M. guiyang* sp. nov., the vulvae were also imaged after being embedded in Arabic gum. Images were captured with a Canon EOS 70D digital camera (20.2 megapixels) mounted on an Olympus CX41 compound microscope and assembled using Helicon Focus 3.10.3 image stacking software (Khmelik et al.

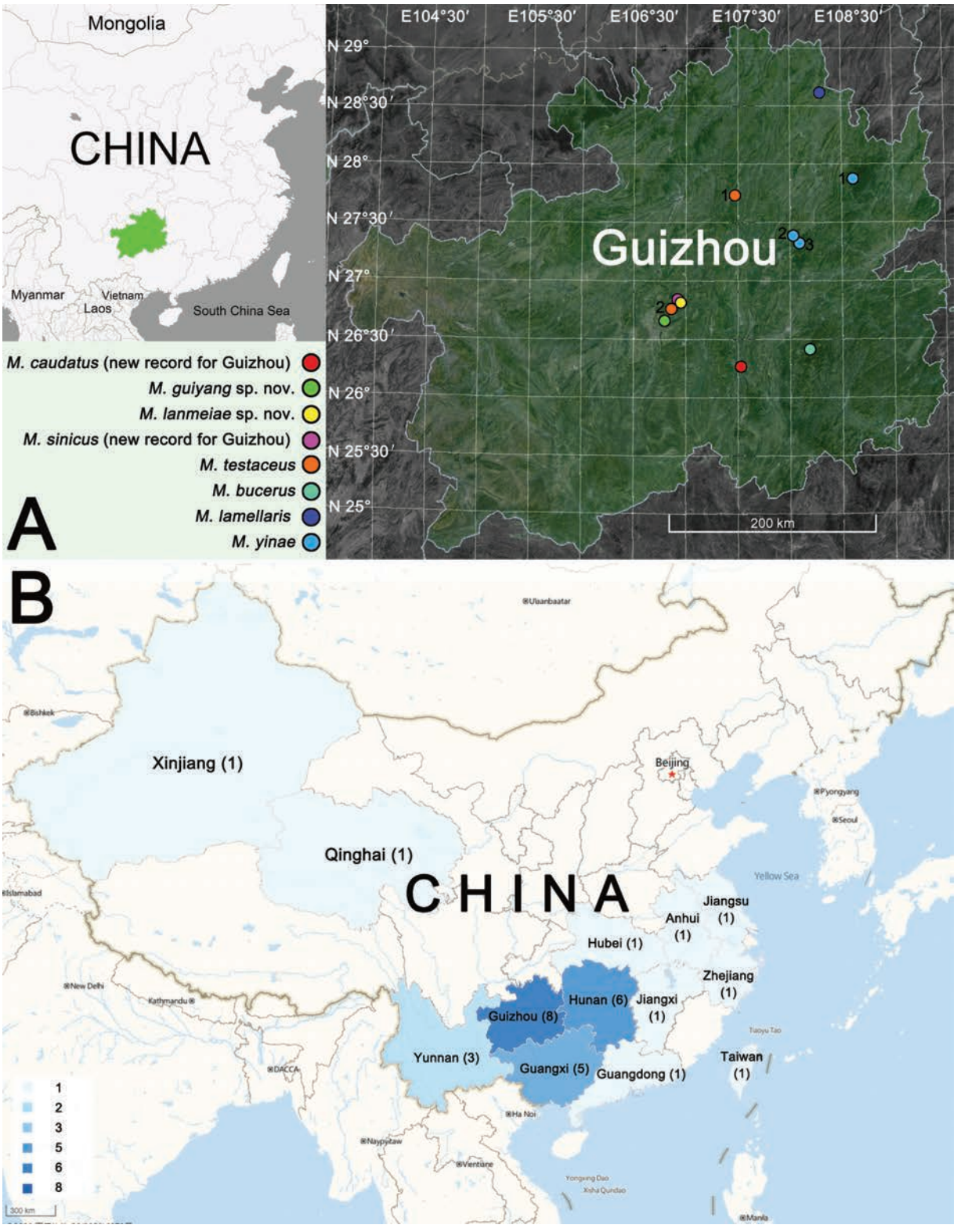

Figure 2. Distribution records of the *Mimetus* species in Guizhou Province (**A**) and species distribution pattern of the genus *Mimetus* in China (**B**). **Note:** In panel **A**, circles of different colors each represent a species. *Mimetus caudatus* Wang, 1990 (scarlet circle: Dunyun City, Xiaoweizhai Town, Yaolin Cave), *M. guiyang* sp. nov. (green circle: Guiyang City, Dongfeng Town), *M. lanmeiae* sp. nov. (yellow circle: Guiyang City, Xinpu Town, Xiangzhigou), *M. sinicus* Song & Zhu, 1993 (purple circle: Guiyang City, Xinpu Town, Xiangzhigou), *M. testaceus* Yaginuma, 1960 (orange circle: 1. Zunyi City; 2. Guiyang City, Shuitian Town, Panlongshan Forest Park), *M. bucerus* Gan, Mi, Irfan, Peng, Ran & Zhan, 2019 (cyan circle: Leishan County, Leigongshan National Nature Reserve), *M. lamellaris* Zeng, Wang & Peng, 2016 (dark blue circle: Yanhe County, Daheba Town, Mayanhe National Nature Reserve), *M. yinae* Gan, Mi, Irfan, Peng, Ran & Zhan, 2019 (light blue circle: 1. Jiangkou County, Dewang Town, Fanjingshan National Nature Reserve; 2. Shiqian County, Ganxi Town, Fuyan Village; 3. Shibing County, Maxi Town, BajiaopingVillage; In panel **B**, the shading of each province on the map and the numbers in parentheses after the province names represent species richness.

2005). All measurements were obtained using an Olympus SZX7 stereomicroscope and are given in millimeters. Eye diameters were measured at the widest part. The total body length does not include the chelicerae and spinnerets. Leg lengths are given as total length (femur, patella + tibia, metatarsus, tarsus). The terminology used in the text and figure legends follows Gan et al. (2019), Benavides and Hormiga (2020), and Liu et al. (2021a, b).

The abbreviations used in the text are: **A** atrium; **AER** anterior eye row; **ALE** anterior lateral eye; **AME** anterior median eye; **BP** basal plate; **C** conductor; **CA** cymbial apex; **CBE** cymbial base extension; **CD** copulatory duct; **CEMP** cymbial ecto-medial process; **CO** copulatory opening; **Cy** cymbium; **E** embolus; **EB** embolar base; **ET** embolar tip; **FD** fertilisation duct; **H** hood; **MOA** median ocular area; **Pc** paracymbium; **PER** posterior eye row; **PLE** posterior lateral eye; **PME** posterior median eye; **Sc** scape; **Sp** spermathecae; **St** subtegulum; **T** tegulum; **TA** tegular apophysis.

The distribution map was generated with ArcGIS 10.5 (ESRI Inc). Locality coordinates for *M. lamellaris*, *M. bucerus*, and *M. yinae* are copied from the original publications (see Zeng et al. 2016 and Gan et al. 2019). Due to a lack of locality coordinates in previous publications, locality coordinates for *M. caudatus*, *M. sinicus*, and *M. testaceus* originated from Google Earth, except for newly examined materials.

In order to obtain the DNA barcodes, a partial fragment of the mitochondrial cytochrome oxidase subunit I (COI) gene was amplified and sequenced using the primers LCOI490 (5'-GGTCAACAAATCATCATAAA-GATATTGG-3') and HCOI2198 (5'-TAAACTTCAGGGTGACCAAAAAAT-3'). However, we were unable to obtain good extractions from *M. guiyang* sp. nov. and *M. caudatus*. For additional information on extraction, amplification, and sequencing procedures, see Benavides et al. (2017). All sequences were analyzed using BLAST and are deposited in GenBank. The accession numbers are provided in Table 2.

Table 1. Checklist of *Mimetus* species from China.

	Species and Known sex	Distribution in China	References
1	*M. bucerus* Gan, Mi, Irfan, Peng, Ran & Zhan, 2019 (♂)	Guizhou	Gan et al. 2019
2	*M. caudatus* Wang, 1990 (♂♀)	Guangxi, Guizhou	Wang 1990; Song et al. 1999; female described in present paper
3	*M. clavatus* Liu, Xu, Hormiga & Yin, 2021 (♂)	Guangxi	Liu et al. 2021a
4	*M. contrarius* (Zeng, Irfan & Peng, 2019) (♂♀)	Yunnan	Zeng et al. 2019
5	*M. dentatus* Liu, Xu, Hormiga & Yin, 2021 (♂♀)	Guangxi	Liu et al. 2021a
6	*M. echinatus* Wang, 1990 (♂♀)	Hunan	Wang 1990; Song et al. 1999; Yin et al. 2012; Zeng et al. 2019
7	*M. juhuaensis* (Xu, Wang & Wang, 1987) (♂♀)	Anhui, Hunan	Xu et al. 1987; Song et al. 1999; Yin et al. 2012; Liu et al. 2021b
8	*M. labiatus* Wang, 1990 (♀)	Hunan	Wang 1990; Song et al. 1999; Yin et al. 2012
9	*M. lamellaris* Zeng, Wang & Peng, 2016 (♂)	Guizhou	Zeng et al. 2016
10	*M. liangkaii* Yao & Liu, 2024 (♂♀)	Jiangxi	Wang et al. 2024
11	*M. lingbaoshanensis* Gan, Mi, Irfan, Peng, Ran & Zhan, 2019 (♂♀)	Yunnan	Gan et al. 2019
12	*M. niveosignatus* Liu, Xu, Hormiga & Yin, 2021 (♂♀)	Guangxi	Liu et al. 2021a
13	*M. ryukyus* Yoshida, 1993 (♂♀)	Taiwan	Yoshida 1993; Song et al. 1999
14	*M. sinicus* Song & Zhu, 1993 (♂♀)	Hubei, Guizhou	Song and Zhu 1993; Song and Li 1997; Song et al. 1999; present paper
15	*M. subulatus* Liu, Xu, Hormiga & Yin, 2021 (♂♀)	Guangdong, Hunan	Liu et al. 2021a
16	*M. testaceus* Yaginuma, 1960 (♂♀)	Zhejiang, Hunan, Hubei, Guizhou, Guangxi	Wang 1990; Chen and Zhang 1991; Song et al. 1999; Yin et al. 2012; present paper
17	*M. tuberculatus* Liang & Wang, 1991 (♀)	Qinghai, Xinjiang	Liang and Wang 1991; Song et al. 1999
18	*M. uncatus* Liu, Xu, Hormiga & Yin, 2021 (♂)	Hunan	Liu et al. 2021a
19	*M. wangi* Zeng, Wang & Peng, 2016 (♂♀)	Yunnan	Zeng et al. 2016
20	*M. yinae* Gan, Mi, Irfan, Peng, Ran & Zhan, 2019 (♂♀)	Guizhou	Gan et al. 2019
21	*M. guiyang* J. S. Zhang, Yu & Xu, sp. nov. (♀)	Guizhou	present paper
22	*M. lanmeiae* Liu, Yu & Xu, sp. nov. (♂)	Guizhou	present paper

Table 2. Voucher specimen information.

Species	Inventory number	Voucher code	Sex	GenBank accession number	Sequence length
M. lanmeiae sp. nov.	MGNU-2022-MIML001	YHGY096	♂	PV213438	558 bp
M. sinicus	MGNU-2022-MIMS003	YHGY079	♂	PV213437	558 bp
	MGNU-2022-MIMS004	YHGY078	♀	PV213436	557 bp
M. testaceus	MGNU-2022-MIMT001	YHGY102	♂	PV213440	558 bp
	MGNU-2022-MIMT002	YHGY080	♀	PV213439	558 bp

Taxonomy

Family Mimetidae Simon, 1881

Genus *Mimetus* Hentz, 1832

Type species. *Mimetus syllepsicus* Hentz, 1832, from the USA and Mexico.

Mimetus caudatus Wang, 1990

Figs 2A, 3–5, 15

Mimetus caudatus Wang 1990: 42, fig. IV.4, 5 (♂, holotype, examined); Song et al. 1999: 73, fig. 30N, O (♂).

Type material. ***Holotype*** • ♂, China: Guangxi Zhuang Autonomous Region: Nanning City, Damingshan Mt., locality coordinates lacking in the original label, 11 VII 1985, J. Wang and Y. Zhang et al. leg. Examined.

Material examined. • 1♂1♀ (MGNU-2014-MIMC001 to 002), China: Guizhou Pro.: Duyun City, Xiaoweizhai Town, Yaolin Village, Yaolin Cave, 26.21°N, 107.53°E, c. 820 m, by hand, 18 VI 2014, P. Long et al. leg.

Diagnosis. Males of *M. caudatus* resemble those of *M. bucerus* and *M. lingbaoshanensis* in having a cylindrical conductor (C) extending outward, and a developed, distinctly prominent cymbial apex (CA) (cymbial apex unobtrusive in all other congeners which with cylindrical conductor distinctly extending, such as *M. echinatus*, *M. juhuaensis*, *M. lamellaris* and *M. yinae*; as in Zeng et al. 2016: figs 1B, C, 2A, B, 5B, C, 6A, B, Liu et al. 2021b: figs 3A–E, 5A–E and Gan et al. 2019: figs 5A, B, 6C, D), but can be easily differentiated from *M. bucerus* and *M. lingbaoshanensis* by: (1) in both pro- and retrolateral views, cymbial apex (CA) triangular (Fig. 3C, D) (*vs.* subuliform in *M. bucerus*, handle-like in *M. lingbaoshanensis*; Gan et al. 2019: figs 1B, C, 2A, B, 3C, D, 4A, B); (2) in retrolateral view, paracymbium (Pc) consisting of a conical basal outgrowth and a blade-shaped distal outgrowth (Fig. 3A, B, D) (*vs.* with a beak-like basal outgrowth and a claviform distal outgrowth in *M. bucerus*, with a claw-shaped basal outgrowth and a subtriangular distal outgrowth in *M. lingbaoshanensis*; Gan et al. 2019: figs 1C, 2B, 3D, 4B); and (3) palpal tibia slightly longer than wide, the ratio of length/width being approximately 1.3 (Fig. 3A–D) (*vs.* distinctly longer than wide, the ratio of length/width is at least 2.8 in *M. bucerus* and 2.0 in *M. lingbaoshanensis*; Gan et al. 2019: figs 1B, C, 2A, B, 3C, D, 4A, B). The female of *M. caudatus* can be distinguished from all other congeners with the exception of *M. lingbaoshanensis* by having a proximally biforked scape (Sc) (scape absent, or present but proximally not forked in other *Mimetus* species, such as *M. yinae* and *M. guiyang* sp. nov.; Gan et al. 2019: figs 5C, D, 6F, G and Fig. 6A, C) and similar vulva, but can be recognised by the Y-shaped scape (Sc) in *M. caudatus* (Fig. 4A, C) (*vs.* V-shaped in *M. lingbaoshanensis*; Gan et al. 2019: figs 3F, 4C) and by the dumbbell-shaped basal plate (Bp) with the posterior margin concave medially in *M. caudatus* (Fig. 4B, D) (*vs.* basal plate labiate, posterior margin slightly prominent medially in *M. lingbaoshanensis*; Gan et al. 2019: figs 3F, G, 4C, D).

Description. Male (MGNU-2014-MIMC001). ***Measurements.*** Total length 5.75. Carapace 2.97 long, 2.21 wide. Abdomen 2.78 long, 2.12 wide. Sternum 1.44 long and 0.95 wide. Labium wider than long. Clypeus height 0.26. Eye sizes and interdistances: AME 0.16, ALE 0.14, PME 0.15, PLE 0.15, AME–AME 0.18, ALE–AME 0.21, PME–PME 0.09, PME–PLE 0.30. MOA 0.50 long, anterior width 0.51, posterior width 0.40. Leg measurements: I 17.23 (4.59, 5.54, 5.06, 2.04), II 13.21 (3.73, 4.38, 3.42, 1.68), III 9.01 (2.78, 2.96, 1.95, 1.32), IV 10.37 (3.32, 3.46, 2.39, 1.20).

Habitus (Figs 4E, 5A–C). Carapace nearly pyriform, light yellowish, with a distinctive anchor-shaped pattern starting from behind PER and almost reaching fovea, a pair of small patches on the lateral margins of the carapace near the coxa II, and a pair of large patches on the lateral margins of the carapace near the coxae III and IV; fovea represented by a small pit; ocular region distinctly narrowed, cervical groove and radial grooves indistinguishable; tegument smooth, clothed with short, sparse setae along radial grooves. Sternum light brown, shaped like a shield. Labium nearly oblong, reddish brown. Endites anteriorly white, posteriorly reddish brown, with dense scopulae on inner margin. Chelicerae dark brown, promargin with 11 peg teeth, retromargin with only one normal tooth. Leg color similar to that of carapace, with irregular brown annuli in the middle parts of femur. Abdomen oval, yellowish white, dorsally covered by many small whitish and large black patches, with many weakly ossified hair bases still remaining, but almost all hairs broken off from body and lost; venter basically light brown, centrally with a V-shaped grayish stripe, posteriorly with two irregular-shaped grayish speckles.

Palp (Fig. 3A–D). Tibia short, < 1/3 of cymbium length, about 1.3 longer than wide. Cymbium (Cy) with basal extension (CBE) and an elongated apex (CA): cymbial base extension (CBE) represented by a semi-circular flange; cymbial apex (CA) shaped like index finger in ventral and dorsal views and triangular in lateral view, ca. 1/3 of cymbium length, pointing dorsal-retrolaterally. Paracymbium (Pc) broad, consisting of a conical basal outgrowth and a blade-shaped distal outgrowth, ca. 1/3 of cymbium length. Tegulum (T) nearly circular, centrally and apically membranous; sperm duct sinuate, forming a loop along tegular margin. Tegular apophysis (TA) sheet-shaped in ventral view and digitiform in prolateral view, located at proximal-prolateral position of tegulum (ca. 8–9 o'clock position of tegulum). Subtegulum (St) located posteriorly to tegulum, without apophysis. Embolus (E) filiform, arising at approximately the 7–8 o'clock position, terminating at ca. 12 o'clock position, with the tip (ET) hidden by conductor. Conductor (C) large, cylindrical, nearly as long as tegulum diameter, proximally partly membranous, apically disc-shaped and strongly sclerotized, dorsally with two hook-shaped apophyses and a sheet-shaped fold.

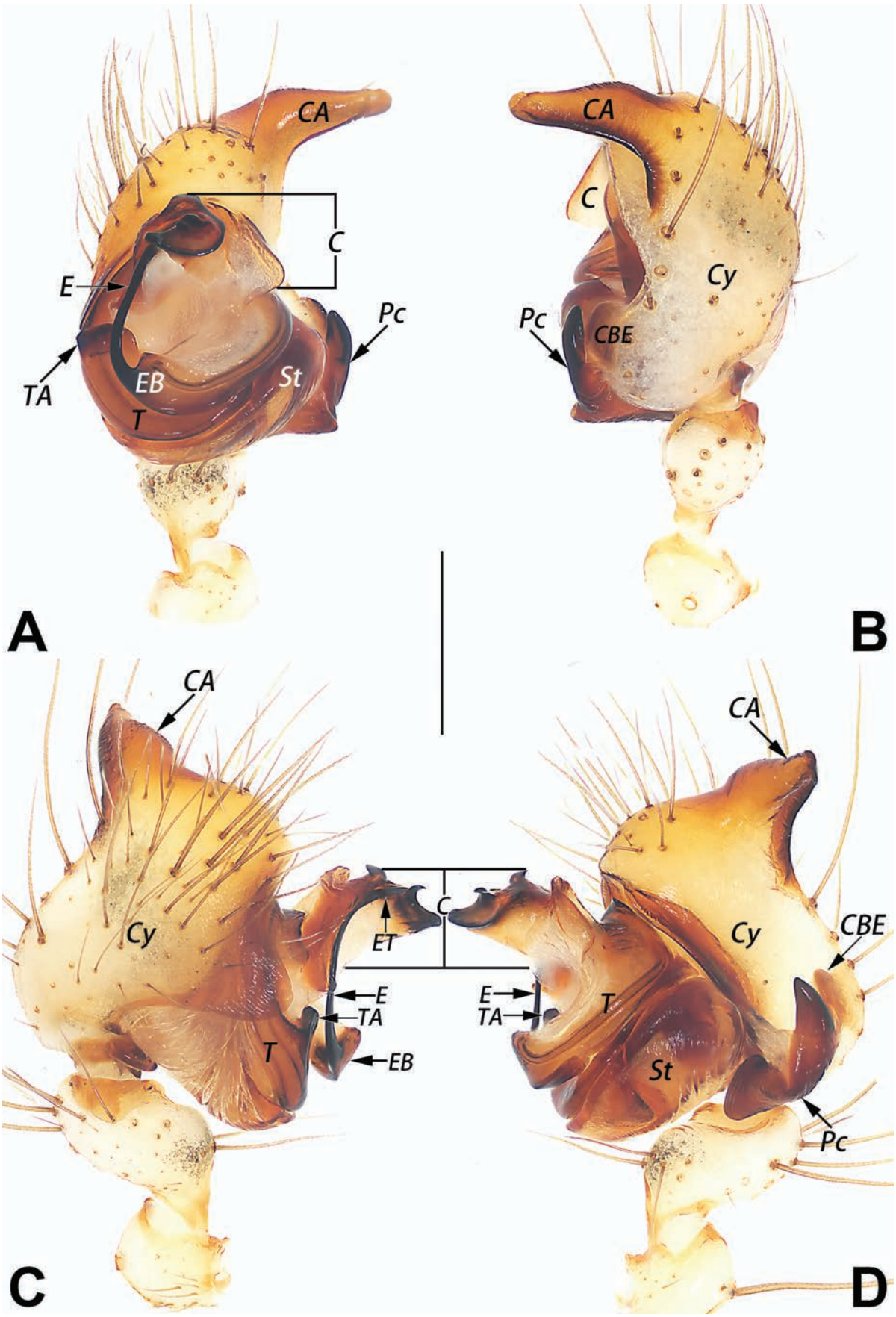

Figure 3. Male palp of *Mimetus caudatus* Wang, 1990 **A.** Ventral view; **B.** Dorsal view; **C.** Prolateral view; **D.** Retrolateral view. Abbreviations: C = conductor; CA = cymbial apex; CBE = cymbial base extension; Cy = cymbium; E = embolus; EB = embolar base; ET = embolar tip; Pc = paracymbium; St = subtegulum; T = tegulum; TA = tegular apophysis. Scale bar: 0.5 mm (equal for **A–D**).

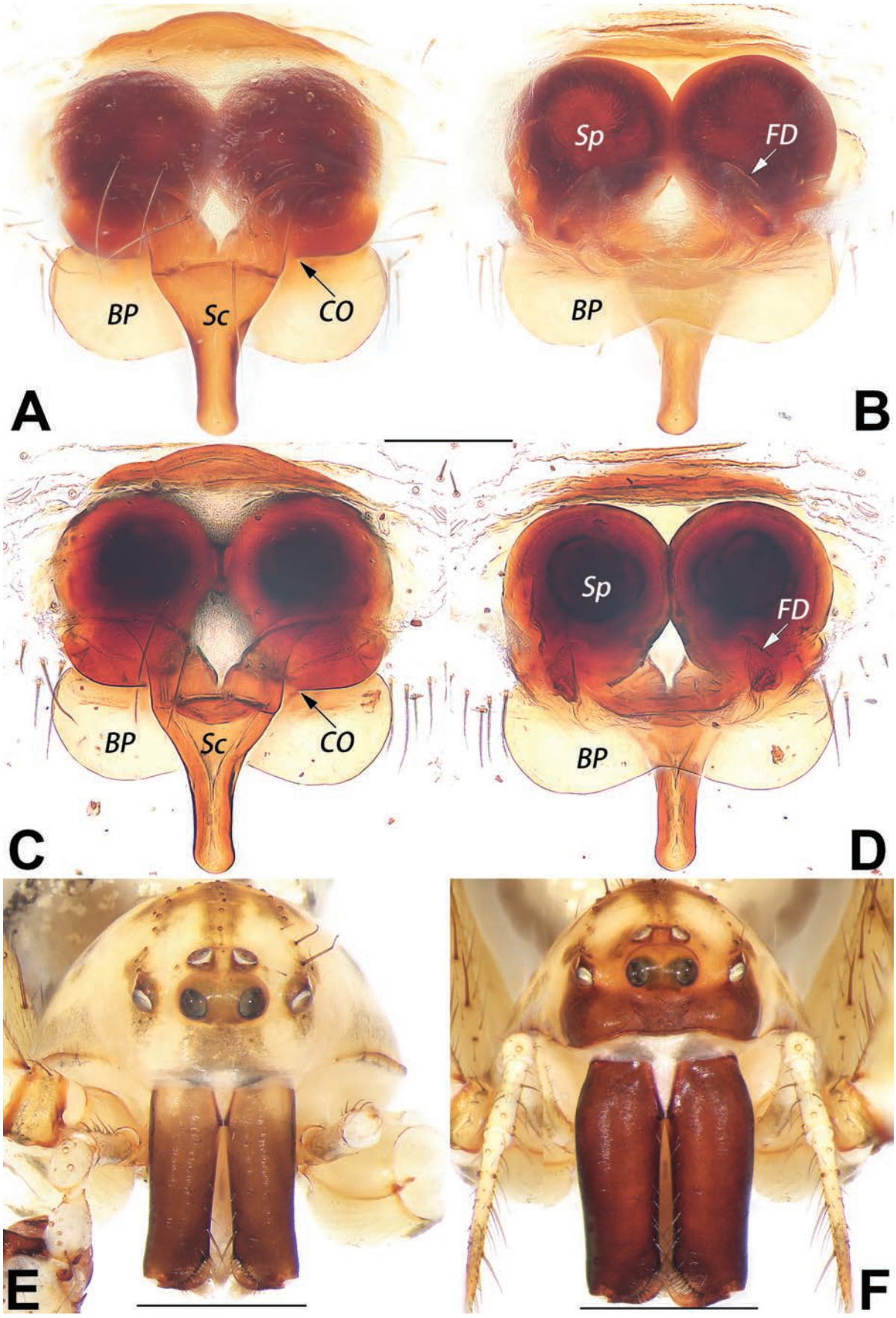

Figure 4. *Mimetus caudatus* Wang, 1990, epigyne (**A–D**) and frontal view of prosoma (**E, F**). **A, B.** Macerated epigyne, ventral and dorsal; **C, D.** Epigyne, macerated and embedded in Arabic gum, ventral and dorsal; **E.** Male; **F.** Female. Abbreviations: BP = basal plate; CO = copulatory opening; FD = fertilisation duct; Sc = scape; Sp = spermathecae. Scale bar: 0.2 mm (equal for **A–D**); 1 mm (equal for **E, F**).

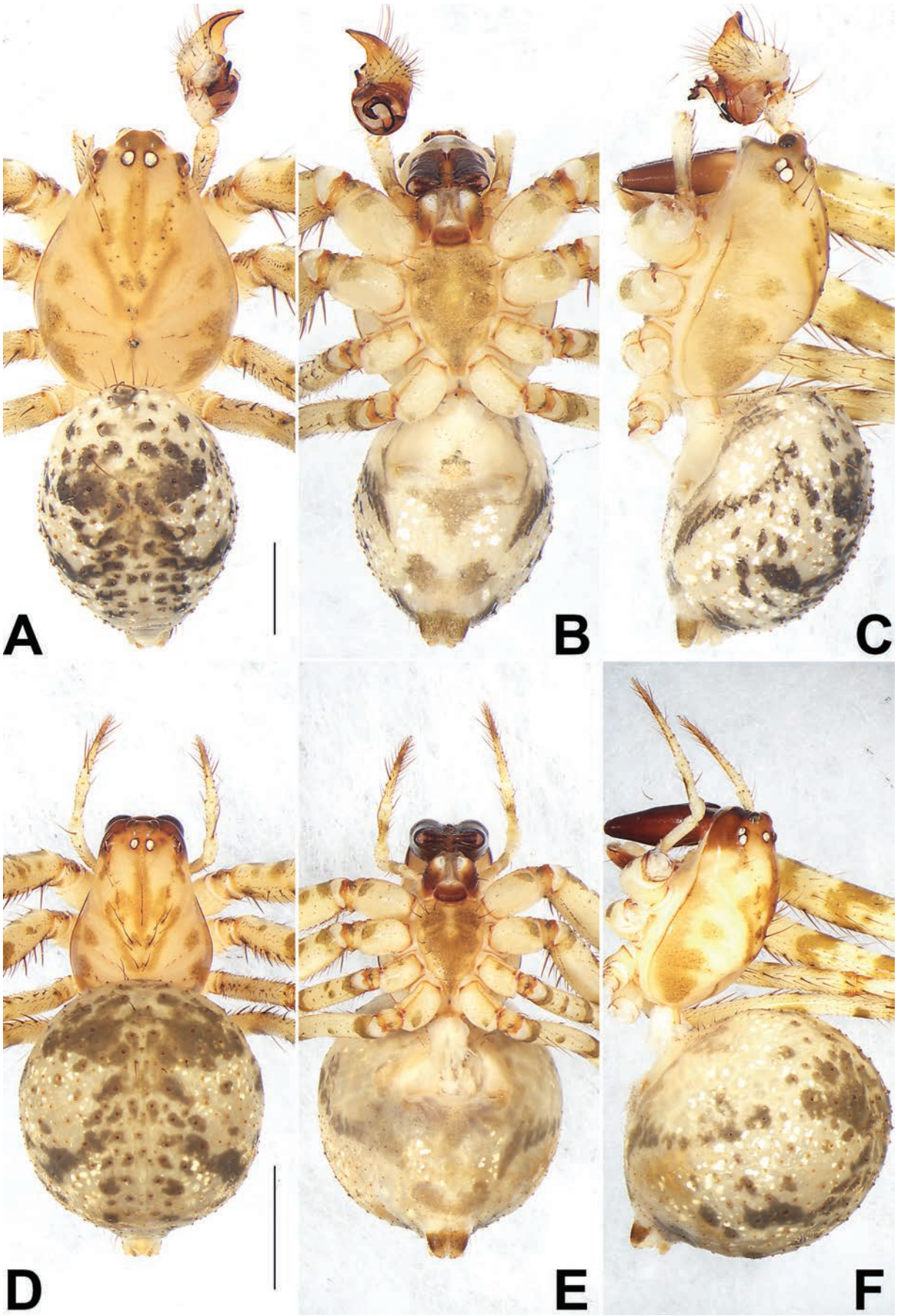

Figure 5. Habitus of *Mimetus caudatus* Wang, 1990, male (**A–C**) and female (**D–F**). **A, D.** Dorsal view; **B, E.** Ventral view; **C, F.** Lateral view. Scale bar: 2 mm (equal for **A–C**, equal for **D–F**).

Female (MGNU-2014-MIMC002). ***Measurements.*** Total length 7.61. Carapace 3.27 long, 2.24 wide. Abdomen 4.34 long, 3.97 wide. Sternum 1.46 long and 1.14 wide. Labium wider than long. Clypeus height 0.35. Chelicerae with 11 teeth on promargin and two on retromargin. Eye sizes and interdistances: AME 0.19, ALE 0.16, PME 0.16, PLE 0.18, AME–AME 0.21, ALE–AME 0.26, PME–PME 0.14, PME–PLE 0.39. MOA 0.55 long, anterior width 0.55, posterior width 0.41. Leg measurements: I 18.10 (4.98, 6.32, 4.83, 1.97), II 14.28 (4.14, 4.92, 3.57, 1.65), III 9.84 (3.05, 3.30, 2.12, 1.37), IV 11.46 (3.68, 3.92, 2.58, 1.68).

Habitus (Figs 4F, 5D–F). Slightly larger and lighter than male, other characters as in male.

Epigyne (Fig. 4A–C). Plate slightly longer than wide, spermathecae (Sp) distinctly visible through transparent integument. Basal plate (BP) broad, ca. 4.5 × wider than its high, with the middle part covered by the scape and with the lateral margins curved and the posterior margin concave medially, shaped like a transverse dumbbell. Scape (Sc) Y-shaped, relatively long, ca. 2/3 of epigyne length, originating near the middle area of epigynal plate, its apex distinctly overpasses the posterior margin of basal plate. Copulatory openings (CO) cambered, located posterior-bilaterally to scape. Copulatory ducts (CD) short barely distinct seen. Spermathecae (Sp) situated anteriorly, balloon-shaped, relatively large, ca. 1.15 ×longer than wide, surface smooth; two spermathecae touching each other. Fertilization duct (FD) membranous, located on dorsal-basal surface of spermathecae.

Natural history. The new materials of *M. caudatus* were found in the entrance zone of the Yaoling Cave.

Distribution. China (Guizhou, Guangxi) (Table 1; Figs 2A, 15).

Mimetus guiyang J. S. Zhang, Yu & Xu, sp. nov.

https://zoobank.org/F13FA58A-1682-4DEB-9509-987FB9FBFBCD

Figs 2A, 6, 14B, 15

Type material. ***Holotype*** • ♀ (MGNU-2017-MIMG001), China: Guizhou Pro.: Guiyang City, Dongfeng Town, 26.64°N, 106.79°E, c. 736 m, pitfall traps, 16 VI 2017–17 VII 2017, H. Yu et al. leg. ***Paratype*** • 1♀ (MGNU-2017-MIMG002), same data as holotype.

Etymology. The specific epithet is derived from the name of the type locality; noun in apposition.

Diagnosis. The female of *M. guiyang* sp. nov. can be distinguished from those of all congeners with the exception of *M. lingbaoshanensis* by having a short and narrow scape (Sc) (scape tip not reaching the posterior margin of the basal plate (Bp), and scape narrower than 1/5 of basal plate width in both species, as in Fig. 6A, C and Gan et al. 2019: 5, figs 3F, 4C, *vs.* scape tip overpassing the posterior margin of basal plate, such as *M. echinatus* and *M. yinae*, or scape tip no less than 1/5 of basal plate width, such as *M. juhuaensis* and *M. labiatus,* as in Wang 1990: fig. IV.1, Zeng et al. 2016: figs 3B, 4B, Gan et al. 2019: figs 5C, 6F, and Liu et al. 2021b: figs 4, 6A). The new species can be differentiated by the scape nearly finger-like, proximally not forked (Figs 6A, C) (*vs.* subtriangular or V-shaped, proximally forked in *M. lingbaoshanensis*; Gan et al. 2019: 5, figs 3F, 4C); and the posterior margin of basal plate's smoothness (Fig. 6A–D) (*vs.* medially slightly prominent in *M. lingbaoshanensis*; Gan et al. 2019: 5, figs 3F, G, 4C, D).

Description. Female (holotype, MGNU-2017-MIMG001). ***Measurements.*** Total length 4.65. Carapace 2.29 long, 1.58 wide. Abdomen 2.36 long, 1.87 wide. Sternum 1.02 long and 0.73 wide. Labium wider than long. Clypeus height 0.26. Eye sizes and interdistances: AME 0.13, ALE 0.12, PME 0.13, PLE 0.12, AME–AME 0.11, ALE–AME 0.16, PME–PME 0.08, PME–PLE 0.23. MOA 0.36 long, anterior width 0.37, posterior width 0.33. Leg measurements: I 11.97 (3.57, 4.17, 2.96, 1.27), II 9.06 (2.79, 3.12, 2.15, 1.00), III 5.49 (1.79, 1.80, 1.14, 0.76), IV 6.86 (2.22, 2.38, 1.51, 0.75).

Habitus (Figs 6E–G, 14B). Carapace nearly pyriform, uniformly yellowish white except cephalic region with a distinctive fan-shaped pattern starting from behind PER and almost reaching fovea; fovea nearly invisible; pars cephalica slightly narrowed, cervical groove and radial grooves indistinct; tegument smooth, clothed with short, sparse setae along the margins of cephalic pattern. Sternum yellowish, shaped like a shield. Labium band-shaped, light reddish brown. Endites anteriorly white, posteriorly colored as that of labium. Chelicerae dark, promargin with 11 peg teeth, retromargin with only one normal tooth. Leg yellowish white, with countless grey spots in the distal parts of femur and conspicuous dark brown annuli in the proximal parts of femur and tibia. Abdomen oval, yellowish white, dorsally covered by several relatively large black patches and small whitish spots; dorsum also with many binate hair bases, all hair bases ossified, among them ca. six or seven pairs relatively large and bubble-shaped, located medially; venter basically light brown, with numerous irregular, silver spots of varying sizes, centrally with a black longitudinal stripe, laterally with a black oblique stripe on each side, posteriorly with a pair of arc-shaped stripes forming a bracket-like pattern.

Epigyne (Fig. 6A–D). Plate nearly as wide as long, through which large spermathecae (Sp) are clearly visible. Hood (H) hemispherical, distinctly large, as wide as epigyne. Basal plate (Bp) large, ca. 1.9 × wider than its high, nearly trapezoidal, with slightly curved posterior and lateral margins, its anterior part hidden by the hood, and its middle part partly covered by the scape. Scape (Sc) finger-like, approximately 2/5 of epigyne length, originating near anterior margin of hood, with its apex distinctly beyond the posterior margin of hood but not reaching the posterior margin of the basal plate. Copulatory openings (CO) indistinct, hidden by the hood. Copulatory ducts (CD) short and barely visible. Spermathecae (Sp) situated anteriorly, egg-shaped, relatively large, ca. 1.2 × longer than wide, surface slightly wrinkled; two spermathecae closely spaced. Fertilization ducts (FD), membranous and curved, located on dorsal-basal surface of spermathecae.

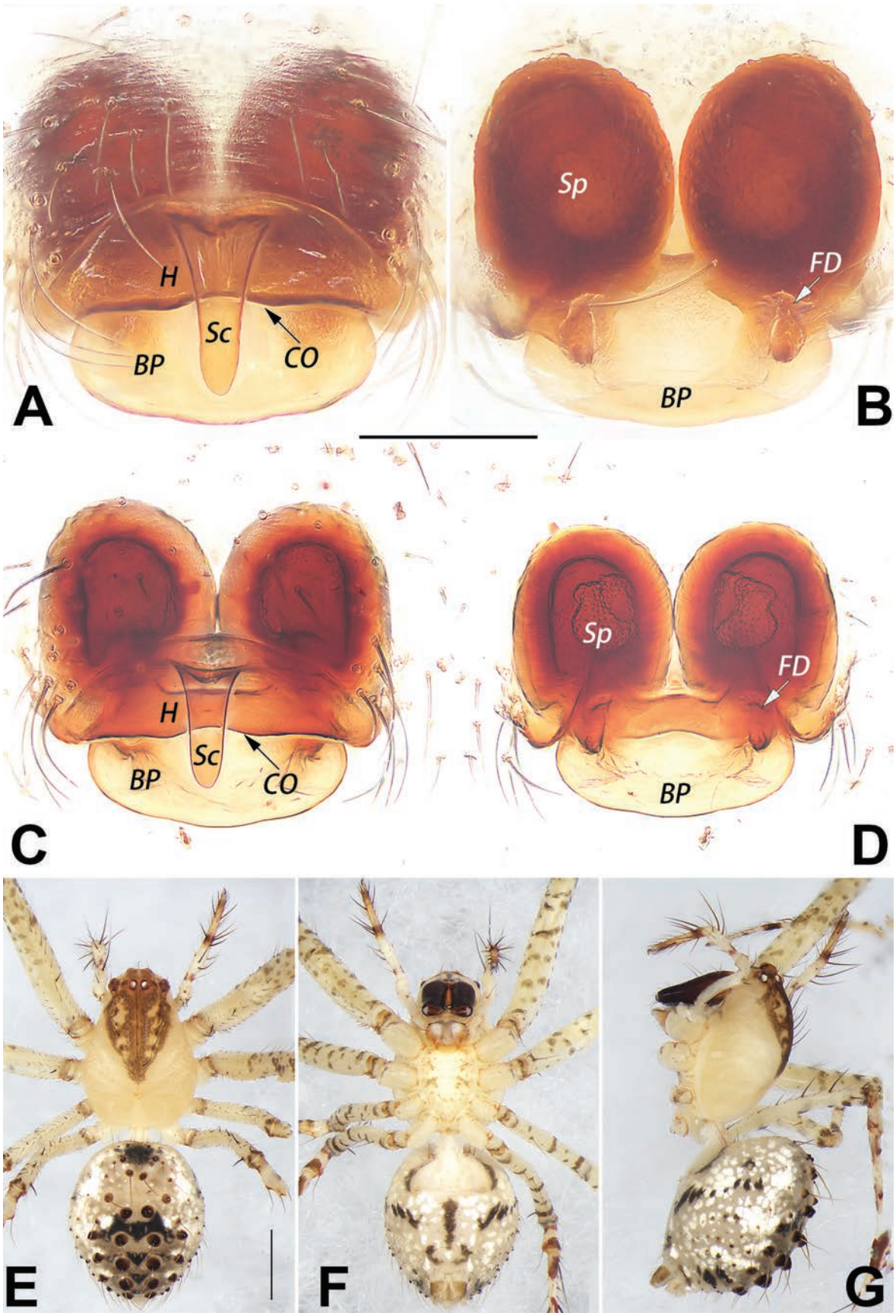

Figure 6. Holotype female of *Mimetus guiyang* sp. nov., epigyne (**A–D**) and habitus (**E–G**). **A, B.** Macerated epigyne, ventral and dorsal; **C, D.** Epigyne, macerated and embedded in Arabic gum, ventral and dorsal; **E.** Dorsal view; **F.** Ventral view; **G.** Lateral view. Abbreviations: BP = basal plate; CO = copulatory opening; FD = fertilisation duct; H = hood; Sc = scape; Sp = spermatheca. Scale bar: 0.2 mm (equal for **A–D**); 1 mm (equal for **E–G**).

Male. Unknown.

Natural history. The types were collected in a pitfall trap set in a masson pine plantation, but the specific biology of *M. guiyang* sp. nov. is not currently clear.

Distribution. Known only from the type locality (Table 1; Figs 2A, 15).

Mimetus lanmeiae Liu, Yu & Xu, sp. nov.

https://zoobank.org/126EF2A2-129C-4DFA-87BD-39D0AC121A71

Figs 2A, 7, 8, 14A, 15

Type material. ***Holotype*** • ♂ (MGNU-2022-MIML001), China: Guizhou Pro.: Guiyang City, Xinpu Town, Xiangzhigou, 26.57°N, 106.93°E, c. 1092 m, by hand, 1 VI 2022, L. Qian leg.

Etymology. The specific name is a matronym in honor of Lanmei Tang, the mother of the collector.

Diagnosis. Male of *M. lanmeiae* sp. nov. resembles that of *M. contrarius* (Zeng et al. 2019: 675, figs 1A–G, 2A–E) in having a C-shaped embolus (E), disc-shaped conductor (C), and elongated, shovel-shaped cymbial apex (CA), but differ by: (1) cymbium (Cy) with an ecto-medial process (CEMP) in the new species (*vs.* CEMP absent in the latter) (cf. Fig. 7A, B, D and Zeng et al. 2019: figs 1C, E, 2B, C); (2) paracymbium (Pc) shaped like water drop, anteriorly with a highly sclerotized thumb-shaped apophysis in the new species (*vs.* nearly triangular, medially with a small tooth-shaped apophysis in the latter) (cf. Fig. 7A, B, D and Zeng et al. 2019: figs 1E, 2C); and (3) palpal tibia approximately 1.4 × longer than wide in the new species (*vs.* palpal tibia distinctly longer than wide, the ratio of length/width is approximately 2.8 in the latter) (cf. Fig. 7A–D and Zeng et al. 2019: figs 1C–E, 2A–C).

Description. Male (holotype, MGNU-2022-MIML001). ***Measurements.*** Total length 2.14. Carapace 0.96 long, 0.86 wide. Abdomen 1.18 long, 1.05 wide. Sternum 0.48 long and 0.49 wide. Labium wider than long. Clypeus height 0.18. Eye sizes and interdistances: AME 0.09, ALE 0.08, PME 0.09, PLE 0.08, AME–AME 0.08, ALE–AME 0.03, PME–PME 0.04, PME–PLE 0.11. MOA 0.24 long, anterior width 0.24, posterior width 0.22. Leg measurements: I 6.2 (1.65, 2.15, 1.61, 0.79), II 4.92 (1.45, 1.65, 1.13, 0.69), III 2.91 (0.85, 0.91, 0.66, 0.50), IV 3.60 (1.12, 2.38, 0.75, 0.53).

Habitus (Figs 8, 14A). Carapace oval, slightly longer than wide, basically yellowish white, with a large black Y-shaped pattern (both lateral margins of pattern are wave-like lines) between ocular area and fovea; fovea inconspicuous; ocular area slightly narrowed, cervical groove and radial grooves invisible; tegument smooth, without setae. Sternum white, heart- or shield-shaped. Labium band-shaped, slightly curved, light reddish brown. Endites anteriorly white, posteriorly colored as that of labium. Chelicerae light reddish brown, promargin with eight peg teeth, retromargin with two small teeth. Leg yellowish white, with several black spots in the distal half of femur. Abdomen round, yellowish white, dorsally with whitish and dark patches, and many weakly ossified hair bases, but almost all hairs have broken off from the body; venter basically yellowish-white, anteriorly with a pair of long, arc-shaped stripes on both sides, extending ca. 1/2 of abdomen length, forming a large, bracket-shaped pattern, posteriorly with a nearly circular black spot.

Palp (Fig. 7A–D). Tibia ca. 1/3 of cymbium length, about 1.4 longer than wide. Cymbium (Cy) with a developed apex (CA), an ecto-medial process (CEMP), and a basal extension (CBE): cymbial apex elongated, ca. 1/3 of cymbium length, nearly triangular in ventral and dorsal views and shovel-shaped in both lateral views, its tip pointing ventro-retrolaterally; ecto-medial process triangular or tooth-shaped, slightly curved, apex sharp and pointing ventro-retrolaterally; cymbial basal extension thumb-like, partly membranous, its tip blunt. Paracymbium (Pc) broad, ca. 2/5 of cymbium length, with a highly sclerotized thumb-shaped apophysis. Tegulum (T) nearly circular, centrally and apically membranous, slightly excavated on prolatero-apical side to accommodate embolus; sperm duct distinct, forming a loop along tegular margin. Tegular apophysis (TA) triangular in ventral view and papilliform in prolateral view, located at proximal-prolateral position of tegulum (ca. 8–9 o'clock position of tegulum). Subtegulum (St) located postero-retrolaterally to tegulum, without apophysis. Embolus (E) C-shaped, arising at 6–7 o'clock position, terminating at ca. 12 o'clock position. Conductor (C) large, disc-shaped, slightly extending outward, membranous centrally and strongly sclerotized marginally, its anterior margin folded to cover the tip of emblous (ET).

Female. Unknown.

Natural history. The holotype of *Mimetus lanmeiae* **sp. nov.** was found on a spider web (Fig. 8D), which may show a mimicry behavior (mimicking the movements of a prey trapped in the host web to attract, attack, and feed upon the resident spider as mentioned in Liu et al. (2021b)).

Distribution. Known only from the type locality (Table 1; Figs 2A, 15).

Mimetus sinicus Song & Zhu, 1993

Figs 2A, 9–11, 14C, D, 15

Mimetus sinicus Song and Zhu 1993: 421, figs 1–5 (♂♀); Song and Li 1997: 400, fig. 1A–E (♂♀); Song et al. 1999: 74, figs 11K, 30H, I, S, T (♂♀).

Material examined. • 5♂♂5♀♀ (MGNU-2022-MIMS001 to 010), China: Guizhou Pro.: Guiyang City, Xinpu Town, Xiangzhigou, 26.79°N, 106.91°E, c. 1092 m, by beating, 31 V 2022, H. Yu et al. leg.

Diagnosis and description. See Song and Zhu (1993). Male palp as in Fig. 9A–C, epigyne as in Fig. 9D, E, habitus as in Figs 10, 14C, D, living specimens as in Fig. 11.

Distribution. China (Guizhou, Hubei) (Table 1; Figs 2A, 15).

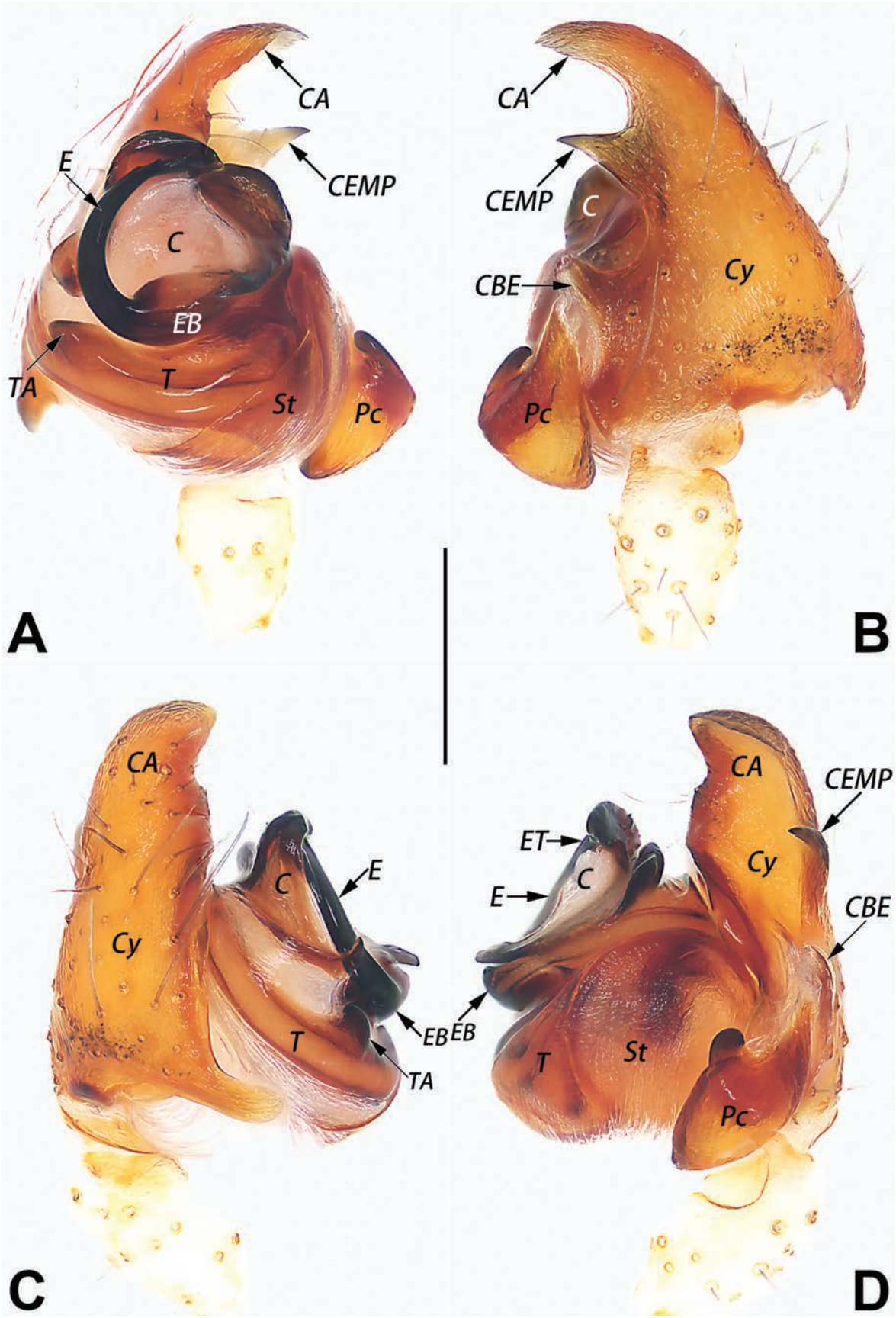

Figure 7. Male palp of the holotype of *Mimetus lanmeiae* sp. nov. **A.** Ventral view; **B.** Dorsal view; **C.** Prolateral view; **D** Retrolateral view. Abbreviations: C = conductor; CA = cymbial apex; CBE = cymbial base extension; CEMP = cymbial ecto-medial process; Cy = cymbium; E = embolus; EB = embolar base; ET = embolar tip; Pc = paracymbium; St = subtegulum; T = tegulum; TA = tegular apophysis. Scale bar: 0.2 mm (equal for **A–D**).

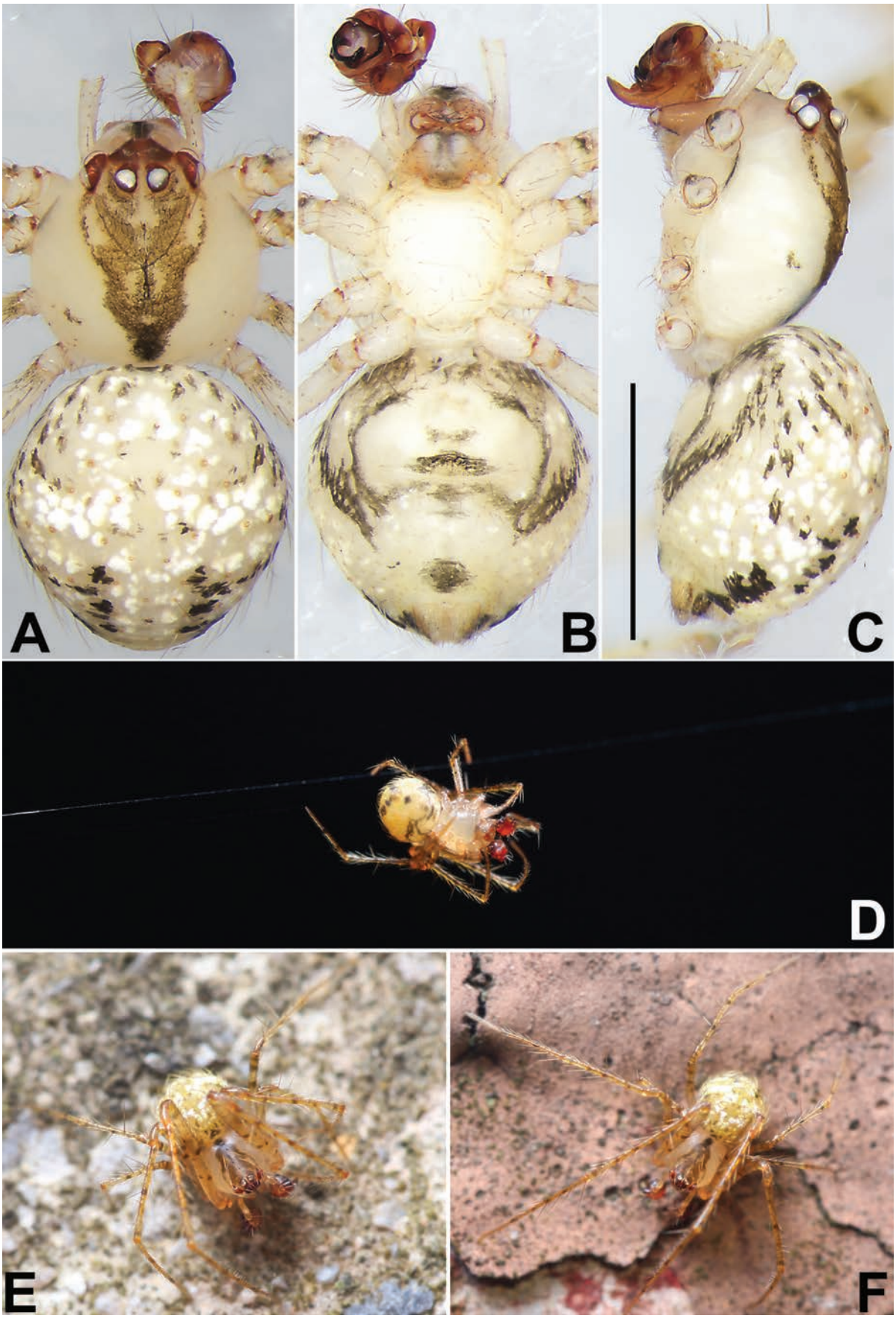

Figure 8. Male holotype of *Mimetus lanmeiae* sp. nov., habitus (**A–D**) and living specimen (**D–F**). **A.** Dorsal view; **B.** Ventral view; **C.** Lateral view; **D.** Spider on web; **E, F.** Spider dropped on the ground. Photographs of living specimen by Q Lu (Shenzhen).Scale bar: 1 mm (equal for **A–C**).

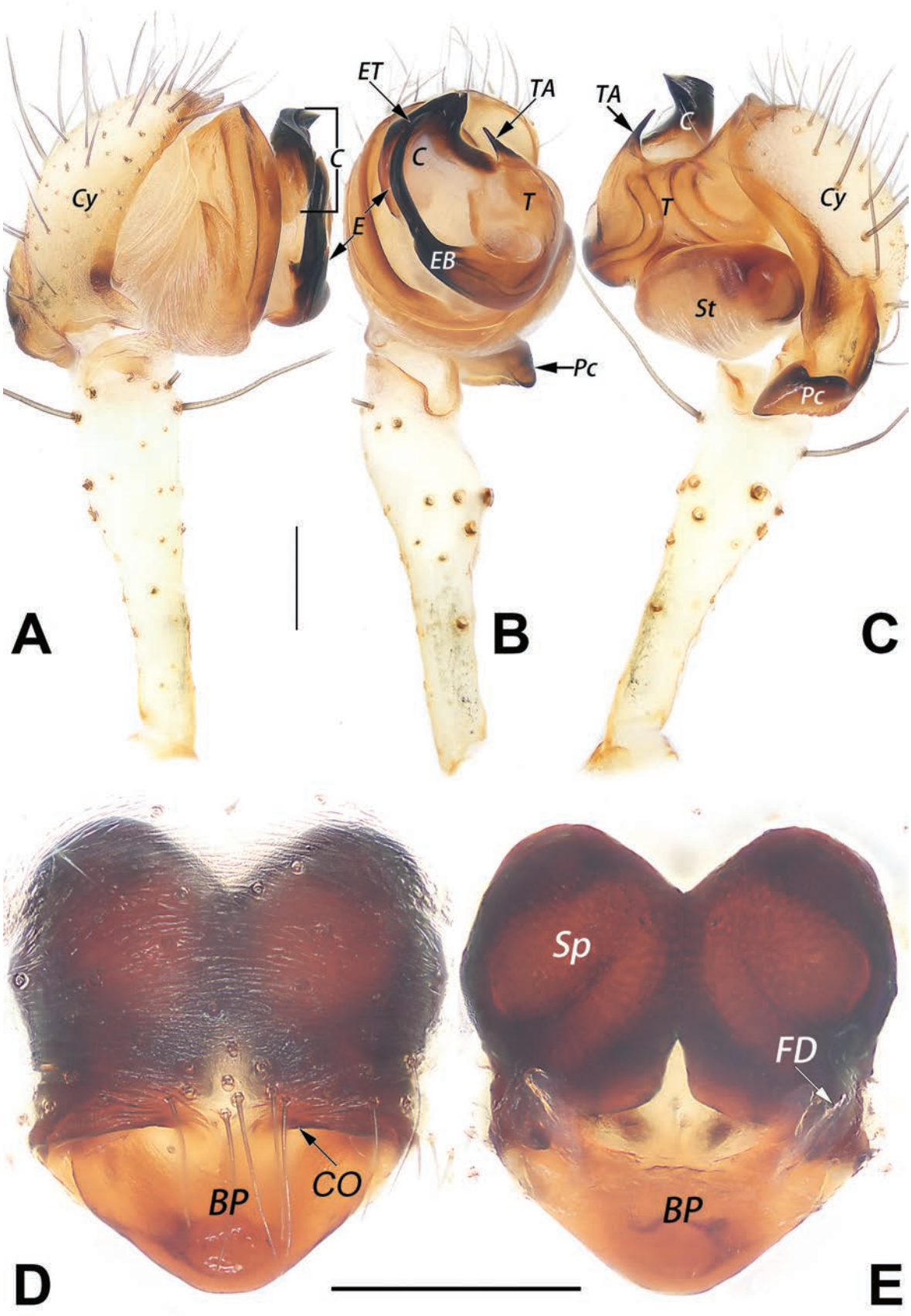

Figure 9. Male palp (**A–C**) and female epigyne (**D, E**) of *Mimetus sinicus* Song & Zhu, 1993. **A–C.** Prolateral, ventral, and retrolateral view; **D–E.** Macerated epigyne, ventral and dorsal. Abbreviations: BP = basal plate; C = conductor; CO = copulatory opening; Cy = cymbium; E = embolus; FD = fertilisation duct; EB = embolar base; ET = embolar tip; Pc = paracymbium; Sp = spermathecae; St = subtegulum; T = tegulum; TA = tegular apophysis. Scale bar: 0.2 mm (equal for **A–C**, equal for **D, E**).

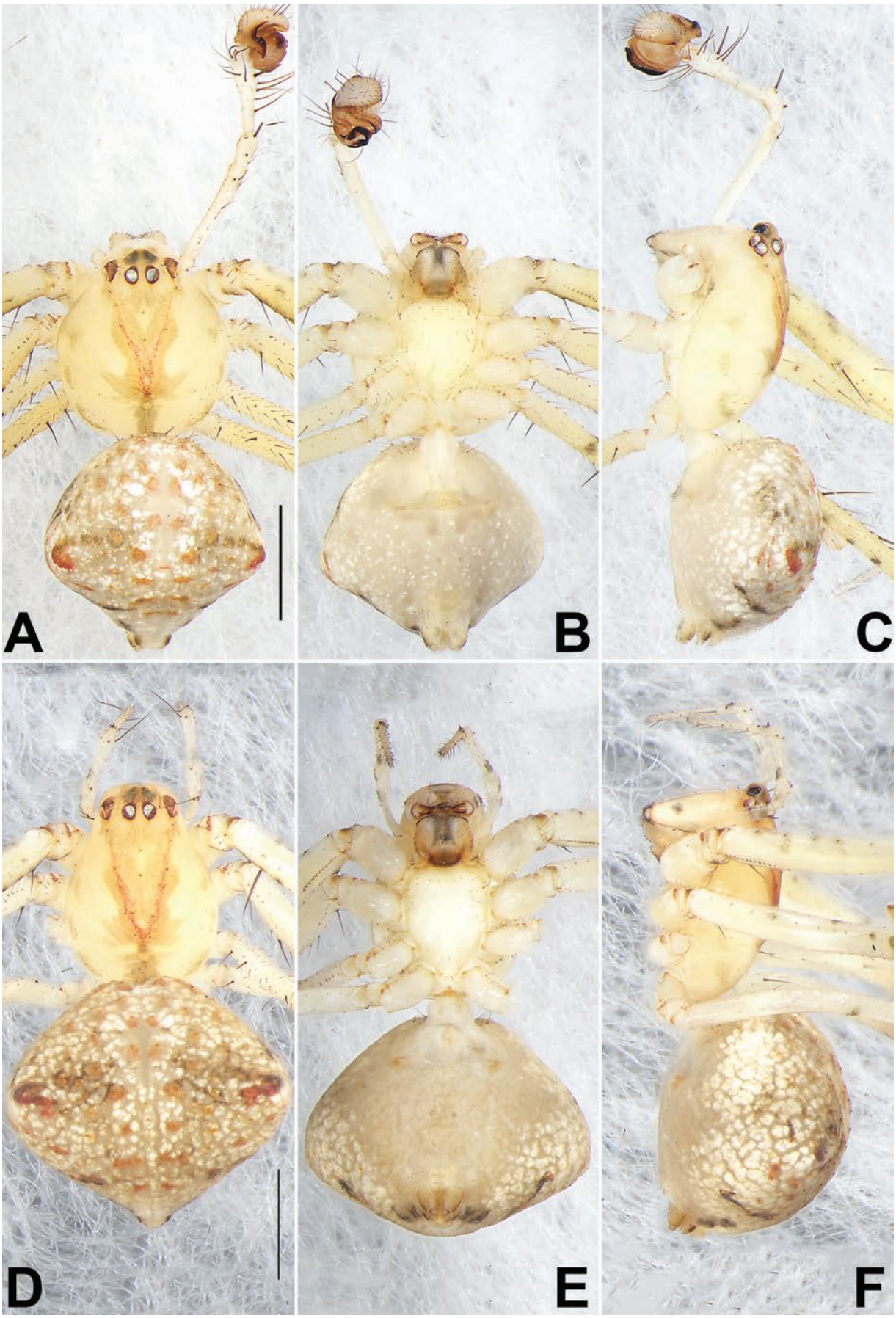

Figure 10. Habitus of *Mimetus sinicus* Song & Zhu, 1993, male (**A–C**) and female (**D–F**). **A, D.** Dorsal view; **B, E.** Ventral view; **C, F.** Lateral view. Scale bar: 1 mm (equal for **A–C**, equal for **D–F**).

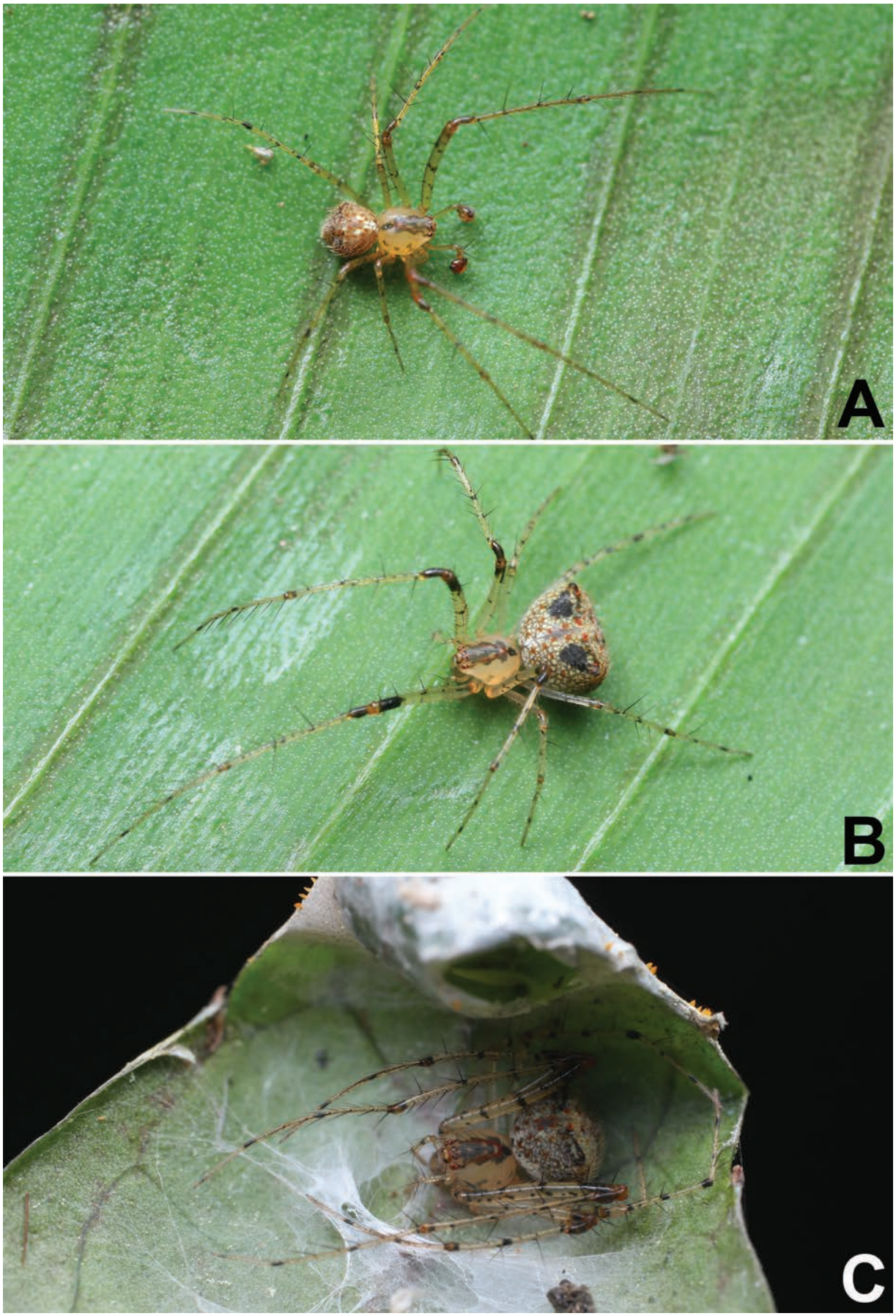

Figure 11. *Mimetus sinicus* Song & Zhu, 1993, male (**A**) and female (**B–C**), living specimens. Photographs of living specimens by Q Lu (Shenzhen).

***Mimetus testaceus* Yaginuma, 1960**

Figs 2A, 12, 13, 14E, F, 15

Mimetus testaceus Yaginuma 1960: append. 3, plate. 15, fig. 93, fig. 101G (♀); Paik 1967: 190, fig. 3, 16–21 (♂♀); Wang 1990: 40, fig. III.5–11 (♂♀); Chen and Zhang 1991: 182, fig. 179.1–5 (♂♀); Song et al. 1999: 74, fig. 30J, K, U, V (♂♀). For a full list of taxonomic references, see WSC (2025).

Material examined. • 2♂♂3♀♀ (MGNU-2022-MIMT001 to 005), China: Guizhou Pro.: Guiyang City, Shuitian Town, Panlongshan Forest Park, 26.74°N, 106.88°E, c. 1072 m, by beating, 2 VI 2022; H. Yu et al. leg.

Diagnosis and description. See Paik (1967). Male palp as in Fig. 12A–C, epigyne as in Fig. 12D, E, habitus as in Figs 13, 14E, F, living specimens as in Fig. 12F, G.

Distribution. China (Hunan, Guangxi, Guizhou, Zhejiang) (Table 1; Figs 2A, 15).

Discussion

The genetic barcode technique (DNA barcodes), based on sequencing of the mitochondrial marker cytochrome c oxidase subunit I (COI), has proven a useful, complementary tool to overcome species limitations and sex matching in taxonomic studies of many spider groups (Barone et al. 2024; Blagoev et al. 2016; Čandek and Kuntner 2015; Xu et al. 2015, 2017; Coddington et al. 2016; Tyagi et al. 2019; Zhang et al. 2021a, b). A preliminary molecular species delimitation was conducted using the DNA barcoding gap method, based on all available COI sequences of the genus *Mimetus* (including both self-sequenced and all sequences downloadable from NCBI). According to the results (unpublished), a distinct gap was observed between intraspecific and interspecific genetic distances, ranging from 4.18% to 6.85% for K2P and from 4.04% to 6.50% for p-distance, indicating that even single-locus analyses based on the COI barcodes, when integrated with morphological data and collection experience, may provide sufficiently reliable species delimitation for *Mimetus*.

Therefore, we prioritize using the COI sequence for sex matching in the present paper. However, the lack of fundamental data (currently, we can obtain COI sequences for only eight *Mimetus* species through NCBI, and among them, only one species, *M. testaceus*, is from China; NCBI 2025) and the inability to obtain high-quality DNA from some specimens (we were unable to obtain good extractions from *M. guiyang* sp. nov. and *M. caudatus*) compel us to seek alternative methods or criteria to solve the issue.

In almost all *Mimetus* spp., there is no significant sexual dimorphism in body size, pattern, and coloration, such as in *M. caudatus* (cf. Figs 4E, 5A–C, and Figs 4F, 5D–F), *M. sinicus* (cf. Figs 10A–C, 11A, 14C, and Figs 10D–F, 11B, C, 14D), and *M. testaceus* (cf. Figs 12F, 13A–C, 14E, and Figs 12G, 13D–F, 14F). Therefore, this relatively low degree of sexual dimorphism can serve as a reference for determining whether specimens of different sexes are conspecific. Furthermore, we used two criteria for matching the opposite sexes: the combined occurrence of males and females in several samples and compatibility of epigyne and male palpal structure.

Up to now, four described *Mimetus* species (*M. caudatus* is excluded) from China are known from males only: *M. bucerus*, *M. clavatus*, *M. lamellaris*, and *M. uncatus* (WSC 2025; Table 1). However, none of them could be matched with *M. guiyang* sp. nov. due to their different habitus: the abdomen dorsally with peculiar, large, bubble-shaped, ossified hair bases in *M. guiyang* sp. nov., but the hair bases are absent or indistinct in *M. bucerus*, *M. clavatus*, *M. lamellaris*, and *M. uncatus* (Gan et al. 2019: fig. 1A; Liu et al. 2021a: figs 9A, B, 20A, B; Zeng et al. 2016: fig. 9A).

According to the WSC (2025), two described species of *Mimetus* from China are known from females only: *M. labiatus* and *M. tuberculatus* (Table 1). However, neither could be matched with *M. lanmeiae* sp. nov. due to their different sizes and habitus. *M. lanmeiae* sp. nov. with a 2.14 mm body length, its abdomen round and smooth, without humps, and the dorsal surface of the abdomen with whitish and dark patches (Fig. 8). In contrast, *M. labiatus* possesses a 5.80 mm body length, its abdomen is elongate-oval and dorsally with several pairs of diagonal, claviform bands (Yin et al. 2012: 199, fig. 53a), and *M. tuberculatus* has a 4.80 mm body length, its abdomen with three pairs of tubercles (Liang and Wang 1991: 61).

Both *M. guiyang* sp. nov. and *M. lanmeiae* sp. nov. were collected from Guiyang City; however, the two can also be considered as separate species due to their different sizes (female with 4.65 mm body length vs. male with 2.14 mm) and their different habitus (abdomen dorsally with many large bubble-shaped hair bases as in Fig. 6E, G, vs. with many small and indistinct hair bases as in Fig. 8A, C). Moreover, there is a great possibility that two new species will be assigned to different species groups or genera in the future (*Mimetus* will likely be split when more data is available). Based on the characters of copulatory organs, Liu et al. (2021b: 574) divided the Chinese *Mimetus* into three types (or groups). It appears that *M. guiyang* sp. nov. and *M. caudatus* should belong to the first type, which presents a distinct set of genitalic characters: basal plate (Bp) of epigynum oblong and scape (Sc) of epigynum conspicuous in female (as shown in Figs 4A–D, 6A–D); conductor (C) cylindrical, strongly sclerotized, and extending outward; embolus (E) originating at the position of 6 o'clock and extending along the conductor (C) in male (Fig. 3A–D). Obviously, *M. lanmeiae* sp. nov. possesses no characters associated with the type (or group), which includes *M. guiyang* sp. nov. and *M. caudatus*, due to lacking the features just mentioned. Consequently, it is currently impossible to discern any obvious derived features that could indicate a close relationship between *M. guiyang* sp. nov. and *M. lanmeiae* sp. nov.

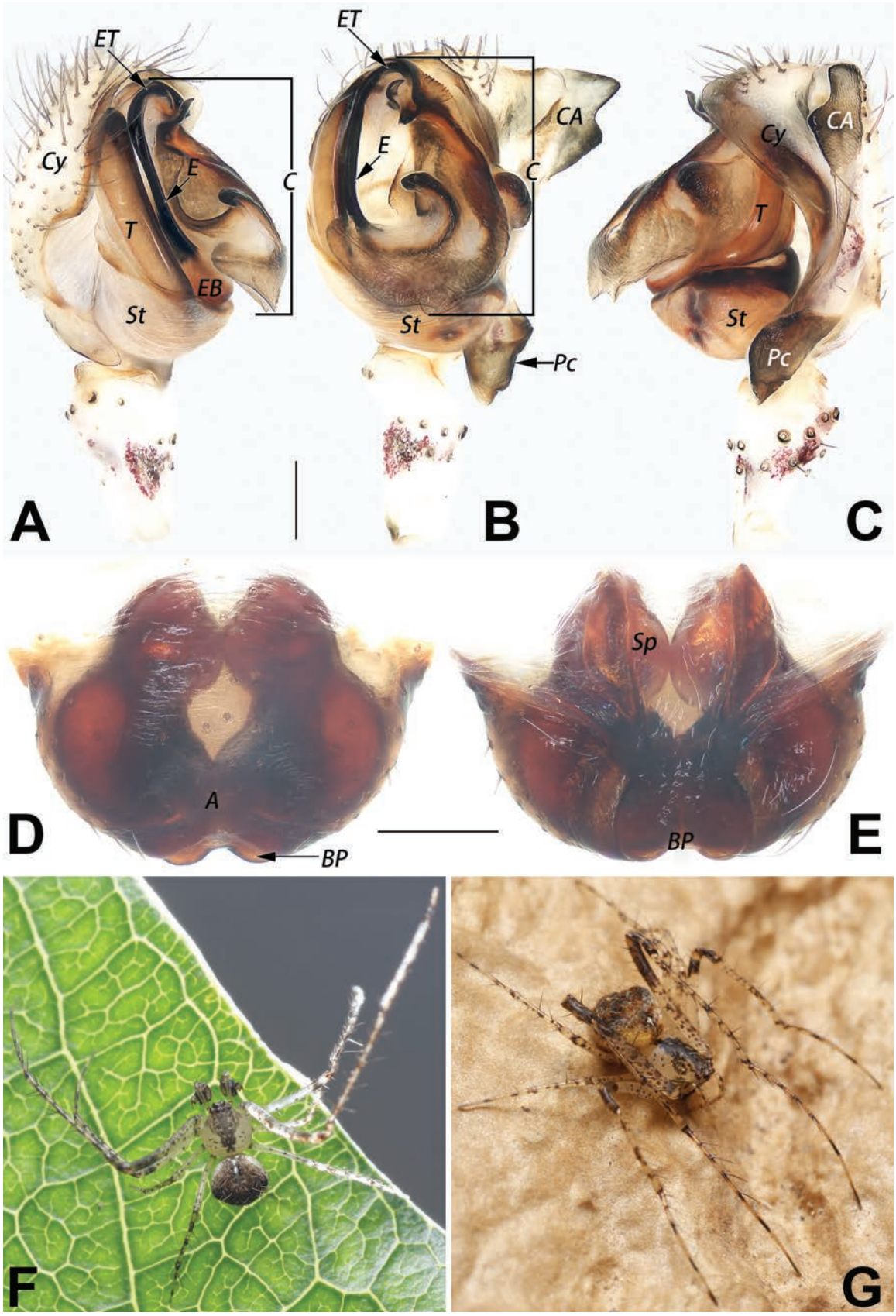

Figure 12. Male palp (**A–C**), female epigyne (**D, E**) and living specimens (**F, G**) of *Mimetus testaceus* Yaginuma, 1960. **A–C.** Prolateral, ventral, and retrolateral view; **D, E.** Macerated epigyne, ventral and dorsal; **F, G.** Male and female Abbreviations: A = atrium; BP = basal plate; C = conductor; CA = cymbial apex; Cy = cymbium; E = embolus; EB = embolar base; ET = embolar tip; Pc = paracymbium; Sp = spermathecae; St = subtegulum; T = tegulum. Photographs of living specimen by Q Lu (Shenzhen). Scale bar: 0.5 mm (equal for **A–C**); 0.2 mm (equal for **D, E**).

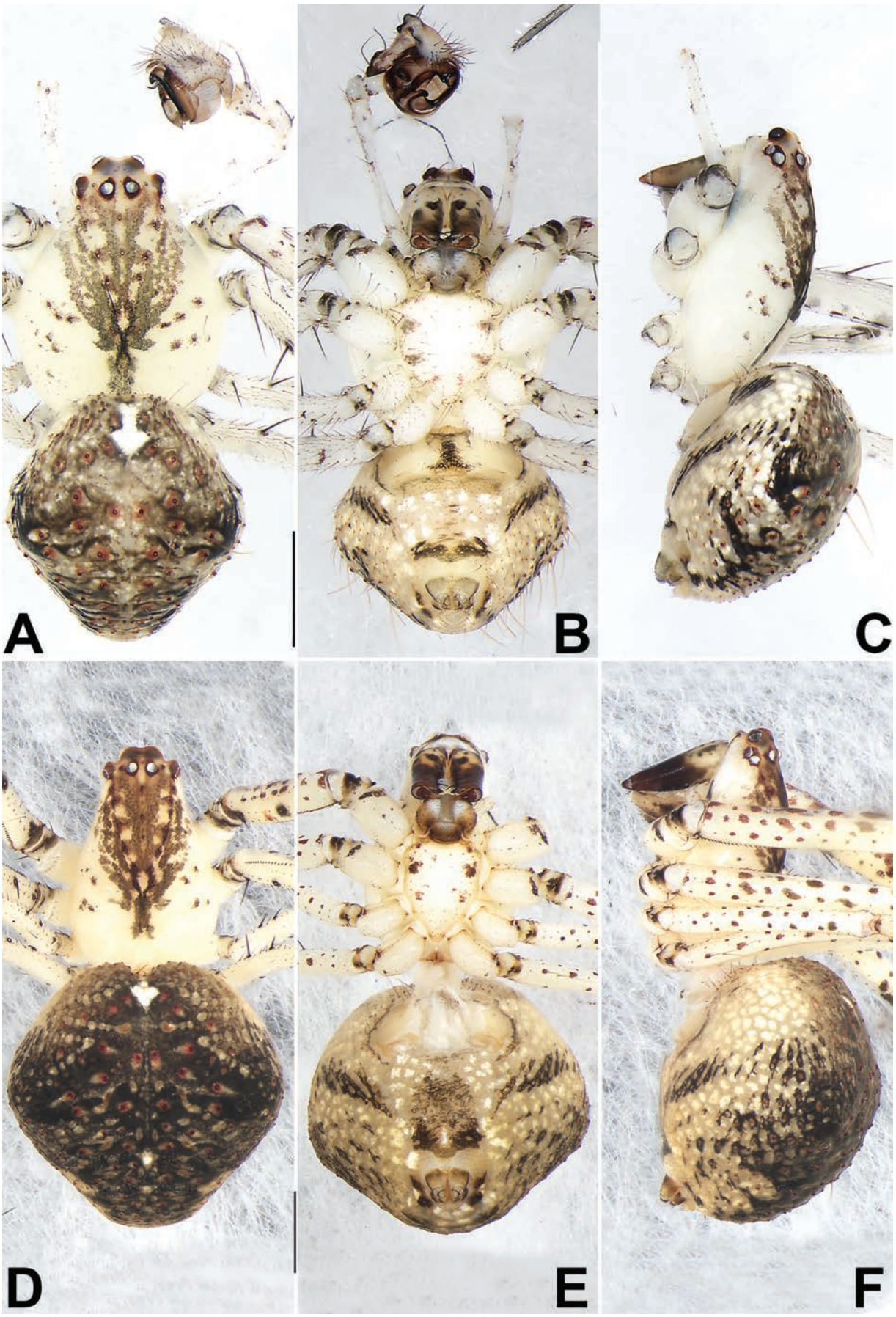

Figure 13. Habitus of *Mimetus testaceus* Yaginuma, 1960, male (**A–C**) and female (**D–F**). **A, D.** Dorsal view; **B, E.** Ventral view; **C, F.** Lateral view. Scale bar: 1 mm (equal for **A–C**, equal for **D–F**).

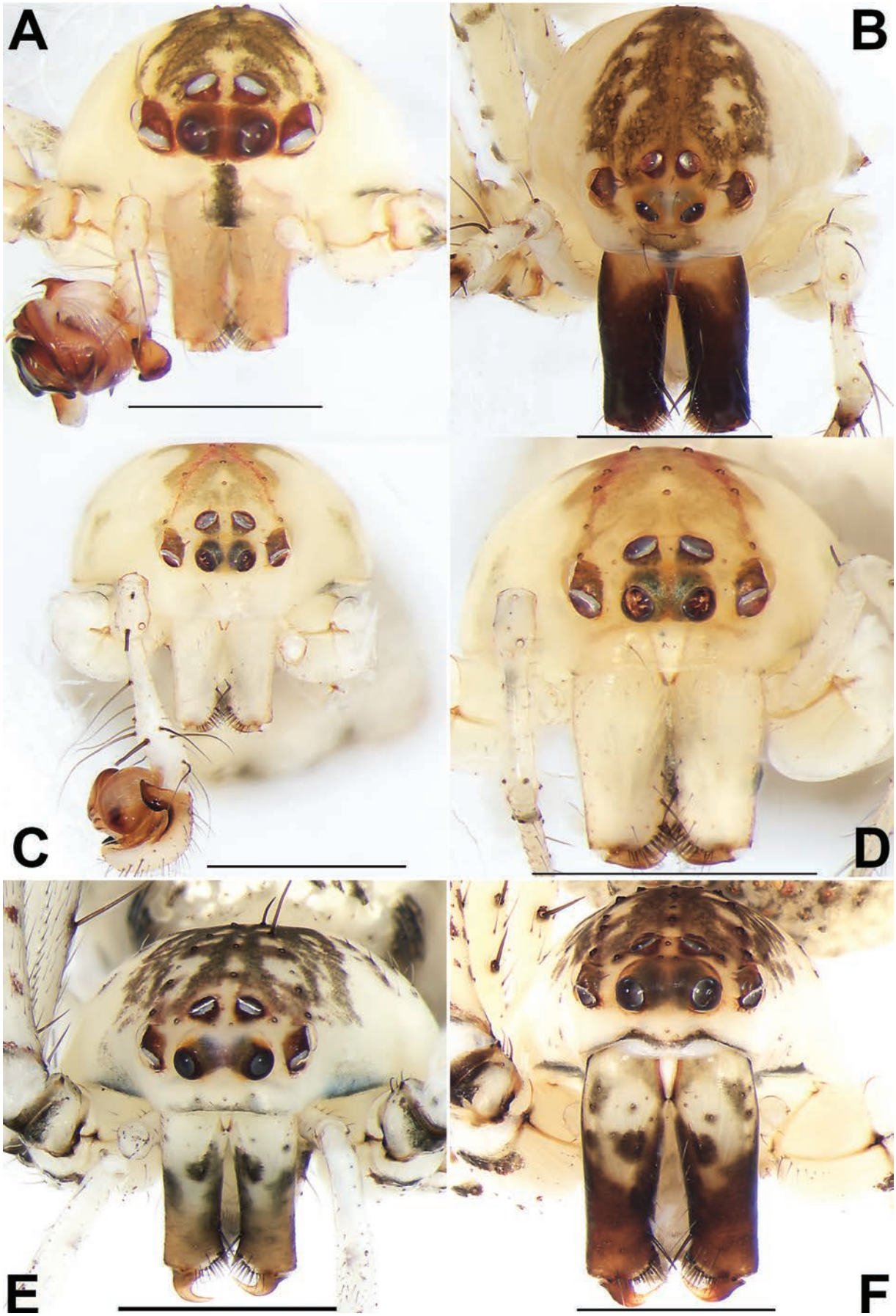

Figure 14. Frontal view of the prosoma of *Mimetus* spp. treated in this paper. **A.** *Mimetus lanmeiae* sp. nov.; **B.** *Mimetus guiyang* sp. nov.; **C, D.** *Mimetus sinicus*, male and female; **E, F.** *Mimetus testaceus*, male and female. Scale bars: 0.5 mm (**A**); 1 mm (**B–F**).

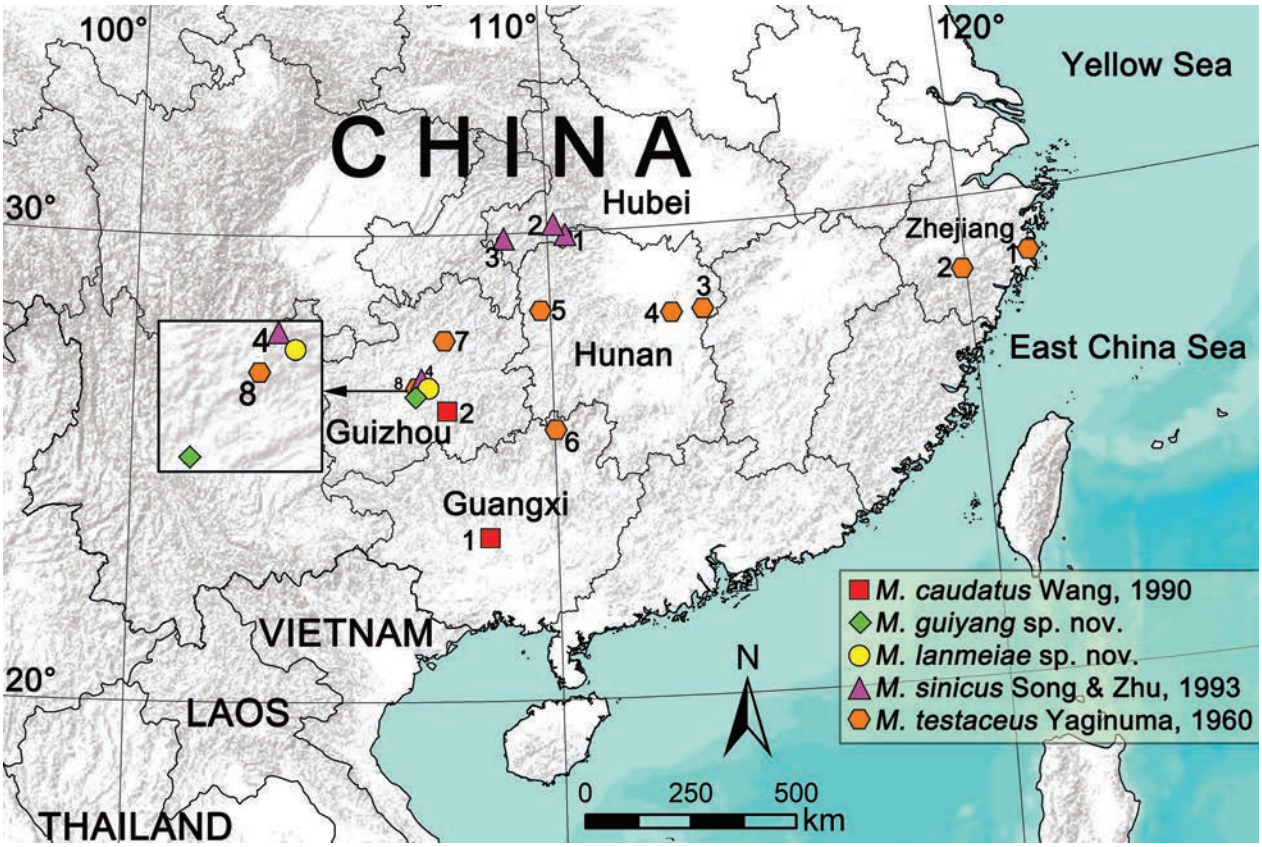

Figure 15. Distribution records of the *Mimetus* species treated in this paper: *Mimetus caudatus* Wang, 1990 (scarlet square: 1. Guangxi Zhuang Autonomous Region, Mt. Daming; 2. Guizhou Province, Dunyun City, Xiaoweizhai Town, Yaolin Cave), *M. guiyang* sp. nov. (green rhombus: Guizhou Province, Guiyang City, Dongfeng Town), *M. lanmeiae* sp. nov. (yellow circle: Guizhou Province, Guiyang City, Xinpu Town, Xiangzhigou), *M. sinicus* Song & Zhu, 1993 (purple triangle: 1. Hubei Province, Hefeng County; 2. Hubei Province, Xuanen County; 3. Hubei Province, Xianfeng County; 4. Guizhou Province, Guiyang City, Xinpu Town, Xiangzhigou), *M. testaceus* Yaginuma, 1960 (orange hexagon: 1. Zhejiang Province, Taizhou City; 2. Zhejiang Province, Lishui City; 3. Hunan Province, Liuyang City; 4. Hunan Province, Mt. Yuelu; 5. Hunan Province, Zhangjiajie City; 6. Guangxi Zhuang Autonomous Region, Longsheng County; 7. Guizhou Province, Zunyi City; 8. Guizhou Province, Guiyang City, Shuitian Town, Panlongshan forest park).

Acknowledgments

We are especially grateful to Danilo Harms (Hamburg, Germany), the subject editor. We thank Gustavo Hormiga (Washington, USA) and Danniella Sherwood (London, UK) for providing constructive comments on the manuscript. We are grateful to Qianle Lu (Shenzhen, China) for his kind help in collecting the specimens and for agreeing to use his image of live specimens. This work was supported by the National Natural Sciences Foundation of China (NSFC-32360123/32060113/31702006/32070429/31772423), the Natural Science Foundation of Guizhou Province (J [2020] 1Y081), the Project of Biodiversity Survey and Assessment in Guiyang (GZZC-2021-018), the Joint Fund of the National Natural Science Foundation of China and the Karst Science Research Center of Guizhou Province (Grant No. U1812401), and the Key Project of Hunan Provincial Department of Education (19A320).

References

Barone ML, Wilson JD, Zapata L, Soto EM, Haddad CR, Grismado C, Izquierdo M, Arias E, Pizarro-Araya J, Briones R, Barriga JE, Peralta L, Ramírez MJ (2024) Genetic barcodes for species identification and phylogenetic estimation in ghost spiders (Araneae: Anyphaenidae: Amaurobioidinae). Invertebrate Systematics 38(11): 1–18. https://doi.org/10.1071/IS24053

Barrantes G, Segura-Hernandez L, Solano-Brenes D (2025) A novel prey capture strategy in pirate spiders (Araneae: Mimetidae). Animal Behaviour 221: 122700. https://doi.org/10.1016/j.anbehav.2023.07.001

Benavides LR, Hormiga G (2016) Taxonomic revision of the Neotropical pirate spiders of the genus *Gelanor* Thorell, 1869 (Araneae, Mimetidae) with the description of five new species. Zootaxa 4064(1): 1–72. https://doi.org/10.11646/zootaxa.4064.1.1

Benavides LR, Hormiga G (2020) A morphological and combined phylogenetic analysis of pirate spiders (Araneae, Mimetidae): evolutionary relationships, taxonomy, and character evolution. Invertebrate Systematics 34(2): 144–191. https://doi.org/10.1071/IS19032

Benavides LR, Giribet G, Hormiga G (2017) Molecular phylogenetic analysis of "pirate spiders" (Araneae, Mimetidae) with the description of a new African genus and the first report of maternal care in the family. Cladistics 33(4): 375–405. https://doi.org/10.1111/cla.12174

Blagoev GA, deWaard JR, Ratnasingham S, deWaard SL, Lu LQ, Robertson J, Telfer AC, Hebert PDN (2016) Untangling taxonomy: a DNA barcode reference library for Canadian spiders. Molecular Ecology Resources 16(1): 325–341. https://doi.org/10.1111/1755-0998.12444

Čandek K, Kuntner M (2015) DNA barcoding gap: reliable species identification over morphological and geographical scales. Molecular Ecology Resources 15(2): 268–277. https://doi.org/10.1111/1755-0998.12304

Chen ZF, Zhang ZH (1991) Fauna of Zhejiang: Araneida. Zhejiang Science and Technology Publishing House, Hangzhou, 356 pp.

Coddington JA, Agnarsson I, Cheng R, Čandek K, Driskell A, Frick H, Gregorič M, Kostanjšek R, Kropf C, Kweskin M, Lokovšek T, Pipan M, Vidergar N, Kuntner M (2016) DNA barcode data accurately assign higher spider taxa. PeerJ 4: e2201. https://doi.org/10.7717/peerj.2201

Cutler B (1972) Notes on the biology of *Mimetus puritanus* Chamberlin (Araneae: Mimetidae). The American Midland Naturalist 87: 554–555. https://doi.org/10.2307/2423592

Gan JH, Mi XQ, Irfan M, Peng XJ, Ran S, Zhan Y (2019) Three new species of the genus *Mimetus* Hentz, 1832 (Araneae: Mimetidae) from Yunnan-Guizhou Plateau of China. European Journal of Taxonomy 525: 1–13. https://doi.org/10.5852/ejt.2019.525

Harms D, Harvey MS (2009a) A review of the pirate spiders of Tasmania (Arachnida, Mimetidae, *Australomimetus*) with description of a new species. Journal of Arachnology 37(2): 188–205. https://doi.org/10.1636/A08-35.1

Harms D, Harvey MS (2009b) Australian pirates: systematics and phylogeny of the Australasian pirate spiders (Araeae: Mimetidae), with a description of the Western Australian fauna. Invertebrate Systematics 23(3): 231–280. https://doi.org/10.1071/IS08015

Heimer S (1986) Notes on the spider family Mimetidae with description of a new genus from Australia (Arachnida, Araneae). Entomologische Abhandlungen, Staatliches Museum für Tierkunde Dresden 49: 113–137.

Hormiga G, Griswold CE (2014) Systematics, phylogeny, and evolution of Orb-weaving Spiders. Annual Review o f Entomology 59: 487–512. https://doi.org/10.1146/annurev-ento-011613-162046

Jackson RR, Whitehouse MEA (1986) The biology of New-Zealand and Queensland pirate spiders (Araneae, mimetidae) – aggressive mimicry, araneophagy and prey specialization. Journal of Zoology 210: 279–303. https://doi.org/10.1111/j.1469-7998.1986.tb03635.x

Khmelik VV, Kozub D, Glazunov A (2005) Helicon Focus version 3.10.3. https://www.heliconsoft.com/heliconsoft-products/helicon-focus/ [accessed on 2 May 2024]

Kloock CT (2001) Diet and insectivory in the "araneophagic" spider, *Mimetus notius* (Araneae: Mimetidae). American Midland Naturalist 146(2): 424–428. https://doi.org/10.1674/0003-0031(2001)146[0424:DAIITA]2.0.CO;2

Kloock CT (2012) Natural history of the pirate spider *Mimetus hesperus* (Araneae; Mimetidae) in Kern county, California. Southwestern Naturalist 57(4): 417–420. https://doi.org/10.1894/0038-4909-57.4.417

Liang TE, Wang JF (1991) A new species of spiders of the genus *Mimetus* in Xinjiang (Araneae: Mimetidae). Journal of August 1st Agricultural College 14(1): 61–62.

Liu JX, Xu X, Hormiga G, Yin HQ (2021a) New species of the pirate spider genus *Mimetus* Hentz, 1832 from China with a cladistic hypothesis on their phylogenetic placement (Araneae, Mimetidae). Zootaxa 5020(1): 1–30. https://doi.org/10.11646/zootaxa.5020.1.1

Liu JX, Xu X, Marusik YM, Yin HQ (2021b) Taxonomic notes on a pirate spider occurring in China (Araneae, Mimetidae). Zootaxa 4974(3): 565–576. https://doi.org/10.11646/zootaxa.4974.3.5

NCBI (2025) National Library of Medicine. The National Center for Biotechnology Information. https://www.ncbi.nlm.nih.gov/ [accessed on 19 January 2025]

Paik KY (1967) The Mimetidae (Araneae) of Korea. Theses collection of Kyungpook University, Korea, 11: 185–196.

Song DX, Li SQ (1997) Spiders of Wuling Mountains area. In: Song DX (Ed.) Invertebrates of Wuling Mountains Area, Southwestern China. Science Press, Beijing, 400–448.

Song DX, Zhu MS (1993) A new species of the genus *Mimetus* from China (Araneae: Mimetidae). Acta Zootaxonomica Sinica 18: 421–423.

Song DX, Zhu MS, Chen J (1999) The spiders of China. Hebei Science and Technology Publishing House, Shijiazhuang, 640 pp.

The People's Government of Guizhou Province (2022) A total of 24,547 species of organisms are known in our province, placing its species richness among the highest in the country. http://www.guizhou.gov.cn/home/gzyw/202205/t20220522_74159825.html [accessed on 12 November 2024]

Tyagi K, Kumar V, Kundu S, Pakrashi A, Prasad P, Caleb John TD, Chandra K (2019) Identification of Indian Spiders through DNA barcoding: Cryptic species and species complex. Scientific Reports 9(14033). https://doi.org/10.1038/s41598-019-50510-8

Wang JF (1990) Study on the spiders of family Mimetidae from south China (Arachnida: Araneae). Acta Zootaxonomica Sinica 15: 36–47.

Wang YB (2021) The Guizhou Model for Biodiversity Conservation. Contemporary Guizhou 43: 18–19.

Wang ZJ, Huang SH, Yao YB, Liu KK (2024) A new species of the genus Mimetus Hentz, 1832 from South China (Araneae: Mimetidae). Acta Arachnologica Sinica 33(2): 102–107. https://doi.org/10.1007/s13131-024-2451-3

WSC (2025) World Spider Catalog. version 25.5. Natural History Museum, Bern. http://wsc.nmbe.ch [accessed on 10 January 2025]

Xu YJ, Wang L, Wang JF (1987) A new species of the genus *Ero* from China (Araneae: Mimetidae). Journal of the Hangzhou Teachers College 1987(2): 65–67.

Xu X, Liu F, Chen J, Li D, Kuntner M (2015) Integrative taxonomy of the primitively segmented spider genus *Ganthela* (Araneae: Mesothelae: Liphistiidae): DNA barcoding gap agrees with morphology. Zoological Journal of the Linnean Society 175(2): 288–306. https://doi.org/10.1111/zoj.12280

Xu X, Liu F, Chen J, Kuntner M, Ono H, Li D (2017) Targeted sampling in Ryukyus facilitates species delimitation of the primitively segmented spider genus *Ryuthela* (Araneae: Mesothelae: Liphistiidae). Zoological Journal of the Linnean Society 181(4): 867–909. https://doi.org/10.1093/zoolinnean/zlx024

Yaginuma T (1960) Spiders of Japan in colour. Hoikusha, Osaka, 186 pp.

Yin CM, Peng XJ, Yan HM, Bao YH, Xu X, Tang G, Zhou QS, Liu P (2012) Fauna Hunan: Araneae in Hunan, China. Hunan Science and Technology Press, Changsha, 1590 pp.

Yoshida H (1993) A new species of the genus *Mimetus* (Araneae: Mimetidae) from the Ryukyus and Taiwan. Proceedings of the Japanese

Society of Systematic Zoology 49: 30–32. https://doi.org/10.2476/asjaa.30.21

Zeng C, Wang C, Peng XJ (2016) Three spider species of the genus *Mimetus* Hentz, 1832 (Araneae, Mimetidae) from China. ZooKeys 626: 125–135. https://doi.org/10.3897/zookeys.626.7918

Zeng C, Irfan M, Peng XJ (2019) First record of the spider genus *Phobetinus* (Araneae: Mimetidae) in China, with the description of a new species. Journal of Asia-Pacific Biodiversity 12(4): 674–677. https://doi.org/10.1016/j.japb.2019.09.003

Zhang JS, Yu H, Li SQ (2021a) Taxonomic studies on the sac spider genus *Clubiona* (Araneae, Clubionidae) from Xishuangbanna Rainforest, China. ZooKeys 1034: 1–163. https://doi.org/10.3897/zookeys.1034.59413

Zhang JS, Yu H, Li SQ (2021b) On the clubionid spiders (Araneae, Clubionidae) from Xishuangbanna, China, with descriptions of two new genera and seven new species. ZooKeys 1062: 73–122. https://doi.org/10.3897/zookeys.1062.66845

Zhao FF, Zhang XY, Liao LF, Nie SH (2021) Variation of soil moisture of its response to climate change in different geomorphological types of Guizhou province. Research of Soil and Water Conservation 28(6): 217–225.

Zhou J, Luo T, An J, Song LX, Lan CT, Yu J, Deng HQ, Xiao N (2023) Advances in amphibian research in Guizhou: A review of 36 years of amphibian diversity and systematic taxonomy. Journal of Guizhou Normal University (Natural Sciences) 41(4): 1–35.

Zoosyst. Evol. 101 (2) 2025, 735–760 | DOI 10.3897/zse.101.144918

PENSOFT

MUSEUM FÜR NATURKUNDE BERLIN

Hidden diversity of *Freyastera* (Asteroidea, Brisingida, Freyellidae) at great depth: Description of new species and remarks on species boundaries

Ruiyan Zhang[1,2], Yadong Zhou[1,2,3], Jingwen Mao[1,2], Chunsheng Wang[1,2,3,4], Dongsheng Zhang[1,2,3,4]

1 *State Key Laboratory of Submarine Geoscience, Second Institute of Oceanography, Ministry of Natural Resources, Hangzhou, 310012, China*
2 *Key Laboratory of Marine Ecosystem Dynamics, Second Institute of Oceanography, Ministry of Natural Resources, Hangzhou, 310012, China*
3 *Southern Marine Science and Engineering Guangdong Laboratory (Zhuhai), Zhuhai 519082, China*
4 *School of Oceanography, Shanghai Jiao Tong University, Shanghai, 200240, China*

https://zoobank.org/4611CD60-658B-42C4-B23C-2DA9185A85E3

Corresponding authors: Dongsheng Zhang (dszhang@sio.org.cn); Chunsheng Wang (wangsio@sio.org.cn)

Academic editor: Pavel Stoev ♦ **Received** 25 December 2024 ♦ **Accepted** 6 March 2025 ♦ **Published** 10 April 2025

Abstract

Freyastera represents the most derived form in the deep-sea starfish order Brisingida, known only at below 2500 m to over 6000 m depth, adapting to the great depth by small body size, reduced number of arms, and simplified body form. Long being remote and rarely investigated, newly collected specimens from the last decade revealed high species diversity of the genus. In this study, a new species, *Freyastera jiaolongi* **sp. nov.**, is described from the southern part of the Kyushu-Palau Ridge. *Freyastera giardi* **comb. nov.** and *Freyastera loricata* **comb. nov.**, formerly belonging to genus *Freyella*, are reassigned to *Freyastera*. The genus is hence revised to include ten species. Key characters of nine *Freyastera* species as well as *Freyella benthophila* (formerly *Freyastera benthophila*) are described and discussed based on an examination of type specimens and new specimens, and a key to *Freyastera* species is provided, aiding in the future identification of *Freyastera*. Phylogenetic analysis using four DNA barcoding genes retrieves a monophyletic *Freyastera*, providing solid support for interspecific phylogeny except at three nodes. Species delimitation analysis results in 11 species units within *Freyastera*, including seven unnamed species pending description. A high diversity of *Freyastera* revealed in the present study suggests a successful adaptation and radiation of the genus at great depth.

Key Words

Deep-sea, phylogeny, species delimitation, taxonomy

Introduction

Genus *Freyastera* Downey, 1986, belonging to the family Freyellidae, order Brisingida, is a group of starfish living exclusively in the deep ocean from lower bathyal to hadal depth. They were known at 2645 m the shallowest (NOAA Ocean Exploration 2024), to 6415 m the deepest (Zhang et al. 2019), being most diverse in the abyssal zone (4000 m to 6000 m) (Galkin and Korovchinsky 1984; Zhang et al. 2019). In contrast to other Brisingida species which possess numerous arms (up to 20), *Freyastera* displays only six long and slender arms with a small disk. A simplification of starfish morphology in relation to the great depth was considered as an adaptive strategy (Mironov et al. 2016) and may be owing to a paedomorphic development, which was also found in several other Brisingida species (Zhang et al. 2024). *Freyastera* is thus an ideal target to investigate the diversification and adaptation of fauna at great depth.

Freyastera was established by Downey in 1986, accommodating four species that were previously classified as *Freyella* Perrier, 1885. McKnight (2006), Zhang et al. (2019), and Zhang et al. (2024) further added three new species and revised the genus, resulting in a total of

seven nominal species of *Freyastera* (Mah 2025). It was once thought that all six-armed freyellids are close to and may belong to *Freyastera* (Mah 1998; Zhang et al. 2019). However, the latest study (Zhang et al. 2024) showed that *Freyastera benthophila* (Sladen, 1889), although having six arms and traditionally classified as *Freyastera* (Downey 1986), was genetically distinct from other *Freyastera* species. Phylogenetic analyses placed it in a clade formed by *Freyella* species, which all have more than six arms (Zhang et al. 2024). This indicated that the possession of six arms is not an autapomorphy of the *Freyastera* clade, and the number of arms should not be considered as the sole character to differentiate *Freyastera* and *Freyella*. *Freyastera benthophila* was reassigned as *Freyella* based on this result (Zhang et al. 2024). This finding has challenged the previous understanding of the boundaries of genera, and the taxonomic position of all the six-armed freyellids needs to be re-evaluated. Furthermore, the same research has provided genetic data of a large number of undescribed species that almost doubled the known diversity of *Freyastera*, but owing to the scope of that study, detailed taxonomic description and discussion of *Freyastera* species were not provided (Zhang et al. 2024).

In the present study, we present the systematic accounts on *Freyastera* and six-armed *Freyella* based on the dataset of Zhang et al. (2024) and additional specimens collected from the latest cruises. A new species, *Freyastera jiaolongi* sp. nov., is described, and two new species combinations are proposed. A diagnostic key and a phylogenetic tree for *Freyastera* species are provided, and boundaries among species using genetic and morphological evidence are investigated, aiding in the future identification of *Freyastera*.

Materials and methods

Sample collection and preservation

A total of 43 *Freyastera* specimens and 26 *Freyella benthophila* specimens were examined in the present study, of which 64 specimens were included in the dataset of Zhang et al. (2024). A majority of the specimens studied were loaned from the following institutes: German Centre for Marine Biodiversity Research, Senckenberg am Meer (DZMB), Institute of Deep-sea Science and Engineering, Chinese Academy of Sciences (IDSSE), P. P. Shirshov Institute of Oceanology, Russian Academy of Sciences (IORAS), Muséum national d'Histoire naturelle (MNHN), Musée Océanographique de Monaco (MOM), Natural History Museum (NHMUK), National Oceanography Centre (NOC), and Université Libre de Bruxelles (ULB). Five additional specimens were collected during Chinese cruises DY68 in 2021, DY80I in 2023, and DY86II in 2024 by HOV *Jiaolong* from the Northwest Pacific. These specimens were photographed on board using a digital camera (Canon EOS 7D), then fixed and preserved in pure ethanol. Collection information of all specimens studied is listed in Suppl. material 1.

Morphological examinations

Specimens were examined under a stereoscope (Zeiss Axio Zoom.V16) or a microscope. The following measurements were obtained for each specimen: r (radius of disk), R (distance between disc center and arm tip), height of disk (Hd), width of arm base (Wb), largest width of arm in genital area (Wg), and length of genital area (Lg). Morphological characters were examined and photographed, sometimes under dry conditions for better observation. Key characters for species delimitation mainly include the armature and spination of the abactinal disk and arm, the form and arrangement of spines on the oral plate and adambulacral plate, the size and arrangement of pedicellariae, the arrangement of inferomarginals and lateral spines, and the form of gonads. Description of species and characters follows Sladen (1889), Perrier (1885, 1894), Koehler (1907, 1908), A.H. Clark (1939), Madsen (1956), Korovchinsky and Galkin (1984), Downey (1986), McKnight (2006), Zhang et al. (2019), and Zhang et al. (2024).

Molecular phylogenetic analysis

DNA extraction, gene amplification, and sequencing procedures were as described in Zhang et al. (2024). Barcoding regions of the mitochondrial cytochrome *c* oxidase subunit I (COI), the mitochondrial 16S ribosomal RNA (16S), the mitochondrial 12S ribosomal RNA (12S), and the nuclear 28S ribosomal RNA (28S) were obtained for phylogenetic analyses and molecular species delimitation. Genetic data from *Freyella attenuata*, *Freyella benthophila*, and *Freyella echinata* published in Zhang et al. 2024, were used as an outgroup. Additional sequences obtained in the present study were submitted to the GenBank repository (see Suppl. material 1 for GenBank accession numbers). Sequences were aligned using the MUSCLE algorithm (Edgar 2004) implemented in Geneious Prime (Kearse et al. 2012). Alignment of 16S was cured in Gblocks 0.91b (Castresana 2000) under less stringent selection options. DAMBE 7 (Xia 2018) was used to test for substitution saturation in the protein-coding gene COI, and saturation was not detected.

Four gene alignments were concatenated, and partitions were set for each gene fragment and each codon position of COI. Phylogenetic trees were constructed using maximum likelihood (ML) and Bayesian inference (BI) methods. ModelFinder (Kalyaanamoorthy et al. 2017), implemented in IQ-TREE v2.0 (Minh et al. 2020), was used for the best model estimation. The following models were selected and used in maximum likelihood analysis: COI (1st codon site: TNe+I; 2nd codon site: F81+F+I; 3rd codon site: HKY+F+G4), 16S (HKY+F+I+G4), 12S (TIM2+F+I+G4), and 28S (HKY+F+I). Maximum likelihood analysis with 100,000 ultrafast bootstrap (Hoang et al. 2018) replicates was run in the IQ-TREE local server. Bayesian reconstruction was conducted using MrBayes v3.2.7 (Huelsenbeck and Ronquist 2001), with four parallel runs of 10,000,000 generations executed with four chains, sampling at every

1,000 generations. The first 25% of trees were discarded as burn-in. TRACER v. 1.7 (Rambaut et al. 2018) was used to check for run convergence. The tree topologies were observed and edited in Figtree v1.4.3.

Species delimitation and genetic distance

Species were delimited primarily based on morphological characters, and the molecular species delimitation tool Assemble Species by Automatic Partitioning (ASAP; Puillandre et al. 2021) was used as a validation method. ASAP uses pairwise genetic distances and a scoring system to define species groups. The Jukes-Cantor (JC69), Kimura (K80), and Simple Distance (p-distances) substitution models were selected on the ASAP web server (https://bioinfo.mnhn.fr/abi/public/asap/) for COI and 16S alignments. COI genetic distances (K2P, Kimura 1980) were calculated in MEGA 11 (Tamura et al. 2021).

Spatial distribution analyses

To evaluate the global and bathymetric distribution of *Freyastera* and closely related species, the coordinates and depth information of type specimens of *Freyastera* and six-armed *Freyella* species were compiled. Together with the information of the non-type specimens examined in the present study, a total of 77 records were used in spatial distribution analyses. The global distribution map was generated using QGIS 3.28.0-Firenze (QGIS Development Team 2024). A bathymetric distribution map was drawn using the R package ggplot2 (Wickham 2016) in RStudio 2023.09.1 (RStudio Team 2024).

Nomenclatural acts

The new names contained in this article are available under the International Code of Zoological Nomenclature. This work and the nomenclatural acts it contains have been registered in ZooBank. Zoobank Life Science Identifier (LSID) for this publication is: urn:lsid:zoobank.org:pub:4611CD60-658B-42C4-B23C-2DA9185A85E3. The LSID registration and any associated information can be viewed in a web browser by adding the LSID to the prefix http://zoobank.org/.

Results

Systematics

Order Brisingida Fisher, 1928
Family Freyellidae Downey, 1986

Genus *Freyastera* Downey, 1986

Type species. *Freyella sexradiata* Perrier, 1885.

Diagnosis. Arms six. Papulae absent. One pair of gonads on each arm. Disk very small, arms extremely long and slender. The first pair of inferomarginal plates appears later on arm, not in contact with the odontophore. Inferomarginal plates and lateral spines generally correspond to every adambulacral plate beyond genital area. Abactinal arm in genital region covered with pavement of spinate plates. Adambulacral plates elongated.

Remarks. *Freyastera* and *Freyella* were redefined by Zhang et al. (2024), with the number of arms and the arrangement of inferomarginal plates as key diagnostic characters. The genus *Freyastera* currently contains seven species (Mah 2025): *Freyastera basketa* Zhang et al., 2019; *Freyastera delicata* Zhang et al., 2019; *Freyastera digitata* McKnight, 2006; *Freyastera mexicana* (A.H. Clark 1939); *Freyastera mortenseni* (Madsen 1956); *Freyastera sexradiata* (Perrier 1885); and *Freyastera tuberculata* (Sladen 1889). A new species, *Freyastera jiaolongi* sp. nov., is described in the present study. Two species previously belonged to *Freyella*, *F. giardi* Koehler, 1907, and *F. loricata* Korovchinsky & Galkin, 1984, are reassigned here to *Freyastera* as new species combinations. The genus is hence composed of 10 species in total. Furthermore, seven unnamed species are included in the molecular analyses: *Freyastera* sp. 2, *Freyastera* sp. 3, *Freyastera* sp. 5, *Freyastera* sp. 6, *Freyastera* sp. 7, *Freyastera* sp. Yap, and *Freyastera* cf. *tuberculata*. Among them, precise identification of *Freyastera* sp. 2, *Freyastera* sp. 7, and *Freyastera* cf. *tuberculata* was not feasible, as they were morphologically similar to *Freyastera tuberculata*, *Freyastera giardi* comb. nov., and *Freyastera loricata* comb. nov. (see *Freyastera tuberculata* species complex). *Freyastera* sp. Yap (RSIOAST0041) was reported based on one broken arm (Zhang et al. 2019), whereas specimens of *Freyastera* sp. 3 (RSIOAST0057), *Freyastera* sp. 5 (RSIOAST0107, RSIOAST0116, RSIOAST0138) (Fig. 14F–G), and *Freyastera* sp. 6 (RSIOAST0124, RSIOAST0125) (Fig. 14H, I) were severely damaged during collection, with only arm fragments available, or kept frozen after collection, which hinders proper morphological identification and description. However, genetic information from these specimens showed high diversity, and species delimitation tools set them as seven species units, distinguishable from other known species with genetic data available. They were therefore included in the present study to discuss the phylogeny and diversity of *Freyastera*. Proper definition and description of these species units need to be done with more specimens in good condition in the future.

The following systematic accounts include a key, diagnoses, illustrations, and remarks on each known *Freyastera* species or species complex based on specimens or photos examined, except one species, *Freyastera digitata* McKnight, 2006. *F. digitata* was described to have an inferomarginal plate corresponding to every 2–3 adambulacral plates (McKnight 2006), but the holotype was broken with only 22 mm of arm left, thus the arrangement of inferomarginal plates beyond the genital area is largely unknown. This species greatly resembles

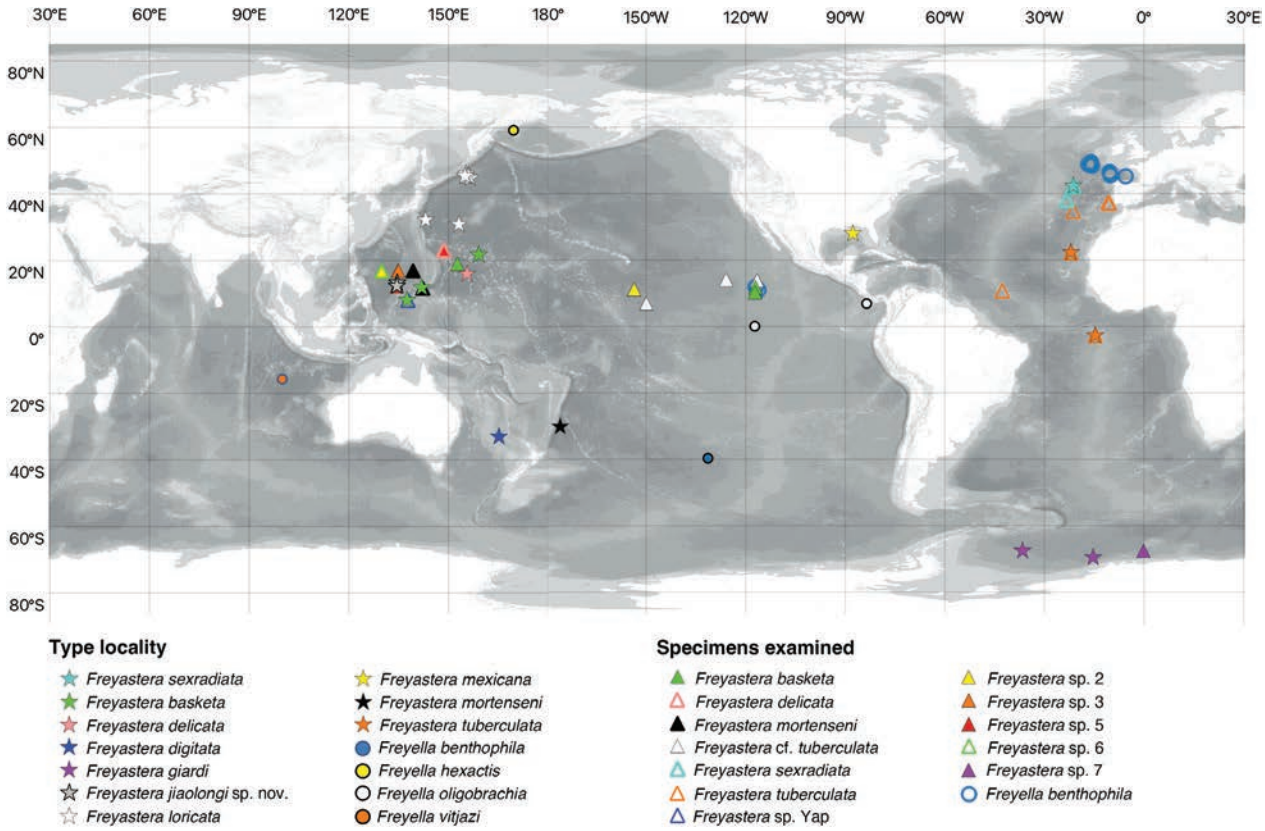

Figure 1. Distribution of *Freyastera* and six-armed *Freyella* specimens examined in the present study and type localities of each species.

Freyella benthophila in the absence of a furrow spine and abactinal plates with several short spinelets. The taxonomic position of *F. digitata* needs to be re-evaluated with further examination of the holotype and other complete specimens. It is thus not included in the diagnostic key of the genus for the time being.

Key to *Freyastera* species

1	large pedicellariae present on abactinal surface of disk and arm genital area, as well as on oral spines	2
–	large pedicellariae absent	3
2	abactinal plate on arm each with one spine	*F. basketa*
–	abactinal plate on arm each with multiple spines	*F. mortenseni*
3	abactinal plate on arm each with multiple spines, not covered by membranous sheath	4
–	abactinal plate on arm each with one spine, covered by membranous sheath	5
4	adambulacral spines 4–5, forming a diagonal row; oral spines 9–12	*F. mexicana*
–	adambulacral spines 2–3; oral spines 4	*F. delicata*
5	furrow spine absent	*F. giardi*/*F. loricata*/*F. tuberculata* (*F. tuberculata* species complex)
–	furrow spine present	6
6	abactinal disk with short spinelets, each surrounded by 2–6 small pedicellariae	*F. jiaolongi* sp. nov.
–	abactinal disk with fairly elongate spines, devoid of pedicellariae	*F. sexradiata*

***Freyastera jiaolongi* sp. nov.**

https://zoobank.org/316a8a05-1665-4602-aa2f-566281c4e451

Figs 2–4, 14A–C

Freyastera sp. 4: Zhang et al. 2024.

Material examined. *Holotype*. RSIOAST0117 (Figs 2, 3), Kyushu-Palau Ridge; 12.330671°N, 134.472114°E, 3523 m; 16 Nov. 2021; cruise DY68, dive JL199. ***Paratype* 1.** RSIOAST0112 (Fig. 3A, D), Kyushu-Palau Ridge; 13.309640°N, 134.591983°E, 3641 m; 13 Nov. 2021; cruise DY68, dive JL197. ***Paratype* 2.** RSIOAST0113 (Fig. 3B, C, E, F), Kyushu-Palau Ridge; 13.310851°N, 134.589032°E, 3541 m; 13 Nov. 2021; cruise DY68, dive JL197. All type specimens were deposited at the Repository of Second Institute of Oceanography, Ministry of Natural Resources, China (SIOMNR) (Suppl. material 1).

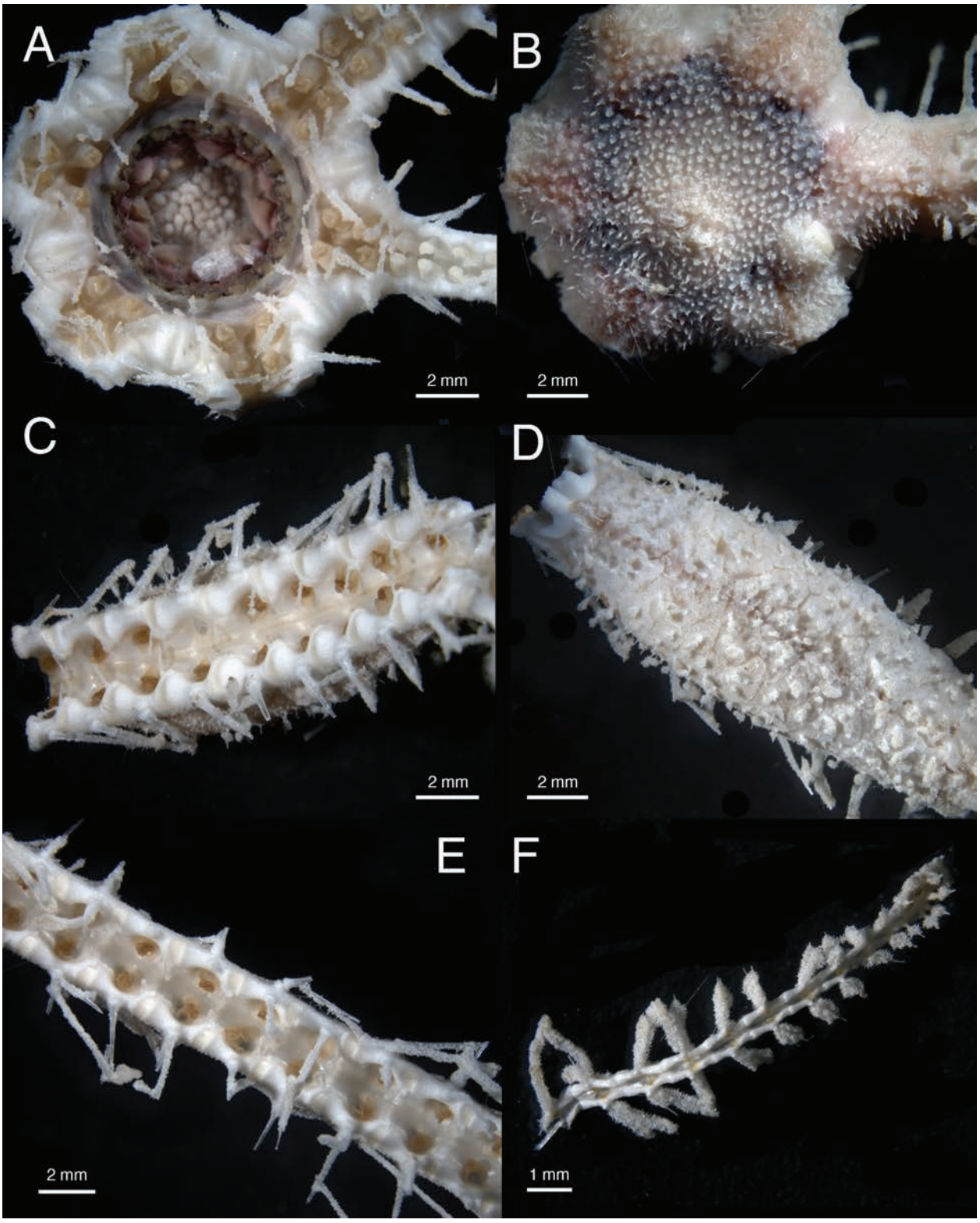

Figure 2. *Freyastera jiaolongi* sp. nov. holotype RSIOAST0117. **A.** Actinal view of disk; **B.** Abactinal view of disk; **C.** Actinal view of arm in genital area; **D.** Abactinal view of arm in genital area; **E.** Actinal view of middle part of arm; **F.** Actinal view of distal part of arm.

Diagnosis. Arms six. Abactinal disk with short hirsute spinelets, about 0.2 mm in length, surrounded by small pedicellariae. Abactinal arm plates each bears one spine, covered with a membranous sheath loaded with small pedicellariae. Pedicellariae on abactinal disk and arm less than 0.1 mm in length. Pedicellariae cluster in pads or transverse bands on abactinal arm beyond genital area. Each adambulacral plate with 1–3 aboral furrow spines and one subambulacral spine. Lateral spines long, corresponding to each adambulacral plate beyond genital area. Oral plate with 1–2 actinostomal spines, one suboral spine, and one aboral spine along the furrow margin.

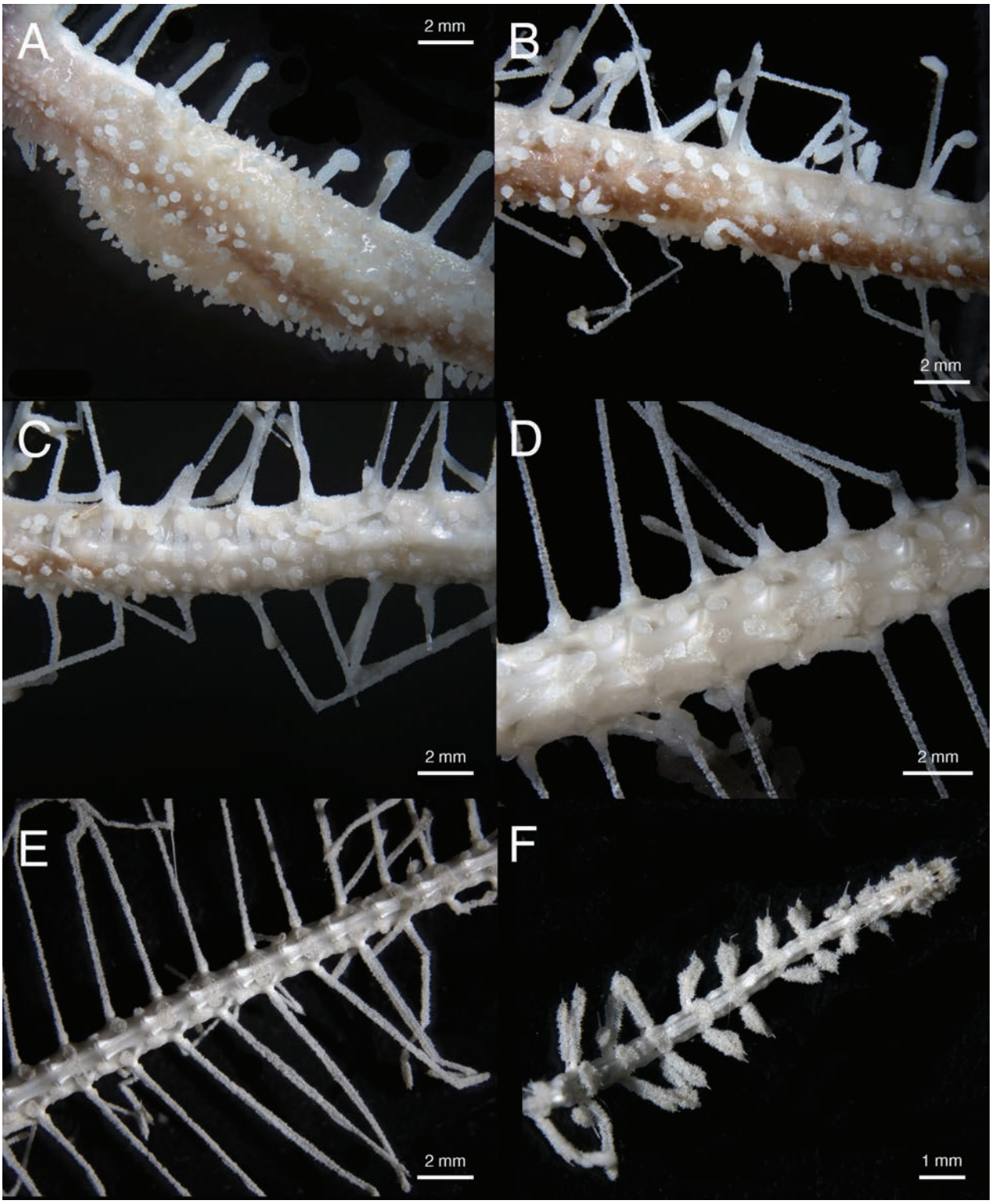

Figure 3. *Freyastera jiaolongi* sp. nov. holotype RSIOAST0117. **A–D.** Abactinal view of arm, from basal part to beyond genital area; **E.** Abactinal view of middle part of arm; **F.** Abactinal view of distal part of arm.

Description. Holotype: a complete specimen, with one arm regenerating. r = 5.5 mm, R about 220 mm. Height of disk 3.5 mm. Arm measures 4 mm at base, 6 mm at the widest part. Genital inflation extends about 13.5 mm. Female. Paratypes: RSIOAST0112 & RSIOAST0113, disks absent, seven detached arms mixed in one jar. Longest arm measures about 230 mm. Arm 4.1 mm wide at base, 4.7 mm at the widest part. Genital inflation extends about 16 mm. Female.

Abactinal surface of disk with small rounded plates, each with one short spinelet measuring about 0.2 mm in length (Fig. 2B). At the base of the spinelets is a circle of 2–6 small pedicellariae, less than 0.1 mm in length. Spinelets are more crowded and longer at center of the

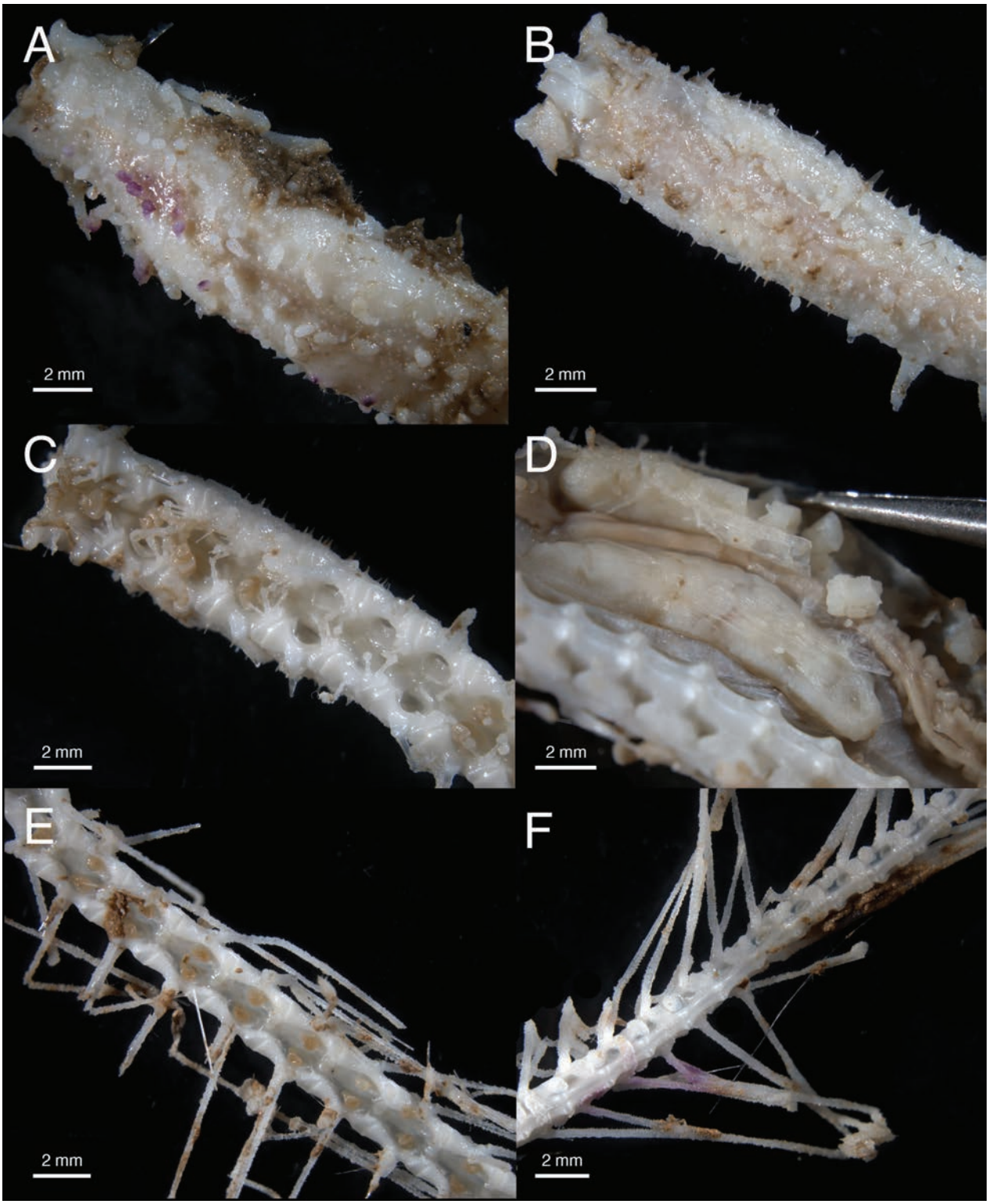

Figure 4. *Freyastera jiaolongi* sp. nov. paratypes. **A, D.** RSIOAST0112; **B, C, E, F.** RSIOAST0AS113. **A, B.** Abactinal view of arm in genital area; **C.** Actinal view of arm in genital area; **D.** Female gonads; **E.** Actinal view of middle part of arm; **F.** Abactinal view of middle part of arm.

disk, where the anus located but obscured by a cluster of spinelets. Madreporite with a subcentral cleavage, 1.3 mm in diameter, rather large and protruding, situated near the interradial margin of the disk above the odontophore. The surface of madreporite also covered with spinelets and small pedicellariae.

Basal part of arm with slight genital inflation. A pair of gonads to each arm. Female gonads encapsulated in a long sac, about 13 mm in length (Fig. 4D). Abactinal armature of arm in the genital area with irregular polygonal-shaped plates, much larger than those on disk (Fig. 2D). Each plate carries one short spine, about

0.5–0.8 mm in length, covered with a tegument loaded with minute pedicellariae (Figs 2D, 3A, 4A, B). A minority of larger plates carry two or even three spines. The surface of arm plates also scattered with small pedicellariae. The abactinal plates do not seem to go far beyond genital area. The spines become shorter at the end of genital area, sheathed with pedicellariae-covered tegument (Fig. 3B, C). Beyond genital area, the pedicellariae cluster in round tegumentary pads (Fig. 3D). At the distal part of the arm, pedicellariae pads or transverse bands occur alternately (Figs 3E, F, 4F).

Adambulacral plate narrow and elongated (Figs 2C, E, 4C). Each bearing one central subambulacral spine and 1–3 small aboral furrow spines. Furrow spines at the base of arm measure less than 1 mm in length, covered with a few scattered small pedicellariae and usually a tuft of pedicellariae at the tip. Furrow spines become fewer and smaller at middle to distal part of arm (Fig. 4E), then disappear. Subambulacral spines sheathed, covered with dense small pedicellariae. Subambulacral spines about 2–2.5 mm in length at base of arm, 4–5 mm at middle part of arm. The first inferomarginal plate occurs at about the 7th adambulacral plate, corresponding to alternate or every third adambulacral plate within the genital area and then to every adambulacral plate beyond about 20th adambulacrals. Inferomarginal plates each bear one long sheathed lateral spine, similar in form to subambulacral spines but much longer, about 20 mm in length at middle part of arm.

Oral plate with 3–4 spines in total (Fig. 2A). One or two actinostomal spines along the proximal margin of the plate, about 1 mm in length. One suboral spine, the most robust of all oral spines, 1.5–2 mm in length, situated not at the center of the plate but near the proximal-furrow margin. One aboral spine similar in size to the actinostomal spine, siting at the distal furrow margin of the plate. All mouth spines with pointed or obtuse tips, covered with minute pedicellariae.

A small crustacean skeleton found in the mouth of the holotype (Fig. 2A).

Etymology. Named after the Chinese manned submersible *Jiaolong* that collected all three specimens of the new species.

Distribution. Northwest Pacific: Kyushu-Palau Ridge. 3523–3641 m.

Remarks. The new species is morphologically most similar to the type species of the genus, *Freyastera sexradiata*, in the armature of abactinal arm plate, adambulacral plate, and oral plate. It differs from *F. sexradiata* mainly in the armature of abactinal disk. In *F. sexradiata* (r = 6 mm), the abactinal surface of disk bears "fairly elongated spines," and pedicellariae are absent from the disk (Perrier, 1894). In the new species (r = 5.5 mm), the abactinal surface of disk is equipped with small hirsute spinelets, about 0.2 mm in length, which are circled by numerous small pedicellariae. The two species are also geographically distant (Fig. 1). *F. sexradiata* is known from the North Atlantic, whereas the new species is distributed in the Kyushu-Palau Ridge in the Philippine Sea. Genetically, the new species is close to another undescribed species, *Freyastera* sp. 5 (COI distance 2.64%–3.52%). The latter was not described here as only fragmented arms were collected, but in these arm fragments, none of the adambulacral plates bear any furrow spines, which is distinguishable from the new species.

Freyastera sexradiata (Perrier, 1885)

Freyella sexradiata: Perrier 1885: 6; 1894: 89; Koehler 1909: 129; Grieg 1921: 30; Mortensen 1927: 129; Fisher 1928: 24; Madsen 1951: 84; Cherbonnier and Sibuet 1972: 1356; Korovchinsky and Galkin 1984: 1213 (in key); Galkin and Korovchinsky 1984: 167.

Freyellidea sexradiata: Fisher 1917: 429.

Freyastera sexradiata: Downey 1986: 40; Clark and Downey 1992: 481; Mah 1998: 87; Mah in Clark and Mah 2001: 318; Dilman 2014: 38; Zhang et al. 2019: 6 (in key).

Material examined. MNHN-IE-2014-165 (***holotype***). MOM-81 0428. (Suppl. material 1).

Diagnosis. Arms six. Abactinal disk plate, each with one fairly elongated spine. Pedicellariae absent on abactinal disk. Abactinal arm plates each bears one spine, covered with a membranous sheath loaded with small pedicellariae. Each adambulacral plate with one small aboral furrow spine and one subambulacral spine. Lateral spines corresponding to each adambulacral plate beyond genital area. Oral plate with two actinostomal spines, one suboral spine, and one aboral spine along the furrow margin.

Distribution. North Atlantic, 4020–5110 m. Type locality: Between the Azores and France, 4060 m.

Remarks. *F. sexradiata* is the type species of the genus. The holotype was examined in the present study, which demonstrates the key characters of the species as described by Perrier (1885, 1894), including having abactinal arm plate with one long spine, adambulacral plate with one subambulacral spine and one small aboral furrow spine, oral plate with two actinostomal spines, one suboral spine, and one aboral furrow spine. The arrangement of inferomarginal plates was not described in *F. sexradiata* (Perrier, 1885, 1894), and the holotype was too broken to be examined for such a character. Based on the drawings in Perrier (1894), the inferomarginal plates appear at each adambulacral plate beyond genital area. Another specimen examined (MOM-81 0428) also has continuous inferomarginal plates beyond genital area. The photos of the holotype of *F. sexradiata* are available on the MNHN collection website (holotype: https://science.mnhn.fr/institution/mnhn/collection/ie/item/2014-165).

Freyastera delicata Zhang et al., 2019

Figs 5, 14D

Freyastera delicata: Zhang et al. 2019: 2; Zhang et al. 2024: 10.

Material examined. RSIOAST0022 (***holotype***). RSIOAST0135 (Figs 5, 14D). (Suppl. material 1).

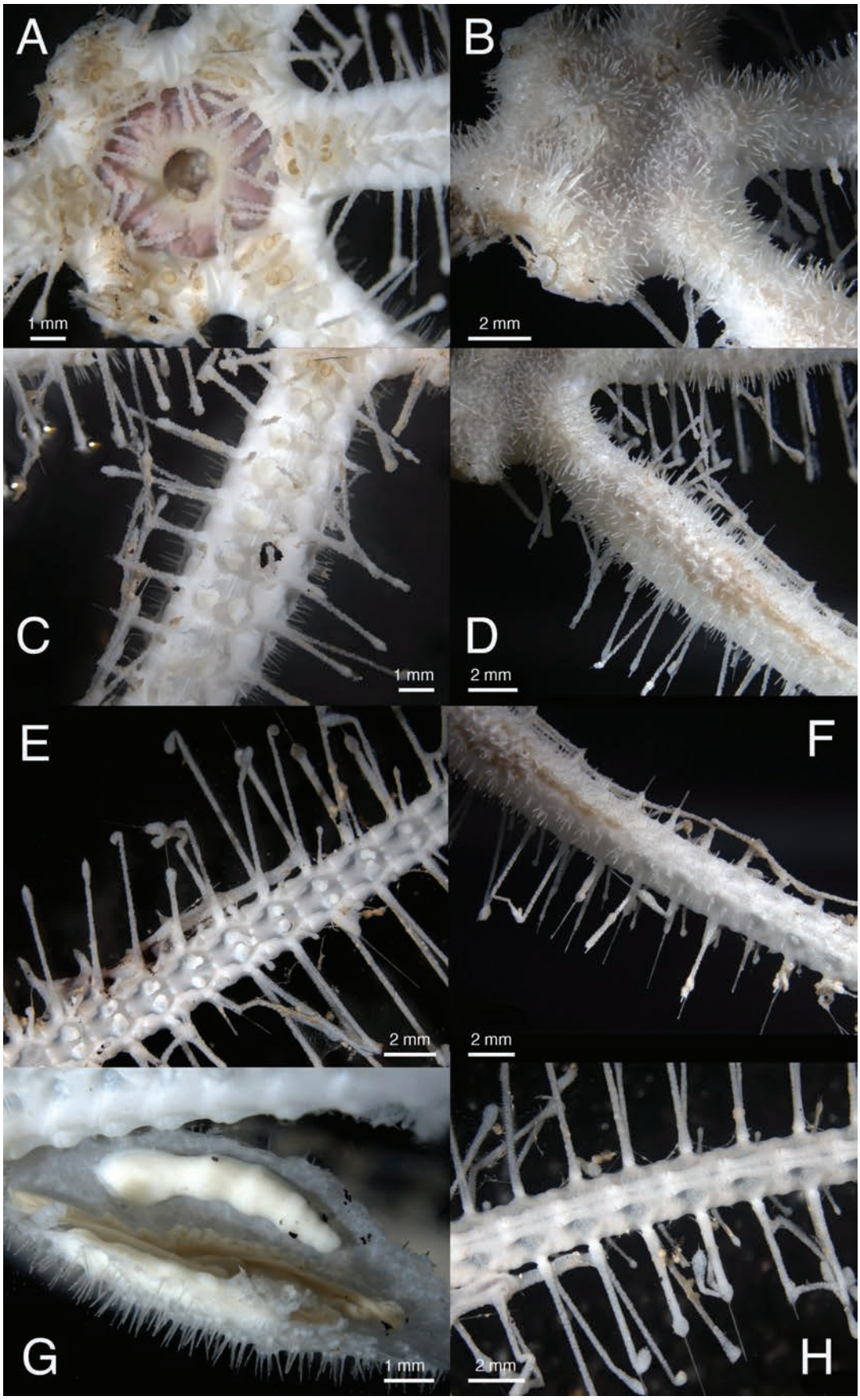

Figure 5. *Freyastera delicata* Zhang et al., 2019, RSIOAST0135. **A.** Actinal view of disk; **B.** Abactinal view of disk; **C.** Actinal view of arm genital area; **D.** Abactinal view of genital area; **E.** Actinal view of middle part of arm; **F.** Abactinal view of arm beyond genital area; **G.** Female gonads; **H.** abactinal view of middle part of arm.

Diagnosis. Arms six. Abactinal disk and arm plate each bears multiple spines (usually 4–8), most measuring 0.5–0.8 mm in length, not covered by membranous sheath. Pedicellariae absent on abactinal surface of disk and arm genital area. Pedicellariae cluster in transverse bands on abactinal arm beyond genital area. One long aboral spine and one subambulacral spine on each adambulacral plate. Proximal subambulacral spines with truncate end. Lateral spine corresponds to every adambulacral plate beyond genital area. Oral plate bears two actinostomal spines, one suboral spine, and one aboral furrow spine.

Distribution. Northwest Pacific: Caiwei Seamount, O-Hakucho Guyot, 3121–4322 m. Type locality: Caiwei Seamount, 4322 m.

Remarks. The species was described based on a single specimen (holotype RSIOAST0022) (Zhang et al. 2019). An additional specimen was examined in the present study, providing information on intraspecific variations of the species. The specimen RSIOAST0135 (Fig. 5) is smaller compared to the holotype, with maximum R = 135 mm, r = 4.1 mm, R/r ≈ 33. The arm measures 3.5 mm wide at the base, whereas the widest part of arm measures 4.6 mm. The genital area is about 9.5 mm in length. Gonads well-developed, female (Fig. 5G). Abactinal arm spines slightly longer than those in the holotype, but not aligned in transverse rows as in the holotype (Fig. 5D). The new specimen shares other characters with the holotype, including having no trace of pedicellariae on abactinal disk and genital area (Fig. 5B, D), mouth plate with two actinostomal spines, one suboral spine, and one aboral furrow spine (Fig. 5A), adambulacral plate with one subambulacral spine and one aboral spine pointing upwardly (Fig. 5C, E), abactinal arm plate with several spines, and arm beyond genital area with transverse bands of pedicellariae (Fig. 5H). The new specimen was found at 3121 m depth from O-Hakucho Guyot, close to the type locality (Fig. 1), but is 1201 m shallower than the depth of the holotype (4322 m).

Freyastera basketa Zhang et al., 2019

Figs 6, 14E

Freyastera basketa: Zhang et al. 2019: 4; Zhang et al. 2024: 2,

Material examined. RSIOAST0038 (***holotype***). RSIOAST0006 (***paratype***); RSIOAST0008 (***paratype***); RSIOAST0039 (***paratype***). RSIOAST0200 (Figs 6A–F, 14E); RSIOAST0201 (Fig. 6 G, H); NHMUK 8963; SO268-2_174_116. (Suppl. material 1).

Diagnosis. Arms 6. Abactinal disk and arm plate each bears one long, sharp spine, about 1 mm in length, not covered by membranous sheath. Enlarged pedicellariae (about 0.3–0.5 mm in length) with curved valves present on oral spines and abactinal surface of disk and arm genital area. Small pedicellariae (less than 0.2 mm in length) cluster in transverse bands on abactinal arm beyond genital area. One aboral furrow spine and one subambulacral spine on each adambulacral plate. Proximal subambulacral spines with truncate end. One lateral spine corresponding to every adambulacral plate beyond genital area. Oral plate bears one actinostomal spine, one suboral spine, and one furrow spine, all covered by large pedicellariae.

Distribution. Northwest Pacific: Mariana Trench, Yap Trench, Lamont Seamount, Pigafetta Basin; Eastern Pacific: Clarion-Clipperton Zone (CCZ). 4137–4991 m. Type locality: Mariana Trench, Yap Trench, Lamont Seamount, 4798–4991 m.

Remarks. This species is characterized by having enlarged pedicellariae with curved valves on oral spines and abactinal surface of disk and arm genital area (Fig. 6A, B, G), and one long, unsheathed spine on each abactinal arm plate. In some specimens, the proximal adambulacral spines are also equipped with large pedicellariae. The large pedicellariae are found in other Brisingida species, such as *Freyella macropedicellaria* Korovchinsky & Galkin, 1984; *Freyella remex* Sladen, 1889; and *Astrocles japonicus* (Korovchinsky 1976), as well as *Freyellaster* species (Zhang et al. 2024). In *Freyastera*, only *F. basketa* and *F. mortenseni* were found to have large pedicellariae. *F. basketa* has rather long, sharp spines on abactinal disk and arms, one to each plate, whereas *F. mortenseni* has several spines on each plate. Furthermore, *F. mortenseni* was reported at greater depth (5850 to 6200 m) than *F. basketa* (4137 to 4991 m). The newly examined specimens extend the distribution range of *F. basketa* to CCZ in the Eastern Pacific (Fig. 1).

Freyastera mortenseni (Madsen, 1956)

Fig. 7

Freyella mortenseni: Madsen 1956: 29; Korovchinsky and Galkin 1984: 1213 (in key); Galkin and Korovchinsky 1984: 166; Mah in Clark and Mah 2001: 322.

Freyastera mortenseni: McKnight 2006: 81; Zhang et al. 2019 (in key); Mah 2022: 15.

Material examined. RSIOAST0102 (Fig. 7); IDSSE-EEB-HX02. (Suppl. material 1).

Diagnosis. Arms 6. Abactinal disk scattered with long, sharp spines. Abactinal arm plates with 1–5 (usually 2–4) spines of similar size and form with those on disk, not covered by membranous sheath. Abactinal arm plates and spines extend beyond genital area. Enlarged pedicellariae (about 0.5 mm in length) with curved valves present on oral spines, proximal adambulacral spines, abactinal surface of disk, and arm genital areas. Small pedicellariae (about 0.1 mm in length) cluster in transverse bands on abactinal arm beyond genital area. Proximal adambulacral plates with one subambulacral spine, one aboral spine, and one furrow spine in a diagonal row. Proximal subambulacral spines with truncate end. Oral plate with one actinostomal spine, one suboral spine, and one aboral furrow spine.

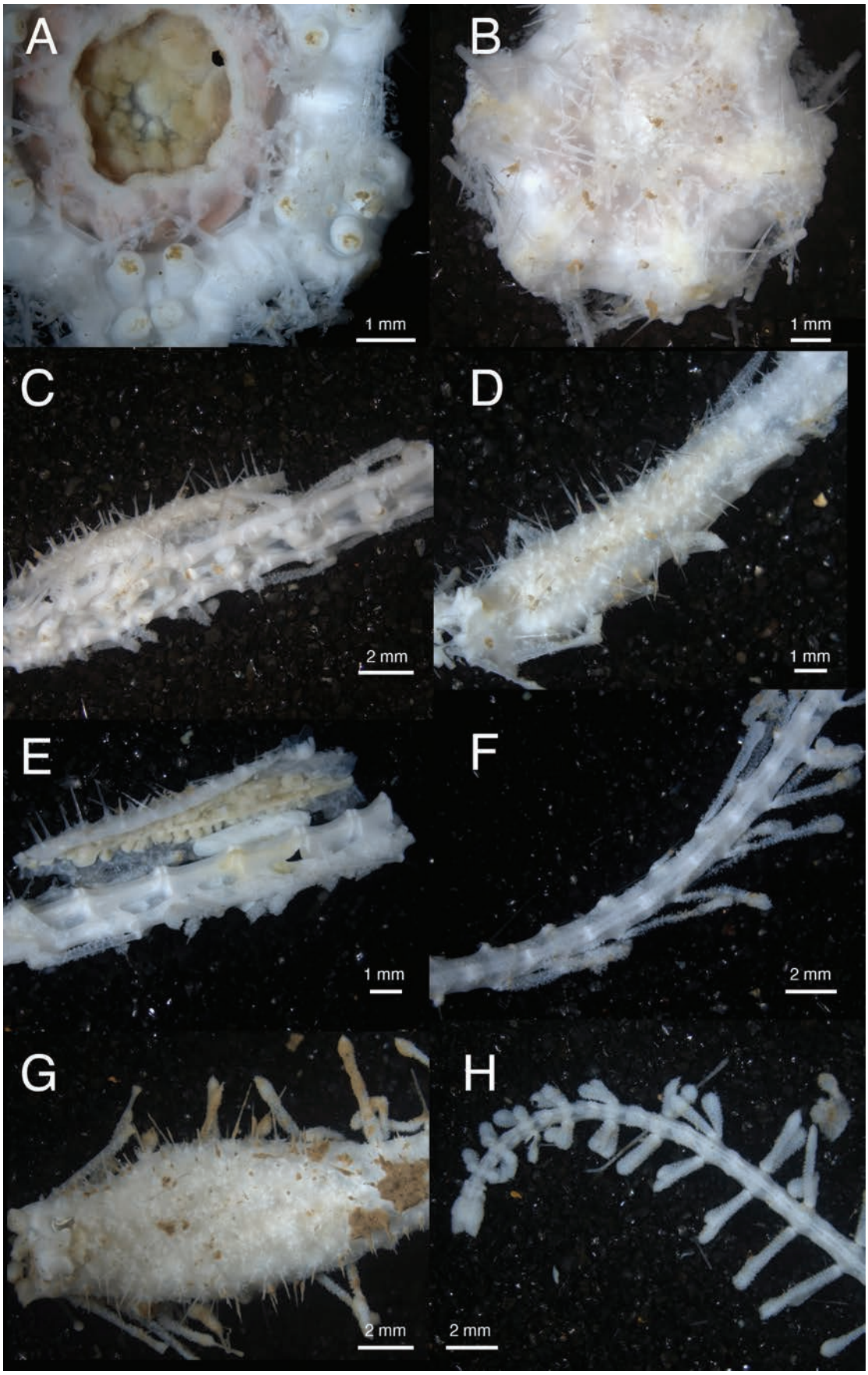

Figure 6. *Freyastera basketa* Zhang et al., 2019. **A–F.** RSIOAST0200; **G–H.** RSIOAST0201. **A.** Actinal view of disk; **B.** Abactinal view of disk; **C.** Actinal view of arm genital area; **D.** Abactinal view of genital area; **E.** Female gonad; **F.** Abactinal view of distal part of arm; **G.** Actinal view of arm genital area; **H.** Distalmost part of arm.

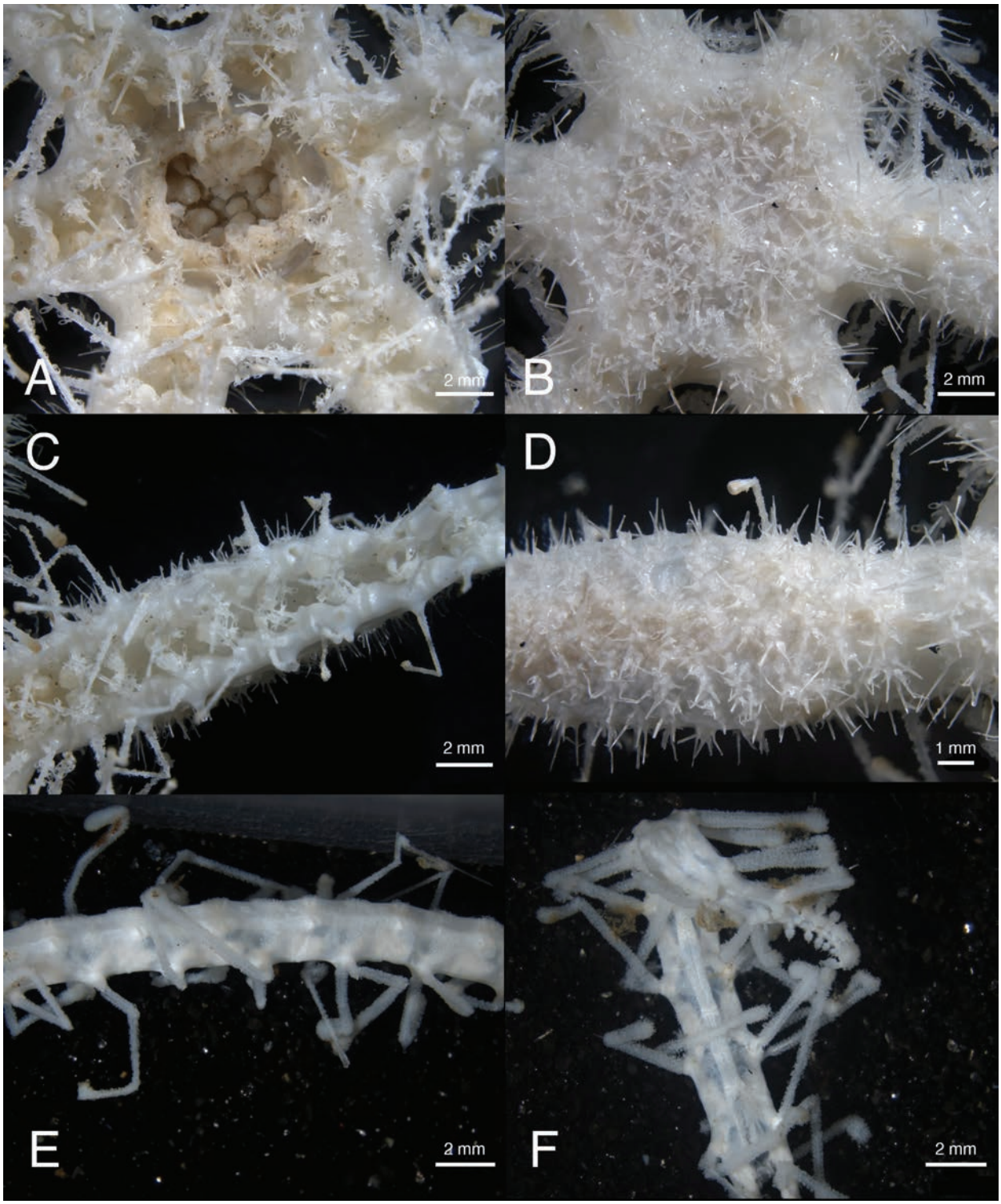

Figure 7. *Freyastera mortenseni* Madsen, 1956, RSIOAST0102. **A.** Actinal view of disk; **B.** Abactinal view of disk; **C.** Actinal view of arm genital area; **D.** Abactinal view of arm genital area; **E.** Abactinal view of middle part of arm; **F.** Distalmost part of arm, tip regenerating.

Distribution. Southwest Pacific: Kermadec Trench; Northwest Pacific: Mariana Trench, Parece Vela basin. 5850–6200 m. Type locality: Kermadec Trench, 5850 m.

Remarks. *F. mortenseni* is characterized by the presence of large pedicellariae on abactinal disk and arm genital area, as well as on oral spines and proximal adambulacral spines (Fig. 7A, B, D). The adambulacral plate of the species carries one subambulacral spine and two aboral spines in an oblique row (Fig. 7C). Beyond genital area, the large pedicellariae are absent; instead, small pedicellariae form transverse bands (Fig. 7E, F). This species is morphologically and phylogenetically close to *F. basketa* (Fig. 12), which also possesses large pedicellariae. The newly examined specimens extend the geographical and depth range of *F. mortenseni*, representing one of the deepest occurrences of *Freyastera*. *F. mortenseni* was also reported in the American Samoa region at 3770 m depth (Mah 2022). However, based on the photos of the specimen investigated

(Mah 2022, Fig. 4C), the large pedicellariae were not present on the oral spines. This specimen, with 1–4 (usually 2–3) sharp spinelets on abactinal plate, three adambulacral spines in a diagonal row, absence of large pedicellariae (based on photo and description), and presence of small pedicellariae on abactinal plates, is potentially a new species that is close to *F. mortenseni* and *F. delicata*.

Freyastera mexicana (A.H. Clark, 1939)

Freyella mexicana: A.H. Clark 1939: 442; Korovchinsky and Galkin 1984:1213 (in key).

Freyastera mexicana: Downey 1986: 38; Clark and Downey 1992: 481; Mah 1998: 87; Mah in Clark and Mah 2001: 318; Pawson et al. 2009: 1191; Zhang et al. 2019 (in key).

Diagnosis (revised from A.H. Clark 1939). Arms six. Abactinal disk plate, each with a single spinelet. Genital region uniformly covered with larger plates, each with usually 2–4 similar spinelets, more or less in a transverse series. Pedicellariae numerous on disk and arms. Each mouth plate with 9–12 spines. First two adambulacral plates united by syzygy. Proximal adambulacrals with a diagonal row of 4 or 5 spines.

Distribution. Only known at type locality: Gulf of Mexico, 2683 m.

Remarks. No specimens of *Freyastera mexicana* were examined in the present study. However, the high-resolution photos of the holotype (USNM E 5602) are available on the collection website of the National Museum of Natural History, US (https://collections.nmnh.si.edu/), allowing for a rough observation of some important characters. The species has a few peculiar characters as described by A.H. Clark (1939), including having a "small unpaired interradial plate between the upper ends of the mouth plates of each pair," the first two adambulacral plates united by syzygy, and a high number of oral spines (9–12). These characters are not common in *Freyastera* or even Freyellidae. Judging from the photos of the holotype, the specimen is generally *Freyastera*-like. Although A.H. Clark noted that the species resembles *Colpaster scutigerula* Sladen, 1889, the most, it does not have the same "interradial plate" (actually inferomarginal plate; see Zhang et al. 2024) inserting in between the mouth plates as in *C. scutigerula*. The oral spines do not seem to be as numerous as described, but this could be owing to damages during examination and long-time preservation. This species resembles *F. delicata* the most but differs from the latter by having numerous small pedicellariae on abactinal disk and arms, as well as having more spines on oral and adambulacral plates. Furthermore, the "syzygy" between the first and second adambulacral plates seems to be obvious from the photos. This structure, redefined as a "partial fusion" by Zhang et al. (2024), was thought to be a character only present in Brisingidae and Brisingasteridae. The nature of such a structure observed in *F. mexicana* needs to be further evaluated to be compared with the partial fusion found in Brisingidae and Brisingasteridae.

Freyastera tuberculata species complex

Diagnosis of the species complex. Arms six. Abactinal disk and arm plate each bears one spine, covered with a membranous sheath loaded with small pedicellariae. Abactinal arm plates extend beyond genital area to over middle part of the arm. Beyond that, small pedicellariae cluster in pads or transverse bands. All pedicellariae small (less than 0.2 mm in length). Adambulacral plate with one subambulacral spine only, furrow spine absent, except in one specimen of *F. giardi*, a few proximal plates with one furrow spine (see Remarks). Oral plate usually with one actinostomal spine and one suboral spine. An additional actinostomal spine and/or aboral spine along the furrow margin may present.

Remarks. The *Freyastera tuberculata* species complex discussed herein includes three known species, *Freyastera giardi* comb. nov., *Freyastera loricata* comb. nov., and *Freyastera tuberculata*, and three undescribed species, *Freyastera* cf. *tuberculata, Freyastera* sp. 2, and *Freyastera* sp. 7.

F. giardi and *F. loricata*, which used to be classified as *Freyella*, are reassigned here to *Freyastera*, as they have inferomarginal plates generally corresponding to every adambulacral plate beyond genital area (Koehler 1908; Korovchinsky and Galkin 1984). They also show similar morphological characters with *F. tuberculata*, which are distinctive from the other *Freyastera* species. These characters include: 1) abactinal disk and arm plate each bear one spine, sheathed and covered with small pedicellariae (Figs 8A, C, 9A, C, E, G); 2) abactinal arm plate extends beyond genital area to over middle part of the arm (Figs 8E, 9I); 3) adambulacral plate absent of furrow spine (only a few proximal plates with one furrow spine in *F. giardi*) (Figs 8F, 9D, H); 4) large pedicellariae absent. It needs to be noted that, in the four syntype specimens of *F. giardi*, only one specimen has furrow spines at a few proximal adambulacral plates (Fig. 8F) (also noted by Koehler 1908). In the other syntype specimens, the furrow spine is absent. The presence of a few furrow spines in one of the syntypes might be an abnormality. As noted by Korovchinsky and Galkin (1984), *F. loricata* is differentiated from *F. tuberculata* in the abactinal coating of arms consisting of plates of irregular shape (rather than hexagonal), the length of the abactinal spines (0.5–0.7 mm instead of 1.25 mm), and the smaller length of the adambulacral plates. However, these differences seem to be trifling, and re-examination of the types shows that the length of abactinal spines in the two species is not much different (Fig. 9A, E). Based on the original descriptions and specimens examined, the three species have rather indistinctive morphological differences and thus are considered here as a species complex. On the other hand, the three species were known from different oceans. *F. tuberculata* was described from the Atlantic; *F. giardi* was known from the Atlantic side of the Southern Ocean; and *F. loricata* was found in the Northwest Pacific near the Kuril-Kamchatka Trench (Fig. 1). Such a great geographical distance may

support them as different species, but to understand the morphological variations among them, more specimens preserved in good conditions need to be studied.

Furthermore, several newly collected specimens examined in the present study were found to have similar morphological characters to the three species above. These include five specimens identified as *Freyastera* cf. *tuberculata* from CCZ (Glover et al. 2016; Amon et al. 2017; Bribiesca-Contreras et al. 2022), a specimen identified as *Freyastera tuberculata* from the Southern Ocean (Moreau et al. 2015, 2018) (here referred to as *Freyastera* sp. 7), and two specimens temporarily named *Freyastera* sp. 2 from CCZ (Bribiesca-Contreras et al. 2022) and the Philippine Sea. *Freyastera* sp. 7 was collected near the type locality of *F. giardi* in the Southern Ocean (Fig. 1), but with only arm fragments, hindering a proper comparison of it with other species. *Freyastera* cf. *tuberculata* and *Freyastera* sp. 2 are genetically close (COI distance 2.73%–3.78%) and were collected from close sites in the CCZ (Fig. 1). A close examination of the specimens fails to identify clear, distinctive morphological differences. As noted by Bribiesca-Contreras et al. (2022), the abactinal disk spines of *Freyastera* cf. *tuberculata* seem to be shorter than those in *Freyastera* sp. 2 (Fig. 10). Although species delimitation results based on genetic data indicate that they should be considered as separate species, more subtle morphological characters or inner skeleton characters need to be examined to know the morphological differences between *Freyastera* cf. *tuberculata* and *Freyastera* sp. 2, which in turn will help to set the boundaries among the species in the *F. tuberculata* species complex.

Freyastera giardi (Koehler, 1907), comb. nov.

Fig. 8

Freyella giardi: Koehler 1907: 145; 1908: 242; Fisher 1940: 75; A.M. Clark 1962: 68; Korovchinsky and Galkin 1984: 1213 (in key); Mah 1998: 89; Mah in Clark and Mah 2001: 321; Moreau et al. 2015: 8; Moreau et al. 2018: 147; Zhang et al. 2019: 6 (in key).

Material examined. NHMUK 1912.11.11.30 (***syntype***) (Fig. 8A–E); MNHN-IE-2014-463 (***syntype***) (Fig. 8F); MOM-INV-0021953 (***syntype***). (Suppl. material 1).

Remarks. *Freyella giardi* was first proposed by Koehler (1907) and described in detail later by the same author (Koehler 1908). As a six-armed species, Koehler (1908) remarked upon its affinity to *F. sexradiata* but did not compare it with *F. tuberculata*. According to the original description and examination of the syntypes, this species has inferomarginal plates and lateral spines generally corresponding to every adambulacral plate beyond genital area. Based on this character and many other characters that *F. giardi* shared with *F. tuberculata* as discussed above, we reassign this species as *Freyastera giardi* comb. nov.

Distribution. Only known at type locality. Weddle Sea. 4572–4791 m.

Freyastera loricata (Korovchinsky & Galkin, 1984), comb. nov.

Fig. 9A–D

Freyella loricata: Korovchinsky and Galkin 1984: 1208; Galkin and Korovchinsky 1984: 167; Mah 1998: 90; Mah in Clark and Mah 2001: 322; Zhang et al. 2019: 7 (in key).

Material examined. ECH00161 (***paratype***) (Fig. 9A–D). (Suppl. material 1).

Remarks. *Freyella loricata* was described based on multiple individuals collected from east of the Kuril-Kamchatka Trench (Korovchinsky and Galkin 1984). Same as *F. giardi*, this species was traditionally classified as *Freyella* but has many shared characters with *Freyastera*, especially with *F. tuberculata*. It has inferomarginal plates and lateral spines that begin at the 7th adambulacral plate, appear at alternate adambulacral plates, and then at every adambulacral plate (Korovchinsky and Galkin 1984); thus, we reassign this species as *Freyastera loricata* comb. nov.

Distribution. Only known at type locality. East of the Kuril-Kamchatka Trench. 4995–5998 m.

Freyastera tuberculata (Sladen, 1889)

Fig. 9E–I

Freyella tuberculata: Sladen 1889: 638; Alcock 1893: 121; Mortensen 1927: 129; Korovchinsky and Galkin 1984: 1214 (in key); Galkin and Korovchinsky 1984: 167.

Freyellidea tuberculata: Fisher 1917: 429; H. L. Clark 1920: 113.

Freyastera tuberculata: Downey 1986: 41; Clark and Downey 1992: 482; Mah 1998: 78; Mah in Clark and Mah 2001: 319; Moreau et al. 2015: 8; Moreau et al. 2018: 147; Zhang et al. 2019: 7 (in key).

Material examined. NHMUK 1890.5.7.1076 (***syntype***) (Fig. 9E–I); NHMUK 1890.5.7.1077 (***syntype***).

Other material. MNHN-IE-2008-1363; MNHN-IE-2017-1819; MNHN-IE-2019-5479; MNHN-IE-2019-5743; MNHN-IE-2019-5745. (Suppl. material 1).

Distribution. Atlantic Ocean; Eastern Pacific; Indian Ocean; Bay of Bengal. 3365–5180 m. Type locality: Atlantic Ocean: between Canary Islands and Cape Verde Islands; between the coast of Africa and the Island of Ascension. 4298–4390 m.

Freyastera cf. *tuberculata*

Freyastera cf. *tuberculata*: Bribiesca-Contreras et al. 2022: 42.

Freyastera cf. *benthophila*: Glover et al. 2016: 17; Amon et al. 2017: 9; GenBank (NHM_413: KU519535; KU519518; KU519550; KU519551).

Material examined. NHMUK 2022.79 (CCZ_087); NHMUK 2022.80 (CCZ_157); NHMUK 9120; NHM_413; SO268-1_64_074. (Suppl. material 1).

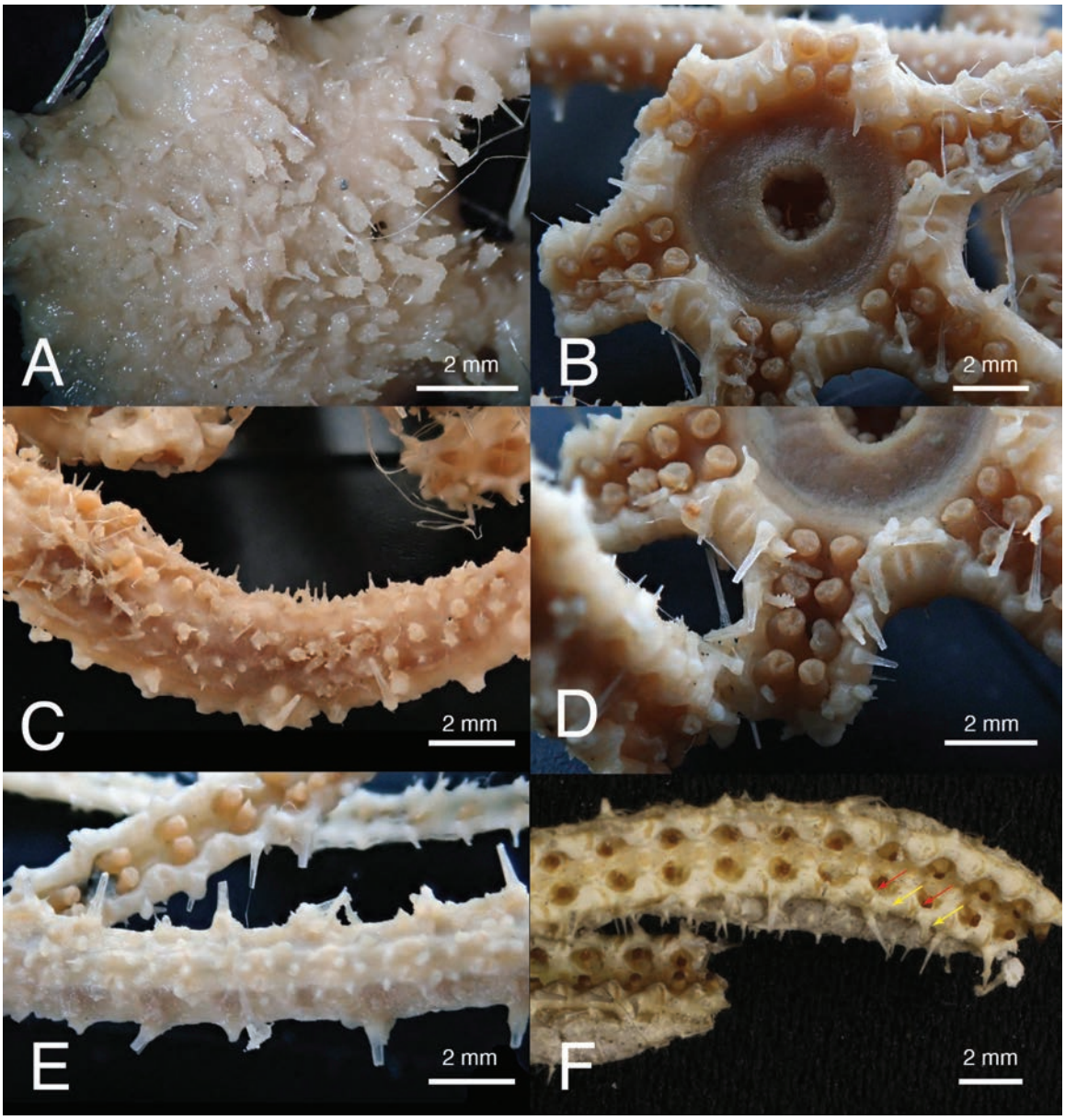

Figure 8. *Freyastera giardi* (Koehler, 1907) type specimens. **A–E.** NHMUK 1912.11.11.30; **F.** MNHN-IE-2014-463. **A.** Abactinal view of disk; **B.** Actinal view of disk; **C.** Abactinal view of arm genital area; **D.** Actinal view of disk and proximal part of arm; **E.** Abactinal view of middle part of arm; **F.** Actinal view of proximal part of arm. Yellow arrows show subambulacral spines; red arrows show aboral furrow spines.

Distribution. Eastern Pacific: Clarion-Clipperton Zone. 4011–5000 m.

Freyastera sp. 2

Fig. 10

Freyastera stet. CCZ_201: Bribiesca-Contreras et al. 2022: 44.

Material examined. NHMUK 2022.81 (Fig. 10 A, B, F) (*Freyastera* stet. CCZ_201); RSIOAST0103 (Fig. 10C–E). (Suppl. material 1).

Distribution. Eastern Pacific: Clarion-Clipperton Zone; Northwest Pacific: Western Philippine Basin. 5204–5900 m.

Freyastera sp. 7

Freyastera tuberculata: Moreau et al. 2015; Moreau et al. 2018.

Material examined. ULB_S59-MT2, multiple broken arms from different individuals. (Suppl. material 1).

Distribution. Weddle Sea, 4648 m.

Genus *Freyella* Perrier, 1885

Type species. *Freyella spinosa* Perrier, 1885, now regarded as a synonym of *Freyella elegans* (Verrill, 1884).

Diagnosis. Arms 6–15. Papulae absent. One pair of gonads on each arm. The first pair of inferomarginal

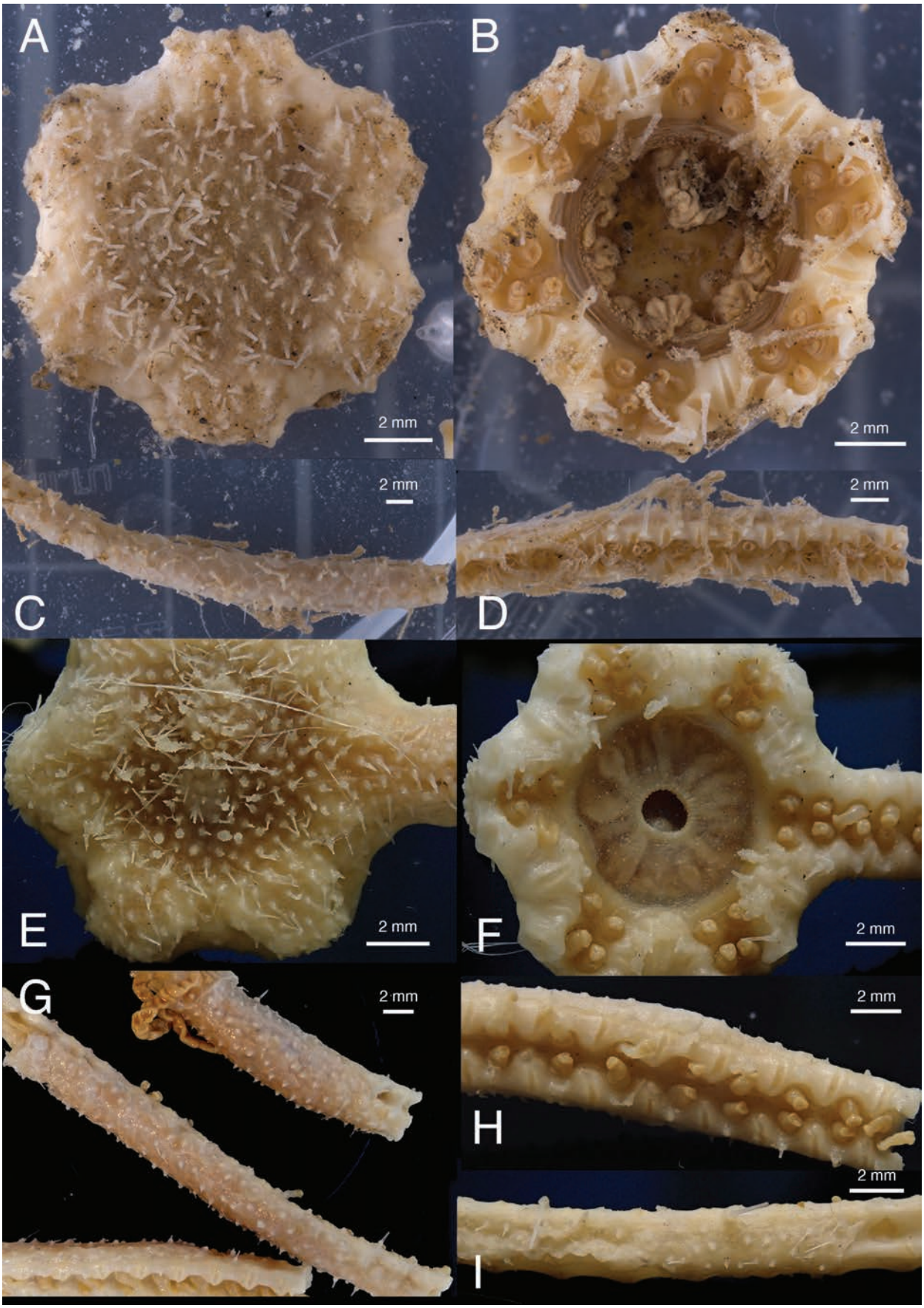

Figure 9. A–D. *Freyastera loricata* (Korovchinsky & Galkin, 1984) type ECH00161 (photos courtesy of Dr. Anna Dilman); **E–I.** *Freyastera tuberculata* (Sladen, 1889) type NHMUK 1890.5.7.1076. **A, E.** abactinal view of disk; **B, F.** Actinal view of disk; **C. G.** Abactinal view of arm genital area; **D, H.** Actinal view of proximal part of arm; **I.** abactinal view of middle part of arm.

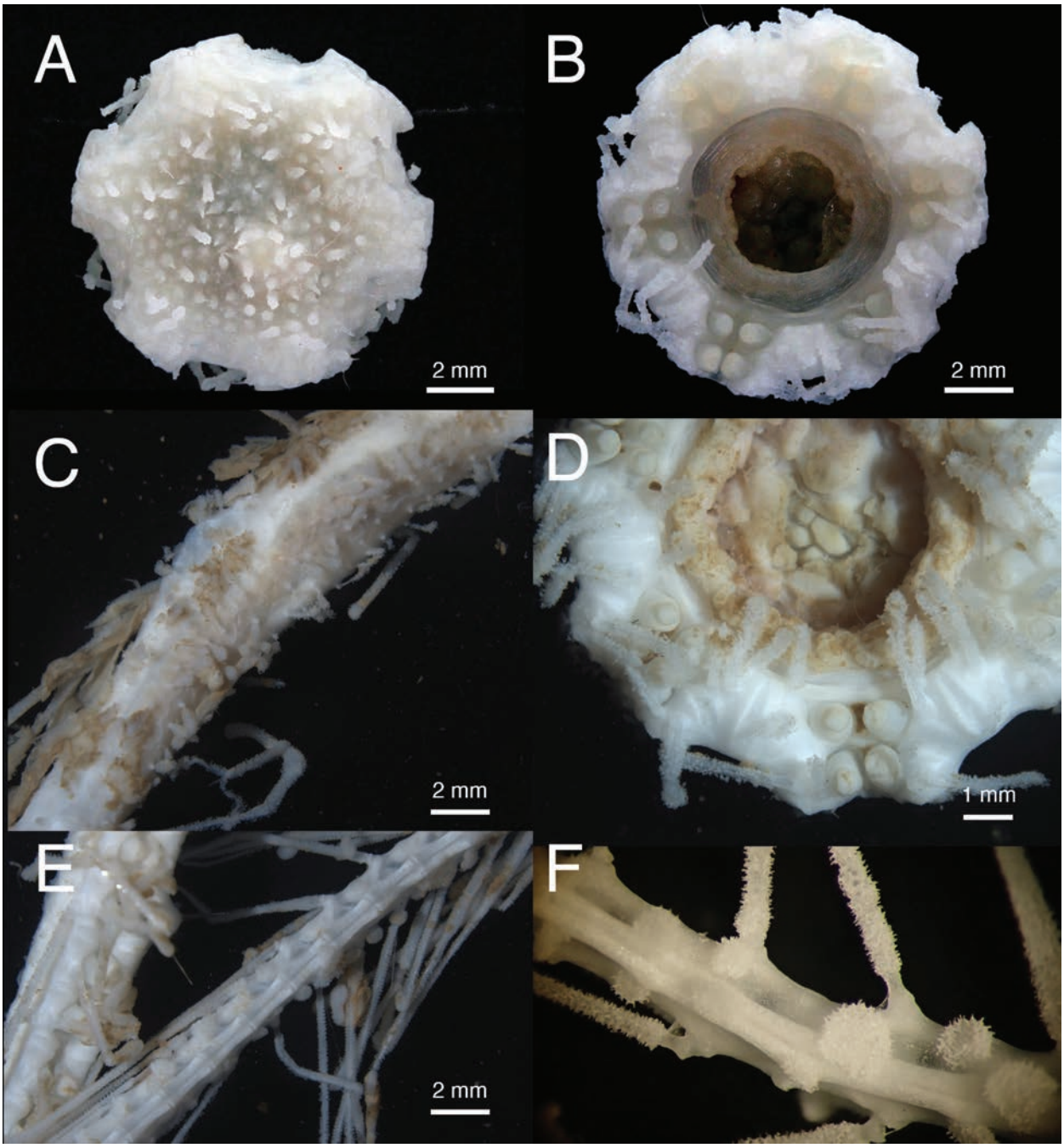

Figure 10. *Freyastera* sp. 2. **A, B, F.** NHMUK 2022.81; **C–E.** RSIOAST0103. **A.** Abactinal view of disk; **B.** Actinal view of disk; **C.** Abactinal view of arm genital area; **D.** Zoom-in view of oral plates; **E.** Abactinal view of middle part of arm; **F.** Zoom-in view of middle part of arm, showing pedicellariae clustered in small pads.

plates not in contact with the odontophore. Inferomarginal plates generally correspond to every 2nd adambulacral plate beyond genital area. Abactinal arm in genital region covered with pavement of spinate plates.

Freyella benthophila Sladen, 1889

Fig. 11

Freyella benthophila: Sladen 1889: 641; Wood-Mason and Alcock 1891: 440; Alcock 1893: 121; Fisher 1928: 24; Madsen 1951: 84; Cherbonnier and Sibuet 1972: 1356; Sibuet 1975: 292; Korovchinsky and Galkin 1984: 1215 (in key); Galkin and Korovchinsky 1984: 165; Zhang et al. 2024: 17.

Freyellidea benthophila: Fisher 1917: 429.

Freyastera benthophila: Downey 1986: 36; McKnight 1993: 173; Mah 1998: 78; Mah in Clark and Mah 2001: 318; Dilman 2014: 38; Moreau et al. 2015: 16; Moreau et al. 2018: 147; Zhang et al. 2019: 7 (in key).

Belgicella racowitzana: Ludwig 1903: 59; Koehler 1907: 141; Koehler 1908: 245; Döderlein 1928: 293; Fisher 1928: 6; Fisher 1940: 75; A.M. Clark 1962: 68; Jangoux and Massin 1986: 91; Mah 1998: 78; Mah in Clark and Mah 2001: 317; Moreau et al. 2015: 5; Moreau et al. 2018: 147.

Material examined. NHMUK 1890.5.7.1078 (***holotype***) (Fig. 11A, B, E, G).

Other material. IA3-2168; MNHN-IE-2008-1057; MNHN-IE-2008-1073; MNHN-IE-2008-1081; MNHN-IE-2017-1829; MNHN-IE-2017-1948; MNHN-IE-2019-5752; MNHN-IE-2022-2192 (Fig. 11D); MNHN-IE-2022-2193; MNHN-IE-2022-2194; MNHN-IE-2022-2195; MNHN-IE-2022-2196; NHMUK 9237 (Fig. 11C, F, H, I); NOC 11908#44; NOC 12930#64; NOC 12930#78; NOC 13200#27; NOC 13200#60; NOC 52701#42; NOC 54901#7; NOC 54902#1; NOC 54903#1; SO268-1_29_014; SO268-2_109_189; SO268-02_99_04. (Suppl. material 1).

Diagnosis. Arms six. Abactinal armature of disk with one primary central plate at center of the disk and a primary interradial plate at each interradius (Fig. 11A–D). Central and interradial primary plates shield-like, much larger than the rest of abactinal disk plates (primary plates present in most specimens examined, but indistinguishable in some individuals). Abactinal disk and arm plates evenly covered with numerous short spinelets and small pedicellariae (Fig. 11G). Beyond genital area, abactinal arm with bands of small pedicellariae. Adambulacral plate with one subambulacral spine. Proximal subambulacral spines with modified tips (truncated or flattened bifurcated) (Fig. 11E, H). Furrow spine absent. Oral plate with 2–3 actinostomal spines and one suboral spine, each covered with membranous sheath, but the tips are bare (Fig. 11E, F). Spines covered with small pedicellariae. Large pedicellariae absent. Inferomarginal plates and lateral spines occur at alternate adambulacral plates beyond genital area (Fig. 11I).

Distribution. North Atlantic, Southern Pacific, Eastern Pacific, Southern Ocean. 2450–5000 m. Type locality: Southern Pacific, 4663 m.

Remarks on *F. benthophila* and other six-armed *Freyella*. *F. benthophila* stands in a peculiar position by having shared morphological characters with both *Freyastera* and *Freyella*. As a species with six arms, it is readily distinguished from other *Freyella* species with more than six arms. Compared with other *Freyastera*, it is differentiated from most species by having many small spinelets on its abactinal disk and arms and distinguished from *Freyastera mortenseni*, *F. delicata*, and *F. mexicana*, which also bears multiple spines on abactinal plates, by the absence of furrow spines and more distantly located inferomarginal plates. Phylogenetic analysis put it within the *Freyella* clade (Fig. 12; Zhang et al. 2024), indicating that having six arms is not an autapomorphy of the *Freyastera* clade.

There are three other six-armed *Freyella* species whose taxonomic position needs to be re-evaluated, including *F. oligobrachia* H.L. Clark, 1920; *F. hexactis* Baranova, 1957; and *F. vitjazi* Korovchinsky & Galkin, 1984. *F. oligobrachia* and *F. vitjazi* have inferomarginals corresponding to alternate adambulacral plates according to their original descriptions; thus, they should be retained within *Freyella*. *F. hexactis* was described to have inferomarginal plates to every third adambulacrals, then to alternate adambulacrals, then at the end of the arm, to each adambulacral plate (Baranova 1957). It is difficult to justify it as either *Freyella* or *Freyastera* simply by this description. However, this species closely resembles *F. oligobrachia* and *F. benthophila*, as was shown in the key in Zhang et al. (2019). It is necessary to examine the types of *F. oligobrachia* and *F. hexactis* to be certain of their generic affinities and their relationship with *F. benthophila*. *F. vitjazi*, on the other hand, could be differentiated from the other six-armed *Freyella* species by having a diagonal line of three spines on each adambulacral plate. These three species are retained as *Freyella* for the time being, but they should be compared with in any future descriptions of six-armed freyellids.

Genetic distances, species delimitation, and phylogeny

The COI genetic distances among 30 *Freyastera* individuals are shown in Table 1. The distance between two specimens of the new species *F. jiaolongi* sp. nov. is 0.45%, whereas intraspecific distances of other *Freyastera* species are between 0% and 1.56%. The distances among the new species and the other *Freyastera* species are between 2.64% and 9.40%. The new species is most closely related to the undescribed species *Freyastera* sp. 5. The largest interspecific distance within *Freyastera* is 10.67%, which is found between *Freyastera mortenseni* and *Freyastera* cf. *tuberculata*.

The species delimitation tool ASAP was used for COI alignment of the 30 *Freyastera* individuals and for 16S alignment of 23 individuals. For COI alignment, a clear barcode gap was shown with the delimitation threshold value (genetic distance) found at 1.9%. The best delimitation result from COI alignment suggested 11 species (ASAP score = 2.00). The same delimitation result was yielded for the 16S alignment (11 species, ASAP score = 2.00).

The phylogenetic tree constructed in the present study (Fig. 12) shows the same topology as the tree in Zhang et al. (2024) for the *Freyastera* clade. Two clades are formed within the genus; one includes *F. basketa* and *F. mortenseni*, and the other includes the remaining nine species. However, the support values of several branches in the bigger clade are not high, especially at the branches of *Freyastera* sp. 6 and *Freyastera* sp. Yap. These two species seem to be derived from the other species and intermediate among the two clades. When only *Freyella benthophila* and *Freyella echinata* were used as outgroup, *F.* sp. 6 and *F.* sp. Yap clustered with the *F. basketa* clade instead, but the support values were also very low. Another species with an uncertain position is *Freyastera* sp. 3. This species clusters with *F. jiaolongi* sp. nov. and *F.* sp. 5 in the ML tree (Fig. 12), but lies outside of a cluster of *F. jiaolongi* sp. nov., *F.* sp. 5, and the *Freyastera* cf. *tuberculata* complex in the BI tree, both with low support values.

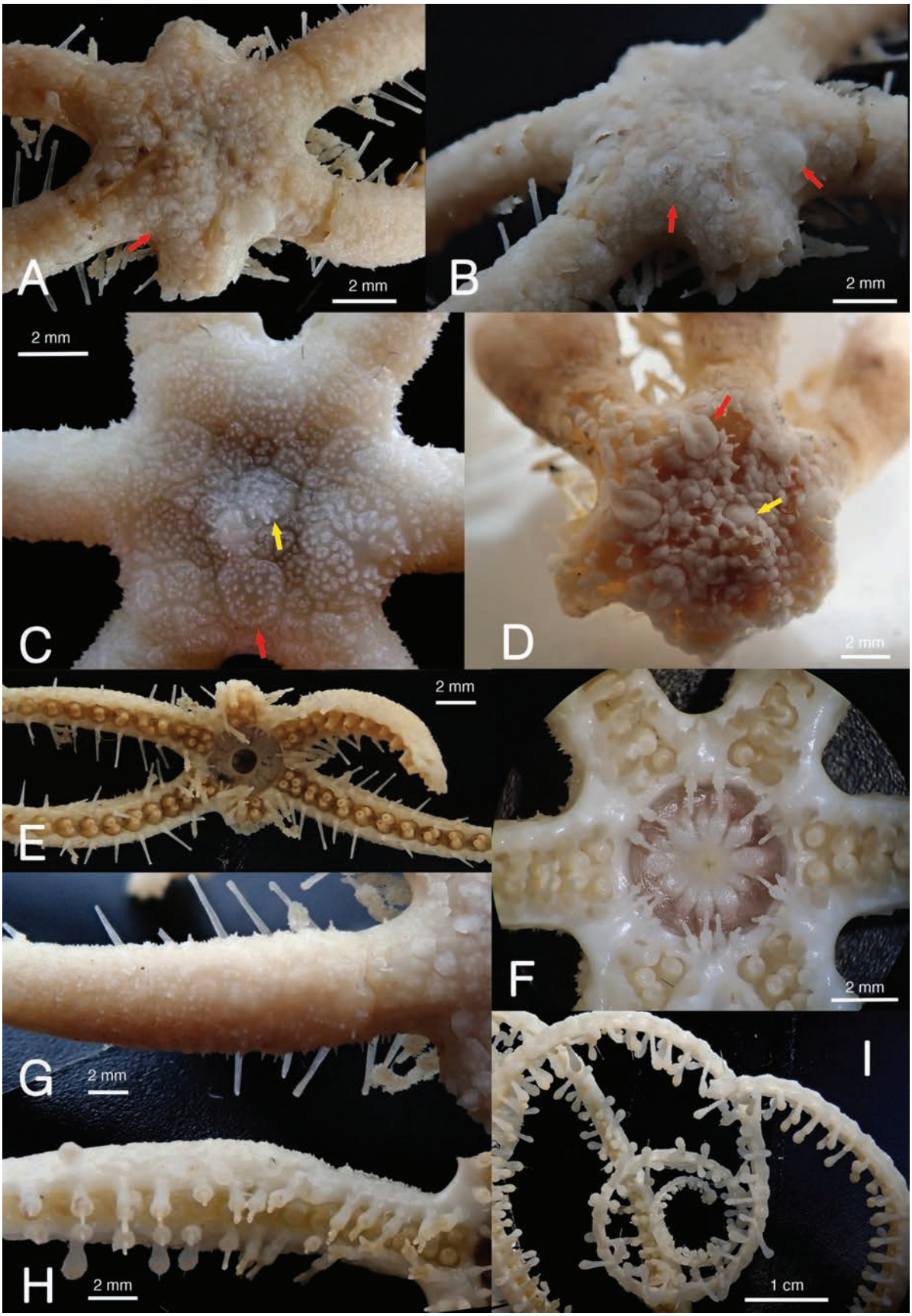

Figure 11. *Freyastera benthophila* Sladen, 1889. **A, B, F, G.** Holotype NHMUK 1890.5.7.1078; **C, F, H, I.** NHM 9237; **D.** MNHN-IE-2022-2192. **A–D.** Abactinal view of disk, red arrows show the primary interradial plates, yellow arrows show the primary central plates; **E.** Actinal view of the specimen; **F.** Actinal view of disk; **G.** Abactinal view of arm genital area, spines mostly lost; **H.** Actinal view of arm genital area; **I.** Distal part of arm.

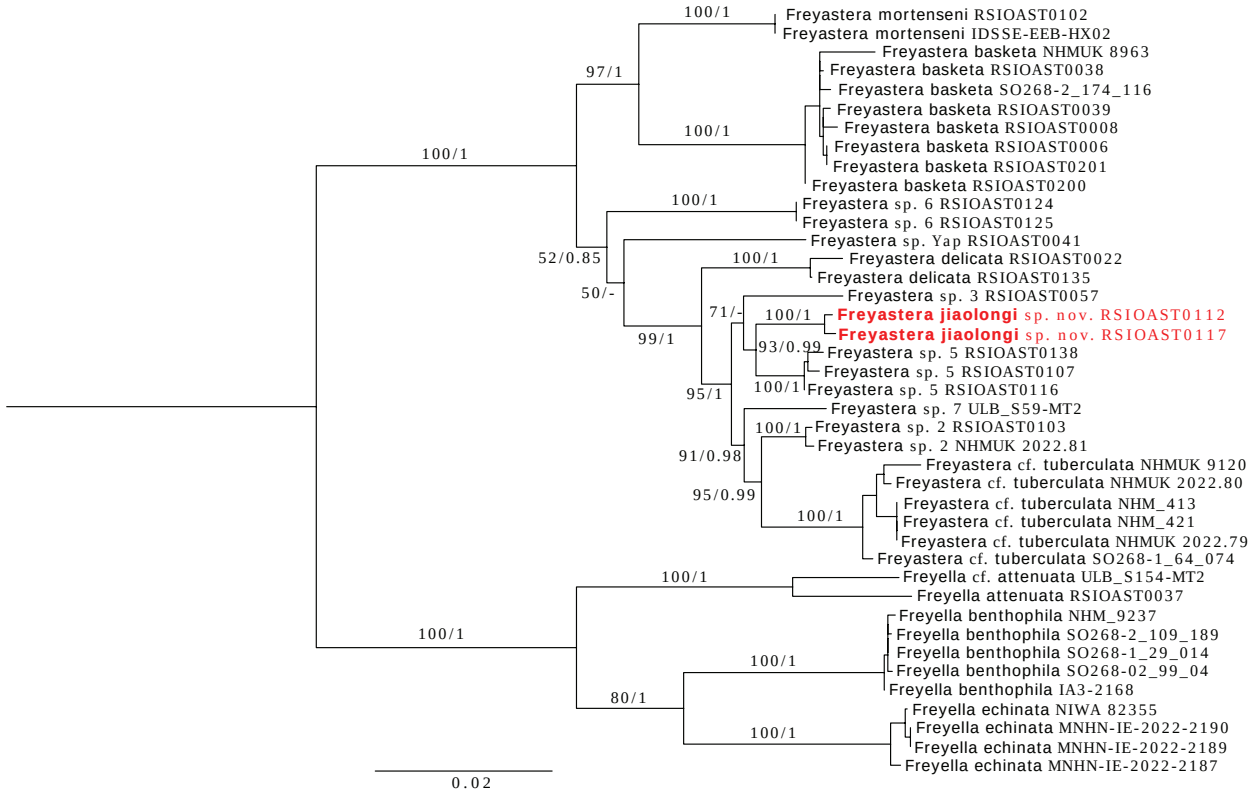

Figure 12. Phylogenetic tree of *Freyastera* using COI, 16S, 12S, and 28S concatenated dataset. Tree topology follows that of the ML tree. Numbers at each node indicate UFBS/PP support values.

Discussion

In this study, a new species, *Freyastera jiaolongi* sp. nov., is described, and two new species combinations, *Freyastera giardi* comb. nov. and *Freyastera loricata* comb. nov., are proposed. Remarks on nine *Freyastera* species and one *Freyella* species and a key to *Freyastera* species are provided based on examination of the type specimens (or photos). Molecular phylogenetic trees based on COI, 16S, 12S, and 28S genes support *Freyastera* as monophyletic and most of the inner lineages with high UFBS/PI values (Fig. 12). The new specimens examined and their genetic data allow for an investigation into the morphological and genetic boundaries among *Freyastera* species. Morphological differences among the known species were demonstrated in the systematics part. Other than the *F. tuberculata* species complex, most *Freyastera* species are well-defined and distinguishable from each other. However, several undescribed species (*Freyastera* sp. 3, *Freyastera* sp. 5, and *Freyastera* sp. 6 (Fig. 12)) were not included in the systematics as specimens were in bad condition for proper description of the species.

Genetic data showed that the COI intraspecific distances of *Freyastera* species are between 0% and 1.56%, which fall within the range of intraspecific distance of Asteroidea obtained in other studies (e.g., Ward et al. 2008; Corstorphine 2010). The interspecific distances among *Freyastera* species are between 2.64% and 10.67%. It needs to be noted that several geographically close species have rather small interspecific distances, such as *Freyastera* cf. *tuberculata* and *Freyastera* sp. 2 (2.73%–3.78%), *Freyastera jiaolongi* sp. nov., and *Freyastera* sp. 5 (2.64%–3.52%). *Freyastera jiaolongi* sp. nov. and *Freyastera* sp. 5, as mentioned in the systematics, are distinguishable in morphology, as the former has furrow spines on adambulacral plates and oral plates, while the latter has no furrow spine at all. *Freyastera* cf. *tuberculata* and *Freyastera* sp. 2 have only subtle differences in morphology as part of the *F. tuberculata* species complex. The small interspecific distances found in these species pairs underline the complexity in the use of a universal threshold value of genetic distance to set the boundaries of species (e.g., 3% in many eDNA studies) (e.g., Laroche et al. 2020; Lanzén et al. 2021). Boundaries among species, especially less-studied deep-sea species, need to be assessed by combining different sources of evidence, including morphology, genetics, biology, and ecology.

Freyastera was believed to be distributed in the global ocean save the Arctic (Zhang et al. 2019). However, as *Freyella benthophila*, a "cosmopolitan" species, was moved out from *Freyastera*, the global distribution of *Freyastera* needs to be re-evaluated. All *Freyastera* specimens examined in the present study and the type localities are found restricted to the Pacific, Atlantic, and the Atlantic part of the Southern Ocean (Fig. 1). The presence of *Freyastera* in the Indian Ocean, on the other hand, is rather dubious. Two records of *Freyastera* were reported from the Bay of Bengal

Table 1. COI pairwise genetic distances (%) of *Freyastera* species. Distances in red color are intraspecific distances.

		1	2	3	4	5	6	7	8	9	10	11	12	13	14	15	16	17	18	19	20	21	22	23	24	25	26	27	28	29
1	*F.* sp. Yap RSIOAST0041																													
2	*F. delicata* RSIOAST0022	5.46																												
3	*F. delicata* RSIOAST0135	5.16	0.59																											
4	*F.* sp. 3 RSIOAST0057	5.83	3.93	3.77																										
5	*F. jiaolongi* sp. nov. RSIOAST0112	6.91	5.27	5.11	3.83																									
6	*F. jiaolongi* sp. nov. RSIOAST0117	6.92	5.15	5.00	3.62	0.45																								
7	*F.* sp. 5 RSIOAST0138	6.24	4.79	4.78	3.20	3.20	3.52																							
8	*F.* sp. 5 RSIOAST0107	6.12	4.22	4.22	3.00	2.90	3.14	0.75																						
9	*F.* sp. 5 RSIOAST0116	5.73	3.92	3.92	2.80	2.64	2.96	0.77	0.31																					
10	*F.* sp. 7 ULB_S59-MT2	5.89	4.74	4.41	3.45	4.25	4.58	3.44	3.60	3.36																				
11	*F.* sp. 2 RSIOAST0103	5.96	4.22	3.91	3.93	4.79	5.01	3.82	3.60	3.59	3.11																			
12	*F.* sp. 2 NHMUK 2022.81	6.07	4.20	3.87	4.04	4.71	5.05	3.86	3.70	3.53	2.93	0.31																		
13	*F. cf. tuberculata* NHMUK 9120	9.14	7.36	7.15	5.44	6.09	6.32	6.49	6.07	5.82	4.81	3.78	3.59																	
14	*F.* cf. *tuberculata* NHM_413	7.10	5.45	5.13	4.33	5.31	5.32	5.13	4.81	4.41	2.97	3.21	2.88	1.38																
15	*F.* cf. *tuberculata* NHM_421	6.87	5.36	5.03	4.23	5.05	5.06	5.03	4.71	4.28	2.98	3.10	2.73	1.38	0.00															
16	*F.* cf. *tuberculata* NHMUK 2022.79	7.07	5.59	5.26	4.31	5.28	5.29	5.10	4.79	4.41	2.95	3.20	2.88	1.37	0.00	0.00														
17	*F.* cf. *tuberculata* SO268-1_64_074	7.40	5.62	5.31	4.24	5.28	5.49	4.78	4.37	4.08	3.27	2.83	2.88	1.17	0.90	0.76	0.90													
18	*F.* cf. *tuberculata* NHMUK 2022.80	7.91	6.24	5.91	4.79	5.77	6.11	5.26	4.94	4.57	3.43	3.35	3.04	0.97	0.75	0.76	0.75	0.75												
19	*F.* sp. 6 RSIOAST0124	5.63	7.24	6.59	6.62	7.73	7.90	6.89	6.91	6.38	6.37	7.41	7.10	9.31	7.76	7.35	7.72	7.72	8.05											
20	*F.* sp. 6 RSIOAST0125	5.74	7.22	6.55	6.55	7.73	7.89	6.89	6.89	6.38	6.37	7.38	7.10	9.31	7.76	7.35	7.72	7.71	8.05	0.00										
21	*F. mortenseni* RSIOAST0102	5.95	7.57	6.92	7.61	8.57	8.58	7.23	6.77	6.90	7.22	7.57	7.44	10.67	8.61	8.38	8.57	8.58	9.25	5.16	5.09									
22	*F. mortenseni* IDSSE-EEB-HX02	5.80	8.67	8.18	8.65	9.15	9.40	7.45	6.98	7.48	8.66	8.18	8.01	10.63	9.95	10.02	9.88	10.15	10.39	6.27	6.27	0.00								
23	*F. basketa* NHMUK 8963	8.47	8.88	8.44	8.20	9.31	8.88	8.63	7.98	8.24	8.43	8.44	8.30	9.34	9.82	9.88	9.99	9.97	10.20	6.94	6.94	6.48	5.57							
24	*F. basketa* RSIOAST0200	7.15	7.48	6.97	6.62	8.00	7.83	6.45	6.28	6.32	6.32	6.79	6.83	9.31	7.64	7.64	7.64	7.29	7.64	6.13	6.13	5.45	5.23	1.39						
25	*F. basketa* SO268-2_174_116	8.25	8.40	7.90	7.77	8.96	8.93	6.85	6.87	7.02	7.19	7.38	7.28	9.85	8.59	8.50	8.59	8.21	8.58	6.21	6.00	6.05	5.66	1.23	0.95					
26	*F. basketa RSIOAST0038*	7.75	7.89	7.41	7.12	8.25	8.23	6.24	6.27	6.56	6.55	6.92	6.93	9.55	8.28	8.22	8.24	7.88	8.23	6.45	6.25	5.81	5.10	1.17	0.62	0.61				
27	*F. basketa* RSIOAST0039	7.75	7.56	7.08	7.12	8.07	8.06	6.40	5.94	6.22	6.55	6.92	6.93	9.55	8.11	8.05	8.07	7.71	8.06	6.45	6.25	5.81	5.34	1.36	0.77	0.76	0.44			
28	*F. basketa* RSIOAST0008	7.92	7.73	7.25	7.29	8.25	8.23	6.40	6.10	6.39	6.72	7.09	7.10	9.77	8.28	8.22	8.24	7.88	8.23	6.62	6.42	5.97	5.57	1.56	0.77	0.76	0.44	0.29		
29	*F. basketa* RSIOAST0006	7.92	7.73	7.25	7.29	8.25	8.23	6.40	6.10	6.39	6.72	7.09	7.10	9.77	8.28	8.22	8.24	7.88	8.23	6.62	6.42	5.97	5.57	1.56	0.77	0.76	0.44	0.29	0.29	
30	*F. basketa* RSIOAST0201	7.95	7.93	7.39	7.56	8.65	8.48	6.85	6.32	6.68	7.03	7.20	7.12	9.79	8.10	8.10	8.10	7.91	8.09	6.52	6.52	6.16	5.87	1.43	0.80	0.80	0.48	0.32	0.32	0.00

(Alcock 1893; Shirayama and Tsuchida 1991), but no descriptions or photos of the specimens were provided. Gerdes et al. (2021) reported a *Freyastera* gen. inc. near the Edmond hydrothermal vent field in the Central Indian Ridge, but according to the photo provided, the specimen has seven arms instead of six, thus is likely to be a *Freyella*. The global distribution and bathymetrical distribution of *Freyastera* species seem to be rather restricted (Fig. 13). No species was found to have a cross-ocean distribution, and the depth range of a species is no larger than 1300 m. *F. basketa* has the widest distribution range from the Yap Trench to the eastern part of CCZ. However, this restricted distribution could also be owing to the insufficiency of data, as only 77 records were included in the map (Fig. 1).

This study reveals high species diversity of *Freyastera*, especially in the Northwest Pacific region, where ten species (including five undescribed ones) were found. On one hand, this might be owing to a greater deep-sea sampling effort in this region. Species found in this region were mostly collected from nine Chinese expeditions starting from 2013 using cutting-edge sampling vehicles such as ROV and HOV (Suppl. material 1), resulting in a fine collection of specimens for biodiversity analysis. On the other hand, the Northwest Pacific harbors high environmental heterogeneity, providing various habitats for different species. The diversity of *Freyastera* in other regions should be further investigated with more samples to be collected in the future. Furthermore, high-resolution cameras mounted on ROV or HOV provided valuable information on the *in situ* environments of *Freyastera* species (Fig. 14). *Freyastera* have been frequently observed by submersibles and deep-tow digital cameras (e.g., Morris et al. 2014; Yu et al. 2014; Glover et al. 2016; Amon et al. 2017; Moreau et al. 2018; Zhang et al. 2019; Zhang et al. 2024; NOAA Ocean Exploration 2024) from the slope or foot of seamounts, abyssal plains, or trenches. Although living at great depth below 3000 m, they were mostly spotted attaching to hard substrate, even when the gross substrate of the environment is soft sediment (Fig. 14A–C, F). *Freyastera* sp. Yap and *Freyastera* sp. 2, on the other hand, might be directly attaching to soft sediment as shown in *in situ* photos (Zhang et al. 2019; Bribiesca-Contreras et al. 2022). Some species, namely, *F. basketa* and *F.* cf. *tuberculata*, were known to be associated with polymetallic nodules in either the CCZ or the Pigafetta basin (Fig. 14E) (Zhang et al. 2019; Glover et al. 2016; Amon et al. 2017; Bribiesca-Contreras et al. 2022), but such an association is not obligate,

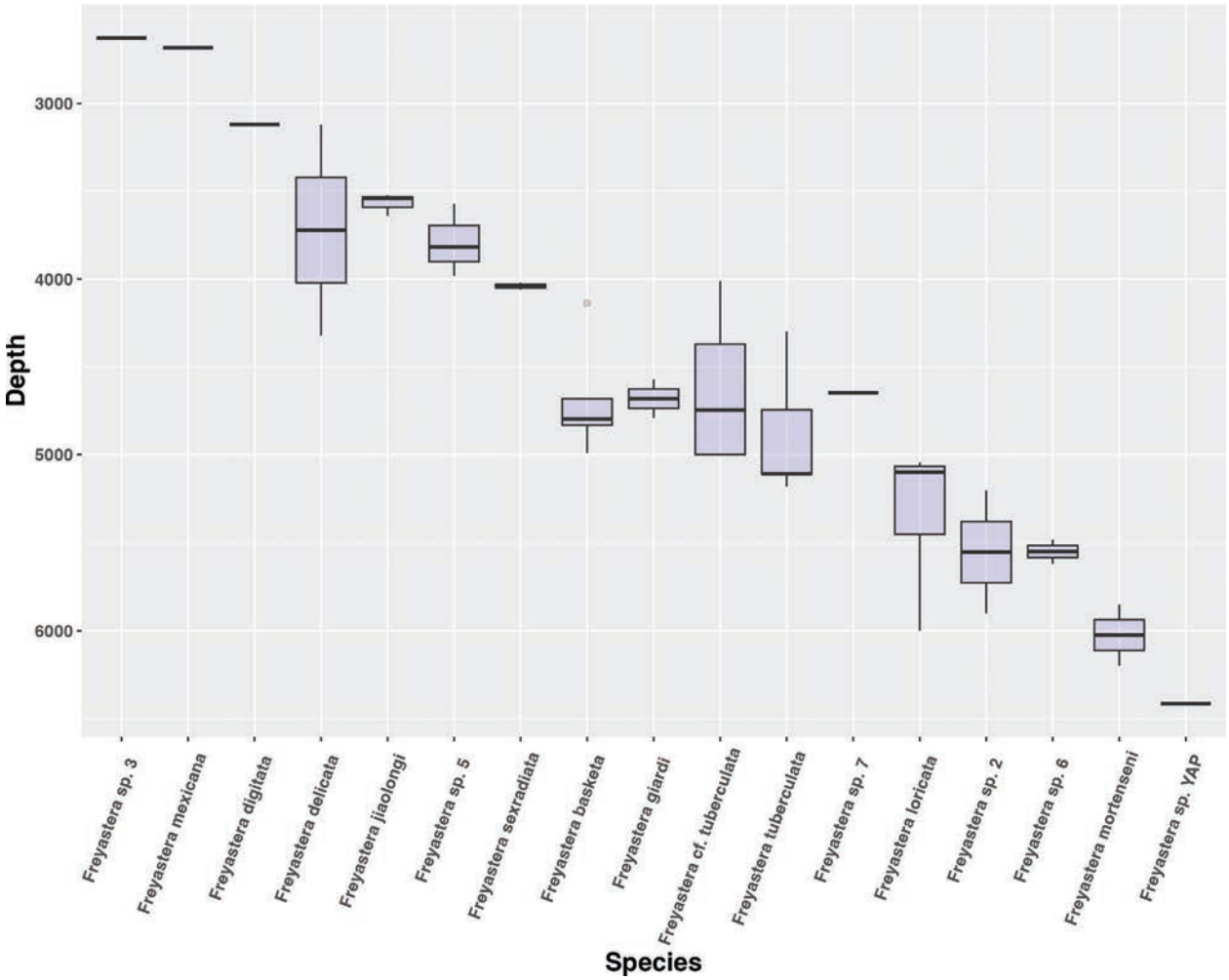

Figure 13. Bathymetric distribution of *Freyastera* species. Data include type localities and specimens examined in the present study.

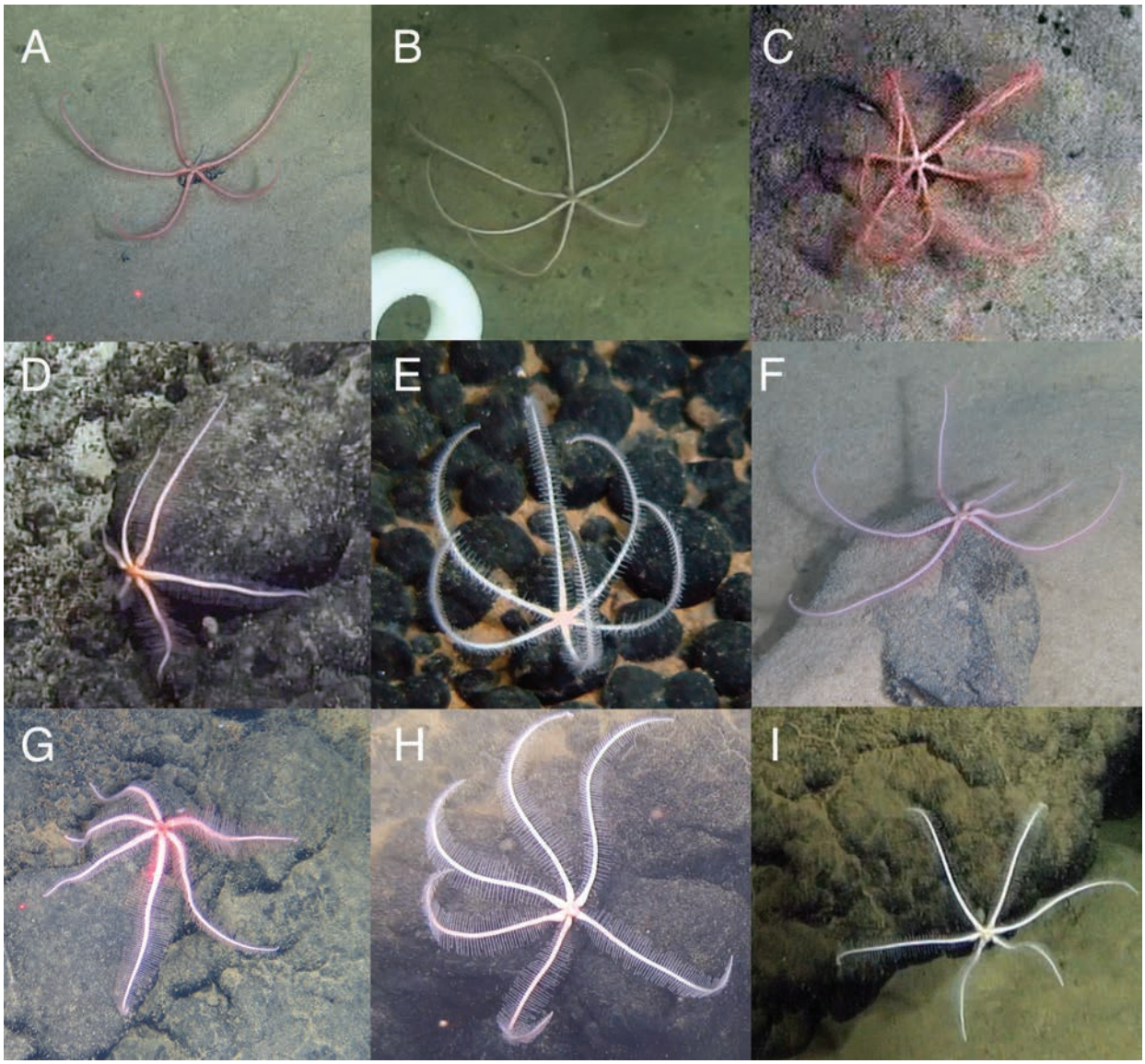

Figure 14. *In situ* photos of *Freyastera* species. **A.** *Freyastera jiaolongi* sp. nov. holotype RSIOAST0117; **B.** *Freyastera jiaolongi* sp. nov. paratype RSIOAST0112; **C.** *Freyastera jiaolongi* sp. nov. paratype RSIOAST0113; **D.** *Freyastera delicata* RSIOAST0135; **E.** *Freyastera basketa* RSIOAST0200; **F.** *Freyastera* sp. 5 RSIOAST0116; **G.** *Freyastera* sp. 5 RSIOAST0107; **H.** *Freyastera* sp. 6 RSIOAST0124; **I.** *Freyastera* sp. 6 RSIOAST0125.

as the same species were also found in non-nodule environments (Zhang et al. 2019). The high diversity of *Freyastera* and its occurrence in various deep-sea environments suggest a successful adaptation and radiation of the genus at great depth.

Acknowledgements

This research was supported by the National Natural Science Foundation of China (42406111), the International Seabed Authority's Sustainable Seabed Knowledge Initiative: One Thousand Reasons Campaign (co-financed by the European Maritime and Fisheries Fund of the European Union, Project 101071214—SSKI-I—EMFAF-2021-ISA-SSKI-IBA), and the UN Ocean Decade Programme Digital DEPTH. We would like to thank all the crew and scientists on board the cruises to collect and preserve the specimens. We are grateful for the following scientists and curators for providing specimens and/or data for this study: Dr. Marc Eléaume, Dr. Agnès Dettaï, Mr. Alexis Martin, Ms. Andréa Filippo, Ms. Sylvie Gonthier from Muséum national d'Histoire naturelle, France (MNHN); Dr. Magdalini Christodoulou, Dr. Saskia Brix (IceAGE project) from German Center for Marine Biodiversity Research (DZMB), Senckenberg am Meer, Germany; Dr. Haibin Zhang, Dr. Jun Liu and Dr. Wendan Mu from Institute of Deep-sea Science and Engineering, Chinese Academy of Sciences (IDSSE); Dr. Anna Dilman from P. P. Shirshov Institute of Oceanology, Russian Academy of Sciences (IORAS); Ms. Michèle Bruni from Musée Océanographique de Monaco (MOM); Dr. Tom White, Dr. Lauren Hughes, Dr. Adrian Glover and Dr. Lupita Bribiesca Contreras from Natural History Museum,

UK (NHMUK); Dr. Tammy Horton from National Oceanography Center, UK (NOC); Dr. Camille Moreau and Dr. Quantin Jossart from Université Libre de Bruxelles, Belgium (ULB). Special thanks to Dr. Dong Sun from the Second Institute of Oceanography, Ministry of Natural Resources (SIOMNR), for his advice on this work.

References

Alcock A (1893) XV.—Natural history notes from H.M. Indian marine survey Steamer 'Investigator,' Commander C. F. Oldham, R. N., commanding.—Series II., No. 7. An account of the collection of deep-sea Asteroidea, Annals and Magazine of Natural History 11(62): 73–121. https://doi.org/10.1080/00222939308677478

Amon DJ, Ziegler AF, Kremenetskaia A, Mah CL, Mooi R, O'Hara T, Pawson DL, Roux M, Smith CR (2017) Megafauna of the UKSRL exploration contract area and eastern Clarion-Clipperton Zone in the Pacific Ocean: Echinodermata. Biodiversity Data Journal 5: e11794. https://doi.org/10.3897/BDJ.5.e11794

Baranova ZI (1957) Echinoderms of the Bering Sea. Investigations of Far-East Seas 4: 149–266. [in Russian]

Bribiesca-Contreras G, Dahlgren TG, Amon DJ, Cairns S, Drennan R, Durden JM, Eléaume MP, Hosie AM, Kremenetskaia A, McQuaid K, D O'Hara T (2022) Benthic megafauna of the western Clarion-Clipperton Zone, Pacific Ocean. ZooKeys 1113: 1. https://doi.org/10.3897/zookeys.1113.82172

Castresana J (2000) Selection of conserved blocks from multiple alignments for their use in phylogenetic analysis. Molecular Biology and Evolution 17: 540–552. https://doi.org/10.1093/oxfordjournals.molbev.a026334

Cherbonnier G, Sibuet M (1972) Résultats scientifiques de la campagne Noratlante: Astérides et Ophiurides. Bulletin du Museum national d'histoire naturelle 102: 1333–1394. [in French] https://doi.org/10.5962/p.272616

Clark HL (1920) Reports on the scientific results of the expedition to the Eastern Tropical Pacific, in charge of Alexander Agassiz, by the US Fish commission Steamer Albatross, from October 1905 to March 1905, Lt. Cmdr. L.M. Garrett, USN, Commanding. XXXII. Asteroidea. Memoirs of the Museum of Comparative Zoology 39(3): 70–154.

Clark AH (1939) Echinoderms of the Smithsonian-Hartford Expedition, 1937, with other West Indian records. Proceedings of the U.S. National Museum 86: 441–456. https://doi.org/10.5479/si.00963801.86-3056.441

Clark AM (1962) Asteroidea. Reports (B.A.N.Z. Antarctic Research Expedition, (1929–1931)). Series B, Zoology and botany, Vol. IX, 104 pp.

Clark AM, Downey ME (1992) Starfishes of the Atlantic. London: Chapman and Hall, 794 pp.

Clark AM and Mah C (2001) An index of names of recent Asteroidea—Part 4: Forcipulatida and Brisingida. Echinoderm studies 6: 229–347.

Corstorphine EA (2010) DNA barcoding of echinoderms: species diversity and patterns of molecular evolution. PhD Thesis, University of Guelph, Guelph, Canada. https://hdl.handle.net/10214/20441

Dilman AB (2014) Deep-sea fauna of European seas: An annotated species check-list of benthic invertebrates living deeper than 2000 m in the seas bordering Europe. Asteroidea. Invertebrate Zoology 11(1): 25–42. https://doi.org/10.15298/invertzool.11.1.05

Döderlein L (1928) Die seesterne der Deutschen Sudpolar-Expedition, 1901–1903. Deutsche Sudpolar Expediiton XIX. Zoologie XI 1901-1903 19(11): 289–301. [in Germany]

Downey ME (1986) Revision of the Atlantic Brisingida (Echinodermata: Asteroidea), with description of a new genus and family. Smithsonian Contributions to Zoology 435: 1–57. https://doi.org/10.5479/si.00810282.435

Edgar RC (2004) MUSCLE: Multiple sequence alignment with high accuracy and high throughput. Nucleic Acids Research 32: 1792–1797. https://doi.org/10.1093/nar/gkh340

Fisher WK (1917) LI.—New genera and species of Brisingidae. Annals and Magazine of Natural History 20(120): 418–431. https://doi.org/10.1080/00222931709487030

Fisher WK (1928) Asteroidea of the North Pacific and adjacent waters. Part 2. Forcipulata (part). Bulletin of the United States National Museum 76: 1–347. https://doi.org/10.5479/si.03629236.145.1

Fisher WK (1940) Asteroidea. Discovery Reports 20: 69–306.

Galkin SV, Korovchinsky NM (1984) Vertical and geographical distribution of the starfishes of the genus Freyella (Brisingidae) with some remarks on their ecology and evolution. Trudy Instituta Okeanologii Akademii Nauk SSSR 119: 164–178. [in Russian with English abstract]

Gerdes K, Kihara TC, Arbizu PM, Kuhn T, Schwarz-Schampera U, Mah CL, Norenburg JL, Linley TD, Shalaeva K, Macpherson E, Gordon D (2021) Megafauna of the German exploration licence area for seafloor massive sulphides along the Central and South East Indian Ridge (Indian Ocean). Biodiversity Data Journal 9: e69955. https://doi.org/10.3897/BDJ.9.e69955

Glover AG, Wiklund H, Rabone M, Amon DJ, Smith CR, O'Hara T, Mah CL, Dahlgren TG (2016) Abyssal fauna of the UK-1 polymetallic nodule exploration claim, Clarion-Clipperton Zone, central Pacific Ocean: Echinodermata. Biodiversity data journal 4(4): e7251. https://doi.org/10.3897/BDJ.4.e7251

Grieg JA (1921) Echinodermata. Report on the Scientific Results of the "Michael Sars" North Atlantic Deep-sea Expedition 1910. Trustees of the Bergen Museum, 1–44.

Hoang DT, Chernomor O, Von Haeseler A, Minh BQ, Vinh LS (2018) UFBoot2: improving the ultrafast bootstrap approximation. Molecular biology and evolution 35(2): 518–522. https://doi.org/10.1093/molbev/msx281

Huelsenbeck JP, Ronquist F (2001) MRBAYES: Bayesian inference of phylogenetic trees. Bioinformatics 17(8): 754–755. https://doi.org/10.1093/bioinformatics/17.8.754

Jangoux M, Massin C (1986) Catalogue commenté des types d'Echinodermes actuels conservés dans les collections nationales belges. Bulletin de l'Institut Royal des Sciences Naturelles de Belgique, Biologie 56: 83–97.

Kalyaanamoorthy S, Minh BQ, Wong TK, Von Haeseler A, Jermiin LS (2017) ModelFinder: fast model selection for accurate phylogenetic estimates. Nature methods 14(6): 587–589. https://doi.org/10.1038/nmeth.4285

Kearse M, Moir R, Wilson A, Stones-Havas S, Cheung M, Sturrock S, Buxton S, Cooper A, Markowitz S, Duran C, Thierer T (2012) Geneious Basic: an integrated and extendable desktop software platform for the organization and analysis of sequence data. Bioinformatics 28(12): 1647–1649. https://doi.org/10.1093/bioinformatics/bts199

Kimura M (1980) A simple method of estimating evolutionary rate of base substitutions through comparative studies of nucleotide se-

quences. Journal of Molecular Evolution 16: 111–120. https://doi.org/10.1007/BF01731581

Koehler R (1907) Asteries, Ophiures et Echinides recueillis dans les mers australes par la “Scotia” (1902–1904). Zoologischer Anzeiger 32(6): 140–147. [in French]

Koehler R (1908) Astéries, Ophiures et Echinides de l’Expedition Antarctique National Ecossaise. Scottish National Antarctic Expedition. Report on the scientific results of the voyage of S.Y. Scotia during the years 1902, 1903, and 1904 5(13): 193–313. [in French]

Koehler R (1909) Echinodermes provenant des campagnes du yacht Princesse-Alise (Astéries, Ophiures, Echinides et Crinoides). Résultats des Campagnes Scientifiques Accomplies sur son Yacht par Albert Ier Prince Souverain de Monaco 34: 25–28. [in French]

Korovchinsky NM (1976) New data on the deep-sea seastars (Asteroidea, Brisingidae) from the North-Western Pacific. Trudy Instituta Okeanologii Akademii Nauk SSSR 99: 165–177. [in Russian with English abstract]

Korovchinsky NM, Galkin SV (1984) New data on the fauna of starfishes of the genus Freyella (Brisingidae). Zoologicheskii Zhurnal 63(8): 1205–1215. [in Russian with English abstract]

Lanzén A, Dahlgren TG, Bagi A, Hestetun JT (2021) Benthic eDNA metabarcoding provides accurate assessments of impact from oil extraction, and ecological insights. Ecological Indicators 130: 108064. https://doi.org/10.1016/j.ecolind.2021.108064

Laroche O, Kersten O, Smith CR, Goetze E (2020) Environmental DNA surveys detect distinct metazoan communities across abyssal plains and seamounts in the western Clarion Clipperton Zone. Molecular Ecology 29(23): 4588–4604. https://doi.org/10.1111/mec.15484

Ludwig H (1903) Seesterne. Résultats du voyage du S.Y. Belgica en 1897-1898-1899. Rapports scientifiques, 1–72. [in Germany]

Madsen FJ (1951) Asteroidea. Reports of the Swedish Deep-sea Expedition 2(6): 73–92.

Madsen FJ (1956) Echinoidea, Asteroidea, and Ophiuroidea from depths exceeding 6000 meters. Galathea Report 2: 23–32.

Mah CL (1998) A phylogeny, taxonomic revision, and natural history of the order Brisingida (Asteroidea). Master’s Thesis, San Francisco State University, San Francisco, US.

Mah CL (2022) New Genera, Species and Occurrences of Deep-Sea Asteroidea (Valvatacea, Forcipulatacea, Echinodermata) collected from the North Pacific Ocean by the CAPSTONE Expedition. Zootaxa 5164(1):1–75. https://doi.org/10.11646/zootaxa.5164.1.1

Mah CL (2025). World Asteroidea Database. *Freyastera* Downey, 1986. [World Register of Marine Species] https://www.marinespecies.org/aphia.php?p=taxdetails&id=123216

McKnight DG (1993) Records of echinoderms (excluding holothurians) from the Norfolk Ridge and Three Kings Rise north of New Zealand. New Zealand Journal of Zoology 20(3): 165–190. https://doi.org/10.1080/03014223.1993.10422858

McKnight DG (2006) The marine fauna of New Zealand, Echinodermata: Asteroidea (Sea-stars). 3. Orders Velatida, Spinulosida, Forcipulatida, Brisingida with addenda to Paxillosida, Valvatida. NIWA Biodiversity Memoir 120: 1–187.

Minh BQ, Schmidt HA, Chernomor O, Schrempf D, Woodhams MD, Von Haeseler A, Lanfear R (2020) IQ-TREE 2: new models and efficient methods for phylogenetic inference in the genomic era. Molecular biology and evolution 37(5): 1530–1534. https://doi.org/10.1093/molbev/msaa015

Mironov AN, Dilman AB, Vladychenskaya IP, Petrov NB (2016) Adaptive strategy of the Porcellanasterid sea stars. Biology Bulletin 43: 503–516. https://doi.org/10.1134/S106235901606011X

Moreau CV, Aguera A, Jossart Q, Danis B (2015) Southern Ocean Asteroidea: a proposed update for the Register of Antarctic Marine Species. Biodiversity Data Journal 3: e7062. https://doi.org/10.3897/BDJ.3.e7062

Moreau C, Mah C, Agüera A, Améziane N, Barnes D, Crokaert G, Eléaume M, Griffiths H, Guillaumot C, Hemery LG, Jażdżewska A. (2018) Antarctic and sub-Antarctic Asteroidea database. ZooKeys 747: 141–156. https://doi.org/10.3897/zookeys.747.22751

Morris KJ, Bett BJ, Durden JM, Huvenne VA, Milligan R, Jones DO, McPhail S, Robert K, Bailey DM, Ruhl HA (2014) A new method for ecological surveying of the abyss using autonomous underwater vehicle photography. Limnology and Oceanography: Methods 12(11): 795–809. https://doi.org/10.4319/lom.2014.12.795

Mortensen T (1927) Handbook of the Echinoderms of the British Isles. Oxford University Press, 471 pp. https://doi.org/10.5962/bhl.title.6841

NOAA Ocean Exploration (2024) NOAA Ocean Exploration Benthic Deepwater Animal Identification Guide, Version 4. NOAA Ocean Exploration. Web application. https://oceanexplorer.noaa.gov/okeanos/animal_guide/animal_guide.html

Pawson DL, Vance DJ, Messing CG, Solís-Marin FA, Mah CL (2009) Echinodermata of the Gulf of Mexico. Gulf of Mexico: origin, waters, and biota 1: 1177–1204.

Perrier E (1885) Premiére note Préliminaire des les Echinodermes, recueillis durant les campagnes de dragages sous-marines du Travailleur et du Talisman. Annales des sciences naturelles, Zoologie 22(8): 1–72. [in French]

Perrier E (1894) Stellérides. Expéditions Scientifiques du Travailleur et du Talisman 3: 1–431. [in French]

Puillandre N, Brouillet S, Achaz G (2021) ASAP: assemble species by automatic partitioning. Molecular Ecology Resources 21(2): 609–620. https://doi.org/10.1111/1755-0998.13281

QGIS Development Team (2024). QGIS Geographic Information System. Open Source Geospatial Foundation Project. http://qgis.osgeo.org

Rambaut A, Drummond AJ, Xie D, Baele G, Suchard MA (2018) Posterior summarization in Bayesian phylogenetics using Tracer 1.7. Systematic biology 67(5): 901–904. https://doi.org/10.1093/sysbio/syy032

RStudio Team (2024) RStudio: Integrated Development Environment for R, Boston, MA. http://www.rstudio.com/

Shirayama Y, Tsuchida E (1991) Benthic studies carried out during the R.V. Hakuho Maru cruise KH-89-2. In: Nemoto, T. and T. Asai. (eds.) Preliminary Report of the Hakuho Maru Cruise KH-89-2 (Around the World Expedition). October 27, 1989-March 5, 1990. Synthetic and Global Studies of Major Oceans in the World. Ocean Research Institute, University of Tokyo, 61–64.

Sibuet M (1975) Astérides abyssales de l’Atlantique sud. (Résultats de la campagne Walda, juin-juillet-août 1971). Bulletin du Muséum National d’Histoire Naturelle, Zoologie 3(289): 281–297. [in French] https://archimer.ifremer.fr/doc/00000/5426/

Sladen WP (1889) Report on the Asteroidea. Report on the Scientific Results of the Voyage of H.M.S. Challenger during the years 1873–1876, Zoology 30(51): 125–174.

Tamura K, Stecher G, Kumar S (2021) MEGA11: molecular evolutionary genetics analysis version 11. Molecular biology and evolution 38(7): 3022–3027. https://doi.org/10.1093/molbev/msab120

Ward RD, Holmes BH, O'Hara TD (2008) DNA barcoding discriminates echinoderm species. Molecular Ecology Resources 8(6): 1202–1211. https://doi.org/10.1111/j.1755-0998.2008.02332.x

Wickham H (2016) ggplot2: Elegant Graphics for Data Analysis. Springer-Verlag New York. [ISBN 978-3-319-24277-4] https://doi.org/10.1007/978-3-319-24277-4

Wood-Mason J, Alcock A (1891) LII. Natural history notes from H. M. Indian marine survey Steamer "Investigator". Series II, No. 1. On the results of deep-sea dredging during the season 1890–91, Annals and Magazine of Natural History 8(48): 427–452. https://doi.org/10.1080/00222939109459221

Xia X (2018) DAMBE7: New and improved tools for data analysis in molecular biology and evolution. Molecular biology and evolution 35(6): 1550–1552. https://doi.org/10.1093/molbev/msy073

Yu OH, Son JW, Ham DJ, Lee GC, Kim KH (2014) The Distribution of Epifaunal Megabenthos Varies with Deep-sea Sediment Conditions in the Korea Deep Ocean Study Area (KODOS) of the North-eastern Pacific. Ocean & Polar Research 36(4): 447–454. [in Korean with English abstract] https://doi.org/10.4217/OPR.2014.36.4.447

Zhang R, Wang C, Zhou Y, Zhang H (2019) Morphology and molecular phylogeny of two new species in genus *Freyastera* (Asteroidea: Brisingida: Freyellidae), with a revised key to close species and ecological remarks. Deep Sea Research Part I: Oceanographic Research Papers 154: 103163. https://doi.org/10.1016/j.dsr.2019.103163

Zhang R, Fau M, Mah C, Eléaume M, Zhang D, Zhou Y, Lu B, Wang C (2024) Systematics of deep-sea starfish order Brisingida (Echinodermata: Asteroidea), with a revised classification and assessments of morphological characters. Molecular Phylogenetics and Evolution 191: 107993. https://doi.org/10.1016/j.ympev.2023.107993

Supplementary material 1

List of specimens studied with geographical information and GenBank accession numbers

Authors: Ruiyan Zhang, Yadong Zhou, Jingwen Mao, Chunsheng Wang, Dongsheng Zhang

Data type: xlsx

Link: https://doi.org/10.3897/zse.101.144918.suppl1

Zoosyst. Evol. 101 (2) 2025, 761–778 | DOI 10.3897/zse.101.142007

PENSOFT

MUSEUM FÜR NATURKUNDE BERLIN

Two new species of *Idas* (Bivalvia, Mytilidae) from sunken wood in the East China Sea: description, phylogenetic position and symbionts

Qiong Wu[1,2], Yi-Tao Lin[3], Jian-Wen Qiu[3], Mei Yu Xu[4], Bing Peng Xing[1]

1 *Third Institute of Oceanography Ministry of Natural Resources, Xiamen, Fujian, China*
2 *College of Life Sciences, Beijing Normal University, Beijing, China*
3 *Department of Biology, Hong Kong Baptist University, Hong Kong, China*
4 *Unaffiliated, Guangzhou, China*

https://zoobank.org/CA51086B-C1D5-4908-B745-612F26276076

Corresponding author: Bing Peng Xing (xingbpeng@gmail.com)

Academic editor: M. Glaubrecht ♦ **Received** 17 November 2024 ♦ **Accepted** 26 March 2025 ♦ **Published** 10 April 2025

Abstract

Mussels of the genus *Idas* (Bathymodiolinae) are small bivalves inhabiting organic falls and cold seep ecosystems. Despite their ecological significance, the taxonomy and phylogeny of *Idas* remain understudied. In this study, 30 *Idas* specimens were collected from a piece of sunken wood in the East China Sea at depths of 460–550 m. DNA barcoding and phylogenetic analysis revealed three distinct clades: 23 specimens matched *Idas* sp. ESU D, previously reported from Japan and the Philippines, five samples clustered with *Idas iwaotakii* (Habe, 1958), and two samples formed a new clade related to *I. iwaotakii*. These findings resulted in the description of two new species, *Idas sinensis* **sp. nov.** and *Idas pacificus* **sp. nov.** We present the complete mitochondrial genomes for both species and investigate the diversity of their symbiotic microbes through full-length 16S rRNA amplicon sequencing. Phylogenetic analyses of mitochondrial genomes further support the taxonomic placement of the new species. The gill-associated microbial communities of these mussels include sulfur-oxidizing SUP05 bacteria, suggesting chemosynthetic symbiosis.

Key Words

Bathymodioline, Chemosynthesis, *Idas*, Mitochondrial genome, Sunken wood

Introduction

Mussels are among the most common organisms found in hydrothermal vent and cold seep ecosystems (Kiel 2010; Xu et al. 2019). However, the origins of deep-sea chemosynthetic symbiotic species remain a subject of debate due to the scarcity of chemosynthetic fossil evidence (Genio et al. 2012). Earlier researchers suggested that these species represent ancient lineages that survived extinction events (Newman 1985; McArthur and Tunnicliffe 1998). In contrast, recent evidence increasingly supports the hypothesis that mollusks in chemosynthetic ecosystems may have originated through adaptive radiation from shallow marine environments. In this context, sunken wood likely served as "stepping stones" facilitating the transition from shallow to deep-sea habitats (Distel et al. 2000; Romano et al. 2020; Altamia et al. 2024). This hypothesis is logically plausible. Geographically, sunken wood, originating from terrestrial sources, is commonly found along continental margins (Pailleret et al. 2007), potentially providing a substrate for mollusks to transition from shallow-water to deep-sea environments (Altamia et al. 2024). Energetically, wood provides an essential food source in the nutrient-scarce deep sea (Pop Ristova et al. 2017). Due to the difficulty of metabolising lignin and cellulose, sunken wood communities generally rely on organisms equipped with specific enzymes that convert these materials into bioavailable forms, with microbes playing an essential role in this process (Turner 1973; Bienhold et al. 2013). As symbiotic dependence increases and digestive tracts degrade, colonization of these environments naturally follows

(Lorion and Samadi 2010). From a redox perspective, the decomposition of plant and animal remains releases hydrogen sulfide, generating reducing conditions similar to those at hydrothermal vents. Such environments provide favorable conditions for benthic organisms to transition into chemosynthetic symbiosis (Distel et al. 2000; Bernardino et al. 2010). Molecular evidence further supports this hypothesis: Samadi et al. (2007) demonstrated that all mytilids associated with seeps, vents, sunken wood, and large animal carcasses form a monophyletic group, with species inhabiting organic falls occupying the basal positions on the phylogenetic tree. However, this hypothesis has been challenged by some opposing evidence. For instance, in the phylogenetic trees constructed by McCowin et al. (2020) and Lorion et al. (2013), *Vulcanidas insolatus* Cosel & B. A. Marshall, 2010,, a vent mussel, appears in a more basal branch than the lineage of wood-fall species. In recent years, with the increasing research into hydrothermal vents and cold seeps, molecular data for bathymodioline mussels from these habitats in waters surrounding China have been increasingly published (Lin et al. 2022; Wang et al. 2022; Li et al. 2023). However, compared to species from vents and seeps, our understanding of species associated with organic falls remains limited (Lorion et al. 2010; Lorion and Samadi 2010).

The genus *Idas* (Bathymodiolinae) was established based on samples collected from the North Atlantic (Jeffreys 1876). Members of *Idas* are small mussels widely distributed in organic fall and cold seep habitats (Lorion et al. 2012). Small bathymodioline mussels, such as those in the genus *Idas*, provide insights into a potential evolutionary pathway from organic falls to vents and seeps (Duperron et al. 2008a). Species of *Idas* are known for their extracellular symbionts and the flexibility of their symbiotic relationships, with some species harboring up to six chemosymbiotic bacteria (Duperron et al. 2008a), with others having lost their symbionts (Rodrigues et al. 2015). However, the diversity of this genus remains poorly understood, with only 14 named species currently recognized (WoRMS 2024). Some specimens considered to be *Idas* have not been formally described (Duperron et al. 2008b; Lorion et al. 2009; Lorion et al. 2012; Rodrigues et al. 2015). Due to morphological convergent evolution and the lack of molecular data, the classification of many bathymodioline species associated with organic falls remains unresolved. Some genera have been confirmed as polyphyletic (Thubaut et al. 2013b; McCowin et al. 2020), and the relationship between *Idas* and *Adipicola* remains unclear (Mietto et al. 2019). This classification mainly follows the works of Altamia et al. (2024), Lin et al. (2022), and Xu et al. (2019). However, some of the genus names employed in these studies, such as "Lignomodiolus" (Thubaut et al. 2013b) and "*Nipponiomodiolus*" (Samadi et al. 2015), remain unresolved and are considered nomena nuda.

The Pacific region is considered to be the origin of deep-sea mussels (Kyuno et al. 2009). Investigating wood-fall mussels in this area can provide crucial insights into the early evolutionary history of deep-sea mussels (Lorion and Samadi 2010). In 2023, we collected a piece of sunken wood from the East China Sea and obtained 30 specimens of *Idas* from it. DNA barcoding revealed that these samples formed three major clades: 23 of these specimens are closely related to *Idas* sp. ESU D, which was collected from Japanese and Philippine waters at depths of 760 to 1760 meters (Lorion et al. 2013). Five samples clustered with *Idas iwaotakii*, while two samples formed a distinct clade, constituting a sister group to *I. iwaotakii*. Apart from *I. iwaotakii*, the morphology of the remaining two species can be distinguished from all known *Idas* species in the Western Pacific region. In this study, we describe these two species based on an integrative analysis of their morphology and molecular phylogenetic position. Additionally, we present the complete mitochondrial genomes of the *Idas* genus for the first time and determine the diversity of their symbionts using full-length bacterial 16S amplicon sequencing. These findings provide valuable data for the biodiversity of wood-fall ecosystems and the gene flow of symbionts in the East China Sea and surrounding regions.

Materials and methods

Sample collection and photography

In April 2023, a piece of sunken wood, approximately 35 cm in length, was collected by a trawler in the East China Sea (30.7°N, 127.8°E) at approximately 460–550 m depth (Suppl. material 1). The wood sample was stored at -30 °C on board. After being transferred to the laboratory, the wood sample was cut open using a saw to collect the specimens inside. The specimens were preserved in 95% ethanol and stored at -80 °C. All type specimens involved in this study are housed in the specimen collection at the Third Institute of Oceanography, Ministry of Natural Resources (TIO).

Photographs were taken using a Leica S9D stereomicroscope and an MC170-HD digital camera.

DNA extraction, PCR amplification, and sequencing

The mantle, adductor muscle, and foot were dissected and used for extraction of the host DNA, while the gill was used to extract bacterial DNA. For some samples that were poorly preserved or too small, the entire soft tissue was used for DNA extraction. Total DNA from all body parts was extracted using the Qiagen DNeasy Blood & Tissue Kit following the manufacturer's instructions, and the DNA quality was assessed using NanoDrop.

The mitochondrial c oxidase subunit I (cox1) and 16S ribosomal RNA (16S) were obtained according to the method described by Meyer (2003), Olu-Le Roy et al. (2007) and Baco-Taylor (2002). The PCR reactions were conducted in 25 μL solution, containing 12.5 μL PCR mixture (Taq plus Master Mix II (Dye Plus)), 1 μL of each

Table 1. PCR primers, reaction conditions, and references.

Gene	Primer F	Primer R	Reaction Condition	Reference
cox1	dgLCO1490: 5′-GGTCAACAAATCATAAAGAYATYGG-3′	dgHCO2198: 5′-TAAACTTCAGGGTGACCAAARAAYCA-3′	95 °C/3min; 95 °C/55s, 45 °C/1min(+0.5 °C/cycle), 72 °C/1min, 15cycle; 95 °C/50s, 49 °C/1min, 72 °C/1min, 20 cycle; 72 °C/10min	Meyer (2003)
cox1	BathCOI-F: 5′-TGTGGTCTGGAATAATTGGAAC-3′	BathCOI-R: 5′-ATAAAAAGATGTATTRAARTGACG-3′	95 °C/3min; 95 °C/35s, 48 °C/35s, 72 °C/70s, 5 cycle; 94 °C/35s, 52 °C/35s, 72 °C/70s, 35cycle; 72 °C/10min	Olu-Le Roy, Von Cosel et al. (2007)
16s rRNA	LRJ-12864: 5′-CTCCGGTTTGAACTCAGATCA-3′	Idas 16SA: 5′-GGARGTASGCCCTGCCCWATGC-3′	95 °C/5min; 95 °C/40s, 55 °C/50s, 72 °C/60s, 34 cycle; 72 °C/10mins	Baco-Taylor (2002)

primer, 2.5 μL template, and 8 μL ultrapure water. Reaction conditions are shown in Table 1. All PCR products were evaluated for amplification efficiency using 1% agarose gel electrophoresis and sequenced at Sangon Biotech (Shanghai) Co., Ltd.. The sequences were aligned and trimmed the ends with low signal strength using SeqMan v. 7.1.0 (DNAStar, U.S.A.).

Phylogenetic analysis

The bathymodioline sequences obtained in this study and sequences of representative species were also obtained from GenBank for phylogenetic analysis. The list of sequences corresponding to those in Lin et al. (2022) (Suppl. material 4). Multiple sequences will be aligned with MAFFT (Katoh and Standley 2013) using the 'auto' strategy and codon (cox1) /normal (16S) alignment mode. The cox1 sequences were further refined using MACSE (Ranwez et al. 2018). Ambiguously aligned fragments were removed using Gblocks (Talavera and Castresana 2007). PhyloSuite (Zhang et al. 2020) was used to concatenate the sequences from different genes. Operational taxonomic units (OTUs) were delimited using the Automatic Barcode Gap Discovery (ABGD) method (Puillandre et al. 2012) via the online tool (https://bioinfo.mnhn.fr/abi/public/abgd/abgdweb.html), based on the COX1 sequence.

The best-fit partition model for both IQ-TREE (Guindon et al. 2010; Nguyen et al. 2015) and MrBayes (Ronquist et al. 2012) was selected using ModelFinder (Kalyaanamoorthy et al. 2017) based on the AIC criterion. For coding sequence (CDS) genes, the codon model was applied, selecting the optimal model for each codon position individually. Bayesian inference phylogenies were inferred using MrBayes (v3.2.6) (Ronquist et al. 2012) under the partition model (2 parallel runs, 2,000,000 generations), with the initial 25% of sampled data discarded as burn-in. Maximum likelihood (ML) phylogenies were inferred using IQ-TREE (Nguyen et al. 2015) under the edge-linked partition model with 5000 ultrafast bootstrap replicates and approximate Bayes test (Anisimova et al. 2011), and the Shimodaira–Hasegawa–like approximate likelihood-ratio test (Guindon et al. 2010). The phylogenetic trees were viewed and edited using iTOL (https://itol.embl.de/) (Letunic and Bork 2021).

Mitochondrial genome sequencing

Total genomic DNA was extracted from three individuals of *I. pacificus* sp. nov. and one individual of *Idas sinensis* sp. nov. using the Qiagen DNeasy Blood & Tissue Kit, following the manufacturer's instructions. The samples were submitted to Shanghai Majorbio Bio-pharm Technology Co., Ltd for library preparation and Illumina sequencing. The DNA was fragmented into random pieces using ultrasound, followed by end-repair, 3′-adenine addition, and adapter ligation. The DNA fragments were then enriched for approximately 400 bp genomic segments using magnetic beads and PCR amplification to generate the sequencing library. The DNA libraries were sequenced on the Novaseq 6000 platform to produce 150 bp paired-end reads. The quality of the sequencing raw data was evaluated using FastQC (Andrews 2010). The sequences were assembled and preliminarily annotated using MitoZ (Meng et al. 2019). Sequencing depth was assessed using Burrows-Wheeler Aligner (BWA) (Li 2013) and Samtools (Danecek et al. 2021).

Protein-coding gene (PCG) boundaries were adjusted by aligning sequences with related species using Nucleotide BLAST (BLASTn) and Protein BLAST (BLASTp) (*Gigantidas vrijenhoeki* S.-J. Jang, P.-T. Ho, S.-Y. Jun, D. Kim & Y.-J. Won, 2020; genbank accession number: NC_068739), and the positions of the start and stop codons were confirmed using SnapGene (v7.1.2). rRNA annotation was performed using MitoZ, with the process completed by calling infernal-1.1.1 (Nawrocki and Eddy 2013; Meng et al. 2019). tRNA annotations were corrected using tRNAscan-SE (Chan et al. 2021). Atp8 was manually annotated between nad3 and s-rRNA using Find Open Reading Frames (ORFs) (Lee et al. 2019). GC skew (= (G–C)/(G+C)) and GC content were calculated and mitochondrial circular plots were generated using proksee (https://proksee.ca/) (Grant et al. 2023). Mitochondrial gene arrangement patterns were determined using PhyloSuite (Zhang et al. 2020) and visualized with iTOL (Letunic and Bork 2021).

Mitochondrial genome-based phylogenetic tree

Mitochondrial genomes of 24 species from GenBank and 2 species (4 individuals) obtained in this study were used for phylogenetic analysis. Three *Mytilus* species were

used as outgroups (Liu et al. 2018; Lee et al. 2019). The concatenated sequences from 12 PCGs and two RNA (rRNA) genes were used to construct the phylogenetic tree. Due to the high variability in tRNA numbers (Lee et al. 2019) and the high variability in atp8 sequences (Zhao et al. 2022), these genes were excluded from the analysis.

The best partitioning scheme and evolutionary models for partitions were selected using PartitionFinder2 (Lanfear et al. 2017) with a greedy algorithm and AIC criterion. All other procedures were the same as for the phylogenetic analysis for the cox1 + 16S data.

16S rRNA amplicon sequencing and data analysis

Since the wood sample was collected by a commercial benthic trawler and stored at -30 °C in a freezer without immediate fixation, it was not possible to perform fluorescence in situ hybridization. The potential symbionts were inferred using full-length 16S rRNA amplicon sequencing. Only a subset of samples with successfully dissected gill tissues were used for this analysis.

PCR reactions and sequencing were performed as a commercial service at Shanghai Majorbio Bio-pharm Technology Co., Ltd. The primers used were 27F(AGRGTTYGATYMTGGCTCAG) and 1492R(RGYTACCTTGTTACGACTT) (Weisburg et al. 1991). Primers were tailed with PacBio barcode sequences to distinguish each sample. The PCR was conducted using an ABI GeneAmp 9700, with Kapa Biosystems KAPA HiFi DNA Polymerase. The reaction mixture consisted of 10 µl 2×Pro Taq, 0.8 µl Forward Primer (5 µM), 0.8 µl Reverse Primer (5 µM), 10 ng/µl Template DNA, and ddH_2O to a total volume of 20 µl. The PCR program included an initial denaturation at 95 °C for 3 minutes, followed by 29 cycles of 95 °C for 30 seconds, 60 °C for 30 seconds, 72 °C for 45 seconds, and a final extension at 72 °C for 10 minutes. PCR products were purified using the AMPure® PB beads (Pacifc Biosciences, CA, USA) and quantified with Qubit 4.0 (Thermo Fisher Scientific, USA).

Purified products were pooled in equimolar and DNA library was constructed using the SMRTbell prep kit 3.0 (Pacifc Biosciences, CA, USA) according to PacBio's instructions. Purified SMRTbell libraries were sequenced on the Pacbio Sequel IIe System (Pacifc Biosciences, CA, USA). High-fidelity (HiFi) reads were obtained from the subreads, generated using circular consensus sequencing via SMRT Link (v11.0). Raw data quality was assessed using fastp (v0.19.6) (Chen et al. 2018). Barcode-CCS recognition was performed using Lima (https://lima.how/). ASV (Amplicon Sequence Variant) information was obtained using DADA2_CCS (Callahan 2022) (https://benjjneb.github.io/dada2/). ASVs aligned to chloroplasts and mitochondria were removed, along with ASVs with a relative abundance below 0.001. Sequences were rarefied to the minimum sample size. Taxonomic annotation was performed using the silva138.1/16s_bacteria database. ASV analyses, including sample filtering and sequence rarefaction, generation of Venn diagrams, community bar plots, and heatmaps, were performed using Majorbio Cloud 2024 (cloud.majorbio.com). ML phylogenetic trees were constructed using PhyloSuite (Zhang et al. 2020) following the same procedures as in the previous section. Microbial functions were predicted using FAPROTAX (Louca et al. 2016).

Results and discussion

Other fauna on the sunken wood

The biological community on the sunken wood is closely related to both the wood species (Pailleret et al. 2007) and the successional stage of the wood-associated community (Bernardino et al. 2010; Bienhold et al. 2013). These factors are crucial for determining the successional stage of the sample and, in turn, inferring the developmental stage of the mussels. However, due to the potential loss of some organisms caused by water flow during trawling (Pailleret et al. 2007), we did not conduct a quantitative assessment of the individual numbers of each species.

The most abundant species on the sunken wood collected in this study was *Pectinodonta aurora* B. A. Marshall, Puillandre, Lambourdière, Couloux & Samadi, 2016, predominantly consisting of mature individuals. The surface of the wood was covered with characteristic feeding pits made by this species (Suppl. material 1). Additionally, members of the families Teredinidae and Xylophagaidae were present, along with their calcareous tubes. Other organisms included small numbers of sea urchins, *Calagrassor* species, and polychaetes, among others. A detailed species list and their respective DNA barcode GenBank accession numbers are provided in Suppl. material 5.

Phylogenetic trees based on cox1 and 16S sequences

The trimmed 16S gene was 404 bp long, and the cox1 sequence was 588 bp long (GenBank accession numbers are listed in Suppl. material 6). The best-fit models according to AIC are provided in Suppl. material 7. The resulting ML and BI phylogenetic trees show some structural differences. Since the ML tree had higher support at the nodes, only the ML tree is presented in the main text, while the BI tree is shown in Suppl. material 2.

Due to some confusion in the systematics of the genera *Idas* and *Adipicola* (Gustafson et al. 1998; Mietto et al. 2019), this study follows Thubaut et al. (2013b), Thubaut et al. (2013a), and Genio et al. (2015) in treating *Adipicola iwaotakii* (Habe, 1958) as *Idas iwaotakii* (Habe, 1958) based on molecular evidence. Therefore, among the recognized species of *Idas*, the following four species have been recorded in the Pacific region: *I. coppingeri* (Murray et al. 1885), *I. indicus* (Smith 1899), *I. washingtonius* (Kyuno et al. 2009; Harbo and Gillespie 2021), and *I. iwaotakii* (Kyuno et al. 2009).

The ABGD analysis revealed that, aside from *Modiolus rumphii* which was used as an outgroup, the remaining sequences could be divided into 51 OTUs. Among these, five OTUs contain more than one sequence that was classified as different species/ESUs in previous studies (Fig. 1: OTU-18, OTU-29, OTU-33, OTU-34 and OTU-45). Both the phylogenetic tree and the ABGD analysis support the clustering of the 30 samples collected in this study into four distinct OTUs (Fig. 1: OTU-47, OTU-48, OTU-49, and OTU-51). Apart from the clade containing *I. iwaotakii*, the other two branches represent the newly described species in this study, temporarily referred to as *Idas* sp. OTU-47 and *I.* sp. OTU-51. Among these, *Idas* sp. OTU-47 forms a sister group with *I. iwaotakii,* while *Idas* sp. OTU-51 is a sister group to *Idas* sp. ESU C. Regarding the clade containing *I. iwaotakii*, sample TIO2023-1816B28 is particularly noteworthy. Although the terminal containing this sample clusters within *I. iwaotakii*, its cox1 sequence shows only 92% similarity to known *I. iwaotakii* sequences. This suggests that the sample may belong to the "species complex within the *Adipicola* (*Idas*) genus" as described by Lorion et al. (2009).

We acknowledge the limitations of using mitochondrial genomes to reconstruct phylogenetic trees. Factors such as incomplete lineage sorting (McGuire et al. 2007; Kimball et al. 2021), introgression, doubly uniparental inheritance (DUI) (Walker et al. 2006; Doucet-Beaupré et al. 2010), maternal inheritance, and recombination can complicate mtDNA interpretations (Rubinoff et al. 2006), making it less suitable as the sole data source for phylogenetic analysis. However, the relatively higher mutation rate of mitochondrial genomes compared to nuclear genomes (Saccone et al. 1999) makes them particularly useful for resolving phylogenetic relationships at lower taxonomic levels. Given the high dispersal potential of organic fall mussel larvae, populations separated by thousands of kilometers may still exhibit close phylogenetic relationships (Fukasawa et al. 2015; DeLeo et al. 2022). Therefore, selecting rapidly evolving genes for phylogenetic tree construction may provide higher resolution in such cases. Furthermore, we compared our phylogenetic tree with that of Lin et al. (2022), which incorporated both mitochondrial and nuclear genes, and found similar topologies, further supporting the reliability of our inferred branching pattern.

General features of the mitochondrial genomes of *Idas pacificus* sp. nov. and *Idas sinensis* sp. nov.

We obtained the mitochondrial genomes of four individuals from the two species, *Idas* sp. OTU-47 and *Idas* sp. OTU-51 (PQ541016–PQ541019, Suppl. material 3). The average sequencing depth of the four samples ranged from 7,915 to 7,940. Among them, the mitochondrial genomes of three *Idas* sp. OTU-51 specimens were assembled into a circular form, with genome sizes ranging from 17,234 bp to 17,480 bp. Each genome includes 23 transfer RNA (tRNA) genes (including 2 trnS and 2 trnL), 13 PCGs, and 2 rRNA genes, with an AT content of 66.67%. The mitochondrial genome of the *Idas* sp. OTU-47 specimen was not circularized, with the assembled portion measuring 17,742 bp. This genome also includes 23 tRNA genes (including 2 trnS and 2 trnL), 13 PCGs, and 2 rRNA genes, with an AT content of 67.91%. The GC skewness values for both species are positive. Except for trnT, all other genes are located on the heavy strand.

Phylogenetic tree and mitochondrial gene arrangement

The topologies of the BI and ML mitochondrial phylogenetic trees are congruent, with the exception of the relationship between *Bathymodiolus marisindicus* and *B. brooks* (Fig. 2). In our phylogenetic analysis, the genera *Bathymodiolus, Idas,* and *Gigantidas* cluster within the subfamily Bathymodiolinae. The clade containing the genus *Modiolus* is sister to Bathymodiolinae, which is consistent with previous analyses (Liu et al. 2018). Both the mitochondrial genome phylogenetic tree and the cox1+16S phylogenetic tree are congruent in topology with those of Xu et al. (2019) in that *Gigantidas japonicus* and *G. securiformis* belong to the genus *Gigantidas* rather than *Bathymodiolus*. Among the species analyzed, the subfamily Bathymodiolinae exhibits shorter branch lengths. Unlike the phylogenetic tree from Lin et al. (2022), the phylogenetic tree based on the 12 PCGs and two rRNA genes reveals a sister relationship between *Bathymodiolus* and *Gigantidas*.

The orders of PCGs and rRNA are relatively conserved within the subfamily Bathymodiolinae and the genus *Modiolus* (Fig. 2), consistent with previous studies (Lee et al. 2019). The arrangement of tRNA genes also exhibits significant conservation within the subfamily Bathymodiolinae. Specifically, the presence of two trnL copies flanking atp8 and one trnS adjacent to rrnL on each side is generally a common characteristic of *Bathymodiolus*, with the exception of *Bathymodiolus brooks*.

Taxonomy

Family Mytilidae Rafinesque, 1815
Genus *Idas* Jeffreys, 1876

Idas sinensis sp. nov.

https://zoobank.org/F28DA47C-082B-40FD-9B47-CECB0BF1D19C

Figs 3H–I, 4F–G

(*Idas* sp. OTU-47 mentioned earlier)

Materials examined. Two specimens collected from the same piece of sunken wood by trawling from a seabed at a depth of 460–550 m (30.7°N, 127.8°E) in April 2023.

Type material. ***Holotype*** • TIO2023-1816B6 (length: 9.3 mm); ***Paratype*** • TIO2023-1816B21 (length: 13.4 mm), with a fractured right valve.

Diagnosis. Shells extremely thin, with internal surface color similar to external surface. Dorsal and ventral margins nearly parallel. Bristles short, brown, mainly concentrated along both sides of ridge in posterior triangular

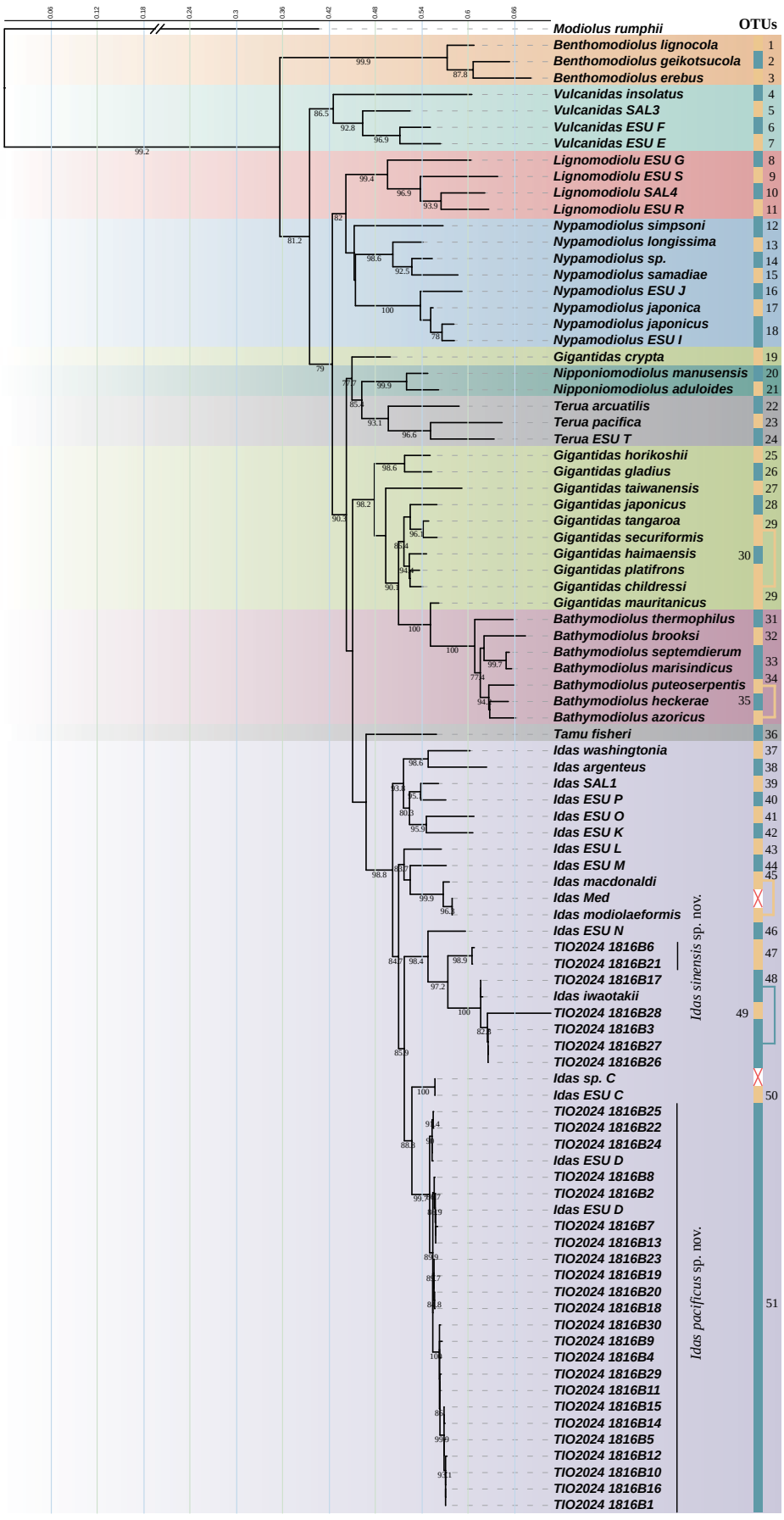

Figure 1. ML phylogenetic tree of the subfamily Bathymodiolinae based on the cox1 and 16S genes. Numbers near the nodes represent bootstrap values (only values >75% are shown). Different genera are distinguished by colors. OTUs are annotated with color blocks and numbers following the species names. Red crosses indicate leaves without cox1 gene data.

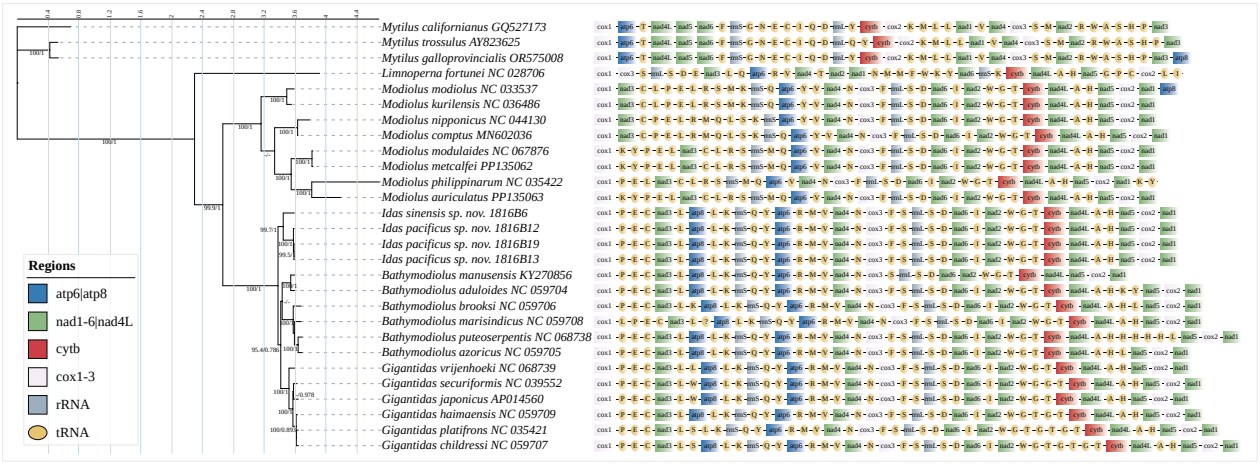

Figure 2. Mitophylogenyinferred using ML and BI methods (based on the concatenated dataset of 12 PCGs and 2 rRNA genes) and gene order for the family Mytilidae. Numbers near the nodes represent ML bootstrap values and BI posterior probabilities (only values >75% and >0.75 are shown, respectively).

area. Shells resemble those of *I. iwaotakii*, but overall outline more elliptical compared to *I. iwaotakii* due to more similar anterior and posterior heights.

Shell morphology. Shells 9.3 mm to 13.4 mm in length, 3.1 mm to 3.9 mm in height (Fig. 3H–I), thin, fragile, deep olive-yellow, semi-transparent, very thin nacreous layer. Highly elongated, elliptical shape with concentric growth lines. Small specimen with rounded anterior and posterior margins; large specimen with broadly triangular posterior margins. Dorsal and ventral margins straight and nearly parallel, with slight incurvature along the ventral outline in larger specimens. Very short, dark brown bristles distributed mainly along the ridge from the posterior margin to the umbo. Umbo extremely anterior. Hinge plate slightly curved, with degenerated anterior hinge teeth (Fig. 4F–G). Inner shell surface smooth, lacking muscle scars. Prodissoconch pink and rounded.

Soft tissue anatomy. The soft tissue was poorly preserved to allow for detailed examination. However, the foot of the specimen preserved in alcohol was purple.

Gill-associated microbes. Only the gill tissues of the holotype (TIO2023-1816B6) could be used for analysis of symbiotic microbes. Among the bacteria associated with the gill, *Pseudohongiella* sp., *Reichenbachiella* sp., and SUP05 cluster were most abundant, representing 70%, 9%, and 7% of the sequences, respectively (Figs 5, 6A).

Habitat and distribution. So far, this species has only been found within wood. It is known only from the East China Sea (30.7°N, 127.8°E).

Etymology. The name *sinensis* – the Latinized form of China, refers to the type locality, within the Chinese EEZ of the East China Sea.

Remarks. *Idas sinensis* sp. nov. exhibits a close morphological and phylogenetic relationship with *I. iwaotakii*, as both species share an elongated shell shape, characterized by nearly parallel dorsal and ventral outlines, a feature that sets them apart from *Idas* species in other clades. The primary difference between these species (for specimens around 1 cm in length) lies in the curvature of the anterior and posterior margins: *Idas sinensis* sp. nov. has a more capsule-shaped outline, while *I. iwaotakii* has a more triangular profile.

Additionally, the Mediterranean species *Idas cristiani* Fr. Giusti, Mietto & Sbrana, 2012 and *Idas emmae* Fr. Giusti, Mietto & Sbrana, 2012 also exhibit an elongated form. However, none of the *Idas sinensis* sp. nov. specimens (9.3 mm and 13.4 mm) have anterior hinge teeth, whereas *I. cristiani* has 5–6 small teeth below the umbo, and *I. emmae* has three. Moreover, *Idas sinensis* sp. nov. has sparser bristles compared to *I. cristiani*, and its shell (H/L = 0.29–0.33) is higher than that of *I. emmae* (H/L = 0.25–0.26) (Giusti et al. 2012).

Idas pacificus sp. nov.

https://zoobank.org/18C6A39C-48B0-429F-803A-6A84CC33D358

Figs 3A–G, 4A–E, 7, 8A

(*Idas* sp. OTU-51 mentioned earlier; *Idas* sp. ESU D, as mentioned by Lorion et al. (2010))

Materials examined. All 23 specimens were collected from a piece of wood by trawling at 460–550 m seabed at 30.7°N, 127.8°E in April 2023.

Type material. ***Holotype*** • TIO2023-1816B14 (length: 10.8 mm); ***Paratypes*** • six specimens, TIO2023-1816B9, TIO2023-1816B12, TIO2023-1816B15, TIO2023-1816B24, TIO2023-1816B29, TIO2023-1816B30

Diagnosis. Adult specimens approximately measure 10 mm in length, resembling the general outline of *Idas ghisottii* Warén & Carrozza, 1990 from the Mediterranean region. Shells with an H/L ratio of about 0.36 to 0.45, maintaining a consistent overall shape across different sizes, though older individuals are slightly more elongated. Umbo located at approximately the anterior 1/7 to 1/9 of the shell length. The triangular area, from the posterior margin to the umbo, near the dorsal margin, is covered with bristles that match the external shell surface color. The base of the bristles is triangular in shape.

Shell morphology. Shells 3.2–10.8 mm in length, 1.4–4.1 mm in height (Fig. 3A–G). Shells thin, olive-yellow,

Figure 3. Specimen photographs of *Idas pacificus* sp. nov. and *Idas sinensis* sp. nov. **A–G.** *Idas pacificus* sp. nov.: **A.** Sample ID: TIO2023-1816B30, paratype, left valve; **B.** Sample ID: TIO2023-1816B29, paratype, left valve; **C.** Sample ID: TIO2023-1816B24, paratype, left valve; **C'.** Dorsal view; **D.** Sample ID: TIO2023-1816B9, paratype, left valve; **E.** Sample ID: TIO2023-1816B12, paratype, left valve; **F.** Sample ID: TIO2023-1816B15, paratype, left valve; **G.** Sample ID: TIO2023-1816B14, holotype, left & right valve; **G'.** Dorsal view; **H, I.** *Idas sinensis* sp. nov.: **H.** TIO2023-1816B21, paratype, left valve; **I.** TIO2023-1816B6, holotype, left & right valve; **I'.** Dorsal view. Scale bar: 2 mm.

semi-transparent, with prominent concentric growth lines. Shells oval, with straight dorsal margin, slightly incurved ventral outline, and rounded posterior margin. Triangular area near dorsal margin, from posterior margin to umbo, sparsely covered with bristles. Umbo located at approximately the anterior 1/7 to 1/9, shifting forward with increasing shell size and tilting slightly forward. Hinge plate slender and straight (Fig. 4A–E). Both inner and outer shell surfaces with pearly luster. Inner shell surface smooth, faint traces of anterior adductor scar and pallial line, difficult to discern under optical microscope. Posterior adductor scar large, nearly circular; anterior adductor scar shallow, curved droplet-shaped (SEM images in Fig. 7C). Pallial sinus indentation small. Prodissoconch pink, rounded, smooth, ~400 μm in diameter.

Soft tissue anatomy. Foot well-developed, approximately 40% of shell length (Fig. 7). Like *I. macdonaldi*, byssal retractors continuous and not divided into posterior and anterior portions (Gustafson et al. 1998). Byssus retractor muscle and pedal retractor muscle fused into a single strand. Cross-section of anterior adductor muscle teardrop-shaped, posterior adductor muscle round. No byssus observed.

Gill-associated microbes. The 13 specimens of *Idas pacificus* sp. nov. share 11 common microbial species

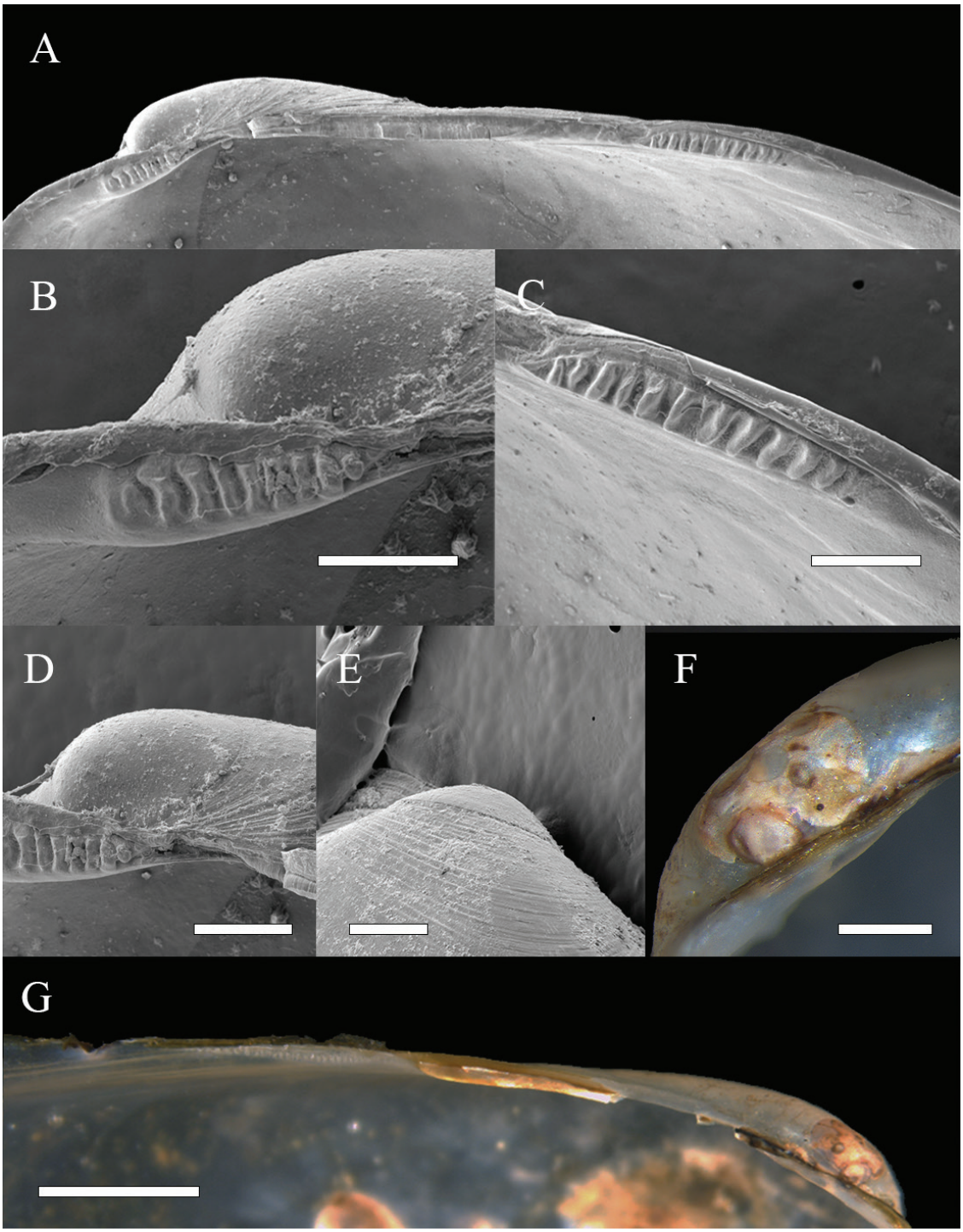

Figure 4. Photographs of the hinge structures and prodissoconch of the specimens of *Idas pacificus* sp. nov. and *Idas sinensis* sp. nov. **A–E.** *Idas pacificus* sp. nov. Sample ID: TIO2023-1816B7, length: 8.3 mm. **A.** Hinge line of specimen; **B.** Hinge denticles located immediately below the umbo; **C.** Hinge denticles located posterior of the ligament; **D.** Prodissoconch; **E.** Ventral view of the larval shell (left valve); **F, G.** *Idas sinensis* sp. nov. Sample ID: TIO2023-1816B6, length: 9.3 mm. hinge line of specimen; **F.** Prodissoconch; **G.** Hinge line of specimen (left valve). Scale bars: 200 μm (**B–E**); 500 μm (**F**); 1 mm (**G**).

(Fig. 6), with 7 of these accounting for more than 1% of the total read abundance. Specifically, three species belong to Gammaproteobacteria, two to Bacteroidia, and two to Campylobacteria. In addition, genetic diversity among symbionts from different *Idas pacificus* sp. nov. specimens is notable, with 11 different SUP05 cluster genotypes detected among the 13 specimens (Fig. 5). ASV2 is the most common SUP05 genotype, dominating in 6 of the specimens where it accounts for over 50% of all SUP05 sequences. In the remaining specimens, the predominant SUP05 genotypes include ASV4, ASV10, ASV96, ASV144, and ASV325.

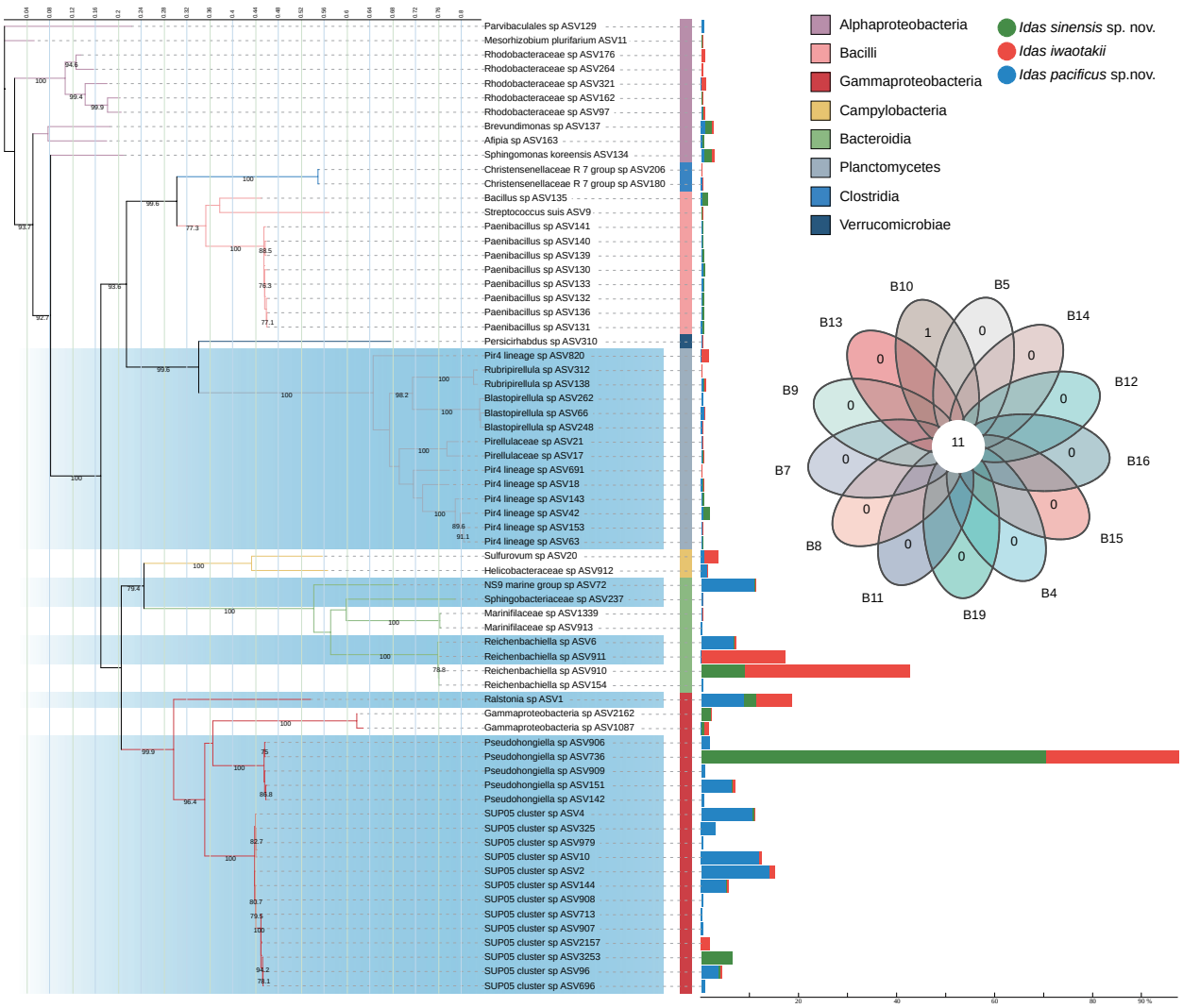

Figure 5. The ML phylogenetic tree of gill-associated microbiota from 16 *Idas* samples obtained in this study. Numbers near the nodes represent bootstrap values (only values >75% are shown). Branches with a blue background indicate bacterial species shared by 13 *Idas pacificus* sp. nov. samples. Stacked bar chart adjacent to the phylogenetic tree shows the relative abundance of each ASV in different species (expressed as the percentage of sequences averaged per individual). Venn diagram displays the symbiont species shared among the 13 *Idas pacificus* sp. nov. individuals.

Habitat and distribution. The *Idas pacificus* sp. nov. specimens lived inside holes in a piece of sunken wood. These holes are typically round, each containing only a single individual. Unlike those of *I. iwaotakii* and *Idas sinensis* sp. nov., the holes occupied by *I. pacificus* sp. nov. are black (Fig. 8A), which may be due to FeS precipitation (Bienhold et al. 2013). This hypothesis is supported by the functional heatmap of the microbes recovered from the gill tissues (Fig. 6B), which showed that *I. pacificus* sp. nov. had a high abundance of sulfur-oxidizing bacteria. Due to the limited samples of *I. iwaotakii* and *Idas sinensis* sp. nov. and the fact that all analyzed *Idas* samples came from the same piece of wood, we could not determine the generality of this phenomenon.

The type specimens were collected from sunken wood in the East China Sea at depths of approximately 460–550 meters. *Idas pacificus* sp. nov. was reported on sunken wood in Philippines and Vanuatu as *Idas* sp. ESU D by Lorion et al. (2009), and experimental bones placed in Japanese waters (Lorion et al. 2013). Comparing our DNA barcode data for *Idas pacificus* sp. nov. with those available on GenBank indicates that it is conspecific to *Idas* sp. ESU D (GenBank Acc. No. HF545116, EU702350, EU350071, EU702358), with K2P distances of 0–0.3%, being smaller than the inter-specific genetic divergence between other species of *Idas* (e.g. 19.8% between *I. argenteus* and *I. washingtonius*, and 2.8% between *I. macdonaldi* and *I. modiolaeformis*, See Suppl. material 8 for details.). Therefore, *Idas pacificus* sp. nov. may be widespread in the Western Pacific, including East China Sea (this study), Santo Island in Vanuatu (Lorion et al. 2009), Bohol Sea (Duperron et al. 2009), and Japanese waters (Lorion et al. 2013), with water depth ranging from 460 to 1764 meters (Duperron et al. 2009; Lorion et al. 2013).

Etymology. Since our comparison with DNA barcode data obtained from GenBank indicates this species

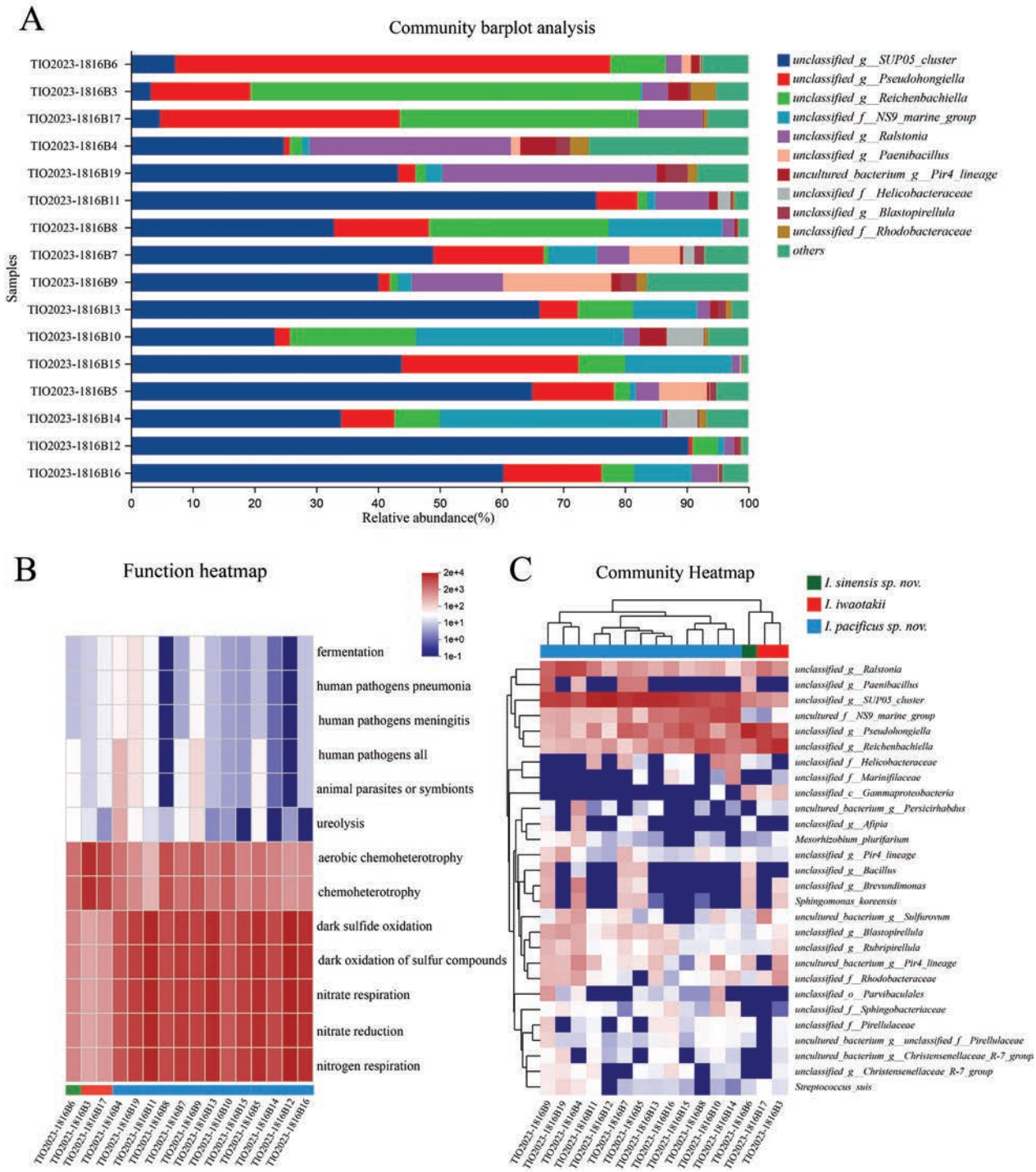

Figure 6. Gill-associated Bacterial Community Analysis of *Idas*. **A.** Relative abundance; **B.** Functional heatmap generated by FAPROTAX; **C.** Community heatmap.

to be widely distributed in the Western Pacific, the name "*pacificus*" was given to the species.

Remarks. *Idas pacificus* sp. nov. is notably different from *I. iwaotakii*, which has a very elongated shape, a sharply pointed posterior margin, and shorter and darker bristles that appear to degrade with increasing size. Bristles are also a key distinguishing feature that separates this species from *I. washingtonius*, *I. coppingeri*, and *I. indicus*. The first two species lack bristles (Murray et al. 1885; Harbo and Gillespie 2021), while *I. indicus* has very short bristles and a more pronounced curvature of the ventral outline (Smith 1899).

Adaptation of *Idas pacificus* sp. nov. and *Idas sinensis* sp. nov. to the sunken wood habitat

Sunken wood provides shelter for a variety of marine organisms, offering both a carbon source and substrate (Altamia et al. 2024). Compared to other Bathymodiolinae species

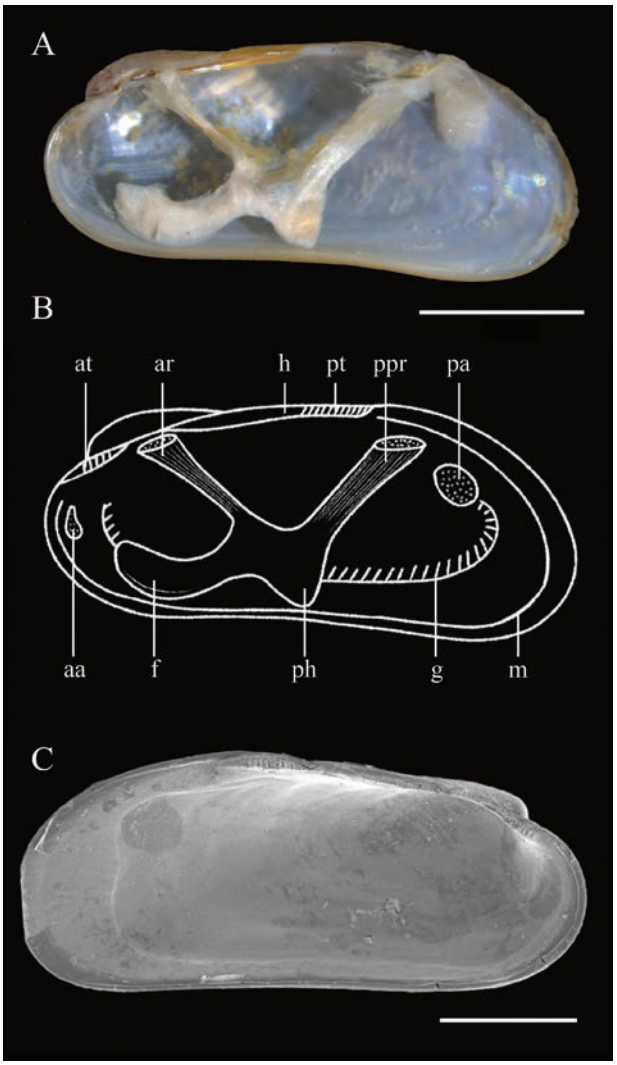

Figure 7. Internal View of *Idas pacificus* sp. nov. **A.** Sample ID: TIO2023-1816B9, lateral view; **B.** Schematic drawing of the right shell and internal structures based on TIO2023-1816B9, the positions of the gill and mantle confirmed across multiple samples; **C.** SEM image showing the anterior adductor scar, pallial line, posterior adductor scar, and pallial sinus, sample ID: TIO2023-1816B7. Note that the posterior margin of the specimen is incomplete. Abbreviations: aa: anterior adductor; ar: anterior byssus retractor; at: anterior hinge teeth; f: foot; g: gill; h: hinge; m: mantle; pa: posterior adductor; ph: pedal heel; ppr: posterior byssus retractor and pedal retractor; pt: posterior hinge teeth. Scale bars: 2 mm.

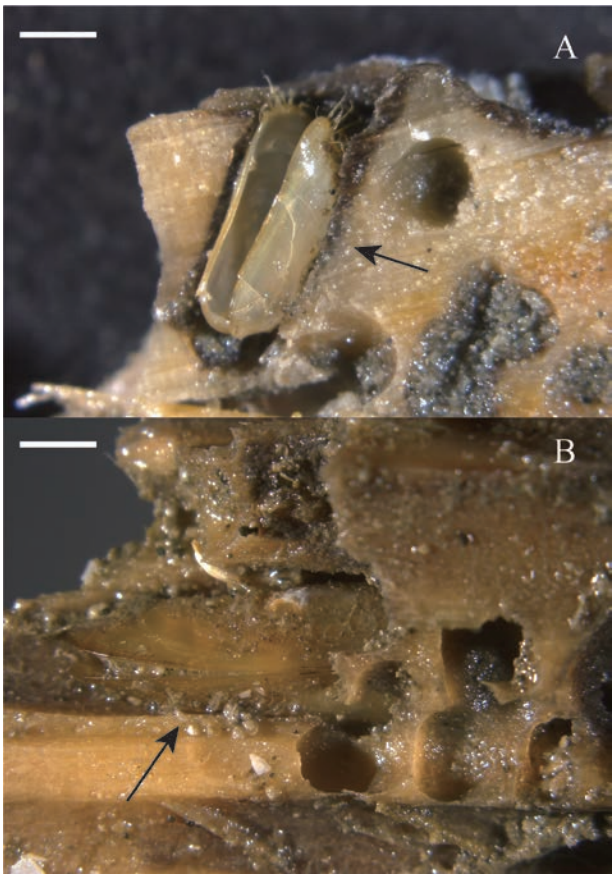

Figure 8. Situ views of the **A.** *Idas pacificus* sp. nov. and **B.** *I iwaotakii*. Both images show the specimens with portions of the wood removed to expose them. Scale bars: 2mm.

inhabiting hydrothermal vents and cold seeps, mussels associated with organic fall ecosystems are generally smaller in size. While hydrothermal vents and cold seeps can vary in size and longevity – ranging from small, short-lived outgassing sites to areas spanning several million square meters (Andrianasolo et al. 2012; Wang et al. 2022), wood fall habitats are typically more localized and transient. Organisms inhabiting these transient environments may need to complete their life cycles within a limited timeframe, and smaller body sizes could represent an adaptation to such constraints.

Both *Idas pacificus* sp. nov. and *Idas sinensis* sp. nov. have thin and fragile shells, which would offer little protection against predators in more exposed environments. However, the sunken wood provides a natural shielding habitat. Altamia et al. (2024) suggested that the bristles of *Idas* species may help keep the valves away from the burrow walls and possibly improve water flow around the animals. This hypothesis may partially explain the differences in bristle development between the two species. *Idas pacificus* sp. nov., with its shorter and more triangular body shape, exhibits more developed bristles, which may enhance stability in cylindrical burrows. Notably, neither species exhibited byssal threads, likely an adaptation to inhabiting wood holes where strong water currents are not a concern.

Diversity of gill-associated microbes

Sample TIO2023-1816B18 was excluded from further analysis due to substantially fewer valid sequences (7,614, compared to > 18,000 in each of the other 16 specimens). A total of 2,853 ASVs were generated across all samples, with an average sequence length of 1,496 bp. After removing chloroplast and mitochondrial sequences and those with an abundance below 0.001, 28 species remained, encompassing 68 ASVs.

We compared the gill-associated bacterial community composition among *Idas pacificus* sp. nov., *I. iwaotakii* and *Idas sinensis* sp. nov. obtained in this study (Figs 5, 6C). All three species harbor *Reichenbachiella*

sp., *Pseudohongiella* sp., and species of the SUP05 cluster in their gills, but the relative abundance and the number of ASVs of these bacteria differ among the three species. Four *Reichenbachiella* sp. ASVs were detected in this study (Fig. 5), with only ASV6 found in *Idas pacificus* sp. nov. and ASV911 exclusively in *I. iwaotakii*. For *Pseudohongiella* sp., its relative abundance reached 30% in *I. iwaotakii* and 70% in *I. sinensis* sp. nov. samples, with ASV736 comprising over 95% of all *Pseudohongiella* sp. sequences in these two species. In contrast, the relative abundance of *Pseudohongiella* sp. in *Idas pacificus* sp. nov. samples was only around 10%, and the proportion of ASV736 sequences was less than 1%.

In *Idas sinensis* sp. nov., the most abundant bacterium is *Pseudohongiella* sp. This bacterium was present in all *Idas* samples examined in this study and showed high relative abundance in the gills of the closely related *I. iwaotakii*. Therefore, we hypothesize that it is likely a gill symbiont of *Idas sinensis* sp. nov. However, since only one specimen was examined for gill-associated bacteria, it remains unclear whether the less abundant bacteria are random associates or symbionts.

In the 14 *Idas pacificus* sp. nov. samples, the relative abundance of the chemosynthetic SUP05 group ranges from 23% to 90%, while in *I. iwaotakii* and *I. sinensis* sp. nov. samples, the maximum relative abundance of the SUP05 group is only 7% (Fig. 6A). Although the SUP05 group is detected in the gills of all three species, there is a marked difference in the dominant ASVs. In *I. iwaotakii*, ASV2157 is the dominant ASV and is found exclusively in this species, while in *I. sinensis* sp. nov., ASV3253 is the dominant ASV and is also unique to this species.

The presence of the same bacterial species, especially those of the chemosynthetic SUP05 group, across different *Idas* species suggests that these are potential symbionts playing crucial roles in the survival of *Idas*. Given that there is substantial evidence indicating that bathymodioline symbionts are primarily acquired through horizontal transmission (Won et al. 2008; Kiel 2010; Romero Picazo et al. 2019; Franke et al. 2021; Lin et al. 2022) and that the piece of wood was only 35 cm long, the likelihood of uneven bacterial distribution due to water flow is minimal. We speculate that different host species may exhibit a preference for specific genotypes of symbionts, or the host may acquire symbionts before colonizing the sunken wood, with genetic differences in the same symbiont species among different *Idas* species arising from bacteria in distinct water masses encountered during the planktonic phase. The variation in the relative abundance of SUP05 may suggest that microbial communities play different roles in different *Idas* hosts.

The SUP05 cluster dominated the gill-associated bacterial community of *Idas pacificus* n. sp. (Figs 5, 6A). These species have been known to be chemosynthetic, obtaining energy through sulfur oxidation (Duperron et al. 2008b) and are common in bathymodiolines, including those of the genera *Idas* (Duperron et al. 2008b), *Adipicola* (Fujiwara et al. 2010), *Nypamodiolus* (Lin et al. 2022) and *Bathymodiolus* (van der Heijden et al. 2012; Raggi et al. 2013).

The function heatmap (Fig. 6B) reveals that, compared to *Idas iwaotakii* and *Idas sinensis* sp. nov., the symbiotic microbes in the gills of *Idas pacificus* sp. nov. show a higher nitrogen and sulfur metabolic potential. By contrast, the symbionts of *I. iwaotakii* exhibit a stronger association with aerobic and general chemoheterotrophy, with *Idas sinensis* sp. nov. showing an intermediate profile. The differences in the relative abundance of SUP05 among different hosts may be a key factor contributing to this variation, as this group can couple sulfide oxidation with nitrate reduction (Callbeck et al. 2018).

The community heatmap (Fig. 6C) also shows a high correlation in bacterial composition between *Idas iwaotakii* and *Idas sinensis* sp. nov. Given that these two species are closely related phylogenetically, their preference for specific bacteria may stem from a shared ancestral lineage. The differentiation in symbiotic microbes among the *Idas* individuals from the same piece of sunken wood could suggest niche differentiation among closely related hosts. However, considering the observed flexibility in symbiont composition among *Idas* species (Duperron et al. 2008a; Rodrigues et al. 2015), the limited number of samples for *Idas iwaotakii* and *Idas sinensis* sp. nov., and the fact that our specimens originated from the same piece of wood, it remains unclear if the symbiont community of these two new species varies with habitat. Further studies are required to investigate these inter- and intra-species variations.

Conclusion

This study describes two new species from sunken wood habitats on the East China Sea: *Idas sinensis* sp. nov. and *Idas pacificus* sp. nov., detailing their morphological characteristics. These findings extend the known distribution and diversity of chemosynthetic mussels. For the first time, we present mitochondrial genome sequences of the *Idas* species and determine their phylogenetic relationships with other bathymodioline mussels. Our results confirm that these mussels from sunken wood are closely related to their counterparts from cold seeps and hydrothermal vents in the *Gigantidas* and *Bathymodiolus* genera. Additionally, we obtained full-length 16S rRNA sequences of the gill-associated bacteria from *I. pacificus* sp. nov., *I. sinensis* sp. nov., and *I. iwaotakii*. Significant differences were observed in the composition of gill symbionts among these species, potentially reflecting ecological niche differentiation. Collectively, our findings highlight the close evolutionary and symbiotic relationships between sunken wood mussels and other chemosynthetic mussels.

Data availability statement

All gene sequences generated in this study have been deposited in the GenBank database under the accession numbers listed in Suppl. material 6.

Acknowledgements

We sincerely thank the anonymous reviewer for their valuable comments, which have greatly benefited our work. For assistance with the identification of sea urchins in the sunken wood fauna, we are grateful to Professor Rich Mooi, Curator Emeritus at the California Academy of Sciences. We acknowledge the financial support provided by the National Key Research and Development Program of China (2022–24, 2022YFC2804001), the Natural Science Foundation of Fujian Province, China (2023J011373), and the Natural Science Foundation of Xiamen, China (3502Z20227252), and the General Research Fund of Hong Kong (12101021).

References

Altamia MA, Appiah-Madson HJ, Falco-Poulin R, Huettel B, Rubin-Blum M, Dubilier N, Gruber-Vodicka HR, Leisch N, Distel DL (2024) Wooden steps to shallow depths: A new bathymodiolin mussel, *Vadumodiolus teredinicola*, inhabits shipworm burrows in an ancient submarine forest. Deep Sea Research Part I: Oceanographic Research Papers 204: 104220. https://doi.org/10.1016/j.dsr.2023.104220

Andrews S (2010) FastQC: a quality control tool for high throughput sequence data. Cambridge, United Kingdom.

Andrianasolo E, Lutz R, Falkowski P (2012) Deep-sea hydrothermal vents as a new source of drug discovery. Studies in Natural Products Chemistry 36: 43–66. https://doi.org/10.1016/B978-0-444-53836-9.00020-7

Anisimova M, Gil M, Dufayard J-F, Dessimoz C, Gascuel O (2011) Survey of branch support methods demonstrates accuracy, power, and robustness of fast likelihood-based approximation schemes. Systematic Biology 60: 685–699. https://doi.org/10.1093/sysbio/syr041

Baco-Taylor AR (2002) Food web structure, succession, and phylogenetics on deep-sea whale skeletons. University of Hawai'i at Manoa.

Bernardino AF, Smith CR, Baco A, Altamira I, Sumida PY (2010) Macrofaunal succession in sediments around kelp and wood falls in the deep NE Pacific and community overlap with other reducing habitats. Deep Sea Research Part I: Oceanographic Research Papers 57: 708–723. https://doi.org/10.1016/j.dsr.2010.03.004

Bienhold C, Pop Ristova P, Wenzhöfer F, Dittmar T, Boetius A (2013) How deep-sea wood falls sustain chemosynthetic life. PLoS One 8: e53590. https://doi.org/10.1371/journal.pone.0053590

Callahan B (2022) DADA2: Fast and accurate sample inference from amplicon data with single-nucleotide resolution (1.16).

Callbeck CM, Lavik G, Ferdelman TG, Fuchs B, Gruber-Vodicka HR, Hach PF, Littmann S, Schoffelen NJ, Kalvelage T, Thomsen S (2018) Oxygen minimum zone cryptic sulfur cycling sustained by offshore transport of key sulfur oxidizing bacteria. Nature Communications 9: 1729. https://doi.org/10.1038/s41467-018-04041-x

Chan PP, Lin BY, Mak AJ, Lowe TM (2021) tRNAscan-SE 2.0: improved detection and functional classification of transfer RNA genes. Nucleic Acids Research 49: 9077–9096. https://doi.org/10.1093/nar/gkab688

Chen S, Zhou Y, Chen Y, Gu J (2018) fastp: an ultra-fast all-in-one FASTQ preprocessor. Bioinformatics 34: i884–i890. https://doi.org/10.1093/bioinformatics/bty560

Danecek P, Bonfield JK, Liddle J, Marshall J, Ohan V, Pollard MO, Whitwham A, Keane T, McCarthy SA, Davies RM (2021) Twelve years of SAMtools and BCFtools. Gigascience 10: giab008. https://doi.org/10.1093/gigascience/giab008

DeLeo DM, Morrison CL, Sei M, Salamone V, Demopoulos AW, Quattrini AM (2022) Genetic diversity and connectivity of chemosynthetic cold seep mussels from the US Atlantic margin. BMC Ecology and Evolution 22: 76. https://doi.org/10.1186/s12862-022-02027-4

Distel DL, Baco AR, Chuang E, Morrill W, Cavanaugh C, Smith CR (2000) Do mussels take wooden steps to deep-sea vents? Nature 403: 725–726. https://doi.org/10.1038/35001667

Doucet-Beaupré H, Breton S, Chapman EG, Blier PU, Bogan AE, Stewart DT, Hoeh WR (2010) Mitochondrial phylogenomics of the Bivalvia (Mollusca): searching for the origin and mitogenomic correlates of doubly uniparental inheritance of mtDNA. BMC Evolutionary Biology 10: 1–19. https://doi.org/10.1186/1471-2148-10-50

Duperron S, Halary S, Lorion J, Sibuet M, Gaill F (2008a) Unexpected co-occurrence of six bacterial symbionts in the gills of the cold seep mussel *Idas* sp. (Bivalvia: Mytilidae). Environmental Microbiology 10: 433–445. https://doi.org/10.1111/j.1462-2920.2007.01465.x

Duperron S, Laurent MC, Gaill F, Gros O (2008b) Sulphur-oxidizing extracellular bacteria in the gills of Mytilidae associated with wood falls. FEMS Microbiology Ecology 63: 338–349. https://doi.org/10.1111/j.1574-6941.2008.00438.x

Duperron S, Lorion J, Samadi S, Gros O, Gaill F (2009) Symbioses between deep-sea mussels (Mytilidae: Bathymodiolinae) and chemosynthetic bacteria: diversity, function and evolution. Comptes Rendus Biologies 332: 298–310. https://doi.org/10.1016/j.crvi.2008.08.003

Franke M, Geier B, Hammel JU, Dubilier N, Leisch N (2021) Coming together – symbiont acquisition and early development in deep-sea bathymodioline mussels. Proceedings of the Royal Society B: Biological Sciences 288: 20211044. https://doi.org/10.1098/rspb.2021.1044

Fujiwara Y, Kawato M, Noda C, Kinoshita G, Yamanaka T, Fujita Y, Uematsu K, Miyazaki J-I (2010) Extracellular and mixotrophic symbiosis in the whale-fall mussel *Adipicola pacifica*: a trend in evolution from extra-to intracellular symbiosis. PLoS One 5: e11808. https://doi.org/10.1371/journal.pone.0011808

Fukasawa Y, Kobayashi-Iwatani H, Kawato M, Kobayashi H, Fujiwara Y, Miyazaki J-I (2015) Dispersal ability and genetic structure in Mytilid mussels of whale-fall communities. Open Journal of Marine Science 5: 295–305. https://doi.org/10.4236/ojms.2015.53025

Genio L, Kiel S, Cunha MR, Grahame J, Little CT (2012) Shell microstructures of mussels (Bivalvia: Mytilidae: Bathymodiolinae) from deep-sea chemosynthetic sites: Do they have a phylogenetic significance? Deep Sea Research Part I: Oceanographic Research Papers 64: 86–103. https://doi.org/10.1016/j.dsr.2012.02.002

Genio L, Rodrigues CF, Guedes IF, Almeida H, Duperron S, Hilario A (2015) Mammal carcasses attract a swarm of mussels in the deep Atlantic: insights into colonization and biogeography of a chemosymbiotic species. Marine Ecology 36: 71–81. https://doi.org/10.1111/maec.12217

Giusti F, Mietto P, Sbrana C (2012) Il genere *Idas* (Mytilidae, Bathymodiolinae) in Mediterraneo, con la descrizione di quattro nuove specie. Bollettino Malacologico: 122–135.

Grant JR, Enns E, Marinier E, Mandal A, Herman EK, Chen C-y, Graham M, Van Domselaar G, Stothard P (2023) Proksee: in-depth characterization and visualization of bacterial genomes. Nucleic Acids Research 51: W484–W492. https://doi.org/10.1093/nar/gkad326

Guindon S, Dufayard J-F, Lefort V, Anisimova M, Hordijk W, Gascuel O (2010) New algorithms and methods to estimate maximum-likelihood phylogenies: assessing the performance of PhyML 3.0. Systematic Biology 59: 307–321. https://doi.org/10.1093/sysbio/syq010

Gustafson RG, Turner RD, Lutz RA, Vrijenhoek RC (1998) A new genus and five new species of mussels (Bivalvia, Mytilidae) from deep-sea sulfide/hydrocarbon seeps in the Gulf of Mexico. Malacologia 40: 63–112.

Harbo R, Gillespie G (2021) A northern range extension of the Washington combmussel, *Idas washingtonius* (Bernard, 1978). The Dredgings 61: 3–4.

Jeffreys JG (1876) XLII. – New and peculiar mollusca of the Pecten, Mytilus, and Arca families procured in the 'Valorous' Expedition. Journal of Natural History 18: 424–436. https://doi.org/10.1080/00222937608682068

Kalyaanamoorthy S, Minh BQ, Wong TK, Von Haeseler A, Jermiin LS (2017) ModelFinder: fast model selection for accurate phylogenetic estimates. Nature Methods 14: 587–589. https://doi.org/10.1038/nmeth.4285

Katoh K, Standley DM (2013) MAFFT multiple sequence alignment software version 7: improvements in performance and usability. Molecular Biology and Evolution 30: 772–780. https://doi.org/10.1093/molbev/mst010

Kiel S (2010) The vent and seep biota: aspects from microbes to ecosystems. Vol. 33, Springer Science & Business Media. https://doi.org/10.1007/978-90-481-9572-5

Kimball RT, Guido M, Hosner PA, Braun EL (2021) When good mitochondria go bad: Cyto-nuclear discordance in landfowl (Aves: Galliformes). Gene 801: 145841. https://doi.org/10.1016/j.gene.2021.145841

Kyuno A, Shintaku M, Fujita Y, Matsumoto H, Utsumi M, Watanabe H, Fujiwara Y, Miyazaki J-I (2009) Dispersal and differentiation of deep-sea mussels of the genus *Bathymodiolus* (Mytilidae, Bathymodiolinae). Journal of Marine Sciences 2009: 625672. https://doi.org/10.1155/2009/625672

Lanfear R, Frandsen PB, Wright AM, Senfeld T, Calcott B (2017) PartitionFinder 2: new methods for selecting partitioned models of evolution for molecular and morphological phylogenetic analyses. Molecular Biology and Evolution 34: 772–773. https://doi.org/10.1093/molbev/msw260

Lee Y, Kwak H, Shin J, Kim S-C, Kim T, Park J-K (2019) A mitochondrial genome phylogeny of Mytilidae (Bivalvia: Mytilida). Molecular Phylogenetics and Evolution 139: 106533. https://doi.org/10.1016/j.ympev.2019.106533

Letunic I, Bork P (2021) Interactive Tree Of Life (iTOL) v5: an online tool for phylogenetic tree display and annotation. Nucleic Acids Research 49: W293–W296. https://doi.org/10.1093/nar/gkab301

Li H (2013) Aligning sequence reads, clone sequences and assembly contigs with BWA-MEM. arXiv 1303.3997:

Li Y-X, Sun Y, Lin Y-T, Xu T, Ip JCH, Qiu J-W (2023) Cold seep macrofauna. In: South China Sea Seeps. Springer Nature Singapore Singapore, 69–88. https://doi.org/10.1007/978-981-99-1494-4_5

Lin Y-T, Kiel S, Xu T, Qiu J-W (2022) Phylogenetic placement, morphology and gill-associated bacteria of a new genus and species of deep-sea mussel (Mytilidae: Bathymodiolinae) from the South China Sea. Deep Sea Research Part I: Oceanographic Research Papers 190: 103894. https://doi.org/10.1016/j.dsr.2022.103894

Liu J, Liu H, Zhang H (2018) Phylogeny and evolutionary radiation of the marine mussels (Bivalvia: Mytilidae) based on mitochondrial and nuclear genes. Molecular Phylogenetics and Evolution 126: 233–240. https://doi.org/10.1016/j.ympev.2018.04.019

Lorion J, Samadi S (2010) Species richness, sampling bias and phylogenetics in deep-sea mussels. Cahiers de Biologie Marine 51: 435.

Lorion J, Duperron S, Gros O, Cruaud C, Samadi S (2009) Several deep-sea mussels and their associated symbionts are able to live both on wood and on whale falls. Proceedings of the Royal Society B: Biological Sciences 276: 177–185. https://doi.org/10.1098/rspb.2008.1101

Lorion J, Buge B, Cruaud C, Samadi S (2010) New insights into diversity and evolution of deep-sea Mytilidae (Mollusca: Bivalvia). Molecular Phylogenetics and Evolution 57: 71–83. https://doi.org/10.1016/j.ympev.2010.05.027

Lorion J, Halary S, Do Nascimento J, Samadi S, Couloux A, Duperron S (2012) Evolutionary history of *Idas* sp. Med, (Bivalvia: Mytilidae), a cold seep mussel bearing multiple symbionts. Cahiers de Biologie Marine 53(1): 77–87.

Lorion J, Kiel S, Faure B, Kawato M, Ho SY, Marshall B, Tsuchida S, Miyazaki J-I, Fujiwara Y (2013) Adaptive radiation of chemosymbiotic deep-sea mussels. Proceedings of the Royal Society B: Biological Sciences 280: 20131243. https://doi.org/10.1098/rspb.2013.1243

Louca S, Parfrey LW, Doebeli M (2016) Decoupling function and taxonomy in the global ocean microbiome. Science 353: 1272–1277. https://doi.org/10.1126/science.aaf4507

McArthur A, Tunnicliffe V (1998) Relics and antiquity revisited in the modern vent fauna. Geological Society, London, Special Publications 148: 271–291. https://doi.org/10.1144/GSL.SP.1998.148.01.15

McCowin MF, Feehery C, Rouse GW (2020) Spanning the depths or depth-restricted: three new species of Bathymodiolus (Bivalvia, Mytilidae) and a new record for the hydrothermal vent Bathymodiolus thermophilus at methane seeps along the Costa Rica margin. Deep Sea Research Part I: Oceanographic Research Papers 164: 103322. https://doi.org/10.1016/j.dsr.2020.103322

McGuire JA, Linkem CW, Koo MS, Hutchison DW, Lappin AK, Orange DI, Lemos-Espinal J, Riddle BR, Jaeger JR (2007) Mitochondrial introgression and incomplete lineage sorting through space and time: phylogenetics of crotaphytid lizards. Evolution 61: 2879–2897. https://doi.org/10.1111/j.1558-5646.2007.00239.x

Meng G, Li Y, Yang C, Liu S (2019) MitoZ: a toolkit for animal mitochondrial genome assembly, annotation and visualization. Nucleic Acids Research 47: e63–e63. https://doi.org/10.1093/nar/gkz173

Meyer CP (2003) Molecular systematics of cowries (Gastropoda: Cypraeidae) and diversification patterns in the tropics. Biological Journal of the Linnean Society 79: 401–459. https://doi.org/10.1046/j.1095-8312.2003.00197.x

Mietto P, Quaggiotto E, Giusti F, Sbrana C (2019) Taxonomic and nomenclatural notes on the genus *Idas* (Bivalvia: Mytilidae). Bollettino Malacologico 55: 116–125.

Murray J, Thomson CW, Nares GS, Thomson FT (1885) Report on the scientific results of the voyage of HMS Challenger during the years 1873–76 under the command of Captain George S. Nares and the late Captain Frank Tourle Thomson. Vol. 2,HM Stationery Office. https://doi.org/10.5962/bhl.title.109677

Nawrocki EP, Eddy SR (2013) Infernal 1.1: 100-fold faster RNA homology searches. Bioinformatics 29: 2933–2935. https://doi.org/10.1093/bioinformatics/btt509

Newman WA (1985) The abyssal hydrothermal vent invertebrate fauna. A glimpse of antiquity? Bulletin of the Biological Society of Washington 6: 231– 242.

Nguyen L-T, Schmidt HA, Von Haeseler A, Minh BQ (2015) IQ-TREE: a fast and effective stochastic algorithm for estimating maximum-likelihood phylogenies. Molecular Biology and Evolution 32: 268–274. https://doi.org/10.1093/molbev/msu300

Olu-Le Roy K, Von Cosel R, Hourdez S, Carney S, Jollivet D (2007) Amphi-Atlantic cold-seep Bathymodiolus species complexes across the equatorial belt. Deep Sea Research Part I: Oceanographic Research Papers 54: 1890–1911. https://doi.org/10.1016/j.dsr.2007.07.004

Pailleret M, Haga T, Petit P, Privé-Gill C, Saedlou N, Gaill F, Zbinden M (2007) Sunken wood from the Vanuatu Islands: identification of wood substrates and preliminary description of associated fauna. Marine Ecology 28: 233–241. https://doi.org/10.1111/j.1439-0485.2006.00149.x

Pop Ristova P, Bienhold C, Wenzhöfer F, Rossel PE, Boetius A (2017) Temporal and spatial variations of bacterial and faunal communities associated with deep-sea wood falls. PLoS One 12: e0169906. https://doi.org/10.1371/journal.pone.0169906

Puillandre N, Lambert A, Brouillet S, Achaz G (2012) ABGD, Automatic Barcode Gap Discovery for primary species delimitation. Molecular ecology 21: 1864–1877. https://doi.org/10.1111/j.1365-294X.2011.05239.x

Rafinesque CS (1815) Analyse de la nature, ou tableau de l'univers et des corps organisés. Aux dépens de l'auteur. https://doi.org/10.5962/bhl.title.106607

Raggi L, Schubotz F, Hinrichs KU, Dubilier N, Petersen JM (2013) Bacterial symbionts of Bathymodiolus mussels and *Escarpia tubeworms* from Chapopote, an asphalt seep in the southern Gulf of Mexico. Environmental Microbiology 15: 1969–1987. https://doi.org/10.1111/1462-2920.12051

Ranwez V, Douzery EJ, Cambon C, Chantret N, Delsuc F (2018) MACSE v2: toolkit for the alignment of coding sequences accounting for frameshifts and stop codons. Molecular Biology and Evolution 35: 2582–2584. https://doi.org/10.1093/molbev/msy159

Rodrigues CF, Laming SR, Gaudron SM, Oliver G, Le Bris N, Duperron S (2015) A sad tale: has the small mussel *Idas argenteus* lost its symbionts? Biological Journal of the Linnean Society 114: 398–405. https://doi.org/10.1111/bij.12431

Romano C, Nunes-Jorge A, Le Bris N, Rouse GW, Martin D, Borowski C (2020) Wooden stepping stones: diversity and biogeography of deep-sea wood boring Xylophagaidae (Mollusca: Bivalvia) in the North-East Atlantic Ocean, with the description of a new genus. Frontiers in Marine Science 7: 579959. https://doi.org/10.3389/fmars.2020.579959

Romero Picazo D, Dagan T, Ansorge R, Petersen JM, Dubilier N, Kupczok A (2019) Horizontally transmitted symbiont populations in deep-sea mussels are genetically isolated. The ISME Journal 13: 2954–2968. https://doi.org/10.1038/s41396-019-0475-z

Ronquist F, Teslenko M, Van Der Mark P, Ayres DL, Darling A, Höhna S, Larget B, Liu L, Suchard MA, Huelsenbeck JP (2012) MrBayes 3.2: efficient Bayesian phylogenetic inference and model choice across a large model space. Systematic Biology 61: 539–542. https://doi.org/10.1093/sysbio/sys029

Rubinoff D, Cameron S, Will K (2006) A genomic perspective on the shortcomings of mitochondrial DNA for "barcoding" identification. Journal of Heredity 97: 581–594. https://doi.org/10.1093/jhered/esl036

Saccone C, De Giorgi C, Gissi C, Pesole G, Reyes A (1999) Evolutionary genomics in Metazoa: the mitochondrial DNA as a model system. Gene 238: 195–209. https://doi.org/10.1016/S0378-1119(99)00270-X

Samadi S, Quéméré E, Lorion J, Tillier A, von Cosel R, Lopez P, Cruaud C, Couloux A, Boisselier-Dubayle M-C (2007) Molecular phylogeny in mytilids supports the wooden steps to deep-sea vents hypothesis. Comptes Rendus Biologies 330: 446–456. https://doi.org/10.1016/j.crvi.2007.04.001

Samadi S, Puillandre N, Pante E, Boisselier MC, Corbari L, Chen WJ, Maestrati P, Mana R, Thubaut J, Zuccon D (2015) Patchiness of deep-sea communities in Papua New Guinea and potential susceptibility to anthropogenic disturbances illustrated by seep organisms. Marine Ecology 36: 109–132. https://doi.org/10.1111/maec.12204

Smith EA (1899) Natural history notes from HM Indian Marine Survey Steamer 'Investigator,'Commander TH Heming, RN – Series III., No. 1. On Mollusca from the Bay of Bengal and the Arabian Sea. Journal of Natural History 4: 11. https://doi.org/10.1080/00222939908678195

Talavera G, Castresana J (2007) Improvement of phylogenies after removing divergent and ambiguously aligned blocks from protein sequence alignments. Systematic Biology 56: 564–577. https://doi.org/10.1080/10635150701472164

Thubaut J, Corbari L, Gros O, Duperron S, Couloux A, Samadi S (2013a) Integrative biology of *Idas iwaotakii* (Habe, 1958), a 'model species' associated with sunken organic substrates. PLoS One 8: e69680. https://doi.org/10.1371/journal.pone.0069680

Thubaut J, Puillandre N, Faure B, Cruaud C, Samadi S (2013b) The contrasted evolutionary fates of deep-sea chemosynthetic mussels (Bivalvia, Bathymodiolinae). Ecology and Evolution 3: 4748–4766. https://doi.org/10.1002/ece3.749

Turner RD (1973) Wood-boring bivalves, opportunistic species in the deep sea. Science 180: 1377–1379. https://doi.org/10.1126/science.180.4093.1377

van der Heijden K, Petersen JM, Dubilier N, Borowski C (2012) Genetic connectivity between north and south Mid-Atlantic Ridge chemosynthetic bivalves and their symbionts. PLoS One 7: e39994. https://doi.org/10.1371/journal.pone.0039994

Walker JM, Curole JP, Wade DE, Chapman EG, Bogan AE, Watters GT, Hoeh WR (2006) Taxonomic distribution and phylogenetic utility of gender-associated mitochondrial genomes in the Unionoida (Bivalvia). Malacologia 48: 265.

Wang X, Guan H, Qiu J-W, Xu T, Peckmann J, Chen D, Feng D (2022) Macro-ecology of cold seeps in the South China Sea. Geosystems and Geoenvironment 1: 100081. https://doi.org/10.1016/j.geogeo.2022.100081

Weisburg WG, Barns SM, Pelletier DA, Lane DJ (1991) 16S ribosomal DNA amplification for phylogenetic study. Journal of Bacteriology 173: 697–703. https://doi.org/10.1128/jb.173.2.697-703.1991

Won Y-J, Jones WJ, Vrijenhoek RC (2008) Absence of cospeciation between deep-sea mytilids and their thiotrophic endosymbionts. Journal of Shellfish Research 27: 129–138. https://doi.org/10.2983/0730-8000(2008)27[129:AOCBDM]2.0.CO;2

WoRMS (2024) WoRMS taxon details: *Idas* Jeffreys, 1876.

Xu T, Feng D, Tao J, Qiu J-W (2019) A new species of deep-sea mussel (Bivalvia: Mytilidae: *Gigantidas*) from the South China Sea: morphology, phylogenetic position, and gill-associated microbes. Deep

Sea Research Part I: Oceanographic Research Papers 146: 79–90. https://doi.org/10.1016/j.dsr.2019.03.001

Zhang D, Gao F, Jakovlić I, Zou H, Zhang J, Li WX, Wang GT (2020) PhyloSuite: An integrated and scalable desktop platform for streamlined molecular sequence data management and evolutionary phylogenetics studies. Molecular Ecology Resources 20: 348–355. https://doi.org/10.1111/1755-0998.13096

Zhao B, Gao S, Zhao M, Lv H, Song J, Wang H, Zeng Q, Liu J (2022) Mitochondrial genomic analyses provide new insights into the "missing" atp8 and adaptive evolution of Mytilidae. BMC Genomics 23: 738. https://doi.org/10.1186/s12864-022-08940-8

Supplementary material 1

Wood substrate from which *Idas* specimens were collected in this study (Sample ID: TIO2023-1816)

Authors: Qiong Wu, Yi-Tao Lin, Jian-Wen Qiu, Mei Yu Xu, Bing Peng Xing

Data type: jpg

Link: https://doi.org/10.3897/zse.101.142007.suppl1

Supplementary material 2

BI phylogenetic tree of the subfamily Bathymodiolinae based on cox1 and 16S genes

Authors: Qiong Wu, Yi-Tao Lin, Jian-Wen Qiu, Mei Yu Xu, Bing Peng Xing

Data type: png

Explanation note: Numbers represent bootstrap values (only those >0.75 are shown).

Link: https://doi.org/10.3897/zse.101.142007.suppl2

Supplementary material 3

The complete mt genome of *Idas sinensis* sp. nov. (Sample ID: TIO2023-1816B6) and *Idas pacificus* sp. nov. (Sample ID:TIO2023-1816B13)

Authors: Qiong Wu, Yi-Tao Lin, Jian-Wen Qiu, Mei Yu Xu, Bing Peng Xing

Data type: png

Link: https://doi.org/10.3897/zse.101.142007.suppl3

Supplementary material 4

GenBank sequences used for phylogenetic tree construction

Authors: Qiong Wu, Yi-Tao Lin, Jian-Wen Qiu, Mei Yu Xu, Bing Peng Xing

Data type: xlsx

Link: https://doi.org/10.3897/zse.101.142007.suppl4

Supplementary material 5

List of animal species associated with wood substrate and their GenBank accession numbers (Excluding *Idas* spp.)

Authors: Qiong Wu, Yi-Tao Lin, Jian-Wen Qiu, Mei Yu Xu, Bing Peng Xing

Data type: xlsx

Link: https://doi.org/10.3897/zse.101.142007.suppl5

Supplementary material 6

List of genbank accession numbers, biosample accession numbers, and sequence read archive (SRA) data obtained in this study

Authors: Qiong Wu, Yi-Tao Lin, Jian-Wen Qiu, Mei Yu Xu, Bing Peng Xing
Data type: xlsx

Link: https://doi.org/10.3897/zse.101.142007.suppl6

Supplementary material 7

The Best-Fit Models According to AIC

Authors: Qiong Wu, Yi-Tao Lin, Jian-Wen Qiu, Mei Yu Xu, Bing Peng Xing
Data type: xlsx

Link: https://doi.org/10.3897/zse.101.142007.suppl7

Supplementary material 8

K2P distances of cox1 genes in *Idas* species

Authors: Qiong Wu, Yi-Tao Lin, Jian-Wen Qiu, Mei Yu Xu, Bing Peng Xing
Data type: xlsx

Link: https://doi.org/10.3897/zse.101.142007.suppl8

Zoosyst. Evol. 101 (2) 2025, 779–790 | DOI 10.3897/zse.101.151083

PENSOFT

für Natur MUSEUM FÜR NATURKUNDE BERLIN

A new tribe, genus, and species of freshwater mussel from the Changjiang River Basin in China (Bivalvia, Unionidae, Unioninae)

Yu-Ting Dai[1*], Zhong-Guang Chen[1*], Shan Ouyang[1], Xiao-Chen Huang[1], Xiao-Ping Wu[1]

1 *School of Life Sciences, Nanchang University, Nanchang 330031, China*

https://zoobank.org/219F8CF1-F488-4B0C-9C65-F8FD98331040

Corresponding authors: Xiao-Chen Huang (xiaochenhuang@hotmail.com); Xiao-Ping Wu (xpwu@ncu.edu.cn)

Academic editor: Matthias Glaubrecht ♦ **Received** 22 February 2025 ♦ **Accepted** 26 March 2025 ♦ **Published** 10 April 2025

Abstract

A new tribe, genus, and species of freshwater mussels, Globunionini Dai, Chen, Huang & Wu, **tribe nov.** and *Globunio mirificus* Chen, Dai, Huang & Wu, **gen. et sp. nov.**, is described from the Changjiang River Basin in China based on comparative morphology and molecular phylogeny. The species presence of a special small-sized and elongated globular, which distinguishes it from all other tribes. The discovery increases the diversity of freshwater mussels in the Changjiang River Basin.

Key Words

Biodiversity, molluscs, phylogeny, taxonomy

Introduction

Freshwater mussels (Mollusca: Bivalvia: Unionida) play an important role in freshwater ecosystems (Graf and Cummings 2007; Huang et al. 2019) and are one of the most threatened freshwater organisms globally (Vaughn 2018; Lopes-Lima et al. 2020; Böhm et al. 2021). China is one of the regions with the highest species diversity of freshwater mussels in the world, with about 100 accepted species recorded and new taxa continuing to be discovered (Heude 1875, 1877a, 1877b, 1878, 1879, 1880a, 1880b, 1881, 1883, 1885; Simpson 1900; He and Zhuang 2013; Graf and Cummings 2021; Guo 2022; Liu et al. 2022; Wu et al. 2022a, 2022b; Chen et al. 2023; Dai et al. 2023, 2024a, 2024b, 2024c, 2024d). The freshwater mussels in China are mainly concentrated in the Changjiang River Basin (Yangtze), with about 70 accepted species recorded (Heude 1875, 1877a, 1877b, 1878, 1879, 1880a, 1880b, 1881, 1883, 1885; Simpson 1900; He and Zhuang 2013; Graf and Cummings 2021; Guo 2022; Chen et al. 2023; Dai et al. 2024a, 2024b). Even in the well-studied middle and lower reaches of the Changjiang River, new freshwater mussels have been continuously discovered in recent years, demonstrating the extremely high diversity in the region (Guo 2022; Chen et al. 2023; Dai et al. 2023, 2024a, 2024b; Wu et al. 2024).

During the surveys in 2022, we discovered a group of freshwater mussel specimens with the special small-sized and elongated-globular shell that did not resemble any known species and were challenging to place in any genus or tribe. Based on a combination of morphology and molecular phylogeny, we describe it as a new tribe, genus, and species of subfamily Unioninae Rafinesque, 1820. The discovery improved the diversity of freshwater mussels in the Changjiang River Basin and showed that even in the central city, there are still yet-to-be-described species of freshwater mussels that exist.

* These authors contributed equally to this work.

Materials and methods

Materials preparation

Specimens were collected from Jiangxi, China, in 2022. Living specimens were initially frozen at -20 °C for 24 hours and subsequently thawed at room temperature for 2 hours to facilitate the extraction of soft parts. The soft parts were then fixed in 95% ethanol. Empty shells were cleaned, dried, and preserved at room temperature. Photographs were taken by camera and edited in Adobe Photoshop CC 2015 (Adobe, San Jose, US). Maps were made in ArcGIS Pro (Esri, Redlands, US).

DNA extraction, sequencing, and mitogenome assembly

Genomic DNA was extracted from muscle preserved in 95% ethanol using a TIANamp Marine Animals DNA Kit (Tiangen Biotech, China). The quality and concentration of the DNA were checked on 1% agarose gel electrophoresis and NanoDrop 2000 (Thermo Scientific, USA). The qualified genomic DNA sample was sent to Novogene (Beijing, China). Two datasets were used for phylogenetic analyses: the partial cytochrome c oxidase subunit 1 (*COI*) sequences and the mitochondrial genomes. The polymerase chain reaction (PCR) systems, conditions, and primer pairs of *COI* are followed by Chen et al. (2023). After quality controls, the library was successfully prepared and sequenced in the Illumina NovaSeq 6000 platform, yielding 12 Gb of data, with 2 × 150 bp paired-end reads. After discarding low-quality reads, clean reads were obtained and assembled de novo using CLC Genomic Workbench v. 12.0 (https://digitalinsights.qiagen.com). Contigs identified as mitogenome sequences were inspected manually for overlap at the beginning and end, resulting in a circular mitogenome. Geneious v. 11.0 (https://www.geneious.com) (Kearse et al. 2012) was used to check the complete mitogenome and analyze nucleotide composition. Strand asymmetry was calculated using the formulas: GC skew = (G−C)/(G+C) and AT skew = (A−T)/(A+T). The initial annotation of the mitogenome was carried out using the MITOS web server (http://mitos.bioinf.uni-leipzig.de/index.py) (Bernt et al. 2013). ARWEN (http://130.235.244.92/ARWEN) (Laslett and Canback 2008) was also used to identify the locations of all tRNA genes. The annotations of two rRNA genes were further refined based on the positions of neighboring genes. PCGs were initially identified using the Open Reading Frame Finder (ORF Finder) implemented on the NCBI website (http://www.ncbi.nlm.nih.gov/orffinder) and BLAST searches (http://blast.ncbi.nlm.nih.gov).

Alignments, partitioning strategies

The *COI* dataset consists of 51 sequences of the family Unionidae and two outgroup taxa (Table 1). The mitochondrial genome dataset consists of 81 sequences (including 12 PCGs (excluding ATP8) and two rRNA genes) of the family Unionidae and nine outgroup taxa (Table 2). The *COI* sequences were aligned using MEGA

Table 1. GenBank accession numbers of the *COI* sequences used in this study.

Species	Locality	Accession number	References
Unioninae Rafinesque, 1820			
Globunio mirificus gen. et sp. nov. 1	Honggutan, Nanchang, Jiangxi, China	PV368604	This study
Globunio mirificus gen. et sp. nov. 2	Honggutan, Nanchang, Jiangxi, China	PV368605	This study
Globunio mirificus gen. et sp. nov. 3	Honggutan, Nanchang, Jiangxi, China	PV368606	This study
Globunio mirificus gen. et sp. nov. 4	Honggutan, Nanchang, Jiangxi, China	PV368607	This study
Globunio mirificus gen. et sp. nov. 5	Honggutan, Nanchang, Jiangxi, China	PV368608	This study
Globunio mirificus gen. et sp. nov. 6	Honggutan, Nanchang, Jiangxi, China	PV368609	This study
Globunio mirificus gen. et sp. nov. 7	Honggutan, Nanchang, Jiangxi, China	PV368610	This study
Globunio mirificus gen. et sp. nov. 8	Honggutan, Nanchang, Jiangxi, China	PV368611	This study
Globunio mirificus gen. et sp. nov. 9	Honggutan, Nanchang, Jiangxi, China	PV368612	This study
Diaurora aurorea (Heude, 1883)	Ji'an, Jiangxi, China	OQ829360*	Chen et al. 2023
Acuticosta chinensis (Lea, 1868)	Jiangxi, China	MG462921	Huang et al. 2019
Schistodesmus lampreyanus (Baird & Adams, 1867)	Jiangxi, China	MG463037	Huang et al. 2019
Schistodesmus spinosus (Simpson, 1900)	Jiangxi, China	MG463046	Huang et al. 2019
Schistodesmus sp.	Hunan, China	MG463043	Huang et al. 2019
Unio pictorum (Linnaeus, 1758)	Europe	KC429109	Sharma et al. 2013
Unio crassus Philipsson, 1788	Poland	KY290446	Burzynski et al. 2017
Tchangsinaia piscicula (Heude, 1874)	Jiangxi, China	MG462977	Huang et al. 2019
Cuneopsis celtiformis (Heude, 1874)	Jiangxi, China	MG462964	Huang et al. 2019
Cuneopsis heudei (Heude, 1874)	Jiangxi, China	MG462970	Huang et al. 2019
Aculamprotula fibrosa (Heude, 1877)	Jiangxi, China	MG462909	Huang et al. 2019
Nodularia douglasiae (Gray, 1833)	China	KX822653	Lopes-Lima et al. 2017
Nodularia breviconcha Lee, Kim, Bogan & Kondo, 2020	South Korea	MT020662	Lopes-Lima et al. 2020

Species	Locality	Accession number	References
Inversiunio yanagawensis (Kondo, 1982)	Japan	MT020654	Lopes-Lima et al. 2020
Inversiunio reinianus (Kobelt, 1879)	Japan	MT020657	Lopes-Lima et al. 2020
Pseudocuneopsis sichuanensis Huang, Dai, Chen & Wu, 2022	Sichuan, China	MZ540966	Wu et al. 2022b
Pseudocuneopsis capitata (Heude, 1874)	Anhui, China	NC042469	Wu et al. 2019
Alasmidonta marginata Say, 1818	U.S.	AF156502	Graf & O'Foighil 2000
Lasmigona compressa (Lea, 1829)	U.S.	AF156503	Graf & O'Foighil 2020
Anodonta anatina (Linnaeus, 1758)	Russia	KX822632	Lopes-Lima et al. 2017
Pseudanodonta complanata (Rossmässler, 1835)	Ukraine	KX822661	Lopes-Lima et al. 2017
Lanceolaria gladiola (Heude, 1877)	Jiangxi, China	KY067441	Unpublished
Lanceolaria oxyrhyncha (Martens, 1861)	Japan	MT020648	Lopes-Lima et al. 2020
Cristaria plicata (Leach, 1814)	Jiangxi, China	MG462956	Huang et al. 2019
Lepidodesma languilati (Heude, 1874)	Jiangxi, China	MG463015	Huang et al. 2019
Sinanodonta woodiana (Lea, 1834)	China	KX822668	Lopes-Lima et al. 2017
Beringiana beringiana (Middendorff, 1851)	Japan	MT020557	Lopes-Lima et al. 2020
*Plethol*ophus *tenuis* (Gray, 1833)	Vietnam	KX822658	Lopes-Lima et al. 2016
Anemina arcaeformis (Heude, 1877)	Jiangxi, China	MG462936	Huang et al. 2019
Amuranodonta kijaensis Moskvicheva, 1973	Russia	MK574204	Bolotov et al. 2020
Parreysiinae Henderson, 1935			
Coelatura aegyptiaca (Cailliaud, 1823)	Egypt	KJ081162	Graf et al. 2014
Indonaia andersoniana (Nevill, 1877)	Myanmar	MF352275	Bolotov et al. 2017
Parreysia nagpoorensis (Lea, 1860)	India	JQ861229	Unpublished
Gonideinae Ortmann, 1916			
Pronodularia japanensis (Lea, 1859)	Japan	LC505454	Fukata and Iigo 2020
Lamprotula leaii (Gray, 1833)	Jiangxi, China	MG462996	Huang et al. 2019
Ambleminae Rafinesque, 1820			
Lampsilis siliquoidea (Barnes, 1823)	U.S.	MH560773	Unpublished
Quadrula quadrula (Rafinesque, 1820)	U.S.	HM230409	Unpublished
Margaritiferidae Henderson, 1929			
Margaritifera dahurica (Middendorff, 1850)	Russia	KJ161516	Bolotov et al. 2015
Gibbosula rochechouartii (Heude, 1875)	Jiangxi, China	MG463022	Huang et al. 2019

X (Kumar et al. 2018) and checked manually. MUSCLE (Edgar 2004) was used for codon alignment of all PCGs implemented in MEGA X (Kumar et al. 2018). MAFFT (Katoh et al. 2019) with the Q-INS-i algorithm was used for the alignment of ribosomal genes (12S and 16S rRNAs). Gblocks (Castresana 2000) were used to exclude ambiguous regions from the alignment of each gene. PartitionFinder (Lanfear et al. 2017) was used to determine the best-fit partitioning schemes and substitution models under greedy search. Predefined data blocks for partitioning scheme searches were designated by gene region (rRNA gene) or codon position (PCG). Branch lengths were allowed to be unlinked, and model selection and partitioning schemes were determined using the AICc method (Table 3).

Phylogenetic analyses

ML analyses were performed in IQ-TREE v. 1.6.12 (Minh et al. 2013) using the Ultrafast bootstrap approach (Minh et al. 2013) with 10,000 iterations. Bayesian inference (BI) analysis was conducted in MrBayes v. 3.2.6 (Ronquist et al. 2012). Four simultaneous runs with four independent Markov Chain Monte Carlo (MCMC) were implemented for 10 million generations, and trees were sampled every 10,000 generations with a burn-in of 25%. The convergence was checked with the average standard deviation of split frequencies < 0.01 and the potential scale reduction factor (PSRF) ~ 1. Trees were visualized in FigTree v.1.4.3 (http://tree.bio.ed.ac.uk/software/figtree/).

Abbreviations

NCU_XPWU: Laboratory of Xiao-Ping Wu, Nanchang University (Nanchang, Jiangxi, China).

Results

COI phylogeny

The alignment of the *COI* gene had lengths of 606 characters. Within these alignments, 260 sites were variable, and 236 sites were parsimony informative. The maximum likelihood and Bayesian analyses produced consistent phylogenies (Figs 1, 2). Although a single gene marker cannot effectively address inter tribes relationships in the subfamily Unioninae, the new species formed an independent branch that does not belong to any tribe. Its systematic position needs further verification through mitochondrial genome phylogenetic analysis.

Table 2. GenBank accession numbers of the mitochondrial genome sequences used in this study.

Species	Accession number
Unioninae Rafinesque, 1820	
Globunio mirificus gen. et sp. nov.	PV394654
Tchangsinaia pisciculus (Heude, 1874)	NC026306
Cuneopsis heudei (Heude, 1874)	NC042471
Cuneopsis rufescens (Heude, 1874)	MZ571512
Cuneopsis celtiformis (Heude, 1874)	MW464617
Cuneopsis demangei Haas, 1929	MZ571513
Pseudocuneopsis capitata (Heude, 1874)	NC042469
Pseudocuneopsis capitata (Heude, 1874)	MZ571517
Pseudocuneposis sichuanensis Huang, Dai, Chen & Wu, 2022	MZ571510
Pseudocuneopsis yemaoi Dai, Chen, Huang & Wu, 2024	OR392755
Pseudocuneopsis yangshuoensis Wu & Liu, 2023	OR392756
Schistodesmus lampreyanus (Baird & Adams, 1867)	NC042470
Schistodesmus spinosus (Simpson, 1900)	MZ571511
Unio crassus Philipsson, 1788	KY290446
Unio delphinus Spengler, 1793	KT326917
Unio pictorum (Linnaeus,1758)	NC015310
Unio tumidus Philipsson, 1788	KY021076
Nodularia breviconcha Lee, Kim, Bogan & Kondo	MT955592
Nodularia douglasiae (Griffith & Pidgeon, 1833)	NC026111
Nodularia fusiformans Wu & Liu, 2024	MT764726
Nodularia nuxpersicae (Dunker, 1848)	OR888962
Nodularia nuxpersicae (Dunker, 1848)	OR888961
Aculamprotula coreana (Martens, 1886)	NC026035
Aculamprotula polysticta (Heude, 1877)	MK728823
Aculamprotula scripta (Heude, 1875)	MF991456
Aculamprotula tientsinensis (Crosse & Debeaux, 1863)	NC029210
Aculamprotula tortuosa (Lea, 1865)	NC021404
Acuticosta chinensis (Lea, 1868)	MF687347
Anodonta anatina (Linnaeus, 1758)	NC022803
Anodonta cygnea (Linnaeus, 1758)	NC036488
Sinanodonta lucida (Heude, 1877)	NC026673
Sinanodonta woodiana (Lea, 1834)	HQ283346
Cristaria plicata (Leach, 1814)	NC012716
Anemina arcaeformis (Heude, 1877)	NC026674
Anemina euscaphys (Heude, 1879)	NC026792
Utterbackia imbecillis (Say, 1829)	NC015479
Utterbackia peninsularis Bogan & Hoeh, 1995	HM856636
Pyganodon grandis (Say, 1829)	NC013661
Lasmigona compressa (Lea, 1829)	NC015481
Lanceolaria gladiola (Heude, 1877)	KY067441
Lanceolaria grayii (Gray, 1833)	NC026686
Lanceolaria lanceolata (Lea, 1856)	NC023955
Lepidodesma languilati (Heude, 1874)	NC029491
Gonideinae Ortmann, 1916	
Sinosolenaia carinata (Heude, 1877)	NC023250
Sinosolenaia oleivora (Heude, 1877)	NC022701
Ptychorhynchus pfisteri (Heude, 1874)	KY067440
Parvasolenaia rivularis (Heude, 1877)	KX966393
Inversidens rentianensis Wu & Wu, 2021	OR823224
Postolata guangxiensis Dai, Huang, Guo & Wu, 2023	OP009366
Microcondylaea bonellii (Férussac, 1827)	NC044111
Monodontina vondembuschiana (Lea, 1840)	NC044112
Pilsbryoconcha exilis (Lea, 1838)	NC044124
Lamprotula gottschei-Schistodesmus.sp	NC023806
Lamprotula leaii (Griffith & Pidgeon, 1833)	NC023346
Lamprotula caveata (Heude, 1877)	NC030336
Pronodularia japanensis (Lea, 1859)	AB055625
Potomida littoralis (Cuvier, 1798)	NC030073
Sinohyriopsis cumingii (Lea, 1852)	NC011763
Sinohyriopsis schlegelii (Martens, 1861)	NC015110
Chamberlainia hainesiana (Lea, 1856)	NC044110
Lens contradens (Lea, 1838)	MW242812
Physunio superbus (Lea, 1843)	MW242814
Hyriopsis bialata Simpson, 1900	MW242816
Rectidens sumatrensis (Dunker, 1852)	MW242818
Lampsilis powellii (Lea, 1852)	NC037720

Species	Accession number
Lampsilis siliquoidea (Barnes, 1823)	NC037721
Lampsilis cardium Rafinesque, 1820	BK010478
Lampsilis ornata (Conrad, 1835)	NC005335
Venustaconcha ellipsiformis (Conrad, 1836)	FJ809753
Leaunio lienosus (Conrad, 1834)	BK010479
Potamilus leptodon (Rafinesque, 1820)	NC028522
Potamilus alatus (Say, 1817)	KU559010
Toxolasma parvum (Barnes, 1823)	NC015483
Popenaias popeii (Lea, 1857)	NC050058
Amblema plicata (Say, 1817)	NC050056
Elliptio complanata (Lightfoot, 1786)	BK010477
Pleurobema oviforme (Conrad, 1834)	NC050057
Quadrula quadrula (Rafinesque, 1820)	NC013658
Uniomerus tetralasmus (Say, 1831)	BK010480
Margaritiferidae Henderson, 1929	
Margaritifera dahurica (Middendorff, 1850)	NC023942
Margaritifera margaritifera (Linnaeus, 1758)	MK421958
Margaritifera falcata (Gould, 1850)	NC015476
Pseudunio marocanus (Pallary, 1918)	KY131953
Cumberlandia monodonta (Say, 1829)	KU873123
Gibbosula rochechouartii (Heude, 1875)	KX378172
Hyriidae Swainson, 1840	
Echyridella menziesii (Gray, 1843)	KU873121
Iridinidae Swainson, 1840	
Mutela dubia (Gmelin, 1791)	KU873120
Mycetopodidae Gray, 1840	
Anodontites trapesialis (Lamarck, 1819)	KU873119

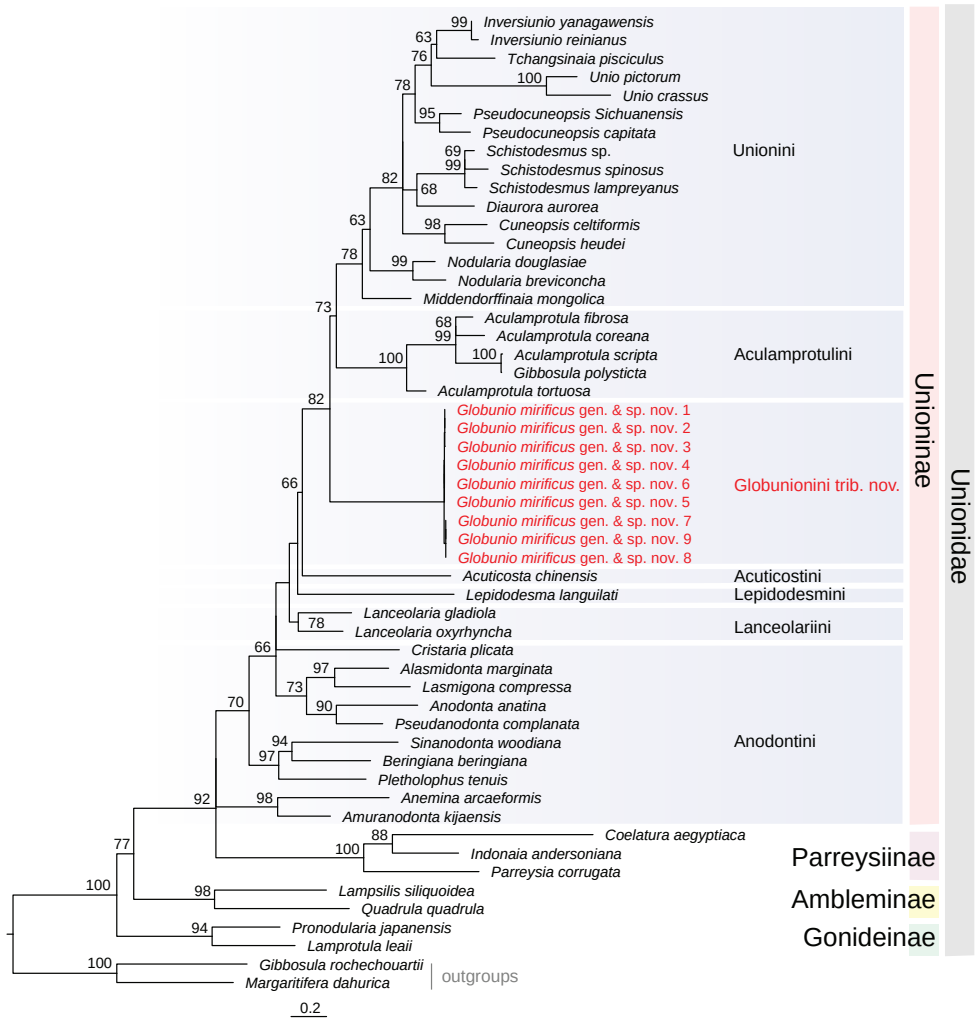

Figure 1. Maximum likelihood tree inferred from *COI* gene sequences. Bootstrap supports are shown on the left of nodes on the tree if greater than 50%.

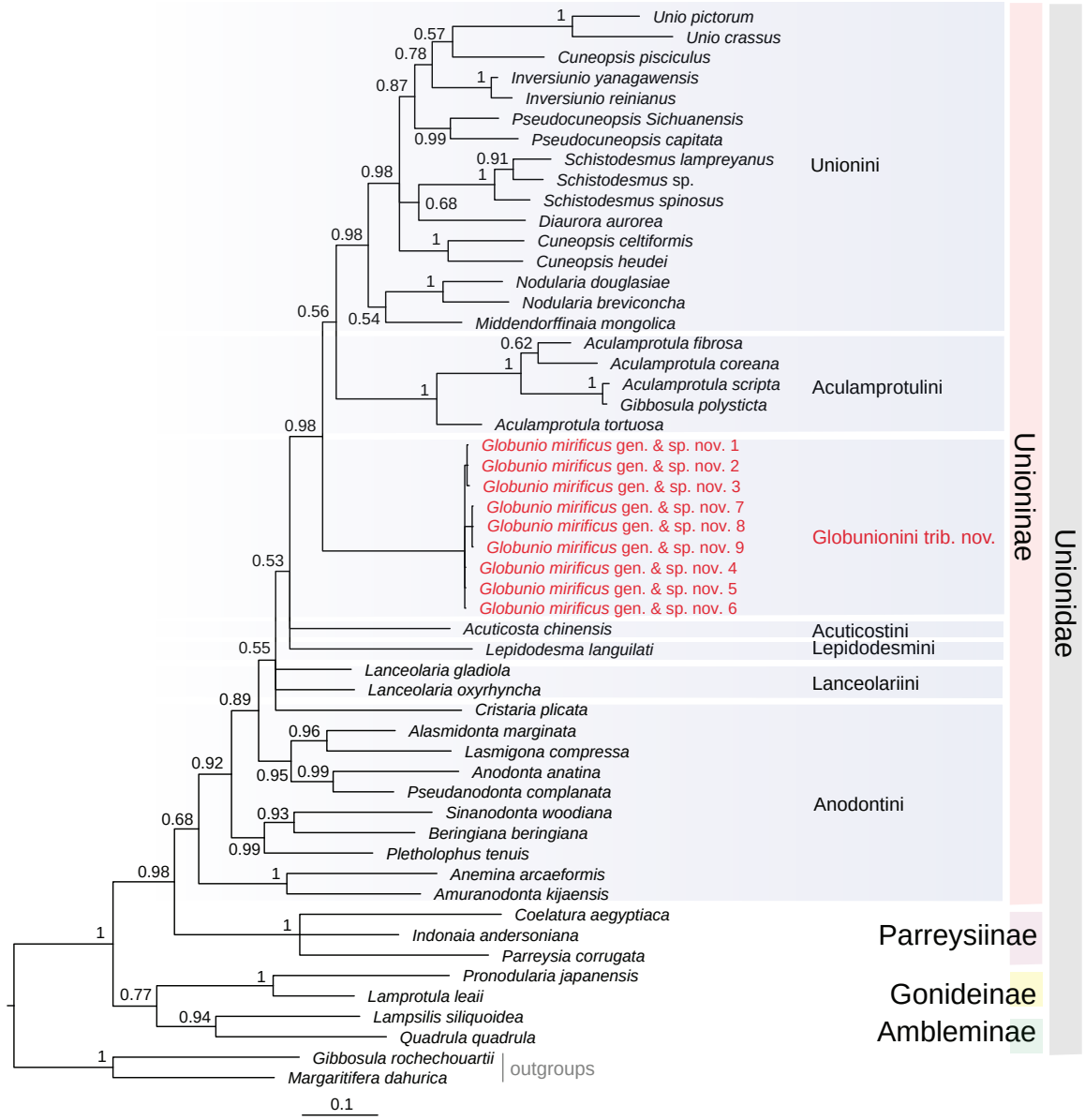

Figure 2. Bayesian inference tree inferred from *COI* gene sequences. Posterior probabilities are shown on the left of nodes on the tree if greater than 50%.

Table 3. Partitioning strategies for the mitogenome dataset (from PartitionFinder2) according to AICc.

Subset	Best Model	Partition scheme
1	GTR+I+G	COX1 codon1, ATP6 codon1, ND4 codon1, ND3 codon1, ND5 codon1, ND4L codon1, CO3 codon1
2	GTR+I+G	ND5 codon2, ND3 codon2, ND4L codon2, COX1 codon2, CO3 codon2, ND4 codon2, ATP6 codon2
3	GTR+I+G	CO2 codon3, ND4L codon3, ND3 codon3, ATP6 codon3, ND4 codon3, ND5 codon3, CO3 codon3, COX1 codon3
4	SYM+I+G	ND1 codon1, CYTB codon1, CO2 codon2, CO2 codon1
5	GTR+I+G	ND1 codon2, ND6 codon2, ND2 codon2, CYTB codon2
6	GTR+G	ND1 codon3, ND6 codon3, CYTB codon3, ND2 codon3
7	GTR+I+G	16S, 12S, ND2 codon1, ND6 codon1

Mitogenome characteristics

The length of the mitogenome is 16,240 bp. The maternal mitogenomes of the new species contain the 13 PCGs typically found in metazoan mitochondrial genomes, the type-specific F-orf described for all Unionida mitogenomes with the DUI system, 22 transfer RNA (tRNA), and two ribosomal RNA (rRNA) genes (Fig. 3A). Most genes were encoded on the light strand (L-strand), whereas 11 genes (COI, COII, COIII, ND3, ND4, ND4L, ND5, ATP6, ATP8, $tRNA^{Asp}$, and $tRNA^{His}$) were located on the heavy strand (H-strand). The location of the F-orf was between ND2 and $tRNA^{Glu}$, and the gene order of the mitogenomes was consistent with other Unioninae and Ambleminae species. The rrnS gene of it was located between $tRNA^{Arg}$ and $tRNA^{Lys}$, while the rrnL gene was located between $tRNA^{Tyr}$

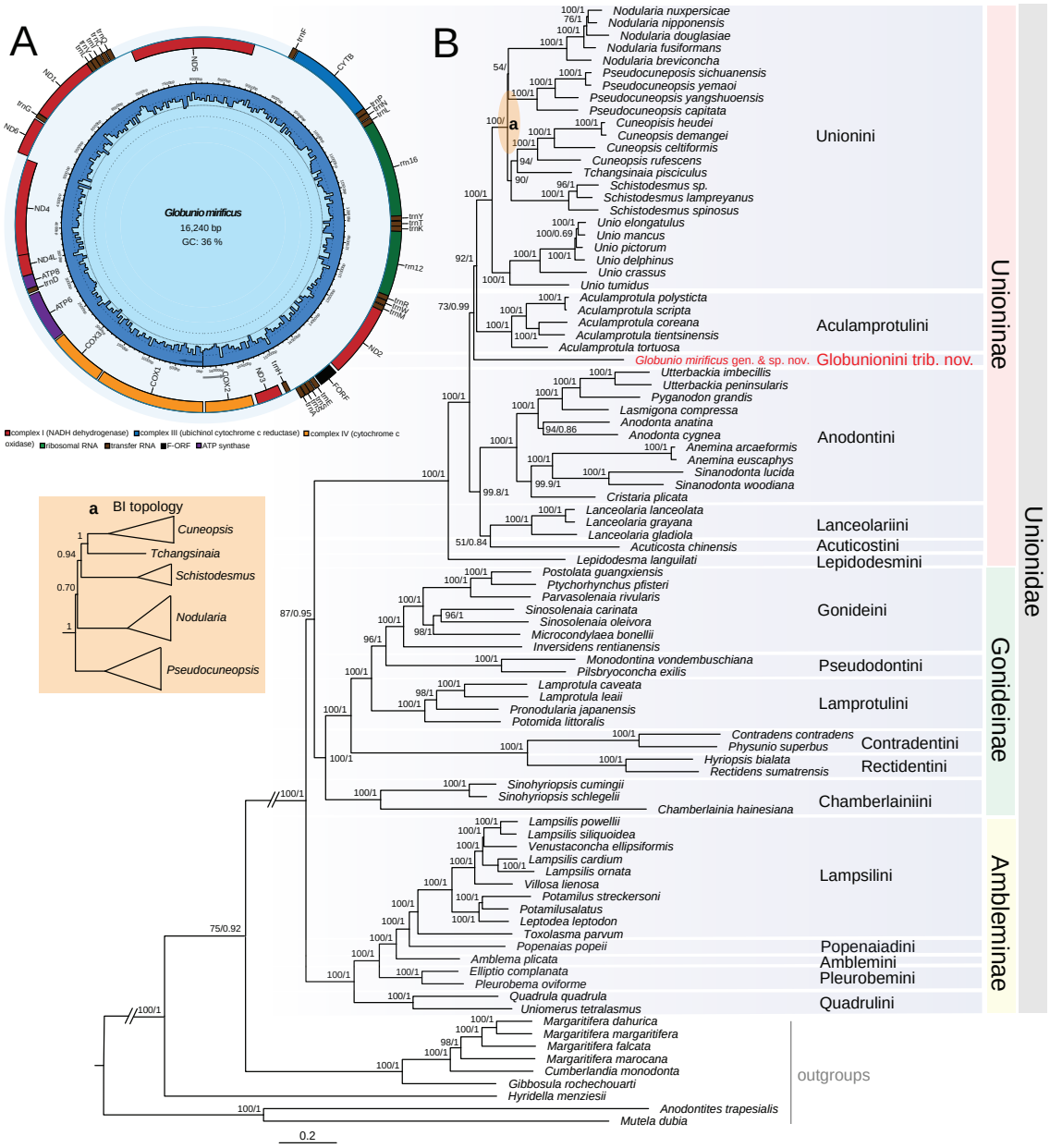

Figure 3. A. Gene map of the F-type mitochondrial genome of *Globunio mirificus* gen. et sp. nov.; **B.** Maximum likelihood and Bayesian inference tree inferred from mitochondrial genome sequences. Bootstrap supports/posterior probabilities are shown on the left/right of nodes on the tree if they are greater than 50%.

and $tRNA^{Leu}$. The overall base composition was A (25.7%), T (38.1%), C (12.2%), and G (24.0%), with the A + T content of 63.8%. Nucleotide asymmetry of the mitochondrial strands was assessed by AT skew and GC skew that were −0.19 and 0.33, respectively.

Mitochondrial phylogeny

The alignment of the mitogenomes had lengths of 11,547 characters. Within these alignments, 7,300 sites were variable, and 6,604 sites were parsimony informative. The maximum likelihood and Bayesian analyses produced largely consistent phylogenies (Fig. 3B). The new species formed an independent branch in the subfamily Unioninae and was sistered with the clade consisting of Unionini + Aculamprotulini with a relatively well support rate (BS/PP = 70/0.99).

Systematics

Family Unionidae Rafinesque, 1820
Subfamily Unioninae Rafinesque, 1820

Tribe Globunionini Dai, Chen, Huang & Wu, tribe nov.
https://zoobank.org/C3AC71B4-5393-4B57-B8C9-5D067E23B3E1

Type genus. *Globunio* Dai, Chen, Huang & Wu, 2024, gen. nov.

Diagnosis. Shell small-sized, elongated-globular, inflated, thick, solid; very wide, with some individuals even wider than height. Anterior extremely short, inflated, and round; posterior long and flat. Anterior margin rounded, dorsal margin straightened, and slope downward at an obtuse angle, usually covered in fine upward wrinkles; ventral margin weakly curved. Umbo inflated, under dorsal margin, almost at the very front of the shell, often eroded.

Vernacular name. 球蚌族 (qiú bàng zú).

Remarks. The new tribe has a special small, thick, and elongated-globular shell, which is completely dissimilar to all other tribes of the subfamily. Its independence was also supported by the molecular phylogeny.

Genus *Globunio* Dai, Chen, Huang & Wu, gen. nov.

https://zoobank.org/88F4B05A-65A8-49E6-A339-DAE71D4DC071

Type species. *Globunio mirificus* Chen, Dai, Huang & Wu, 2024, sp. nov.

Diagnosis. Same as the tribe.

Etymology. The species is made from the Latin g*lob* for globular, and unio for the unionid type genus.

Vernacular name. 球蚌属 (qiú bàng shǔ).

Globunio mirificus Chen, Dai, Huang & Wu, sp. nov.

https://zoobank.org/C2C368AA-A510-4FDC-B58C-C037009B42CB

Figs 4, 6C, D

Holotype. 24_NCU_XPWU_GM01, ♀, Honggutan District [红谷滩区], Nanchang City [南昌市], Jiangxi Province [江西省], China, 24.68146°N, 109.69794°E, leg. Zhong-Guang Chen & Yu-Ting Dai, September 2022.

Paratypes. n = 10, 24_NCU_XPWU_GM02, Honggutan District [红谷滩区], Nanchang City [南昌市], Jiangxi Province [江西省], China, 24.68146°N, 109.69794°E, leg. Zhong-Guang Chen, December 2021; 24_NCU_XPWU_GM03–11, other information same as holotype.

Diagnosis. Same as the tribe.

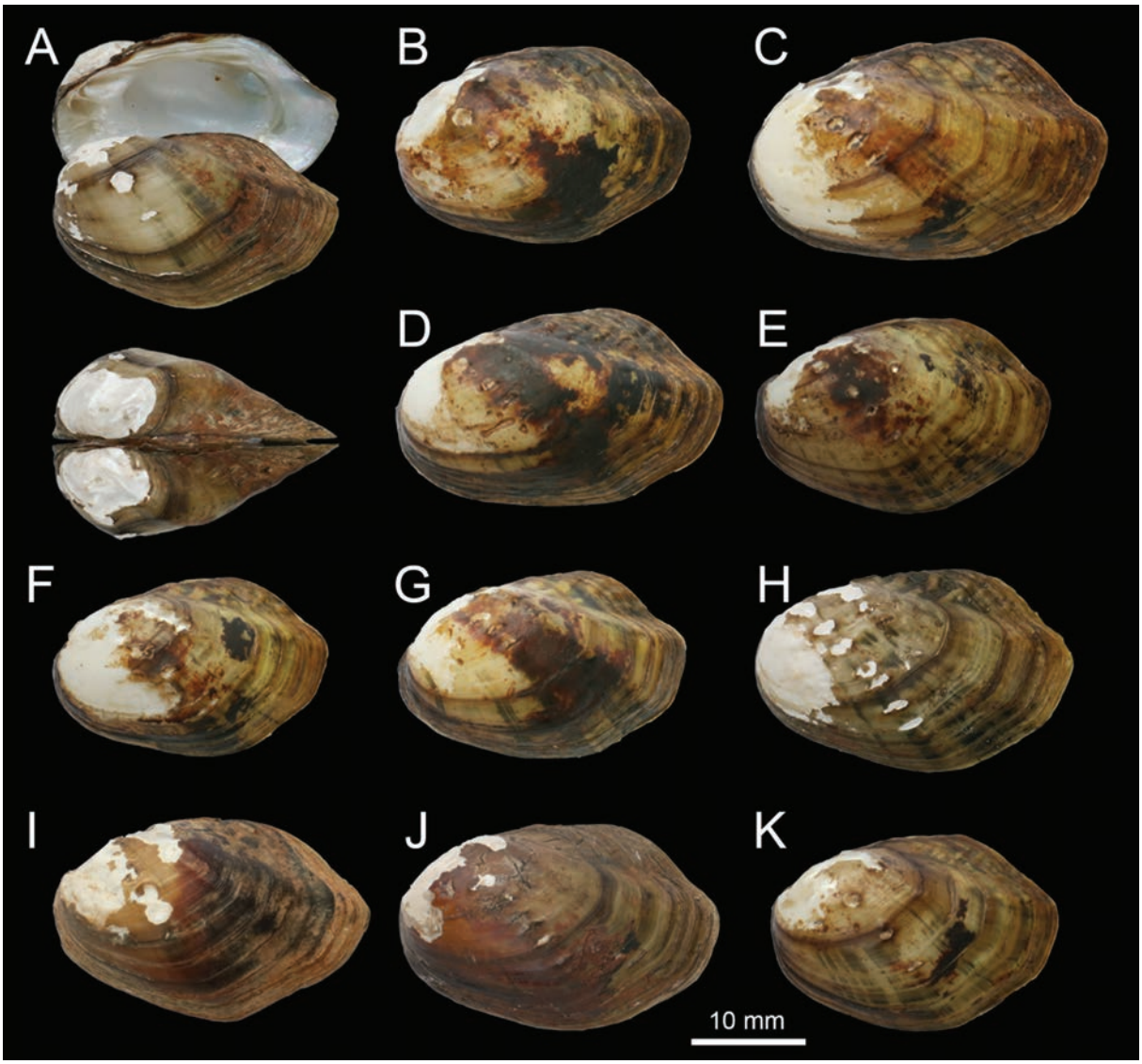

Figure 4. *Globunio mirificus* gen. et sp. nov. **A.** Holotype; **B–K.** Paratypes.

Description. Shell small-sized, elongated-globular, inflated, thick, solid. Anterior extremely short, inflated, and round; posterior long and flat. Anterior margin rounded, dorsal margin straightened, and slope downward at an obtuse angle, usually covered in fine upward wrinkles; ventral margin weakly curved. Umbo inflated, under dorsal margin, almost at the very front of the shell, often eroded. Central of shell with two rows of posterior dorsal spines (usually detached with only attachment marks), the anterior row longer and the posterior row shorter. Periostracum yellowish-green with olive-green rays and several thick growth lines. Hinge short and strong. Hinge developed. Left valve with two pseudocardinal teeth, anterior tooth small, triangular-shaped, posterior tooth well-developed, rectangular-shaped; right valve with a single well-developed, pyramidal pseudocardinal tooth. Both valves with two lateral teeth: left valve external weak, internal well-developed; right valve external well-developed, internal weak. Mantle attachment scars on the pallial line obvious. Anterior adductor muscle scars deep, samll; posterior adductor muscle scars shallow, orbicular-shaped. Umbo cavity open, deep. Nacre milky white.

Measurements. Shell length 15.07–32.37 mm, width 9.83–21.54 mm, height 13.06–19.30 mm.

Etymology. The species is named after the Latin *mirificus* for remarkable, referring to the remarkable shell morphology of this species.

Vernacular name. 奇异球蚌 (qí yì qiú bàng).

Distribution and ecology. Known from three localities of the Changjiang River Basin: the Ganjiang River at Nanchang, the Dongtinghu Lake at Yueyang, and the Qingyijiang River at Wuhu (Fig. 5). Living in the slow-flowing rivers and lakes with muddy and sandy substrates alongside dozens of other freshwater mussels (Fig. 6).

Discussion

Of all freshwater mussels of subfamily Unioninae, only partial species of Aculamprotulini have a somewhat similar elongated-globular shell with the new species. However, the new species has a much smaller (shell length < 35 mm), more expanded, and symmetric shell, while Aculamprotulini has a larger (shell length > 100 mm), flatter, and asymmetrical shell. A thorough examination of type specimens and more than 100 live animals of the new species has revealed that individuals over 15 mm frequently exhibit severe corrosion. This finding serves as a reliable indicator of the animals' advanced age, thereby confirming their status as adults rather than juveniles of other species. The new species is one of the smallest freshwater mussels in China.

The type locality of the new species was located in the central city of Nanchang, a region that has been extensively surveyed for freshwater mussels in China. However, due to the general lack of sensitivity amongst researchers to freshwater mussel classification, this species was overlooked for a considerable period. Its distribution in densely populated areas poses a significant threat to its survival. The preference of microhabitats with flowing and fine sediment, resulting in a very narrow distribution of the new species in the Ganjiang River. However, all the sediment at its type locality was completely excavated in 2023 for the construction of a water plant (Fig. 6B). Surveys conducted between 2023 and 2025, following the

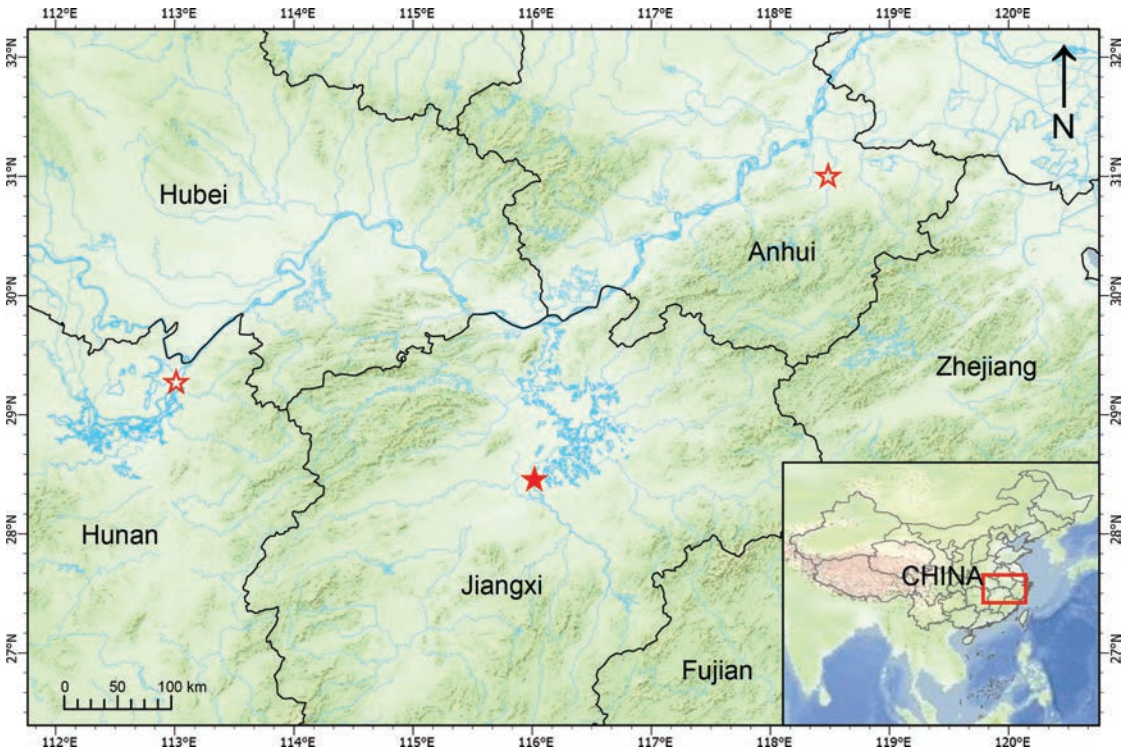

Figure 5. Distribution of *Globunio mirificus* gen. et sp. nov. Solid star: type locality; hollow stars: other localities.

Figure 6. Habitats and live animals of *Globunio mirificus* gen. et sp. nov. **A.** Type locality, Ganjiang River at Honggutan of Nanchang in 2022; **B.** Type locality, Ganjiang River at Honggutan of Nanchang in 2023; **C, D.** Live animals.

completion of the water plant, failed to recover any live animals. Furthermore, the construction of multiple dams (called the Ganfuweilyu Project) in the lower reaches of the Ganjiang River in 2024, resulting in the storage of water, has led to an increase in the average water level by 10 meters, thereby transforming the river into a static reservoir. This has led to concerns regarding the survival of new species that are dependent on flowing microhabitats. In addition to the type locality, the new species has also been discovered in Hunan and Anhui. The population size in Anhui is relatively large, but only empty shells have been found in Hunan. Protective measures such as artificial reproduction and ex situ conservation should be implemented for this species in order to save its declining population.

Acknowledgements

We thank Zheng-Jie Lou (Hangzhou) and Zhe-Hao Wu (Nanchang) for assistance in collecting specimens. This study was supported by the National Natural Science Foundation of China under Grant No. 32360132 and No. 31772412.

References

Bernt M, Donath A, Jühling F, Externbrink F, Florentz C, Fritzsch G, Pütz J, Middendorf M, Stadler PF (2013) Mitos: Improved de novo metazoan mitochondrial genome annotation. Molecular Phylogenetics and Evolution 69: 313–319. https://doi.org/10.1016/j.ympev.2012.08.023

Böhm M, Dewhurst-Richman NI, Seddon ML, Albrecht C, Allen D (2021) The conservation status of the world's freshwater molluscs. Hydrobiologia 848: 3231–3254. https://doi.org/10.1007/s10750-020-04385-w

Bolotov IN, Bespalaya YV, Vikhrev IV, Aksenova OV, Aspholm PE, Gofarov MY, Klishko OK, Kolosova YS, Kondakov AV, Lyubas AA, Paltser IS, Konopleva ES, Tumpeesuwan S, Bolotov NI, Voroshilova IS (2015) Taxonomy and Distribution of Freshwater Pearl Mussels (Unionoida, Margaritiferidae) of the Russian Far East. PLoS ONE 10(5): e0122408. https://doi.org/10.1371/journal.pone.0122408

Bolotov IN, Vikhrev IV, Kondakov AV, Konopleva ES, Gofarov MY, Aksenova OV, Tumpeesuwan S (2017) New taxa of freshwater mussels (Unionidae) from a species-rich but overlooked evolutionary hotspot in Southeast Asia. Scientific Reports 7(1): 11573. https://doi.org/10.1038/s41598-017-11957-9

Bolotov IN, Kondakov AV, Konopleva ES, Vikhrev IV, Aksenova OV, Aksenov AS, Bespalaya YV, Borovskoy AV, Danilov PP, Dvoryankin

GA, Gofarov MY, Kabakov MB, Klishko OK, Kolosova YS, Lyubas AA, Novoselov AP, Palatov DM, Savvinov GN, Solomonov NM, Spitsyn VM, Sokolova SE, Tomilova AA, Froufe E, Bogan AE, Lopes-Lima M, Makhrov AA, Vinarski MV (2020) Integrative taxonomy, biogeography and conservation of freshwater mussels (Unionidae) in Russia. Scientific Reports 10(3072): 1–20. https://doi.org/10.1038/s41598-020-59867-7

Burzynski A, Soroka M, Mioduchowska M, Kaczmarczyk A, Sell J (2017) The complete maternal and paternal mitochondrial genomes of *Unio crassus*: Mitochondrial molecular clock and the overconfidence of molecular dating. Molecular Phylogenetics and Evolution 107: 605–608. https://doi.org/10.1016/j.ympev.2016.12.007

Castresana J (2000) Selection of conserved blocks from multiple alignments for their use in phylogenetic analysis. Molecular Biology and Evolution 17(4): 540–552. https://doi.org/10.1093/oxfordjournals.molbev.a026334

Chen ZG, Dai YT, Ouyang S, Huang XC, Wu XP (2023) Unveiling the identity of *Diaurora* Cockerell, 1903 (Bivalvia, Unionidae): morphology, molecular phylogenetics, and the description of a new species. Zookeys 1173: 131–144. https://doi.org/10.3897/zookeys.1173.106148

Dai YT, Huang XC, Wu CHZ, Chen ZG, Guo L, Shu SY, Ouyang S, Wu XP (2023) Multilocus and mitogenomic phylogenetic analyses reveal a new genus and species of freshwater mussel (Bivalvia, Unionidae) from Guangxi, China. Invertebrate Systematics 37(2): 152–166. https://doi.org/10.1071/IS22048

Dai YT, Chen ZG, Cheng YZ, Huang XC, Ouyang S, Shu FY, Wu XP (2024a) Molecular phylogeny reveals a new genus and species of freshwater mussel (Bivalvia, Unionidae, Gonideinae) from Jiangxi, China. Zoosystematics and Evolution 100(4): 1419–1429. https://doi.org/10.3897/zse.100.135217

Dai YT, Chen ZG, Hu CL, Ning PF, Ouyang S, Huang XC, Wu XP (2024b) Taxonomic reassessment of *Scabies* (Bivalvia, Unionidae) species in China based on multilocus and mitogenomic phylogenetic analyses. Invertebrate Systematics 38: 24020. https://doi.org/10.1071/IS24020

Dai YT, Chen ZG, Hu CL, Ouyang S, Huang XC, Wu XP (2024c) Description of a new freshwater mussel species of *Plethobophus*, Simpson, 1900 (Bivalvia, Unionidae) from Guangdong, China. Zoosystematics and Evolution 100(4): 1191–1200. https://doi.org/10.3897/zse.100.131019

Dai YT, Chen ZG, Peng KJ, Ouyang S, Huang XC, Wu XP (2024d) Revisiting the genus *Pseudocuneopsis* (Bivalvia, Unionidae): Morphology, mitochondrial phylogenomics, and the description of a new species. Zoologica Scripta 53(3): 323–337. https://doi.org/10.1111/zsc.12647

Edgar RC (2004) Muscle: Multiple sequence alignment with high accuracy and high throughput. Nucleic Acids Research 32(5): 1792–1797. https://doi.org/10.1093/nar/gkh340

Fukata Y, Iigo M (2020) The complete mitochondrial genome of freshwater mussel *Pronodularia japanensis* (Gonideinae, Unionidae, Unionida) from Tochigi Prefecture, Japan, and its phylogenetic analysis. Mitochondrial DNA, Part B, Resources 5(2): 1215–1217. https://doi.org/10.1080/23802359.2020.1730726

Graf DL, Cummings KS (2007) Review of the systematics and global diversity of freshwater mussel species (Bivalvia, Unionoida). Journal of Molluscan Studies 73(3): 291–314. https://doi.org/10.1093/mollus/eym029

Graf DL, Cummings KS (2021) A 'big data' approach to global freshwater mussel diversity (Bivalvia, Unionoida), with an updated checklist of genera and species. Journal of Molluscan Studies 87(1): eyaa034. https://doi.org/10.1093/mollus/eyaa034

Graf DL, O'Foighil D (2000) The evolution of brooding characters among the freshwater pearly mussels (Bivalvia, Unionoidea) of North America. The Journal of Molluscan Studies 66(2): 157–170. https://doi.org/10.1093/mollus/66.2.157

Graf DL, Geneva AJ, Pfeiffer III JM, Chilala AD (2014) Phylogenetic analysis of *Prisodontopsis* Tomlin, 1928 and *Mweruella* Haas, 1936 (Bivalvia, Unionidae) from Lake Mweru (Congo basin) supports a Quaternary radiation in the Zambian Congo. The Journal of Molluscan Studies 80(3): 303–314. https://doi.org/10.1093/mollus/eyu012

Guo L (2022) Unionoida. The Straits Publishing, China, 256 pp. [In Chinese]

He J, Zhuang ZM (2013) The Freshwater Bivalves of China. ConchBooks, Germany, 198 pp.

Heude PM (1875) Conchyliologie fluviatile de la province de Nanking et de la Chine centrale. Premier Fascicule. Librairie F. Savy, France, 8 pp. [In French] https://doi.org/10.5962/bhl.title.14450

Heude PM (1877a) Conchyliologie fluviatile de la province de Nanking et de la Chine centrale. Deuxième Fascicule. Librairie F. Savy, France, 8 pp. [In French]

Heude PM (1877b) Conchyliologie fluviatile de la province de Nanking et de la Chine centrale. Troisième Fascicule. Librairie F. Savy, France, 8 pp. [In French]

Heude PM (1878) Conchyliologie fluviatile de la province de Nanking et de la Chine centrale. Quatrième Fascicule. Librairie F. Savy, France, 8 pp. [In French]

Heude PM (1879) Conchyliologie fluviatile de la province de Nanking et de la Chine centrale. Cinquième Fascicule. Librairie F. Savy, France, 8 pp. [In French]

Heude PM (1880a) Conchyliologie fluviatile de la province de Nanking et de la Chine centrale. Sixième Fascicule. Librairie F. Savy, France, 8 pp. [In French]

Heude PM (1880b) Conchyliologie fluviatile de la province de Nanking et de la Chine centrale. Dixième Fascicule. Librairie F. Savy, France, 8 pp. [In French]

Heude PM (1881) Conchyliologie fluviatile de la province de Nanking et de la Chine centrale. Septième Fascicule. Librairie F. Savy, France, 8 pp. [In French]

Heude PM (1883) Conchyliologie fluviatile de la province de Nanking et de la Chine centrale. Huitième Fascicule. Librairie F. Savy, France, 8 pp. [In French]

Heude PM (1885) Conchyliologie fluviatile de la province de Nanking et de la Chine centrale. Neuvième Fascicule. Librairie F. Savy, France, 8 pp. [In French]

Huang XC, Su JH, Ouyang JX, Ouyang S, Zhou CH, Wu XP (2019) Towards a global phylogeny of freshwater mussels (Bivalvia, Unionida): Species delimitation of Chinese taxa, mitochondrial phylogenomics, and diversification patterns. Molecular Phylogenetics and Evolution 130: 45–59. https://doi.org/10.1016/j.ympev.2018.09.019

Katoh K, Rozewicki J, Yamada KD (2019) MAFFT online service: Multiple sequence alignment, interactive sequence choice and visualization. Briefings in Bioinformatics 20(4): 1160–1166. https://doi.org/10.1093/bib/bbx108

Kearse M, Moir R, Wilson A, Stones-Havas S, Cheung M, Sturrock S, Buxton S, Cooper A, Markowitz S, Duran C, Thierer T, Ashton B, Meintjes P, Drummond A (2012) Geneious basic: An integrated and extendable desktop software platform for the organization and analysis of sequence data. Bioinformatics 28(12): 1647–1649. https://doi.org/10.1093/bioinformatics/bts199

Kumar S, Stecher G, Li M, Knyaz C, Tamura K (2018) Mega X: Molecular evolutionary genetics analysis across computing platforms. Molecular Biology and Evolution 35(6): 1547–1549. https://doi.org/10.1093/molbev/msy096

Lanfear R, Frandsen PB, Wright AM, Senfeld T, Calcott B (2017) Partitionfinder 2: New methods for selecting partitioned models of evolution for molecular and morphological phylogenetic analyses. Molecular Biology and Evolution 34(3): 772–773. https://doi.org/10.1093/molbev/msw260

Laslett D, Canback B (2008) ARVEN: A program to detect tRNA genes in metazoan mitochondrial nucleotide sequences. Bioinformatics 24(2): 172–175. https://doi.org/10.1093/bioinformatics/btm573

Liu XJ, Liu YY, Wu RW, Zanatta DT, Lopes-Lima M, Gonçalves DV, Bogan A, Ouyang S, Wu XP (2022) Systematics, distribution, biology, and conservation of freshwater mussels (Bivalvia, Unionida) in China. Aquatic Conservation Marine and Freshwater Ecosystems 32(5): 859–895. https://doi.org/10.1002/aqc.3799

Lopes-Lima M, Froufe E, Do VT, Ghamiz M, Mock KE, Kebapçı Ü, Klishko O, Kovitvadhi S, Kovitvadhi U, Paulo OS, Pfeiffer III JM, Raley M, Riccardi N, Şereflişan H, Sousa R, Teixeira A, Varandas S, Wu X, Zanatta DT, Zieritz A, Bogan AE (2017) Phylogeny of the most species-rich freshwater bivalve family (Bivalvia, Unionida, Unionidae): Defining modern subfamilies and tribes. Molecular Phylogenetics and Evolution 106: 174–191. https://doi.org/10.1016/j.ympev.2016.08.021

Lopes-Lima M, Hattori A, Kondo T, Hee Lee J, Ki Kim S, Shirai A, Hayashi H, Usui T, Sakuma K, Toriya T, Sunamura Y, Ishikawa H, Hoshino N, Kusano Y, Kumaki H, Utsugi Y, Yabe S, Yoshinari Y, Hiruma H, Tanaka A, Sao K, Ueda T, Sano I, Miyazaki JI, Gonçalves DV, Klishko OK, Konopleva ES, Vikhrev IV, Kondakov AV, Yu Gofarov M, Bolotov IN, Sayenko EM, Soroka M, Zieritz A, Bogan AE, Froufe E (2020) Freshwater mussels (Bivalvia, Unionidae) from the Rising Sun (Far East Asia): Phylogeny, systematics, and distribution. Molecular Phylogenetics and Evolution 146(2): 106755. https://doi.org/10.1016/j.ympev.2020.106755

Minh BQ, Nguyen MAT, von Haeseler A (2013) Ultrafast approximation for phylogenetic bootstrap. Molecular Biology and Evolution 30: 1188–1195. https://doi.org/10.1093/molbev/mst024

Ronquist F, Teslenko M, van der Mark P, Ayres DL, Darling A, Höhna S, Larget B, Liu L, Suchard MA, Huelsenbeck J (2012) Mrbayes 3.2: Efficient bayesian phylogenetic inference and model choice across a large model space. Systematic Biology 61: 539–542. https://doi.org/10.1093/sysbio/sys029

Simpson CT (1900) Synopsis of the naiades, or pearly fresh-water mussels. Proceedings of the United States National Museum 22(1205) 501–1044. https://doi.org/10.5479/si.00963801.22-1205.501

Vaughn CC (2018) Ecosystem services provided by freshwater mussels. Hydrobiologia 810: 15–27. https://doi.org/10.1007/s10750-017-3139-x

Wu RW, Liu XJ, Wang S, Roe KJ, Ouyang S, Wu XP (2019) Analysis of mitochondrial genomes resolves the phylogenetic position of Chinese freshwater mussels (Bivalvia, Unionida). ZooKeys 812(6): 23–46. https://doi.org/10.3897/zookeys.812.29908

Wu RW, Liu XJ, Kondo T, Ouyang S, Wu XP (2021) New species of the genus *Inversidens* Haas, 1911 (Unionoida, Unionidae, Gonideinae) from Jiangxi Province, China. Zookeys 1054: 85–93. https://doi.org/10.3897/zookeys.1054.69075

Wu RW, Liu XJ, Guo L, Zhou CH, Ouyang S, Wu XP (2022a) DNA barcoding, multilocus phylogeny and morphometry reveal phenotypic plasticity in the Chinese freshwater mussel *Lamprotula caveata* (Bivalvia, Unionidae). Ecology and Evolution 12(7): e9035. https://doi.org/10.1002/ece3.9035

Wu XP, Dai YT, Yin N, Shu FY, Chen ZG, Guo L, Zhou CH, Ouyang S, Huang XC (2022b) Mitogenomic phylogeny resolves *Cuneopsis* (Bivalvia, Unionidae) as polyphyletic: The description of two new genera and a new species. Zoologica Scripta 51(2): 173–184. https://doi.org/10.1111/zsc.12527

Wu RW, Liu LL, Zhang LP, Liu XJ, Hu ZK, Jin DD, Zhang ZP, Wu XP, Xie ZC, Li ZF, Lopes-Lima M (2024) Diversity, morphology, and phylogeny of freshwater mussels of the genus *Nodularia* (Bivalvia, Unionidae) from China, with descriptions of four new species. Zoologica Scripta 53(5): 594–613. https://doi.org/10.1111/zsc.12677

Zoosyst. Evol. 101 (2) 2025, 791–804 | DOI 10.3897/zse.101.137781

PENSOFT

MUSEUM FÜR NATURKUNDE BERLIN

Taxonomic status and phylogenetic analyses based on complete mitochondrial genome and microscopic ossicles: Redescription of a controversial tropical sea cucumber species (Holothuroidea, *Holothuria* Linnaeus, 1767)

Chenghao Jia[1,2], Zening Xu[1,3], Fengping Li[1,2], Liuna Chen[3], Aimin Wang[1,3], Fei Gao[1,3]

1 *State Key Laboratory of Marine Resource Utilization in South China Sea, Hainan University, Haikou, Hainan, China*
2 *School of Ecology, Hainan University, Haikou, Hainan, China*
3 *School of Marine Biology and Fisheries, Hainan University, Haikou, Hainan, China*

https://zoobank.org/1374FED0-9868-49BF-9924-C5C513A3BC93

Corresponding author: Fei Gao (gaofeicas@126.com)

Academic editor: Pavel Stoev ♦ **Received** 24 September 2024 ♦ **Accepted** 19 March 2025 ♦ **Published** 15 April 2025

Abstract

To explore the taxonomic status of a tropical sea cucumber species with controversy, we conducted an investigation into its morphological characteristics (external form and ossicles) and mitochondrial genome and rearranged the historical materials of the species and its confusing species. The species was first described in the middle of the 18th century but later synonymized with *Bohadschia ocellata* Jaeger, 1833, *Holothuria hamata* Pearson, 1913, or *Holothuria kurti* Ludwig, 1891, by different scholars. The observed ossicles encompassed multiple types, including buttons, C-shaped ossicles, rods, and tables, with a distinct subtype identified as tack-like tables. Ventral and dorsal body walls exhibited similar table and button ossicle shapes. The mitogenome contained 13 protein-coding genes (PCGs), 2 ribosomal RNAs (rRNAs), and 22 transfer RNA (tRNA) genes, with a sequence length of 15,797 bp. Subsequent construction of a phylogenetic tree using Bayesian inference (BI) and maximum likelihood (ML) methods indicated that the species was grouped into a separate branch firstly with *Holothuria* (*Theelothuria*) *spinifera* Théel, 1886, so suggesting its taxonomic classification under subgenus *Theelothuria* Deichmann, 1958. Based on the data of this study and previous literature, we suggested that the Latin name for this species should tentatively be "*Holothuria ocellata* Jaeger, 1833 *sensu* Théel 1886." The morphologic and genomic information in the current study could be valuable in further biological studies of this sea cucumber species.

Key Words

Mitochondrial genome, molecular phylogenetics, ossicles, taxonomy, tropical sea cucumber

Introduction

Holothuroidea, commonly known as holothuroids or sea cucumbers, includes about 1700 species worldwide (Reich 2017; Harini et al. 2024). These species are one of the largest and most diverse groups of benthic invertebrates in the intertidal and subtidal zones, constituting the vast majority of total biomass in slope and abyssal benthic systems (Slater and Chen 2015). Within this class, the family Holothuriidae comprises 45 genera and approximately 778 species (WoRMS 2023a), and it has also emerged as one of the most significant benthic taxa due to its substantial economic and ecological value in aquaculture, pharmacy, or high biodiversity (Purcell et al. 2012; Soliman et al. 2019). However, due to morphological similarities or the brevity of descriptions in some previous literature predating the mainstream adoption of Linnaean classification, the taxonomic status of certain species has long been subject to dispute.

Sea cucumber *Holothuria ocellata* Jaeger, 1833, also known as *Bohadschia ocellata* Jaeger, 1833, is a subject of controversy. This species inhabits the Indo-West Pacific region and exhibits a wide bathymetric distribution from 0 to 270 m (Clark and Rowe 1971; Guille et al. 1986; Liao 1997; Teo and Ng 2009). While some authors asserted it belongs to the genus *Holothuria* Linnaeus, 1767 (Heding 1939; Liao 1980; Liao 1997), others recognized it as a member of the genus *Bohadschia* Jaeger, 1833 (Kim et al. 2013; Patantis et al. 2019). Still others argued that *H. ocellata* is synonymous with other sea cucumber species like *Holothuria hamata* Pearson, 1913, or *Holothuria kurti* Ludwig, 1891 (Aydin et al. 2019; Moazzam and Moazzam 2020; Purcell et al. 2023). The databases that are widely referenced present different results. WoRMS (https://www.marinespecies.org/) acknowledges the validity of *B. ocellata*, but the NCBI taxonomy database (https://www.ncbi.nlm.nih.gov/Taxonomy/Browser) recognizes the validity of *H. ocellata*. Before reaching a conclusion, we use the appellation of "*Holothuria ocellata*" in this study.

Besides the external morphology, the traditional morphological classification of sea cucumbers is mainly based on the structure of ossicles within their body wall, which is part of the sea cucumber's calcified endoskeleton (Aydin and Erkan 2015). However, due to the variability and multiformity of ossicles within the same species, the morphological analysis often leads to the wrong species identification of holothuroids (Massin et al. 2000; Utzeri et al. 2020). In addition, hybridization events among related species may also lead to animals with mixed morphological features, which might add confounding factors (Uthicke et al. 2005; Yoshida et al. 2012; Kim et al. 2013). Thus, to improve the accuracy of species identification, molecular information is necessary to complement and ascertain the taxonomic status of sea cucumbers (Dettaï et al. 2011; Aydin and Erkan 2015; Valente et al. 2015). Among molecular technologies, the mitochondrial genome is an excellent tool for species identification, which has been widely utilized in the work of sea cucumber species identification (Utzeri et al. 2020; Sun et al. 2021; Ma et al. 2022; Li et al. 2022).

In this study, as a first step for identifying the species of obtained samples, we provided a detailed description of the external morphology and ossicle structure for *H. ocellata* using microscopy inspection. Then, we sequenced the complete mitochondrial genome of this species and compared it with the other complete mitochondrial sequences of other holothuroid species. Through integrating morphological observation and molecular biological methods, along with comparison to other literature, we aim to clarify the taxonomic history and position of this sea cucumber species. The produced molecular and morphological results have addressed a gap in the phylogenetic analysis of *H. ocellata* and have provided important classification and identification data for this species.

Materials and methods

Sample collection and preservation

The sea cucumber sample (Fig. 1) was collected by diving from the coastal waters of Wenchang in China in August 2022 and was transported alive to the laboratory in fresh seawater. The sample was identified based on morphological characteristics and DNA barcoding before alcohol preservation, and the individual was chosen for mitogenome sequencing. Muscle tissues were placed in 95% ethanol at -20 °C for further study.

Microscopic analyses of the ossicles and calcareous ring

To verify the identity of the specimen, both optical microscopy and scanning electron microscopy were used to observe and analyze the types and sizes of ossicles in the body wall, tentacle, tube feet, and papillae. The ossicles were extracted using the method modified by Teo and Ng (2009). Three tissue pieces weighing about 1 g were collected from each target site and rinsed with distilled water. Then, 8% sodium hypochlorite was added to each sample and shocked to digest for approximately 3–5 min. After white particles appeared at the bottom of the tube, undigested tissue pieces were picked out and left to stand for 5 minutes. An appropriate amount of turbid liquid was absorbed with white particles and placed on a slide. We used the light microscope to preliminarily observe these samples and confirmed different types of ossicles. Then, the other turbid liquid was dropped on the conductive tape and stoved in a drying oven, followed by gold spray treatment with an ion sputtering apparatus. A scanning electron microscope (SEM; HITACHI, S-4800) was used to observe and photograph these samples. The size of the ossicles in the photographs was measured by the soft ruler and converted to actual lengths based on the scale bars. Ten individuals from each ossicle were randomly selected for measurement. The calcareous ring was observed and depicted with the stereoscopic microscope. The size of the calcareous ring in the photographs was measured by the soft ruler and converted to actual lengths based on the scale bars.

DNA extraction and sequencing

According to the manufacturer's protocol, the total DNA of the sea cucumber was extracted using the TIANamp Marine Animal DNA Kit (TIANGEN, Beijing, China). The DNA library was sequenced by Origingene Co., Ltd. (Shanghai, China) using the Illumina NovaSeq™ 6000 platform with an insert size of 300–500 bp. Approximately 9.09 GB of raw data from *Holothuria ocellata* were generated with 150-base-pair paired-end read lengths. The quality control and assessment of data

Figure 1. Dorsal (**A**) and ventral (**B**) views of *H. ocellata*.

were used by Cutadapt v1.16 and FASTQC v0.11.4, respectively (Martin 2011). The mitogenome was assembled by NOVOPLASTY v4.2 with default parameters (Dierckxsens et al. 2017).

Sequence annotation and analysis

The mitogenome of *H. ocellata* was annotated by the MITOS WEBSERVER (Donath et al. 2019) (http://mitos2.bioinf.uni-leipzig.de/index.py). The graphical circle map of the mitogenome was drawn using the online PROKSEE tool (Stothard et al. 2019) (https://proksee.ca/). The relative synonymous codon usage (RSCU) was conducted using CODONW v1.4.4 (http://codonw.sourceforge.net). The blank region of the mitogenome was defined as the control region (D-loop) and compared with the mitogenome of the reference species to determine the control region. The TRNASCAN-SE tool was used to identify the tRNA gene and predict the secondary structure diagram of tRNA (Chan and Lowe 2019). The composition skewness of each segment was calculated by the following formulas: AT-skew = (A − T) / (A + T); GC-skew = (G − C) / (G + C) (Perna and Kocher 1995).

Phylogenetic analysis

Besides the sequence obtained in this study, mitogenomes of 35 previously sequenced sea cucumber species in the class Holothuroidea and 2 previously sequenced starfish species in the class Asteroidea (with the latter as the outgroup taxon) were used in the phylogenetic analyses. We extracted the nucleotide sequences of the 13 protein-coding genes from each mitogenome as the dataset to construct the phylogenetic tree. Sequences were extracted and concatenated by PHYLOSUITE v1.2.3 (Zhang et al. 2020; Xiang et al. 2023), and these sequences were aligned and refined through MAFFT v7.505 and MACSE v2.06 (Katoh and Standley 2013; Ranwez et al. 2018). Ambiguously aligned fragments of 13 alignments were removed in batches based on GBLOCKS with the default parameter settings (Talavera and Castresana 2007). MODELFINDER v2.2.0 was used to select the best-fit model through the BIC criterion (Kalyaanamoorthy et al. 2017). Maximum likelihood (ML) phylogenies were inferred by IQ-TREE v2.2.0 under the model automatically selected by the 'Auto' option for 20000 ultrafast bootstraps (Guindon et al. 2010; Minh et al. 2013; Nguyen et al. 2015). Bayesian inference (BI) phylogenies were inferred through MRBAYES v3.2.7a under the GTR+I+G+F model (2 parallel runs, 200000 generations), with the initial 25% of sampled data discarded as burn-in (Ronquist et al. 2012).

To determine whether the species belongs to the genus *Bohadschia* or to *Holothuria*, we selected the mitochondrial sequence fragments of all *Bohadschia* and some *Holothuria* from NCBI to perform the phylogenetic tree. 13 *rrnL* genes and 9 *cox1* genes, including sequences from this study, were selected to build Neighbor-Joining (NJ) phylogenetic trees based on two genes, respectively. Sequences were aligned by SEQMAN from DNASTAR software (USA). The trees were constructed, and the distances between and within groups were determined by MEGA v5.0 (Tamura et al. 2011) with 1000 bootstrap replicates based on genetic distances calculated with the Kimura-2-parameter (K2P) model by the same software.

Results

Morphological characters

The specimen, in the state of natural extension, is 24.35 ± 0.3 cm long and 5 ± 0.2 cm wide. The body is cylindrical, tapering at both ends. The bivium presents convex (Fig. 1A), while the trivium presents flattened (Fig. 1B). The mouth is ventral, and the anus is located in a terminal. The dorsal color is grayish on both sides and yellowish-brown in the middle, interspersed with tan spots. The whole dorsal surface is covered with conic papillae, which are milky at the tip and brown at the base. Each papilla is usually surrounded by a narrow light-grey band and a white band from inside to outside, although the white band may be absent or non-significant in some papillae. The ventral has a lighter color and slightly flatter shape than the dorsal. The ventral papillae are arranged in 3–4 bands, concentrated in the middle of the trivium, showing a trend of spreading to the interambulacrum on both sides. Papillae on the sides of the ventral are prominent in size, arranged along the sides of the body to form the dorsoventral junction with a number of 41 or 42 on each side.

Microscopic analyses of the ossicles and calcareous ring

The body wall of the specimen has four major ossicle types, including multiple buttons, C-shaped ossicles, rods, and tables. Ventral/dorsal body walls have similar table and button types. The majority of the buttons are knobbed, yet the minority are smooth and nearly oval, usually with 3 pairs of holes, 30–68 μm in length and 30–40 μm in width (Fig. 2A, B). Some buttons are long ellipsoids with up to 4–7 pairs of holes, 63–88 μm in length, and 27–38 μm in width (Fig. 2C, D). The paired holes of most buttons are symmetrical and similar in size to each other. Tables are intact with nearly circular discs with smooth or wavy margins. There are basically two types of typical tables: 1) the disc is convex with a larger size of 81–136 μm in diameter, with dozens of holes in the circumferential margin; the spire is moderate in length, relatively thin, and terminating in a cluster of spines (Fig. 2E, F); 2) the disc is convex with a smaller size, 64–82 μm in diameter, with 8–12 holes in the circumferential margin; the spire is moderate in length, relatively thick, and terminating in a cluster of spines (Fig. 2G, H). The rods in the body wall are commonly composed of simple spicules, which are smooth and elongated, with a wide range of length variations, 131–496 μm long (Fig. 2I). The C-shaped ossicles in the body wall are commonly C-form, smooth, and elongated, with a wide range of length variations, 200–300 μm long (Fig. 2K). Tentacles with spiny rods, 232–376 μm long (Fig. 2P–R).

Ossicles of papillae and tube feet include rods, perforated plates, and tables. The morphology of rods is diverse and complex, with spines present or not and thicknesses different (Fig. 2I–J). Most perforated plates, measuring up to 200 μm in length, have perforations in the middle, and some plates are perforated throughout their whole length (Fig. 2L–O). The type of tables in papillae is basically consistent with those of the body wall or tube feet, except for the tack-like tables. The tack-like tables, only found in papillae, with concave bottoms, are few in number, standing up to 240 μm high, and have a tall attenuating spire with several cross-beams, resembling the shape of a nail (Fig. 2S, T).

Calcareous ring, with radial plates obviously larger than interradial ones; radial plates with anterior concave and obviously posterior bifurcation; interradial plates with cuspate anteriorly (Suppl. material 1).

Mitogenome composition and characteristics

The complete mitochondrial genome of the sea cucumber (GenBank No. OQ731944) is 15,797 bp in length (Fig. 3). The mitogenome contains 37 typical genes (13 PCGs, 22 tRNAs, and 2 rRNAs) and 2 control regions. Most mitochondrial genes are encoded on the H-strand, except for nad6 and 5 tRNA genes (*trn*S2, *trn*Q, trnA, *trn*V, and *trn*D) that are encoded on the L-strand (Table 1). The nucleotide composition of mitogenomes has a higher A+T bias of 59.01%, and all PCGs show negative GC-skew except for *nad6* (Table 2).

The number of PCGs in mitogenomes is consistent with the general findings on the mitogenomes in Holothuriidae species. Twelve PCGs (*cox1*, *cox2*, *cox3*, *atp8*, *atp6*, *nad1*, *nad2*, *nad3*, *nad4*, *nad4l*, *nad5*, and *cob*) are coded on the heavy strand (H-strand), while the remaining one (*nad5*) is coded on the light strand (L-strand). All 13 PCGs collectively encode 3696 amino acids. All PCGs use the initiation codon ATG. The termination codons TAA and TAG are commonly observed, although the incomplete termination codon T is found in *cox2* and *nad4* in the mitogenome.

We calculated the relative synonymous codon usage (RSCU) of the mitogenome (Table 3, Fig. 4), and the results showed that the frequency of NNA and NNC (N represents A, T, C, G) is higher than NNT and NNG. The most frequent amino acids in the coding sequences of mitochondrial proteins are Leu1, Phe, and Ile (> 290) (Table 3). Moreover, the minimally used amino acid in the mitogenomes is Trp (< 30).

Similar to the most holothuroids, the mitogenome of *Holothuria ocellata* has one *rrnS* (12S rRNA) and one *rrnL* (16S rRNA) gene. The *rrnS* gene is located between *trnF* and *trnE*, and the *rrnL* gene is located between *nad2* and *cox1*. In the *H. ocellata* mitogenome, the A+T content of rRNA is 59.82%. The AT-skew of rRNA is strongly positive, whereas the GC-skew is slightly negative, indicating that the contents of A and C are higher than those of T and G in the rRNA, respectively. And there are

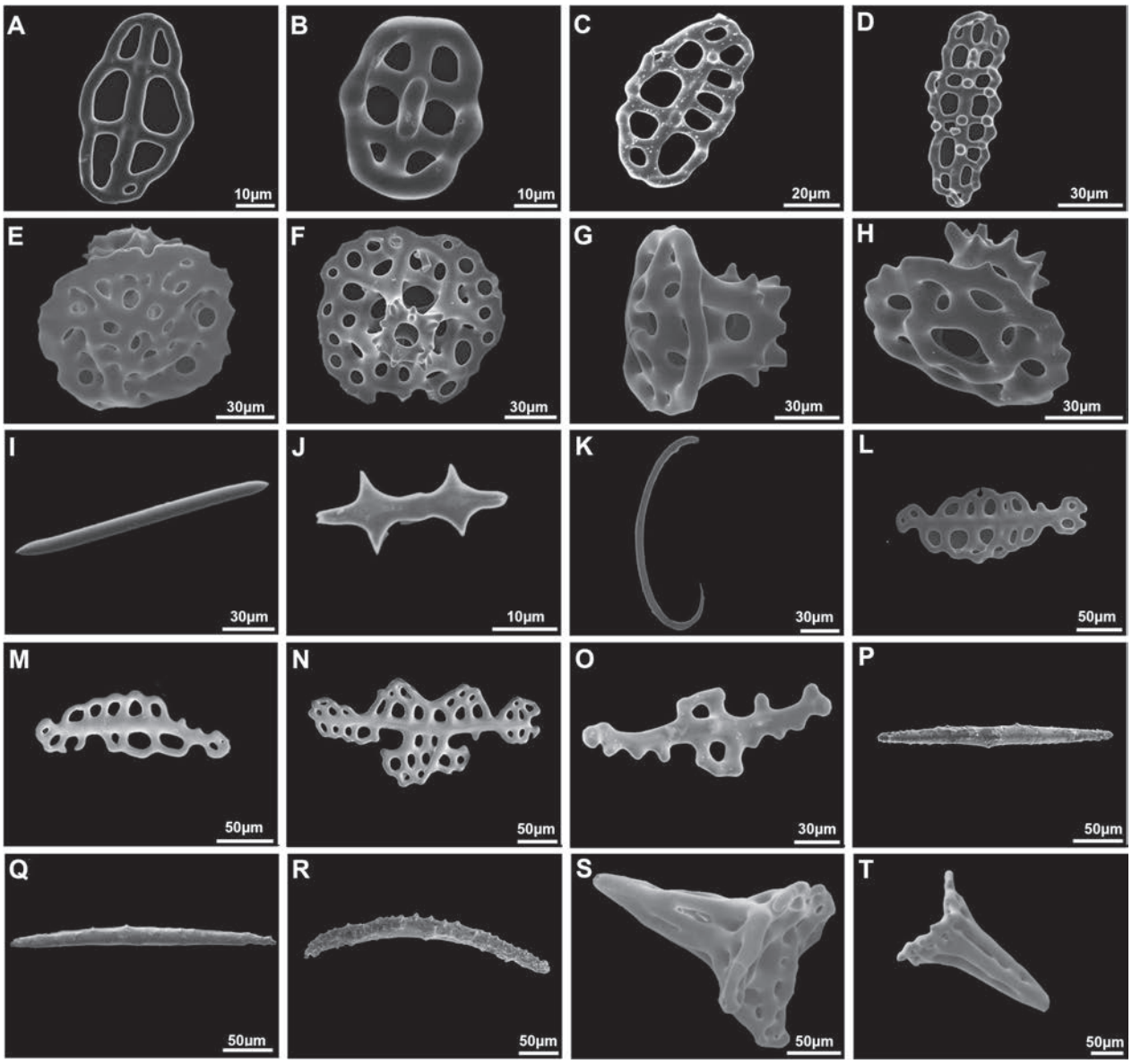

Figure 2. *H. ocellata*: scanning electron microscopy images of ossicles. **A, B.** Buttons with 3 pairs of holes; **C, D.** Buttons with 4–7 pairs of holes; **E, F.** Tables with larger discs; **G, H.** Tables with smaller discs; **I, J.** Rods in papillae, tube feet, or body wall; **K.** C-shaped ossicles in the body wall; **L-O.** Perforated plates of papillae, or tube feet; **P–R.** Rods in tentacles; **S, T.** Tack-like tables of papillae.

22 tRNA genes. The secondary clover-leaf structures of tRNA genes identified in the mitogenome are shown in Fig. 5. These tRNA genes vary in length from 57 bp to 75 bp. All predicted tRNAs display the typical clover-leaf secondary structure, except for *trnS1*.

Phylogenetic analysis

Phylogenetic relationships are constructed based on the sequences of 13 PCGs of 38 mitogenomes using BI and ML methods. The phylogenetic trees constructed by the two methods are consistent with high intermediate bootstrap values, and the topological structure of the trees is entirely the same (Fig. 6A). The results showed that 10 *Holothuria* sequences formed a monophyletic group in both ML and BI analyses. Moreover, *H. ocellata* formed a sister group with *Holothuria* (*Theelothuria*) *spinifera* Théel, 1886, and both divided with *Bohadschia argus* Jaeger, 1833.

Using the NJ method, the unrooted phylogenetic trees of the *rrnL* and *cox1* genes both indicated that *Holothuria* and *Bohadschia* species form a monophyletic group, respectively (Fig. 6B, C). *Holothuria* and *Bohadschia* sequences are observably divided from each other. Besides, the tree of *rrnL* showed the *Holothuria ocellata* sequence obtained in this study clusters with the *H. ocellata* sequence from NCBI. And the tree of *cox1* showed the *H. ocellata* sequence is divided with *Bohadschia ocellata* sequences from NCBI.

Table 1. Summary of the genes in the *H. ocellata* mitogenome.

Gene	Strand	Location	Size (bp)	Start codon	Stop codon	Anticodon
cox1	H	1-1557	1557	ATG	TAG	
trnR	H	1564-1632	69			TCG
nad4l	H	1633-1929	297	ATG	TAA	
cox2	H	1931-2618	688	ATG	T	
trnK	H	2619-2686	68			CTT
atp8	H	2687-2854	168	ATG	TAA	
atp6	H	2884-3531	648	ATG	TAA	
cox3	H	3534-4316	783	ATG	TAA	
trnS2	L	4315-4385	71			TGA
nad3	H	4404-4748	345	ATG	TAA	
nad4	H	4753-6109	1357	ATG	T	
trnH	H	6111-6176	66			GTG
trnS1	H	6189-6245	57			GCT
nad5	H	6477-8081	1605	ATG	TAA	
nad6	L	8100-8588	489	ATG	TAG	
cob	H	8597-9739	1143	ATG	TAG	
trnF	H	9742-9812	71			GAA
rrnS	H	9812-10633	822			
trnE	H	10631-10699	69			TTC
trnT	H	10701-10769	69			TGT
trnP	H	11252-11319	68			TGG
trnQ	L	11316-11385	70			TTG
trnN	H	11386-11455	70			GTT
trnL1	H	11456-11527	72			TAG
trnA	L	11527-11595	69			TGC
trnW	H	11596-11665	70			TCA
trnC	H	11666-11727	62			GCA
trnV	L	11728-11797	70			TAC
trnM	H	11816-11885	70			CAT
trnD	L	11891-11960	70			GTC
trnY	H	11961-12028	68			GTA
trnG	H	12028-12102	75			TCC
trnL2	H	12103-12173	71			TAA
nad1	H	12174-13145	972	ATG	TAG	
trnI	H	13168-13235	68			GAT
nad2	H	13236-14279	1044	ATG	TAA	
rrnL	H	14243-15665	1423			

Table 2. Compositions and skewness of *H. ocellata* mitogenomes.

Region	A%	T%	G%	C%	A + T (%)	G + C (%)	AT-Skew	GC-Skew
whole	31.47	27.54	16.46	24.52	59.01	40.98	0.067	-0.197
PCGs	28.73	29.70	16.54	25.03	58.43	41.57	-0.017	-0.204
cox1	27.87	27.49	18.24	26.40	55.36	44.64	0.007	-0.183
nad4l	28.62	30.64	11.45	29.29	59.26	40.74	-0.034	-0.438
cox2	31.24	24.96	16.59	27.20	56.20	43.79	0.112	-0.242
atp8	37.50	27.98	13.69	20.83	65.48	34.52	0.145	-0.207
atp6	31.33	28.09	12.96	27.62	59.42	40.58	0.055	-0.361
cox3	27.33	27.59	17.75	27.33	54.92	45.08	-0.005	-0.212
nad3	29.28	27.25	16.52	26.96	56.53	43.48	0.036	-0.240
nad4	31.73	25.88	15.06	27.34	57.61	42.40	0.102	-0.290
nad5	29.78	30.78	16.01	23.43	60.56	39.44	-0.016	-0.188
nad6	17.18	45.40	25.56	11.86	62.58	37.42	-0.451	0.366
cob	28.26	30.62	16.36	24.76	58.88	41.12	-0.040	-0.204
nad1	26.34	32.82	16.87	23.97	59.16	40.84	-0.110	-0.174
nad2	28.93	31.51	15.61	23.95	60.44	39.56	-0.043	-0.211
tRNAs	31.06	28.42	21.02	19.50	59.48	40.52	0.044	0.038
rRNAs	37.59	22.23	18.98	21.20	59.82	40.18	0.257	-0.055

Table 3. Codon numbers and relative synonymous codon usages in 13 PCGs of *H. ocellata*.

Codon	Count	RSCU	Codon	Count	RSCU	Codon	Count	RSCU	Codon	Count	RSCU
UUU(F)	143	0.97	UCU(S)	53	1.18	UAU(Y)	44	0.85	UGU(C)	18	1.00
UUC(F)	151	1.03	UCC(S)	86	1.92	UAC(Y)	60	1.15	UGC(C)	18	1.00
UUA(L)	138	1.34	UCA(S)	71	1.58	UAA(*)	7	0.22	UGA(*)	82	2.59
UUG(L)	28	0.27	UCG(S)	18	0.40	UAG(*)	6	0.19	UGG(W)	23	1.00
CUU(L)	108	1.05	CCU(P)	46	1.07	CAU(H)	17	0.42	CGU(R)	9	0.37
CUC(L)	92	0.89	CCC(P)	46	1.07	CAC(H)	64	1.58	CGC(R)	6	0.24
CUA(L)	209	2.03	CCA(P)	70	1.63	CAA(Q)	56	1.38	CGA(R)	49	2.00
CUG(L)	42	0.41	CCG(P)	10	0.23	CAG(Q)	25	0.62	CGG(R)	9	0.37
AUU(I)	78	0.64	ACU(T)	53	0.87	AAU(N)	31	0.81	AGU(S)	15	0.33
AUC(I)	61	0.50	ACC(T)	89	1.45	AAC(N)	46	1.19	AGC(S)	26	0.58
AUA(I)	226	1.86	ACA(T)	88	1.44	AAA(K)	98	1.26	AGA(R)	68	2.78
AUG(M)	74	1.00	ACG(T)	15	0.24	AAG(K)	57	0.74	AGG(R)	6	0.24
GUU(V)	63	1.18	GCU(A)	62	0.94	GAU(D)	17	0.55	GGU(G)	26	0.47
GUC(V)	57	1.07	GCC(A)	121	1.83	GAC(D)	45	1.45	GGC(G)	39	0.70
GUA(V)	79	1.48	GCA(A)	70	1.06	GAA(E)	63	1.29	GGA(G)	110	1.98
GUG(V)	15	0.28	GCG(A)	12	0.18	GAG(E)	35	0.71	GGG(G)	47	0.85

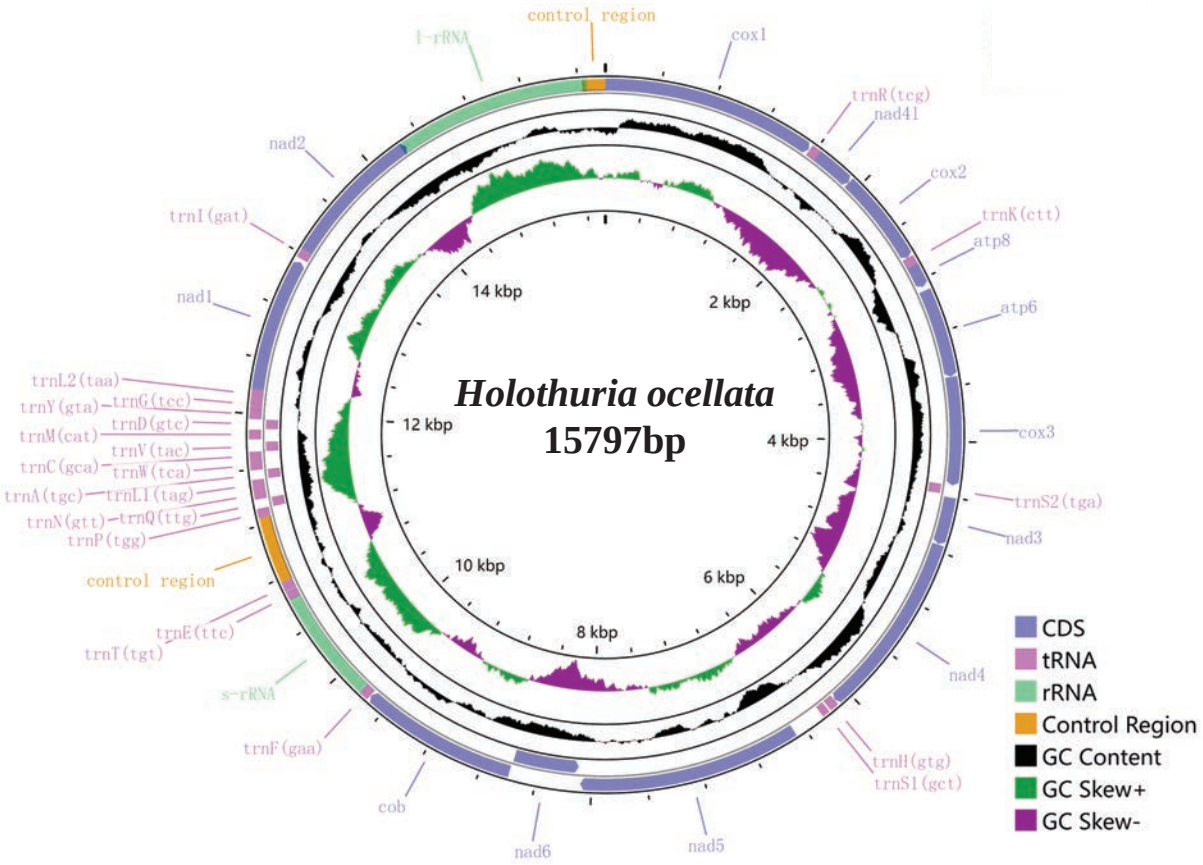

Figure 3. Mitochondrial genome maps of *H. ocellata*. Genes encoded on the heavy or light strands are shown outside or inside the circular gene map, respectively.

Discussion

Comparative analysis of suspected synonyms

vs. B. ocellata Jaeger, 1833

The controversy regarding the nomenclature of two sea cucumber species (*H. ocellata* / *B. ocellata*) stems from the blurry original nomenclators. Jaeger (1833) first found a sea cucumber species and classified it into the subgenus *Holothuria*, tribes *Bohadschia*, the latter being subordinate to the former, and named this species "*ocellata*." With the continuous progress of sea cucumber taxonomy, both *Holothuria* and *Bohadschia* have evolved into independent and valid genera (WoRMs 2023b, c). Due to the lack of an initial description and the continuous change

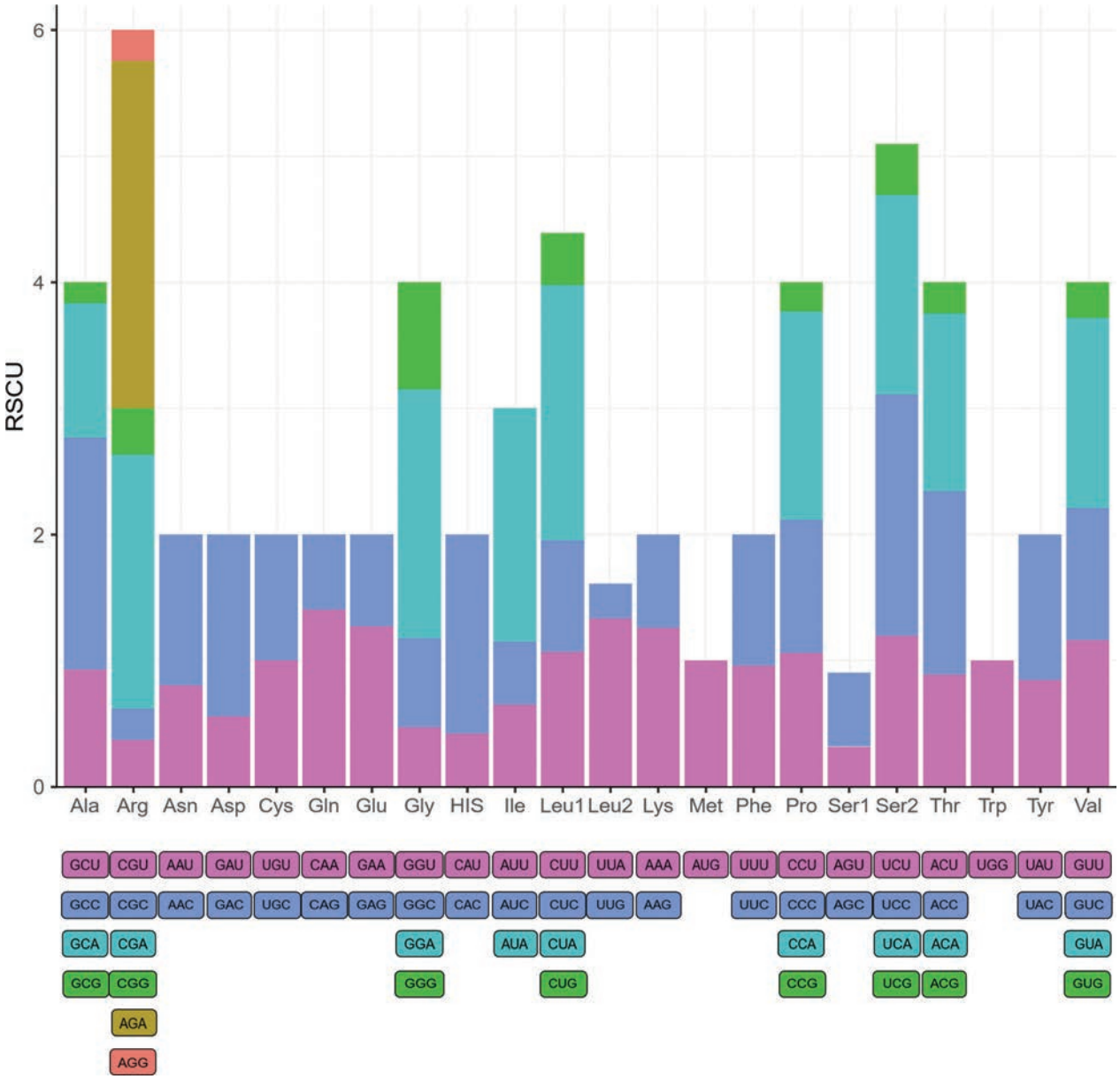

Figure 4. The relative synonymous codon usage (RSCU) in *H. ocellata* mitogenome. Codon families are labeled on the x-axis. The termination codon is not given.

of classification status, subsequent scholars had different opinions and controversies about this sea cucumber species. Some scholars continued to use *H. ocellata* as the name of the species they observed (Semper 1868; Pearson 1913; Heding 1939; Clark 1946; Rowe 1969; Liao 1980; Liao 1997; Teo and Ng 2009; Kamarudin et al. 2010). Conversely, some scholars used *B. ocellata* as the name of the species they found (Kim et al. 2013; Patantis et al. 2019; Javanmardi et al. 2020).

In this study, based on morphological characters and mitochondrial genome sequences, we believe that the two current Latin names, "*Holothuria ocellata*" and "*Bohadschia ocellata*," represent two different species, respectively. Firstly, compared with the descriptions and figures of *B. ocellata* provided by Purcell et al. (2023), these two species have obviously different ossicles and spots: 1) The types of ossicles in *H. ocellata* include buttons and tables, while *B. ocellata* has none of these; 2) Compared to *H. ocellata*, the spots of *B. ocellata* are irregular and differ greatly in size or shape. Finally, after identifying this classification problem between *H. ocellata* and *B. ocellata*, we subsequently selected the mitochondrial sequences of all *Bohadschia* and some *Holothuria* from NCBI and performed two phylogenetic trees based on *rrnL* and *cox1* genes. The result showed a clear separation between the sequences of *H. ocellata* and *B. ocellata*. Furthermore, the phylogenetic tree based on the sequences of 13 PCGs also proved that *H. ocellata* does not belong to the genus *Bohadschia*. For the above reasons, rather than synonyms, it is reasonable to consider *H. ocellata* and *B. ocellata* as two different species.

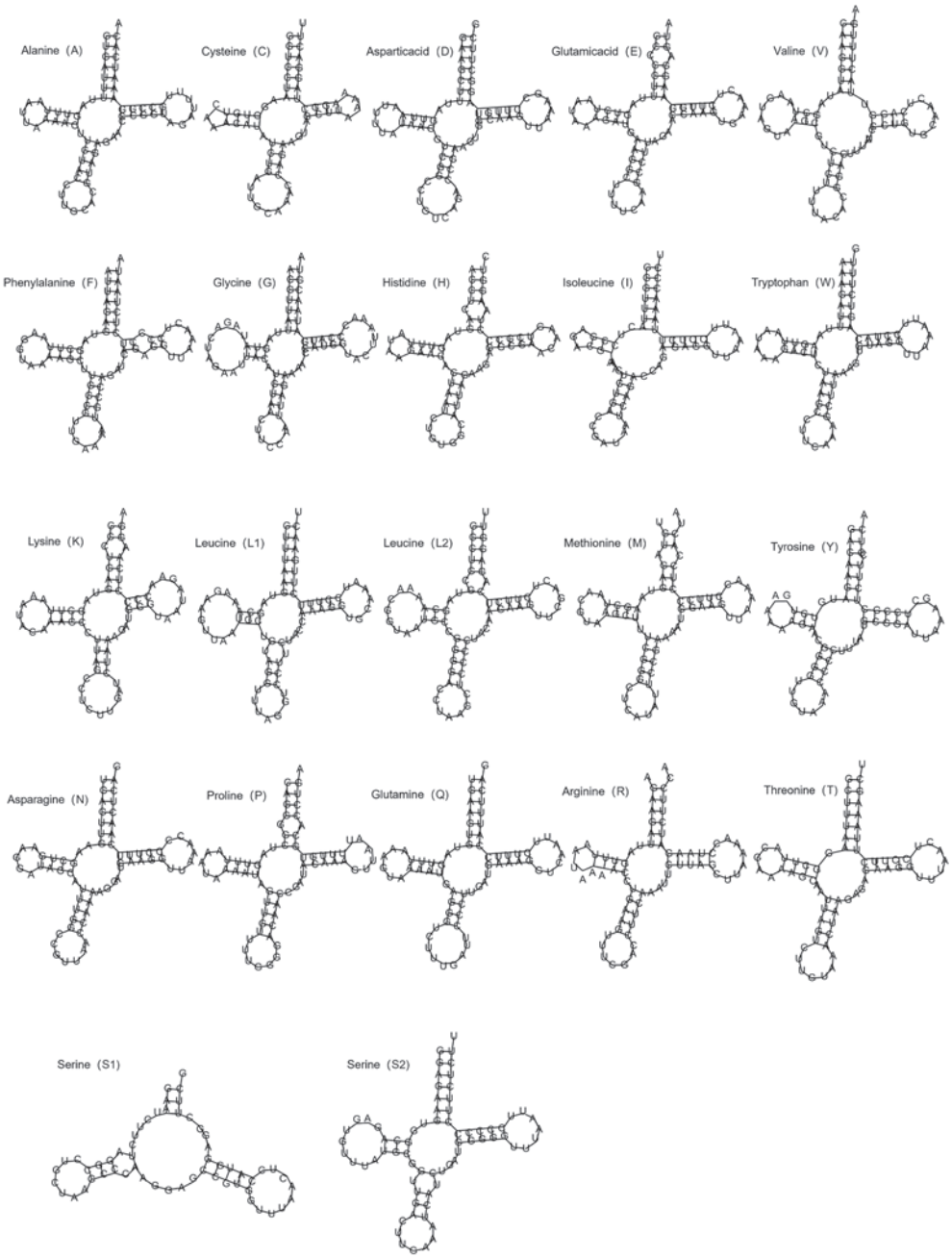

Figure 5. Inferred secondary structures of the 22 tRNA genes of *H. ocellata* mitogenomes.

vs. H. kurti Ludwig, 1891

Due to the similar external morphology between *H. kurti* and a small specimen of *H. ocellata*, some scholars have regarded them as the same species (Liao and Clark 1995; Liao 1997). The sea cucumber *H. kurti* was first found by Sluiter (1889) and initially named "*Holothuria lamperti* Sluiter, 1889" (Ludwig 1891). Because of a naming duplication with "*Holothuria lamperti* Ludwig, 1886," Ludwig (1891) subsequently renamed the sea cucumber species as "*Holothuria kurti* Ludwig, 1891." In 1901, Sluiter described the ossicles of *H. kurti* for the first time and identified a table with cross-shaped chassis (synallactid-type table) as the characteristic of this species. Pearson (1913) compared the ossicles between *H. kurti* and *H. ocellata*, utilizing the differences in the types of tables as the basis for distinguishing the two species. Liao (1980, 1997) suggested that *H. kurti* might be the juvenile of *H. ocellata*, as he observed that the juveniles of *H. ocellata* had a similar synallactid-type table. In the meanwhile, he also found some large synallactid-type tables in the

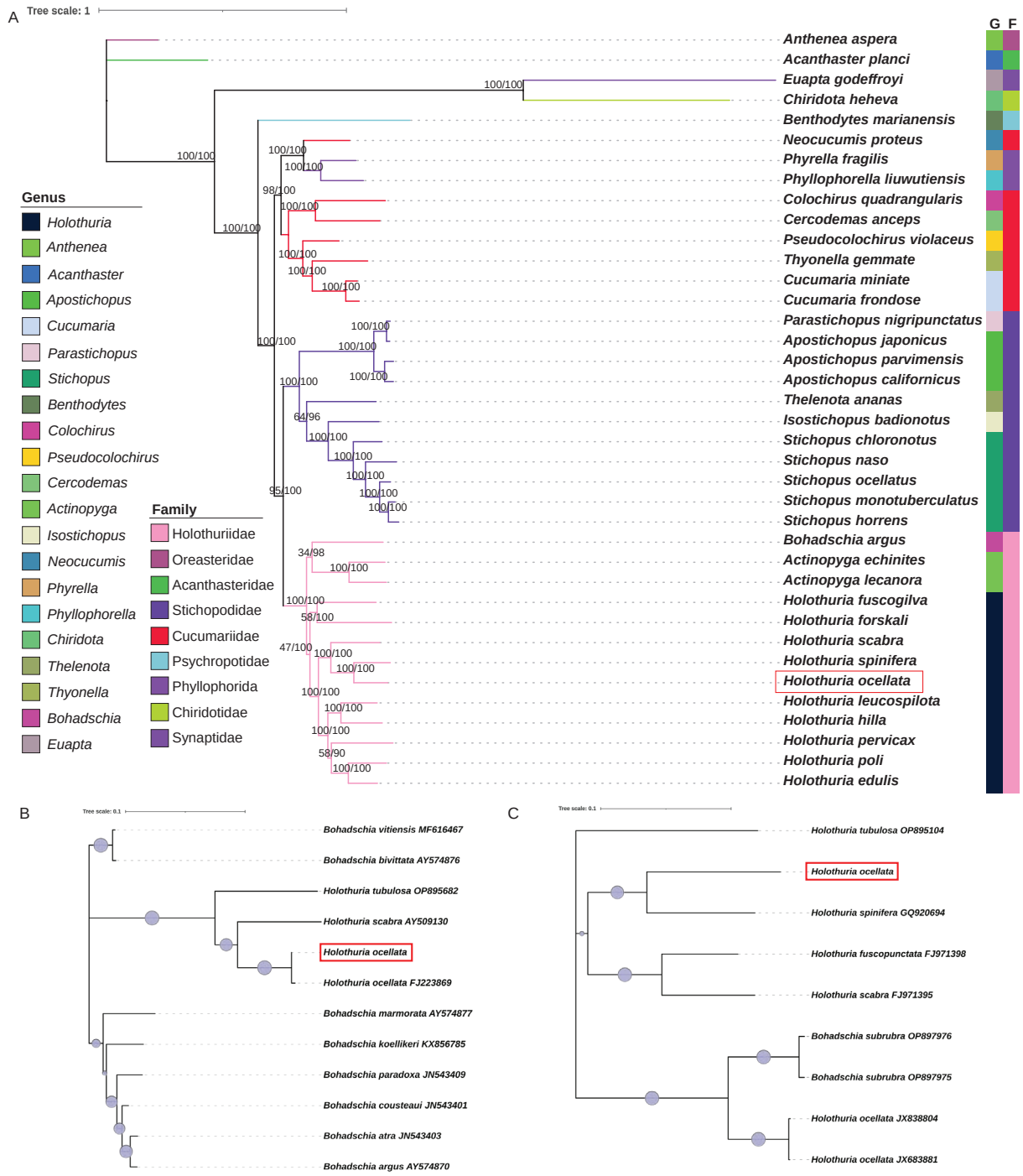

Figure 6. A. Phylogenetic tree of 36 Holothuroidea sequences constructed by Bayesian inference (BI) and maximum likelihood (ML) methods based on concatenated sequences of 13 PCGs. Asteroidea species were used as the outgroup; **B**. Phylogenetic tree of 12 *Holothuria* and *Bohadschia* sequences constructed by Neighbor-Joining (NJ) methods based on concatenated sequences of the *rrnL* gene; **C**. Phylogenetic tree of 9 *Holothuria* and *Bohadschia* sequences constructed by Neighbor-Joining (NJ) methods based on concatenated sequences of the *cox1* gene. The species in the red frame indicates the sequences generated in this study.

adults of *H. ocellata*. In previous studies, some sea cucumber species were also found to have their ossicles of adult individuals that were quite different from juvenile individuals (Gosliner et al. 1990; Massin et al. 2000; Soliman et al. 2019), which seemed to verify the credibility of Liao's conclusion. However, Samyn and Vandenspiegel (2016) disagreed with the conclusion; they collected some specimens of *H. kurti* and found that these samples were over 7 cm long and had mature gonads; they thought that *H. kurti* and *H. ocellata* were two different species. Besides, it is indeed true that scholars did not find tack-like tables in the papillae of *H. kurti*, which were found in the sample we collected in this study (Fig. 2O, P). For the above reasons,

we agree with the view of Samyn and Vandenspiegel (2016). It is reasonable to consider that *H. ocellata* and *H. kurti* are different species. We also hope that more molecular biological data on *H. kurti* will be available in the future to verify and support this conclusion.

***vs. H. hamata* Pearson, 1913**

The samples obtained in this study were similar in external form and ossicle types to the species found by Teo and Ng (2009), which they thought these samples were *H. ocellata*. However, some authors suggested that Teo and Ng's (2009) samples should be *H. hamata* (Aydin et al. 2019; Moazzam and Moazzam 2020). We do not agree with the point of Aydin et al. (2019) because: 1) *H. hamata*, as re-described by Aydin et al. (2019), has lateral papillae ± 20 in number on each side. However, *H. ocellata,* no matter which samples obtained from the current study or those of Teo and Ng (2009), exhibits approximately ± 40 lateral papillae on each side; 2) Tables of the body wall in *H. hamata* mainly have a spiny disc, whereas *H. ocellata* mainly has tables with a disc of smooth or wavy margin (Fig. 2E–H). Besides, Pearson (1913) first described the characteristics of both *H. hamata* and *H. ocellata* simultaneously. According to Pearson's records, *H. ocellata* had the Cuvierian tubules, while *H. hamata* did not. This discrepancy further certifies that these two sea cucumbers are different species.

Discussion on the classification status of Holothuria ocellata based on the mitochondrial genome

The complete mitochondrial genome of *H. ocellata* has a similar A-T content with the other holothuroid mitogenomes analyzed in the previous study (Utzeri et al. 2020; Sun et al. 2021; Li et al. 2022; Ma et al. 2022). The comparison of the gene order showed that *H. ocellata* has the same gene position on mtDNA as that of all other *Holothuria*, suggesting a common ancestral condition and a closer evolutionary relationship. The taxonomic controversy about *H. ocellata* centers on its subgenus: Jaeger (1833) initially thought it belonged to subgenus *Holothuria,* and some authors considered it as subgenus *Metriatyla* Rowe, 1969 (Rowe 1969; Cannon and Silver 1986). Moreover, some scholars have proposed that it should be classified into the subgenus *Theelothuria* based on the further study of ossicles (Liao 1997; Lane et al. 2000). The result of phylogenetic analysis indicated that *H. ocellata* preferentially forms a sister group with *H. spinifera* before clusters with *Holothuria scabra* Jaeger, 1833 (Fig. 6A). Besides, the result of phylogenetic analysis also indicated that *H. ocellata* preferentially forms a sister group with *H. spinifera* before clusters with *Holothuria tubulosa* Gmelin, 1791 (Fig. 6C). That means, compared to *H. scabra* and *H. tubulosa*, the member of subgenus *Metriatyla* and subgenus *Holothuria, H. ocellata* is more closely related to *H. spinifera*, which belongs to subgenus *Theelothuria*. In early studies, some scholars also found that *H. ocellata* is closely related to the species of subgenus *Theelothuria*: Théel (1886) considered *H. ocellata* to be doubtlessly nearly allied to *H. squamifera*; Pearson (1913) also found that *H. ocellata* and *H. spinifera* were exceedingly similar in morphology; and either *H. squamifera* or *H. spinifera*, both sea cucumber species, belong to subgenus *Theelothuria*. Because of that, it is reasonable to believe that *H. ocellata* should be classified within the subgenus *Theelothuria*.

The suggestion of formal Latin names about *H. ocellata*

Due to the lack of original descriptions and the difficulties in retrieving ancient references, identifying whether *B. ocellata* or *H. ocellata* refers to the same species discovered by Jaeger (1833) presents a challenge. Fortunately, Samyn and Vandenspiegel (2016) examined the holotype of *Bohadschia ocellata* Jaeger, 1833, and concluded that this is a valid *Bohadschia* species. In addition, the validity of the classification status of *B. ocellata* was certified by WoRMS. Because of that, we can assume that the species discovered by Jaeger was *Bohadschia ocellata*. Semper (1868) found a sea cucumber species and recorded it as *H. ocellata*, only citing Jaeger's descriptions without further explanation. Théel (1886), the third recorder of *H. ocellata*, not only gave a detailed description but also made hand-drawn pictures of appearance and ossicles. After comparing the description and the hand-drawn images of the species, we found them to be largely consistent with the samples obtained in this study. We speculated that Théel's (1886) record should be considered the actual first discovery of *H. ocellata*. According to the relevant provisions of the International Code of Zoological Nomenclature and considering the current classification of *H. ocellata*, we propose that it should be given a new formal Latin name. However, due to the absence of type specimens found by Théel (1886), it is not appropriate to give this species a new name directly by ourselves. Because of that, the full Latin name of this species should tentatively be "*Holothuria ocellata* Jaeger, 1833 *sensu* Théel 1886," which means "specimens belonging to the species that Théel 1886 called *Holothuria ocellata*" and distinguishes it from "*Bohadschia ocellata* Jaeger, 1833."

Conclusion

In this study, the complete mitochondrial genome of *H. ocellata* was characterized for the first time, and the morphology of this species, including its external form and ossicles, was further described. After careful consideration of the obtained data and comparison with previous references, we clarified the classification history and current status of *H. ocellata*. Finally, we suggest that the

full Latin name of this species should be "*Holothuria ocellata* Jaeger, 1833 *sensu* Théel 1886." The present study demonstrates the significant advantage of coupling ossicle data with molecular data to confirm species identification. Furthermore, the complete mitogenome sequence of *H. ocellata* Jaeger, 1833 *sensu* Théel 1886, will serve as a valuable genomic resource for further studies on holothuroid species. In addition, we recommend the continuation of broader taxonomy studies of holothuroids, employing a combination of "morphology + molecular analysis," to provide valuable information for taxonomy and evolutionary biology studies.

Acknowledgments

We sincerely thank the reviewer and editor for their critique and suggestions. At the same time, we are especially grateful to Dr. Elie Saliba and Dr. Zhengsen Yu for their detailed explanation and advice on the nomenclatural theory. This work was supported by the National Key Research and Development Program of China (2022YFD2401303), the Hainan Provincial Natural Science Foundation of China (321RC1023), and the National Natural Science Foundation of China (42166005; 42076097).

References

Aydin M, Erkan S (2015) Identification and some biological characteristics of commercial sea cucumber in the Turkey coast waters. International Journal of Fisheries and Aquatic Studies 3(1): 260–265. https://api.semanticscholar.org/CorpusID:29850036

Aydin M, Gurlek M, Samyn Y, Erguden D, Turan C (2019) First record of a Lessepsian migrant: the sea cucumber *Holothuria* (*Theelothuria*) *hamata* Pearson, 1913. Zootaxa 4551(1): 94–100. https://doi.org/10.11646/zootaxa.4551.1.7

Cannon L, Silver H (1986) Sea cucumbers of northern Australia. Queensland Museum, Queensland, 60 pp.

Chan P, Lowe T (2019) tRNAscan-SE: Searching for tRNA genes in genomic sequences. Methods in Molecular Biology 1962: 1–14. https://doi.org/10.1007/978-1-4939-9173-0_1

Clark H (1946) The echinoderm fauna of Australia: its composition and its origin. Carnegie Institution, Washington, 429–430.

Clark A, Rowe F (1971) Monograph of shallow-water Indo-West Pacific echinoderms. British Museum Press, Britain, 238 pp.

Dettaï A, Adamowizc S, Allcock L, Arango C, Barnes D, Barratt I, Chenuil A, Couloux A, Cruaud C, David B (2011) DNA barcoding and molecular systematics of the benthic and demersal organisms of the CEAMARC survey. Polar Science 5: 298–312. https://doi.org/10.1016/j.polar.2011.02.002

Dierckxsens N, Mardulyn P, Smits G (2017) NOVOPlasty: De novo assembly of organelle genomes from whole genome data. Nucleic Acids Research 45(4): e18. https://doi.org/10.1093/nar/gkw955

Donath A, Jühling F, Al-Arab M, Bernhart SH, Reinhardt F, Stadler P, Middendorf M, Bernt M (2019) Improved annotation of protein-coding genes boundaries in metazoan mitochondrial genomes. Nucleic Acids Research 47: 10543–10552. https://doi.org/10.1093/nar/gkz833

Gosliner T, Behrens D, Wicksten M (1990) Special resemblance, aposematic coloration and mimicry in opisthobranch gastropods. In Wicksten M (Ed.) Adaptive coloration in invertebrates. Texas A&M University Sea Grant College Program, College Station, 127–138. https://repository.library.noaa.gov/view/noaa/12371

Guille A, Laboute P, Menon J (1986) Handbook of the sea-stars, sea-urchins, and related echinoderms of New-Caledonia Lagoon. Orstom, Paris, 238 pp.

Guindon S, Dufayard J, Lefort V, Anisimova M, Hordijk W, Gascuel O (2010) New algorithms and methods to estimate maximum-likelihood phylogenies: assessing the performance of PhyML 3.0. Systematic biology 59(3): 307–321. https://doi.org/10.1093/sysbio/syq010

Harini R, Natarajan V, Sunil CK (2024) Sea cucumber significance: Drying techniques and India's comprehensive status. Journal of Food Science 89(7): 3995–4018. https://doi.org/10.1111/1750-3841.17153

Heding S (1939) The holothurians of the Iranian Gulf. In: Jessen K, Spärck R (Eds) Danish Scientific Investigations in Iran. Munksgaard, Copenhagen, 113–137. https://lib.ugent.be/catalog/rug01:001652091

Jaeger GF (1833) De Holothuriis. Gessnerianis, Turici, 19 pp.

Javanmardi S, Rezaei Tavabe K, Moradi S, Abed-Elmdoust A (2020) The effects of dietary levels of the sea cucumber (*Bohadschia ocellata* Jaeger, 1833) meal on growth performance, blood biochemical parameters, digestive enzymes activity and body composition of Pacific white shrimp (*Penaeus vannamei* Boone, 1931) juveniles. Iranian Journal of Fisheries Sciences 19: 2366–2383. https://doi.org/10.1016/j.jtcme.2017.06.007

Kalyaanamoorthy S, Minh B, Wong T, Von Haeseler A, Jermiin L (2017) ModelFinder: Fast model selection for accurate phylogenetic estimates. Nature methods 14: 587–589. https://doi.org/10.1038/nmeth.4285

Kamarudin K, Rehan A, Hashim R, Usup G (2010) An update on diversity of sea cucumbers (Echinodermata, Holothuroidea) in Malaysia. Malayan Nature Journal 62(3): 315–334. https://api.semanticscholar.org/CorpusID:55884321

Katoh K, Standley D (2013) MAFFT multiple sequence alignment software version 7: improvements in performance and usability. Molecular biology and evolution 30(4): 772–780. https://doi.org/10.1093/molbev/mst010

Kim S, Kerr A, Paulay G (2013) Colour, confusion, and crossing: resolution of species problems in *Bohadschia* (Echinodermata: Holothuroidea). Zoological Journal of the Linnean Society 168: 81–97. https://doi.org/10.1111/zoj.12026

Lane D, Marsh L, Vandenspiegel D, Rowe F (2000) Echinoderm fauna of the South China Sea: an inventory and analysis of distribution patterns. The Raffles Bulletin of Zoology 8(8): 459–493. https://lkcnhm.nus.edu.sg/wp-content/uploads/sites/10/app/uploads/2017/04/s08rbz459-493.pdf

Li Z, Ma B, Li X, Lv Y, Jiang X, Ren C, Hu C, Luo P (2022) The complete mitochondrial genome of *Stichopus naso* (Aspidochirotida, Stichopodidae, *Stichopus*) and its phylogenetic position. Genes 13(5): 825. https://doi.org/10.3390/genes13050825

Liao Y (1980) The aspidochirote holothurians of China with erection of a new genus. In: Jangoux M (Ed.) Echinoderms: Present and past. Taylor & Francis, London, 115–120. https://doi.org/10.1201/9781003078913

Liao Y (1997) Fauna Sinica: Echinoderma: Holothuroidea. Science Press, Beijing, 99–100, 150–152, 154–156. [in Chinese]

Liao Y, Clark AM (1995) The Echinoderms of Southern China. Science Press, Beijing, 614 pp.

Ludwig H (1891) Die Seewalzen. In: Bronn H (Ed.) Klassen und Ordnungen des Thierreichs. Smithsonian Libraries, Washington, 329–330. https://www.biodiversitylibrary.org/item/44497

Ma B, Li Z, Lv Y, E Z, Fang J, Ren C, Luo P, Hu C (2022) Analysis of complete mitochondrial genome of *Bohadschia argus* (Jaeger, 1833) (Aspidochirotida, Holothuriidae). Animals 12(11): 1437. https://doi.org/10.3390/ani12111437

Martin M (2011) Cutadapt removes adapter sequences from high-throughput sequencing reads. EMBnet Journal 17: 10–12. https://doi.org/10.14806/ej.17.1.200

Massin C, Mercier A, Hamel J (2000) Ossicle change in *Holothuria scabra* with a discussion of ossicle evolution within the Holothuriidae (Echinodermata). Acta Zoologica 81: 77–91. https://doi.org/10.1046/j.1463-6395.2000.00039.x

Minh B, Nguyen M, Von Haeseler A (2013) Ultrafast approximation for phylogenetic bootstrap. Molecular biology and evolution 30: 1188–1195. https://doi.org/10.1093/molbev/mst024

Moazzam M, Moazzam N (2020) Annotated checklist of sea cucumbers from Pakistan with new records of *Holothuria* (*Theelothuria*) *hamata* (Pearson, 1913) and *Stichopus herrmanni* (Semper, 1868). In: Eeckhaut I (Ed.) SPC Beche-de-mer Information Bulletin 40. Secretariat of the Pacific Community, Noumea, 32–39. https://coastfish.spc.int/en/publications/bulletins/beche-de-mer/512

Nguyen L, Schmidt H, Von Haeseler A, Minh B (2015) IQ-TREE: A fast and effective stochastic algorithm for estimating maximum-likelihood phylogenies. Molecular biology and evolution 32(1): 268–274. https://doi.org/10.1093/molbev/msu300

Patantis G, Dewi A, Fawzya Y, Nursid M (2019) Identification of Beche-de-mers from Indonesia by molecular approach. Biodiversitas Journal of Biological Diversity 20: 537–543. https://doi.org/10.13057/biodiv/d200233

Pearson J (1913) Notes on the Holothurioidea of the Indian Ocean. The genus *Holothuria*. Spolia Zeylanica 9: 49–190. https://doi.org/10.5962/bhl.part.7317

Perna N, Kocher T (1995) Patterns of nucleotide composition at fourfold degenerate sites of animal mitochondrial genomes. Journal of molecular evolution 41(3): 353–358. https://doi.org/10.1007/BF01215182

Purcell S, Samyn Y, Conand C (2012) Commercially important sea cucumbers of the world; FAO, Rome, 28–29.

Purcell S, Lovatelli A, González-Wangüemert M, Solís-Marín F, Samyn Y, Conand C (2023) Commercially important sea cucumbers of the world. FAO, Rome, 42–43.

Ranwez V, Douzery E, Cambon C, Chantret N, Delsuc F (2018) MACSE v2: Toolkit for the alignment of coding sequences accounting for frameshifts and stop codons. Molecular biology and evolution 35(10): 2582–2584. https://doi.org/10.1093/molbev/msy159

Reich M (2017) First report of sea cucumbers (Echinodermata, Holothuroidea) from the latest Cretaceous of Bavaria, Germany. Zitteliana 89: 285–289.

Ronquist F, Teslenko M, Van Der Mark P, Ayres D, Darling A, Höhna S, Larget B, Liu L, Suchard M, Huelsenbeck J (2012) MrBayes 3.2: Efficient Bayesian phylogenetic inference and model choice across a large model space. Systematic biology 61(3): 539–542. https://doi.org/10.1093/sysbio/sys029

Rowe F (1969) A review of the family Holothuriidae (Holothuroidea: Aspidochirotida). Bulletin of the British Museum of Natural History, Zoology 18(4): 119–170. https://doi.org/10.5962/bhl.part.18419

Samyn Y, Vandenspiegel D (2016) Sublittoral and bathyal sea cucumbers (Echinodermata, Holothuroidea) from the Northern Mozambique Channel with description of six new species. Zootaxa 4196(4): 451–497. https://doi.org/10.11646/zootaxa.4196.4.1

Slater M, Chen J (2015) Sea cucumber biology and ecology. In: Brown N, Eddy S (Eds) Echinoderm Aquaculture. John Wiley & Sons, Inc., Hoboken, 47–55. https://doi.org/10.1002/9781119005810.ch3

Sluiter CP (1901) Die Holothurien der Siboga Expedition. Sboga Exped. 44: 1–142. https://doi.org/10.5962/bhl.title.85348

Soliman T, Reimer J, Kawamura I, Van Der Meij S, Reijnen B, Paulay G (2019) Description of the juvenile form of the sea cucumber *Thelenota anax* H.L. Clark, 1921. Marine Biodiversity 49: 547–554. https://doi.org/10.1007/s12526-017-0820-2

Stothard P, Grant J, Van Domselaar G (2019) Visualizing and comparing circular genomes using the CGView family of tools. Briefings in Bioinformatics 20(4): 1576–1582. https://doi.org/10.1093/bib/bbx081

Sun S, Sha Z, Xiao N (2021) The first two complete mitogenomes of the order Apodida from deep-sea chemoautotrophic environments: New insights into the gene rearrangement, origin and evolution of the deep-sea sea cucumbers. Comparative Biochemistry and Physiology D: Genomics and Proteomics 39: 100839. https://doi.org/10.1016/j.cbd.2021.100839

Talavera G, Castresana J (2007) Improvement of phylogenies after removing divergent and ambiguously aligned blocks from protein sequence alignments. Systematic biology 56(4): 564–577. https://doi.org/10.1080/10635150701472164

Tamura K, Peterson D, Peterson N, Stecher G, Nei M, Kumar S (2011) MEGA5: Molecular evolutionary genetics analysis using maximum likelihood, evolutionary distance, and maximum parsimony methods. Molecular biology and evolution 28(10): 2731–2739. https://doi.org/10.1093/molbev/msr121

Teo S, Ng C (2009) New record of a sea cucumber, *Holothuria ocellata* (Jaeger, 1833) (Holothuroidea, Aspidochirotida, Holothuriidae) in Singapore. Nature in Singapore 2: 411–414.

Théel H (1886) Holothuroidea. Part 2. Report of the Scientific Results of the Voyage of the "Challenger". Zoology 14(38–39): 178–179. https://www.biodiversitylibrary.org/item/194597

Uthicke S, Purcell S, Blockmans B (2005) Natural hybridization does not dissolve species boundaries in commercially important sea cucumbers. Biological Journal of the Linnean Society 85: 261–270. https://doi.org/10.1111/j.1095-8312.2005.00489.x

Utzeri V, Ribani A, Bovo S, Taurisano V, Calassanzio M, Baldo D, Fontanesi L (2020) Microscopic ossicle analyses and the complete mitochondrial genome sequence of *Holothuria* (*Roweothuria*) *polii* (Echinodermata, Holothuroidea) provide new information to support the phylogenetic positioning of this sea cucumber species. Marine genomics 51: 100735. https://doi.org/10.1016/j.margen.2019.100735

Valente S, Serrão E, González-Wangüemert M (2015) West versus East Mediterranean Sea: origin and genetic differentiation of the sea cucumber *Holothuria polii*. Marine Ecology 36: 485–495. https://doi.org/10.1111/maec.12156

WoRMS (2023a) Holothuriidae Burmeister, 1837. https://www.marinespecies.org/aphia.php?p=taxdetails&id=731943

WoRMS (2023b) *Holothuria* Linnaeus, 1767. https://www.marinespecies.org/aphia.php?p=taxdetails&id=123456

WoRMS (2023c) *Bohadschia* Jaeger, 1833. https://www.marinespecies.org/aphia.php?p=taxdetails&id=204900

Xiang C, Gao F, Ivan J, Lei H, Hu Y, Zhang H, Zou H, Wang G, Zhang D (2023) Using PhyloSuite for molecular phylogeny and tree-based analyses. iMeta 13: e87. https://doi.org/10.1002/imt2.87

Yoshida W, Ishida S, Ono K, Izumi S, Hasegawa K (2012) Developmental styles and larval morphology of hybridized sea cucumbers (Echinodermata, Holothuroidea). Invertebrate reproduction and development 56: 249–259. https://doi.org/10.1080/07924259.2011.601140

Zhang D, Gao F, Jakovlić I, Zou H, Zhang J, Li W, Wang G (2020) PhyloSuite: An integrated and scalable desktop platform for streamlined molecular sequence data management and evolutionary phylogenetics studies. Molecular Ecology Resources 20: 348–355. https://doi.org/10.1111/1755-0998.13096

Supplementary material 1

Additional information

Authors: Chenghao Jia, Zening Xu, Fengping Li, Liuna Chen, Aimin Wang, Fei Gao

Data type: tif

Link: https://doi.org/10.3897/zse.101.137781.suppl1

Zoosyst. Evol. 101 (2) 2025, 805–812 | DOI 10.3897/zse.101.151802

PENSOFT

MUSEUM FÜR NATURKUNDE BERLIN

A new genus and species of freshwater mussel from the Pearl River Basin in Guangxi, China (Bivalvia, Unionidae, Gonideinae)

Yu-Ting Dai[1*], Zhong-Guang Chen[1*], Fan Li[2], Xiao-Chen Huang[1], Shan Ouyang[1], Xiao-Ping Wu[1]

1 *School of Life Sciences, Nanchang University, Nanchang 330031, China*

2 *Laboratory of Ecological Security and Biodiversity Conservation of Cities on the Yangtze River Delta, Shanghai Natural History Museum, Branch of Shanghai Science and Technology Museum, Jingan, Shanghai 200000, China*

https://zoobank.org/25394CCD-7B64-4BBF-A4CA-76D28B9B7391

Corresponding authors: Fan Li (lfaqua@gmail.com); Xiao-Ping Wu (xpwu@ncu.edu.cn)

Academic editor: M. Glaubrecht ♦ **Received** 2 March 2025 ♦ **Accepted** 27 March 2025 ♦ **Published** 17 April 2025

Abstract

A new genus and species of freshwater mussels, *Guiunio rarus* Chen, Li, Dai & Wu, **gen. et sp. nov.**, is described from the Pearl River Basin in China based on comparative morphology and molecular phylogeny. The new taxon belongs to the tribe Gonideini and can be distinguished from other genera by a unique combination of characteristics: shell medium-sized, moderately thick, flat, long, sub-glossy, opaque; anterior small, rounded and short; posterior extremely expanded, wide and long, with an indistinct obtuse angle in the middle of posterior margin; papillae on flap margin highly degraded. The validity of it is further supported by the molecular phylogenetic analysis based on *COI, 16S* and *28S* sequences.

Key Words

Biodiversity, molluscs, phylogeny, taxonomy

Introduction

Freshwater mussel is a group of large benthic animal that play an important role in freshwater ecosystems (Graf and Cummings 2007; Huang et al. 2019; Liu et al. 2022). China is a diversity hotspot of freshwater mussels, with about 100 accepted species recorded and new taxa continuing to be discovered (Heude 1875, 1877a, 1877b, 1878, 1879, 1880a, 1880b, 1881, 1883, 1885; Simpson 1900; He and Zhuang 2013; Graf and Cummings 2021, 2025; Guo 2022; Liu et al. 2022, 2023, 2024; Wu et al. 2021, 2022, 2024; Chen et al. 2023; Dai et al. 2023, 2024a, 2024b, 2024c, 2024d; MolluscaBase eds. 2025). The majority of studies on Chinese freshwater mussels are concentrated in the Changjiang River Basin (Yangtze) (Heude 1875, 1877a, 1877b, 1878, 1879, 1880a, 1880b, 1881, 1883, 1885; Zeng et al. 1981, 1985; Zeng and Liu 1989; Liu and Wu 1991; Wu et al. 1994, 1999, 2000, 2017, 2018, 2021, 2022; Shu and Wu 2004; Ouyang et al. 2011; Xiong et al. 2011, 2012; Xiao et al. 2012; Chen et al. 2023; Dai et al. 2024a, 2024d), with very few focusing on the Pearl River Basin (Dai et al. 2023, 2024b, 2024c; Liu et al. 2023, 2024; Wu et al. 2024). The Pearl River is the southernmost large river in China, located between the Changjiang River and the Red River. The recurrence of connectivity events throughout the history of the region has resulted in the fish community of the Pearl River Basin exhibited by both the local and the Changjiang River Basin's characteristics (Huang et al. 2017; Sun et al. 2022). However, the freshwater mussel community here remains a subject of limited knowledge due to the absence of systematic studies. Some sporadic studies have revealed the unique composition of freshwater mussels and several as yet undescribed species in the region (Dai

* These authors contributed equally to this work.

et al. 2023, 2024b, 2024c; Liu et al. 2023, 2024; Hou et al. 2025). There are substantial regions here that have not yet been the subject of exploration and research.

Subfamily Gonideinae Ortmann, 1916, encompasses small to large freshwater mussels from East Europe, West Asia, East Asia, Southeast Asia, and North America (Graf and Cummings 2025; MolluscaBase eds. 2025). The shell morphology of the subfamily exhibits significant phenotypic plasticity and convergence, making it difficult to classify based solely on morphology reliably (Zieritz and Aldride 2009; Inoue et al. 2013). China represents a diversity hotspot of the subfamily, harboring about 10 genera and 30 accepted species (Graf and Cummings 2025; MolluscaBase eds. 2025), and new taxa being discovered continuously (Wu et al. 2021; Dai et al. 2023, 2024a).

During the surveys in 2024, we discovered a group of freshwater mussel specimens with the special expanded posterior that did not resemble any known species and were challenging to place in any genus. Based on a combination of morphology and molecular phylogeny, we describe it as a new genus and species of subfamily Gonideinae. The discovery improved the diversity of freshwater mussels in the Pearl River Basin, leading to a more comprehensive understanding of the endemic species in the region.

Materials and methods

Specimens were collected from Guaangxi in China in 2024. Living specimens were initially frozen at -20 °C for 24 hours and subsequently thawed at room temperature for 2 hours to facilitate the extraction of soft parts. The soft parts were then fixed in 70% ethanol. Empty shells were cleaned, dried, and preserved at room temperature. Photographs were taken by camera and edited with Adobe Photoshop CC 2015 (Adobe, San Jose, US). Maps were made in ArcGIS Pro (Esri, Redlands, US).

Genomic DNA was extracted from foot tissues preserved in 70% ethanol using a TIANamp Marine Animals DNA Kit (Tiangen Biotech, China). The quality and concentration of the DNA were checked on 1% agarose gel electrophoresis and NanoDrop 2000 (Thermo Scientific, USA). Partial cytochrome c oxidase subunit 1 (*COI*), 16S ribosomal RNA (*16S*) and 28S ribosomal RNA (*28S*) were amplified and sequenced for molecular phylogenetic analyses. Polymerase chain reaction (PCR) systems, conditions and primer pairs were followed Dai et al. (2024a). The *COI* sequences were aligned using MEGA v. 6.0 (Tamura et al. 2013), and the *16S* and *28S* sequences were aligned using MAFFT v. 7 (Katoh et al. 2019) by the Q-INS-i algorithm. The accession numbers of other species and newly obtained sequences are given in Table 1.

Phylogenies reconstructed by the dataset combined three genes using Maximum Likelihood (ML) and Bayesian Inference (BI). Five species of Unioninae Rafinesque, 1820 and Margaritiferidae Henderson, 1929 were used as the outgroups for rooting the trees. The best-fit model for each gene and gene partition was calculated by PartitionFinder2 v. 1.1 (Lanfear et al. 2017), based on the corrected Akaike Information Criterion (AICc) and using a heuristic search algorithm. The program proposed the division of the concatenated dataset into three partitions, comprising partitions for the *16S* and *28S* genes and each of the three codon positions of the *COI* gene. The best-fit model was determined to be GTR+I+G for the first and second codon positions of *COI*, as well as for *16S* and *28S*, while GTR+G was selected for the third position of *COI*. ML analyses were performed in IQ-TREE v. 1.6.12 (Minh et al. 2013) using the Ultrafast bootstrap approach (Minh, et al. 2013) with 10,000 iterations. Bayesian inference (BI) analysis was conducted in MrBayes v. 3.2.6 (Ronquist et al. 2012). Four simultaneous runs with four independent Markov Chain Monte Carlo (MCMC) were implemented for 10 million generations, and trees were sampled every 10,000 generations with a burn-in of 25%. The convergence was checked with the average standard deviation of split frequencies <0.01 and the potential scale reduction factor (PSRF) ~ 1. Trees were visualized in FigTree v.1.4.3 (http://tree.bio.ed.ac.uk/software/figtree/).

Abbreviations: NCU_XPWU: Laboratory of Xiao-Ping Wu, Nanchang University (Nanchang, Jiangxi, China); aam: anterior adductor muscle; pam: posterior adductor muscle; ea: excurrent aperture; ia: incurrent aperture; pia: papillae of the incurrent aperture; pea: papillae of the excurrent aperture; ig: inner gills; og: outer gills; m: mantle; lp: labial palps; vm: visceral mass; f: foot.

Results

Phylogenetic analyses

The sequence dataset consisting of 55 *COI*, 55 *16S* and 55 *28S* sequences from 50 species, including with five outgroup taxa, was employed for phylogenetic analyses (Table 1). The alignments of *COI, 16S* and *28S* genes had a length of 606, 516 and 457 characters, respectively. Within these alignments, 258, 235 and 168 sites were variable, and 238, 198 and 154 sites were parsimony informative. The Bayesian and Maximum Likelihood analyses produced same phylogenies (Fig. 1). The new species was sistered with genus *Cosmopseudodon* Haas, 1920 with relatively well support rate (BS/PP = 70/0.92).

Systematics

Family Unionidae Rafinesque, 1820
Subfamily Gonideinae Ortmann, 1916
Tribe Gonideini Ortmann, 1916

Genus *Guiunio* Dai, Chen, Li & Wu, gen. nov.
https://zoobank.org/8C80C6EF-3A7F-4568-8F8A-DC55228FE620

Type species. *Guiunio rarus* Chen, Li, Dai & Wu, sp. nov.

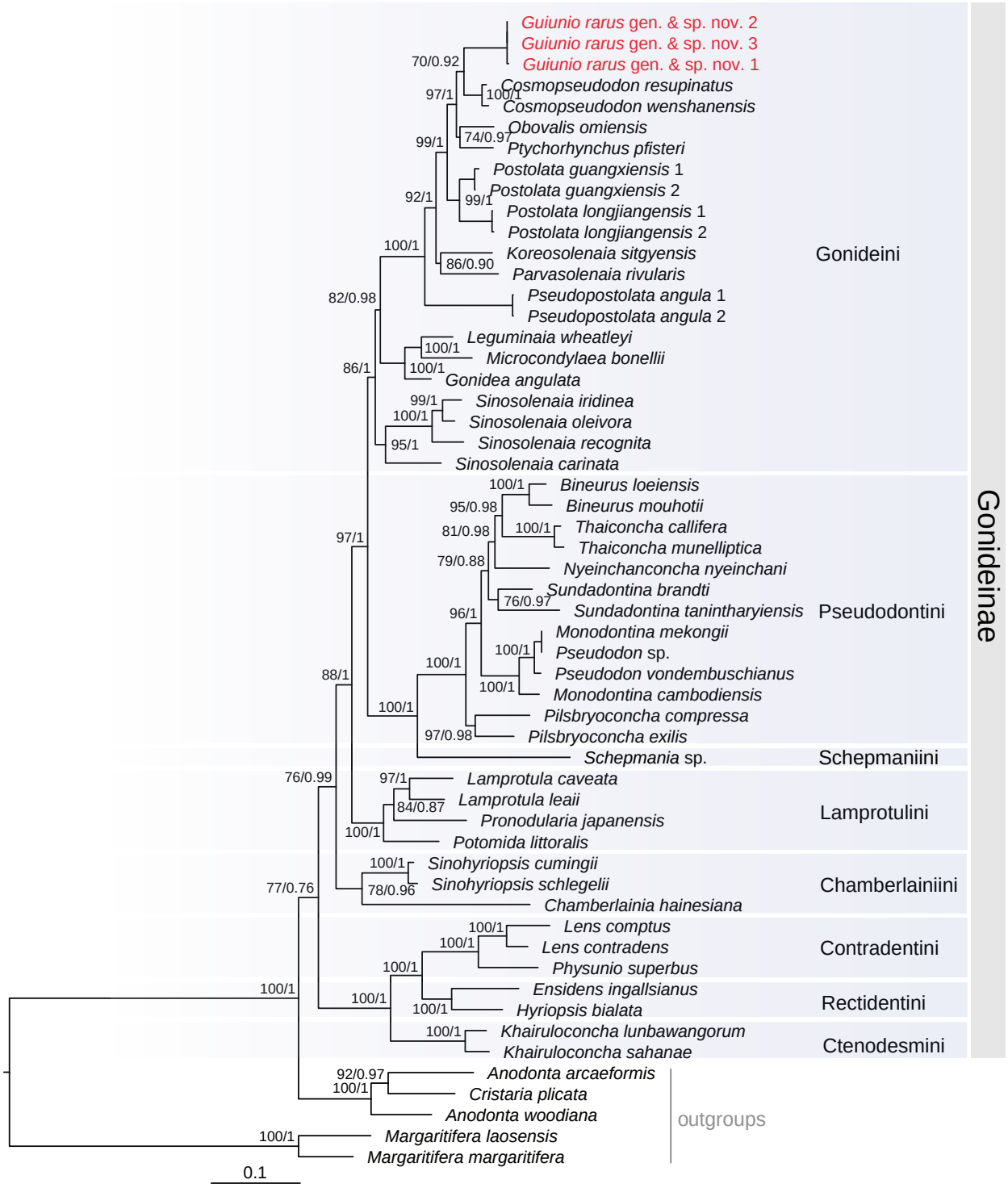

Figure 1. Maximum Likelihood tree and Bayesian inference tree inferred from *COI, 16S* and *28S* genes sequences. Bootstrap supports/posterior probabilities are shown on the left/right of nodes on the tree if greater than 50%.

Diagnosis. Shell medium-sized, moderately thick, flat, long, sub-glossy, opaque. Anterior small, rounded and short; posterior extremely expanded, wide and long, with an indistinct obtuse angle in the middle of posterior margin. Umbo inflated, slightly higher at the hinge line, located at 1/4 of the dorsal margin, with concentric square carving. Periostracum yellowish green to brown with thin growth lines. Papillae on flap margin highly degraded.

Description. Shell medium-sized, moderately thick, flat, long, sub-glossy, opaque. Anterior small, rounded and short; posterior extremely expanded, wide and long, with an indistinct obtuse angle in the middle of posterior margin. Dorsal margin slightly curved downwards and truncated in behind; ventral margin weakly curved or retuse. Umbo inflated, slightly higher the hinge line, located at 1/4 of the dorsal margin, with concentric square carving. Periostracum

Table 1. Genbank accession numbers of sequences used in this paper.

Species	*COI*	*16S*	*28S*
UNIONIDAE Rafinesque, 1820			
Gonodeinae Ortmann, 1916			
Gonideini Ortmann, 1916			
Guiunio rarus gen. et sp. nov.	PV368601	PV368859	PV368862
Guiunio rarus gen. et sp. nov.	PV368602	PV368860	PV368863
Guiunio rarus gen. et sp. nov.	PV368603	PV368861	PV368864
Obovalis omiensis	MT020684	LC223994	MT020830
Obovalis omiensis	LC518995	LC223994	MT020830
Obovalis omiensis	LC518996	LC223995	LC519064
Obovalis omiensis	LC518997	LC519045	LC519065
Ptychorhynchus pfisteri	MG463036	KY067440	MG595564
Ptychorhynchus pfisteri	MG463034	KY067440	MG595563
Ptychorhynchus pfisteri	MG463035	KY067440	MG595562
Parvasolenaia rivularis	MG463100	KX966393	MG595626
Sinosolenaia carinata	MG463087	NC_023250	MG595616
Sinosolenaia oleivora	MG463090	NC_022701	MG595617
Sinosolenaia iridinea	MG463091	MT477834	MG595618
Sinosolenaia recognita	MG463092	KY561653	MG595619
Leguminaia wheatleyi	MN402614	MN396725	MN396721
Microcondylaea bonellii	KX822652	KT966473	KX822609
Gonidea angulata	MN402615	MN396726	MN396722
Koreosolenaia sitgyensis	MT020682	GQ451859	MT020817
Postolata guangxiensis	OP009379	OP020466	OP020470
Postolata guangxiensis	OP009380	OP020467	OP020470
Postolata guangxiensis	OP009381	OP020468	OP020470
Postolata guangxiensis	OP009382	OP020469	OP020471
Postolata guangxiensis	OP009383	OP020467	OP020472
Postolata guangxiensis	OP009384	OP020468	OP020470
Postolata guangxiensis	OP009385	OP020469	OP020471
*Postolata longjiangensis**	PP786557	PP786405	PP786407
*Postolata longjiangensis**	PP786557	PP786406	PP786407
*Postolata longjiangensis**	PP786558	PP786405	PP786407
*Postolata longjiangensis**	PP786558	PP786406	PP786407
Pseudopostolata angula	PQ189757	PQ201945	PQ201943
Pseudopostolata angula	PQ189757	PQ201945	PQ201944
Cosmopseudodon resupinatus	PP079436	PP079964	PP080006
Cosmopseudodon wenshanensis	PP079444	PP079972	PP080014
Pseudodontni Frierson, 1927			
Pseudodon mekongi	KX865861	KX865632	KX865733
Pseudodon vondembuschianus	KP795029	KP795052	MZ684028
Pseudodon cambodjensis	KP795028	NC_044112	KP795011
Bineurus loeiensis	KX865879	KX865650	KX865750
Bineurus mouhotii	KX865876	KX865647	KX865747
Sundadontina tanintharyiensis	MN275057	MN307248	MN307189
Sundadontina brandti	MN275058	MN307249	MN307190
Pilsbryoconcha exilis	KP795024	NC_044124	KP795007
Pilsbryoconcha compressa	KX865875	KX865646	KX865746
Thaiconcha callifera	KX865862	KX865633	KX865734
Thaiconcha munelliptica	MN275063	MN307252	MN307193
Nyeinchanconcha nyeinchani	KP795025	KP795050	KP795008
Lamprotulini Modell, 1942			
Lamprotula caveata	MG462991	NC_030336	MG595518
Lamprotula leaii	MN402616	MN396727	MN396723
Potomida littoralis	MN402617	MN396728	MN396724
Pronodularia japanensis	KX822659	AB055625	KX822615
Chamberlainiini Bogan, Froufe & Lopes-Lima in Lopes-Lima et al., 2017			
Sinohyriopsis schlegelii	MT020706	EF507846	MT020836
Sinohyriopsis cumingii	MG463086	NC011763	MG595613
Chamberlainia hainesiana	KX822635	NC_044110	KX822592
Rectidentini Modell, 1942			
Hyriopsis bialata	KX051274	MT993644	MT993697
Ensidens ingallsianus	MT993541	MT993687	MT993739
Contradentini Modell, 1942			
Lens contradens	MG581991	MT993693	MT993745
Lens comptus	KX865928	KX865682	KX865799
Physunio superbus	MG582020	MT993689	MT993741
Schepmaniini Lopes-Lima, Pfeiffer & Zieritz, 2021			
Schepmania sp.	MZ678755	MZ684082	MZ684035
Ctenodesmini Pfeiffer, Zieritz, Rahim & Lopes-Lima, 2021			
Khairuloconcha lunbawangorum	MN900790	MZ684078	MN902294
Khairuloconcha sahanae	MZ678752	MZ684079	MZ684024
Unioninae Rafinesque, 1820			
Anemina arcaeformis	NC_026674	NC_026674	MG595457
Cristaria plicata	NC_012716	NC_012716	MG595484
Sinanodonta woodiana	HQ283346	HQ283346	MG595604
MARGARITIFERIDAE Henderson, 1929			
Gibbosula laosensis	JX497731	KC845943	KT343741
Margaritifera margaritifera	KX550089	KX550091	KX550093

yellowish green to brown with thin growth lines. Posterior slope with an indistinct low secondary posterior ridge end in the angle on the posterior margin. Growth lines arranged in irregular concentric circles. Hinge long. Ligament short and strong. Beak cavities shallow, open. Mantle attachment scars on the pallial line obvious. Anterior adductor muscle scars irregularly oval, deep, smooth; posterior adductor muscle scars long oval, smooth. Left valve with two pseudocardinal teeth, posterior tooth elevated pyramidal or degenerated; anterior tooth thick and pyramidal. Right valve also with one pseudocardinal tooth, low triangular. Lateral teeth of both valves long and thin. Nacre light orange to white.

Mantle light brown, aperture margins black, papillae on flap margin highly degraded. Gills light brown, inner gills slightly longer and wider than outer gills. Labial palps-rown, distally pointed and irregularly fan-shaped in appearance. Visceral mass grayish white, foot light orange.

Etymology. The species is made from the *Gui* for the abbreviation for Guangxi and *unio* for the unionid type genus.

Vernacular name. 桂蚌属 (gùi bàng shǔ).

Guiunio rarus Chen, Li, Dai & Wu, sp. nov.

https://zoobank.org/EE9A0840-BD0E-4568-9951-939B8E6D0DDF

Fig. 2

Type material. ***Holotype*** • 25_NCU_XPWU_GR001, Zhongduhe River [中渡河], Luzhai County [鹿寨县], Liuzhou City [柳州市], Guangxi Zhuang Autonomous Region [广西壮族自治区], China, 24.60754°N, 109.80318°E, leg. Fan Li, January 2024.

Paratypes • n = 2, 25_NCU_XPWU_GR002–003, other information same as holotype.

Diagnosis. Same as the genus.

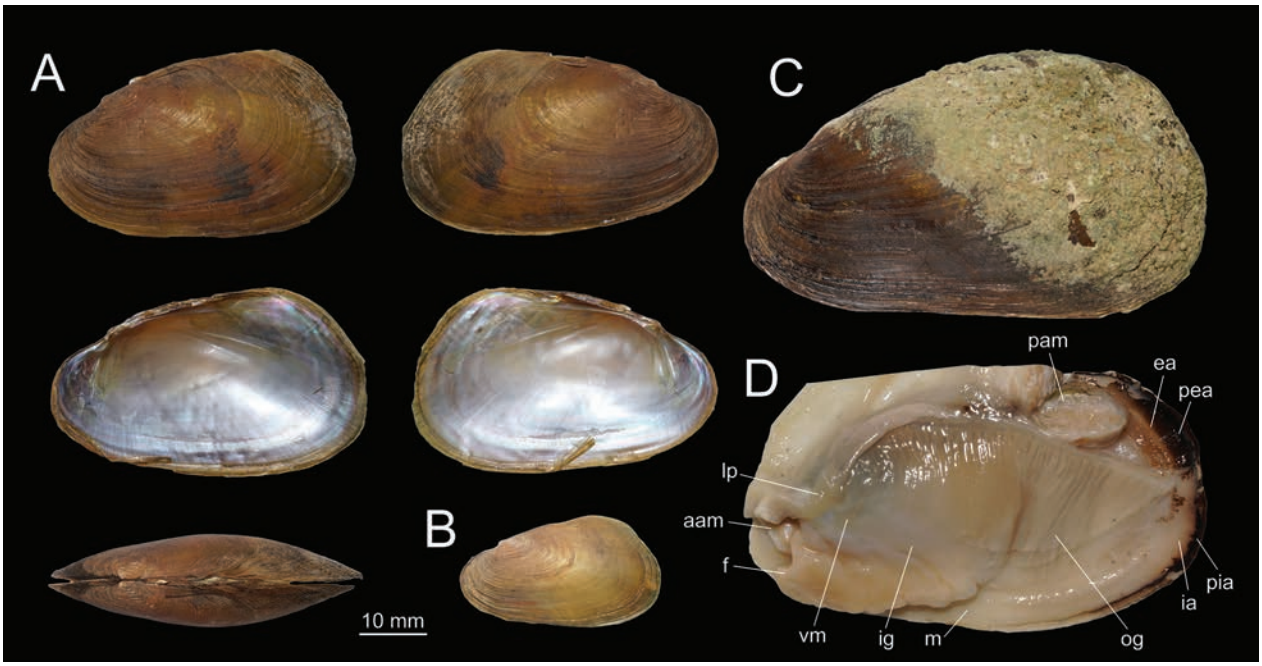

Figure 2. *Guiunio rarus* gen. et sp. nov. **A.** Holotype; **B, C.** Paratypes; **D.** Soft anatomy.

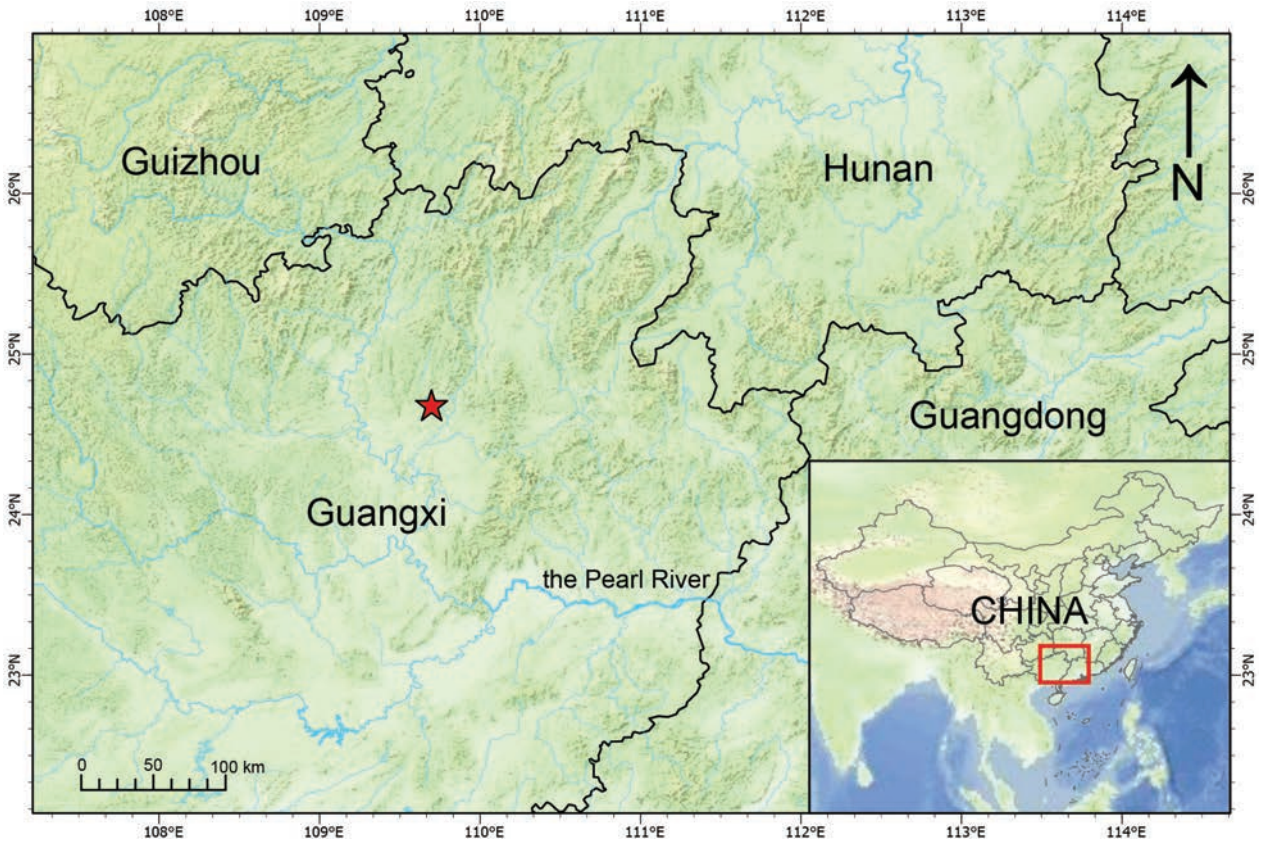

Figure 3. Distribution of *Guiunio rarus* gen. et sp. nov.

Description. Same as the genus.

Measurements. Holotype: shell length 50.0 mm, height 29.4 mm, width 14.2 mm. Paratypes: shell length 32.2–72.3 mm, height 18.1–42.2 mm, width 7.8–26.2 mm.

Etymology. The species is named after Latin *rarus* for rare, referring to the rarity of it.

Vernacular name. 稀有桂蚌 (xī yǒu gùi bàng).

Distribution and ecology. Known from the type locality only (Fig. 3). Living in the slow flowing stream with muddy and sandy bottom alongside *Cristaria plicata* (Leach, 1814), *Nodularia douglasiae* (Gray, 1833) and *Lanceolaria gladiola* (Heude, 1877). In addition, the new

species was associated with a yet-to-be-described species of *Rhodeus* Agassiz, 1832, which may be laying eggs in the gills of it (all type specimens of the new species were collected during the dry season in winter, so no fish eggs were observed in the gills). It is an occasional species in the type locality, accounting for less than 1/20 of the population of all freshwater mussels.

Discussion

Despite the fact that only three type specimens were collected after an extended period of collection, molecular phylogeny and morphological comparison offer robust support for its independence. Molecular phylogenetic results supported placing the new genus in tribe Gonideini Ortmann, 1916. Within the tribe, the new genus is only similar to *Parvasolenaia* Huang & Wu, 2019 by having an extremely expanded posterior, but differs by the thicker, opaque and sub-glossy shell (vs. thinner, semi-transparent and glossy shell), and the highly degraded papillae on flap margin (vs. with developed papillae on flap margin). The new genus was sistered with *Cosmopseudodon* in the phylogenetic tree, but differs by the extremely expanded posterior (vs. narrowed), the absence of an incision at the posterior (vs. presence) and the highly degraded papillae on flap margin (vs. with distinct papillae on flap margin). Within the subfamily, the new genus was similar to *Trapezoideus* Simpson, 1900, *Yaukthwa* Bolotov, Konopleva, Vikhrev, Lopes-Lima, Bogan, Lunn, Chan, Win, Aksenova, Gofarov, Tomilova & Kondakov, 2019, and *Lens* Simpson, 1900 of tribe Contradentini Modell, 1942 by the similar shell shape, but differs by the oblique dorsal margin without developed wing, the more blunt posterior margin and the different distribution (southern China vs. Indochina). The convergent evolution of shell morphology among different groups in Unionida is a common phenomenon (Huang et al. 2018; Wu et al. 2020, 2022; Dai et al. 2024b), which may be attributable to adaptation to similar habitat environments.

The distribution of both the new species and a yet-to-be-described species of *Rhodeus* is confined to the same river, representing the second documented instance of sympatric occurrence between a new freshwater mussel and a new bitterling (Wu et al. 2022). Southern China is a hotspot for the both freshwater mussels and bitterlings (Guo 2022; Li 2025), and the special mutually beneficial symbiotic relationship between them may have driven their coevolution.

Acknowledgements

This study was supported by the National Natural Science Foundation of China under Grant No.32360132, No.31772412, and the Laboratory of Ecological Security and Biodiversity Conservation of Cities on the Yangtze River Delta, Shanghai Science and Technology Museum.

References

Chen ZG, Dai YT, Ouyang S, Huang XC, Wu XP (2023) Unveiling the identity of *Diaurora* Cockerell, 1903 (Bivalvia, Unionidae): morphology, molecular phylogenetics, and the description of a new species. Zookeys 1173: 131–144. https://doi.org/10.3897/zookeys.1173.106148

Dai YT, Huang XC, Wu CHZ, Chen ZG, Guo L, Shu SY, Ouyang S, Wu XP (2023) Multilocus and mitogenomic phylogenetic analyses reveal a new genus and species of freshwater mussel (Bivalvia: Unionidae) from Guangxi, China. Invertebrate Systematics 37(2): 152–166. https://doi.org/10.1071/IS22048

Dai YT, Chen ZG, Cheng YZ, Huang XC, Ouyang S, Shu FY, Wu XP (2024a) Molecular phylogeny reveals a new genus and species of freshwater mussel (Bivalvia, Unionidae, Gonideinae) from Jiangxi, China. Zoosystematics and Evolution 100(4): 1419–1429. https://doi.org/10.3897/zse.100.135217

Dai YT, Chen ZG, Hu CL, Ning PF, Ouyang S, Huang XC, Wu XP (2024b) Taxonomic reassessment of *Scabies* (Bivalvia: Unionidae) species in China based on multilocus and mitogenomic phylogenetic analyses. Invertebrate Systematics 38, IS24020. https://doi.org/10.1071/IS24020

Dai YT, Chen ZG, Hu CL, Ouyang S, Huang XC, Wu XP (2024c) Description of a new freshwater mussel species of *Plethol*o*phus*, Simpson, 1900 (Bivalvia, Unionidae) from Guangdong, China. Zoosystematics and Evolution 100(4): 1191–1200. https://doi.org/10.3897/zse.100.131019

Dai YT, Chen ZG, Peng KJ, Ouyang S, Huang XC, Wu XP (2024d) Revisiting the genus *Pseudocuneopsis* (Bivalvia, Unionidae): Morphology, mitochondrial phylogenomics, and the description of a new species. Zoologica Scripta 53(3): 323–337. https://doi.org/10.1111/zsc.12647

Graf DL, Cummings KS (2007) Review of the systematics and global diversity of freshwater mussel species (Bivalvia: Unionoida). Journal of Molluscan Studies 73(3): 291–314. https://doi.org/10.1093/mollus/eym029

Graf DL, Cummings KS (2021) A 'big data' approach to global freshwater mussel diversity (Bivalvia: Unionoida), with an updated checklist of genera and species. Journal of Molluscan Studies 87(1): eyaa034. https://doi.org/10.1093/mollus/eyaa034

Graf DL, Cummings KS (2025) The MUSSEL Project. http://www.mussel-project.net/ [Accessed 01 March 2025]

Guo L (2022) Unionoida. The Straits Publishing, China, 256 pp. [In Chinese]

He J, Zhuang ZM (2013) The Freshwater Bivalves of China. ConchBooks, Germany, 198 pp.

Heude PM (1875) Conchyliologie fluviatile de la province de Nanking et de la Chine centrale. Premier Fascicule. Librairie F. Savy, France, 8 pp. [In French] https://doi.org/10.5962/bhl.title.14450

Heude PM (1877a) Conchyliologie fluviatile de la province de Nanking et de la Chine centrale. Deuxième Fascicule. Librairie F. Savy, France, 8 pp. [In French]

Heude PM (1877b) Conchyliologie fluviatile de la province de Nanking et de la Chine centrale. Troisième Fascicule. Librairie F. Savy, France, 8 pp. [In French]

Heude PM (1878) Conchyliologie fluviatile de la province de Nanking et de la Chine centrale. Quatrième Fascicule. Librairie F. Savy, France, 8 pp. [In French]

Heude PM (1879) Conchyliologie fluviatile de la province de Nanking et de la Chine centrale. Cinquième Fascicule. Librairie F. Savy, France, 8 pp. [In French]

Heude PM (1880a) Conchyliologie fluviatile de la province de Nanking et de la Chine centrale. Sixième Fascicule. Librairie F. Savy, France, 8 pp. [In French]

Heude PM (1880b) Conchyliologie fluviatile de la province de Nanking et de la Chine centrale. Dixième Fascicule. Librairie F. Savy, France, 8 pp. [In French]

Heude PM (1881) Conchyliologie fluviatile de la province de Nanking et de la Chine centrale. Septième Fascicule. Librairie F. Savy, France, 8 pp. [In French]

Heude PM (1883) Conchyliologie fluviatile de la province de Nanking et de la Chine centrale. Huitième Fascicule. Librairie F. Savy, France, 8 pp. [In French]

Heude PM (1885) Conchyliologie fluviatile de la province de Nanking et de la Chine centrale. Neuvième Fascicule. Librairie F. Savy, France, 8 pp. [In French]

Hou KY, Liu XY, Zhang LP, Liu GP, Wu RW (2025) Revisiting the genus *Nodularia* (Bivalvia, Unionidae): Mitochondrial phylogenomics and the description of a new species. Zoosystematics and Evolution 101(1): 35–44. https://doi.org/10.3897/zse.101.139762

Huang SP, Zhao YH, Chen IS, Shao KT (2017) A new species of *Microphysogobio* (Cypriniformes: Cyprinidae) from Guangxi Province, southern China. Zoological Studies 56: e8. https://doi.org/10.6620/ZS.2017.56-08

Huang XC, Wu RW, An CT, Xie GL, Su JH, Ouyang S, Zhou CH, Wu XP (2018) Reclassification of Lamprotula rochechouartii as *Margaritifera rochechouartii* comb. nov. (Bivalvia: Margaritiferidae) revealed by time-calibrated multilocus phylogenetic analyses and mitochondrial phylogenomics of Unionoida. Molecular Phylogenetics and Evolution 120: 297–306. https://doi.org/10.1016/j.ympev.2017.12.017

Huang XC, Su JH, Ouyang JX, Ouyang S, Zhou CH, Wu XP (2019) Towards a global phylogeny of freshwater mussels (Bivalvia: Unionida): Species delimitation of Chinese taxa, mitochondrial phylogenomics, and diversification patterns. Molecular Phylogenetics and Evolution 130: 45–59. https://doi.org/10.1016/j.ympev.2018.09.019

Inoue K, Hayes DM, Harris JL, Christian AD (2013) Phylogenetic and morphometric analyses reveal ecophenotypic plasticity in freshwater mussels obovaria jacksoniana and villosa arkansasensis (bivalvia: Unionidae). Ecology and Evolution 3(8): 2670–2683. https://doi.org/10.1002/ece3.649

Katoh K, Rozewicki J, Yamada KD (2019) MAFFT online service: multiple sequence alignment, interactive sequence choice and visualization. Briefings in Bioinformatics 20(4): 1160–1166. https://doi.org/10.1093/bib/bbx108

Lanfear R, Frandsen PB, Wright AM, Senfeld T, Calcott B (2017) Partitionfinder 2: New methods for selecting partitioned models of evolution for molecular and morphological phylogenetic analyses. Molecular Biology and Evolution 34(3): 772–773. https://doi.org/10.1093/molbev/msw260

Li F (2025) Freshwater fishesof China. The Straits Publishing, China, 762 pp. [In Chinese]

Liu YY, Wu XP (1991) The further description of *Solenaia carinatus* (Lamellibranchia: Unionidae). Acta Zootaxonomica Sinica 16(1): 122–123 [In Chinese]

Liu XJ, Liu YY, Wu RW, Zanatta DT, Lopes-Lima M, Gonçalves DV, Bogan A, Ouyang S, Wu XP (2022) Systematics, distribution, biology, and conservation of freshwater mussels (Bivalvia: Unionida) in China. Aquatic Conservation Marine and Freshwater Ecosystems 32(5): 859–895. https://doi.org/10.1002/aqc.3799

Liu LL, Zhang LP, Jin DD, Wang HT, Liu XJ, Wu RW (2023) Molecular and morphological evidence reveals a hidden new taxon in the endemic genus *Pseudocuneopsis* (Bivalvia, Unionidae) from China. ZooKeys 1179: 219–229. https://doi.org/10.3897/zookeys.1179.109817

Liu LL, Zhang LP, Hou KY, Ning LY, Wu RW (2024) Addition to the known diversity of Chinese freshwater mussels: integrative description of a new species of *Postolata* Dai et al., 2023 (Bivalvia, Unionidae, Gonideinae). Zoosystematics and Evolution 100(3): 769–778. https://doi.org/10.3897/zse.100.126069

Minh BQ, Nguyen MAT, von Haeseler A (2013) Ultrafast approximation for phylogenetic bootstrap. Molecular Biology and Evolution 30: 1188–1195. https://doi.org/10.1093/molbev/mst024

Tamura K, Stecher G, Peterson D, Filipski A, Kumar S (2013) MEGA6: Molecular evolutionary genetics analysis version 6.0. Molecular Biology and Evolution 30: 2725–2729. https://doi.org/10.1093/molbev/mst197

MolluscaBase [Eds] (2025) MolluscaBase. https://www.molluscabase.org/ [Accessed 01 March 2025]

Ouyang S, Qi T, Xiao JZ, Xu L, Han YY, Wu XP (2011) Species Diversity and Abundance of Freshwater Molluscks in the Middle Reaches of Gan River and the Surrounding Branches. Journal of Nanchang University (Engineering & Technology) 33(01): 1–6. [In Chinese]

Ronquist F, Teslenko M, van der Mark P, Ayres DL, Darling A, Höhna S, Larget B, Liu L, Suchard MA, Huelsenbeck J (2012) Mrbayes 3.2: Efficient bayesian phylogenetic inference and model choice across a large model space. Systematic Biology 61: 539–542. https://doi.org/10.1093/sysbio/sys029

Shu FY, Wu XP (2004) Investigation of bivalves resources in main branch lake inlet of the Gan River. Territory & Tatural Resources Study 3: 80–81. [In Chinese]

Simpson CT (1900) Synopsis of the naiades, or pearly fresh-water mussels. Proceedings of the United States National Museum 22(1205): 501–1044. https://doi.org/10.5479/si.00963801.22-1205.501

Sun ZX, Li XJ, Tang WQ, Zhao YH (2022) A new species of the gudgeon genus *Huigobio* Fang, 1938 (Cypriniformes: Cyprinidae) from the Yangtze River Basin, southern China. Zoological Research 43(1): 33−39. https://doi.org/10.24272/j.issn.2095-8137.2021.168

Wu XP, Ouyang S, Hu QY (1994) Bivalves (Mollusca) of the Poyang Lake. Journal of Nanchang University (Natural Science) 18(3): 249–252. [In Chinese]

Wu XP, Liang YL, Wang HZ, Ouyang S (1999) Morphological characters of glochidia of Unionidae and the taxonomic significance. Acta Hydrobiologica Sinica 23(supplement): 139–147. https://doi.org/10.3724/issn1000-3207-1999-2-141-1

Wu XP, Liang YL, Wang HZ, Xie ZC, Ouyang S (2000) Distribution and species diversity of freshwater Mollusca of lakes along mid-lower reaches of the Yangtze River. Journal of Lake Science 12: 111–118. [In Chinese] https://doi.org/10.18307/2000.0203

Wu RW, Gao BY, Lan ZC, Zhang MH, Ouyang S, Wu XP (2017) Predicting local colonization and extinction rates of freshwater mussels based on biological traits in a case of Lake Poyang. Journal of Lake Sciences 29(3): 678–686. [In Chinese] https://doi.org/10.18307/2017.0317

Wu RW, Liu YT, Wang S, Liu XJ, Zanatta DT, Roe KJ, Song XL, An CT, Wu XP (2018) Testing the utility of DNA barcodes and a preliminary phylogenetic framework for Chinese freshwater mussels (Bivalvia: Unionidae) from the middle and lower Yangtze River. PLOS ONE 13(8): e0200956. https://doi.org/10.1371/journal.pone.0200956

Wu RW, Kim KS, Xie GL, Ouyang S, Wu XP (2020) Phylogenetic position of *Aculamprotula polysticta*, comb. res. (Bivalvia: Unionidae) inferred from phylogenetic relationships in Unionida. Invertebrate Systematics 34: 192–199. https://doi.org/10.1071/IS19036

Wu RW, Liu XJ, Kondo T, Ouyang S, Wu XP (2021) New species of the genus *Inversidens* Haas, 1911 (Unionoida, Unionidae, Gonideinae) from Jiangxi Province, China. Zookeys 1054: 85–93. https://doi.org/10.3897/zookeys.1054.69075

Wu XP, Dai YT, Yin N, Shu FY, Chen ZG, Guo L, Zhou CH, Ouyang S, Huang XC (2022) Mitogenomic phylogeny resolves *Cuneopsis* (Bivalvia: Unionidae) as polyphyletic: The description of two new genera and a new species. Zoologica Scripta 51(2): 173–184. https://doi.org/10.1111/zsc.12527

Wu RW, Liu LL, Zhang LP, Bogan AE, Niu GY, Jin DD, Wu XP, Liu XJ (2024) Taxonomic revision of two species in the genus *Ptychorhynchus* Simpson, 1900 (Bivalvia: Unionidae: Gonideinae), with description of a new species. Invertebrate Systematics 38: IS24014. https://doi.org/10.1071/IS24014

Xiao JZ, Liu XM, Liu YB, Xu L, Ouyang S, Chen JK, Lei GC, Wu XP (2012) Distribution and abundance of freshwater mussels along the middle and lower reaches of the GanJiang River, Jiangxi. Resources and Environment in the Yangtze Basin 21(11): 1330–1335. [In Chinese]

Xiong LF, Ouyang S, Chen TH, Qi T, Wu XP (2011) The comparative study of resource status on freshwater mussel in two lakes of different usage in Poyang Lake area. Journal of Shanghai Ocean University 20(2): 204–210. [In Chinese]

Xiong LF, Ouyang S, Wu XP (2012) Fauna and standing crop of freshwater mussels in Poyang Lake, China. Chinese Journal of Oceanology and Limnology 30(01): 124–135. https://doi.org/10.1007/s00343-012-1070-6

Zeng HQ, Liu YY (1989) A new species of the genus *Acuticosta* from Sichuan Province, China (Lamellibranchia: Unionidae). Acta Zootaxonomica Sinica 14(4): 404–407. [In Chinese]

Zeng HQ, Su LD, Xie SG (1981) On the freshwater mollusks in Chongqing, China. Journal of the southwest teachers college 2: 78–82. [In Chinese]

Zeng HQ, Xie SG, Su LD (1985) On the freshwater mollusks in eastern Sichuan, China. Journal of the southwest teachers college 1: 71–79. [In Chinese]

Zieritz A, Aldride D (2009) Identification of ecophenotypic trends within three european freshwater mussel species (bivalvia: Unionoida) using traditional and modern morphometric techniques. Biological Journal of the Linnean Society 98(4): 814–825. https://doi.org/10.1111/j.1095-8312.2009.01329.x

Zoosyst. Evol. 101 (2) 2025, 813–853 | DOI 10.3897/zse.101.137663

PENSOFT

MUSEUM FÜR NATURKUNDE BERLIN

Across trench and ridge: description of five new species of the *Haploniscus belyaevi* Birstein, 1963 species complex (Isopoda, Haploniscidae) from the Kuril-Kamchatka Trench region

Henry Knauber[1,2], Tilman Schell[3], Angelika Brandt[1,2], Torben Riehl[1,2]

1 *Senckenberg Research Institute and Natural History Museum, Department of Marine Zoology, Section Crustacea, Senckenberganlage 25, 60325 Frankfurt, Germany*

2 *Johann Wolfgang Goethe University Frankfurt, Department of Biological Sciences, Institute of Ecology, Evolution and Diversity, Max-von-Laue-Str. 13, 60438 Frankfurt, Germany*

3 *LOEWE-Centre for Translational Biodiversity Genomics (LOEWE-TBG), 60438 Frankfurt, Germany*

https://zoobank.org/1764B434-B419-4430-B297-6D6380572DFB

Corresponding author: Henry Knauber (henry.knauber@senckenberg.de)

Academic editor: Luiz F. Andrade ♦ **Received** 23 September 2024 ♦ **Accepted** 11 March 2025 ♦ **Published** 22 April 2025

Abstract

Integrative taxonomy provides a valuable approach to discover and unravel even morphologically almost indiscernible species, such as those forming "cryptic" species complexes. The six members of the recently discovered *Haploniscus belyaevi* species complex (short: *belyaevi*-complex) from the abysso-hadal Kuril-Kamchatka Trench (KKT) region in the Northwest Pacific Ocean are taxonomically described herein. The eponymous *Haploniscus belyaevi* is redescribed alongside new descriptions of the five closely related species *Haploniscus apaticus* **sp. nov.**, *H. erebus* **sp. nov.**, *H. hades* **sp. nov.**, *H. kerberos* **sp. nov.**, and *H. nyx* **sp. nov.** The morphological differences between these species are most eminent in the rostral and pleotelson morphology of the adult males. Alongside light-microscopical drawings, CLSM scans, and 16S and COI barcodes, these species descriptions are complemented by the first genomic data of deep-sea haploniscid isopods. Geometric morphometrics was applied to quantify interspecific and intraspecific morphological differences of the pleotelson considering the pronounced sexual dimorphism. The distributional range of the *belyaevi*-complex covers a large geographical area, ranging across the greater KKT region and extending beyond large-scale geomorphological barriers such as the KKT and the Kuril Island Ridge, turning these into promising species to study differentiation processes in the deep sea.

Key Words

Asellota, biological systematics, CLSM, genomics, Janiroidea, mitogenome, Peracarida, Sea of Okhotsk

Introduction

Attempts to catalogue the biodiversity of the largest yet least explored biome of the world, the deep sea, have been ongoing for decades and remain far from complete. Estimations suggest up to 91% of marine species are yet to be discovered (Mora et al. 2011; but see also Appeltans et al. 2012). Species complexes – closely related taxa that often exhibit minuscule morphological differences (e.g., "cryptic" species) – are numerous amongst many phyla and taxonomic groups, e.g., Bivalvia (Goffredi et al. 2003), Crinoidea (McLaughlin et al. 2023), Decapoda (Silva et al. 2021), or Isopoda (Schnurr et al. 2018). Yet, the discovery of marine biodiversity is especially complicated by a high proportion of species that are difficult to discriminate, including "cryptic" species as well as those with relatively strong phenotypic plasticity, di- and polymorphisms, and significant morphological changes during their ontogenetic development (e.g., Knowlton 1993; Vrijenhoek 2009; Riehl et al. 2012). However, an

integrative taxonomic framework has proven useful in discriminating "cryptic" species and revealing new species even in such difficult cases.

For deep-sea biodiversity studies, where sample sizes are commonly small in light of low abundances and patchy distributions, species are often represented by only a few individuals (Rex and Etter 2010). Yet, as explained above, without knowing the full phenotypic variability, cataloging species richness can be a challenge. Johannsen et al. (2020) faced such a situation, leading Knauber et al. (2022) to use an integrative taxonomic approach to study patterns of phenotypic variation in a species of haploniscid isopods from the Kuril-Kamchatka Trench region in the Northwest Pacific Ocean. Initially believed to represent a single species, *Haploniscus belyaevi* Birstein, 1963, the collected material turned out to comprise at least six distinct species, five of which were new to science (see also Johannsen et al. 2020).

Haploniscidae Hansen, 1916, is a relatively common and cosmopolitan family of asellote isopods inhabiting soft sediments in the deep sea. Haploniscids occur from shallow to hadal depths. Currently, over 120 species of haploniscid isopods are known to science (Boyko et al. 2023), and a major taxonomic revision of the family has been called for, as relationships are largely unresolved and the largest genus, *Haploniscus* (Richardson, 1908), serves as a repository for species that lack clear apomorphies or affinities to the remaining genera. The discovery of the *belyaevi*-complex is by no means the first record of a species complex within this family: Brökeland and Raupach (2008) and Brökeland (2010a) described two other species complexes within the Haploniscidae, emphasizing the need for a major taxonomic revision of the systematically unstructured family.

In this study the newly discovered species of the *belyaevi*-complex are formally described, and *H. belyaevi* is redescribed with new neotypes assigned. Besides classical morphological methods and DNA barcoding, geometric morphometric analyses and genome sequencing were utilized, two approaches novel for haploniscid species descriptions.

Methods

Study area and sampling

The study region covers the central part of the Kuril-Kamchatka Trench (KKT) in the Northwest Pacific Ocean (NWP) and adjacent abyssal seabed, also including the marginal Sea of Okhotsk (SO). Located in a highly productive area, the KKT extends from the Japanese island Hokkaido in the southwest alongside the Kuril Island Ridge (KIR) to the coasts of the Russian peninsula Kamchatka in the northeast. With depths of up to 9,600 m (Dreutter et al. 2020), the KKT represents one of the deepest hadal regions in the Pacific Ocean and forms a link between the Japan and Aleutian Trenches. Neighboring the trench to the southeast are vast abyssal plains of the open NWP, while the marginal SO and its Kuril Basin (3,374 m max. depth) in the northwest are separated from the KKT and the NWP by the Kuril Islands. Several bathyal straits, such as the Bussol Strait (2,350 m sill depth) or Krusenstern Strait (1,920 m sill depth), allow for the exchange of water and potentially deep-sea fauna between the KKT and the SO (Tyler 2002; Malyutina et al. 2018). Between 2012 and 2016, the benthos of both the KKT and the SO has been investigated during three successive deep-sea expeditions, namely the KuramBio (KB), KuramBio II (KBII), and SokhoBio (SKB) campaigns (Brandt and Malyutina 2013; Malyutina et al. 2015; Brandt 2016). These expeditions aimed to complement the inventory of the benthic biodiversity of the greater KKT region established in the mid-twentieth century by Russian investigators (Monin 1983; Golovan et al. 2019; Brandt et al. 2020), understand species ranges and turnover and their driving forces, and investigate potential barrier effects of the KKT and the KIR on deep-sea fauna. The distribution map was created using QGIS 3.28 with GRASS 7.8.7 (GRASS Development Team 2020; QGIS.org 2020).

All haploniscid samples examined for this study were collected during the SokhoBio (Sea of Okhotsk Biodiversity Studies; Malyutina et al. 2018) campaign on board the RV *Akademik M.A. Lavrentyev* in 2015 and the KuramBio II (Kuril Kamchatka Biodiversity Studies II, Brandt 2016) campaign on board the RV *Sonne* in the KKT and SO regions. The samples referred to in this study were collected using a box corer (BC; Hessler and Jumars 1974), an Agassiz trawl (AGT; Agassiz 1880), and an epibenthic sledge with 300 µm-meshed cod ends (Brenke 2005; EBS; Brandt et al. 2013). The collected sediment was sieved on board using 300 µm-meshed metal sieves and filtered with –20 °C precooled, filtered seawater to remove fine sediment fractions. Thereafter, samples were bulk fixed in chilled 96% ethanol and kept chilled at all times to prevent DNA degradation, following Riehl et al. (2014).

Taxonomy

Following recent publications on the sexual dimorphic haploniscid isopods, the species descriptions focus on the adult males as holotypes (see Fig. 1), while adult females are used and described as paratypes (Brökeland and Raupach 2008; Brökeland 2010a; Brökeland and Svavarsson 2017). The designation and nomenclature of ontogenetic stages follow Knauber et al. (2022).

The material was examined using a stereomicroscope, the Leica M60, to assign type specimens for subsequent taxonomic analysis. To designate a type locality for each novel species, special emphasis was laid on selecting holo- and paratype specimens from the same or neighboring sampling areas, which also include the specimens used for genome analyses (see below). Voucher photos were taken using a LEICA M165C equipped with a LEICA DMC5400 camera utilizing the LAS-X software. Taxonomic drawings of each specimen were prepared using a Leica DM 2500 LED microscope equipped with a *camera lucida*. While pereopods, pleopods, and mouthparts were dissected, the

antennae were illustrated *in situ* to prevent potential damage to the head of the type specimens. To prepare the specimens for drawing and confocal laser scanning microscopy (CLSM), they were transferred from 70–96% EtOH to a 1:1 solution of 70% EtOH and glycerin and set aside for two days, letting the ethanol evaporate slowly to avoid potential shrinking of the specimens. Subsequently, they were transferred to 80% glycerin, and temporary slides were prepared following the method of Wilson (2008). The resulting pencil drawings were digitalized using the Adobe Illustrator 27.2 software, following Coleman (2003).

For the CLSM, the samples were stained using Congo Red dissolved in 70% denatured EtOH while remaining in glycerine following Michels and Büntzow (2010). After placing the samples on temporary slides, scans were conducted using a Leica DM2500 with a Leica TCS SPE II and the LEICA LAS X 3.5.5.19976 software at a resolution of 2480 × 2480 pixels. Post-production of the resulting CLSM scans was carried out in Adobe Photoshop 24.1.1 and Adobe Illustrator 27.2.

Based on the voucher images, CLSM scans, and digitalized drawings, all specimens were measured using the measuring tool in Adobe Acrobat Pro, building upon the standards of Hessler (1970). The body length was measured from a lateral view under consideration of potential body curvature from the frontal margin of the head to the posterior medial margin of the pleotelson, thus excluding rostrum and pleotelsonic processes from the total body length. All other measurements regarding body segment lengths were taken from the dorsal habitus drawings along the specimens' midline. Generally, the total length of appendages like antennae or pereopods was measured along the midline of each segment.

For the species description, a taxonomic character database for the Haploniscidae developed in the DELTA system (Dallwitz 1980; Dallwitz et al. 1999) was used (SOSA et al. 2024). The preparation of the taxonomic characters and their character states within the DELTA database included literature research on haploniscid taxonomy papers with special emphasis on characters used for species delimitation. Morphological terminology was based on Brökeland and Svavarsson (2017) with modifications. Setae were named after Riehl and Brandt (2010).

Molecular diagnoses based on barcodes of the mitochondrial large ribosomal RNA subunit (16S) and the cytochrome-c-oxidase subunit I (COI) were prepared using the online tool DeSigNate (Hütter et al. 2020), only focusing on alignment positions with a discriminative power of 1.0.

The material of the herein described species is deposited at the Senckenberg Museum Frankfurt, Germany (SMF), the Zoological Museum Hamburg, Germany (ZMH), and the Museum of Institute of Marine Biology, Vladivostok, Russia (MIMB).

Haploniscid species description standards

Historically, janiroidean species descriptions became more and more lengthy over time, as taxonomists attempted to describe new species in a complete and detailed fashion, often incorporating characters without species delimitating potential. Leaning on a recent description template (SOSA et al. 2024), this study prioritized the illustration of characters over their extensive description in the form of text. To achieve this, the focus was on apomorphic characters useful for species delimitation, whilst most plesiomorphic characters and such of descriptive nature were only omitted from the descriptions. Characters omitted from the text comprise the mostly plesiomorphic mouthparts, pleopods III–V, and most setation patterns on antennae, pereopods, and pereonites. Nevertheless, all these structures have been depicted in the provided illustrations, considering the possibility that future reassessments may still discover their value in species delimitation. Likewise, recurring features were only presented once in text form, such as in the case of the pereopods. The description of the female paratypes with a more uniform morphology is restricted to characters in which these specimens differ from their male counterparts. Pereopod I was drawn and described due to more pronounced setation patterns in its distal segments in comparison to the remaining pereopods, of which only pereopods II and VI were depicted, as pereopods II through VII differ only in length and length-dependent ratios. With pereopod II being the shortest and pereopod VI the longest of these otherwise uniform legs, we solely depict their extremes.

The species descriptions also feature molecular diagnoses based on 16S and COI barcodes to facilitate differentiation on molecular data.

Geometric morphometrics

Most haploniscid species can be told apart based on the morphology of the antenna, the rostrum, and the pleotelson, of which the latter is the easiest to study in a standardized way. Therefore, the pleotelson shape was studied from a ventral view using geometric morphometrics (GM) and a combination of CLSM scans and photographs. Due to a low specimen count for several of the herein discussed species, these analyses were restricted to adult specimens of *H. belyaevi*, *H. kerberos* sp. nov., and *H. hades* sp. nov. The CLSM scans and photographs were then processed and statistically analyzed using the tps software suite (Rohlf 2015) and MorphoJ 1.07a (Klingenberg 2011) following the approach described in Casaubon and Riehl (2024). Subsequently, Adobe Illustrator 27.2 was used to adjust the resulting plot.

Genome sequencing

Genome sequencing was conducted for five of the six members of the *belyaevi* complex, alongside another haploniscid species, *H. hydroniscoides* Birstein, 1963, for means of comparison. Given the low available specimen count for *H. nyx* sp. nov., no specimen of this species was chosen for genome sequencing. DNA isolation was conducted at Loewe TBG, Frankfurt, Germany, while sequencing was carried out by Novogene in Cambridge, UK.

A thorough description of the methods used for the nuclear and mitochondrial genome assembly can be found in Suppl. material 1. In brief, nuclear genome assemblies were conducted using Spades 3.15.0 (Prjibelski et al. 2020) and Platanus 1.2.4 (Kajitani et al. 2014) after quality filtering with Trimmomatic 0.39 (Bolger et al. 2014). From the resulting contigs, contamination and sequences with mitochondrial origin were filtered out, and final assemblies were assessed regarding quality with Quast (Gurevich et al. 2013) and BUSCO 5.5.0 (Manni et al. 2021). Raw Illumina reads were used alongside available COI sequences from the respective specimens (BOLD acc. no. NWPHA090-20, NWPHA107-20, NWPHA138-20, NWPHA223-20, NWPHA267-20, NWPHA268-20) as a seed for input in NOVOplasty 4.2 (Dierckxsens et al. 2017) to assemble the mitochondrial genome of each sample. The annotation of the mitochondrial genomes was conducted by manually combining and curating annotations from GeSeq (Tillich et al. 2017) and MITOS2 (Donath et al. 2019) in Geneious Prime 2020.2.3 (https://www.geneious.com) per species. Mitogenome data of two preliminary species of the munnopsid genus *Notopais* were extracted from GenBank (Benson et al. 2012; acc. no. OL661185 and OL661186) as an outgroup for subsequent analyses on interspecific divergence. Thereafter, matrices of pairwise distances were calculated for the resulting mitogenome dataset using MEGA11 v11.0.11 (Tamura et al. 2021).

Abbreviations

A—Antenna; **Ceph**—Cephalothorax; **Md**—Mandible; **Mxp**—Maxilliped; **P**—Pereopod; **Plp**—Pleopod; **Plt**—Pleotelson; **Prn**—Pereonite.

Results

Taxonomy

Family Haploniscidae Hansen, 1916
Genus *Haploniscus* Richardson, 1908

Haploniscus belyaevi species complex

Composition. *Haploniscus belyaevi* Birstein, 1963, *H. apaticus* sp. nov., *H. erebus* sp. nov., *H. hades* sp. nov., *H. kerberos* sp. nov., *H. nyx* sp. nov.

Diagnosis. Haploniscidae with a dorsoventrally elliptical body, non-conglobating; tergite surfaces tuberculate, ornamentation evenly distributed, convex cross-section of tergites broken by slight, uneven elevations at the muscle attachment points of pereopods, elevated areas without ornamentation (see Fig. 1). Ceph trapezoidal, tuberculate; anterolateral angles rounded, not projecting; acute rostrum, basally with ventral bulge. At least Prn 1 posterior tergite margin through Prn 5 anterior tergite margin delicately serrated, setose; at least Prn 2 anterolateral angle through Prn 4 posterolateral angle with minute, acute projections; Prn 1–7 posterolateral angles asetose; Prn 7 of similar shape as previous Prns; Prn 7 and Plt tergites medially conjoint, segment borders not expressed. Plt dorsally with a pair of tubercles; posterolateral processes tapering to acute tips. AII article 3 slightly longer than wide, dorsal projection oriented anteriorly; article 5 with elongated and acute distolateral projection. Mandible palp distinctly longer than mandible, palp article 2 curved. All P carpi, propodi, and dactyli dorsal margins fringed by comb-like scale rows. Male Plp I proximal part trapezoid; lateral lobes indistinct, fused with medial lobes. Male Plp II protopod distal margin with continuous row of elongated simple setae, lateral margin with 1–3 short simple setae, endopod stylet very long, distinctly longer than protopod. Female operculum anteriorly with median bulge, otherwise circular, smooth. Uropods cylindrical, projecting caudally beyond posterior Plt apex, recessed in sternal fold laterally to anal valve.

Remarks. Species of the *belyaevi*-complex can be easily recognized amongst congeners by the two antennal spines located on the third and fifth peduncular articles of the second antennae. While antennal spines on the third article are fairly common amongst haploniscids, the presence of a second, large, and distal spine on the antennal fifth article is a unique feature of the *belyaevi*-complex. The rostral process of the *belyaevi*-complex, despite minor interspecific differences, could only be confused with the rostrum of *H. profundicolus* (Birstein 1971) and is otherwise conspicuously different from other haploniscids from the Northwest Pacific Ocean. Outside of the NWP, similar rostrum shapes also featuring a ventral bulge can be found in *H. hamatus* Lincoln, 1985, and *H. ampliatus* Lincoln, 1985. As common for the Haploniscidae, also the species of the *belyaevi*-complex show a pronounced sexual dimorphism. The adult males are highly distinct (see Fig. 1), while the adult female counterparts look much more alike, especially in terms of their overall body and pleotelson shapes. As the species-specific characters of rostrum and pleotelson only fully emerge in the adult male stages, assigning manca and female stages remains difficult when only morphological characters are considered. A noteworthy observation regarding ontogenetic changes within this species complex is that the antennal spines on the fifth article are minute in ovigerous females, much smaller than in preceding stages, and to a degree that they are almost unnoticeable. A visualization of the molecular variation within the complex is provided in Table 1 (16S) and Table 2 (COI). The mitochondrial genome contains the expected 13 protein-coding genes and two rRNAs in a conserved order (see 4.3 Genomics) for all member species of the complex. Detailed station data on sampling locations of the *belyaevi*-complex and its member species are provided in Table 3.

Table 1. Overview of molecular variation in the 16S gene within members of the *belyaevi*-complex. Numbers in brackets following a species name refer to the specimen count used for the molecular diagnosis analysis. Bold letters with a grey background indicate apomorphic nucleotides at the given position. Letters in brackets indicate heterogeneous base calls at that position. n lists the number of apomorphic nucleotides for each species in the respective gene sequence.

Taxon	25	56	64	66	71	150	155	156	173	204	206	219	228	243	249	312	342	350	355	358	n
H. apaticus sp. nov. (8)	A	A	A	G	T	A	G	A	A	T	A	G	T	T	T	T	T	G	A	T	0
H. erebus sp. nov. (14)	A	**G**	**G**	**T**	**G**	**-**	**A**	**T**	A	**A**	**G**	G	A	**C**	T	T	**C**	**A**	**G**	**C**	14
H. belyaevi (31)	A	A	A	G	T	A	G	A	A	T	A	G	(T)	T	**C**	T	T	G	A	T	1
H. hades sp. nov. (27)	T	A	C	A	T	G	G	A	A	T	A	**A**	A	T	T	T	T	G	A	T	1
H. kerberos sp. nov. (22)	T	A	C	A	T	G	G	A	**G**	T	A	G	**G**	T	T	T	T	G	A	T	2
H. nyx sp. nov. (3)	**G**	A	A	A	T	A	G	A	A	T	A	G	T	T	T	**C**	T	G	A	T	2

Table 2. Overview of molecular variation in the COI gene within members of the *belyaevi*-complex. Numbers in brackets following a species name refer to the specimen count used for the molecular diagnosis analysis. Bold letters with a grey background indicate apomorphic nucleotides at the given position. Letters with a red background indicate incomplete base call information due to shorter sequence reads. Letters in brackets indicate heterogeneous base calls at that position. n lists the number of apomorphic nucleotides for each species in the respective gene sequence.

Taxon	61	69	91	103	124	148	151	154	193	199	206	211	217	220	232	256	268	284	286	298
H. apaticus sp. nov. (3)	A	**T**	T	A	T	A	C	C	T	A	C	G	G	**A**	A	A	G	C	T	G
H. erebus sp. nov. (8)	A	C	**T**	A	T	A	**T**	**T**	T	A	C	G	G	C	A	A	**T**	**T**	**A**	A
H. belyaevi (6)	A	C	**T**	**A**	**T**	A	C	C	T	**G**	C	G	G	C	A	A	G	C	T	G
H. hades sp. nov. (27)	A	C	T	**G**	T	A	C	C	T	A	C	**A**	**T**	C	**C**	**G**	(G)	C	T	G
H. kerberos sp. nov. (21)	**T**	C	**C**	A	T	A	C	C	T	A	C	G	G	C	A	A	G	C	T	**C**
H. nyx sp. nov. (3)	A	C	T	A	**C**	**G**	C	C	**C**	A	**T**	G	G	C	A	A	G	C	T	A
Taxon	**301**	**304**	**313**	**328**	**334**	**346**	**349**	**352**	**364**	**370**	**376**	**385**	**388**	**409**	**412**	**418**	**430**	**436**	**442**	**451**
H. apaticus sp. nov. (3)	G	T	A	C	T	T	G	C	**A**	G	C	T	A	T	**G**	C	A	C	T	A
H. erebus sp. nov. (8)	**C**	T	**G**	C	T	T	G	**T**	G	G	**G**	**C**	**C**	A	T	**T**	A	**A**	T	**T**
H. belyaevi (6)	G	T	A	C	**C**	T	G	C	G	(G)	**T**	T	A	**C**	**A**	C	A	C	T	A
H. hades sp. nov. (27)	A	A	A	**T**	T	T	**A**	C	**C**	**C**	C	T	T	A	T	C	A	T	**C**	A
H. kerberos sp. nov. (21)	A	A	A	C	T	**G**	G	C	T	G	C	T	T	A	(C)	C	**G**	T	T	A
H. nyx sp. nov. (3)	A	**C**	A	C	**G**	**C**	G	C	T	G	C	T	A	T	C	C	A	T	T	A
Taxon	**469**	**472**	**475**	**481**	**496**	**499**	**502**	**508**	**520**	**553**	**556**	**562**	**565**	**571**	**592**	**607**	**625**	**628**	**649**	**n**
H. apaticus sp. nov. (3)	**G**	C	**A**	A	G	T	A	G	T	T	**C**	A	A	T	A	T	A	G	A	7
H. erebus sp. nov. (8)	C	**G**	**G**	A	(G)	T	**G**	T	T	T	T	**G**	**G**	T	A	T	A	G	A	19
H. belyaevi (6)	T	(T)	T	A	G	T	A	T	T	T	T	A	A	T	**G**	T	A	G	A	6
H. hades sp. nov. (27)	**A**	(A)	(T)	A	G	**C**	A	(A)	T	A	T	(T)	A	**C**	A	A	(G)	A	A	13
H. kerberos sp. nov. (21)	C	A	(T)	A	G	T	A	G	T	A	T	C	A	T	A	**G**	**T**	G	**G**	8
H. nyx sp. nov. (3)	T	C	T	**G**	**T**	T	A	**C**	**C**	**G**	**G**	A	A	T	A	T	G	**C**	A	14

Haploniscus belyaevi Birstein, 1963

Figs 1–5, 26

Neotype. SKB Hap46, adult male (stage VI), 3.4 mm, MIMB 50300.

Paraneotypes. SKB Hap04, adult female (stage IV; genome), SMF 56521; SKB Hap24, adult female (stage IV), 3.2 mm, MIMB 50294; SKB Hap06, adult male (stage VI), 3.6 mm, SMF 56523.

Type material. As pointed out by Knauber et al. (2022), the original male syntype of *H. belyaevi* as depicted in the original species description was lost. Instead, the species' type material is lumped together with additional material of *Haploniscus menziesi* Birstein, 1963. Most specimens are in poor condition, lacking either the distal AII with the characteristic spine on the fifth peduncular article or the pleotelson, rendering identification beyond genus level difficult. Three specimens can be identified as members of the *belyaevi*-complex, yet, as all of them are (ovigerous) female stages, allocation to one of the herein described member species of the *belyaevi*-complex remains uncertain. The type material is missing associated information about the sampling locality, and as the original description by Birstein does not define a type locality, *H. belyaevi* does not possess a definite type locality.

Based on I) the lack of a definite type locality, II) the presence of multiple haploniscid species in the type material of *H. belyaevi*, III) the absence of the original male syntype, and IV) uncertainty about where the material at hand stems from and whether it represents the type material, *H. belyaevi* is considered a *nomen dubium*. In an attempt to resolve the taxonomic identity of *H. belyaevi*, the species is therefore defined by the illustrations depicted in the original description by Birstein (1963),

Table 3. SokhoBio (LV71) and KuramBio II (SO250) stations, where members of the *Haploniscus belyaevi*-complex were sampled. EBS = Epibenthic Sledge; AGT = Agassiz Trawl.

Station	Depth [m]	Gear	Date	Latitude, Longitude
LV71 01-08	3307	EBS	2015-07-10	46°08.8'N, 145°59.2'E
LV71 02-07	3352	EBS	2015-07-13	46°40.9'N, 147°28.5'E
LV71 04-09	3365	EBS	2015-07-17	47°13.6'N, 149°39.2'E
LV71 04-10	3366	EBS	2015-07-17	47°12.2'N, 149°36.7'E
LV71 07-03	3296	EBS	2015-07-22	46°54.6'N, 151°05.3'E
LV71 07-04	3287	EBS	2015-07-22	46°59.4'N, 151°05.4'E
LV71 09-06	3502	EBS	2015-07-26	46°16.1'N, 152°00.0'E
LV71 09-07	3374	EBS	2015-07-26	46°16.2'N, 152°03.1'E
LV71 10-06	4469	EBS	2015-07-28	46°07.7'N, 152°09.7'E
LV71 10-07	4469	EBS	2015-07-29	46°07.8'N, 152°10.3'E
LV71 11-06	3206	EBS	2015-08-01	45°35.3'N, 146°24.7'E
SO250 008	5136	EBS	2016-08-19	43°49.55'N, 151°46.25'E
SO250 010	5120	EBS	2016-08-20	43°49.43'N, 151°46.96'E
SO250 020	8191	AGT	2016-08-23	45°51.32'N, 153°50.08'E
SO250 028	6051	EBS	2016-08-25	45°54.43'N, 152°47.02'E
SO250 030	6181	EBS	2016-08-27	45°56.38'N, 152°56.70'E
SO250 040	7081	EBS	2016-08-29	45°38.00'N, 152°55.95'E
SO250 042	7123	EBS	2016-08-30	45°39.62'N, 152°56.39'E
SO250 065	5755	EBS	2016-09-09	45°09.85'N, 153°43.34'E
SO250 085	5265	EBS	2016-09-15	45°02.26'N, 151°02.14'E
SO250 086	5493	AGT	2016-09-15	45°00.43'N, 151°06.01'E
SO250 087	5492	EBS	2016-09-16	45°00.76'N, 151°05.53'E
SO250 097	6575	EBS	2016-09-18	44°05.68'N, 151°24.88'E
SO250 098	6446	AGT	2016-09-19	44°05.53'N, 151°24.25'E

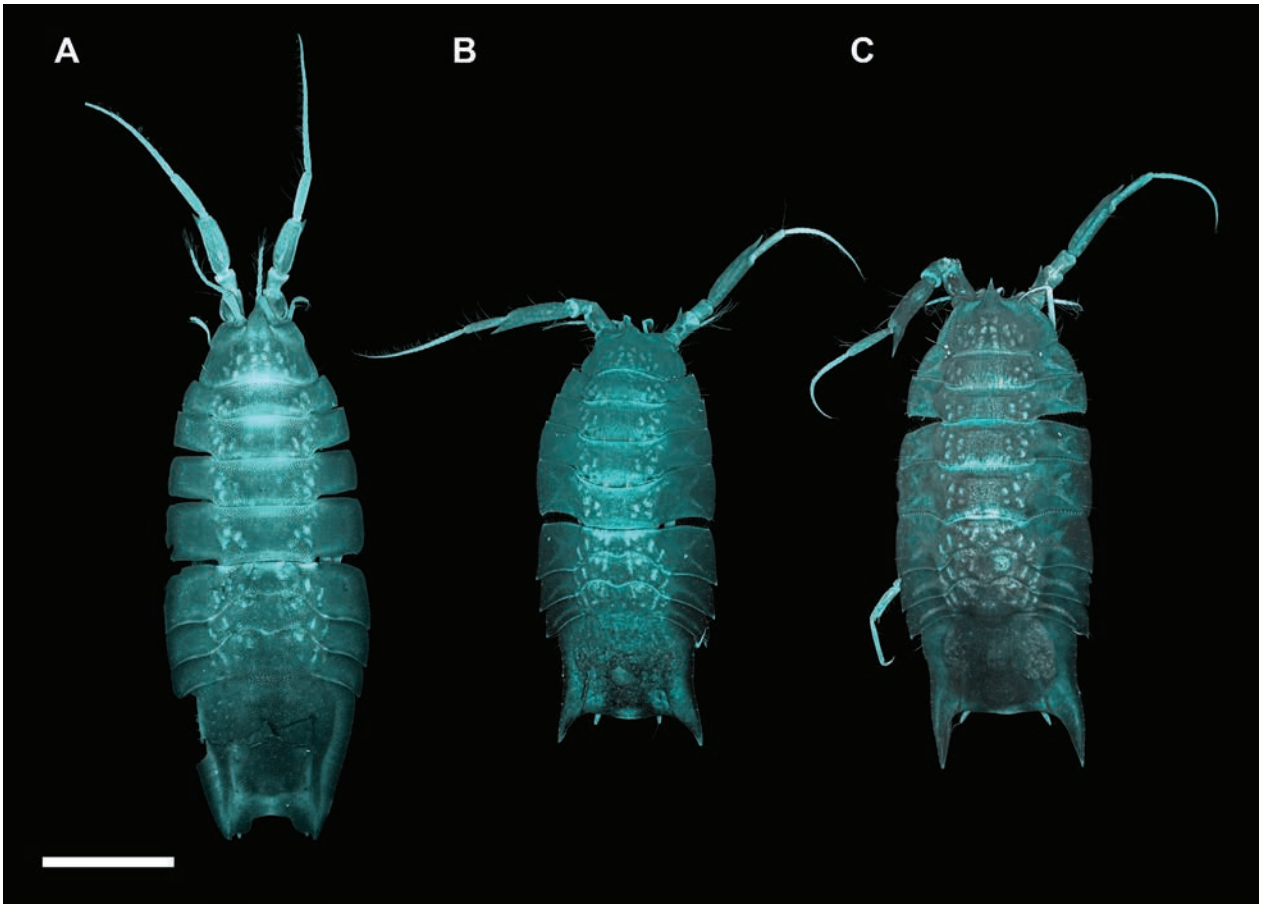

Figure 1. Morphological plasticity of adult males within the *Haploniscus belyaevi* species complex from Knauber et al. (2022). Dorsal habitus CLSM scans of *H. hades* sp. nov. (**A**), *H. belyaevi* (**B**), and *H. erebus* sp. nov. (**C**). Scale bar: 1 mm.

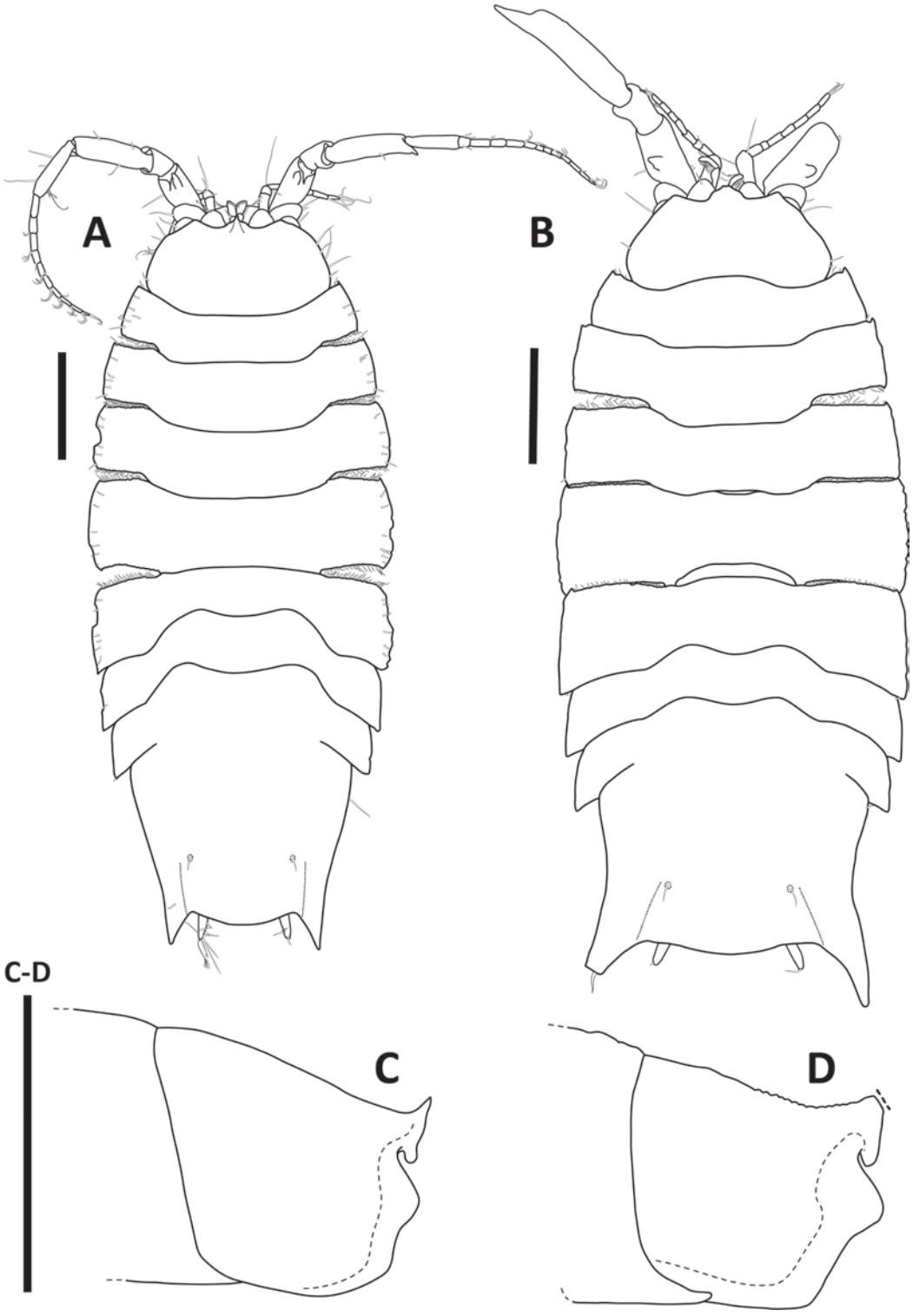

Figure 2. *Haploniscus belyaevi* Birstein, 1963 female paraneotype SKB Hap24 (**A, C**); male neotype, SKB Hap46 (**B, D**). **A, B.** Habitus, dorsal view; **C, D.** Head, lateral view. Scale bars: 0.5 mm.

and a male neotype alongside additional paratypes were assigned from recent material of the SokhoBio expedition (compare *H.* SO-KIR from Knauber et al. 2022), which exhibit a strong morphological resemblance to *H. belyaevi* as featured in the original description. This goes alongside the designation of a type locality, which is in the vicinity of a "Vityaz" station, where *H. belyaevi* was historically sampled.

Type locality. LV71–09–07, RV "Akademik M. A. Lavrentyev", SokhoBio expedition, EBS, 3374 m, 46°12.2'N, 152°03.1'E, Northwest Pacific, abyssal branch of the Kuril-Kamchatka Trench into the Bussol Strait.

Further records. St. LV71–01–08: SKB Hap25 (manca) MIMB 50295; St. LV71–04–09: SKB Hap39 (manca) SMF 56556, SKB Hap42 (manca) MIMB 50297, SKB Hap43 (manca) MIMB 50298, SKB Hap60 (adult

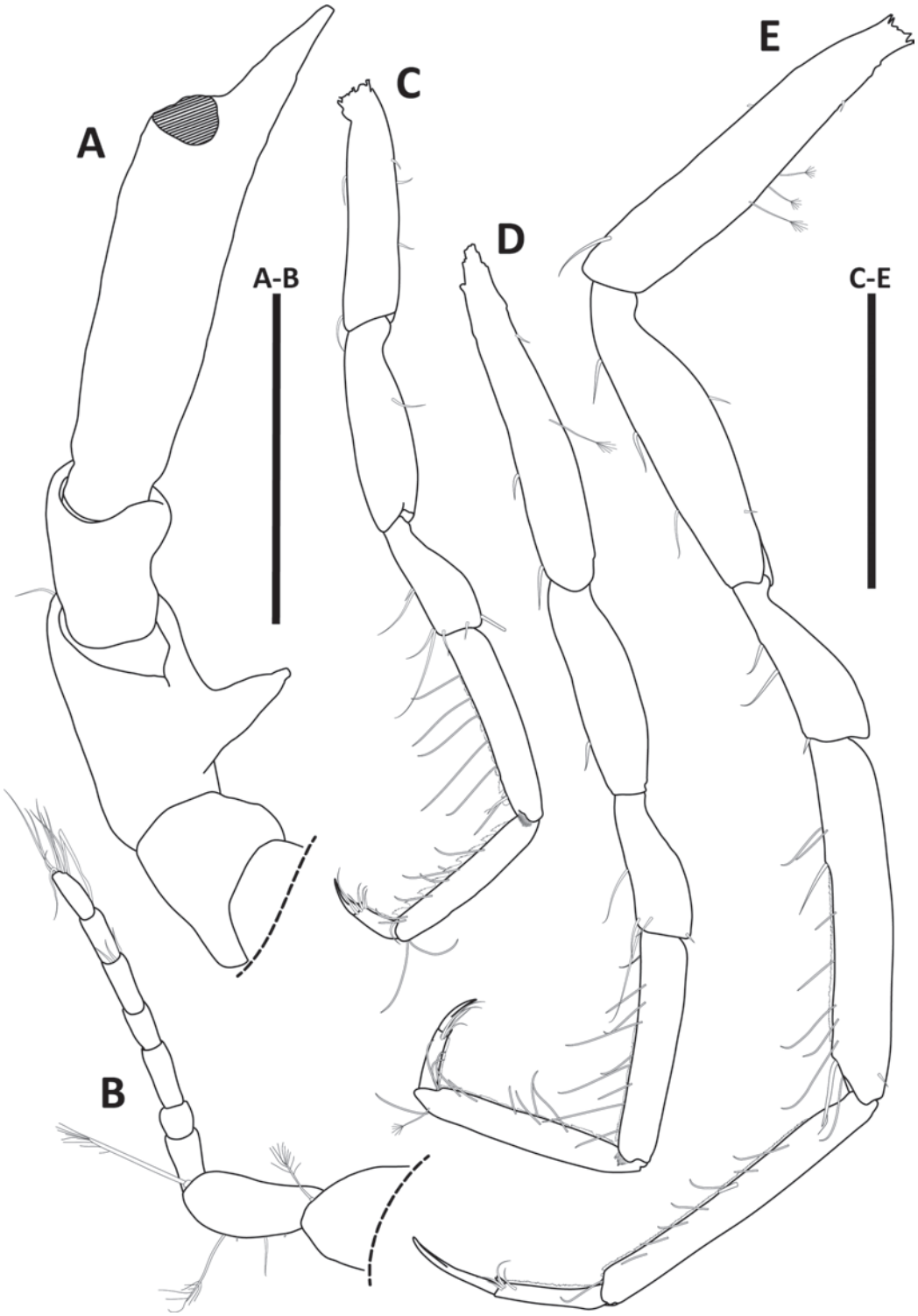

Figure 3. *Haploniscus belyaevi* Birstein, 1963 male neotype, SKB Hap46. **A.** Antenna II; **B.** Antenna I; **C.** Pereopod I; **D.** Pereopod II; **E.** Pereopod VI. Scale bars: 0.4 mm.

female) MIMB 50305, SKB Hap61 (adult female) MIMB 50306; St. LV71–04–10: SKB Hap07 (adult male) SMF 56524, SKB Hap17 (adult female) SMF 56534, SKB Hap38 (manca) SMF 56555; St. LV71–07–03: SKB Hap12 (manca) SMF 56529, SKB Hap19 (adult male) SMF 56536, SKB Hap20 (manca) MIMB 50293, SKB Hap56 (adult male) MIMB 50302, SKB Hap57 (adult female) SMF 56574, SKB Hap58 (adult male) MIMB 50303, SKB Hap59 (adult male) MIMB 50304; St. LV71–07–04: SKB Hap03 (adult female) MIMB 50292, SKB Hap40 (adult female) MIMB 50296, SKB Hap41 (adult female) SMF 56558, SKB Hap44 (manca) MIMB 50299, SKB Hap45 (manca) SMF 56562; St. LV71–09–06: SKB Hap15 (manca) SMF 56532, SKB Hap23 (adult female) SMF 56540; St. LV71–09–07: SKB Hap05 (adult male) SMF 56522, SKB Hap16 (manca) SMF 56533,

Figure 4. *Haploniscus belyaevi* Birstein, 1963 male neotype, SKB Hap46. **A.** Maxillipeds; **B.** Right mandible; **C.** Left mandible; **D.** Maxilla II; **E.** Maxilla I; **F.** Maxillipeds, detail of distomedial margins of endites; **G.** Left mandible, detail of incisor, *lacinia mobilis*, and molar process; **H.** Right mandible, detail of incisor and molar process. Scale bars: 0.1 mm.

SKB Hap32 (adult male) SMF 56549, SKB Hap33 (manca) SMF 56550, SKB Hap47 (adult male) MIMB 50301.

Distribution. Northwest Pacific, Sea of Okhotsk, Kuril Basin, and abyssal regions to the northwest of the Kuril-Kamchatka Trench, depth 3299–3386 m. Given its occurrence on both sides of the Kuril Island Ridge, it might be possible that this species' lowest bathymetric limit might lie even shallower, as it most likely dispersed across the Bussol Strait in one or other direction with a maximum depth of 2,350 m. The original species description of *H. belyaevi* depicts a distributional range extending far into the KKT area, yet despite sampling these areas during the above-mentioned expeditions, *H. belyaevi* was solely recorded in the vicinity of the Bussol Strait. One can therefore only hypothesize that Birstein, potentially due to limited material, lumped the distributional patterns

Figure 5. *Haploniscus belyaevi* Birstein, 1963 male neotype, SKB Hap46. **A.** Pleopod I; **B.** Pleopod II, ventral view; **C.** Pleopod II, dorsal view; **D.** Pleopod III; **E.** Pleopod IV; **F.** Pleopod V. Scale bar: 0.25 mm.

of multiple *belyaevi*-complex members together, not realizing that he was dealing with multiple species. Visualized in Fig. 27.

Synonymy. *Haploniscus* SO-KIR (see Knauber et al. 2022).

Diagnosis. The species differs from other members of the *belyaevi*-complex in the following characters: rostrum curved upwards, anteriorly flat; Prn 1 anterior tergite margin delicately serrated, setose; Prn 1 anterolateral angles with minute acute projection; posterolateral processes short, more than 0.10 Plt length, curved in males, oriented posteriorly.

Molecular diagnosis. Differing in the 16S gene from other species of the *belyaevi*-complex in the nucleotide C (position 249 of the alignment) as well as the nucleotides G (199), C (334), T (376), C (409), A (412), and G (592) of the COI gene.

Description. Male. ***Body*** (Figs 1B, 2B) length 2.3 width; subrectangular; anterior body length (Ceph–Prn 4) 1.0 posterior body length (Prn 5–Plt); lateral margin interrupted between Prn 7 and Plt, otherwise continuous.

Cephalothorax (Figs 1B, 2B, D) length 0.38 width, 0.10 body length, width 0.58 body width; frontal margin width 0.50 Ceph width; rostrum curved upwards, frontally plane.

Pereonite 1 (Figs 1B, 2B) anterior tergite margin through Prn 5 anterior tergite margin delicately serrated, setose; Prn 1–5 anterolateral angles slightly projecting; Prn 1–4 posterolateral angles slightly projecting; Prn 4 lateral margin length 1.04 Prn 5 lateral margin length.

Pleotelson (Figs 1B, 2B, 26H) length 0.74 width, 0.25 body length, rectangular, posterior margin rounded, convex; tergite surface smooth; with posterolateral

tergal ridge between uropod insertion and posterolateral process; posterolateral processes short, 0.31 Plt length, curved, oriented posteriorly.

Antenna I (Fig. 3B) length 0.17 body length; flagellum with 5 articles.

Antenna II (Fig. 3A) length 0.31 body length (without missing peduncular article 6 and flagellum); article 3 dorsal projection triangular, projection length 0.30 article 3 length; article 5 projection length 0.28 article 5 length; flagellum with 17 articles (inferred from male paratype).

Mandible (Fig. 4B, C) incisor with 5 cusps, left Md *lacinia mobilis* with 4 cusps.

Maxillipeds (Fig. 4A) with 3 coupling hooks each.

Pereopod I (Fig. 3C) length 0.40 body length. **PII** (Fig. 3D) length 0.49 body length. **PIII** length 0.53 body length. **PIV** length 0.53 body length. **PV** length 0.64 body length. **PVI** (Fig. 3E) length 0.71 body length; P lengths gradually increasing from PI to PVI, PVII shorter than PVI.

Pleopod I (Figs 5A, 26H) medial lobes subtriangular, projecting caudolaterally; separated at the apex by a narrow gap.

Pleopod II (Fig. 5B, C) protopod semi-circular, with distal lobe extending beyond protopod distal margin; endopod stylet 1.6 protopod length.

Female. Differs from male in the following characters:

Body (Fig. 2A) length 2.3 width; oval; anterior body length (Ceph–Prn 4) 0.95 posterior body length (Prn 5–Plt).

Cephalothorax (Fig. 2A, C) length 0.48 width, 0.13 body length, width 0.60 body width; frontal margin width 0.47 Ceph width.

Pereonite (Fig. 2A) 4 lateral margin length 1.05 Prn 5 lateral margin length.

Pleotelson (Figs 2A, 26G) length 0.83 width, 0.27 body length, trapezoidal; posterolateral processes 0.20 Plt length, straight.

Antenna I (Fig. 2A) length 0.16 body length; flagellum with 4 articles.

Antenna II (Fig. 2A) length 0.57 body length; flagellum with 12 articles.

Operculum (Fig. 26G) Length 1.0 width, 0.77 Plt length; distal margin with numerous, evenly distributed long setae.

Haploniscus apaticus Knauber & Riehl, sp. nov.

https://zoobank.org/2E90065E-FCEE-470C-9AE0-B173281E7677

Figs 6–9, 26

Holotype. SKB Hap08, adult male (stage VI), 3.3 mm, MIMB 50307.

Paratypes. SKB Hap18, adult female (stage IV), 3.2 mm, MIMB 50308; SKB Hap48, adult female (stage IV; genome), SMF 56565.

Type locality. St. LV71–04–10, RV "Akademik M. A. Lavrentyev", SokhoBio expedition, EBS, 3366 m, 47°12.2'N, 149°36.7'E, Northwest Pacific, Sea of Okhotsk, Kuril Basin.

Further records. St. LV71–02–07: SKB Hap27 (manca) SMF 56544, SKB Hap36 (manca) MIMB 50309; St. LV71–04–09: SKB Hap55 (manca) MIMB 50310, SKB Hap62 (adult male) SMF 56579; St. LV71–10–07: SKB Hap02 (adult female) SMF 56519.

Distribution. Northwest Pacific, Sea of Okhotsk, Kuril Basin, depth 3351–3366 m. Visualized in Fig. 27.

Etymology. "*apaticus*" is a Latinized adjective derived from "Apate", the goddess of deceit in Greek mythology. This name refers to this species' lack of a pronounced sexual dimorphism, e.g., in the pleotelson shape, and overall inconspicuous morphology, keeping it hidden amongst its sibling species until recently. *Haploniscus apaticus* can be interpreted in English as "deceitful or deceptive *Haploniscus*."

Synonymy. *Haploniscus* SO-SO (see Knauber et al. 2022).

Diagnosis. Differs from other species of the *belyaevi*-complex in the following characters: Prn 4 lateral margin longer than Prn 5 lateral margin; Plt posterolateral processes straight, oriented posterolaterally; PV–VII lengths distinctly exceeding PI–IV lengths.

Molecular diagnosis. differing in the COI gene from other species of the *belyaevi*-complex in the nucleotides T (position 69 of the alignment), A (220), A (364), G (412), G (469), A (475), and C (556).

Description. Male. ***Body*** (Fig. 6B) length 2.5 width; oval; anterior body length (Ceph–Prn 4) 1.0 posterior body length (Prn 5–Plt); lateral margin interrupted between Prn 7 and Plt, otherwise continuous.

Cephalothorax (Fig. 6B, D) length 0.41 width, 0.10 body length, width 0.59 body width; frontal margin width 0.48 Ceph width; rostrum curved upwards.

Pereonite 1 (Fig. 6B) posterior tergite margin through Prn 5 anterior tergite margin delicately serrated, setose; Prn 2–5 anterolateral angles slightly projecting; Prn 1–4 posterolateral angles slightly projecting; Prn 4 lateral margin length 1.17 Prn 5 lateral margin length.

Pleotelson (Figs 6B, 26J) length 0.79 width, 0.25 body length, trapezoidal, posterior margin rounded, convex; tergite surface smooth; with posterolateral tergal ridge between uropod insertion and posterolateral process; posterolateral processes short, 0.35 Plt length, straight, oriented posterolaterally.

Antenna I (Fig. 7E) length 0.16 body length; flagellum with 5 articles.

Antenna II (Fig. 7A) length 0.69 body length; article 3 dorsal projection triangular, projection length 0.38 article 3 length; article 5 projection length 0.43 article 5 length; flagellum with 19 articles.

Mandible (Fig. 8B, C) incisor with 5 cusps, left Md *lacinia mobilis* with 4 cusps.

Maxillipeds (Fig. 8A) left Mxp with 4 coupling hooks; right Mxp with 3 coupling hooks.

Pereopod II (Fig. 7C) length 0.34 body length. **PIII** length 0.35 body length. **PIV** length 0.37 body length.

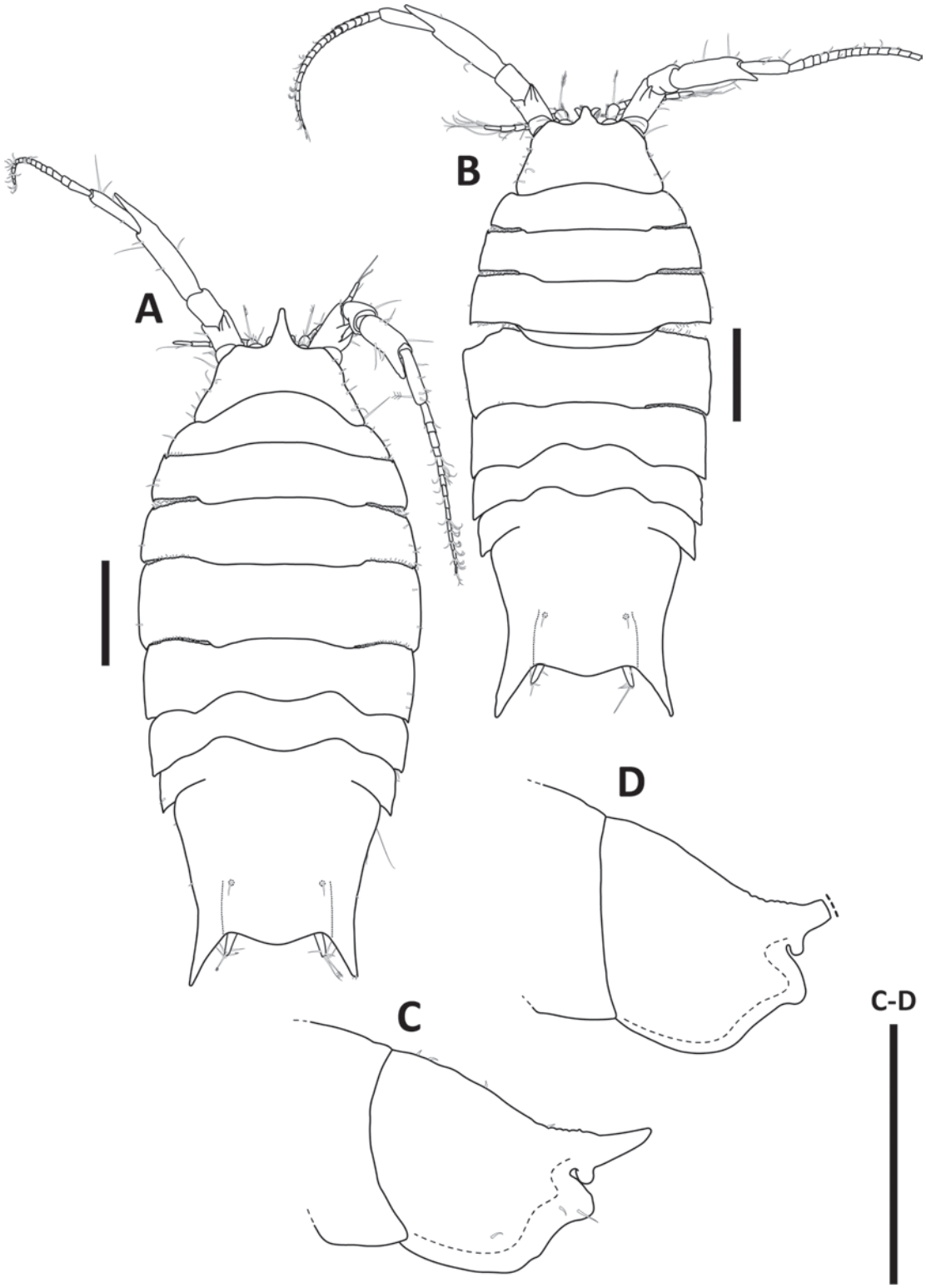

Figure 6. *Haploniscus apaticus* sp. nov. female paratype, SKB Hap18 (**A, C**); male holotype SKB Hap08 (**B, D**). **A, B.** Habitus, dorsal view; **C, D.** Head, lateral view. Scale bars: 0.5 mm.

PV length 0.64 body length. **PVI** (Fig. 7D) length 0.68 body length. **PVII** length 0.62 body length; PV–VII lengths distinctly exceeding PI–IV lengths, PVII shorter than PVI.

Pleopod I (Figs 9A, 26J) medial lobes subtriangular, projecting caudolaterally; adjoining at the apex.

Pleopod II (Fig. 9B, C) protopod semi-circular, with distal lobe extending beyond protopod distal margin; endopod stylet 1.8 protopod length.

Female. Differs from male in the following characters:

Body (Fig. 6A) length 2.4 width; anterior body length (Ceph–Prn 4) 0.95 posterior body length (Prn 5–Plt).

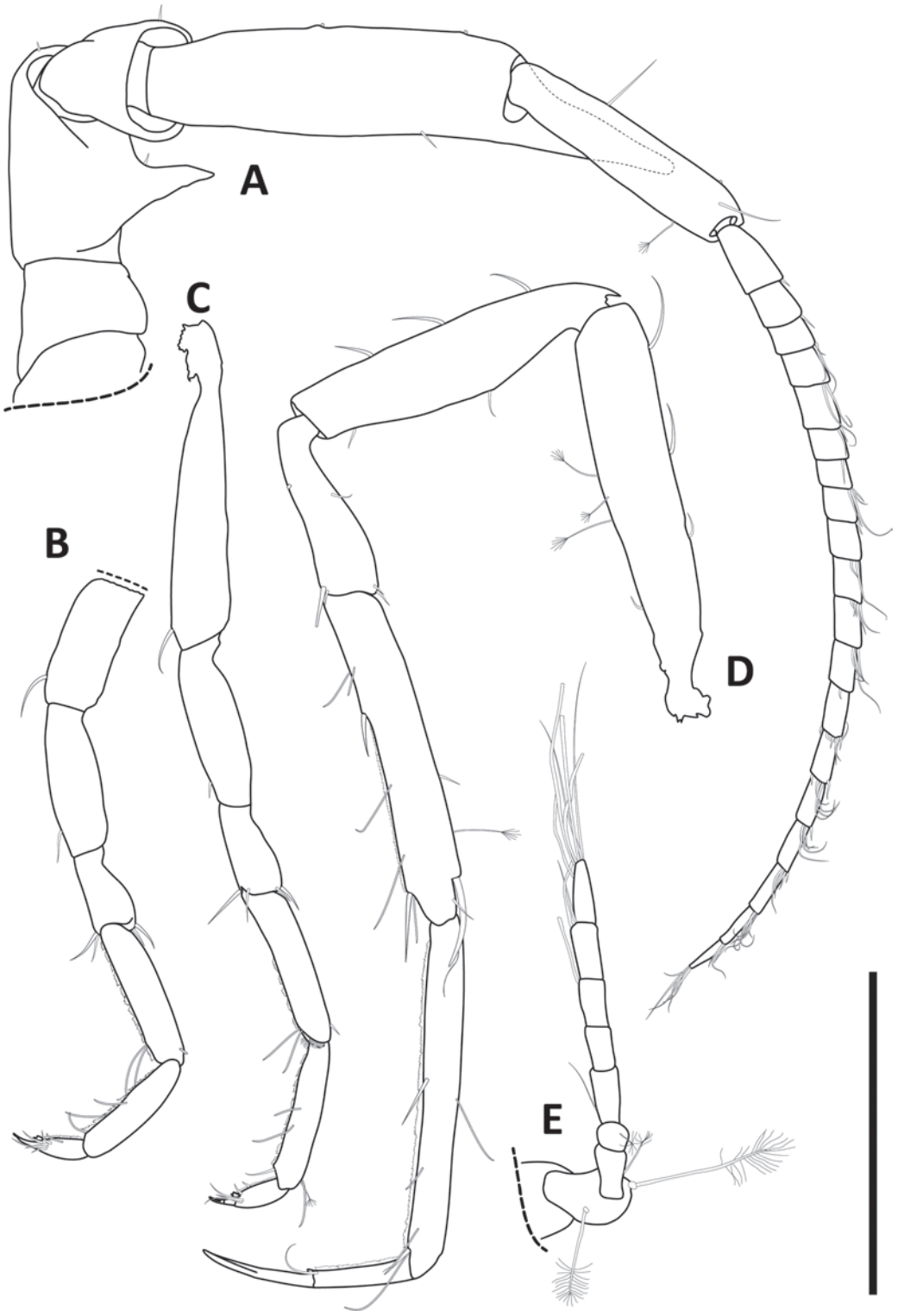

Figure 7. *Haploniscus apaticus* sp. nov. male holotype, SKB Hap08. **A.** Antenna II; **B.** Pereopod I; **C.** Pereopod II; **D.** Pereopod VI; **E.** Antenna I. Scale bar: 0.4 mm.

Cephalothorax (Fig. 6A, C) length 0.26 width, 0.07 body length, width 0.60 body width; frontal margin width 0.51 Ceph width.

Pereonite 4 (Fig. 6A) lateral margin length 1.24 Prn 5 lateral margin length.

Pleotelson (Figs 6A, 26I) length 0.81 width, 0.25 body length; posterolateral processes 0.32 Plt length.

Antenna I (Fig. 6A) length 0.14 body length; flagellum with 4 articles.

Antenna II (Fig. 6A) length 0.63 body length; flagellum with 16 articles.

Operculum (Fig. 26I) length 0.97 width, 0.81 Plt length; distal margin with numerous, evenly distributed long setae; lateral margins with fewer, evenly distributed short setae.

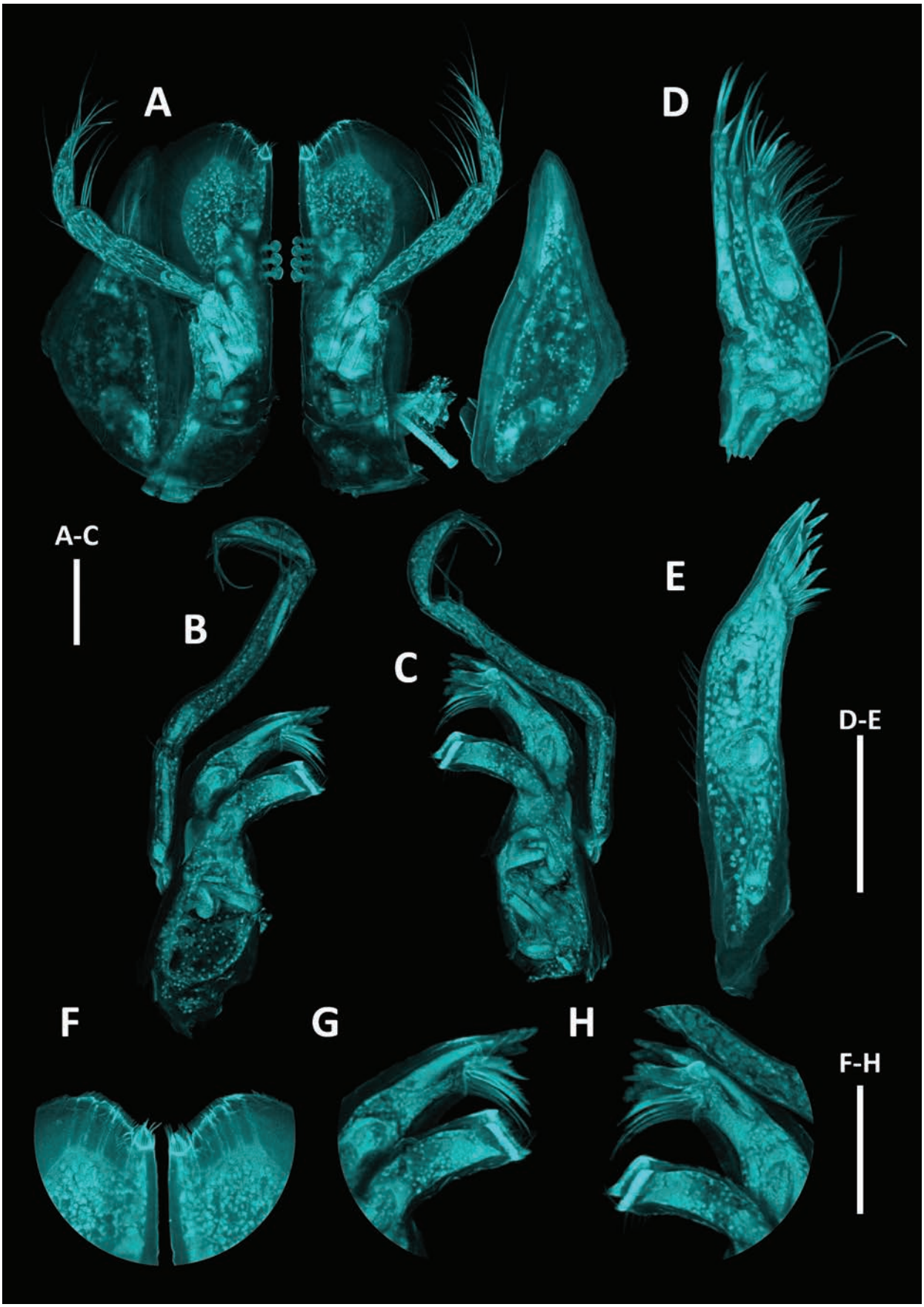

Figure 8. *Haploniscus apaticus* sp. nov. male holotype, SKB Hap08. **A.** maxillipeds; **B.** Right mandible; **C.** Left mandible; **D.** Maxilla II; **E.** Maxilla I; **F.** Maxillipeds, detail of distomedial margins of endites; **G.** Right mandible, detail of incisor and molar process; **H.** Left mandible, detail of incisor, *lacinia mobilis*, and molar process. Scale bars: 0.1 mm.

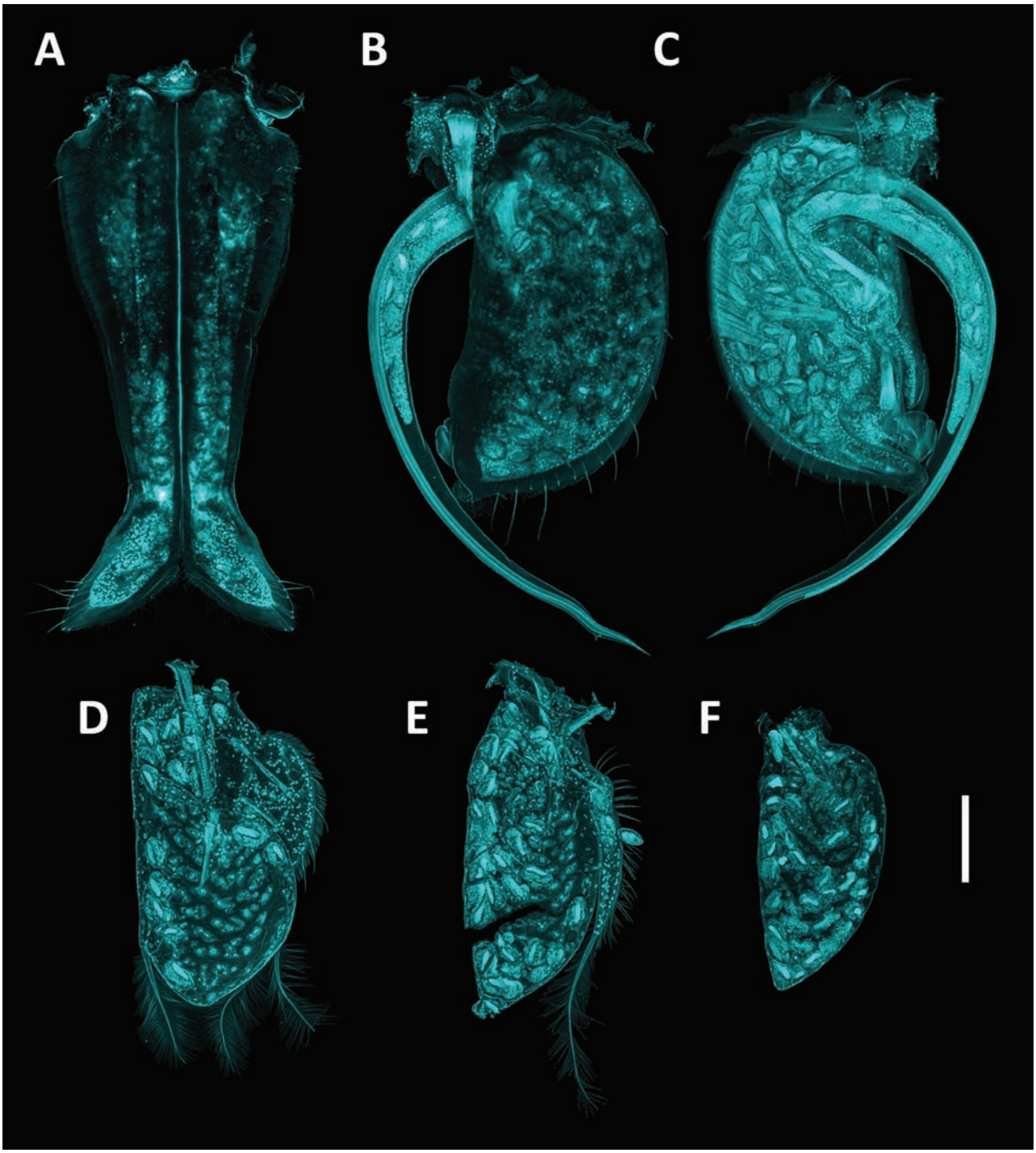

Figure 9. *Haploniscus apaticus* sp. nov. male holotype, SKB Hap08. **A.** Pleopod I; **B.** Pleopod II, ventral view; **C.** Pleopod II, dorsal view; **D.** Pleopod III; **E.** Pleopod IV; **F.** Pleopod V. Scale bar: 0.25 mm.

Haploniscus erebus Knauber & Riehl, sp. nov.

https://zoobank.org/0CA1699A-04CF-4332-A6B8-F9AA1DD108B4

Figs 1, 10–13, 26

Holotype. SKB Hap54, adult male (stage VI), 3.3 mm, MIMB 50317.

Paratypes. SKB Hap49, adult female (stage IV; genome), SMF 56566; SKB Hap50, adult female (stage IV), 3.3 mm, MIMB 50315.

Type locality. St. LV71–02–07, RV "Akademik M. A. Lavrentyev", SokhoBio expedition, EBS, 3352 m, 46°40.9'N, 147°28.5'E, Northwest Pacific, Sea of Okhotsk, Kuril Basin.

Further records. St. LV71–02–07: SKB Hap26 (manca) MIMB 50312, SKB Hap28 (manca) MIMB 50313; St. LV71–04–09: SKB Hap10 (manca) MIMB 50311; St. LV71–04–10: SKB Hap09 (manca) SMF 56526; St. LV71–11–06: SKB Hap29 (manca) MIMB 50314, SKB Hap30 (manca) SMF 56547, SKB Hap31 (manca) SMF 56548, SKB Hap51 (manca) MIMB 50316, SKB Hap52 (manca) SMF 56569, SKB Hap53 (manca) SMF 56570, SKB Hap63 (manca) SMF 56580.

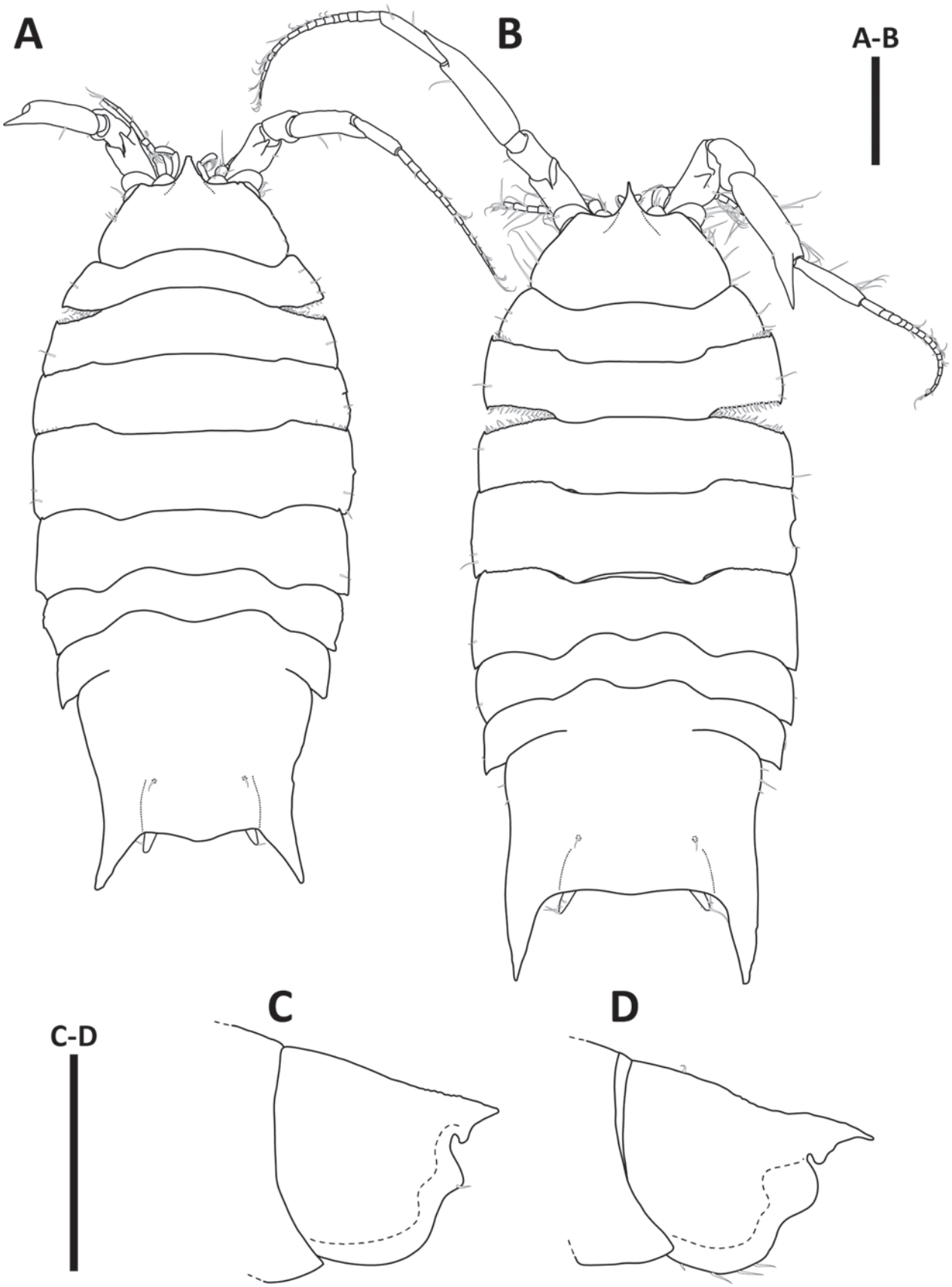

Figure 10. *Haploniscus erebus* sp. nov. female paratype, SKB Hap50 (**A, C**); male holotype SKB Hap54 (**B, D**). **A, B.** Habitus, dorsal view; **C, D.** Head, lateral view. Scale bars: 0.5 mm.

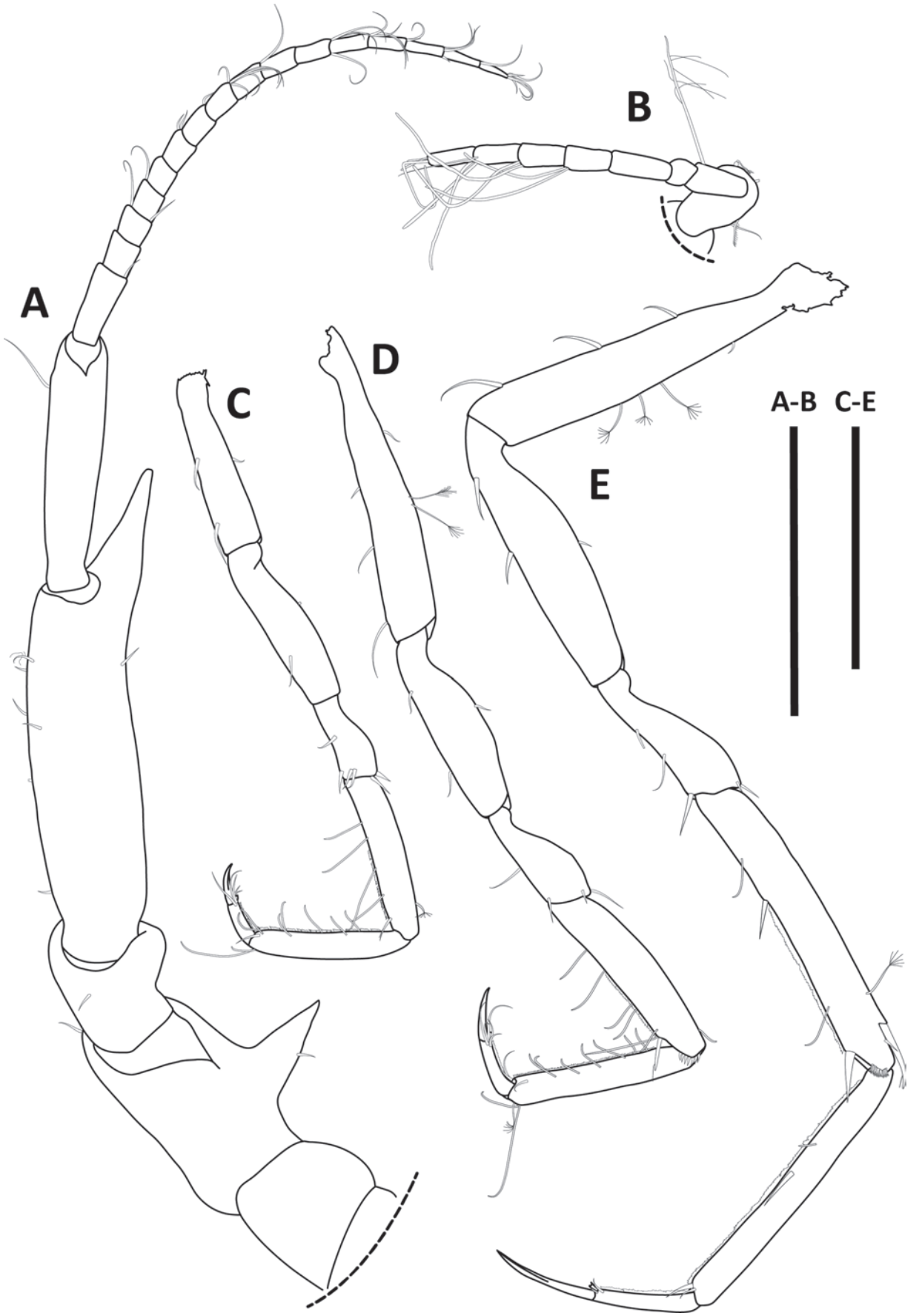

Figure 11. *Haploniscus erebus* sp. nov. male holotype, SKB Hap54. **A.** Antenna II; **B.** Antenna I; **C.** Pereopod I; **D.** Pereopod II; **E.** Pereopod VI. Scale bars: 0.4 mm.

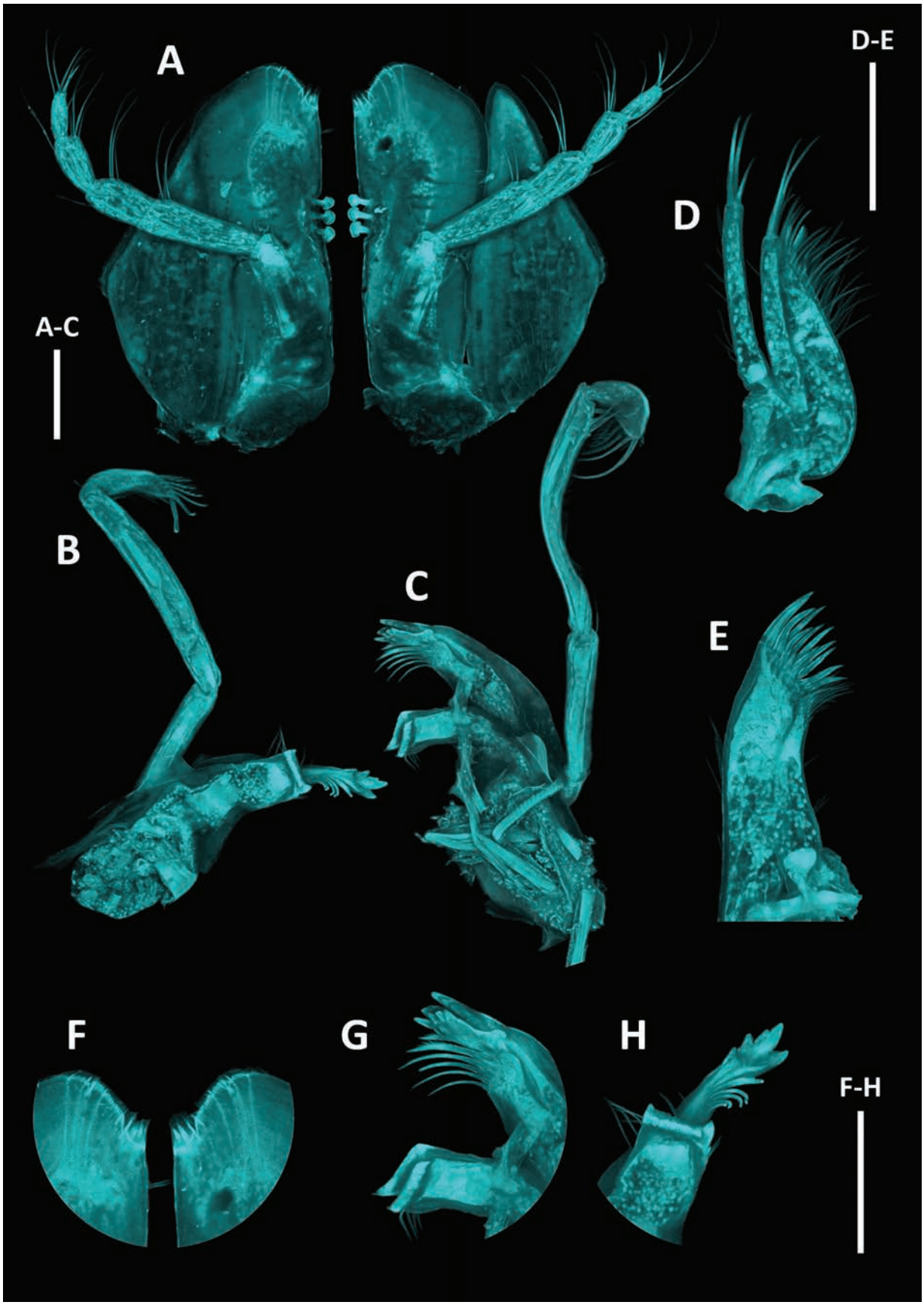

Figure 12. *Haploniscus erebus* sp. nov. male holotype, SKB Hap54. **A.** Maxillipeds; **B.** Right mandible; **C.** Left mandible; **D.** Maxilla II; **E.** Maxilla I; **F.** Maxilliped, right, detail of distomedial margin of endite; **G.** Maxilliped, left, detail of distomedial margin of endite; **H.** Right mandible, detail of incisor and molar process; **I.** Left mandible, detail of incisor, *lacinia mobilis*, and molar process. Scale bars: 0.1 mm.

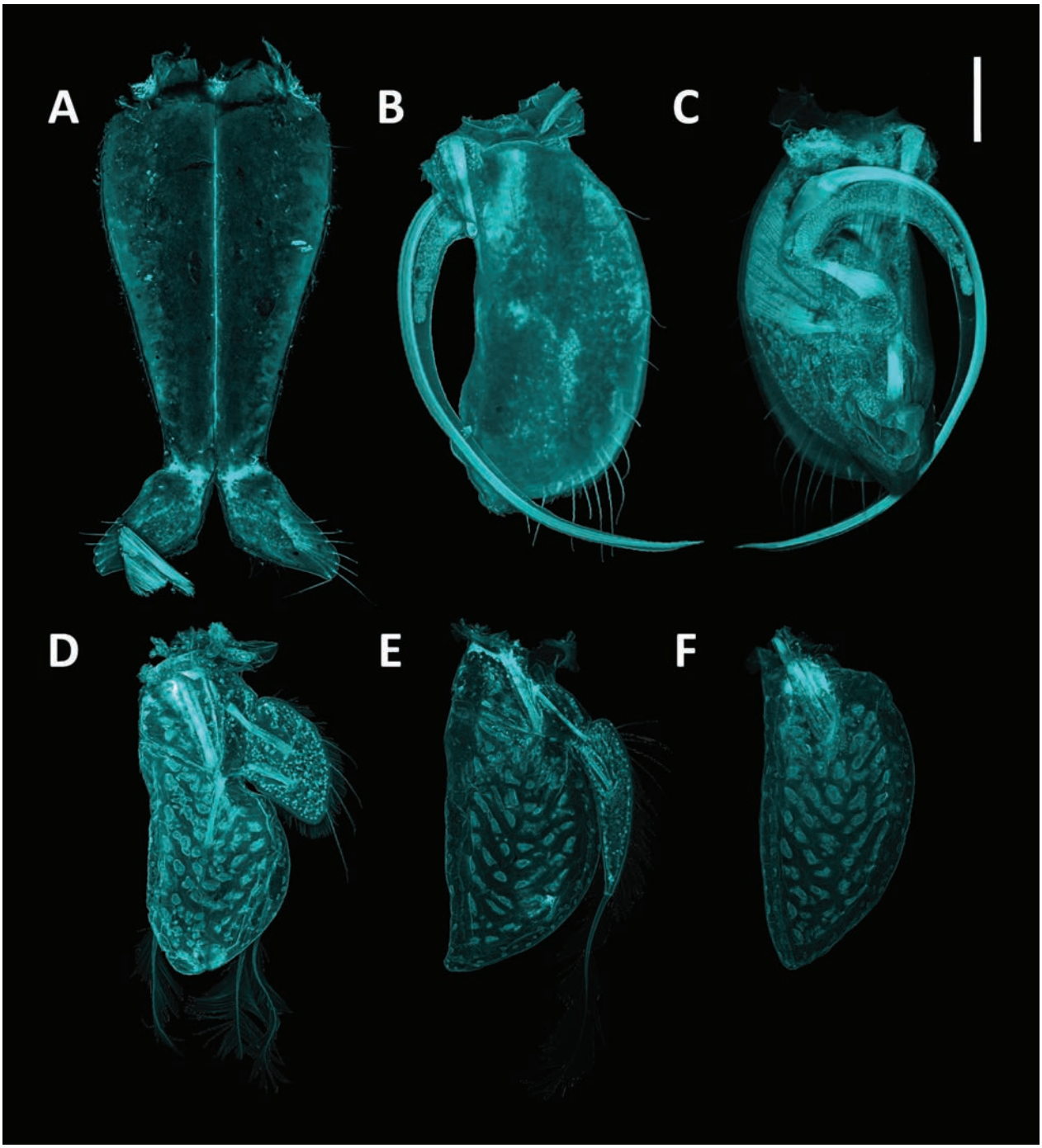

Figure 13. *Haploniscus erebus* sp. nov. male holotype, SKB Hap54. **A.** Pleopod I; **B.** Pleopod II, ventral view; **C.** Pleopod II, dorsal view; **D.** Pleopods III; **E.** Pleopod IV; **F.** Pleopod V. Scale bar: 0.25 mm.

Distribution. Northwest Pacific, Sea of Okhotsk, Kuril Basin, depth 3210–3366 m. Visualized in Fig. 27.

Etymology. From "Erebus" (Ancient Greek: Ἔρεβος), the Greek mythological personification of darkness. It is a noun in apposition.

Synonymy. *Haploniscus* aff. *belyaevi* (see Knauber et al. 2022).

Diagnosis. *Haploniscus erebus* sp. nov. differs from other species of the *belyaevi*-complex in the following characters: rostrum straight, near triangular in lateral view; Plt shape rectangular, posterior margin straight in males; posterolateral processes long, more than 0.50 Plt length in males, straight, oriented posteriorly.

Molecular diagnosis. Differing in the 16S gene from other species of the *belyaevi*-complex in the nucleotides G (position 56 of the alignment), G (64), T (66), G (71), - (150), A (155), T (156), A (204), G (206), C (243), C (342), A (350), G (355), and C (358) as well as the nucleotides T (151), T (154), T (268), T (284), A (286), C (301), G (313), T (352), G (376), C (385), C (388), T (418), A (436), T (451), G (472), G (475), G (502), G (562), and G (565) of the COI gene.

Description. Male. ***Body*** (Figs 1C, 10B) length 2.2 width; subrectangular; anterior body length (Ceph–Prn 4) 1.1 posterior body length (Prn 5–Plt); lateral margin interrupted between Prn 7 and Plt, otherwise continuous.

Cephalothorax (Figs 1C, 10B, D) length 0.45 width, 0.13 body length, width 0.61 body width; frontal margin width 0.50 Ceph width; rostrum straight, near triangular laterally.

Pereonite 1 (Figs 1C, 10B) posterior tergite margin through Prn 5 anterior tergite margin delicately serrated, setose; Prn 2–5 anterolateral angles slightly projecting; Prn 2–4 posterolateral angles slightly projecting; Prn 4 lateral margin length 0.89 Prn 5 lateral margin length.

Pleotelson (Figs 1C, 10B, 26B) length 0.64 width, 0.23 body length, rectangular, posterior margin straight; tergite surface smooth; with posterolateral tergal ridge between uropod insertion and posterolateral process; posterolateral processes long, 0.53 Plt length, straight, oriented posteriorly.

Antenna I (Fig. 11B) length 0.18 body length; flagellum with 6 articles.

Antenna II (Fig. 11A) length 0.68 body length; article 3 dorsal projection triangular, projection length 0.42 article 3 length; article 5 projection length 0.28 article 5 length; flagellum with 16 articles.

Mandible (Fig. 12B, C) incisor with 5 cusps, left Md *lacinia mobilis* with 5 cusps.

Maxillipeds (Fig. 12A) with 3 coupling hooks each.

Pereopod I (Fig. 11C) length 0.43 body length. **PII** (Fig. 11D) length 0.49 body length. **PIII** length 0.58 body length. **PIV** length 0.60 body length. **PV** length 0.75 body length. **PVI** (Fig. 11E) length 0.81 body length. **PVII** length 0.79 body length; P lengths gradually increasing from PI to PVI, PVII shorter than PVI.

Pleopod I (Figs 13A, 26B) medial lobes subtriangular, projecting caudolaterally; separated at the apex by a narrow gap.

Pleopod II (Fig. 13B, C) protopod semi-circular, with distal lobe extending beyond protopod distal margin; endopod stylet 1.8 protopod length.

Female. Differs from male in the following characters:

Body (Fig. 10A) length 2.3 width; oval; anterior body length (Ceph–Prn 4) 0.99 posterior body length (Prn 5–Plt).

Cephalothorax (Fig. 10A, C) length 0.36 width, 0.09 body length, width 0.59 body width; frontal margin width 0.55 Ceph width.

Pereonite 4 (Fig. 10A) lateral margin length 1.0 Prn 5 lateral margin length.

Pleotelson (Figs 10A, 26A) length 0.74 width, 0.24 body length, trapezoidal, posterior margin rounded, convex; posterolateral processes short, 0.34 Plt length, oriented posterolaterally.

Antenna I (Fig. 10A) length 0.14 body length; flagellum with 4 articles.

Antenna II (Fig. 10A) length 0.61 body length; flagellum with 13 articles.

Operculum (Fig. 26A) length 0.93 width, 0.81 Plt length; distal margin with numerous, evenly distributed long setae; lateral margins with fewer, evenly distributed short setae.

Haploniscus hades Knauber & Riehl, sp. nov.

https://zoobank.org/07F6AD09-20C0-4726-B3B7-774BCFC5785F

Figs 1, 14–17, 26

Holotype. KBII Hap137, adult male (stage VI), 3.7 mm, SMF 56419.

Paratypes. KBII Hap104, adult female (stage IV; genome), SMF 56388; KBII Hap213, adult female (stage IV), 2.4 mm, SMF 56495.

Type locality. St. SO250–042, RV "Sonne", KuramBio II expedition, EBS, 7123 m, 45°39.62'N, 152°56.39'E, Northwest Pacific, hadal Kuril-Kamchatka Trench near Bussol Strait.

Further records. St. SO250–020: KBII Hap116 (adult female) SMF 56399; St. SO250–028: KBII Hap208 (adult male) SMF 56490; St. SO250–030: KBII Hap209 (manca) SMF 56491, KBII Hap210 (adult female) SMF 56492; St. SO250–040: KBII Hap220 (ovigerous female) SMF 56502, KBII Hap221 (ovigerous female) SMF 56503, KBII Hap231 (manca) SMF 56513, KBII Hap232 (manca) SMF 56514; St. SO250–042: KBII Hap105 (manca) SMF 56389, KBII Hap106 (manca) SMF 56390, KBII Hap165 (adult male) SMF 56447, KBII Hap198 (manca) SMF 56480, KBII Hap230 (manca) SMF 56512; St. SO250–086: KBII Hap226 (adult male) SMF 56508; St. SO250–097: KBII Hap201 (manca) SMF 56483, KBII Hap204 (adult male) SMF 56486, KBII Hap205 (adult female) SMF 56487, KBII Hap206 (ovigerous female) SMF 56488, KBII Hap214 (manca) SMF 56496, KBII Hap215 (adult female) SMF 56497, KBII Hap216 (adult male) SMF 56498, KBII Hap217 (adult female) SMF 56499, KBII Hap227 (manca) SMF 56509, KBII Hap233 (manca) SMF 56515, KBII Hap234 (manca) SMF 56516; St. SO250–098: KBII Hap203 (manca) SMF 56485.

Distribution. Northwest Pacific, Kuril-Kamchatka Trench, depth 5493–8191 m. Visualized in Fig. 27.

Etymology. The specific epithet "*hades*" is a noun in apposition derived from "Hades" (Ancient Greek: Ἅιδης), the god and ruler of the underworld in Greek mythology. This name refers to this species distributional range within the hadal depths of the Kuril-Kamchatka Trench and the novel feature of the pleotelson posterior margin tergal plates projecting above the uropods in males. These render the uropods "invisible" from dorsal view, reminiscent of Hades' cap of invisibility.

Synonymy. *Haploniscus* KKT hadal (see Knauber et al. 2022).

Diagnosis. *Haploniscus hades* sp. nov. differs from other species of the *belyaevi*-complex in the following characters: rostrum curved upwards, basally with dorsal bulge in males; Plt with posterolateral tergal ridge on posterolateral process and posterior margin tergal plates projecting above uropods (solely present in sister species *H. kerberos* sp. nov. otherwise); AII article 3 dorsal projection hook-shaped; Plp I distally with hook-shaped projection.

Molecular diagnosis. Differing in the 16S gene from other species of the *belyaevi*-complex in the nucleotide A (position 219 of the alignment) as well as the nucleotides

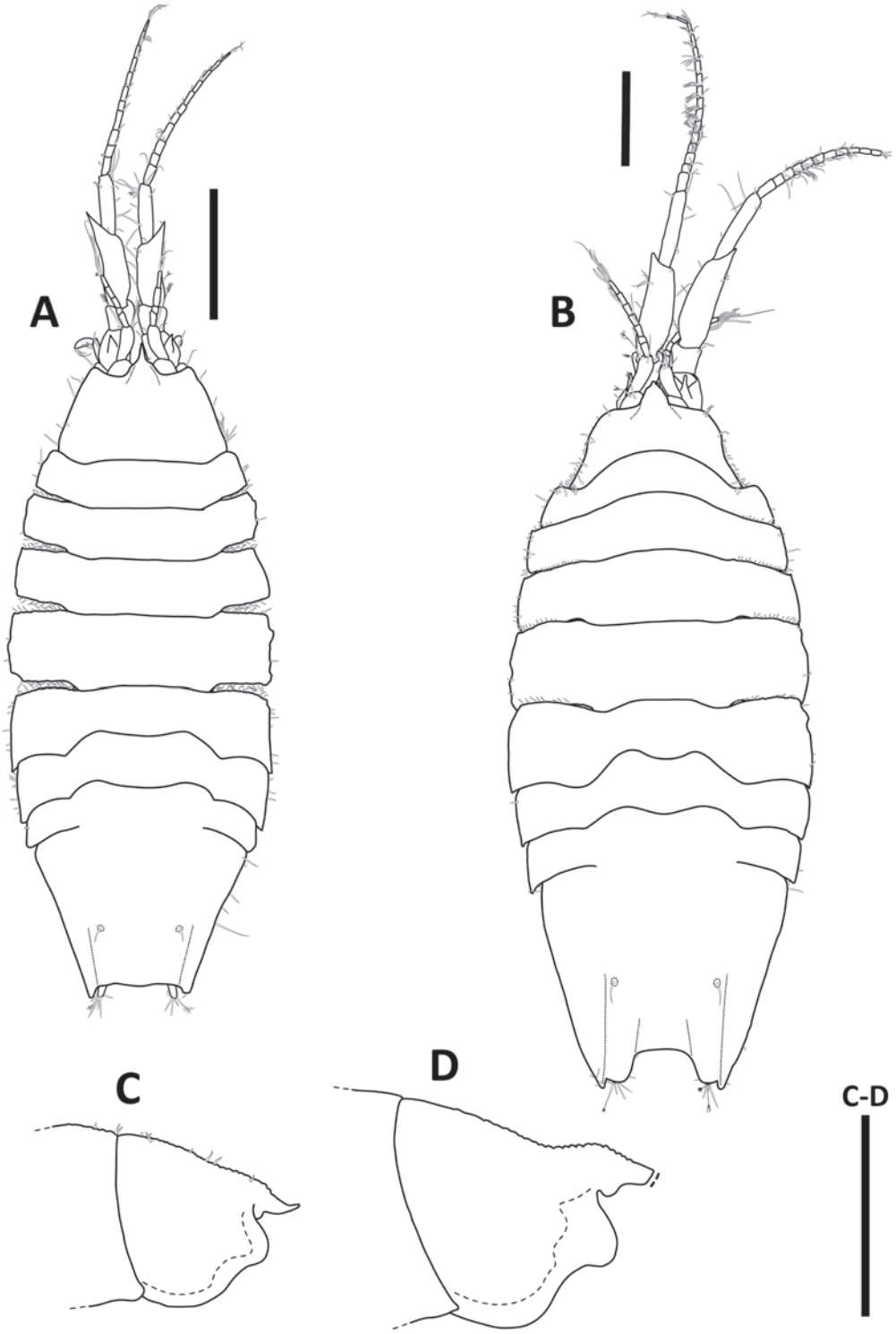

Figure 14. *Haploniscus hades* sp. nov. female paratype, KBII Hap213 (**A, C**); male holotype KBII Hap137 (**B, D**). **A, B.** Habitus, dorsal view; **C, D.** Head, lateral view. Scale bars: 0.5 mm.

G (103), A (211), T (217), C (232), G (256), T (328), A (349), C (364), C (370), C (442), A (469), C (499), and C (571) of the COI gene.

Description. Male. ***Body*** (Figs 1A, 14B) length 2.3 width; oval; anterior body length (Ceph–Prn 4) 0.84 posterior body length (Prn 5–Plt); lateral margin continuous.

Cephalothorax (Figs 1A, 14B, D) length 0.28 width, 0.07 body length, width 0.56 body width; frontal margin width 0.53 Ceph width; rostrum curved upwards, basally with dorsal bulge.

Pereonite 1 (Figs 1A, 14B) posterior tergite margin through Prn 5 anterior tergite margin delicately serrated, setose; Prn 2–4 anterolateral angles slightly projecting; Prn 2–4 posterolateral angles slightly projecting; Prn 4 lateral margin length 0.89 Prn 5 lateral margin length; Prn 5 anterolateral angle not projecting, rectangular.

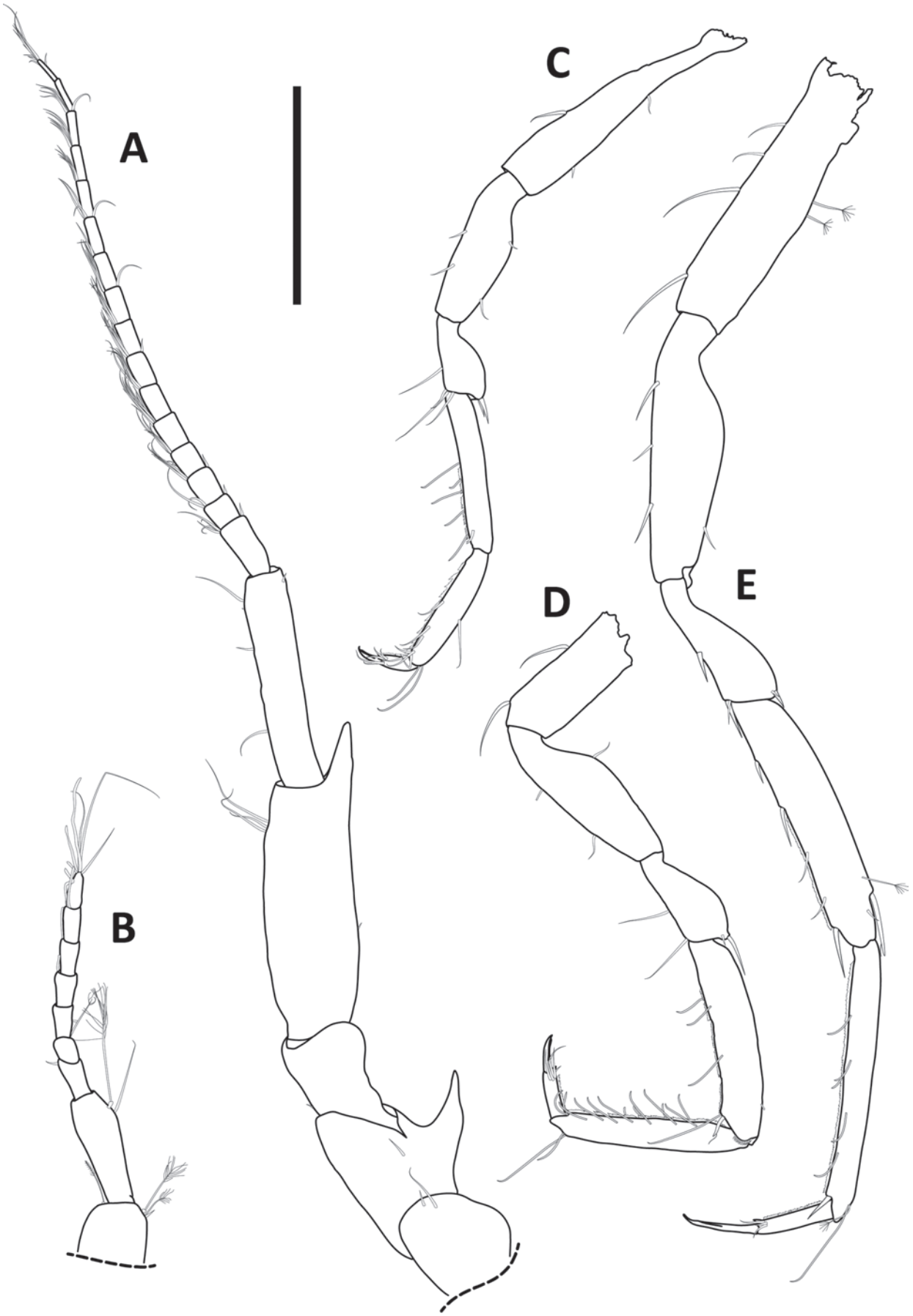

Figure 15. *Haploniscus hades* sp. nov. male holotype, KBII Hap137. **A.** Antenna II; **B.** Antenna I; **C.** Pereopod I; **D.** Pereopod II; **E.** Pereopod VI. Scale bar: 0.4 mm.

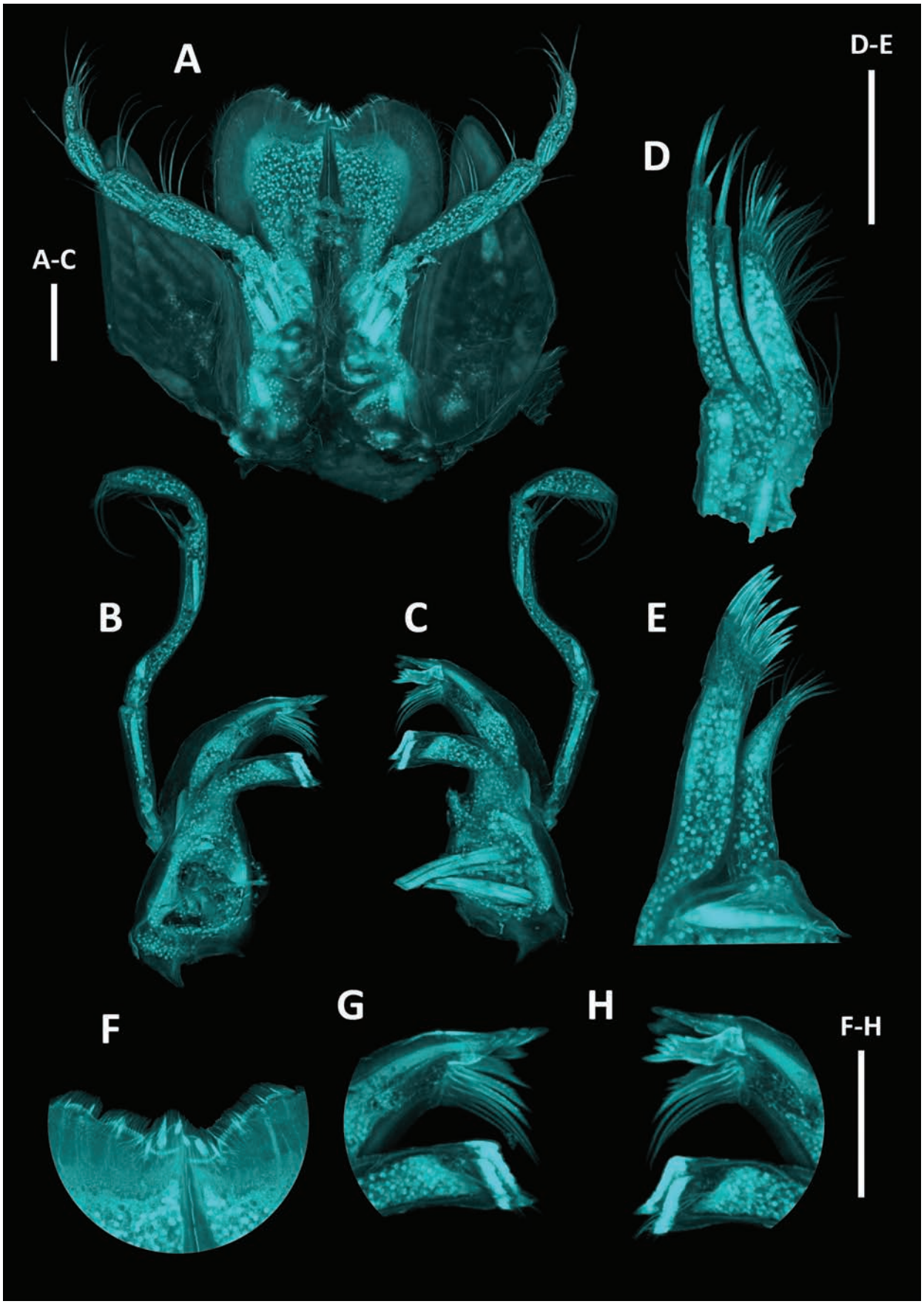

Figure 16. *Haploniscus hades* sp. nov. male holotype, KBII Hap137. **A.** Maxillipeds; **B.** Right mandible; **C.** Left mandible; **D.** Maxilla II; **E.** Maxilla I; **F.** Maxillipeds, detail of distomedial margins of endites; **G.** Right mandible, detail of incisor and molar process; **H.** Left mandible, detail of incisor, *lacinia mobilis*, and molar process. Scale bars: 0.1 mm.

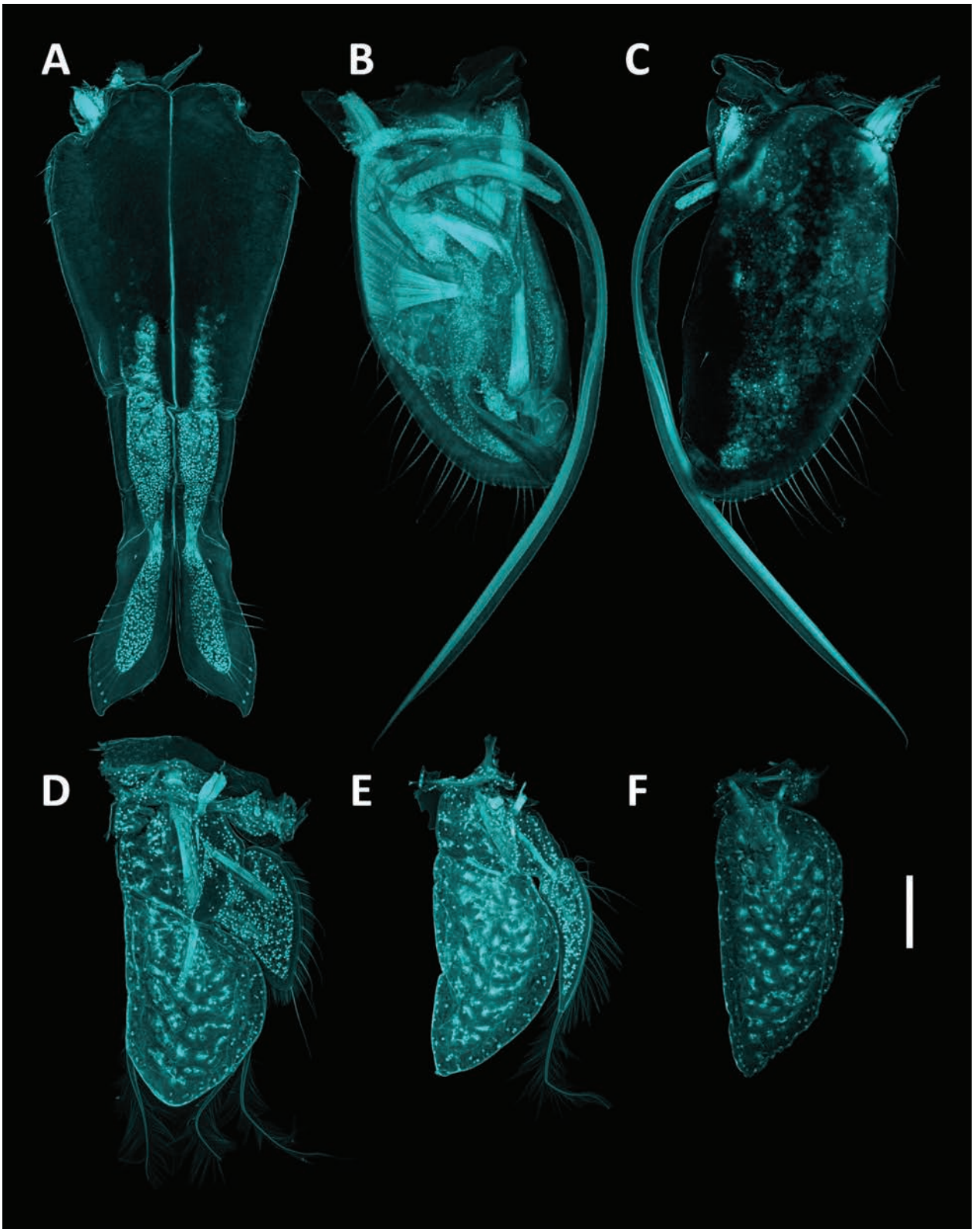

Figure 17. *Haploniscus hades* sp. nov. male holotype, KBII Hap137. **A.** Pleopod I; **B.** Pleopod II, dorsal view; **C.** Pleopod II, ventral view; Pleopod III; **D.** Pleopod IV; **E.** Pleopod V. Scale bar: 0.25 mm.

Pleotelson (Figs 1A, 14B, 26F) length 0.75 width, 0.27 body length, trapezoidal, posterior margin concave; tergite surface tuberculate, less distinct than in remaining body; with posterolateral tergal ridge on posterolateral process and posterior margin tergal plates projecting above uropods; posterolateral processes minute, 0.04 Plt length, straight, oriented posteriorly.

Antenna I (Fig. 15B) length 0.17 body length; flagellum with 6 articles.

Antenna II (Fig. 15A) length 0.67 body length; article 3 dorsal projection hook-shaped, projection length 0.39 article 3 length; article 5 projection length 0.26 article 5 length; flagellum with 16 articles.

Mandible (Fig. 16B, C) incisor with 6 cusps, left Md *lacinia mobilis* with 5 cusps.

Maxillipeds (Fig. 16A) with 3 coupling hooks each.

Pereopod I (Fig. 15C) length 0.41 body length. **PIII** length 0.53 body length. **PIV** length 0.54 body length. **PV** length 0.67 body length. **PVI** (Fig. 15E) length 0.70 body length. **PVII** length 0.69 body length; P lengths gradually increasing from PI to PVI, PVII shorter than PVI.

Pleopod I (Figs 17A, 26F) medial lobes convexly rounded, tapering to an obtuse point; distally with hook-shaped projection; separated at the apex by a narrow gap.

Pleopod II (Fig. 17B, C) protopod elongated, suboval; endopod stylet 2.0 protopod length.

Female. Differs from male in the following characters:

Body (Fig. 14A) length 2.4 width; anterior body length (Ceph–Prn 4) 1.0 posterior body length (Prn 5–Plt).

Cephalothorax (Fig. 14A, C) length 0.52 width, 0.14 body length, width 0.63 body width; frontal margin width 0.55 Ceph width.

Pereonite 4 (Fig. 14A) lateral margin length 0.93 Prn 5 lateral margin length.

Pleotelson (Figs 14A, 26E) length 0.75 width, 0.25 body length, posterior margin straight; posterolateral processes 0.08 Plt length.

Antenna I (Fig. 14A) length 0.15 body length; flagellum with 4 articles.

Antenna II (Fig. 14A) length 0.70 body length; flagellum with 11 articles.

Operculum (Fig. 26E) length 1.1 width, 0.74 Plt length; distal margin with numerous, evenly distributed long setae; lateral margins with up to 3 short setae each.

Haploniscus kerberos Knauber & Riehl, sp. nov.

https://zoobank.org/29F19A6D-3FCA-4F9E-9454-170905F09E5E

Figs 18–21, 26

Holotype. KBII Hap136, adult male (stage VI), 3.1 mm, SMF 56418.

Paratypes. KBII Hap122, adult female (stage IV; genome), SMF 56405; KBII Hap123, adult female (stage IV), 2.4 mm, SMF 56406.

Type locality. St. SO250–010, RV "Sonne", KuramBio II expedition, EBS, 5120 m, 43°49.43'N, 151°46.96'E, Northwest Pacific, abyssal plains southeast of the Kuril-Kamchatka Trench.

Further records. St. LV71–10–06: SKB Hap13 (manca) MIMB 50318; St. LV71–10–07: SKB Hap01 (ovigerous female) SMF 56518, SKB Hap22 (adult male) SMF 56539, SKB Hap37 (adult male) MIMB 50319; St. SO250–008: KBII Hap200 (manca) SMF 56482, KBII Hap219 (adult female) SMF 56501, KBII Hap229 (manca) SMF 56511; St. SO250–010: KBII Hap119 (adult male) SMF 56402, KBII Hap120 (adult male) SMF 56403, KBII Hap121 (adult female) SMF 56404, KBII Hap135 (ovigerous female) SMF 56417, KBII Hap228 (manca) SMF 56510; St. SO250–065: KBII Hap211 (manca) SMF 56493, KBII Hap212 (manca) SMF 56494; St. SO250–085: KBII Hap222 (adult male) SMF 56504, KBII Hap223 (adult male) SMF 56505, KBII Hap224 (adult male) SMF 56506; St. SO250–087: KBII Hap218 (ovigerous female) SMF 56500, KBII Hap225 (adult male) SMF 56507, KBII Hap235 (ovigerous female) SMF 56517.

Distribution. Northwest Pacific, abyssal regions adjacent to the Kuril-Kamchatka Trench, depth 4469–5755 m. Visualized in Fig. 27.

Etymology. As a noun in apposition, the epithet "*kerberos*" refers to "Kerberos" (Ancient Greek Κέρβερος) from Greek mythology, the creature guarding the gates of the underworld. This name relates to this species' distributional range, which, according to the available data, is limited to the abyssal plains adjacent to the hadal Kuril-Kamchatka Trench.

Synonymy. *Haploniscus* KKT abyssal (see Knauber et al. 2022).

Diagnosis. *Haploniscus kerberos* sp. nov. is highly similar to *H. hades* sp. nov. in also possessing the characteristic Plt shape with posterolateral tergal ridges terminating on the posterolateral processes and the posterior margin tergal plates projecting above the uropods. It differs from its sister species in the following characters: rostrum basally without dorsal bulge in males (basally with dorsal bulge in *H. hades* sp. nov.) and AII article 3 dorsal projection triangular (hook-shaped in *H. hades* sp. nov.).

Molecular diagnosis. differing in the 16S gene from other species of the *belyaevi*-complex in the nucleotides G (position 173 of the alignment) and G (228), as well as the nucleotides T (61), C (91), C (298), G (346), G (430), G (607), T (625), and G (649) of the COI gene.

Description. Male. ***Body*** (Fig. 18B) length 2.5 width; oval; anterior body length (Ceph–Prn 4) 1.1 posterior body length (Prn 5–Plt); lateral margin continuous.

Cephalothorax (Fig. 18B, D) length 0.35 width, 0.08 body length, width 0.59 body width; frontal margin width 0.54 Ceph width; rostrum curved upwards.

Pereonite 1 (Fig. 18B) posterior tergite margin through Prn 5 anterior tergite margin delicately serrated, setose; Prn 2–4 anterolateral angles slightly projecting; Prn 2–4 posterolateral angles slightly projecting; Prn 4 lateral margin length 0.92 Prn 5 lateral margin length; Prn 5 anterolateral angle not projecting, rectangular.

Pleotelson (Figs 18B, 26D) length 0.68 width, 0.22 body length, trapezoidal, posterior margin concave; tergite surface tuberculate, less distinct than in remaining body; with posterolateral tergal ridge on posterolateral process and posterior margin tergal plates projecting above uropods; posterolateral processes minute, 0.09 Plt length, straight, oriented posteriorly.

Antenna I (Fig. 19B) length 0.20 body length; flagellum with 6 articles.

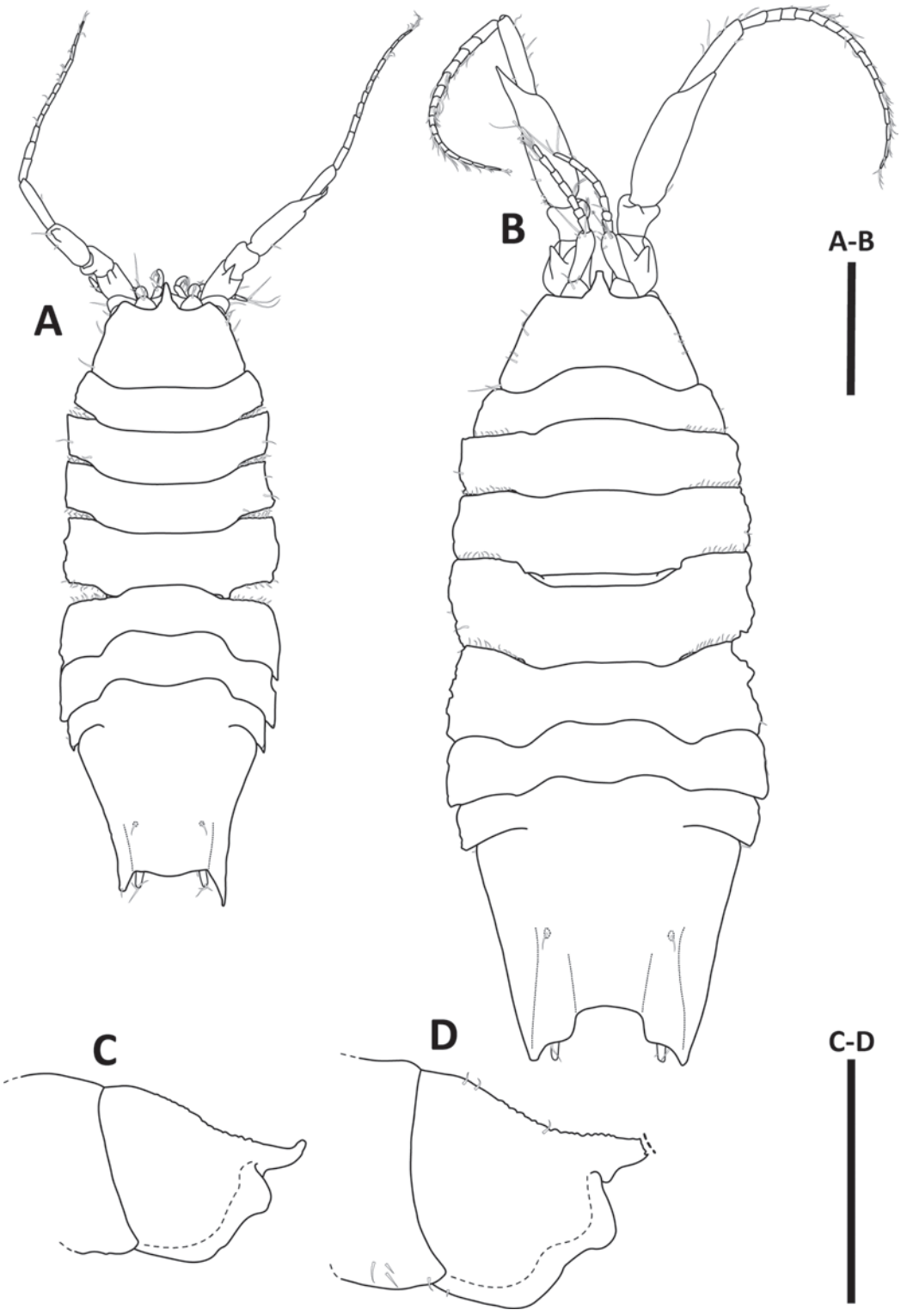

Figure 18. *Haploniscus kerberos* sp. nov. female paratype, KBII Hap123 (**A, C**); male holotype KBII Hap136 (**B, D**). **A, B.** Habitus, dorsal view; **C, D.** Head, lateral view. Scale bars: 0.5 mm.

Antenna II (Fig. 19A) length 0.77 body length; article 3 dorsal projection triangular, projection length 0.31 article 3 length; article 5 projection length 0.22 article 5 length; flagellum with 16 articles.

Mandible (Fig. 20B, C) incisor with 5 cusps, left Md *lacinia mobilis* with 4 cusps.

Maxillipeds (Fig. 20A) with 3 coupling hooks each.

Pereopod I (Fig. 19D) length 0.43 body length. **PVI** (Fig. 19C) length 0.70 body length; P lengths gradually increasing from PI to PVI, PVII shorter than PVI.

Pleopod I missing.

Pleopod II (Fig. 21A, B) protopod elongated, suboval; endopod stylet 2.0 protopod length.

Female. Differs from male in the following characters:

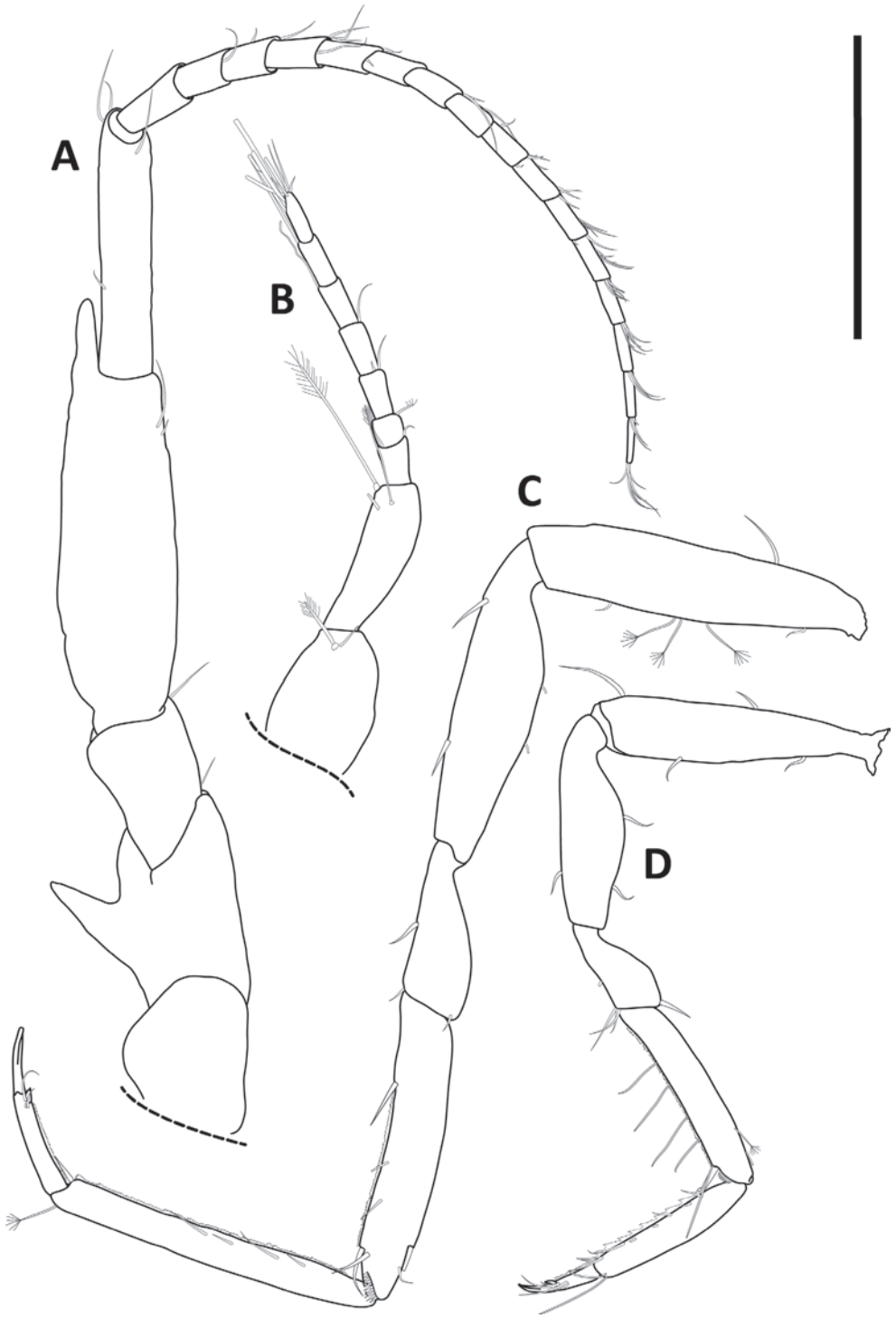

Figure 19. *Haploniscus kerberos* sp. nov. male holotype, KBII Hap136. **A.** Antenna II; **B.** Antenna I; **C.** Pereopod VI; **D.** Pereopod I. Scale bar: 0.4 mm.

Body (Fig. 18A) length 2.7 width; anterior body length (Ceph–Prn 4) 0.94 posterior body length (Prn 5–Plt).

Cephalothorax (Fig. 18A, C) length 0.50 width, 0.12 body length, width 0.66 body width; frontal margin width 0.55 Ceph width.

Pereonite 4 (Fig. 18A) lateral margin length 0.80 Prn 5 lateral margin length.

Pleotelson (Figs 18A, 26C) length 0.84 width, 0.24 body length, posterior margin rounded, convex; with posterolateral tergal ridge between uropod insertion and posterolateral process; posterolateral processes short, 0.23 Plt length.

Antenna I (Fig. 18A) length 0.14 body length; flagellum with 4 articles.

Antenna II (Fig. 18A) length 0.67 body length; flagellum with 12 articles.

Operculum (Fig. 26C) length 1.1 width, 0.75 Plt length; distal margin with numerous, evenly distributed long setae; lateral margins with 2 short setae each.

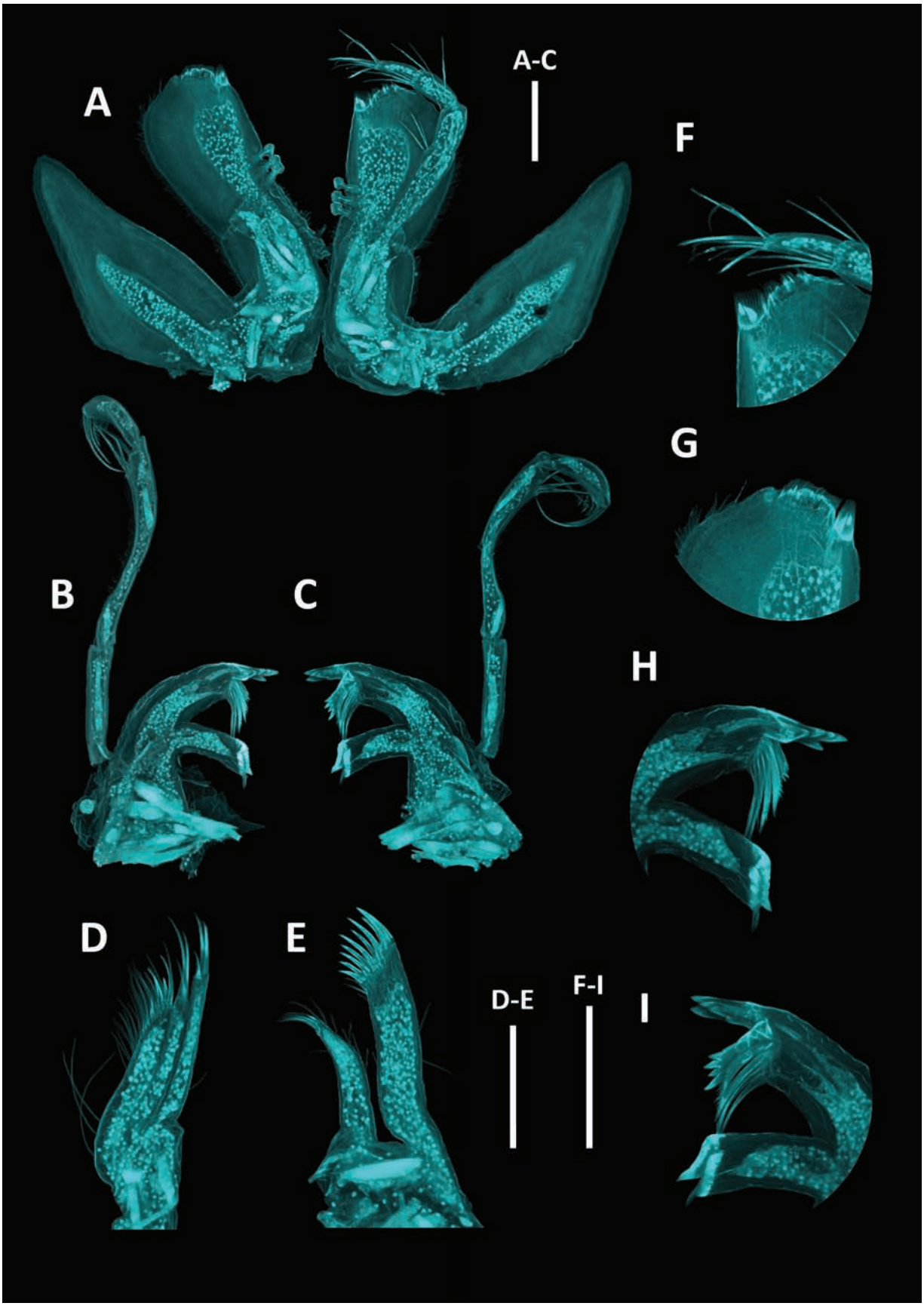

Figure 20. *Haploniscus kerberos* sp. nov. male holotype, KBII Hap136. **A.** Maxillipeds; **B.** Right mandible; **C.** Left mandible; **D.** Maxilla II; **E.** Maxilla I; **F.** Left maxilliped, detail of distomedial margin of endite; **G.** Right maxilliped, detail of distomedial margin of endite; **H.** Right mandible, detail of incisor and molar process; **I.** Left mandible, detail of incisor, *lacinia mobilis*, and molar process. Scale bars: 0.1 mm.

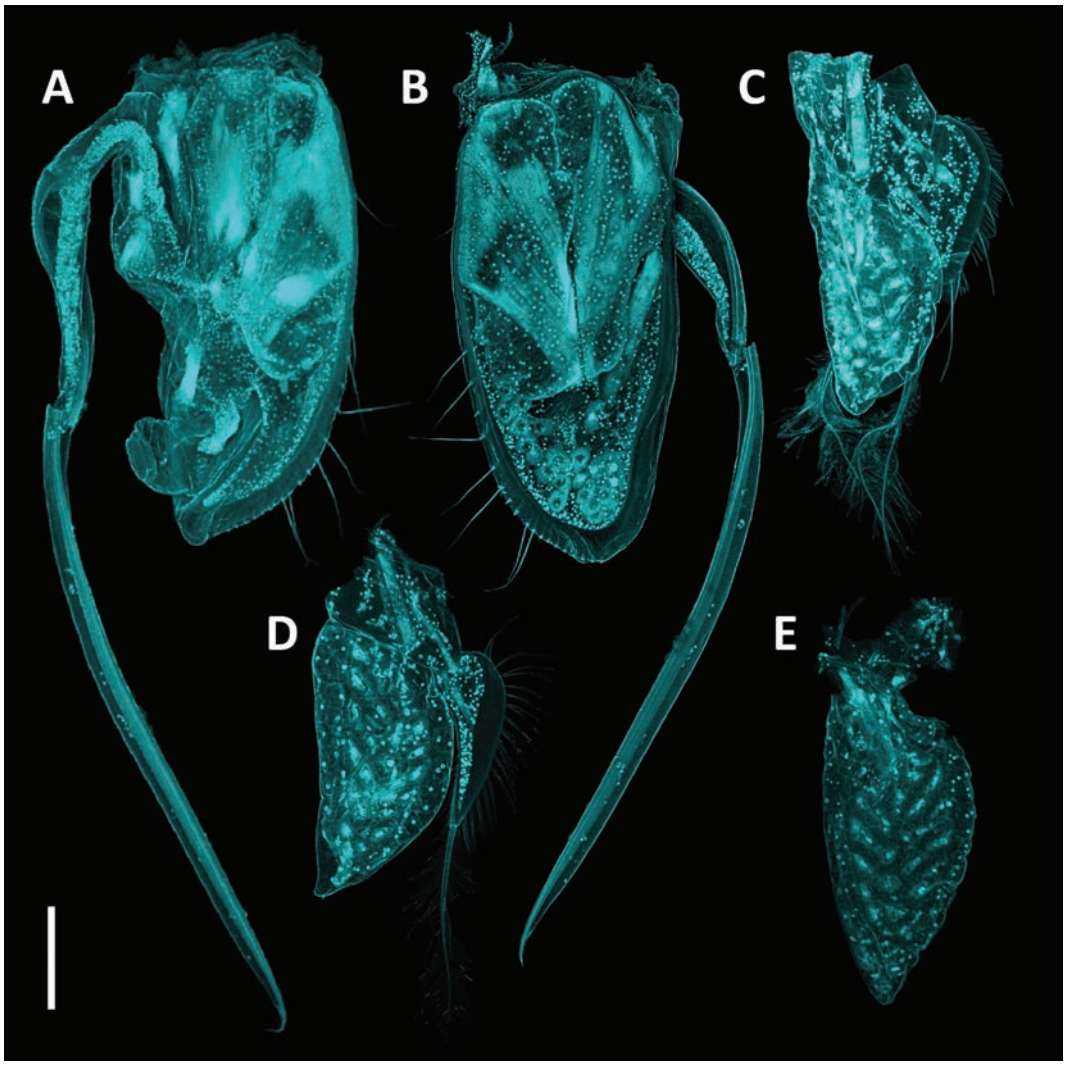

Figure 21. *Haploniscus kerberos* sp. nov. male holotype, KBII Hap136. **A.** Pleopod II, dorsal view; **B.** Pleopod II, ventral view; **C.** Pleopod III; **D.** Pleopod IV; **E.** Pleopod V. Scale bar: 0.25 mm.

Haploniscus nyx Knauber & Riehl, sp. nov.

https://zoobank.org/3AA34260-5C82-45B8-BC35-3779AEE6657E
Figs 22–26

Holotype. SKB Hap34, adult male (stage VI), 3.4 mm, MIMB 50320.

Paratypes. SKB Hap21, adult female (stage IV), 3.0 mm, MIMB 50321.

Type locality. St. LV71–10–07, RV "Akademik M. A. Lavrentyev", SokhoBio expedition, EBS, 4469 m, 46°07.8'N, 152°10.3'E, Northwest Pacific, abyssal branch of the Kuril-Kamchatka Trench into the Bussol Strait.

Further records. St. LV71–10–07: SKB Hap35 (adult male), SMF 56552.

Distribution. Only known from type locality. Northwest Pacific, abyssal region adjacent to the Kuril-Kamchatka Trench to the northwest, depth 4769 m. Visualized in Fig. 27.

Etymology. The epithet "*nyx*," a noun in apposition, is derived from "Nyx" (Ancient Greek Νύξ), the goddess of the night in Greek mythology.

Synonymy. *Haploniscus* SO-WTA (see Knauber et al. 2022).

Diagnosis. *Haploniscus nyx* sp. nov. differs from other species of the *belyaevi*-complex in the following character: pleotelson posterior margin concave in males; Plp I medial lobes convexly rounded, tapering to an obtuse point, distally without a hook-shaped protrusion.

Molecular diagnosis. differing in the 16S gene from other species of the *belyaevi*-complex in the nucleotides G (position 25 of the alignment) and C (312) as well as the nucleotides C (124), G (148), C (193), T (206), C (304), G (334), C (346), G (481), T (496), C (508), C (520), G (553), G (556), and C (628) of the COI gene.

Description. Male. ***Body*** (Fig. 22B) length 2.2 width; subrectangular; anterior body length (Ceph–Prn 4) 0.99 posterior body length (Prn 5–Plt); lateral margin continuous.

Cephalothorax (Fig. 22B, D) length 0.30 width, 0.07 body length, width 0.55 body width; frontal margin width 0.46 Ceph width; rostrum curved upwards.

Pereonite 1 (Fig. 22B) posterior tergite margin through Prn 5 anterior tergite margin delicately serrated, setose;

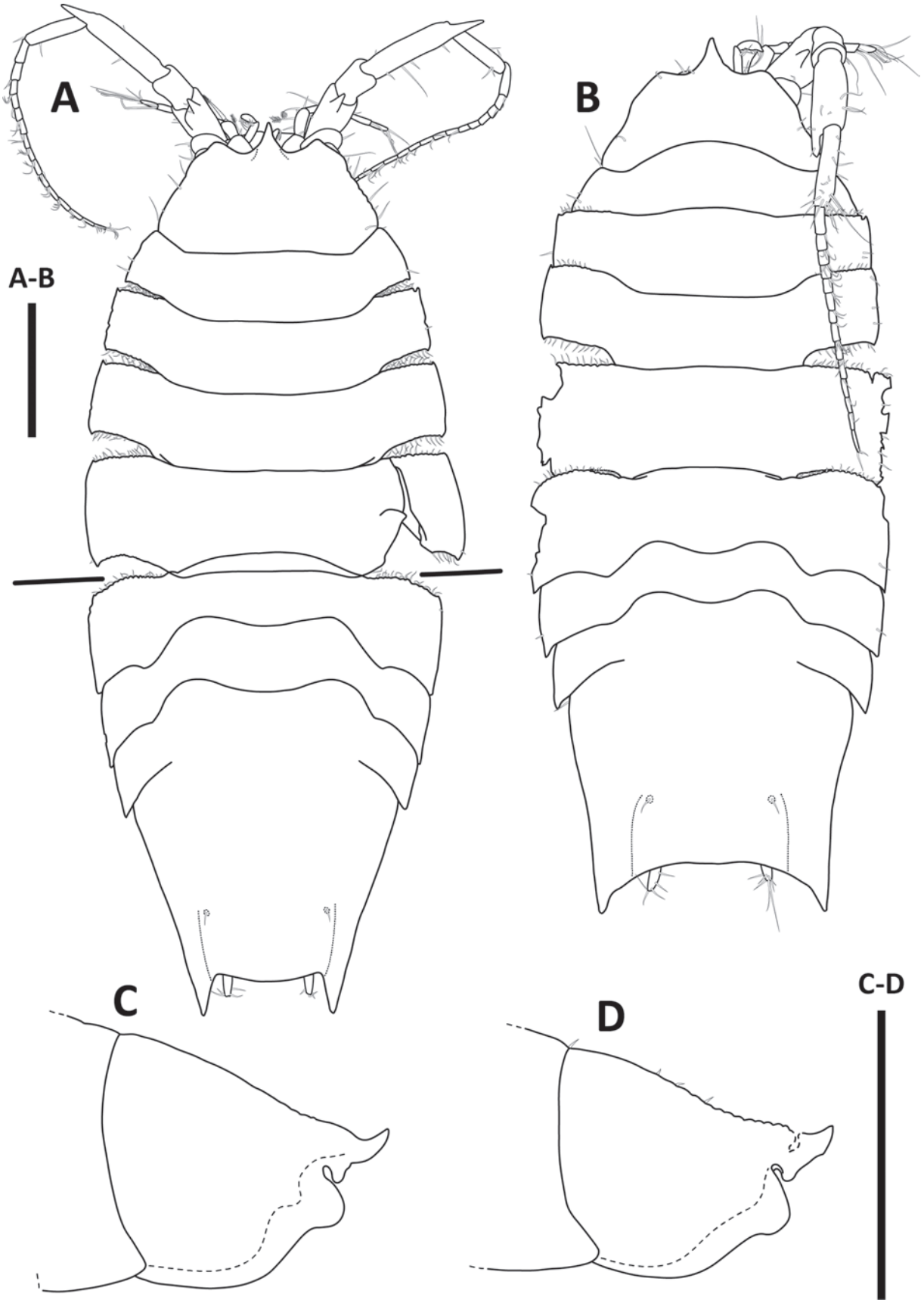

Figure 22. *Haploniscus nyx* sp. nov. female paratype, SKB Hap21 (**A, C**); male holotype SKB Hap34 (**B, D**). **A, B.** Habitus, dorsal view; **C, D.** Head, lateral view. Scale bars: 0.5 mm. Due to pronounced body curvature, the habitus drawing of the female paratype was prepared by two separate drawings, stitching them together along the illustrated line.

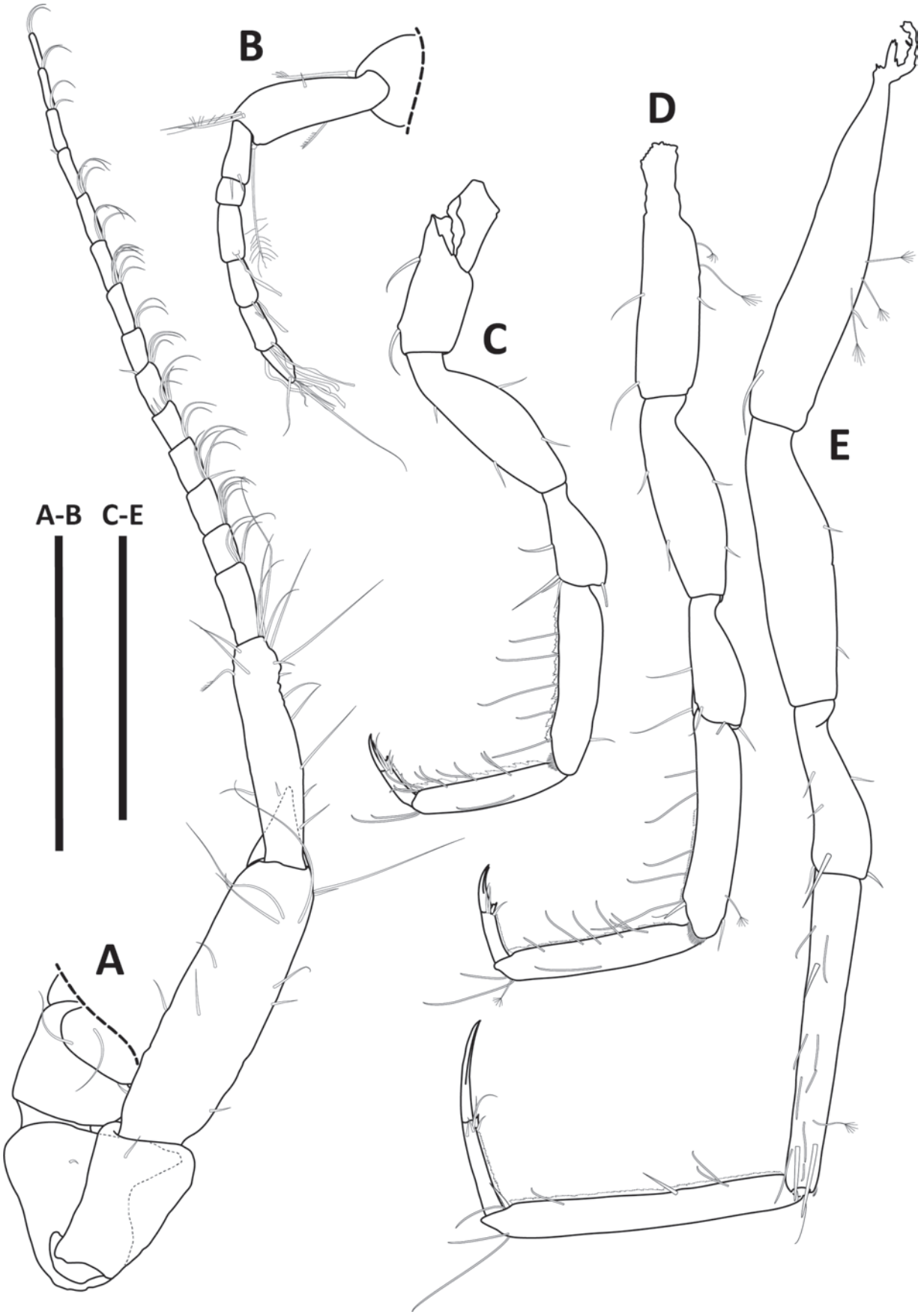

Figure 23. *Haploniscus nyx* sp. nov. male holotype, SKB Hap34. **A.** Antenna II; **B.** Antenna I; **C.** Pereopod I; **D.** Pereopod II; **E.** Pereopod VI. Scale bars: 0.4 mm.

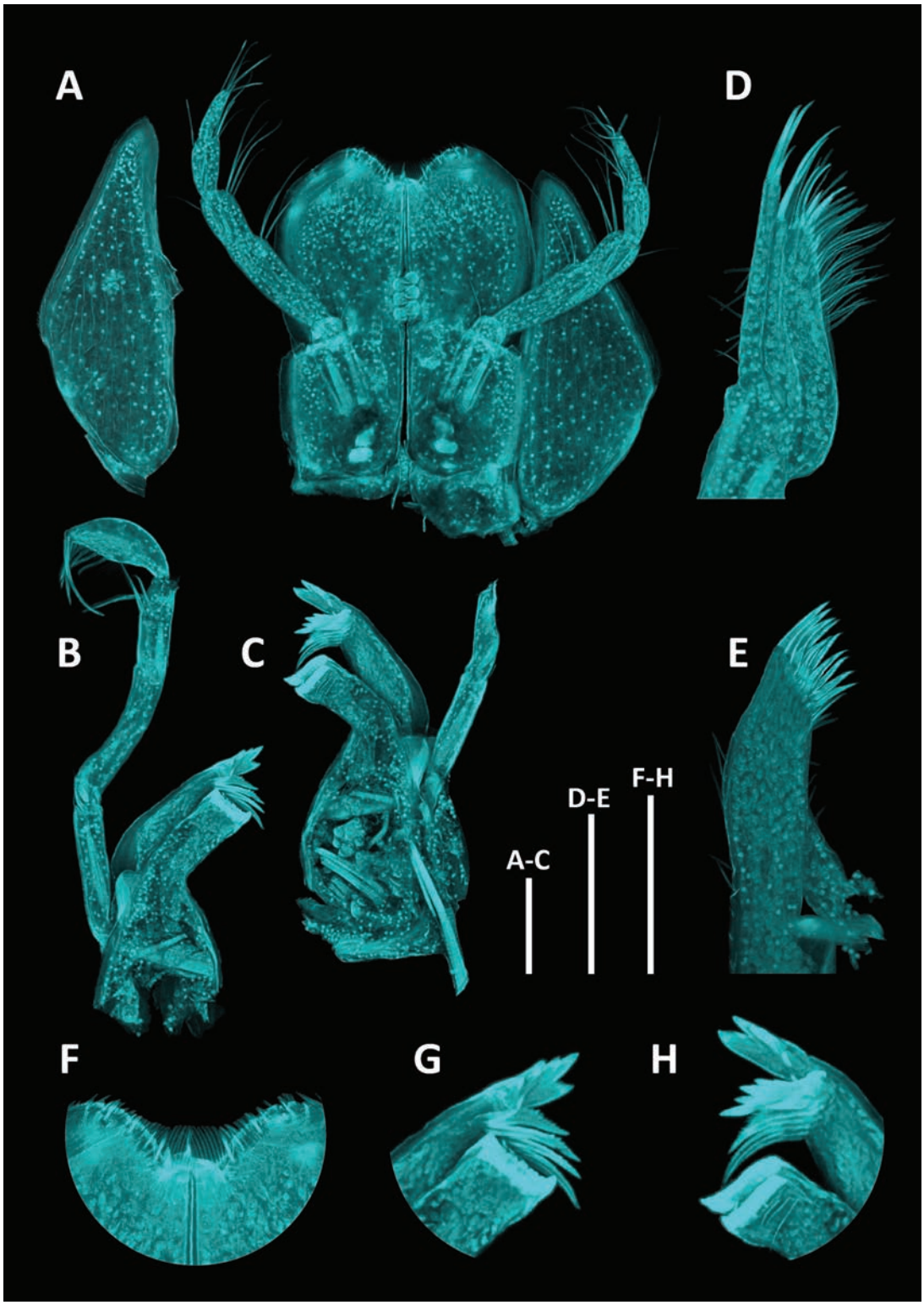

Figure 24. *Haploniscus nyx* sp. nov. male holotype, SKB Hap34. **A.** Maxillipeds; **B.** Right mandible; **C.** Left mandible; **D.** Maxilla II; **E.** maxilla I; **F.** Maxillipeds, detail of distomedial margins of endites; **G.** Right mandible, detail of incisor and molar process; **H.** Left mandible, detail of incisor, *lacinia mobilis*, and molar process. Scale bars: 0.1 mm.

Prn 2–5 anterolateral angles slightly projecting; Prn 1–4 posterolateral angles slightly projecting; Prn 4 lateral margin length 1 Prn 5 lateral margin length.

Pleotelson (Figs 22B, 26L) length 0.72 width, 0.23 body length, trapezoidal, posterior margin concave; tergite surface smooth; with posterolateral tergal ridge between uropod insertion and posterolateral process; posterolateral processes minute, 0.13 Plt length, straight, oriented posteriorly.

Antenna I (Fig. 23B) length 0.16 body length; flagellum with 5 articles.

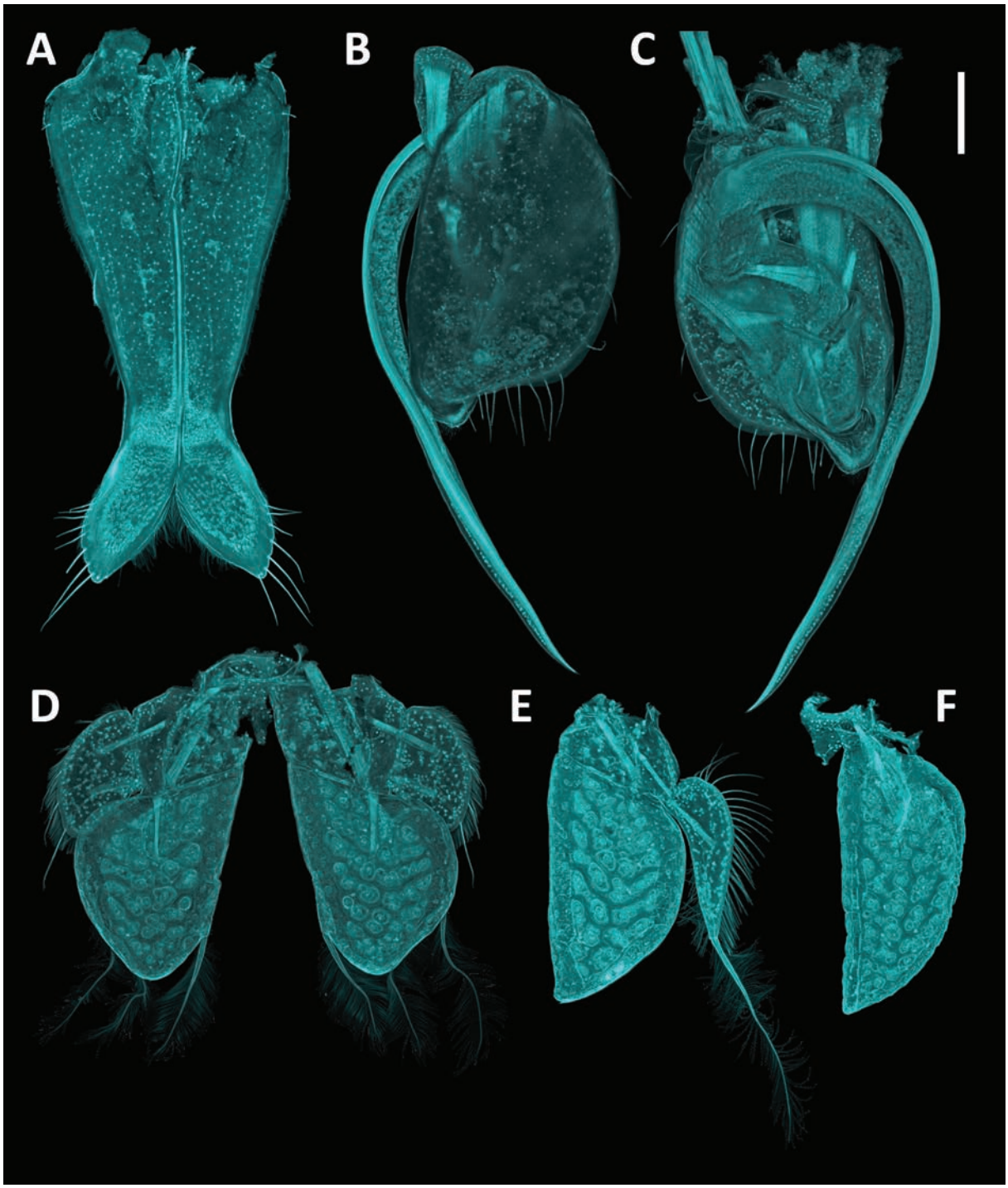

Figure 25. *Haploniscus nyx* sp. nov. male holotype, SKB Hap34. **A.** Pleopod I; **B.** Pleopod II, ventral view; **C.** Pleopod II, dorsal view; **D.** Pleopods III; **E.** Pleopod IV; **F.** Pleopod V. Scale bar: 0.25 mm.

Antenna II (Fig. 23A) length 0.61 body length; article 3 dorsal projection triangular, projection length 0.36 article 3 length; article 5 projection length 0.23 article 5 length; flagellum with 15 articles.

Mandible (Fig. 24B, C) incisor with 5 cusps, left Md *lacinia mobilis* with 4 cusps.

Maxillipeds (Fig. 24A) with 3 coupling hooks each.

Pereopod I (Fig. 23C) length 0.37 body length. **PII** (Fig. 23D) length 0.45 body length. **PIII** (Fig. 23E) length 0.52 body length. **PV** length 0.65 body length. **PVI** length 0.70 body length; P lengths gradually increasing from PI to PVI, PVII shorter than PVI.

Pleopod I (Figs 25A, 26L) medial lobes convexly rounded, tapering to an obtuse point; adjoining at the apex.

Pleopod II (Fig. 25B, C) protopod semi-circular, with distal lobe extending beyond protopod distal margin; endopod stylet 2.1 protopod length.

Female. Differs from male in the following characters:

Body (Fig. 22A) length 2.1 width; oval; anterior body length (Ceph–Prn 4) 0.98 posterior body length (Prn 5–Plt).

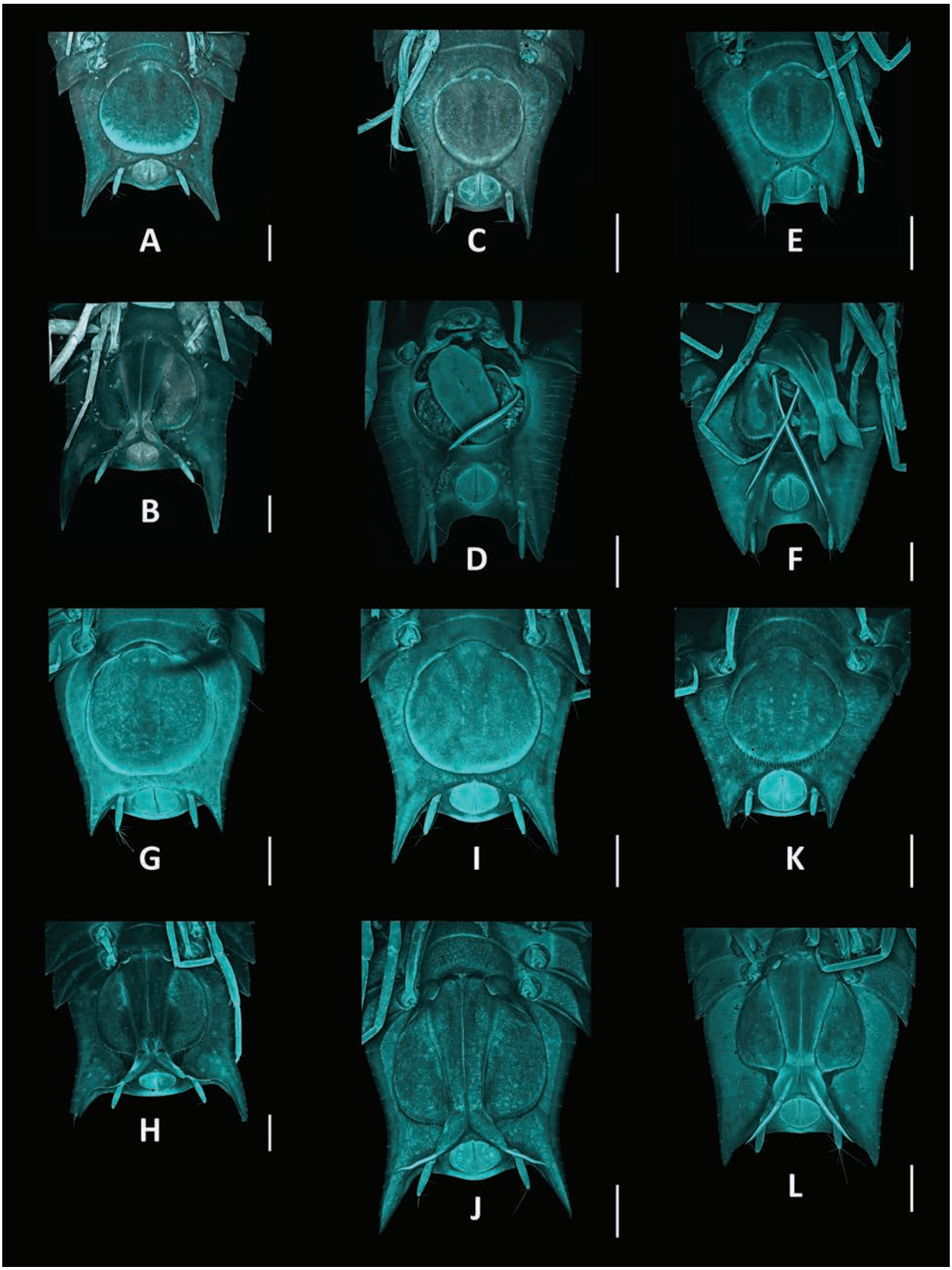

Figure 26. Comparison of pleotelson shapes amongst adult male and female members of the *Haploniscus belyaevi* species complex (CLSM). *H. erebus* sp. nov. female (**A**) and male (**B**) from Knauber et al. (2022); *H. kerberos* sp. nov. female (**C**) and male (**D**); *H. hades* sp. nov. female (**E**) and male (**F**); *H. belyaevi* female (**G**) and male (**H**); *H. apaticus* sp. nov. female (**I**) and male (**J**); *H. nyx* sp. nov. female (**K**) and male (**L**). Scale bars: 0.5 mm.

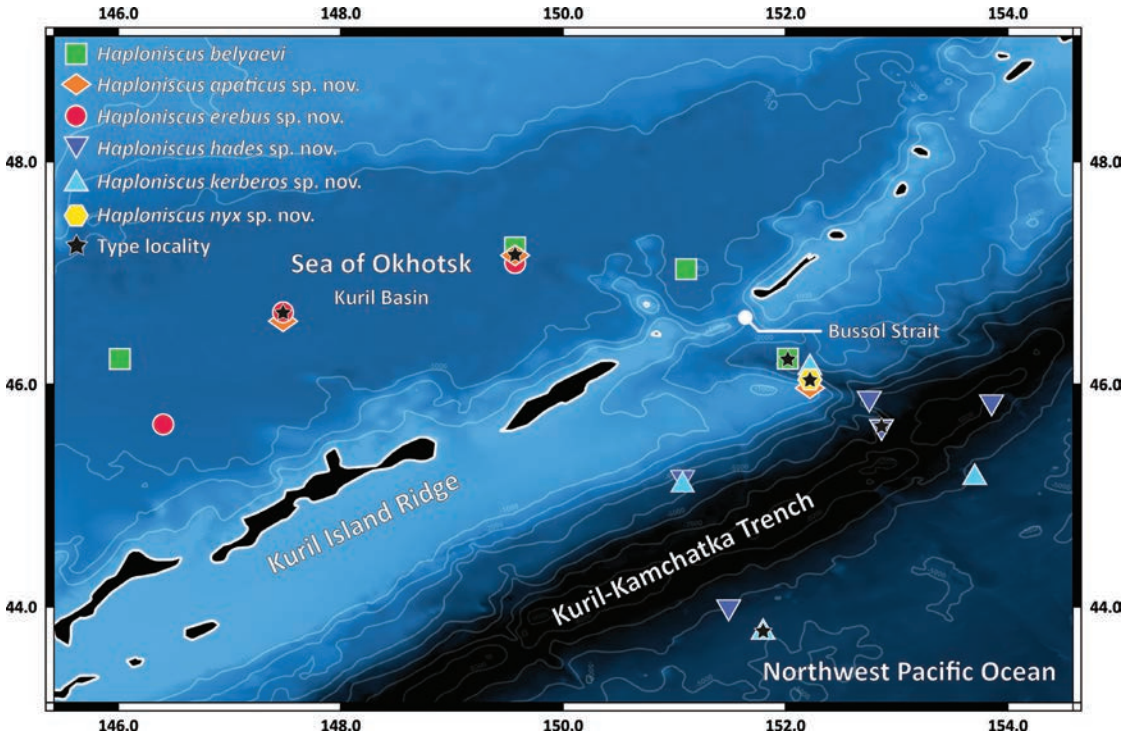

Figure 27. Distribution of haploniscid species of the *belyaevi*-complex in the greater Kuril-Kamchatka Trench and Sea of Okhotsk area of the Northwest Pacific. Stars indicate each species type locality.

Cephalothorax (Fig. 22A, C) length 0.46 width, 0.12 body length, width 0.55 body width; frontal margin width 0.46 Ceph width.

Pereonite 4 (Fig. 22A) lateral margin length 1.05 Prn 5 lateral margin length.

Pleotelson (Figs 22A, 26K) length 0.83 width, 0.27 body length, posterior margin rounded, convex; posterolateral processes short, 0.19 Plt length.

Antenna I (Fig. 22A) length 0.16 body length; flagellum with 4 articles.

Antenna II (Fig. 22A) length 0.50 body length; flagellum with 15 articles.

Operculum (Fig. 26K) length 0.98 width, 0.66 Plt length; distal margin with numerous, evenly distributed long setae; lateral margins with fewer, evenly distributed short setae.

Identification key to the species of the *Haploniscus belyaevi* species complex based on adult male stages

1 Anterolateral angle of Prn 5 not projecting; Plt posterior margin with tergal plates projecting above uropods, covering them almost completely from dorsal view; Plt with posterolateral tergal ridge terminating on posterolateral process; Plp II elongated, suboval, without distal lobe extending beyond protopod distal margin 2

– Anterolateral angle of Prn 5 with minute acute projection; Plt posterior margin without projecting tergal plates, uropods clearly visible from dorsal view; Plt with posterolateral tergal ridge terminating between uropod insertion and posterolateral process; Plp II semi-circular, with distal lobe extending beyond protopod distal margin 3

2 (1) Rostrum basally with pronounced dorsal bulge; All article 3 dorsal projection hook-shaped..... *Haploniscus hades* sp. nov.

– Rostrum basally without dorsal bulge; All article 3 dorsal projection triangular ..... *Haploniscus kerberos* sp. nov.

3 (1) Rostrum straight ..... *Haploniscus erebus* sp. nov.

– Rostrum curved upwards 4

4 (3) Rostrum anteriorly flat; Prn 1 anterolateral angle with minute, acute projection; Prn 1 anterior margin delicately serrated, setose; Plt rectangular, posterolateral processes curved..... *Haploniscus belyaevi* Birstein, 1963

– Rostrum anteriorly not flat; Prn 1 anterolateral angle not projecting; Plt trapezoidal, posterolateral processes straight..... 5

5 (4) Lateral margin of Prn 4 longer than of Prn 5; Plt posterior margin convex, posterolateral processes oriented posterolaterally; PV–VII lengths distinctly exceeding PI–IV lengths; Plp I medial lobes subtriangular, projecting caudolaterally ..... *Haploniscus apaticus* sp. nov.

– Prn 4 and Prn 5 lateral margins of equal length; Plt posterior margin concave, posterolateral processes oriented posteriorly; P lengths gradually increasing from PI to PVI; Plp I medial lobes convexly rounded, tapering to an obtuse point ..... *Haploniscus nyx* sp. nov.

Geometric morphometrics

The canonical variate analysis of the pleotelson shapes of *H. kerberos* sp. nov., *H. hades* sp. nov., and *H. belyaevi* revealed the distinction of six groups defined by the species and sex of the analyzed specimens (Fig. 28). A Procrustes ANOVA confirmed that the conducted pleotelson shape analysis was highly significant ($p < 0.01\%$). The male pleotelson shapes of *H. kerberos* sp. nov. and *H. hades* sp. nov. are quite similar, yet distinct, as indicated by their close positioning next to one another, while *H. belyaevi* is far off. The latter species also exhibits the strongest differentiation between male and female pleotelson shapes of any of the three analyzed species. The female pleotelson shape of *H. belyaevi* is much more similar to the ones of the other female specimens of *H. kerberos* sp. nov. and *H. hades* sp. nov. than to its respective males. For *H. kerberos* sp. nov. and *H. hades* sp. nov., male and female specimens are also located much closer to one another.

Genomics

The resulting nuclear genome assemblies are very fragmented, which is expected given their respective low coverage. Statistics of the final assemblies after filtering are shown in Table 4.

All assembled mitochondrial genomes contain the expected 13 protein-coding genes and two rRNAs. The gene order is conserved among the assembled mitochondrial genomes and references, with the sole exception of KBII Hap154, belonging to *Haploniscus hydroniscoides*, having ND6 and 16S rRNA switched (Fig. 29A; not observed in all references) as well as 12S rRNA before ND1 (Fig. 29B; only observed in the reference of *Ichthyoxenos japonensis*).

Levels of intraspecific divergence within the *belyaevi*-complex ranged between 5.5 and 20.5% (Table 5). In comparison, *H. hydroniscoides* scored higher *p*-distances in relation to the *belyaevi*-complex, ranging between 36.1 and 36.7%. Interspecific divergence to the two outgroup species of *Notopais* amounted to 51.7–52%.

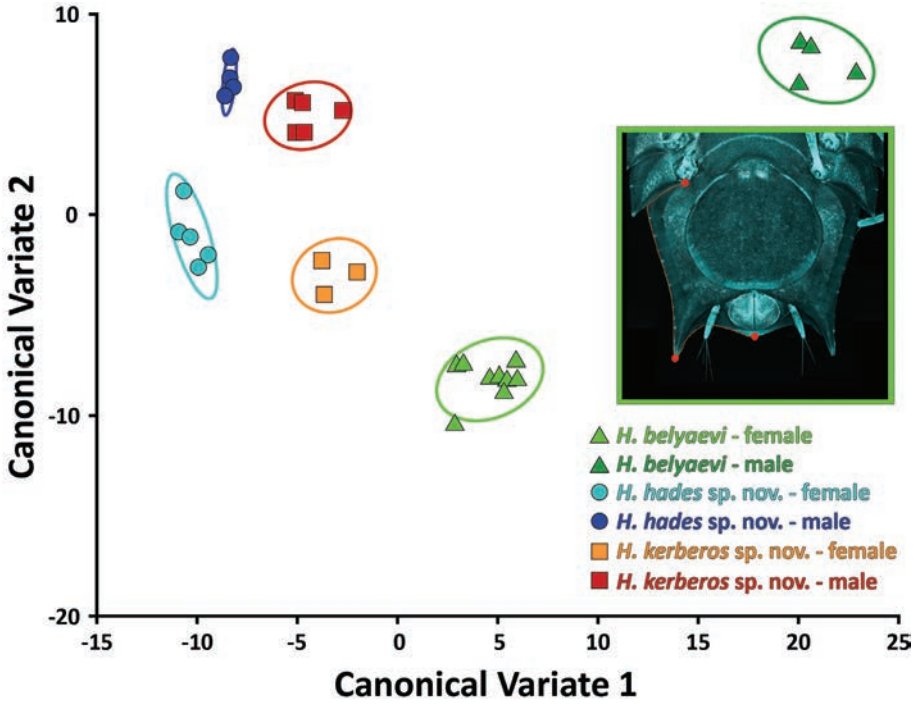

Figure 28. Scatter plot displaying the geometric morphometric analyses of the pleotelson shape from *H. belyaevi*, H. *kerberos* sp. nov., and *H. hades* sp. nov. for both sexes. The underlying data for this analysis stem from landmarking the pleotelson outline from a ventral view using CLSM images and photographs, as illustrated on the right

Table 4. Statistics of the *de novo* assemblies after filtering.

Sample	KBII Hap104	KBII Hap122	KBII Hap154	SKB Hap04	SKB Hap48	SKB Hap49
Species	***H. hades* sp. nov.**	***H. kerberos* sp. nov.**	***H. hydroniscoides***	***H. belyaevi***	***H. apaticus* sp. nov.**	***H. erebus* sp. nov.**
Assembler	Spades	Spades	Spades	Platanus	Spades	Platanus
#contigs	647436	610536	568443	26068249	698293	26259349
Total length	877079199	916542958	776628239	1667875350	699113445	2126489036
N50	3054	3254	3931	875	2107	1036
GC (%)	32.46	32.52	33.24	32.14	31.93	32.16
BUSCO arthropoda _ odb10 (N = 1013)	C:24.5% [S:24.0%, D:0.5%], F:38.9%, M:36.6%	C:24.2% [S:23.5%, D:0.7%], F:42.3%, M:33.5%	C:28.4% [S:26.5%, D:1.9%], F:38.0%, M:33.6%	C:9.1% [S:9.0%, D:0.1%], F:34.0%, M:56.9%	C:19.6% [S:19.3%, D:0.3%], F:39.2%, M:41.2%	C:12.0% [S:12.0%, D:0.0%], F:37.3%, M:50.7%

Figure 29. Overview of the mitochondrial genome alignment. The alignments were created from assembled sequences and available references in the regions of ND6 and 16S rRNA (**A**) as well as ND1 and 12S rRNA (**B**). Hap04 = *H. belyaevi*; Hap48 = *H. apaticus* sp. nov.; Hap49 = *H. erebus* sp. nov.; Hap104 = *H. hades* sp. nov.; Hap122 = *H. kerberos* sp. nov.; Hap154 = *H. hydroniscoides*.

Table 5. Interspecific divergence within the *belyaevi*-complex and outgroup species. Uncorrected *p*-distances between mitogenomes of the analyzed *belyaevi*-complex members, *H. hydroniscoides* and two outgroup species of the munnopsid genus *Notopais*.

Taxon	*H. hades* sp. nov.	*H. kerberos* sp. nov.	*H. belyaevi*	*H. apaticus* sp. nov.	*H. erebus* sp. nov.	*H. hydroniscoides*	*Notopais* sp. c
H. kerberos sp. nov.	0.066						
H. belyaevi	0.205	0.198					
H. apaticus sp. nov.	0.204	0.199	0.055				
H. erebus sp. nov.	0.203	0.197	0.154	0.156			
H. hydroniscoides	0.363	0.361	0.367	0.364	0.361		
Notopais sp. c	0.598	0.595	0.597	0.598	0.593	0.567	
Notopais sp. p	0.517	0.517	0.518	0.52	0.52	0.497	0.489

Discussion

The present study builds upon the efforts of Knauber et al. (2022), which laid the groundwork for delimitating the closely related species of the *Haploniscus belyaevi* species complex using integrative taxonomy. The close relationships and corresponding overlapping morphological variation of these species made it necessary to reach beyond traditional taxonomic concepts for the Haploniscidae to successfully delineate the members of the *belyaevi*-complex. Our findings demonstrate that the novel species described herein can be told apart more or less clearly based on morphology and molecular data.

Morphological and molecular variation within the belyaevi-complex

The application of reciprocal illumination (Hennig 1965; Lienau et al. 2006) in the *belyaevi*-complex revealed that the primary morphological distinguishing features comprise the shapes of the antennae, the cephalothorax (particularly the rostrum), and the pleotelson (specifically the posterolateral processes). Conversely, other anatomical features, such as the pleopods III–V or the mouthparts, have historically been described in greater detail, yet reportedly exhibit comparatively small variation in the herein described species and the Haploniscidae as a whole (Park 2000; Leese and Brenke 2005; e.g., Brökeland 2010a). While these appendages are illustrated herein to allow for future investigations, their description was shortened as currently their diagnostic value remains low. Instead, the species descriptions were complemented with molecular data using barcode-based molecular diagnoses and mitogenomic data. Levels of interspecific divergence between members of the *belyaevi*-complex using mitogenomic data were of similar magnitude as the ones using COI barcode data (compare Knauber et al. 2022) with slight deviations. The most notable difference between interspecific divergence levels based on mitogenomic and COI barcode data is found between the *belyaevi*-complex and *H. hydroniscoides*, which served as an outgroup in the study from 2022 and herein: interspecific divergence was over 10% higher between those two groups in the mitogenomic data than in the COI data.

Implications for the taxonomy of the Haploniscidae

The phenotypic plasticity of the *belyaevi*-complex is in line with the observation of ontogenetic changes and sexual dimorphism observed in various other studies on haploniscid taxonomy (Brökeland and Raupach 2008; Brökeland 2010b; Brix et al. 2011; Knauber et al. 2022). It underscores the importance of integrative approaches, including the combined consideration of morphological and molecular data as well as novel analysis techniques. As species complexes are relatively common among the Haploniscidae (Brökeland and Raupach 2008; Brökeland 2010a; Knauber et al. 2022), such methodologically broad attempts to uncover their diversity seem essential.

The Haploniscidae, especially the genus *Haploniscus*, reportedly require substantial taxonomic revision (Lincoln 1985; Brökeland 2010a). Historically, taxonomic work on this group has relied on very detailed and extensive descriptions of morphological characters, many of which as of now seem to have low or no diagnostic and species delimitating value. Following these standards to describe everything in great detail renders the description of novel species into a time-consuming endeavor. This issue is further exacerbated by a large number of haploniscid species still awaiting description (unpublished data). In order to resolve the haploniscid taxonomy and complement the species catalogue of this family, future studies should, therefore, carefully evaluate the information content and diagnostic power of the wide range of available data to effectively achieve these aims.

Complementing the belyaevi-complex

Preliminary data from recent sampling campaigns in the North Pacific Aleutian and Japan Trenches in the course of the AleutBio (Brandt 2022) and Hakuho Maru campaigns (Brandt et al. 2024) indicate that the *belyaevi*-complex also occurs there (Knauber, unpublished data). Haploniscid specimens bearing the distinct distal spine on article 5 of the second antenna have been recovered from both of these trenches. Their specific taxonomic affiliation, whether they pertain to the species treated here or represent novel members of the *belyaevi*-complex, remains unclear so far.

Similarly, Gamó (1989) illustrated an immature specimen from the Okinawa Trough, also possessing the characteristic spine on the second antenna. Due to the ontogenetic variability of haploniscid isopods, a species assignment of this juvenile specimen based solely on these illustrations is impossible. Unfortunately, scrutinizing this specimen further is unfeasible as it has been destroyed during analysis. Regardless, this record shows the biogeographic range of the *belyaevi*-complex extends way beyond the greater KKT area.

Outlook

The species composition and biogeographic distribution of the *belyaevi*-complex will be complemented based on novel specimens in the foreseeable future. Given the *belyaevi*-complex's prevalence in the NWP, its composition and distinct distribution (Knauber et al. 2022) raise questions about how these closely related species dispersed and differentiated. Studying the *belyaevi*-complex in an integrative context on a larger scale might thus provide valuable insights into the processes and underlying factors shaping benthic faunal differentiation and distribution patterns in the deep NWP.

Conclusion

The species of the Haploniscidae described herein belong to a complex of closely related species – the first of its kind reported for this isopod family from the Northwest Pacific Ocean. While morphologically diagnostic characters are mostly limited to the relatively distinct adult males, these species exhibit varying biogeographical ranges tied to large-scale bathymetric features. New means of morphological and molecular methods, including the first mitogenomic data for haploniscid isopods, aided in their delineation and might be beneficial for future taxonomic studies on the to-be-revised Haploniscidae and the study of species differentiation in the abysso-hadal Northwest Pacific.

Data availability statement

The associated (meta-)data to these haploniscid records, made available by Knauber et al. (2022) in the Barcode of Life Data System (BoLD System; Ratnasingham and Hebert 2007) available at dx.doi.org/10.5883/DS-NWPHA22, GenBank (Benson et al. 2012) accession numbers OM782497 to OM782662, National Center for Biotechnology Information (NCBI, (Sayers et al. 2022) available at BioProject PRJNA1100257, Ocean Biogeographic Information System (OBIS; Grassle 2000) available at https://ipt.iobis.org/obis-deepsea/resource?r=deep-sea_haploniscid_isopods and Zenodo (European Organization For Nuclear Research, OpenAIRE 2013) available at http://doi.org/10.5281/zenodo.6553796, will be updated accordingly.

Acknowledgements

We thank the crews of the RVs *Sonne* and *Akademik M.A. Lavrentyev* for their work and help in collecting the samples analyzed within this study as well as all scientists, student helpers, and technicians who sorted and managed the collected samples during the international KuramBio II and SokhoBio projects. Special thanks to Anchita Casaubon for her help with geometric morphometrics. The authors also want to thank Damian Baranski and Carola Greve for their help regarding the sequencing lab work. This is contribution #27 of the Senckenberg Ocean Species Alliance (SOSA).

The SokhoBio expedition was organized with financial support from the Russian Science Foundation (Project No. 14-50-00034). Material sorting was funded by the BMBF (German Ministry of Education and Research) grant 03G0857A to Angelika Brandt, University of Hamburg, now Senckenberg Museum, Frankfurt, Germany. Funding for the KuramBio II expedition was provided by the PTJ (Projektträger Jülich) BMBF grant 03G0250A to Angelika Brandt. Further support for these projects was provided by the Russian Foundation for Basic Research (projects 13-04-02144, 16-04-01431), the Council of the President of the Russian Federation (project MK-2599.2013.4), Russian Federation Government grant No 11. G34.31.0010, and a grant of the Presidium of the Far East Branch of RAS (12–I–P30–07). Sequencing was financed through the Holotype Sequencing Project of the LOEWE Centre for Translational Biodiversity Genomics (TBG; grant number LOE WE/1/10/519/03/03.001(0014)/52 of the Hessen State Ministry of Higher Education, Research and the Arts (HMWK)).

References

Agassiz A (1880) Report of the dredging cruise of the U.S. steamer Blake, Commander Bartlett, during the summer of 1880. Science 1: 314–314. https://doi.org/10.1126/science.os-1.27.314-a

Appeltans W, Ahyong ST, Anderson G, Angel MV, Artois T, Bailly N, Bamber R, Barber A, Bartsch I, Berta A, Błażewicz-Paszkowycz M, Bock P, Boxshall G, Boyko CB, Brandão SN, Bray RA, Bruce NL, Cairns SD, Chan T-Y, Cheng L, Collins AG, Cribb T, Curini-Galletti M, Dahdouh-Guebas F, Davie PJF, Dawson MN, De Clerck O, Decock W, De Grave S, de Voogd NJ, Domning DP, Emig CC, Erséus C, Eschmeyer W, Fauchald K, Fautin DG, Feist SW, Fransen CHJM, Furuya H, Garcia-Alvarez O, Gerken S, Gibson D, Gittenberger A, Gofas S, Gómez-Daglio L, Gordon DP, Guiry MD, Hernandez F, Hoeksema BW, Hopcroft RR, Jaume D, Kirk P, Koedam N, Koenemann S, Kolb JB, Kristensen RM, Kroh A, Lambert G, Lazarus DB, Lemaitre R, Longshaw M, Lowry J, Macpherson E, Madin LP, Mah C, Mapstone G, McLaughlin PA, Mees J, Meland K, Messing CG, Mills CE, Molodtsova TN, Mooi R, Neuhaus B, Ng PKL, Nielsen C, Norenburg J, Opresko DM, Osawa M, Paulay G, Perrin W, Pilger JF, Poore GCB, Pugh P, Read GB, Reimer JD, Rius M, Rocha RM, Saiz-Salinas JI, Scarabino V, Schierwater B, Schmidt-Rhaesa A, Schnabel KE, Schotte M, Schuchert P, Schwabe E, Segers H, Self-Sullivan C, Shenkar N, Siegel V, Sterrer W, Stöhr S, Swalla B, Tasker ML, Thuesen EV, Timm T, Todaro MA, Turon X, Tyler S, Uetz P, van der Land J, Vanhoorne B, van Ofwegen LP, van Soest RWM, Vanaverbeke J, Walker-Smith G, Walter TC, Warren A, Williams GC, Wilson SP, Costello MJ (2012) The Magnitude of Global Marine Species Diversity. Current Biology 22: 2189–2202. https://doi.org/10.1016/j.cub.2012.09.036

Benson DA, Cavanaugh M, Clark K, Karsch-Mizrachi I, Lipman DJ, Ostell J, Sayers EW (2012) GenBank. Nucleic Acids Research 41: D36–D42. https://doi.org/10.1093/nar/gks1195

Birstein JA (1963) Deep water isopods (Crustacea, Isopoda) of the north-western part of the Pacific Ocean. Nauka Publishing House, USSR Academy of Sciences, P.P. Shirshov Institute of Oceanography, Moscow, 317 pp.

Birstein JA (1971) Additions to the fauna of isopods (Crustacea: Isopoda) of the Kuril-Kamchatka Trench. Part 2. Asellota-2. Trudy Instituta Okeanologii Akademiya Nauk SSR, 162–238.

Bolger AM, Lohse M, Usadel B (2014) Trimmomatic: a flexible trimmer for Illumina sequence data. Bioinformatics 30: 2114–2120. https://doi.org/10.1093/bioinformatics/btu170

Boyko CB, Bruce NL, Hadfield KA, Merrin KL, Ota Y, Poore GCB, Taiti S, Schotte M, Wilson GDF (2023) World Register of Marine Species - Database: Haploniscidae Hansen, 1916. World register of marine species. http://www.marinespecies.org/aphia.php?p=taxdetails&id=118254#sources [March 7, 2018]

Brandt A (2016) Kuril Kamchatka Biodiversity Studies II - RV Sonne SO250, Tomakomai-Yokohama (Japan), 16.08.-26.09.2016. University of Hamburg, Hamburg, Germany. Cruise report, 174 pp.

Brandt A (2022) SO293 AleutBio (Aleutian Trench Biodiversity Studies) Cruise Report. Cruise report, 209 pp. https://doi.org/10.48433/cr_so293

Brandt A, Malyutina M (2013) The German-Russian deep-sea expedition KuramBio (Kurile Kamchatka Biodiversity Studies) to the Kuril-Kamchatka Trench and abyssal plain on board of the R/V Sonne. Vladivostok, Russia. Cruise report, 100 pp. http://oceanrep.geomar.de/36686/ [March 28, 2018]

Brandt A, Elsner N, Brenke N, Golovan O, Malyutina MV, Riehl T, Schwabe E, Würzberg L (2013) Epifauna of the Sea of Japan collected via a new epibenthic sledge equipped with camera and environmental sensor systems. Deep Sea Research Part II: Topical Studies in Oceanography 86–87: 43–55. https://doi.org/10.1016/j.dsr2.2012.07.039

Brandt A, Brix S, Riehl T, Malyutina M (2020) Biodiversity and biogeography of the abyssal and hadal Kuril-Kamchatka trench and adjacent NW Pacific deep-sea regions. PrOce 181: 102232. https://doi.org/10.1016/j.pocean.2019.102232

Brandt A, Bergmeier F, Casaubon A, Kano Y, Kelch A, Knauber H, Okamoto K, Ohta M, Shiraki S, Yamamoto D, Kojima S (2024) Benthos meets plankton: Isopods sampled in the Japan Trench by means of plankton nets fixed to large bottom trawls. Marine Biodiversity. https://doi.org/10.21203/rs.3.rs-3801343/v1

Brenke N (2005) An epibenthic sledge for operations on marine soft bottom and bedrock. Marine Technology Society Journal 39: 10–21. https://doi.org/10.4031/002533205787444015

Brix S, Riehl T, Leese F (2011) First genetic data for species of the genus *Haploniscus* Richardson, 1908 (Isopoda: Asellota: Haploniscidae) from neighbouring deep-sea basins in the South Atlantic. Zootaxa 2838: 79–84. https://doi.org/10.11646/zootaxa.2838.1.5

Brökeland W (2010a) Description of four new species from the *Haploniscus unicornis* Menzies, 1956 complex (Isopoda: Asellota: Haploniscidae). Zootaxa 2536: 1–35. https://doi.org/10.11646/zootaxa.2536.1.1

Brökeland W (2010b) Redescription of *Haploniscus rostratus* (Menzies, 1962) (Crustacea: Peracarida: Isopoda) with observations on the postmarsupial development, size ranges and distribution. Zootaxa 2521: 1–25. https://doi.org/10.11646/zootaxa.2521.1.1

Brökeland W, Raupach MJ (2008) A species complex within the isopod genus *Haploniscus* (Crustacea: Malacostraca: Peracarida) from the Southern Ocean deep sea: a morphological and molecular approach. Zoological Journal of the Linnean Society 152: 655–706. https://doi.org/10.1111/j.1096-3642.2008.00362.x

Brökeland W, Svavarsson J (2017) Distribution of haploniscids (Isopoda, Asellota, Haploniscidae) in Icelandic waters, with description of *Haploniscus astraphes* n. sp. from the Iceland basin and the Southeast Atlantic Ocean. Zootaxa 4231: 301–326. https://doi.org/10.11646/zootaxa.4231.3.1

Casaubon A, Riehl T (2024) Shape matters: investigating the utility of geometric morphometric techniques in the deep-sea isopod family Macrostylidae (Isopoda: Asellota). Frontiers in Marine Science 11. https://doi.org/10.3389/fmars.2024.1380594

Coleman CO (2003) "Digital inking": How to make perfect line drawings on computers. Organisms, Diversity and Evolution 3: 303–304. https://doi.org/10.1078/1439-6092-00081

Dallwitz MJ (1980) A general system for coding taxonomic descriptions. Taxon, 41–46. https://doi.org/10.2307/1219595

Dallwitz MJ, Paine TA, Zurcher EJ (1999) User's guide to the DELTA Editor.

Dierckxsens N, Mardulyn P, Smits G (2017) NOVOPlasty: de novo assembly of organelle genomes from whole genome data. Nucleic acids research 45: e18–e18. https://doi.org/10.1093/nar/gkw955

Donath A, Jühling F, Al-Arab M, Bernhart SH, Reinhardt F, Stadler PF, Middendorf M, Bernt M (2019) Improved annotation of protein-coding genes boundaries in metazoan mitochondrial genomes. Nucleic Acids Research 47: 10543–10552. https://doi.org/10.1093/nar/gkz833

Dreutter S, Steffen M, Arbizu PM, Brandt A (2020) Will the "top five" deepest trenches lose one of their members? Progress in Oceanography 181: 102258. https://doi.org/10.1016/j.pocean.2019.102258

European Organization For Nuclear Research, OpenAIRE (2013) Zenodo. https://doi.org/10.25495/7GXK-RD71

Gamó S (1989) Some bathyal cumacean and isopod crustaceans from the Okinawa Trough, the East China Sea, with descriptions of a new genus and five new species. Bulletin of the Biogeographical Society of Japan 44: 20.

Goffredi S, Hurtado L, Hallam S, Vrijenhoek R (2003) Evolutionary relationships of deep-sea vent and cold seep clams (Mollusca: Vesicomyidae) of the "*pacifica/lepta*" species complex. Marine Biology 142: 311–320. https://doi.org/10.1007/s00227-002-0941-3

Golovan OA, Błażewicz M, Brandt A, Jażdżewska AM, Jóźwiak P, Lavrenteva AV, Malyutina MV, Petryashov VV, Riehl T, Sattarova VV (2019) Diversity and distribution of peracarid crustaceans (Malacostraca) from the abyss adjacent to the Kuril-Kamchatka Trench. Marine Biodiversity 49: 1343–1360. https://doi.org/10.1007/s12526-018-0908-3

GRASS Development Team (2020) Geographic Resources Analysis Support System (GRASS) Software. Open Source Geospatial Foundation. http://grass.osgeo.org [August 31, 2020]

Grassle JF (2000) The Ocean Biogeographic Information System (OBIS): an online, worldwide atlas for accessing, modeling and mapping marine biological data in a multidimensional geographic context. Oceanography 13: 5–7. https://doi.org/10.5670/oceanog.2000.01

Gurevich A, Saveliev V, Vyahhi N, Tesler G (2013) QUAST: quality assessment tool for genome assemblies. Bioinformatics 29: 1072–1075. https://doi.org/10.1093/bioinformatics/btt086

Hansen HJ (1916) Crustacea Malacostraca, III. V. The order Isopoda. In: The Danish Ingolf-Expedition. Copenhagen, 1–262.

Hennig W (1965) Phylogenetic systematics. Annual review of entomology 10: 97–116. https://doi.org/10.1146/annurev.en.10.010165.000525

Hessler RR (1970) 15 The Desmosomatidae (Isopoda, Asellota) of the Gay Head-Bermuda transect. University of California Press, 185 pp. https://escholarship.org/uc/item/1mn198vx [March 27, 2020]

Hessler RR, Jumars PA (1974) Abyssal community analysis from replicate box cores in the central North Pacific. Deep Sea Research and Oceanographic Abstracts 21: 185–209. https://doi.org/10.1016/0011-7471(74)90058-8

Hütter T, Ganser MH, Kocher M, Halkic M, Agatha S, Augsten N (2020) DeSignate: detecting signature characters in gene sequence alignments for taxon diagnoses. BMC Bioinformatics 21: 151. https://doi.org/10.1186/s12859-020-3498-6

Johannsen N, Lins L, Riehl T, Brandt A (2020) Changes in species composition of Haploniscidae (Crustacea: Isopoda) across potential barriers to dispersal in the Northwest Pacific. Progress in Oceanography: 180. https://doi.org/10.1016/j.pocean.2019.102233

Kajitani R, Toshimoto K, Noguchi H, Toyoda A, Ogura Y, Okuno M, Yabana M, Harada M, Nagayasu E, Maruyama H (2014) Efficient de novo assembly of highly heterozygous genomes from whole-genome shotgun short reads. Genome research 24: 1384–1395. https://doi.org/10.1101/gr.170720.113

Klingenberg CP (2011) MorphoJ: an integrated software package for geometric morphometrics. Molecular Ecology Resources 11: 353–357. https://doi.org/10.1111/j.1755-0998.2010.02924.x

Knauber H, Silberberg JR, Brandt A, Riehl T (2022) Evolution and biogeography of the *Haploniscus belyaevi* species complex (Isopoda: Haploniscidae) revealed by means of integrative taxonomy. Systematics and Biodiversity 20: 1. https://doi.org/10.1080/14772000.2022.2099477

Knowlton N (1993) Sibling species in the sea. Annual review of ecology and systematics 24: 189–216. https://doi.org/10.1146/annurev.es.24.110193.001201

Leese F, Brenke N (2005) *Chauliodoniscus coronatus* sp. nov., a new deep-sea species from the Angola Basin (Crustacea, Isopoda, Asellota, Janiroidea, Haploniscidae). Organisms Diversity & Evolution 5: 189–201. https://doi.org/10.1016/j.ode.2004.11.003

Lienau EK, DeSalle R, Rosenfeld JA, Planet PJ (2006) Reciprocal Illumination in the Gene Content Tree of Life. Systematic Biology 55: 441–453. https://doi.org/10.1080/10635150600697416

Lincoln RJ (1985) The marine fauna of New Zealand deep-sea Isopoda Asellota family Haploniscidae. New Zealand Oceanographic Institute Memoir Vol. 94, 55 pp.

Malyutina MV, Brandt A, Ivin VI (2015) The Russian-German deep-sea expedition SokhoBio (Sea of Okhotsk Biodiversity Studies) to the Kurile Basin of the Sea of Okhotsk on board of the R/V Akademik M. A. Lavrentyev. Vladivostok, Russia. Cruise report, 102 pp.

Malyutina MV, Chernyshev AV, Brandt A (2018) Introduction to the SokhoBio (Sea of Okhotsk Biodiversity Studies) expedition 2015. Deep Sea Research Part II 154: 1–9. https://doi.org/10.1016/j.dsr2.2018.08.012

Manni M, Berkeley MR, Seppey M, Simão FA, Zdobnov EM (2021) BUSCO update: novel and streamlined workflows along with broader and deeper phylogenetic coverage for scoring of eukaryotic, prokaryotic, and viral genomes. Molecular Biology and Evolution 38: 4647–4654. https://doi.org/10.1093/molbev/msab199

McLaughlin EL, Wilson NG, Rouse GW (2023) Resolving the taxonomy of the Antarctic feather star species complex *Promachocrinus 'kerguelensis*' (Echinodermata: Crinoidea). Invertebrate Systematics 37: 498–527. https://doi.org/10.1071/IS22057

Michels J, Büntzow M (2010) Assessment of Congo red as a fluorescence marker for the exoskeleton of small crustaceans and the cuticle of polychaetes. Journal of Microscopy 238: 95–101. https://doi.org/10.1111/j.1365-2818.2009.03360.x

Monin AS (1983) The Research Vessel "Vityaz" and her Expeditions (1949–1979). Nauka Publishing House, USSR Academy of Sciences, P.P. Shirshov Institute of Oceanography, Moscow, 392 pp.

Mora C, Tittensor DP, Adl S, Simpson AGB, Worm B (2011) How Many Species Are There on Earth and in the Ocean? PLOS Biology 9: e1001127. https://doi.org/10.1371/journal.pbio.1001127

Park J-Y (2000) A revision of the isopod genus Mastigoniscus (Asellota, Haploniscidae) with descriptions of three new species. Zoosystematics and Evolution 76: 195–229. https://doi.org/10.1002/mmnz.20000760204

Prjibelski A, Antipov D, Meleshko D, Lapidus A, Korobeynikov A (2020) Using SPAdes De Novo Assembler. Current Protocols in Bioinformatics 70: e102. https://doi.org/10.1002/cpbi.102

QGIS.org (2020) QGIS Geographic Information System. Open Source Geospatial Foundation Project. http://qgis.org [August 31, 2020]

Ratnasingham S, Hebert PDN (2007) BOLD: The Barcode of Life Data System (www.barcodinglife.org). Molecular Ecology Notes 7: 355–364. https://doi.org/10.1111/j.1471-8286.2007.01678.x

Rex MA, Etter RJ (2010) Deep-sea biodiversity: pattern and scale. Harvard University Press, Boston, MA, 354 pp.

Richardson H (1908) Some new Isopoda of the superfamily Aselloidea from the Atlantic coast of North America. Proceedings of the United States National Museum, 71–86. https://doi.org/10.5479/si.00963801.35-1633.71

Riehl T, Brandt A (2010) Descriptions of two new species in the genus *Macrostylis* Sars, 1864 (Isopoda, Asellota, Macrostylidae) from the Weddell Sea (Southern Ocean), with a synonymisation of the genus *Desmostylis* Brandt, 1992 with *Macrostylis*. ZooKeys 57: 9–49. https://doi.org/10.3897/zookeys.57.310

Riehl T, Wilson GDF, Hessler RR (2012) New Macrostylidae Hansen, 1916 (Crustacea: Isopoda) from the Gay Head-Bermuda transect with special consideration of sexual dimorphism. Zootaxa 3277: 1–26. https://doi.org/10.11646/zootaxa.3277.1.1

Riehl T, Brenke N, Brix S, Driskell A, Kaiser S, Brandt A (2014) Field and laboratory methods for DNA studies on deep-sea Isopod Crustaceans. Polish Polar Research 35: 203–224. https://doi.org/10.2478/popore-2014-0018

Rohlf FJ (2015) The tps series of software. Hystrix 26: 9–12. https://doi.org/10.4404/hystrix-26.1-11264

Sayers EW, Bolton EE, Brister JR, Canese K, Chan J, Comeau DC, Connor R, Funk K, Kelly C, Kim S, Madej T, Marchler-Bauer A, Lanczycki C, Lathrop S, Lu Z, Thibaud-Nissen F, Murphy T, Phan L, Skripchenko Y, Tse T, Wang J, Williams R, Trawick BW, Pruitt KD, Sherry ST (2022) Database resources of the national center for biotechnology information. Nucleic Acids Research 50: D20–D26. https://doi.org/10.1093/nar/gkab1112

Schnurr S, Osborn KJ, Malyutina M, Jennings R, Brix S, Driskell A, Svavarsson J, Arbizu PM (2018) Hidden diversity in two species complexes of munnopsid isopods (Crustacea) at the transition between the northernmost North Atlantic and the Nordic Seas. Marine Biodiversity 48: 813–843. https://doi.org/10.1007/s12526-018-0877-6

SOSA, Brandt A, Chen C, Engel L, Esquete P, Horton T, Jażdżewska A, Johannsen N, Kaiser S, Kihara T, Knauber H, Kniesz K, Landschoff J, Lörz A-N, Machado F, Martínez-Muñoz C, Riehl T, Serpell-Stevens A, Sigwart J, Tandberg AH, Tato R, Tsuda M, Vončina K, Watanabe H, Wenz C, Williams J (2024) Ocean Species Discoveries 1–12 — A primer for accelerating marine invertebrate taxonomy. Biodiversity Data Journal 12: e128431. https://doi.org/10.3897/BDJ.12.e128431

Silva CNS, Murphy NP, Bell JJ, Green BS, Duhamel G, Cockcroft AC, Hernández CE, Strugnell JM (2021) Global drivers of recent diversification in a marine species complex. Molecular Ecology 30: 1223–1236. https://doi.org/10.1111/mec.15780

Tamura K, Stecher G, Kumar S (2021) MEGA11: Molecular Evolutionary Genetics Analysis Version 11. Molecular Biology and Evolution 38: 3022–3027. https://doi.org/10.1093/molbev/msab120

Tillich M, Lehwark P, Pellizzer T, Ulbricht-Jones ES, Fischer A, Bock R, Greiner S (2017) GeSeq–versatile and accurate annotation of organelle genomes. Nucleic Acids Research 45: W6–W11. https://doi.org/10.1093/nar/gkx391

Tyler PA (2002) Deep-sea eukaryote ecology of the semi-isolated basins off Japan. Journal of Oceanography 58: 333–341. https://doi.org/10.1023/A:1015817910449

Vrijenhoek RC (2009) Cryptic species, phenotypic plasticity, and complex life histories: Assessing deep-sea faunal diversity with molecular markers. Deep Sea Research Part II: Topical Studies in Oceanography 56: 1713–1723. https://doi.org/10.1016/j.dsr2.2009.05.016

Wilson GDF (2008) A review of taxonomic concepts in the Nannoniscidae (Isopoda, Asellota), with a key to the genera and a description of *Nannoniscus oblongus* Sars. Zootaxa 1680: 1–24. https://doi.org/10.11646/zootaxa.1680.1.1

Supplementary material 1

Genome Sequencing-Methods

Authors: Tilman Schell
Data type: pdf
Explanation note: Detailed overview about the methods used for genome assembly.

Link: https://doi.org/10.3897/zse.101.137663.suppl1

Zoosyst. Evol. 101 (2) 2025, 855–874 | DOI 10.3897/zse.101.147368

PENSOFT

für Natur MUSEUM FÜR NATURKUNDE BERLIN

On the border of Europe and Asia: *Gobio uralensis*, a new species of gudgeons (Cypriniformes, Gobionidae) from the Caspian Sea basin

Ilya S. Turbanov[1,2,3], Aleksey A. Bolotovskiy[1], Oleg N. Artaev[1], Aleksandr A. Gandlin[2], Marina A. Levina[2], Ekaterina D. Vasil'eva[4], Boris A. Levin[2]

1 *Papanin Institute for Biology of Inland Waters Russian Academy of Sciences, Borok, Russia*
2 *A.N. Severtsov Institute of Ecology and Evolution of the Russian Academy of Sciences, Moscow, Russia*
3 *Cherepovets State University, Cherepovets, Russia*
4 *Zoological Museum, Moscow State University, Moscow, Russia*

https://zoobank.org/6F4C6617-F13E-4C9C-9113-938C862467D2

Corresponding authors: Ilya S. Turbanov (turba13@mail.ru); Boris A. Levin (borislyovin@gmail.com)

Academic editor: Nicolas Hubert ♦ **Received** 21 January 2025 ♦ **Accepted** 21 March 2025 ♦ **Published** 22 April 2025

Abstract

A new species of cypriniform fish was discovered during studies of the riverine fish fauna of the Caspian Sea basin, employing an integrative taxonomy approach. The Ural gudgeon is herein described as a new species from the Ural River system, which is considered a geographical boundary between Europe and Asia. The new species is distinguished from the other gudgeon species by a combination of morphological characters and genetic data. Morphologically, it is very similar to *Gobio volgensis* from the Volga basin. Genetically, however, it is closer to *G. acutipinnatus*, which occurs in the upper Irtysh River (Ob' River system), and to *G. multipunctatus* from the Lake Alakol basin in Central Asia (*p*-distance = 0.037; COI mtDNA). Therefore, the Ural gudgeon, which is endemic to the Ural River system, is of Asian rather than European origin. The biogeography of freshwater aquatic animals in the region is discussed in relation to paleogeographic events and connections between the Caspian Sea and Ob' drainages.

Key Words

Biogeography, DNA barcoding, endemics, freshwater fish, genetics, taxonomy

Introduction

According to modern taxonomic concepts, gudgeons of the genus *Gobio* Cuvier, 1816 (Gobionidae, Cypriniformes) comprise 47 valid species (Fricke et al. 2025; Fang et al. 2025). The genus *Gobio* Cuvier, 1816 (Gobionidae, Cypriniformes) is widely distributed across Eurasia. Its range extends from the Iberian Peninsula in the west, including Portugal, and covers most of Europe, except for the central and northern parts of the Scandinavian Peninsula, the Kola Peninsula, Northern Karelia, and the Arctic coast of European Russia. In the east, it reaches Korea and Sakhalin Island. The genus is also found in Siberian rivers, ranging from the Ural Mountains to the Lena and Kolyma river basins. However, it does not extend to the Arctic coast, with its northern limit around 65°N. In Southeast Asia, the range of *Gobio* includes China and extends westward along the southern border of Central Asia, encompassing northern Afghanistan and adjacent regions of the Middle East within the Caspian Sea basin. The range also includes the Caucasus and Asia Minor in the southwest (Bănărescu and Nalbant 1973; Fricke et al. 2025).

The type species *Gobio gobio* (Linnaeus, 1758) was, until recently, considered a morphologically variable species comprising several subspecies and intraspecific forms, distributed across much of Northern Eurasia, from the Iberian Peninsula to the Far East and northeastern Siberia (Berg, 1949; Bănărescu et al. 1999). However, revisions of European fishes have been proposed based on

phylogenetic (Kottelat 1997) and evolutionary (Mayden 2002) species concepts. It has been hypothesized that multiple distinct gudgeon species exist under the name *G. gobio*. A comprehensive revision of the genus cannot be resolved through examination of museum material – often old and poorly preserved – but requires direct comparison of freshly collected, well-preserved specimens (Kottelat 1997; Mayden 2002). Subsequently, based on morphological, karyological, and molecular genetic data, several gudgeon species within the genus *Gobio* were described as new (Vasil'eva et al. 2004, 2005, 2023; Doadrio and Madeira 2004; Freyhof and Naseka 2005; Kottelat and Persat 2005; Naseka et al. 2006; Xie 2007; Mendel et al. 2008; Turan et al. 2012, 2016, 2017, 2018; Li 2015). Additionally, molecular genetic analyses have confirmed the validity of several other species within the genus and revealed the hybrid origin of some populations (Doadrio and Madeira 2004; Yang et al. 2006; Mendel et al. 2008; Tang et al. 2011; Takács et al. 2014, 2021; Aksu and Bektaş 2019; Sheraliev et al. 2020; Zangl et al. 2020; etc.).

As part of efforts to document the ichthyofauna of Russia, we investigated gudgeons of the genus *Gobio* in the Ural River basin and adjacent drainage systems. The Ural River, the third longest river in Europe, has a total length of 2,428 km and a catchment area of 231,000 km^2. It flows through Russia and Kazakhstan, representing the boundary between Europe and Asia. The river originates in the Ural Ridge of the Southern Urals and drains into the northeastern Caspian Sea (Davydov 1936).

Studies of *Gobio* gudgeons in the Ural River basin have a history spanning more than a century. The earliest record of gudgeons in the region appears in Kessler (1877), who cited *Gobio fluviatilis* Cuvier, 1842 (now considered a junior synonym of *G. gobio*). Subsequent researchers (Navozov 1912; Berg 1914; Bening 1938; Tikhiy 1938; Kozhin 1949; Shaposhnikova 1964; Mitrofanov 1988; Zinovyev and Baklanov 2007; Magazov and Rechkalov 2007; Chibilev and Debelo 2009; Shevchenko 2018) reported the presence of *G. gobio* in the Ural River and its tributaries. Notably, *Gobio volgensis* Vasil'eva, Mendel, Vasil'ev, Lusk & Lusková, 2008 – originally described from the Volga River basin (Mendel et al. 2008) – was also reported from the Ural River delta (Bogutskaya et al. 2013). Based on comparative morphological analysis, Martynova and Vasil'eva (2021) assigned gudgeons from six populations in the Ural River basin to *G. volgensis*.

Based on a study of gudgeons from various parts of the Ural River basin, Shaposhnikova (1964) demonstrated their morphological heterogeneity. According to her observations, the population inhabiting the upper reaches of the Ural River is morphologically closer to gudgeons (identified as *G. gobio*) from the Northern Dvina basin (part of the Arctic Ocean catchment in European Russia), which are now referred to as *G. volgensis* (our data). In contrast, the population from the steppe tributaries of the middle Ural River more closely resembles the Siberian gudgeon *Gobio sibiricus* Nikolsky, 1936 – identified in the cited work as *Gobio gobio cynocephalus* Dybowski, 1869 – from the Ob' and Yenisei basins. Subsequent authors (Mitrofanov 1988; Chibilev and Debelo 2009) also suggested that gudgeons from the Ural River basin differ from typical *G. gobio*, although no dedicated studies have been conducted to confirm this.

Thus, the taxonomy of gudgeons from the Ural River basin remains unresolved, with all previous conclusions based solely on morphological data. In the absence of molecular genetic data, there is insufficient evidence to determine whether the Ural gudgeons belong to any of the species inhabiting adjacent basins. Our study, based on extensive sampling and an integrative taxonomic approach, enabled us to formally describe the Ural gudgeons as a distinct species.

Materials and methods

Sampling

Material for this study was collected by the authors in the Ural River basin and adjacent basins of the Volga and Ob' rivers in Russia during 2020–2021. Sampling sites are shown in Fig. 1. Type specimens and additional material of the newly described species were collected from nine localities in the Ural River basin. Comparative material was collected from basins adjacent to the Ural River. *G. volgensis* specimens were obtained from four localities in the Volga River basin, and *G. sibiricus* from three localities in the Ob' River basin. Additionally, *Gobio acutipinnatus* Menshikov, 1939, from Kazakhstan was included in the comparative material, comprising a type series (syntypes) from Lake Markakol (Menshikov 1939), deposited in the Zoological Institute of the Russian Academy of Sciences. Sample characteristics are provided in the subsequent description of the new species and comparative remarks.

Fish were caught using a frame net and a seine net with a mesh size of 6–8 mm. Individuals were euthanized in a solution of clove oil and photographed in an aquarium under artificial lighting. Photographs were taken using a Nikon D5300 camera with a Nikkor 60mm f/2.8G lens (Nikon Corporation, Tokyo, Japan), and a physical white swatch was used for color correction. Tissues (pectoral or pelvic fins) were taken from some specimens (DNA vouchers) and placed in 96% ethanol for subsequent DNA extraction in the laboratory. Then, most of the specimens were preserved in 10% formalin, while some (usually small individuals) were preserved in 96% ethanol. In the laboratory, formalin samples were rinsed in running water and then transferred to 70% ethanol.

The types (holotype, some paratypes), additional, and comparative material were deposited at the Fish Collection of the Papanin Institute for Biology of Inland Waters of the Russian Academy of Sciences, Borok, Russia (**IBIW_FS**); the remaining paratypes (see below) were deposited at the Zoological Institute of the Russian Academy of Sciences, Saint Petersburg, Russia (**ZISP**), and the Zoological Museum of the Moscow State University, Moscow, Russia (**ZMMU**).

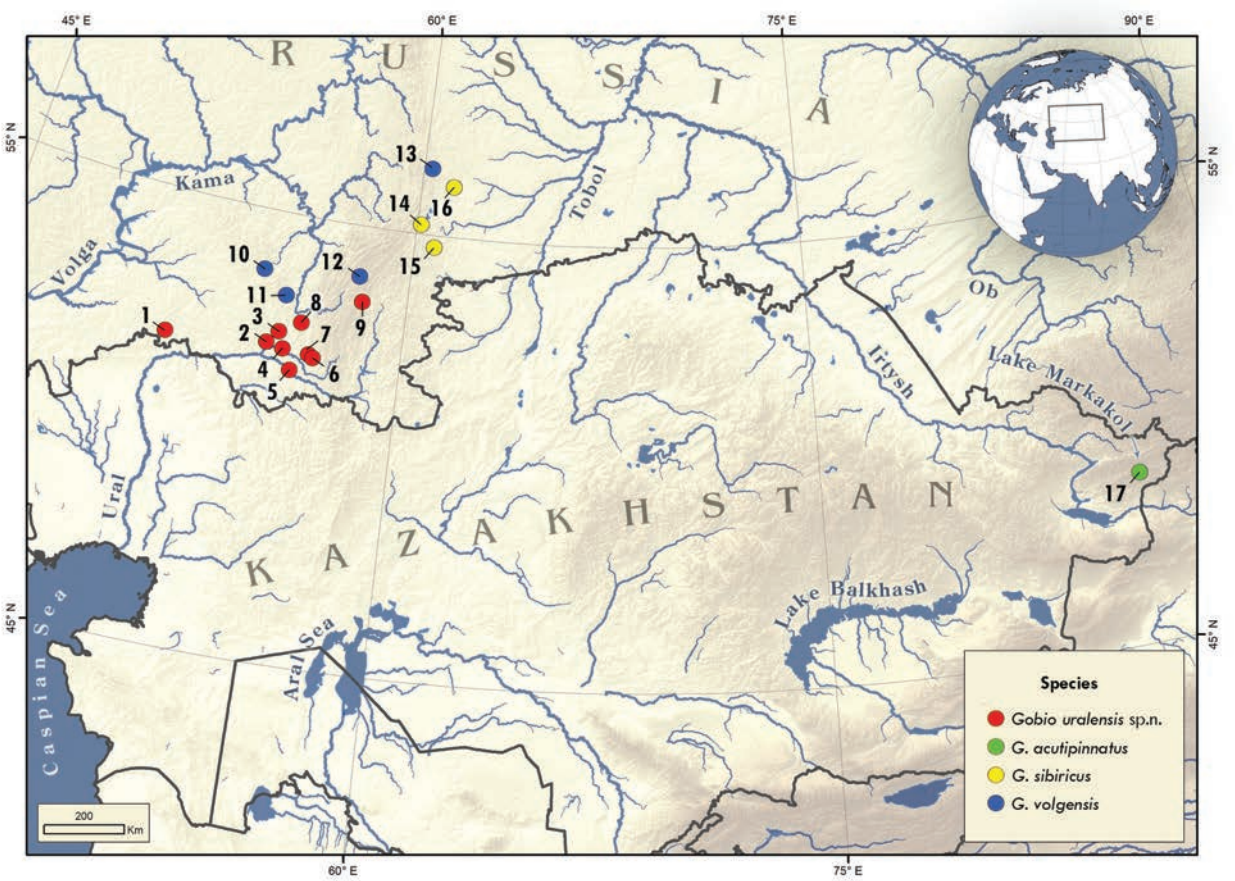

Figure 1. Map of localities of *Gobio* spp. sampled for this study: 1. Bolshoy Kizil River; 2. Chagan River; 3. Ural River; 4. Sakmara River; 5. Kargalka River; 6. Bolshoy Yushatyr River; 7. Nakas River; 8. Uskalyk River; 9. Assel River; 10. Dyoma River; 11. Ashkadar River; 12. Belaya River; 13. Chusovaya River; 14. Kushtumga River; 15. Koelga River; 16. Sinara River; 17. Lake Markakol.

Comparative material

Gobio volgensis: • 6 spec. (IBIW_FS_467) 101.1–129.7 mm SL, Russia, Sverdlovsk Region, Polevskoy Distr., near Kosoy Brod, Chusovaya River, 56.4799°N, 60.3270°E, 23 Aug. 2020, O.N. Artaev, A.A. Bolotovskiy, I.V. Pozdeev, I.S. Turbanov leg. • 4 spec. (IBIW_FS_468) 92.4–117.3 mm SL, same data (see above), 29 May 2021, O.N. Artaev, A.A. Bolotovskiy, A.V. Kutuzov leg. • 1 spec. (IBIW_FS_469) 98.8 mm SL, 1 spec. (IBIW_FS_470) 79.5 mm SL, Russia, Republic of Bashkortostan, Beloretsky Distr., near Sermenevo, Belaya River, 53.8679°N, 58.0977°E, 24 Aug. 2020, O.N. Artaev, A.A. Bolotovskiy, I.V. Pozdeev, I.S. Turbanov leg.• 26 spec. (IBIW_FS_471) 67.4–100.8 mm SL, Russia, Republic of Bashkortostan, Fyodorovsky Distr., near Zlataustovka, Ashkadar River, 53.1802°N, 55.5203°E, 26 Aug. 2020, O.N. Artaev, A.A. Bolotovskiy, I.S. Turbanov leg. • 8 spec. (IBIW_FS_472) 68.8–87.4 mm SL, Russia, Republic of Bashkortostan, Miyakinsky Distr., near Kanbekovo, Dyoma River, 53.6641°N, 54.5435°E, 27 Aug. 2020, O.N. Artaev, A.A. Bolotovskiy, I.S. Turbanov leg. ***Gobio sibiricus***: • 1 spec. (IBIW_FS_473) 78.1 mm SL, 12 spec. (IBIW_FS_474) 24.0–62.4 mm SL, Russia, Chelyabinsk Region, Miass Distr., near Severnye Pechi, Kushtumga River, 55.2105°N, 60.1570°E, 23 May 2020, O.N. Artaev, A.A. Bolotovskiy, I.V. Pozdeev, I.S. Turbanov leg. • 10 spec. (IBIW_FS_477) 54.6–84.4 mm SL, Russia, Chelyabinsk Region, Chebarkulsky Distr., near Zvyagino, Koelga River, 54.7327°N, 60.7620°E, 27 May 2021, O.N. Artaev, A.A. Bolotovskiy, A.V. Kutuzov leg. • 13 spec. (IBIW_FS_475) 53.0–94.7 mm SL, 3 spec. (IBIW_FS_476) 40.8–56.7 mm SL, Russia, Chelyabinsk Region, Kaslinsky Distr., near Bulzi (abandoned Yugo-Konevo), Sinara River, 56.1209°N, 61.2691°E, 27 May 2021 O.N. Artaev, A.A. Bolotovskiy, A.V. Kutuzov leg. ***Gobio acutipinnatus***: Syntypes • 7 spec. (ZISP 26865) 82.2–102.9 mm SL, Kazakhstan, East Kazakhstan Region, Kurshim Distr., Lake Markakol, ca. 48.7555°N, 85.7642°E, 21 July 1936, M.I. Menshikov leg. • 3 spec. (ZISP 7831) 101.79–110.21 mm SL, same locality (see above), 1887, Suworcev leg.

Morphological studies

Morphological and morphometric characters were selected based on previous studies on the taxonomy of the genus *Gobio* (Bănărescu et al. 1999; Vasil'eva et al. 2004; Freyhof and Naseka 2005). A total of 18 meristic characters and 31

morphometric indices, along with several proportional relationships and two qualitative characters, were investigated. Individual measurements were taken as described by Hubbs and Lagler (1946). All measurements were taken point-to-point using a digital caliper and recorded to the nearest 0.1 mm by a single operator to ensure consistency, following the recommendations of Mina et al. (2005). Standard length (SL) was measured from the tip of the snout to the end of the hypural complex. Lateral head length (HL) was measured to include the skin flap. All indices are given as percentages of standard length (SL) unless otherwise noted.

External meristic characters were counted on both sides. The count of lateral line scales includes all pored scales, from the first one just behind the supracleithrum to the posterior-most scale on the caudal-fin base (hypural). The total number of lateral line scales, as well as the transverse scales above and below the lateral line, were counted. These correspond to horizontal scale rows located below the origin of the dorsal fin and above the origin of the pelvic fin, respectively. The last two branched rays, articulated on a single pterygiophore in the dorsal and anal fins, are noted as "1½". For the description of the type and additional material of new species, the number of unbranched rays in the dorsal and anal fins was counted. The number of outer gill rakers on the first gill arch was counted on the right side of the specimens. Meristic characters (except for the axial skeleton) and qualitative characters (breast squamation and coloration) were examined using an MC-2-ZOOM stereomicroscope (Micromed, Saint Petersburg, Russia). Axial skeleton was examined using radiographs. Vertebral counts were made following Naseka (1996), using PRDU (v.II) X-ray equipment (ELTECH-Med, St. Petersburg, Russia). Images of pharyngeal teeth were obtained using a JEOL JSM-6510LV scanning electron microscope (JEOL, Tokyo, Japan). Abbreviations used are **A** – number of branched rays of anal fin, **D** – number of branched rays of dorsal fin, **P** – number of branched rays of pectoral fin, **V** – number of branched rays of pelvic fin, **LLt** – total number of lateral line scales, **LL** – number of lateral line scales to hypural, **GR** – number of gill rakers on the outer side of the first gill arch, **up LL** – number of scales above lateral line in horizontal rows below the dorsal fin origin, **down LL** – number of scales between lateral line and the pelvic fin origin, **CPS** – number of circumpeduncular scales, **Vert.** – total vertebrae, Va – abdominal vertebrae, **VpreD** – predorsal abdominal vertebrae, **Vi** – intermediate vertebrae, **Vc** – caudal vertebrae, **VpreA** – preanal caudal vertebrae, **VpostA** – postanal caudal vertebrae.

Statistical procedures were carried out with the R statistics using packages: *ggplot2*, *rstatix*, *tidyverse*, and *MASS*. The pattern of morphological variation was analyzed using Linear Discriminant Analysis (LDA). The results of LDA were assessed using the Wilks' Lambda and F-test statistics. The significant differences in morphometric and meristic characters were tested using the Kruskal-Wallis test followed by Dunn's post hoc test with Bonferroni correction.

In total, morphological analysis was performed on 170 specimens: *G. volgensis* – 46, *G. sibiricus* – 37, *G. acutipinnatus* – 10 (7 for radiographs), and new species – 77 specimens.

Molecular and phylogenetic study

DNA was isolated by the salt-extraction method (Aljanabi and Martinez 1997) from ethanol-fixed tissues. Molecular genetic studies were conducted on 58 samples: new species – 29, *G. volgensis* – 23, *G. sibiricus* – six specimens (see Suppl. material 1). As comparative phylogenetic material, we obtained six COI sequences from several other *Gobio* species (*G. cynocephalus, G. macrocephalus* Mori, 1930, *G. multipunctatus* Vasil'eva, Mamilov & Sharakhmetov, 2023, *G. holurus* Fowler, 1976, *G. krymensis* Bănărescu & Nalbant, 1973, and *G. sarmaticus* Berg, 1949) as well as included sequences from GenBank – *G. cynocephalus, G. nigrescens* (Keyserling, 1861), *G. macrocephalus, G. artvinicus* Turan, Japoshvili, Aksu & Bektaş, 2016, *G. caucasicus* Kamensky, 1901, *G. acutipinnatus, G. kizilirmakensis* Turan, Japoshvili, Aksu & Bektaş, 2016, *G. sakaryaensis, G. lozanoi, G. occitaniae, G. holurus, G. lepidolaemus, G. sibiricus, G. ohridanus, G. skadarensis* Karaman, 1937, *G. gobio, G. balcanicus* Dimovski & Grupche, 1977, *G. bulgaricus* Drensky, 1926, *G. kovatschevi* Chichkoff, 1937 and *G. volgensis* (Triantafyllidis et al. 2011; Geiger et al. 2014; Knebelsberger et al. 2015; Mousavi-Sabet et al. 2016; Yang et al. 2016; Corse et al. 2017; Friedrich et al. 2018; Li et al. 2018; Aksu and Bektaş 2019; Sheraliev et al. 2020; Yi and Fu 2020; Behrens-Chapuis et al. 2021; Sheraliev and Peng 2021; and unpublished sequences in GenBank – https://www.ncbi.nlm.nih.gov/) (see Suppl. material 1).

Mitochondrial cytochrome *c* oxidase subunit I (COI mtDNA) barcode region was amplified using M13-tailed primer cocktail: FishF2_t1: 5′-TGT AAA ACG ACG GCC AGT CGA CTA ATC ATA AAG ATA TCG GCA C-3′, FishR2_t1: 5′-CAG GAA ACA GCT ATG ACA CTT CAG GGT GAC CGA AGA ATC AGA A-3′, VF2_t1: 5′-TGT AAA ACG ACG GCC AGT CAA CCA ACC ACA AAG ACA TTG GCA C-3′, and FR1d_t1: 5′-CAG GAA ACA GCT ATG ACA CCT CAG GGT GTC CGA ARA AYC ARA A-3′ (Ivanova et al. 2007). PCR conditions for COI followed protocols from Ivanova et al. (2007).

Sequencing of the PCR products purified by ethanol and ammonium acetate (3 M) precipitation was conducted using the Applied Biosystems 3500 DNA sequencer (Thermo Fisher Scientific, USA) with primers M13F 5′-GTA AAA CGA CGG CCA GT-3′ M13R-pUC 5′- CAG GAA ACA GCT ATG AC-3′ for COI.

DNA chromatograms were checked for errors in FinchTV 1.4.0 (Rothgänger et al. 2006), and the DNA sequences were aligned using the ClustalW algorithm in MEGA7 (Kumar et al. 2016). Phylogenetic analysis was performed on COI (627 bp) sequences. Only unique haplotypes were used in downstream phylogenetic analyses.

The Bayesian phylogenetic analysis was performed in a Bayesian statistical framework implemented in BEAST v.1.10.4 (Hill and Baele 2019) with 2×10^7 MCMC generations (10% burn-in) and parameters sampled every 2000 steps. The substitution models by codon position for Bayesian analysis were selected in PartitionFinder v.2.1.1 (Lanfear et al. 2016) with the greedy algorithm (Lanfear et al. 2012) (Suppl. material 2). Maximum likelihood phylogenies were inferred using IQ-TREE v.2.2.0 (Nguyen et al. 2015) in PhyloSuite v.1.2.3 (Zhang et al. 2020; Xiang et al. 2023) under the Edgelinked partition model for 1000 ultrafast (Minh et al. 2013) bootstraps. ModelFinder v.2.2.0 (Kalyaanamoorthy et al. 2017) in PhyloSuite v.1.2.3 was used to select the best-fit partition model (edge-linked) using the AICc criterion (Suppl. material 2).

The average intra-group as well as the average pairwise intergroup *p*-distances using concatenated COI sequences data set were calculated using the MEGA7 program (Kumar et al. 2016) with 1000 bootstrap replicas.

Map visualization

The map was created using the QGIS software v.3.34. Digital elevation model visualized based on GMTED2010, 30 sec. resolution (Danielson and Gesch 2011); river systems – HydroATLAS v.1.0 (Linke et al. 2019).

Results

Phylogenetic relationships and genetic distance

The phylogenetic Bayesian tree of the genus *Gobio* shows (Fig. 2) that the gudgeon from the Ural River basin forms its own lineage and is a sister (with a high support) to *G. acutipinnatus* from the upper Irtysh River and its tributaries (Ob' River basin, Arctic Ocean catchment) and *G. multipunctatus* from the Emel River (Lake Alakol basin; enclosed water system). Genetic *p*-distances to these species are 0.037 ± 0.007 and 0.037 ± 0.008, respectively (Table 1). Being combined together, the aforementioned species form a clade that is sister to a clade of the Caucasian species *G. caucasicus* from the Kura River (Caspian Sea basin) and *G. artvinicus* from the Chorokh (Çoruh) and Natanebi rivers (Black Sea basin) – although this node is weaker supported. ML-tree (Suppl. material 3) supported the same phylogenetic relationships of the Ural gudgeon, *G. acutipinnatus*, *G. multipunctatus*, and *G. caucasicus-artvinicus* lineages. The results obtained confirm that the Ural gudgeon is an independent new species.

Noteworthy, this new species is genetically distant from geographically neighboring species – *G. volgensis* from the Volga River basin (*p*-distance = 0.059 ± 0.009) and *G. sibiricus* from the rivers of the Ob' River basin (0.047 ± 0.008) (Table 1). Intraspecific divergence of the Ural gudgeon (0.001) is comparable to that in other species (Table 1). Below we provide a description of this species.

Systematics

Class Actinopteri Cope, 1871
Order Cypriniformes Bleeker, 1859
Family Gobionidae Bleeker, 1863
Genus *Gobio* Cuvier, 1816

***Gobio uralensis* sp. nov.**

https://zoobank.org/25D6334F-3234-4D62-A90D-4B4C85C4BB0F
Figs 3, 4, 8A
(English name – Ural gudgeon, Russian name – уральский пескарь)

Gobio fluviatilis non Cuvier, 1842 – Kessler 1877: 298.

Gobio gobio (non Linnaeus, 1758) – Navozov 1912: 263; Berg 1914: 428 (part.); Bening 1938: 237; Tikhiy 1938: 307; Berg 1949: 640 (part.); Kozhin 1949: 374 (part.); Shaposhnikova 1964: 78; Mitrofanov 1988: 6, fig. 1 (part.); Kottelat 1997: 60 (part.); Bănărescu et al. 1999: 81 (part.); Zinovyev and Baklanov 2007: 54 (part.); Magazov and Rechkalov 2007: 87 (part.); Chibilev and Debelo 2009: 101 (part.); Shevchenko 2018: 122–123.

Gobio volgensis non Vasil'eva, Mendel, Vasil'ev, Lusk & Lusková, 2008 – Bogutskaya et al. 2013: 176, figs 35a, 36a (part.); Martynova and Vasil'eva 2021: 529 (part.), figs 1, 2; Vasil'eva et al. 2023: 503 (part.).

Type material. ***Holotype*** • (IBIW_FS_454) 97.7 mm SL, Russia, Republic of Bashkortostan, Abzelilovsky Distr., near Ryskuzhino, Bolshoy Kizil River, 53.3161°N, 58.3351°E, 24 Aug. 2020, O.N. Artaev, A.A. Bolotovskiy, I.V. Pozdeev, I.S. Turbanov leg. ***Paratypes*** • 4 spec. (IBIW_FS_455) 70.3–110.4 mm SL, 3 spec. (ZISP 57042) 69.8–73.4 mm SL, 3 spec. (ZMMU P-24633) 68.1–75.7 mm SL, same data as holotype.

Additional material. • 7 spec. (IBIW_FS_456) 40.9–64.4 mm SL, same data as holotype and paratypes • 4 spec. (IBIW_FS_457) 34.8–42.7 mm SL, Russia, Orenburg Region, Pervomaysky Distr., near Lyashevo, Chagan River, 51.8514°N, 51.4965°E, 22 May 2021, O.N. Artaev, A.A. Bolotovskiy, A.V. Kutuzov leg. • 1 spec. (IBIW_FS_458) 72.5 mm SL, Russia, Orenburg Region, Saraktashsky Distr., near Krasnogor, Ural River, 51.5591°N, 56.1224°E, 23 May 2021, O.N. Artaev, A.A. Bolotovskiy, A.V. Kutuzov leg. • 5 spec. (IBIW_FS_459) 38.9–50.3 mm SL, 32 spec. (IBIW FS_465) 27.9–39.9 mm SL, Russia, Orenburg Region, Saraktashsky Distr., near Nikolskoe, Sakmara River, 52.0018°N, 55.7371°E, 24 May 2021, O.N. Artaev, A.A. Bolotovskiy, A.V. Kutuzov leg. • 2 spec. (IBIW_FS_460) 85.0–87.5 mm SL, Russia, Orenburg Region, Sakmarsky Distr., near Svetlyi, Kargalka River, 52.0835°N, 55.1283°E, 24 May 2021, O.N. Artaev, A.A. Bolotovskiy, A.V. Kutuzov leg. • 11 spec. (IBIW_FS_461) 47.2–80.2 mm SL • 15 spec. (IBIW FS_466) 33.7–47.6 mm SL, Russia, Orenburg Region, Oktyabrsky Distr., Oktyabrskoe, Bolshoy Yushatyr River, 52.3631°N, 55.5008°E, 24 May 2021, O.N. Artaev, A.A. Bolotovskiy, A.V. Kutuzov leg. • 1 spec. (IBIW_FS_462) 71.8 mm SL, Russia, Republic of Bashkortostan, Kugarchinsky Distr., near Aznagulovo, Nakas River, 52.6431°N, 56.2436°E, 24 May 2021, O.N.

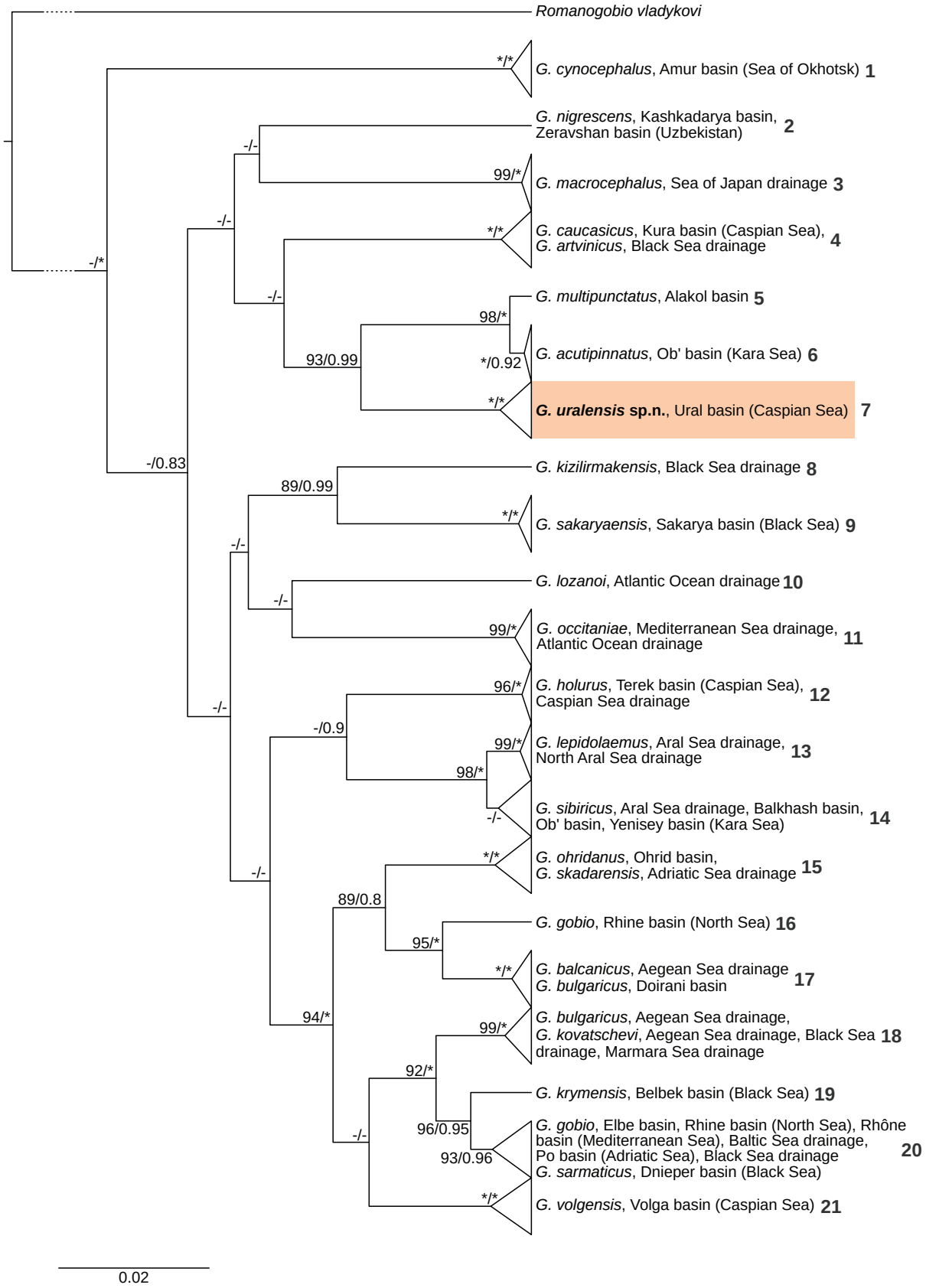

Figure 2. BI consensus tree of COI mtDNA sequences representing all available *Gobio* species in GenBank combined with our data set. *Gobio uralensis* sp. nov. is highlighted by color. Bootstrap values/posterior probabilities above 80/0.8 are shown; asterisks represent 100/1 bootstrap/posterior probability values. The scale bar is in expected substitutions per site. The nodes with multiple specimens collapsed to a triangle, with the horizontal depth indicating the level of divergence within the node. Lineage numbers are given by the bold numbers from 1 to 21.

Artaev, A.A. Bolotovskiy, A.V. Kutuzov leg. • 17 spec. (IBIW_FS_463) 57.9–82.1 mm SL, Russia, Republic of Bashkortostan, Zianchurinsky Distr., near Verkhniy Muinak, Uskalyk River, 51.9687°N, 56.6878°E, 25 May 2021, O.N. Artaev, A.A. Bolotovskiy, A.V. Kutuzov leg. • 5 spec. (IBIW_FS_464) 37.2–81.4 mm SL, Russia, Republic of Bashkortostan, Zianchurinsky Distr., upstream Itkulovo, Assel River, 51.9047°N, 56.8683°E, 25 May 2021, O.N. Artaev, A.A. Bolotovskiy, A.V. Kutuzov leg.

Etymology. The adjective *uralensis* comes from the name of the Ural River, which literally means lives in the basin of this river.

Diagnosis. *Gobio uralensis* sp. nov. is distinguished by a combination of characters, none of which is unique, as follows: predorsal length 47.4–52.6% SL; postdorsal length 36.3–42.1% SL; body depth 17.4–23.7% SL; prepelvic length 49.8–56.8% SL; preanal length 70.2–75.2 SL; snout length 40.9–48.8% HL; interorbital width 22.3–29.6% HL; ratio of caudal peduncle length to caudal peduncle depth 2.0–2.8; pharyngeal teeth in two rows, 3.5–5.3; anal fin branched rays $6^{1}/_{2}$; number of lateral line scales 39–45, mean 42.1; 12 (mode) predorsal vertebrae; the breast between the pectoral fins is naked; lower lip is interrupted in middle, with a notch between narrower anterior and widening posterior parts.

Description. General appearance shown in Fig. 3. Morphometric and meristic data are given in Tables 2–4. Largest recorded specimen – 110.4 mm SL.

Morphometrics. The body and the caudal peduncle are moderately compressed; the minimum body depth is somewhat greater than the width of the caudal peduncle at the level of the last anal ray. Predorsal length is somewhat more than postdorsal length. The distance between pectoral and pelvic-fin origins is somewhat more than the distance between pelvic and anal-fin origins. The anus is closer to the insertion of the anal fin than to the origin of the pelvic fins; the pelvic fin reaches beyond the anus. Barbels are moderately long; they are usually less than 1/3 of the head length and reach up to the middle of the eye but never reach to its posterior edge. Paired fins are moderately long: pectoral fins never reach the pelvic fin insertion; ventral fins never reach the anal fin insertion. The eye is large with a diameter of 17.6–25.2% of the head length, an eye diameter of 2.2–3.3 times in head depth, and 1.0–1.5 times in interorbital width. The snout is pointed; its length is somewhat longer than the postorbital length. Caudal peduncle is 2.0–2.8 times longer than depth.

Meristics. Dorsal fin margin is concave, with 3 unbranched and $7^{1}/_{2}$ branched rays (only one specimen had $8^{1}/_{2}$ rays); anal fin margin is concave or straight, with 3 unbranched and $6^{1}/_{2}$ branched rays; pectoral fin branched ray numbers vary within 13–17 (mode 16 and 15 in left and right, respectively); and pelvic fin branched ray numbers vary within (5) 6–8 (mode 7). The shape of the caudal fin is variable; the two lobes are sharpened or rounded, with a notch in the middle. Body is covered by scales. Lateral line includes 39–45 total scales (mode 42) and 11–15 circumpeduncular scales (mode 12). Two-five gill rakers (modes 4 and 5) on outer side of first gill arch. Pharyngeal teeth are in two rows, 3.5–5.3, slightly hooked at tip (Fig. 4).

Total vertebrae 39–42 (mode 40), 20–22 (mode 21) abdominal, including 11–13 predorsal and 18–21 (mode 19) caudal, including 1–3 preanal and 16–19 postanal vertebrae. The radiograph of the holotype is given in Fig. 5.

Qualitative characters. The breast in front of the posterior edge of the base of the pectoral fins usually lacks scales; some individuals have 1–3 scales along the midline towards the throat [character state 1 following Naseka et al. (2006)] (Fig. 8A).

Coloration. Body is dark olive-brown above, merging into a light silvery underside. There are large, more or less rounded 6–14 (often 10) blotches on flank located along the lateral line. The color of the fins corresponds to the color of the body with several rows of small dark dots on the dorsal and caudal fins. Live coloration is given in Figs 3A, D, E, 8A.

Distribution. The type specimens were collected from the Bolshoy Kizil River, a tributary of the Ural River, near Ryskuzhino (53.3161°N, 58.3351°E), Republic of Bashkortostan, Russia (see Fig. 6). All other gudgeons genetically confirmed as the same species were caught in different locations in the Ural River basin (see materials). Although we suppose that the whole Ural River basin is inhabited by the Ural gudgeon, one may not exclude that some parts of the extended Ural drainage are inhabited by other species. According to Shaposhnikova (1964), the gudgeon is widespread throughout the Ural River. The gudgeon is especially abundant in the mountain tributaries of the Ural and in its upper reaches, where it is numerous in riffles and sandbanks; this is partly confirmed by the data of Martynova and Vasil'eva (2021) as well as by our observations.

Biology. In the Ural River near Orenburg, the gudgeon spawns from the middle of the twentieth days of April to early or mid-May, but individual spawning specimens are caught throughout the summer (Navozov 1912). Spawning is multiple (Shaposhnikova 1964). In all areas of the Ural basin, regardless of the time of year, larvae of Tendipedidae (Insecta: Diptera) are the main food item beginning from the first year of life. In addition, larvae of Heleidae (Insecta: Diptera), Oligochaeta (Annelida), larvae of Ephemeroptera (Insecta), Gastropoda (Mollusca), plant remnants, and diatom algae were also detected. In juveniles (up to 47 mm), Cladocera and Copepoda (Crustacea) as well as diatoms and other algae predominated in the food bolus (Shaposhnikova 1964).

Comparative remarks. As we have already noted above, in the earliest faunal studies, the gudgeons from the Ural River basin were identified as *Gobio gobio*. However, according to the latest data, *G. gobio* is distributed in the basins of the Atlantic Ocean, the North, Baltic and White Seas (including Great Britain and the upper Danube basin), but not in the Caspian Sea basin (Dyldin et al. 2023). At the same time, *G. gobio* is well differentiated from *G. uralensis* sp. nov. by a narrow lower lip with no interception between the anterior and posterior parts (vs. the lower lip is interrupted in the middle, with

Table 1. Genetic *p*-distances between *Gobio* spp. for COI mtDNA sequences. The averages of interspecies distances are given below the diagonal, the standard errors are given above the diagonal, and the intraspecies divergence is given in a diagonal in bold. Lineage numbers (from 1 to 21) are given in parentheses after the species name.

	***G. acutipinnatus* (6)**	***G. artvinicus* (4)**	***G. balcanicus* (17)**	***G. bulgaricus* (18)**	***G. bulgaricus* (17)**	***G. caucasicus* (4)**	***G. cynocephalus* (1)**	***G. gobio* (16)**	***G. gobio* (20)**	***G. holurus* (12)**	***G. kizilirmakensis* (8)**	***G. kovatschevi* (18)**	***G. krymensis* (19)**
G. acutipinnatus (6)	**0.001**	0.008	0.009	0.009	0.009	0.008	0.010	0.009	0.009	0.008	0.009	0.009	0.009
G. artvinicus (4)	0.049	**0.004**	0.008	0.008	0.008	0.002	0.009	0.008	0.008	0.008	0.008	0.008	0.008
G. balcanicus (17)	0.056	0.051	**0.003**	0.002	0.008	0.008	0.010	0.006	0.007	0.008	0.009	0.007	0.007
G. bulgaricus (18)	0.058	0.049	0.003	—	0.008	0.008	0.010	0.006	0.007	0.009	0.009	0.007	0.007
G. bulgaricus (17)	0.056	0.051	0.041	0.043	—	0.008	0.009	0.008	0.005	0.009	0.009	0.003	0.006
G. caucasicus (4)	0.048	0.004	0.049	0.049	0.049	**0**	0.009	0.008	0.008	0.008	0.008	0.008	0.008
G. cynocephalus (1)	0.074	0.062	0.073	0.071	0.068	0.063	**0.005**	0.010	0.009	0.009	0.009	0.009	0.009
G. gobio (16)	0.060	0.048	0.022	0.022	0.038	0.046	0.069	—	0.007	0.008	0.009	0.007	0.007
G. gobio (20)	0.053	0.042	0.032	0.034	0.019	0.040	0.062	0.029	**0.000**	0.008	0.008	0.004	0.003
G. holurus (12)	0.050	0.049	0.052	0.053	0.053	0.047	0.069	0.047	0.046	**0.002**	0.008	0.009	0.008
G. kizilirmakensis (8)	0.063	0.053	0.061	0.059	0.054	0.056	0.065	0.059	0.050	0.052	—	0.008	0.008
G. kovatschevi (18)	0.053	0.045	0.035	0.037	0.006	0.043	0.061	0.035	0.013	0.049	0.048	**0**	0.005
G. krymensis (19)	0.055	0.049	0.032	0.035	0.021	0.048	0.065	0.033	0.008	0.047	0.046	0.014	—
G. lepidolaemus (13)	0.048	0.046	0.048	0.049	0.050	0.045	0.068	0.050	0.044	0.041	0.057	0.047	0.045
G. lozanoi (10)	0.061	0.053	0.056	0.057	0.062	0.051	0.069	0.053	0.056	0.057	0.065	0.056	0.054
G. macrocephalus (3)	0.046	0.047	0.050	0.052	0.055	0.045	0.077	0.047	0.044	0.051	0.066	0.052	0.050
G. multipunctatus (5)	0.004	0.047	0.053	0.054	0.053	0.046	0.073	0.056	0.050	0.050	0.059	0.049	0.051
G. nigrescens (2)	0.071	0.067	0.075	0.077	0.067	0.065	0.080	0.070	0.061	0.065	0.065	0.064	0.059
G. occitaniae (11)	0.055	0.047	0.049	0.049	0.049	0.046	0.069	0.048	0.046	0.047	0.048	0.043	0.043
G. ohridanus (15)	0.061	0.057	0.033	0.035	0.045	0.056	0.076	0.038	0.038	0.057	0.064	0.040	0.037
G. sakaryaensis (9)	0.069	0.052	0.066	0.069	0.056	0.053	0.082	0.065	0.057	0.061	0.048	0.053	0.057
G. sarmaticus (20)	0.053	0.041	0.032	0.033	0.019	0.040	0.061	0.029	0.000	0.045	0.049	0.013	0.008
G. sibiricus (14)	0.048	0.042	0.044	0.046	0.043	0.041	0.063	0.044	0.038	0.035	0.052	0.040	0.039
G. skadarensis (15)	0.061	0.054	0.032	0.032	0.040	0.053	0.074	0.035	0.035	0.053	0.061	0.035	0.037
G. uralensis sp. nov. (7)	0.037	0.045	0.056	0.057	0.054	0.043	0.077	0.059	0.052	0.055	0.060	0.054	0.056
G. volgensis (21)	0.064	0.059	0.037	0.038	0.042	0.056	0.073	0.045	0.031	0.055	0.065	0.035	0.034

a groove between narrower anterior and wider posterior parts in *G. uralensis* sp. nov.); its minimum body depth always exceeds 30% of the length of the head and 40% of the length of the caudal peduncle (Vasil'eva et al. 2023).

Geographically, the two species closest to the new species are the Siberian gudgeon *G. sibiricus* (Figs 7C, D, 8C), distributed from the Ob' to Lena basins (including the Nura River in Kazakhstan), and *G. volgensis* (Figs 7A, B, 8B), known from the Volga River basin.

In turn, the new species is morphologically almost indistinguishable from the Volga gudgeon; therefore, the Ural populations were previously identified as *G. volgensis* (Vasil'eva et al. 2023). According to the materials of this study, *G. volgensis* from the Chusovaya, Belaya, Ashkadar and Dema rivers (neighboring rivers of the Volga River basin to the typical habitats of the Ural gudgeon) have a slightly higher total number of lateral line scales – a range 41–45 and median of 42.5 (vs. a range 39–45, median of 42 in *G. uralensis* sp. nov.), as well as a higher number of scales above lateral line – a range 5–6.5 and median of 6 (vs. a range 4–6, median of 5.5 in *G. uralensis* sp. nov.). Besides, small differences in the mean values of some morphometric characters are observed between the combined samples of both species (see Table 3).

Contrast to *G. uralensis* sp. nov. the minimum body depth in *G. sibiricus*, always exceeds 30% of the length of the head and 40% of the length of the caudal peduncle (vs. usually exceeds the half of caudal peduncle length) and the number of blotches on flank along the lateral line in this species varies from 6 to 11 (vs. usually less than 10) (Vasil'eva et al. 2023). In addition, according to the materials of the present study, *G. sibiricus* from the Kushtumga, Koelga, and Sinara rivers (neighboring rivers of the Ob' River basin to the typical habitats of the Ural gudgeon) has a fewer number of lateral line scales to hypural and total number of lateral line scales (ranges 36–40 and 40–43, medians 39 and 42, respectively, vs. ranges 36–42 and 39–45, medians 37.5 and 41 in *G. uralensis* sp. nov.) and a smaller number of predorsal vertebrae (range 11–13, median 12 vs. range 10–12, median 11 in *G. uralensis* sp. nov.). Besides, small differences in the mean values of some morphometric characters are observed between the combined samples of both species (see Table 3).

Table 1. Continued.

	G. lepidolaemus (13)	*G. lozanoi* (10)	*G. macrocephalus* (3)	*G. multipunctatus* (5)	*G. nigrescens* (2)	*G. occitaniae* (11)	*G. ohridanus* (15)	*G. sakaryaensis* (9)	*G. sarmaticus* (20)	*G. sibiricus* (14)	*G. skadarensis* (15)	*G. uralensis* sp. nov. (7)	*G. volgensis* (21)
G. acutipinnatus (6)	0.009	0.009	0.008	0.002	0.010	0.009	0.010	0.010	0.009	0.008	0.009	0.008	0.010
G. artvinicus (4)	0.008	0.008	0.008	0.008	0.009	0.008	0.009	0.009	0.008	0.007	0.009	0.008	0.009
G. balcanicus (17)	0.008	0.009	0.008	0.009	0.010	0.009	0.007	0.010	0.007	0.008	0.006	0.009	0.007
G. bulgaricus (18)	0.008	0.009	0.009	0.009	0.010	0.009	0.007	0.010	0.007	0.008	0.006	0.009	0.007
G. bulgaricus (17)	0.009	0.009	0.009	0.009	0.009	0.008	0.008	0.010	0.005	0.008	0.007	0.009	0.008
G. caucasicus (4)	0.008	0.008	0.008	0.008	0.009	0.008	0.009	0.009	0.008	0.007	0.009	0.008	0.009
G. cynocephalus (1)	0.010	0.010	0.010	0.010	0.010	0.010	0.010	0.010	0.009	0.009	0.010	0.010	0.010
G. gobio (16)	0.009	0.008	0.008	0.009	0.010	0.008	0.007	0.010	0.007	0.008	0.007	0.009	0.008
G. gobio (20)	0.008	0.009	0.008	0.009	0.009	0.008	0.007	0.010	0.000	0.008	0.007	0.009	0.007
G. holurus (12)	0.008	0.009	0.008	0.008	0.009	0.008	0.009	0.009	0.008	0.007	0.009	0.008	0.009
G. kizilirmakensis (8)	0.009	0.009	0.009	0.009	0.009	0.008	0.010	0.008	0.008	0.008	0.009	0.009	0.009
G. kovatschevi (18)	0.009	0.009	0.008	0.009	0.009	0.008	0.008	0.009	0.004	0.008	0.007	0.009	0.007
G. krymensis (19)	0.009	0.009	0.008	0.009	0.009	0.008	0.008	0.010	0.003	0.008	0.007	0.009	0.007
G. lepidolaemus (13)	**0.002**	0.009	0.009	0.009	0.010	0.009	0.009	0.010	0.008	0.003	0.009	0.008	0.008
G. lozanoi (10)	0.061	**0**	0.009	0.009	0.010	0.008	0.010	0.009	0.009	0.009	0.009	0.009	0.010
G. macrocephalus (3)	0.060	0.068	**0.002**	0.008	0.009	0.008	0.009	0.010	0.008	0.008	0.008	0.009	0.009
G. multipunctatus (5)	0.051	0.057	0.045	—	0.010	0.009	0.010	0.010	0.009	0.008	0.009	0.007	0.010
G. nigrescens (2)	0.066	0.075	0.066	0.067	**0**	0.010	0.011	0.011	0.009	0.009	0.010	0.010	0.010
G. occitaniae (11)	0.058	0.051	0.047	0.051	0.069	**0.003**	0.009	0.009	0.008	0.008	0.009	0.009	0.009
G. ohridanus (15)	0.056	0.067	0.058	0.057	0.080	0.057	**0**	0.010	0.007	0.009	0.003	0.010	0.008
G. sakaryaensis (9)	0.067	0.061	0.068	0.065	0.083	0.056	0.067	**0.003**	0.010	0.009	0.010	0.010	0.010
G. sarmaticus (20)	0.043	0.056	0.044	0.049	0.061	0.046	0.038	0.057	—	0.008	0.007	0.009	0.007
G. sibiricus (14)	0.008	0.054	0.054	0.047	0.061	0.052	0.050	0.061	0.038	**0.002**	0.008	0.008	0.008
G. skadarensis (15)	0.051	0.065	0.055	0.057	0.077	0.055	0.008	0.065	0.035	0.045	**0.004**	0.009	0.007
G. uralensis sp. nov. (7)	0.048	0.067	0.057	0.037	0.070	0.059	0.067	0.070	0.051	0.047	0.064	**0.001**	0.009
G. volgensis (21)	0.048	0.070	0.061	0.060	0.077	0.059	0.044	0.066	0.031	0.043	0.041	0.059	**0.003**

LDA analysis explained 86.88% of shape variations by the first LD axis and 13.12% by the second LD axis for all specimens of three species examined above. LDA of morphometric characters shows that *G. uralensis* sp. nov. together with *G. volgensis* is strongly different from *G. sibiricus* by LD1 in the following features: length caudal peduncle/depth caudal peduncle, interorbital length/eye diameter, and depth caudal peduncle/SL (Fig. 9). *Gobio uralensis* sp. nov. is slightly overlapping with *G. volgensis* by LD2 in the following features: head depth through nape/eye diameter, interorbital length/eye diameter, and length caudal peduncle/depth caudal peduncle. Specimens of *G. volgensis* are located mainly on the positive side of LD2, while specimens of *G. uralensis* sp. nov. are situated mainly on the negative side of LD2. The statistic values for LDA were as follows: Wilks' Lambda = 0.037001, approx. F (62, 160) = 10.835, $p < 0.0001$, indicating good species discrimination. Coefficients of linear discriminants see Suppl. material 4.

Further morphological comparison with a number of geographically close gudgeon species distributed out of the Volga and Ob' basins has been done based on literature data (except for *G. acutipinnatus*, some features of which were studied by authors using materials from the ZISP collection).

Another gudgeon species indicated in the literature for the Ob' River basin is *G. acutipinnatus* (Fig. 7E). This species was described from Lake Markakul in the Irtysh basin in Kazakhstan but today is also recorded for the water bodies of Russia, Mongolia, and China (Kottelat 2006; Yang et al. 2016; Yi and Fu 2020; Fricke et al. 2025). Compared to *G. acutipinnatus* from Lake Markakul (ZISP collection, 10 specimens), based on the materials of this study, *G. uralensis* sp. nov. has significantly (Kruskal-Wallis test, see Table 4) more pectoral fin branched rays, median 15.5 (vs. median 14.25), more total lateral line scales, median 42 (vs. median 41.5), and fewer scales below lateral line, median 3.75 (vs. median 4).

Compared to *G. lepidolaemus* Kessler, 1872 from the Zeravshan and Syr-Darya rivers based on the materials of Nikolsky (1936), *G. uralensis* sp. nov. has a greater number of lateral line scales (39–45, mean 42.1 vs. 36–42, mean 39.6) and anal fin branched rays $6^1/_2$ (vs. $5^1/_2$).

Figure 3. Lateral view of *Gobio uralensis* sp. nov.: **A–C.** Bolshoy Kizil River near Ryskuzhino (**A, B.** Holotype; **C.** Paratype); **D.** Uskalyk River near Verkhniy Muinak; **E.** Ural River near Krasnogor (right side, inverted image). **A, D, E.** Live coloration; **B, C.** After fixation in 10% formalin (5 months), then transferred to 70% ethanol. Scale bar: 10 mm.

Compared to *Gobio nigrescens* from the Hari River based on the materials of Mousavi-Sabet et al. (2016), *G. uralensis* sp. nov. has longer head (as % of SL) 25.6–30.0 (vs. 22.3–25.8), more predorsal lenght 47.4–52.6 (vs. 43.3–45.4), more prepelvic length 49.9–56.8 (vs. 46.4–50.7), and more preanal length 70.2–75.2 (vs. 67.1–69.1), less depth of caudal peduncle 7.2–8.8 (vs. 8.3–9.3), less body width 12.7–17.8 (vs. 17.3–18.7), has shorter cau-

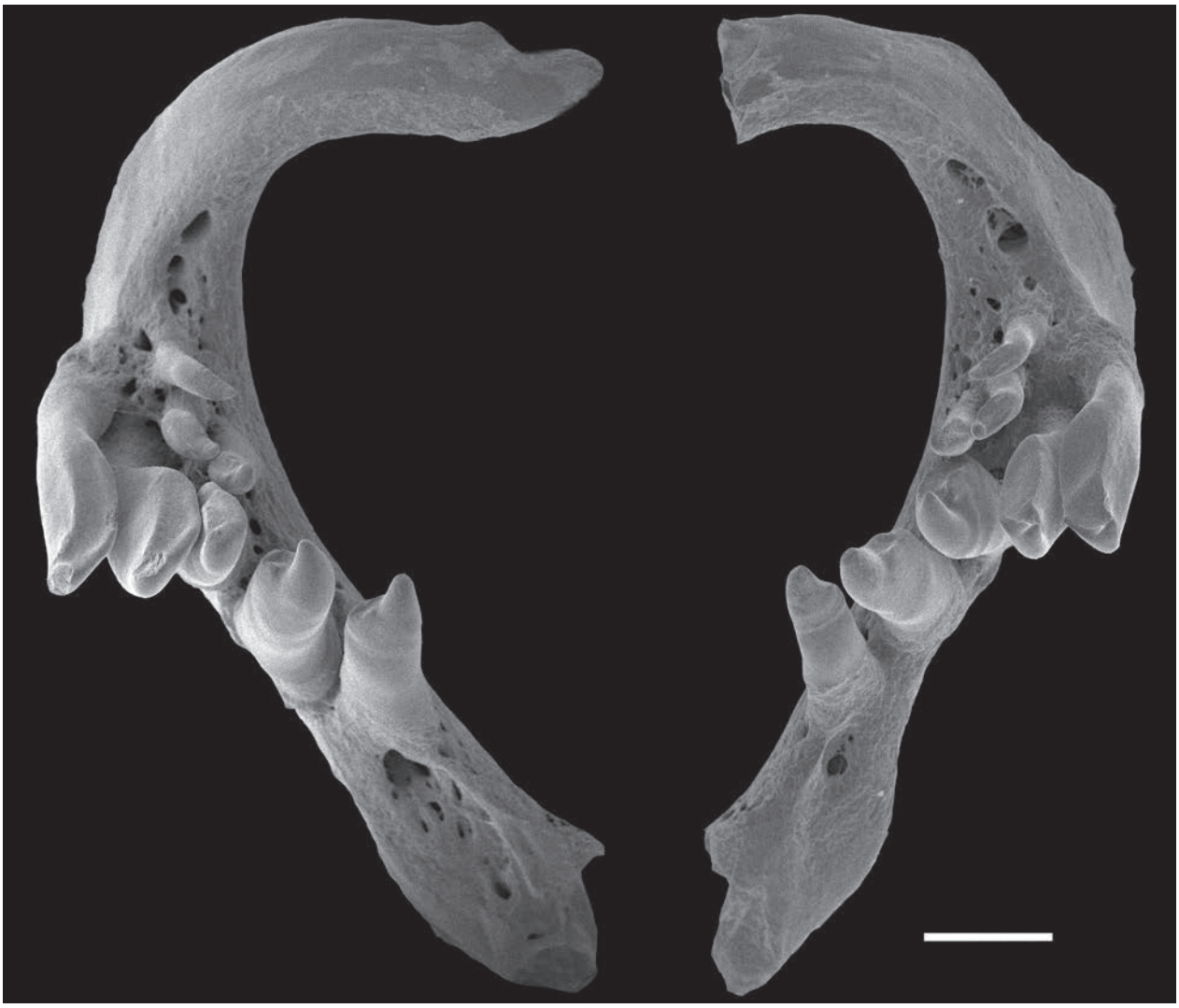

Figure 4. Dentition of pharyngeal bones (3.5–5.3) of *Gobio uralensis* sp. nov. Scale bar: 0.5 mm.

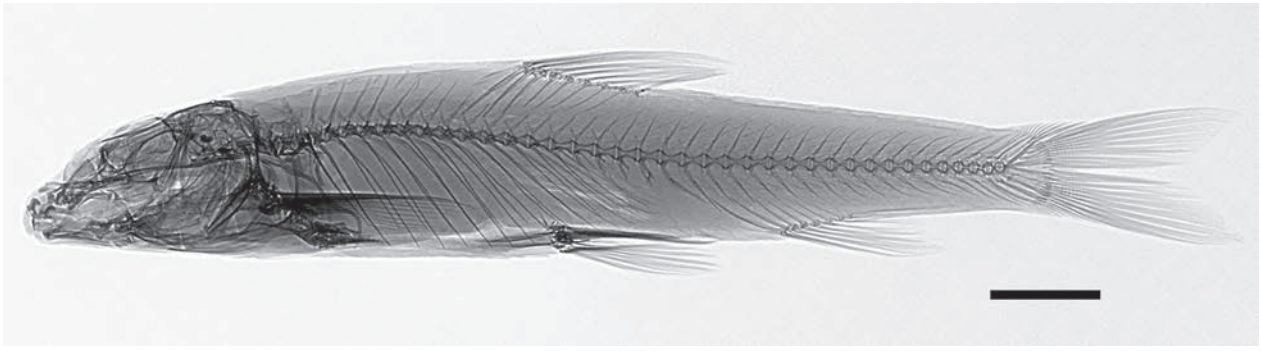

Figure 5. Radiograph of *Gobio uralensis* sp. nov., holotype: Scale bar: 10 mm.

dal peduncle 16.3–22.8 (vs. 21–24), has less head depth (in percent of HL) 52.6–62.0 (vs. 65–69), less interorbital width (in percent of HL) 22.3–29.6 (vs. 34–41), more snout length (in percent of HL) 40.9–48.8 (vs. 35–40), less anal fin branched rays $6^{1}/_{2}$ (vs. $5^{1}/_{2}$) and less circumpeduncular scales 11–15 (vs. 16).

Compared to *Gobio latus* Anikin, 1905 from Lake Issyk-Kul based on the materials of Berg (1949), *G. uralensis* sp. nov. has more numbers of pharyngeal teeth in minor row – 3.5–5.3 (vs. 2.5–5.2).

Compared to *Gobio multipunctatus* from the Emel River, Lake Alakol basin based on the materials of Vasil'eva et al. (2023), *G. uralensis* sp. nov. has less depth of caudal peduncle 7.2–8.8 (vs. 8.0–10.0), shorter caudal peduncle 16.3–22.8 (vs. 20.2–24.9), less dorsal fin depth 18.2–23.1 (vs. 21.8–26.2), more number of pharyngeal teeth in mi-

Table 2. Morphometric data of *Gobio uralensis* sp. nov. (holotype and paratypes, n = 11).

Character	holotype	paratypes			
		mean	min	max	SD
SL (mm)	97.7	77.9	70.3	110.4	–
In percent of SL:					
Head length (HL)	27.4	27.4	26.4	28.6	0.72
Body depth at dorsal-fin origin	18.3	19.1	18.3	19.9	0.51
Depth of caudal peduncle	7.8	8.0	7.3	8.5	0.34
Body width at dorsal-fin origin	14.7	15.4	14.7	16.2	0.47
Width of caudal peduncle at posterior anal-fin ray	8.2	8.5	7.7	9.2	0.47
Predorsal length	49.8	49.6	47.4	52.2	1.35
Postdorsal length	39.5	39.6	36.6	42.1	1.40
Prepelvic length	52.8	52.6	50.4	54.3	1.21
Preanal length	73.6	73.0	70.2	74.6	1.20
Distance between pectoral and pelvic-fin origins	26.7	26.8	26.0	29.0	0.90
Distance between pelvic and anal-fin origins	22.0	20.9	19.3	22.2	1.05
Distance between anus and anal-fin origin	7.7	7.8	6.8	8.8	0.67
Caudal peduncle length	21.0	20.5	19.0	21.9	0.87
Dorsal-fin base length	11.8	12.6	11.8	13.8	0.69
Dorsal-fin depth	20.4	20.3	18.2	21.1	0.77
Anal-fin base length	8.1	7.4	6.7	8.0	0.49
Anal-fin depth	15.2	15.7	14.9	17.3	0.75
Pectoral fin length	20.0	19.4	17.5	21.1	1.07
Pelvic fin length	16.0	15.5	13.9	16.4	0.69
In percent of HL:					
Head depth at nape	57.5	57.0	54.5	58.6	1.12
Head depth at eye	45.5	46.9	45.4	49.3	1.34
Snout length	41.8	43.7	40.9	46.6	1.86
Eye diameter	19.0	19.7	18.1	21.7	1.05
Postorbital distance	40.0	41.6	39.9	45.0	1.70
Maximum head width	58.6	59.4	56.5	62.1	1.54
Interorbital width	26.5	25.9	22.3	29.6	2.05
Barbel length	22.8	23.1	17.5	28.0	2.92
Ratios:					
Interorbital width/eye diameter	1.4	1.3	1.2	1.5	0.08
Snout length/eye diameter	2.2	2.2	1.9	2.6	0.19
Head depth at nape/eye diameter	3.0	2.9	2.7	3.2	0.16
Caudal peduncle length/depth	2.7	2.6	2.2	2.8	0.16

nor row – 3.5–5.3 (vs. 2.5–5.2), and has less black blotch numbers on body—often 10 (vs. usually more than 12).

Compared to *Gobio holurus* from the rivers of the western part of the Caspian basin based on the materials of Freyhof and Naseka (2005), *G. uralensis* sp. nov. has a naked breast between the pectoral fins (vs. the scaled breast). Compared to *G. holurus* from the Podkumok and Sunzha rivers (Berg 1914), *G. uralensis* sp. nov. has longer head (as % of SL) 25.6–30.0 (vs. 23.8–24.7), less postdorsal length 36.3–42.1 (vs. 42.6–43.1), more dorsal fin depth 18.2–23.1 (vs. 16.1–17.9), more anal fin depth 14.9–18.0 (vs. 13.9–14.1), and more ratio of caudal peduncle length to caudal peduncle depth 2.0–2.8 (vs. 1.9–2.0).

Discussion

According to our study, the Ural River basin is inhabited by a distinct species, *Gobio uralensis* sp. nov., currently known only from this riverine basin (Fig. 1). Our results show that *G. uralensis* sp. nov. differs significantly from *G. sibiricus* in many morphological characters (Fig. 9, Tables 3, 4) but is poorly distinguishable from the Caspian species *G. volgensis* (Fig. 9, Tables 3, 4). The latter, in turn, shares notable morphological similarities with *G. gobio* (Mendel et al. 2008). For this reason, gudgeons from the Ural basin were likely attributed to *G. volgensis* based on morphological analysis (Bogutskaya et al. 2013; Martynova and Vasil'eva 2021). The most reliable way to distinguish morphologically similar (or cryptic) species of the genus *Gobio* is through molecular genetic analysis (Mendel et al. 2008; this study). Based on DNA barcoding results, *G. uralensis* sp. nov. differs significantly from all other species of the genus, including the geographically neighboring *G. volgensis* (*p*-distance = 0.059 ± 0.009) and *G. sibiricus* (0.047 ± 0.008). At the same time, *G. uralensis* sp. nov. is genetically closer to Central Asian gudgeon species, namely *G. acutipinnatus* from the upper reaches of the Irtysh River (Ob' River basin; 0.037 ± 0.007) and *G. multipunctatus* from the Emel River in the Lake Alakol basin (0.037 ± 0.008) (see Table 1, Fig. 2).

Table 3. Morphometric characters for *Gobio* spp. (including the type series for *G. uralensis* sp. nov.) from three neighboring basins – range (mean ± standard deviation). Significant differences ($p < 0.05$) between populations are indicated with different lowercase letters (the non-parametric Kruskal-Wallis test followed by the Dunn's post hoc test). Green color shows the significant differences between *G. uralensis* sp. nov. and *G. volgensis*, yellow color shows significant differences between *G. uralensis* sp. nov. and *G. sibiricus*, and blue color shows significant differences between *G. uralensis* sp. nov., *G. volgensis*, and *G. sibiricus*.

Character	*G. volgensis* (n = 46)	*G. uralensis* sp. nov. (n = 77)	*G. sibiricus* (n = 37)
In percent of SL:			
Head length (HL)	25.3–29.7 (27.8 ± 1.04)[a]	25.6–30.0 (27.9 ± 1.10)[a]	26.9–30.9 (28.6 ± 0.94)[b]
Body depth at dorsal–fin origin	17.0–22.0 (19.2 ± 1.23)[a]	17.4–23.7 (19.8 ± 1.31)[a]	19.3–25.3 (22.6 ± 1.32)[b]
Caudal peduncle depth	7.6–9.5 (8.4 ± 0.43)[a]	7.2–8.8 (8.1 ± 0.40)[b]	8.9–10.9 (9.9 ± 0.50)[c]
Body width at dorsal–fin origin	11.6–16.6 (13.8 ± 1.23)[a]	12.7–17.8 (14.8 ± 1.17)[b]	13.3–19.0 (15.7 ± 1.35)[b]
Width of caudal peduncle at posterior anal–fin ray	6.1–9.5 (7.7 ± 0.90)	6.6–9.2 (7.7 ± 0.68)	6.7–9.2 (7.9 ± 0.72)
Predorsal length	42.2–51.5 (49.2 ± 1.50)[a]	47.4–52.6 (50.5 ± 1.30)[b]	48.8–53.5 (51.5 ± 1.09)[b]
Postdorsal length	38.2–44.4 (40.8 ± 1.47)[a]	36.3–42.1 (39.4 ± 1.22)[b]	37.6–42.6 (40.0 ± 1.28)[ab]
Prepelvic length	49.0–53.2 (51.0 ± 1.17)[a]	49.9–56.8 (52.0 ± 1.43)[b]	49.8–54.4 (52.2 ± 1.32)[b]
Preanal length	67.3–75.1 (71.8 ± 1.53)[a]	70.2–75.2 (73.0 ± 1.21)[b]	71.2–82.0 (74.4 ± 2.15)[c]
Distance between pectoral and pelvic–fin origins	20.6–26.6 (24.4 ± 1.40)	21.7–29.0 (25.2 ± 1.40)	23.1–27.1 (24.7 ± 1.28)
Distance between pelvic and anal–fin origins	18.9–24.0 (21.4 ± 1.13)[a]	19.3–25.1 (21.5 ± 1.23)[a]	19.9–23.8 (22.3 ± 1.08)[b]
Distance between anus and anal–fin origin	5.9–9.8 (7.9 ± 0.97)	5.5–9.5 (7.6 ± 0.85)	5.5–9.0 (7.6 ± 0.80)
Length of caudal peduncle	18.6–22.9 (20.8 ± 1.04)[a]	16.3–22.8 (19.6 ± 1.27)[b]	17.0–21.8 (18.6 ± 1.13)[c]
Dorsal–fin base length	10.6–14.7 (12.8 ± 0.83)[a]	11.8–14.6 (13.1 ± 0.73)[ab]	11.2–14.8 (13.4 ± 0.77)[b]
Dorsal–fin depth	18.9–23.3 (21.6 ± 1.12)[a]	18.2–23.1 (21.1 ± 1.08)[a]	20.72–25.34 (23.4 ± 1.31)[b]
Anal–fin base length	6.7–9.3 (7.5 ± 0.60)[a]	6.7–9.9 (8.0 ± 0.67)[b]	7.6–9.8 (8.6 ± 0.49)[c]
Anal–fin depth	13.6–18.2 (16.0 ± 0.87)[a]	14.9–18.0 (16.2 ± 0.78)[a]	16.1–19.9 (18.0 ± 0.94)[b]
Pectoral fin length	17.3–23.5 (20.5 ± 1.30)[a]	17.5–22.1 (19.8 ± 1.12)[a]	19.5–24.3 (22.0 ± 1.17)[b]
Pelvic fin length	1.2–17.6 (16.0 ± 2.36)[a]	13.9–17.5 (15.9 ± 0.82)[a]	16.1–20.2 (17.8 ± 0.85)[b]
In percent of HL:			
Head depth at nape	48.6–62.7 (56.0 ± 3.15)[a]	52.6–62.0 (56.5 ± 2.09)[a]	55.9–62.4 (59.6 ± 1.88)[b]
Head depth at eye	40.9–54.5 (48.2 ± 2.81)	43.4–54.9 (48.2 ± 3.08)	45.3–51.2 (49.1 ± 1.69)
Snout length	33.6–48.4 (43.1 ± 2.72)[a]	40.9–48.8 (44.8 ± 2.01)[b]	39.6–47.0 (43.4 ± 1.86)[a]
Eye diameter	18.3–26.6 (21.1 ± 1.59)	17.6–25.2 (21.0 ± 1.82)	18.9–22.9 (21.1 ± 1.05)
Postorbital distance	35.9–43.4 (40.8 ± 1.63)[a]	38.8–46.7 (41.5 ± 1.87)[ab]	38.2–45.2 (42.4 ± 1.92)[b]
Maximum head width	49.1–65.3 (58.3 ± 3.20)[a]	51.8–66.4 (59.0 ± 3.05)[a]	57.0–67.6 (61.8 ± 3.02)[b]
Interorbital width	21.4–31.3 (25.8 ± 2.23)[a]	22.3–29.6 (25.9 ± 1.56)[a]	27.9–33.0 (30.4 ± 1.45)[b]
Barbel length	20.2–30.0 (24.7 ± 2.37)[a]	15.9–32.6 (24.7 ± 3.28)[a]	22.4–35.5 (27.7 ± 3.89)[b]
Ratios:			
Interorbital width/eye diameter	1.0–1.6 (1.2 ± 0.16)[a]	1.0–1.5 (1.2 ± 0.13)[a]	1.2–1.6 (1.4 ± 0.11)[b]
Snout length/eye diameter	1.6–2.5 (2.1 ± 0.23)	1.7–2.6 (2.2 ± 0.21)	1.8–2.4 (2.1 ± 0.13)
Head depth at nape/eye diameter	2.1–3.2 (2.7 ± 0.24)[a]	2.2–3.3 (2.7 ± 0.28)[ab]	2.5–3.1 (2.8 ± 0.17)[b]
Caudal peduncle length/depth	2.1–2.9 (2.5 ± 0.18)[a]	2.0–2.8 (2.4 ± 0.19)[a]	1.6–2.3 (1.9 ± 0.15)[b]

The range of the Ural gudgeon remains uncertain. Currently, its distribution is reliably defined only for the localities sampled in this study. We assume that *G. uralensis* sp. nov. may be distributed throughout the entire Ural River basin, including the Kazakhstan's part of the basin.

It is noteworthy that the small genetic distance between *G. acutipinnatus* and *G. multipunctatus* (0.004 ± 0.002) (see Table 1, Fig. 2) suggests that they may represent different populations of the same species. This issue can be clarified through molecular analysis, including specimens of *G. acutipinnatus* from its type locality, Lake Markakul. The specimens previously identified as *G. acutipinnatus* (Yang et al. 2016; Yi and Fu 2020) are from the Chinese section of the Irtysh River and may actually refer to a different species – possibly the recently described *G. multipunctatus*. Moreover, according to the study describing *G. multipunctatus* (Vasil'eva et al. 2023), this species is not native to the Lake Alakol basin in Kazakhstan, although it was originally described from that region. This reflects a broader issue: the ongoing introduction and establishment of alien species in Kazakhstan, including in the Lake Alakol basin (Mamilov et al. 2015, 2022, 2024; Sharakhmetov 2022). Thus, the taxonomic status of the gudgeons inhabiting the Central Asian region remains unclear and requires further research.

Gobio uralensis sp. nov. is genetically closer to the geographically distant *G. acutipinnatus* and *G. multipunctatus* (see Fig. 1), that is likely explained by paleogeographic factors and ancient hydrological connections between the Ural and Irtysh river basins. Several basins are between these riverine systems, including the Nura and Sarysu rivers, the rivers and water bodies of the Irgiz-Turgai trough, the Emba and Uil rivers, and numerous smaller lake and river systems. Most of these are currently endorheic (drainless), but during high-water years, they may overflow into the Ob' or Caspian Sea basins (Davydov 1936). Part of these modern basins was, during the Late Pliocene and Pleistocene, composed of glacial-sub-

Table 4. Meristic characters of the studied *Gobio* spp. Significant differences ($p < 0.05$) between populations are indicated with different lowercase letters (the non-parametric Kruskal-Wallis test followed by the Dunn's post hoc test). Green color shows significant differences between *G. uralensis* sp. nov. and other *Gobio* species. Abbreviations: lim – limits; M – mean; SD – standard deviation.

Characters	K-U	*G. acutipinnatus* (n = 10)			*G. sibiricus* (n = 37)			*G. uralensis* sp. nov. (n = 77)			*G. volgensis* (n = 46)		
	p	lim	M	SD	lim	M	SD	lim	M	SD	lim	M	SD
D	0.441	7–7	7.0	0.00	7–7	7.0	0.00	7–8	7.0	0.11	7–8	7.0	0.21
A	0.441	6–6	6.0	0.00	6–6	6.0	0.00	6–6	6.0	0.00	5–6	6.0	0.15
P	0.00257*	13–16	14.4^{a}	0.84	14–17	15.0^{ab}	0.69	13–17	15.3^{b}	0.91	13–17	15.4^{b}	0.66
V	0.0604	7–7	7.00	0.00	7–8	7.0	0.11	5–8	7.0	0.29	7–8	7.2	0.31
LL	<0.0001*	37–42	38.6^{ab}	0.98	36–40	37.8^{a}	0.82	36–42	38.9^{b}	0.93	37–42	38.9^{b}	0.85
LLt	<0.0001*	40–44	41.6^{a}	0.89	40–43	41.3^{a}	0.80	39–45	42.1^{b}	0.86	41–45	42.6^{c}	0.84
up LL	<0.0001*	5–7	5.6^{ab}	0.53	5–6	5.5^{a}	0.46	4–6	5.5^{a}	0.46	5–6.5	5.9^{b}	0.27
down LL	0.0133*	3–5	4.0^{a}	0.24	3–4	3.7^{ab}	0.38	3–5	3.6^{b}	0.47	3–4.5	3.8^{ab}	0.32
CPS	0.0341*	11–15	12.6^{ab}	1.17	12–14	12.3^{a}	0.58	11–15	12.6^{ab}	0.85	12–15	12.9^{b}	0.93
Blotches on flank	0.313	9–11	10.2	0.67	7–11	8.2	0.83	6–14	9.6	1.30	7–12	9.2	0.88
GR	0.109	–	–	–	3–5	3.7	0.67	2–5	3.8	1.20	2–5	3.2	0.73
Vert.	0.000974*	40–41	40.1^{ab}	0.38	39–41	39.9^{a}	0.64	39–42	40.30^{b}	0.67	40–42	40.5^{b}	0.66
Va	0.152	21–22	21.1	0.38	20–22	21.0	0.58	20–22	21.0	0.56	20–22	21.2	0.47
VpreD	0.00592*	11–12	11.3^{ab}	0.49	10–12	11.2^{a}	0.53	11–13	11.6^{b}	0.54	10–12	11.4^{ab}	0.55
Vi	0.736	3–5	3.9	0.69	3–5	4.1	0.52	3–5	4.0	0.71	3–5	4.0	0.71
Vc	0.0101*	18–20	19.0^{ab}	0.58	18–20	18.9^{a}	0.60	18–21	19.3^{b}	0.65	18–21	19.3^{b}	0.56
VpreA	0.599	2–3	2.1	0.38	1–3	2.0	0.69	1–3	1.9	0.50	1–3	1.9	0.58
VpostA	0.00173*	16–18	16.9^{ab}	0.69	16–18	17.0^{a}	0.70	16–19	17.4^{b}	0.65	16–19	17.5^{b}	0.62

Figure 6. Type locality of *Gobio uralensis* sp. nov. – Bolshoy Kizil River near Ryskuzhino (53.3161°N, 58.3351°E, 24 Aug. 2020).

pond lake and riverine systems that were repeatedly connected via the Irgiz-Turgai trough, facilitating two-way flow between the Ob' and Caspian Sea basins (Kvasov 1975; Grosswald 1999). Paleohydrological connections might facilitate the historical dispersal of ancestral gudgeon lineages, followed by geographical isolation. At present, no genetic data are available for gudgeons inhabiting the water bodies of the Irgiz-Turgai trough. It is possible that gudgeons belonging to lineages closely related to *G. uralensis* and *G. acutipinnatus* inhabit or formerly inhabited other water bodies in southern Siberia and northern Central Asia, between Lake Markakol and the Ural basin.

Faunistic relationships between the Arctic Ocean and Caspian Sea basins have been a subject of zoological interest since the work of Berg (1928). Makhrov et al. (2020) summarized recent data and demonstrated, using multiple examples, that faunal exchanges between these basins have occurred in both directions and at various times. We provide examples of faunal dispersal between the Caspian Sea and Siberian river basins – particularly the Ob' River and its tributary, the Irtysh River – as the gudgeons examined in this study exhibit a similar pattern of past dispersal. The so-called *baerii*-like mitotype (similar to the mtDNA haplotypes of the Siberian sturgeon *Acipenser baerii* Brandt, 1869) was detected in approximately 30% of Russian sturgeons (*Acipenser gueldenstaedtii* Brandt, 1833; Acipenseriformes: Acipenseridae) from the North Caspian basin (Ural and Volga rivers) (Birstein et al. 2000; Jenneckens et al. 2000; Timoshkina et al. 2009). Water bodies in the southwestern Irtysh basin are inhabited by gastropod mollusks of Ponto-Caspian origin – the genus *Caspiohydrobia* Starobogatov, 1970 (Gastropoda: Hydrobiidae) (Andreeva 1987). Bivalves of the genus *Unio* Philipsson, 1788 (Bivalvia: Unionidae), recorded in the upper Irtysh basin and its tributary, the Uy River, likely reflect the presence of a refugium in the upper reaches of the basin, further supporting the hypothesis of ancient faunal exchange between the Caspian and Ob' basins (Andreeva et al. 2009; Bolotov et al. 2020). The vectors and timing of ancient aquatic animal dispersal remain incompletely understood. It is assumed that the ancestor of the Siberian sturgeon (*A. baerii*) colonized Siberian rivers from the Ponto-Caspian basin (Birstein and DeSalle 1998; Birstein et al. 2000), later surviving glaciation in a refugium, presumably Lake Baikal (Barmintseva and Mugue 2017), where it speciated. A subsequent recolonization of the Caspian basin by *A. baerii* likely occurred during one of the last Pleistocene glacial-interglacial cycles (Timoshkina et al. 2009). The mollusks *Caspiohydrobia* and *Unio* also clearly have Caspian origins upon colonizing the Irtysh basin (Makhrov et al. 2020).

Figure 7. Lateral view of *Gobio* spp. (comparative material): **A, B.** *G. volgensis* (**A.** Chusovaya River near Kosoy Brod; **B.** Buzuluk River near Fedorovka (right side, inverted image)); **C, D.** *G. sibiricus* (**C.** Koelga River near Zvyagino; **D.** Sinara River near Bulzi), **E.** *G. acutipinnatus*, syntype ZISP 26865 (Lake Markakol). **A–D.** Live coloration; **E.** Preserved specimen of 1936 year. Scale bar: 10 mm.

In contrast, reverse colonization is exemplified by the Siberian taimen *Hucho taimen* (Pallas, 1773) (Salmoniformes: Salmonidae), which entered the Caspian basin from Siberia in the Late Pleistocene, likely via paleohydrological connections through the Chusovaya River (Marić et al. 2014), originating in Siberia. The Chusovaya River has served as a bi-directional corridor for faunal exchange between Europe and Asia, as seen from

Figure 8. Breast and belly view of *Gobio* spp.: **A.** *G. uralensis* sp. nov., Ural River near Krasnogor; **B.** *G. volgensis*, Schegrinka River near Jidobuzhi; **C.** *G. sibiricus*, Koelga River near Zvyagino. Scale bar: 10 mm.

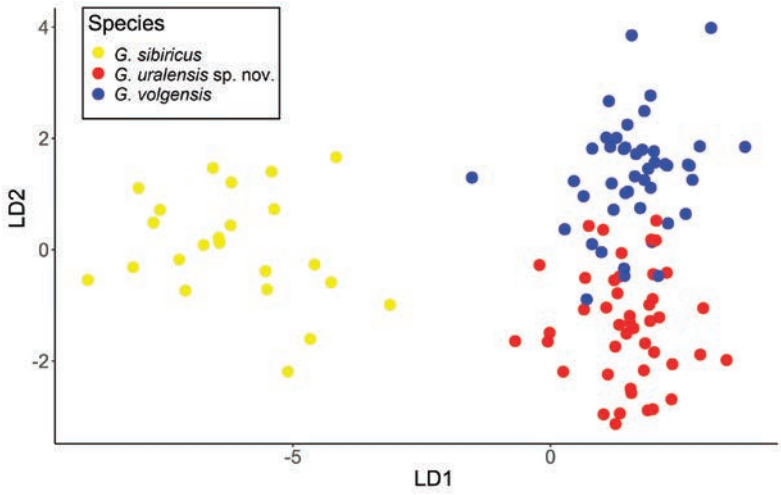

Figure 9. Linear Discriminant Analysis (LDA) of *Gobio uralensis* sp. nov. (n = 77), *G. volgensis* (n = 46), and *G. sibiricus* (n = 37) based on 31 morphometric indexes and ratios.

the Northern minnow *Phoxinus isetensis* (Georgi, 1775) (Cypriniformes: Leuciscidae), which migrated from the Caspian to the Ob' basin (Artaev et al. 2024). An issue on the route of colonization of the Ural River basin by the proto-lineage of *G. uralensis* sp. nov. is still unclear.

In summary, our study demonstrates that the Ural River – a major river forming the boundary between Europe and Asia – is inhabited by an endemic gudgeon species, here described as *G. uralensis* sp. nov. Notably, *G. uralensis* sp. nov. is the only endemic fish species known from the Ural River basin. To better understand the evolutionary origin of the Ural gudgeon and the zoogeographic relationships between Asia and Europe, it is essential to clarify the phylogenetic affinities and taxonomic status of *Gobio* species inhabiting the region of historic paleohydrological connections between the Ob' and Caspian Sea basins – specifically, the Nura and Sarysu rivers, the Irgiz-Turgai trough, and the Emba and Uil rivers. However, genetic data on fish from this region are currently limited (see Suppl. material 1).

Acknowledgments

The authors are very grateful to Ivan Pozdeev (Perm, Russia) and Alexey Kutuzov (Borok, Russia) for their assistance in collecting the material and to all reviewers for their valuable comments that significantly improved the manuscript. This study was supported by the Russian Science Foundation, grant no. 24-44-20019 "Fishes of the Caspian Sea basin: genetic diversity, evolution, and biogeography."

References

Aksu I, Bektaş Y (2019) Mitochondrial phylogeny and biogeography of the genus *Gobio* (Teleostei: Cyprinidae) in Turkey. Zoology in the Middle East 65(2): 128–141. https://doi.org/10.1080/09397140.2019.1586126

Aljanabi SM, Martinez I (1997) Universal and rapid salt-extraction of high quality genomic DNA for PCR-based techniques. Nucleic Acids Research 25(22): 4692–4693. https://doi.org/10.1093/nar/25.22.4692

Andreeva SI (1987) Mollusks of the genus *Caspiohydrobia* Starobogatov, 1970 (Gastropoda, Pyrgulidae) of the water bodies of Kazakhstan. Mollusks. Results and prospects of their research. Eighth All-Union Conference on the Study of Mollusks. Leningrad, 178–180 pp. [In Russian]

Andreeva SI, Vinarski MV, Karimov AV (2009) The first record of *Unio* species (Bivalvia: Unionidae) in the Irtysh River basin (Western Siberia, Russia). Mollusca 27: 87–91.

Artaev ON, Bolotovskiy AA, Turbanov IS, Gandlin AA, Kutuzov AV, Levina MA, Melentev DA, Pozdeev IV, Borisov MYa, Levin BA (2024) Forgotten for two centuries: redescription of *Phoxinus isetensis* (Georgi, 1775) (Cypriniformes, Leuciscidae) – the most widespread minnow in Europe. Zoosystematics and Evolution 100(3): 1155–1173. https://doi.org/10.3897/zse.100.126702

Bănărescu P, Nalbant TT (1973) Pisces, Teleostei, Cyprinidae (Gobioninae). Das Tierreich, Lieferung 93. Walter de Guryter, Berlin, 1–304.

Bănărescu P, Šorić VM, Economidis PS (1999) *Gobio gobio* (Linnaeus, 1758). In: Bănărescu P (Ed.) The freshwater fishes of Europe. Vol. 5/I, Cyprinidae 2. Part. 1. *Rhodeus* to *Capoeta*. AULA-Verlag, Wiebelsheim, 81–134.

Barmintseva AE, Mugue NS (2017) Natural genetic polymorphism and phylogeography of siberian sturgeon *Acipenser baerii* Brandt, 1869. Russian Journal of Genetics 53(3): 358–368. https://doi.org/10.1134/S1022795417030024

Behrens-Chapuis S, Herder F, Geiger MF (2021) Adding DNA barcoding to stream monitoring protocols – What's the additional value and congruence between morphological and molecular identification approaches? PLoS ONE 16(1): e0244598. https://doi.org/10.1371/journal.pone.0244598

Bening AL (1938) Materials on hydrobiology of the Ural River. Bol'shaya Emba. Vol. 2. Academy of Sciences of the USSR, Leningrad-Moscow, 153–258. [In Russian]

Berg LS (1914) Fauna of Russia and neighboring countries based mainly on the collections of the Zoological Museum of the Imperial Academy of Sciences in St. Petersburg. Fish (Marsipobranchii and Pisces). Vol. III, Part 2. Ostariophysi. Petrograd, Izdatelstvo Imperatorskoj Akademii Nauk, 337–704. [In Russian]

Berg LS (1928) On the origin of northern elements in the Caspian fauna. Doklady Akademii nauk SSSR 7, 107–112. [In Russian]

Berg LS (1949) Freshwater fishes of the U.S.S.R. and adjacent countries. Part 2. Izdatelstvo Akademii Nauk SSSR, Leningrad, 456 pp. [In Russian]

Birstein VJ, DeSalle R (1998) Molecular phylogeny of Acipenserinae. Molecular Phylogenetics and Evolution 9(1): 141–155. https://doi.org/10.1006/mpev.1997.0443

Birstein VJ, Doukakis P, DeSalle R (2000) Polyphyly of mtDNA lineages in the Russian sturgeon, *Acipenser gueldenstaedtii*: forensic and evolutionary implications. Conservation Genetics 1(1): 81–88. https://doi.org/10.1023/A:1010141906100

Bogutskaya NG, Kijaschko PV, Naseka AM, Orlova MI (2013) Identifications keys for fish and invertebrates. Vol. 1. Fish and molluscs. KMK Scientific Press Ltd., St. Petersburg-Moscow, 543 pp.

Bolotov IN, Kondakov AV, Konopleva ES, Vikhrev IV, Aksenova OV, Aksenov AS, Bespalaya YV, Borovskoy AV, Danilov PP, Dvoryankin GA, Gofarov MY, Kabakov MB, Klishko OK, Kolosova YS, Lyubas AA, Novoselov AP, Palatov DM, Savvinov GN, Solomonov NM, Spitsyn VM, Sokolova SE, Tomilova AA, Froufe E, Bogan AE, Lopes-Lima M, Makhrov AA, Vinarski MV (2020) Integrative taxonomy, biogeography and conservation of freshwater mussels (Unionidae) in Russia. Scientific Reports 10: 3072–20. https://doi.org/10.1038/s41598-020-59867-7

Chibilev AA, Debelo PV (2009) Fishes of the Ural-Caspian region. Series: Natural diversity of the Ural-Caspian region. Vol. 2. Ural Branch of the Russian Academy of Sciences, Ekaterinburg, 228 pp. [In Russian]

Corse E, Meglécz E, Archambaud G, Ardisson M, Martin JF, Tougard C, Chappaz R, Dubut V (2017) A from-benchtop-to-desktop workflow for validating HTS data and for taxonomic identification in diet metabarcoding studies. Molecular Ecology Resources 17(6): e146–e159. https://doi.org/10.1111/1755-0998.12703

Danielson JJ, Gesch DB (2011) Global multi-resolution terrain elevation data 2010 (GMTED2010). US Geological Survey Open-File Report 2011-1073. https://doi.org/10.3133/ofr20111073

Davydov LK [Ed] (1936) Handbook of water resources of the USSR. Vol. 12. Urals and Southern Urals. Part 1. Main Directorate of the Hydrometeorological Service of the USSR, State Hydrological Institute, Editorial and Publishing Department of the Hydrometeorological Service of the USSR, Leningrad-Moscow, 664 pp. [In Russian]

Doadrio I, Madeira MJ (2004) A new species of the genus *Gobio* Cuvier, 1816 (Actynopterigii, Cyprinidae) from the Iberian Peninsula and southwestern France. Graellsia 60(1): 107–116. https://doi.org/10.3989/graellsia.2004.v60.i1.197

Dyldin YuV, Orlov AM, Hanel L, Romanov VI, Fricke R, Vasil'eva ED (2023) Ichthyofauna of the Fresh and Brackish Waters of Russia and Adjacent Areas: Annotated List with Taxonomic Comments. 2. Order Cypriniformes, Suborders Catostomoidei, Cobitoidei and Cyprinoidei. Journal of Ichthyology 63(4): 636–686. https://doi.org/10.1134/S0032945223040045

Fang Y, Sun Z, Zhao Y (2025) Taxonomic revision on the *Gobio* group in the Yellow River drainage, with discussion on the validity of the genus *Acanthogobio* (Cypriniformes, Gobionidae). Zoosystematics and Evolution 101(2): 661–679. https://doi.org/10.3897/zse.101.144134

Freyhof J, Naseka A (2005) *Gobio delyamurei*, a new gudgeon from Crimea, Ukraine (Teleostei: Cyprinidae). Ichthyological Exploration of Freshwaters 16(4): 331–338.

Fricke R, Eschmeyer WN, Van der Laan R [Eds] (2025) Eschmeyer's Catalog of Fishes: Genera, Species, References. http://

researcharchive.calacademy.org/research/ichthyology/catalog/fishcatmain.asp [Electronic version accessed 18.01.2025]

Friedrich T, Wiesner C, Zangl L, Daill D, Freyhof J, Koblmueller S (2018) *Romanogobio skywalkeri*, a new gudgeon (Teleostei: Gobionidae) from the upper Mur River, Austria. Zootaxa 4403(2): 336–350. https://doi.org/10.11646/zootaxa.4403.2.6

Geiger MF, Herder F, Monaghan MT, Almada V, Barbieri R, Bariche M, Berrebi P, Bohlen J, Casal-Lopez M, Delmastro GB, Denys GPJ, Dettai A, Doadrio I, Kalogianni E, Kärst H, Kottelat M, Kovačić M, Laporte M, Lorenzoni M, Marčić Z, Özuluğ M, Perdices A, Perea S, Persat H, Porcelotti S, Puzzi C, Robalo J, Šanda R, Schneider M, Šlechtová V, Stoumboudi M, Walter S, Freyhof J (2014) Spatial heterogeneity in the Mediterranean Biodiversity Hotspot affects barcoding accuracy of its freshwater fishes. Molecular Ecology Resources 14(6): 1210–1221. https://doi.org/10.1111/1755-0998.12257

GenBank (2025) GenBank. https://www.ncbi.nlm.nih.gov/

Grosswald MG (1999) Catastrophic megafloods in Eurasia and the polar ice sheets. Nauchnyi mir, Moscow, 120 pp. [In Russian]

Hill V, Baele G (2019) Bayesian estimation of past population dynamics in BEAST 1.10 using the Skygrid coalescent model. Molecular biology and evolution 36(11): 2620–2628. https://doi.org/10.1093/molbev/msz172

Hubbs CL, Lagler KF (1946) Fishes of the Great Lakes Region. University of Michigan Press, Ann Arbor, xv + 213 pp.

Ivanova NV, Zemlak TS, Hanner RH, Hebert (2007) PDbUniversal primer cocktails for fish DNA barcoding. Molecular Ecology Notes 7(4): 544–548. https://doi.org/10.1111/j.1471-8286.2007.01748.x

Jenneckens I, Meyer J-N, Debus L, Pitra C, Ludwig A (2000) Evidence of mitochondrial DNA clones of Siberian sturgeon, *Acipenser baerii*, within Russian sturgeon, *Acipenser gueldenstaedtii*, caught in the River Volga. Ecology Letters 3(6): 503–508. https://doi.org/10.1111/j.1461-0248.2000.00179.x

Kalyaanamoorthy S, Minh BQ, Wong TKF, von Haeseler A, Jermiin LS (2017) ModelFinder: fast model selection for accurate phylogenetic estimates. Nature Methods 14(6): 587–589. https://doi.org/10.1038/nmeth.4285

Kessler KF (1877) The Aralo-Caspian Expedition. Vol. IV. Fishes found and encountered in the Aral-Caspian-Pontic ichthyological region. St. Petersburg, i–xxviii + 1–360. [Pls. 1–8] [In Russian] https://doi.org/10.5962/bhl.title.159366

Knebelsberger T, Dunz AR, Neumann D, Geiger MF (2015) Molecular diversity of Germany's freshwater fishes and lampreys assessed by DNA barcoding. Molecular Ecology Resources 15(3): 562–572. https://doi.org/10.1111/1755-0998.12322

Kottelat M (1997) European freshwater fishes. An heuristic checklist of the freshwater fishes of Europe (exclusive of former USSR), with an introduction for non-systematists and comments on nomenclature and conservation. Biologia, Bratislava 52(Suppl 5): 1–271.

Kottelat M (2006) Fishes of Mongolia. A check-list of the fishes known to occur in Mongolia with comments on systematics and nomenclature. The World Bank, Washington, 103 pp.

Kottelat M, Persat H (2005) The genus *Gobio* in France, with redescription of *G. gobio* and description of two new species (Teleostei: Cyprinidae). Cybium 29(3): 211–234.

Kozhin NI (1949) Gudgeon – *Gobio gobio* (Linne). In: Berg LS, Bogdanov AS, Kozhin NI, Rase TS (Eds) Commercial fish of the USSR. Food Industry Publishing House, 374–375. [In Russian]

Kumar S, Stecher G, Tamura K (2016) MEGA7: Molecular Evolutionary Genetics Analysis version 7.0 for bigger datasets. Molecular Biology and Evolution 33(7): 1870–1874. https://doi.org/10.1093/molbev/msw054

Kvasov DD (1975) Late Quaternary history of large lakes and inland seas of Eastern Europe. Nauka, Leningrad, 278 pp. [In Russian]

Lanfear R, Calcott B, Ho SY, Guindon S (2012) PartitionFinder: combined selection of partitioning schemes and substitution models for phylogenetic analyses. Molecular biology and evolution 29(6): 1695–1701. https://doi.org/10.1093/molbev/mss020

Lanfear R, Frandsen PB, Wright AM, Senfeld T, Calcott B (2016) PartitionFinder 2: new methods for selecting partitioned models of evolution formolecular and morphological phylogenetic analyses. Molecular biology and evolution 34(3): 772–773. https://doi.org/10.1093/molbev/msw260

Li Z-Q (2015) Fishes of the Yellow River & Beyond. The Sueichan Press, Taiwan, 640 pp. [In Chinese]

Li Y, Cao K, Fu C (2018) Ten fish mitogenomes of the tribe Gobionini (Cypriniformes: Cyprinidae: Gobioninae). Mitochondrial DNA Part B 3(2): 803–804. https://doi.org/10.1080/23802359.2018.1467236

Linke S, Lehner B, Dallaire CO, Ariwi J, Grill G, Anand M, Beames P, Burchard-Levine V, Maxwell S, Moidu H, Tan F, Thieme M (2019) Global hydro-environmental sub-basin and river reach characteristics at high spatial resolution. Scientific Data 6(283): 283. https://doi.org/10.1038/s41597-019-0300-6

Magazov OA, Rechkalov VV (2007) Ichthyofauna of reservoirs of the Chelyabinsk region. Bulletin of Chelyabinsk State University 6: 85–94. [In Russian]

Makhrov AA, Vinarski MV, Gofarov MYu, Dvoryankin GA, Novoselov AP, Bolotov IN (2020) Faunal exchanges between the Arctic Ocean and Caspian basins: history and current processes. Zoologicheskii Zhurnal 99(10): 1124–1139.

Mamilov NSh, Dan'ko EK, Sansyzbaev EM (2015) Eightbarbel loach is a new alien species in fish fauna of Kazakhstan. Zoological Yearbook of Kazakhstan and Central Asia. Selevinia 23: 133–135.

Mamilov NSh, Konysbaev TG, Belyaev AI, Vasil'eva ED (2022) Exotic fish species in the Lake Balkhash basin (Kazakhstan). Inland Water Biology 1: 101–104. https://doi.org/10.1134/S1995082922010084

Mamilov NSh, Tursynali M, Khassengaziyeva GK, Urban J, Bartunek D, Sharakhmetov SE, Sapargaliyeva N, Urgenishbayeva Z, Kegenova GB, Kozhabaeva E, Baimukanov M, Levin B (2024) Alien rainbow trout *Oncorhynchus mykiss* in the Balkhash basin (Kazakhstan, Central Asia): 50 years of naturalization. Animals 14: 3013. https://doi.org/10.3390/ani14203013

Marić S, Alekseyev S, Snoj A, Askeyev O, Askeyev I, Weiss S (2014) First mtDNA sequencing of Volga and Ob basin taimen *Hucho taimen*: European populations stem from a late Pleistocene expansion of *H. taimen* out of western Siberia and are not intermediate to *Hucho hucho*. Journal of Fish Biology 85(2): 530–539. https://doi.org/10.1111/jfb.12428

Martynova AL, Vasil'eva ED (2021) Problems of taxonomy and diagnostics of gudgeons of the genus *Gobio* (Cyprinidae) from Ural, Siberia, Kazakhstan and the Amur River basin. Journal of Ichthyology 61(5): 685–700. https://doi.org/10.1134/S0032945221050106

Mayden RL (2002) On biological species, species concepts and individuation in the natural world. Fish and Fisheries 3(3): 171–196. https://doi.org/10.1046/j.1467-2979.2002.00086.x

Mendel J, Lusk S, Vasil'eva ED, Vasil'ev VP, Lusková V, Ekmekci FG, Erk'akan F, Ruchin A, Koščo J, Vetešník L, Halačka K,

Šanda R, Pashkov AN, Reshetnikov SI (2008) Molecular phylogeny of the genus *Gobio* Cuvier, 1816 (Teleostei: Cyprinidae) and its contribution to taxonomy. Molecular Phylogenetics and Evolution 47(3): 1061–1075. https://doi.org/10.1016/j.ympev.2008.03.005

Menshikov MI (1939) On the ichthyofauna of lake Marka-Kul. Scientific Memoirs of the University of Perm 3(2): 119–142. [+ 2 Pls.] [In Russian, English summary]

Mina MV, Levin BA, Mironovsky AN (2005) On the possibility of using character estimates obtained by different operators in morphometric studies of fish. Journal of Ichthyology 45(4): 284–294.

Minh BQ, Nguyen MA, von Haeseler A (2013) Ultrafast approximation for phylogenetic bootstrap. Molecular Biology and Evolution 30(5): 1188–1195. https://doi.org/10.1093/molbev/mst024

Mitrofanov VP (1988) Genus *Gobio* Cuvier, 1917 – gudgeon. In: Mitrofanov VP, Dukravets GM, Mel'nikov VA, Baimbetov AA, et al. (Eds) Fishes of Kazakhstan. Vol. 3. Cyprinidae (continued). Nauka, Alma-Ata, 5–23. [In Russian]

Mousavi-Sabet H, Ganjbakhsh B, Geiger MF, Freyhof J (2016) Redescription of *Gobio nigrescens* from the Hari River drainage (Teleostei: Cyprinidae). Zootaxa 4114(1): 71–80. https://doi.org/10.11646/zootaxa.4114.1.4

Naseka AM (1996) Comparative study on the vertebral column in the Gobioninae (Cyprinidae, Pisces) with special reference to its systematics. Publicaciones Especiales – Instituto Español de Oceanografía 21: 149–167.

Naseka AM, Erk'akan F, Küçük F (2006) A description of two new species of the genus *Gobio* from Central Anatolia (Turkey) (Teleostei: Cyprinidae). Zoosystematica Rossica 15(1): 185–194. https://doi.org/10.31610/zsr/2006.15.1.185

Navozov N (1912) Materials on the ichthyofauna of the Ural River basin. Vestnik rybopromishlennosti, 8–10: 252–253. [In Russian]

Nguyen LT, Schmidt HA, von Haeseler A, Minh BQ (2015) IQ-TREE: a fast and effective stochastic algorithm for estimating maximum-likelihood phylogenies. Molecular Biology and Evolution 32(1): 268–274. https://doi.org/10.1093/molbev/msu300

Nikolsky GV (1936) Sur la variabilité géographique de *Gobio gobio* (L.) du nord-est de Kazachstan et de la Sibérie occidentale. Trudy Zoologičeskogo Instituta Akademii Nauk SSSR 3: 457–473. [In Russian, with French summary]

Rothgänger J, Weniger M, Weniger T, Mellmann A, Harmsen D (2006) Ridom TraceEdit: A DNA trace editor and viewer. Bioinformatics 22(4): 493–494. https://doi.org/10.1093/bioinformatics/btk002

Shaposhnikova GKh (1964) Biology and distribution of fish in the rivers like the Ural River. Nauka, Moscow, 170 pp. [In Russian]

Sharakhmetov SE (2022) Diversity of the ichthyofauna of the rivers of the southern macroslope of the Tarbagatai ridge (Alakol basin, Kazakhstan). Eurasian Journal of Ecology 70(1): 108–120. https://doi.org/10.26577/EJE.2022.v70.i1.10

Sheraliev B, Peng Z (2021) Molecular diversity of Uzbekistan's fishes assessed with DNA barcoding. Scientific Reports 11(1): 16894. https://doi.org/10.1038/s41598-021-96487-1

Sheraliev B, Allayarov S, Peng Z (2020) First records of *Gobio nigrescens* and *Gobio sibiricus* (Cypriniformes: Gobionidae) from the Amu Darya River basin, Uzbekistan. Journal of Applied Ichthyology 36(2): 235–239. https://doi.org/10.1111/jai.14019

Shevchenko AM (2018) Modern trends in the change in the composition of the ichthyofauna of the upper reaches of the Ural River basin. Materials on flora and fauna of the Republic of Bashkortostan 18: 119–129. [In Russian]

Takács P, Bihari P, Erös T, Specziár A, Szivák I, Bíró P, Csoma E (2014) Genetic heterogeneity reveals on-going speciation and cryptic taxonomic diversity of stream-dwelling gudgeons (Teleostei, Cyprinidae) in the Middle Danubian hydrosystem (Hungary). PLoS ONE 9(5): e97278. https://doi.org/10.1371/journal.pone.0097278

Takács P, Ferincz Á, Imecs I, Kovács B, Nagy AA, Ihász K, Vitál Z, Csoma E (2021) Increased spatial resolution of sampling in the Carpathian basin helps to understand the phylogeny of central European stream-dwelling gudgeons. BMC Zoology 6(1): 1–11. https://doi.org/10.1186/s40850-021-00069-7

Tang KL, Agnew MK, Chen W-J, Hirt MV, Raley ME, Sado T, Schneider LM, Yang L, Bart HL, He S, Liu H, Miya M, Saitoh K, Simons AM, Wood RM, Mayden RL (2011) Phylogeny of the gudgeons (Teleostei: Cyprinidae: Gobioninae). Molecular Phylogenetics and Evolution 61(1): 103–124. https://doi.org/10.1016/j.ympev.2011.05.022

Tikhiy M.I. (1938) Use and ecology of fishes of the Ural River concerning the river regulation project. Bol'shaya Emba. Vol. 2. Academy of Sciences of the USSR, Leningrad-Moscow, 259–366. [In Russian]

Timoshkina NN, Barmintseva AE, Usatov AV, Mugue NS (2009) Intraspecific genetic polymorphism of Russian sturgeon *Acipenser gueldenstaedtii*. Genetika 45(9): 1250–1259. https://doi.org/10.1134/S1022795409090117

Triantafyllidis A, Bobori D, Koliamitra C, Gbandi E, Mpanti M, Petriki O, Karaiskou N (2011) DNA barcoding analysis of fish species diversity in four north Greek lakes. Mitochondrial DNA 22 (Suppl 1): 37–42. https://doi.org/10.3109/19401736.2010.542242

Turan D, Ekmekçi FG, Luskova V, Mendel J (2012) Description of a new species of genus *Gobio* from Turkey (Teleostei: Cyprinidae). Zootaxa 3257(1): 56–65. https://doi.org/10.11646/zootaxa.3257.1.4

Turan D, Japoshvili B, Aksu İ, Bektaş Y (2016) Description of two new species of the genus *Gobio* (Teleostei: Cyprinidae) from the Black Sea coast of Turkey. Zoology in the Middle East 62(2): 112–124. https://doi.org/10.1080/09397140.2016.1182779

Turan D, Kaya Ç, Bayçelebi E, Aksu İ, Bektaş Y (2017) *Gobio baliki*, a new gudgeon from Turkey (Teleostei: Cyprinidae). Zootaxa 4350(2): 284–290. https://doi.org/10.11646/zootaxa.4350.2.4

Turan D, Kaya Ç, Bayçelebi E, Aksu İ, Bektaş Y (2018) Description of *Gobio fahrettini*, a new gudgeon from Lake Ilgın basin, Central Anatolia (Teleostei: Gobionidae). Ichthyological Exploration of Freshwaters 28(4): 365–373.

Vasil'eva ED, Vasil'ev VP, Kuga TI (2004) On taxonomy of gudgeons of the genus *Gobio* (Gobioninae, Cyprinidae) of Europe: a new species of gudgeon *Gobio kubanicus* sp. nov. from the Kuban River basin. Voprosy Ikhtiologii 44(6): 766–782. [In Russian]

Vasil'eva ED, Vasil'ev VP, Boltachev AR (2005) Taxonomic relationships among gudgeons (*Gobio*, Gobioninae, Cyprinidae) of Crimea. Voprosy Ikhtiologii 45(6): 768–781. [In Russian]

Vasil'eva ED, Mamilov NSh, Sharakhmetov SE (2023) Gudgeon from the Emel River and problems of the gudgeon taxonomy (Genus *Gobio*, Cyprinidae) in Kazakhstan and Siberia. Voprosy Ikhtiologii 63(5): 499–513. [In Russian] https://doi.org/10.31857/S0042875223050156

Xiang C-Y, Gao F, Jakovlić I, Lei H-P, Hu Y, Zhang H, Zou H, Wang G-T, Zhang D (2023) Using PhyloSuite for molecular phylogeny and tree-based analyses. iMeta 2(1): e87. https://doi.org/10.1002/imt2.87

Xie Y-H (2007) Freshwater fishes in northeast region of China. Publishing Company in Chinese characters, 529 pp. [In Chinese, with English summary]

Yang J, He S, Freyhof J, Witte K, Liu H (2006) The phylogenetic relationships of the Gobioninae (Teleostei: Cyprinidae) inferred from mitochondrial cytochrome *b* gene sequences. Hydrobiologia 553(1): 255–266. https://doi.org/10.1007/s10750-005-1301-3

Yang T, Meng W, Zhang R, Gao T, Cai L, Hai S, Zhou Q (2016) DNA barcoding of fishes in Irtysh River China. Russian Journal of Genetics 52(9): 969–976. https://doi.org/10.1134/S1022795416090167

Yi T, Fu C (2020) Two mitochondrial genomes of freshwater gudgeons in the genus *Gobio* (Cypriniformes: Gobionidae). Mitochondrial DNA Part B 5(3) 3054–3055. https://doi.org/10.1080/23802359.2020.1797569

Zangl L, Daill D, Gessl W, Friedrich T, Koblmüller S (2020) Austrian gudgeons of the genus *Gobio* (Teleostei: Gobionidae): a mixture of divergent lineages. Journal of Zoological Systematics and Evolutionary Research 58(1): 327–340. https://doi.org/10.1111/jzs.12340

Zhang D, Gao F, Jakovlić I, Zou H, Zhang J, Li WX, Wang GT (2020) PhyloSuite: An integrated and scalable desktop platform for streamlined molecular sequence data management and evolutionary phylogenetics studies. Molecular Ecology Resources 20(1): 348–355. https://doi.org/10.1111/1755-0998.13096

Zinovyev EA, Baklanov MA (2007) The fauna of fishes and its unusual elements in water basins of Chelyabinsk and Kurgan regions. Perm University Heralds 5(10): 53–56. [In Russian, with English summary]

Supplementary material 1

Material for genetic studies

Authors: Ilya S. Turbanov, Aleksey A. Bolotovskiy, Oleg N. Artaev, Aleksandr A. Gandlin, Marina A. Levina, Ekaterina D. Vasil'eva, Boris A. Levin

Data type: xlsx

Link: https://doi.org/10.3897/zse.101.147368.suppl1

Supplementary material 2

The best partition schemes generated by ModelFinder v.2.2.0 (ML) and PartitionFinder v.2.1.1 (BI)

Authors: Ilya S. Turbanov, Aleksey A. Bolotovskiy, Oleg N. Artaev, Aleksandr A. Gandlin, Marina A. Levina, Ekaterina D. Vasil'eva, Boris A. Levin

Data type: docx

Link: https://doi.org/10.3897/zse.101.147368.suppl2

Supplementary material 3

ML phylogenetic tree of COI mtDNA sequences representing all available species in GenBank combined with our data set

Authors: Ilya S. Turbanov, Aleksey A. Bolotovskiy, Oleg N. Artaev, Aleksandr A. Gandlin, Marina A. Levina, Ekaterina D. Vasil'eva, Boris A. Levin

Data type: docx

Link: https://doi.org/10.3897/zse.101.147368.suppl3

Supplementary material 4

Coefficients of linear discriminants based on LDA

Authors: Ilya S. Turbanov, Aleksey A. Bolotovskiy, Oleg N. Artaev, Aleksandr A. Gandlin, Marina A. Levina, Ekaterina D. Vasil'eva, Boris A. Levin

Data type: docx

Link: https://doi.org/10.3897/zse.101.147368.suppl4

Zoosyst. Evol. 101 (2) 2025, 875–885 | DOI 10.3897/zse.101.139075

PENSOFT

für Natur MUSEUM FÜR NATURKUNDE BERLIN

Discovery and taxonomic exploration of *Metopa propoda* sp. nov., a new species of Stenothoidae Boeck, 1871 (Amphipoda, Amphilochoidea) from a seamount of the Caroline Plate, Western Pacific

Yan-Rong Wang[1,2], Zhong-Li Sha[1,2,3,4]

1 *Laboratory of Marine Organism Taxonomy and Phylogeny, Institute of Oceanology, Chinese Academy of Sciences, Qingdao 266071, China*
2 *College of Biological Sciences, University of Chinese Academy of Sciences, Beijing 100049, China*
3 *Laboratory for Marine Biology and Biotechnology,Qingdao Marine Science and Technology Center, Qingdao 266237, China*
4 *Shandong Province Key Laboratory of Experimental Marine Biology, Institute of Oceanology, Chinese Academy of Sciences, Qingdao, China*

https://zoobank.org/CCF17ADF-D1A0-44E5-A68A-5E6B30D51C85

Corresponding author: Zhong-Li Sha (shazl@qdio.ac.cn)

Academic editor: Luiz F. Andrade ♦ **Received** 11 October 2024 ♦ **Accepted** 31 January 2025 ♦ **Published** 24 April 2025

Abstract

A new stenothoid species, *Metopa propoda* **sp. nov.**, is described from a seamount of the Western Pacific. The new species differs from all other congeneric species by the mature males having a large rectangular notch in the palmar corner of the gnathopod 2. One mitochondrial gene (COI) was used to analyze the validity of *Metopa propoda* **sp. nov.** An identification key of the Pacific *Metopa* species, including this new species, is provided.

Key Words

COI, deep sea, morphology, taxonomy

Introduction

The large amphipod family Stenothoidae Boeck, 1871 comprises 354 species and subspecies within 50 genera (Horton et al. 2024; Navarro-Mayoral et al. 2024) and is found at depths ranging from subtidal zones to over 3000 meters (Krapp-Schickel 2015; Krapp-Schickel and Vader 2015). This family is regarded as one of the most challenging among all amphipod families (Tandberg 2011) and is characterized by a vestigial coxa 1 that is covered by following coxae, a shield-like coxa 4 that is enlarged and not posterodorsally excavate, and a uniramous uropod 3 (Barnard and Karaman 1991). Among all stenothoid genera, the genus *Metopa* Boeck, 1871, has long been considered polyphyletic (Barnard and Karaman 1991; Krapp-Schickel and Koenemann 2006; Tandberg 2011; Tandberg and Vader 2023).

Following *Stenothoe* Dana, 1852, the *Metopa* is the second largest genus in the family Stenothoidae, encompassing 56 accepted species (Krapp-Schickel 2009; Tandberg 2011; Tandberg and Vader 2023; Horton et al. 2024). Krapp-Schickel and Vader (2015) categorized *Metopa* into three groups based on the shape of the palmar corner of gnathopod 1, noting that the palmar shape of gnathopod 2 is not meaningful for cladistic analysis (Tandberg 2011; Krapp-Schickel and Vader 2015). Fifteen *Metopa* species have been reported from the Western Pacific, occurring at depths up to 2300 meters (Pirlot 1933; Gurjanova 1948, 1952, 1955; Krapp-Schickel 2009). Among these, only *M. abyssi* Pirlot, 1933, and *M. torbeni* Krapp-Schickel, 2009, have been found in the tropical Western Pacific, at depths of 100 m and 54 m, respectively (Pirlot 1933; Krapp-Schickel 2009).

During a biodiversity survey of seamounts in the Caroline Plate, several stenothoid specimens were collected. After careful examination, these specimens were identified as belonging to the genus *Metopa*. The present study describes a new *Metopa* species, highlights the

morphological distinctions between the new species and other congeneric species, and provides an identification key to all Pacific species of the genus.

Materials and methods

Specimens were collected from seamounts in the Caroline Plate of the Western Pacific by the research vessel KEXUE with Remote Operated Vehicle (ROV) FAXIAN. The animals were sorted on board and fixed in 96% ethanol, then transferred to 75% ethanol in the laboratory for further study. All material is deposited at the Marine Biological Museum of Chinese Academy of Sciences (MBMCAS), Qingdao, China. External morphology and internal anatomy were examined, dissected, and photographed under a microscope (ZEISS Discovery V20). Line drawings were completed by the software Adobe Photoshop CS6 with a graphics tablet (Wacom PTH 851). Length measurement was made along the outline of the animal, beginning from the anterior margin of the head to the posterior margin of the telson.

Genomic DNA of *Metopa propoda* sp. nov. was obtained from one specimen using Illumina HiSeq sequencing. At least 3 μg of genomic DNA was used for sequencing library construction. Paired-end libraries were prepared following Illumina's standard genomic DNA library preparation procedure (insert size of ~400 bp). Purified genomic DNA was sheared into smaller fragments with a desired size by Covaris, and blunt ends were generated by using T4 DNA polymerase. After adding an "A" base to the 3' end of the blunt phosphorylated DNA fragments, adapters were ligated to the ends of the DNA fragments. The desired fragments were purified through gel electrophoresis and then selectively enriched and amplified by PCR. The index tag was introduced into the adapter at the PCR stage, as appropriate, and we did a library quality test. Finally, the qualified Illumina paired-end library was used for Illumina Nova-Seq 6000 sequencing (150 bp*2, Shanghai Biozeron Co., Ltd). The raw paired-end reads were trimmed and quality controlled by Trimmomatic with parameters (SLIDINGWINDOW:4:15 MINLEN:75) (v. 0.36 http://www.usadellab.org/cms/uploads/supplementary/Trimmomatic). Clean data obtained by the above quality control processes were used to do further analysis. One gene (COI, 1534 bp) was BLASTed and deposited in GenBank (for accession numbers, see Table 1).

The sequences obtained were aligned using MEGA 6 (Tamura et al. 2013). The phylogenetic tree was constructed with maximum likelihood (ML), and the ML analyses were conducted online using W-IQ-TREE (http://iqtree.cibiv.univie.ac.at/) (Trifinopoulos et al. 2016), with clade support evaluated via 10,000 ML bootstrap replications. A total of fifty described and undescribed species within Stenothoidae and two outgroup taxa of Iphimediidae Boeck, 1871, were used for assessing the hypothesis that the specimen is a distinct new species by multiple species delimitation methods. The Bayesian implementation of the Poisson Tree Processes (bPTP) species delimitation model was employed as per Zhang et al. (2013), conducted on the web server of the Heidelberg Institute for Theoretical Studies, Germany (http://species.h-its.org/), using BI phylogenetic trees as the input data. The alignment from the fast-evolving COI gene was uploaded to the online server of Assemble Species by Automatic Partitioning (ASAP) method (https://bioinfo.mnhn.fr/abi/public/asap) with the model of Jukes-Cantor (JC69) with default settings (Puillandre et al. 2021). The Automated Barcode Gap Discovery (ABGD) analysis using a web-based interface (https://bioinfo.mnhn.fr/abi/public/abgd/abgdweb.html) as described by Puillandre et al. (2012). The analysis was conducted using the Kimura 2-parameter substitution model (TS/TV = 2.0), with a prior range for maximum intraspecific divergence set between 0.001 and 0.1, encompassing 10 recursive steps, and a relative gap width (X) of 1.0.

Systematic account

Order Amphipoda Latreille, 1816
Suborder Amphilochidea Boeck, 1871
Superfamily Amphilochoidea Boeck, 1871
Family Stenothoidae Boeck, 1871
Subfamily Stenothoinae Boeck, 1871
Genus *Metopa* Boeck, 1871

***Metopa propoda* sp. nov.**

https://zoobank.org/F5C694B2-6134-4A5D-8482-DDCFCA933B98

Figs 1–3

Material examined. *Holotype*. Western Pacific • 1 male, 6.1 mm; an unnamed seamount in Caroline Plate; M6091, 10°04'N, 140°9–15'E; depth 985–2016 m; 2–11 Jun. 2019; collected by a team of ROV "FAXIAN"; MBM 286611.

***Paratype*.** Western Pacific • 1 male, 4.3 mm; an unnamed seamount in Caroline Plate; M6091, 10°04'N, 140°9–15'E; depth 985–2016 m; 2–11 Jun. 2019; collected by a team of ROV "FAXIAN"; MBM 286611; 9 females, 2.3–4.5 mm; an unnamed seamount in Caroline Plate; M6091, 10°04'N, 140°9–15'E; depth 985–2016 m; 2–11 Jun. 2019; collected by a team of ROV "FAXIAN"; MBM 286821.

Description. *Head*. Head length subequal to pereonite 1 and 2 combined. Interantennal lobe strongly projecting, broadly rounded. Eyes rounded. Antenna 1 and 2 sexual dimorphisms. In female antenna 1, subequal to or slightly longer than antenna 2, peduncular articles 1 and 2 of equal length, flagellum 12–13 articles, accessory flagellum absent; antenna 2 peduncular article 5 the longest, flagellum 3/4 length of peduncular article 5, with 7–8 articles. In males, antenna 1 is shorter than antenna 2, primary flagellum article 1 longest, article 2 half-length of article 1 (based on male paratype); antenna 2 with flagellum shorter than half-length of peduncular article 5.

Table 1. Details of species and GenBank accession numbers used in this study.

Genus	Species	voucher/isolate	COI
Metopa Boeck, 1871	*M. propoda* **sp. nov.**	MBM 286611	PQ287283
	Metopa sp.	NUN-0300	MG320561
	M. boeckii	08PROBE-0337	MG319126
	M. boeckii	DZMB-HH 54716 c	MG264880
	M. boeckii	DZMB-HH 54693	MG264843
	M. boeckii	DZMB-HH 54688	MG264763
	M. cistella	BCAMP0079	MG310759
	M. alderi	MT03961	KT209338
	M. alderi	MT03958	KT208542
	M. rubrovittata	MT03932	KT209277
	M. rubrovittata	MT03929	KT209052
	M. rubrovittata	MT03931	KT208825
	M. rubrovittata	MT03930	KT208695
Parametopella Gurjanova, 1938	*P. cypris*	SERCINVERT2582	OQ323416
	P. cypris	SERCINVERT2541	OQ323322
	P. cypris	SERCINVERT2544	OQ323121
	P. cypris	SERCINVERT2543	OQ322893
	P. cypris	SERCINVERT2602	OQ322697
Stenothoe Dana, 1852	*S. nhatrangensis*	B	MH128324
	S. nhatrangensis	A	MH128323
	S. valida	SERCINVERT2483	OQ322684
	Stenothoe sp.	M3.Oa-3-Ssp	OQ417149
	S. gallensis	ABC-9	OL311534
	S. gallensis	ABC-5	OL311530
	S. gallensis	ABC-14	OL311539
	Stenothoe sp.	M1.c-89-Sts	MZ504220
	Stenothoe sp.	PD008SHx1	MT317094
	Stenothoe sp.	PD034GA2	MT317092
	Stenothoe sp.	PD034Gx1	MT317091
	S. marina	Crust 18897V	MG934996
	S. marina	MT02094	KT209198
	S. marina	MT02093	KT208537
	S. monoculoides	MT03107	KT209271
	S. monoculoides	MT03925	KT209192
	S. monoculoides	MT03934	KT208458
	S. monoculoides	MT03935	KT208446
Stenula Barnard, 1962	*Stenula* sp.	SFCM9-003	HM422231
	Stenula sp.	SFCM9-001	HM422230
Wollastenothoe	*W. minuta*	nl2	PP595991
	Stenothoidae sp.	BCC2010-045	MG321169
	Stenothoidae sp.	NUN-0004	MG320587
	Stenothoidae sp.	NUN-0003	MG317721
	Stenothoidae sp.	CCNUN604	MG317164
	Stenothoidae sp.	NUN-0139	MG313209
	Stenothoidae sp.	NUN-0066	MG311622
	Stenothoidae sp.	BIOUG<CAN>:BCC2010-046	HQ945467
	Stenothoidae sp.	BMBM-0990	MH242980
	Stenothoidae sp.	BMBM-0994	MH242979
	Stenothoidae sp.	BMBM-0998	MH242981
	Stenothoidae sp.	31	EF989710
Iphimedia Rathke, 1843	*I. obesa*	Crust 17980V	MG935235
	I. obesa	Crust 17979V	MG935137

Mouthparts. Right mandible incisor with four large teeth; lacinia mobilis serrate edge broader than that of the incisor, with 9 teeth; palp 3-articulate, basal article quadrangular, second one the longest, very short and small third article carrying one long distal seta. Left mandible incisor with 11 teeth unequal in size, lacinia mobilis absent. Maxilla 1 palp with one article, with row of 4 robust setae in distal 1/4 length of medial margin and 3 setae subapically. Maxilla 2 plates in ordinary tandem position. Maxilliped inner plate fused with apical notch and small marginal setae; outer plate visible as acute tooth-shaped prolongation; dactylus subequal in length to article 3.

Coxa 2 tongue-shaped, with marginal setae; coxa 3 larger than coxa 2, rectangular; coxa 4 not excavated, about 1.3 times wider than long.

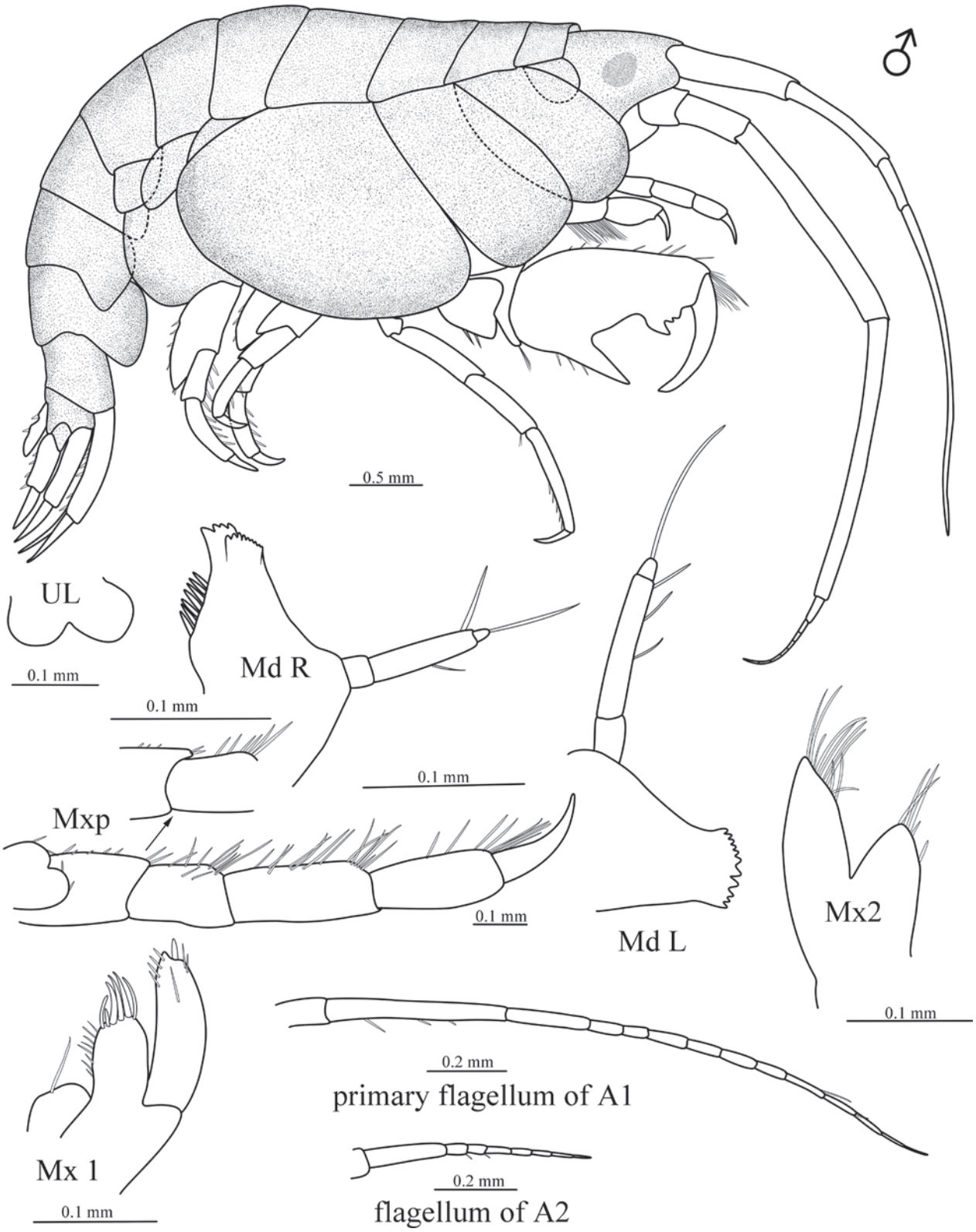

Figure 1. *Metopa propoda* sp. nov. male holotype (MBM 286611). UL. upper lip; LL. lower lip; Md L. left mandible (not showing molar and palp); Md R. right mandible; Mx1. maxilla 1; Mx2. maxilla 2; Mxp. right maxilliped; A1. antenna 1; A2. antenna 2.

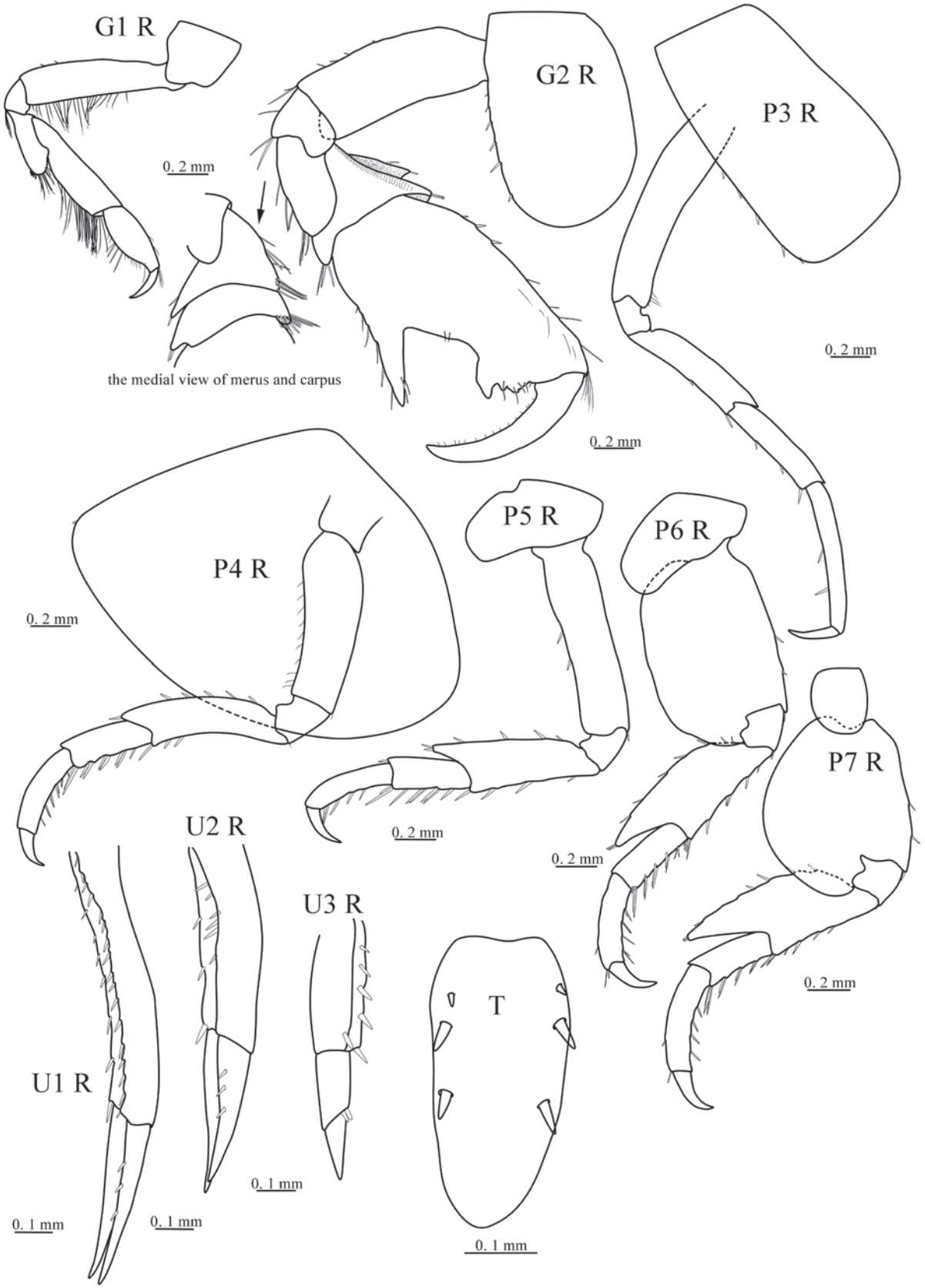

Figure 2. *Metopa propoda* sp. nov. male holotype (MBM 286611). G1 R. right gnathopod 1; G2 R. right gnathopod 2 (arrow showing the medial view of merus and carpus); P3 R. right pereopod 3; P4 R. right pereopod 4; P5 R. right pereopod 5; P6 R. right pereopod 6; P7 R. right pereopod 7; U1 R. right uropod 1; U2 R. right uropod 2; U3 R. right uropod 3; T. telson.

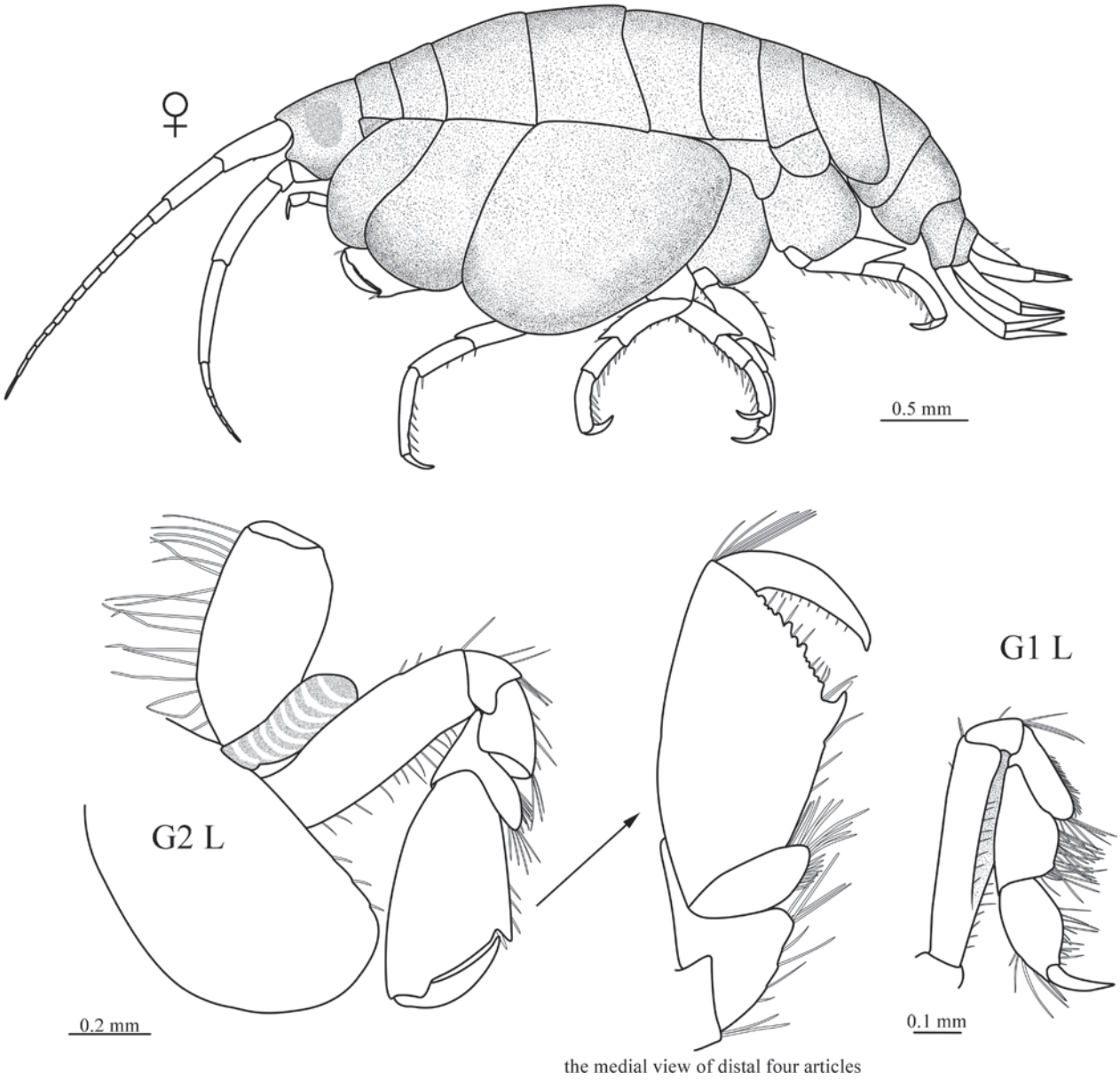

Figure 3. *Metopa propoda* sp. nov. female paratype (MBM 286821). G1 R. right gnathopod 1; G2 R. right gnathopod 2 (arrow showing the medial view of merus to dactylus).

Gnathopods and pereopods. Gnathopod 1 sexual dimorphism, propodus suboval and narrow, palm not defined; carpus in female wider and shorter than that of in male, longer than propodus, proximally narrower than distally; merus projecting under carpus, all articles beset with groups of short setae. Gnathopod 2 sexual dimorphism, female propodus slightly widening distally, hind margin subequal in length to palm, which is defined by a shallow notch and not very strong tooth and has many small serrations next to dactylus insertion; dactylus somewhat shorter than length of palm; carpus in lateral view wider than long, triangular, in medial view oval-shaped; merus not lobate, in lateral view rectangular, in medial view triangular. Gnathopod 2 male propodus hind margin shorter than palm, which is defined by a very large rectangular excavation and strong thumb-shaped palmar corner and has 4 small serrations; carpus in lateral view triangular, dorsal margin with row of stridulating knobs, in medial view rectangular, with anterodistal acute projection; merus not lobate. Pereopod 3 longer than pereopod 4, all articles elongate and weak, distal three articles with setae on posterior margin. Pereopod 4 with posterior margin of merus, carpus, and propodus with a few transverse rows of small setae; merus somewhat curved. Pereopod 5 basis rectilinear; merus to propodus anterior margin with several transverse rows of small setae; merus wider than carpus, with shortly lengthened posterodistally. Pereopod 6 and 7 bases widened with rounded posterodistal lobe; merus with lengthened posterodistally hardly reaching to distal margin of carpus; merus to propodus of both armed as in pereopod 5.

Uropods and telson. Uropod 1 peduncle much longer than subequal rami, with short robust setae on peduncle and outer ramus; inner ramus unarmed with setae. Uropod 2 peduncle longer than rami, with short robust setae; outer

ramus slightly longer than inner one, armed with robust setae; inner ramus unarmed. Uropod 3 peduncle subequal to ramus; article 1 of ramus slightly longer than spine-shaped robust article 2. Telson tongue-shaped, distally rounded, with three marginal robust setae on each side dorsally.

Etymology. The species is named for the large rectangular notch on the palmar corner of gnathopod 2.

Distribution. Presently known only from a seamount of the Caroline Plate at a depth of 985–2016 meters.

Remarks. According to the diagnostic key by Barnard and Karaman (1991), *M. propoda* sp. nov. definitely belongs to the genus *Metopa* for having the basis of pereopods 6 and 7 similarly expanded, the palp of maxilla 1 only 1-articulate, and the mandibular palp 3-articulate. Krapp-Schickel and Vader (2015) classified members of the genus *Metopa* into three groups based on the shape of the palmar corner on the gnathopod 1. *M. propoda* sp. nov. belongs to the N group, characterized by a palmar corner angle of 150–160°. Therefore, the present new species is in the similar group to the following four Pacific species: *M. abyssi* Pirlot, 1933; *M. exigua* Krapp-Schickel, 2009; *M. layi* Gurjanova, 1948; and *M. uschakovi* Gurjanova, 1948 (Krapp-Schickel 2009; Krapp-Schickel and Vader 2015).

Metopa propoda sp. nov. can be distinguished from these four species by the large rectangular notch in the palmar corner of the gnathopod 2 in mature males. Additionally, the new species differs from *M. abyssi* in having antenna 1 that is shorter or equal in length to antenna 2, rather than longer; the inner plate of the maxilliped is fused; and the merus prolongation of pereopods 5–7 does not reach the distal margin of the carpus (Pirlot 1933, fig. 54). It differs from *M. exigua* by having antenna 1 shorter or equal in length to antenna 2, a fused inner plate of the maxilliped, the merus prolongation of pereopods 6 and 7 nearly reaching the distal margin of the carpus, and the rami of uropod 2 being equal in length (Krapp-Schickel 2009). It differs from *M. layi* in that the peduncle of uropod 3 is equal in length to the ramus, whereas in *M. layi*, the peduncle is distinctly shorter than the ramus (Gurjanova 1948, fig. 49). It differs from *M. uschakovi* in that the articles of the ramus of uropod 3 are equal in length, whereas in *M. uschakovi*, article 1 is much shorter than article 2 (Gurjanova 1948, fig. 55). A key (modified from Krapp-Schickel and Vader 2015) to the Pacific species of *Metopa* is provided below.

The phylogenetic trees produced by ML analyses (Fig. 4) show that *Metopa* species cluster together with four unidentified Stenothoidae species and *Wollastenothoe minuta* Gouillieux & Navarro-Mayoral, 2024, with moderate support (BP = 66%). The *Stenothoe* species form a clade with one unidentified *Stenula* species and *Parametopella cypris* Holmes, 1905, also with moderate support (BP = 85%). The remaining two unidentified *Stenothoe* J.L. Barnard, 1962 species. and one Stenothoidae species are grouped into another moderately supported clade (BP = 87%). The species delimitation based on ABGD, ASAP, and bPTP methods has confirmed the identification of the new species (Fig. 5).

Identification key to the Pacific species of *Metopa*

1	Gnathopod 1 with palmar corner 120°, propodus widened	2
–	Gnathopod 1 simple, with palmar corner absent, propodus hind margin straight	10
–	Gnathopod 1 normal, palmar corner 150–160°, propodus hind margin rounded	14
2	Hind margin of propodus of gnathopod 2 longer than palm	3
–	Hind margin of propodus of gnathopod 2 shorter than or subequal to palm	5
3	Carpus of gnathopod 2 carrying acute, triangular lobe posterodistally	*M. majuscula* Gurjanova, 1948
–	Carpus of gnathopod 2 normal, not lobate	4
4	Article 2 of ramus of uropod 3 longer than article 1	*M. timonovi* Gurjanova, 1955
–	Article 2 of ramus of uropod 3 shorter than article 1	*M. colliei* Gurjanova, 1948
5	Merus of gnathopod 2 carrying large lobe anterodistally`	*M. mirifica* Gurjanova, 1952
–	Merus of gnathopod 2 not lobate	6
6	Body carinate	*M. eupraxiae* Krapp-Schickel, 2009
–	Body not carinate (not sure for *M. kobjakovae*)	7
7	Telson richly spinose	*M. kobjakovae* Gurjanova, 1955
–	Telson with at most several marginal robust setae on each side	8
8	Eyes absent; antenna 1 longer than antenna 2	*M. samsiluna* J.L. Barnard, 1966
–	Eyes present; antenna 1 shorter than antenna 2	9
9	Dactylus of gnathopod 2 shorter than palm	*M. japonica* Gurjanova, 1952
–	Dactylus of gnathopod 2 equal to palm	*M. bulychevae* Gurjanova, 1955
10	All peduncular articles of antenna 1 subequal in length	*M. angustimana* Gurjanova, 1948
–	Basal two peduncular articles of antenna 1 much longer than article 3	11
11	Palmar corner of gnathopod 2 not defined	*M. torbeni* Krapp-Schickel, 2009
–	Palmar corner of gnathopod 2 defined by a pronounced tooth	12
12	Carpus of gnathopod 1 subequal in length to propodus	*M. cistella* Barnard, 1969
–	Carpus of gnathopod 1 longer than propodus	13

13 Palm of gnathopod 2 nearly smooth ..... *M. dawsoni* J.L. Barnard, 1962
– Palm of gnathopod 2 carrying large tooth ..... *M. koreana* Gurjanova, 1952
14 Peduncle of uropod 3 shorter than ramus 15
– Peduncle of uropod 3 subequal to ramus 17
15 Article 1 of ramus of uropod 3 shorter than article 2 ..... *M. uschakovi* Gurjanova, 1948
– Articles of ramus of uropod 3 subequal in length 16
16 Inner plate of maxilliped not fused ..... *M. abyssi* Pirlot, 1933
– Inner plate of maxilliped fused ..... *M. layi* Gurjanova, 1948
17 Antenna 1 shorter than or subequal to antenna 2 ..... *M. propoda* sp. nov.
– Antenna 1 longer than antenna 2 ..... *M. exigua* Krapp-Schickel, 2009

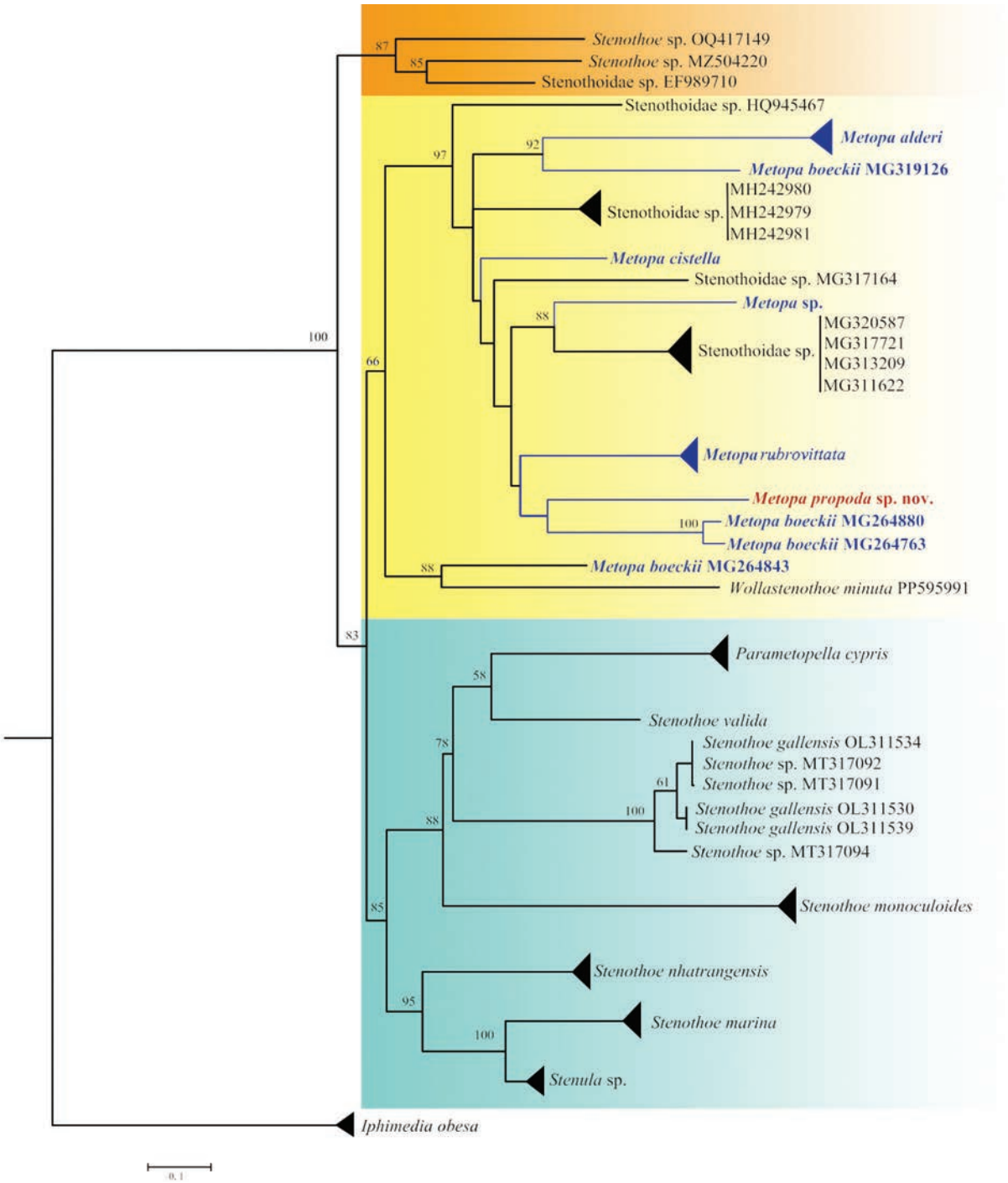

Figure 4. The maximum-likelihood (ML) tree shows the relationships between *Metopa propoda* sp. nov. and other Stenothoidae COI sequences. The numbers at each node represent bootstrap values (BP). *M. propoda* sp. nov. is highlighted in bold and red, and the other *Metopa* species are highlighted in bold and blue.

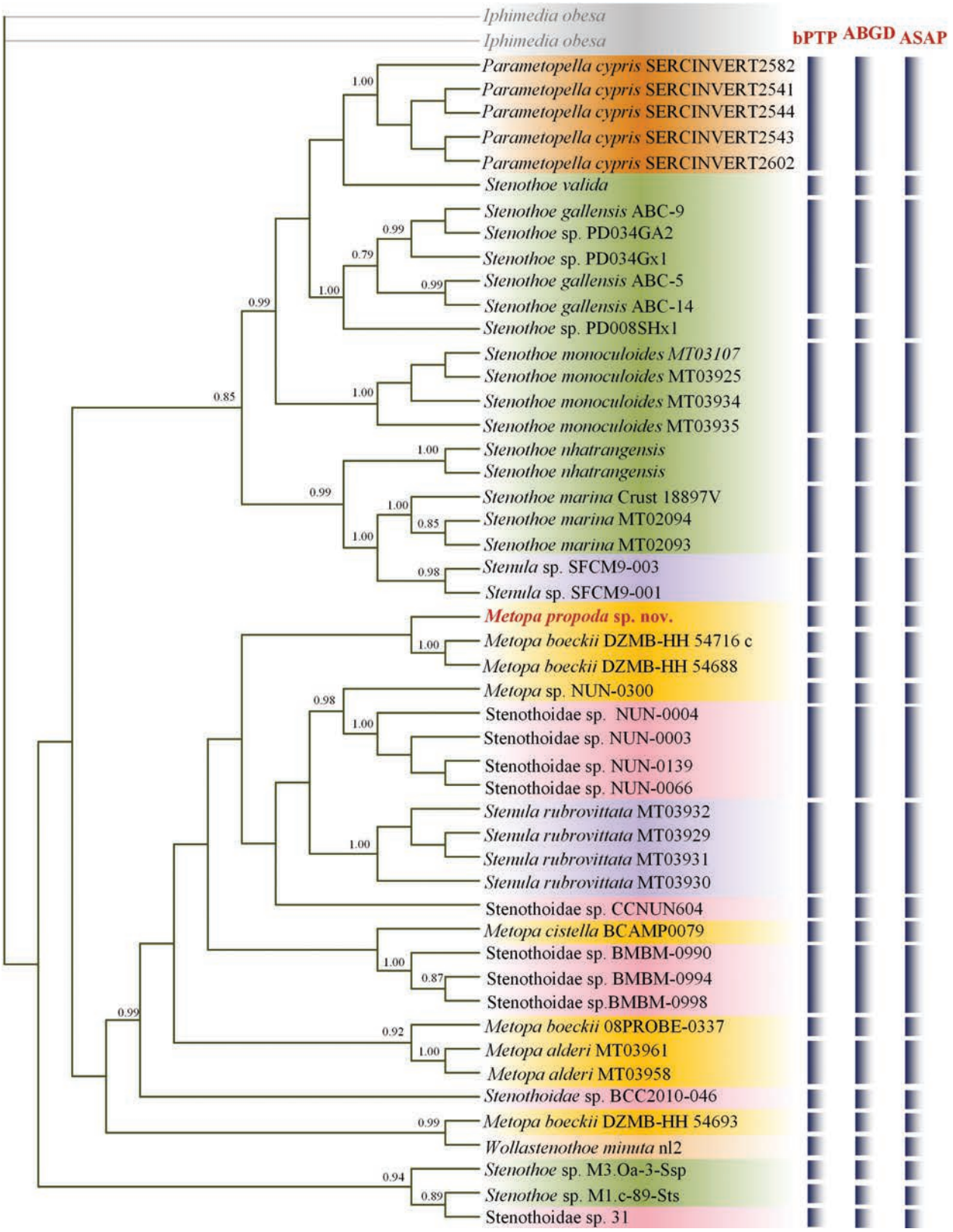

Figure 5. Bayesian inference (BI) Phylogenetic tree based on COI showing the phylogenetic relationship between *Metopa propoda* sp. nov. and related stenothoids. Numbers adjacent to nodes refer to BI posterior probability (>70). Putative species identified by DNA-based species delimitation methods [Bayesian implementation of the Poisson Tree Processes (bPTP), Automated Barcode Gap Discovery (ABGD), and Assemble Species by Automatic Partitioning (ASAP)] applied on the COI tree/distance matrices are indicated by bars on the concatenated tree.

Discussion

Nineteen *Metopa* species, including *M. propoda* sp. nov., have been reported in the Pacific, with all of them found in the northern Pacific (Gurjanova 1948, 1952, 1955; Barnard 1962, 1966, 1969; Krapp-Schickel 2009; Krapp-Schickel and Vader 2015). Five of these species are found in deep waters, including *M. angustimana* Gurjanova, 1948 (Peter the Great Gulf, 351 m), *M. bulychevae* Gurjanova, 1955 (Japan Sea, 414 m), *M. koreana* Gurjanova, 1952 (off Korea, 1100 m), *M. mirifica* Gurjanova, 1952 (Kuril Islands, 2300 m), and *M. propoda* sp. nov. (Seamount in Caroline Plate, 985–2016 m) (Gurjanova 1948, 1952, 1955). However, only the present new species was found in the deep waters of the tropical Pacific (4–5 °C).

The results of the present study validate *M. propoda* sp. nov. and reveal a close relationship between the new species and *M. boeckii* G.O. Sars, 1892, given the existing Stenothoidae molecular sequences. *Metopa boeckii* was redescribed by Tandberg (2010) and was distributed from the Arctic to the Atlantic at depths of 10–170 m. The present study reveals that *M. boeckii* showed intraspecific variation considerably exceeding the values commonly used for amphipod species delimitation (Fig. 5), indicating potential cryptic diversity (Jażdżewska et al. 2018) or misidentification, as *M. boeckii* had been confused with *M. borealis* G.O. Sars, 1883, and *M. bruzelii* (Goës, 1866) (Tandberg 2010).

The genus *Metopa* has long been considered polyphyletic (Barnard and Karaman 1991). Phylogenetic studies based on both morphological characters and molecular sequences have shown that it is not monophyletic (Krapp-Schickel and Koenemann 2006; Tandberg 2011; Navarro-Mayoral et al. 2024). Morphologically, *Metopa* has a close relationship with *Metopoides* Della Valle, 1893; *Proboloides* Della Valle, 1893; *Prometopa* Schellenberg, 1926; and *Stenothoe* Dana, 1852 (Barnard and Karaman 1991). However, the genus *Metopa* does not show a close relationship with *Stenothoe* species in the present study (Fig. 4) and Navarro-Mayoral et al. (2024). The Stenothoidae shows to be a controversial amphipod family, calling for further taxonomic and phylogenetic studies.

Acknowledgements

This work was supported by the National Natural Science Foundation of China (42306110), the National Science Foundation for Distinguished Young Scholars (42025603), the NSFC Innovative Group Grant (42221005), and the Biological Resources Programme of the Chinese Academy of Sciences.

References

Barnard JL (1962) Benthic marine Amphipoda of southern California. 3 Families Amphilochidae, Leucothoidae, Stenothoidae, Argissidae, Hyalidae. Pacific Naturalist 3: 116–163.

Barnard JL (1966) Submarine canyons of southern California. Part V. Systematics: Amphipoda. Allan Hancock Pacific Expeditions 27: 1–166.

Barnard JL (1969) Gammaridean Amphipoda of the rocky intertidal of California: Monterey Bay to La Jolla. United States National Museum Bulletin 258: 1–230. https://doi.org/10.5479/si.03629236.258.1

Barnard JL, Karaman GS (1991) The families and genera of marine gammaridean Amphipoda (except marine gammaroids). Records of the Australian Museum, Supplement 13 (part 2): 419–866. https://doi.org/10.3853/j.0812-7387.13.1991.367

Gurjanova E (1948) Amphipoda Tixogo Okeana II. Stenothoidae dal'Nevostchnykh Morei, Notebook of the Academician Sergei Aleksevich Zernov (Hydrobiologist), 287–325.

Gurjanova E (1952) Novye vidy bokoplavov (Amphipoda,Gammaridea) iz dal'nevostochnykh morei. Akademii Nauk SSSR. Trudy Zoologicheskogo Instituta 12(17): 171–194.

Gurjanova E (1955) Novye vidy bokoplavov (Amphipoda, Gammaridea) iz severnoi chasti Tikhogo okeana (=Tikhogo) Okeana. Zoological Institute Ak. Nauk SSSR 18: 166–218.

Horton T, Lowry J, De Broyer C, Bellan-Santini D, Copilas-Ciocianu D, Corbari L, Costello MJ, Daneliya M, Dauvin JC, Fišer C, Gasca R, Grabowski M, Guerra-García JM, Hendrycks E, Hughes L, Jaume D, Jazdzewski K, Kim YH, King R, Krapp-Schickel T, LeCroy S, Lörz AN, Mamos T, Senna AR, Serejo C, Souza-Filho JF, Tandberg AH, Thomas JD, Thurston M, Vader W, Väinölä R, Valls Domedel G, Vonk R, White K, Zeidler W (2024) World Amphipoda Database. Metopa Boeck, 1871. Accessed through: World Register of Marine Species. https://www.marinespecies.org/aphia.php?p=taxdetails&id=101764 [on 2024-09-19]

Jażdżewska AM, Corbari L, Driskell A, Frutos I, Havermans C, Hendrycks E, Hughes L, Lörz AN, Bente Stransky, Tandberg AHS, Vader W, Brix S (2018) A genetic fingerprint of Amphipoda from Icelandic waters - the baseline for further biodiversity and biogeography studies. ZooKeys 23: 55–73. https://doi.org/10.3897/zookeys.731.19931

Krapp-Schickel T (2009) New and poorly described stenothoids (Crustacea, Amphipoda) from the Pacific Ocean. Memoirs of Museum Victoria 66: 95–116. https://doi.org/10.24199/j.mmv.2009.66.12

Krapp-Schickel T (2015) Minute but constant morphological differences within members of Stenothoidae: The *Stenothoe gallensis* – group with four new members, keys to *Stenotho*e world-wide, a new species of *Parametopa* and *Sudanea* n. gen. (Crustacea, Amphipoda). Journal of Natural History 49: 1–69. https://doi.org/10.1080/00222933.2015.1021873

Krapp-Schickel T, Koenemann S (2006) Cladistic analysis of the family Stenothoidae (Amphipoda, Crustacea). Contributions to Zoology 74: 169–188. https://doi.org/10.1163/18759866-0750304006

Krapp-Schickel T, Vader W. (2015) "Stenothoids living with or on other animals (Crustacea, Amphipoda)." Zoosystematics and Evolution 91: 215–246. https://doi.org/10.3897/zse.91.5715

Navarro-Mayoral S, Gouillieux B, Fernandez-Gonzalez V, Tuya F, Lecoquierre N, Bramanti L, Terrana L, Espino F, Flot J-F, Haroun R, Otero-Ferrer F (2024) "Hidden" biodiversity: a new amphipod genus dominates epifauna in association with a mesophotic black coral forest. Coral Reefs 43: 655–672. https://doi.org/10.1007/s00338-024-02491-y

Pirlot JM (1933) Les amphipodes de l'expédition du Siboga. Deuxième partie. Les amphipodes gammarides. II. Les amphipodes de la mer profonde. 1. (Lysianassidae, Stegocephalidae, Stenothoidae, Pleu-

stidae, Lepechinellidae). Siboga-Expeditie. Uitkomsten op zoologisch, botanisch, oceanographisch en geologisch gebied verzameld in Nederlandsch Oost-Indie 1899–1900 aan boord H.M. Siboga 33: 115–167.

Puillandre N, Lambert A, Brouillet S, Achaz G (2012) ABGD, Automatic Barcode Gap Discovery for Primary Species Delimitation. Molecular Ecology 21: 1864–1877. https://doi.org/10.1111/j.1365-294X.2011.05239.x

Puillandre N, Brouillet S, Achaz G (2021) ASAP: Assemble species by automatic partitioning. Molecular Ecology Resources 21: 609–620. https://doi.org/10.1111/1755-0998.13281

Tamura K, Stecher G, Peterson D, Filipski A, Kumar S (2013) MEGA6: Molecular Evolutionary Genetics Analysis version 6.0. Molecular Biology and Evolution 30: 2725–2729. https://doi.org/10.1093/molbev/mst197

Tandberg AHS (2010) A redescription of *Metopa* species (Amphipoda, Stenothoidae) based on the type material. 3. Natural History Museum, Oslo (NHM) 2465. Zootaxa 2465: 1–94. https://doi.org/10.11646/zootaxa.2465.1.1

Tandberg AHS (2011) Studies on the Amphipod Genus *Metopa* (Stenothoidae): Taxonomy, Ecology, Phylogeny. PhD thesis, University of Tromsø. [ISBN: 978-82-8266-024-2]

Tandberg AHS, Vader W (2023) A new stenothoid (Crustacea: Amphipoda: Stenothoidae) from a shallow water hydroid polyp in British Columbia, Canada. Records of the Australian Museum 75: 559–565. https://doi.org/10.3853/j.2201-4349.75.2023.1893

Trifinopoulos J, Nguyen LT, von Haeseler A, Minh BQ (2016) W-IQTREE: A fast online phylogenetic tool for maximum likelihood analysis. Nucleic Acids Research 44: 232–235. https://doi.org/10.1093/nar/gkw256

Zhang J, Kapli P, Pavlidis P, Stamatakis A (2013) A general species delimitation method with applications to phylogenetic placements. Bioinformatics 29: 2869–2876. https://doi.org/10.1093/bioinformatics/btt499

Zoosyst. Evol. 101 (2) 2025, 887–906 | DOI 10.3897/zse.101.136290

PENSOFT

für Natur MUSEUM FÜR NATURKUNDE BERLIN

A needle in a haystack: Rediscovery and revised description of *Ichnotropis microlepidota* Marx, 1956, from the central highlands of Angola

Max Benito[1], Werner Conradie[2,3,4], Pedro Vaz Pinto[5,6,7,8], Javier Lobón-Rovira[5,6]

1 *Universidad Internacional Menéndez Pelayo, Calle de Isaac Peral 23, 28040 Madrid, Spain*
2 *Port Elizabeth Museum, 23 Beach Road, Humewood, Gqeberha, South Africa*
3 *School of Natural Resource Management, Nelson Mandela University (George Campus), George, South Africa*
4 *National Geographic Okavango Wilderness Project, Wild Bird Trust, Okavango, South Africa*
5 *CIBIO, Centro de Investigação em Biodiversidade e Recursos Genéticos, InBIO Laboratório Associado, Campus de Vairão, Universidade do Porto, 4485-661 Vairão, Portugal*
6 *BIOPOLIS Program in Genomics, Biodiversity and Land Planning, CIBIO, Campus de Vairão, 4485-661 Vairão, Portugal*
7 *TwinLab CIBIO/ISCED, Instituto Superior de Ciências da Educação da Huíla, Rua Sarmento Rodrigues s/n, Lubango, Angola*
8 *Fundação Kissama, Rua 60 Casa 560, Lar do Patriota, Luanda, Angola*

https://zoobank.org/4DFDA337-6ADD-4AC4-AD3C-D50C6222C32D

Corresponding author: Javier Lobón-Rovira (j.lobon.rovira@cibio.up.pt)

Academic editor: Johannes Penner ♦ **Received** 3 September 2024 ♦ **Accepted** 21 February 2025 ♦ **Published** 25 April 2025

Abstract

Ichnotropis is a genus of small and elusive ground-dwelling lizards mostly distributed in the savannas and woodlands south of the Congo River. The genus comprises six nominal species and three subspecies; however, the phylogenetic hypothesis of this group and the taxonomical status of several taxa remain unresolved. Among these species, *Ichnotropis microlepidota* stands out, as it is only known from the type series since its discovery in the 1950s in the crop of a Chanting Goshawk in Mount Moco, in the central highlands of Angola. Consequently, due to the lack of a precise locality and its similar morphology to other species, the taxonomic status of this species has been debated by several authors. Thanks to the collection of new material across the Angolan territory, we take the opportunity to revise the group, using molecular and morphological techniques. Thus, we here provide the first phylogenetic hypothesis of the group in Angola and therefore a phylogenetic placement of *I. microlepidota*. As a result, we validate the taxonomic status of this elusive species and demonstrate that it represents a distinct taxon within the *bivittata* group, differing by 14.99% *16S* uncorrected p-distance from *I. bivittata*. Furthermore, we undertake an updated description of this species, providing additional external and internal (i.e., cranial osteology) morphological features that can be used to compare *I. microlepidota* with other members of the group. Finally, we identified two candidate new species from Angola and corroborated the importance of the central highlands of Angola as an important center of endemism in the western slope of Central Africa.

Key Words

Africa, CT scan, endemic, grasslands, herpetology, Lacertidae, Mount Moco

Introduction

Among reptiles, lizards have the highest proportion of species known only from their type localities, type series, or both combined, with several species known from a single specimen (Meiri et al. 2018). This is due to different factors, such as difficult-to-detect or elusive species (i.e., strictly fossorial species or canopy specialists), cryptic species that are challenging to identify or to distinguish from others in the field, or species that distribute across conflict zones and consequently are poorly surveyed or currently inaccessible (Tolley et al. 2016; Meiri et al. 2018).

Nonetheless, despite the growing number of recent rediscoveries (Rodrigues et al. 2013; Prates et al. 2017; Solano-Zavaleta et al. 2017; Wang et al. 2017; Baptista et al. 2020; Putra et al. 2020; Bates et al. 2023; Cowan et al. 2024), many species remain 'lost' and needs further investigation (Meiri et al. 2018; Lindken et al. 2024).

Notwithstanding, while Africa hosts nine out of the 34 biodiversity hotspots in the world, its biodiversity remains poorly known and understudied (Böhm et al. 2013; Deikumah et al. 2014; Tolley et al. 2016). This is mainly a consequence of political pressure and social instability in the continent, the difficult access to many areas, and the lack of resources in the territory (Rydén et al. 2020; Ogwu et al. 2022). All these situations have hampered scientific surveys in this still poorly explored continent. The case of Angola is remarkable. After the war of independence (1961–1975), it suffered nearly a 40-year-long civil war (1975–2002) that almost completely precluded any fieldwork or biodiversity research (Marques et al. 2018; Baptista et al. 2019).

The first herpetological surveys in Angola date from the 19th century during the colonial era, led mainly by European and western countries, like Portugal, England, the United States of America, or Germany (Marques et al. 2018; Baptista et al. 2019). In the last decade, political stabilization in Angola has motivated numerous expeditions to previously understudied or poorly explored areas across the country. Consequently, access to new material, coupled with the advancement of molecular techniques and morphological analysis, has led to the description of several new taxa (Conradie et al. 2012a, b, 2013, 2020, 2022a, b; Stanley et al. 2016; Ceríaco et al. 2018, 2020a, b, d, e, 2021, 2024; Branch et al. 2019a, b, c, 2021; Marques et al. 2019, 2020a, b, 2022b, 2023a, b, 2024a, b; Hallermann et al. 2020; Nielsen et al. 2020; Baptista et al. 2021, 2023; Lobón-Rovira et al. 2021b, 2022, 2024b; Parrinha et al. 2021; Wagner et al. 2021; Bates et al. 2023), several new species records (Marques et al. 2018, 2022a, 2023a, b, 2024a; Butler et al. 2019; Conradie et al. 2021, 2022b, 2023; Lobón-Rovira et al. 2022, 2024a, c) and some species rediscoveries (Branch et al. 2018; Baptista et al. 2020; Bates et al. 2023). However, some groups are better known than others, with some groups still poorly studied in Angola (e.g., *Ichnotropis, Agama* ~ Conradie, 2024, or *Leptopelis* ~ Baptista, 2024).

The family Lacertidae comprises ~370 species distributed in the more arid regions of Europe, Africa, and Asia (Uetz et al. 2025). Notably, southern Africa represents a high center for lacertid diversity (Branch 1998), which includes eight different genera, of which six are present in Angola: *Ichnotropis, Heliobolus, Holaspis, Meroles, Nucras,* and *Pedioplanis* (Branch et al. 2019a). In recent years, some of these genera have undergone taxonomic revisions in Angola (i.e., *Heliobolus* ~Marques et al. 2022b, *Nucras* ~Baptista et al. 2020; Branch et al. 2019a and *Pedioplanis* ~Conradie et al. 2012b; Parrinha et al. 2021). However, other groups like *Ichnotropis* have never been studied in detail, mainly due to the lack of fresh material and the highly problematic taxonomy of the group (van den Berg 2017).

Ichnotropis is a genus of small-sized African lizards (van den Berg 2017) with a wide distribution in the southern and eastern rim of the Congo River Basin, ranging from South Africa to Gabon in the west and northwards to the eastern coast of Tanzania. Exceptionally, *Ichnotropis chapini* Schmidt, 1919, has only been recorded from Adra, northern Democratic Republic of the Congo (DRC), close to the border with South Sudan, and seems to be isolated from all other *Ichnotropis* species (Schmidt 1919; Edwards et al. 2013; Engleder et al. 2013; van den Berg 2017). *Ichnotropis* lizards normally inhabit dry woodland savanna habitats, although they are also present in sandy deserts and even in relatively humid environments (van den Berg 2017).

This genus contains a total of six recognized species (*I. bivittata* Bocage, 1866, *I. capensis* (Smith, 1838), *I. chapini* Schmidt, 1919, *I. grandiceps* Broadley, 1967, *I. microlepidota* Marx, 1956, and *I. tanganicana* Boulenger, 1917) and several subspecies with questionable validity (e.g., *I. b. pallida* Laurent, 1964, *I. c. nigrescens* Laurent, 1952, and *I. c. overlaeti* Laurent, 1964). Six of these taxa have been recorded within Angolan territory (i.e., *I. b. bivittata, I. b. pallida, I. c. capensis, I. c. overlaeti, I. microlepidota,* and *I.* cf. *grandiceps*) (Marques et al. 2018; Conradie et al. 2022b). Not surprisingly, these elusive lizards have been poorly studied, with some of the species being only known from their type series, such as *I. microlepidota, I. tanganicana,* and *I. chapini* (van den Berg 2017). In addition, the lack of fresh material has prevented phylogenetic studies from exploring interspecific relationships of this group. Rarity in the observations of these lizards can be due to the fact that several sympatric species display a unique 'annual' reproductive strategy, in which their breeding cycles happen asynchronously, thus reducing competition between them (Broadley 1967, 1974, 1979; Jacobsen 1987) and potentially between juveniles and adults. Therefore, due to the above-mentioned elusive character of these lizards, information about their general ecology and biology in most of their representatives remains unknown or poorly understood.

Morphologically, the genus can be subdivided into two main groups, the *capensis* group, which only includes *I. capensis* and subspecies, and the *bivittata* group, which includes *I. bivittata, I. microlepidota,* and *I. tanganicana* (Boulenger 1921; Marx 1956; van den Berg 2017). *Ichnotropis chapini* is believed to be part of the *capensis* group (Schmidt 1919). The *capensis* group is characterized by having a more elongated and sharper snout than the species in the *bivittata* group (i.e., *I. bivittata, I. microlepidota,* and *I. tanganicana*), prefrontal scales usually not in contact with anterior supraocular scales, and well-defined head striations (Boulenger 1921; Marx 1956). On the other hand, the *bivittata* group normally has prefrontal scales in contact with the anterior supraocular, weakly defined head striations, and a much shorter and rounded snout (Boulenger 1921; Marx 1956). It is unclear to which of these groups *I. grandiceps* belongs, but it is considered closely related to *I. capensis* (Broadley 1967). Of all six recognized species, the taxonomic placement and validity

of *I. microlepidota* has been the most controversial and discussed in recent years (Mayer 2013; Edwards et al. 2013; van den Berg 2017).

Ichnotropis microlepidota was described in 1956, when five specimens (FMNH 74283–74287) were removed from the crop of a Dark Chanting Goshawk (*Melierax metabates*) that was collected from the base of Mount Moco, Huambo Province, during a bird survey (Marx 1956). However, some authors have questioned the validity of this species and its distribution, suggesting that these specimens may have been transported by the goshawk from another locality (van den Berg 2017). Nevertheless, a series of apomorphic characters in *I. microlepidota*, which support its taxonomic recognition, including prefrontals in contact with anterior supraoculars, a row of smaller scales separating the supraciliaries from the supraoculars, and a more rounded snout, has motivated some authors to consider the species as related to the *bivitatta* group (Marx 1956; Edwards et al. 2013; van den Berg 2017). However, *I. microlepidota* differs from *I. bivitatta* by having smaller-sized dorsal scales, having more scales around midbody (43–50 vs. 32–39), and a lower number of subdigital lamellae under the fourth toe (16–17 vs. 19–21) (Marx 1956). It is noteworthy that prior to Marx's examination, Parker (1936) recorded a juvenile *Ichnotropis* from Mount Moco (1500–1900 m. a.s.l.), which he tentatively identified as *I. bivittata*, but noted some different characters (specifically, smaller scales and higher midbody scale rows [45–56]) that indicated it possibly being a distinct species from *I. bivittata*. Since then, no more individuals have been found. Therefore, the taxonomic status of *I. microlepidota* remains the subject of debate, as highlighted by Edwards et al. (2013), who suggested that resolution could only come through new material enabling a phylogenetic revision of this enigmatic genus.

The Central Highlands of Angola are represented by an archipelago of Afromontane forest pockets surrounded by montane grasslands with numerous peaks exceeding 2000 m. a.s.l. (Lobón-Rovira and Bauer 2021). Therefore, it is noteworthy to mention an *Ichnotropis* specimen photographed in Mount Namba that was documented in van den Berg (2020) as possibly being *I. microlepidota*. Although finally it could not be properly identified from the pictures, and the specimen was tentatively assigned to *I. bivittata*. This record should be taken into consideration due to Mount Namba having similar or identical habitat traits as Mount Moco and that they already share some endemic species (e.g., *Bitis heraldica* Boulenger, 1887 (Ceríaco et al. 2020c)).

With this work we aim to shed light on the taxonomic status of *I. microlepidota* and provide an updated phylogenetic hypothesis of this group in Angola. To achieve this goal, we implemented a robust phylogenetic analysis to revisit the taxonomic status of the different taxa recorded from Angola, based on the most complete molecular data, internal (3D osteological reconstruction of the skull), external morphological data, and distribution. This helped us to provide a phylogenetic placement of *I. microlepidota,* but also to corroborate if this species is part of the *bivittata* group as previously thought or, in contrast, if the species is more closely related to the *capensis* group.

Materials and methods

Sampling

Material of *Ichnotropis* spp. (specimens and tissue samples) has been collected across the Angolan territory between 2012 and 2021. Target sites included Mount Moco Special Reserve, Huambo Province, and Calandula (=Duque de Braganca), Malanje Province, for being the type localities of *I. microlepidota* and *I. bivittata*, respectively. In October 2020, an adult male, morphologically identified as *I. microlepidota*, was collected at Mount Moco (-12.4554, 15.1632). Nevertheless, despite the fact that we failed to collect fresh topotypic material of *I. bivittata*, additional material of *I. bivittata, I. capensis,* and *I.* cf. *grandiceps* was collected across the territory (Table 1) (Baptista et al. 2019; Conradie et al. 2023). The final dataset included 38 newly collected specimens of four Angolan *Ichnotropis* spp. (Table 1). Tissue samples and/or vouchers were collected. Vouchers were euthanized with an injection of tricaine methanesulphonate (MS222) (Conroy et al. 2009). After euthanasia, liver or muscle samples were collected for the phylogenetic analyses and stored in 95–99% ethanol. The individuals were fixed in 10% formalin, after which they were transferred to 70% ethanol for long-term storage in the Museu de História Natural e da Ciência—Universidade do Porto (MHNC-UP), Porth Elizabeth Museum (PEM), and Fundação Kissama Collection (FKH) herpetological collections. For each sample collected, the locality was recorded using the WGS84 coordinate datum.

Phylogenetic data

We extracted DNA from newly collected material using the EasySpin Genomic DNA Tissue Kit (Citomed, Portugal), following the manufacturer´s protocols. Concentrations were 5 µl PCR Master Mix, 0.4 µl of each primer, 3.2 µl H2O, and 1–3 µl DNA (DNA elution was adjusted to extraction results). Two mitochondrial genes, a partial mitochondrial ribosomal gene (*16S* rRNA; 511 bp) and a mitochondrial encoded gene *ND4* (802 bp), and two partial fragments of a nuclear gene (*RAG-1* ~985 bp and *c-mos* ~337 bp) were generated for most of the tissue samples detailed in Table 1. Primer and PCR reaction details are summarized in Table 2. The prepared PCR products were purified and sequenced at the Centre for Molecular Analysis (CTM-CIBIO, Porto, Portugal) and Macrogen Corp. (Amsterdam, Netherlands). Sequences were checked and edited using Geneious Prime v.2024.0.5 (http://www.geneious.com/) and aligned using the MUSCLE plugin for Geneious. All sequences have been deposited in GenBank (Table 1).

Table 1. List of material used for the phylogenetic analyses, including information on their catalog number, field number, country, localities, decimal geographic coordinates, and GenBank ascension numbers. Abbreviations: Aaron M. Bauer field numbers (AMB), California Academy of Sciences (CAS), Krystal Tolley field numbers (KTH, RSP, WP), Museu de História Natural e da Ciência - Universidade do Porto (MHNCUP), Ninda Baptista field numbers (NB), Pedro Vaz Pinto field numbers (P, L series), Port Elizabeth Museum (PEM), Stuart V. Nielsen field numbers (SVN), Thomas Branch field numbers (TB), Werner Conradie field numbers (WC, ANG). Missing data or unavailable information is indicated as Missing Data (–).

Species	Catalog No.	Field Number	Country	Locality	Latitude, Longitude	*16S*	*ND4*	*RAG1*	*C-mos*	Source
I. aff. grandiceps	PEM R23306	WC-3969	Angola	4 km upstream from Cuanavale River source	-13.5080, 18.8973	PV357715	PV412835	PV412862	PV390640	This work
I. aff. grandiceps	PEM R23420	WC-4816	Angola	Cuando River source	-13.0035, 19.1275	PV357716	PV412836	–	–	This work
I. aff. grandiceps	PEM R23362	WC-4056	Angola	drive to Cuanavale camp from Samanunga village	-13.0380, 18.8298	PV357717	PV412837	PV412863	–	This work
I. aff. grandiceps	PEM R23279	WC-3994	Angola	Cuanavale River source	-13.0903, 18.8940	PV357718	PV412838	PV412864	–	This work
I. b. bivittata	–	NB0675	Angola	Luando Integral Nature Reserve	-10.2772, 16.9533	PV357719	PV412839	PV412865	PV390641	This work
I. b. bivittata	–	P1-318	Angola	Cambau	-9.9633, 15.1706	PV357720	PV412840	PV412866	PV390642	This work
I. b. bivittata	PEM R23525	WC-4515	Angola	west of Cuito town on Aludungo rd.	-12.3278, 16.9067	PV357721	–	PV412867	–	This work
I. b. pallida	PEM R17934	KTH09-075	Angola	7 km East of Humpata	-14.9820, 13.4352	HF547775	HF547731	HF547694	–	Edwards et al. 2012
I. capensis	PEM R23530	WC-4585	Angola	Kembo River source	-13.1095, 19.0061	PV357722	PV412841	PV412868	PV390643	This work
I. capensis	PEM R23500	WC-4618	Angola	Kembo River source lake	-13.1360, 19.0453	PV357723	PV412842	PV412869	–	This work
I. capensis	PEM R20009	WC12-A191	Angola	HALO Cuito Cuanavale office	-15.1392, 19.1436	PV357724	PV412843	–	–	This work
I. capensis	PEM R20495	ANG-311	Angola	8.5 km north of Rito	-16.6232, 19.0535	PV357725	PV412844	–	–	This work
I. capensis	PEM R22069	L18	Angola	Gambos, Foster's farm	-15.8500, 14.6833	PV357726	PV412845	–	–	This work
I. capensis	–	NB0771	Angola	Bicuar National Park	-15.2435, 14.8915	PV357727	PV412846	PV412870	PV390644	This work
I. capensis	–	NB0772	Angola	Bicuar National Park	-15.2435, 14.8915	PV357728	PV412847	PV412871	PV390644	This work
I. capensis	–	NB0779	Angola	Bicuar National Park	-15.1048, 14.8403	PV357729	PV412848	PV412872	PV390644	This work
I. capensis	–	NB1116	Angola	Cusseque	-13.6851, 17.0795	PV357730	PV412849	–	PV390647	This work
I. capensis	PEM R27394	WC-6797	Angola	Quembo River bridge camp	-13.5275, 19.2806	PV357731	PV412850	PV412873	PV390648	This work
I. capensis	–	NB1123	Angola	Cusseque	-13.6782, 17.0832	PV357732	PV412851	–	PV390649	This work
I. capensis	–	NB1124	Angola	Cusseque	-13.6776, 17.0836	PV357733	PV412852	–	–	This work
I. capensis	–	NB1138	Angola	Cusseque	-13.6858, 17.0796	PV357734	–	–	–	This work
I. capensis	–	ABC2	Namibia	Katima Mulilo	-17.7000, 24.0000	JX962898	–	JX963023	JX962916	Engleder et al. 2013
I. capensis	CAS 209602	AMB 6007	South Africa	KwaZulu-Natal, Kosi Bay	-26.9400, 32.8200	DQ871149	–	DQ871207	–	Makokha et al. 2007
I. capensis	–	AMB 6001	Namibia	Road to Tsumkwe	-19.4600, 19.7200	DQ871148	–	DQ871206	–	Makokha et al. 2007
I. aff. capensis	PEM R19903	TB44	Angola	Camp Chiri, Miombo forest/camp	-9.3969, 20.4319	PV357735	PV412853	PV412874	–	This work
I. aff. capensis	PEM R23531	WC-4560	Angola	Sombanana village river	-12.3071, 18.6235	PV357736	PV412854	PV412875	–	This work
I. aff. capensis	MHNCUP-REP0984	P9-035	Angola	Mona Quimbundo – Tahal	-10.0583, 19.8056	PV357737	PV412855	–	–	This work
I. aff. capensis	PEM R19905	TB46	Angola	Camp Chiri, Miombo forest/camp	-9.3969, 20.4319	PV357738	PV412856	PV412876	–	This work
I. aff. capensis	–	P3-059	Angola	Cuemba	-12.1707, 18.2257	PV357739	PV412857	–	PV390650	This work
I. aff. capensis	PEM R23996	WC-6291	Angola	Lake Tchanssengwe	-12.4140, 18.6442	PV357740	PV412858	–	–	This work
I. aff. capensis	PEM R23409	WC-4557	Angola	Lungue Bungue River camp bridge crossing	-12.5835, 18.6660	PV357741	PV412859	PV412877	–	This work
I. microlepidota	MHNCUP-REP 0983	P0-044	Angola	Moco – Canjonde	-12.4554, 15.1632	PV357742	PV412860	PV412878	PV390651	This work

Species	Catalog No.	Field Number	Country	Locality	Latitude, Longitude	*16S*	*ND4*	*RAG1*	*C-mos*	Source
M. squamulosus	–	WP125	South Africa	Rooipoort Nature Reserve	-28.5937, 24.2100	HF547778	HF547738	HF547701	–	Edwards et al. 2012
M. squamulosus	–	RSP373	South Africa	Venetia Limpopo Reserve	-22.2661, 29.3329	HF547777	HF547737	HF547699	–	Edwards et al. 2012
M. squamulosus	PEM R19626	SVN362	South Africa	Lapalala Game Reserve, Landmanslust	-23.8759, 28.3061	HF547776	HF547736	HF547697	–	Edwards et al. 2012
M. squamulosus	–	ABH9	Tanzania	Laela	-8.7500, 32.1833	JX962897	–	EF632221	EF632266	Engleder et al. 2013
M. squamulosus	–	ABH3	Mozambique	unknown	–	JX962896	–	JX963022	JX962915	Engleder et al. 2013

Table 2. Primer details and PCR protocols used to generate sequences for this study. The PCR column denotes the number of repeated cycles/annealing temp (°C) used in the PCR.

Gene	Primer	Length (bp)	Reference	Sequence	PCR
16S	16S-L	511	Palumbi 1996	5'-CGCCTGTTTATCAAAAACAT-3'	40 / 54
	16S-H			5'-TGACTGCAGAGGGTGACGGGCGGTGTGT-3'	
c-mos	G73_69	337	Whiting et al. 2003	5'-GCGGTAAAGCAGGTGAAGAAA-3'	40 / 54
	G74_70			5'-TGAGCATCCAAAGTCTCCAATC-3'	
ND4	ND4 (ND4F)	802	Arévalo et al. 1994	5'-CACCTATGACTACCAAAAGCTCATGTAGAAGC-3'	40 / 58
	Leu (ND4R)			5'-CATTACTTTTACTTGGATTTGCACCA-3'	
RAG-1	f1aFw	985	Wiens et al. 2010	5'-CAGCTGYAGCCARTACCATAAAAT-3'	40 / 50–54
	r2Rv			5'-CTTTCTAGCAAAATTTCCATTCAT-3'	

Phylogenetic analyses

We used phylogenetic reconstructions to place *I. microlepidota* in an evolutionary context and to provide an updated phylogenetic hypothesis of the group for Angola. For these analyses, we combined the newly generated sequences and supplemented them with previously published sequence data of *Ichnotropis* spp. (i.e., Edwards et al. 2013; Engleder et al. 2013) downloaded from GenBank, using *Meroles squamulosus* as an outgroup (Table 1) for being a close-related member of the sister genus *Meroles* (Engleder et al. 2013). Phylogenetic analyses were run using Bayesian inference (BI) and maximum likelihood (ML) approaches using a concatenated dataset of the four genes. The partitioning schemes were assessed using PartitionFinder2 (Lanfear et al. 2017), and the best substitution model of sequence evolution was selected using ModelFinder in IQ-Tree v2.3.4 (Minh et al. 2021) with the Bayesian information criterion (BIC). We partitioned the combined dataset by gene, as suggested in PartitionFinder2. The best substitution models were TIM2+F+G4 (*16S*), TPM2u+F+I+G4 (*ND4*), K2P (*c-mos*), and K2P+G4 (*RAG-1*). Maximum likelihood (ML) analysis was performed in IQ-Tree v2.3.4 (Trifinopoulos et al. 2016) with four partitions of the concatenated dataset and 1000 bootstrap replicates following the ultrafast bootstrap approximation method (UFBoot) (Hoang et al. 2018). Bootstrap values of 95% or higher for the ML analysis were considered as strongly supported (Huelsenbeck and Hillis 1993). The Bayesian inference analysis was conducted with MrBayes v3.2.7 (Ronquist et al. 2012) on CIPRES (Miller et al. 2010) with four partitions of the concatenated dataset. The final BI analysis was run for 10×10^6 generations of the Metropolis coupled Markov chain Monte Carlo [(MC)3], sampled every 1000 generations. Convergence was assessed by examining the effective sample size (ESS) values using Tracer 1.7 (Rambaut et al. 2014), where all parameter values had ESS values > 200, and 25% of the trees generated were discarded as burn-in to generate a 50% majority rule consensus tree in MrBayes. We set the substitution model space with the option lset nst=mixed rates=invgamma. Bootstrap analyses (BS) with 1000 pseudoreplicates were used to evaluate relative branch support. Posterior probabilities (PP) were used to assess nodal support, and PP ≥ 0.95 was considered strongly supported. Finally, we used *16S* uncorrected pairwise sequence divergences (p-distance) to inspect intra- and interspecific variation, calculated in MEGA v.10.1.7 (Kumar et al. 2018).

External morphological data

For the external morphological analyses, we examined a total of 135 specimens of *Ichnotropis* from Angola, the Democratic Republic of the Congo (DRC), Namibia, and South Africa (Suppl. material 1: table S1). This material included 25 newly collected materials from Angola and 110 historical materials from across Africa deposited in the British Museum of Natural History, UK (BMNH), Field Museum of Natural History, USA (FMNH), the Royal Belgian Institute of Natural Sciences, Belgium (RBINS), the Royal Museum of Central Africa, Belgium (RMCA), and the Porth Elizabeth Museum, South Africa (PEM). Historical material from RBINS and RMCA, including the types of *I. c. overlaeti* and *I. c. nigrescens*, was included. We also included the type series of *I. microlepidota*, which is deposited in the Field Museum of Natural History (FMNH). In addition, we compared high-resolution images of the types.

We recorded morphometric measurements as follows: snout-vent length (SVL, from tip of snout to anterior cloaca opening), tail length (TL, from tip of tail to posterior cloaca opening), occipital-snout length (HL, from posterior end of occipital to tip of snout), head width (HW, at widest point), head height (HH, at highest point), snout to front of arm (S-FL, from tip of snout to anterior insertion of forelimb), snout to eye distance (SE, from tip of snout to anterior corner of eye), eye diameter (ED), eye to eye distance (EE, from anterior corner of eye to anterior corner of eye), tympanum width (Tymp-L, at its widest), fore limb length (FLL, from elbow to wrist), hind limb length (HLL, from knee to heel), inner limb length (IL, distance between inguinal and axillary regions), hind foot length (HFL, from ankle to tip of fourth toe excluding claw), lower jaw length (LJL, anterior edge of jaw bone to tip of lower jaw), fourth finger length (FFL, excluding claw), fourth toe length (FTL, excluding claw), anterior SO (length of anterior supraorbital scale), distance between anterior supraocular to second loreal (SO-L, measurement between the closest point of the anterior supraocular to the posterior edge of the second loreal), frontal scale width (FNW, at its widest point), frontal scale length (FNL). The meristic data collected was: number of upper labials (UL) for which we counted scales in anteriorly and posteriorly of the subocular, number of lower labials (LL), number of chin shields (including the number in direct contact), number of supraciliaries, longitudinal rows of ventral scales at midbody; transverse number of ventral scales (from line between posterior side of fore limbs to groin), scales around midbody (including ventral scales), number of granular scales separating supraorbital from the supraciliaries, rows of scales between anterior supraocular and second supraciliaries, number of scales separating anterior supraocular from posteriorly loreal, number of rows of scales between upper labials and temporal shield, number of subdigital lamellae from the base of the digit to tip of toe before the claw starts on the fourth toe and the number of femoral pores on the left and right side. We also examined if the occipital scale extended past the parietal scales, if there was contact between prefrontal scales and anterior supraocular, contact between supraoculars and supraciliaries, contact between frontonasal and supraciliaries, and if the anterior loreal scale was divided or not. All data was collected using a Leica LD2500 or Nikon SMZ1270 dissecting microscope, and measurements were taken in millimeters (mm) with a digital caliper (accuracy of 0.01 mm).

Morphological analyses

We used different datasets for the different analyses, defined as follows: Dataset 1, which included all specimens on which most morphological traits have been recorded (48 specimens), and Dataset 2, which included all the specimens (135 specimens; Suppl. material 1: table S1). First, to explore the main morphological differences among Angolan *Ichnotropis* species, we conducted two Principal Component Analyses (PCAs). The first analysis was performed using Dataset 1, while the second excluded the effect of head shape differences by removing head-related variables (HL, HW, and HH) from Dataset 1. These variables were size-corrected using SVL as a covariate, and the residuals were subsequently used in the PCAs. Following Branch et al. (2014), variables with communalities > 0.5 were retained in the PCA. A varimax rotation was applied, and principal components (PCs) with eigenvalues > 1.0 were extracted. The resulting PC scores were saved and used as input variables for a multivariate analysis of variance (MANOVA), with species as the fixed factor. Post-hoc pairwise comparisons were conducted using Tukey's HSD test to identify which variables explained the main morphological differences in the first two PCAs (Branch et al. 2014). Secondly, to explore other potential diagnostic characters between species, we tested the morphological variation in Dataset 2 across different taxa using permutational ANOVAs (PERMANOVAs) with the package RRPP (Collyer and Adams 2018) implemented in RStudio v.2023.09.1+494 (RStudio Team, 2022). Variables were size-corrected (SVL) and log-transformed prior to the analyses to mitigate the effects of size and multicollinearity. Finally, we used standard boxplots to visually represent those variables that showed significant differences between *I. microlepidota* and any other species.

Osteological data and comparisons

To identify potential diagnostic characters on the cranial elements of *Ichnotropis microlepidota*, we visually compare the high-resolution X-ray computed tomography (HRCT) scan of *I. microlepidota* (MHNCUP-REP0983) with material of *I. bivittata* (RCMA 14641, formerly the holotype of *I. c. nigrescens fide* Conradie et al. in prep.; and MCZ-R39726) (Suppl. material 1: table S2). HRCT was performed at the Royal Museum of Central Africa (RMCA) CT facilities and at Centro de Instrumentación Científica of Granada (CIC). The cranium of *Ichnotropis bivittata* (MCZ-R39726) was downloaded from the Morphosource platform (https://www.morphosource.org). Detailed parameters for each CT scan are defined in Suppl. material 1: table S2. All specimens were regarded as adults to avoid potential ontogeny variation of the skull elements. To guarantee we used adult specimens for the cranial comparisons, we checked the femoral pore development, as they are feebly visible or not completely developed in juveniles and subadults. The 3D segmentation models for the skulls were generated for articulated skulls using Avizo Lite 2019.1 (Thermo Fisher Scientific). To facilitate visualization, individual bone units of the cranium and jaws were colored following the same color palette as Lobón-Rovira and Bauer (2021). Bones not included

in Lobón-Rovira and Bauer (2021) were included in the pallet and are defined in Suppl. material 1: table S3. Annotations were made manually in Adobe Photoshop v.25.7.0 (Adobe Systems Incorporated 2019). CT scan raw data (.tiff files) have been deposited in MorphoSource (www.morphosource.org; Suppl. material 1: table S2).

Results

Phylogenetic analyses

Both phylogenetic analyses (ML and BI) retrieved the same topology, although with different support strengths for some nodes. The phylogenetic analyses recovered five well-supported operational taxonomic units (OTUs) (Fig. 1) that are consistent with the pairwise comparisons of the *16S* uncorrected p-distances (4.57%–17.80%, Table 3).

The different phylogenetic reconstructions recovered a well-supported monophyletic group that includes individuals morphologically identified as *Ichnotropis* aff. *grandiceps.* This group clusters with a larger group (PP: 0.99, BS: 89%) that includes all the other members of the *Ichnotropis* genus (Fig. 1). The large clade includes two well-differentiated subclades, here identified as the *capensis* and *bivittata* groups (PP: 0.99, BS: 97%). The *capensis* group includes two well-supported subclades (PP: 1.00, BS: 100%) that differ genetically from each other by > 4.5% (*16S* uncorrected p-distance). The two main subclades recovered here in the *capensis* group represented a well-defined geographic distribution with one subclade (namely *I. capensis*) from central to the southern half of the Angolan territory, northeastern Namibia, and eastward to coastal South Africa, and a second subclade (namely *I.* aff. *capensis*) distributed in the northeastern half of the Angolan territory (Fig. 8). Within the *bivittata* group, the phylogenetic analyses retrieved two subclades that differ by a minimum of 14.83% (*16S* uncorrected p-distance, Table 3), including both subspecies of *I. bivittata* (namely, *I. b. bivittata* and *I. b. pallida*) and *I. microlepidota*, that were recovered as sister taxa (PP: 0.99, BS: 97%, Fig. 1). The two subspecies of *I. bivittata* differ by 4.03% (*16S* uncorrected p-distance, Table 3).

Morphological analyses

The results of the two PCAs explained a considerable portion of the variation in the three principal components in both analyses (69.5% and 68.65%, respectively). On the first PCA, the highest proportion of the variation in the PC1 is explained by the HL and S-FL, and in the PC2 by the HW and the Tymp_L (Suppl. material 1: table S4).

When we remove the HL, HW, and HH from the PCA analysis (PCA2; Suppl. material 1: table S4), the PC1 is explained by the S-FL and the HLL, and in the PC2 by the ED and the Tymp_L.

Nevertheless, in both analyses, the multivariate means on PC1 show no differences between the species (MANOVA PCA1 p value = 0.639; MANOVA PCA2 p value = 0.297) as shown in Fig. 2. The PC2 shows two main groupings exploring differently the morphospace (MANOVAs p value = 0.000). These results are supported by the *post hoc* pairwise comparison (Tukey's HSD) that does not show a significative difference in the PC1 (HL and S-FL) between species, but it does in several species pairs in the PC2 (e.g., HW and Tymp_L in *I. microlepidota–I.* aff. *capensis* $p < 0.05$) (Suppl. material 1: table S5).

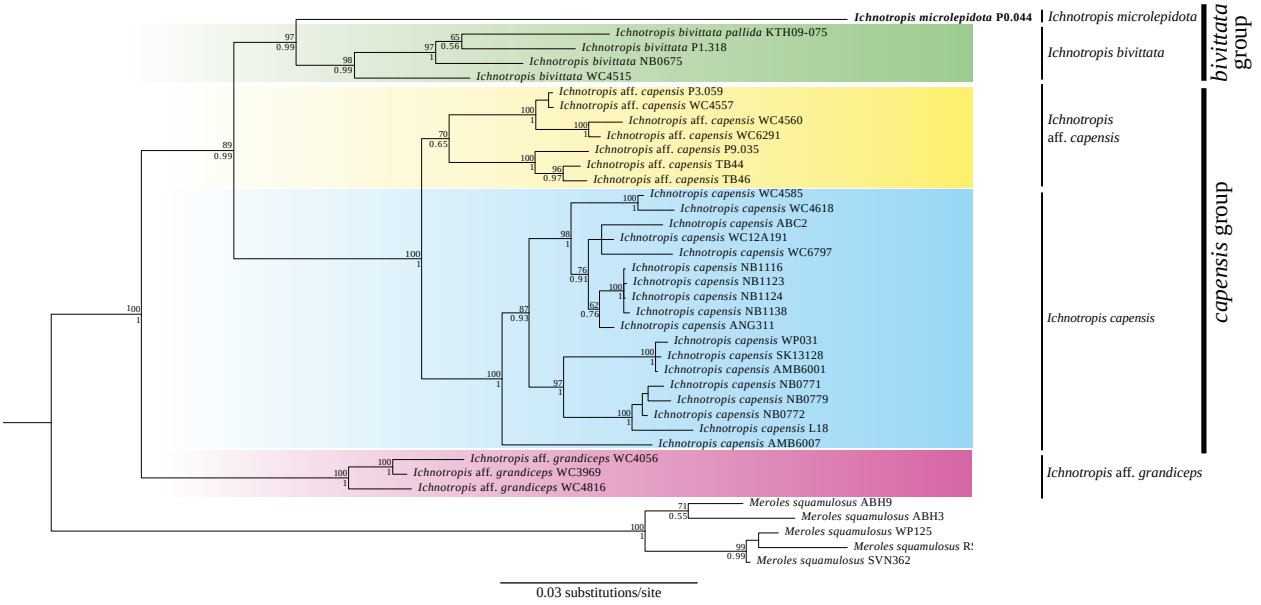

Figure 1. Bayesian inference tree based on concatenated dataset including 2635 bp of two mitochondrial (*16S, ND4*) and two nuclear-encoded (*C-mos, RAG1*) markers. Nodes are labeled with ML bootstrap values (BS) above and BI posterior probability (PP) below.

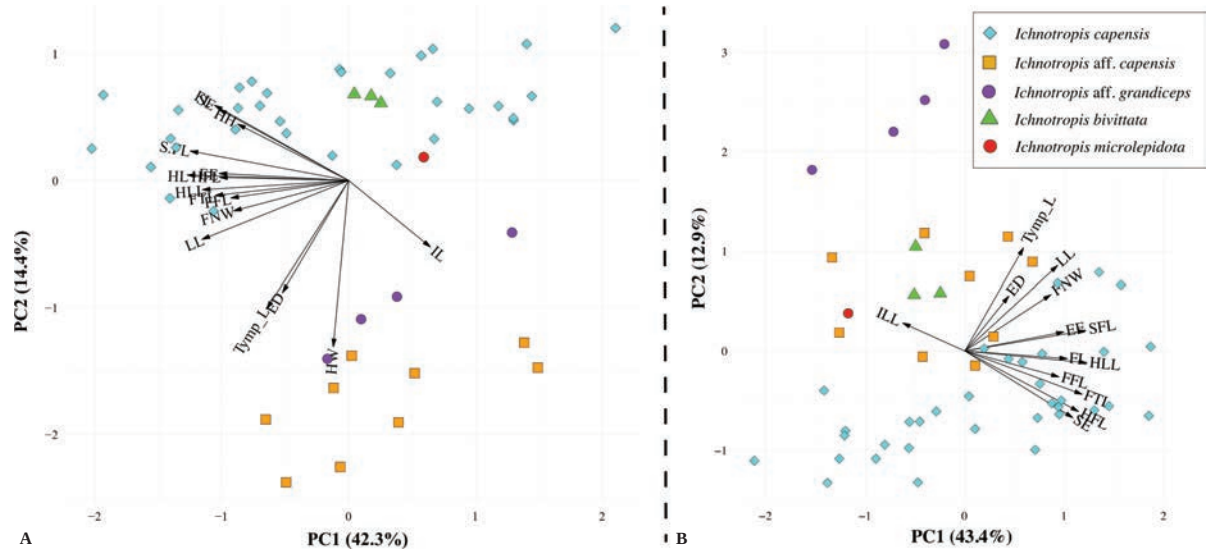

Figure 2. A. PCA plot of the first principal component (PC1) versus the second principal component (PC2) on Dataset 1 including all the morphological variables; **B.** PCA plot of the first principal component (PC1) versus the second principal component (PC2) of Dataset 1, excluding the three main morphological variables of the head (i.e., HL, HW, HH). Species are represented by different color and symbol included in the legend. For abbreviations see the Materials and Methods section. For loadings of all axes and explained variance, see Suppl. material 1: tables S4, S5.

Table 3. Percent sequence divergence for *16S* (uncorrected pairwise distances) between and within *Ichnotropis* species included on the phylogenetic analyses and *Meroles squamulosus*. Bold values on the diagonal depict mitochondrial divergence within species.

ID	1	2	3	4	5	6	7
1. *Ichnotropis microlepidota*	**n/c**						
2. *Ichnotropis bivittata bivittata*	14.83	**3.37**					
3. *Ichnotropis bivittata pallida*	15.50	4.03	**n/c**				
4. *Ichnotropis capensis*	16.23	8.50	9.13	**3.64**			
5. *Ichnotropis* aff. *grandiceps*	17.80	6.70	7.85	9.26	**1.30**		
6. *Ichnotropis* aff. *capensis*	15.88	6.76	7.68	4.57	8.72	**1.95**	
7. *Meroles squamulosus*	24.69	14.29	14.74	19.00	14.74	17.69	**3.25**

Despite the fact that the PERMANOVAs did not retrieve many additional significant results for the continuous measurements (Suppl. material 1: table S6), it recovers some additional significative differences not highlighted by the PCA analyses (Suppl. material 1: table S6). Thus, the main morphological differences between *I. microlepidota* and other *Ichnotropis* members are the SVL, three main head measurements (i.e., HL, HW, and HH), the S-FL, and the Tymp_L (Fig. 3, Suppl. material 1: table S6). For example, significant differences in head length (HL) have been found when compared to *I. capensis* (ANOVA: $F_{1,27}$ = 14.630; *p*-value = 0.001), *I.* aff. *grandiceps* (ANOVA: $F_{1,14}$ = 11.478; p-value = 0.008), and *I. bivittata* (ANOVA: $F_{1,21}$ = 10.335; *p*-value = 0.013), in the head width (HW) with *I.* aff. *grandiceps* (ANOVA: $F_{1,14}$ = 19.166; *p*-value = 0.000) and *I. capensis* (ANOVA: $F_{1,27}$ = 8.271; *p*-value = 0.037) and in the head height (HH) with *I.* aff. *grandiceps* (ANOVA: $F_{1,14}$ = 10.201; *p*-value = 0.015) (Fig. 3, Suppl. material 1: table S6). In addition, the results on the comparison of the meristic data show a marginal difference between *I. microlepidota* and the other members of the group (like midbody scales or lamellae under the fourth toe; Fig. 3), being exceptionally divergent when compared to *I.* aff. *grandiceps* in most of the meristic measurements (Fig. 3). Meristic comparison showed main differences in the midbody scale count, which is higher in *I. microlepidota* than in the other *Ichnotropis* species (43–50 vs. 32–39 in *I. bivittata*, 30–41 in *I. capensis*, 34–41 in *I.* aff. *Capensis*, and 43–48 in *I.* aff. *grandiceps*) and in the number of lamellae under the fourth toe, which conversely seems lower in *I. microlepidota* (16–19 vs. 18–20 in *I. bivittata*, 18–26 in *I. capensis*, 19–24 in *I.* aff. *capensis*, and 19–24 in *I.* aff. *grandiceps*) (Fig. 3). It is worth noticing that although not as high as in *I. microlepidota*, the number of scales around the midbody is also higher in *I.* aff. *grandiceps* than in the other species (excluding *I. microlepidota*).

The osteological comparison of the skulls of *I. microlepidota* and *I. bivittata* allows us to identify a few potential diagnostic characters between species. While the *I. microlepidota* cranium presents a more rounded shape in dorsolateral view, with a broader lateral profile and taller dorsoventral profile, the skull in both *I. bivittata* skulls presents a slenderer and more elongated overall shape (Fig. 4). In addition, the skull in *I. microlepidota* presents a shorter and more robust jugal bone than in the other two species, a broader and more longitudinally compressed

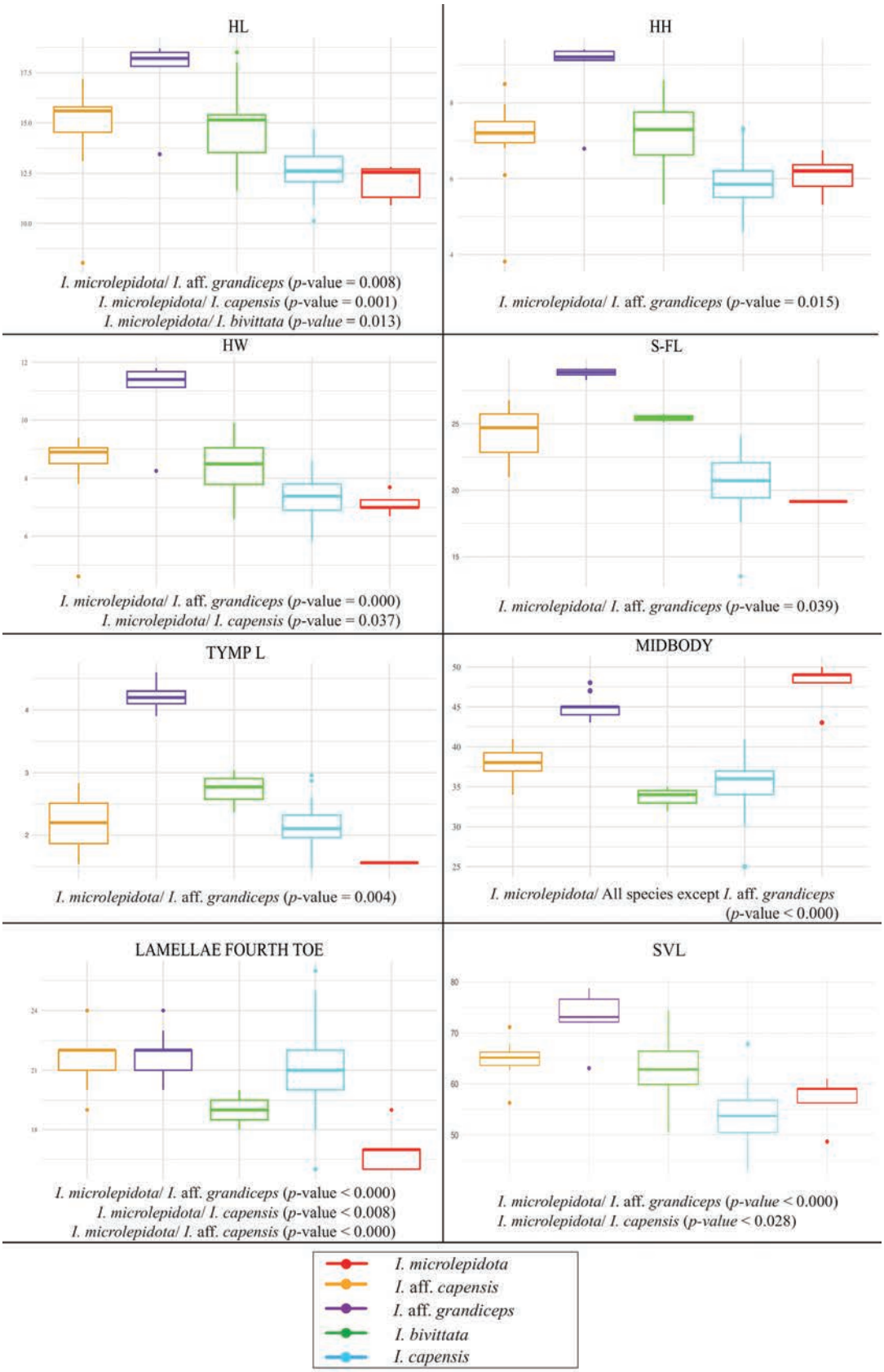

Figure 3. Boxplot (top whisker – maximum value; lower whisker – minimum value; bold horizontal line – median; box – 1st and 3rd quartile) displaying meristic measurements of *Ichnotropis* species. Different colors depict records of different species within *Ichnotropis*; see inset for color explanations. Significative values between *I. microlepidota* and other *Ichnotropis* species are highlighted under the graphics. For all ANOVA results see Suppl. material 1: table S6. For abbreviations see the Materials and Methods section.

maxilla and dentary bones in their lateral view, and a more downfacing and compressed premaxilla in its lateral view with a larger distance between the posterior ends of both pterygoid bones and jugals when compared to *I. bivittata*. Furthermore, the parietal bone is wider than longer in *I. microlepidota*, while in *I. bivittata*, the parietal presents a broader lateral profile. Finally, striation in the dorsal view of skulls seems to be more prominent in *I. microlepidota*, with a rougher-looking surface on almost all bones in the dorsal view of the skulls (Fig. 4).

Overall, due to the morphological and phylogenetic differences that support the taxonomic recognition of *I. microlepidota*, coupled with the lack of accurate morphological information about the species (e.g., coloration in life, osteology) and the taxonomic confusion around this taxon, we take the opportunity to provide an updated description (below) of *I. microlepidota*, aiming to provide an accurate description and comparison with other members of the group that could be useful for future taxonomic decisions on this group.

Ichnotropis microlepidota Marx, 1956

Figs 4–6, Table 4, Suppl. material 1: tables S1, S7

Holotype. FMNH 74285, adult male, collected at the foot of Mount Moco, Huambo Province, Angola, on 19 September 1954 by Gerd Heinrich.

Paratypes. FMNH 74283–84, adult females, with the same collecting information as the holotype; FMNH 74286–7, adult males, with the same collecting information as the holotype.

New additional material. MHNCUP-REP0983, adult male, collected at Mount Moco, Huambo Province, Angola (-12.4554, 15.1632), 2300 m a.s.l., on 18 October 2020 by Pedro Vaz Pinto.

Additional referred material. A juvenile specimen collected at Mount Moco, Huambo Province, Angola, 1500–1900 m a.s.l., in March 1934 by Karl Jordan (Parker 1936).

Updated description. Measurements and meristic data are summarized in Suppl. material 1: table S1. *Ichnotropis microlepidota* is a medium-sized lizard species (maximum SVL = 61.00 mm, mean 56.8 ± 4.8). 4 upper labials anteriorly to the subocular (mostly 2–3 posteriorly to the subocular), 7–8 (mostly 7) lower labials, and 5 pairs of chin shields, from which the first three pairs are in contact. Rostral with slight insertion between nasals. Single rhomboid frontonasal scale, slightly wider than longer. Undivided anterior loreal scale, which is smaller than the larger posterior loreal. Prefrontal scales longer than wider and in contact with supraoculars. Single row of scales between posterior loreal and anterior supraocular scales. Four supraciliaries on each side, which can be in contact or not with the anterior supraoculars. Three supraoculars, with the first (anterior one) being the largest,

Table 4. Summary of external morphological data of all species within the *Ichnotropis* genus. Measurements are shown in millimeters (mm) (average and standard deviations). Juveniles are excluded from these summary statistics. For individual measurements, see Suppl. material 1: table S8. Abbreviations are detailed in the Materials and Methods section. Missing data or unavailable information is indicated as not available (N/A).

Species	*I. bivittata*	*I. capensis*	*I. aff. capensis*	*I. aff. grandiceps*	*I. microlepidota*
N (males/females)	**(N = 10/6)**	**(N = 50/39)**	**(N = 9/3)**	**(N = 3/2)**	**(N = 3/2)**
SVL	62.4 ± 6.9	53.5 ± 4.9	65.3 ± 2.4	74.9 ± 3.1	56.8 ± 4.8
HL	14.9 ± 1.8	12.7 ± 0.9	15.2 ± 1.2	18.3 ± 0.4	11.8 ± 0.8
HW	8.4 ± 1	7.3 ± 0.6	8.8 ± 0.5	11.5 ± 0.3	7 ± 0.2
HH	7.2 ± 0.9	5.9 ± 0.6	7.2 ± 0.6	9.3 ± 0.1	5.9 ± 0.6
S-FL	25.4 ± 0.3	20.9 ± 1.7	24.4 ± 1.8	28.8 ± 0.4	19.14
SE	6.4 ± 0.1	6 ± 0.4	5.4 ± 0.9	6.4 ± 0.4	4.85
ED	2.9 ± 0.1	2.2 ± 0.4	3.7 ± 1.0	3.2 ± 0.3	2.62
EE	4.6 ± 0.1	4.2 ± 0.4	4.4 ± 1.1	3.2 ± 0.3	3.62
Tymp-L	2.7 ± 0.3	2.2 ± 0.3	2.2 ± 0.6	4.2 ± 0.3	1.56
FLL	7 ± 1.2	6.2 ± 0.7	7.5 ± 0.5	8.3 ± 0.6	5.45
HL	10.1 ± 1.5	10.6 ± 1.1	12.6 ± 1	13.4 ± 0.4	7.43
ILL	26.2 ± 4	25.1 ± 3.4	29.8 ± 1.4	36.3 ± 2.4	22.53
HFL	14.8 ± 1	16 ± 1.8	18.4 ± 1.8	16.4 ± 1.9	12
LJL	16.4 ± 0.9	13.4 ± 1.4	16.5 ± 1.9	21.6 ± 1.5	13.32
FFL	4 ± 0.4	3.9 ± 0.5	3.9 ± 0.6	5 ± 0.5	3.56
FTL	7.4 ± 0.6	8.4 ± 0.9	8.8 ± 1.2	9.8 ± 0.7	6.28
FNW	2 ± 0.3	1.8 ± 0.2	2.2 ± 0.1	2.6 ± 0.2	1.54
FNL	4.3 ± 0.6	2.3 ± 1	2.7 ± 1.1	2.1 ± 0.2	3.29
UL	4 ± 0	4.1 ± 0.2	4.1 ± 0.2	4.6 ± 0.5	4 ± 0
LL	6.3 ± 0.6	6.6 ± 0.6	6.2 ± 0.4	6.2 ± 0.3	7.6 ± 0.5
Chin shields	5 ± 0	5.2 ± 0.5	5 ± 0	4.9 ± 0.2	5 ± 0
SC	3 ± 0	3.9 ± 0.9	4 ± 0	5.1 ± 0.2	4 ± 0
Ventral plates longitudinal	24.8 ± 3.6	25.3 ± 2.4	28.4 ± 1.6	27.8 ± 1.8	25.4 ± 1.5
Ventral plates transverse	8.8 ± 1.1	8.8 ± 0.9	9.2 ± 0.4	10 ± 0	8.8 ± 1.1
Midbody	34 ± 1.2	35.5 ± 2.7	38.2 ± 1.9	44.8 ± 1.9	47.8 ± 2.8
Lamellae fourth toe	19.3 ± 1.2	21.3 ± 1.9	21.8 ± 1	21 21.2 ± 1.3	17 ± 1.2
FP	8.8 ± 0.9	10.1 ± 1.1	10.9 ± 0.8	12 12.2 ± 0.8	1 1.3 ± 0.8

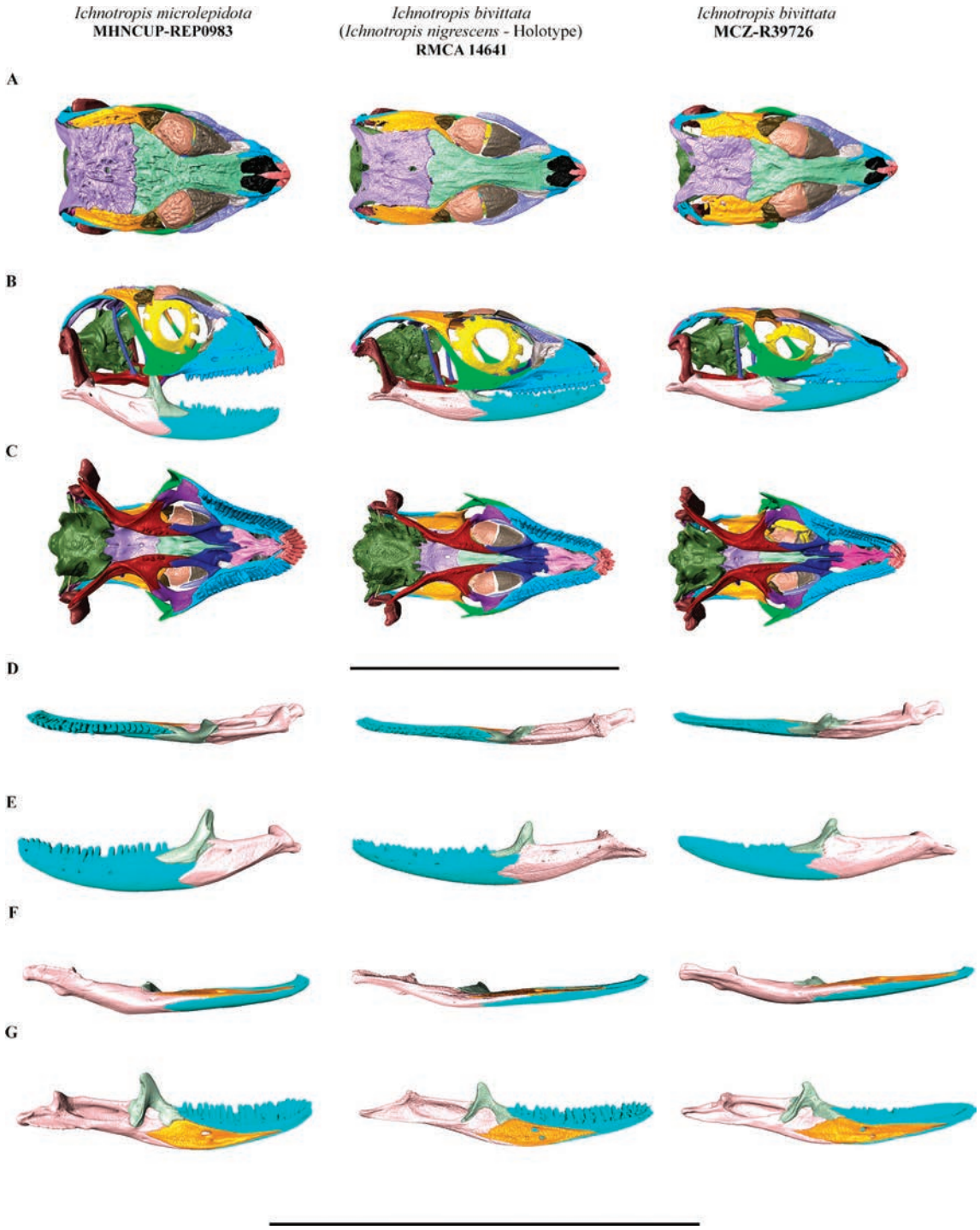

Figure 4. Comparative visualization of the skulls of *Ichnotropis microlepidota* (MHNCUP-REP0983) and *I. bivittata* (RMCA 14641; MCZ-R39726) (from left to right). Detail of the skull in **A.** Dorsal; **B.** Lateral, and **C.** Ventral views; and lower jaws in **D.** Dorsal; **E.** Lateral; **F.** Ventral, and **G.** Medial views. For the color palette, see Suppl. material 1: table S3. Scale bars: 10 mm.

followed by a slightly smaller second supraocular and a third one, which is the smallest. Eight rows of temporal scales between temporal shield and upper labials. Temporal shields half the length of parietals. Parietals twice as long than broad. Frontal scale 2–3 times longer than wide. Semicircular-shaped occipital scales slightly extending past the parietal scales. Head shields heavily striated. Dorsal scalation is composed of small, heavily keeled, rounded scales slightly elongated towards the back. High number of scales around the midbody (43–50, mean 47.8 ± 2.8). Middorsal scales slightly larger than dorsal scales and lack keeling towards the venter. Ventral pholidosis with large hexagonal scales that lack keeling. 23–27 ventral plates in the longitudinal section and between 8–10 in the transverse section. Tail scalation is formed by elongated and keeled scales pointing towards the tail tip and disposed in rings (Fig. 5). Subdigital lamellae 16–19. Femoral pores 9–12 per side.

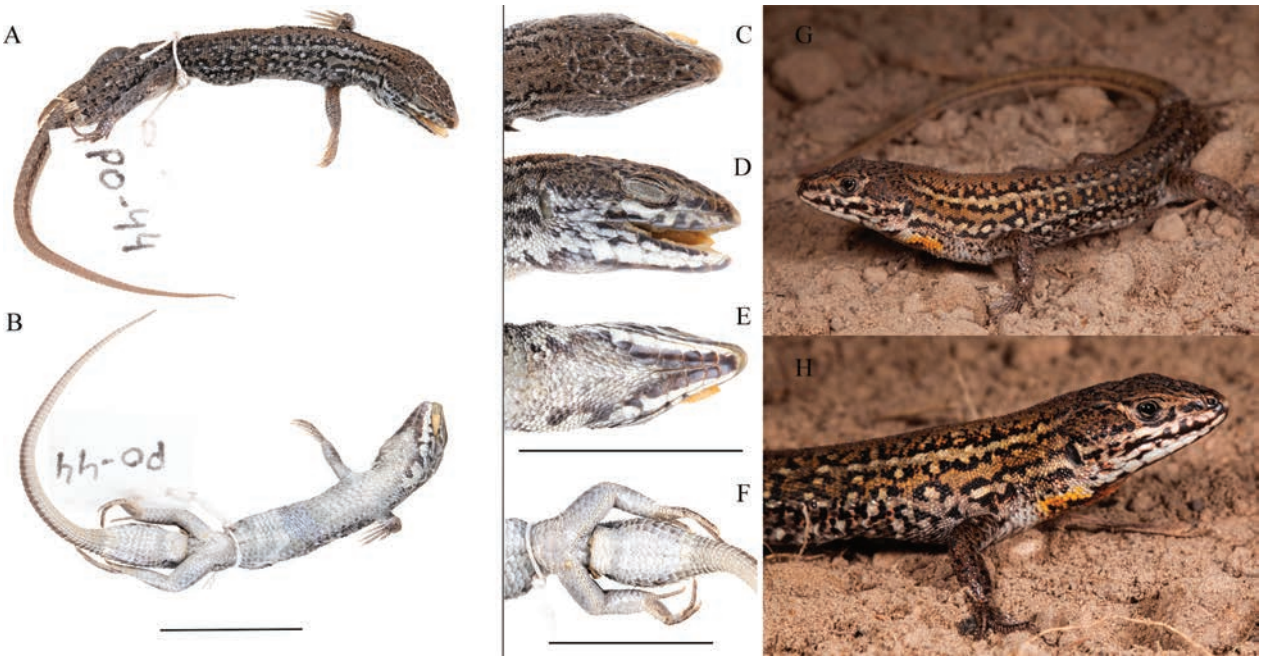

Figure 5. Specimen of *Ichnotropis microlepidota* (MHNCUP-REP0983) from Mount Moco, Huambo Province, Angola. (**A, B**) Dorsal and ventral view of the preserved specimen. Details of the head of the preserved specimen in (**C**) dorsal, (**D**) lateral, and (**E**) ventral view. (**F**) Detail of pelvic region and hind limbs. Scale bars represent 15 mm. In life pictures of the full body (**G**) and detail of the head (**H**). Photos by Max Benito and Pedro Vaz Pinto.

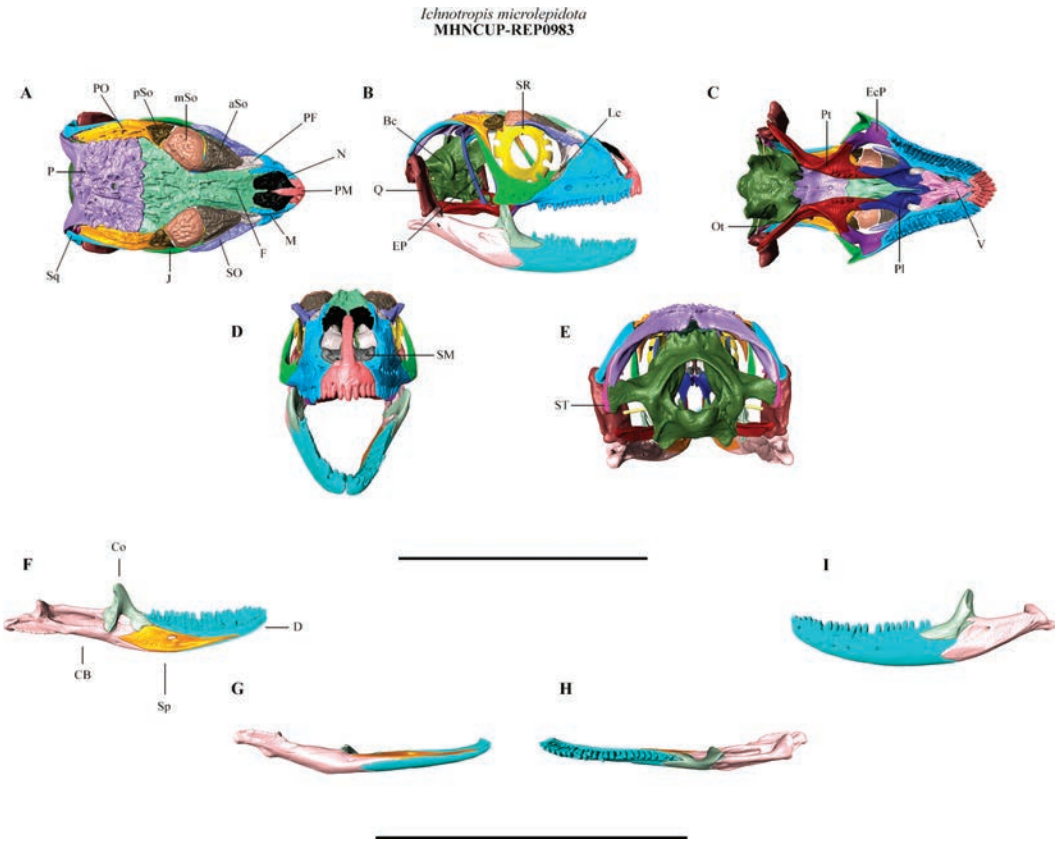

Figure 6. Detailed views in **A.** Dorsal; **B.** Lateral; **C.** Ventral; **D.** Frontal; **E.** Posterior of skull, and **F.** Medial; **G.** Ventral; **H.** Dorsal; **I.** Lateral view of the right jaw of *Ichnotropis microlepidota* (MHNCUP-REP0983). Abbreviations: aSo, anterior supraocular; Bc, braincase; Co, coronoid; CB, compound bone; D, dentary; EcP, ectopterygoid; EP, epipterygoid; F, frontal; J, jugal; Lc, lacrimal; M, maxilla; mSo, middle supraocupar; N, nasal; Ot, otostape; P, parietal; PF, prefrontal; Pl, palatine; PM, premaxilla; PO, postorbital; pSo, posterior supraocular; Pt, pretygoid; Q, quadrate; SM, septomaxilla; SO, supraorbital; Sp, splenial; Sq, squamosal; SR, sclerotic ring; ST, supratemporal; V, vomer. Scale bars represent 10 mm.

The cranium presents on its overall a rounded shape on its lateral and dorsal view (Fig. 6A, B). Frontal and parietal bones fused and separated by the fronto-parietal suture (Fig. 6A). Both bones are heavily striated in their dorsal view. Pineal foramen present in the medial section of the parietal bone. Postorbital bones prominent, in tight contact with the postocular, frontal, parietal, and squamosal bones. Supratemporal bone present, located as a splinter of a bone between the squamosal and the posterolateral process of the parietal (Fig. 6E). Nasal bones paired (Fig. 6D). Lacrimal bone present and unfused with the maxilla (Fig. 6B). A large jugal bone present in contact with the lacrimal bone, ectopterygoid, and postorbital bone. Braincase elements fused. Otostapes unperforated. The sclerotic rings comprise 14 ossicles with similar shape and size. Vomer bones paired (Fig. 6C). A robust lower jaw with a high and prominent coronoid bone (Fig. 6F–I). Compound bone and surangular bones fused. Splenial bone large in contact with compound bone, coronoid, and dentary. Nine premaxillary tooth loci, 20 maxillary tooth loci, and 22–23 dentary tooth loci.

Comparative diagnosis. This species can be differentiated from *I. bivittata* by having higher number of scales around the midbody (43–50 vs. 32–39 in *I. bivittata*) and a lower number of subdigital lamellae under the fourth toe (16–19 vs. 18–20 in *I. bivittata*). Furthermore, *I. bivittata* presents narrowly yellow-spaced spots above the front limbs, while *I. microlepidota* lacks this dorsolateral spotting. Furthermore, *I. microlepidota* presents anterior suboculars, which can be in contact or not with the supraciliaries, while in *I. bivittata*, they are always separated. Moreover, it differs from the *capensis* group by having a more rounded and shorter snout, prefrontals in contact with the anterior supraoculars, a higher number of scales around the midbody (43–50 vs. 30–41 in *I. capensis* and 34–41 in *I.* aff. *capensis*), a lower number of subdigital lamellae under the fourth toe (16–19 vs. 18–26 in *I. capensis* and 19–24 in *I.* aff. *capensis*), and for lacking a lateral orange band in adult males, which is highly conspicuous in adult males from the *capensis* group. It also differs from *I.* aff. *grandiceps* in the number of lamellae under the fourth toe (16–19 vs. 19–24 in *I.* aff. *grandiceps*) and for the same orange band in adult males as in the *capensis* and *bivittata* groups. In addition, *I. microlepidota* can be differentiated from *I. bivittata* based on a few osteological characters as follows: broader cranium dorsoventrally, with a taller dorsoventral profile, a shorter and more robust jugal bone, a more downfacing and laterally compressed premaxilla, and longitudinally compressed maxilla and dentary bones in *I. microlepidota versus* a narrower and shorter cranial profile in I. *bivittata*. The skull of *I. bivittata* presents an overall rounded shape in its lateral and dorsal view. Parietal and frontal bones separated by the fronto-parietal suture, and both with low striation in their dorsal view. The pineal foramen situated in the medial to anterior section of the parietal. Elongated jugal bones in their lateral view, in contact with lacrimal bone, ectopterygoid, and the postorbital bone. Otostapes unperforated. The sclerotic rings comprise 14 ossicles with similar shape and size. Nasal and vomer bones paired. An elongated lower jaw formed by coronoid, dentary, splenial, and fused compound bones, all of them in contact. Nine premaxillary tooth loci, 20 maxillary tooth loci, and 23 dentary tooth loci. (Fig. 4).

Coloration in life (Fig. 5G–H). The dorsal pattern consists of a light brown dorsal band that reaches from behind the head to the posterior limbs, surrounded by two discontinuous bands consisting of black blotches. The pattern on the lateral side of the body consists of two light cream to yellow bands from ear opening height extending towards the back. Between them, a row of consecutive pairs of white ocelli surrounded by external black sections. Under the lower lateral band, another row of continuous single ocelli. The head is brown on top, sprinkled with black markings on most of the scales. Mouth opening is surrounded by a black coloration, which turns white to the upper part of the upper labials and to the lower part of the lower labials. The first row of chin shields is fully black, and rows 2–5 are half white (towards the outside) and half black. The gular coloration consists of a light orange color, some black scales, and two conspicuous bright yellow-orange speckles under the posterior end of both lower jaws. Ventral coloration is immaculate white.

Variation. Meristic and morphometric data are summarized in Suppl. material 1: table S1. The new individual of *I. microlepidota* (MHNCUP-REP0983) has a smaller snout-vent length when compared to the type series (Suppl. material 1: table S1). Sexual dimorphism appears in the head height (HH), higher in males than in females (6.2 ± 0.5 vs. 5.3 ± 0), in the head length (HL), longer in males (12.1 ± 1 vs. 11.5 ± 0.2), in the scales around the midbody, higher in females (49–50 vs. 43–49), and in the number of ventral scales in transversal view, higher in males (8–10 vs. 8). In addition, the newly collected material presents a proportionally larger HH (Suppl. material 1: table S1) when compared to the type series, probably a consequence of the decomposition stage of the type series when they were found.

Distribution and habitat. *Ichnotropis microlepidota* represents a micro-endemic Angolan species only known to occur at Mount Moco, Huambo Province (Fig. 8). The type series (holotype and paratypes) were found in the crop of a goshawk, which was collected at the base of Mount Moco. However, the locality may lack precision given that the bird could have captured the lizard elsewhere. The habitats at Mount Moco include open montane and fire-prone grasslands with scattered bushes and trees, rocky outcrops, and remnants of Afromontane forest in deep gullies (Fig. 7). The montane grasslands start at around 1800 m a.s.l. but are most prominent above 2100 m a.s.l. and are formed by a thick layer of grass and small bushes as well as many rocks underneath. The grass species present in those grasslands are *Festuca* spp., *Monocymbium ceresiiforme, Themeda triandra, Tristachya inamoena, Tristachya bequertii, Hyparrhenia andongensis,*

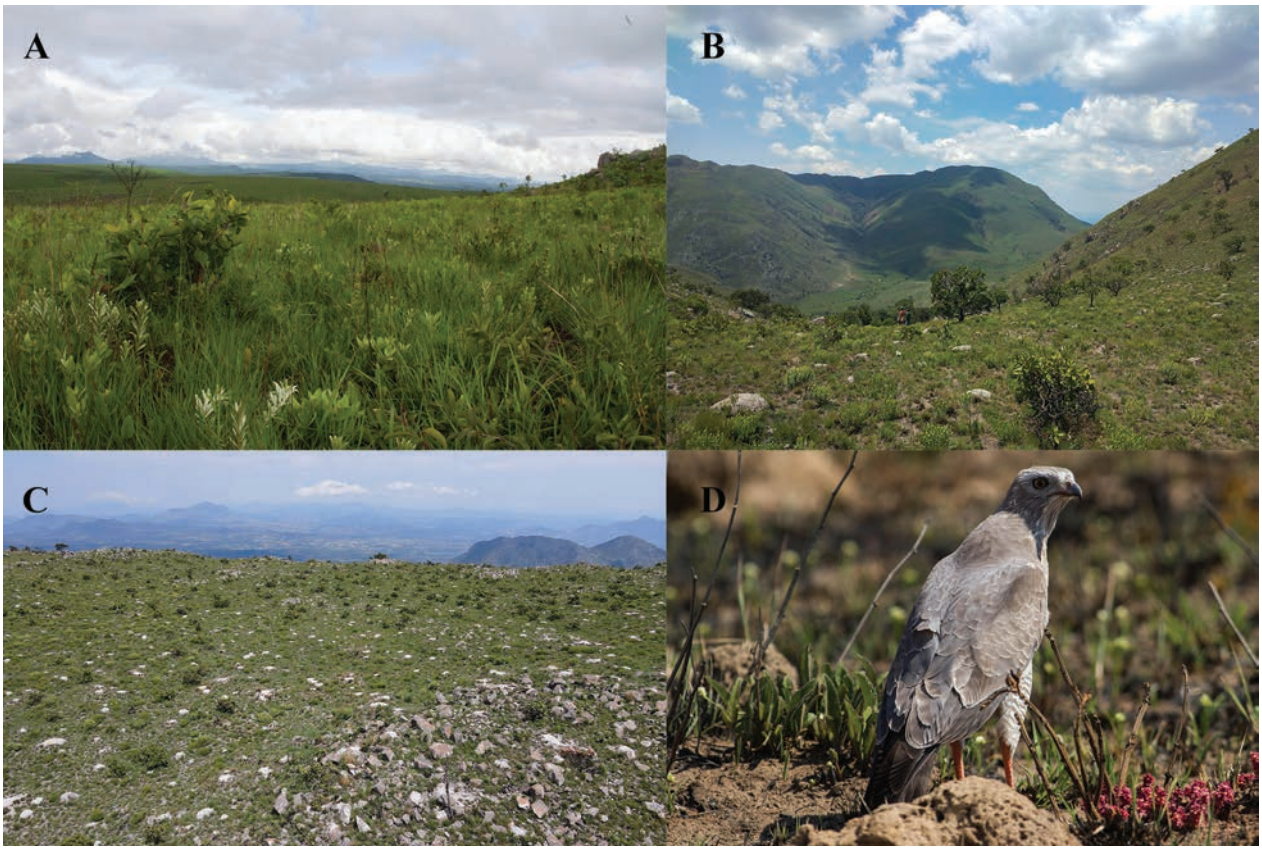

Figure 7. A–C. Habitat of *Ichnotropis microlepidota* in Mount Moco, Huambo Province; **D.** Dark Chanting Goshawk (*Melierax metabates*) from Mount Moco. Photos by Pedro Vaz Pinto.

and *Hyparrhenia quarrei*, among others (Mills et al. 2011). Shrub cover usually includes species such as *Cliffortia* spp., *Erica* spp., *Philippia benguelensis, Protea trichophylla, Stoebe vulgaris*, and *Xerophyta* spp., although the last ones mainly appear in rocky outcrops (Mills et al. 2011).

Natural history. *Ichnotropis microlepidota* is a ground-dwelling lizard with diurnal habits. The specimen reported here (MHNCUP-REP0983) was found during the day on top of an exposed small rock in open montane grassland habitat, with thick vegetation cover. Few reptile species were observed in the area, but at least one Viperidae species has been previously recorded in the region and same habitat, namely the endemic *Bitis heraldica*, which may prey on *Ichnotropis microlepidota*. Other reptile species recorded nearby but associated with rocky or wetland habitat included *Crotaphopeltis hotamboeia, Cordylus momboloensis, Trachylepis albopunctata, Trachylepis sulcata, Panaspis cabindae, Agama* cf. *schacki*, and *Afroedura wulfhaackei*.

Conservation status. The species is listed as Data Deficient (DD) on the IUCN Red List (Ceríaco et al. 2020c). This is a consequence of the lack of information about the distribution of this species and the specific threats that menace the sites where it occurs. Even with the collection of this new individual of *I. microlepidota* (MHNCUP-REP0983), this information is still incomplete, and therefore, it is likely that this species will remain listed as Data Deficient (DD).

Discussion

Although most lacertid genera in Angola have been recently revised and several new species have been described (Conradie et al. 2012b; Branch et al. 2019b; Baptista et al. 2020; Parrinha et al. 2021; Marques et al. 2022b), *Ichnotropis* has been neglected as a consequence of the lack of fresh material to evaluate the species relationships in a phylogenetic context. Therefore, the relationships between the genus members and the taxonomical status of some of them, such as *I. microlepidota*, have been the subject of debate. The access to newly collected topotypical material from Mount Moco and additional fresh material from different sites across the Angolan territory has allowed us to verify the taxonomic status of the species, but also to better assess the relationships of *I. microlepidota* with other members of this group, providing the first phylogenetic placement of *I. microlepidota.*

Morphologically, the new material of *I. microlepidota* (MHNCUP-REP0983) from Mount Moco agreed with the original description of *I. microlepidota* (Marx 1956). In addition, the genetic information has allowed us to demonstrate that *I. microlepidota* represents a distinct taxon within the *bivittata* group, which conforms a monophyletic clade containing *I. bivittata* and *I. microlepidota* as sister species. Although the nodal support within this group is sufficient, further sampling efforts are needed to obtain new fresh material within the group to provide a larger and more robust phylogenetic hypothesis.

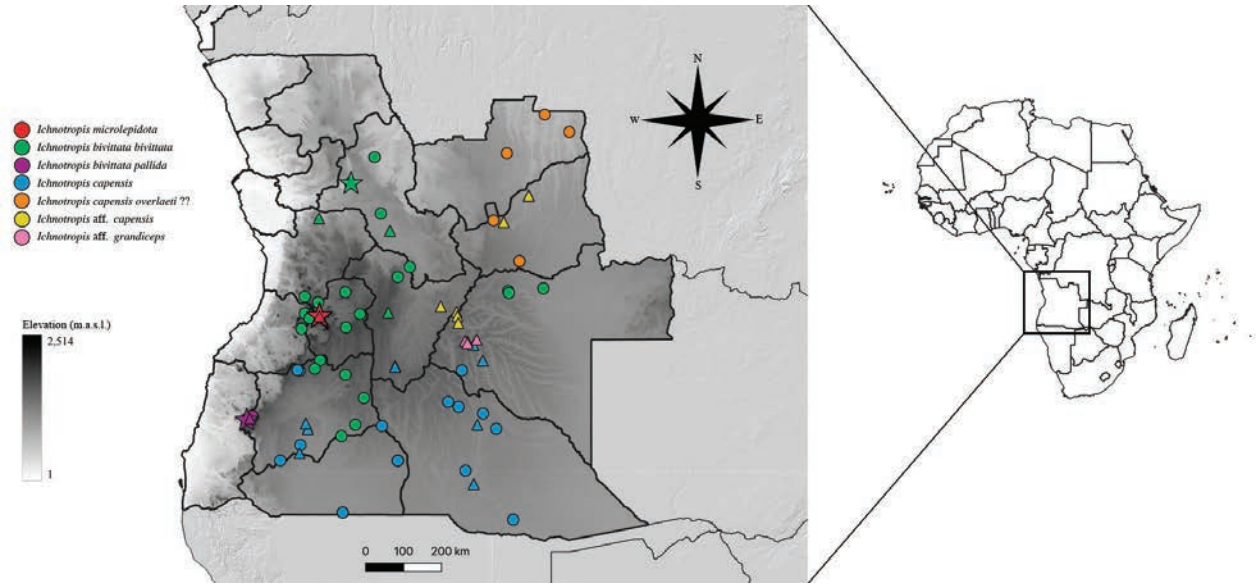

Figure 8. Geographic distribution of *Ichnotropis* within Angolan territory, on a greyscale elevation map (Fick and Hijmans 2017). Different colors depict records of different species within *Ichnotropis*; see the inset for color explanations. Circles represent historical records, triangles denote newly collected material, and start denotes type localities.

The phylogenetic reconstruction recovered three main groups among Angolan *Ichnotropis*, including five different taxa (*I.* aff. *grandiceps*, *I. capensis*, *I.* aff. *capensis*, *I. bivittata*, and *I. microlepidota*). Even though the two subspecies of *I. bivittata* show relevant mitochondrial distances in the *16S* gene (4.03%), we cannot confirm whether the *I. b. pallida* subspecies represents a valid species or not due to the lack of sufficient genetic and morphological material for this work. Therefore, further sampling is recommended to clarify the taxonomy of this subspecies. Moreover, we failed to retrieve any genetic lineage that can be ascribed to *I. c. overlaeti* (see below regarding the status of this subspecies) in Angola (Marques et al. 2018). On the other hand, our phylogenetic and morphological analyses retrieve a highly divergent clade within the *capensis* group that represents a candidate new species (namely, *I.* aff. *capensis*). In addition, detailed examination of the type series of *I. c. overlaeti* and *I. c. nigrescens* challenges the validity of these two subspecies and places them in the *bivittata* group. Thus, the taxonomic status of this candidate new species cannot be resolved in this work due to taxonomic inconsistencies found in the original description and the detailed examination of the type series of *I. c. overlaeti* and *I. c. nigrescens*. Consequently, a detailed revision of this entire group is still needed to shed light on the taxonomy of all *Ichnotropis*.

External morphology seems to be very conserved among *Ichnotropis* species, and few characters are reliable enough to identify species. However, the new material has allowed us to provide unequivocal diagnostic character between *I. microlepidota* and other *Ichnotropis* species in terms of scalation, coloration, and morphometry. In addition, we identified some diagnostic characters on the skull between *I. microlepidota* and I. *bivittata*. However, previous works have already shown that lizard species can display significant intraspecific osteological variation (e.g., Lobón-Rovira 2024a), and therefore the cranial diagnostic characters here proposed must be taken with caution due to the low series used for this osteological comparison. In addition, despite the fact that morphology is very conserved in this group, *I. microlepidota* can be easily distinguished morphologically and genetically from *I. bivittata* (the only species occurring in sympatry), and therefore guarantees the taxonomic status of this species.

Color polymorphism is known for being highly prevalent among and within Lacertidae. This has led to dismissing coloration as a reliable diagnostic character to use to distinguish between different taxa (Brock et al. 2022). However, the large series of material examined in this work have allowed us to assess coloration features that we consider worth mentioning, which could be useful when identifying *I. microlepidota* from other *Ichnotropis* species (namely, the lack of a red/orange lateral band in adult males and the presence of consecutive rows of black encircled white ocelli). Moreover, the narrowly spaced yellow spots above the forelimbs present in *I. bivittata* and absent in *I. microlepidota* are a key coloration feature to take into consideration to differentiate the two species. These spots are the reason for finally identifying the doubtful individual in van den Berg (2020) as *I. bivittata* and not *I. microlepidota*.

The results of this work represent another example of the importance of the central highlands as the main center of endemism in southwestern Africa for amphibians and reptiles (Bauer et al. 2023; Lobón-Rovira 2024a) as well as underline the importance of Mount Moco as an important conservation area (Gonçalves et al. 2019; Branch et al. 2021; Lobón-Rovira et al. 2021a; Conradie et al. 2022c; Baptista et al. 2023; Bates et al. 2023).

In addition, we consider that this elusive species might exist in other areas with similar habitat traits, such as Mount Namba, and consequently we highlight the importance of further surveys on the central highlands aiming to shed light on the distribution and conservation status of this still poorly known endemic lizard.

It must be highlighted that the conservation status of this species remains unclear due to the lack of data about its distribution and relative abundance (Ceríaco et al. 2020c). However, the grassland habitat in Mount Moco is highly threatened by intentionally provoked bushfires to create suitable land portions for agriculture and livestock, which affects possible suitable habitat for this species (Cáceres et al. 2013). Furthermore, montane grasslands seem to play a crucial role in complicating the detectability of this species and others in this area, which are also rarely found in surveys, such as the Angolan adder (*Bitis heraldica*) (Ceríaco et al. 2020d). Consequently, this highlights again the importance of continuing fieldwork in these remote and poorly explored areas of Angola to shed light on the conservation status of this endemic species.

To conclude, this work demonstrates the taxonomic status of a poorly known and endemic Angolan species but also provides the first revision of this group in Africa. We here provide crucial genetic material for key species of this group (i.e., *I. microlepidota*) that can help to solve future taxonomic questions on this group. Therefore, this work can help to better understand the evolutionary history of elusive ground lizards and serve as a foundation for future studies in this group.

Acknowledgements

Work supported by National Funds through FCT-Fundação para a Ciência e a Tecnologia in the scope of the project LA/P/0048/2020. This work was only possible due to the institutional collaboration with the Ministry of Environment of the Republic of Angola (MINAMB), and in particular, the support received by Dr. Miguel Xavier, Director of Instituto Nacional de Biodiversidade e Conservação (INBC). We also acknowledge the remarkable logistical assistance of Fundaçao Kissama, especially Vlady Russo. JLR is currently supported by Associação BIOPOLIS CIBIO Base FUI 2020–2023 - UIDB1 50027 i2020. We thank CTM staff (especially Susana Lopes, Sofia Mourão, and Patrícia Ribeiro) at CIBIO for their tireless work and support in the lab. This work was partially supported by the Synthesis+ BE-TAF Project 2022 Grant obtained by JLR. We thank Garin Cael and Olivier Pauwels, from RMCA and RBINS, respectively, for their kind support providing relevant material deposited in their respective herpetological museums. WC thanks the Wild Bird Trust, which administrates the National Geographic Okavango Wilderness Project (2015–2019 National Geographic Society grant), and Chris Brooks, who organized the SAREP Aquatic Biodiversity Survey of the upper Angola Catchments of the Cubango-Okavango River Basin (May 2012) and the lower Cuito and Cuando River basins (April 2013). Material was collected and exported under the following export permits issued by the Angolan Ministry of Environment Institute of Biodiversity (MINAMB): 31/GGPCC/2016, 151/INBAC/MINAMB/2019). WC further thanks Chad Keates for processing the samples collected by him.

References

Baptista NL (2024) Conservation biogeography of Angolan amphibians. [PhD Thesis]. Porto: Faculdade de Ciências da Universidade do Porto.

Baptista NL, Conradie W, Vaz Pinto P, Branch WR (2019) The amphibians of Angola: Early studies and the current state of knowledge. In: Huntley BJ, Russo V, Lages F, Ferrand N (Eds) Biodiversity of Angola. Science & Conservation: A Modern Synthesis. Springer, Cham, 24–281.

Baptista NL, Tolley KA, Bluhm M, Finckh M, Branch WR (2020) Rediscovery, range extension, habitat and phylogenetic relation of the endemic Scaled Sandveld Lizard *Nucras scalaris* Laurent, 1964 (Sauria: Lacertidae) in the central Angolan plateau. African Journal of Herpetology 69(1): 12–28. https://doi.org/10.1080/21564574.2020.1778108

Baptista NL, Pinto PV, Keates C, Edwards S, Roedel MO, Conradie W (2021) A new species of red toad, *Schismaderma* Smith, 1849 (Anura: Bufonidae), from central Angola. Zootaxa 5081(3): 301–332. https://doi.org/10.11646/zootaxa.5081.3.1

Baptista NL, Pinto PV, Keates C, Lobón-Rovira J, Edwards S, Rödel MO (2023) Two new *Poyntonophrynus* species (Anura: Bufonidae) highlight the importance of Angolan centers of endemism. Vertebrate Zoology 73: 991–1031. https://doi.org/10.3897/vz.73.e103935

Bates MF, Lobón-Rovira J, Stanley EL, Branch WR, Pinto PV (2023) A new species of green-eyed *Cordylus* Laurenti, 1768 from the west-central highlands of Angola, and the rediscovery of *Cordylus angolensis* (Bocage, 1895) (Squamata: Cordylidae). Vertebrate Zoology 73: 599–646. https://doi.org/10.3897/vz.73.e95639

Bauer AM, Ceríaco LMP, Marques MP, Becker FS (2023) Highland reptiles of Angola and Namibia. Namibian Journal of Environment 8: 259–276.

Bocage JVB (1866) Lista dos reptis das possessões portuguezas d`Africa occidental que existem no Museu de Lisboa. - Jornal de Sciencias Mathematicas, Physicas e Naturaes, Academia Real das Sciencias de Lisboa 1(1): 37–56.

Böhm M, Collen B, Baillie JEM, Bowles P, Chanson J, Cox N, Hammerson G, Hoffmann M, Livingstone SR, Ram M, Rhodin AGJ, Stuart SN, van Dijk PP, Young BE et al. (2013) The conservation status of the world's reptiles. Biological Conservation 157: 372–385. https://doi.org/10.1016/j.biocon.2012.07.015

Boulenger GA (1887) Catalogue of the lizards in the British Museum (Natural History). Vol. III. Lacertidae. - London, 1887: I-XII + 1–118.

Boulenger GA (1917) XXII.—Descriptions of new lizards of the family Lacertidæ. Annals and Magazine of Natural History 19(111): 277–279. https://doi.org/10.1080/00222931709486935

Boulenger GA (1921) Monograph of the Lacertidae. Vol. II. - British Museum (Natural History). Department of Zoology, London, 451 pp.

Branch WR (1998) Field guide to snakes and other reptiles of southern Africa, Struik Publishers, Cape Town, South Africa, 160–176.

Branch WR, Bayliss J, Tolley KA (2014) Pygmy chameleons of the *Rhampholeon platyceps* complex (Squamata: Chamaeleonidae): Description of four new species from isolated 'sky islands' of northern Mozambique. Zootaxa 3814(1): 1–36. https://doi.org/10.11646/zootaxa.3814.1.1

Branch WR, Baptista N, Pinto PV (2018) Angolan amphisbaenians: rediscovery of *Monopeltis luandae* Gans 1976, with comments on the type locality of *Monopeltis perplexus* Gans 1976 (Sauria: Amphisbaenidae). Herpetology Notes 11: 603–606.

Branch WR, Conradie W, Vaz Pinto P, Tolley K (2019a) Another Angolan Namib endemic species: a new *Nucras* Gray, 1838 (Squamata: Lacertidae) from south-western Angola. Amphibian & Reptile Conservation 12(2): 85–95. https://zenodo.org/doi/10.5281/zenodo.3731976

Branch WR, Baptista N, Keates C, Edwards S (2019b) Rediscovery, taxonomic status, and phylogenetic relationships of two rare and endemic snakes (Serpentes: Psammophiinae) from the south-western Angolan plateau. Zootaxa 4590(3): 342–366. https://doi.org/10.11646/zootaxa.4590.3.2

Branch WR, Baptista N, Pinto PV, Conradie W (2019c) The reptiles of Angola – history, diversity, endemism and hotspots. In: Huntley BJ, Ferrand N (Eds) Biodiversity of Angola. Science & Conservation: A Modern Synthesis. Springer, Cham, 283–326.

Branch WR, Schmitz A, Lobón-Rovira J, Baptista NL, António T, Conradie W (2021) Rock island melody: A revision of the *Afroedura bogerti* Loveridge, 1944 group, with descriptions of four new endemic species from Angola. Zoosystematics and Evolution 97(1): 55–82. https://doi.org/10.3897/zse.97.57202

Broadley DG (1967) The life cycles of two sympatric species of *Ichnotropis* (Sauria: Lacertidae). Zoologica Africana 3(1): 1–2. https://doi.org/10.1080/00445096.1965.11447347

Broadley DG (1974) Field studies on 'annual lizards' of the genus Ichnotropis. The Rhodesia science news 8, 309 pp.

Broadley DG (1979) A field study of two sympatric "annual" lizards (genus Ichnotropis) in Rhodesia. South African Journal of Zoology 14(3): 133–138. https://doi.org/10.1080/02541858.1979.11447662

Brock KM, McTavish EJ, Edwards DL (2021) Color polymorphism is a driver of diversification in the lizard family Lacertidae. Systematic Biology 71(1): 24–39. https://doi.org/10.1093/sysbio/syab046

Butler BO, Ceríaco LM, Marques MP, Bandeira S, Júlio T, Heinicke M P, Bauer AM (2019) Herpetological survey of Huíla Province, southwest Angola, including first records from Bicuar National Park. Herpetological Review 50(2): 225–240.

Cáceres A, Santos P, Tchalo F, Mills M, Melo M (2013) Human use of natural resources and the conservation of the afromontane forest in Mount Moco, Angola. Journal of Sustainable Development in Africa 15(3): 91–101.

Ceríaco LM, Marques MP, Bandeira S, Agarwal I, Stanley EL, Bauer AM, Heinicke MP, Blackburn DC (2018) A new earless species of *Poyntonophrynus* (Anura, Bufonidae) from the Serra da Neve inselberg, Namibe province, Angola. ZooKeys 780: 109–136. https://doi.org/10.3897/zookeys.780.25859

Ceríaco LM, Agarwal I, Marques MP, Bauer AM (2020a) A review of the genus *Hemidactylus* Goldfuss, 1820 (Squamata: Gekkonidae) from Angola, with the description of two new species. Zootaxa 4746(1): 1–71. https://doi.org/10.11646/zootaxa.4746.1.1

Ceríaco LMP, Heinicke MP, Parker K, Marques MP, Bauer AM (2020b) A review of the African snake-eyed skinks (Scincidae: *Panaspis*) from Angola, with the description of a new species. Zootaxa 4747(1): 77–112. https://doi.org/10.11646/zootaxa.4747.1.3

Ceríaco LMP, Baptista NL, Conradie W (2020c) *Ichnotropis microlepidota*. The IUCN Red List of Threatened Species 2020: e. T44929734A44929746. [Accessed on 27 July 2024]

Ceríaco LM, Tolley KA, Marques MP, Heinicke MP, Bauer AM (2020d) A dwarf among giants: phylogenetic position of the elusive Angolan Adder (*Bitis heraldica*) and biogeographic affinities of Angolan Afromontane regions. African Journal of Herpetology 69(1): 108–118. https://doi.org/10.1080/21564574.2020.1782484

Ceríaco LMP, Agarwal I, Marques MP, Bauer AM (2020e) A correction to a recent review of the genus *Hemidactylus* Goldfuss, 1820 (Squamata: Gekkonidae) from Angola, with the description of two additional species. Zootaxa 4861(1): 92–106. https://doi.org/10.11646/zootaxa.4861.1.6

Ceríaco LM, Santos BS, Marques MP, Bauer AM, Tiutenko A (2021) Citizen Science meets specimens in old formalin filled jars: a new species of Banded Rubber Frog, genus *Phrynomantis* (Anura, Phrynomeridae) from Angola. Alytes 38(1–4): 18–48.

Ceríaco LM, Marques MP, Parrinha D, Tiutenko A, Weinell JL, Butler BO, Bauer AM (2024) The *Trachylepis* (Squamata: Scincidae) of Angola: an integrative taxonomic review with the description of seven new species. Bulletin of the American Museum of Natural History 465: 1–153. https://doi.org/10.1206/0003-0090.465.1.1

Collyer ML, Adams DC (2018) RRPP: An r package for fitting linear models to high-dimensional data using residual randomization. Methods in Ecology and Evolution 9(7): 1772–1779. https://doi.org/10.1111/2041-210X.13029

Conradie W (2024) Herpetofaunal diversity and affiliations of the unexplored south-eastern Angola. [PhD Thesis]. South Africa: Nelson Mandela University, 640 pp.

Conradie W, Branch WR, Measey GJ, Tolley KA (2012a) A new species of *Hyperolius* Rapp, 1842 (Anura: Hyperoliidae) from the Serra da Chela mountains, southwestern Angola. Zootaxa 3269(1): 1–17. https://doi.org/10.11646/zootaxa.3269.1.1

Conradie W, Measey GJ, Branch WR, Tolley KA (2012b) Revised phylogeny of African sand lizards (*Pedioplanis*), with the description of two new species from south-western Angola. African Journal of Herpetology 61(2): 91–112. https://doi.org/10.1080/21564574.2012.676079

Conradie W, Branch WR, Tolley KA (2013) Fifty shades of grey: giving colour to the poorly known Angolan Ashy reed frog (Hyperoliidae: *Hyperolius cinereus*), with the description of a new species. Zootaxa 3635(3): 201–223. https://doi.org/10.11646/zootaxa.3635.3.1

Conradie W, Deepak V, Keates C, Gower DJ (2020) Kissing cousins: a review of the African genus *Limnophis* Günther, 1865 (Colubridae: Natricinae), with the description of a new species from north-eastern Angola. African Journal of Herpetology 69(1): 79–107. https://doi.org/10.1080/21564574.2020.1782483

Conradie W, Baptista NL, Verburgt L, Keates C, Harvey J, Julio T, Neef G (2021) Contributions to the herpetofauna of the Angolan Okavango-Cuando-Zambezi river drainages. Part 1: Serpentes (snakes).

Conradie W, Keates C, Baptista NL, Lobón-Rovira J (2022a) Taxonomical review of *Prosymna angolensis* Boulenger, 1915 (Elapoidea, Prosymnidae) with the description of two new species. ZooKeys 1121: 97–143. https://doi.org/10.3897/zookeys.1121.85693

Conradie W, Keates C, Verburgt L, Baptista NL, Harvey J, Julio T, Neef G (2022b) Contributions to the herpetofauna of the Angolan Okavango-Cuando-Zambezi River drainages. Part 2: Lizards (Sauria), chelonians, and crocodiles.

Conradie W, Schmitz A, Lobón-Rovira J, Becker FS, Vaz Pinto P, Hauptfleisch ML (2022c) Rock island melody remastered: two new species in the *Afroedura bogerti* Loveridge, 1944 group from Angola and Namibia. Zoosystematics and Evolution 98(2): 435–453. https://doi.org/10.3897/zse.98.86299

Conradie W, Keates C, Verburgt L, Baptista NL, Harvey J (2023) Contributions to the herpetofauna of the Angolan Okavango-Cuando-Zambezi river drainages. Part 3: Amphibians.

Conroy CJ, Papenfuss T, Parker J, Hahn NE (2009) Use of Tricaine Methanesulfonate (MS222) for Euthanasia of Reptiles. Journal of the American Association for Laboratory Animal Science 48: 28–32.

Cowan O, Conradie W, Keates C, Telford NS, Petford M, Egan V, Tolley KA (2024) Lost lizards: The importance of targeted surveys in filling knowledge gaps for reptile conservation in South Africa. Journal for Nature Conservation 84: 126790. https://doi.org/10.1016/j.jnc.2024.126790

Deikumah JP, McAlpine CA, Maron M (2014) Biogeographical and taxonomic biases in tropical forest fragmentation research. Conservation Biology 28(6): 1522–1531. https://doi.org/10.1111/cobi.12348

Edwards S, Branch WR, Vanhooydonck B, Herrel A, Measey GJ, Tolley KA (2013) Taxonomic adjustments in the systematics of the southern African lacertid lizards (Sauria: Lacertidae). Zootaxa 3669(2): 101–114. https://doi.org/10.11646/Zootaxa.3669.2.1

Engleder A, Haring E, Kirchhof S, Mayer W (2013) Multiple nuclear and mitochondrial DNA sequences provide new insights into the phylogeny of South African Lacertids (Lacertidae, Eremiadinae). Journal of Zoological Systematics and Evolutionary Research 51(2): 132–143. https://doi.org/10.1111/jzs.12012

Fick SE, Hijmans RJ (2017) WorldClim 2: new 1-km spatial resolution climate surfaces for global land areas. International Journal of Climatology 37(12): 4302–4315. https://doi.org/10.1002/joc.5086

Gonçalves FM, Braine D, Bauer AM, Valério H, Marques MP, Ceríaco LM (2019) Rediscovery of the poorly known Angolan Adder, *Bitis heraldica* (Bocage, 1889) (Serpentes: Viperidae): New records, live photographs and first case history of envenomation. Herpetological Review 50(2): 241–246.

Hallermann J, Ceríaco LMP, Schmitz A, Ernst R, Conradie W, Verburgt L, Marques MP, Bauer AM (2020) A review of the Angolan House snakes, genus *Boaedon* Duméril, Bibron and Duméril (1854) (Serpentes: Lamprophiidae), with description of three new species in the *Boaedon fuliginosus* (Boie, 1827) species complex. African Journal of Herpetology 69(1): 29–78. https://doi.org/10.1080/21564574.2020.1777470

Hoang DT, Chernomor O, Von Haeseler A, Minh BQ, Vinh LS (2018) UFBoot2: improving the ultrafast bootstrap approximation. Molecular Biology and Evolution 35(2): 518–522. https://doi.org/10.1093/molbev/msx281

Huelsenbeck JP, Hillis DM (1993) Success of phylogenetic methods in the four-taxon case. Systematic Biology 42(3): 247–264. https://doi.org/10.1093/sysbio/42.3.247

Jacobsen NHG (1987) Notes on Reproduction in Ichnotropis squamulosa and Interspecific competition with Ichnotropis capensis in the Transvaal. The Journal of the Herpetological Association of Africa 33: 51–63.

Kumar S, Stecher G, Li M, Knyaz C, Tamura K (2018) MEGA X: Molecular evolutionary genetics analysis across computing platforms. Molecular Biology and Evolution 35: 1547–1549. https://doi.org/10.1093/molbev/msy096

Lanfear R, Frandsen PB, Wright AM, Senfeld T, Calcott B (2017) PartitionFinder 2: new methods for selecting partitioned models of evolution for molecular and morphological phylogenetic analyses. Molecular Biology and Evolution 34(3): 772–773.

Laurent RF (1952) Batraciens et reptiles récemment acquis par le Musée du Congo Belge. Revue Zoologique et Botanique Africaine 45(3, 4): 198–203.

Laurent RF (1964) Reptiles et Amphibiens de l'Angola (Troisième contribution). Publicações culturais da Companhia de Diamantes de Angola 67: 11–165.

Lindken T, Anderson CV, Ariano-Sánchez D, Barki G, Biggs C, Bowles P, Chaitanya R, Cronin DT, Jähnig SC, Jeshcke JM, Kennerley RJ, Lacher T, Swandby JL, Liu C, Long B, Mallon DP, Martin GM, Meiri S, Pasachnik S, Reynoso VH, Stanford CB, Stephenson PJ, Tolley K, Carvajal OT, Waldien DL, Woinarski J, Evans T (2024) What factors influence the rediscovery of lost tetrapod species?. Global Change Biology 30(1): e17107. https://doi.org/10.1111/gcb.17107

Lobón-Rovira J (2024a) Inferring the evolutionary trends in Southern Africa geckos: from wide to local perspective. Ph.D. Thesis. University of Porto, Porto, 524 pp.

Lobón-Rovira J, Bauer AM (2021) Bone-by-bone: A detailed skull description of the White-headed dwarf gecko *Lygodactylus picturatus* (Peters, 1870). African Journal of Herpetology 70(2): 75–94. https://doi.org/10.1080/21564574.2021.1980120

Lobón-Rovira J, Conradie W, Buckley Iglesias D, Ernst R, Veríssimo L, Baptista NL, Pinto PV (2021) Between sand, rocks and branches: An integrative taxonomic revision of Angolan *Hemidactylus* Goldfuss, 1820, with description of four new species. Vertebrate Zoology 71: 465–501. https://doi.org/10.3897/vz.71.e64781

Lobón-Rovira J, Conradie W, Baptista NL, Pinto PV (2022) A new species of feather-tailed leaf-toed gecko, *Kolekanos* Heinicke, Daza, Greenbaum, Jackman & Bauer, 2014 (Squamata, Gekkonidae) from the poorly explored savannah of western Angola. ZooKeys 1127: 91–116. https://doi.org/10.3897/zookeys.1127.84942

Lobón-Rovira J, Bauer AM, Pinto PV, Trape JF, Conradie W, Kusamba C, Júlio T, Cael G, Stanley EL, Hughes DF, Behangana M, Masudi FM, Pauwels OP, Greenbaum E (2024b) Integrative revision of the *Lygodactylus gutturalis* (Bocage, 1873) complex unveils extensive cryptic diversity and traces its evolutionary history. Zoological Journal of the Linnean Society 201(2): 447–492. https://doi.org/10.1093/zoolinnean/zlad123

Lobón-Rovira J, Baptista NL, Clark T, Verburgt L, Jongsma G, Conradie W, Veríssimo L, Pinto PV (2024c) Filling the gaps: herpetological checklist of Mayombe National Park and Cabinda Province (Angola) shed light on one of the most unexplored corners of tropical Central Africa. African Journal of Herpetology 2025: 1–59.

Makokha JS, Bauer, AM, Mayer W, Matthee CA (2007) Nuclear and mtDNA-based phylogeny of southern African sand lizards, Pedioplanis (Sauria: Lacertidae). Molecular Phylogenetics and Evolution 44(2): 622-633. https://doi.org/10.1016/j.ympev.2007.04.021

Marques MP, Ceríaco LM, Blackburn DC, Bauer AM (2018) Diversity and distribution of the amphibians and terrestrial reptiles of Angola: atlas of historical and bibliographic records (1840–2017). California Academy of Sciences.

Marques MP, Ceriaco LM, Stanley EL, Bandeira S, Agarwal I, Bauer AM (2019) A new species of girdled lizard (Squamata: Cordylidae) from the Serra da Neve Inselberg, Namibe Province, southwestern Angola. Zootaxa 4668(4): 503–524. https://doi.org/10.11646/zootaxa.4668.4.4

Marques MP, Ceriaco LM, Buehler MD, Bandeira S, Janota JM, Bauer AM (2020a) Description of a new long-tailed skink (Scincidae: *Trachylepis*) from Angola and the Democratic Republic of the Congo. Zootaxa 4568(1): 51–68. https://doi.org/10.11646/zootaxa.4568.1.3

Marques MP, Ceríaco LM, Buehler MD, Bandeira S, Janota JM, Bauer AM (2020b) A revision of the Dwarf Geckos, genus *Lygodactylus* (Squamata: Gekkonidae), from Angola, with the description of three new species. Zootaxa 4583(3): 301–352. https://doi.org/10.11646/zootaxa.5555.3.1

Marques MP, Parrinha D, Santos BS, Bandeira S, Butler BO, Sousa ACA, Bauer AM, Wagner P (2022a) All in all it's just another branch in the tree: A new species of *Acanthocercus* Fitzinger, 1843 (Squamata: Agamidae), from Angola. Zootaxa 5099(2): 221–243. https://doi.org/10.11646/zootaxa.5099.2.4

Marques MP, Ceríaco LM, Heinicke MP, Chehouri RM, Conradie W, Tolley A, Bauer AM (2022b) The Angolan bushveld lizards, genus *Heliobolus* Fitzinger, 1843 (Squamata: Lacertidae): Integrative taxonomy and the description of two new species. Vertebrate Zoology 72: 745–769. https://doi.org/10.3897/vz.72.e85269

Marques MP, Parrinha D, Ceríaco LM, Brennan IG, Heinicke MP, Bauer AM (2023a) A new species of thick-toed gecko (*Pachydactylus*) from Serra da Neve and surrounding rocky areas of southwestern Angola (Squamata: Gekkonidae). Vertebrate Zoology 73: 325–343. https://doi.org/10.3897/vz.73.e101329

Marques MP, Parrinha D, Tiutenko A, Lopes-Lima M, Bauer AM, Ceríaco LM (2023b) A new species of African legless skink, genus *Acontias* Cuvier, 1816 "1817" (Squamata: Scincidae) from Serra da Neve inselberg, south-western Angola. African Journal of Herpetology 72(2): 145–162. https://doi.org/10.1080/21564574.2023.2246487

Marques MP, Parrinha D, Lopes-Lima M, Tiutenko A, Bauer AM, Ceríaco LM (2024a) An island in a sea of sand: a first checklist of the herpetofauna of the Serra da Neve inselberg, southwestern Angola. ZooKeys 1201: 167–217. https://doi.org/10.3897/zookeys.1201.120750

Marques MP, Parrinha D, Lopes-Lima M, Tiutenko A, Bauer AM, Ceríaco LM (2024b) A treasure trove of endemics: two new species of snake-eyed skinks of the genus Panaspis Cope, 1868 (Squamata, Scincidae) from the Serra da Neve Inselberg, southwestern Angola. Evolutionary Systematics 8: 167–182. https://doi.org/10.3897/evolsyst.8.121103

Marx H (1956) A new lacertid lizard from Angola. Publication (Chicago Natural History Museum), 802 pp.

Mayer W (2013) Kommentierte Lacertiden-Liste für Europa, Afrika, den Nahen Osten inklusive der Arabischen Halbinsel und Asien. Lacertidae (Eidechsen Online) 7: 81–141.

Meiri S, Bauer AM, Allison A, Castro-Herrera F, Chirio L, Colli G, Das I, Doan TM, Glaw F, Grismer LL, Hoogmoed M, Kraus F, LeBreton M, Meirte D, Nagy ZT, Nogueira CC, Oliver P, Pauwels OSG, Pincheira-Donoso D, Shea G, Sindaco R, Tallowin OJS, Torres-Carvajal O, Trape JF, Uetz P, Wagner P, Wang Y, Ziegler T, Roll U (2018) Extinct, obscure or imaginary: the lizard species with the smallest ranges. Diversity and Distributions 24(2): 262–273. https://doi.org/10.1111/ddi.12678

Miller MA, Pfeiffer W, Schwartz T (2010) Creating the CIPRES science gateway for inference of large phylogenetic trees. In: Gateway Computing Environments Workshop 2010: 1–8.

Mills MS, Olmos F, Melo M, Dean WRJ (2011) Mount Moco: its importance to the conservation of Swierstra's Francolin *Pternistis swierstrai* and the Afromontane avifauna of Angola. Bird Conservation International 21(2): 119–133. https://doi.org/10.1017/S0959270910000493

Minh BQ, Dang CC, Vinh LS, Lanfear R (2021) QMaker: fast and accurate method to estimate empirical models of protein evolution. Systematic Biology 70(5): 1046–1060. https://doi.org/10.1093/sysbio/syab010

Nielsen SV, Conradie W, Ceríaco LMP, Bauer AM, Heinicke MP, Stanley EL, Blackburn DC (2020) A new species of Rain Frog (Brevicipitidae, *Breviceps*) endemic to Angola. ZooKeys 979: 133–160. https://doi.org/10.3897/zookeys.979.56863

Ogwu MC, Izah SC, Iyiola AO (2022) An Overview of the Potentials, Threats and Conservation of Biodiversity in Africa. In: Chibueze Izah S (Eds) Biodiversity in Africa: Potentials, Threats and Conservation. Sustainable Development and Biodiversity 29. Springer, Singapore.

Palumbi SR (1996) The polymerase chain reaction. In: Hillis D, Moritz C, Mable B (Eds) Molecular Systematics. 2nd edn. Sunderland: Sinauer Associates, 205–247.

Parker HW (1936) Dr. Karl Jordan's expedition to South-West Africa and Angola: herpetological collection. Novitates Zoologicae 40: 115–146.

Parrinha D, Marques MP, Heinicke MP, Khalid F, Parker KL, Tolley KA, Childers JL, Conradie W, Bauer AM, Ceríaco LM (2021) A revision of Angolan species in the genus *Pedioplanis* Fitzinger (Squamata: Lacertidae), with the description of a new species. Zootaxa 5032(1): 1–46. https://doi.org/10.11646/zootaxa.5032.1.1

Prates I, Melo-Sampaio PR, de Oliveira Drummond L, Teixeira Jr M, Rodrigues MT, Carnaval AC (2017) Biogeographic links between southern Atlantic Forest and western South America: rediscovery, re-description, and phylogenetic relationships of two rare montane anole lizards from Brazil. Molecular Phylogenetics and Evolution 113: 49–58. https://doi.org/10.1016/j.ympev.2017.05.009

Putra CA, Amarasinghe AT, Hikmatullah D, Scali S, Brinkman J, Manthey U, Ineich I (2020) Rediscovery of Modigliani's nose-horned lizard, *Harpesaurus modiglianii* Vinciguerra, 1933 (Reptilia: Agamidae) after 129 years without any observation. *Taprobanica:* The Journal of Asian Biodiversity 9(1): 3–11. https://doi.org/10.47605/tapro.v9i1.216

Rambaut A, Suchard MA, Xie D, Drummond AJ (2014) Tracer Version 1.6. http://beast.bio.ed.ac.uk/Tracer

Rodrigues MT, Teixeira Jr M, Dal Vechio F, Amaro RC, Nisa C, Camacho A, Damasceno R, Roscito J, Nunes PMS, Recoder RS (2013) Rediscovery of the earless microteiid lizard *Anotosaura collaris* Amaral, 1933 (Squamata: Gymnophthalmidae): a redescription complemented by osteological, hemipenial, molecular, karyological, physiological and ecological data. Zootaxa 3731(3): 345–370. https://doi.org/10.11646/zootaxa.3731.3.5

Ronquist F, Teslenko M, van der Mark P, Ayres DL, Darling A, Hohna S, Larget B, Liu L, Suchard MA, Huelsenback JP (2012) MrBayes 3.2: Efficient Bayesian phylogenetic inference and model choice across a large model space. Systematic Biology 61: 539–542. https://doi.org/10.1093/sysbio/sys029

RStudio Team (2022) RStudio: Integrated Development Environment for R. RStudio, PBC, Boston, MA. http://www.rstudio.com

Rydén O, Zizka A, Jagers SC, Lindberg SI, Antonelli A (2020) Linking democracy and biodiversity conservation: Empirical evidence and research gaps. Ambio 49: 419–433. https://doi.org/10.1007/s13280-019-01210-0

Schmidt KP (1919) Contributions to the herpetology of the Belgian Congo based on the collection of the American Museum Congo Expedition, 1909–1915 (39). American Museum of Natural History.

Smith A (1838) Contributions to the Natural History of Southern Africa. Art. VIII. Magazine of natural history, London 2(14): 92–94.

Solano-Zavaleta I, De la Luz NMC, Clause AG (2017) Solving a 50-year mystery: Rediscovery of Mesaspis antauges (Squamata: Anguidae). Zootaxa 4303(4): 559–572. https://doi.org/10.11646/zootaxa.4303.4.7

Stanley EL, Ceríaco LM, Bandeira S, Valerio H, Bates MF, Branch WR (2016) A review of *Cordylus machadoi* (Squamata: Cordylidae) in southwestern Angola, with the description of a new species from the Pro-Namib desert. Zootaxa 4061(3): 201–226. https://doi.org/10.11646/zootaxa.4061.3.1

Trifinopoulos J, Nguyen LT, von Haeseler A, Minh BQ (2016) W-IQ-TREE: A fast online phylogenetic tool for maximum likelihood analysis. Nucleic Acids Research 44: 232–235. https://doi.org/10.1093/nar/gkw256

Tolley KA, Alexander GJ, Branch WR, Bowles P, Maritz B (2016) Conservation status and threats for African reptiles. Biological Conservation 204: 63–71. https://doi.org/10.1016/j.biocon.2016.04.006

Uetz P, Freed P, Aguilar R, Reyes, F, Kudera J, Hosek J (2025) The Reptile Database. http://www.reptile-database.org [accessed 01/03/2025]

van den Berg MP (2017) An annotated bibliographic history of *Ichnotropis* Peters, 1854 (Reptilia, Lacertidae) with remarks on the validity of some of the including species. Lacertidae (Eidechsen Online) 4: 60–138.

van den Berg MP (2020) Could this be the first live image of *Ichnotropis microlepidota*? Lacertidae (Eidechsen Online) 2: 14–18.

Wagner P, Butler BO, Ceríaco LM, Bauer AM (2021) A new species of the *Acanthocercus atricollis* complex (Squamata: Agamidae). Salamandra 57(4).

Wang K, Ren J, Jiang K, Yuan Z, Siler CD (2017) Rediscovery of the enigmatic Mountain Dragon, *Japalura yulongensis* (Reptilia: Sauria: Agamidae), with notes on its natural history and conservation. Zootaxa 4318(2): 351–363. https://doi.org/10.11646/zootaxa.4318.2.8

Whiting AS, Bauer AM, Sites Jr JW (2003) Phylogenetic relationships and limb loss in sub-Saharan African scincine lizards (Squamata: Scincidae). Molecular phylogenetics and evolution 29(3): 582–598. https://doi.org/10.1016/S1055-7903(03)00142-8

Wiens JJ, Kuczynski CA, Townsend T, Reeder TW, Mulcahy DG, Sites Jr JW (2010) Combining phylogenomics and fossils in higher-level squamate reptile phylogeny: molecular data change the placement of fossil taxa. Systematic Biology 59(6): 674–688. https://doi.org/10.1093/sysbio/syq048

Supplementary material 1

Morphological measurements of all individuals

Authors: Max Benito, Werner Conradie, Pedro Vaz Pinto, Javier Lobón-Rovira

Data type: docx

Explanation note: Information on the individuals used for the skull segmentations; color pallete used in the skull segmentations for bones not included in Lobón-Rovira and Bauer (2021); Principal component analysis (PCA) loadings, ANOVA analysis results; list of individuals used for the genetic work and distribution (map), with information about their museum and field numbers, localities, coordinates and source.

Link: https://doi.org/10.3897/zse.101.136290.suppl1